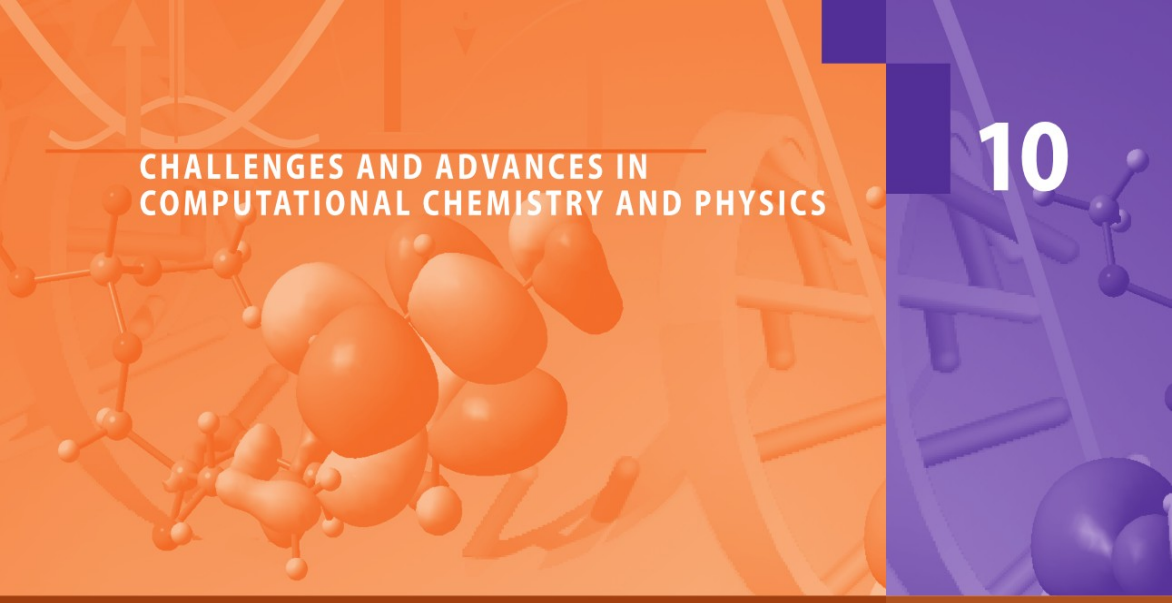

CHALLENGES AND ADVANCES IN COMPUTATIONAL CHEMISTRY AND PHYSICS

10

Series Editor J. Leszczynski

Volume Editors M. Barysz · Y. Ishikawa

Relativistic Methods for Chemists

Springer

Relativistic Methods for Chemists

CHALLENGES AND ADVANCES IN COMPUTATIONAL CHEMISTRY AND PHYSICS

Volume 10

Series Editor:

JERZY LESZCZYNSKI
Department of Chemistry, Jackson State University, U.S.A.

For further volumes:
http://www.springer.com/series/6918

Relativistic Methods for Chemists

Edited by

Maria Barysz
Nicolaus Copernicus University, Toruń, Poland

Yasuyuki Ishikawa
University of Puerto Rico, San Juan, USA

Springer

Editors
Prof. Maria Barysz
Nicolaus Copernicus University
Inst. Chemistry
Dept. Quantum Chemistry
Gagarin Street 7
87-100 Toruń
Poland
teomjb@chem.uni.torun.pl

Prof. Yasuyuki Ishikawa
University of Puerto Rico
Dept. Chemistry
P.O. Box 23346
San Juan PR 00931-3346
USA
yishikawa@uprrp.edu

ISBN 978-1-4020-9974-8 e-ISBN 978-1-4020-9975-5
DOI 10.1007/978-1-4020-9975-5
Springer Dordrecht Heidelberg London New York

Library of Congress Control Number: 2010926093

Cover design: WMXDesign GmbH

Printed on acid-free paper

Springer is part of Springer Science+Business Media (www.springer.com)

PREFACE

Relativistic effects are responsible for a number of well-known chemical phenomena. For instance, the effect on the adsorption energy of carbon monoxide on platinum low-index surfaces is so pronounced that the adsorption energy cannot be described by non-relativistic theory based on the Schrödinger equation. Relativistic effects on Pt–C bond shortening and CO adsorption energy obtained in calculations that include the relativistic correction, and corresponding calculations that exclude the correction, are found dramatic. The adsorption energy increases by about 50% when relativity is included. They point up the importance of accounting for relativistic effects in a general theory of atomic and molecular electronic structure.

In the last 3 decades, a great deal of effort has been expended to develop quasi-relativistic and fully relativistic electronic structure theory to account for these chemical phenomena. With the increasing use of quasi-relativistic and fully relativistic quantum chemical calculations on heavy-atom-containing molecules, there is an obvious need to provide experts' reviews of the concept and computational methods. This volume has the ambitious aim of addressing both experimentalists and theoreticians interested in the area of relativistic effects in atomic and molecular systems and processes and in their consequences for the interpretation of the heavy element's chemistry. The book will include chapters covering basic theory, computational methods, and experimental aspects of interest for chemists. It describes the essential details of the theoretical methods to account for relativistic effects and place them into the context of modern applications, of broad interest to experimentalists and theoretical chemists in both academia and industry.

All the authors are renowned experts in their fields and many topics covered in this volume represent the forefront of today's science.

The leading chapters of the book will concentrate on theory at the intermediate level, starting with the explanatory article intended to show the importance of the relativistic theory and relativistic 'thinking' in chemistry and molecular physics. This introductory chapter will outline the basic features of the transition from non-relativistic to relativistic methods and will be followed by several chapters explaining the most promising recent development in relativistic theories for chemistry and their computational implementations. These chapters cover the all-electron methods in the framework of the two- and four-component relativistic approaches, the relativistic density functional approaches, and more approximate techniques based on the idea of relativistic pseudopotentials.

The several chapters are focused on the relativistic methods for molecular calculations and the problems discussed include relativistic two-component theory, density functional theory, pseudopotentials and correlations. These chapters will be mostly addressed to experimentalists with only general background in theory and to the computational chemists without training in relativistic methods. The reliability of different methods used in relativistic calculations on heavy molecules will be thoroughly discussed. This should bridge the gap between recent developments in relativistic computational methods and their understanding and use by experimentalists. A separate chapter will focus on the interplay between relativistic effects and electron correlation. Both these effects need to be accounted for in calculations aiming at high reliability of the computed data.

In contrast to recently published books on relativistic theories for atoms and molecules, the present volume is developed at the intermediate level to be of interest for broader audience. The different chapters in the volume are explanatory rather than formal and primarily address the understanding of relativistic computational methods. The book is designed for those who are not highly versed in these methods and are willing to acquire the basic knowledge of the relativistic computing and associated problems of importance for the heavy element chemistry. The discussion of the possible future applications of relativistic computational methods in modeling of new materials, design of efficient catalysts, and in biochemistry-oriented spin-forbidden photochemical processes is provided in a chapter. The book is designed to address equally well needs of students, postgraduates, and researchers.

We owe a considerable debt to our publishers who have been very helpful and understanding. In particular, we would like to thank Dr. Sonia Ojo and Ms. Claudia Thieroff at Springer Publishers for their support and encouragement.

Toruń, Poland
San Juan, PR
October 2009

Maria Barysz
Yasuyuki Ishikawa

CONTENTS

CHAPTER 1

AN INTRODUCTION TO RELATIVISTIC QUANTUM CHEMISTRY

W.H. EUGEN SCHWARZ*

Theoretical and Computational Chemistry Laboratory, Tsing Hua University, Beijing 100084, China
e-mail: schwarz@chemie.uni-siegen.de

"Those who understand nothing else than chemistry,
don't understand chemistry either"
G. C. Lichtenberg (1793), natural scientist and writer [129]

Abstract: Chemistry is governed by the shell structure of the atoms. This holds in particular concerning the periodic system of chemical elements. Non-relativistic quantum chemistry describes the motion of electrons and nuclei and their mutual interactions to a first approximation. It reproduces a large fraction of chemistry of the more important lighter elements sufficiently well. A significant amount of chemical insight can already be gained from the analysis of the atomic one-electron orbitals. However, while valence electrons have 'non-relativistically small' energies, they become 'relativistically fast' in the neighborhood of heavy nuclei. The importance of relativistic effects in the atomic valence shells increases approximately as Z^2. Relativity significantly changes the chemical trends at the bottom of the periodic table. The relativistic effects of the valence electrons can be classified as direct and indirect ones. The direct ones are due to the increase of the effective mass with velocity, to the change of the electric nuclear attraction of a spinning electron, and to the magnetic spin-orbit coupling. The indirect effects on the valence electrons are due to the relativistic changes of nuclear shielding and Pauli repulsion by the inner orbitals. The changes of the radial, the angular, and the quaternionic phase behavior of the relativistic atomic valence orbitals modify the atomic bonding properties, the energetics, the structure and properties of the molecules.

Keywords: Relativistic effects in chemistry, Chemical concepts, Heavy elements, Spin, Molecular spin-orbitals and spinors, Mechanics, Electrodynamics, Velocity-mass effect, Spin-orbit coupling, Darwin effect, Double perturbation theory, Picture change, Direct effects, Indirect effects, Structure effects

* Permanent address: Theoretical Chemistry Group, University, D-57068 Siegen, Germany

M. Barysz and Y. Ishikawa (eds.), *Relativistic Methods for Chemists*,
Challenges and Advances in Computational Chemistry and Physics 10,
DOI 10.1007/978-1-4020-9975-5_1,

1.1. MOTIVATION

The world of our daily experience seems continuous and classical, but the material world is indeed *quantized and relativistic*. So to speak, there are no relativistic and quantum corrections to the real world, there are only non-relativistic and non-quantum approximations by our common perception. Macroscopic chemistry is essentially determined by the continuously and classically looking statistical laws, but with the basis in relativistic discreteness. Atoms and molecules are governed, and their chemistry is explainable, by the laws of relativistic quantum field theory. Several reviews of relativistic quantum chemistry have appeared during the past 35 years [1–8]. The first two excellent textbooks in this special field were recently published [9, 10]. More than 14,000 papers in the field have been collected by Pyykkö [11, 12].

The father of relativistic quantum mechanics [13] and the author of the first book entitled Quantum Chemistry [14] both mistakenly assumed that the chemically active valence electrons behave non-relativistically [15, 134]. Both argued that the valence energies are small and therefore the potential and kinetic contributions should be small, too. The preconception "that a satisfactory description of the atom can be obtained without Einstein's revolutionary theory" [16] died out only very slowly in the communities of both physicists and chemists. However, valence electrons, diving into the atomic cores, become relativistically fast near nuclei[1] with a large Coulomb charge (direct relativistic effects), and all valence electrons are subject to the relativistic modifications of the inner atomic cores (indirect relativistic effects). Common non-relativistic quantum chemistry deviates numerically from the facts of heavy and medium heavy elements, and sometimes even of the light elements (e.g. the so-called 'spin-forbidden' processes, see Figure 1-1). Relativistic

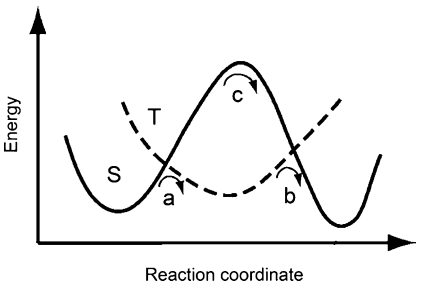

Figure 1-1. A double spin-flip (at **a** and **b**) between the molecular potential energy surfaces of the singlet ground state (**S**, solid line) and the triplet intermediate state (**T**, dashed line) can reduce the non-relativistic activation energy (at **c**) drastically, even for medium heavy atomic molecules

[1] In principle there are no local contributions to property expectation-values in holistic quantum mechanics. However, choosing a specific integral representation, discussion of local contributions to this integral can still give physical insight, see below Section 1.3 and Footnote 11.

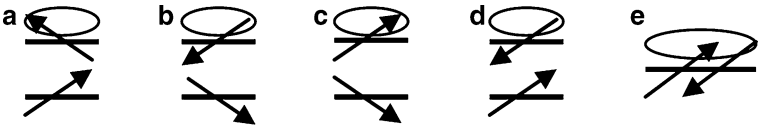

Figure 1-2. Quantum mechanics offers the description of point particles with intrinsic properties. The simplest options are spin-$^1/_2$ fermions. They possess, in addition to mass and charge, an intrinsic angular and magnetic momentum. As any angular momentum vector in three-dimensional space, the spin has only two well-defined components (a consequence of Heisenberg's Uncertainty Principle) and is never vertically aligned (not $\pm 90^\circ$) but tilted up or down by about $\pm 35^\circ$ only, with undefined horizontal direction. Two independent spins can point (**a**) both upwards, (**b**) both downwards, (**c**) both sidewards – in different directions, this is a triplet of spin-states, traditionally called "parallel" – or (**d**) exactly anti-parallel, one singlet spin-state. Two fermions (**e**) in the same position-state (orbital) can only be in a singlet spin-state due to Pauli's Exclusion Principle

quantum chemistry is required even at the qualitative level to explain the heavier elements' chemistry and the structure of the periodic table [1–3, 17].

In Section 1.1, we will touch on quantization in Section 1.1.1, on relativity in Section 1.1.2, then on relativistic quantum mechanics in Section 1.1.3, on common quantum chemistry in Section 1.1.4, and finally on relativistic quantum chemistry in Section 1.1.5. The atomic units used here are defined in Section 1.1.6. Section 1.2 is devoted to the three concepts of quantization, spin (Figure 1-2) and relativity. An exemplary application to the simplest model, the one-electron hydrogen atom, and then to the more realistic many electron atoms is presented in Section 1.3. The analysis of atomic valence orbitals yields a significant amount of insight into the physical mechanisms influencing the chemical behavior of matter. On this background, we can develop the basic concepts of relativistic molecular quantum chemistry in Section 1.4. Subsequent chapters in this volume will fill this conceptual framework with theoretical, algorithmic and numerical details. We also refer to the more recent reviews mentioned above, in particular to the two textbooks on relativistic quantum chemistry [9,10], to the comprehensive Festschrift edited by Schwerdtfeger [6,7] on the occasion of the 60th birthday of the doyen of relativistic theoretical chemistry, Pekka Pyykkö, and to the B.A. Heß memorial issue of 'Chemical Physics' edited by Dolg and van Wüllen [18].

1.1.1. Quantization

The idea that the material world is discrete dates back to some Greek natural philosophers 25 centuries ago. But only two centuries ago, Dalton discovered the first quantitative empirical *chemical* indications of the discreetness of matter. Half a century later, the particle picture started to become also *physically* corroborated by statistical and mechanical theories and laws, derived by Clausius, Boltzmann, Maxwell and others. The discreetness of interactions (by real and virtual photons), and of stationary state energies and of rotational motions were invented since 1900 by Planck, Einstein, Haas and Bohr et al. This led after 1925 to the invention of non-relativistic quantum mechanics by Heisenberg, Schrödinger, Born, Jordan, Dirac and colleagues.

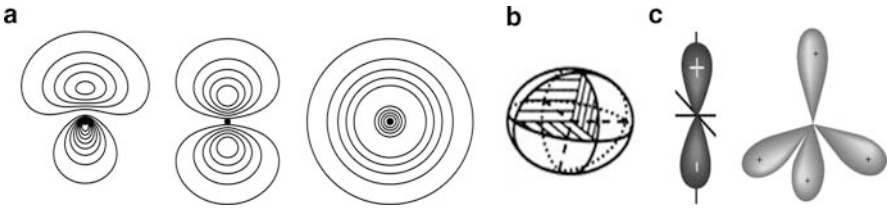

Figure 1-3. (**a**) Probability density distribution of electronic non-relativistic sp^3-hybrid and p_z AOs and relativistic $p_{1/2}$ AOs, in a plane, (**b**) envelope of a nuclear probability density distribution in a crystal, in 3-D, (**c**) common graphical icons symbolizing a p_z and four sp^3 AOs, used to illustrate chemical discussions of bonding and reactions

Observable variables were replaced by Hermitean operators, e.g. for real position $\boldsymbol{x} \rightarrow \hat{\boldsymbol{x}} = x\cdot$, for canonical conjugate momentum $\boldsymbol{p} \rightarrow \hat{\boldsymbol{p}} = -\mathrm{i}\hbar \cdot \mathrm{d}/\mathrm{d}x$ (and, later, for matter field amplitude $\varphi \rightarrow \hat{\varphi} = \varphi \cdot \hat{a}_\varphi$, where $\hat{a}_\varphi$ destroys one particle described by orbital φ). The measurable values a_i of observable variable a had to be represented by value-distributions with amplitude $\varphi(a)$, with average expectation value $\bar{a}$ and value-scattering Δa. This sounds very ordinary, since it is in some sense quite similar to the distribution of measured values in classical experimental science. The concept of real sharp values of observables is only a construct of classical physical theory. On this quantum-physical basis, the quantum-chemical research project was initiated around 1930 by Heitler, London, Hund, Mulliken, Slater, Pauling, Hellmann et al. [19–21, 131]. Electrons are now represented by orbitals, and nuclei by nuclear distributions (Figure 1-3).

1.1.2. Relativity

Einstein's so-called principle of special relativity of 1905 [133] states that all natural laws of mechanics and electrodynamics have the same mathematical form, independent of any forceless linear motion of the coordinate reference frame. The concept already holds in classical mechanics, though assuming an infinitely large (instead of a large finite) limiting velocity. The classical approximation was in accord with several naive preconceptions, such as the absoluteness of space and time distances, the algebraic additivity of velocities, the dependence of the velocity of light on the motions of source and observer, or the constancy of the gravitational and inertial masses.

However, Galilee[2] – Newton's mechanics (with unlimited maximum velocity), and Maxwell's electrodynamics (with a finite critical velocity) were basically inconsistent with each other. The principle of relativity imposes severe constraints on the form of the natural laws. And it turned out that the basic laws of physics correspond just to the simplest mathematical expressions fulfilling these constraints (Figure 1-4). The principle of relativity fixes the explicit form of the transformation

[2] We use the English modification of Galileo Galelei's name.

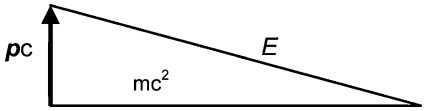

Figure 1-4. The structure of relativistic laws: A scalar 'time-related' variable (e.g. the total energy E) is the Pythagorean sum of a scalar constant (here the rest-mass energy mc^2) and a 'space-related' three-dimensional vectorial variable (here $\boldsymbol{p}c$): $E^2 = (mc^2)^2 + (\boldsymbol{p}c)^2$

of time and space coordinates (Lorentz transformation) up to a critical maximum velocity parameter. This parameter is the velocity of the electromagnetic interaction in vacuum (the velocity of light c). It is finite and must be determined experimentally [22].

1.1.3. Relativistic Quantum Field Theory for Electrons

In 1928, Dirac [13] formulated a relativistic 'Schrödinger equation' linear in time, the Dirac equation, which required the existence of an electronic spin (Figure 1-5). The respective eigen-energies for electrons were either seriously above and below zero. It took the work of many theoretical physicists during half a century, among them Dirac, Feynman, Schwinger, Tomonaga and Dyson, to develop a conceptually consistent approach. Electrons, electron–positron pairs and virtual photons around the nuclei together build up the atoms, the molecules and the more complex forms of matter. This quantum electro-dynamical (QED) theory is not that complicated, if compared to the standard model of elementary particle physics. Quite accurate numbers can be obtained by computational approximations to QED [24]. It is the most accurate of all theories of natural science, 'the jewel of theoretical physics', which governs and explains a large amount of chemistry, among other branches of science.

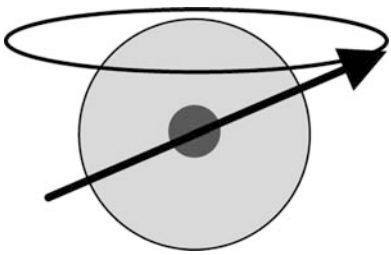

Figure 1-5. In a relativistic quantum theory of fermions, point charge and point mass are distributed around each other by the order of the Compton length (1/137 Bohr $\approx$ 0.4 pm) causing the Darwin effect, and giving rise to spin-orbit coupling effects

1.1.4. Quantum Chemistry

The individual empirical findings of chemistry can be numerically reproduced or predicted (computational chemistry), and the trends can be rationalized or explained (theoretical chemistry), by an appropriate and skillful combination of classical mechanical, quantum mechanical and statistical mechanical theories [25–28], and later chapters in this book]. This holds in principle, though problems concern accuracy and reliability [134].[3] In experimental chemistry, it is less common than in physics or crystallography to perform statistical error analyses of the raw data and of the data deduced from the measurements (error propagation). And concerning estimates or guesses of the systematic errors, they are anyhow somewhat 'subjective'. The systematic errors may be due to the limitations of the experimental procedures, or due to the bias in the theoretical prescription for the experimental raw data in order to reconstruct physically meaningful 'measured values' from them.

On the side of computational chemistry, systematic errors can be due to oversimplifying the theory (in order to construct understandable, clear and simple models) and due to applying too crude numerical procedures (in order to save computational expense or human work time). Most common are the use of too restricted one- and many-electron basis sets, the application of non-convergent perturbation expansions, or the use of too strongly simplified Hamiltonians.[4] The amount of systematic errors seems to correlate with the expertise of the respective research groups; the commercial 'black box' program packages cannot be used as black-box problem solvers. Statistical errors usually play a minor role in computational chemistry, but they also occur, for instance in Monte Carlo type approaches or in approaches of screening out all small contributions (integrals) or all lower decimal digits.

Theoretical and computational chemistry can be applied at different levels. Ordinary chemists think within a non-quantum non-relativistic framework. Nuclei, atoms, molecules, complexes etc. are viewed as classical (stick and ball or space-filling calotte) particles. The chemically active electronic systems are represented by individualized and localized 'chemist's orbitals' in space. A proper quantum chemical counterpart is the lowest order Born–Oppenheimer (BO) approximation

[3] In his famous, often-cited dictum, [134] expressed four ideas: First – The fundamental physical laws for a 'mathematical theory of chemistry' are completely known. (It is not clear whether Dirac realized that a 'mathematical theory of chemistry' comprises only a fraction of chemistry. Another question is which proper chemists, computational chemists, theoretical chemists or philosophers of chemistry are aware of this significant aspect.) Second – the relativistic theory is incomplete. (This is still valid, but the left-over problems are mainly relevant to elementary particle physics and cosmology. Most chemically relevant problems of the physical theory of relativity are now solved.) Third – relativity is irrelevant to chemistry. (Now, we know it better.) Fourth – The two main and permanent problems of theoretical chemistry are to develop computational approaches to calculate reasonably accurate observable values, and to derive interpretational tools for a physical understanding of the complex chemical processes in matter.

[4] This comprises the approximation of static and dynamic two-electron correlations, the neglect of non-adiabatic electron-nuclear couplings, the neglect of relativistic electron dynamics, or the neglect of environmental perturbations by 3K cosmic background radiation, or perturbations by the condensed phase surroundings.

for the nuclei and the so-called 'independent particle' or molecular and crystal orbital (MO, CO) approximation for the electrons.[5] At best, the many-electron correlations are somewhat accounted for in this 'single quasi-particle' model, e.g. within a Kohn–Sham orbital density-functional approach. And at best, the molecular orbitals are orthogonally chosen and localized as far as possible to approach the chemical views. Observable values of a molecule are then usually representable in a quasi-classical manner as sums of contributions from single and pairs of nuclei, from single and pairs of electronic orbitals and from nucleus–orbital interactions. In such a nuclear-Born–Oppenheimer electronic-orbital model, we may speak of distinguishable nuclear probability ellipsoids and orbital densities (Figure 1-3 left and middle) instead of indistinguishable nuclei and electrons. In many cases, this approximation causes only small numerical errors, despite of the basic conceptual change from the quantum to the classical world [29].

In cases that are more ambitious, this 'chemical' model must be improved in four different directions, depending on the required accuracy and reliability of the results, on the molecular system at hand, and on the properties in question. (1) The nuclei must be described by nuclear orbitals or wave packets, in uncorrelated or differently correlated ways. (2) Nonadiabatic or diabatic nuclear–electron couplings must be accounted for. (3) Two- and multi-electron correlations due to electron–electron interactions must be described explicitly. (4) The consequences of the strongly relativistic behavior of electrons in the strong fields around heavy nuclei, including spin-dependent energy contributions, must be allowed for.

1.1.5. Relativistic Quantum Chemistry

In many cases, electron correlation (point 3) is the most important one. A reliable non-relativistic orbital model (applying sufficiently extended orbital basis sets) and a reliable representation of electron correlation (extended configuration mixing) should have first priority. In the cases of heavy elements, of high accuracy demands, of spin-forbidden optical or reactive processes, etc., relativity (point 4) must also be accounted for in some manner.

1.1.5.1. Fractional Relativistic Corrections

The fractional difference $\delta^{\mathrm{rel}} P_i = \Delta^{\mathrm{rel}} P_i / P_i$ of property values P_i between the non-relativistic approximation and relativistic reality, i.e. the fractional non-relativistic error, is commonly called the fractional relativistic correction. $\delta^{\mathrm{rel}} P$ is often of the order of $(\alpha Z)^2 = \gamma^2$, where Z is the nuclear charge and $\alpha \approx 1/137$ is Sommerfeld's fine structure constant.

$$\delta^{\mathrm{rel}} P_i = \Delta^{\mathrm{rel}} P_i / P_i \approx a(i, hs, g) \cdot (Z/137)^2 \tag{1-1}$$

[5] One should distinguish between an expansion which can give, in principle, the correct value, and an approximation consisting only of the first term of the expansion. There are the lowest-order BO approximation and the BO expansion. There are the Hartree, Hartree–Fock and Kohn–Sham orbital approximations and the post-independent-particle expansions.

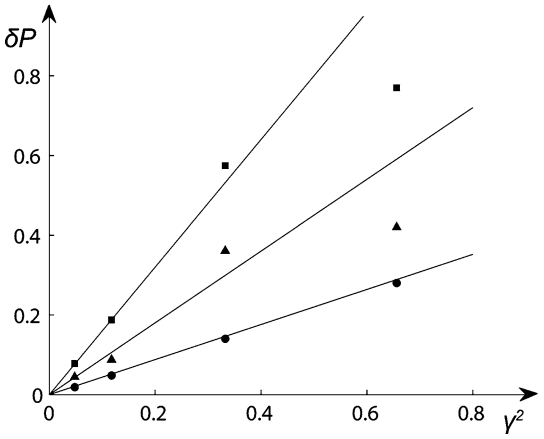

Figure 1-6. Coinage metal hydride molecules $_{29}$Cu-H, $_{47}$Ag-H, $_{79}$Au-H and $_{111}$EkaAu-H. Fractional relativistic property correction $\delta^{\mathrm{rel}}P$ versus $\gamma^2 = (\alpha Z)^2$, ● for bond length contraction ($P = -R_\mathrm{e}$, line is $\delta P = a\gamma^2, a = 0.4$), ▲ for increase of dissociation energy ($P = D_\mathrm{e}, a = 0.9$) and ■ for increase of stretching force constant ($P = k, a = 1.6$). Higher order contributions of γ^2 seem important for high Z values

$a(i, hs, g)$ is an approximate constant for the given property i (such as bond length, dissociation energy, or some spectroscopic parameter) of the homologous series hs (molecule type) from the rows of the periodic table of group g (such as C, Si, Ge, Sn, Pb or Cu, Ag, Au). $\Delta^{\mathrm{rel}}P/P$ typically increases by factors of 2–4 from row to row down in a group. The a-factors are of the order of unity. A few examples are given in Figures 1-6 and 1-7. In the fourth row of the periodic table (the light transition metals Sc–Cu and the 4sp-elements Zn–Kr), $(Z/137)^2$ is in the range of several percent. $\delta^{\mathrm{rel}}P$ may reach 10–100% and even more in the sixth and seventh rows (lanthanoids and actinoids,[6] heavy transition metals and heavy main group elements), see Reiher and Wolf [10], Dyall and Fægri [9], Schwerdtfeger [6, 7], Pyykkö [2,3,12], Schwarz et al. [30], and later chapters in this book. Of course, rule of thumb (1-1) is not applicable to so-called (non-relativistically) spin-forbidden optical or molecular-reaction processes, since the whole effect is purely relativistic.

1.1.5.2. Historical Development

This was quite slow at the beginning. Chemical relativistic effects were systematically investigated not before the 1960s, first in atoms, then in solids (see, e.g. [31–33, 135]), and only finally in molecules. Already in 1935, Swirles [132] concluded "that for heavy atoms the relativistic correction will be of importance".

[6] The IUPAC recommends lanthanoids and actinoids instead of former lanthanides and actinides. '-ides' are usually anionic compounds such as halides, sulfides, etc. See http://en.wikipedia.org/wiki/Lanthanoid.

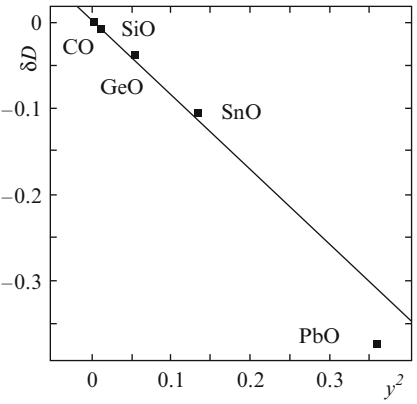

Figure 1-7. Group-14 monoxide molecules $_6$CO, $_{14}$SiO, $_{32}$GeO, $_{50}$SnO and $_{82}$PbO. Fractional relativistic property correction $\delta^{\text{rel}}P$ versus $\gamma^2 = (\alpha Z)^2$, for dissociation energy decrease ($a = -0.86$) (After Wang and Schwarz [108])

This was substantiated from time to time by numerical calculations on atoms. Williams [34] noted that the relativistic corrections to the charge density become remarkable near the nucleus already for a comparatively light atom (Cu, Z = 29). Mayers [35] investigated Hg ($Z = 80$) and first elaborated on the direct and indirect relativistic changes of energies and radii of the inner and outer atomic shells of different angular momenta (see Section 1.3).

Electronic computers made comprehensive investigations feasible. Herman and Skillman [36] determined approximate relativistic contributions to the orbital energies of all atoms. Fricke [1, 37, 38] extended the periodic system of chemical elements up to $Z = 184$. They showed that the structure of the system begins to change more and more for the heavy and superheavy elements.[7] Various relativistic atomic orbital corrections of all atoms up to $Z = 120$ were numerically and graphically displayed by Desclaux [39]. Rosén and Ellis [40] and Desclaux and Pyykkö [41] were the first to supplement their extensive atomic calculations by relativistic single molecule investigations. Since then the number of publications per year in the new field of relativistic quantum chemistry has more than doubled each decade, and has reached several hundreds to one thousand in recent years. Pyykkö's Account with Desclaux [4] on "Relativity and the Periodic System of Elements" and his Chemical Review [3] on "Relativistic Effects in Structural Chemistry" were instrumental in drawing the attention of the real chemists onto the field. Still, many chemists believe that the empirical experience form the lighter half of the elements can be extrapolated without drastic relativistic modifications. One aim of this volume is to foster heavy element chemistry through a sound quantum chemical basis.

[7] Let 'superheavy' be defined as $Z > 100$.

1.1.5.3. Targets of Relativistic Quantum Chemistry

One can distinguish six different aims: (i) Further development of theoretical concepts and models. (ii) Improvement of numerical techniques. (iii) Numerical calculation of properties of chemically known heavy atomic compounds, for instance concerning reaction mechanisms, dominating species in solution equilibria, NMR parameters etc. (iv) Prediction of unknown chemical compounds of known elements, such as environmentally safe actinoid complexes, catalytically active Au cluster compounds or novel Hg(IV) compounds. (v) Prediction of unknown compounds of unknown or recently synthesized short-lived superheavy nuclei. (vi) Last but not least the derivation, explanation or rationalization of trends in the chemistry of heavy elements. Most publications, including the subsequent reviews in this book, approach two or more of these targets.

1.1.5.4. Periodic Trends

The periodic table of chemical elements is one of the most prominent icons of chemistry and one of the great achievements of science and culture [17]. Periodic tables were created to systematically order the empirical findings of chemistry. Most of the data concern the more abundant and more important chemicals. Just the lighter half of all elements, say up to $Z = 54$ (Xe), and then only a dozen of the heavier ones, among them Ba, W, Pt, Au, Hg, Pb, Th and U, practically and historically determined the structure of the periodic system. Fleck described already in 1935 [122], how so-called 'scientific facts' without or against sufficient empirical basis are sometimes 'created' by communities of scientists and then taught to all students.

Several aspects of the periodic tables are nice examples for the creation of non-existing chemical facts. The primary and secondary periodicities and the horizontal and vertical trends in the periodic system embrace the light-element-biased chemical wisdom. The chemical regularities are governed by the energetic *and* spatial order of the outer core *and* valence orbitals of the elemental *atoms in compounds*, being determined by the nuclear attractions, the electron repulsions, and the kinematical effects under the constraints of the Pauli principle. For the lighter elements, for which the non-relativistic approximation of theory works comparatively well, the respective variations with nuclear charge Z are rather smooth and can be easily interpolated.

However, it turns out that in reality, which is mapped by a relativistic theory, the trends of many chemical properties bend away for higher Z-values. Extrapolation into the high Z region is not reliable. This happens, because the electronic motions and interactions exhibit a more complex behavior than to be expected in the non-relativistic regime [2–4, 42]. Particularly important parameters of the elements are the atomic radii, the ionization potentials and the common valence numbers. In general, the ionization potentials decrease in a group of elements down the periodic table, but this trend changes in the lowest row(s) for groups 1, 2 and 6–14 (Figure 1-8). There is a common increase of atomic radii down the periodic table,

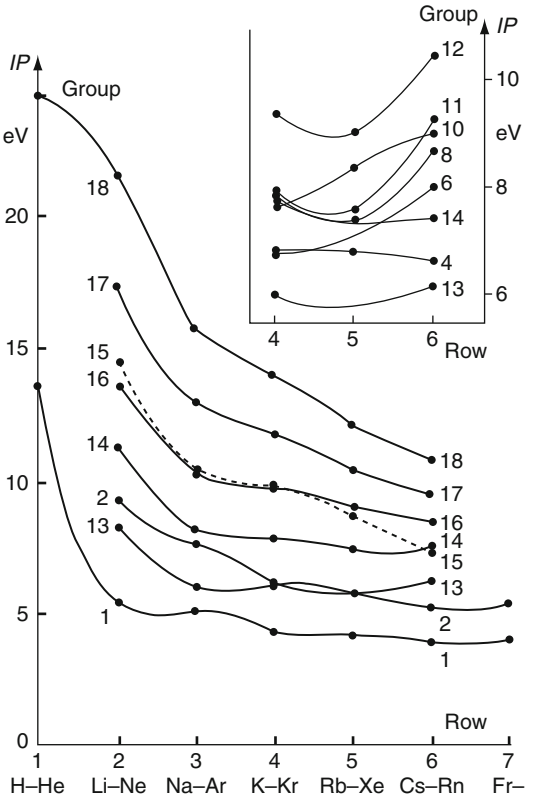

Figure 1-8. Atomic ionization potentials (IP/eV) of the elements versus the group number in the periodic system, with changes of trends in rows 6 and 7 for groups 1, 2 and 6 through 14 (After Schwarz [41])

again with several exceptions at the bottom. For instance, while for decades the radii of Cu^+, Ag^+ and Au^+ were given as about 46, 67 and 137 pm, more reasonable values are 46, 67 and 58(!) pm, respectively [43]. According to Pyykkö and Atsumi [44] the superheavy elements E111 (Eka-Au = Rg) through E114 (Eka-Pb) have smaller single-bond covalent radii than Au through Pb, respectively. And concerning the valence numbers, the six heavy main group elements Hg, Tl, Pb, Bi, Po, At exhibit a pronounced tendency to particularly low values (Hg^0, Tl^1, Pb^2, Bi^3, Po^2, At^1). More examples are found in Chapters 2, 3, 7, and 11.

The chemistry of heavy and superheavy elements cannot even qualitatively be understood or rationalized without accounting for the relativistic kinematics of the core *and* valence electrons. In order to obtain chemically reliable numbers from quantum chemical calculations, the relativistic behavior of the electrons must be considered already for medium heavy elements, and concerning spectroscopy, even for light elements (see subsequent Chapters).

1.1.6. Units and Numbers

In the formulas, we will use the following atomic units: electronic *charge* e (≈–96485.3 C/mol), electronic rest-*mass* m (≈1/1822.888u, u = chemical atomic mass unit = g/mol), Bohr *length* a_0(≈52.9177 pm), Hartree atomic *energy* unit E_h=2 E_R Rydberg units (≈27.21138 eV ≈ 26255.00 kJ/mol, 1 eV≈96.48535 kJ/mol), the *angular momentum* unit ħ (=Planck's constant h, divided by 2π) and the *velocity* unit αc (c = vacuum velocity of light = 2.99792458·$\times 10^{10}$ cm/s; α ≈ 1/137.036 is Sommerfeld's fine structure constant). This corresponds to a dielectric constant $\varepsilon_0 = 1/4\pi$. Sometimes, we will write out the units such as e or m to make the physics clearer.

Constants like e, m, c or i ($i^2 = -1$) are represented by standard letters, variable values (a, b, …, x, y, z), functions ($f(t)$) and integer indices (i, j, …) by italics. Three-dimensional vectors are printed bold ($\boldsymbol{r} = (x, y, z)$), and operators with a hat ($\hat{H}$). The derivative operation is $\partial/\partial t$ or $\partial/\partial \boldsymbol{r} = (\partial/\partial x, \partial/yx, \partial/\partial z) = \nabla$. We use the electromagnetic Gauss convention, so that the magnetic potential $\boldsymbol{A}$ and field $\boldsymbol{B}$ appear with pre-factors 1/c. The nuclear charge is Z, and γ means $Z/c = \alpha Z$.

Only a few decimal figures are experimentally obtainable as approximations to the *real* values in theory. Empirically there is only a finite set of *rational* decimal numbers. In addition to the single real numbers, the equations of physics may contain compound variables, namely for the compact representation of sets of equations, reflecting the mathematical structure in these equations. There occur the *complex* numbers ($z = a + ib$), the *quaternion* numbers ($y = a + ib + jc + kd$, with $i^2 = j^2 = k^2 = ijk = -1$, i.e. ij = –ji = k, jk = –kj = i, ki = –ik = j), the three-dimensional *vectors* with Euclidean norm ($|\boldsymbol{r}| = xx^* + yy^* + zz^*$, where * means complex conjugation) and the *four-vectors*, here written as (t, $\boldsymbol{r}$).

1.2. FROM THREE BASIC CONCEPTS TO THE DIRAC EQUATION

Three concepts form the basis of an accurate description of single electrons around nuclei, namely by the Dirac equation: (1) relativistic invariance, (2) quantization, and (3) the existence of spin. We introduce the Lorentz coordinates transformation in Section 1.2.1 and derive the relativistically correct expressions for effective mass and energy in Section 1.2.2. Upon quantization, we arrive in Section 1.2.3 at non-relativistic and relativistic wave equations for spinless particles, namely the Schrödinger and Klein–Gordon equations. In Section 1.2.4 we admit spin and rationalize the non-relativistic and relativistic equations for particles with spin ½, the Levy-Leblond and Dirac equations. All these wave equations can be represented in different equivalent forms. In Section 1.2.5 we comment on the so-called 'picture changes'. A short summary is given in Section 1.2.6.

1.2.1. Principle of Invariance: The Lorentz Transformation

Galilee and Newton (early and late seventeenth century) found that one cannot distinguish between rest and constant linear motion in force-field-free space.

The laws in two different (time, space)-coordinate systems $(t, \boldsymbol{r})$ and $(t', \boldsymbol{r}')$, moving with constant velocity v against each other, should have the same form. This principle of invariance was later called principle of 'relativity'. The simplest type of coordinate transformation $\hat{T}$ is a linear one (for simplicity, we assume at first a one-dimensional space r):

$$\begin{pmatrix} t' \\ r' \end{pmatrix} = \hat{T}(v) \cdot \begin{pmatrix} t \\ r \end{pmatrix} = \begin{bmatrix} a(v) & b(v) \\ d(v) & e(v) \end{bmatrix} \cdot \begin{pmatrix} t \\ r \end{pmatrix} \tag{1-2}$$

The four transformation coefficients a, b, d, e, depending on the velocity v, can be determined through the following conditions:

(i) The transformation for negative velocity should compensate the transformation for positive velocity:

$$\hat{T}(v) \cdot \hat{T}(-v) = 1. \tag{1-3}$$

(ii) The catenation of two individual transformations for parallel velocities v_1 and v_2 should correspond to the transformation of their 'formal sum' $v_{1+2} = v_1 \oplus v_2 = v_2 \oplus v_1$:

$$\hat{T}(v_1) \cdot \hat{T}(v_2) = \hat{T}(v_2) \cdot \hat{T}(v_1) = \hat{T}(v_1 \oplus v_2). \tag{1-4}$$

(iii) The transformation of the origin should correspond to a linear shift in time, $r = v \cdot t$:

$$d(v) = -v \cdot e(v). \tag{1-5}$$

(iv) The transformation should be consistent with inversion symmetry of space:

$$a(-v) = a(v), b(-v) = -b(v), d(-v) = -d(v), e(-v) = e(v). \tag{1-6}$$

The solution for $\hat{T}(v)$, the Lorentz transformation, contains still an undetermined parameter c of the dimension of a velocity:

$$\hat{T}(v) = \frac{1}{\sqrt{1 - v^2/\mathrm{c}^2}} \cdot \begin{bmatrix} 1 & -v/\mathrm{c}^2 \\ -v & 1 \end{bmatrix} \tag{1-7}$$

Consistency with electrodynamics requires c to be the vacuum velocity of light. Theory still does not offer a value for it, so it must be determined experimentally.

The 'formal summation' of (parallel) velocities yields:

$$v_1 \oplus v_2 = (v_1 + v_2)/(1 + v_1 \cdot v_2/\mathrm{c}^2). \tag{1-8}$$

The 'sum' of two small velocities $v_i \ll c$ is just the algebraic sum, $v_1 \oplus v_2 \approx v_1 + v_2$. For two large velocities $v_i \lesssim c$, the sum remains below c, $v_1 \oplus v_2 \lesssim c$. The constant vacuum-velocity of light denotes the upper limit of mechanical velocities.

1.2.2. Relativity and the Natural Laws for Mechanics and Electrodynamics

1.2.2.1. Relativistic Mechanics

We can now search for other expressions that are invariant under Lorentz transformations. The first simplest example is the proper time duration (Eigenzeit) τ of the relative motion of a point from (0,**0**) to (t, $\boldsymbol{r}$), as detected by an external observer. The value of τ is defined by

$$\tau = t \cdot \sqrt{1 - v^2/c^2} \tag{1-9}$$

τ is the time observed at the position of the moving point by the moving observer himself (i.e. for $v = 0$ and $\boldsymbol{r}$ = constant). It differs from t, as observed by an observer, who sees the point moving. The difference is of the order of $(v/c)^2$. An object, suddenly accelerated, and then moving with constant velocity, ages more slowly, $\tau < t$ (time dilatation), as compared to the non-accelerated observer. τ according to Eq. (1-9) does not change under a Lorentz transformation (1-2, 1-7). $\tau(t, \boldsymbol{r}) = \tau'(t', \boldsymbol{r}')$ for all observers seeing the point moving with velocities $\boldsymbol{v}$ and $\boldsymbol{v}'$.

The canonical conjugate variables of t and $\boldsymbol{r}$ are energy E and momentum $\boldsymbol{p}$. In a relativistic framework, $\boldsymbol{p}$ is defined as

$$\boldsymbol{p} = m \cdot d\boldsymbol{r}/d\tau = m\boldsymbol{v}/\sqrt{1 - v^2/c^2} = m_{\text{eff}} \cdot \boldsymbol{v}. \tag{1-10}$$

m is the rest-mass of the particle, and the effective moving mass is

$$\boxed{m_{\text{eff}} = m/\sqrt{1 - v^2/c^2}.} \tag{1-11}$$

The effective inertial mass increases with the velocity squared (Figure 1-9).

It is natural next to define the value of the energy-momentum four-vector (E, $\boldsymbol{p}$) as another invariant under Lorentz transformations:

$$Inv = E^2 - \boldsymbol{p}^2 \cdot c^2. \tag{1-12}$$

where *Inv* turns out to be equal to $E_0{}^2 = m^2c^4$. This may be rewritten as (Figure 1-4)

$$\boxed{E^2 = m^2c^4 + \boldsymbol{p}^2c^2.} \tag{1-13}$$

Taking the square root of (1-13) and expanding in a power series yields

$$E = \sqrt{m^2c^4 + \boldsymbol{p}^2c^2} = mc^2 + {}^1\!/_2\boldsymbol{p}^2/m - {}^1\!/_8\boldsymbol{p}^4/m^3c^2 \cdots \tag{1-14a}$$

$$= mc^2 + {}^1\!/_2 m\boldsymbol{v}^2 + {}^3\!/_8 m\boldsymbol{v}^4/c^2 \ldots \tag{1-14b}$$

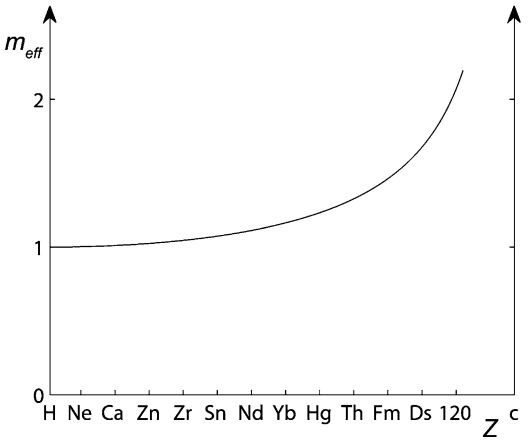

Figure 1-9. Effective mass m_{eff} of an electron on a 1s Bohr orbit in the field of nuclear charge $Z = 1$, 10(10)120, c. In the case of a point nucleus, the classical velocity is $\alpha Z \cdot c$, and m_{eff} would diverge against ∞ for $Z \rightarrow c \approx 137$ au

where Eq. (1-10) has been inserted. The total relativistic mechanical energy of a moving rest-mass m is the Pythagorean sum of the rest-mass energy mc^2 and the momentum energy $\boldsymbol{p}c$ (Figure 1-4). This can be approximated by the algebraic sum of the rest-mass energy $+mc^2$, the non-relativistic kinetic energy $+{}^1/_2 m\boldsymbol{v}^2$, a first-order relativistic correction $+{}^3/_8 m\boldsymbol{v}^4/c^2$, and higher-order terms. The kinetic energy increases faster with velocity than in the non-relativistic approximation, and the velocity (bounded by $v < c$) increases more slowly upon application of an accelerating force. Namely, the effective inertial mass (1-11) increases upon acceleration, and the velocities can only converge from below towards the limit c. The first important relativistic effect in atoms, molecules and crystals is the electronic mass–velocity effect. It will be discussed in Section 1.3. Neglecting terms of order $1/c^2$ yields the non-relativistic approximation to the energy, Eq. (1-15), with reference energy $E_0 = mc^2$.

$$E^{\text{n-rel}} = E_0 + {}^1/_2 m\boldsymbol{v}^2 = E_0 + \boldsymbol{p}^2/2m \tag{1-15}$$

1.2.2.2. Mechanics in Electromagnetic Fields

The directly measurable[8] electric and magnetic field strengths $\boldsymbol{F}, \boldsymbol{B}$ are compactly represented by the electromagnetic four-potential $(V, \boldsymbol{A})$. $V(t, \boldsymbol{r})$ is the electric scalar potential and $\boldsymbol{A}(t, \boldsymbol{r})$ is called the magnetic vector potential. The field strengths are related to the potentials [126] by

$$\boldsymbol{F} = -\partial/\partial \boldsymbol{r} \cdot V - \partial/\partial ct \cdot \boldsymbol{A}, \quad \boldsymbol{B} = \partial/\partial \boldsymbol{r} \times \boldsymbol{A}. \tag{1-16}$$

Only electric potential *differences* have a physical meaning, the zero of the potential scale can be chosen arbitrarily. Even more general so-called gauge-transformations

[8] This means without accounting for any quantum interference effects.

can be applied to an electromagnetic four-potential $(V, \boldsymbol{A})$ without changing the observable effects. Such gauge-transformations are achieved by arbitrary, differentiable functions $g(t, \boldsymbol{r})$:

$$V \rightarrow V' = V - (\partial/\partial ct)g(t, \boldsymbol{r}); \tag{1-17a}$$

$$\boldsymbol{A} \rightarrow \boldsymbol{A}' = \boldsymbol{A} + (\partial/\partial x, \partial/\partial y, \partial/\partial z)g(t, \boldsymbol{r}) \tag{1-17b}$$

The choice of $g(t, \boldsymbol{r})$ is guided in a given case by the desire to obtain a simple or elegant final formula. A specific $(V, \boldsymbol{A})$ cannot be an observable. However, the *set* of all $(V, \boldsymbol{A})$ connected by all admissible g is indeed an observable [45]. An objective observable in natural science is a mathematical object in a theory, which is uniquely derivable from empirical data. Scholars, who know, what is going on in experimental data acquisition, know that observables are not purely empirically observable. This is the so-called 'theory-ladenness' of all empirical facts. An energy-difference is an observable represented by one real number. An electromagnetic potential is an observable, represented by a gauge-invariant *set* of individually gauge-dependent analytical functions.

In order to combine electrodynamics of some electromagnetic potential $(V, \boldsymbol{A})$ with mechanics of a particle of mass m and charge q, one has to subtract $q \cdot (V, \boldsymbol{A})$ from $(E, \boldsymbol{p}\mathrm{c})$. For electrons, $q = -\mathrm{e}$. The relativistic energy expression then reads

$$[\mathrm{mc}^2]^2 = [E + \mathrm{e} \cdot V(t, \boldsymbol{r})]^2 - [\boldsymbol{p} \cdot \mathrm{c} + \mathrm{e} \cdot \boldsymbol{A}(t, \boldsymbol{r})]^2 \quad \text{or} \tag{1-18a}$$

$$E = -\mathrm{e} \cdot V(t, \boldsymbol{r}) + \mathrm{c} \cdot \{\mathrm{m}^2\mathrm{c}^2 + [\boldsymbol{p} + \mathrm{e}/\mathrm{c} \cdot \boldsymbol{A}(t, \boldsymbol{r})]^2\}^{1/2}, \tag{1-18b}$$

and the non-relativistic one

$$E^{\text{n-rel}} = -e \cdot V(t, \boldsymbol{r}) + \mathrm{mc}^2 + [\boldsymbol{p} + \mathrm{e}/\mathrm{c} \cdot \boldsymbol{A}(t, \boldsymbol{r})]^2/2\mathrm{m}. \tag{1-19}$$

The factors e/c in Eqs. (1-18) and (1-19) depend on the choice of the mechanical and electro-magnetic units. They are related to relativity in the sense that a changing electric field creates a magnetic field and vice versa, and such fields propagate in space with velocity c. Maxwell's equations for the electromagnetic potentials or fields (expressed by the four-potential $(V, \boldsymbol{A})$ or the field strength tensor $\{\boldsymbol{F}, \boldsymbol{B}\}$) require a finite wave-velocity c and a non-vanishing electromagnetic coupling parameter 1/c. So to say, Maxwell's electrodynamics was Lorentz invariant 'from the outset'. With infinitely large c, one would obtain vanishing electromagnetic induction. Galilee–Newton's transformation of space and time, i.e. the Lorentz transformation for $\mathrm{c} \rightarrow \infty$, corresponds to a reasonable approximation of mechanics at 'ordinary' velocities, and to electrostatics, magnetostatics and to weak and slowly varying currents and fields, but without induction or Lorentz force. In order to combine incompatible Galilee-invariant mechanics and Lorentz-invariant electrodynamics, Lorentz and others developed the so-called Lorentz-transformation at the end of the nineteenth century. Einstein then reformulated mechanics in 1905 to obtain a comprehensive and consistent picture of electrodynamics *and* mechanics.

1.2.3. Relativistic and Non-relativistic Wave Equations

The common (non-unique) quantization rules prescribe to replace the observable variables a,c in some classical equation $f(a,c) = 0$ by respective linear-Hermitean operators $\hat{a}, \hat{c}$. They act on state functions or state vectors Ψ in Hilbert space. The relation for numerical function $f(a,c) = 0$ is replaced by the operator equation $f(\hat{a},\hat{c}) \cdot \Psi = 0$. The operators for canonically conjugated observable pairs a,b (such as t,E or $\boldsymbol{r}$, $\boldsymbol{p}$) should fulfill the Heisenberg commutation rule:

$$[\hat{a},\hat{c}] = \hat{a}\cdot\hat{c} - \hat{c}\cdot\hat{a} = \pm \mathrm{i}\hbar\cdot \tag{1-20}$$

The replacement rules are somewhat flexible. In the so-called space-time representation they read:

$$t \to \hat{t}{=}t\cdot,\ E \to \hat{E} = +\mathrm{i}\hbar\cdot\partial/\partial t\cdot$$
$$\boldsymbol{r} \to \hat{\boldsymbol{r}}{=}\hat{\boldsymbol{r}}\cdot,\ \boldsymbol{p} \to \hat{\boldsymbol{p}} = -\mathrm{i}\hbar\cdot\partial/\partial\boldsymbol{r}\cdot = -\mathrm{i}\hbar\cdot\nabla\cdot = -\mathrm{i}\hbar\cdot(\partial/\partial x, \partial/\partial y, \partial/\partial z)\cdot \tag{1-21}$$

1.2.3.1. Nonrelativistic Wave Equation without Spin

Quantization of non-relativistic energy expression (1-19) by replacement (1-21) yields the *Schrödinger equation* (1-22):

$$\boxed{\mathrm{i}\hbar\cdot\partial/\partial t\cdot = [\mathrm{E}_0 + \mathrm{e}\cdot V(t,\boldsymbol{r})] + [\hat{\boldsymbol{p}}\text{–}\mathrm{e}/\mathrm{c}\cdot\boldsymbol{A}(t,\boldsymbol{r})]^2/2\mathrm{m}\cdot(\text{acting on }\psi\,(t,\boldsymbol{r})).} \tag{1-22}$$

The spinless scalar quantum state function $\psi(t,\boldsymbol{r})$ describes the deterministic development of spinless particles in time under the action of an electromagnetic potential in the non-relativistic mechanical limit. The compound ^{12}C and ^{4}He nuclei and $\pi^{o,\pm}$ mesons and anti-mesons and the elementary Higgs boson (predicted in high energy physics) are spin-zero particles. However, the compound deuteron ^{2}H, ^{6}Li, ^{14}N etc. and the elementary photon are spin-1 particles. And the compound proton, neutron, ^{13}C etc. and in particular the elementary electron (and neutrinos and quarks) are known to be spin-$^1/_2$ particles (spin quantum number $s = {}^1/_2$) with intrinsic mechanical angular momentum

$$|\boldsymbol{S}| = \sqrt{{}^1/_2({}^1/_2+1)}\,\hbar, \tag{1-23}$$

The description of non-zero spin particles will be discussed in the next paragraph.

1.2.3.2. Relativistic Wave Equation without Spin

Quantization of the relativistic energy expression (1-13) with electromagnetic potentials (Eq. 1-18b) yields

$$\boxed{\begin{aligned}&[\mathrm{i}\hbar\cdot\partial/\partial t + \mathrm{e}\cdot V(t,\boldsymbol{r})]^2\cdot \\ &\qquad = \mathrm{m}^2\mathrm{c}^4\cdot + [\hat{p}\cdot\mathrm{c} + \mathrm{e}\cdot\boldsymbol{A}(t,\boldsymbol{r})]^2\cdot(\text{acting on }\psi\,(t,\boldsymbol{r}))\end{aligned}} \tag{1-24}$$

Equation (1-24) is called the *Klein–Gordon equation.* It was first considered by Schrödinger in 1925, and first published in 1926/1927 by Oskar Klein [128], Walter Gordon [123], and also by several others [46]. It describes spin-zero particles correctly in the relativistic regime [47, 121]. For large c and neglecting terms of order $1/c^2$, one obtains the non-relativistic counterpart, the Schrödinger equation (1-22).

Different equivalent forms of classical equations for numerical variables give rise to non-equivalent quantum mechanical operator-equations, since the operators do not commute: $a \cdot c = c \cdot a$ for real or complex (though not for quaternionic) numbers a,c, while in general $\hat{a}\cdot\hat{c} \neq \hat{c}\cdot\hat{a}$ for operators or matrices $\hat{a}, \hat{c}$. For instance, the square-root energy expression (1-18b) yields, for vanishing magnetic potential,

$$[\mathrm{i}\hbar \cdot \partial/\partial t + \mathrm{e} \cdot V(t,\mathbf{r})] \cdot = \sqrt{\mathrm{m}^2\mathrm{c}^4 - \mathrm{c}^2\nabla^2} \cdot (\text{acting on } \psi\ (t,\boldsymbol{r})). \quad (1\text{-}25)$$

This so-called square-root or relativistically corrected Schrödinger equation (1-25) is no longer equivalent to Eq. (1-24) [48].

In the equations above, the energy E is given by $E^2 = f(t,\boldsymbol{r},\boldsymbol{p}) > 0$ or $E = \pm\sqrt{f(t,\boldsymbol{r},\boldsymbol{p})}$. In either case, the energies are (for small momenta and potentials) near $+\mathrm{mc}^2$ and $-\mathrm{mc}^2$. These so-called positive and negative energy solutions describe particles and antiparticles, respectively, with positive or negative wave-frequency $\pm\omega = \pm E/\hbar$ in the time-dependent factor $\mathrm{e}^{\pm\mathrm{i}\omega t}$ of a stationary state function $\psi(t,\boldsymbol{r})$. Multiplying an equation for negative frequency or energy by –1, one obtains an equation with positive energy, positive rest-mass and kinetic energy, but for opposite charge. That is, antiparticles have opposite charge and positive energy.

The Klein–Gordon operator (1-24) acts on scalar 1-component wavefunctions $\psi(t,\boldsymbol{r})$, as in the Schrödinger case (1-22). In order to describe particles and antiparticles by the same equation, one needs something like a quadratic equation with a double-valued square-root solution. One does *not* need two different components in the wavefunction to describe particles and antiparticles. The Klein–Gordon equation is such a 1-component equation for spin-0 particles and antiparticles. However, one can transform a scalar equation containing $\partial^2/\partial t^2$ into a coupled system of two equations looking rather similar to Schrödinger equations with terms linear in $\partial/\partial t$, but with a 2-component wavefunction [47]. The 1-component Klein–Gordon equation (second order in time) and the two coupled 2-component Schrödinger-like equations (first order in time, Feshbach–Villars representation, see [49]) are of course equivalent.

1.2.4. The Natural Occurrence of Spin

Classically, point like particles such as electrons or quarks cannot have internal structure without internal divergences. Because of Heisenberg's uncertainty principle for position and momentum of a point, and because position of charge and position of mass are different observables, point-particles can exhibit internal structure in quantum mechanics [49]. The operators in non-relativistic equation (1-22) and relativistic equation (1-24) act on scalar type wavefunctions. They can

be generalized to cover also the cases of spin > 0. The internal structure is then represented by multi-component wavefunctions.

The operators are multiplied by mathematical objects of unit norm that act on such multi-component wavefunctions. The general strategy is to choose the irreducible representation matrices of the non-relativistic Galilee group or the relativistic Poincaré group as basis for the operators. For spin-$^1/_2$ (or higher spin) particles, four-dimensional (higher-dimensional) matrices appear in the wave equations of such approaches [50, 51].

The wavefunction for spin-$^1/_2$ particles has four complex (or eight real) components, although there are only two independent ones, describing the α and β spins. Two of the four complex components are dependent on the other two. Therefore, the 4-component spin-$^1/_2$ wave equation can be transformed to a two-component equation (although usually not in explicit form, but iteratively, in complex cases at least on the computer). The result looks like a 'simple' wave equation (depending on the approach: like a non-relativistic Schroedinger equation or like a free-particle Dirac equation) with corrections for the kinetic energy, for the potential energy and for mixed contributions. On one hand, two-component formulations are fully equivalent to the relativistic Dirac representation; on the other hand, the two-component representations are often formulated only approximately. Anyhow, it has become customary to call them all quasi-relativistic.

We stress again that the appearance of a spin is a quantum phenomenon, connected with the fact that operators need not commute and that the causal law for the development of states in time is a wave equation. In contrast, the existence of particle–antiparticle pairs is a relativistic phenomenon, connected with the two signs of the root expression for the relativistic energy $\omega\hbar = \pm|E| = \pm(mc^2+\varepsilon)$. ε means the conventional energy relative to the energy of an electron or positron at rest in field-free space.

1.2.4.1. Relativistic Wave Equation with Spin

While the group-theoretical approach of Levy-Leblond is rather involved, Dirac [25] arrived quite early at the correct relativistic wave equation for spin-$^1/_2$ particles by applying a simple heuristic strategy. He searched for a modified Klein–Gordon equation that is linear in space–time derivatives. To this end, he introduced constant matrices α_i, β, obeying the relations $\alpha_i^2 = \beta^2 = \mathbf{1}_4$[9] and $\alpha_i\alpha_j + \alpha_j\alpha_i = \alpha_i\beta + \beta\alpha_i = 0_4$ (anti-commutativity). If the β and α_i were just numbers (or one-dimensional matrices), the relations were contradictory, and one could not explicitly solve and linearize the square root of Eq. (1-25) to obtain the *Dirac equation* (1-26),

$$\boxed{1\cdot(E+e\cdot V)\cdot = \sqrt{1\cdot m^2c^4 + 1\cdot(\hat{\boldsymbol{p}}c + e\boldsymbol{A})^2}\cdot = \left[\beta\cdot mc^2 + \alpha\cdot(\hat{\boldsymbol{p}}c + e\boldsymbol{A})\right]\cdot} \tag{1-26}$$

which acts on a multi-component 'spinor wavefunction'.

[9] $\mathbf{0}_4$ and $\mathbf{1}_4$ mean the 4×4 zero- and unit-matrices.

To show the principle, we assume a two-dimensional space for simplicity (instead of the real three-dimensional one). In this case, just three matrices α'_1, α'_2, β' are sufficient, and they only need to be 2×2 to obey the required relations; they act on two-component spinor wavefunctions. This can easily be verified by the reader. The matrices are known as the Pauli spin-matrices σ_i, and $\mathbf{1}_2$ is the 2×2 unit matrix:

$$\alpha'_1 = \sigma_x = \begin{pmatrix} 0 & 1 \\ 1 & 0 \end{pmatrix}, \quad \alpha'_2 = \sigma_y = \begin{pmatrix} 0 & -\mathrm{i} \\ \mathrm{i} & 0 \end{pmatrix}, \quad \beta' = \sigma_z = \begin{pmatrix} 1 & 0 \\ 0 & -1 \end{pmatrix} \tag{1-27}$$

Of course, any unitarily transformed set of these Pauli matrices can also be used. In the case of the real three-dimensional space, one needs one α-matrix more, and then all matrix operators must be at least four-dimensional to fulfill the required anticommutation relations. The respective 4×4 Dirac matrices can be constructed with the help of the Pauli matrices:

$$\boldsymbol{\alpha}_j = \begin{pmatrix} \mathbf{0}_2 & \boldsymbol{\sigma}_j \\ \boldsymbol{\sigma}_j & \mathbf{0}_2 \end{pmatrix}, \quad \beta = \begin{pmatrix} \mathbf{1}_2 & \mathbf{0}_2 \\ \mathbf{0}_2 & -\mathbf{1}_2 \end{pmatrix}, \quad \gamma = \begin{pmatrix} \mathbf{1}_2 & \mathbf{0}_2 \\ \mathbf{0}_2 & \mathbf{1}_2 \end{pmatrix} = \mathbf{1}_4 \tag{1-28}$$

The Dirac equation (1-26), which describes relativistic spin-½ particles correctly, then reads explicitly, with $\boldsymbol{\sigma} = (\sigma_x, \sigma_y, \sigma_z)$:

$$\begin{pmatrix} \mathbf{1}_2 \cdot (\mathrm{mc}^2 - \mathrm{e}V - E) & \boldsymbol{\sigma} \cdot (\hat{\boldsymbol{p}}\mathrm{c} + \mathrm{e}A) \\ \boldsymbol{\sigma} \cdot (\hat{p}\mathrm{c} + \mathrm{e}A) & -\mathbf{1}_2 \cdot (\mathrm{mc}^2 + \mathrm{e}V + E) \end{pmatrix} \cdot \begin{pmatrix} \varphi_2 \\ \chi_2 \end{pmatrix} = \mathbf{0} \tag{1-29}$$

The Dirac equation and its transformed form (1-29) are system of 2 + 2 coupled equations. Each of the two lines contains the 2×2 Pauli spin-matrices. The upper and lower component functions φ_2 and χ_2 are each a 2-component object, ${\varphi_2}^+ = (\varphi_\alpha, \varphi_\beta)$ and ${\chi_2}^+ = (\chi_\alpha, \chi_\beta)$, referring to α (up) and β (down) spin. (These α and β symbols have nothing to do with the Dirac matrices $\boldsymbol{\alpha}_\mathrm{i}$, β, γ, nor with the fine-structure constant α.) The two spin-components of the wavefunction, i.e. the dependence of the wavefunction on the spin directions α and β, in addition to the dependence on the space coordinates x, y, z, are really needed for spin-½ particles. It is somewhat accidental that the Dirac equation describes α and β spin of positive energy states (electrons) and negative energy states (positrons) just with the help of $2 \cdot 2 = 4$ components. Indeed, the 4-component Dirac equation (1-26) or (1-29) can be transformed to a two-component equation for a negatively charged particle and a similar two-component equation for a positively charged particle ([10, 52, 53], and later chapters). The 'picture change' between 2- and 4-component representations will be further discussed in the next Section.

One can shift the energy zero of electronic states by $-\mathrm{mc}^2$, $\varepsilon = E - \mathrm{mc}^2$, to obtain 'ordinary' energies ε for ordinarily bound electrons. If one then divides the second

line of Eq. (1-26) by c, and uses $c\chi$ instead of χ, one obtains the following set of equations equivalent to Eq. (1-26) or Eq. (1-29):

$$\begin{pmatrix} -\mathbf{1}_2 \cdot (\mathrm{e}V + \varepsilon) & \sigma \cdot (\hat{p} + \mathrm{e}/\mathrm{c} \cdot A) \\ \sigma \cdot (\hat{p} + \mathrm{e}/\mathrm{c} \cdot A) & -\mathbf{1}_2 \cdot (2\mathrm{m} + (\mathrm{e}V + \varepsilon)/\mathrm{c}^2) \end{pmatrix} \cdot \begin{pmatrix} \phi_2 \\ \mathrm{c}\chi_2 \end{pmatrix} = \mathbf{0} \qquad (1\text{-}30)$$

1.2.4.2. Non-relativistic Wave Equation with Spin

For small $(\mathrm{e}V - \varepsilon)/2\mathrm{mc}^2$, this term may be treated as a relativistic correction, or just may be neglected. In the latter case, one obtains a 4-component non-relativistic equation for electrons with spin, the Levy-Leblond equation [50]. Upon elimination of $\mathrm{c}\chi$, one obtains a two-component Schrödinger-like equation with spin, acting on the two-component spinor wavefunction φ_2. We call it the *two-component Levy-Leblond equation* (1-31).

$$\boxed{1_2 \cdot \left[-\mathrm{e} \cdot V - \varepsilon + (\hat{\boldsymbol{p}} + \mathrm{e}/\mathrm{c} \cdot \boldsymbol{A})^2/2\mathrm{m}\right] \cdot + \mathrm{e}\hbar/2\mathrm{mc} \cdot \sigma \cdot \boldsymbol{B} \cdot = 0_2 \cdot} \qquad (1\text{-}31)$$

Here the useful Dirac–Landau relation

$$(\boldsymbol{\sigma} \cdot \boldsymbol{A})(\boldsymbol{\sigma} \cdot \boldsymbol{B}) = (\boldsymbol{A} \cdot \boldsymbol{B}) + \mathrm{i} \cdot \mathrm{Det}[\boldsymbol{\sigma}, \boldsymbol{A}, \boldsymbol{B}] \qquad (1\text{-}32)$$

has been used, where $\mathrm{Det}[\boldsymbol{\sigma}, \boldsymbol{A}, \boldsymbol{B}] = \boldsymbol{\sigma} \cdot \boldsymbol{A} \times \boldsymbol{B} = \boldsymbol{\sigma} \times \boldsymbol{A} \cdot \boldsymbol{B}$. $\mathrm{e}\hbar/2\mathrm{mc} = \mu_\mathrm{B}$ is called the Bohr magneton. Equations (1-30) and (1-31) can be obtained directly, by the tedious Galilee-group-theoretical approach applied to the non-relativistic Hamiltonian [50]. That is, non-relativistic quantum theory with external electromagnetic fields offers the natural possibility of particles with intrinsic angular momentum (here with $s = 1/2$, $S_z = \pm\hbar/2$) and with coupling to a magnetic field as by a classical magnetic dipole moment of 1 Bohr magneton. This corresponds to a gyromagnetic ratio $\gamma = \mu_\mathrm{B}/S_z = \mathrm{e}/\mathrm{mc}$, which is 'anomalous', namely twice that of the classical or quantum mechanical value e/2mc of a freely orbiting point charge. The coupling of a spin to a magnetic field had been introduced somewhat ad hoc already by Pauli in 1927 [54].

1.2.4.3. Gauge Transformations

The energy term $(\boldsymbol{p} + \mathrm{e}/\mathrm{c} \cdot \boldsymbol{A})^2/2\mathrm{m}$ in Eq. (1-31) combines three contributions (i) the non-relativistic kinetic energy $T = \boldsymbol{p}^2/2\mathrm{m}$, (ii) the paramagnetic energy $\mathrm{e}/\mathrm{mc} \cdot (\boldsymbol{p} \cdot \boldsymbol{A} + \boldsymbol{A} \cdot \boldsymbol{p})$ and (iii) the diamagnetic energy $\mathrm{e}^2/2\mathrm{mc}^2 \cdot \boldsymbol{A}^2$. Upon gauge transformation with gauge function g, the paramagnetic term changes linearly with g, whilst the diamagnetic term changes according to $(\boldsymbol{A} + \boldsymbol{\nabla} g)^2$, i.e. contains a term quadratic in g. This has two consequences. First, only the sums of the para- and dia-magnetic energy shifts by a magnetic field are measurable and theoretically well defined. The partitioning into a para- and a dia-magnetic contribution is not unique and depends on the choice of the gauge g. Second, the expectation value of the magnetic energy depends on the Hamiltonian containing g and g^2 *and*

on the wavefunction. If the gauge of the four-potential (V, $\boldsymbol{A}$) is changed, also the phase of the wavefunction $\boldsymbol{\varphi}$ for the particle in this potential changes:

$$\boldsymbol{\varphi}' = \exp(-\mathrm{ie}/\hbar\mathrm{c} \cdot g) \cdot \boldsymbol{\varphi}. \tag{1-33}$$

In principle, for 'exact' calculations, the gauge transformation of the wavefunction and of the Hamiltonian in an integral expression for the expectation values let these values invariant. However, this does no longer hold for approximate calculations. In practical calculations of interactions of molecules with electromagnetic fields and radiation, the results depend less or more on the chosen gauge. It is a challenge to find gauges, which minimize the gauge sensitivity of the approximate results for some given type of problems (for details see Chapter 12).

Each equation of systems (1-29) or (1-30) consists of two lines. The α and β lines can be mixed, corresponding to a change of the reference axis for the spin. The upper and lower component eigenfunctions of system (1-29), φ and χ, are sometimes called the large and small components, because for small energies ε and large distances from the nuclei, $\varphi/\chi \sim \mathrm{c}^2$. However, whether φ or χ (or $\mathrm{c}\chi$ in Eq. 1-30) is larger near the nuclei depends on the angular momenta and the potentials [10,55]. The two individual equations of systems (1-29) or (1-30) can also be arbitrarily linear-combined. It changes the ratios of the upper and lower components and corresponds to a (unitary) equivalence-transformation of the Dirac matrices 1_4, $\boldsymbol{\alpha}_i$ and β. As Eqs. (1-19) and (1-30) clearly demonstrate, both wavefunction components are in general equally important for the energy, irrespective of their norms. For very large energies, $\varphi \sim \pm\chi$, depending on the sign of E, which defines the electronic or positronic character of the state function. At least in general, the upper and lower components of a relativistic four-component function should not be identified with electronic and positronic components, respectively, except one has performed a unitary transformation of the Dirac equation towards two uncoupled two-component spinor equations, one for $E \sim +\mathrm{mc}^2$ (electrons) and the other one for $E \sim -\mathrm{mc}^2$ (positrons).

1.2.5. Picture Changes

Any wave equation can be unitarily transformed with the help of a unitary operator or matrix $\hat{U}$ ($\hat{U}\hat{U}^+ = \hat{U}^+\hat{U} = 1$),

$$\hat{H}\Psi = E\Psi \rightarrow (\hat{U}^+\hat{H}\hat{U})(\hat{U}^+\Psi) = \hat{H}'\Psi' = E\Psi'. \tag{1-34}$$

This is the so-called "picture change". The operators of *all* other observables must of course be simultaneously transformed, too, for instance the operator of the space coordinates $\boldsymbol{r}$, which appear in the electronic charge density distribution $\rho(\boldsymbol{r}) = \mathrm{e} \cdot \Psi^*(\boldsymbol{r}) \cdot \Psi(\boldsymbol{r})$ and in dipole moment and transition-dipole moment expressions.

$$\hat{\boldsymbol{r}} \rightarrow \hat{\boldsymbol{r}}' = (\hat{U}^+\hat{\boldsymbol{r}}\hat{U}). \tag{1-35}$$

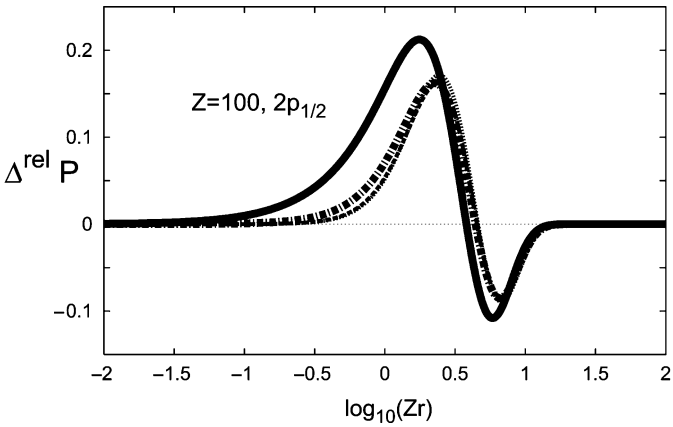

Figure 1-10. Relativistic change of radial density, $\Delta^{\mathrm{rel}}\mathrm{P} = (\rho^{\mathrm{rel}} - \rho^{\mathrm{n\text{-}rel}}) \cdot r^2$ (in au/$10^6\alpha^2$), of the $2p^1/_2$ spinor of Fm($Z = 100$) versus $\log_{10}(Z \cdot r)$. —— charge density in the Dirac picture; - - - - - - particle density in the two-component picture (After Autschbach and Schwarz [59])

An equivalent viewpoint is the transformation of the density operator $\hat{\rho}(\boldsymbol{r})$ to $\hat{\rho}'(\boldsymbol{r}) = \hat{U}^+\hat{\rho}(\boldsymbol{r})\hat{U}$ [56]. In the Dirac picture, $\boldsymbol{r}$ is the position of charge coupled to the electromagnetic potential and ρ is the charge density, while in the transformed picture, it is $\boldsymbol{r}'$ and ρ'. On the other hand, simple $\boldsymbol{r}$ in the transformed picture means something like position of mass [56–59]. Figure 1-10 presents $\rho - \rho^{\mathrm{n\text{-}rel}}$ and $\rho' - \rho^{\mathrm{n\text{-}rel}}$ for a $2p^1/_2$ spinor and a large nuclear charge. The picture-change of the density distribution, i.e. the difference between the relativistic charge and mass densities, is pronounced near the nuclei. It is qualitatively different for different *nlj* quantum numbers and for large or small nuclear charges Z.

Such 'picture transformations' are common in quantum chemistry. It is also a 'picture change' if we go from the all-electron representation of a molecule to the valence-only representation by replacing the atomic core electrons by atomic effective-core potentials (ECP) or pseudo-potentials (PP) [60, 61, Chapter 6] i.e. from the valence orbitals to the valence-pseudo-orbitals with less inner nodes in the atomic core regions. Another example of a picture change is the change between the four-component Dirac representation and respective two-component representations:

$$(\hat{H}_D - E) \cdot \Psi = \begin{pmatrix} \mathbf{1}_2 \cdot (\mathrm{mc}^2 - \mathrm{e}V - E) & \boldsymbol{\sigma} \cdot (\hat{\boldsymbol{p}}\mathrm{c} + \mathrm{e}\boldsymbol{A}) \\ \boldsymbol{\sigma} \cdot (\hat{\boldsymbol{p}}\mathrm{c} + \mathrm{e}\boldsymbol{A}) & -\mathbf{1}_2 \cdot (\mathrm{mc}^2 + \mathrm{e}V + E) \end{pmatrix} \cdot \begin{pmatrix} \phi_2 \\ \chi_2 \end{pmatrix}$$
$$= \mathbf{0} \rightarrow \qquad (1\text{-}36)$$

$$(\hat{H}' - E) \cdot \Psi' = \begin{pmatrix} \hat{H}_+ - E & \mathbf{0}_2 \\ \mathbf{0}_2 & \hat{H}_- - E \end{pmatrix} \cdot \begin{pmatrix} \phi' & \mathbf{0}_2 \\ \mathbf{0}_2 & \chi' \end{pmatrix} = \mathbf{0}_4, \qquad (1\text{-}37)$$

where, for the particular case $E \sim +\mathrm{mc}^2$, $\hat{H}_+$ and charge e in the electromagnetic potential terms describe electrons in a *convenient* two-component way (and for case

$E \sim -mc^2$ positrons in an 'unusual' way, whilst $\hat{H}_-$ is then more convenient for positrons). Explicit expressions for Hamiltonians (containing potential terms) cannot be given. Either the matrix elements of $\hat{H}_+$ can be computed numerically by computer iteration of some implicit equation, or one can develop series expansions for the matrix elements in powers of $\alpha = 1/c$, nuclear charge Z or potential V (see later chapters).

We present the lowest order approximation to $[\hat{H}_+ - \varepsilon]$, obtained in the framework of 'direct Dirac perturbation theory' (DPT), as applied to Eq. (1-30) [62, 63]:

$$\left[\hat{H}_+ - \varepsilon\right]\cdot = \left[-e\cdot \boldsymbol{V} + \hat{\boldsymbol{p}}^2/2m - \varepsilon + (-\hat{\boldsymbol{p}}(eV+\varepsilon)\hat{\boldsymbol{p}} + \sigma\cdot\nabla\boldsymbol{V}\times\nabla)/4m^2c^2\right]\cdot \tag{1-38}$$

The first two terms in the right brackets are the electrostatic potential energy and the non-relativistic kinetic energy T_0. The last terms of order $\alpha^2/4$ are the lowest order relativistic corrections. The term $\sim\boldsymbol{\sigma}\cdot\boldsymbol{\nabla V}\times\boldsymbol{\nabla}$ is the spin-orbit coupling. The other term $\sim -\boldsymbol{p}(eV+\varepsilon)\boldsymbol{p}$ is spin-independent. In the present representation, the respective energy contribution can be written as an expectation value of the non-relativistic wavefunction Ψ^o:

$$\Delta^{\text{spin-indep}}\varepsilon(\text{DPT}) = \alpha^2/4\cdot\langle\Psi^o|-2(\varepsilon+eV)T + (\boldsymbol{\nabla V})\boldsymbol{\nabla}|\Psi^o\rangle \tag{1-39}$$

The historical, numerically quite sensitive Pauli expression can be recovered by inserting the non-relativistic Schrödinger equation and integrating by parts:

$$\Delta^{\text{spin-indep}}\varepsilon(\text{Pauli}) = \alpha^2/4\cdot\langle -{}^1\!/_2\boldsymbol{p}^4 - {}^1\!/_2(\boldsymbol{\nabla}^2 V)\rangle \tag{1-40}$$

The partitioning of the energy into spin-independent contributions of order α^{-2} (i.e. mc^2), α^0 (non-relativistic potential and kinetic energies), α^2 (Eqs. 1-39 or 1-40), α^4 etc. and spin-dependent contributions of order α^2, α^4 etc. is picture-independent. Further, one can split up the spin-independent contribution of order α^2 into a mass–velocity term and the so-called non-classical Darwin or Zitterbewegung term. The latter term is absent in the Klein–Gordon theory for spin-0 particles. A point particle with spin has an internal structure with positional uncertainty that reduces the electron–nuclear attraction. The operators for positions of charge and of mass of spin-$^1/_2$ particles differ, in any picture, at the order of α^2 by terms dependent on the spin operators [58]. The DPT and Pauli forms of the mass–velocity and Darwin terms in Eqs. (1-39) and (1-40) look different, but give the same numerical values, provided exact zeroth order wavefunctions are applied. The value of the Darwin term can also be obtained as the limit of the spin-orbit coupling energy of $j = l + {}^1\!/_2$ for continuous $l \to 0$ [64].

Many further representations can also be generated. They differ in their sensitivities on errors in the wavefunction. The Pauli form is rather sensitive due to the singularities at the origins of the nuclear Coulomb potentials. Franke and Kutzlnigg [65] have shown that representation (1-39) is less sensitive than (1-40), i.e. superior.

Finally, it seems necessary to stress the triviality that perturbation expressions such as (1-38)–(1-40) should never be applied in variational approaches.

1.2.6. Summary

The theoretically derivable relativistic wave equations for spin-0 and spin-$^1/_2$ particles, respectively, are the one-component Klein–Gordon equation (1-24) and the at least two-component equivalents of the Dirac equation (1-26/1-37). Letting $c \rightarrow \infty$, or $\alpha \rightarrow 0$, one obtains approximate non-relativistic equations, namely the one-component Schrödinger equation (1-22) for spin-0 and the two-component Levy-Leblond (or Pauli) equation (1-31) for spin-$^1/_2$. The appearance of particles and antiparticles is a relativistic phenomenon. E-values around and above $+mc^2$ represent electronic states, round and below $-mc^2$ positronic states. The physical energy is at best defined as $|E| = |\omega\hbar|$.

Any system of equations for massive ($m > 0$) spin-s particles and antiparticles of multiplicity $M = 2s + 1$ must comprise at least M equations for an M-component wavefunction, with wave-frequency $\omega \gg 0$ for particles and $\omega \ll 0$ for antiparticles. The wave equations may be formulated with more lines than the number of spin-components, sometimes locking or being more simple and elegant, such as the four-component Dirac equation in comparison to its two-component equivalents (see later chapters). Two-component representations such as by $\hat{H}_+$ in Eq. (1-37) may be more convenient for the numerical computation or for the explanation of the physical mechanism of electronic states. It depends on the type of the four-to-two components transformation, whether the spectrum of the constructed Hamiltonian $\hat{H}_+$ contains only the electronic solutions, or the electronic positive-energy solutions, and also the positronic negative-energy solutions though in an inconvenient manner [52].

The definition of particles and antiparticles is not unique. One may choose a basis of free waves with $E^+ > +mc^2$ for electrons and with $E^- < -mc^2$ for positrons. Another option is the single-particle states in the field of the clamped, naked nuclei. The best choice is a basis of self-consistent field (SCF) orbitals of the molecule under investigation, with orbital energies $E^+ \gg -mc^2$ for electronic states and with $E^- < -mc^2$ for positronic states. This is an unproblematic definition for all 'chemically reasonable' Z values.[10] The complete sum of Dirac many-electron energies and quantum field corrections is independent of the choice of the $e^- - e^+$ one-particle basis. The choice of electronic (single or multiple configuration) SCF orbitals leads to comparatively small quantum electrodynamical (QED) corrections, i.e. the Dirac approach alone without e^--e^+ pair corrections ('no-pair approximation') is already quite good [66–69, 124, 125].

We can distinguish between quantum effects, relativistic effects and quantum relativistic effects. The possibility of an internal spin of a point particle with

[10] For Z larger than about 165, the electronic 1s level dives into the positronic continuum of the extended nucleus, with spontaneous electron–positron pair production.

'anomalous' gyromagnetic ratio ∼2 is a *quantum* effect [50, 51]. It is connected to Heisenberg's uncertainty concerning the charge and mass distributions of a spinning point particle, which differ from each other in strong fields by the order of the Compton length $\lambda_C = h/mc$ [49,58,59, Chapter 12]. It is a consequence of electromagnetic coupling $\sim e/c \cdot \boldsymbol{A}$, and in this sense it is a *relativistic quantum field* effect. The place, where a factor $\alpha = 1/c$ appears in the equations, depends on the choice of the electromagnetic units. For an alternative convention than used above see Chapter 12, Section 12.2.5. The increase of inertial mass with velocity (Eq. 1-11), the reduced kinetic energy expression in terms of the momenta (Eq. 1-14a) or increased in terms of the velocities (Eq. 1-14b) are *relativistic mechanical* effects.

When electrons move in the field of nuclei, there are four genuine lowest-order *quantum relativistic* effects [43,70]. (i) The coupling of the internal spin structure to the strong inhomogenity of the nuclear electric field, i.e. the Darwin effect $\sim\alpha^2$. It influences the Dirac solutions for spin-$^1/_2$, though not the Klein–Gordon or square-root solutions for spin-0 (e.g. [48]). (ii) The coupling of the spinning electron to magnetic (or moving electric) fields, the spin-orbit coupling $\sim\alpha^2$. It is mainly due to the nuclear field; specific two-electron contributions in many-electron atoms and molecules will be mentioned below. (iii) The quantum field theoretical coupling to virtual excitations of the electromagnetic vacuum (vacuum fluctuations) and to virtual excitations of the electron–positron vacuum (vacuum polarizations) $\sim\alpha^3$. (iv) 'Weak interactions' between the electron and a nucleus. The latter are orders of magnitude smaller, but have been suggested as origin of chirality in biomolecules [71,72]; for a different view see [93]). At higher than second order of α, the coupling of the various mechanisms prevents such simple partitioning; in reality there is only the total relativistic energy.

1.3. DIRAC SOLUTIONS FOR HYDROGEN AND OTHER ATOMS

The hydrogen atom is the only atom that has no occupied core shells and is also not influenced by any two-electron interactions. So it is an exceptional one among all atoms, forming an unusually small cation and a somewhat atypical covalence. On the other hand, due to its simple structure, it is particularly useful to explain some of the basic chemical phenomena and concepts. A simplified H-atom model with an infinitely heavy point-nucleus without any internal structure (no nuclear spin) and with all QED effects suppressed can be solved in closed form at the semi-classical Bohr, at the non-relativistic Schrödinger and at the relativistic Dirac levels. In Sections 1.3.1–1.3.3 we discuss its relativistic orbital energies, orbital functions and orbital radii. Some common paradoxical relations are analyzed in Section 1.3.4.

Atoms with occupied inner shells are chemically more realistic examples. The electronic shielding effects on the orbitals are discussed in Sections 1.3.5–1.3.7, and the relativistic two-electron interactions in Section 1.3.8. The smaller quantum electrodynamical and weak-interaction effects and the finite extension of the nuclear charge distribution are finally mentioned in Section 1.3.9.

1.3.1. Relativistic Orbital Energies of the Simplified H-Atom Model

The Dirac energy values of the simplified one-electron atom (ion) with nuclear point charge Z, clamped at the coordinate origin, are known since Gordon [73], see also Bethe and Salpeter [74]:

$$E_{nk}(Z) = \mathrm{mc}^2 \cdot [\{1 + \gamma^2/(n + \sqrt{k^2 - \gamma^2} - |k|)^2\}^{-1/2} - 1] \qquad (1\text{-}41)$$

Here and in the following, $\gamma = Z/c$; $n = n_\mathrm{r} + l$ are the principal, radial and angular orbital quantum numbers; $k = \pm(l + 1/2 \pm 1/2)$, and $j = l \pm 1/2$ is the total (orbital and spin) angular momentum quantum number. The formula for the eigen-energies of the Klein–Gordon equation is similar, except for replacing the spin-dependent k-quantum number by spin-independent $\lambda = +(l + 1/2 + 0)$ [47]. The non-relativistic energetic degeneracy of the hydrogenic orbitals, for instance $E(3\mathrm{s}) = E(3\mathrm{p}_{\mathrm{x,y,z}}) = E(3\mathrm{d}_{\mathrm{xy,xz,yz,zz,xx-yy}})$, is partially removed. Orbitals with different angular momentum are subject to different mass–velocity and spin-orbit effects, e.g. $E(3\mathrm{s}) = E(3\mathrm{p}1/2) < E(3\mathrm{p}3/2) = E(3\mathrm{d}3/2) < E(3\mathrm{d}5/2)$. That is the hydrogen orbital energies depend only on n and j (or $|k|$). The four lowest states are

$$\begin{aligned} &1\mathrm{s}1/2 : n = 1, k = -1, l = 0, j = 1/2, \\ &2\mathrm{s}1/2 : n = 2, k = -1, l = 0, j = 1/2, \\ &2\mathrm{p}1/2 : n = 2, k = +1, l = 1, j = 1/2, \\ &2\mathrm{p}3/2 : n = 2, k = -2, l = 1, j = 3/2. \end{aligned} \qquad (1\text{-}42)$$

We expand the energies in powers of γ (e.g. [75]):

$$\begin{aligned} &1\mathrm{s}1/2 : && E = -Z^2/2 \cdot (1 + 1/4\gamma^2 + 1/8\gamma^4 + \ldots) && \delta\varepsilon = 4/16\gamma^2 + 16/256\gamma^4 \cdots \\ &2\mathrm{s}1/2, 2\mathrm{p}1/2 : && E = -Z^2/8 \cdot (1 + 5/16\gamma^2 + 21/128\gamma^4 + \ldots) && \delta\varepsilon = 5/16\gamma^2 + 17/256\gamma^4 \cdots \\ &2\mathrm{p}3/2 : && E = -Z^2/8 \cdot (1 + 1/16\gamma^2 + 1/128\gamma^4 + \ldots) && \delta\varepsilon = 1/16\gamma^2 + 1/256\gamma^4 \ldots \end{aligned} \qquad (1\text{-}43)$$

The first factors $\sim Z^2$ are the non-relativistic energies E^0. $\delta\varepsilon = (E - E^0)/E$ are the fractional relativistic energy stabilizations, they are of the order of a fraction of $+\gamma^2$. This is the 'relativistic orbital stabilization'. For Z-values of the lighter transition elements (Sc to Cu), $\delta\varepsilon$ is in the 1% range; of the second transition row elements (Y to Ag) in the few-% range; of the lanthanoids (La to Lu) in the 5% range; and of the actinoids (Ac to Lr) over 10%. For many chemical purposes, relativistic corrections to first order in γ^2 are sufficient for the first two transition rows of the periodic table; the second order is needed from the lanthanoids onwards; and third *and* higher order terms (i.e. the full energy) are required from the actinoids onwards. For more details, see [76] and [75].

1.3.2. Relativistic Atomic Spinors

When discussing the four-component complex relativistic spinor wavefunctions, one should keep in mind that the upper and lower components have no absolute meaning but depend on the chosen representation. We will use the standard Dirac representation with matrices as given in Eq. (1-28).

1.3.2.1. $s^1/_2$ Spinors

At first, we discuss the simplest case, $1s^1/_{2+}$. The explicit form for a point nucleus reads:

$$1s^1/_{2+} : N \cdot r^{-d} \cdot e^{-Zr} \cdot \begin{pmatrix} (i\gamma/d) \cdot \alpha \\ 0 \\ (z/r) \cdot \alpha \\ (x + iy)/r \cdot \beta \end{pmatrix}, d = 1-\sqrt{1-\gamma^2} \approx {}^1/_2\gamma^2. \quad (1\text{-}44)$$

N is the normalization factor, r the nuclear-electronic distance. The factor r^{-d} increases strongly for small r. The electron is nearer to the nucleus than in the non-relativistic limit ('relativistic orbital contraction') and the Coulomb potential energy becomes more negative ('relativistic orbital stabilization'), in particular for large Z values. For unrealistic point nuclei, the wavefunctions even diverge towards ∞ for $r \to 0$. However, for real extended nuclei, the wavefunction becomes smooth and Gaussian-like inside the nucleus, without any cusp or singularity (Figure 1-11). Typical nuclear radii are

$$R_N \approx 1^1/_4 \, A^{1/3} \text{ fm}, \quad (1\text{-}45)$$

where A is the nuclear mass number. Nuclei are about 10^{-5} times smaller than the whole atoms. For the heaviest nuclei, the probability of a '1s electron' being inside the nucleus approaches the ‰-range. In the non-relativistic limit, $c \to \infty$, d vanishes and the function becomes $r^0 \cdot e^{-Zr} = 1 \cdot e^{-Z \cdot r}$, just the non-relativistic 1s orbital.

The lower components of the $1s^1/_2$ spinor are smaller than the upper ones by a factor of $d/\gamma \approx \gamma/2$. For small nuclear charges Z, this is a large ratio. This is so for all spinors with $j = l + s$. In the non-relativistic limit, the lower components would contribute nothing to the charge density. But the lower components are always important for the energy (since they are multiplied by terms of order mc^2 and $\boldsymbol{p}c$) and for other expectation values containing the factor c in front of the lower components.

The angular behavior of the lower components is different from that of the upper ones. If the upper component is a $j = l + s$ function ($s^1/_2$, $p^3/_2$, etc.), the lower component is a $j = (l + 1) - s$ function ($p^1/_2$, $d^3/_2$, etc.). In the present case ($l = 0$), the upper component is of gerade type ($1s^1/_{2+} = s\alpha$), and the lower

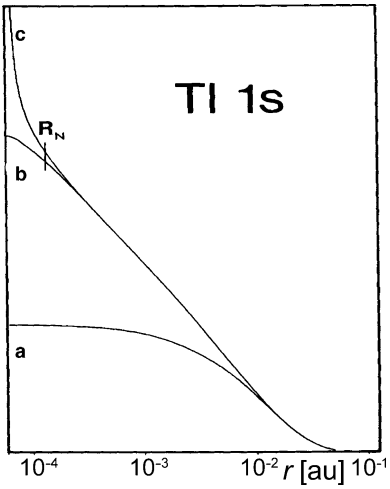

Figure 1-11. Values of 1s wavefunctions of the Tl atom ($Z = 81$) versus nuclear distance r (log-scale for r in au). (**a**) Non-relativistic (the difference between finite and point nuclei is not visible), (**b**) relativistic, finite nucleus with radius R_N, and (**c**) relativistic, point nucleus (After Schwarz and Wallmeier [98])

component is ungerade ($1p^1/_{2+} = p_0\alpha + \sqrt{2}\, p_{+1}\beta$). With '*nlj*' type, we will denote a two-component spinor $\sim$'x,y,z'$^l \cdot r^{n-l-1}$ with spin and orbital angular momenta coupled to $j = l \pm s$. For instance, '$1p^1/_{2+}$' means a function with a factor of type 'x,y,z'$/r$. This factor changes steeply inside the nucleus (for a point nucleus, it jumps); around $r = 0$, the lower component changes along the x axis from -1β to $+1\beta$, along the y axis from $-i\beta$ to $+i\beta$, and along the z axis from -1α to $+1\alpha$. The other spin state $1s^1/_{2-}$ with dominant β instead of α spin is the complex conjugate function, with α replaced by β and β replaced by $-\alpha$ (note the negative sign). Along any axis, the upper component of 1s has no zero, while the lower component has a zero at $r = 0$.

1.3.2.2. $p^3/_2$ Spinors

Another simple case is $l = 1$, $j = \ell + {}^1/_2$, i.e. $2p^3/_2$. For a point nucleus, we have:

$$2p^3/_2, {}^3/_2 : N' \cdot r^{d'} \cdot e^{-Zr/2} \cdot \begin{pmatrix} 4/\gamma \cdot {}'2p_{3/2}{}' \\ i \cdot {}'2d_{3/2}{}' \end{pmatrix}, d' = \sqrt{4-\gamma^2} - 1 \approx 1 - {}^1/_4\gamma^2. \quad (1\text{-}46)$$

'2p' and '2d', respectively, denote factors of type '$\sim x,y,z$' and '$\sim xy, \ldots /r$' around the nucleus. The upper 2p ungerade component has a node inside the nucleus, with an extremely steep slope (infinite for the point nucleus), much steeper than in the non-relativistic limit. Note that the exponent d' of prefactor $r^{d'}$ is smaller than 1. Again, the relativistic spinor is more contracted than the non-relativistic orbital. The lower 2d gerade component approaches zero inside the nucleus as a quite sharp parabola and rises comparatively steeply outside the nucleus.

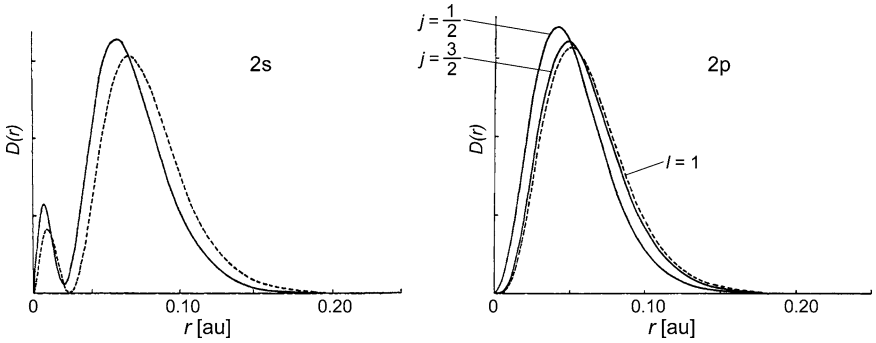

Figure 1-12. Radial densities $D(r) = 4\pi r^2|\Psi|^2$ of spinors of Hg($Z = 80$) versus nuclear distance r in au. (*Full curves*) relativistic, (*dashed*) non-relativistic, (*left*) 2s, and (*right*) relativistic 2p($j = \frac{1}{2}$) and 2p($j = \frac{3}{2}$), and non-relativistic 2p($l = 1$) (After Burke and Grant [76])

The higher $ns1/2$ spinors with $n > 1$ and the higher $np3/2$ spinors with $n > 2$ have slightly more complicated and (for upper and lower components) more different r-dependent factors. In general, the lower component χ has one zero more than the upper component φ, their nodes interlacing each other. Since the charge density is $\rho = |\varphi|^2 + |\chi|^2$, it nowhere vanishes but has minima near the points, where the larger upper component vanishes (see Figure 1-12 left). The shell structure of the hydrogenic spinors becomes less pronounced for increasing Z.

While $\rho(\boldsymbol{r})$ in the four-component Dirac picture means the charge density at $\boldsymbol{r}$, $\rho(\boldsymbol{r})$ has a slightly different meaning in the two-component picture, where the position of charge is not $\boldsymbol{r}$ but $U^+\boldsymbol{r}U$ [58, 59] (Chapter 12).

1.3.2.3. $p1/2$ Spinors

The simplest example of a $j = l - s$ spinor with a lower $j = (l-1) + s$ component is $2p1/2_+$, for a point nucleus:

$$2p1/2_+ : N'' \cdot r^{-d} \cdot e^{-Zr/2d''} \cdot \begin{pmatrix} i(r + O(\gamma^2)) \cdot {}'1p_{1/2}{}' \\ O(\gamma) \cdot (r - O(\gamma^0)) \cdot {}'1s_{1/2}{}' \end{pmatrix},$$

$$d'' = \sqrt{1 - d/2} \approx 1 - 1/8\gamma^2. \tag{1-47}$$

Both r-dependent factors r^{-d} and $e^{-Zr/2d''}$ rise faster towards the nucleus then in the non-relativistic case (r^0 and $e^{-Zr/2}$). The relativistic orbital contraction and energetic stabilization is comparatively large for $p1/2$ spinors, in particular in comparison to $p3/2$ spinors, which do not differ that much in energy and radial distribution for the non-relativistic p orbitals (Figure 1-12 right). At large and medium r, the upper ungerade term in the parentheses of formula (1-47) behaves as $r \cdot 1p \sim 2p \sim$ 'x,y,z', whilst the lower gerade term behaves as γ(r–const) $\cdot$ 1s, i.e. radially as a small 2s component. However, for $r \to 0$, the upper term behaves

as $\gamma^2 \cdot 1p \sim \gamma^2 \cdot$ 'z'$/r$, whilst the lower term behaves as $\gamma \cdot 1s \sim \gamma \cdot \text{const}$. The upper component is the smaller one near the nucleus. This holds for all $j = l$–s spinors.

The non-relativistic p-orbitals are completely degenerate and can be easily mixed. The electric fields in molecules then stabilize real oriented ones such as p_z along the z-axis, which can well overlap with orbitals with same spin from neighbor atoms on the z-axis. The relativistic spin-orbit interaction, however, couples real and imaginary, and also α and β spin contributions. For instance, a $p^1/_{2+}$ spinor is $(p_x\beta + ip_y\beta + p_z\alpha)/\sqrt{3}$ and has a non-directional spherical charge density distribution $\rho = f(x^2 + y^2 + z^2) = f(r^2)$ (Figure 1-3a); the wavefunction is inherently complex and spin-mixed. In general, spin-orbit coupling will weaken covalent overlap bonding [77, 78], for details see Section 1.4.3.

1.3.3. Relativistic Changes of Orbital Radii

The atomic orbital radii $r = \langle(\varphi, \chi)||\hat{\boldsymbol{r}}||(\varphi, \chi)\rangle$ had been investigated, e.g., by Burke and Grant [76] and Andrae [79]. For the fractional relativistic orbital contraction $\delta\rho = (r - r^0)/r$ with respect to the non-relativistic value r^0, one obtains to first order in γ^2

$$\begin{aligned} &1s : \delta\rho \approx -1/3\gamma^2 && (1/3 \approx 0.33), \\ &2s : \delta\rho \approx -35/96\gamma^2 && (35/96 \approx 0.36), \\ &2p^1/_2 : \delta\rho \approx -42/96\gamma^2 && (42/96 \approx 0.44), \\ &2p^3/_2 : \delta\rho \approx 1/10\gamma^2 && (1/10 = 0.10). \end{aligned} \tag{1-48}$$

In both cases, for orbital energies and for orbital radii, the percent-effects increase from 1s to 2s and $2p^1/_2$, but for large n, l, j finally become smaller. The largest fractional energy stabilization and contraction occurs for $j = 1/2$ at 2s,$2p^1/_2$, for $j = 3/2$ at $3p^3/_2, 3d^3/_2$, for $j = 5/2$ at $5d^5/_2, 5f^5/_2$. This is the rule for hydrogenic orbitals, which also applies to the innermost core orbitals of heavy (neutral or nearly neutral) atoms in chemical compounds, i.e. for the case of x-ray spectroscopy. The relations for the relativistic corrections of energies and radii of the outer atomic core and valence shells are different, see below.

1.3.4. Paradoxical Relations

In order to *explain* complex physical phenomena, one must introduce theoretical simplifications and construct a transparent model. There may be two completely different reasons for a model correctly reproducing some aspects of the real situation. Either the basic aspect of the physics of the system under consideration is correctly represented by the applied model, and the approximation influences only negligibilities in the given context. Or two significant errors accidentally happen to cancel each.

1.3.4.1. The Bohr Model of the H Atom

A typical example of the latter situation is Bohr's model of the hydrogen atom. Obviously, the H atom is an object in three-dimensional space. However, Bohr treated it as a two-dimensional, planar, planetary object. One spatial dimension is missing. This seriously affects the consequences of Heisenberg's uncertainty relation, which determines the size of the unit cell in position-momentum phase space and, thereby, the quantum-kinetic energy. To compensate for the missing radial quantization, Bohr had to choose the minimal angular momentum value, which is $0\hbar$ for the lowest rotationless states, as $1\hbar$. In the case of the H atom, these two errors cancel exactly, while they do not do so for $H_2{}^+$ or He or H_2. Since the semiclassical H atom is such a nice simple model, which is commonly referred to in elementary quantum chemical explanations, we will consider it, too. However, we should not be embarrassed, if it does not correctly work out.

In the H atom, there is equilibrium between the Coulomb attraction Ze^2/r^2 and the centrifugal force $m_{\text{inert}} \cdot v^2/r$ (m_{inert} is the longitudinal and transversal inertial mass, to be distinguished from the angular momentum quantum number m). Upon angular momentum quantization, $L_z = m_{\text{inert}} \cdot v \cdot r = m\hbar$, we get two equations for the two unknown variables v and r. We note that Bohr's quantum number (here denoted by m) has the meaning of a quantum number for fixed-axis rotation, though not that of Schrödinger's principle quantum number n. Setting $e = \hbar = 4\pi\varepsilon_o = 1$, the velocity of light is $c \approx 137$. When we exchange the two different quantum numbers m and n, we obtain for velocity v, radius r and energy E of the hydrogenic orbit:

$$v = Z/n, r = n^2/Zm_{\text{inert}}, E = -T = -\tfrac{1}{2}V = -Z^2 m_{\text{inert}}/2n^2. \quad (1\text{-}49)$$

For m_{inert} = electronic rest-mass m, these are the non-relativistic values for the hydrogenic states. With the relativistic effective mass of Eq. (1-11), we obtain

$$v = Z/n, r = n^2\sqrt{1-\gamma^2/n^2}/Z\text{m}, E = -T = \tfrac{1}{2}V = -Z^2\text{m}/2n^2\sqrt{1-\gamma^2/n^2}. \quad (1\text{-}50)$$

The model qualitatively explains that relativity contracts the orbital radius and stabilizes the energy. Eqs. (1-11) and (1-50) are frequently cited to rationalize the direct relativistic effects. However, the numerical values of the 'relativistic Bohr model' are incorrect, even the trend with respect to increasing n is not correct. The Bohr model predicts $\delta r \approx -\gamma^2/2n^2$ and $\delta\varepsilon \approx +\gamma^2/2n^2$, i.e. approximately the same percent age for orbital contraction and for orbital stabilization, and both effects decreasing for increasing quantum number squared. However, the true hydrogenic effects are larger for the radii than for the energies. And the largest percentages of relativistic effects occur for some small n value, depending on the property (E, r, ...), though not for the smallest n, compare [75] and [80]. The relativistic spinless Bohr model also deviates from the spinless Klein–Gordon model, where the lowest energy varies as $E = -Z^2/2 \cdot (1 + \tfrac{5}{8}\gamma^2 \ldots)$, though the deviation is smaller than from the Dirac spin model.

1.3.4.2. The Dirac Hydrogen Atom

Another astonishing situation of rather common logical structure is displayed in Table 1-1. The expression for the relativistic kinetic-energy correction at lowest order of α is $-(\alpha^2/8)\cdot \boldsymbol{p}^4$, see Eq. (1-14a). The expectation value of the electronic momentum in the hydrogenic ground state is, at lowest order, $\langle|\boldsymbol{p}|\rangle = Z$. It is, however, purely accidental that the relativistic lowest order energy correction for hydrogen is just $-(\alpha^2/8)\cdot Z^4$. Whilst $\langle|\boldsymbol{p}|\rangle = Z$, and $\langle|\boldsymbol{p}^2|\rangle = Z^2$, $\langle|\boldsymbol{p}^4|\rangle = \langle|2(\varepsilon - V)\boldsymbol{p}^2|\rangle = \langle|4(\varepsilon - V)^2|\rangle = 5Z^4$! The $\boldsymbol{p}^4$ operator, applied to a hydrogenic 1s orbital with a cusp at the origin, yields also a δ-contribution at the origin. Indeed, $-5\cdot(\alpha^2/8)\cdot Z^4$ is the correct lowest order energy correction for the spinless hydrogenic Klein–Gordon system. The mass–velocity stabilization for the Dirac system, i.e. for the H atom with a spinning electron, is the same.

However, the charge versus mass distribution of an electron near to the nucleus due to its spin-structure causes an averaging over the Coulomb potential that reduces the nuclear-electronic attraction in particular for states with finite probability at the Coulomb singularity. This Darwin correction to the potential energy of spinning point charges is $+{}^1\!/_2\alpha^2 Z^4$ and yields a value of $-{}^1\!/_8\alpha^2 Z^4$ for the total relativistic energy correction at lowest order of α. (For non-s states, the Darwin correction is smaller, of order α^4.)

The lowest order *total* energy can be obtained from the 'unperturbed' non-relativistic wavefunction Ψ^0 and the lowest order correction of the Hamiltonian, $\Delta^{\mathrm{rel}}\hat{\mathrm{H}}$. However, for other expectation values, for instance of the potential and kinetic energy contributions, also the lowest order correction to the wavefunction, $\Delta^{\mathrm{rel}}\Psi$, is needed. Since the total energy is stationary, it is not changed at this order; the kinetic and potential energy changes due to the relativistic change of the wavefunction are of opposite value, $\pm\alpha^2 Z^4$. As a result, the kinetic energy *expectation value* increases by $+{}^3\!/_8\alpha^2 Z^4$, despite the negative term in the Hamiltonian *operator expression* $(-{}^1\!/_8\alpha^2\boldsymbol{p}^4)$. And the potential energy *expectation value* decreases by $-{}^1\!/_2\alpha^2 Z^4$, despite the positive Darwin term in the Hamiltonian *operator expression*, namely because of the relativistic relaxation of the wavefunction.

Table 1-1 Kinetic, potential and total energies of the hydrogenic 1s ground state for nuclear charge Z: Non-relativistic approximation (n-rel), the two contributions of lowest order in α due to relativistic corrections of Hamiltonian ($\Delta^{\mathrm{rel}}\hat{\mathrm{H}}$) and of the wavefunction ($\Delta^{\mathrm{rel}}\Psi$), and the total lowest order energy correction (Δ rel) in comparison to Bohr's model ($\Delta\mathrm{rel}_{\mathrm{Bohr}}$)

Energies	n-rel	$\langle\Psi^0\lvert\Delta^{\mathrm{rel}}\hat{\mathrm{H}}\rvert\Psi^0\rangle$	$\langle\Psi^0\lvert\hat{\mathrm{H}}^0\rvert\Delta^{\mathrm{rel}}\Psi\rangle$ + c.c	Δrel	$\Delta\mathrm{rel}_{\mathrm{Bohr}}$
Kinetic	$+Z^2/2$	$-{}^5\!/_8\,\alpha^2 Z^4$	$+\alpha^2 Z^4$	$+{}^3\!/_8\,\alpha^2 Z^4$	$(-{}^1\!/_8 + {}^1\!/_4 =)$ $+{}^1\!/_8\,\alpha^2 Z^4$
Potential	$-Z^2$	$+{}^1\!/_2\,\alpha^2 Z^4$	$-\alpha^2 Z^4$	$-{}^1\!/_2\,\alpha^2 Z^4$	$(0 - {}^1\!/_4 =) - {}^1\!/_4\,\alpha^2 Z^4$
Total	$-Z^2/2$	$-{}^1\!/_8\,\alpha^2 Z^4$	0	$-{}^1\!/_8\,\alpha^2 Z^4$	$-{}^1\!/_8\,\alpha^2 Z^4$

The kinetic and potential energy values are in accord with the relativistic virial theorem [30, 81]:

$$E_{\text{kin}} = -E - \partial E / \partial \ln \alpha, \qquad (1\text{-}51)$$
$$E_{\text{pot}} = 2E + \partial E / \partial \ln \alpha.$$

Here, we have defined the kinetic and potential energies in the Dirac picture as $E_{\text{pot}} = \langle \mathrm{e}V_{\text{i}} \rangle$ and $E_{\text{kin}} = E - E_{\text{pot}} = \langle (\beta - 1_4)\mathrm{mc}^2 + \boldsymbol{\alpha p}\mathrm{c} \rangle$, yielding

$$E = \langle (\beta - 1_4)\mathrm{mc}^2 \rangle, E_{\text{pot}} = E - E_{\text{kin}} = -\langle \boldsymbol{\alpha p}\mathrm{c} \rangle. \qquad (1\text{-}52)$$

The momentum term $\langle \boldsymbol{\alpha p}\mathrm{c} \rangle$ is approximately twice the kinetic energy.

1.3.4.3. Covalent Bond Formation, Singlet Triplet Splitting and More

There are many other examples of such paradoxical mechanisms with similar logical and mathematical structure. First, we mention the mechanism of covalent bond formation [82, 83]. Upon overlap of two open shell atoms and concomitant electron sharing, the bonding electrons of two atoms get more space in the bond direction. Due to Heisenberg's uncertainty principle, the bond-parallel component of the momentum uncertainty, and thereby the kinetic energy *density functional* are reduced. The simple MO model of frozen AOs yields a reduced molecular energy. However, the reduced kinetic energy 'pressure' results in a contractive relaxation of the bond orbital, until the kinetic energy *expectation value* has increased, as required by the virial theorem.

Another example is given by the two-electronic singlet and triplet states. The uncorrelated Coulomb repulsion of two electrons in a spin-triplet state $(J - K)$ is reduced in comparison to the singlet state $(J + K)$, because of Pauli's antisymmetry requirement. The result is a contraction of the electronic triplet shell, with increased electron-nuclear attraction energy as compared to the singlet state. Often the triplet has an even higher inter-electronic repulsion energy than the singlet $(J - K)_{\text{triplet}} > (J + K)_{\text{singlet}}$.

Such counterintuitive examples, where the 'driving force' is of one sign, but where the relaxation of the system upon the 'intended' change causes an effect of the opposite sign, are rather ubiquitous. This 'anti-LeChatelier' behavior, where the intended change is not just moderated, but at the end even inverted, depends on the details of the system, i.e. whether some parameter values are below or above respective critical values. This behavior does not only occur in quantum mechanics, but also in classical mechanics, biology and ecology, economy and financing. Its understanding is important for both sensible discussions in science and in daily life.

1.3.5. Orbitals in Many-Electron Atoms: Small Angular Momenta

The electron in a hydrogen-like ion everywhere 'feels' the same full nuclear charge Z. In more typical, heavier, many-electron atoms, the effective nuclear charge

$Z_{\text{eff}}(r)$ at distance r from the nucleus is reduced through shielding by the inner (and to some extent also by the outer) electron density. The inner electron density consists of the density of the inner *nlj* shells, *and* of the inner tails of core-penetrating outer shells (mainly valence s and p). Z_{eff} at small r, near the nucleus, is nearly Z, but decreases in an exponential manner for larger r. Therefore, we must distinguish the atomic orbitals according to their radial behavior, in particular according to their angular momenta. $s_{1/2}$ and $p_{1/2}$ orbitals ($l = 0$ and 1) always have some density near the nucleus, whilst the centrifugal force acting on d and f orbitals keeps them away. We must also distinguish between the lowest orbital of a given angular momentum ('primogenic' orbitals 1s, 2p, 3d, 4f, i.e. *nl* with $n = l + 1$) and the higher ones (*nl* with $n > l + 1$). The former ones 'feel' the centrifugal force $\sim l(l+1)/r^3$, whilst the latter ones feel the centrifugal force *and* the Pauli repulsion by the lower occupied subshell(s) of same l-value [84–86].

The hydrogenic orbitals in the Coulomb potential $V(\mathrm{r}) = -Z/r$ of an unscreened nucleus obey the virial theorem in the simple form

$$V + 2T = 0, V = 2E, T = -E. \tag{1-53}$$

However, atomic orbitals in the strongly screened potential of real many-electron atoms obey the generalized virial theorem:

$$\langle r \cdot \partial V/\partial r \rangle + 2T = 0, \tag{1-54}$$

which corresponds, in the case of outer valence orbitals, to

$$V + T \approx 0, |V| \gg |E|, T \gg -E \tag{1-55}$$

Figure 1-13 shows that a higher atomic orbital with several inner nodes contains about 90% of its integrated density S in the outer diffuse spatial shell, and in each more inner shell there is about one order of magnitude less charge. The same holds for the total orbital energy E, which comes mainly from the outer spatial shell.[11] However, despite the smaller and smaller density contributions from the inner spatial shells, each spatial shell contributes a similar amount of potential or kinetic energy. Classically, the valence electron increases its speed when it dives into the atomic core, where the increasing kinetic energy compensates for the disappearing screening of the nuclear attraction. This explains, why valence electrons have a comparatively small energy, but may still be relativistically fast.

[11] Of course, quantum mechanics is a holistic theory without physically defined local contributions to an observable expectation value. However, in a concrete calculation of a physical value, or in a specific explanation of the physical mechanism, one applies one specific formula chosen from a gauge-invariant set. This then gives one of the many complementary, internally consistent pictures of physical realty. For instance, we here choose $+1/2\ {}_{\mathrm{a}}\int^{\mathrm{e}} \mathrm{d}\boldsymbol{r} \cdot |\nabla\Psi(\boldsymbol{r})|^2$ with positive definite integrand for local contributions of the kinetic energy T. It gives a somewhat different picture than $-1/2\ {}_{\mathrm{a}}\int^{\mathrm{e}} \mathrm{d}\boldsymbol{r} \cdot (\Psi^* \cdot \nabla^2\Psi)$. For the total energy we choose ${}_{\mathrm{a}}\int^{\mathrm{e}} \mathrm{d}\boldsymbol{r} \cdot (\Psi^* \cdot \hat{\mathrm{H}}\Psi) = E \cdot {}_{\mathrm{a}}\int^{\mathrm{e}} \mathrm{d}\boldsymbol{r} \cdot \rho(\boldsymbol{r})$. In the present Figures, a means the nuclear position, $r = 0$, and e corresponds to the upper integration limit plotted on the abscissa.

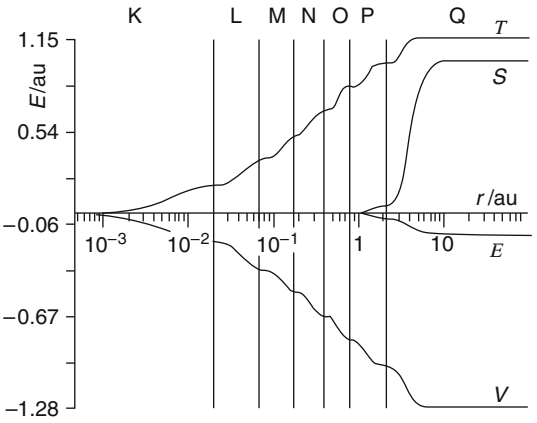

Figure 1-13. 7s spinor $\varphi(r)$ of a U atom (2-component picture) over a logarithmic r-scale: Radial integration over spatial shells K (corresponding to n = 1), L, M, N, O, P, Q ($\sim n = 7$) from the nucleus (r = 0) up to r, ${}_0\int^r \mathrm{d}\boldsymbol{r}' \cdot f(\boldsymbol{r}')$, $\mathrm{d}\boldsymbol{r}' = 4\pi r'^2 \mathrm{d}r'$. T: non-relativistic kinetic energy from $f = 1/2 \cdot |\nabla\varphi|^2$; S: density from $f = |\varphi|^2 = \rho$; V: potential energy from $f = V_{\mathrm{scf}} \cdot \rho$; E: total energy from $f = E\rho$.[11] The vertical lines indicate the minima of the ns orbital densities, which all nearly coincide (After Schwarz et al. [130])

1.3.5.1. Direct and Indirect Relativistic Effects

Whilst the total energy of the atomic valence shell dominantly stems from the outer atomic region, and the kinetic and potential energy contributions from all atomic spatial shells, the 'direct' relativistic energies from the corrections to the potential and kinetic energy operators originate only in the neighborhood of the nucleus, namely for s valence orbitals in the spatial K shell (*D*, *MV* and *DIR* in Figures 1-14 and 1-15), for p valence shells in the spatial K and L shells (*DIR* and *SO* in Figures 1-16 and 1-17), for d valence shells in the spatial L and M shells (*DIR* and *SO* in Figure 1-20 below), and for f valence shells in the spatial M and N shells (*DIR* and *SO* in Figure 1-21).

In addition to these stabilizing, contracting, 'direct' relativistic effects, known from the hydrogen atom, there appear additional 'indirect' relativistic effects in many-electron atoms [2, 3, 35, 87]. The $s^1/_2$ and $p^1/_2$ orbitals contract significantly, in many-electron atoms fractionally even more than in hydrogen-like one-electron systems. The contraction looks like a linear shift on a logarithmic r-scale, with a concomitant increase of the relativistic amplitude maxima, see Figure 1-18. Thereby, the nuclear charge becomes relativistically better shielded. The relativistic self-consistent field (scf) is less attractive than the non-relativistic one. The respective change $\Delta^{\mathrm{ind}} V_{\mathrm{scf}} = V_{\mathrm{scf}}{}^{\mathrm{rel}} - V_{\mathrm{scf}}{}^{\mathrm{n\text{-}rel}}$ due to the $s^1/_2$ and $p^1/_2$ contraction acts in a repulsive manner, in particular on orbitals not coming near to the nuclei such as d and f orbitals, and on weakly bound orbitals such as the virtual frontier orbitals. This indirect de-stabilization is distributed over all shielding shells, see *IND* in Figures 1-14 1-16, 1-20 and 1-21.

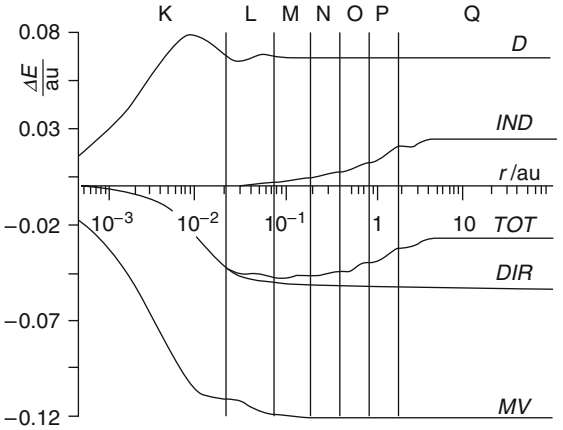

Figure 1-14. 7s orbital φ of a U atom: Radial energy integration (compare legend of Figure 1-13). D: relativistic Darwin potential energy correction from $f = \alpha^2/4 \cdot [(\varphi V_{\mathrm{scf}} \Delta\varphi) - V_{\mathrm{scf}}(\nabla\varphi)^2]$; MV: relativistic kinetic energy mass–velocity correction from $f = -\alpha^2/8 \cdot (\Delta\varphi)^2$; DIR: the respective sum; IND: relativistic energy correction due to the relativistic change of the nuclear screening potential from $f = \Delta^{\mathrm{rel}} V_{\mathrm{scf}} \varphi^2$; TOT: total relativistic orbital energy correction (After Schwarz et al. [130])

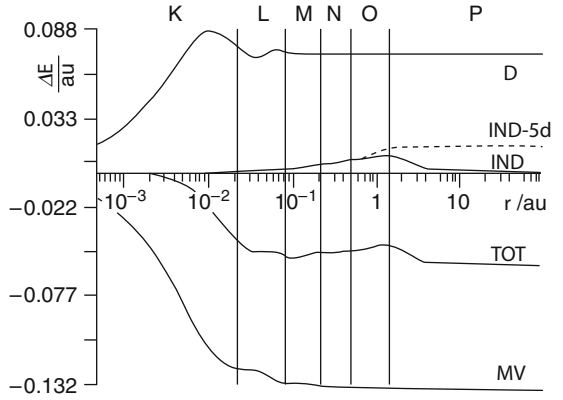

Figure 1-15. 6s orbital of an Au atom: Radial energy integration (compare legends of Figures 1-13 and 1-14). D: relativistic Darwin potential energy correction; MV: relativistic kinetic energy mass–velocity correction; IND: relativistic energy correction due to the relativistic change of the nuclear screening potential; TOT: total relativistic orbital energy correction. IND-$5d$ (dashed curve): IND without the screening by the $5d^{10}$ shell (After Schwarz et al. [130])

Since the direct relativistic effects occur in the immediate vicinity of the nuclei, they are hydrogen-like and increase as $\alpha^2 Z^4$. However, the total orbital *energies*, being produced in the outer shielded region, are reduced by the total scf shielding. Therefore, the fractional relativistic corrections of order $\alpha^2 Z^2$ become *larger* for most orbitals in many-electron atoms as compared to the hydrogen-like orbitals in the field of a naked nucleus. In particular, the percent-changes of the valence orbital

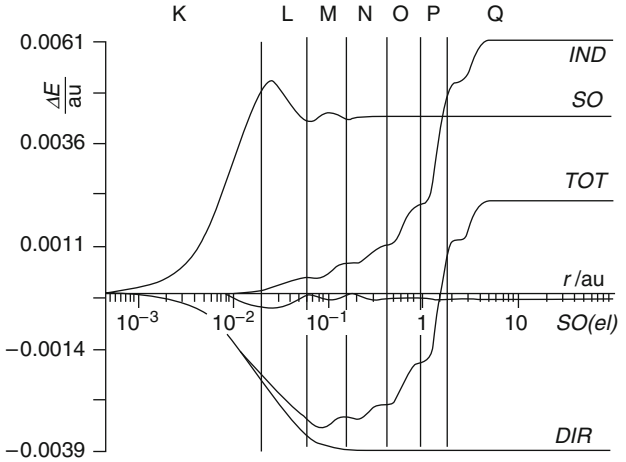

Figure 1-16. 7p orbital of a U atom (spin-averaged): Radial energy integration (compare legends of Figures 1-13 and 1-14). DIR: direct relativistic energy correction (kinetic velocity–mass plus potential Darwin terms); IND: dominant energy correction from of the relativistic change of the screening potential; TOT: the respective sum; SO: spin-orbit coupling energy from $f = \alpha^2/4 \cdot [(\boldsymbol{\sigma} \times \boldsymbol{\nabla}\varphi)V_{\text{scf}}(\boldsymbol{p}\varphi)]$, V_{scf} comprizing the nuclear Coulomb and the electron screening potentials; $SO(el)$: contribution from nuclear screening by the other electrons (After Schwarz et al. [130])

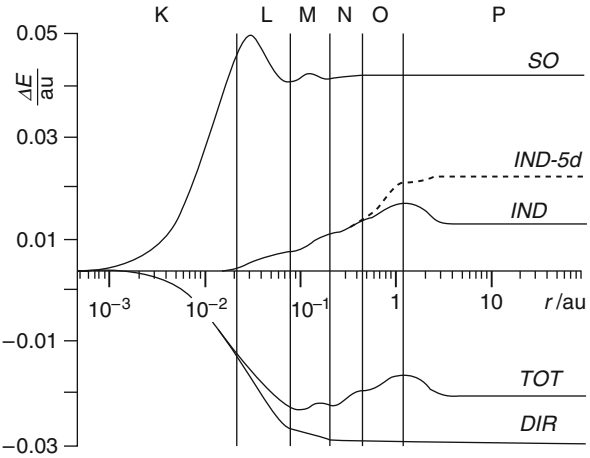

Figure 1-17. 6p orbital of a Pb atom (spin-averaged): Radial energy integration (compare legends of Figures 1-13 and 1-14). DIR: direct relativistic energy correction (kinetic velocity–mass plus potential Darwin terms); IND: energy correction from of the relativistic change of the screening potential; TOT: the respective sum; SO: spin-orbit coupling energy. IND-$5d$ (*dashed curve*): IND without the screening by the $5d^{10}$ shell (After Schwarz et al. [130])

energies and of the valence ionization potentials do *not* decrease with increasing n (as they do for hydrogen, i.e. from $n = 2$ onwards for $j = {}^1/_2$, from $n = 3$ onwards for $j = {}^3/_2$ and from $n = 5$ onwards for $j = {}^5/_2$, noted in Section 1.3.3).

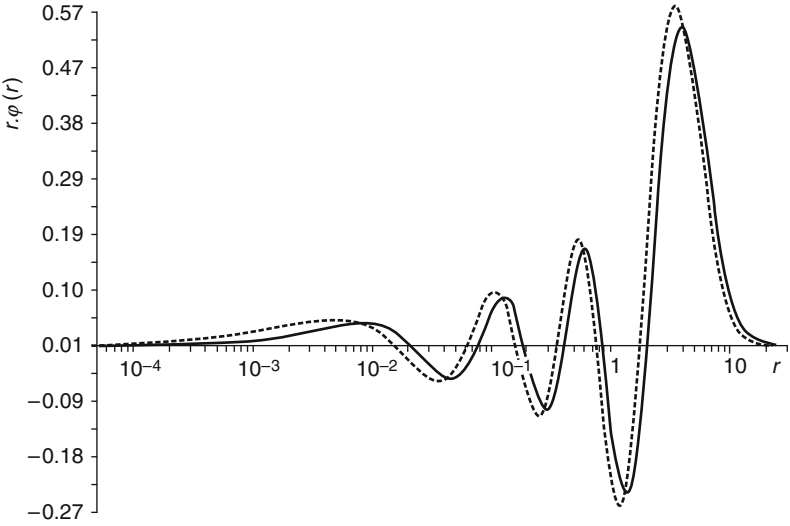

Figure 1-18. Upper component of the 7s radial Dirac spinor of a U atom, $r\varphi(r)$, over a logarithmic r-scale. - - - - - relativistic, —— non-relativistic (After Schwarz et al. [130])

The relativistic numerical atomic scf calculations of Desclaux [39] have shown that the fractional relativistic orbital *energy stabilizations* of $ns^1/_2$ and $np^1/_2$ increase with increasing n and are particularly large in the lowest row of the periodic system of elements with the largest valence principal quantum numbers. The fractional relativistic $ns^1/_2$ and $np^1/_2$ orbital *radius contractions*, however, still behave nearly hydrogen-like, being largest for 2sp.

One can still read the statement that only the *innermost* s and p core orbitals are stabilized and contracted due to direct relativistic effects, the outer s and p valence orbitals being indirectly stabilized because of the orthogonality requirement on the contracted inner orbitals of same l value. Baerends et al. [58] have shown, however, that the orthogonality constraint of the valence orbital on the contracted inner core orbitals has just the opposite effect. The Pauli exclusion effect caused by the relativistically contracted core orbitals squeezes the valence orbitals of same angular momentum more efficiently out of the atomic core, slightly *expanding* the valence orbital.

When discussing relativistic orbital contractions and expansions, one should also not mix up different pictures. $\boldsymbol{r}$ describes the position of the charge in the four-component Dirac picture and occurs in expressions for the electric dipole moment, for the optical dipole transition moment or for the electric field gradients. The $\boldsymbol{r}$ in two-component pictures (i.e. in two-component pseudo-potential or Douglas–Kroll–Heß or regular-approximation or Pauli approaches) has a somewhat different meaning, see Figure 1-10 [56–59, 87, 88], Chapters 4 and 12.

Concerning the trends within a row of the periodic table, i.e. upon increasing the nuclear charge and the number of valence electrons one by one, the $s^1/_2$ and

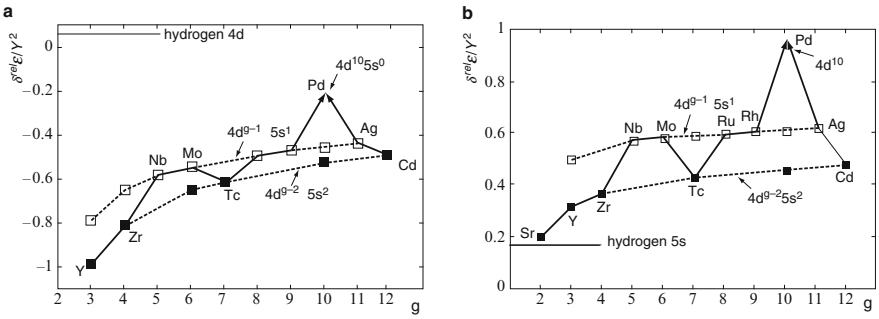

Figure 1-19. Fractional relativistic correction factors for the valence orbital energies, $\delta^{\mathrm{rel}}\varepsilon/\gamma^2$, of the neutral transition metal atoms of row 5 in group $g = 2$(Sr) through $g = 12$ (Cd). (**a**) Relativistic de-stabilization of 4d. (**b**) Relativistic stabilization of 5s. Values for valence electron configurations $4d^{g-2}5s^2$ and $4d^{g-1}5s^1$ are connected by dotted lines (After Autschbach et al. 2002)

$p^1/_2$ valence orbitals become relativistically more or less stabilized, depending on whether the added electron-density-distribution is sitting more inside or more outside the s or p valence-density distribution. The largest relativistic stabilization of the s valence shell occurs, when the d and f shells are just being filled up, that is for $(n-1)d^{10}ns^k$ or $(n-2)f^{14}(n-1)d^{10}ns^k$ configurations: Concerning atoms without (partial) charge, for $d^{10}s^0$ in Ni, Pd, Pt, Ds; for $d^{10}s^1$ in Cu, Ag, Au, Rg; and for $d^{10}s^2$ in Zn, Cd, Hg, Uub. The fractional relativistic s valence stabilization begins in each row near a hydrogen-like value, increases in the d and f blocks of the periodic system (Figure 1-19b), and then goes down again in the p block. The relativistic s valence stabilization also decreases upon increase of the s population. The largest relativistic s valence stabilizations of up to $1 \cdot \gamma^2$ are obtained in groups 10, 11 and 12, where it is largest for given s population, see Figure 1-19b [39,42,89, Figure 3-1 in this book]. This phenomenon is called 'the gold maximum'.

The reason for these trends is the *indirect stabilization*, which is less often discussed than the indirect de-stabilization. The stabilization is due to the (indirect) expansion of the d and f orbitals and affects the outermost s valence orbitals in the middle of the periodic table (Figure 1-15) and the outermost p valence orbitals on the right side of the periodic table (Figure 1-17). In some cases (e.g. for Au 6s, though not for U 7s, Figure 1-14), the indirect stabilization nearly cancels the more common indirect de-stabilization.

1.3.6. Orbitals in Many-Electron Atoms: Higher Angular Momenta

The situation for d and f orbitals is quite different. The direct relativistic stabilization is smaller, but more importantly, the indirect shielding de-stabilization is much larger, see Figures 1-20 and 1-21. Due to the centrifugal force for $l = 2$ and 3, these orbitals are kept outside the innermost core shells and feel a large, relativistically improved nuclear shielding. Consequently, the d and f valence orbitals are no longer stabilized as in the hydrogenic case, but are de-stabilized and spatially extended.

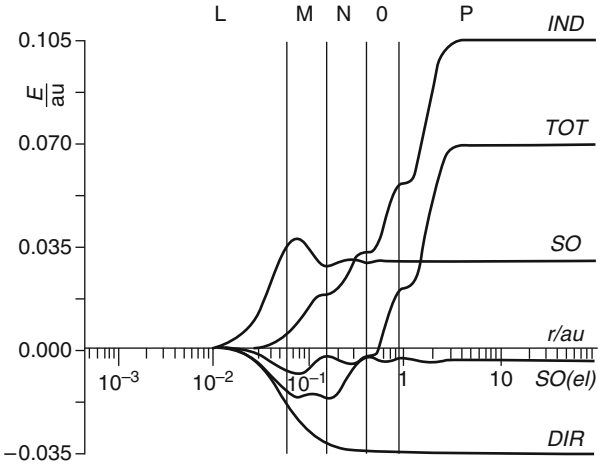

Figure 1-20. 6d orbital of a U atom (spin-averaged): Radial energy integration (compare legends of Figures 1-13 and 1-14). DIR: relativistic kinetic velocity–mass plus potential Darwin energy correction; energy correction from of the relativistic change of the screening potential, IND; the respective sum, TOT; the spin-orbit coupling energy, SO; the contribution from nuclear screening by the other electrons, SO(el) (After Schwarz et al. [130])

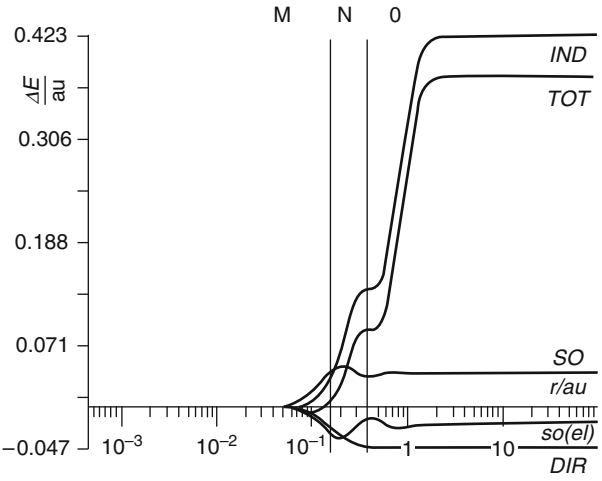

Figure 1-21. 5f orbital of a U atom (spin-averaged): Radial energy integration (compare legends of Figures 1-12 and 1-13). Relativistic kinetic velocity–mass plus potential Darwin energy correction, DIR; energy correction from of the relativistic change of the screening potential, IND; the respective sum, TOT; the spin-orbit coupling energy, SO; the contribution from nuclear screening by the other electrons, $SO(el)$ (After Schwarz et al. [130])

In addition, there is the spin-orbit splitting into more stable and compact, and into less stable and less compact components, one $p^1/_2$ versus two $p^3/_2$ components, two $d^3/_2$ versus three $d^5/_2$ components, and three $f^5/_2$ versus four $f^7/_2$ components, respectively. The nuclear spin-orbit splittings are partially shielded, too, by the inner electron density, by a few percent up to about one third (Figures 1-16, 1-20, and 1-21).

The $d^3/_2$ and $d^5/_2$ valence levels are most de-stabilized, when the d shell is beginning to become populated, i.e. in group 3 of the periodic system, in particular after the inner f shell has been filled up. The fractional averaged d orbital de-stabilizations are around $0.9\gamma^2$ for Sc, Y, Lu and Lr, but decrease for higher nuclear charges (Figure 1-19a). The $d^3/_2$ levels are eventually stabilized again, when they become inner core levels for larger Z values, whilst the $d^5/_2$ levels remain de-stabilized. The orbital shapes and the radial expectation values do not differ that much from the hydrogenic behavior. At the beginning of the transition series, $d^3/_2$ is slightly expanded by a fraction of $0.3–0.4\gamma^2$, while it begins to be more and more contracted when it becomes a core level. The $d^5/_2$ orbitals are more expanded than the $d^3/_2$ ones, by fractions of $0.5–0.6\gamma^2$. As a result, significant spin-orbit splittings show up, which increase along the transition series from groups 3 to 11, namely from $\sim$0.1 to $\sim 0.3\gamma^2$ for the orbital energies and from $\sim$0.1 to $\sim 0.15\gamma^2$ for the orbital radii.

The fractional indirect de-stabilizations dominate even more over the direct relativistic stabilizations for the 4f and 5f valence orbitals in the lanthanoid and actinoid groups. The fractional energy effects range from 1 to $1.5\gamma^2$, with spin-orbit splittings from 0.1 to $0.2\gamma^2$. The respective orbital radii expansions range from 0.1 to $0.15\gamma^2$, with spin-orbit splittings from 0.05 to $0.08\gamma^2$.

1.3.7. Orbitals in Many-Electron Atoms: The $p^3/_2$ Valence Orbital

In contrast to the $s^1/_2$ and $p^1/_2$ valence orbitals, which are relativistically stabilized and contracted, the $p^3/_2$ orbitals become at first somewhat de-stabilized and expanded along the rows from groups 13 through 18, with largest indirect effects in the noble gas atoms ($\delta E \sim -0.3\gamma^2$, $\delta r \sim +0.05\gamma^2$). Then, as core orbitals for higher nuclear charges, the direct effects increase faster than the indirect effects, and finally the $p^3/_2$ becomes stabilized, too.

The weighted $p^1/_2$–$p^3/_2$ average orbital energies $\bar{E}$ in the valence shell show slight stabilizations for the lighter and earlier p-block elements, and de-stabilizations for the heavier and later ones. The $p^1/_2$–$p^3/_2$ spin-orbit splittings form an important aspect of the p valence shell properties. They increase from group 13 ($\Delta^{so}E/\bar{E} \sim {}^1/_4$ to ${}^1/_2\gamma^2$ for the light to the heavy atoms) to group 18 ($\Delta^{so}E/\bar{E}$ up to $1\gamma^2$). The fractional spin-orbit difference of the p orbital radii of the noble gasses is $\Delta^{so}\langle r\rangle/\langle r\rangle_{ave} \sim {}^1/_3\,\gamma^2$).

While the hydrogenic model (Eq. 1-41) predicts a small increase and than a decrease of the fractional relativistic orbital stabilization $\delta E \sim \gamma^2/n$ for increasing main quantum number n, the $\delta E/\gamma^2$ values of valence orbitals of many-electron

atoms do not decrease. Similarly, the fractional spin-orbit splitting $\Delta^{so}E/E$ varies as $\gamma^2/2l(l+1)$ in hydrogen-like systems, i.e. decreases with increasing squared angular momentum. However, in many-electron atoms $\Delta^{so}E/E\gamma^2$ decreases only weakly for increasing l. When the p, d and f shells are just becoming occupied, $\Delta^{so}E/E\gamma^2$ is about 0.3, 0.2 and 0.1, respectively, while for nearly filled p, d and f shells, $\Delta^{so}E/E\gamma^2$ is about 1, $^2/_3$ and $^1/_2$.

The pattern of relativistic atomic orbital energy and radii changes is even more complex than the pattern for the non-relativistic shells. In particular, energies and radii vary in different manners. In rows 6 and 7 $(\alpha Z)^2$ is about 0.16–0.4 and 0.4–0.74, respectively. Relativistic effects become qualitatively important in the valence shells of the heavy elements.

1.3.8. The Relativistic Two-Electron Interaction

Two points concerning the representation of the electromagnetic interaction must be distinguished [9, 10]). The first point is the gauge of the electromagnetic potential $(V, \boldsymbol{A})$. In order to obtain concrete compact formulas, one needs an appropriate choice for the gauge function $g(t, \boldsymbol{r})$, see Eq. (1-17). Depending on the choice, some terms in the Hamiltonian cancel. The two most common choices are the Coulomb and the Lorentz gauge.

In the Coulomb gauge, one assumes for a free field in a space without any charges ($\rho = 0$) and currents ($\boldsymbol{j} = 0$):

$$V^0(t, \boldsymbol{r}) = 0, \nabla \boldsymbol{A}^0(t, \boldsymbol{r}) = 0, \tag{1-56}$$

leading to

$$\nabla^2 V(t, \boldsymbol{r}) = -4\pi\rho(t, \boldsymbol{r}), \partial^2 \boldsymbol{A}/\partial^2 t = 4\pi\alpha^2 \cdot \boldsymbol{j}(t, \boldsymbol{r}) \tag{1-57}$$

in the case of non-vanishing external charge and current distributions ρ and $\boldsymbol{j}$.

Another common gauge is the Lorentz gauge, where one assumes in a space free of charges and currents:

$$\nabla^2 V(t, \boldsymbol{r}) = \alpha^2 \cdot \partial^2 V^0/\partial^2 t, \nabla \boldsymbol{A}^0(t, \boldsymbol{r}) = -\alpha^2 \cdot \partial V^0/\partial t \tag{1-58}$$

leading to

$$\begin{aligned} \nabla^2 V(t, \boldsymbol{r}) - \alpha^2 \cdot \partial^2 V/\partial^2 t &= -4\pi \cdot \rho(t, \boldsymbol{r}), \\ \nabla^2 \boldsymbol{A}(t, \boldsymbol{r}) - \alpha^2 \cdot \partial^2 \boldsymbol{A}/\partial^2 t &= -4\pi \cdot \boldsymbol{j}(t, \boldsymbol{r}). \end{aligned} \tag{1-59}$$

The second point is the chosen picture for the relativistic matter field (wavefunction). The formulas (1-56–1-59) refer to the case of the Dirac picture, where $\boldsymbol{r}$ means the position of charge, and where the mass-dependent kinetic energy takes the simple, non-classical form $(\beta mc^2 + \boldsymbol{\alpha} \cdot \boldsymbol{p}c)$. A reasonable approximation to the electromagnetic interaction between two moving charges q_1 and q_2 at distance

r_{12} then takes a comparatively simple form in Lorentz gauge. The so-called Gaunt operator reads:

$$V_{12} = \mathrm{q}_1 \cdot \mathrm{q}_2 \cdot (\mathbf{1}_4 \cdot \mathbf{1}_4 – \boldsymbol{\alpha}_1 \cdot \boldsymbol{\alpha}_2)/r_{12} \cdot \exp(\mathrm{i}\alpha \cdot \omega_{12} \cdot r_{12}). \qquad (1\text{-}60)$$

The two terms in the first parentheses in Eq. (1-60) describe the Coulombic charge and the magnetic spin-and-current contributions, respectively. The last exponential factor may be looked upon as the retardation effect, i.e. caused by the finite velocity by which the electromagnetic interaction is exchanged between the two charges. It contributes to exchange and correlation terms [10]. $\omega\hbar$ is the energy difference of the interacting orbitals, i.e. the energy transferred by the photon between the two particles. The retardation terms are usually negligible for valence shells, but contribute to core excited states, where ω_{12} is large for core-valence correlation-exchange-terms. They also contribute to the long-range van der Waals interactions, where r_{12} is large. The leading $-\mathrm{C}_6/R^6$ term of the van der Waals attraction becomes damped to $-\mathrm{C}_7'/R^7$ due to the finite time R/c needed for electromagnetic interaction.

In the Coulomb gauge and small $\omega_{12} \cdot r_{12}$, one obtains the so-called Breit operator [10]:

$$V_{12} = \mathrm{q}_1 \cdot \mathrm{q}_2 \cdot (\mathbf{1}_4 \cdot \mathbf{1}_4 - 1/2[\boldsymbol{\alpha}_1 \cdot \boldsymbol{\alpha}_2 + (\boldsymbol{\alpha}_1 \cdot \boldsymbol{r}_{12})(\boldsymbol{\alpha}_2 \cdot \boldsymbol{r}_{12})/{r_{12}}^2])/r_{12}. \qquad (1\text{-}61)$$

The Dirac $\boldsymbol{\alpha}$ matrices couple the upper and lower components of the wavefunction and introduce a factor $\alpha = 1/\mathrm{c}$ each into the expectation values. The $\boldsymbol{\alpha}_1 \cdot \boldsymbol{\alpha}_2$ terms describe the relativistic lowest order corrections $\sim\alpha^2$ to the instantaneous Coulomb interaction. The term $-\mathrm{q}_1\boldsymbol{\alpha}_1 \cdot \mathrm{q}_2\boldsymbol{\alpha}_2/r_{12}$ is called the magnetic Gaunt interaction. Different authors attach different physical meanings to the difference between Eqs. (1-60) and (1-61), which is $\sim{}^1\!/_2\,[\boldsymbol{\alpha}_1 \cdot \boldsymbol{\alpha}_2 – (\boldsymbol{\alpha}_1 \cdot \boldsymbol{r}_{12})(\boldsymbol{\alpha}_2 \cdot \boldsymbol{r}_{12})/{r_{12}}^2]$. It is either called the lowest order retardation contribution or the change-of-gauge contribution. The controversy originates in the fact that Newtonian mechanics and Maxwellian electrodynamics are not compatible. If one chooses the non-relativistic representation, all electro-magnetic couplings disappear, in particular the $\boldsymbol{\alpha} \cdot \boldsymbol{\alpha}$ terms in Eqs. (1-60) and (1-61). In the relativistic representation, combining the appropriately gauge transformed exact wavefunction (Eq. 1-33) with expression (1-60) with $\omega = 0$, or (1-61), respectively, would give the same numerical results. Different gauges lead to different complementary pictorial explanations of the underlying physics.

In the two-component picture, $\boldsymbol{r}$ means the position of mass, and the mass-dependent energy takes the relativistically corrected Newtonian form $\mathrm{mc}^2 + \boldsymbol{p}^2/2\mathrm{m} + \mathcal{O}(\alpha^2)$. Upon unitary transformation of the Dirac equation for two particles including the electromagnetic interaction according to Eq. (1-61), many terms cancel each other, but one still obtains a long expression for the electron–electron interaction:

$$V_{12} = +1/r_{12} – \alpha^2/2r_{12}[\mathrm{MOO} + \mathrm{TED} + \mathrm{SOO1} + \mathrm{SOO2} + \mathrm{SS}]. \qquad (1\text{-}62)$$

The first two terms in the brackets are spin-free; MOO is the magnetic dipole orbit–orbit interaction,

$$\mathrm{MOO} = \boldsymbol{p}_1 \cdot \boldsymbol{p}_2 + 1/{r_{12}}^2(\boldsymbol{r}_{12}(r_{21} \cdot \boldsymbol{p}_1) \cdot \boldsymbol{p}_2); \tag{1-63}$$

TED is the Darwin correction to the two-electron Coulomb repulsion $1/r_{12}$,

$$\mathrm{TED} = 2\pi r_{12}\delta(r_{12}). \tag{1-64}$$

The next two terms are the magnetic-dipole spin-own-orbit interactions, i.e. the orbiting of one electron around the other, in addition to their orbiting around the nucleus,

$$V_{\mathrm{nucso}} = +Z\alpha^2/2 \cdot ([\boldsymbol{s}_1 \cdot \boldsymbol{r}_1 \times \boldsymbol{p}_1]/r_1^3 + [\boldsymbol{s}_2 \cdot \boldsymbol{r}_2 \times \boldsymbol{p}_2]/r_2^3). \tag{1-65}$$

SOO1 refers to the electron's orbiting around the other electron,

$$\mathrm{SOO1} = 1/{r_{12}}^2[(\boldsymbol{s}_1 \cdot \boldsymbol{r}_{12} \times \boldsymbol{p}_1) + (\boldsymbol{s}_2 \cdot \boldsymbol{r}_{21} \times \boldsymbol{p}_2)]; \tag{1-66}$$

SOO2 is the magnetic dipole interaction of one electron's spin with the other electron's orbit,

$$\mathrm{SOO2} = 2/{r_{12}}^2[(\boldsymbol{s}_1 \cdot \boldsymbol{r}_{21} \times \boldsymbol{p}_2) + (\boldsymbol{s}_2 \cdot \boldsymbol{r}_{12} \times \boldsymbol{p}_1)]. \tag{1-67}$$

The two-electron terms $\sim -1 \cdot \alpha^2$ screen the electron-nuclear terms $\sim +Z \cdot \alpha^2$, corresponding to the difference between the nuclear Coulomb potential $-Z/r$ and the scf potential V_{scf}. Finally, there is the spin–spin interaction,

$$\mathrm{SS} = [8\pi/3(\boldsymbol{s}_1 \cdot \boldsymbol{s}_2)\delta(r_{12}) - (\boldsymbol{s}_1 \cdot \boldsymbol{s}_2)/{r_{12}}^2 - 3(\boldsymbol{s}_1 \cdot \boldsymbol{r}_{12})(\boldsymbol{s}_2 \cdot \boldsymbol{r}_{21})/r_{12}^4]. \tag{1-68}$$

The three terms in the brackets correspond to the classical expression for the interaction of two dipoles in the limit of point-dipoles. The relativistic contributions to the two-electron interactions contribute dominantly to the inner-shell correlation energy of heavy atoms [127].

1.3.9. Smaller Effects: Nuclear Size, QED and Weak Interaction

1.3.9.1. Extended Nuclei

Real nuclei are not point-like, but spherically or non-spherically extended. This has several consequences. The weak singularity of the relativistic Coulomb-point-charge wavefunction disappears; the wavefunctions behave Gaussian-like in the nuclear region. The inner orbital levels become somewhat de-stabilized what is relevant for the calculation of core-excited states (x-ray spectroscopy), in particular for heavy nuclei. The artifactual limitation of the Dirac–Coulomb point-charge model to $Z < 137$ disappears. Since relativistic wavefunctions are quite compact in the

neighborhood of the nuclei, finite-nucleus effects are much more pronounced in the relativistic regime as compared to the non-relativistic approximation (Figure 1-11).

Valence properties, which mainly depend on the outer valence density distribution (bond energies) or on the atomic outer density parts (polarizability, dispersion) are only weakly affected by the type and details of the nuclear charge distribution. However, electric or magnetic properties which probe the distribution of the electrons close to the nucleus are more sensitive.

Different models for the nuclear charge distribution [90] have been investigated. In atomic calculations using numerical grid techniques, all nuclear models are equally easy to apply. In molecular and basis set applications, the nuclear charge model should lead to a simple expression of the electrostatic potential, and the respective eigen-solutions should be well representable in the basis set. For instance, the sharp discontinuity of the density distribution at the surface of the 'uniformly charged sphere' model causes problems in the relativistic regime, where sharp boundaries are not admissible anyhow [91]. Also, simple exponential nuclear-charge models cause problems. The best compromise seems to be a Gaussian charge distribution, although the nuclear surface is too 'soft':

$$\rho_{\mathrm{nuc}}(r) = (\pi R_{\mathrm{nuc}}^2)^{-3/2}\, Z\, exp{-}(r/R_{\mathrm{nuc}})^2 \tag{1-69}$$

R_{nuc} is the nuclear radius in this model; a good rule of thumb is

$$R_{\mathrm{nuc}}/10^{-5}\text{Å} = 0.57 + 0.836\sqrt[3]{A}, \tag{1-70}$$

where A is the nuclear mass number.

The dominant energetic effect of a finite size nucleus (fsn) is the de-stabilization of the 1s level, strongly increasing with nuclear charge,

$$\Delta^{\mathrm{fsn}}E_{1\mathrm{s}} \approx 10^2 \text{ au } (\alpha Z)^7 \tag{1-71}$$

For Hg, for instance, the effect is about +2 au or +55 eV, which is large but only 2/3‰ of the total 1s binding energy. Specific effects weighing the nuclear region may be influenced more, such as hyperfine and Mössbaur splittings, electric field gradients, or quantum electrodynamical and parity non-conserving shifts. The non-sphericity of some nuclei (nuclear spin ≥ 1), which couples to $j \geq 3/2$ the Chapter by orbitals, may play a role in specific cases. For further details, see Andrae [90] and Chapter 12.

1.3.9.2. Vacuum Polarization

Quantum electrodynamics [24, 140, 141] plays a role not only in the interaction of two moving and spinning electrons, but also in the electron–nuclear interaction, even if the nucleus is treated as a stationary 'external' source of an electromagnetic potential [71]. The two lowest-order effects $\sim\alpha^3$ are the repulsive vacuum fluctuation and the somewhat smaller attractive vacuum polarization. The latter is related to the creation of virtual electron–positron pairs in the vicinity of the nucleus. The

respective vacuum polarization can be modeled by the Uehling potential, which is somewhat stronger decaying than $-\alpha/r$, in particular for r values larger than 0.1α.

1.3.9.3. Electronic Self-energy

The vacuum fluctuation or self-energy effect results from the zero-point oscillations of the quantized electromagnetic potential. No simple state-independent expression has been derived. The effect originates also in the neighborhood of the nuclei and has been semi-empirically modeled by a nuclear-peaked Gaussian fit-potential $\sim+\mathrm{B}(Z)\cdot\exp(-\beta(Z)\cdot r^2)$ [92]. Vacuum fluctuations overcompensate the vacuum polarizations; together with higher order terms they are called the Lamb shift. The Lamb shift is largest for the 1s level and deceases with increasing n,l,j. Hyperfine splittings and indirect nuclear spin-spin coupling constants of heavy atoms are modified in the percent range.

1.3.9.4. Parity Violation

The by far smallest effect so far considered in the quantum chemical literature is the parity-changing interaction between electrons and nuclei through the Z_0 bosons, interchanged between the quarks in the nuclei. At very high energies and short distances, the electric and the so-called weak interactions become similarly important. A reasonable approximation to the coupling operator at the 'low' energies near the nuclei is $\mathrm{G}\cdot Q\cdot\rho_{\mathrm{nuc}}(\boldsymbol{r})\cdot\gamma_5$, where G is the electro-weak coupling constant, Q the 'weak charge' of the nucleus, $\rho_{\mathrm{nuc}}(\boldsymbol{r})$ the nuclear density at electronic position $\boldsymbol{r}$, and γ_5 is a Dirac 4×4 matrix, that mixes the upper and lower components of the electronic 4-component wavefunction having opposite parities (see Eqs. 1-44, 1-46, and 1-47). The effects are of the order of 10^{-21} in hydrogen, but scale at least as Z^5. Small energy differences between otherwise degenerate α and β spin components or contributions to parity-forbidden optical transitions of atoms have been detected and calculated. Tiny energy differences of left and right-handed molecular isomers have been predicted [72]. There is the speculation that some statistical enhancement mechanism may explain the predominance of one of the two chiralities in carbohydrates and amino acids from the biosphere. On the other hand, if sufficiently complex molecular systems have the inherent tendency to become chiral, no additional exotic mechanism to generate chirality is needed [93, 94].

1.4. RELATIVISTIC CHANGES OF MOLECULES

The chemically most important parameters of molecules and crystals are the geometric equilibrium structure R_{e} from $(\partial E/\partial R)|_{Re}=0$, the rigidity of the structure, i.e. the force constants $k_{\mathrm{e}}=(\partial^2E/\partial R^2)|_{Re}$(or vibrational frequencies), and the bond energies defined through atomization energies $AE=E(R_{\mathrm{e}})$–$\mathrm{E}(\infty)$. E here means the total energy, and R_{e} internuclear lengths and angles. In addition, one needs reaction barrier energies, long range interaction forces, spin coupling constants for

non-relativistically 'spin-forbidden' processes, and spectroscopic constants (such as NMR chemical shifts and nuclear spin–spin coupling constants, Chapter 12) to support analytical investigations.

The practical chemist wants to know reliable data of (heavy atomic) compounds, i.e. one should determine the relativistic energy hypersurfaces $E(R)$ and other properties, see Chapters 2, 3, 8, 11, and 12. Various computational approaches to this aim are discussed in Chapters 4–7, 10. No serious problems occur in numerical grid calculations of the four-component Dirac equation 'other than computational expense', which however is prohibitive for molecules. Therefore, numerical approaches are only applied to atoms and at most to diatomic or small hydrogen containing molecules.

Most relativistic molecular investigations are performed within the approximation of the finite basis-set expansion. The solution of the four-component Dirac equation poses two specific problems [95]. First, the energy spectrum is not bounded from below. So there is no lower bound for variational calculations, and one must search for saddle points of the energy functional. This causes particular problems in the case, where one does not have a single equation, but a *set of coupled equations* as the Dirac equation. If the coupling of the upper and lower components of the Dirac wavefunction is not correctly reproduced [96–98], large errors can be introduced. This also happens, if the Schroedinger second order differential equation is replaced by two coupled first-order equations. Accordingly, the first computational efforts went quite astray, e.g. Malli and Oreg [136]. The problems are now under control by the use of so-called kinetically balanced basis sets [99]. Second, the *two-electron interaction* introduces the positron–electron continuum around every bound state. This problem, called continuum dissolution or Brown–Ravenhall disease, can be eliminated by 'no-pair' approaches. Defining electrons through positive-energy mean-field or natural orbitals, the pair-creation corrections are minimized [66]. Both problems do not show up in the common two-component approaches, such as the ZORA, the DKH method or the relativistic effective-core or pseudo-potential methods.

If one has already sufficient understanding of light atomic chemistry, one might like to make educated guesses of the relativistic corrections in the heavy atomic domain. Below we will outline some general relativistic trends. Both computationally and conceptually, one may distinguish between scalar and spinor approximations. In the scalar approaches one applies non-relativistic concepts and program structures, but using relativistic spin-averaged values from ab-initio or semi-empirical electron dynamics. In the spinor approaches the orbital functions $\varphi(\boldsymbol{r})$, which can in general be chosen as real, are to be replaced by complex and spin-dependent quaternion functions (in the two-component approaches): $(\varphi_1\alpha(\boldsymbol{r}), \mathrm{i}\cdot\varphi_2\alpha(\boldsymbol{r}), \varphi_3\beta(\boldsymbol{r}), \mathrm{i}\cdot\varphi_4\beta(\boldsymbol{r}))$, and by bi-quaternions or bi-spinors (in the Dirac four-component approaches), see Chapter 9.

In this final section, we also survey the mechanisms of relativistic molecular changes, mainly in the context of covalent bonding. (Relativistic modifications of strongly polar bonds had been discussed, e.g., by Schwerdtfeger et al. [100], or Schwarz [42].) In Section 1.4.1, we point out that the relativistic corrections for molecules consist of two contributions, the relativistic change at the non-relativistic

equilibrium structure, and the change related to the relativistic structure change. In Section 1.4.2 we elaborate on the fact that relativistic changes of molecular properties can be theoretically described by whole sets of different, though equivalent formulas that give rise to different, complementary physical explanations. In Section 1.4.3 we mention the large differences and the respective consequences of non-relativistic real spin-orbitals and relativistic complex spin-mixed and spin-split spinors. We conclude in Section 1.4.4 with a survey of the periodic system of elements, with the structure of the atomic shells and the changes due to non-relativistic and relativistic shell effects at the bottom of the periodic table. In this section we present some general qualitative and conceptual outlines, while the concrete details are unfolded in the subsequent chapters.

1.4.1. Always Two Different Relativistic Contributions

The chemically relevant molecular properties are differences or derivatives with respect to geometric parameters or electric or magnetic field strengths. We are interested in their relativistic corrections. In general, up to $Z \approx 70$, i.e. up to the lanthanoids, the lowest order relativistic correction is sufficient to qualitatively understand the physical mechanisms and their trends. For chemically reliable numbers, and even for the qualitative trends of higher Z values, one must live with the fact that only the full relativistic approach gives satisfactory results. The convergence in terms of α^2 is unsatisfactory for high Z values.

When we are interested in molecular equilibrium structures averaged over the vibrational ground state, represented by R_o, the harmonic approximation to the potential surface is usually insufficient because of the common anharmonicity of the potential curves. Therefore, in order to gain some understanding, we will approximate the energy function by a cubic expression in R, and (for simplicity) the relativistic correction by terms in α^2. We here discuss the general framework. Numerical examples of specific molecules are found in subsequent chapters.

Let ΔR be the deviation from the (vibrationless) non-relativistic equilibrium bond length (or bond angle) $R_e^{\text{n-rel}}$, let $k^{\text{n-rel}}$ be the non-relativistic force constant, and $a^{\text{n-rel}}$ the non-relativistic anharmonicity. The non-relativistic approximation to the energy function ('potential curve or hypersurface') is then given by

$$E^{\text{n-rel}}(\Delta R) \approx E_o^{\text{n-rel}} + k^{\text{n-rel}}/2 \cdot \Delta R^2 - a^{\text{n-rel}}/6 \cdot \Delta R^3. \tag{1-72}$$

The respective relativistic correction is

$$\Delta^{\text{rel}} E(\Delta R) \approx \Delta^{\text{rel}} E_o + (\partial \Delta^{\text{rel}} E/\partial R) \cdot \Delta R + \Delta^{\text{rel}} k/2 \cdot \Delta R^2 - \Delta^{\text{rel}} a/6 \cdot \Delta R^3. \tag{1-73}$$

1.4.1.1. Molecular Structures

An approximate relativistic correction to the *equilibrium-structure* is then

$$\Delta^{\text{rel}} R_e \approx -(\partial \Delta^{\text{rel}} E/\partial R)/k \cdot (1 - a \cdot (\partial \Delta^{\text{rel}} E/\partial R)/2k^2). \tag{1-74}$$

The leading term is the change of the relativistic energy correction $\Delta^{\text{rel}}E$ with the structure parameter R, divided by the force constant k. We call it the 'direct' contribution. Since the relative relativistic corrections of the force constants $\Delta^{\text{rel}}k/k$ are sometimes as large as $+10\gamma^2$, it is better to use the relativistic force constant than its non-relativistic approximation, even in semi-quantitative discussions. The same holds for the anharmonicity constant a. The anharmonicity term in the parentheses is sometimes qualitatively non-negligible, in particular in heavy atomic systems. This second term shall be called the 'structure' contribution. Each contribution has 'direct relativistic' and 'indirect relativistic' contributions (Section 1.3.5).

1.4.1.2. Bond Energies

The bond energy BE is the difference between molecular energies E at R_e and at infinity. Its relativistic change depends on the relation of the relativistic corrections of the bonded system *and* of the dissociation products. The latter may have different leading configurations in the dissociated state and in the bonded molecule. One may also refer to some common diabatic dissociation products, which may be different from their ground states, i.e. in heterolytic decompositions. The bond energy is not a 'local' property of the molecule.[12] In particular in heavy atomic molecules, there are two similarly important contributions. First, there is the difference of the relativistic energy corrections of the atoms and of the molecule at non-relativistic equilibrium $R_e^{\text{n-rel}}$, $\Delta^{\text{rel}}BE(R_e^{\text{n-rel}})$, the 'direct' energy difference. Second, there is the change of the molecular energy due to the difference of non-relativistic and relativistic equilibrium structures (the 'structure' contribution)

$$\Delta^{\text{rel}}BE_{\text{eq}} \approx \Delta^{\text{rel}}BE(R_e^{\text{n-rel}}) - (\partial\Delta^{\text{rel}}E/\partial R)^2/2k. \tag{1-75}$$

1.4.1.3. Force and Other Constants

The relativistic correction of the *force constant*, and of other molecular properties, are also made up of two contributions, the 'direct' one (∂P^{dir}) at non-relativistic equilibrium, and the 'structure' change ($\partial P^{\text{struct}}$), basically the change of the non-relativistic property upon the relativistic change of structure. Both terms are of same order α^2, i.e. they are of comparable importance even for light systems:

$$\Delta^{\text{rel}}k \approx \Delta^{\text{rel}}k(R_e^{\text{n-rel}}) + (\partial\Delta^{\text{rel}}E/\partial R)\cdot \text{a}/k. \tag{1-76}$$

In Table 1-2 we present results for H_2^+. For small $Z = 1$, the relativistic 'structure' contributions to bond energy and bond lengths are negligible, but to other properties (force constant, anharmonicity) they are appreciable, and here even dominant.

There are some chemical rules of thumb that for similar systems, the shorter the bond length, the larger (more negative) the bond energy, and the stronger the force

[12] This has sometimes been called the 'sausage phenomenon', reminding of the carnival song 'everything has an end, only the sausage (and the molecular potential curve) has two ends.

Table 1-2 Fractional relativistic property changes $\partial P = \Delta^{\text{rel}} P/\gamma^2 P = \partial P^{\text{dir}} + \partial P^{\text{struct}}$ of $H_2{}^+(Z = 1, \gamma = \alpha)$ for P = bond energy BE, bond length R_e, force constant $k = \partial^2 E/\partial R^2$, and unharmonicity $a = -\partial^3 E/\partial R^3$, using the DPT approach of Rutkowski et al. [103]

P	Value	∂P^{dir}	$\partial P^{\text{struct}}$	∂P
BE(eV)	−2.774	+0.132	+0.001	+0.133
R_e(Å)	1.057	−0.349	+0.000	−0.349
k(N cm^{-1})	1.592	−1.116	+1.768	+0.652
a (Ncm^{-2})	7.631	−0.752	+1.706	+0.954

constant (Gordy's and Badger's rules). However, these rules are sometimes violated when applied to relativistic corrections. Relativistic bond length contractions are rather frequent; nevertheless, the force constant is sometimes relativistically decreased. Relativistic bond energy stabilizations and destabilizations are rather 'statistically' distributed because of the 'sausage effect'. In the case of $H_2{}^+$, the 'direct' contributions to k and a are just opposite to the naive expectations, and only the overcompensation by the 'structure' contribution restores the simple rules in the present case [30,101–103]. For more examples from electromagnetic properties, see Chapter 12.

1.4.2. Multiple Perturbation Theory

The term $(\partial \Delta^{\text{rel}} E/\partial R)$ in the preceding equations is the simplest example of a higher order mixed term of multiple perturbation theory. It is of lowest order in relativity ($\sim\alpha^2$) and of lowest order in structure-change ($\sim\Delta R$). Such terms are generally represented by different 'gauge-dependent' expressions, which offer different complementary physical interpretations. For more details, see Schwarz et al. [104], Rutkowski and Schwarz [102], Rutkowski et al. [103], and Chapter 12.

We expand the relativistic Hamiltonian around the non-relativistic equilibrium structure in powers of α^2 and ΔR:

$$\hat{H} = \hat{H}^{00} + \alpha^2 \cdot \hat{H}^{10} + \Delta R \cdot \hat{H}^{01} + \alpha^2 \cdot \Delta R \cdot \hat{H}^{11} + \ldots \tag{1-77}$$

Subtleties of this expansion were discussed by Rutkowski et al. [103]. $\hat{H}^{10}$ contains the relativistic correction terms of DPT (e.g., Eq. 1-39), $\hat{H}^{11}$ consists of the respective $\partial/\partial R$ derivatives, and $\hat{H}^{01}$ is the $\partial/\partial R$ derivative of the non-relativistic Hamiltonian (i.e. the Hellmann–Feynman force). The mixed second order perturbation energy is

$$(\partial \Delta^{\text{rel}} E/\partial R) = \langle \Psi^{00} | \hat{H}^{11} | \Psi^{00} \rangle + 2\text{Re}\langle \Psi^{10} | \hat{H}^{01} | \Psi^{00} \rangle = \tag{1-78a}$$

$$= \langle \Psi^{00} | \hat{H}^{11} | \Psi^{00} \rangle + 2\text{Re}\langle \Psi^{01} | \hat{H}^{10} | \Psi^{00} \rangle = \text{etc.} \tag{1-78b}$$

Table 1-3 Relativistic bond length contraction of Au_2 (in Å)

Calculational approach	All electron ab initio	Valence electron RECP	Valence electron RPP
$\langle\Psi^{00}\vert\hat{H}^{11}\vert\Psi^{00}\rangle$	+0.0	−0.5	−0.4
$2\mathrm{Re}\langle\Psi^{10}\vert\hat{H}^{01}\vert\Psi^{00}\rangle$	−0.4	+0.1	+0.0
Sum	−0.4	−0.4	−0.4

There are two contributions to the mixed second order perturbation energy $\partial\Delta^{\mathrm{rel}}E/\partial R$. The first 'direct' contribution $\langle\Psi^{00}\vert\hat{H}^{11}\vert\Psi^{00}\rangle$ is due to the change of the Hamiltonian by the two 'perturbations', here relativity and structure-change. The second term can be expressed in many different forms according to the so-called interchange theorem. Only the sum, i.e. the value of $(\partial\Delta^{\mathrm{rel}}E/\partial R)$, is well-defined, the magnitudes of the different contributions depend of the chosen picture and calculational approach (four-component Dirac, direct Dirac perturbation theory DPT, two-component Douglas–Kroll–Heß DKH, or relativistic effective-core pseudo-potential RECP), see Table 1-3. In the Dirac four-component approach, $\hat{H}^{11} = \partial^2(-Z/|R-r|)/\partial R\partial\alpha^2 = 0$, in the RECP approach, $\hat{H}^{11} = \partial(\Delta^r\hat{V}_{recp})/\partial R \neq 0$, and in the DPT approach, too, $\hat{H}^{11} \neq 0$, namely $\hat{H}^{11} = \partial(\boldsymbol{\sigma}\,\boldsymbol{p}V_{\mathrm{nuc}}\boldsymbol{\sigma}\,\boldsymbol{p}/4)/\partial R$.

The first form of the second contribution in Eq. 1-78a, $2\mathrm{Re}\langle\Psi^{10}\vert\hat{H}^{01}\vert\Psi^{00}\rangle$, is the non-relativistic nuclear Hellmann–Feynman force acting on the relativistic change of the molecular electron density distribution,

$$\Delta^{\mathrm{rel}}\rho_{\mathrm{mol}} = \Delta^{\mathrm{rel}}\rho_{\mathrm{ats}} + \Delta^{\mathrm{rel}}\rho_{\mathrm{def}} \tag{1-79}$$

$\Delta^{\mathrm{rel}}\rho_{\mathrm{ats}}$ is the sum of the atomic relativistic density changes, and $\Delta^{\mathrm{rel}}\rho_{\mathrm{def}}$ is the relativistic change of the molecular bond deformation density. The conjecture that atomic valence orbital contraction would cause bond length contraction is obviously too simple-minded. Core orthogonalization, overlap interference, renormalization, polarization and deformation of the valence orbitals upon bond formation in the relativistic and non-relativistic regimes contribute in a complex manner to $\Delta^{\mathrm{rel}}\rho_{\mathrm{def}}$ [101, 105]. In particular, the Hellmann–Feynman force weighs different parts of space very differently, the main bond-force contributions being due to tiny density polarizations near the nuclei [106]. For more details see Rutkowski, Schwarz et al. [42, 101–104].

The second form of the second contribution in Eq. (1-78b) is $2\mathrm{Re}\langle\Psi^{01}\vert\hat{H}^{10}\vert\Psi^{00}\rangle$. It describes the relativistic energy contribution ($\hat{H}^{10}$) of the 'non-relativistic bond deformation density', i.e. of $(\Psi^{01*}\Psi^{00} + \Psi^{00*}\Psi^{01}) \sim \partial\rho_{\mathrm{mol}}(\boldsymbol{r})/\partial R$. Snijders and Pyykkö [107] have rationalized that the Pauli exclusion principle will, on the average, keep most overlapping density of atom A out of the core region of atom B, and vice versa, when bond A–B is formed. But the core orthogonality has the result

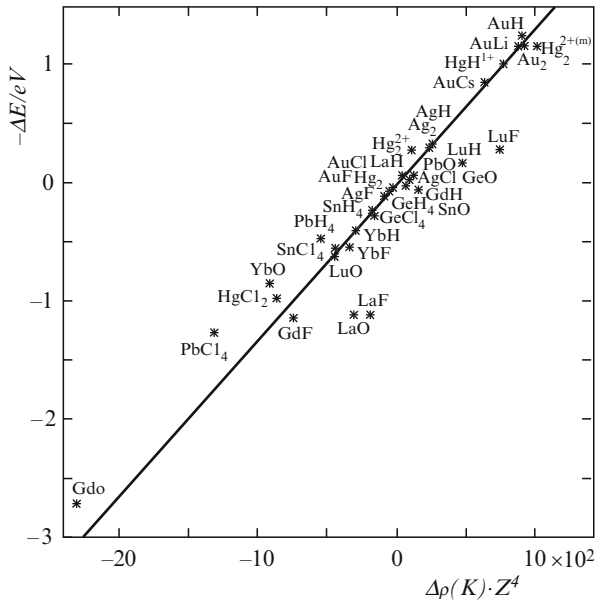

Figure 1-22. Relativistic bond energy corrections ΔE^{of} 35 s–p bonded molecules versus electron density pile up in the K shell upon bond formation, $\Delta\rho(K)$, multiplied by Z^4 (After Schwarz et al. [30])

that in small regions of space, e.g. near the nuclei, the density increases. These are just the regions where the relativistic Hamiltonian creates stabilizing energy contributions [106]. Accordingly, relativistic bond length contractions occur rather frequently, even for relativistically expanded valence shells, see Schwarz et al. [104]. In Figure 1-22 the relativistic bond energy correction $\Delta^{\text{rel}}BE_{\text{eq}}$ (here denoted by ΔE, negative value means relativistic stabilization) is plotted against the electron density pile up in the K shell upon bond formation, $\Delta\rho(K)$, multiplied by Z^4, the order of the relativistic corrections. The correlation line is $\Delta E = 0.9\alpha^2 \cdot \Delta\rho(K\text{i} \cdot Z^4$ [30, 108, 109].

1.4.3. Atomic Spinors and Molecular Quaternions

In stationary non-relativistic quantum chemistry, one may usually assume without restriction that the molecular spin-orbitals occur in pairs, $(\varphi\alpha(\boldsymbol{r}), 0)$ and $(0, \varphi\beta(\boldsymbol{r}))$, with a single real spatial part $\varphi(\boldsymbol{r})$, with arbitrary phase $+1$ or -1. In the relativistic regime, an even degeneracy follows from Kramers' time reversal symmetry for single (and odd-numbered) electronic states, see Chapter 9. In the two-component formalism, the molecular spinors occur in orthogonal quaternionic pairs $(\varphi_1\alpha(\boldsymbol{r}), \text{i} \cdot \varphi_2\alpha(\boldsymbol{r}), \varphi_3\beta(\boldsymbol{r}), \text{i} \cdot \varphi_4\beta(\boldsymbol{r}))$ and $(\varphi_3\alpha(\boldsymbol{r}), -\text{i} \cdot \varphi_4\alpha(\boldsymbol{r}), -\varphi_1\beta(\boldsymbol{r}), \text{i} \cdot \varphi_2\beta(\boldsymbol{r}))$, consisting of four different real space functions $\varphi_i(\boldsymbol{r})$. The one-electron density matrix is now in the general case complex, self-adjoint and spin-dependent. Of course, for

common closed shell molecules in field-free space, the 'one-matrix' is still spin-symmetric and real. Each spinor may carry an arbitrary phase factor $e^{-i\eta}$, and in the case of closed shell states, the Kramers pair may be unitarily mixed. One may choose the free mixing factors to generate spinors with minimal spin-mixture and minimal imaginary contribution to look most similar to the common nonrelativistic orbitals. Anyhow, the molecular spinors carry in general some $\boldsymbol{r}$-dependent complex spin admixture, corresponding to an $\boldsymbol{r}$-dependent variation of spin direction. Accordingly, one can no longer choose a universal axis for the spin in spin-density functional theory (the so-called collinear spin approximation), which has been noted by Autschbach and Ziegler [110] and van Wüllen [111].

The forms of $s^3/_2$, $p^1/_2$ and $p^3/_2$ type atomic spinors were given in Eqs. (1-44), (1-47) and (1-46), respectively. The largest difference in complex, angular and spin-appearance between non-relativistic atomic orbitals and relativistic spinors occurs for the $p^1/_2$ ones. The latter have a spherical electron density (Figure 1-3a). To first order, the valence-$p^1/_2$ spinors are doubly occupied in Pb and Eka-Pb ($_{114}$Uuq); they form, because of relativistic energy stabilization, a quasi-closed shell. The valence-$s^1/_2$ spinors of Hg, Eka-Hg ($_{112}$Uub) and subsequent elements also form relativistically stabilized shells. This enhances the so-called inert pair effect of the heaviest main-group elements, which have a particular tendency to form compounds of valence and oxidation numbers of 2 or 4 below their group numbers (Hg^0, Tl^I, Pb^{II}, Bi^{III}, $Po^{II,IV}$).

Since $p^1/_2$ spinors are a complex $\alpha - \beta$-spin mixture of p_x, p_y, p_z, $(p_x\beta + i \cdot p_y\beta + p_z\alpha)$ and $(-p_x\alpha + i \cdot p_y\alpha + p_z\beta)$, s-p hybridization and the formation of p–p–σ bond orbitals is severly hampered, see Pitzer [137, 138], Grant and Pyper [112], Pyper [77], and Hafner et al. [78]. The constructive interference of partially occupied non-relativistic p_x, p_y and p_z orbitals gives rise to one σ and two π bonds. Two $p^1/_2$ spinors with strong spin-orbit coupling (dominating over the molecular field) can even yield either a $1/3\sigma$–$2/3\pi^*$ or a $2/3\pi$–$1/3\sigma^*$ interaction, with reduced bonding or antibonding power. Pairs of $p^3/_2$ spinors on two overlapping atoms with dominating spin-orbit coupling yield one π and one $2/3\pi$–$1/3\sigma^*$ interaction. Therefore, the bond energies and bond lengths of heavy p-block elements are significantly influenced by spin-orbit coupling, i.e. they are usually expanded, with softened vibrations and reduced bond energies (Figure 1-23).

Although the bond-angle force constants are usually smaller than the bond-stretching force constants, only few remarkable spin-orbit triggered bond-angle changes are known. It has been shown by Schwarz et al. [113] that in the case of only one heavy (Hv) and two light (Lt) atoms, the spin-orbit effects on the bond angle of Lt-Hv-Lt are partially compensated, so that only a small overall effect is left over. On the other hand, van Wüllen and Langermann [114] have shown more recently that large bond-angle changes occur when the spin-orbit couplings of three heavy atoms Hv, Hw, Hu contribute to the Hv-Hw-Hu angle. See also Kaupp and v. R. Schleyer [115].

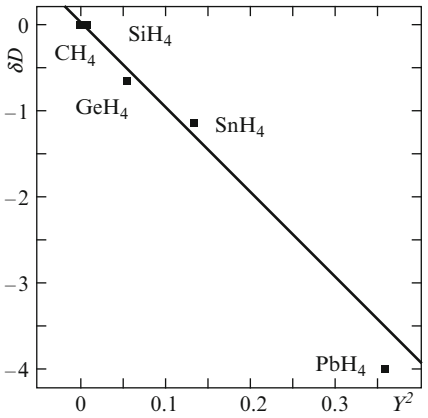

Figure 1-23. Relativistic weakening of the bond energy BE of group-14 tetrahydrides, $\delta D = \Delta^{\mathrm{rel}} BE_{\mathrm{eq}}/BE$ versus γ^2 (After Schwarz et al. [30])

1.4.4. The Periodic System of Elements and Its Natural End

1.4.4.1. Classical Considerations, Periodicity

Through elementary ordering principles, the unlimited number of static and reactive properties of stuffs is reduced to few millions of pure substances and finally to about a hundred different elements. The invention and systematic arrangement of the elements as the conservation principles of chemistry culminated in the construction of the periodic table about 140 years ago. The comprehensive physical explanation and understanding of the periodic system developed in rather slow steps until recent years [17, 84, 116, 139]. The identity of the chemical elements resides in the nuclear charges, while the chemical characteristics are determined by the energetic and spatial parameters of the electronic shells of bonded atoms. Several points are relevant, which are often insufficiently appreciated in discussions of general chemistry. We first mention these points and then point out, where relativity plays a role.

Both the outer core orbitals and the occupied and virtual valence orbitals play a role. Pyykkö [117] had coined the term 'primogenic' for the lowest orbital of a given angular momentum (Section 1.3.5). A primogenic valence orbital does not endure the Pauli repulsion by occupied core orbitals of same angular momentum. 2p is comparatively contracted, i.e. of similar size than the 2s, and it undergoes stronger 2s–2p hybridization than ns-np for $n > 2$ of the heavier main group elements [85]. 3d is also comparatively contracted and less apt to covalent overlap binding than the nd shells for $n > 3$ of the heavier transition metals. Similarly, 4f is particularly deep in the atomic core and acts as an ionic spectator orbital, mainly expanding the 5sp core shell if more occupied, while 5f participates significantly more in the early actinoids. The same is to be expected for the 5g, which would become occupied in the yet non-existing eighth row of the periodic table.

While s and p orbitals smoothly contract for increasing Z in the series of neutral or weakly charged atoms, the higher angular momentum d and f orbitals at first

remain outside the atomic core. They feel only a strongly shielded nuclear charge; they are weakly bounded and of spatially extended Rydberg type; they hardly contribute to chemical bonding. For instance, 3d plays little role in the chemistry of P through K. However, at some critical Z value, the orbital 'collapses' into the core and is then much more energetically bound[13] and spatially compact. This happens for the $(n–1)$d orbitals in row n of the periodic table around group 3 [118, 119]. For the alkali metals, $n\mathrm{s} < np < (n–1)\mathrm{d}$, energetically and spatially. For the heavier alkaline earth metals,[14] $n\mathrm{s} < (n–1)\mathrm{d} < n\mathrm{p}$. The actually 'standard' valence-orbital energy sequence $(n–1)\mathrm{d} < n\mathrm{s} < n\mathrm{p}$ is realized for *all* other heavier elements. The $(n–2)$f orbital collapse occurs in row n around groups 4–5, and the $(n–3)$g orbital collapse around groups 6–7 [1, 116].

IR–Vis–UV spectroscopy of unbound atoms in vacuum detects low energy states that may be spatially rather extended. The atomic Rydberg orbitals, such as 3d in potassium or 4s in the light transition atoms have diameters of $3^1/_2$ to 4 Å. Upon inserting an atom with an occupied Rydberg orbital into a molecule or condensed phase, the diffuse Rydberg orbital overlaps with many doubly occupied orbitals of adjacent atoms and becomes destabilized and depopulated [120]. Rydberg orbitals are unimportant in qualitative quantum chemistry. The leading electron configuration of chemically bonded atoms often differs from the configuration, from which the atomic ground state derives. For example, for bonded carbon, the chemically dominant configuration is usually $1\mathrm{s}^2 2\mathrm{s}^1 2\mathrm{p}^3$, in contrast to the parent configuration $1\mathrm{s}^2 2\mathrm{s}^2 2\mathrm{p}^2$ of the unperturbed atomic ground state $^3\mathrm{P}^\mathrm{e}_\mathrm{o}$. The chemically dominant configurations of the transition metals of groups $G = 3$ through 10 are $(n-1)\mathrm{d}^G n\mathrm{s}^0$, throughout, usually differing from the parent configurations $(n-1)\mathrm{d}^{G-k} n\mathrm{s}^k$, $\mathrm{k} = 1$ or 2, of the free-atomic ground states.

Periodicity is impressed on the Z-ordered array of elements by the appearance of closed shells that are both energetically stable *and* separated by a large gap from the next higher orbital level.[15] These are the noble gasses with $1\mathrm{s}^2$ or $n\mathrm{p}^6$ shells ($n = 2 - 5$ or 6). Nuclear shielding modifies the hydrogenic energy-sequence only slightly for the *inner core* shells:

$$1\mathrm{s} \ll 2s < 2\mathrm{p}^1/_2 < 2\mathrm{p}^3/_2 \ll 3\mathrm{s} < 3\mathrm{p}^1/_2 < 3\mathrm{p}^3/_2 < 3\mathrm{d}^3/_2 < 3\mathrm{d}^5/_2 \ll 4\mathrm{s} \text{ etc.} \tag{1-80}$$

where $<$ means a little higher, and $\ll$ significantly higher. The outer *valence shells* with low angular momenta are much more strongly perturbed by nuclear shielding:

$$n\mathrm{s} < n\mathrm{p} \ll n\mathrm{d} \lll n\mathrm{f} \cdots \ll \text{hydrogen-like high-}l\text{ states} \tag{1-81}$$

---

[13] We here define the orbital energy of a many-electron open-shell atom as the difference of the *configuration average energies* of the neutral and the ionized species.

[14] These few elements are the only ones, where the ubiquitous so-called $(n + l, n)$ text book rule holds!

[15] A (separated) shell is stable, because its energy is low and therefore filled up. Chemists sometimes apply the inverted pseudo-logics: A shell becomes stable by filling it up.

For most heavy, bonded atoms (except the first ones in a period), the energetic sequence in the *valence shell* is therefore different from the $(n + l, n)$-rule taught in chemistry textbooks:

$$(n-1)\mathrm{p}_{3/2} \ll (n-2)\mathrm{f}_{5/2,7/2} < (n-1)\mathrm{d}_{3/2,5/2} < n\mathrm{s} < n\mathrm{p}_{1/2} < n\mathrm{p}_{3/2} \ll \quad (1\text{-}82)$$

Orbital energy gaps develop above the 1s and 2p, 3p, etc. frontier orbital levels. Atoms with $1s^2$, $2p^6$, $3p^6$, etc. shells form the noble gasses. The preceding elements with np vacancies are strongly electronegative; the subsequent elements with weakly bound ns electrons are strongly electropositive. The strong variation of elemental properties from groups 16 (chalcogenides) to 17 (halogenides) to 18–0 (noble gases) to 1 (alkali metals) to 2 (alkaline earth metals) fixes the period lengths. The closed ns^2 shells of the metals of groups 2 and 12 are not inert because of the nearby $(n-1)$d and np shells. The closed $(n-1)d^{10}$ shells of the metals of group 10 are not inert because of nearby ns.

1.4.4.2. Relativistic Aspects

The chemical properties of the elements are qualitatively explainable by the energies and radii of the atomic orbitals. The physical explanation of chemistry then consists of two steps. Most simply, one takes the orbital parameters as empirically given, and rationalizes the vast amount of chemical trends. More deeply, one can derive the orbital parameters from first principles. The upper half of the periodic table contains most of the important elements and for them, non-relativistic quantum mechanics with spin is sufficient. The results, however, cannot be extrapolated into the region of the heavier elements. Non-relativistic quantum chemistry is qualitatively correct up to the third or fourth row. The lowest order relativistic corrections $\sim(\alpha Z)^2 = \gamma^2$ work well up to the lanthanoids. Because of the strongly nonlinear dependence of the atomic orbital parameters for higher Z values, extrapolation of the empirical data will not lead to reliable predictions in the seventh, not to speak of the eighth row. Trend changes in the sixth row had already been mentioned in the introduction. At least from this row onwards, where the relativistic effects become larger than a few percent, the different non-relativistic (electron correlation and solvent effects) and relativistic corrections can no longer be separated in a linear, additive, first order perturbation-theoretic manner, since cross terms contribute significantly.

Non-relativistic as well as relativistic aspects modify the structure of the periodic system from row 6 onwards. An important point is the fundamental gap between the $(n-1)$p and $(n-2)$f, $(n-1)$d, ns, np levels. Relativistic scalar and spin-orbit effects raise the $(n-2)$f and $(n-1)$d levels, lower the $ns_{1/2}$ and $np_{1/2}$ levels, reduce the $(n-1)p_{3/2} - ns$ gap, and split the $(n-2)$f, $(n-1)$d, and np levels. Together with the non-relativistically decreasing orbital-energy gaps for increasing row number or main quantum number n, the exceptional inertness of the p^6 configuration gets lost for the heaviest noble gasses. In addition, the atomic shell structure (visible in plots of the radial electron density $r^2 \cdot \rho(r)$ or the density Laplacian $\Delta\rho(r)$ for shells 1 through 4) becomes washed out.

From bismuth ($_{83}$Bi) onwards, the lifetimes of the nuclei are finite for all isotopes and decrease irregularly for increasing Z values (at a very rough average, by factors of $^1/_3$–$^1/_4$ from Z to Z+ 1). If the lifetime of the most stable isotope is less than a year (for $_{85}$At, $_{86}$Rn, $_{87}$Fr, and from $_{100}$Fm onwards), the radiation damage will quickly damage solid compounds. Experimental tracer investigations are complemented by theoretical predictions (Chapter 11). For elements Eka-Tl ($_{113}$Uut) and Eka-Pb ($_{114}$Uuq) the lifetimes reach the 1s-range; these and the heavier elements seem unamenable to traditional chemical investigation. Single fleeting molecules of elements with lifetimes in the ms to μs range such as Eka-Rn ($_{118}$Uuo) and the following ones will be even hard to investigate spectroscopically. Ordinary chemistry seems to end with the seventh period, first because of the short nuclear lifetime and second because of the nearly continuous bands of severely spin-orbit coupled atomic valence spinors. The construction of periodic tables by naive extrapolation into the region of three- or even four-digit Z values appears senseless.

ACKNOWLEDGMENTS

WHES thanks Professors J. Autschbach (Buffalo) and M. Reiher (Zürich) for improving comments. He expresses his gratitude to Professor Jun Li (Beijing) for financial support and generous hospitality and to B.Sc. Chen Guo (Beijing) for significant technical help.

REFERENCES

1. Fricke, B.: Struct. Bond. **21**, 89–144 (1975)
2. Pyykkö, P.: Adv. Quant. Chem. **11**, 353–409 (1978)
3. Pyykkö, P.: Chem. Rev. **88**, 563–594 (1988)
4. Pyykkö, P., Desclaux, J.P.: Acc. Chem. Res. **12**, 276–281 (1979)
5. Balasubramanian, K., Pitzer, K.S.: Adv. Chem. Phys. **67**, 287–319 (1987)
6. Schwerdtfeger, P. (ed.): Relativistic Electronic Structure Theory, Part 1, Fundamentals. Elsevier, Amsterdam (2002)
7. Schwerdtfeger, P. (ed.): Relativistic Electronic Structure Theory, Part 2, Applications. Elsevier, Amsterdam (2004)
8. Heß, B.A. (ed.): Relativistic Effects in Heavy-Element Chemistry and Physics. Wiley, Chichester, GB (2003)
9. Dyall, K.G., Fægri, K.: Introduction to Relativistic Quantum Chemistry. Oxford University Press, Oxford, GB (2007)
10. Reiher, M., Wolf, A.: Relativistic Quantum Chemistry. Wiley-VCH, Weinheim (2009)
11. Pyykkö, P.: Relativistic Theory of Atoms and Molecules, 3 vols. Springer, Berlin (1986–1993–2000)
12. Pyykkö, P.: DATABASE 'RTAM', Version 14.1; http://rtam.csc.fi/ (2009)
13. Dirac, P.A.M.: Proc. Roy. Soc. Lond. A **117**, 610–624 (1928)
14. Hellmann, H.: Einführung in die Quantenchemie. Deuticke, Leipzig and Wien (1937); Gel'man G Kvantovaya Khimiya. ONTI, Moscow/Leningrad (1937)
15. Hellmann, H. alias Gel'man, G.: Front Nauki Tekh. (Russian) **6**, 34–48; **7**, 39–50 (1936)

16. Glashow, S.L.: Interactions: A Journey Through the Mind of a Particle Physicist and the Matter of This World. Warner Books, New York (1988)
17. Wang, S.G., Schwarz, W.H.E.: Angew. Chem. **121**, 3456–3467 (2009); Angew. Chem. Int. Ed. **48**, 3404–3415
18. Dolg, M., van Wüllen, C. (eds.): Chem. Phys. **311**, issue 1–2 (2005)
19. Rocke, A.J.: Chemical Atomism in the Nineteenth Century. Ohio State University Press, Columbus, OH (1984)
20. Simonyi, K.: Kulturgeschichte der Physik. Urania-Verlag, Leipzig (1990)
21. Hocking, T.D., Carson, C.: The History of Modern Physics. University of California, Berkeley, CA (2005)
22. Sexl, R., Urbantke, H.K.: Relativity, Groups, Particles. Springer, Vienna (2001)
23. Greiner, W., Reinhardt, J.: Theoretische Physk, vol.7. Quantenelektrodynamik. Harry Deutsch, Thun (1984)
24. Greiner, W., Reinhardt, J., Müller, B.: Theoretical physics, vol.4. Quantum Electrodynamics. Springer, Berlin (1992)
25. Cook, D.B.: Handbook of Computational Quantum Chemistry. Oxford University Press, Oxford, GB (1998)
26. Young, D.C.: Computational Chemistry. Wiley, New York (2002)
27. Lewars, E.: Computational Chemistry. Kluwer, Dordrecht (2004)
28. Helgaker, T., Klopper, W., Tew, D.P.: Mol. Phys. **106**, 2107–2143 (2008)
29. Giulini, D., Joos, E., Kiefer, C., Kupsch, J., Stamatescu, I.O., Zeh, H.D.: Decoherence and the Appearance of a Classical World in Quantum Theory. Springer, Heidelberg (2002)
30. Schwarz, W.H.E., Rutkowski, A., Wang, S.G.: Int. J. Quant. Chem. **57**, 641–653 (1996)
31. Mackintosh, A.R.: Bull. Am. Phys. Soc. **11**, 215 (1966)
32. Onodera, Y., Okazaki, M.: J. Phys. Soc. Jpn **21**, 1273–1281 (1966)
33. Loucks, T.L.: Augmented Plane Wave Method. Benjamin, New York (1967)
34. Williams, A.O.: Phys. Rev. **58**, 723–726 (1940)
35. Mayers, D.F.: Proc. Roy. Soc. Lond. A **241**, 93–109 (1957)
36. Herman, F., Skillman, S.: Atomic Structure Calculations. Prentice-Hall, Englewood Cliffs, NJ (1963)
37. Fricke, B., Waber, J.T.: Actin. Rev. **1**, 433 (1971)
38. Fricke, B., Greiner, W., Waber, J.T.: Theor. Chim. Acta **21**, 235–260 (1971)
39. Desclaux, J.P.: At. Data Nucl. Data Tabs. **12**, 311406 (1973)
40. Rosén, A., Ellis, D.E.: Chem. Phys. Lett. **27**, 595–599 (1974)
41. Desclaux, J.P., Pyykkö, P.: Chem. Phys. Lett. **29**, 534–539 (1974)
42. Schwarz, W.H.E.: In Z.B. Maksić (ed.) The Concept of the Chemical Bond, pp. 593–643. Springer, Berlin (1990)
43. Liao, M.S., Schwarz, W.H.E.: Acta Cryst. B **50**, 9–12 (1994)
44. Pyykkö, P., Atsumi, M.: Chem Eur J **15**, 186–197 (2009)
45. Feynman, R.P., Leighton, R.B., Sands, M.: The Feynman Lectures on Physics, vol 2. Addison-Wesley, Reading, MA (1964 seq.)
46. Kragh, H.: Am. J. Phys. **52**, 1024–1033 (1984)
47. Greiner, W.: Theoretical physics, vol. 3. Relativistic Quantum Mechanics. Springer, Berlin (1990); Greiner, W.: Theoretische Physik, vol. 6: Relativistische Quantenmechanik. Harry Deutsch, Thun (1990)
48. Kissel-Phillip, M., Schwarz, W.H.E.: Phys. Rev. A **38**, 6027–6033 (1988)
49. Döring, W.: Atomphysik und Quantenmechanik, vol.3. Anwendungen. Walter de Gruyter, Berlin (1979)
50. Levy-Leblond, J.M.: Commun. Math. Phys. **6**, 286–311 (1967)

51. Hurley, W.J.: Phys. Rev. D **3**, 2339–2347; **4**, 3605–3616 (1971)
52. Reiher, M., Wolf, A.: J. Chem. Phys. **121**, 2037–2047, 10945–10956 (2004)
53. Sadlej, A.J.: Struct. Chem. **18**, 757–767 (2007)
54. Pauli, W.: Z. Physik. **43**, 601–623 (1927)
55. Berestetskii, V.B., Lifshitz, E.M., Pitayevskii, L.P.: Relativistic quantum theory. In: L.D. Landau, E.M. Lifshitz (eds.) Course of Theoretical Physics, vol 4a. Permagon, New York (1971 seq.)
56. Mastalerz, R., Lindh, R., Reiher, M.: Chem. Phys. Lett. **465**, 157–164 (2008)
57. Newton, T.D., Wigner, E.P.: Rev. Mod. Phys. **21**, 400–406 (1949)
58. Baerends, E.J., Schwarz, W.H.E., Schwerdtfeger, P., Snijders, J.G.: J Phys B 23, 3225–3240 (1990)
59. Autschbach, J., Schwarz, W.H.E.: Theor. Chem. Acc. **104**, 82–88 (2000)
60. Schwarz, W.H.E.: Theor. Chim. Acta **23**, 147–154 (1971)
61. Hafner, P., Schwarz, W.H.E.: Chem. Phys. Lett. **65**, 537–541 (1979)
62. Rutkowski, A.: J. Phys. B **19**, 149–158, 3431–3441, 3443–3455 (1986)
63. Kutzelnigg, W.: In: Schwerdtfeger (ed.) Relativistic Electronic Structure Theory, Part 2, Applications, pp. 664–757. Elsevier, Amsterdam (2004)
64. Condon, E.U., Shortley, G.H.: The Theory of Atomic Spectra. University Press, Cambridge, GB (1935)
65. Franke, R., Kutzlnigg, W.: Chem. Phys. Lett. **199**, 561–566 (1992)
66. Mittleman, M.H.: Phys. Rev. A **24**, 1167–1175 (1981)
67. Sucher, J.: Phys. Rev. A **22**, 348–362 (1980)
68. Sucher, J.: Phys. Scripta. **36**, 271–281 (1987)
69. Esteban, M.J., Lewin, M., Séré: Bull. Am. Math. Soc. **45**, 535–593 (2008)
70. Itzykson, C., Zuber, J.B.: Quantum Field Theory. McGraw-Hill, New York (1980 et seq.)
71. Sapirstein, J.: In: Schwerdtfeger, P. (ed.): Relativistic Electronic Structure Theory, Part 1, Fundamentals, pp. 468–522. Elsevier, Amsterdam (2002)
72. Berger, R.: In: Schwerdtfeger (ed.) Relativistic Electronic Structure Theory, Part 2, Applications, pp. 188–288. Elsevier, Amsterdam (2004)
73. Gordon, W.: Z. Physik. **48**, 11–14 (1928)
74. Bethe, H.A., Salpeter, E.E.: Quantum Mechanics of One- and Two-Electron Atoms. Springer, Berlin (1957)
75. Molzberger, K., Schwarz, W.H.E.: Theor. Chim. Acta **94**, 213–222 (1996)
76. Burke, V.M., Grant, I.P.: Proc. Phys. Soc. Lond. **90**, 297–314 (1967)
77. Pyper, N.C.: Chem. Phys. Lett. **73**, 385–392; **74**, 554–561 (1980)
78. Hafner, P., Habitz, P., Ishikawa, Y., Wechsel-Trakowski, E., Schwarz, W.H.E.: Chem. Phys. Lett. **80**, 311–315 (1981)
79. Andrae, D.: J. Phys. B **30**, 4435–4451 (1997)
80. Desclaux, J.P.: In: Schwerdtfeger (ed.) Relativistic Electronic Structure Theory, Part 2, Applications, pp. 1–22. Elsevier, Amsterdam (2004)
81. Rutkowski, A., Schwarz, W.H.E., Koslowski, R.: Theor. Chim. Acta **87**, 75–87 (1993)
82. Bitter, T., Ruedenberg, K., Schwarz, W.H.E.: J. Comp. Chem. **28**, 411–422 (2007)
83. Ruedenberg, K., Schmidt, M.W.: J. Phys. Chem. A **113**, 1954–1968 (2009)
84. Pyykkö, P.: Int. J. Quant. Chem. **85**, 18–21 (2001)
85. Kutzelnigg, W.: Angew. Chem. **96**, 262–286 (1984); Angew. Chem. Int. Ed **23**, 272–295
86. Schwarz, W.H.E.: Theor. Chim. Acta **15**, 235–243 (1969)
87. Rose, S.J., Grant, I.P., Pyper, N.C.: J Phys B **11**, 1171–1176 (1978)
88. Hafner, P., Schwarz, W.H.E.: J. Phys. B **11**, 217–233, 2975–2999 (1978)
89. Autschbach, J., Siekierski, S., Seth, M., Schwerdtfeger, P., Schwarz, W.H.E.: J. Comp. Chem. **23**, 804–813 (2002)
90. Andrae, D.: Phys. Rep. **336**, 413–525 (2000)

91. Ishikawa, Y., Koc, K., Schwarz, W.H.E.: Chem. Phys. **225**, 239–246 (1997)
92. Pyykkö, P., Zhao, L.B.: J. Phys. B **36**, 1469–1478 (2003)
93. Siegel, J.S.: Chirality **10**, 24–27 (1998)
94. Avetisov, V., Goldanski, V.: Proc. Natl. Acad. Sci. USA **93**, 11435–11442 (1996)
95. Schwarz, W.H.E., Wechsel-Trakowski, E.: Chem. Phys. Lett. **85**, 94–97 (1982)
96. Rosicky, F., Mark, F.: Theor. Chim. Acta **54**, 35–51 (1979)
97. Mark, F., Schwarz, W.H.E.: Phys. Rev. Lett. **48**, 673–676 (1982)
98. Schwarz, W.H.E., Wallmeier, H.: Mol. Phys. **46**, 1045–1061 (1982)
99. Grant, I.P.: Phys. Rev. A **25**, 1230–1232 (1982)
100. Schwerdtfeger, P., Dolg, M., Schwarz, W.H.E., Bowmaker, G.A., Boyd, P.D.W.: J. Chem. Phys. **91**, 1762–1774 (1989)
101. Schwarz, W.H.E.: Phys. Scripta. **36**, 403–411 (1987)
102. Rutkowski, A., Schwarz, W.H.E.: Theor. Chim. Acta **76**, 391–410 (1990)
103. Rutkowski, A., Rutkowska, D., Schwarz, W.H.E.: Theor. Chim. Acta **84**, 105–114 (1992)
104. Schwarz, W.H.E., Chu, S.Y., Mark, F.: Mol. Phys. **50**, 603–623 (1983)
105. van Weezenbeck, E.M., Baerends, E.J., Snijders, J.G.: Theor. Chim. Acta **81**, 139–155 (1991)
106. Autschbach, J., Schwarz, W.H.E.: J. Phys. Chem. A **B**, 6039–6046 (2000)
107. Snijders, J.G., Pyykkö, P.: Chem. Phys. Lett. **75**, 5–8 (1980)
108. Wang, S.G., Schwarz, W.H.E.: J. Mol. Struct. (THEOCHEM) **338**, 347–362 (1995)
109. Wang, S.G., Liu, W.J., Schwarz, W.H.E.: J. Phys. Chem. **106**, 795–803 (2002)
110. Autschbach, J., Ziegler, T.: J. Chem. Phys. **113**, 9410–9418 (2000)
111. van Wüllen, C.: J. Comp. Chem. **23**, 779–785 (2002)
112. Grant, I.P., Pyper, N.C.: Nature **265**, 715–717 (1977)
113. Schwarz, W.H.E., Rutkowski, A., Collignon, G.: In: S. Wilson, I.P. Grant, B.L. Gyorffy (eds.) The Effects of Relativity on Atoms, Molecules, and the Solid State, pp. 135–148. Plenum, New York (1991)
114. van Wüllen, C., Langermann, N.: J. Chem. Phys. **126**, 114106 (2007)
115. Kaupp, M., Schleyer, P.v.R.: J. Am. Chem. Soc. **115**, 1061–1073 (1993)
116. Schwarz, W.H.E., Wang, S.G.: Int. J. Quant. Chem. online since Sept. 22 (2009)
117. Pyykkö, P.: Phys. Scripta **20**, 647–651 (1979)
118. Connerade, J.P.: Contemp. Phys. **19**, 415–448 (1978)
119. Connerade, J.P.: J. Phys. B **24**, L109–L115 (1991)
120. Wang, S.G., Qiu, Y.X., Fang, H., Schwarz, W.H.E.: Chem. Eur. J. **12**, 4101–4114 (2006)
121. Cohen-Tannoudji, C., Diu, B., Laloé, F.: Quantum Mechanics. Wiley, New York (1977)
122. Fleck, L.: Entstehung und Entwicklung einer wissenschaftlichen Tatsache. Schwabe, Basel (1935); The Genesis and Development of a Scientific Fact. University of Chicago Press, Chicago, IL (1979)
123. Gordon, W.: Z. Physik. **40**, 117–133 (1926)
124. Hardekopf, G., Sucher, J.: Phys. Rev. A **30**, 703–711 (1984)
125. Hardekopf, G., Sucher, J.: Phys. Rev. A **31**, 2020–2029 (1985)
126. Jackson, J.D.: Classical Electrodynamics. Wiley, New York (1962 et seq.)
127. Karwowski, J., Styszynski, J., Schwarz, W.H.E.: J. Phys. B **25**, 2763–2764 (1992); J Phys B **24**, 4877–4886 (1991)
128. Klein, O.: Z. Physik. **41**, 407–442 (1927)
129. Lichtenberg, G.C.: Sudelbuch No. 860, in (2000) The Waste Books. New York Review of Books, New York (1793)
130. Schwarz, W.H.E., van Wezenbeek, E.M., Baerends, E.J., Snijders, J.G.: J. Phys. B **22**, 1515–1530 (1989)

131. Schwarz, W.H.E., Andrae, D., Arnold, S.R., Heidberg, J., Hellmann, H., Hinze, J., Karachalios, A., Kovner, M.A., Schmidt, P.C., Zülicke, L.: Bunsenmagazin **1**, 10–21, 60–70 (1999); http://www.tc.chemie.uni-siegen.de/hellmann/hh-engl_with_figs.pdf
132. Swirles, B.: Proc. R. Soc. Lond. A **152**, 625–649 (1935)
133. Einstein, A.: Ann. Physik **17**, xx–yy, zz–vv (1905)
134. Dirac, P.A.M.: Proc. Roy. Soc. Lond. A **123**, 714–733 (1929)
135. Mattheiss, L.F.: Phys. Rev. **151**, 450–464 (1966)
136. Malli, G., Oreg, J.: Chem. Phys. Lett. **69**, 313–314 (1980)
137. Pitzer, K.S.: J. Chem. Phys. **63**, 1032–1033 (1975)
138. Pitzer, K.S.: Acc. Chem. Res. **12**, 272–276 (1979)
139. Schwarz, W.H.E., Rich, R.L.: J. Chem. Educ. **87**, in press (2010)
140. Salam, A.: Int. Rev. Phys. Chem. **27**, 405–448 (2008)
141. Cohen-Tannoudji, C., Dupont-Roc, J., Grynberg, G.: Photons and Atoms. Introduction to Quantum Electrodynamics. Wiley, New York (1989)

CHAPTER 2

RELATIVISTIC EFFECTS AND THE CHEMISTRY OF THE HEAVIER MAIN GROUP ELEMENTS

JOHN S. THAYER

Department of Chemistry, University of Cincinnati, Cincinnati, OH 45221-0172
e-mail: thayerj@email.uc.edu

Abstract: This chapter reviews possible experimental aspects of relativistic effects in heavier Main Group elements and their compounds. Attention is focused on the sixth, seventh and eighth Period elements, for which the relativistic contribution to their physical and chemical properties is significant. Superheavy elements through Z = 120 are also discussed. This review may increase interest of theoreticians in chemistry-oriented problems that require use of relativistic methods of quantum chemistry.

Keywords: Relativistic effects, Sixth, seventh and eight periodic elements, Superheavy elements

2.1. BACKGROUND

2.1.1. Introduction to Relativistic Effects

The theory of relativistic effects in Chemistry is discussed in detail elsewhere [1–9]. A simple introduction will be given here. Einstein's Theory of Special Relativity states that the mass of any moving object changes as its velocity changes:

$$m = m_0[1 - (v/c)^2]^{-1/2} \tag{2-1}$$

where m_0 is the mass at zero velocity. Under ordinary conditions, the term $(v/c)^2$ is so small that any relativistic effects would be insignificant. However, if v becomes sufficiently large, the ratio m/m_0 becomes appreciably larger than unity.

The Bohr model for a hydrogen-like species (a one-electron cation of general formula ${}_ZA^{(Z-1)+}$) will illustrate this. According to this model, the electron would obey the following equations for its velocity, energy, and its orbital radius [10]:

$$v = (2\pi e^2/nh)Z \tag{2-2}$$

$$E = -(2\pi^2 e^4/n^2h^2)mZ^2 \tag{2-3}$$

$$r = Ze^2/mv^2 \tag{2-4}$$

M. Barysz and Y. Ishikawa (eds.), *Relativistic Methods for Chemists*,
Challenges and Advances in Computational Chemistry and Physics 10,
DOI 10.1007/978-1-4020-9975-5_2,

where **n** is a quantum number, **e** is the charge on the electron, **h** is Planck's constant and **Z** is the atomic number of the nucleus. Equation (2-2) enables the calculation of the electron velocity for any element. Substituting this calculated velocity into Eq. (2-1) gives the ratio m_r/m_0, where m_r is the *relativistic mass* for the electron. Calculated values of this ratio for the ground state ($n = 1$) of selected elements are shown in Table 2-1.

Elements of the first three periods show ratio changes of less than 1%; corresponding ratios for elements in the Fourth Period vary from 0.9% to 3.6%. For the Fifth Period elements, the ratios show changes of ca. 8%. Only for the Sixth and Seventh Period elements does this ratio exceed 10%; these elements show the greatest relativistic effects. Energy changes resulting from replacement of m_0 by m_r increase as Z increases (Eq. (2-3)). Since the orbit radius is inversely proportional to m (Eq. (2-4)), it will *decrease* as Z increases. It has been proposed that relativistic effects might even depend on higher powers of Z, especially for the heaviest elements [11].

The figures in Table 2-1 suggest a steady increase for m_r/m_0 across each given period. More exact calculations indicate otherwise [12]. Across the Sixth Period, the relativistic radius for the 6s orbital slowly decreases between Cs and Ir, then

Table 2-1 Calculated m/m_0 values for the electron in $E^{(Z-1)+}$ ions of groups 1, 2, 11–18

Group 1	Group 2	Group 11	Group 12
H 1.000027			
Li 1.00024	Be 1.00042		
Na 1.0032	Mg 1.0038		
K 1.0092	Ca 1.011	Cu 1.023	Zn 1.025
Rb 1.038	Sr 1.041	Ag 1.064	Cd 1.067
Cs 1.091	Ba 1.095	Au 1.22	Hg 1.23
Fr 1.29	Ra 1.30	Rg 1.69	112 1.72
119 1.99	120 2.05		
Group 13	Group 14	Group 15	Group 16
B 1.00067	C 1.00095	N 1.0013	O 1.001
Al 1.0045	Si 1.0052	P 1.0060	S 1.0068
Ga 1.026	Ge 1.028	As 1.030	Se 1.032
In 1.070	Sn 1.073	Sb 1.077	Te 1.080
Tl 1.24	Pb 1.25	Bi 1.25	Po 1.26
113 1.75	114 1.79	115 1.82	116 1.86
Group 17	Group 18		
	He 1.00011		
F 1.0021	Ne 1.0027		
Cl 1.007	Ar 1.0087		
Br 1.034	Kr 1.036		
I 1.084	Xe 1.087		
At 1.27	Rn 1.28		
117 1.90	118 1.95		

drops sharply, passes through a minimum at Au, and subsequently increases from Au to Rn. This has become known as the "Group 11 maximum" [13], A similar trend also occurs for the following period, although there the maximum occurs at element 112 ("eka-mercury") [13].

2.1.2. Intraatomic Changes

2.1.2.1. Orbital Energies

s–Orbitals decrease substantially in energy when relativistic effects are considered; p–orbitals also decrease, but to a lesser extent. This enhances their nuclear shielding effect, causing d– and f–orbitals to increase in energy. As a result, energy differences among orbitals change, often drastically, for the heavier elements, compared to what might be expected by extrapolation from their lighter congenors.

2.1.2.2. Subshell Splittings

As a result of spin-orbit interaction, subshells with $l > 0$ will split into two subgroups of $l - 1/2$ and $l + 1/2$, the former being lower in energy. Figure 2-1 shows this for the 5d, 6s and 6p subshells. The energies for these various splittings depend on the specific element, and increase as Z increases.

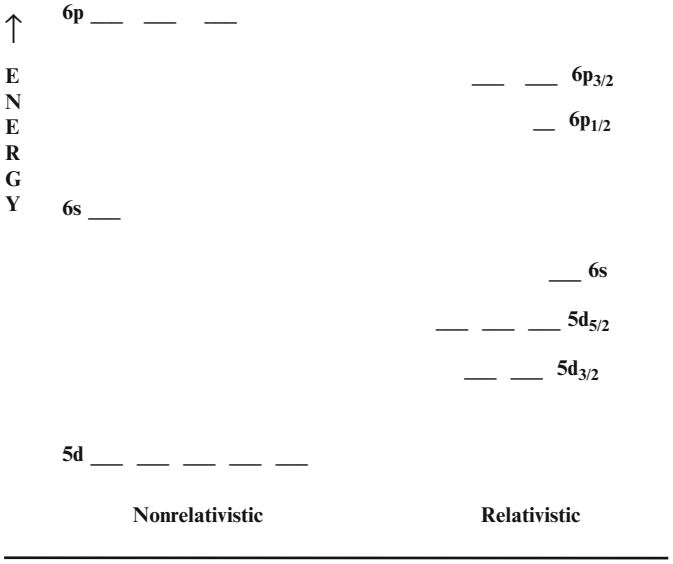

Figure 2-1. Relativistic and nonrelativistic energy level diagrams for the 5d, 6s and 6p sublevels of sixth period elements (Reproduced from [1] with permission from *Journal of Chemical Education*. Copyright ©2005 Division of Chemical Education Inc)

2.1.2.3. Radial Changes

If a relativistic mass is calculated and used to calculate the radius of the electron's orbit, the resulting value will decrease. Since relativistic effects are strongest for s orbitals, these will shrink the most. Such shrinkage is termed the *orbital contraction* [5, 6, 8, 9]. This causes changes in bond lengths and other inter-atomic separations.

2.1.3. Chemical Effects

All physical and chemical properties ultimately depend on the energies and spatial distributions of electrons in the atoms involved. For heavier elements, the relativistic effect approach must be used to give accurate descriptions for such properties.

Physical properties (bond lengths, transition energies, polarizations, etc.) have been extensively investigated for their relativistic alterations. The two best known macroscopic examples are the low melting point of mercury [4] and the unusual color of gold [8]. Other examples are discussed elsewhere in this volume.

Chemical properties also are changed by relativistic effects. The best known example is the so-called Inert Pair Effect [1, 8]. This term was originally coined to describe the reluctance of Sixth Period elements (Hg-Rn) to use the 6s electrons in bonding, and remains the most common example of relativistic effects mentioned in general textbooks. Other species affected are mentioned either slightly or not at all; species such as intermetallic compounds, semiconductors, metal clusters etc.

The Sixth Period elements can be studied directly (with difficulty for Po, At and Rn) and effects of relativity measured For the superheavy elements, where actual chemical studies are few and where relativistic effects are expected to be strong, theoretical studies of such effects can be used to predict physical and/or chemical properties, providing guidelines for future investigation.

For the purposes of this article the "heavier Main Group elements" are those of the Sixth and Seventh Periods. Pt and Au (along with their heavier congenors Ds and Rg) are not Main Group elements, but are included in this article because their strong and well-studied relativistic properties provide a convenient starting point for comparison discussion.

2.2. SIXTH PERIOD ELEMENTS

2.2.1. s-Block Elements

2.2.1.1. Cesium

Cesium behaves like a typical Group I metal, and examples of relativistic effects are few. Like Na, K, and Rb, Cs forms an alkalide anion Cs^- [14]. One paper reports that triatomic $Cs_3{}^{3-}$ may form in solid lattices of certain cesides [15].

2.2.1.2. Barium

In the intermetallic compound Ba_2Pt [16], one of the two 6s electrons of barium is transferred to platinum while the other remains in the barium band, indicative of the increased stability of the 6s subshell. Experimentally observed polarizabilities of both Ba and Ba_2 agreed well with calculated relativistic values [17].

2.2.2. d-Block Elements

2.2.2.1. Introduction

These elements show the strongest relativistic effects in the Sixth Period. All three metals can use both d-electrons and s-electrons in their bonding. The color of gold, unique among the elements, arises from elevated energies of the 5d electrons, shifting those wavelengths required for their excitation to into the visible region of the electromagnetic spectrum [3, 8]. The liquidity of mercury at ordinary temperatures, unusual among metals, results from relativistically lowered energy of the 6s electrons, weakening Hg-Hg interatomic attractions [4].

2.2.2.2. Platinum$\{5d_{3/2}{}^4 5d_{5/2}{}^5 6s^1\}$

General The electron configuration of platinum differs from the $4d^{10}$ configuration of its lighter congenor palladium and reflects relativistic changes in both the energies of the 6s subshell and the $5d_{5/2}$ spinor. This in turn leads to substantial differences in their chemistries.

Platinide Ions Addition of two electrons to a platinum atom forms the platinide anion Pt^{2-} found in the salt Cs_2Pt [14, 18]. This deep red solid adopts the Ni_2In structure with each Pt atom surrounded by nine Cs atoms in a tricapped trigonal prism [18]. Band structure investigations gave results consistent with an ionic formulation [16, 18].

The ion $Pt_2{}^{2-}$ would be the first member of an isoelectronic series that continues with Au_2 and $Hg_2{}^{2+}$. BaPt did not contain this ion, but formed chains having Pt-Pt bonds [18, 19]. Charge transfer studies indicated that each barium atom transferred only one electron to the platinum; the compound was described as "the first example of a Zintl-phase where the polyatomic structure is established by a transition element" [19]. Ba_3Pt_2 contained Pt-Pt dumbbells in the solid state [19], while Ba_2Pt has a $CdCl_2$ structure with isolated platinide ions and has been proposed to have a charge assignment $(Ba^{2+})_2Pt^{2-} \bullet 2e^-$ [16]. Electrochemical and X-ray photoelectron spectroscopy investigations have confirmed the formation of negative oxidation states for platinum [20].

Higher Oxidation States Common oxidation states for Pt are $+2$ and $+4$. The $+6$ state is found in platinum hexafluoride, PtF_6, which earned a niche in chemical history as the first species to form a dioxygenyl salt, $O_2{}^+ PtF_6{}^-$ [21] and a xenon compound $Xe^+PtF_6{}^-$ [22]. The ground state structure of PtF_6 [23, 24]

has a regular octahedral structure and a closed-shell ground state. This compound has a high electron affinity (ca 7 eV) [25], and forms both PtF_6^- and PtF_6^{2-} ions. The latter has had its detachment spectrum studied by a relativistic approach [26]. No Pd(VI) compounds have been reported; apparently there is not enough relativistic destabilization of its 4d electrons to allow their oxidation.

Platinum pentafluoride is a deep-red solid that disproportionates readily upon heating [27]:

$$2\,PtF_5 \xrightarrow{\Delta} PtF_4 + PtF_6 \tag{2-5}$$

Theoretical studies indicated that platinum octafluoride, PtF_8, would be unstable towards loss of F_2 [27].

Laser ablation of atomic platinum in an Ar-O_2 mixture at 10 K gave evidence for the formation of PtO_3 with D_{3h} symmetry [28]. Theoretical calculations indicate that Pt atoms should be able to combine with noble gas atoms to form species of formula Ng-Pt-Ng in the gas phase or in a matrix [29].

Platinum Clusters Investigation of $\{Pt(CO)(AuR)_8\}^{2+}$ (R = triphenylphosphine) indicated that 5d orbitals from both Pt and Au contributed to the HOMO [30]. Similar studies on effects of mixed Au-Pt species (e.g. $PtAu^+$) in the dehydrogenation of methane revealed that the HOMO formed primarily from gold and showed enhanced interaction with the LUMO σ* of methane, when compared to the corresponding interaction for Pt^+ [31]. Ionization spectroscopy showed that bond energies of Pt_2 and Pt_2^+ were 3.14 and 3.26 eV respectively [32], indicating significant 5d contributions to these Pt-Pt bonds.

2.2.2.3. Gold $\{5d^{10}6s^1\}$

General The roles of relativistic effects in the properties of gold have been extensively reported [2, 3, 6, 8, 16, 33]. These effects expand the chemistry of gold well beyond "normal" limits for Group 11 elements (the "Coinage Metals") and give a remarkably rich chemistry to a "noble metal."

Auride Salts and Au–Au Bonds The outer shell configuration of gold predicts an oxidation state of +1, also found for other Group 11 elements. However, enhanced stability of the 6s orbital allows formation of both *auride* anion, Au^-, and the molecule Au_2. Comparable species are known for the alkali metals, but *alkalide* compounds require stabilizing ligands for isolation [34]. The silver counterpart, *argentide* ion, Ag^- has been prepared by electrochemistry in liquid ammonia solution [35]. Yellow CsAu dissolved readily in liquid ammonia; however, slow removal of solvent resulted in crystallization of an intensely blue solid $CsAu{\bullet}NH_3$ [33, 36]. The presence of auride anion as a distinct entity has been verified by various techniques, including ^{197}Au Mössbauer spectroscopy [16]. A colorless salt $(Me_4N)^+\,Au^-$ {Me = methyl} was prepared from CsAu by ion exchange and was isostructural with the corresponding bromide [16]. Auride ion has been suggested to be an analog of halide ions [16]. Two examples of this analogy:

1. Gold undergoes disproportionation in base:

$$2\,Cs_2O + 5\,Au \rightarrow [CsAu]_4\,[Cs_3AuO_2] \tag{2-6}$$

This compares to:

$$Cl_{2\,(aq)} + 2\,OH^-_{(aq)} \rightarrow Cl^-_{(aq)} + ClO^-_{(aq)} + H_2O \tag{2-7}$$

The product was described as "intergrowths of slabs corresponding to the binary aurides and to the ternary aurates(I)" [37]. The presence of two different oxidation states of gold was verified by ^{197}Au Mössbauer spectroscopy [16]. The electronic structure of auride ion has been studied [38].

2. Auride ion shows hydrogen bonding:

$\{Rb([18]crown\text{-}6)(NH_3)_3\}^+\,\{Au{\bullet}NH_3\}^-$, when studied by X-ray crystallography, was found to have a Au–H distance of 258 pm, comparable to corresponding H-Br and H-I hydrogen-bond distances of 249 and 272 pm [39].

Hydrolysis of the model species $Au(OH_2)^+$, when compared to the hydrolysis of analogous Cu(I) and Ag(I) species, showed marked relativistic effects [40]. Inclusion of relativistic corrections for AuCN increased the bond order of the Au-C bond [41,42]. Au_2 showed a dissociation energy of 2.34 eV [3] (= 225.8 kJ/mol), making it considerably more stable than Ag_2 [43] or the corresponding alkali metal dimers. The Au-Au bond length was shortened by some 35 pm by inclusion of relativistic effects [3].

Unusual Gold Compounds Au(III) compounds with oxygen and the halogens are well known, and less reactive than Cu(III) or Ag(III) analogs. Gold pentafluoride, Au_2F_{10} [44], is a powerful oxidizing agent and readily forms AuF_6^- salts, including $[O_2]^+\,[AuF_6]^-$. A compound with stoichiometry AuF_7, stable at room temperature, has been reported [45]. Theoretical studies suggested the formula $AuF_5\,F_2$ [46]! If verified, this would be the first example of difluorine acting as a Lewis base in a condensed phase [46].

Another surprising class of ionic gold compounds contains Au-Xe cations with $Sb_2F_{11}^-$ counterions [47–49]. Examples reported to date are

$AuXe_4^{2+}$ (a square-planar Au(II) derivative), *cis*-$AuXe_2^{2+}$ (also square planar, with bridging fluorides), an unstable *trans*-isomer, the F-bridging species $XeAuFAuXe^{3+}$ [47, 49], and the unusual ion $(F_3As)AuXe^+$, containing a linear As-Au-Xe framework [48, 50]. All these show varying degrees of fluoride bridging, contain the unusual Au^{2+} ion, and apparently involve d-d electron pair donation from Xe [49]. Studies on chemical bonds between Au(I) and noble gases indicated an appreciable charge transfer from the noble gas to Au [50–54].

Gold Clusters and Aurophilic Interactions Gold has an extensive cluster chemistry, as exemplified by Au_{55} [55] and $Au_2Te_{12}^{4-}$ [56]. Gold nanoclusters have

low-symmetry structures due to relativistic effects [57]. In mixed Cu-Au species, pure Au clusters were more stable than mixed clusters when the total number of atoms was less than 12 [58].

Closed-shell interactions have considerably extended the chemistry of gold and other elements. The term "aurophilicity", originally coined by Schmidbaur [59], describes interactions between filled 5d subshells of adjacent gold atoms [60, 61]. Relativistically enhanced energy of Au(I) 5d electrons makes such interactions comparable in energy to hydrogen bonding [60, 61]. The compound $M(C_6F_5)\{N(H) = CPh_2$ (M = Ag, Au), displayed both types of bonding [62]. For the gold species, both types were almost equal in energy; in the silver species, hydrogen bonding was stronger, indicating that 'argentophilicity' is weaker than its gold counterpart. Both aurophilic attraction and relativistic effects were predicted to stabilize the cluster species $W@Au_{12}$ [63], a possible analogue to C_{60}. This prediction has been confirmed by experimental observation of $W@Au_{12}$ and its molybdenum counterpart [64]. Investigation indicated strong 6s – $5d_{5/2}$ hybridization in the tungsten cluster, whose structure is icosahedral (overall symmetry I_h) with the tungsten atom surrounded by gold atoms [64]. Gold clusters have been investigated for their role in absorbing and catalyzing the oxidation of carbon monoxide [65, 66].

2.2.2.4. *Mercury* $\{5d^{10}6s^2\}$

General Unlike gold, the outermost electrons of mercury comprise a completely filled subshell. As Norrby pointed out, gold and mercury are "next-door neighbors in the Periodic Table but have dramatically different properties" [4]. There is an s^2–s^2 interaction [60]; dimeric Hg_2 has a bond length of 363 pm (compared 416 pm for the sum of the van der Waals radii) and a bond energy of 0.0434 eV. The first ionization energy of Hg is higher than most other metals of the Sixth Period (Table 2-2),

Table 2-2 First ionization energies for fourth, fifth and sixth row elements of groups 8 through 18 (All values are taken from The Elements (Emsley J. ed) Clarendon, Oxford, 2nd edn, 1991 and have units of kJ/mol)

8	9	10	11
Fe 759.3	Co 760.0	Ni 736.7	Cu 745.4
Ru 711	Rh 720	Pd 805	Ag 731.0
Os 840	Ir 880	Pt 870	Au 890.1
12	13	14	15
Zn 745.4	Ga 578.8	Ge 762.1	As 947.0
Cd 867.6	In 558.3	Sn 708.6	Sb 833.7
Hg 1007.0	Tl 589.3	Pb 715.5	Bi 703.2
16	17	18	
Se 940.9	Br 1139.9	Kr 1350.7	
Te 869.2	I 1008.4	Xe 1170.4	
Po 812	At 930	Rn 1037	

due to relativistic stabilization of the 6s subshell. Consequently, Hg^{2+} ion very electrophilic, and Hg(II) compounds differ in many respects from their Zn and Cd counterparts for this reason. The configuration also suggests that Hg(0) would be less likely to gain electrons to form anionic species than either Pt(0) or Au(0).

Polyatomic Cations Mercurous ion, Hg_2^{2+}, has been studied theoretically [67–70]. This ion is isoelectronic with Au_2 and Pt_2^{2-}. In the gas phase, it was slightly unstable towards dissociation [70]; however, a large heat of hydration stabilizes it in aqueous solution. The monatomic species Hg^+ formed only under high energy conditions and dimerized in a second-order reaction with a rate constant of 4.0×10^9 L/mol•s [68]. Stability of the Hg-Hg bond depended very much on the attached group [70–72]: ligands with electronegativities above 2.5 formed stable compounds, while those below that value caused disproportionation. Pure crystals of mercurous halides needed to be prepared by sublimation [71]. Diorganodimercury compounds have never been isolated because the Hg-Hg bond in such compounds was too weak [69, 70]. Mercurous complexes of formula $[M_2Hg_2L_3](PF_6)_2$ (M = Pt, Pd; L = 2,9-bis(diphenylphosphino)-1,10-phenanthroline) [72] had one mercury atom linked to two N atoms and two Pd(Pt) atoms as well as to the other mercury; spectroscopic evidence indicated that the Hg-Hg unit was spinning rapidly [72].

Other polyatomic mercury cations (e.g. Hg_3^{2+}, Hg_3^{4+}, Hg_4^{2+}) are also known [73–75]. The linear Hg_3^{2+} cation, formed by disproportionation,

$$2Hg_2Cl_2 \rightarrow Hg_3^{2+} + HgCl_2 + 2Cl^- \tag{2-8}$$

contributed to the photoluminescence of Hg_2Cl_2, as did Hg_3^{4+}, believed to form by the reaction [73]

$$Hg_2Cl_2 + HgCl_2 \rightarrow Hg_3^{4+} + 4Cl^- \tag{2-9}$$

Hg_2^{2+} and Hg_3^{2+} both formed complexes with benzene, in which the benzene molecules interacted with mercury atoms at the end of the chain [74]. Both cations also occurred in the three-dimensional framework of $[Hg_{11}As_4](GaBr_4)_4$ [76], and showed large Hg-Hg coupling constants in their crown ether complexes [77]. The triangular cation Hg_3^{4+} formed complexes with bis(diphenylphosphinomethane): each mercury atom was bonded to two other mercury atoms and two phosphorus atoms [78, 79]. Extended structures for mercurous-oxy cations [80] and Hg-P linkages [81] have also been reported.

Higher Oxidation States As with platinum and gold, mercury can lose electrons from its 5d subshell, albeit reluctantly. An early report of trivalent mercury [82] has never been verified and must be considered doubtful. Theoretical attention has been given to HgF_4 and its derivatives [83–86]. In 2007, HgF_4 was finally prepared and

isolated in inert-gas matrices [87]. It has a square-planar structure with a $5d^8$ configuration, making it isoelectronic with AuF_4^{1-} and PtF_4^{2-}. Infrared spectroscopy of HgF_4 in neon showed a peak at 703 cm^{-1}, assigned to the degenerate E_u stretching mode of HgF_4 [87]. Similar experiments involving ZnF_2/F_2 or $HgCl_2/Cl_2$ in Ne matrices gave no evidence for the formation of either ZnF_4 or $HgCl_4$ [87]. Theoretical studies indicated that many potential Hg(IV) complexes would be thermodynamically unstable [88], but might possess a sufficiently high activation energy barrier to enable their detection. Other studies indicate that HgF_3 by itself would probably be unstable [86], but the dimeric molecule Hg_2F_6 or complexes such as HgF_4^- might be more stable.

Both HgH_4 and HgH_6 have been proposed as possible candidates for higher-valence mercury compounds [88]. The isoelectronic species PtD_4^{2-} [89] and AuH_4^- [90, 91] have been reported; they have square-planar $5d^8$ structures.

The involvement of 5d electrons in d_π π^* backbonding in mercury cyanides has been proposed on the basis of their photoelectron spectra [92].

Mercury Clusters and Amalgams Mercury has an extensive cluster chemistry [1, 93]. Polyatomic mercury cations have already been discussed. Anionic clusters have been reported: Na_3Hg contains the square planar species Hg_6^{4-} [93], while electron transfer has been reported for alkaline earth metal-mercury intermetallic compounds [94]. Bonding varies according to whether the clusters are cationic, neutral or anionic [93, 95]: both cationic and anionic clusters show Hg-Hg σ – bonding, while neutral clusters show van der Waal's bonding. Bonding in neutral clusters seems also to depend on the cluster size [1, 95, 96].

2.2.3. p-Block Elements

2.2.3.1. Introduction

For the elements Tl-Rn, 6p-electrons become the dominant contributors to bonding, while the 5d electrons become part of the core and the 6s electrons reacted only under oxidizing conditions. Oxidation states involving 6s electrons become increasingly less stable from thallium to astatine, and disappear entirely for radon. Table 2-3 shows examples of compounds for these elements in their most positive oxidation states. The roles of relativistic effects and ligands (especially H and the halogens) has been discussed by Schwerdtfeger [97], who noted a sharp change between Pb and Bi for the oxidizing power of the highest oxidation state. In the elements bismuth through radon, the energy of the $6p_{1/2}$–$6p_{3/2}$ spinor separation becomes increasingly important in determining oxidation state stability.

Because of their radioactivity, the chemistry of Po, At and Rn is less developed than other Sixth Period elements.

Table 2-3 Some stable compounds for Thallium through Radon in their highest oxidation states (Reproduced from [1] with permission from *Journal of Chemical Education*; copyright ©2005, Division of Chemical Education, Inc.)

Element	Compounds
Tl(III)	TlX_3 (X = F-Br), TlX_4^-, Tl_2E_3 (E = O, S, Se) R_4Tl^-, R_3Tl, R_2Tl^+, $C_6H_5Tl(OAc)$
Pb(IV)	PbX_4, PbX_6^{2-} (X = F,Cl), PbO_2, PbO_3^{2-}, PbO_8^{6-}, R_4Pb, R_3PbA, R_2PbA_2, $C_6H_5Pb(OAc)_3$, R_6Pb_2
Bi(V)	BiF_5, BiF_6^-, BiF_7^{2-}, Bi_2O_5(?), BiO_3^- R_6Bi^-, R_5Bi, R_4Bi^+, Ar_3BiA_2
Po(VI)	PoF_6(?), PoO_3(?)
At(VII)	AtO_4^- (?)
Rn(VIII)	None reported

A – anion, R – alkyl and/or aryl group, Ar – aryl group, (?) – existence uncertain

2.2.3.2. *Thallium* $\{6s^2 6p_{1/2}{}^1\}$

General The electron configuration predicts two oxidation states: +1("thallous") and +3 ("thallic"). The +1 state, isoelectronic with Hg(0), is the more stable state, forming numerous salts. Tl^+ is much the same size of Rb^+ (ionic radii are 159 and 149 pm respectively), and is quite toxic. Compounds in the +3 state are covalent, and readily reduced to the +1 state. TlI_3 is actually $Tl^+ I_3^-$, but addition of iodide ion produces TlI_4^-, containing Tl(III). Stable Tl(III) compounds contain bonds to electronegative elements and/or organic groups (Table 2-3).

Thallides Relativistic effect theory predicts that Tl^- should be isoelectronic with Pb(0) and have a filled $6p_{1/2}$ spinor. Both KTl and CsTl are known compounds but do not have monatomic thallide ions; their stoichiometry is actually M_6Tl_6 [98,99] ! The $Tl_6{}^{6-}$ octahedra show D_{4h} symmetry due to tetragonal distortion [98]. Other binary alkali metal-thallide compounds have been reported [100,101]. $BaTl_3$ shows Tl-Tl interactions involving 6p orbitals [99]. Various anionic Tl clusters have also been reported [98], including the new phase $Na_9K_{16}Tl_{25.25}$, which contains $Tl_9{}^{9-}$ clusters [102].

Thallium-Thallium Bonds and Heteroatomic Clusters Both the Au_2 molecule and the mercurous ion, $Hg_2{}^{2+}$, show distinct metal-metal covalent bonds; the corresponding isoelectronic thallium species would be $Tl_2{}^{4+}$. No salts containing such an ion have yet been reported. Halides of the formula TlX_2 are actually mixed-valence species $Tl^+TlX_4^-$ having the NiAs structure [103]. Theoretical studies on E_2X_4 (E = B-Tl; X = H, F-I) indicated that the Tl-Tl bond would be the weakest in the series [104]. Thallium forms fewer compounds of this type than do other Group 13 elements [104, 105]. The Tl-Tl bond occurs in the cluster species $Tl_{0.8}Sn_{0.6}Mo_7O_{11}$ [106]. Three compounds of formula $[(R_3Si)_3Si]_4Tl_2$ have been

reported, where $R = Me$ [107], t-Bu [108] or a t-Bu/Ph mixture [109]. All are colored and decompose at 20° [107], 52° [108] and 125° [109] respectively. Tl-Tl bond lengths in these compounds vary from 2.881 to 2.966 Ĺ [107–109].

2. Tl(I)-Tl(I) interactions have been reported in some pentaorganocyclopentadienylthallium(I) compounds, with Tl-Tl bond lengths exceeding 3.3 Ĺ [110–112]. The bonding appears to be another example of "metallophilic interactions" [60,112–114]. Larger clusters have been reported, containing covalently bonded Tl atoms with bond lengths around 2.92 Ĺ [109, 115].

A model study of Au(I)-Tl(I) complexes showed that metallophilic attraction occurred and that the charge on Tl was more positive than on Au [116]. In clusters of Tl with coinage metals, Au_2Tl_2 was the most stable [117]. Compounds of formula $Tl_3Ag_3E_2S_6$ (E = As,Sb) showed certain very short Tl-Ag separations, indicating strong metallophilic interactions [118].

2.2.3.3. Lead $\{6s^26p''^2\}$

General The relativistically stabilized $6p''$ spinor is completely filled, causing lead metal to be unreactive; its first ionization energy is higher than that for either Tl or Bi (Table 2-2). Predicted oxidation states are +2 ("plumbous") and +4 ("plumbic"). Pb(II) compounds tend to be ionic with some covalent character; Pb(IV) compounds are rarer, polar covalent, and usually good oxidizing agents. Pb-Pb bonds are less numerous than for lighter Group 14 elements and occur in organolead compounds or cluster species. The marked difference in stability for Pb(IV) with inorganic versus organic substituents has been discussed by Kaupp and Schleyer [119]. They suggested that bonds to electronegative substituents deplete the 6p-orbitals more than the 6s orbitals, weakening their ability to enter into hybridization.

Plumbides and Some Inorganic Lead Compounds Various anionic lead clusters have been reported [120–123], of which the best known is probably Pb_9^{4--}. Unlike Pt and Au, but like Hg and Tl, Pb does not form monatomic anions. Relativistic theory suggests that formation of Pb^{4--} might not be energetically favorable, since the additional electrons would have to go into the higher energy $6p_{3/2}$ spinor. Studies on alkali metal-lead alloys indicate that, for Li and Na, the stable compounds nearest in stoichiometry to the 4:1 ratio are $Li_{22}Pb_5$ and $Na_{15}Pb_4$ respectively [122].

Plumbane, PbH_4, has been extensively studied [7, 119, 124–127]. Infrared spectra at 3.5 K indicated that it had T_d symmetry [125]. The hydride Pb_2H_4 was also observed, and was assigned a *trans*-ring C_{2h} structure with two-bridging H atoms [125], in contrast to structures for ethylene or its Si and Ge analogs. Plumbane has only a transient existence at 25°, but is stable enough to allow its use in lead analysis by hydride generation [128].

The tetrahaloplumbanes, PbX_4, have also received theoretical investigations [127, 129–131]. Only the fluoride is stable at 25°C; the chloride decomposes slowly at that temperature, while the bromide and iodide have never been reported. Salts containing $PbCl_6^{2-}$ ion have been isolated and are stable at room temperature [132]. This ion has a yellow color, attributed to relativistic stabilization of the a_{1g} LUMO [133]. Solution studies on $PbBr_2$–Br_2–Br^--H_2O systems led to a claim

for both $PbBr_4$ and $PbBr_6^{2-}$ formation [134, 135], but that claim has not been verified. Advances in scientific techniques make it probable that $PbBr_4$ and PbI_4 could be formed and identified at low temperatures—probably by matrix trapping—and that the corresponding PbX_6^{2-} salts might be stable enough for detection and/or isolation.

Steric effects from the lone pair on Pb(II) can be diminished by relativistic contraction. In the ternary oxide $SnWO_4$, the electron pair on Sn(II) interacts strongly with the 2p orbitals on oxygen, affecting its crystalline structure [136]; the 6s electron pair in $PbWO_4$ shows a markedly lower interaction.

Organolead Compounds Organolead compounds represent the most common examples of stable Pb(IV) derivatives, with, however, considerable variation in their thermal and chemical stability. In a comparative study of bond energies in the series $(CH_3)_2M$ ($M = Au^-$, Hg, Tl^+, Pb^{2+}), the energy rose from Au to Hg, then decreased from Hg to Tl to Pb [137], due to relativistic effects. The presence of organic groups adds thermal stability to Pb-halogen bonds. For example, all triphenyllead halides are stable solids, melting at temperatures above 140° [138a]; diphenyllead dibromide decomposes above 250°, while the corresponding iodide melts smoothly at 103°. Phenyllead trichloride decomposes below 0°, but the derived salts tetraphenylphosphonium phenyltetrachloroplumbate(IV) and bis(tetramethylammonium phenylpentachloroplumbate(IV) are stable up to 137° and 108° respectively [138a]. Corresponding alkyllead compounds are less stable thermally, but trimethyllead bromide and iodide are both known, and dimethyllead dibromide has been isolated as an unstable white solid [138a]. The highly sterically hindered compound bis {2,4,6-tris[bis(trimethylsilyl)-methyl]phenyldibromoplumbane is monomeric in the crystalline state [139], unlike diphenyllead dihalides, which are polymeric as solids.

The previously mentioned series Pt_2^{2-} Au_2, Hg_2^{2+}, Tl_2^{4+} should continue with Pb_2^{6+}. No such ion has yet been reported; however, the hexaorganodiplumbanes, R_6Pb_2, containing Pb-Pb bonds, may be considered as derivatives. Hexamethyldiplumbane decomposes slowly at room temperature, while hexaphenyldiplumbane melts at 170° with decomposition [138a]. Pentaphenyl [tris(trimethylsilyl)methyl]diplumbane melts at 143°, but changes from yellow to green at 134° [140]. Cyclotriplumbanes are also known [141, 142], and unusual organolead cluster compounds, containing Pb-C_6H_5 σ-bonds, have been reported [143, 144].

Pb(II) also forms organo derivatives. Plumbylenes, R_2Pb:, usually polymerise to a cycloplumbane [145, 146]

$$n\ R_2Pb :\rightarrow (R_2Pb)_n \tag{2-10}$$

but, if the organic group is sufficiently bulky, a diplumbene can form [145]

$$2\ R_2Pb :\rightarrow R_2Pb = PbR_2 \tag{2-11}$$

and, for extremely bulky groups, the monomeric plumbylene can actually be isolated [146]. Like Tl(I), Pb(II) can form compounds with cyclopentadiene; $(\eta^5\text{-}C_5H_5)_2Pb$ (plumbocene) and numerous derivatives have been reported [147]. Plumbocene is polymeric as a solid but has a monomeric bent structure in the gas phase, reflecting the steric influence of the Pb 6s electrons.

2.2.3.4. Bismuth $\{6s^2 6p_{1/2}{}^2 6p_{3/2}{}^1\}$

General Decreasing stability of the highest oxidation state for Sixth Period elements continues with bismuth. Table 2-3 shows fewer compounds of Bi(V) than for either Pb(IV) or Tl(III). Inorganic Bi(V) species usually behave as strong oxidizing agents. Organobismuth(V) compounds are the most numerous examples for this oxidation state.

Inorganic Bismuth Compounds The "standard" oxidation states for Group 15 elements are -3, $+3$ and $+5$. Bismuth forms compounds in all three states. The -3 state is found in various bismuthides, such as Na_3Bi. Some reactions for this compound in liquid ammonia have been reported [148]:

$$Na_3Bi + 3\ AgI \rightarrow Bi + 3\ Ag + 3\ NaI \tag{2-12}$$

$$Na_3Bi + BiI_3 \rightarrow 2\ Bi + 3\ NaI \tag{2-13}$$

$$Na_3Bi + 2\ Bi \rightarrow Na_3Bi_3 \tag{2-14}$$

These reactions are all consistent with the presence of Bi^{3-} but do not necessarily prove that this ion exists as a monomer in the solid state. In species such as $M_{11}Bi_{10}$ ($M = Sr$, Ba) there are Bi^{3-} ions, but also $Bi_2{}^{4-}$ and $Bi_4{}^{4-}$ [149]. Apparently, the monomeric anion does exist for Bi, unlike Pb.

Bismuth forms a $+1$ oxidation state by loss of the electron from the $6p_{3/2}$ spinor, but might also form a -1 oxidation state by adding one electron to form the half-filled $6p_{3/2}$ spinor. No compounds for the latter configuration have yet been reported, but it is predicted to have two bound states [150]. Bismuth monohalides BiX contain bismuth clusters [151]. Bi^+ion does occur in solution [152, 153] and in $Bi_{10}Hf_3Cl_{18}$ [154]. Mixed-valence compounds, such as BiI{which contains both Bi(0) and Bi(II)}, are also known [155]. A compound containing the Bi_2 molecule has been reported [156, 157]

Stable inorganic compounds of Bi(V) contain fluorine or oxygen. The ions $BiF_6{}^-$ and $BiF_7{}^{2-}$ have been reported [158]. Other pentahalides are predicted to be unstable towards reductive elimination of halogen [159], but they may be detectable at low temperatures in an inert matrix, and salts containing $BiCl_6{}^-$ may be isolable.

Bismuth Clusters Unlike thallium and lead, bismuth usually forms cationic clusters [160–162], although some neutral ones are also known [161, 163]. Homoleptic Bi cationic clusters are electrophilic and require weakly basic counterions for stability. $Bi_9{}^{5+}$ is isoelectronic with $Pb_9{}^{4-}$, but the bismuth cluster has a tricapped trigonal prism structure whereas the lead cluster (along with its Group 14 congenors)

has a monocapped square antiprism structure [161]. The electrophilic nature of bismuth clusters appears in the aromatic planar cation $[Fe(Bi_5)]^+$ [164]. A mixed Bi-Te cluster cation has been reported [165]. Solid compounds of bismuth with other Group 15 elements show a decrease in the band gap due to the relativistic lowering of the 6s electrons on Bi [166, 167].

Organobismuth Compounds Bismuth forms organo derivatives in both +3 and +5 states. The latter has a restricted range of stability: no Bi(V) derivatives containing only one or two organo ligands are known, and compounds with three organo ligands exist only when the inorganic groups are halogens or oxygen. Tetraarylbismuthonium salts, $Ar_4Bi^+ X^-$ have been isolated; tetramethylbismuthonium ion formed from the β-decay of $^{210}Pb(CH_3)_4$ [168]. Pentaphenylbismuth and other pentaarylbismuth compounds are known [169, 170], and the unstable pentamethylbismuth has been reported [169]. Hexaorganobismuthates have also been prepared [169, 171]. The color for pentaarylbismuth compounds was attributed to its square pyramidal structure and to lowering of the HOMO-LUMO separation in this structure due to relativistic effects [133, 170]. However, pentamethyl-bismuth has a trigonal bipyramidal structure and also a violet color [169], so other factors may be involved.

No organo compounds containing Bi(V)–Bi(V) bonds have been reported. The ion Bi_2^{8+}, predicted by continuation of the aforementioned dimeric series starting with Pt_2^{2-}, does not yet have any derivatives reported; one might expect any organo derivative of stoichiometry R_8Bi_2 to decompose rapidly under ordinary conditions:

$$R_8Bi_2 \rightarrow R_3Bi + [R_5Bi] \rightarrow 2\ R_3Bi + R_2 \qquad (2\text{-}15)$$

Possibly such a compound may be prepared if the attached groups are very large, as with Tl and Pb. Covalently bonded dibismuth(III) compounds R_4Bi_2 are known [138b, 172], some of which are thermochromic (change color upon melting). Bond angles are close to 90°, indicating that the Bi atoms use p-orbitals for bonding, and that the lone pair is predominantly situated in the 6s orbital. Thermochromic dibismuthines, like their antimony analogues [172], show intermolecular closed-shell interactions in the solid state.

2.2.3.5. Polonium $\{6s^2 6p_{1/2}{}^2 6p_{3/2}{}^2\}$

General The chemistry of polonium is more extensive than textbooks indicate [173, 174], although its radioactivity has hampered investigation. α-Polonium is the only elemental allotrope that has a simple cubic structure, attributed to relativistic effects [175]. Declining stability of the highest oxidation state continues: the oxidation state of +6 for Po is has only two examples. The +4 state is the dominant one, and +2 is well represented. Various polonides in the −2 state are also known.

Inorganic Chemistry: Positive Oxidation States The +6 state is currently represented by PoF_6 and PoO_3, neither of which has been isolated in macroscopic

quantities. A volatile fluoride was reported for the reaction of Po with fluorine, but was not characterized [176]., Calculations indicate that inclusion of relativistic effects should weaken the Po-F bond in PoF_6 [177]. PoI_6 was reported to form and decompose in the vapor phase [178, 179]. Possibly Po(VI), like other high oxidation states, may be stabilized by anion formation, e.g. PoF_8^{2-} or PoO_6^{6-}.

The +4 state includes numerous characterized compounds similar to tellurium in their chemical behavior. Po(IV) resembles corresponding Zr, Hf and Rf species in forming diketonate complexes [180]. Po(IV) is stable in aqueous solution over a wide pH range, enabling both anion exchange [181] and hydration [182] studies.

The +2 state occurs in various compounds [174a] and is more widespread than the isoelectronic +1 state for bismuth. Most of these compounds are readily oxidized to the +4 state. Tracer work using ^{210}Po indicate that Po^{2+} can be coprecipitated with a variety of M^{+2} salts [183].

While a +3 state has been claimed [173], these claims have never been verified [174a]. The +5 state occurred when ^{222}Rn underwent α-decay in the presence of water vapor or nitrogen dioxide [184]. In the latter case, electron transfer occurred:

$$PoO_2^{+} + NO_2 \rightarrow PoO_2 + NO_2^{+} \tag{2-16}$$

From this reaction, the ionization energy of PoO_2 has been estimated as 10.44 ± 0.05 eV [184].

Inorganic Chemistry: Zero or Negative Oxidation States Polonium metal vaporizes as Po_2 molecules [174a, 185], and its partial pressures have been calculated over a wide temperature range [185].

Hydrogen polonide is a volatile molecule, studied for its bonding properties [186, 187]. When water vapor was exposed to ^{210}Po, the levels of volatilized polonium increased sharply due to H_2Po formation [188, 189].

Various metal polonides have been prepared [174a, 190]. PbPo received particular attention because its volatility enabled it to vaporize from a lead-bismuth eutectic coolant in nuclear reactors [191]. Energy band analysis for this compound indicated that it was a semimetal rather than a direct-gap semiconductor [192]. This was also true for ZnPo, CdPo and HgPo, being attributed to relativistic effects [193]. These compounds had a strong ionic character; metal polonides, especially Na_2Po [174a], apparently contain the monomeric Po^{2-} ion. No homoleptic polonium clusters have yet been reported, even though both Bi and Te form clusters.

Organopolonium Compounds These compounds have been reviewed [174b]. Organo derivatives are known for both Po(II) and Po(IV). Arylpolonium(IV) compounds can be formed by β decay of ^{210}Bi precursors [194]

$$Ar_3BiX_2 \rightarrow \left[Ar_3PoX_2^{+}\right] \rightarrow Ar_3PoX + Ar_2PoX_2 \tag{2-17}$$

with the product ratio depending on the nature of X. A similar reaction using pentaphenylbismuth gave a mixture of di- and tetraphenylpolonium [194]. The endohedral compound Po@C_{60} has been prepared and proposed as a candidate for radiotracer and radiopharmaceutical work [195, 196].

Volatilization of polonium is reported to occur through bacterial methylation and release of dimethylpolonide [197, 198].

2.2.3.6. Astatine {$6s^2 6p_{1/2}{}^2 6p_{3/2}{}^3$}

General Astatine is a member of the halogens, and its chemistry is much like iodine [199, 200]. Due to its radioactivity and the short half-lives of its isotopes (^{210}At has the longest $t_{1/2}$: 8.1 h), investigations have been limited. Most recent work has concentrated on the use of ^{211}At (t″ 7.2 h) in radiotherapy [200, 201]. Like the other halogens, astatine would be expected to show oxidation states of −1, +1, +3, +5 and +7. Relativistic effects modify their relative stabilities. The highest oxidation state of +7 has not been verified in any detected compound; earlier claims for perastatate ion, AtO_4^- [199] have not been verified. Even the +5 state seems to be limited to astatate ion and a few organoastatine compounds [199, 200]. An oxidation state of +3 would be predicted from the electron configuration and by extension from Bi(I) and Po(II). Some organo derivatives are known [199, 200]. The molecule AtF_3 has been investigated; the FAtF bond angle increases relative to the corresponding bond angle in IF_3 due to relativistic effects [202, 203].

Two stable states are +1 and −1, corresponding to loss or gain of one electron by the high energy $6p_{3/2}$ spinor. Calculated values for polonium, astatine and radon appear in Table 2-3, showing a steadily increasing gap between the $6p_{1/2}$ and $6p_{3/2}$ spinors [204], which would be expected to enhance the resistance of At in the +1 state to oxidation.

Astatides Astatide anion, At^-, resembles iodide anion in its general chemical behavior, although it was not always retained when coprecipitated with iodide [199]. Astatide formed a complex with Hg(II) in aqueous solution; as might be expected, astatide was a softer base than iodide and formed stronger complexes [205]. It also formed complexes with chelated Rh(III) and Ir(III), which might serve as precursors to radiopharmaceuticals [206]. Liquid-liquid extraction experiments showed high separation factors for astatide ion [207].

Hydrogen astatide, HAt, has been extensively studied for its properties [208–211]. Its dissociation energy is 2.52 eV (HI = 3.19 eV) and the molecular dipole moment is 0.22D (HI = 0.47D) [211]. A value of 0.06D has been calculated, with the negative end on the hydrogen atom, indicating that this molecule should be named astatine hydride [211].

Like iodine, astatine would be expected to form polyhalides; only a few, such as AtI_2^-, have so far been reported [199].

2.2.3.7. Radon $\{6s^2 6p_{1/2}{}^2 6p_{3/2}{}^4\}$

General Radon, a member of Group 18, is the last element of the Sixth Period; relativistic trends across that Period reach their culmination here. Reported chemical reactions for this element are few [212, 213].

No compounds in the +8 state have been reported or even claimed. RnF_8 is predicted to be unstable towards loss of fluorine [214]. By analogy with Xe, the most likely Rn(VIII)compound to be isolated would probably be Ba_2RnO_6, the radon analog of barium perxenate.

Two recent studies on RnF_6 [214, 215] indicated that the molecule should be stable to loss of fluorine, and that relativistic effects actually weakened the Rn-F bond! Theoretical calculations indicate that RnF_6 and the isoelectronic ions $AtF_6{}^-$ and $PoF_6{}^{2-}$ should have regular octahedral structures because relativistic contraction removes any stereochemical distortion from the 6s electron pair [216]. Chemical species containing Rn(VI), such as RnO_3 and certain derivatives, have been claimed [213], but these claims have not been confirmed. RnF_4 is also predicted to be stable, but has yet to be prepared [214].

Radon(II) and Rn(0) Compounds The +2 oxidation state is the only one for which compounds have been prepared and characterized. This state, isoelectronic with At(I), corresponds to the loss of half the electrons in the $6p_{3/2}$ spinor. RnF_2 and RnF^+ derivatives (e.g. $[RnF^+][SbF_6{}^-]$) are known [213]; in fact, formation of involatile compounds of this type has been proposed as a method for removing gaseous radon from air [217]:

$$Rn_{(g)} + 2\ O_2{}^+\ SbF_{6(s)} \rightarrow RnF^+Sb_2F_{11}{}^-(s) + 2\ O_{2(g)} \qquad (2\text{-}18)$$

Trichlorotrifluoroethane solutions of RnF_2 passed through specially prepared columns displaced protons, sodium ion and potassium ion from salts, indicating that Rn can exist as a cation in solution [218].

Radon gas has been predicted to interact with bromide ion [219] and to form a monomeric carbonyl RnCO [220].

2.3. SEVENTH AND EIGHTH PERIOD ELEMENTS

2.3.1. General

All elements in these Period are radioactive. Some have yet to be prepared; others have such short half-lives that their chemical behavior has yet to be investigated. All these elements are predicted to show strong relativistic effects. As of this writing, only francium, radium and element 112 have observed chemical properties. For those elements whose chemistry still remains to be determined, a few selected predictions will be presented.

2.3.2. s-Block Elements

2.3.2.1. Introduction

Francium and radium have only s electrons in their outermost shell. The increased stabilization of these electrons would be expected to alter their properties in comparison to those of the lighter elements. Such alterations do appear, but have not been extensively investigated. Calculated values for electronegativities of the ions $Fr^{+}$and Ra^{2+} show that they increase, relative to those of Cs^{+} and Ba^{2+}, rather than decrease as might be expected [221].

2.3.2.2. Francium

The short half-life for this element (the most stable isotope, ^{223}Fr, has $t_{1/2}$ = 21.8 min) has hampered chemical investigation. Some selected physical properties have been reported, all of which deviate from the trends for Li through Cs. Ionization energy [222] is higher for Fr than for Cs, as is the electron affinity [223] and the polarizability of the anion [224]. Investigation into alkali metal homo- and heterodiatomic molecules showed that the dipole moment for CsFr indicated Cs^{+} Fr^{-} polarization [225]; by contrast, other heteroatomic dialkalis have the heavier alkali metal atom at the positive end of the dipole. This reflects a greater relativistic stabilization of the Fr 7s subshell compared to the Cs 6s subshell. Similarly, there was more covalent character in FrO_2 than in the other alkali metal superoxides, attributed to increased interaction between 6p orbitals on Fr and orbitals on oxygen [226]. Potential energy curves and transport coefficients for Fr with the rare gases have been determined spectroscopically [227].

2.3.2.3. Radium

There exists a substantial literature on radium, almost all dealing with its radioactivity, environmental occurrence or use in medical treatment. An investigation into hydrolysis of Ra^{2+} showed that the value for the first hydrolysis constant was the same as for Ba^{2+}, despite the larger size of radium [228]. Studies on both RaF_2 [229] and $RaAt_2$ [230] indicate that the 6s and 6p orbitals on Ra participate in the bonding, creating a degree of covalency in the bonding. A study of a radium amalgam indicated stronger Ra-Hg interactions than were found in the Ba-Hg system [231].

2.3.3. Superheavy Elements

2.3.3.1. Introduction

Elements having $Z > 103$, are occasionally termed *transactinide elements* or *translawrencium elements*. Much of the work done on these elements is described in a book by Schädel [232], and in two papers [233, 234]. This article will discuss the elements darmstadtium ($Z = 110$) through unbinilium ($Z = 120$). Some theoretical

studies for elements in this series have been reported [235,236]. At the time of this writing, actual chemical studies have only been reported for ununbium (Z = 112).

2.3.3.2. *Darmstadtium*

In a study of MF_6 (M = Pd,Pt,Ds), a 10Dq value of $34,625.6\,cm^{-1}$ was predicted for Ds, compared to $29,471.7\,cm^{-1}$ for Pt [237]. Two reports on DsC [238,239] and one on $DsCl_4$ [240] support the placement of Ds in Periodic Group 10. Calculations indicate that DsF_6 would have an O_h symmetry [24].

2.3.3.3. *Roentgenium*

Roentgenium is predicted to have a ground state of $6d^97s^2$, compared to the expected $6d^{10}7s^1$ [241], reflecting enhanced relativistic stabilization of the 7s subshell and destabilization of the $6d_{5/2}$ spinor. Theoretical studies indicated that Rg(I) is a "softer" base than Au(I), making it the "softest metal ion" [242]. Studies on Group 11 monohydrides, MH (M = Cu,Ag,Au,Rg) indicated that Au-H had a shorter bond length than Ag-H, due to relativistic effects, and that Rg-H was shorter still [243]. The dissociation energy for Rg_2 was calculated to be less than the corresponding energy of Au_2 [43]. The Rg-C bond length in RgCN was predicted to be less than the corresponding Au-C bond length [41,42].

2.3.3.4. *Element 112 (Ununbium, Eka-Mercury)*

This element has received considerable attention due to an expected strong stabilization of the assumed outer shell configuration $7s^2$, making it less reactive than mercury, and possibly inert [244]. The atomic structure and properties of this element have been calculated and compared to those of mercury [245].

Adsorption/desorption investigations on a gold surface, using the radioisotopes $^{283}112$, ^{185}Hg and ^{219}Rn, showed that element 112 behaved like a metal rather than like a noble gas [246–248]. From these experiments, workers estimated the boiling point of element 112 to be 357^{+112}_{-108} K [248], compared to 629.7 K for Hg and 211.4 K for Rn. Fully relativistic studies on (112)X and HgX (X = Pd,Cu,Ag,Au) showed a decrease of 15–20 kJ/mol in bonding for (112)X relative to HgX [249]. This was attributed to decreased contribution of the 7s orbital (compared to the 6s orbital on Hg) due to stronger relativistic effects.

2.3.3.5. *Element 113 (Ununtrium, Eka-Thallium)*

Calculations on the linkage between element 113 and element 117 indicated that this bond would be weaker than the Tl-At bond and that, when spin-orbit effects were included, element 113 became more electronegative than element 117 [250]. The strong relativistic stabilization of the 7s orbital for this element suggests that the oxidation state of −1 should be more stable than for Tl [251].

2.3.3.6. Element 114 (Ununquadium, Eka-Lead)

Element 114 has attracted attention because its outer shell configuration $7s^2 7p_{1/2}{}^2$ should be exceptionally stable, making it less reactive than lead.

Ionization potentials and excitation energies have been calculated for element 114 and its lighter homologs [252]. The +4 oxidation state is expected to be unstable, except possibly for $(114)F_4$ [253]. Ion exchange behavior of Pb in hydrohalic acids was proposed as a homolog for the corresponding behavior of element 114 [254, 255].A study on mixed metal-metal species indicated that element 114 would form weaker bonds than Pb [256] and would show lower adsorption on surfaces [257]. Density functional theoretical calculations indicate that element 114 would be more electronegative than Pb [258].

2.3.3.7. Element 115 (Ununpentium, Eka-Bismuth)

An early paper on this element [259] predicted that element 115 would have an outer shell configuration analogous to that of Bi, that the oxidation state of +1 would become more important (with a standard reduction potential of −1.5 V), and that the aqueous chemistry of the +3 state would resemble that of Bi^{+3}. Another paper confirmed the importance of the +1 state and suggests cluster compounds might form [162].

2.3.3.8. Element 116 (Ununhexium, Eka-Polonium)

A study of the Group 16 dihalides reported that spin-orbit coupling was so strong in element 116 that its dihalides would be linear rather than bent [260]. The bond angle in $(116)H_2$ was found to be larger than expected, and the authors suggest the possibility of "supervalent" hybridization involving the 8s orbital [261]. Subshell and spinor energy splittings for this element are larger than for polonium (Table 2-4), suggesting that the oxidation states of +2 and −2 may be correspondingly more stable.

Table 2-4 Selected calculated spinor energies (All values taken from [204]. Reproduced [with modifications] from [1] with permission from the *Journal of Chemical Education*; copyright © 2005 by the Division of Chemical Education Inc.)

	Calculated energies, eV		
Element	$np_{3/2}$	$np_{1/2}$	ns
Sixth row	−8.22	−10.98	−22.04
Po	−9.33	−12.80	−25.53
At	−10.45	−14.70	−29.16
Rn			
Seventh row			
(116)	−6.69	−14.67	−27.16

2.3.3.9. Element 117 (Ununseptium, Eka-Astatine)

Element 117 has been estimated to have a boiling point of 618 K [262], comparable to that for At(610 K) and considerably higher than for I(457.5 K). As previously mentioned, element 117 became less electronegative than element 113 in the compound (113)(117) [250, 263]. Spin-orbit effects in the molecule H(117) caused the bond to become unusually long and unusually strong [264]. The species $(117)_2$ has been studied [265].

2.3.3.10. Element 118 (Ununoctium, Eka-Radon)

Element 118 has been estimated to have a boiling point of 247 K [262], compared to 211 K for Rn and 166 K for xenon. It may also be the first rare gas with an electron affinity [266]. The compound $(118)F_4$ is predicted to have a tetrahedral structure rather than a square planar structure [267, 268].

2.3.3.11. Element 119 (Ununennium, Eka-Francium)

Calculations predicted that Element 119 would have higher values for the first ionization energy [222] and electron affinity [223] than francium.

2.3.3.12. Element 120 (Unbinilium, Eka-Radium)

Little is known of this element. Relativistic trends predict that it is likely to be more covalent, less ionic than radium; a +1 state might be isolable. Vibrational excitations for $^{292}120$ have been reported [269].

2.4. CONCLUSIONS

Advances in chemical theory, combined with great enhancement of computer capabilities during the last 20 years, have resulted in a near-exponential growth in understanding and applications of relativity theory to chemistry. Corresponding advances in experimental techniques have also grown, though more slowly. Compounds that once were considered too unstable to exist can now be prepared and studied; HgF_4 is an example.

The heavier Main Group elements have been somewhat neglected by comparison to their lighter congenors. Growing interest in these elements over recent years has changed that, and there is likely to be a surging growth in this area in coming years. Realization of all the physical properties and chemical systems that can be predicted by relativity theory, plus the ability to apply it, will play a large part in this.

Synthesis of the superheavy elements has spurred development of "single atom techniques" for their chemical investigation, which in turn have been guided by predictions generated from relativity. Very soon the first true compound(s) of element 112 will be reported, with element 114 following soon thereafter. Subsequently, as more stable nuclides from the "Island of Stability" are synthesized, their compounds will also be prepared.

Relativistic effects have a much greater role in the chemistry of Main Group elements than has generally been realized. Hopefully, this article and this volume will do much to correct that lack of awareness.

ACKNOWLEDGMENTS

I thank Mr. John Tebo, librarian, and the staff of the Oesper Chemistry-Biology Library of the University of Cincinnati, for their in-valuable help in obtaining materials for this article. I thank Dr. John Moore, editor, and the Journal of Chemical Education for permission to reproduce material from an earlier paper. I thank Drs Maria Barysz and Yasuyuki Ishikawa for their invitation to contribute this article.

REFERENCES

1. Thayer, J.S.: Relativistic effects and the chemistry of the heaviest main-group elements. J. Chem. Educ. **82**, 1721–1729 (2005)
2. Pitzer, K.S.: Relativistic effects on chemical properties. Acc. Chem. Res. **12**, 271–276 (1977)
3. Pyykkö, P., Desclaux, J.P.: Relativity and the periodic system of elements. Acc. Chem. Res. **12**, 276–281 (1977)
4. Norrby, L.J.: Why is mercury liquid? J. Chem. Educ. **68**, 110–113 (1991)
5. Hess, B.A.: Relativistic Effects in Heavy-Element Chemistry and Physics. Wiley, Chichester (UK) (2003)
6. Balasubramanian, K.: Relativistic Effects in Chemistry. Wiley, New York (1997)
7. Schwerdtfeger, P.: Relativistic effects in molecular structures of s- and p-Block elements. In: A. Domenicano, I. Hargittai (eds.) Strength from Weakness: Structural Consequences of Weak Interactions in Molecules, Supermolecules and Crystals, pp. 169–190. Kluwer, Dordrecht, The Netherlands (2002)
8. Pyykkö, P.: Relativistic effects in structural chemistry. Chem. Rev. **88**, 563–594 (1988)
9. Schwerdtfeger, P. (ed.).: Relativistic Electronic Structure Theory, vol. 2. Elsevier, Amsterdam, The Netherlands (2004)
10. Douglas, B., McDaniel, D.H., Alexander, J.J.: Concepts and Models of Inorganic Chemistry, 3rd edn., pp. 10–12. Wiley, New York (1994)
11. Onoe, J.: Atomic number dependence of relativistic effects on chemical bonding. Adv. Quantum Chem. **37**, 311–323 (2000)
12. Desclaux, J.P.: Relativistic Dirac-Fock expectation values for atoms with $Z = 1$ to $Z = 120$. Atom. Data Nucl. Data **12**, 374–383 (1973)
13. Schwerdtfeger, P.: Relativistic effects in properties of gold. Heteroatom Chem. **13**, 578–584 (2002)
14. Huang, R.H., Ward, D.L., Kuchenmeister, M.E., Dye, J.L.: The crystal structures of two cesides show that Cs^- is the largest monatomic ion. J. Am. Chem. Soc. **109**, 5561–5563 (1987)
15. Ichimura, A.S., Huang, R.H., Xie, Q., et al.: One-dimensional zig-zag chains of Cs^-: The structure and properties of Li^+ (Cryptand[2.1.1])Cs^- and Cs^+ (Cryptand[2.2.1])Cs^-. J. Phys. Chem. B **110**, 12293–12301 (2006)
16. Jansen, M.: Effects of relativistic motion on the chemistry of gold and platinum. Solid State Sci. **7**, 1464–1474 (2005)
17. Schäfer, S., Mehring, M., Schäfer, R.: Polarizabilities of Ba and Ba_2: Comparison of molecular beam experiments with relativistic quantum chemistry. Phys. Rev. A **76**, 052515/1–5 (2007)

18. Karpov, A., Nuss, J., Wedig, U., Jansen, M.: Cs_2Pt: A Platinide(-II) exhibiting complete charge separation. Angew. Chem. Int. Ed. Engl. **42**, 4818–4821 (2003)
19. Karpov, A., Nuss, J., Wedig, U., Jansen, M.: Covalently bonded $[Pt]^-$ chains in BaPt: Extension of the Zintl-Klemm concept to anionic transition metals? J. Am. Chem. Soc. **126**, 14123–14128 (2004)
20. Ghilane, J., Lagrost, C., Guilloux-Viry, M., et al.: Spectroscopic evidence of platinum negative oxidation states at electrochemically reduced surfaces. J. Phys. Chem. C **111**, 5701–5707 (2007)
21. Bartlett, N., Lohmann, D.H.: Fluorides of the noble metals. II. Dioxygenyl hexafluoroplatinate(V) $O_2{}^+[PtF_6{}^-]$. J. Chem. Soc. 5253–5261 (1962)
22. Bartlett, N.: Xenon hexafluoroplatinate(V) $Xe^+[PtF_6{}^-]$. Proc. Chem. Soc. (June 1962) 218 (1962)
23. Alvarez-Thon, L., David, J., Arratia-Pérez, R., Seppelt, K.: Ground state of octahedral platinum hexafluoride. Phys. Rev. A **77**, 034502/1–4 (2008)
24. David, J., Fuentealba, P., Restrepo, A.: Relativistic effects on the hexafluorides of group 10 metals. Chem. Phys. Lett. **457**, 42–44 (2008)
25. Wesendrup, R., Schwerdtfeger, P.: Structure and electron affinity of platinum fluorides. Inorg. Chem. **40**, 3351–3354 (2001)
26. Pernpointer, M., Cederbaum, L.S.: $PtF_6{}^{2-}$ dianion and its detachment spectrum: A fully relativistic study. J. Chem. Phys. **126**, 144310/1–7 (2007)
27. Bartlett, N., Lohmann, D.H.: Fluorides of the noble metals. Part III. The fluorides of platinum. J. Chem. Soc. 619–626 (1964)
28. Bare, W.D., Citra, A., Chertihin, G.V., Andrews, L.: Reaction of laser-ablated platinum and palladium atoms with dioxygen. Matrix infrared spectra and density functional calculations of platinum oxides and palladium complexes. J. Phys. Chem. A **103**, 5456–5462 (1999)
29. Ono, Y., Taketsugu, T., Noro, T.: Theoretical study of Pt-Ng and Ng-Pt-Ng (Ng = Ar,Kr,Xe). J. Chem. Phys. **123**, 204321/1–5 (2005)
30. Boča, R.: Platinum-centered octakis(Triphenylphosphinegold) clusters: A relativistic MO study. Int. J. Quantum Chem. **57**, 735–740 (1996)
31. Xia, F., Cao, Z.: Relativistic DFT studies of dehydrogenation of methane by Pt cationic clusters: Cooperative effect of bimetallic clusters. J. Phys. Chem. A **110**, 10078–10083 (2006)
32. Taylor, S., Lemire, G.W., Hamrick, Y.M., et al.: Resonant two-photon ionization spectroscopy of jet-cooled Pt_2. J. Chem. Phys. **89**, 5517–5523 (1988)
33. Pyykkö, P.: Relativity, gold, closed-shell interactions and $CsAu{\bullet}NH_3$. Angew. Chem. Int. Ed. Engl. **41**, 3573–3578 (2002)
34. Huang, R.H., Huang, S.Z., Dye, J.L.: Syntheses and structures of six compounds that contain the sodium anion. J. Coord. Chem. **46**, 13–31 (1998)
35. Tran, N.E., Lagowski, J.J.: Metal ammonia solutions: Solutions containing argentide ions. Inorg. Chem. **40**, 1067–1068 (2001)
36. Mudring, A.V., Jansen, M., Daniels, J., Krämer, S., Mehring, M., Ramalho, J.P.P., Romero, A.H., Parrinello, M.: Cesiumauride ammonia(1/1), $CsAu{\bullet}NH_3$: A crystalline analogue to alkali metals dissolved in ammonia? Angew. Chem. Int. Ed. Engl. **41**, 120–124 (2002)
37. Mudring, A.V., Jansen, M.: Base-induced disproportionation of elemental gold. Angew. Chem. Int. Ed. Engl. **39**, 3066–3067 (2000)
38. Belpassi, L., Tarantelli, F., Sgamellotti, A., Quiney, H.M.: The electronic structure of alkali aurides. A four-component Dirac-Kohn-Sham study. J. Phys. Chem. A **110**, 4543–4554 (2006)
39. Nuss, H., Jansen, M.: $[Rb([18]crown\text{-}6)(NH_3)_3]Au{\bullet}NH_3$: Gold as acceptor in $N\text{-}H\cdots Au^-$ hydrogen bonds. Angew. Chem. Int. Ed. Engl. **45**, 4369–4371 (2006)
40. Barysz, M., Leszczyński, J., Bilewicz, A.: Hydrolysis of the heavy metal cations: Relativistic effects. Phys. Chem. Chem. Phys. **6**, 4553–4557 (2004)

41. Lee, D.-K., Lim, I.S., Lee, Y.S., Jeung, G.-H.: Relativistic effects on the ground state properties of group 1 and group 11 cyanides estimated from quantum chemical calculations. Int. J. Mass Spectrom. **271**, 22–29 (2008)
42. Zaleski-Ejgierd, P., Patzschke, M., Pyykkö, P.: Structure and bonding of the MCN moleucles, M = Cu,Ag,Au,Rg. J. Chem. Phys. **128**, 224303/1–11 (2008)
43. Kullie, O., Zhang, H., Kolb, D.: Relativistic and non-relativistic local-density functional benchmark results and investigations on the dimers Cu_2 Ag_2 Au_2 Rg_2. Chem. Phys. **351**, 106–110 (2008)
44. Hwang, I., Seppelt, K.: Gold pentafluoride: Structure and fluoride ion affinity. Angew. Chem. Int. Ed. Engl. **40**, 3690–3693 (2001)
45. Riedel, S., Kaupp, M.: Has AuF_7 been made? Inorg. Chem. **45**, 1228–1234 (2006)
46. Himmel, D., Riedel, S.: After 20 years, theoretical evidence that "AuF_7" is actually $AuF_5 \bullet F_2$. Inorg. Chem. **46**, 5338–5342 (2007)
47. Drews, T., Seidel, S., Seppelt, K.: Gold-Xenon complexes. Angew. Chem. Int. Ed. Engl. **41**, 454–456 (2002)
48. Hwang, I., Seidel, S., Seppelt, K.: Gold(I) and mercury(II) xenon complexes. Angew. Chem. Int. Ed. Engl. **42**; 4392–4395 (2003)
49. Seppelt, K.: Metal-Xenon complexes. Z. Anorg. Allg. Chem. **629**, 2427–2430 (2003)
50. Pyykkö, P.: Predicted chemical bonds between rare gases and Au^+. J. Am. Chem. Soc. **117**, 2067–2070 (1995)
51. Belpassi, L., Infante, I., Tarantelli, F., Visscher, L.: The chemical bond between Au(I) and the noble gases. Comparative study of NgAuF and $NgAu^+$ ($Ng = Ar$, Kr, Xe) by density functional and coupled cluster methods. J. Am. Chem. Soc. **130**, 1048–1060 (2008)
52. Lovallo, C.C., Klobukowski, M.: Transition metal-noble gas bonding: The next frontier. Chem. Phys. Lett. **368**, 589–593 (2003)
53. Berski, S., Latajka, Z., Andrés, J.: The nature of the Au-Rg bond in the $[AuRg_4]^{2+}$ (Rg = Ar,Kr,Xe) molecules. Chem. Phys. Lett. **356**, 483–489 (2002)
54. Zeng, T., Klobukowski, M.: Relativistic model core potential study of the Au^+ Xe system. J. Phys. Chem. A **112**, 5236–5242
55. Boyen, H.G., Kästle, G., Weigl, F., et al.: Oxidation-resistant Gold-55 clusters. Science **297**, 1533–1536 (2002)
56. Dhingra, S.S., Haushalter, R.C.: Synthesis and structure of the new gold polytelluride anion $[Au_2Te_{12}]^{4-}$. Inorg. Chem. **33**, 2735–2737 (1994)
57. Huang, W., Ji, M., Dong, C.-D., et al.: Relativistic effects and the unique low-symmetry structures of gold nanoclusters. ACSNANO **2**, 897–904 (2008)
58. Lordeiro, R.A., Guimarães, F.F., Belchior, J.C., Johnston, R.L.: Determination of main structural compositions of nanoalloy clusters of Cu_xAu_y (x + y ? 30) using a genetic algorithm approach. Int. J. Quantum Chem. **95**, 112–125 (2003)
59. Scherbaum, F., Grohmann, A., Huber, B., Krüger, C., Schmidbaur, H.: Aurophilicity as a consequence of relativistic effects. Angew. Chem. Int. Ed. Engl. **27**, 1544–1546 (1988)
60. Pyykkö, P.: Strong closed-shell interactions in inorganic chemistry. Chem. Rev. **97**, 597–636 (1997)
61. Bardají, M., Laguna, A.: Gold chemistry: The aurophilic attraction. J. Chem. Educ. **76**, 201–203 (1999)
62. Codina, A., Fernández, E.J., Jones, P.G., et al.: Do aurophilic interactions compete against hydrogen bonds? Experimental evidence and rationalization based on *ab Initio* calculations. J. Am. Chem. Soc. **124**, 6781–6786 (2002)

63. Pyykkö, P., Runeberg, N.: Icosahedral WAu_{12}: A predicted closed-shell species, stabilized by aurophilic attraction and relativity and in accordance with the 18-electron rule. Angew. Chem. Int. Ed. Engl. **41**, 2174–2176 (2002)
64. Li, X., Kiran, B., Li, J., et al.: Experimental observation and confirmation of icosahedral $W@Au_{12}$ and $Mo@Au_{12}$ molecules. Angew. Chem. Int. Ed. Engl. **41**, 4786–4789 (2002)
65. Schwerdtfeger, P., Lein, M., Krawczyk, R.P., Jacob, C.R.: The adsorption of CO on charged and neutral Au and Au_2: A comparison between wave-function based and density functional theory. J. Chem. Phys. **128**, 124302/1–9 (2008)
66. Chang, C.M., Cheng, C., Wei, C.M.: CO oxidation on unsupported Au_{55}, Ag_{55} and $Au_{25}Ag_{30}$ nanoclusters. J. Chem. Phys. **128**, 124710/1–4 (2008)
67. Neisler, R.P., Pitzer, K.S.: The dipositive dimeric ion $Hg_2{}^{2+}$: A theoretical study. J. Phys. Chem. **91**, 1084–1087 (1987)
68. Horváth, O., Mikó, I.: Photoredox chemistry of mercury ions in aqueous ethanol solutions. J. Photochem. Photobiol. **128**, 33–38 (1999)
69. Schwerdtfeger, P., Boyd, P.D.W., Brienne, S., et al.: The mercury-mercury bond in inorganic and organometallic compounds. A theoretical study. Inorg. Chim. Acta. **213**, 233–246 (1993)
70. Liao, M.-S., Zhang, Q.: Hg-Hg bonding in mercurous $Hg(I)_2L_2$ compounds: The influence of ligand electronegativity. J. Mol. Struct. (Theochem). **358**, 195–203 (1995)
71. Singh, N.B., Marshall, G., Gottlieb, M., et al.: Purification and characterization of mercurous halides. J. Cryst. Growth **106**, 62–67 (1990)
72. Catalano, V.J., Malwitz, M.A., Noll, B.C.: Pd(0) and Pt(0) metallo-cryptands encapsulating a spinning mercurous dimer. Inorg. Chem. **41**, 6553–6559 (2002)
73. Kunkely, H., Vogler, A.: On the origin of the photoluminescence of mercurous chloride. Chem. Phys. Lett. **240**, 31–34 (1995)
74. Ulvenlund, S., Rosdahl, J., Fischer, A., Schwerdtfeger, P., Kloo, L.: Hard acid and soft acid base stabilisation of di- and trimercury cations in benzene solution – a spectroscopic, X-ray scattering and quantum chemical study. Eur. J. Inorg. Chem. 633–642 (1999)
75. Gaston, N., Schwerdtfeger, P., von Issendorff, B.: Photoabsorption spectra of cationic mercury clusters. Phys. Rev. A **74**, 043203/1–9 (2006)
76. Olenev, A.V., Shevelkov, A.V.: The Hg_3^{2+} group as a framework unit in a host-guest compound. Angew. Chem. Int. Ed. Engl. **40**, 2353–2354 (2001)
77. Autschbach, J., Igna, C.D., Ziegler, T.: A theoretical study of the large Hg-Hg spin coupling constants in $Hg_2{}^{2+}$, Hg_3^{2+}, and $Hg_2{}^{2+}$– crown ether complexes. J. Am. Chem. Soc. **125**, 4937–4942 (2003)
78. Mason, W.R.: MCD spectra for metal-centered transitions in the $Hg_3(dppm)_3^{4+}$ cluster complex. Inorg. Chem. **36**, 1164–1167 (1997)
79. Mühlecker-Knoepfler, A., Ellmerer-Müller, E., Konrat, R., et al.: Synthesis and crystal structure of the subvalent mercury cluster [*triangulo*-$Hg_3(\mu$-dmpm$)_4$] $[O_3SCF_3]_4$. J. Chem. Soc., Dalton Trans. 1607–1610 (1997)
80. Meyer, G., Nolte, M., Berners, R.: Nanometer channels and cages within the extended basic mercurous cations $[(Hg_2)_3(OH)_2]^{4+}$ and $[(Hg_2)_2O]^{2+}$ Z. Anorg. Allg. Chem. **632**, 2184–2186 (2006)
81. Shevelkov, A.V., Mustyakimov, M.Y., Dikarev, E.V., Popovkin, B.A.: $(Hg_2P)_2HgBr_4$: A phosphorus analogue of the Millon's base salts. J. Chem. Soc. Dalton Trans. 147–148 (1996)
82. Deming, R.L., Allred, A.L., Dahl, A.R., et al.: Tripositive mercury. Low temperature electrochemical oxidation of 1,4,8,11-Tetraazacyclo-tetradecanemercury(II) tetrafluoroborate. J. Am. Chem. Soc. **98**, 4132–4137 (1976)

83. Kaupp, M., Dolg, M., Stoll, H., von Schnering, H.G.: Oxidation state + IV in group 12 chemistry. *Ab Initio* study of Zinc(IV), Cadmium(IV) and Mercury(IV) fluorides. Inorg. Chem. **33**, 2122–2131 (1994)
84. Liu, W., Franke, R., Dolg, M.: Relativistic *abIinitio* and density functional theory calculations on the mercury fluorides: Is HgF_4 thermodynamically stable? Chem. Phys. Lett. **302**, 231–239 (1999)
85. Riedel, S., Straka, M., Kaupp, M.: Can weakly coordinating anions stabilize mercury in its oxidation state + IV? Chem. Eur. J. **11**, 2743–2755 (2005)
86. Riedel, S., Kaupp, M., Pyykkö, P.: Quantum chemical study of trivalent group 12 fluorides. Inorg. Chem. **47**, 3379 (2008)
87. Wang, X., Andrews, L., Riedel, S., Kaupp, M.: Mercury is a transition metal: The first experimental evidence for HgF_4. Angew. Chem. Int. Ed. Engl. **46**, 8371–8375 (2007)
88. Pyykkö, P., Straka, M., Patzschke, M.: HgH_4 and HgH_6: Further candidates for high-valent mercury compounds. Chem. Commun. 1728–1729 (2002)
89. Bronger, W.: Complex transition metal hydrides. Angew. Chem. Int. Ed. Engl. **30**, 759–768 (1991)
90. Wang, X., Andrews, L.: Gold is noble but gold hydride anions are stable. Angew. Chem. Int. Ed. Engl. **42**, 5201–5206 (2003)
91. Andrews, l., Wang, X.: Infrared spectra and structures of the stable CuH_2^-, AgH_2^-, AuH_2^- and AuH_4^- anions and the AuH_2 molecule. J. Am. Chem. Soc. **125**, 11751–11760 (2003)
92. Burroughs, P., Evans, S., Hamnett, A., et al.: Evidence from the photoelectron spectra of some mercury(II) compounds for the involvement of the inner 5d electrons in covalent bonding JCS. Chem. Comm. 921–922 (1974)
93. Deiseroth, H.J.: Discrete and extended metal clusters in alloys with mercury and other group 12 elements. In: M. Driess, H. Nöth (eds.) Molecular Clusters of the Main Group Elements, pp. 169–187. Wiley, Weinheim (2004)
94. Tkachuk, A.V., Mar, A.: Alkaline-earth metal mercury intermediates. Inorg. Chem. **47**, 1313–1318 (2008)
95. Tomilin, O.B., Akamova, L.V., Yudin, P.A., Terekhin, II.: Electronic structure and stability of bulky mercury clusters. J. Struct. Chem. **42**, 519–525 (2001)
96. Moyano, G.E., Wesendrup, R., Söhnel, T., Schwerdtfeger, P.: Properties of small- to medium-sized mercury clusters from a combined *ab initio,* density-functional, and simulated-annealing study. Phys. Rev. Lett. **89**, 103401/1–4 (2002)
97. Schwerdtfeger, P., Heath, G.A., Dolg, M., Bennett, M.A.: Low valencies and periodic trends in heavy element chemistry. A theoretical study of relativistic effects and electron correlation effects in group 13 and period 6 hydrides and halides. J. Am. Chem. Soc. **114**, 7518–7527 (1992)
98. Dong, Z.C., Corbett, J.D.: CsTl: A new example of tetragonally compressed Tl_6^{6-} octahedra. Electronic effects and packing requirements in the diverse structures of ATl (A = Li, Na, K, Cs). Inorg. Chem. **35**, 2301–2306 (1996)
99. Costa Cabral, B.J., Martins, J.L.: *Ab initio* molecular dynamics of liquid K-Tl. J. Non-cryst. Solids **312–314**, 69–73 (2002)
100. Kaskeff, S., Dong, Z.C., Klem, M.T., Corbett, J.D.: Synthesis and structure of the metallic K_6Tl_{17}: A layered tetrahedral star structure related to that of Cr_3Si. Inorg. Chem. **42**, 1835–1841 (2003)
101. Seo, D.K., Corbett, J.D.: Synthesis, structure and bonding of $BaTl_3$: An unusual competition between clusters and classical bonding in the thallium layers. J. Am. Chem. Soc. **124**, 415–420 (2002)
102. Li, B., Corbett, J.D.: $Na_9K_{16}Tl_{\sim 25}$: A new phase containing naked icosahedral cluster fragments Tl_9^{9-}. J. Clust. Sci. **19**, 331–340 (2008)
103. Thiele, G., Rink, W.: Die Konstitution des valenzgemischten Thalliumchlorid-bromids und ber Mischkristalle im system $TlCl_2/TlBr_2$ Z. Anorg. Allg. Chem. **414**, 47–55 (1975)

104. Szabó, A., Kovács, A., Frenking, G.: Theoretical studies of inorganic compounds. 34. Energy decomposition analysis of E-E bonding in planar and perpendicular X_2E-EX_2 (E = B,Al,Ga,In,Tl; X = H,F,Cl,Br,I). Z. Anorg. Allg. Chem. **631**, 1803–1809 (2005)
105. Uhl, W.: Organoelement compounds possessing Al-Al, Ga-Ga, In-In, and Tl-Tl single bonds. In: R. West, A.F. Hill (eds.) Advances in Organometallic Chemistry, vol. 51, pp. 53–108. Academic Press, Amsterdam (2004)
106. Dronskowski, R., Simon, A.: $PbMo_5O_8$ and $Tl_{0.8}Sn_{0.6}Mo_7O_{11}$, novel clusters of molybdenum and thallium. Angew. Chem. Int. Ed. Engl. **28**, 758–760 (1989)
107. Henkel, S., Klinkhammer, K.W., Schwarz, W.: Tetrakis(hypersilyl)-dithallium(*Tl-Tl*): A divalent thallium compound. Angew. Chem. Int. Ed. Engl. **33**, 681–683 (1994)
108. Wiberg, N., Amelunxen, K., Nöth, H., Schmidt, M., Schwenk, H.: Tetrasupersilyldiindium(*In-In*) and tetrasupersilyldithallium(*Tl-Tl*): $(tBu_3Si)_2M$-$M(SitBu_3)_2$ (M = In,Tl). Angew. Chem. Int. Ed. Engl. **35**, 65–67 (1996)
109. Wiberg, N., Blank, T., Amelunxen, K., et al.: Ditrielanes $(R_3Si)_2E - E(SiR_3)_2$ and heterocubanes $(R_3Si)_4E_4Y_4$ (R = tBu, Ph; E = Al, Ga, In, Tl; Y = O,S,Se). Eur. J. Inorg. Chem. **34**, 341–350 (2002)
110. Schumann, H., Janiak, C., Pickard, J., Börner, U.: Pentabenzylcyclopentadienylthallium(I): Synthesis and structure of a dimeric organothallium compound with Tl-Tl interactions. Angew. Chem. Int. Ed. Engl. **26**, 789–790 (1987)
111. Schumann, H., Janiak, C., Khani, H.: Cyclopentadienylthallium(I) compounds with bulky cyclopentadienyl ligands. J. Organomet. Chem.. **330**, 347–355 (1987)
112. Janiak, C., Hoffmann, R.: $Tl^I - Tl^I$ interactions in the molecular state—an MO analysis. Angew. Chem. Int. Ed. Engl. **28**, 1688–1690 (1989)
113. Janiak, C., Hoffmann, R.: $Tl^I - Tl^I$ and In^I-In^I interactions: From the molecular to the solid state. J. Am. Chem. Soc. **112**, 5924–5946 (1990)
114. Schwerdtfeger, P.: Metal-metal bonds in Tl(I)-Tl(I) compounds: Fact or fiction? Inorg. Chem. **30**, 1660–1663 (1991)
115. Wiberg, N., Blank, T., Lerner, H.W., et al.: $R_4^*Tl_3Cl$ and $R_6^*Tl_6Cl_2$(R = t-Bu_3Si)— the first compounds with larger clusters containing covalently linked thallium atoms. Angew. Chem. Int. Ed. Engl. **40**, 1232–1235 (2001)
116. Fernández, E.J., Laguna, A., López-de-Luzuriaga, J.M., et al.: Theoretical study of the aggregation of $d^{10}s^2$ Au(I)-Tl(I) complexes in extended un-supported chains. J. Mol. Struct. Theor. Chem. **851**, 121–126 (2008)
117. Liu, F.L., Zhao, Y.F., Li, X.Y., Hao, F.Y.: *Ab Initio* study of the struc-ture and stability of M_nTl_n (M = Cu,Ag,Au; n = 1, 2) clusters. J. Mol. Struct. Theor. Chem. **809**, 189–194 (2007)
118. Karanović, L., Poleti, D., Balić-Žuni, T., et al.: Two new examples of very short thallium-transition metal contacts: $Tl_3Ag_3Sb_2S_6$ and $Tl_3Ag_3A_2S_6$. J. Alloy. Compd. **457**, 66–74 (2008)
119. Kaupp, M., Schleyer, P.v.R.: *Ab Initio* study of structures and stabilities of substituted lead compounds. Why is inorganic lead chemistry dominated by Pb^{II} but organolead chemistry by Pb^{IV}? J. Am. Chem. Soc. **115**, 1061–1073 (1993)
120. Edwards, P.A., Corbett, J.D.: Stable homopolyatomic anions. Synthesis and crystal structures of salts containing the pentaplumbide(2-) and pentastannide(2-) anions. Inorg. Chem. **16**, 903–907 (1977)
121. Molina, L.M., López, M.J., Rubio, L.C., et al.: Pure and mixed Pb clusters of interest for liquid ionic alloys. In: J.R. Sabin, M.C. Zerner, E. Brändas, J.M. Seminario (eds.) Advances in Quantum Chemistry, vol. 33, pp. 329–348. Academic, San Diego, CA (1999)
122. Molina, L.M., Alonso, J.A., Stott, M.J.: Octet composition in alkali-Pb solid alloys. Phys. Rev. B **66**, 165427–1–165427–8 (2002)

123. Liu, S., Corbett, J.D.: Synthesis, structure and properties of four ternary compounds: CaSr*Tt*,*Tt*=. Si,Ge,Sn,Pb. J. Solid. State. Chem. **179**, 830–835 (2006)
124. Schwerdtfeger, P., Silberfach, H., Miehlich, B.: Relativistic effects in molecules: Pseudopotential calculations for PbH^+, PbH, PbH2, and PbH4. J. Chem. Phys. **90**; 762–767 (1989)
125. Wang, X., Andrews, L.: Infrared spectra of group 14 hydrides in solid hydrogen: Experimental observation of PbH_4, Pb_2H_2 and Pb_2H_4. J. Am. Chem. Soc. **125**, 6581–6587 (2003)
126. Malli, G.L., Siegert, M., Turner, D.P.: Relativistic and electron cor-relation effects for molecules of heavy elements: *Ab Initio* relativistic coupled-cluster calculations for PbH_4. Int. J. Quantum Chem. **99**, 940–949 (2004)
127. Wang, S.G., Schwartz, W.H.E.: Relativistic effects of p-Block molecules. J. Mol. Struct. (Theor Chem). **338**, 347–362 (1995)
128. Dos Santos, E.J., Herrmann, A.B., Frescura, V.L.A., et al.: Determination of lead in sediments and sewage sludge by on-line hydride generation axial-view inductively-coupled plasma optical-emission spectrometry using slurry sampling. Anal. Bioanal. Chem. **388**, 863–868 (2007)
129. Escalante, S., Vargas, R., Vela, A.: Structure and energetics of group 14 (IV-A) halides: A comparative density functional-pseudopotential study. J. Phys. Chem. A **103**, 5590–5601 (1999)
130. Seth, M., Faegri, K., Schwerdtfeger, P.: The stability of the oxidation state + 4 in group 14 compounds from carbon to element 114. Angew. Chem. Int. Ed. Engl. **37**, 2493–2495 (1998)
131. Giju, K.T., De Proft, F., Geerlings, P.: Comprehensive study of density functional theory based properties for group 14 atoms and functional groups $-XY_3$ (X = C, Si, Ge, Sn, Pb, Element 114; $Y = CH_3$, H, F, Cl, Br, I, At). J. Phys. Chem. A **109**, 2925–2936 (2005)
132. Salyulev, A.B., Vovkotrub, E.G., Strekalovskii, V.N.: The interaction of divalent lead compounds with chlorine. Russ. J. Inorg. Chem. **37**, 109–110 (1992)
133. El-Issa, B.D., Pyykkö, P., Zanati, H.M.: MS Xα studies on the colors of $BiPh_5$, $PbCl_6^{2-}$, and WS_4^{2-}: Are relativistic effects on the LUMO important? Inorg. Chem. **30**, 2781–2787 (1991)
134. Basinski, A., Lenarcik, B.: Investigation of the $PbBr_2 - Br_2 - Br^-$ - H_2O system. I. Solubility method. Rocz. Chem. **38**, 1035–1044; Chem. Abstr. **62**, 15487 (1964)
135. Lenarcik, B., Basinski, A.: Investigation of the $PbBr_2$-Br_2- Br^- - H_2O system. III. Equilibria of complex formation between Pb^{++} and Br^-, Br_2 and Br^-, and among Pb^{++}, Br^- and Br_2. Rocz. Chem. **40**, 165–176; Chem. Abstr. **65**, 1460 (1965)
136. Stoltzfus, M.W., Woodward, P.M., Seshadri, R. et al.: Structure and bonding in $SnWO_4$, $PbWO_4$ and $BiVO_4$: Lone pairs vs inert pairs. Inorg. Chem. **46**, 3839–3850 (2007)
137. Schwerdtfeger, P.: On the anomaly of the metal-carbon bond strength in $(CH_3)_2M$ compounds of the heavy elements M = Au^-, Hg, Tl^+, Pb^{2+}. Relativistic effects in metal-ligand force constants. J. Am. Chem. Soc. **112**, 2818–2820 (1990)
138. (a) The Dictionary of Organometallic Compounds, 2nd edn, vol. 3, pp. 2851–2880. Chapman & Hall, London; (b) vol. 1, pp. 721–747 (1995)
139. Kano, N., Tokitoh, N., Okazaki, R.: Synthesis and X-ray crystal structure of Bis{2,4,6-tris[bis(trimethylsilyl)methyl]phenyl}dibromoplumbane. Organometallics **16**, 2748–2750 (1997)
140. Mallela, S.P., Myrczek, J., Bernal, I., Geanangel, R.A.: Crystal and molecular structure of pentaphenyl[tris(trimethylsilyl)methyl]diplumbane. J. Chem. Soc. Dalton. Trans. 2891–2894 (1993)
141. Stabenow, F., Saak, W., Marsmann, H., Weidenbruch, M.: Hexa-arylcyclotriplumbane: A molecule with a homonuclear ring system of lead. J. Am. Chem. Soc. **125**, 10172–10173 (2003)
142. Koch, R., Bruhn, T., Weidenbruch, M.: Theoretical group 14 chemistry. 4. Cyclotriplumbanes: Relativistic and substituent effects. J. Chem. Theor. Comput. **1**, 1298–1303 (2005)
143. Klinkhammer, K.W., Xiong, Y., Yao, S.: Molecular lead clusters-from unexpected discovery to rational synthesis. Angew. Chem. Int. Ed. Engl. **43**, 6202–6204 (2004)
144. Liu, H., Xing, X., Sun, S., et al.: Pb_m-Phenyl (m = 1–5) complexes: An anion photoelectron spectroscopy and density functional study. J. Phys. Chem. A **110**, 8688–8694 (2006)

145. Tokitoh, N., Okazaki, R.: Recent topics in the chemistry of heavier congenors of carbenes. Coord. Chem. Rev. **210**, 251–277 (2000)
146. Spikes, G.H., Peng, Y., Fettinger, J.C., Power, P.P.: Synthesis and characterization of the monomeric sterically encumbered diaryls $E\{C_6H_3{-}2,6\text{-}(C_6H_3{-}2,6\text{-}Pr^i_2)_2\}_2$ (E = Ge, Sn, Pb). Z. Anorg. Allg. Chem. **632**, 1005–1010 (2006)
147. Jutzi, P., Burford, N.: Structurally diverse π-Cyclopentadienyl complexes of the main group elements. Chem. Rev. **99**, 969–990 (1999)
148. Watt, G.W., Moore, T.E.: Some reactions of trsodium monobismuthide in liquid ammonia. J. Am. Chem. Soc. **70**, 1197–1200 (1948)
149. Derrien, G., Tillard-Charbonnel, M., Manteghetti, A., et al.: Synthesis and crystal structure of $M_{11}X_{10}$ compounds, M = Sr, Ba and X = Sb, Bi. Electronic requirements and chemical bonding. J. Solid State Chem. **164**, 169–175 (2002)
150. Eliav, E., Kaldor, U., Ishikawa, Y.: The relativistic coupled-cluster method: Transition energies of bismuth and Eka-Bismuth. Mol. Phys. **94**, 181–187 (1998)
151. Ruck, M.: From the metal to the molecule – ternary bismuth subhalides. Angew. Chem. Int. Ed. Engl. **40**, 1182–1193 (2001)
152. Bjerrum, N.J., Boston, C.R., Smith, G.P.: Lower oxidation states of bismuth. Bi^+ and Bi_5^{3+} in molten salt solutions. Inorg. Chem. **6**, 1162–1172 (1967)
153. Kuznetsov, A.N., Popovkin, B.A., Henderson, W., et al.: Monocations of bismuth and indium in arene media: A spectroscopic and EXAFS investigation. J. Chem. Soc. Dalton. Trans. 1777–1781 (2000)
154. Friedman, R.M., Corbett, J.D.: Synthesis and structural characterization of bismuth(1+) nonabismuth(5+) hexachlorohafnate(IV), Bi^+ $Bi_9^{5+}(HfCl_6{}^{2-})_3$. Inorg. Chem. **12**, 1134–1139 (1973)
155. Norman, N.C. (ed.).: Chemistry of Arsenic, Antimony and Bismuth, pp. 86–87. Blackie Academic & Professional, London (1998)
156. Huttner, G., Weber, U., Zsolnai, L.: Bl_2, das Bismuth-Homolog des Stickstoffs, als Komplexligand in $Bi_2[W(CO)_5]$. Z. Naturforsch. B **37**, 707–710 (1982)
157. Esterhuysen, C., Frenking, G.: Comparison of side-on and end-on coordination of E_2 ligands in complexes $[W(CO)_5E_2]$ (E = N, P, As, Sb, Bi, Si^-, Ge^-, Sn^-, Pb^-). Chem. Eur. J. **9**, 3518–3529 (2003)
158. Drake, G.W., Dixon, D.A., Sheehy, J.A., et al.: Seven-coordinated pnicogens. Synthesis and characterization of the SbF_7^{2-} and BiF_7^{2-} dianions and a theoretical study of the AsF_7^{2-} dianion. J. Am. Chem. Soc. **120**, 8392–8400 (1998)
159. Breidung, J., Thiel, W.: A systematic *Ab Initio* study of the group V trihalides MX_3 and pentahalides MX_5 (M = P-Bi, X = F-I). J. Comput. Chem. **13**, 165–176 (1991)
160. Kuznetsov, A.N., Kloo, L., Lindsjö, M., et al.: *Ab Initio* calculations on bismuth cluster polycations. Chem. J. Eur. **7**, 2821–2828 (2001)
161. Krossing, I.: Homoatomic cages and clusters of the heavier group 15 elements: Neutral species and cations. In: M. Driess, H. Nöth (eds.) Molecular Clusters of the Main Group Elements, pp. 209–229. Wiley, Weinheim, Germany (2004)
162. Smith, G.P., Davis, H.L.: Relationships between the chemistry and spectroscopy of bismuth and that anticipated for element 115. Inorg. Nucl. Chem. Lett. **9**, 991–996 (1973)
163. Yuan, H.K., Chen, H., Kuang, A.L., et al.: Density-functional study of small neutral and cationic bismuth clusters. J. Chem. Phys. **128**, 094305/1–10 (2008)
164. Lein, M., Frunzke, J., Frenking, G.: A novel class of aromatic compounds: Metal-centered planar cations $[Fe(Sb_5)]^+$ and $[Fe(Bi_5)]^+$. Angew. Chem. Int. Ed. Engl. **42**, 1303–1306 (2002)
165. Beck, J., Dolg, M., Schlüter, S.: $Bi_4Te_4{}^{4+}$– A cube-shaped polycationic main group element cluster. Angew. Chem. Int. Ed. Engl. **40**, 2287–2289 (2001)

166. Ferhat, M., Zaoui, A.: Structural and electrical properties of III-V bismuth compounds. Phys. Rev. B **73**, 5107/1–7 (2006)
167. Saidi-Houat, N., Zaoui, A., Ferhat, M.: Structural stability of thallium-V compounds. J. Phys.: Condens. Matter. **19**, 106221/1–18 (2007)
168. Duncan, J.F., Thomas, F.G.: β-decay of radioactive lead tetramethyl. J. Inorg. Nucl. Chem. **29**, 869–890 (1967)
169. Neumüller, B., Dehnicke, K.: Blue-violet pentamethylbismuth. Angew. Chem. Int. Ed. Engl. **33**, 1726–1727 (1994)
170. Seppelt, K.: Structure, color and chemistry of pentaarylbismuth compounds. In: F.G.A. Stone, R. West (eds.) Advances in Organometallic Chemistry, vol. 34, pp. 207–217. Academic Press, San Diego, CA (1992)
171. Wallenhauser, S., Leopold, D., Seppelt, K.: Hexacoordinate organobismuth compounds. Inorg. Chem. **32**, 3948–3951 (1993)
172. Ashe, A.J.: Thermochromic distibines and dibismuthines. In: F.G.A. Stone, R. West (eds.) Advances in Organometallic Chemistry, vol. 30, pp. 77–97. Academic, San Diego, CA (1990)
173. Bagnall, K.W.: Chemistry of the Rare Radioelements, pp. 3–94. Butterworths, London (1957)
174. Zingaro, R.A.: (a) Polonium: Inorganic chemistry, pp. 3338–3341; (b) Polonium: Organometallic chemistry, pp. 3341–3343. In: R.B. King (ed.) Encyclopedia of Inorganic Chemistry, vol. 6. Wiley, Chichester, UK (1994)
175. Legut, D., Friák, M., Šob, M.: Why is polonium simple cubic and so highly anisotropic? Phys. Rev. Lett. **99**, 016402/1–4 (2007)
176. Weinstock, B., Chernick, C.L.: The preparation of a volatile polonium fluoride. J. Am. Chem. Soc. **82**, 4116–4117 (1960)
177. Onoe, J.: Relativistic effects on covalent bonding: Role of individual valence atomic orbitals. J. Phys. Soc. Japan **66**, 2328–2336 (1997)
178. Abakumov, A.S., Malyshev, M.L.: Dissociation of polonium iodides and vapor pressure in the polonium-iodine system. Radiokhimiya **18**, 894–901 (1976); Chem. Abstr. **86**, 60689s (1977)
179. Abakumov, A.S., Malyshev, M.L.: Possibility of the pyrochemical removal of radiogenic lead from polonium by the use of volatile polonium iodides. Radiokhimiya (5), 776–778; Chem. Abstr. **94**, 94988u (1980)
180. Bilewicz, A.: Adsorption of Zr^{4+}, Hf^{4+}, Rf^{4+} and Po^{4+} diketonate complexes on hydrophobized glass surface. J. Radioanal. Nucl. Chem. **247**, 407–410 (2001)
181. Suganuma, H.: Anion exchange of the chemical species of tracer concentrations of polonium(IV) in chloride solutions. J. Radioanal. Nucl. Chem. **191**, 265–272 (1995)
182. Ayala, R., Martinez, J.M., Pappalardo, R.R., et al.: Po(IV) hydration: A quantum chemical study. J. Phys. Chem. B **112**, 5416–5422 (2008)
183. Zikovsky, L.: Precipitation and solubility of some polonium compounds. J. Radioanal. Nucl. Chem. **227**, 171–172 (1998)
184. Chu, K.D., Hopke, P.K.: Neutralization kinetics for polonium-218. Environ. Sci. Technol. **22**, 711–717 (1988)
185. Eichler, B.: Volatility of polonium PSI-Bericht (02-12) a 1-52. Chem. Abstr. **137**, 146192h (2002)
186. Dubillard, S., Rota, J.B., Saue, T., Faegri, K.: Bonding and analysis using localized relativistic orbitals: Water, the ultrarelativistic case and the heavy homologues H_2X (X = Te, Po, eka-Po). J. Chem. Phys. **124**, 154307/1–14 (2006)
187. Sumathi, K., Balasubramanian, K.: Electronic states and potential energy surfaces of H_2Te, H_2Po and their positive ions. J. Chem. Phys. **92**, 6604–6619 (1990)
188. Petryanov, I.V., Borisov, N.B., Churkin, S.L., et al.: Generation and isolation of a gaseous fraction of polonium from its solid preparations. Dokl. Akad. Nauk. SSSR **322**, 557–559; Chem. Abstr. **116**, 160875f (1992)

189. Buongiorno, J., Larson, C., Czerwinski, K.R.: Speciation of polonium released from molten lead-bismuth. Radiochim. Acta. **91**, 153–158 (2003)
190. Witteman, W.G., Giorgi, A.L., Vier, D.T.: The preparation and identification of some intermetallic compounds of polonium. J. Am. Chem. Soc. **64**, 434–440 (1960)
191. Miura, T., Obara, T., Sekimoto, H.: Experimental verification of thermal decomposition of lead polonide. Ann. Nucl. Energy **34**, 926–930 (2007)
192. Rabii, S., Lasseter, R.H.: Band structure of PbPo and trends in the Pb chalcogenides. Phys. Rev. Lett. **33**, 703–705 (1974)
193. Boukra, A., Zaoui, A., Ferhat, M.: Ground state structures in the polonium-based II-VI compounds. Solid State Commun.. **141**, 523–528 (2007)
194. Wiles, D.R.: The radiochemistry of organometallic compounds. In: F.G.A. Stone, R. West (eds.) Advances in Organometallic Chemistry, vol. 11, pp. 207–252. Academic, New York (1973)
195. Ohtsuki, T., Ohno, K.: Formation of $Po@C_{60}$. Phys. Rev. B **72**, 153411/1–3 (2005)
196. Chi, M., Han, P., Fang, X., et al.: Density functional theory of polonium-doped endohedral fullerenes $Po@C_{60}$. J. Mol. Struct. Theor. Chem. **807**, 121–124 (2007)
197. Thayer, J.S.: Biological methylation of less-studied elements. Appl. Organomet. Chem. **16**; 677–691 (2002)
198. Momoshima, N., Fukuda, A., Ishida, A., Yoshinaga, C.: Impact of microorganisms on polonium volatilization. J. Radioanal. Nucl. Chem. **272**, 413–417 (2007)
199. Aten, A.H.W.: The chemistry of astatine. In: H.J. Emeleus, A.G. Sharpe (eds.) Advances in Inorganic Chemistry, vol. 6, pp. 207–223. Academic, San Diego, CA (1964)
200. Brown, I.: Astatine: Its organonuclear chemistry and biomedical application. In: H.J. Emeleus, A.G. Sharpe (eds.) Advances in Inorganic Chemistry, vol. 31, pp. 43–88. Academic, San Diego, CA (1987)
201. Blower, P.J.: Inorganic pharmaceuticals: Astatine. Annu. Rep. Prog. Chem. Sect. A **96**, 655 (2000)
202. Schwerdtfeger, P.: Second-order Jahn-Teller distortions in group 17 fluorides EF_3 (E = Cl, Br, I, At). Large relativistic bond angle changes in AtF_3. J. Phys. Chem. **100**, 2968–2973 (1996)
203. Bae, C., Han, Y.K., Lee, Y.S.: Spin-orbit and relativistic effects on structures and stabilities of group 17 fluorides EF_3 (E = I, At and Element 117): Relativity induced stability for the D_{3h} structure of $(117)F_3$. J. Phys. Chem. A **107**, 852–858 (2003)
204. Pyykkö, P., Lohr, L.L.: Relativistically parameterized exrended Hückel calculations. 3. Structure and bonding for some compounds of uranium and other heavy elements. Inorg. Chem. **20**, 1950–1959 (1981)
205. Pruszyński, M., Bilewicz, A., Was, B., Petelenz, B.: Formation and stability of astatide-mercury complexes. J. Radioanal. Nucl. Chem. **268**, 91–94 (2006)
206. Pruszyński, M., Bilewicz, A., Zalutsky, M.R.: Preparation of Rh[16aneS$_4$-diol]^{211}At and Ir[16aneS$_4$-diol]^{211}At complexes as potential precursors for astatine radiopharmaceuticals. Part 1: Synthesis. Bioconjug. Chem. **19**, 958–965 (2008)
207. Roy, K., Lahiri, S.: Production and separation of astatine radionuclides: Some new addition to astatine chemistry. Appl. Radiat. Isot. **66**, 571–576 (2008)
208. Baran, E.J.: Vibrational properties for hydrogen astatide, HAt. Z. Naturforsch. A **59**, 133–135 (2004)
209. Saue, T., Faegri, K., Gropen, O.: Relativistic effects on the bonding of heavy and superheavy hydrogen halides. Chem. Phys. Lett. **263**, 360–366 (1996)
210. Stewart, M., Rösler Bickelhaupt, F.M.: Proton affinities in water of maingroup-element hydrides—effects of hydration and methyl substitution. Eur. J. Inorg. Chem. 3646–3654 (2007)
211. Dolg, M., Küchle, W., Stoll, H., et al.: *Ab Initio* pseudopotentials for Hg to Rn II. Molecular calculations on the hydrides of Hg to At and the fluorides of Rn. Mol. Phys. **74**, 1265–1285 (1991)
212. Vasilescu, I.J.: On the existence, structure and properties of radon compounds. Rev. Roum. Chim. **12**, 835–838 (1967)

213. Holloway, J.H., Hope, E.G.: Recent advances in noble-gas chemistry. In: A.G. Sykes (ed.) Advances in Inorganic Chemistry, vol. 46, pp. 51–100. Academic, San Diego, CA (1999)
214. Malli, G.L.: Relativistic all-electron Dirac-Fock calculations on RnF_6 and its ions. J. Mol. Struct (Theor Chem). **537**, 71–77 (2001)
215. Filatov, M., Cremer, D.: Bonding in radon hexafluoride: An unusual relativistic problem? Phys. Chem. Chem. Phys. **5**, 1103–1105 (2003)
216. Kaupp, M., van Wüllen, Ch., Franke, R., et al.: The structure of XeF_6 and compounds isoelectronic with it. A challenge to computational chemistry and to the qualitative theory of the chemical bond. J. Am. Chem. Soc. **118**, 11939–11950 (1996)
217. Stein, L., Hohorst, F.A.: Collection of radon with solid oxidizing reagents. Environ. Sci. Technol. **16**, 419–422 (1982)
218. Stein, L.: New evidence that radon is a metalloid element: Ion-exchange reactions of cationic radon. J. Chem. Soc., Chem. Commun. 1631–1632 (1985)
219. Buchachenko, A.A., Klos, J., Szczesniak, M.M., et al.: Interaction potentials for B-Rg (Rg = He-Rn): Spectroscopy and transport coefficients. J. Chem. Phys. **125**, 064305/1–12 (2006)
220. Malli, G.L.: Prediction of the existence of radon carbonyl: RnCO. Int. J. Quantum Chem. **90**, 611–615.
221. Li, K., Xue, D.: Estimation of electronegativity values of elements in different valence states. J. Phys. Chem. A **110**, 11332–11337 (2006)
222. Eliav, E., Vilkas, M.J., Ishikawa, Y., Kaldor, U.: Ionization potentials of alkali atoms: Towards meV accuracy. Chem. Phys. **311**, 163–168 (2005)
223. Landau, A., Eliav, E., Ishikawa, Y., Kaldor, U.: Benchmark calculations of electron affinities of the alkali atoms sodium to eka-Francium. J. Chem. Phys. **115**, 2389–2392 (2001)
224. Lupinetti, C., Thakkar, A.J.: Polarizabilities of the alkali anions Li^- to Fr^-. J. Chem. Phys. **125**, 194317/1–7 (2006)
225. Aymar, M., Dulieu, O., Spiegelman, F.: Electronic properties of francium diatomic compounds and prospects for cold molecule formation. J. Phys. B: At. Mol. Opt. **39**, S905-S927 (2006)
226. Lee, E.P.F., Wright, T.G.: Ground electronic states of $RbO_2{}^+$, $CsO_2{}^+$ and FrO_2: The ionization energies of RbO_2 and CsO_2. J. Phys. Chem. A **109**, 3257–3261 (2005)
227. Hickling, H.L., Viehland, L.A., Shepherd, D.T., et al.: Spectroscopy of $M^+ \bullet Rg$ and transport coefficients of M^+ in Rg (M = Rb-Fr; Rg = He-Rn). Phys. Chem. Chem. Phys. **6**, 4233–4239 (2004)
228. Zielińska, B., Bilewicz, A.: Influence of relativistic effects on hydrolysis of Ra^{2+}. J. Radioanal. Nucl. Chem. **266**, 339–341 (2005)
229. Lee, E.P.F., Soldán, P., Wright, T.G.: The heaviest group 2 difluoride, RaF_2: Geometry and ionization energy. Inorg. Chem. **40**, 5979–5984 (2001)
230. Lee, E.P.F., Wright, T.G.: The heaviest group 2 dihalide: $RaAt_2$. Chem. Phys. Lett. **374**, 176–182 (2003)
231. Gumiński, C.: The Hg-Ra (Mercury-Radium) system. J. Phase. Equil. Diff. **26**, 80 (2005)
232. Schädel, M. (ed.).: The Chemistry of the Superheavy Elements. Kluwer, Dordrecht (2003)
233. Pershina, V.: The chemistry of the superheavy elements and relativistic effects. In: P. Schwerdtfeger (ed.) Relativistic Electronic Structure, vol. 2, pp. 1–80. Elsevier, Amsterdam (2004)
234. Kemsley, J.: Extreme elements. Chem. Eng. News. (June), 42–43 (2008)
235. Bonchev, D., Kamenska, V.: Predicting the properties of the 113–120 transactinide elements. J. Phys. Chem. **85**, 1177–1186 (1981)
236. Han, Y.K., Bae, C., Son, S.K., Lee, Y.S.: Spin-orbit effects on the transactinide p-Block element monohydrides MH (M = Element 113–118). J. Chem. Phys. **112**, 2684–2691 (2000)
237. David, J., Fuentealba, P., Restreppo, A.: Relativistic effects on the hexafluorides of group 10 metals. Chem. Phys. Lett. **457**, 42–44 (2008)

238. Patzschke, M., Pyykkö, P.: Darmstadtium carbonyl and carbide resemble platinum carbonyl and carbide. Chem. Commun. 1982–1983 (2004)
239. De Macedo, L.G.M., Sambrano, J.R., De Souza, A.R., Borin, A.C.: All electron fully relativistic Dirac-Fock calculation for darmstadtium carbide using prolapse free basis set. Chem. Phys. Lett. **440**, 367–371 (2007)
240. Ionova, G.V., Ionova, I.S., Mikhalko, V.K., et al.: Halides of tetravalent transactinides (Rg,Db,Sg,Bh,Hs,Mt, 110th Element): Physicochemical properties. Russ. J. Coord. Chem. **30**, 352–359 (2004)
241. Eliav, E., Kaldor, U., Schwerdtfeger, P., et al.: Ground state electron configuration of element 111. Phys. Rev. Lett. **73**, 3203–3206 (1994)
242. Hancock, R.D., Bartolotti, L.J., Kaltsoyannia, H.: Density functional theory-based prediction of some aqueous-phase chemistry of superheavy element 111. Roentgenium(I) is the "Softest" metal ion. Inorg. Chem. **45**, 10780–10785 (2006)
243. Seth, M., Schwerdtfeger, P., Dolg, M., et al.: Large relativistic effects in molecular properties of the hydride of superheavy element 111. Chem. Phys. Lett. **250**, 461–465 (1996)
244. Gaston, N., Opahle, I., Gäggeler, H.W., Schwerdtfeger, P.: Is Eka-Mercury (Element 112) a group 12 metal? Angew. Chem. Int. Ed. Engl. **46**, 1663–1666 (2007)
245. Guang, L.J., Zhong, D.C., Jun, Y.Y., et al.: The atomic structure and the properties of ununbium(Z = 112) and mercury(Z = 80). Sci. China G **50**, 707–715 (2007)
246. Eichler, R., Aksenov, N.V., Belozerov, A.V., et al.: Confirmation of the decay of ^{283}112 and first indication for Hg-like behavior of element 112. Nucl. Phys. A **787**, 373c-380c (2007)
247. Eichler, R., Aksenov, N.V., Belozerov, A.V., et al.: Chemical characterization of element 112. Nature **447**, 72–75 (2007)
248. Eichler, R., Aksenov, N.V., Belozerov, A.V., et al.: Thermochemical and physical properties of element 112. Angew. Chem. Int. Ed. Engl. **47**, 3262–3266 (2008)
249. Pershina, V., Bastug, T., Jacob, T., et al.: Intermetallic compounds of the heaviest elements: The electronic structure and bonding of dimers of element 112 and its homolog Hg. Chem. Phys. Lett. **365**, 176–183 (2002)
250. Bae, C., Choi, Y.J., Lee, Y.S.: Two-component spin-orbit calculations for the heterodiatomic molecules TlAt and (113)(117) with relativistic effective core potentials. Chem. Phys. Lett. **375**, 65–71 (2003)
251. Eliav, E., Kaldor, U., Ishikawa, Y., et al.: Calculated energy levels of thallium and eka-thallium(Element 113). Phys. Rev. A **53**, 3926–3933 (1996)
252. Yu, Y.J., Dong, C.Z., Li, J.G., Fricke, B.: The excitation energies, ionization potentials and oscillator strengths of neutral and ionized species of Uuq (Z = 114) and the homolog elements Ge,Sn and Pb. J. Chem. Phys. **128**, 124316/1–7 (2008)
253. Seth, M., Faegri, K., Schwerdtfeger, P.: The stability of the oxidation state +4 in group 14 compounds from carbon to element 114. Angew. Chem. Int. Ed. Engl. **37**, 2493–2496 (1998)
254. Guseva, L.I.: A study of ion-exchange behavior of Pb in dilute HBr solutions, aimed to evaluate the possibility of on-line isolation of element 114. ^{228}Ra – ^{212}Pb generator. Radiochemistry **49**, 92–96 (2007)
255. Guseva, L.I.: A comparative study of ion-exchange behavior of Hf and Pb as homologs of elements 104(Rf) and 114, respectively, in solutions of hydrohalic acids. Relativistic Effects Radiochem. **50**, 186–190 (2008)
256. Pershina, V., Anton, J., Fricke, B.: Intermetallic compounds on the heaviest elements and their homologs: The electronic structure and bonding of MM', where M = Ge,Sn,Pb, and element 114 and M' = Ni,Pd,Pt,Cu,Ag,Au,Sn,Pb and element 114. J. Chem. Phys. **127**, 134310/1–9 (2007)
257. Pershina, V., Borschevsky, A., Eliav, E., Kaldor, U.: Prediction of the adsorption behavior of elements 112 and 114 on inert surfaces from *Ab Initio* Dirac-Coulomb atomic calculations. J. Chem. Phys. **128**, 024707/1–9 (2008)

258. Giju, K.T., De Proft, F., Geerlings, P.: Comprehensive study of density functional theory based properties for group 14 atoms and functional groups, -XY_3 (X = C, Si, Ge, Sn. Pb, Element 114; Y = CH_3, H, F, Cl, Br, I, At). J. Phys. Chem. A **109**, 2925–2936 (2005)
259. Keller, O.L., Nestor, C.W., Fricke, B.: Predicted properties of the superheavy elements. III. Element 115, eka-bismuth. J. Phys. Chem. **78**, 1945–1949 (1974)
260. Van Wüllen, C., Langermann, N.: Gradients for two-component quasirelativistic methods. Application to dihalogenides of element 116. J. Chem. Phys. **126**, 114106/1–9 (2007)
261. Nash, C.S., Crockett, W.W.: An anomalous bond angle in (116)H_2. Theoretical evidence for supervalent hybridization. J. Phys. Chem. A **110**, 4619–4621 (2006)
262. Takahashi, N.: Boiling points of the superheavy elements 117 and 118. J. Radioanal. Nucl. Chem. **251**, 299–301 (2002)
263. Faegri, K., Saue, T.: Diatomic molecules between very heavy elements of group 13 and group 17: A study of relativistic effects on bonding. J. Chem. Phys. **115**, 2456–2464 (2001)
264. Nash, C.S., Bursten, B.E.: Spin-orbit effects on the electronic structure of heavy and superheavy hydrogen halides. J. Phys. Chem. A **103**, 632–636 (1999)
265. Mitin, A.V., van Wüllen, C.: Two-component relativistic density-functional calculations of the dimers of the halogens from bromine through element 117 using core potential and all-electron methods. J. Chem. Phys. **124**, 064305/1–7 (2006)
266. Eliav, E., Kaldor, U., Ishikawa, Y., Pyykkö, P.: Element 118: The first rare gas with an electron affinity. Phys. Rev. Lett. **77**, 5350–5352 (1996)
267. Nash, C.S., Bursten, B.E.: Spin-orbit effects, VSEPR theory and the electronic structures of heavy and superheavy group IVA hydrides and group VIIIA tetrafluorides. A partial role reversal for elements 114 and 118. J. Phys. Chem. A **103**, 402–410 (1999)
268. Han, Y.K., Lee, Y.S.: Structures of RgF_n (Rg = Xe, Rn and Element 118. n = 2,4) calculated by two-component spin-orbit methods. A spin-orbit induced isomer of (118)F_4. J. Phys. Chem. A **103**, 1104–1108 (1999)
269. Mişicu, Ş., Bürvenich, T., Cornelius, T., Greiner, W.: Collective ex-citations of the element Z = 120. Phys. Atom. Nucl. **66**, 1552–1556 (2003)

CHAPTER 3

WHY DO WE NEED RELATIVISTIC COMPUTATIONAL METHODS?

Chemical Intuition Versus Experimental and Theoretical Results

JACEK STYSZYŃSKI

Instytut Fizyki, Uniwersytet Szczeciński, Wielkopolska 15, 70-51 Szczecin, Poland,
fax: +48/91/444-12-26
e-mail: jstysz@wmf.univ.szczecin.pl

Abstract: Inclusion of relativistic effects is required for proper description of atomic and molecular properties, when electrons approach the region of space with high potential energy near the nuclei. The effects become particularly important for the systems with heavy and very heavy atoms leading to significant changes in the energetic structure of the molecule and in the values of spectroscopic molecular parameters, influencing the mechanism and character of the bonds. This chapter reviews the relativistic *ab initio* all electron four component calculations for molecular systems, whose results show that in many cases the nonrelativistic description is inadequate and cannot explain certain trends of properties observed and that the inclusion of relativistic effects is mandatory for correct predictions of molecular properties.

Keywords: Relativistic four component methods, Dirac-Fock method relativistic corrections, Electron correlation, Correlation-relativistic cross terms, Spectroscopic constants

3.1. INTRODUCTION

Relativistic theory of atoms and molecules can be considered as a simplification of the description provided by quantum electrodynamics in which particles interact by exchange of photons. The effective Hamiltonian for an N-electron system derived from this description can be written as a sum of N one-electron Dirac operators for an electron moving in the classical field of nucleons, Coulomb interelectron repulsion term and Breit operator representing relativistic corrections to this interaction. Such a Hamiltonian is known in literature as the Dirac-Coulomb-Breit Hamiltonian (DCB). The omission of the Breit operator leads directly to the Dirac-Coulomb Hamiltonian (DC). The techniques and methods used to solve the DCB (DC) eigenvalue problem were derived as a analogue of methods of solving the Schrödinger equation for N-electron system.

M. Barysz and Y. Ishikawa (eds.), *Relativistic Methods for Chemists*,
Challenges and Advances in Computational Chemistry and Physics 10,
DOI 10.1007/978-1-4020-9975-5_3,

The relativistic self consistent field (SCF) formalism for atoms was derived in 1935 by Bertha Swirles [1] and later reformulated using Racah's tensor operators by I.P. Grant [2]. This allowed construction of programs solving the Dirac-Fock (DF) equations for atoms in their general multiconfigurational version: Multiconfigurational Dirac-Fock Package (MCDF). One of them was developed by Desclaux and coworkers [3], while the other by the Oxford group of Grant [4]. These two programs in principle permit accurate solutions of the DF and MCDF equations for atoms and became standard tools in atomic physics.

For molecular systems, numerical solution of the DF equations is in practice impossible (except for diatomic molecules) and their algebraic form, the Dirac-Fock-Roothan (DFR) equations, have to be solved. A closed shell molecular Dirac-Fock equations was first proposed by Malli and Oreg [5], who expanded molecular spinors as a linear combination of atomic four-component spinors. The crucial point in developing a relativistic four-component methods for molecules was the introduction of the so called *kinetic balance* condition [6–9], which determines the relation between basis set functions of large and small component of a one electron spinor. This relation ensures the convergence to the non-relativistic limit upon enlarging the value of the speed of light c to infinity and enables the correct separation of an approximate one electron Hamiltonian spectrum into electron (positive-energy) and positron (negative-energy) part. One should also be aware that in relativistic calculations a more physical model of finite nucleus is used, which removes a weak singularity at the origin for the radial part of one electron spinors, which characterizes the solutions of Dirac equation for point nucleus potential. The *ab initio* all electron four-component relativistic DFR programs were developed at a number of research centres, some of the programs were distributed freely to academic users. The MOLFDIR program package [10] was developed by the group of Nieuwpoort in Groningen. Its first closed shell version, written by P. J. C. Aerts was ready in 1984. L. Visscher implemented the correlated methods in this package: the general multi-reference CI (MRCI) and the coupled cluster method (CC). In this way a range of correlation treatments in the four component formalism has been developed, from no correlation in the DF method, through the second-order Møller-Plesset perturbation theory (MP2), the configuration interaction with single and double substitutions (CISD), the coupled cluster with single and double substitutions (CCSD) to the most recent method, perturbatively corrected for the effect of triple excitations (CCSD(T)). The DIRAC program package implements the direct SCF method. Its first version was programmed by T. Saue. At present, DIRAC is probably the most advanced relativistic four component molecular code [11], developed by the international community of relativistic quantum chemists, with the same range of electron correlation treatment as the MOLFDIR package, additionally equipped with the code to calculate various molecular properties including the propagator method within the Random Phase Approximation (RPA).

Inclusion of relativistic effects is required for proper description of atomic and molecular properties when electrons approach the region of space near nuclei with high potential energy. These effects become particularly important for systems with heavy and super heavy ($Z >= 104$) elements. There are many methods which

take into account relativistic effects in approximate ways, such as perturbation theory, relativistic pseudo-potential or density functional methods. All these methods can be derived from the DCB equation and therefore solution of this equation provides direct reference results for more approximate treatment of relativistic effects. This chapter presents results of the *ab initio* all electron four component calculations for molecular systems, which prove that in many cases the nonrelativistic description is just inadequate and cannot explain certain trends of properties observed and the inclusion of relativistic effects is mandatory for correct predictions of molecular properties. In these calculations the basis sets for large and small components fulfilling the kinetic balance conditions have been used. The commonly used symbols of basis sets are employed, i.e. TZ – triple zeta, VTZ – valence triple zeta, pVTZ – polarized valence triple zeta, aug-pVTZ – the latter one augmented with extra diffuse functions, etc.

The relativistic effects can be analyzed in terms of direct and indirect effects. The direct relativistic effects (the effects of dynamics) are responsible for the radial contraction and energetic stabilization of the $s_{1/2}$ and $p_{1/2}$ shells as well as for the spin-orbit splitting of shells with $l > 0$ into subshells with $\mathrm{j} = l - 1/2$ and $\mathrm{j} = l + 1/2$. The indirect relativistic effects (i.e. the effects of potential) are consequences of a more efficient screening of the d and f electrons by inner electrons occupying the contracted $s_{1/2}$ and $p_{1/2}$ orbitals and lead to the radial expansion of the d and f shells accompanied by their energetic destabilization. For $p_{3/2}$ subshells both effects approximately cancel.

The values of the relativistic effects for a given quantity X are usually calculated as a difference between the relativistic and nonrelativistic values of this quantity, i.e. $\Delta\mathrm{X} = \mathrm{X(rel)} - \mathrm{X(nrel)}$ calculated at the same level of theory. Therefore, most relativistic all electron four component calculations reported here are accompanied by the corresponding calculations with the nonrelativistic version of the same method. The prefix DC indicates the relativistic version of given method, for example DC-CCSD stands for the relativistic four component CCSD method.

3.2. ENERGETIC STRUCTURE AND SPECTROSCOPIC CONSTANTS

3.2.1. Diatomic Molecules

3.2.1.1. Coinage Metal Molecules

Coinage metal atoms are well known many electron systems in which relativistic effects are particularly pronounced. This phenomenon is due to the interplay of direct and indirect relativistic effects and leads to the so-called "maximum for gold rule" [12, 13]. According to this rule, for a given row of the periodic table, relativistic effects on bond distances and fundamental frequencies are the largest for the molecules containing group 11 atoms. Dyall and Fægrii [14] plotted (see Figure 3-1) the relative shrinkage of the mean radius and the relative eigenvalue decrease of the 6s orbital across the sixth row of the periodic table. They explained the trend

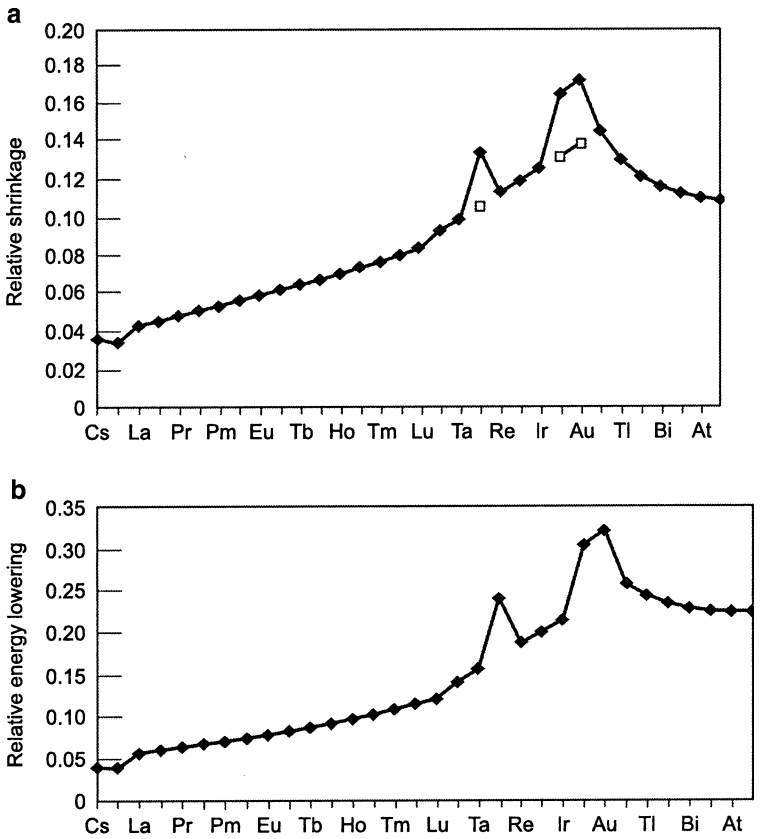

Figure 3-1. Variation in the relative mean radius (**a**) and the relative eigenvalue (**b**) of the *6s* orbital across the sixth row of the periodic table (Figure 22.1 [p. 456] from "Introduction to Relativistic Quantum Chemistry" by Dyall, K.G. and Fægri, Jr., K. [2007]. By permission of Oxford University Press, Inc.)

observed as the interplay of the direct (contraction of 6s orbital and its energetic stabilization) and indirect (the weakening screening of the 6s shell due to the filling of the valence d and f shells and their spatial expansion) relativistic effects. In these considerations the conventional free atom configuration with two electrons on the 6s orbital has been used, except for W, Pt and Au, for which one 6s-electron was assumed. The electronic configuration with singly occupied 6s orbital additionally increases the direct relativistic effects, which explains the pronounced peaks obtained for these atoms. Results obtained for the $5d^n6s^2$ configurations of W, Pt and Au lead to the regular behaviour of relative decrease in the mean radius of the 6s orbital. A combination of the above mentioned effects makes the molecules containing coinage metal atoms particularly interesting objects to study the role of relativistic effects for correct prediction of the energetic structure and spectroscopic properties of molecules as well as for testing different calculation methods taking into account the relativistic effects.

Table 3-1 Bond length R_e, fundamental frequency ν_e and dissociation energy D_e of CuH, AgH and AuH calculated using the nonrelativistic and relativistic HF and MP2 methods. For comparison experimental values are also given

Molecule	Ref.	Method	R_e(Å)	ν_e(cm^{-1})	D_e(eV)
CuH	[16]	HF	1.569	1,642	1.416
		DF	1.541	1,699	1.477
		MP2	1.454	2,024	2.585
		DC-MP2	1.428	2,101	2.711
	[19]	Expt.	1.463	1,941	2.85
AgH	[15]	HF	1.774	–	1.23
		DF	1.697	–	1.31
	[16]	HF	1.779	1,473	1.126
		DF	1.700	1,605	1.233
		MP2	1.663	1,699	1.986
		DC-MP2	1.585	1,873	2.195
	[18]	DF	1.691	–	1.439
	[19]	Expt.	1.618	1,760	2.39
AuH	[15]	HF	1.80	–	1.11
		DF	1.64	–	1.53
	[16]	HF	1.831	1,464	1.084
		DF	1.570	2,067	1.778
		MP2	1.711	1,695	1.901
		DC-MP2	1.497	2,496	3.114
	[17]	DF	1.570	2,091	1.778
		DC- CISD	1.531	2,296	2.864
	[19]	Expt.	1.524	2,305	3.36

Lee and McLeen [15] in their pioneer paper have reported results of the Dirac-Fock calculations on the AgH and AuH molecules. In their study they have exploited the Slater type uncontracted basis sets of DZ quality, which fulfil the kinetic balance condition for large and small components. Table 3-1 presents the values of bond length R_e, fundamental frequency ν_e and dissociation energy D_e obtained by Lee and McLeen using the HF and DF methods. Coinage metal hydrides have also been studied using the four component methods by Collins et al. [16], Saue and Visscher [17] and Mohanty and Parpia [18]. Results of their calculations are also given in Table 3-1. Collins et al. used the four component DF and MP2, while Saue and Visscher the DF and CI methods. Results of Mohanty and Parpia were obtained with the DF method. These authors used different basis sets that satisfied the kinetic balance condition. Table 3-2 gives the relativistic corrections to spectroscopic constants of CuH, AgH and AuH. The values presented in both tables show that the inclusion of relativistic effects leads to the bond length contraction by about 0.03, 0.08 and 0.21–0.26 Å, for CuH, AgH and AuH, respectively. Taking into account the relativistic effects increases the values of the fundamental frequency ν_e and dissociation energy D_e. For AuH these effects are large, 600–800 cm^{-1} for ν_e and 0.7–1.2 eV for D_e, which shows that the relativistic effects are important for the series of coinage metal hydrides. A comparison with experiments shows that

Table 3-2 Relativistic corrections to spectroscopic properties from Table 3-1

Molecule	Ref.	Method	ΔR_e(Å)	$\Delta\nu_e(cm^{-1})$	ΔD_e(eV)
CuH	[16]	DF	−0.028	57	0.061
		DC-MP2	−0.026	77	0.126
AgH	[15]	DF	−0.077	–	0.080
	[16]	DF	−0.079	132	0.107
		DC-MP2	−0.078	174	0.209
AuH	[15]	DF	−0.160	–	0.420
	[16]	DF	−0.261	603	0.694
		DC-MP2	−0.214	801	1.213
	[17]	DF	−0.261	627	0.694

the nonrelativistic results are far from the experimental values [19]. The calculation errors for R_e, ν_e and D_e obtained by Collins et al. [16] using nonrelativistic and relativistic versions of the SCF and MP2 methods are given in Figure 3-2. As shown, the error increases across the series for nonrelativistic SCF calculations. A similar behaviour is observed for the correlated MP2 results. The inclusion of relativistic effects changes this trend, while the error is smaller and not increasing. The error in the bond length grows from 7% to 20% (HF) and 1% to 12% (MP2) across the series, while it remains approximately constant, about 5% (DF) and 2% (DC-MP2), when relativity is included. It is worth noticing slightly different values of the relativistic corrections for R_e, ν_e and D_e obtained using SCF and correlated methods, which indicates that the relativistic and correlation effects are not independent.

Lærdahl, Saue and Fægri [20] studied the properties of the coinage metal fluorides. They have performed the four-component DF and MP2 calculations for the ground states ($^1\Sigma^+$) of CuF, AgF and AuF using uncontracted dual family basis sets. The basis set for the fluorine atom was generated for the negative ion F^- for proper description of strongly polar bond in the coinage metal fluorides. In the correlated calculations the active space of virtual spinors was restricted to those with energy smaller than 100 a.u., while the active occupied space included 18 (MP2/a) and 26 (MP2/b) valence electrons. Table 3-3 presents the values of the bond lengths R_e and the vibrational frequencies ν_e obtained by Lærdahl et al. [20] for the ground state of the CuF, AgF and AuF molecules. Table 3-4 contains the values of relativistic corrections for the spectroscopic constants from Table 3-3. As follows, the relativistic effects shorten the bond length by 0.02, 0.04 and 0.18 Å on the SCF level and by 0.03, 0.05 and 0.2 Å on the correlated level. The relativity increases the values of the vibrational frequencies ν_e. This effect is the largest for AuF and equals 85 cm^{-1} (DF) and 127 cm^{-1} (MP2). It is worth noting that in contrast to the coinage metal hydrides, the electron correlation increases the value of relativistic corrections for the fluorides. For example, the bond length contraction ΔR_e for AuF increases from 0.178 Å (DF) to 0.204 Å (MP2). A comparison of the values of the relativistic bond length contraction for AuH and AuF also shows that the inclusion of electron correlation leads to a much smaller difference in ΔR_e at the MP2 level. The extension of the active space from 18 to 26 electrons leads to a significant change in the values of

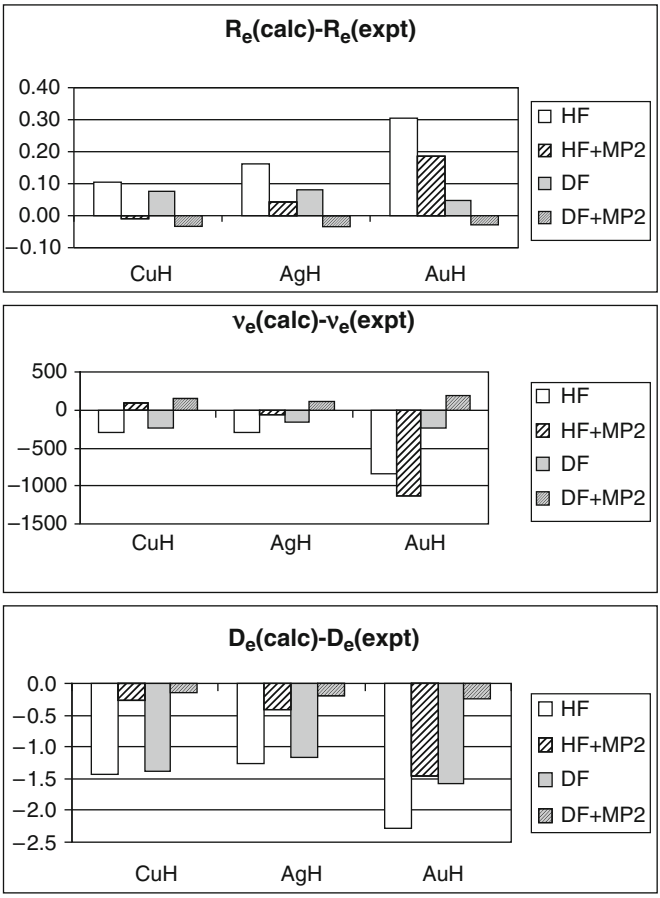

Figure 3-2. Comparison of the calculated and experimental values of the bond length R_e(Å), fundamental frequency ν_e(cm^{-1}) and dissociation energy D_e(eV) of the coinage metal hydrides (From [16])

the spectroscopic constants of the series of CuF, AgF and AuF molecules. A comparison with experiment can be made only for the first two members of the series, since the experimental data [19] for the AuF molecule are not available. The errors in the calculations of the bond distance R_e and vibrational frequency ν_e of the CuF and AgF molecules are given in Figure 3-3. Again, we can notice that for the nonrelativistic methods the error for R_e increases, when going from lighter to heavier molecules, while the inclusion of relativistic effects reduces the value of the error.

Saue and coworkers studied the effect of relativity on the spectroscopic constants of the homologous series CuCs, AgCs and AuCs. The results of that study were published in two papers: Saue et al. [21] and Fossgaard et al. [22]. The authors performed nonrelativistic and four-component relativistic SCF, MP2 and CCSD(T) calculations employing uncontracted dual family Gaussian basis sets. They correlated 38 electrons: *4d5s5p6s* of the Cs atom and *(n-1)s(n-1)p(n-1)d* electrons of the

Table 3-3 Bond lengths R_e and fundamental frequencies ν_e for the CuF, AgF and AuF molecules obtained by Lærdahl et al. [20] using the nonrelativistic and relativistic versions of SCF and MP2 methods [20]. MP2/a and MP2/b correspond to the results obtained with 18 and 26 valence electrons, respectively, included in the active occupied space. Experimental values taken from Huber, Herzberg [19]

Molecule	Method	R_e(Å)	ν_e(cm^{-1})
CuF	HF	1.823	563
	MP2/a	1.754	606
	MP2/b	1.751	612
	DF	1.805	572
	DC-MP2/a	1.728	627
	DC-MP2/b	1.725	633
	Expt.	1.745	623
AgF	HF	2.069	472
	MP2/a	2.033	491
	MP2/b	2.026	496
	DF	2.029	491
	DC-MP2/a	1.987	515
	DC-MP2/b	1.977	521
	Expt.	1.983	513
AuF	HF	2.146	443
	MP2/a	2.113	458
	MP2/b	2.103	463
	DF	1.968	528
	DC-MP2/a	1.916	571
	DC-MP2/b	1.899	590

Table 3-4 Relativistic corrections to the bond length and harmonic frequency of CuF, AgF and AuF obtained by Lærdahl et al. [20] using DF and MP2 methods

Molecule	Method	ΔR_e(Å)	$\Delta\nu_e$(cm^{-1})
CuF	DF	−0.018	9
	DC-MP2/a	−0.026	21
	DC-MP2/b	−0.026	21
AgF	DF	−0.040	19
	DC-MP2/a	−0.046	24
	DC-MP2/b	−0.049	25
AuF	DF	−0.178	85
	DC-MP2/a	−0.197	113
	DC-MP2/b	−0.204	127

M atom (M = Cu, Ag and Au). In this way the core-valence correlation effects were partially taken into account. The bond distances R_e, harmonic frequencies ν_e, anharmonic constants $\nu_e x_e$ and dissociation energies D_e obtained by these authors

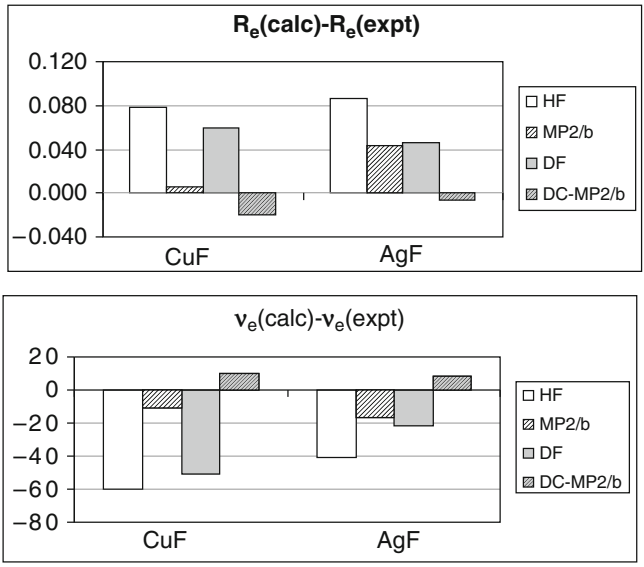

Figure 3-3. The difference between the calculated and experimental values of bond length R_e(Å) and vibrational frequency ν_e(cm^{-1}) for the CuF and AgF molecules (From [20])

are given in Table 3-5, while the relativistic corrections to these quantities are given in Table 3-6. As follows from these data, the relativity is responsible for the contraction of the bond. This effect is large and increasing along the series of the CsM molecules (M = Cu, Ag, Au). On the DF level, the contraction is 0.09, 0.18 and 0.41 Å for CuCs, AgCs and AuCs, respectively, while on the CCSD(T) level the corresponding numbers are: 0.08, 0.14 and 0.31 Å. The electron correlation for these molecules reduces the relativistic contraction of the bond length. The inclusion of the relativistic effects increases the values of the fundamental frequencies and covalent dissociation energy. The increase in ν_e is small for AuCs around 22 cm^{-1}, while the increase in D_e is 1.18 eV at the CCSD(T) level. The results show the relativistic strengthening of the bond. In particular for CsAu the dissociation energy is almost doubled. The value of D_e obtained at the DC-CCSD(T) level of theory agrees very well with the experimental value of 2.53 eV [22, 23]. The relativistic effect on anharmonicity is negligible and the trend is difficult to identify because of the small numerical values describing this property as well as its sensitivity to the approximate energy values. Figure 3-4 presents the ratio of relativistic and nonrelativistic CCSD(T) values of the spectroscopic constants R_e, ν_e and D_e for the MCs (M = Cu, Ag and Au) series. We can see from this figure that the stabilization of the bond is accompanied by a relativistic bond length contraction. The electron correlation further strengthens and contracts the bond and causes an increase in the values of the fundamental frequencies. Differences between the correlated and SCF results obtained by the nonrelativistic and relativistic calculations are given in Table 3-7. As indicated by these data the electron correlation effect on bond length is huge and

Table 3-5 Bond length R_e, fundamental frequency ν_e, anharmonic constant $\nu_e x_e$ and covalent dissociation energy D_e^{cov} obtained by Fossgaard et al. [22] for the CuCs, AgCs and AuCs molecules

Molecule	Method	R_e(Å)	$\nu_e(cm^{-1})$	$\nu_e x_e(cm^{-1})$	D_e^{cov}(eV)
CuCs	HF	3.638	79	0.2	0.95
	DF	3.545	83	0.2	0.98
	MP2	3.207	104	0.5	1.48
	DC-MP2	3.125	109	0.1	1.55
	CCSD(T)	3.277	97	0.2	1.31
	DC-CCSD(T)	3.198	102	0.1	1.36
AgCs	HF	3.817	64	0.1	0.94
	DF	3.641	71	0.1	1.16
	MP2	3.376	85	0.1	1.43
	DC-MP2	3.230	96	0.2	1.70
	CCSD(T)	3.459	79	0.0	1.26
	DC-CCSD(T)	3.316	88	0.2	1.51
AuCs	HF	3.826	57	0.1	1.11
	DF	3.413	79	0.1	2.31
	MP2	3.522	71	0.1	1.46
	DC-MP2	3.204	94	0.3	2.66
	CCSD(T)	3.571	68	0.1	1.34
	DC-CCSD(T)	3.263	89	0.2	2.52
	Expt.[a]	–	–	–	2.53

[a]Estimated by Fossgaard et al. [22] using results of [23]

Table 3-6 Relativistic corrections to R_e, ν_e, $\nu_e x_e$ and D_e^{cov} from Table 3-5 for the CuCs, AgCs and AuCs molecules

Molecule	Method	ΔR_e(Å)	$\Delta\nu_e(cm^{-1})$	$\Delta\nu_e x_e(cm^{-1})$	ΔD_e^{cov} (eV)
CuCs	DF	−0.093	4	0.0	0.03
	DC-MP2	−0.082	6	−0.4	0.07
	DC-CCSD(T)	−0.079	5	−0.1	0.05
AgCs	DF	−0.176	7	0.0	0.22
	DC-MP2	−0.146	11	0.1	0.27
	DC-CCSD(T)	−0.143	10	0.2	0.25
AuCs	DF	−0.413	22	0.0	1.20
	DC-MP2	−0.318	23	0.2	1.20
	DC-CCSD(T)	−0.308	22	0.1	1.18

decreases along the CuCs-AgCs-AuCs series of molecules. A similar effect is noted for the covalent dissociation energy.

Fossgaard et al. [22] analyzed the nonrelativistic and relativistic SCF solutions using projection analysis [24], in which the occupied molecular orbitals (MO) are projected onto the orbitals of the neutral atomic fragments M and Cs. This method allows unambiguous expression of MOs in terms of the atomic orbitals [22]. The projection coefficients for the six upper occupied molecular orbitals of CuCs, AgCs and AuCs are given in Table 3-8. For all three molecules HOMO is an almost

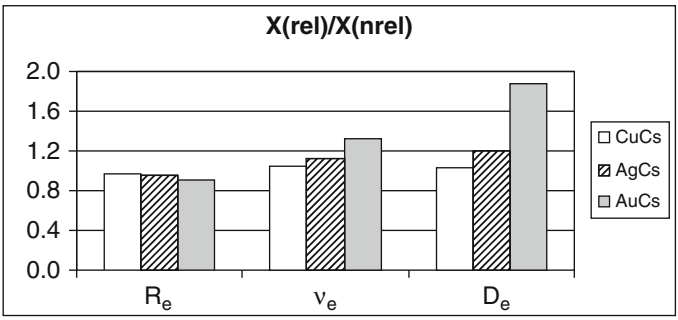

Figure 3-4. Relativistic effects for R_e, ν_e and D_e for a series of the CuCs, AgCs and AuCs molecules calculated using the CCSD(T) method (From [22])

Table 3-7 Differences $\delta X = X(corr) - X(SCF)$ between the correlated and SCF results of Fossgaard et al. [22] from Table 3-5

Molecule	Method	δR_e (A)	$\delta\nu_e(cm^{-1})$	$\delta\nu_e x_e(cm^{-1})$	δD_e^{cov} (eV)
CuCs	MP2	−0.431	24	0.4	0.53
	DC-MP2	−0.420	26	0.0	0.57
	CCSD(T)	−0.361	18	0.0	0.36
	DC-CCSD(T)	−0.347	19	−0.1	0.38
AgCs	MP2	−0.441	21	0.1	0.49
	DC-MP2	−0.411	25	0.1	0.54
	CCSD(T)	−0.358	15	−0.1	0.32
	DC-CCSD(T)	−0.325	17	0.1	0.35
AuCs	MP2	−0.304	14	0.0	0.35
	DC-MP2	−0.209	15	0.2	0.35
	CCSD(T)	−0.255	11	0.0	0.23
	DC-CCSD(T)	−0.150	11	0.1	0.21

pure *ns* orbital of M (Cu, Ag and Au) with a small contribution of Cs$6s$. Five lower MOs are nonbonding $(n-1)d$ orbitals of M. The analysis of Fossgaard et al. [22] has shown that the MCs molecules (M = Cu, Ag, Au) have highly polar bonds with a substantial electron transfer from cesium to copper, silver or gold. The projection analysis results are in qualitative agreement with the conclusions drawn from the Mulliken population analysis [22].

3.2.1.2. Transition Metal Hydrides

Transition metal atoms with their partly filled *nd* orbitals being in close proximity to $(n+1)s$ and $(n+1)p$ ones, posses a large number of low-lying atomic states with strong configurational mixing. Therefore, inclusion of nondynamical and dynamic correlation is required for the correct prediction of the energetic structure of such atomic systems. We can expect the relativistic effects to be also important for these systems, because of the large direct and indirect effects (relativistic contraction of $(n+1)s$ and the expansion of *nd* orbital). For example, the spin-orbit splitting for

Table 3-8 Projection coefficients c_{ji} for six upper occupied MOs of CuCs, AgCs and AuCs obtained using the DF method (From [22])

	ω	1/2	3/2	1/2	3/2	5/2	1/2
CuCs	ε(a.u.)	−0.4120	−0.4117	−0.3982	−0.3980	−0.3980	−0.1581
	Cs(total)	0.0010	0.0000	0.0010	0.0000	0.0000	0.2300
	$6s_{1/2}$	0.0040	0.0000	0.0050	0.0000	0.0000	0.3410
	Cu(total)	0.9990	1.0000	0.9990	1.0000	1.0000	0.7490
	$3d_{3/2}$	1.0000	1.0000	0.0110	0.0050	0.0000	0.0070
	$3d_{5/2}$	0.0110	0.0050	1.0000	1.0000	1.0000	0.0090
	$4s_{1/2}$	0.0040	0.0000	0.0060	0.0000	0.0000	0.8060
AgCs	ε(a.u.)	−0.4543	−0.4529	−0.4297	−0.4290	−0.4279	−0.1576
	Cs(total)	0.0010	0.0000	0.0010	0.0000	0.0000	0.2240
	$6s_{1/2}$	0.0040	0.0000	0.0050	0.0000	0.0000	0.3350
	Ag(total)	0.9990	1.0000	0.9990	1.0000	1.0000	0.7560
	$4d_{3/2}$	1.0000	1.0000	0.0140	0.0240	0.0000	0.0080
	$4d_{5/2}$	0.0130	0.0240	1.0000	1.0000	1.0000	0.0110
	$5s_{1/2}$	0.0050	0.0000	0.0070	0.0000	0.0000	0.8110
AuCs	ε(a.u.)	−0.3961	−0.3932	−0.3310	−0.3293	−0.3268	−0.1902
	Cs(total)	0.002	0.000	0.002	0.000	0.000	0.123
	$6s_{1/2}$	0.006	0.000	0.009	0.000	0.000	0.217
	Au(total)	0.997	1.000	0.995	0.998	1.000	0.861
	$5d_{3/2}$	0.999	1.000	0.011	0.021	0.000	0.013
	$5d_{5/2}$	0.011	0.020	0.999	0.999	1.000	0.028
	$6s_{1/2}$	0.012	0.000	0.025	0.000	0.000	0.897

the $^3D(5d^9 6s^1)$ state of the platinum atom (Z = 78) is of an order of $10,000\,cm^{-1}$, while the singlet-triplet splitting for this configuration is only of $3,800\,cm^{-1}$. Thus, we can predict that relativistic effects will influence the character and mechanism of bonding in the molecules containing a platinum atom. Visscher et al. [25] reported results of the all electron four-component calculations, in which electron correlation was included by means of the CI method. They studied platinum hydride, the simplest molecule with the platinum — hydrogen bond. In their calculations the authors used nonrelativistic basis sets with extra tight functions. The Pt basis set was augmented with diffuse and polarization functions and subjected to general contraction.

According to Mulliken [26], they assumed that the Pt electrons in platinum hydride retain their n, l and $|m_l|$ quantum numbers and that the σ bond is created by *1s* electron of H and *6s* electron of Pt. Thus, the electron configuration of the PtH molecule can be written as $1s^2 2s^2 2p^6 \ldots 5d^9\sigma^2$. There are three terms corresponding to this electron configuration: $^2\Sigma$, $^2\Pi$ and $^2\Delta$. However in the relativistic description, the *5d* shell splits into $5d_{3/2}$ and $5d_{5/2}$ and we obtain two relativistic electron configurations with nine d electrons: $5d^4_{3/2}5d^5_{5/2}\sigma^2_{1/2}$ and $5d^3_{3/2}5d^6_{5/2}\sigma^2_{1/2}$. According to Table 3-9, we have two groups of allowed terms ($\Omega = |M_J|$) corresponding to the above two-electron configurations: $\Omega = 1/2, 3/2, 5/2$ and $\Omega = 1/2, 3/2$. It can be expected that the lower group of states are ordered

Table 3-9 Nonrelativistic and relativistic electron configurations and the corresponding terms for the ground state of platinum hydride

Nonrelativistic		Relativistic	
Electron configuration	Term	Electron configuration	Term
$5d^9\sigma^2 \equiv d^1$	$^2\Sigma$ $^2\Sigma_{1/2}$	$5d^4_{3/2}5d^5_{5/2}\sigma^2_{1/2} \equiv d^1_{5/2}$	$\Omega = 1/2, 3/2, 5/2$
$\lvert m_\ell \rvert = 0, 1, 2$	$^2\Pi$ $^2\Pi_{1/2}, {}^2\Pi_{3/2}$	$\lvert m_j \rvert = 1/2, 3/2, 5/2$	
$s = 1/2$	$^2\Delta$ $^2\Delta_{3/2}, {}^2\Delta_{5/2}$	$5d^3_{3/2}5d^6_{5/2}\sigma^2_{1/2} \equiv d^1_{3/2}$	$\Omega = 1/2, 3/2$
		$\lvert m_j \rvert = 1/2, 3/2$	

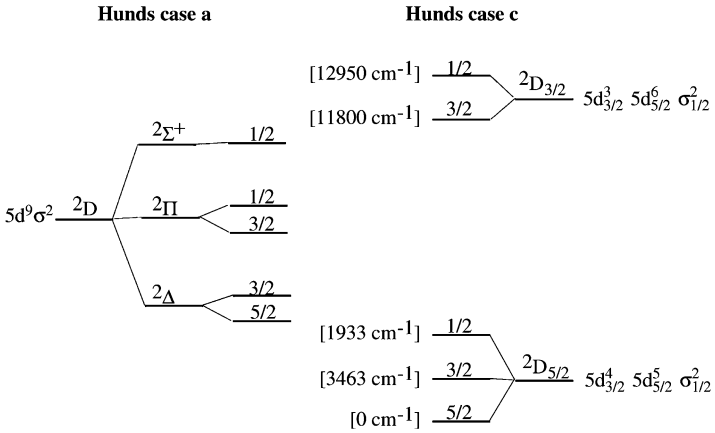

Figure 3-5. Nonrelativistic ($\Lambda\Sigma$) and relativistic ($\omega\omega$) terms obtained assuming a simple σ(s-s) bonding in the PtH molecule. In parentheses the excitation energies T_e obtained from relativistic CISD calculations are given (Reprinted with permission from L. Visscher, T. Saue, W. C. Nieuwpoort, K. Fægri, O. Gropen, J. Chem. Phys. 99, 6704 (1993). Copyright 1993, American Institute of Physics)

as $5/2 < 3/2 < 1/2$ (with $\Omega = 5/2$ the ground state), while two upper states are ordered as $3/2 < 1/2$. The nonrelativistic and relativistic terms from Table 3-9 corresponding to $5d^9\sigma^2$ configuration of platinum hydride are presented in Figure 3-5. However, it must be realized that this bonding scheme can be perturbed by *5d* participation in the bond, which can change the ordering of states. Additionally, for a strong spin-orbit coupling, a mixing between the $\Lambda\Sigma$ states with the same Ω number can be expected. Therefore, for PtH we should rather use $\omega\omega$ coupling for description of molecular states and characterize them using the quantum number Ω.

Visscher et al. [25] performed all electron four-component DF calculations and used the resulting molecular orbitals in relativistic RAS CI calculations of the five lower states of PtH. Molecular parameters of PtH calculated using the DF and CI methods are presented in Table 3-10. The Mulliken population analysis of the DF wave function has proved a significant participation of Pt*5d* orbitals in the Pt-H bond, which changes the order of the three lower states of PtH from

Table 3-10 Molecular properties of PtH calculated by (a) Visscher et al. [25] and (b) Dyall [28] using DF and post DF methods

Method	State	R_e (Å)	ν_e(cm^{-1})	$\nu_e x_e$(cm^{-1})	D_e (eV)	T_e (eV)
DF (a)	5/2	1.548	2,251	69	2.28	0.00
	1/2	1.568	2,095	70	1.96	0.32
	3/2	1.581	2,044	69	1.86	0.41
DF (b)	5/2	1.551	2,234	–	2.03	0.00
	1/2	1.573	2,094	–	1.69	0.34
	3/2	1.584	2,080	–	1.61	0.42
	3/2(2)	1.577	2,162	–	0.60	1.43
	1/2(2)	1.590	2,097	–	0.47	1.55
DC-CISD (a)	5/2	1.518	2,458	63	2.98	0.00
	1/2	1.526	2,419	66	2.74	0.24
	3/2	1.542	2,313	65	2.54	0.44
	3/2(2)	1.540	2,365	62	2.73	1.46
	1/2(2)	1.562	2,277	64	2.58	1.61
Expt. (c), (d), (e)	5/2	1.528	2,378	–	3.6	0.00
	1/2			–		
	3/2	1.520	2,265	–		0.41
	3/2(2)	–	2,349	–	–	1.45
	1/2(2)	–	–	–	–	–

(c) Scullman et al. [29, 30] and references therein
(d) McCarthy et al. [31]
(e) Squires [32]

$5/2 < 3/2 < 1/2$ to $5/2 < 1/2 < 3/2$. The values of the corresponding excitation energies T_e are given in Table 3-10 as well as in Figure 3-5 (in cm^{-1}) and they confirm the change in the order (similar change in the energetic order of the d-type orbitals was observed by Wang and Schwarz [27] for the ground state of the first row transition metal dihalides). The population analysis set up in terms of the nonrelativistic functions σ, π and δ confirms a strong mixing of nonrelativistic configurations corresponding to a given Ω state. It is worth mentioning that the parameters characterising molecular properties of PtH obtained on the DF level agree very well with those of DF calculations reported by Dyall [28]. As follows from Table 3-10, electron correlation is important and responsible for the shortening of the bond length R_e and an increase in the dissociation energy D_e and harmonic frequency ν_e. The CI results show good agreement with experimental data [29–32]. The difference in R_e is close to 0.01 Å, while that in $\nu_e - 80\,cm^{-1}$ for the $\Omega = 5/2$ ground state of PtH. For the three lower states, the weight of the DF reference configuration in the CI expansion is 90%, while for the other configurations it is less then 0.4%. This indicates that in contrast to the platinum atom, static correlation is not important in the PtH molecule. It should be emphasised that the unusual stability of the Pt-H bond ($R_e = 1.518$ Å, $D_e = 2.98$ eV) can be explained in terms of the relativistic stabilization of the *6s* orbital of platinum.

Table 3-11 Bond distances and excitation energies of PdH obtained by Sjøvoll et al. [33] using the nonrelativistic and relativistic versions of the MR-CISD method

Method	State	R_e (Å)	T_e (eV)
Nrel	$^2\Sigma$	1.59	0.00
	$^2\Delta$	1.68	0.97
	$^2\Pi$	1.76	1.09
Rel	1/2(1)	1.53	0.00
	5/2(1)	1.60	0.67
	3/2(1)	1.63	0.85
	3/2(2)	1.63	1.20
	1/2(2)	1.68	1.28

A similar mechanism of bonding as in PtH takes place in palladium hydride (palladium belongs to the same group of the periodic table). Again we can assume that electrons of Pd in the PdH molecule can be characterized by n, l and $|m_l|$ quantum numbers and that the Pd-H bond is created mainly by *5s* and *1s* electrons of Pd and H, respectively. For the $4d^9\sigma^2$ electron configuration, assuming the $\Lambda\Sigma$ coupling scheme we can find five states: $^2\Sigma_{1/2}, ^2\Pi_{1/2}, ^2\Pi_{3/2}$ and $^2\Delta_{3/2}, ^2\Delta_{5/2}$, while within the $\omega\omega$ scheme we will obtain the states with $\Omega = 1/2, 3/2, 5/2$ and $\Omega = 1/2, 3/2$. Sjøvoll et al. [33] performed series of calculations, including those by the four-component DF and RAS CI methods, for the palladium hydride molecule. They have used basis sets with nonrelativistically optimized exponents augmented with relativistic (tight) functions. The values of the bond distances and excitation energies obtained by Sjøvoll et al. [33] are given in Table 3-11. The PdH molecule, similarly as the PtH one, turned out to be single configurational with the weight of reference determinant in CI expansion of more than 90% for a given state. The population analysis of the DC wave function shows that the bonding has strong d- and p-contributions. The 1/2(1), 1/2(2) and 5/2(1) states may be characterized as almost pure $1\sigma^2 2\sigma^1 1\pi^4 1\delta^4$, $1\sigma^2 2\sigma^2 1\pi^3 1\delta^4$ and $1\sigma^2 2\sigma^2 1\pi^4 1\delta^3$ configurations, respectively. However the states 3/2(1) and 3/2(2) are mixtures of $1\sigma^2 2\sigma^2 1\pi^3 1\delta^4$ and $1\sigma^2 2\sigma^2 1\pi^4 1\delta^3$ states. From the excitation energies T_e given in Table 3-11 we conclude that, unlike for PtH, the ground state of the PdH molecule is $\Omega = 1/2$ and the states are grouped like 1:2:2. This grouping is due to the weaker spin-orbit splitting in the palladium atom as compared to those in platinum and participation of the *4p*- and *4d*-orbitals of palladium in the bonding. The relativistic effect leads to a substantial bond contraction and lower excitation energies.

The relativistic effects turned out also to be crucial for a reasonable description of the energetic structure of other transition-metal molecules: cadmium hydride and its ions. Eliav, Kaldor and Hess [34] studied spectroscopic parameters of the CdH, CdH^+ and CdH^- molecules applying the relativistic Fock-space coupled cluster method with single and double excitations of 18 external electrons to include core-valence polarization. In their four-component calculations they have exploited

Table 3-12 Spectroscopic parameters of CdH, CdH^+ and CdH^- obtained by Eliav et al. [34] using the nonrelativistic and relativistic versions of the Fock space coupled cluster method

State	Method	R_e(Å)	ν_e(cm^{-1})	$\nu_e x_e$(cm^{-1})	D_e(eV)	IP (eV)	T_e (eV)	EA (eV)
				CdH^+				
$X\,^1\Sigma^+$	CCSD	1.758	1,625	42.4	1.812	–	–	–
	DC-CCSD	1.709	1,672	35.3	1.908	–	–	–
	Expt.[a]	1.667	1,771	35.4	2.081	–	–	–
				CdH				
$X\,^2\Sigma^+$	CCSD	1.820	1,386	30.3	0.867	7.081	–	–
	DC-CCSD	1.778	1,370	37.2	0.703	7.273	–	–
	Expt.[a]	1.781	1,337	–	0.68	–	–	–
$A\,^2\Pi$	CCSD	1.765	1,571	41.2	–	–	2.553	–
$A\,^2\Pi_{1/2}$	DC-CCSD	1.702	1,652	38.9	–	–	2.688	–
$A\,^2\Pi_{3/2}$		1.701	1,659	39.2	–	–	2.811	–
$A\,^2\Pi_{1/2}$	Expt.[a]	1.669	1,677	–	–	–	2.742	–
$A\,^2\Pi_{3/2}$	Expt.[a]	1.657	1,758	38.6	–	–	2.866	–
$C\,^2\Sigma^+$	CCSD	1.763	1,560	31.6	–	–	4.650	–
	DC-CCSD	1.709	1,654	48.1	–	–	4.780	–
	Expt.[a]	1.68	1,567	50	–	–	4.984	–
				CdH^-				
$X\,^1\Sigma^+$	CCSD	1.847	1,442	35.7	–	–	–	0.456
	DC-CCSD	1.806	1,389	42.0	–	–	–	0.442

[a]Expt. – experimental values from Huber and Herzberg [19]

Table 3-13 Relativistic corrections to the spectroscopic parameters from Table 3-12 obtained using the DC-CCSD method for the CdH^+, CdH and CdH^- molecules (From [34])

State	R_e (Å)	ν_e(cm^{-1})	$\nu_e x_e$(cm^{-1})	D_e(eV)	IP (eV)	T_e (eV)	EA (eV)
			CdH^+				
$X\,^1\Sigma^+$	−0.049	47	−7.1	0.096	–	–	–
			CdH				
$X\,^2\Sigma^+$	−0.042	−16	6.9	−0.164	0.192	–	–
$A\,^2\Pi_{1/2}$	−0.063	81	−2.3	–	–	0.135	–
$A\,^2\Pi_{3/2}$	−0.064	88	−2.0	–	–	0.258	–
$C\,^2\Sigma_0^+$	−0.054	94	16.5	–	–	0.131	–
			CdH^-				
$X\,^1\Sigma^+$	−0.041	−53	6.3	–	–	–	−0.014

basis sets with nonrelativistic exponents. Table 3-12 gives the values of the bond length R_e, harmonic frequency ν_e, anharmonic constant $\nu_e x_e$, dissociation energy D_e, ionization potential IP, excitation energy T_e and electron affinity EA for the ground and excited states of CdH, CdH^+ and CdH^-. Table 3-13 contains relativistic corrections to the parameters from Table 3-12. As follows from both tables, for the ground state of CdH^+ the relativistic corrections are responsible for a significant bond strengthening with a bond contraction of 0.05 Å, an increase in the dissociation

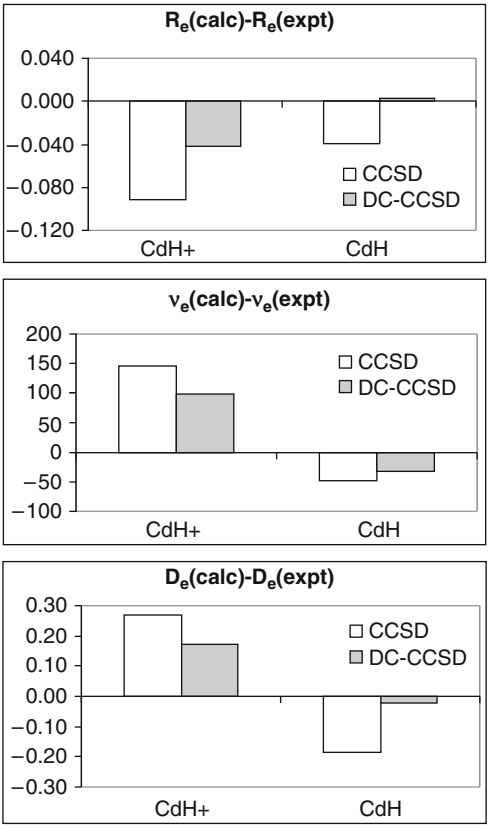

Figure 3-6. Differences between the calculated and experimental values of bond length R_e(Å), harmonic frequency ν_e(cm^{-1}) and dissociation energy D_e(eV) for the ground state of the CdH^+ and CdH molecules (From [34])

energy by 0.1 eV and an increase in the fundamental frequency by 47 cm^{-1}. For CdH we observe also a contraction of the bond by 0.04 Å, while the dissociation energy and harmonic frequency are decreased by 0.16 eV and 16 cm^{-1}, respectively. The coupled cluster results for the ground states of CdH^+, CdH and CdH^- agree well with the corresponding experimental values [19]. It is worth emphasising that relativistic effect reduces the error by about one order of magnitude as illustrated in Figure 3-6.

3.2.1.3. Di- and Inter-halogens

Diatomic molecules containing halogen atoms, presented on the diagram in Figure 3-7 were the subjects of very accurate benchmark calculations using the four-component SCF and post SCF methods [24, 35–39]. The analysis performed for a series of dihalogens, interhalogens and hydrogen halides using a series of correlated

	F	Cl	Br	I	At	(117)
F	F_2					
Cl	ClF	Cl_2				
Br	BrF	BrCl	Br_2			
I	IF	ICl	IBr	I_2		
At	*AtF*	*AtCl*	*AtBr*	*AtI*	At_2	
(117)	(117)F	(117)Cl	(117)Br	(117)I	(117)At	$(117)_2$
H	HF	HCl	HBr	HI	HAt	H(117)

Figure 3-7. Diagram presenting a series of halogen diatomic molecules analyzed using all electron four-component DF and post DF methods (molecules, whose names are written in Italic have not been studied yet)

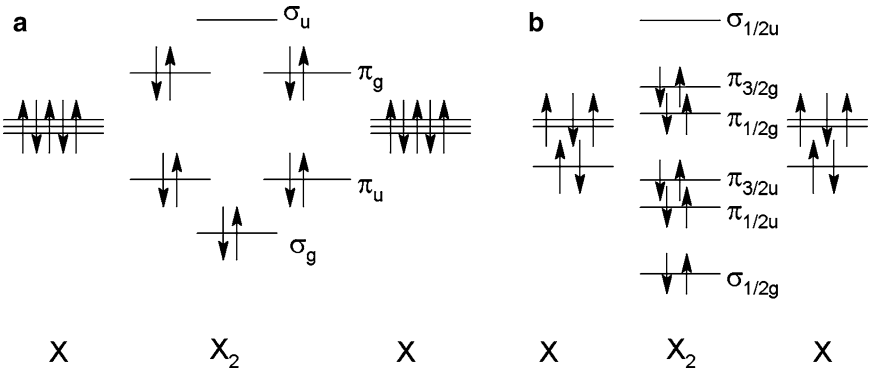

Figure 3-8. Molecular orbitals of the X_2 molecule obtained as linear combinations of atomic *np* orbitals in the nonrelativistic (**a**) and relativistic (**b**) approaches

methods, which exploited a series of basis sets, gave insight to relativistic changes that occur in the bonding and allowed identification of the trends across the series, with increasing atomic number of atoms making the molecules.

Visscher and Dyall [35] studied the relativistic and correlation effects on the spectroscopic properties of dihalogens: F_2, Cl_2, Br_2, I_2 and At_2. They performed a series of calculations using the DF, MP2, CISD and CCSD methods and exploiting basis sets of VDZ and VTZ quality. These basis sets, augmented with extra diffuse functions, were also used by Visscher et al. [36] and de Jong et al. [37], who studied the spectroscopic properties of hydrogen halides and interhalogens, respectively. To understand the mechanism of bonding in dihalogen and interhalogen molecules, let us consider the linear combinations of valence p orbitals of both halogen atoms of the X_2 molecule as shown in Figure 3-8. There are six such combinations: σ_g, π_u, π_u, π_g, π_g and σ_u. In the relativistic description the p orbitals split into $p_{1/2}$ and $p_{3/2}$. Since the large component of the atomic spinor p_{j,m_j} can be expanded into the nonrelativistic spin-orbitals $p_{l,m_l}\alpha$ and $p_{l',m_{l'}}\beta$, we can express the large

component of the relativistic molecular spinors in terms of the σ and π molecular orbitals. However, since the large component of the molecular spinor is a mixture of σ and π orbitals, we can talk only about the approximate σ and π character of the relativistic molecular orbitals. For the dihalogen molecule X_2, the six possible linear combinations can be labelled as $\sigma_{1/2g}$, $\pi_{1/2u}$, $\pi_{3/2u}$, $\pi_{1/2g}$, $\pi_{3/2g}$, $\sigma_{1/2u}$. If the energy difference between $p_{1/2}$ and $p_{3/2}$ is small, the molecular orbitals have pure σ or π character. However, for increasing spin-orbit splitting of the atomic p orbitals, the admixtures of π and σ in the σ and π orbitals, respectively, become increasingly important. The degree of mixing can be obtained from the population analysis of the DF solutions. For the homonuclear molecules, the *gerade* or *ungerade* symmetry of molecular spinors makes them partially bonding and antibonding. The formation of diatomic molecular spinors from a linear combination of atomic spinors (LCAS) is discussed in details in Chapter 22 of the book by Dyall and Fægrii [14]. For the series of dihalogens we observe increasing antibonding contribution of $\sigma_{1/2u}$ in the $\pi_{1/u}$ molecular orbital: 0.00%, 0.01%, 0.2%, 1% and 10% for F_2, Cl_2, Br_2, I_2 and At_2, respectively. It is also displayed in Figure 3-9.

Molecular bonding can be analyzed in similar way for the hydrogen halide molecules. Figure 3-10 presents the molecular orbitals formed as linear combinations of the valence *np* orbitals of the halogen atom and *1s* orbital of hydrogen. Those combinations are labelled σ, π, π and σ^* in the nonrelativistic description, while $\sigma_{1/2}$, $\pi_{1/2}$, $\pi_{3/2}$ and $\sigma_{1/2}{}^*$ in the relativistic one. The relativistic molecular orbitals have no pure σ and π character and the degree of mixing depending on the spin-orbit splitting of atomic p orbitals can be determined from the population analysis of molecular solutions. The admixture of the $\pi_{1/2}$ orbital into the $\sigma_{1/2}$ orbital determined by such an analysis is 0.01%, 0.02%, 0.34%, 1.6% and 18% for HF, HCl, HBr, HI and HAt, respectively. This increasing $\pi_{1/2}$ contribution in the $\sigma_{1/2}$ orbital is also displayed in Figure 3-9. Tables 3-14–3-16 give the values of the bond distance R_e, harmonic frequency ν_e and dissociation energy D_e and the corresponding relativistic corrections for the dihalogen molecules X_2, obtained using the nonrelativistic and relativistic versions of SCF and post SCF

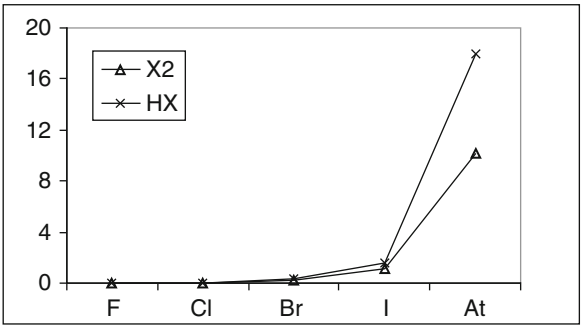

Figure 3-9. Gradual increase in the percentage of the $\sigma^*(\pi)$ character in the first $\omega = 1/2u$ ($\omega = 1/2$) molecular orbital of the X_2 (HX) series of molecules, X = F, Cl, Br, I and At

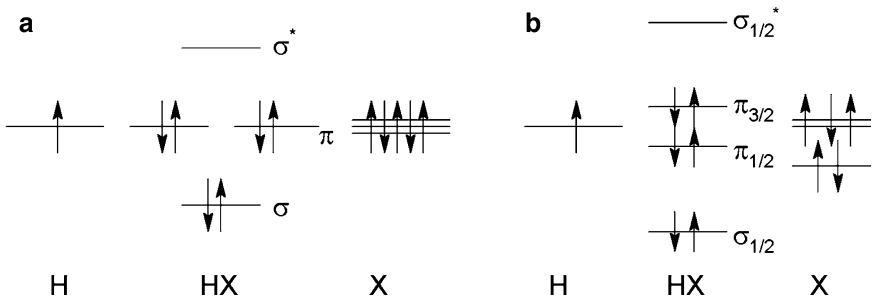

Figure 3-10. Molecular orbitals of the HX molecule, obtained as linear combinations of the atomic X*np* and H1s orbitals in the nonrelativistic (**a**) and relativistic (**b**) approaches

Table 3-14 Bond distance R_e for the dihalogen molecules obtained by Visscher and Dyall [35] at various levels of theory

Method	F_2	Cl_2	Br_2	I_2	At_2
			R_e (Å)		
HF	1.329	1.984	2.279	2.681	2.904
DF	1.329	1.985	2.277	2.682	2.973
DF + Br	1.329	1.985	2.278	2.683	2.974
MP2	1.398	1.997	2.291	2.686	2.914
DC- MP2	1.398	1.998	2.291	2.688	2.984
CISD	1.371	1.997	2.292	2.691	2.919
DC-CISD	1.371	1.997	2.292	2.693	2.993
CCSD	1.395	2.009	2.307	2.704	2.934
DC-CCSD	1.395	2.010	2.306	2.708	3.022
CCSD(T)	1.416	2.018	2.315	2.712	2.942
DC-CCSD(T)	1.416	2.019	2.315	2.717	3.046
Expt.[a]	1.412	1.987	2.281	2.666	–

[a]Experimental values from Huber and Herzberg [19]

methods with pVTZ basis sets. As shown by these data, the relativistic effects lead to a destabilization of the bond. These effects are negligible for lighter molecules, up to Br_2. However, the bond length expansion for I_2 calculated using the CCSD(T) method is 0.006 Å and the decrease in the dissociation energy is 13 kcal/mol. The values of these effects for the At_2 molecule are 0.1 Å and 24 kcal/mol, respectively. Taking into account the relativistic effects causes a lowering in the harmonic frequency on the CCSD(T) level by 11 and 46 cm^{-1} for I_2 and At_2, respectively. The increase in the relativistic corrections with Z for dihalogens is plotted in Figure 3-11. As it can be seen from this figure and from the corresponding tables, the ASO approximation, in which the relativistic effect on dissociation energy is obtained by correcting the nonrelativistic results for the spin-orbit splitting of atomic asymptote only, gives correct results for lighter molecules, up to I_2. In At_2 this simple model, assuming that the spin-orbit coupling is completely quenched in the molecule, fails, indicating that scalar and spin-orbit effects in molecule should be taken into account.

Table 3-15 Harmonic frequency ν_e and dissociation energy D_e for the dihalogen molecules obtained by Visscher and Dyall [35] at various levels of theory

Method	F_2	Cl_2	Br_2	I_2	At_2
		ν_e (cm^{-1})			
HF	1,267	613	354	237	169
DF	1,266	612	351	228	131
DF + Br	1,266	612	350	228	132
MP2	1,017	578	336	230	164
DC-MP2	1,016	576	333	221	126
CISD	1,110	585	338	229	163
DC-CISD	1,110	584	335	220	125
CCSD	1,013	562	324	222	158
DC-CCSD	1,012	561	321	212	116
CCSD(T)	919	546	316	217	154
DC-CCSD(T)	920	544	312	206	108
Expt.[a]	917	560	325	215	–
		D_e (kcal/mol)			
HF	−25.3	26.5	23.4	23.8	22.2
DF	−26.3	24.5	15.7	9.2	−8.2
DF + Br	−26.2	24.5	15.8	9.3	−8.1
MP2	42.3	56.9	49.5	45.6	42.1
DC-MP2	41.5	55.0	42.5	32.2	15.0
CISD	11.8	32.1	29.1	26.8	24.7
DC-CISD	10.9	30.3	22.3	14.3	0.9
CCSD	28.3	48.6	42.9	39.5	36.4
DC-CCSD	27.5	46.8	36.0	26.7	11.4
CCSD(T)	34.8	52.3	46.1	42.3	39.0
DC-CCSD(T)	34.0	50.4	39.2	29.6	14.6
Expt.[a]	38.2	58.0	45.9	35.9	-

[a]Experimental values from Huber and Herzberg [19]

Visscher and Dyall [35] in their study correlated 14 valence electrons of the X_2 molecule, however de Jong et al. [40] performed calculations for the I_2 molecule using the same basis set but correlating also the electrons from the 4d inner shell. Their CCSD(T) results show that inclusion of the core-valence effects additionally shortens the bond by 0.02 Å and causes an increase in the dissociation energy by 2 kcal/mol and harmonic frequency by 11 cm^{-1}. It indicates that core-valence effects are important for correct prediction of spectroscopic constants of dihalogens.

A comparison of theory and experiment can be done for all the molecules except At_2, for which experimental data are not available. The differences between the calculated and experimental values [19] of the spectroscopic constants of the F_2, Cl_2, Br_2 and I_2 molecules are displayed in Figures 3-12–3-14. As follows from the figures, the agreement between the calculated and experimental values is good. The difference in the bond length changes with the method but does not exceed a few tenth of Å. The differences in the harmonic frequency and dissociation energy

Table 3-16 Relativistic corrections to R_e, ν_e and D_e for the dihalogen molecules obtained by Visscher and Dyall [35] at various levels of theory

	F_2	Cl_2	Br_2	I_2	At_2
			ΔR_e (Å)		
DF	0.000	0.001	−0.002	0.001	0.069
DF + Br	0.000	0.001	−0.001	0.002	0.070
DC- MP2	0.000	0.001	0.000	0.002	0.070
DC-CISD	0.000	0.000	0.000	0.002	0.074
DC-CCSD	0.000	0.001	−0.001	0.004	0.088
DC-CCSD(T)	0.000	0.001	0.000	0.005	0.104
			$\Delta\nu_e(cm^{-1})$		
DF	−1	−1	−3	−9	−38
DF + Br	−1	−1	−4	−9	−37
DC- MP2	−1	−2	−3	−9	−38
DC-CISD	0	−1	−3	−9	−38
DC-CCSD	−1	−1	−3	−10	−42
DC-CCSD(T)	1	−2	−4	−11	−46
			ΔD_e (kcal/mol)		
DF	−1.0	−2.0	−7.7	−14.6	−30.4
DF + Br	−0.9	−2.0	−7.6	−14.5	−30.3
DC- MP2	−0.8	−1.9	−7.0	−13.4	−27.1
DC-CISD	−0.9	−1.8	−6.8	−12.5	−23.8
DC-CCSD	−0.8	−1.8	−6.9	−12.8	−25.0
DC-CCSD(T)	−0.8	−1.9	−6.9	−12.7	−24.4
ASO[a]	−0.8	−1.7	−7.0	−14.5	−45.0

[a] ASO – the nonrelativistic results corrected for the spin-orbit splitting of atomic asymptote

are of an order of a few cm^{-1} and a few kcal/mol, respectively. However, perhaps more interesting is the unexpected trend observed for R_e, which can be formulated as follows: the better and the more advanced the correlation method used, the worse the agreement with experiment. For example, for I_2 the best agreement is obtained on the HF level, while the worst on the CCSD(T) one. This behavior of the computational error can be attributed to the incompleteness of the basis sets used in calculations or the neglect of the core-valence electron correlation. We will discuss this problem in the next subsection of this chapter.

It is interesting to notice that the DF method and post DF methods give slightly different values of relativistic corrections for spectroscopic properties of the dihalogen molecules, which proves that relativistic and correlation effects are not simply additive. We can estimate the value of the correlation-relativistic cross terms for the dissociation energy as the difference between the relativistic corrections to D_e obtained on the DF and on the correlated levels:

$$\delta^x D_e = \Delta D_e^{rel}(corr) - \Delta D_e^{rel}(DF). \tag{3-1}$$

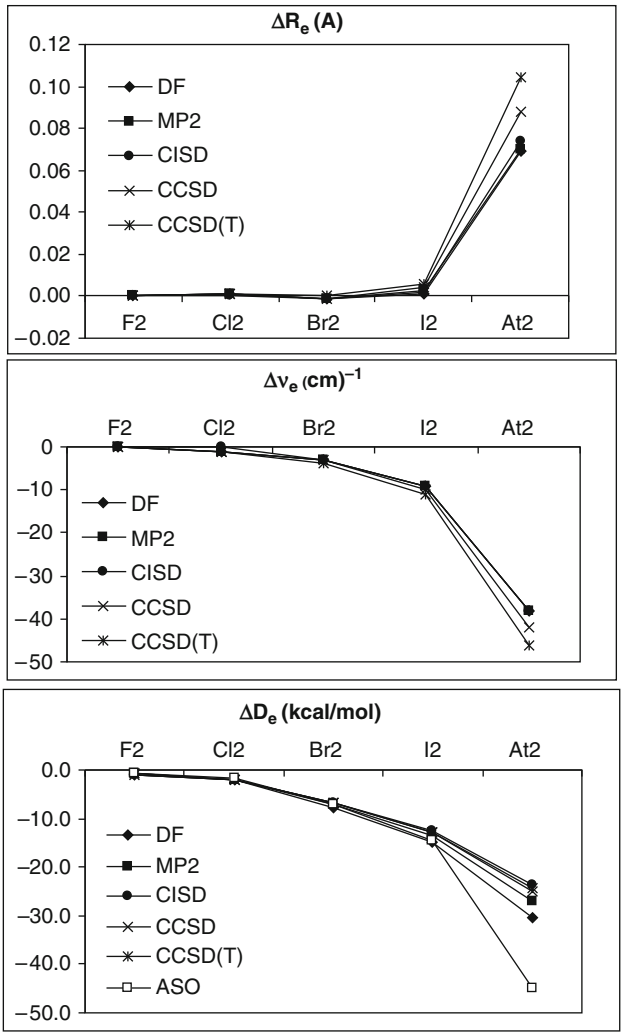

Figure 3-11. Relativistic corrections to bond length R_e, harmonic frequency ν_e and dissociation energy D_e for a series of dihalogen molecules (From [35])

The values of the $\delta^x D_e$ cross terms are displayed in Figure 3-15, which indicates that these effects are small for the light elements, but grow fast with Z and for At_2 are of about 6 kcal/mol, which makes 25% of the relativistic corrections to D_e calculated using the CCSD(T) method.

Similar trends have been observed by de Jong et al. [37] for the series of interhalogen molecules listed in the columns of the diagram in Figure 3-7. They performed a series of four-component calculations (DF, MP2, CCSD) exploiting the basis sets used by Visscher and Dyall for dihalogens, augmented by the extra diffuse

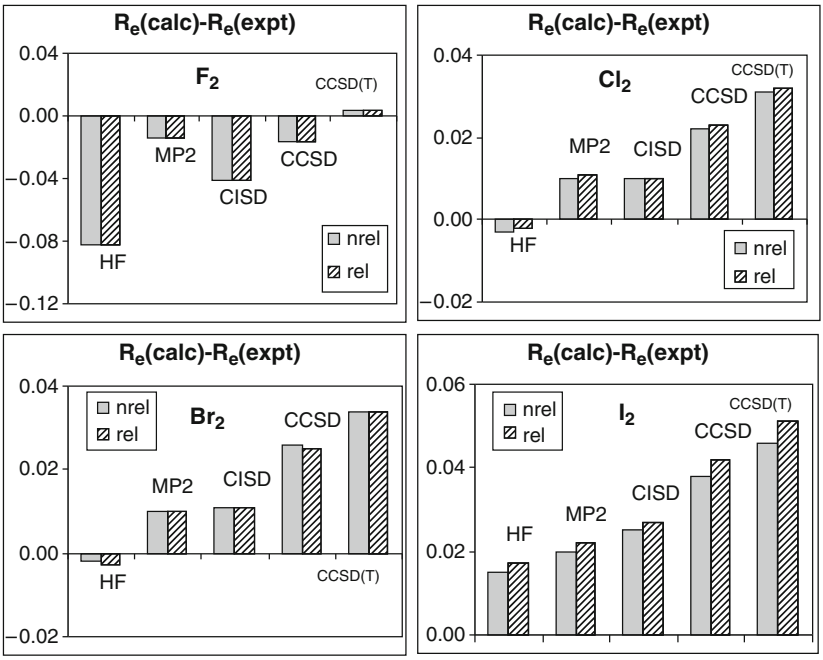

Figure 3-12. Differences (in Å) between the calculated and experimental values of bond length R_e of dihalogen molecules F_2, Cl_2, Br_2 and I_2 (From [35])

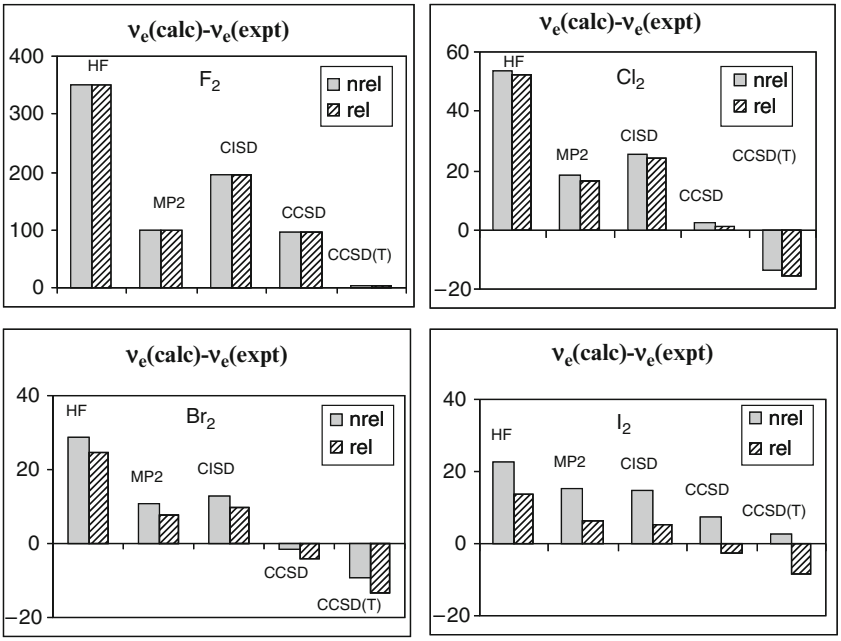

Figure 3-13. Differences (in cm^{-1}) between the calculated and experimental values of harmonic frequency ν_e of dihalogen molecules F_2, Cl_2, Br_2 and I_2 (From [35])

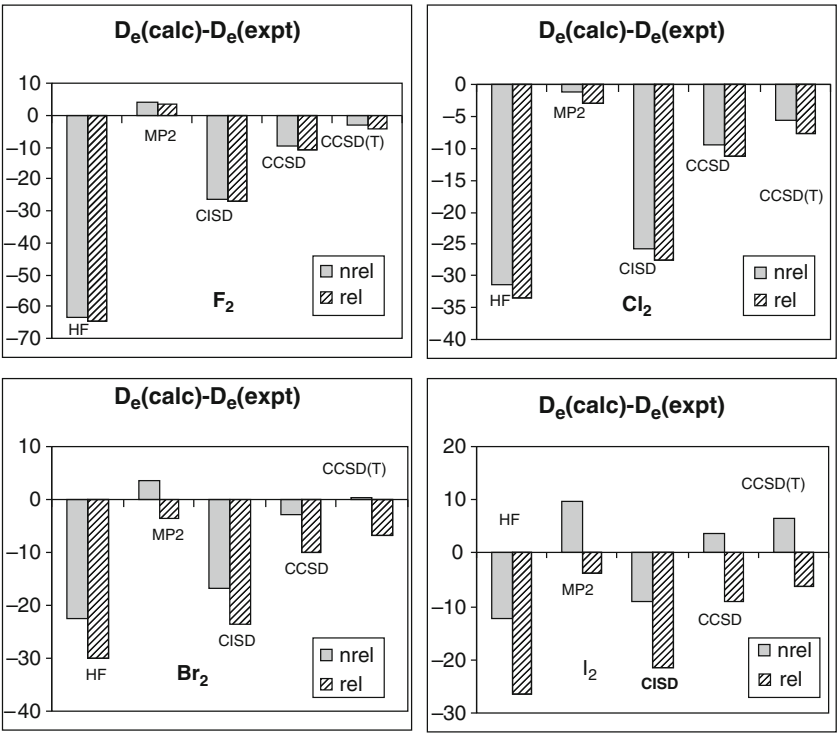

Figure 3-14. Differences (in kcal/mol) between the calculated and experimental values of dissociation energy D_e of dihalogen molecules F_2, Cl_2, Br_2 and I_2 (From [35])

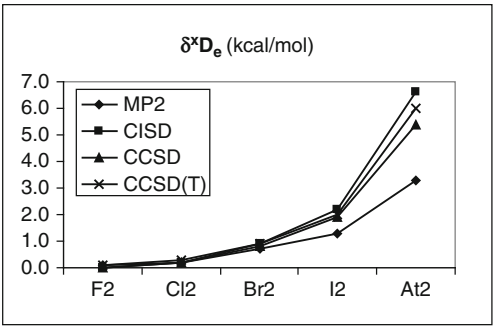

Figure 3-15. The correlation-relativistic cross terms for D_e of dihalogens obtained using different correlated methods (From [35])

functions [36]. In correlated calculations, the excitations of 14 valence electron were taken into account. The values of the spectroscopic constants calculated by de Jong et al. [37] for the XY molecules, X, Y = F, Cl, Br and I are given in Table 3-17, while the corresponding relativistic corrections are given in Table 3-18. To analyze the trends, we can divide the set of the XY molecules into a several series in such a

Table 3-17 Spectroscopic constants of interhalogens calculated by de Jong et al. [37] at various levels of theory using pVTZ basis sets

Method	ClF	BrF	IF	BrCl	ICl	IBr
			R_e(Å)			
HF	1.590	1.716	1.876	2.129	2.319	2.472
DF	1.590	1.718	1.886	2.130	2.326	2.475
DF + Br	1.590	1.719	1.887	2.131	2.327	2.476
MP2	1.637	1.759	1.916	2.143	2.330	2.483
DC-MP2	1.637	1.762	1.928	2.144	2.338	2.486
CCSD	1.632	1.754	1.910	2.156	2.341	2.497
DC-CCSD	1.633	1.757	1.921	2.157	2.349	2.501
CCSD(T)	1.645	1.765	1.920	2.165	2.349	2.506
DC-CCSD(T)	1.645	1.769	1.932	2.166	2.359	2.511
Expt.	1.628	1.759	1.91	2.136	2.321	2.469
			$\nu_e(cm^{-1})$			
HF	918	777	703	487	424	295
DF	915	771	680	483	411	287
DF + Br	915	771	680	483	411	287
MP2	809	699	645	458	405	283
DC-MP2	808	693	624	455	392	275
CCSD	814	705	654	446	395	275
DC-CCSD	814	699	632	443	383	266
CCSD(T)	781	679	634	433	385	267
DC-CCSD(T)	780	673	611	429	372	258
Expt.	786	671	610	444	384	269
			D_e(kcal/mol)			
HF	17.1	20.1	30.1	26.1	29.1	25.7
DF	15.2	14.9	20.7	21.1	20.9	14.5
DF + Br	15.2	15.0	20.9	21.2	21.0	14.6
MP2	68.1	70.1	78.1	55.1	56.1	50.5
DC-MP2	66.4	66.3	70.5	50.9	49.1	40.4
CCSD	56.1	59.1	66.1	48.1	49.1	44.0
DC-CCSD	54.7	54.5	58.8	43.2	41.7	34.1
CCSD(T)	61.1	63.1	70.5	51.2	52.3	47.1
DC-CCSD(T)	59.4	59.1	63.1	46.9	45.2	37.4
Expt.	66.3	64.7	67.3	52.1	50.2	42.3

way that each series starts with a dihalogen molecule, while the remaining members are obtained by replacing one atom of X_2 by a heavier halogen atom Y. In this way we will obtain: F_2, ClF, BrF, IF; Cl_2, BrCl, ICl and Br_2, IBr etc., which correspond to the columns in the diagram in Figure 3-7. The relativistic corrections to R_e, ν_e and D_e for the series of interhalogen atoms are displayed in Figure 3-16. Similarly like for dihalogens, the relativistic effect weakens the bond. We observe an increase in the bond length and a decrease in the dissociation energy and in the harmonic frequency. Again, these effects are small for light molecules but increase for the molecules containing heavier elements. For example for the IF molecule, the

Table 3-18 Relativistic corrections to spectroscopic constants of interhalogens calculated by de Jong et al. [37] at various levels of theory using pVTZ basis sets

Method	ClF	BrF	IF	BrCl	ICl	IBr
			ΔR_e(Å)			
DF	0.000	0.003	0.010	0.001	0.007	0.003
DF + G	0.000	0.003	0.011	0.001	0.008	0.004
MP2	0.001	0.003	0.011	0.001	0.008	0.004
CCSD	0.001	0.003	0.011	0.001	0.009	0.004
CCSD(T)	0.001	0.003	0.012	0.001	0.010	0.005
			$\Delta\nu_e$(cm^{-1})			
DF	−2	−6	−23	−3	−13	−8
DF + G	−3	−6	−23	−4	−13	−8
MP2	−1	−6	−21	−3	−12	−8
CCSD	−1	−6	−21	−4	−13	−8
CCSD(T)	−1	−6	−23	−4	−13	−9
			ΔD_e(kcal/mol)			
DF	−1.5	−4.6	−8.8	−4.9	−8.2	−11.2
DF + G	−1.5	−4.5	−8.7	−4.8	−8.1	−11.0
MP2	−1.4	−4.0	−7.4	−4.5	−7.4	−10.1
CCSD	−1.4	−4.1	−7.6	−4.4	−7.2	−9.8
CCSD(T)	−1.4	−4.0	−7.4	−4.3	−7.1	−9.7
ASO	−1.3	−4.0	−7.8	−4.5	−8.3	−11.0

corrections obtained using the correlated method are of an order of 0.01 Å, 20 cm^{-1} and 7.5 kcal/mol for R_e, ν_e and D_e, respectively. The ASO approximation estimates correctly the relativistic corrections to the dissociation energy for lighter systems. However, for the molecules containing iodine atom, the relativistic shift in the D_e is by over 1 kcal/mol smaller then the ASO values. Inclusion of the Breit correction does not change in practice the values of the spectroscopic constants. The values of the correlation-relativistic cross terms for the dissociation energy of the interhalogen molecules are presented in Figure 3-17. As for dihalogens, they are small for light molecules but grow fast and become not negligible (up to 20% of the total relativistic correction) for heavier systems.

The theoretical values can be compared with the experimental data [19] also given in Table 3-17. The differences between the experimental and theoretical values obtained on the correlated level do not exceed 0.05 Å, 45 cm^{-1} and 12 kcal/mol for R_e, ν_e and D_e, respectively. These differences are plotted in Figures 3-18–3-20. Similarly as for the dihalogen molecules, the differences in the bond length reveal the unexpected tendency: the more advanced the method of inclusion of electron correlation, the worse the agreement between the calculated and the experimental values of R_e. This problem will be discussed in the next subsection of this chapter.

3.2.1.4. Hydrogen Halides

Visscher et al. [36] studied the relativistic and correlation effects on the properties of the molecules of hydrogen halides: HF, HCl, HBr, HI and HAt. The molecules

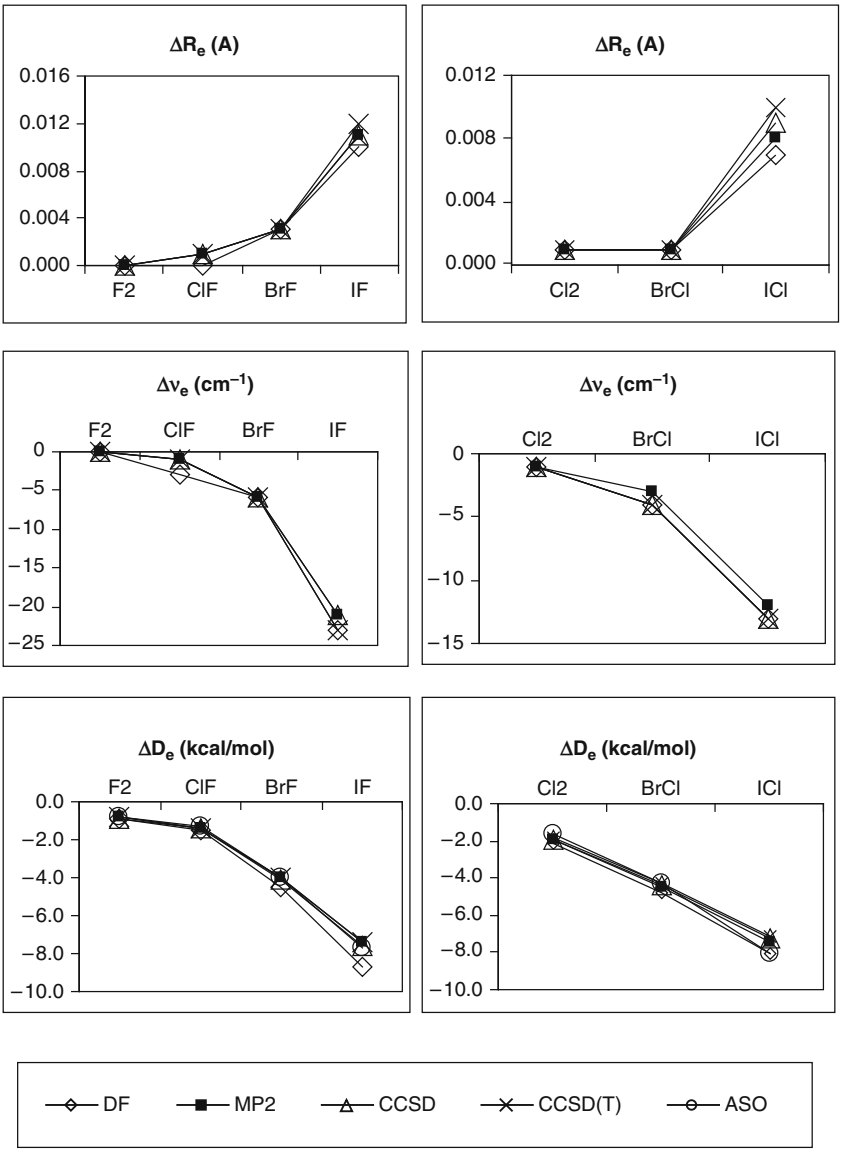

Figure 3-16. Variation in relativistic corrections to spectroscopic constants of interhalogen molecules obtained at various levels of theory (From [35, 37])

containing a hydrogen atom bonded to a heavy atom pose a feasible computational problem to most methods, yet giving some insight to the changes in the bonding caused by the relativistic effects. The authors used the DF, MP2, CISD and CCSD methods to calculate the energetic structure and spectroscopic properties of these diatomic systems. Thus they got a range of correlation treatments,

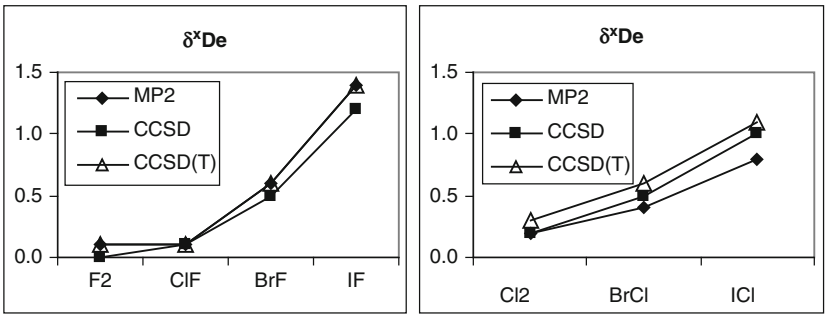

Figure 3-17. The correlation-relativistic cross terms for D_e of interhalogens obtained using different correlated methods (From [35, 37])

from no correlation in the DF method to a fairly high level of correlation in the CCSD(T) method. In their calculations the authors used the basis sets of Dyall and Visscher [35] for dihalogens, but augmented with extra diffuse functions to describe the electronegativity of the halogen atom in the molecule. In the post DF methods the authors correlated eight valence electrons of hydrogen and halide atoms.

For the hydrogen halide molecules we can assume a simple model of bonding as already explained at the beginning of the previous subsection (see Figure 3-10 and its description in the text). The results of the calculations are given in Tables 3-19 and 3-20. Table 3-19 displays the values of the bond distances R_e, harmonic frequencies ν_e and dissociation energies D_e, calculated using different methods with aug-pVTZ basis sets, while Table 3-20 presents the relativistic corrections obtained as the differences between the corresponding relativistic and nonrelativistic values. These corrections for the series of hydrogen halides are also displayed in Figure 3-21. As follows, the relativistic effects are negligible for the light molecules HF and HCl. They do not change the bond length, decrease the harmonic frequency by a few cm^{-1} and the dissociation energy by up to 1 kcal/mol. The effects grow up with increasing atomic number of the halogen atom. Thus, the bond is contracted by about 0.002 and 0.004 Å for HBr and HI, respectively. However, for the heaviest member of the series, HAt, we observe the opposite effect, i.e. the expansion of the bond by 0.01 Å (on the CCSD(T) level). This trend can also be noted in Figure 3-21: from HF to HI the relativistic bond length contraction increases, while for HAt we observe a change in the trend and a significant bond length expansion. This observation can be explained in terms of the two effects: the contraction of the p shell responsible for a decrease in the bond length is counteracted by the spin-orbit coupling, which leads to a mixing of the occupied π orbitals with the σ^* orbital, thus weakening the bond and increasing the bond length. The above trend has been confirmed by the DF calculations of Saue et al. [24] for the HI, HAt and H(117) molecules. The results for HI and HAt obtained by these authors agree very well with those of Visscher et al., while the relativistic bond length expansion for H(117) of 0.13 Å is a continuation of the trend noted for HAt.

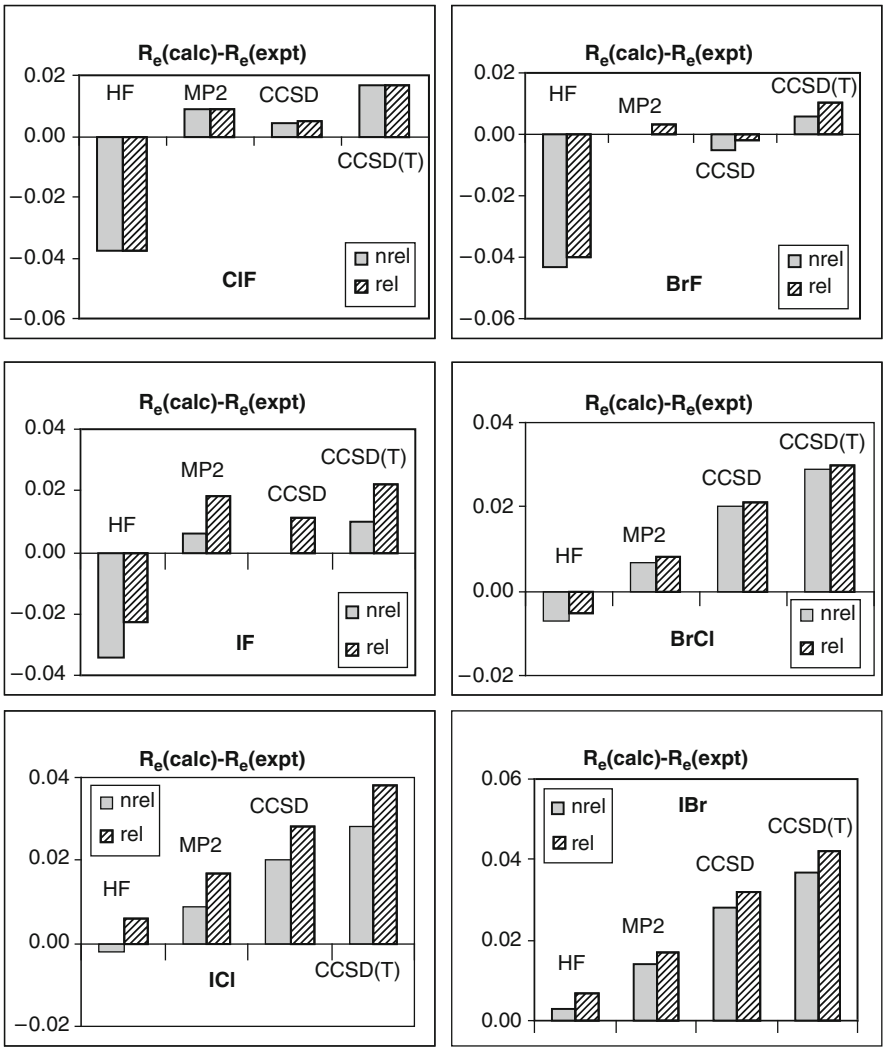

Figure 3-18. Differences between the theoretical and experimental values of the bond distance R_e(Å) for interhalogen molecules calculated at various levels of theory (From [37])

The relativistic effects on the harmonic frequency and on the dissociation energy cause a monotonic decrease in both these parameters. They grow with Z of the halogen atoms and are more pronounced in the methods treating the electron correlation on higher levels. For the CCSD(T) calculations for the HAt molecule, the decrease in ν_e and D_e, is 216 cm^{-1} and 18 kcal/mol, respectively. The Breit correction to the two-electron interaction (not included in the tables) gives only a marginal change in the parameters calculated.

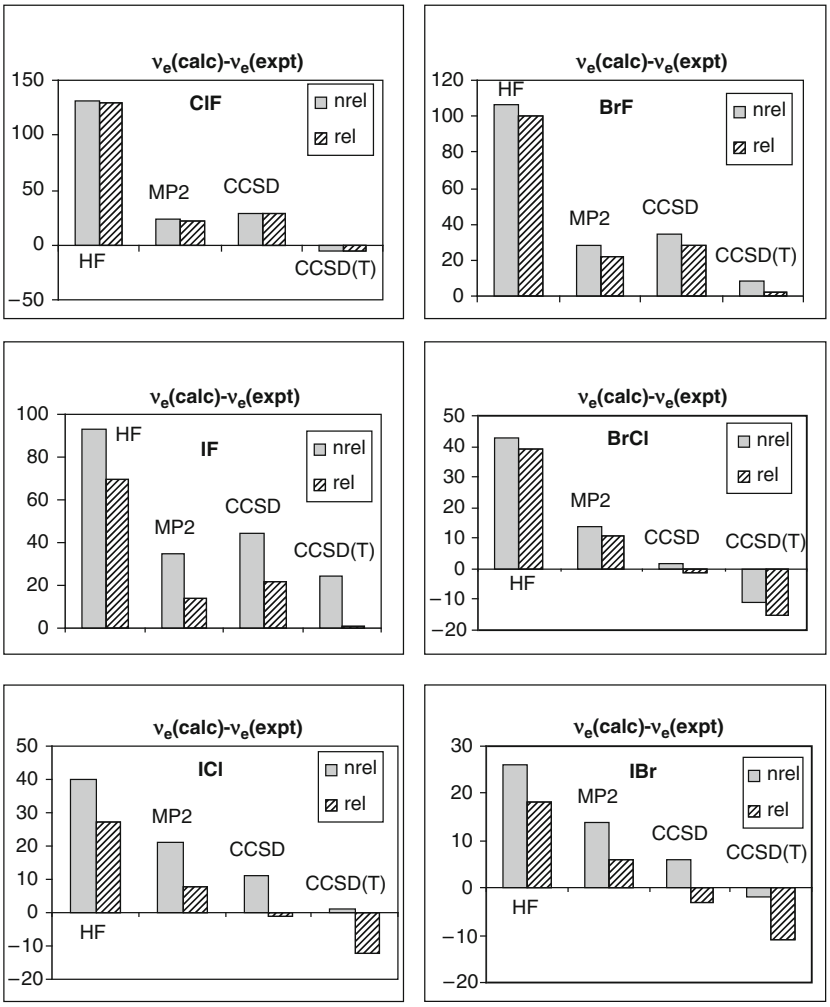

Figure 3-19. Differences between the theoretical and experimental values of the fundamental frequency $\nu_e(\mathrm{cm}^{-1})$ for interhalogen molecules calculated at various levels of theory (From [37])

Similarly as for the series of dihalogens and interhalogens, we can estimate the values of the correlation-relativistic cross terms for the dissociation energy of the HX molecules, X = F, Cl, Br, I and At. They are small for light molecules and increase with Z of the X atom, as shown in Figure 3-22. For HAt they are of about 3 kcal/mol, which makes about 16% of the relativistic correction to D_e obtained on the CCSD(T) level.

Another interesting aspect of these calculations is revealed from a comparison between the theoretical results and the experimental values. We can compare them only for the first four members of the series, for which experimental data are

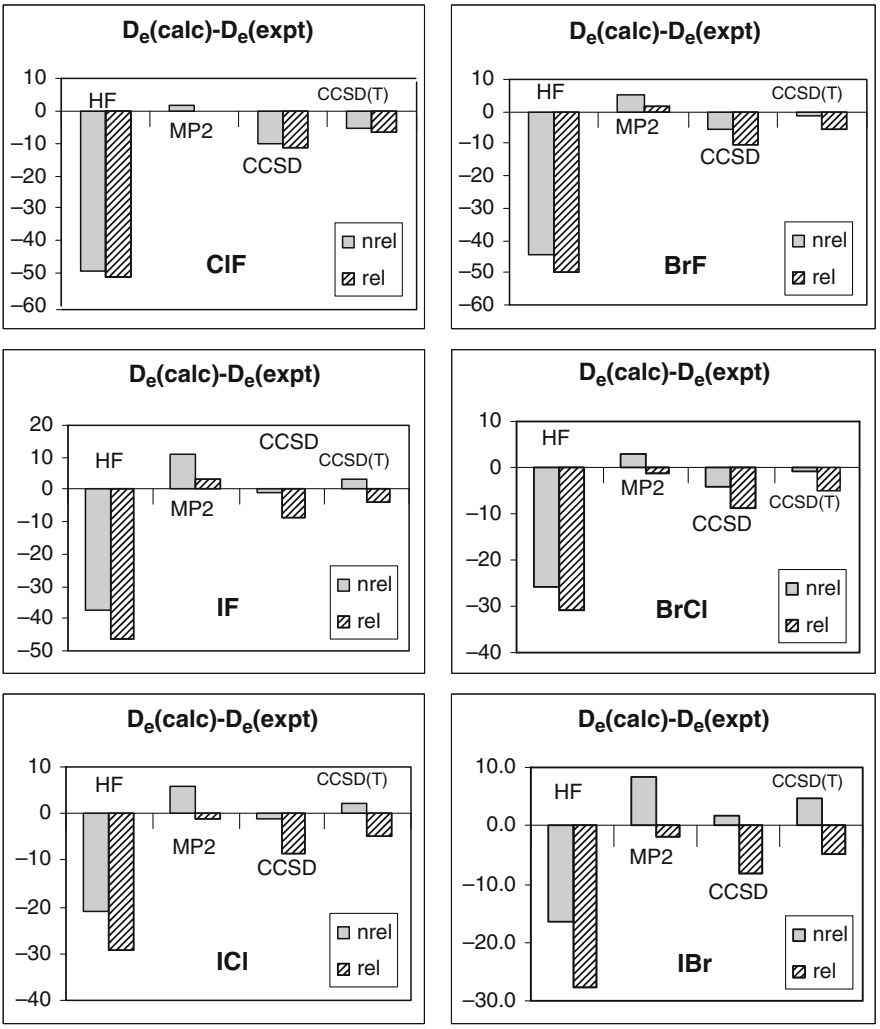

Figure 3-20. Differences between the theoretical and experimental values of the dissociation energy D_e(kcal/mol) for interhalogen molecules calculated at various levels of theory (From [37])

available [19]. Figures 3-23–3-25 show differences between the experimental and the calculated values of spectroscopic constants. Similarly as for the dihalogen and interhalogen molecules, we observe an interesting trend for the bond length values R_e: the better the correlation method used, the worse the agreement with experiment. As already mentioned, such trend can be a consequence of the truncation of the basis set and the neglect of the core-valence electron correlation. This problem was discussed by Styszyski and Kobus [38, 39]. In the calculations reported in these works,

Table 3-19 Spectroscopic properties of hydrogen halides calculated by Visscher et al. [36] at various levels of theory

	HF	HCl	HBr	HI	HAt
			R_e(Å)		
HF	0.899	1.267	1.408	1.611	1.713
DF	0.899	1.267	1.406	1.603	1.715
MP2	0.922	1.275	1.415	1.616	1.719
DC-MP2	0.922	1.275	1.413	1.610	1.723
CCSD	0.918	1.277	1.419	1.623	1.727
DC-CCSD	0.918	1.277	1.417	1.617	1.737
CISD	0.915	1.274	1.415	1.619	1.723
DC-CISD	0.915	1.273	1.414	1.613	1.731
CCSD(T)	0.921	1.279	1.421	1.625	1.73
DC-CCSD(T)	0.921	1.279	1.419	1.620	1.739
Expt.	0.917	1.275	1.414	1.609	–
			$\nu_e(cm^{-1})$		
HF	4,466	3,136	2,795	2,457	2,306
DF	4,464	3,132	2,784	2,429	2,112
MP2	4,123	3,044	2,724	2,404	2,258
DC-MP2	4,121	3,041	2,711	2,373	2,070
CCSD	4,169	3,014	2,679	2,351	2,198
DC-CCSD	4,168	3,011	2,664	2,314	1,983
CISD	4,223	3,049	2,711	2,382	2,228
DC-CISD	4,222	3,046	2,697	2,347	2,017
CCSD(T)	4,124	2,991	2,660	2,334	2,182
DC-CCSD(T)	4,123	2,988	2,645	2,297	1,966
Expt.	4,138	2,991	2,648	2,309	–
			D_e(kcal/mol)		
HF	101.2	81.1	69.2	58.0	52.0
DF	100.5	79.9	64.9	49.4	30.7
MP2	142.9	104.1	89.7	76.0	69.1
DC-MP2	142.3	103.0	85.7	68.2	49.9
CCSD	136.1	102.2	89.1	76.5	70.0
DC-CCSD	135.5	101.1	85.2	68.8	51.6
CISD	133.4	100.1	87.2	74.6	68.2
DC-CISD	132.8	99.0	83.2	66.9	49.7
CCSD(T)	138.0	103.4	90.2	77.4	70.8
DC-CCSD(T)	137.4	102.3	86.3	69.9	52.6
Expt.	141.2	106.5	90.4	73.6	–

the electron correlation is examined in two steps. In the first step, called the core-valence 1 (CV1), the eight valence electrons of the HX molecule and the outermost core electrons are included, resulting in N = 10, 16, 26, 26 and 26 correlated electrons in HF, HCl, HBr, HI and HAt, respectively. In the second step, the core valence 2 (CV2), the next inner shell is also included. This increases N to 18, 36, 44 and 58, respectively, as explained in Table 3-21. Table 3-22 presents the values of

Table 3-20 Relativistic corrections to spectroscopic constants of hydrogen halides calculated by Visscher et al. [36] at various levels of theory

	F	HCl	HBr	HI	HAt
			ΔR_e(Å)		
DF	0.000	0.000	−0.002	−0.007	0.002
MP2	0.000	0.000	−0.002	−0.006	0.004
CCSD	0.000	0.000	−0.002	−0.006	0.009
CISD	0.000	0.000	−0.002	−0.006	0.008
CCSD(T)	0.000	0.000	−0.002	−0.005	0.010
			$\Delta\nu_e$(cm^{-1})		
DF	−1	−3	−12	−29	−194
MP2	−2	−3	−13	−31	−188
CCSD	−2	−3	−14	−37	−215
CISD	−1	−3	−14	−35	−211
CCSD(T)	−2	−3	−15	−37	−216
			ΔD_e(kcal/mol)		
DF	−0.6	−1.2	−4.4	−8.6	−21.3
MP2	−0.6	−1.1	−4.0	−7.9	−19.3
CCSD	−0.6	−1.1	−3.9	−7.6	−18.4
CISD	−0.6	−1.1	−3.9	−7.7	−18.5
CCSD(T)	−0.6	−1.1	−3.9	−7.5	−18.2
ASO	−0.39	−0.8	−3.5	−7.3	−23.0

the bond length, harmonic frequency and dissociation energy of hydrogen halides obtained for CV1 and CV2 calculations. For the sake of comparison, the results of the plain valence calculations (V) with only eight valence electrons included for each molecule in the correlated method are also given. As follows from the table, the inclusion of the core spinors in the correlation calculations brings an additional shortening (relative to the results with the valence electrons only) of R_e. This effect is of ∼0.002 Å for the HF molecule and it increases by one order of magnitude for heavier molecules (it amounts to 0.02 Å for HAt). The core-valence correlation increases the values of the harmonic frequency and dissociation energy in comparison with the results obtained for the valence electrons only. This increase, depending on the method and the number of correlated shells, is of order of a few tens of cm^{-1} and of 1–3 kcal/mol for ν_e and D_e, respectively. The relativistic corrections to the bond length R_e are given in Table 3-23. They are consistent with the results obtained for the valence electron only (V) calculations except the HAt molecule, for which we observe the differences of 0.01 Å. The relativistic effects on the harmonic frequency vary with different levels of inclusion of the core shell electrons in the correlation calculation. For the HF, HCl and HBr molecules the differences between V, CV1 and CV2 approximations are equal to several cm^{-1} and change in an irregular way.

However, for the HI and HAt the values of the relativistic corrections change in a systematic way: for the HI molecule they are −37, −32 and −24 cm^{-1}, while for the HAt molecule −191, −180 and −179 cm^{-1}, in the V, CV1 and CV2 approximations, respectively. The values of the relativistic corrections to the dissociation energy

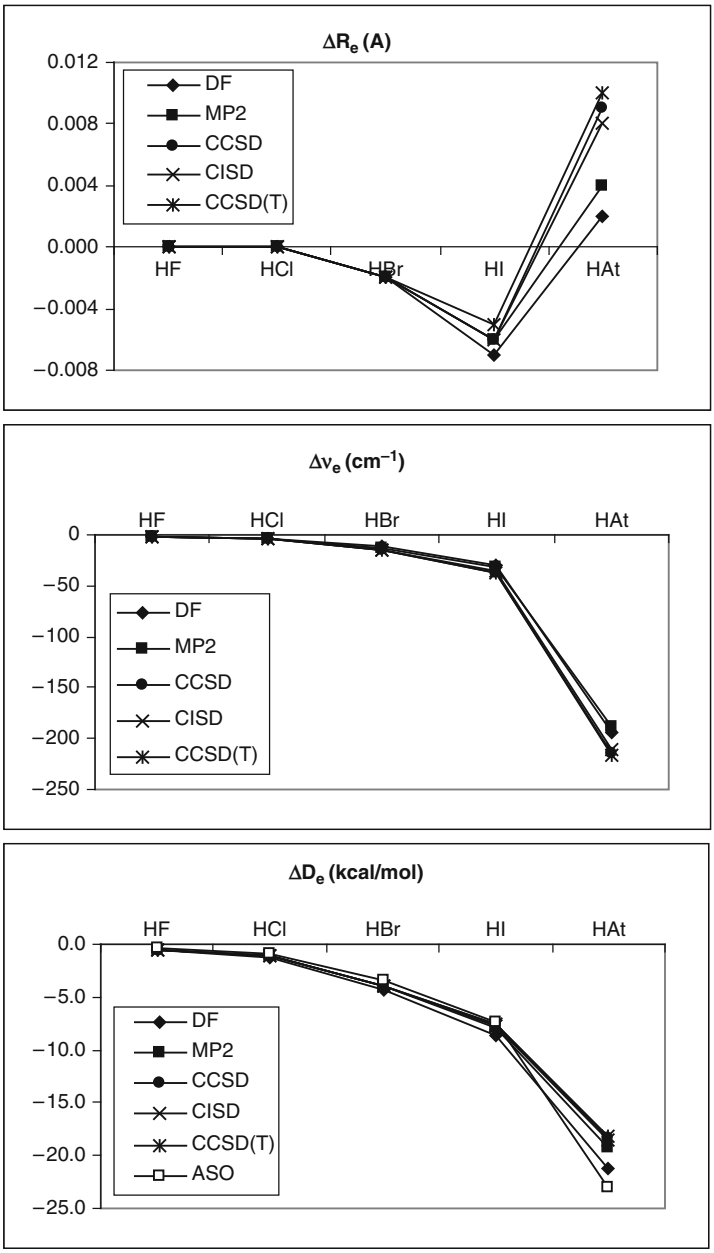

Figure 3-21. Relativistic corrections to spectroscopic constants of hydrogen halides calculated at various levels of theory (From [36])

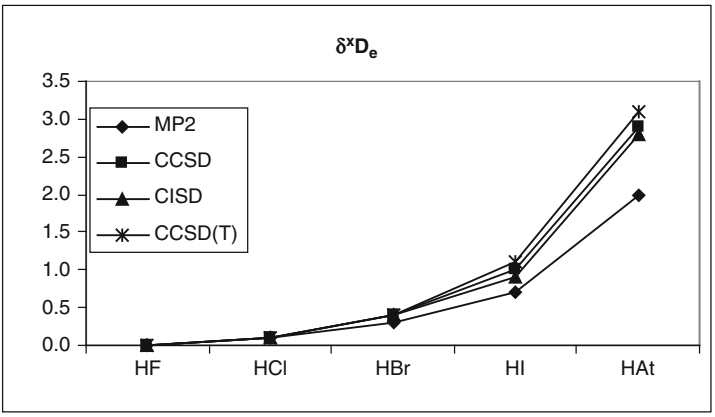

Figure 3-22. The correlation-relativistic cross terms for the dissociation energy of hydrogen halides calculated at various levels of theory (From [36])

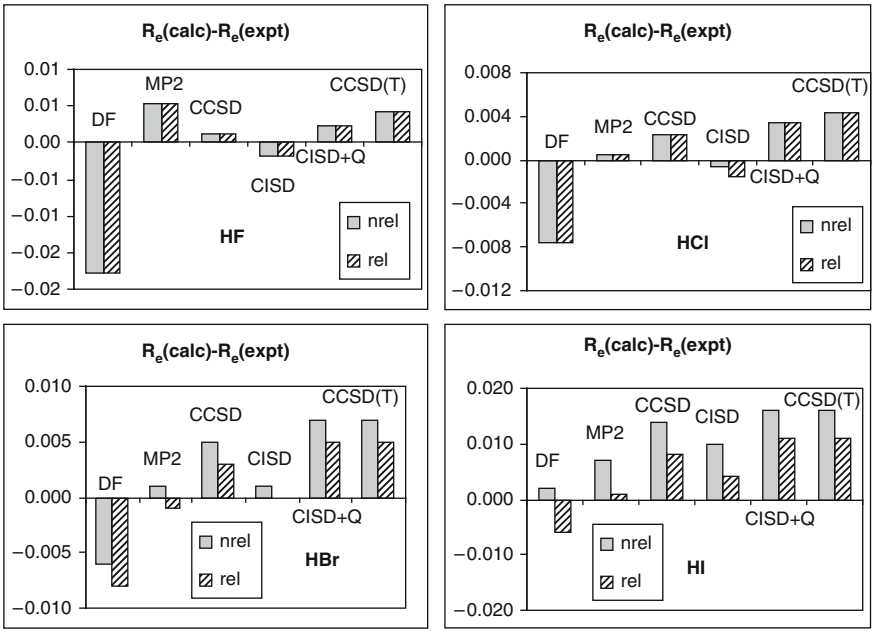

Figure 3-23. Differences between the theoretical and experimental values of the bond length R_e(Å) for the hydrogen halides molecules calculated at various levels of theory (From [36])

of halogen halides obtained on the CV1 and CV2 levels of inclusion of core-valence correlation are consistent with the DF and post DF results with the valence electrons only (V).

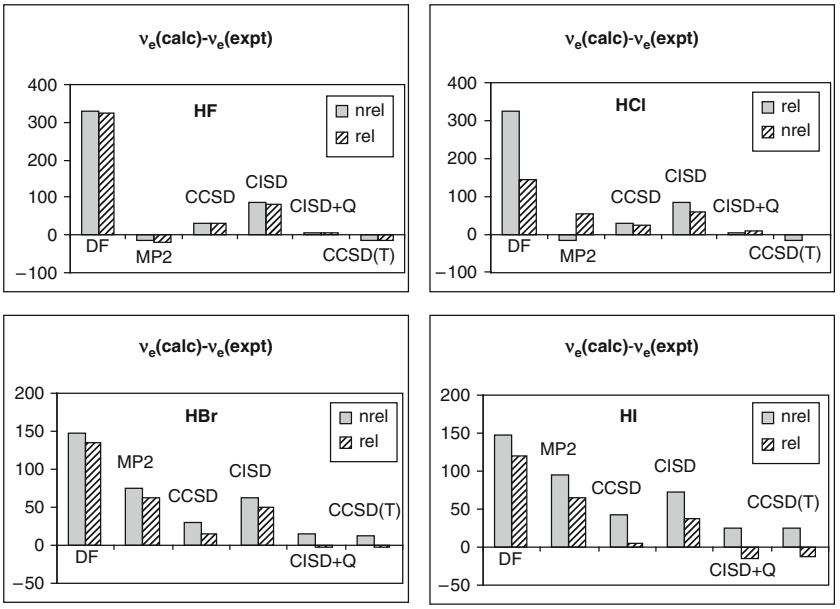

Figure 3-24. Differences between the theoretical and experimental values of the harmonic frequency $\nu_e(cm^{-1})$ for the hydrogen halides molecules calculated at various levels of theory (From [36])

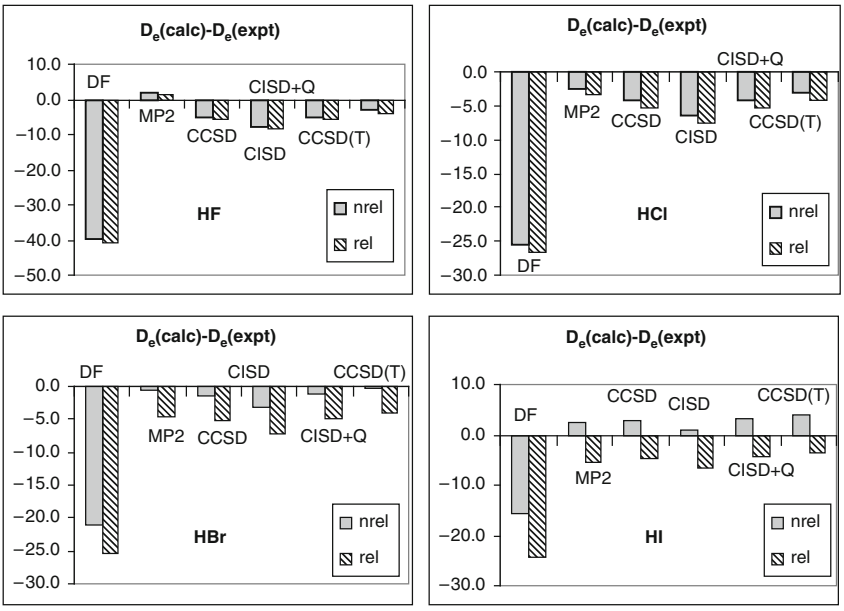

Figure 3-25. Differences between the theoretical and experimental values of the dissociation energy D_e(kcal/mol) for the hydrogen halides molecules calculated at various levels of theory (From [36])

Table 3-21 Subshells of halogen atoms X and the number of electrons included in the correlated calculations of Styszyński and Kobus [38, 39] for the HX molecules

	HF	HCl	HBr	HI	HAt
V	$2s^2 2p^5$	$3s^2 3p^5$	$4s^2 4p^5$	$5s^2 5p^5$	$6s^2 6p^5$
N(V)	8	8	8	8	8
CV1	$1s^2$	$2s^2 2p^6$	$3s^2 3p^6 3d^{10}$	$4s^2 4p^6 4d^{10}$	$5s^2 5p^6 5d^{10}$
N(CV1)	10	16	26	26	26
CV2		$1s^2$	$1s^2 2s^2 2p^6$	$3s^2 3p^6 3d^{10}$	$4s^2 4p^6 4d^{10} 4f^{14}$
N(CV2)		18	36	44	58

The inclusion of core-valence electron correlations substantially improves the agreement between the theoretical results and experiment and changes the trend obtained when only eight valence electrons are involved in the correlated methods. This is illustrated in Figure 3-26 showing the differences between the calculated and experimental values of the bond distance R_e for the HCl molecule. The theoretical values presented there were obtained with the inclusion of valence electrons (a) Cl$3s^2 3p^5$ and electrons of subsequent inner subshells: (b) $2p^6$, (c)$2s^2 2p^6$, (d)$1s^2$. As implied by the data in this figure, the core-valence effects for R_e cause a qualitative change in the picture and improve the agreement with experiment, which is the better the more inner electrons are taken into account. Finally, when all electrons are included, the theory-experiment agreement for the CCSD(T) method is excellent. Figures 3-27 and 3-28 present the differences in the harmonic frequency and dissociation energy. The inclusion of the core-valence effects only slightly changes the theory-experiment differences, but it does not change the tendencies which remain the same as for the correlated calculations with valence electrons only. Therefore, for the remaining hydrogen halide molecules, we present in Figure 3-29 the corresponding differences in the bond length R_e only and omit the analogous figures for ν_e and D_e. The inclusion of the core electrons in the correlation calculations for the hydrogen halide molecules substantially changes the values of the bond lengths and improves the agreement with experiment. If core-valence correlation is properly included, then the wrong trend obtained when only valence electrons are correlated in the post DF calculations, is reversed to the expected one: the more advanced the method of electron correlation inclusion, the better the agreement with experimental values.

3.2.1.5. Super Heavy Molecules

Systems containing heavy and super heavy elements are particularly interesting for studying the relativistic effects on the energetic structure and bonding in molecules, because of large values of these effects. Super heavy elements are yielded in nuclear synthesis reactions producing a small number of short lifetime atoms. Therefore, chemical experiments with such elements are extremely difficult and theoretical calculations can be a source of very useful information. On the other hand, the calculations for super heavy system with many electrons are not trivial and require enormous computer resources and CPU time.

Table 3-22 Spectroscopic constants of hydrogen halides calculated by Styszyński and Kobus [38, 39] at different levels of approximation

Method		F		HCl		HBr		HI		HAt	
		Nrel	Rel	Nrel	Rel	Nrel	Rel	Nrel	Rel	Nrel	Rel
						R_e(Å)					
MP2	v	0.922	0.922	1.275	1.275	1.415	1.413	1.616	1.610	1.724	1.723
	cv1	0.920	0.920	1.271	1.271	1.403	1.400	1.605	1.600	1.712	1.701
	cv2	–	–	1.271	1.271	1.402	1.399	1.604	1.598	1.712	1.698
CCSD	v	0.918	0.918	1.277	1.277	1.419	1.417	1.623	1.617	1.732	1.737
	cv1	0.916	0.916	1.273	1.273	1.407	1.406	1.612	1.607	1.721	1.715
	cv2	–	–	1.273	1.272	1.407	1.405	1.611	1.605	1.720	1.712
CCSD(T)	v	0.921	0.921	1.279	1.279	1.421	1.419	1.625	1.620	1.735	1.739
	cv1	0.919	0.919	1.275	1.275	1.410	1.408	1.614	1.609	1.723	1.718
	cv2	–	–	1.275	1.275	1.409	1.407	1.613	1.607	1.723	1.715
						ν_e(cm^{-1})					
MP2	v	4,123	4,120	3,044	3,041	2,724	2,711	2,404	2,373	2,234	2,070
	cv1	4,136	4,134	3,057	3,062	2,774	2,778	2,439	2,414	2,232	2,083
	cv2	–	–	3,058	3,064	2,776	2,782	2,443	2,426	2,233	2,084
CCSD	v	4,169	4,167	3,014	3,011	2,679	2,664	2,351	2,314	2,174	1,983
	cv1	4,184	4,182	3,028	3,033	2,727	2,727	2,388	2,358	2,179	2,002
	cv2	–	–	3,029	3,035	2,729	2,731	2,392	2,369	2,181	2,004
CCSD(T)	v	4,124	4,122	2,991	2,988	2,660	2,645	2,334	2,297	2,158	1,966
	cv1	4,139	4,137	3,004	3,009	2,707	2,706	2,369	2,337	2,161	1,981
	cv2	–	–	3,005	3,010	2,708	2,710	2,373	2,348	2,162	1,983

(continued)

Table 3-22 (continued)

Method		F		HCl		HBr		HI		HAt	
		Nrel	Rel	Nrel	Rel	Nrel	Rel	Nrel	Rel	Nrel	Rel
					D_e(kcal/mol)						
MP2	v	144.4	143.8	105.6	104.5	91.5	87.5	78.1	70.4	71.1	53.1
	cv1	145.4	144.9	106.9	105.6	94.3	90.3	80.5	72.9	73.5	56.9
	cv2	–	–	107.0	105.8	94.4	90.5	80.7	73.3	73.6	57.3
CCSD	v	137.4	136.8	103.7	102.6	90.8	86.9	78.4	70.9	71.9	54.7
	cv1	138.5	137.9	105.1	103.7	93.1	89.1	80.4	72.9	74.0	57.7
	cv2	–	–	105.1	103.9	93.2	89.3	80.6	73.3	74.1	58.1
CCSD(T)	v	139.3	138.7	105.0	103.9	92.0	88.1	79.4	72.0	72.9	55.8
	cv1	140.4	139.8	106.4	105.0	94.4	90.4	81.6	74.2	75.1	59.1
	cv2	–	–	106.4	105.2	94.5	90.6	81.7	74.6	75.2	59.5

Table 3-23 Relativistic effects on spectroscopic constants of hydrogen halides obtained by Styszyński and Kobus [38, 39] at various levels of approximation

Method		HF	HCl	HBr	HI	HAt
			ΔR_e(Å)			
MP2	v	0.0000	−0.0001	−0.002	−0.006	−0.001
	cv1	−0.0001	0.0000	−0.003	−0.006	−0.012
	cv2	–	−0.0004	−0.003	−0.007	−0.014
CCSD	v	−0.0001	−0.0001	−0.002	−0.006	0.004
	cv1	−0.0001	0.0000	−0.002	−0.005	−0.006
	cv2	–	−0.0004	−0.003	−0.006	−0.008
CCSD(T)	v	−0.0001	−0.0001	−0.002	−0.005	0.004
	cv1	−0.0001	0.0001	−0.002	−0.005	−0.005
	cv2	–	−0.0003	−0.002	−0.006	−0.007
			$\Delta\nu_e$(cm^{-1})			
MP2	v	−2	−3	−13	−31	−164
	cv1	−2	5	4	−25	−149
	cv2	–	6	7	−17	−149
CCSD	v	−2	−3	−14	−37	−191
	cv1	−2	5	0	−30	−177
	cv2	–	6	3	−23	−177
CCSD(T)	v	−2	−3	−15	−37	−191
	cv1	−2	4	−1	−32	−180
	cv2	–	6	2	−24	−179
			ΔD_e(kcal/mol)			
MP2	v	−0.6	−1.1	−4.0	−7.7	−18.0
	cv1	−0.6	−1.4	−4.0	−7.6	−16.6
	cv2	–	−1.2	−3.8	−7.4	−16.3
CCSD	v	−0.6	−1.1	−4.0	−7.5	−17.2
	cv1	−0.6	−1.4	−4.0	−7.5	−16.3
	cv2	–	−1.2	−3.9	−7.3	−16.0
CCSD(T)	v	−0.6	−1.1	−3.9	−7.4	−17.1
	cv1	−0.6	−1.4	−4.0	−7.4	−16.0
	cv2	–	−1.2	−3.8	−7.2	−15.8

Saue et al. [24] performed the relevant calculations for H(117), Sethe et al. [41] for HTl, H(113) and F(113), Fægri and Saue [42] for diatomic molecules of very heavy of group 13 and 17 atoms: TlAt, Tl(117), (113)At and (113)(117). The basis sets used by Saue et al. [24] for H and (117) and by Seth et al. [41] for H, F, Tl were derived by energy optimization in nonrelativistic atomic calculations and further augmented by extra tight functions, while the basis set used by Seth et al. for (113) were optimized in relativistic calculations. Fægri and Saue [42] used both types of basis sets. The results of DF, MP2 and CCSD(T) calculations for hydrides and fluorides of group 13 and 17 atoms are presented in Table 3-24. The correlated calculations were performed taking into account the valence electron excitations. Since in nonrelativistic and relativistic calculations Seth et al. [41] used the active space of different size, the values of relativistic correction obtained on the correlated

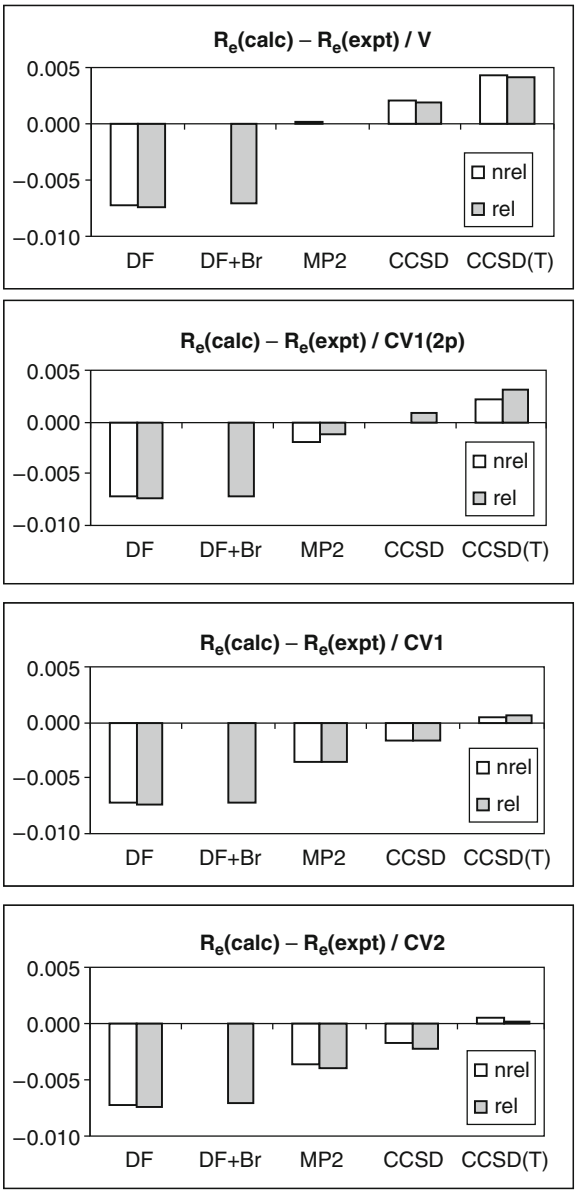

Figure 3-26. Differences between the calculated and experimental bond length values R_e(Å) for HCl obtained using the DF, DF + Br, MP2, CCSD and CCSD(T) methods for various levels of core electrons inclusion (From [38])

level given in Table 3-25 should be considered as a crude estimation only. The theory-experiment agreement for the HTl molecule is good. The CCSD(T) method gives the 0.015 Å difference in the bond length R_e, which is probably due to the

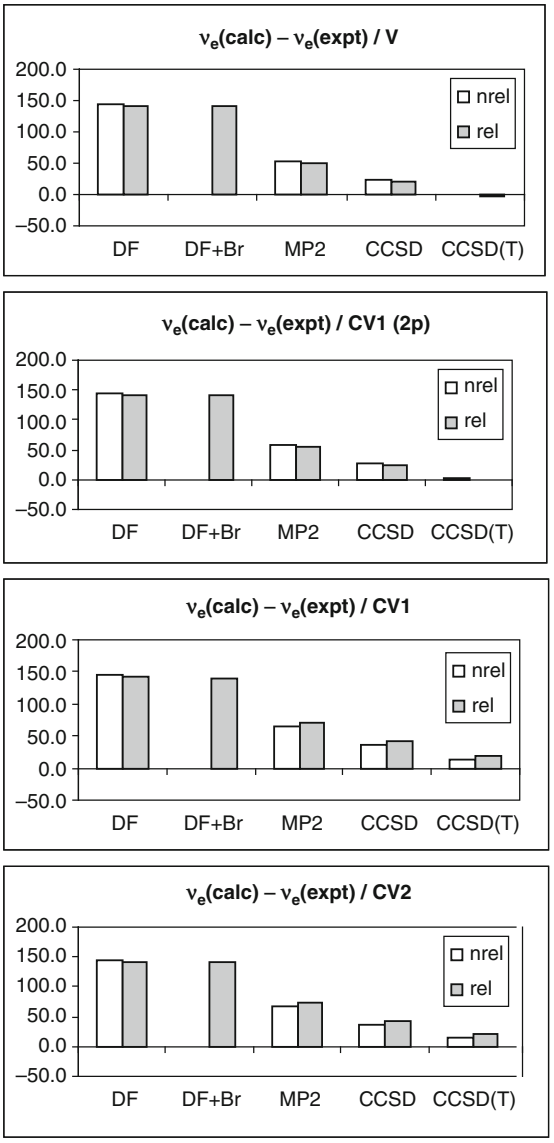

Figure 3-27. Differences between the calculated and experimental harmonic frequency values $\nu_e(cm^{-1})$ for HCl obtained using the DF, DF + Br, MP2, CCSD and CCSD(T) methods for various levels of core electrons inclusion (From [38])

neglect of the core-valence correlation effects. The relativistic effects on bonding in hydrides of super heavy atoms are dramatic and cause a shortening of the bond by 0.38 Å for H(113), while extending the bond by 0.13 Å for H(117). These opposite

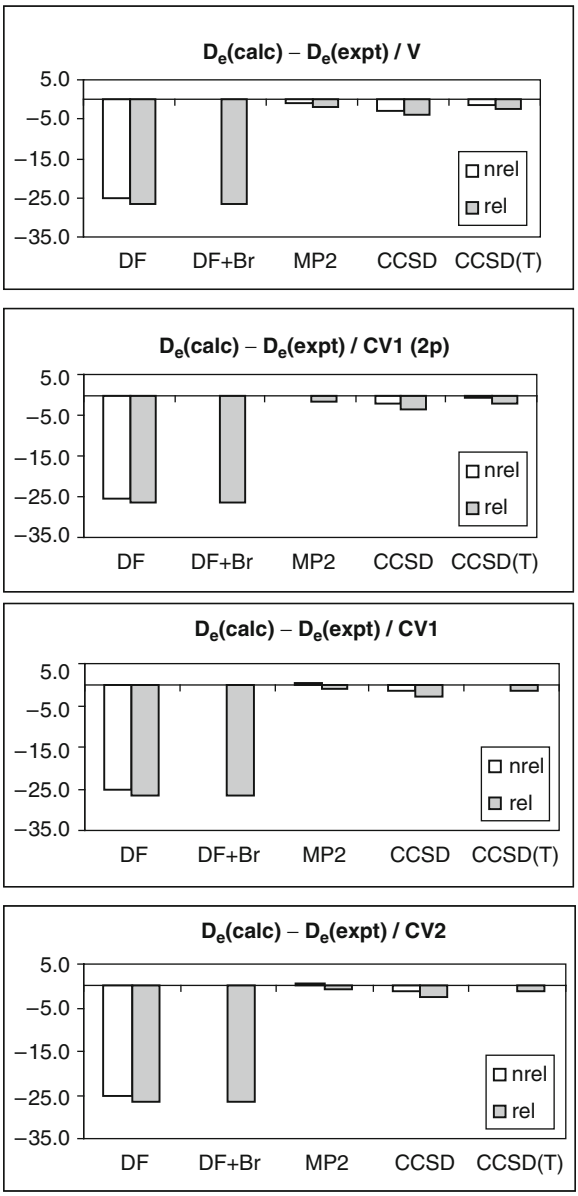

Figure 3-28. Differences between the calculated and experimental dissociation energy values D_e(kcal/mol) for HCl obtained using the DF, DF + Br, MP2, CCSD and CCSD(T) methods for various levels of core electrons inclusion (From [38])

effects my by rationalized as a result of a competition between the scalar and spin-orbit relativistic effects, which has been previously assumed to explain the change in the trend of variation in ΔR_e for the hydrogen halide series. The large contraction of

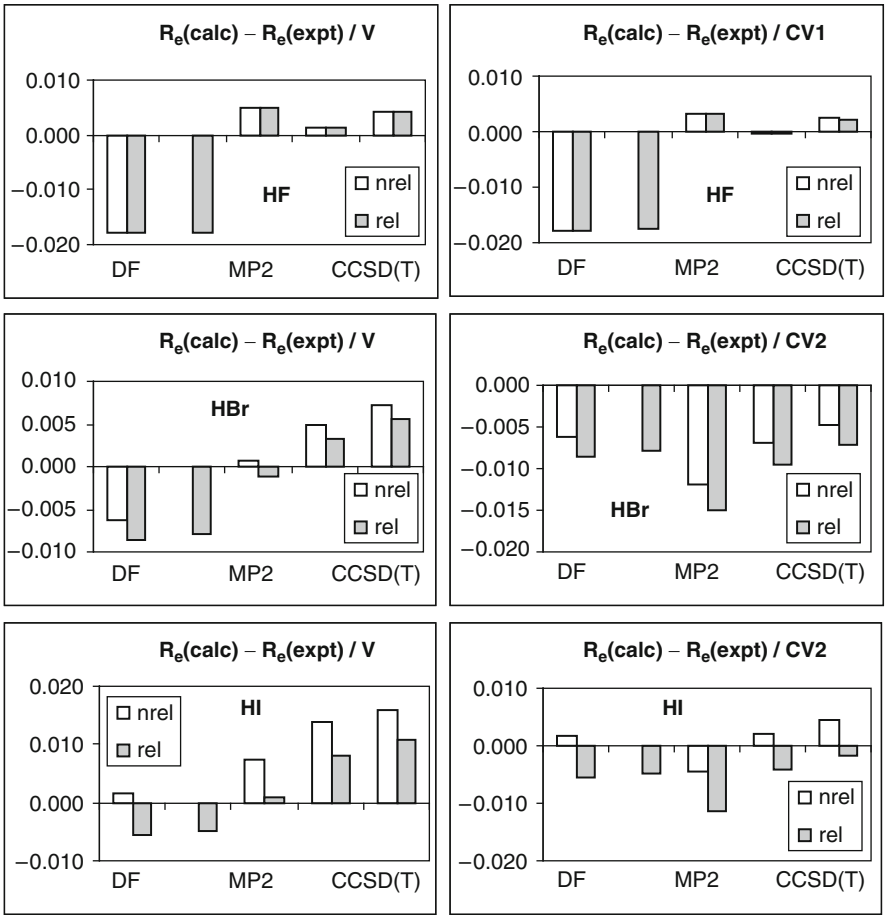

Figure 3-29. Differences between the calculated and experimental bond length values R_e(Å) for HF, HBr and HI obtained using the DF, DF + Br, MP2, CCSD and CCSD(T) methods for various levels of inclusion of core electrons (From [38])

the H-(113) bond is due to the spin-orbit splitting of *7p* shell and a large contraction of $7p_{1/2}$ orbital participating in the bond. On the other hand, an increased contribution of $7p_{3/2}$ to the bond in H(117) is responsible for the bond length expansion. The inclusion of relativistic effects increases by 278 cm^{-1} the value of the fundamental frequency in H(113) and decreases it by 285 cm^{-1} in H(117). Moreover, for H(113) the dissociation energy decreases by ∼1 eV and the dipole moment by ∼1 D. The relativistic effects on R_e and ν_e of F(113) are smaller due to the ionic character of the bond in this molecule.

Results of the calculations by Fægri and Saue [42] for TlAt, Tl(117), (113)At and (113)(117) are presented in Tables 3-26 and 3-27. The authors obtained the relativistic results within the DF approach, while the nonrelativistic ones were obtained

Table 3-24 Spectroscopic properties of the HTl, H(113), F(113) and H(117) molecules obtained at various levels of theory. Negative value of dipole moment corresponds to negative charge of the heavier atom

Molecule	Ref.	Method	R_e(Å)	$\nu_e(cm^{-1})$	D_e (eV)	μ_e(D)
HTl	[41]	DF	1.869	1,449	1.17	−0.94
		DC-MP2	1.862	1,431	1.83	−1.39
		DC-CCSD(T)	1.885	1,371	2.07	−1.22
		Expt.	1.870	1,389	2.06	–
H(113)	[41]	HF	2.082	1,412	1.77	0.53
		DF	1.704	1,690	0.50	−0.17
		MP2	2.059	1,388	2.19	1.24
		DC-MP2	1.757	1,476	1.20	0.28
		CCSD(T)	2.077	1,345	2.52	0.99
		DC-CCSD(T)	1.789	1,357	1.44	0.19
H(117)	[24]	HF	1.849	1816	–	–
		DF	1.978	1531	–	–
F(113)	[41]	HF	2.203	485	3.73	3.34
		DF	2.167	461	0.64	–
		MP2	2.219	462	5.37	4.14
		DC-MP2	2.180	478	2.77	–
		CCSD(T)	2.215	468	5.36	3.81
		DC-CCSD(T)	2.187	463	2.52	–

Table 3-25 Relativistic corrections to spectroscopic properties from Table 3-24 (From [24,41])

Molecule	Method	ΔR_e(Å)	$\Delta\nu_e(cm^{-1})$	ΔD_e(eV)	$\Delta\mu_e$(D)
H(113)	DF	−0.378	278	−1.270	−0.700
	DC-MP2	−0.302	88	−0.99	−0.96
	DC-CCSD(T)	−0.288	13	−1.08	−0.80
H(117)	DF	0.129	−285	–	–
F(113)	DF	−0.036	−24	−3.090	−3.340
	DC-MP2	−0.039	16	−2.60	–
	DC-CCSD(T)	−0.028	−5	−2.84	–

using the standard HF method and solving the four-component Lèvy-Leblond (L-L) equations [14], generated by the nonunitary transformation of the four-component spinor and by letting the speed of light $c \to \infty$. The values of the spectroscopic parameters of the XY molecules, X = Tl, (113) and Y = At, (117) obtained by these authors are given in Table 3-26. The values of the estimated relativistic corrections to these parameters are included in Table 3-27.

We can assume a simple bonding mechanism in the XY molecules, in which the bond is created by the valence *s* orbital of group 13 atom X and the valence *p* orbital of group 17 atom Y. The energies of the valence orbitals of the Tl, (113), At and (117) atoms are displayed in Figure 3-30. The relative contribution of the valence $np_{1/2}$ and $np_{3/2}$ orbitals to the bonding is determined by the energy splitting and

Table 3-26 Spectroscopic properties of diatomic molecules of very heavy elements of group 13 and 17 calculated by Fægri and Saue [42]. Negative value of dipole moment corresponds to negative charge of group 17 atom

Molecule	Method	R_e(Å)	ν_e(cm^{-1})	μ(D)
TlAt	HF	3.069	116	–
	L-L	3.057	113	−4.32
	DF[a]	2.987	115	–
	DF	2.977	116	−4.37
Tl(117)	HF	3.234	99	–
	L-L	3.235	99	−4.46
	DF[a]	3.113	95	–
	DF	3.112	98	−1.67
(113)At	HF	3.209	103	–
	L-L	3.206	102	−4.79
	DF[a]	2.970	114	–
	DF	2.948	114	−2.24
(113)(117)	HF	3.373	96	–
	L-L	3.391	83	−4.99
	DF[a]	3.056	102	–
	DF	3.044	101	1.80

[a]Results obtained with basis sets of nonrelativistically optimised exponents but augmented with extra tight exponents

Table 3-27 Relativistic corrections to spectroscopic properties from Table 3-26 estimated as a difference between the relativistic (DF) and the corresponding nonrelativistic (HF, L-L) values (From [42])

Molecule	Method	ΔR_e(Å)	$\Delta\nu_e$(cm^{-1})	$\Delta\mu$(D)
TlAt	DF[a]-HF	−0.082	−1	–
	DF[a]-(L-L)	−0.070	2	–
	DF-HF	−0.092	0	–
	DF-(L-L)	−0.080	3	−0.05
Tl(117)	DF[a]-HF	−0.121	−4	–
	DF[a]-(L-L)	−0.122	−3	–
	DF-HF	−0.122	−1	–
	DF-(L-L)	−0.123	−1	2.79
(113)At	DF[a]-HF	−0.239	10	–
	DF[a]-(L-L)	−0.236	12	–
	DF-HF	−0.261	11	–
	DF-(L-L)	−0.258	12	2.55
(113)(117)	DF[a]-HF	−0.317	6	–
	DF[a]-(L-L)	−0.336	19	–
	DF-HF	−0.329	5	–
	DF-(L-L)	−0.347	18	6.79

[a]Results obtained with basis sets of nonrelativistically optimised exponents but augmented with extra tight exponents

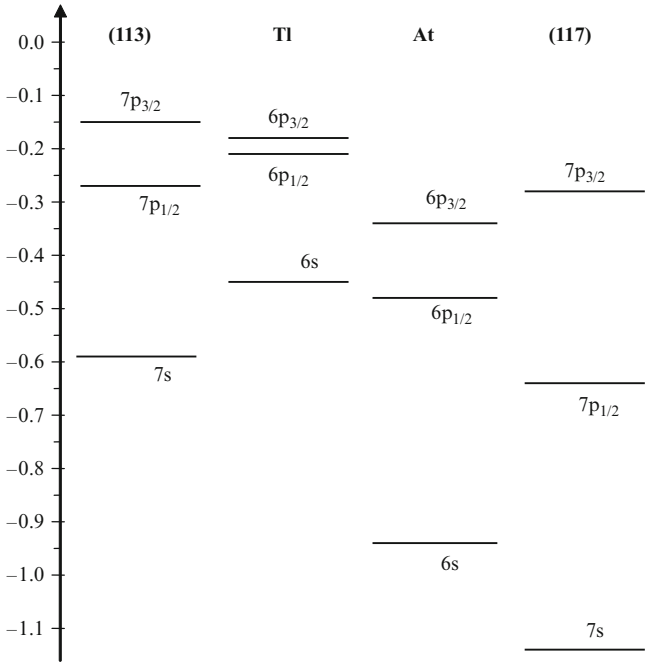

Figure 3-30. Valence *nsnp* atomic energy levels for group 13 and 17 atoms

different spatial extents of these two groups of orbitals [42]. Stabilization of the $Ynp_{1/2}$ orbital increases the $Ynp_{3/2}$ contribution to the bonding, which leads to an expansion of the bond due to the increased size of the $Ynp_{3/2}$ orbital. On the other hand, the stabilization of the $Xp_{1/2}$ orbital induces its greater participation in the bonding and leads to a dramatic contraction of the bond length. The finial effect is a resultant of these two opposite effects. The above mechanism describes also the bonding in hydrides of group 13 and 17 atoms, if we substitute the valence *s* orbital by *1s* orbital of the hydrogen atom. Therefore, in hydrides of very heavy halides, where the bonding is dominated by $np_{3/2}$, we observe the final bond expansion by 0.002 and 0.13 Å, for HAt and H(117), respectively. In the diatomic XY molecules of group 13 and 17 atoms the final effect is the contraction of the bond as can be seen from Table 3-27. These effects are large, for example, 0.26 and 0.35 Å for (113) At and (113)(117), respectively. The increasing involvement of the $np_{3/2}$ orbital of Y results in a decreased participation of group 17 elements in the bond and in changing the dipole moment μ from -4.37 D in TlAt to -1.67 D in Tl(117). The negative sing of μ corresponds to the negative charge of the group 17 atom. In (113)At again we have an increased group 13 participation in the bond and $\mu = -2.24$ D. Finally, in the (113)(117) molecule, both stabilization of (113)$7p_{1/2}$ orbital and destabilization of (117)$7p_{3/2}$ orbital result in a more pronounced participation of the (113) atom in the bond and gives a transfer of electron charge from the (117) to (113) atom, leading to the dipole moment $\mu = +1.80$ D.

3.2.2. Polyatomic Molecules

3.2.2.1. $PtCH_2^+$

Cationic platinum carbene is the most likely reaction product between Pt^+ and CH_4 and it is the key molecule for subsequent C-C coupling reactions. Heinemann et al. [43] postulated that the Pt^+ mediated activation of methane ($Pt^+ + CH_4 \rightarrow PtCH_2^+ + H_2$) can occur due to a relativistic strengthening of the Pt^+–CH_2 bond. In their paper, they evaluated the interplay of relativistic and correlation effects on the structure and the bond strength of Pt^+–CH_2. They used basis sets of roughly triple-zeta quality with extra polarization functions for Pt and performed DF and relativistic MP2 calculations with 15 valence electrons included in the active space, assuming C_{2v} symmetry. Figure 3-31 presents the valence molecular orbitals of $PtCH_2^+$ formed from the *5d*, *6s* orbitals of Pt^+ (^{2}D) and the a_1, b_1 orbitals of CH_2. The ground state of methylene is $^3B_1$, while its first excited state is $^1A_1$, with the energy difference (MP2) of 16 kcal/mol. The authors expected these two lowest electronic states of CH_2 to mix upon binding to Pt^+ and considered three extreme bonding situations. Relativistic effects, influencing the ordering of the valence *5d* and *6s* orbitals of Pt with respect to each other and relative to the orbitals of methylene, may change the bonding mechanism in $PtCH_2^+$.

The population analysis of the nonrelativistic wave function allows an interpretation of $PtCH_2^+$ as an electrostatic complex with the *5s/6d* hybridization due to the donation of the lone pair into the axial hybrid. Analysis of the relativistic results leads to an increase in the Pt*6s* occupation accompanied by the depletion of the *5d* occupation, which can be attributed to the stabilization of the *6s* orbital and

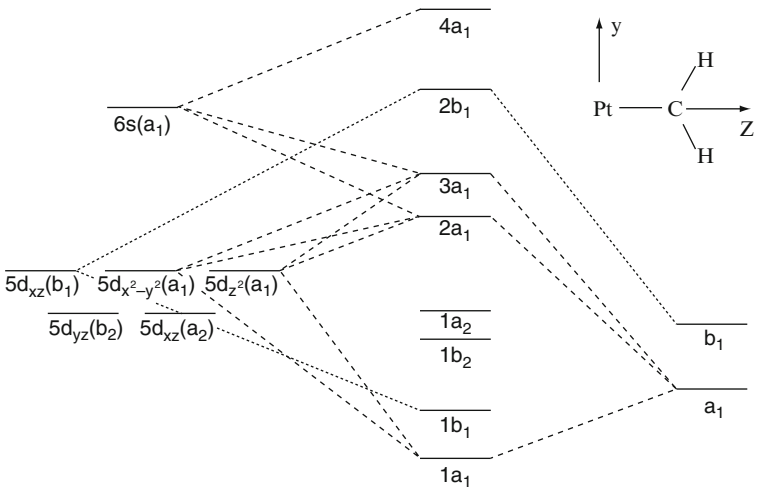

Figure 3-31. Qualitative molecular orbital diagram for $PtCH_2^+$ (Reprinted with permission from C. Heinemann, H. Schwarz, W. Koch, K. Dyall, J. Chem. Phys. 104, 4642 (1996). Copyright 1996, American Institute of Physics)

Table 3-28 Optimised geometry parameters and bond dissociation energy (BDE) for the $PtCH_2^+$ molecule and relativistic corrections to them calculated by Heinemann et al. [43] at various levels of theory. Bond lengths are given in Å, bond angles in degrees and BDE in kcal/mol

Method	R_1(Pt-C)	R_2(C-H)	Θ(Pt-C-H)	α(H-C-H)	BDE[a]
HF	2.243	1.083	125.2	109.6	20.1
DF	1.935[b]	1.107	120.2	119.6	47.2
MP2	1.898	1.090	121.8	116.4	50.6
DC-MP2	1.787	1.089	120.4	119.2	100.8
expt.	–	–	–	–	113.3[c]
Δ^{rel}(DF)	−0.307	0.023	−5.0	10.0	27.1
Δ^{rel}(DC-MP2)	−0.111	−0.001	−1.4	2.8	50.2

[a] $BDE = E(Pt^+) + E(CH_2) - E(PtCH_2^+)$
[b] Optimised with the R(C-H) and Θ(Pt-C-H) parameters kept frozen
[c] Derived by Heinemann et al. [43] from experimental data of [44]

destabilization of the *5d* orbitals. In other words, the excited $5d^8\,6s^1$ configuration mixes into the wave function leading to a twofold electron pair formation with the CH_2 group, i.e. to the formation of the Pt-C double bond. The relativistic effects favour the formation of a double bond and change the bond order from one to two. Table 3-28 gives the values of the optimized geometry parameters. As shown, the relativistic effects are dramatic and stabilize the cationic platinum carbene. They shorten the bond by 0.3 and 0.1 Å on DF and MP2 level of theory, respectively. The bond contraction is three times smaller on the correlated level than in the DF method. Inclusion of the relativistic effects decreases the Pt-C-H angle by 5° and 1.4° and increases the bond dissociation energy (BDE) relative to that of Pt^+ and CH_2 in their electronic ground states by 27 kcal/mol and 50 kcal/mol on the DF and MP2 level of theory, respectively. The influence of both relativistic effects and electron correlation is shown to be highly significant in the calculation of BDE and their incorporation leads to doubling of its value. The inclusion of electron correlation improves the agreement with experiment [44]. However, the authors conclude that the MP2 method performs fortuitously well because of the oscillating behaviour of the perturbation series. In this case the relativistic and correlation effects are strongly nonadditive.

3.2.2.2. UF_6

De Jong and Nieuwpoort [45] studied the influence of relativistic and correlation effects on the electronic structure and spectroscopic properties of the uranium hexafluoride molecule. They derived for uranium a contracted basis set of dual family type (i.e. basis set, which consists of a two sets of exponents and the $(l + 2)$-exponents form a subset of the *l*-exponents set [46]) augmented with extra tight and diffuse functions. The molecular calculations for the ground state $^1A_{1g}$ of UF_6 were performed using the DF and CISD methods and assuming O_h symmetry. The energies of valence spinors obtained from the DF calculations are graphically presented

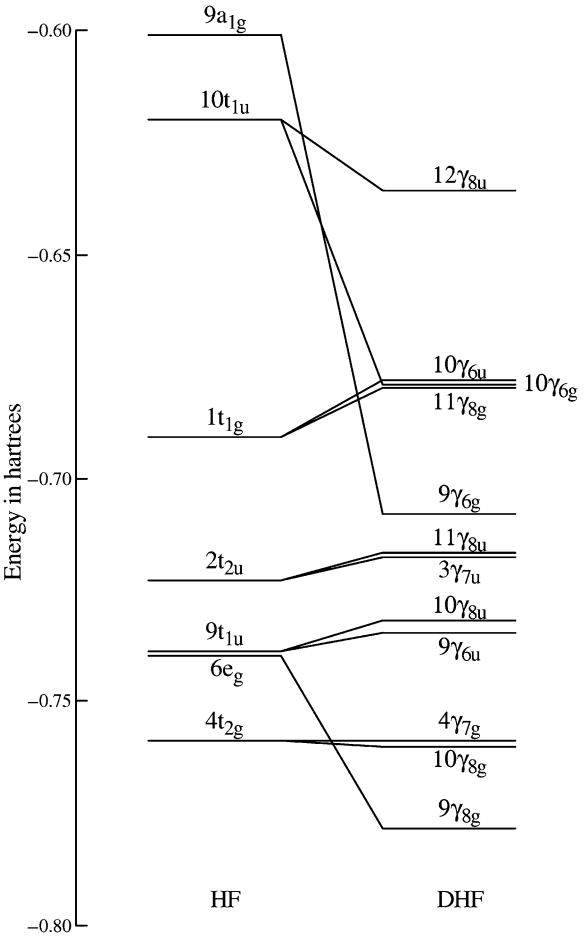

Figure 3-32. Nonrelativistic (HF) and relativistic (DHF) energies (in a.u.) of valence orbitals of UF_6 (Figure 1 from W. A. de Jong and W. C. Nieuwpoort, International Journal of Quantum Chemistry, Vol. 58, No. 2, 1996, 203–216. Reprinted with permission of John Wiley and Sons, Inc.)

in Figure 3-32. For the sake of comparison, the energies of the nonrelativistic HF spinors are also given. As implied by the figure, the relativistic effects change the value and the order of orbital energies. The HOMO orbital $9a_{1g}$ in the HF calculations is of U$6s_{1/2}$ character and shifts down ($9\gamma_{6g}$) in energy. The next one below, the $10t_{1u}$ orbital with a large amount of U$6p$ character, splits into the $12\gamma_{8u}$ and $10\gamma_{6u}$ orbitals. Both effects reflect the relativistic atomic effects in the uranium atom: a strong contraction (12.4 eV) of the $6s_{1/2}$ shell and a large spin orbit splitting (9.7 eV) of the *6p* shell. The DF results indicate the $12\gamma_{8u}$ orbital to be HOMO as shown in Figure 3-32. The molecular orbitals with a significant U6*s* contribution are antibonding in the nonrelativistic description and due to a strong contraction of

Table 3-29 Bond length, atomization energy and electron affinity of UF_6 obtained by de Jong and Nieuwpoort [45]

	R_e(Å)	D_e(eV)	EA (eV)
HF	1.995	9.0	8.9
DF	1.994	23.1	6.4
DF + Br	–	22.7	6.5
DC-CISD	–	–	5.3
Expt.[a]	1.999	31.9	5.1
Δ^{rel}(DF)	−0.001	14.1	−2.5
Δ^{expt}(DF)	0.005	8.8	−1.3
Δ^{expt}(CISD)	–	–	−0.2

[a]Experimental results of Compton [48]
Δ^{rel}(DF) = X(DF) – X(HF)
Δ^{exp}(DF) = X(DF) – X(expt.)
Δ^{exp}(CISD) = X(DC-CISD) – X(expt.)

the U$6s$ orbitals, become nonbonding in the relativistic description. This means that DF calculations imply a stronger bonding. The same occurs for the U$6p$ orbitals but this effect is smaller. The large (∼8 eV) upward shift in the energy of U$5f$ (due to a more effective screening of the nucleus by contracted inner s and p orbitals) is also reflected in the upward shift of the corresponding molecular orbitals ($9\gamma_{6u}$, $10\gamma_{8u}$) with large $5f$ character. This effect for the U$6d$ orbitals is much smaller. These conclusions are in agreement with the DF results reported by Malli and Styszyski [47]. In Table 3-29 the values of the bond length R_e, the atomization energy D_e into seven atoms and the electron affinity EA obtained by de Jong and Nieuwpoort [45] are given. Their results agree well with the experiment. The relativistic corrections to the bond length are small and cause its contraction by 0.001 Å. On the other hand, we observe a dramatic increase in the atomization energy by 14 eV. The small relativistic contraction of the bond length, in spite of increased bonding energy, is consistent with the relativistic effects on the molecular orbitals with a significant U$6s$ contribution. The electron affinity calculated on the DC-CISD level agrees well with the experimental result of Compton [48].

3.2.2.3. CUO

Laser ablation matrix infrared experiments have made it possible to synthesize small actinide molecules like CUO. In such experiments, laser ablated uranium atom contacts with CO, which breaks the triple C-O bond. Adrews et al. [49, 50] suggested that due to the interaction with the noble gas (Ar, Kr) matrix, the ground state of the gas phase molecule is changed from $^1\Sigma_0{}^+$ to $^3\Phi_2$, which leads to a large vibration frequency shift in the C-U stretching.

Infante and Visscher [51] reported the energy distance between the two lowest lying states $^1\Sigma_0{}^+$ and $^3\Phi_2$ of CUO calculated by different four-component methods. In the calculations by the DF, CCSD, CCSD(T) and MR-CCSD methods they exploited the basis sets of de Jong [52] and Fægrii [53] for the uranium

Table 3-30 Optimised values of the bond distances R_{CU} and R_{UO} for the $^3\Phi_2$ and $^1\Sigma_0^+$ states of the CUO molecule and adiabatic energy difference $\Delta E_2 = E(^3\Phi_2) - E(^1\Sigma_0^+)$ calculated by Infante and Visscher [51] at various levels of theory

State	R_{CU}(Å)	R_{UO} (Å)	Method	Act. space	ΔE_2(kJ/mol)
$^1\Sigma_0^+$	1.772	1.808	DF	–	−36.8
$^3\Phi_2$	1.889	1.842	CCSD	12e	2.5
				22e	34.3
				34e	49.8
			CCSD(T)	12e	3.3
				22e	40.6
				34e	58.2
			MR-CCSD	12e	23.0
				22e	34.3
				34e	57.3

atom and cc-pVTZ basis sets for carbon and oxygen. The CC calculations were performed for different sizes of the active space by inclusion of 12, 22 and 34 valence and subvalence electrons in the correlated calculations. In this way the core-valence correlation effects were partly taken into account. The set of virtual orbitals was restricted to those with the orbital energy below 10 a.u. Since in the triplet state there is one electron less participating in the bond relative to those in the singlet state, the authors expected these two states to have different R_{CU} (and R_{UO}) bond distances. Therefore, they computed the energy of a given state assuming the geometry optimized for that state, rather then the common optimized geometry. Table 3-30 gives the bond lengths R_{CU}, R_{UO} and the energy difference $\Delta E_2 = E(^3\Phi_2) - E(^1\Sigma_0{}^+)$ calculated at various levels of theory. The correlation energy changes the value of ΔE_2 from −36.8 to 58.2 kJ/mol for the largest active space of 34 electrons, i.e. makes it positive. It fits with the experimental picture in which the interaction with a number of noble gas atoms is required to change the ground state. Spin-orbit coupling splits the $^3\Phi$ state into $^3\Phi_2$, $^3\Phi_3$ and $^3\Phi_4$ and lowers the lowest $^3\Phi_2$ component by 40 kJ/mol, however the correlation energy stabilizes the $^1\Sigma_0{}^+$ state more (by almost 100 kJ/mol) than the $^3\Phi_2$ state. The result of Infante and Visscher is in contrast to the earlier accurate CASPT2 calculations of Roos et al. [54], who predicted $^3\Phi_2$ as the ground state (both with and without approximate inclusion of the spin-orbit coupling) in contradiction to the experimental findings of the inversion of the ground state relative to the gas phase.

3.3. ELECTRIC PROPERTIES OF MOLECULES

An important contribution to the development of *ab initio* all electron four-component methods for molecules was the paper by Visscher et al. [55], in which the four-component random phase approximation (RPA) method was described and implemented in the RELCCSD code. The authors applied this method to the

calculation of the frequency dependent dipole polarizabilities $\alpha(\omega)$ of H_2O, SnH_4 and Hg. The relativistic corrections to $\alpha(\omega)$ of the water molecule are small, of about 0.1% of the corresponding nonrelativistic values and are becoming significant (a few per cent) for a heavier molecule of tin tetrahydride. The relativistic corrections to the frequency-dependent polarizability $\alpha(\omega)$ of mercury are very large (50% and more), change its value significantly and give two (instead of one in nonrelativistic case) excitation peaks, due to the spin-orbit splitting which makes the transition $^1S_0 \rightarrow ^3 P_1$ allowed.

3.3.1. Electric Properties of Interhalogens

The RPA method implemented by Visscher et al. [55] was used by de Jong et al. [37] in their calculation of electric properties of interhalogens. They studied the relativistic effects on the electric dipole and quadrupole moments and the static dipole polarizability of the XY series, X, Y = F, Cl, Br, I. These parameters were calculated assuming the experimental bond length and the quadrupole moment was computed relative to the centre of mass of the molecule. The dipole and quadrupole moments were calculated as expectation values, while the dipole polarizability as a response property using the propagator method within the RPA approach. The correlation effects were estimated by means of CISD calculations. The calculations were performed with the pVDZ and pVTZ basis sets used in the calculations of spectroscopic properties of the HX and XY molecules as described earlier in this chapter. The values of the electric dipole moment μ_z, quadrupole moment Θ_{zz} and static dipole polarizability α_{zz} for the series of interhalogen molecules XY, X, Y = F, Cl, Br and I, calculated using the relativistic DF and CISD methods and exploiting the pVTZ basis sets are given in Table 3-31. All quantities are in atomic units. For the sake of comparison, the corresponding nonrelativistic and experimental values [56–64] are also given in Table 3-31. The relativistic corrections to the electric properties of XY are presented in Table 3-32 and in Figure 3-33. As implied by the data, the electric dipole moment undergoes a relativistic increase for all the molecules. This effect becomes increasingly important for the heavier molecules. For the iodine containing molecules this contribution is 10–20% of the total value. The theoretical CISD results overestimate the experimental values by 5–9%. The inclusion of the correlation effects significantly improves the agreement with experiment. The computation error bars for μ_z and Θ_{zz} are marked in Figure 3-34. The relativistic effects on quadrupole moment show monotonic behavior and are large for iodine containing molecules IF and ICl. The Θ_{zz} values of the two lightest molecules are within the wide error bars of the experimental data. The inclusion of relativistic effects leads to an increase in α_{zz} except for the IF molecule, in which a significant decrease is found. This increase is significant for BrCl, IF, ICl and IBr, with the largest relativistic effect on IBr. Figure 3-35 presents the correlation-relativistic crossterms

Table 3-31 Dipole moments μ_z, quadrupole moments Θ_{zz} and static dipole polarizability α_{zz} calculated by de Jong et al. [37] for interhalogen molecules. The positive sign of μ_z corresponds to X^+Y^- polarity

	ClF	BrF	IF	BrCl	ICl	IBr
			μ_z(a.u.)			
HF	0.438	0.644	0.790	0.201	0.425	0.243
DF	0.444	0.680	0.900	0.234	0.548	0.340
CISD	0.378	0.569	0.709	0.194	0.405	0.226
DC-CISD	0.383	0.601	0.810	0.224	0.518	0.313
Expt.	0.3494[a]	0.559[c]	0.766[d]	0.204[e]	0.49[f]	0.290[h]
	0.346[b]	–	–	–	0.475[g]	0.286[i]
			Θ_{zz} (a.u.)			
HF	0.828	0.382	0.059	2.515	2.313	3.696
DF	0.836	0.349	−0.189	2.533	2.123	3.772
CISD	0.912	0.557	0.255	2.535	2.352	3.722
DC-CISD	0.922	0.534	0.045	2.560	2.196	3.815
Expt.	1.00[b]	0.68[b]	–	–	–	–
	0.65[b]	0.91[b]	–	–	–	–
			α_{zz} (a.u.)			
HF	22.18	27.97	36.30	51.55	64.98	78.85
DF	22.20	27.96	35.85	51.82	65.49	80.38

[a]Experimental value of Davis and Muenter [56]
[b]Experimental value of Ewing et al. [57]
[c]Experimental value of Nair et al. [58]
[d]Experimental value of Nair et al. [60]
[e]Experimental value of Nair et al. [59]
[f]Experimental value of of Herbst and Steinmetz [61]
[g]Experimental value of Durand et al. [62]
[h]Experimental value of Tiemann and Dreyer [63]
[i]Experimental value of Nair and Hoeft [64]

Table 3-32 Relativistic effects on electric properties of interhalogens from Table 3-31 (From [37])

	ClF	BrF	IF	BrCl	ICl	IBr
			$\Delta\mu_z$ (a.u.)			
DF	0.006	0.036	0.111	0.033	0.123	0.097
DC-CISD	0.005	0.032	0.101	0.030	0.112	0.087
			$\Delta\Theta_{zz}$ (a.u.)			
DF	0.009	−0.033	−0.248	0.018	−0.191	0.076
DC-CISD	0.010	−0.023	−0.210	0.025	−0.156	0.093
			$\Delta\alpha_{zz}$ (a.u.)			
DF	0.02	−0.01	−0.46	0.27	0.51	1.53

contributing to electric dipole and quadrupole moments. These effects are small, of a few tenth of a.u., but increase fast and we may expect them to be not negligible for interhalogens with heavy and superheavy atoms At and (117).

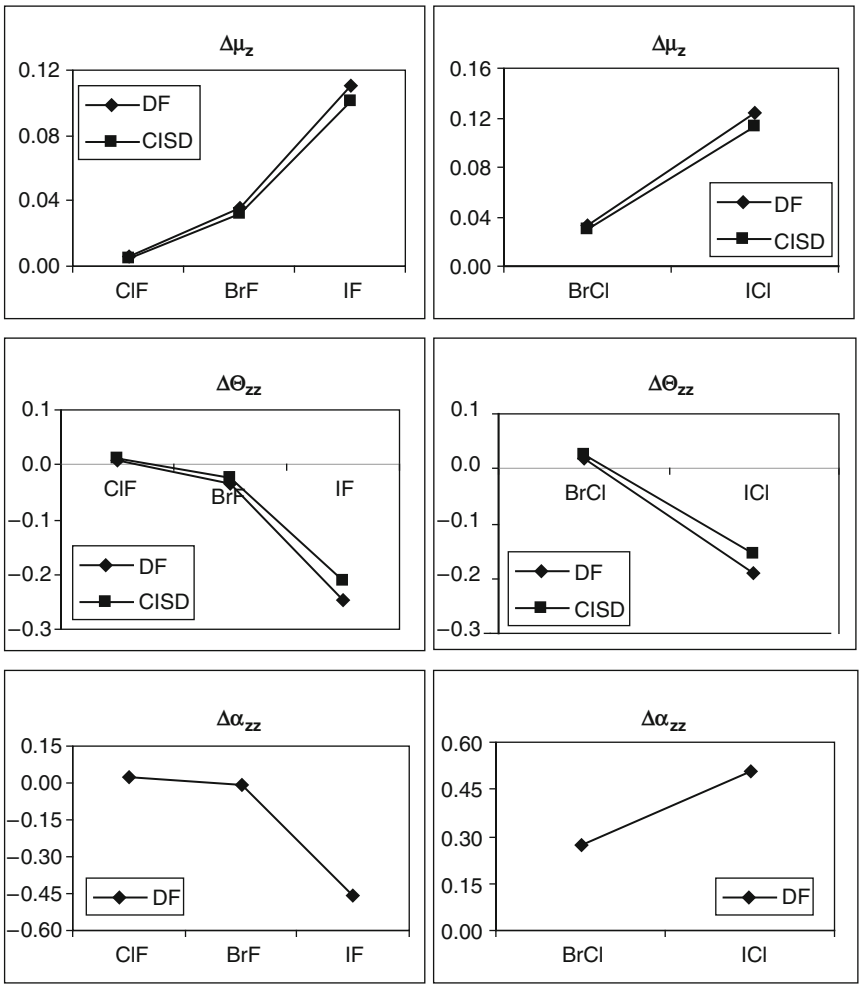

Figure 3-33. Relativistic effects (in a.u.) on dipole moment μ_z, quadrupole moment Θ_{zz} and dipole polarizability α_{zz} of interhalogens (From [37])

3.3.2. Electric Field Gradient and Quadrupole Moments

The nuclear quadrupole moment (NQM) is a quantity describing the nonspherical distribution of the nuclear charge. It can be determined from the molecular calculations by combining the experimental nuclear quadrupole coupling constants (NQCC) available from microwave spectroscopy and the electric field gradients (EFG) calculated according to the formula:

$$Q(X) = k\frac{\nu_Q(X)}{q(X)}, \tag{3-2}$$

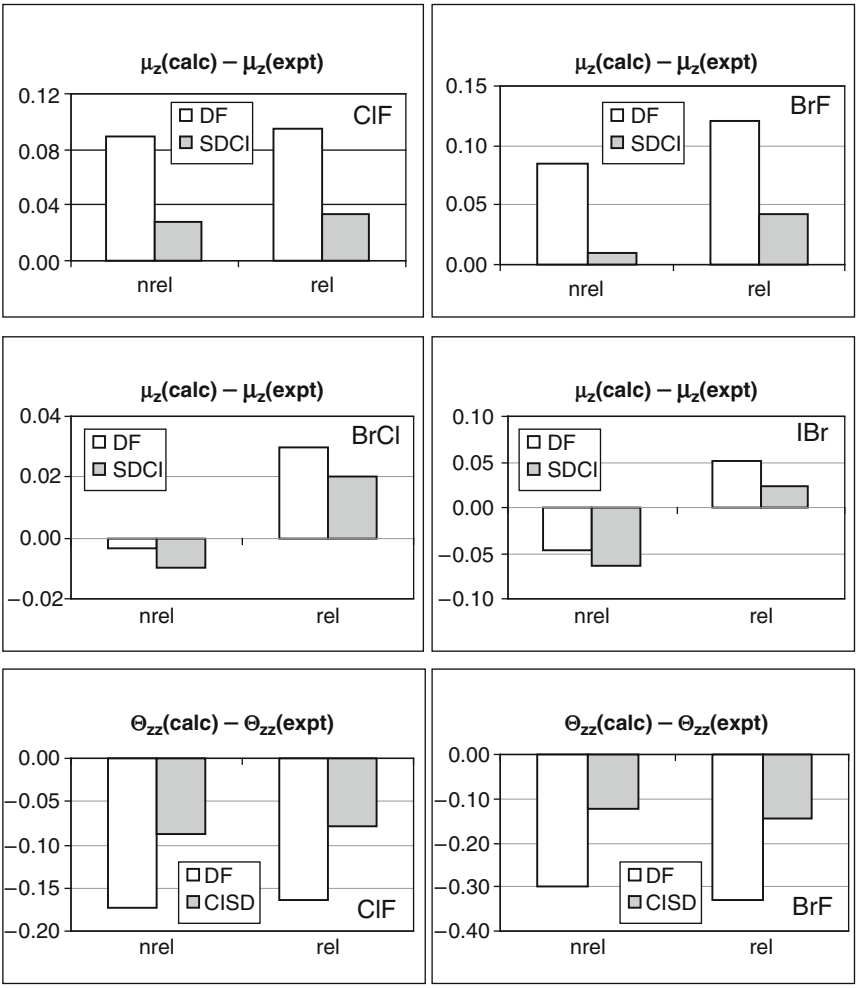

Figure 3-34. Differences (in a.u.) between the calculated and experimental values of electric properties of interhalogens (From [37])

where $\nu_Q(X)$ is NQCC in MHz, q(X) is EFG (in a.u.) at the position of the nucleus X, Q(X) is NCM in barns and the conversion factor $k = 1/234.9647$. For the nuclei for which highly accurate experimental NQCC are available, the accuracy of NCM is determined by the quality of calculated EFG. Visscher's group published a series of papers in which the state of art of the relativistic molecular calculations of EFG and new recommended values of NQM are reported. Such calculations require an advanced level of inclusion of not only relativistic effects but also electron correlation. In the molecular approach the values of NQM are usually derived for a series of molecules containing the atom of interest and then they are averaged for a given method. Van Stralen and Visscher [65] determined NQM of ^{115}In on the

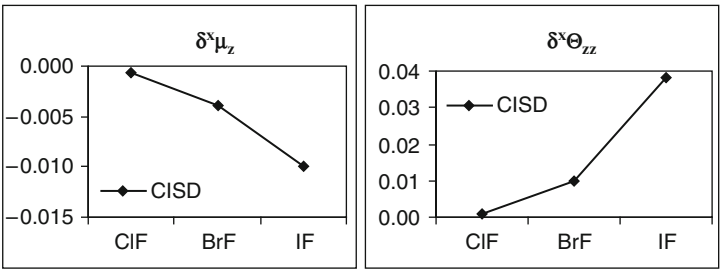

Figure 3-35. Correlation-relativistic cross terms (in a.u.) for the electric dipole and quadrupole moments of interhalogens (From [37])

Table 3-33 Electric field gradient (in a.u.) values at the In nucleus in a series of indium halides calculated by van Stralen and Visscher [65] at various levels of theory. DF-benchmark results were obtained using the basis sets for indium and halogen atoms for which the EFG on In was converged within 0.001 a.u; the remaining results were obtained using smaller basis sets, for which EFG convergence within 0.01 a.u. was obtained

Method	InF	InCI	InBr	InI
HF	−3.990	−3.671	−3.553	−3.462
DF	−4.425	−4.067	−3.910	−3.762
DF-benchmark	−4.432	−4.074	−3.914	−3.754
DC-MP2	0.404	0.449	0.441	0.438
DC-CCSD	0.326	0.347	0.318	0.309
DC-CCSD(T)	0.420	0.422	0.405	0.400

basis of the calculations for indium halides: InF, InCl, InBr, InI. Accurate calculations of EFGs have to take into account the core and valence polarization, which in turn requires large basis sets. To optimize the exponents of the basis set for the indium atom, the authors used the DF energy criterion for the ground state of In. In the next step, the convergence of EFG as a function of basis set extension with extra polarization, diffuse and tight functions, was studied. For halide atoms the basis sets of triple zeta quality were used. On the correlated level van Stralen and Visscher performed a thorough analysis of the core correlation and the effect of truncation of the virtual spinors. They came to the conclusion, that both relativistic and correlation contributions to EFG at the In nucleus in indium halides are of roughly the same magnitude but of the opposite sign. Therefore, due to the near cancellation of both contributions, they observe a fortuitous agreement between the HF and DC-CCSD(T) values. The values of EFG at the indium nucleus in various indium halides are presented in Table 3-33. The values of the nuclear quadrupole moments of In obtained using the calculated EFGs are given in Table 3-34 and in Figure 3-36. Average values of NQMs derived from different molecules and their average absolute deviations (AAD) are given in the last column of this table. As follows, the relativistic effect and electron correlation reduce substantially the values of these deviations. The small value of AAD at the DC-CCSD(T) level indicates

Table 3-34 Nuclear quadrupole moments of ^{115}In (in mb) derived by van Stralen and Visscher [65] from a series of indium halides at various levels of theory

Method	InF	InCI	InBr	InI	Average
HF	775.7	764.7	760.2	746.7	761.8 (8.4)
DF	699.4	690.2	690.9	687.2	691.9 (3.7)
DC MP2	768.3	774.6	777.6	779.7	775.1 (3.6)
DC CCSD	753.7	750.7	751.1	750.6	751.5 (1.1)
DC CCSD(T)	771.4	768.8	769.6	770.8	770.2 (1.0)

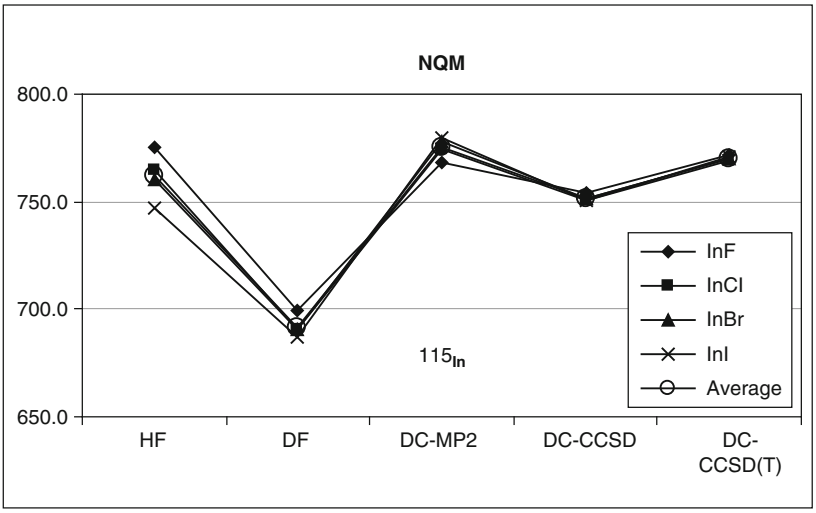

Figure 3-36. NQMs of ^{115}In derived from different indium halides using different methods (From [65])

the quality of these calculations. Therefore, the authors used these results to recommend the new value of nuclear quadrupole moment of ^{115}In as Q(^{115}In) = 770(8) millibarn (mb).

In another paper van Stralen and Visscher [66] calculated NQM of ^{127}I in thorough relativistic molecular calculations on nine closed-shell diatomic molecules: HI, IF, ICl, IBr, I_2, CuI, AgI, AuI and TlI. The recommended value of NQM obtained by them is 696(12) mb. A separate paper of Belpassi and coworkers [67] was devoted to NQM of gold. They report relativistic calculations of EFG at gold atom in six molecules: AuF, XeAuF, KrAuF, ArAuF, (OC)AuF and AuH. On the basis of these results the authors obtained NQM of gold as Q(^{197}Au) = 510(15) mb. Pernpointner and Visscher [68] investigated different approaches to the calculation of EFG, they calculated EFG for a series of diatomic molecules: AlF, AlCl, AlBr, GaF, GaCl, GaBr and derives new values of NQM for ^{27}Al and ^{69}Ga. The values of NQM they recommended are 146.0(0.4) and 171(2) mb, for Al and Ga respectively. The values of the nuclear quadrupole moments derived in the fully relativistic four-component framework are collected in Table 3-35.

Table 3-35 Nuclear quadrupole moments (in mb) of the nucleus X derived from fully relativistic four component calculations of the EFG at nucleus X performed for different series of molecules containing atom X

X	Ref.	Q(X)	Uncertainty[a]
^{27}Al	[68]	146	0.4
^{69}Ga	[68]	171	2
^{115}In	[65]	770	8
^{127}I	[66]	696	12
^{197}Au	[67]	510	15

[a]Estimated uncertainty for calculated Q(X)

3.4. CONCLUSIONS

The calculations reported in this chapter have shown that the inclusion of the relativistic effects leads to a significant change in the values of spectroscopic molecular parameters. For the coinage metal hydrides a contraction of the bond length and an increase in the values of the fundamental frequency and of the dissociation energy are observed. For AuH these effects are large, 0.3 Å, 800 cm^{-1} and 1 eV, for R_e, ν_e and D_e respectively. The difference between the experimental and theoretical results increases across the CuH-AgH and AuH series, however the inclusion of relativistic effects reduces this discrepancy and keeps it not growing. Similar trends were observed for the MF and MCs series, where M = Cu, Ag and Au. For example, the relativistic effects almost doubled the value of the dissociation energy for AuCs.

The study of the energetic structure of the PtH and PdH molecules has shown that relativistic effects influence both the character and the mechanism of bonding and because of the mixing of nonrelativistic states with the same Ω quantum number, the $\omega\omega$-coupling scheme should be used for the description of molecular states. This mixing leads to a change in the order of the molecular states for PtH. The relativistic contraction and the energetic stabilization of the *6s* orbital of Pt is responsible for the unusual stability of the Pt-H bond, while the higher value of the spin-orbit splitting in Pt when compared to that in Pd, influences the pattern of grouping of molecular states for the PdH and PtH molecules. For the series of diatomic molecules with halogen atoms (X_2, XY and HX; X, Y = F, Cl, Br, I, At) the increasing relativistic effects on the spectroscopic constants of these molecules have been evidenced. For di- and inter-halogens a relativistic expansion of the bond length was obtained, while for hydrogen halides the contraction (for HF, HCl, HBr and HI) and expansion (for HAt) were found. The change in the trend can be explained as a result of the competition between the scalar and the spin-orbit relativistic effects. This mechanism is even more pronounced for the molecules with superheavy elements of group 13 and 17 of the periodic table. The relativistic admixture of antibonding $\sigma^*(\pi^*)$ orbital to bonding $\pi(\sigma)$ orbitals weakens the bond in the X_2, XY and HX molecules.

Although the relativistic effects grow fast with the atomic number of atoms making the molecule, the electron correlation remains always important for the correct prediction of molecular parameters and its inclusion usually improves the agreement

of theory with experiment. The different values of relativistic corrections obtained on DF and post DF level of theory indicate that the relativistic and correlation effects are not additive and should be considered simultaneously. The increasing values of the correlation-relativistic cross terms estimated for the diatomic molecules containing halogen atoms illustrate this conclusion. Moreover, the proper description of the core-valence electron correlation is also important for these molecules and changes the trend obtained when the correlation effects are included in the valence shell only.

The relativistic effects in dihalogen molecules containing superheavy elements are responsible for dramatic changes in the spectroscopic constants of these systems. The bond contraction for H(113) and (113)(117) is almost 0.4 Å and the bond length expansion for H(117) is 0.1 Å. Relativistic effects lead to different polarizations of group 13 and 17 diatomic molecules which result in a dramatic change in the value of dipole moment of the (113)(177) molecule from −4.99 to 1.80 (the negative value corresponds to the negative charge of the (117) atom). The relativistic effects in $PtCH_2^+$ are also large; they favour the formation of a double bond and change the bond order from one to two, shorten the bond by 0.3 Å and double the value of the bond dissociation energy. These effects stabilize the bonding in the UF_6 molecule (due to the relativistic contraction of the U*6s* orbital involved in the antibonding molecular orbitals) and are responsible for the change in the order of molecular energy levels of UF_6, which significantly influences the assignment of lines in the photoelectron spectrum. The relativistic correction to the atomization energy of UF_6 is 14 eV. The state of art calculations of electric field gradient for the series of molecules containing the atom of interest, which take into account both electron correlation (with core and valence polarization) and relativistic effects, lead to significantly more accurate values of nuclear quadrupole moments of various nuclei.

The calculation results obtained in the last 2 decades (see Appendix for a list of molecules for which *ab initio* four-component calculations have been performed) have proved that in many cases the inclusion of relativistic effects is mandatory for proper description of the energetic structure of many electron systems and leads to a better agreement of theory with experiment. We have discussed only the examples of *ab initio* all electron four component methods assuming that N-electron molecular system is described by the Dirac-Coulomb-Breit Hamiltonian. These methods are much more expensive when compared to their nonrelativistic counterparts because of large basis set required for molecular calculations. On the other hand, the four component DF and post DF calculations are considered to be the most accurate and supply the results which can serve as benchmark results necessary for testing or for calibration of less advanced methods.

APPENDIX

Styszyński [69] listed the molecules whose energetic structure and spectroscopic constants have been determined by the *ab initio* all-electron four-component methods. Table 3-36 gives the list of the molecules, methods, year of publication and references to the relevant calculations.

Table 3-36 The molecules whose energetic structure and spectroscopic constants have been determined by the four-component methods (From "Badanie efektów relatywistycznych w molekułach. Metody czteroskładnikowe" by J. Styszyński (2007). By permission of Wydawnictwo Naukowe Uniwersytetu Szczecińskiego)

Molecule	DF	DF + Br	MP2	CISD	CISD(Q)	CCSD	CCSD + T	CCSD(T)
CuH	1995 [16]							
AgH	1982 [15]		1995 [16]					
	1995 [16]							
	1996 [18]							
AuH	1982 [15]		1995[16]	1996 [17]				
	1995 [16]							
	1996 [17]							
HO	1995 [70]							
HS	1995 [70]							
HSe	1995 [70]							
HTe	1995 [70]							
HPo	1995 [70]							
GeO	1992 [71, 72]							
SnO	1992 [71, 72]							
PbO	1993 [71–73]							
ThO	1997 [74]							
PtH, PtH^+	1993 [25, 28]			1993 [25]				
PdH	1997 [33]			1997 [33]				
CdH, $CdH^{\pm}$	1998 [34]					1998 [34]		
PtCu	2005 [75]		2005 [75]	2005 [75]				
PtAg	2005 [75]		2005 [75]	2005 [75]				
PtAu	2005 [75]		2005 [75]	2005 [75]				
CuCl				1997 [76, 77]				
CuBr				1997 [77]				
CuI				1997 [77]				
CuF	1997 [20]		1997 [20]					
AgF	1997 [20]		1997 [20]					
AuF	1997 [20]		1997 [20]					
CsAu	1997 [21]		2003 [22]					2003 [22]
	2003 [22]							
CsAg	2003 [22]		2003 [22]					2003 [22]
CsCu	2003 [22]		2003 [22]					2003 [22]
KF	1993 [78]							
RbF	1993 [78]							
CsF	1993 [78]							
GdF	1997 [79]							
GdF_2	1998 [80]							
FO		1996 [81]				1996 [81]	1996 [81]	1996 [81]
ClO		1996 [81]				1996 [81]	1996 [81]	1996 [81]

(continued)

Table 3-36 (continued)

Molecule	DF	DF + Br	MP2	CISD	CISD(Q)	CCSD	CCSD + T	CCSD(T)
$O_2^{\pm}$		1996 [81]				1996 [81]	1996 [81]	1996 [81]
F_2	1996 [35]	1996 [35]	1996 [35]	1996 [35]		1996 [35]		1996 [35]
Cl_2	1996 [35]	1996 [35]	1996 [35]	1996 [35]		1996 [35]		1996 [35]
Br_2	1996 [35]	1996 [35]	1996 [35]	1996 [35]		1996 [35]		1996 [35]
	1997 [82]							1997 [82]
I_2	1996 [35]	1996 [35]	1996 [35]	1996 [35]		1996 [35]		1996 [35]
	1997 [82]							1997 [82]
								1997 [40]
At_2	1996 [35]	1996 [35]	1996 [35]	1996 [35]		1996 [35]		1996 [35]
	1997 [82]							1997 [82]
HF	1996 [36]	1996 [36]	1996 [36]	1996 [36]	1996 [36]	1996 [36]	1996 [36]	1996 [36]
			2000 [38]			2000 [38]		2000 [38]
HCl	1996 [36]	1996 [36]	1996 [36]	1996 [36]	1996 [36]	1996 [36]	1996 [36]	1996 [36]
			2000 [38]			2000 [38]		2000 [38]
HBr	1996 [36]	1996 [36]	1996 [36]	1996 [36]	1996 [36]	1996 [36]	1996 [36]	1996 [36]
			2000 [38]			2000 [38]		2000 [38]
HI	1992 [83]	1996 [36]	1996 [36]	1996 [36]	1996 [36]	1996 [36]	1996 [36]	1996 [36]
	1996 [36]		2000 [38]			2000 [38]		2000 [38]
	1996 [24]							
HI^+	1992 [83]							
HAt	1992 [83]	1996 [36]	1996 [36]	1996 [36]	1996 [36]	1996 [36]	1996 [36]	1996 [36]
	1996 [36]		2003 [39]			2003 [39]		2003 [39]
	1996 [24]							
HAt^+	1992 [83]							
HUus	1996 [24]							
ClF	1998 [37]	1998 [37]	1998 [37]			1998 [37]		1998 [37]
BrF	1998 [37]	1998 [37]	1998 [37]			1998 [37]		1998 [37]
BrCl	1998 [37]	1998 [37]	1998 [37]			1998 [37]		1998 [37]
IF	1998 [37]	1998 [37]	1998 [37]			1998 [37]		1998 [37]
ICl	1998 [37]	1998 [37]	1998 [37]			1998 [37]		1998 [37]
IBr	1998 [37]	1998 [37]	1998 [37]			1998 [37]		1998 [37]
H_2O	1994 [84, 85]		1998 [86]					
	1998 [86]							
H_2S	1994 [84, 85]							
H_2Se	1994 [84, 85]							
H_2Te	1994 [84, 85]							
H_2Po	1994 [84, 85]							
H_2Pt	1993 [28]					1995 [87]		
$PtCH_2$	1996 [43]		1996 [43]					
CH_4	1991 [88]	1992						
	1992							
SiH_4	1991 [88]	1992 [89]						
	1992 [89]							
GeH_4	1991 [88]	1992 [89]						
	1992 [89]							

Table 3-36 (continued)

Molecule	DF	DF + Br	MP2	CISD	CISD(Q)	CCSD	CCSD + T	CCSD(T)
SnH_4	1991 [88]	1992 [89]						
	1992 [89]							
PbH_4	1991 [88]	1992 [89]						
	1992 [89]							
XeF	1997 [90]	1997 [90]						
XeF_2	1995 [91]	1995 [91]				2008 [92]	2008 [92]	2008 [92]
	1997 [90]	1997 [90]						
	2008 [92]							
XeF_4	1995 [93]	1995 [93]						
	1997 [90]	1997 [90]						
XeF_6	1997 [90]	1997 [90]						
ThF_4	1994 [94]	1994 [94]						
$RfCl_4$	1998 [95]	1998 [95]						
UF_6	1996 [47]	1996 [47]		1996 [45]				
	1996 [45]	1996 [45]						
EuO_6^{9-}	1992 [96]							
	1995 [97]							
CoF_6^{2-}	1994 [98]			1994 [98]				
RhF_6^{2-}	1994 [98]			1994 [98]				
IrF_6^{2-}	1994 [98]			1994 [98]				
TlH	1999 [41]		1999 [41]					1999 [41]
(113)H	1999 [41]		1999 [41]					1999 [41]
(113)F	1999 [41]		1999 [41]					1999 [41]
TlAt	2001 [42]							
Tl(117)	2001 [42]							
(113)At	2001 [42]							
(113)(117)	2001 [42]							
(110)C	2007 [99]		2007 [99]			2007 [99]		2007 [99]

REFERENCES

1. Swirles, B.: Proc. R. Soc. A **152**, 625 (1935)
2. Grant, I.P.: Adv. Phys. **19**, 747 (1970)
3. Desclaux, J.P.: Comput. Phys. Commun. **9**, 31 (1975)
4. Dyall, K.G., Grant, I.P., Johnson, C.T., Parpia, F.A., Plummer, E.P.: Comput. Phys. Commun. **55**, 425 (1989)
5. Malli, G.L., Oreg, J.: J. Chem. Phys. **63**, 830 (1975)
6. McLean, A.D., Lee, Y.S.: In: R. Carbo (ed.) Current Aspects of Quantum Chemistry. Elsevier, Amsterdam (1982)
7. Schwarz, W.H.E.: Chem. Phys. Lett. **85**, 94 (1982)
8. Mark, F., Schwarz, W.H.E.: Phys. Rev. Lett. **48**, 673 (1982)
9. Pestka, G., Bylicki, M., Karwowski, J.: In: S. Wilson, P.J. Grout, J. Maruani, G. Delgado-Barrio (eds.) Frontiers in Quantum Systems in Chemistry and Physics. Springer, The Netherlands (2008)
10. Visscher, L., Visser, O., Aerst, P.J.A, Merenga, H., Nieuwpoort, W.C.: Comput. Phys. Commun. **81**, 120 (1994)

11. Jensen, H.J.A., Saue, T., Visscher, L., Bakken, V., Eliav, E., Enevoldsen, T., Fleig, T., Fossgaard, O., Helgaker, T., Lærdahl, J., Larsen, C.V., Norman, P., Olsen, J., Pernpointner, M., Pedersen, J.K., Ruud, K., Salek, P., van Stralen, J.N.P., Thyssen, J., Visser, O., Winther, T.: Dirac, a Relativistic Ab initio Electronic Structure Program, Release DIRAC04.0 (2004)
12. Pyykko, P., Desclaux, J.P.: Acc. Chem. Res. **12**, 276 (1979)
13. Pyykko, P.: Chem. Rev. **88**, 563 (1988)
14. Dyall, K.G., Fægri, K.: Introduction to Relativistic Quantum Chemistry. Oxford University Press, New York (2007)
15. Lee, Y.S., McLean, A.D.: J. Chem. Phys. **76**, 735 (1982)
16. Collins, C.L., Dyall, K.G., Schaefer, H.F.: J. Chem. Phys. **102**, 2024 (1995)
17. Saue, T., Visscher, L.: The Electronic Structure of Au, Au^- and AuH. http://rugch5.chem.-rug.nl:80/∼luuk/AuH.html. Accessed 16 January 1996 (1996)
18. Mohanty, P.R.K., Parpia, F.A.: Phys. Rev. A **54**, 2863 (1996)
19. Huber, K., Herzberg, G.: Constants of Diatomic Molecules. Reinhold, New York (1979)
20. Lærdahl, J.K., Saue, T., Fægri, K.J.: Theor. Chem. Acc. **97**, 177 (1997)
21. Saue, T., Fægri, K., Helgaker, T., Gropen, O.: Mol. Phys. **91**, 937 (1997)
22. Fossgaard, O., Gropen, O., Eliav, E., Saue, T.: J. Chem. Phys. **119**, 9355 (2003)
23. Busse, B., Weil, K.G.: Ber. Bunsen. Phys. Chem. **85**, 309 (1981)
24. Saue, T., Fægri, K., Gropen, O.: Chem. Phys. Lett. **263**, 360 (1996)
25. Visscher, L., Saue, T., Nieuwpoort, W.C., Fægri, K., Gropen, O.: J. Chem. Phys. **99**, 6704 (1993)
26. Mulliken, R.S.: Rev. Mod. Phys. **4**, 1 (1932)
27. Wang, S.G., Schwarz, W.H.E.: J. Chem. Phys. **109**, 7252 (1998)
28. Dyall, K.G.: J. Chem. Phys. **98**, 9678 (1993)
29. Scullman, R., Cederbalk, P.: J. Phys. B **10**, 3659 (1977)
30. Gustafsson, G., Scullman, R.: Mol. Phys. **67**, 981 (1989)
31. McCarthy, M.C., Field, R.W., Engelman, Jr. R., Bernath, P.F.: J. Mol. Spectrosc. **158**, 208 (1993)
32. Squires, R.R.: J. Am. Chem. Soc. **107**, 4385 (1985)
33. Sjowoll, M., Fægri, H., Gropen, O., Almlof, J., Saue, T., Olsen, J., Helgaker, T.: J. Chem. Phys. **107**, 5496 (1997)
34. Eliav, E., Kaldor, U., Hess, B.: J. Chem. Phys. **108**, 3409 (1998)
35. Visscher, L., Dyall, K.G.: J. Chem. Phys. **104**, 9040 (1996)
36. Visscher, L., Styszyński, J., Nieuwpoort, W.C.: J. Chem. Phys. **105**, 1987 (1996)
37. de Jong, W.A., Styszyński, J., Visscher, L., Nieuwpoort, W.C.: J. Chem. Phys. **108**, 5177 (1998)
38. Styszyński, J.: Chem. Phys. Lett. **317**, 351 (2000)
39. Styszyński, J., Kobus, J.: Chem. Phys. Lett. **369**, 441 (2003)
40. de Jong, W.A., Visscher, L., Nieuwpoort, W.C.: J. Chem. Phys. **107**, 9046 (1997)
41. Seth, M., Schwerdtfeger, P., Fægrii, K.: J. Chem. Phys. **111**, 6422 (1999)
42. Fægri, K., Saue, T.: J. Chem. Phys. **115**, 2456 (2001)
43. Heinemann, C., Schwarz, H., Koch, W., Dyall, K.G.: J. Chem. Phys. **104**, 4642 (1996)
44. Irikura, K.K., Beauchamp, J.L.: J. Am. Chem. Soc. **113**, 2769 (1991)
45. de Jong, W.A., Nieuwpoort, W.C.: Int. J. Quantum Chem. **58**, 203 (1996)
46. Fægri, Jr. K.: Theor. Chem. Acc. **105**, 252 (2001)
47. Malli, G.L., Styszyński, J.: J. Chem. Phys. **104**, 1012 (1996)
48. Compton, R.N.: J. Chem. Phys. **66**, 4478 (1977)
49. Andrews, L., Liang, B.Y., Li, J., Bursten, B.E.: J. Am. Chem. Soc. **125**, 3126 (2003)
50. Andrews, L., Liang, B.Y., Li, J., Bursten, B.E.: New J. Chem. **28**, 289 (2004)
51. Infante, I., Visscher, L.: J. Chem. Phys. **121**, 5783 (2004)
52. de Jong, W.A., Visscher, L., Nieuwpoort, W.C.: J. Mol. Struct.: Theochem **458**, 41 (1999)
53. Fægri, K.: (2009)

54. Roos, B.O., Widmark, P.O., Gagliardi, L.: Faraday Discuss. **124**, 57 (2003)
55. Visscher, L., Saue, T., Oddershede, J.: Chem. Phys. Lett. **274**, 181 (1997)
56. Davis, R.E., Muenter, J.S.: J. Chem. Phys. **57**, 2836 (1972)
57. Ewing, R.E., Tigelaar, H.L., Flygare, W.H.: J. Chem. Phys. **56**, 1957 (1972)
58. Nair, K.P.R., Hoeft, J., Tiemann, E.: J. Mol. Spectrosc. **78**, 506 (1979)
59. Nair, K.P.R., Hoeft, J., Tiemann, E.: Chem. Phys. Lett. **58**, 153 (1978)
60. Nair, K.P.R., Hoeft, J., Tiemann, E.: Chem. Phys. Lett. **60**, 253 (1979)
61. Herbst, E., Steinmetz, W.: J. Chem. Phys. **56**, 5342 (1972)
62. Durand, A., Loison, J.C., Vigue, J.: J. Chem. Phys. **106**, 477 (1997)
63. Tiemann, E., Dreyer, A.: Chem. Phys. **23**, 231 (1977)
64. Nair, K.P.R., Hoeft, J.: J. Mol. Struct. **79**, 227 (1982)
65. van Stralen, J.N.P., Visscher, L.: J. Chem. Phys. **117**, 3103 (2002)
66. van Stralen, J.N.P., Visscher, L.: Mol. Phys. **101**, 2115 (2003)
67. Belpassi, L., Tarantelli, F., Sgamellotti, A., Quiney, H.M., van Stralen, J.N.P., Visscher, L.: J. Chem. Phys. **126**, 064314 (2007)
68. Pernpointner, M., Visscher, L.: J. Chem. Phys. **114**, 10389 (2001)
69. Styszyński, J.: Badanie efektów relatywistycznych w molekułach. Metody czteroskładnikowe. Wydawnictwo Naukowe Uniwersytetu Szczeciskiego, Szczecin (2007)
70. Pisani, L., Clementi, E.: J. Chem. Phys. **103**, 9321 (1995)
71. Dyall, K.G.: Chem. Phys. Lett. **196**, 178 (1992)
72. Dyall, K.G.: J. Chem. Phys. **98**, 2191 (1993)
73. Matsuoka, O., Pisani, L., Clementi, E.: Chem. Phys. Lett. **202**, 13 (1993)
74. Watanabe, Y., Matsuoka, O.: J. Chem. Phys. **107**, 3738 (1997)
75. Abe, M., Mori, S., Nakajima, T., Hirao, K.: Chem. Phys. **311**, 129 (2005)
76. Sousa, C., de Jong, W.A., Broer, R., Nieuwpoort, W.C.: J. Chem. Phys. **106**, 7162 (1997)
77. Sousa, C., de Jong, W.A., Broer, R., Nieuwpoort, W.C.: Mol. Phys. **92**, 677 (1997)
78. Dyall, K.G., Partridge, H.: Chem. Phys. Lett. **206**, 565 (1993)
79. Tatewaki, H., Matsuoka, O.: J. Chem. Phys. **106**, 4558 (1997)
80. Tatewaki, H., Matsuoka, O.: Chem. Phys. Lett. **283**, 161 (1998)
81. Visscher, L., Lee, T.J., Dyall, K.G.: J. Chem. Phys. **105**, 8769 (1996)
82. Visscher, L.: Theor. Chem. Acc. **98**, 68 (1997)
83. Matsuoka, O.: J. Chem. Phys. **97**, 2271 (1992)
84. Pisani, L., Clementi, E.: J. Comput. Chem. **15**, 466 (1994)
85. Pisani, L., Clementi, E.: J. Chem. Phys. **101**, 3079 (1994)
86. Quiney, H.M., Skaane, H., Grant, I.P.: Chem. Phys. Lett. **290**, 473 (1998)
87. Visscher, L., Dyall, K.G., Lee, T.J.: Int. J. Quantum Chem.: Quantum Chem. Symp. **29**, 411 (1995)
88. Dyall, K.G., Taylor, P.R., Fægri, K., Partridge, H.: J. Chem. Phys. **95**, 2583 (1991)
89. Visser, O., Visscher, L., Aerts, P.J.C., Nieuwpoort, W.C.: Theor. Chim. Acta **81**, 405 (1992)
90. Styszyński, J., Cao, X., Malli, G.L., Visscher, L.: J. Comput. Chem. **18**, 601 (1997)
91. Malli, G.L., Styszyński, J., da Silva, A.B.F.: Int. J. Quantum Chem. **55**, 213 (1995)
92. Haiduke, R.L.A., Filho, H.P.M., da Silva, A.B.F.: Chem. Phys. **348**, 89 (2008)
93. Styszyński, J., Malli, G.L.: Int. J. Quantum Chem. **55**, 227 (1995)
94. Malli, G.L., Styszyński, J.: J. Chem. Phys. **101**, 10736 (1994)
95. Malli, G.L., Styszyński, J.: J. Chem. Phys. **109**, 4448 (1998)
96. Visser, O., Visscher, L., Aerts, P.J.C., Nieuwpoort, W.C.: J. Chem. Phys. **96**, 2910 (1992)
97. Dijkstra, F., de Jong, W.A., Nieuwpoort, W.C.: Int. J. Quantum Chem.: Quantum Chem. Symp. **29**, 609 (1995)
98. Visscher, L., Nieuwpoort, W.C.: Theor. Chim. Acta **88**, 447 (1994)
99. de Macedo, L.G.M., Sambrano, J.R., de Souza, A.R., Borin, A.C.: Chem. Phys. Lett. **440**, 367 (2007)

CHAPTER 4

TWO-COMPONENT RELATIVISTIC THEORIES

MARIA BARYSZ

Institute of Chemistry, N. Copernicus University, 87 100 Toruń, Gagarina 7, Poland
e-mail: teomjb@chem.uni.torun.pl

Abstract: This review describes a variety of two-component methods of relativistic quantum chemistry. It starts with the description of elimination of the small component and the Pauli expansion and followed by the regular approximation method. Then the two-component methods of relativistic quantum chemistry based on the unitary transformation of the Dirac Hamiltonian are reviewed. After discussing the Douglas–Kroll–Hess method and its generalizations the main emphasis is put on the infinite-order two-component method (IOTC). The transition from the Dirac formalism to any two-component approximation is accompanied by the change of all operators, including those which correspond to external perturbations and lead to properties of different orders. This so-called change of picture problem is given some attention as well. The back-transformation of the two-component wave function to the four-component spinor and the quality of the resulting four-component wave function is discussed. Finally some discussion of the two-electron terms is presented.

Keywords: Dirac equation, Elimination of small component, Regular approximation, Douglas–Kroll–Hess method, Infinite-order Two-component (IOTC) method, Change of picture, Relativistic interactions

4.1. INTRODUCTION

For relatively light elements the electronic structure of their compounds is studied in terms of solutions of the non-relativistic equation, i.e., the Schrödinger equation. For stationary states these solutions are the eigenstates of the electronic Schrödinger Hamiltonian:

$$H_S = \sum_{i=1}^{n} \left\{ -\frac{1}{2}\nabla_i^2 + \sum_{A=1}^{N} \left(-\frac{Z_A}{r_{Ai}}\right) \right\} + \sum_{i<j} \frac{1}{r_{ij}} \tag{4-1}$$

where the terms in the bracket represents the one particle kinetic and the potential energy operators. The last term is the two-electron Coulomb potential operator.

M. Barysz and Y. Ishikawa (eds.), *Relativistic Methods for Chemists*,
Challenges and Advances in Computational Chemistry and Physics 10,
DOI 10.1007/978-1-4020-9975-5_4,

Most of the analysis of these solutions and the methods of approximation are rooted in solutions of the non-relativistic one-electron problem with the Hamiltonian.

$$h_S = -\frac{1}{2}\nabla^2 + V_{ext} \tag{4-2}$$

where V_{ext} is the external potential. The simplest case is that of the Coulomb interaction with a single nucleus of charge Z_A,

$$V_{ext} = -\frac{Z_A}{r_A} \tag{4-3}$$

If the electron spin is taken into account each solution of the one-electron Schrödinger equation is doubled and leads to two spin-orbitals, $\boldsymbol{u_{k1}} = \psi_k\alpha$ and $\boldsymbol{u_{k2}} = \psi_k\beta$, where α and β are the so-called spin functions which correspond to the 1/2 and $-1/2$ values of the so called spin quantum number m_s, respectively. Hence, the Schrödinger equation which includes some information about spin can be interpreted in terms of the 2×2 matrix Hamiltonian's,

$$\boldsymbol{h_S} = \begin{pmatrix} h_S & 0 \\ 0 & h_S \end{pmatrix}. \tag{4-4}$$

with solutions

$$\boldsymbol{h_S\phi_k} = \epsilon_k\boldsymbol{\phi_k} \tag{4-5}$$

where

$$\boldsymbol{\phi_k} = c_1\begin{pmatrix} \psi_k \\ 0 \end{pmatrix} + c_1\begin{pmatrix} 0 \\ \psi_k \end{pmatrix} \tag{4-6}$$

Since h_S does not include spin operators one can choose two independent solutions

$$\boldsymbol{u_{k1}} = \begin{pmatrix} \psi_k \\ 0 \end{pmatrix} \tag{4-7}$$

and

$$\boldsymbol{u_{k2}} = \begin{pmatrix} 0 \\ \psi_k \end{pmatrix} \tag{4-8}$$

which correspond to the usual spin-orbitals of the spin-restricted method of non-relativistic quantum chemistry.

With the increasing value of the nuclear charge Z_A the relativistic effects become of increasing importance. In consequence the one-electron Schrödinger Hamiltonian needs to be replaced by its appropriate relativistic counterpart which is the Dirac Hamiltonian, h_D, which will be defined later.

Once we know the solution of the Dirac equation for a single electron moving in the external potential it is tempting to build the relativistic theory of many-electron systems in a similar way as the non-relativistic theory is built, i.e., by combining the one-electron Dirac Hamiltonian for each electron with the Coulomb interaction between electrons,

$$H_{DC} = \sum_{i=1}^{N} h_D(i) + \sum_{i<j} \frac{1}{r_{ij}} \tag{4-9}$$

This is the simplest approximation to the true relativistic Hamiltonian of a many particle system which would follow from quantum electrodynamics. The one-electron part of Eq. (4-9) is fully consistent with all requirements of the relativistic theory of a particle moving in some external potential. However, the Coulomb interaction term in Eq. (4-9) assumes that the interaction is instantaneous like in non-relativistic theory. Hence, as a whole the Hamiltonian (4-9) is not fully relativistic.

Leaving aside for a moment the problem of the relativistic Hamiltonian for many particle systems we learn from [1,2] that the central issue is the form of h_D.

Unlike the non-relativistic one-electron Hamiltonian, h_D leads to the stationary eigenvalue problem which is defined in terms of mutually coupled first-order differential equations. These are usually written in the matrix operator form

$$h_D \Psi_D = \epsilon_D \Psi_D \tag{4-10}$$

where

$$h_D = c\boldsymbol{\alpha}\boldsymbol{p} + \boldsymbol{\beta}mc^2 + (V - mc^2)I = \begin{pmatrix} V & c\boldsymbol{\sigma}\boldsymbol{p} \\ c\boldsymbol{\sigma}\boldsymbol{p} & V - 2mc^2 \end{pmatrix}, \tag{4-11}$$

where V is the external potential of the Coulomb type, or alternatively a potential derived from an extended nuclear charge distribution.

$$\boldsymbol{\alpha} = \begin{pmatrix} \mathbf{0} & \boldsymbol{\sigma} \\ \boldsymbol{\sigma} & \mathbf{0} \end{pmatrix}, \boldsymbol{\beta} = \begin{pmatrix} \mathbf{I} & \mathbf{0} \\ \mathbf{0} & -\mathbf{I} \end{pmatrix}, \tag{4-12}$$

with

$$\mathbf{0} = \begin{pmatrix} 0 & 0 \\ 0 & 0 \end{pmatrix}, \mathbf{I} = \begin{pmatrix} 1 & 0 \\ 0 & 1 \end{pmatrix} \tag{4-13}$$

and

$$\sigma_x = \begin{pmatrix} 0 & 1 \\ 1 & 0 \end{pmatrix}, \sigma_y = \begin{pmatrix} 0 & -i \\ i & 0 \end{pmatrix}, \sigma_z = \begin{pmatrix} 1 & 0 \\ 0 & -1 \end{pmatrix} \tag{4-14}$$

are the Pauli matrices. Except for a factor of $\frac{1}{2}$, the $\sigma_{x,y,z}$ matrices can be viewed as $\boldsymbol{s_x}$, $\boldsymbol{s_y}$ and $\boldsymbol{s_z}$ spin operators, respectively, with the spin functions of the form of two-dimensional column vectors. Then,

$$s_z = \frac{1}{2}\sigma_z \tag{4-15}$$

$$s_z \begin{pmatrix} 1 \\ 0 \end{pmatrix} = \frac{1}{2} \begin{pmatrix} 1 \\ 0 \end{pmatrix} \tag{4-16}$$

$$s_z \begin{pmatrix} 0 \\ 1 \end{pmatrix} = -\frac{1}{2} \begin{pmatrix} 0 \\ 1 \end{pmatrix} \tag{4-17}$$

Moreover, in order to get electronic binding energies from Eq. (4-10) directly comparable to the non-relativistic theory the energy scale is shifted by the rest mass energy mc^2 of the electron.

The 4×4 matrix form of the Dirac equation (4-10) gives for each energy state four solutions which are arranged into a four-component column vector referred to as the 4-spinor. Each of these solutions can be written as

$$\Psi_D = \begin{pmatrix} \psi^L \\ \psi^S \end{pmatrix}, \tag{4-18}$$

where the upper and lower two components Ψ^L and Ψ^S are spinors originating from the electronic and positronic degrees of freedom.

In the limit of $c \rightarrow \infty$ the lower component vanishes and Ψ^L terms into non-relativistic solutions the Eq. (4-5). Simultaneously the Dirac energy for these solutions becomes equal to the non-relativistic energy. For a free electron the limit $c \rightarrow \infty$ would correspond to positive energy states. For this reason the part of the Dirac spectrum which has the Schrödinger non-relativistic limit for $c \rightarrow \infty$ is referred to as the positive energy spectrum and is associated with the dominant contribution of Ψ^L in the Ψ_D-spinor (4-18).

The solutions of the Dirac equation have four components and manipulating them in the many-electron theory based on the Dirac–Coulomb Hamiltonian is quite cumbersome.

Moreover, the use of the Dirac Hamiltonian (4-11) requires considerably larger computational resources compared to the use of the Schrödinger Hamiltonian.

The four-component relativistic Dirac wave function contains information about positive- and negative-energy states of the system. In chemical applications, one is usually concerned with the electronic (or positive-energy) states only. Therefore, some reduction of the four-component wave function seems to be preferred. The history of this 'reduction' goes back to the period before the Dirac equation. The first step in this direction appears to have been made by Pauli in the form of a quasi-relativistic Hamiltonian known as the Pauli Hamiltonian [1, 2]. This Hamiltonian can be approximately derived from the Dirac Hamiltonian by using the fact that in the non-relativistic limit the 'large' (the upper) 2-vector part of the Dirac 4-spinor becomes the electronic (positive energy) solution with spin. On this basis one could expect that there is some representation of the Dirac Hamiltonian which completely separates the positive and negative energy spectra and permits to focus all attention on the electronic part only.

Actually the 2-spinor formalism may not be that much an approximation as far as relativistic quantum chemistry is concerned. The idea of this separation goes back to Foldy and Wouthuysen [3]. The exact separation of the two spectra would be equivalent to the transformation of the Dirac 4-spinors into either electronic or positronic 2-spinors. Alternatively, this means that the 4×4 Dirac Hamiltonian is to be block-diagonalized, i.e., brought into the form of the direct sum of two 2×2 matrix Hamiltonian's, one of them corresponding to the electronic spectrum and the other one referring solely to the positronic eigenvalues. Once this is achieved most problems of the relativistic quantum chemistry can be formulated solely in terms of electronic 2-spinors. The positronic solutions can be simply abandoned. Obviously, they will be needed in all cases which may involve the electron–positron pair creation processes, i.e., whenever the given problem needs to be considered in the framework of quantum electrodynamics [4–6]. However, for the majority of problems encountered in relativistic quantum chemistry the use of the advanced apparatus of the quantum field theory does not seem to be urgently required [7].

4.2. THE TWO-COMPONENT METHODOLOGY

In this Section we describe the general ideas of the two-component methods. We start with the method of the elimination of the small component and the ZORA ansatz followed by the Douglas–Kroll approximation and the Douglas–Kroll–Hess methods. The main discussion will be based on the Infinite Order Two-Component method (IOTC) which seems to be the best available exact two-component method.

4.2.1. Elimination of the Small Component and the Pauli Expansion

Since $\boldsymbol{\alpha}$ and $\boldsymbol{\beta}$ are block matrices, the Dirac equation (4-10) can be factored out in two equations.

$$\begin{aligned} (c\boldsymbol{\sigma}\boldsymbol{p})\Psi^S + V\Psi^L &= E\Psi^L \\ (c\boldsymbol{\sigma}\boldsymbol{p})\Psi^L + (-2mc^2 + V)\Psi^S &= E\Psi^S \end{aligned} \tag{4-19}$$

Here Ψ^L and Ψ^S are large and small two-component wave functions that include the α and β spin functions. The latter equation can be solved for Ψ^S.

$$\Psi^S = (E + 2mc^2 - V)^{-1} c\boldsymbol{\sigma p}\Psi^L \tag{4-20}$$

Equation (4-20) or approximations to this equation can be used as an ansatz for the small component. The Pauli expansion results from taking $2mc^2$ out of the denominator of Eq. (4-20) for the elimination of the small component (ESC).

$$(E + 2mc^2 - V)^{-1} = (2mc^2)^{-1} \left(1 + \frac{E - V}{2mc^2}\right)^{-1} \tag{4-21}$$

By inserting it into Eq. (4-20) and then into the Dirac equation (4-19), modified but still exact Dirac equations are obtained.

$$(V - E)\Psi^L + \frac{1}{2m}(\boldsymbol{\sigma p}) \left(1 + \frac{E - V}{2mc^2}\right)^{-1} (\boldsymbol{\sigma p})\Psi^L = \mathbf{0} \tag{4-22}$$

We may obtain relativistic corrections by expanding the right side of Eq. (4-21) in the Taylor series.

$$\left(1 + \frac{E - V}{2mc^2}\right)^{-1} = 1 - \frac{E - V}{2mc^2} + \cdots \tag{4-23}$$

The problem with this expansion is, that it is only valid when $E - V \ll 2mc^2$, however in the region of atom close to the nucleus where $V \to -\infty$ for r $\to 0$ this is not fulfilled. Inserting (4-23) in (4-22), using the vector identity

$$(\boldsymbol{\sigma u})(\boldsymbol{\sigma v}) = (\boldsymbol{uv}) + i\boldsymbol{\sigma}(\boldsymbol{u} \times \boldsymbol{v}) \tag{4-24}$$

and assuming the Coulomb potential $-Z/r$ one obtains, after renormalization of the large component of the wave function, the non-relativistic limit through terms of the order of $\frac{1}{c^2}$ [2, 8–10]:

$$\left[\frac{\boldsymbol{p}^2}{2m} + V - \frac{\boldsymbol{p}^4}{8m^3c^2} + \frac{Z\boldsymbol{sl}}{2m^2c^2r^3} + \frac{Z\pi\delta(\boldsymbol{r})}{2m^2c^2}\right]\Psi^L = E\Psi^L \tag{4-25}$$

Equation (4-25) is called the two-component Pauli equation. The first two terms are the non-relativistic kinetic and potential energy operators, the $\boldsymbol{p}^4$ term is called the mass-velocity correction, and is due to the dependence of the electron mass on the velocity. The next is the *spin–orbit* term ($\boldsymbol{s}$ is the electron spin and $\boldsymbol{l}$ is the angular momentum operator $\boldsymbol{r} \times \boldsymbol{p}$), which corresponds to an interaction of the electron spin with the magnetic filed generated by the orbital movement of the electron. The last term involving the δ function is the Darwin correction, which corresponds

to the correction that can be interpreted as the result of the oscillation of the electron around its mean position, referred also as Zwitterbewegung. The mass–velocity and Darwin corrections are often called the scalar (spin-free) relativistic corrections. Due to the singular behaviour of Pauli operators the Pauli Hamiltonian is not bounded from below and can only be used as first-order corrections to the non-relativistic calculations.

4.2.2. Regular Approximations (RA)

The Pauli expansion results from taking $2mc^2$ out of the denominator of the equation for the elimination of the small component. The problem with this is that both E and V can potentially be larger in magnitude than $2mc^2$ and so expansion (4-23) is not valid in some region of space. An alternative way is to extract from the denominator (4-21) the operator $(2mc^2 - V)$, which is always positive definite for the nuclear potential and is always greater than $2mc^2$. With this choice we may eliminate the small component by writing the Eq. (4-22)

$$(V - E)\Psi^L + \frac{1}{2m}(\boldsymbol{\sigma p})\frac{2mc^2}{2mc^2 - V}\left(1 + \frac{E}{2mc^2 - V}\right)^{-1}(\boldsymbol{\sigma p})\Psi^L = \mathbf{0} \quad (4\text{-}26)$$

The minimum value of the potential is zero, so the power series is now valid everywhere for energies $|E| < 2mc^2$. This range covers all the electron bound states, and continuum states up to an energy of $2mc^2$.

In the development of the Pauli Hamiltonian, truncation of the power series expansion of the inverse operator after the first term gives the non-relativistic Hamiltonian.

The zero-order term is obtained by setting the expression $(1 + \frac{E}{2mc^2 - V})^{-1}$ in Eq. (4-26) to **1** and after the Taylor expansion of $(2mc^2 - V)^{-1}$. The zero-order Hamiltonian is

$$H^{ZORA} = V + \frac{1}{2m}(\boldsymbol{\sigma p})\left(1 + \frac{V}{2mc^2} + \frac{V^2}{4m^2c^4} + \cdots\right)(\boldsymbol{\sigma p}) \quad (4\text{-}27)$$

This Hamiltonian first developed by Chang et al. [11], is often referred to as the CPD Hamiltonian. The method was further developed by van Lenthe et al. [12, 13] and the name given was the zeroth-order regular approximation (ZORA).

The first term in the bracket of Eq. (4-27) is the non-relativistic kinetic energy T. Commuting $\boldsymbol{\sigma p}$ to the right and using the vector identity (4-24), the second term gives

$$(\boldsymbol{\sigma p}\ V)(\boldsymbol{\sigma p}) = V\boldsymbol{p^2}\ + (\boldsymbol{p}V)\boldsymbol{p} + \hbar\boldsymbol{\sigma}\ (\boldsymbol{\nabla}V)\boldsymbol{\times p} \quad (4\text{-}28)$$

This operator contains the Pauli spin–orbit operator and part, but not all of the spin-free relativistic correction [10]. What is missing, compared with the Pauli expansion in (4-25) is the term which gives rise to the mass–velocity correction and part of the

Darwin term. Since the missing term is positive for the bound states, ZORA will give energies that are too low. The ZORA advantage over the Pauli expansion is the fact that the ZORA energy (contrary to the Pauli energy) is bounded from below for $Z < c$, and hence variationally stable. However one minor drawback of ZORA is that it is not gauge independent, (i.e.), a change of the zero in the energy scale does affect the results. Solutions to this problem have been proposed [14–16]. The further development of the regular approximation is based on the expansion of the inverse operator $\frac{1}{2mc^2-V+E}$ in Eq. (4-20)

$$\frac{1}{2mc^2 - V + E} = \frac{1}{2mc^2 - V}\left[1 + \frac{E}{2mc^2 - V}\right]^{-1} = \sum_{k=0}^{\infty} \frac{(-E)^k}{(2mc^2 - V)^{k+1}} \quad (4.29)$$

While the ZORA Hamiltonian ($k = 0$) is E-independent, higher order approximations involve E-dependent operators what makes it difficult to apply. In the contents of the Regular Approximation, the other methods based on the elimination of the small component (ESC) must be mentioned, mainly the normalized elimination of the small component (NESC) proposed by Dyall [17].

4.2.3. Unitary Transformations of the Dirac Hamiltonian

In solving the Dirac equation, it would be desirable to use as much as possible of the well-established techniques known from non-relativistic theory. However, as we have discussed above we quickly encounter a problem with the variational principle, since our master equation (4-10) describes both electronic and positronic states. The latter have much lower energies, and any attempt to minimize the energy without additional constraints is likely to result in a positronic-like solution. To avoid such a collapse, one must first take necessary precautions to ensure that the solutions are constrained to a space of proper electron-like solutions. This would be accomplished if one could find a unitary transformation of the 4×4 Eq. (4-10) that would de-couple the large and the small component and bring it on a block-diagonal form. It was the idea of Foldy and Wouthuysen [3] to completely separate the electronic and positronic solutions of the Dirac equation by the van Vleck-type (unitary) transformation of the Dirac Hamiltonian:

$$\mathrm{H}_D^{\mathcal{U}} = \mathcal{U}^\dagger \mathrm{H}_D \mathcal{U}, \quad (4\text{-}30)$$

i.e.,

$$\mathrm{H}_D^{\mathcal{U}} = \begin{pmatrix} \mathrm{h}_+ & 0 \\ 0 & \mathrm{h}_- \end{pmatrix}. \quad (4\text{-}31)$$

Such a transformation converts the 4×4 Dirac equation (4-10) into two separate eigenvalue problems. The one which corresponds to what is called the positive (electronic) part of the spectrum:

$$\mathrm{h}_+ \psi_+ = \epsilon_+ \psi_+, \tag{4-32}$$

where ψ_+ is the upper 2-spinor of the transformed four-component function:

$$\Psi_D^{\mathcal{U}} = \mathcal{U}^\dagger \Psi_D = \begin{pmatrix} \psi_+ \\ 0 \end{pmatrix}, \tag{4-33}$$

and should convert into the two-component non-relativistic Schrödinger equation in the limit of $c \to \infty$ (or $\alpha = 1/c \to 0$).

The FW transformation $\mathcal{U}$ of Eq. (4-30) can be specified in a number of different forms [18, 19]. The most common are the exponential and the square root forms [20]. Moreover, it can be also expressed as a product of subsequent unitary transformations:

$$\mathcal{U} = \mathcal{U}_0 \mathcal{U}_1 \ldots \tag{4-34}$$

Until recently this way of composing the final transformation $\mathcal{U}$ seemed to be of particular importance for the development of non-singular two-component relativistic Hamiltonians and this is the way how we are going to define it in this review.

The one-step transformation can be easily determined in the case of a free Dirac particle [3, 21–24] and has the following form:

$$\mathcal{U}_0 = \begin{pmatrix} \mathrm{A} & \alpha\mathrm{AB} \\ \alpha\mathrm{AB} & -\mathrm{A} \end{pmatrix}, \qquad \mathcal{U}_0{}^\dagger \mathcal{U}_0 = \mathrm{I}, \tag{4-35}$$

where

$$\mathrm{A} = \sqrt{\frac{e_p + 1}{2e_p}}, \qquad \mathrm{B} = \frac{1}{e_p + 1} \boldsymbol{\sigma p}, \tag{4-36}$$

and

$$e_p = \sqrt{1 + \alpha^2 p^2}. \tag{4-37}$$

When applied to the free-particle Dirac Hamiltonian this transformation brings it into diagonal form:

$$\mathcal{U}_0{}^\dagger \begin{pmatrix} 0 & c\boldsymbol{\sigma p} \\ c\boldsymbol{\sigma p} & -2c^2 \end{pmatrix} \mathcal{U}_0 = \begin{pmatrix} \mathrm{T}_p & 0 \\ 0 & -2c^2 - \mathrm{T}_p \end{pmatrix}, \tag{4-38}$$

where

$$\mathrm{T}_p = c^2(e_p - 1). \tag{4-39}$$

The atomic units has been used in the above equations. Thus the free-particle positive and negative energy spectra become fully separated. In other words one may say that fpFW of Eq. (4-35) accounts for all 'kinetic' relativistic effects. Simultaneously, there is no power expansion involved and one may expect that if the same transformation were applied to the Hamiltonian (4-11) the strongly divergent operators would not appear in the transformed Hamiltonian. In the traditional FW transformation of the Dirac Hamiltonian [1, 3, 20], the essentially singular operators arise either from high powers of p^2 or from their action on the Coulombic term V. This observation leads immediately to the conclusion that one may considerably profit by carrying out a preliminary free-particle Fouldy–Wouthuyse (fpFW) transformation of the Hamiltonian (4-11). Obviously, this transformation will not block-diagonalize H_D. In a general case to build the exact two-component formalism would mean that the next step is to define the complementary transformation U_1 which would fully block-diagonalize H_1, i.e.,

$$\mathcal{U}_1^\dagger \mathrm{H}_1 \mathcal{U}_1 = \mathcal{U}_1^\dagger \mathcal{U}_0^\dagger \mathrm{H}_D \mathcal{U}_0 \mathcal{U}_1 = \begin{pmatrix} \mathrm{h}_+ & 0 \\ 0 & \mathrm{h}_- \end{pmatrix}. \tag{4-40}$$

Usually, this block-diagonalization is achieved only approximately and one of the possibilities is that used by Douglas, Kroll and Hess [25–28]. A general description of the method will be presented in the next Section.

4.2.3.1. Douglas–Kroll–Hess Approximation

Although the unitary matrix U in Eq. (4-30) can be given in closed-form, what will be shown later in this review, historically, the first was the strategy introduced in 1974 by Douglas and Kroll [23] and followed by B.A. Hess [25, 26] who found the efficient way of handling the matrix elements of the two-component Douglas–Kroll Hamiltonian. B.A. Hess defined the unitary transformation U as the sequence of two transformations $U_1 U_0$. The inter most first unitary transformation U_0 was, chosen to be the fpFW transformation. The decoupling of the Dirac Hamiltonian in the framework of the Douglas–Kroll transformation was achieved by an expansion of the Hamiltonian in ascending powers of the external potential V, whereby the off-diagonal terms, which are called odd terms were removed to a certain order in V. What is referred to as the Douglas–Kroll–Hess (DKH) method corresponds to the approximate unitary transformation U_1 which makes the block of the partly block-diagonalized Hamiltonian accurate through the certain order of V. The resulting approximate two-component approximation to h_+ exact through the terms of the order of V^2 has been thus referred to as the DKH2 method. Since than the Douglas–Kroll–Hess (DKH2) numerical method became the very successful two-component computational tool of the relativistic quantum chemistry.

In the past few years several attempts have been made to formulate approximate two-component DK-type relativistic theories of the higher than the second-order with respect to the external potential. The third-order (DKH3) scheme has been proposed by Nakajima and Hirao [29] and recently generalized Douglas–Kroll–Hess (DKHn) transformation [30–32] up to any predefined order in the external potential has been formulated as well. The idea of the generalized DKHn method is to decompose the overall unitary transformation U into a sequence of simpler unitary transformations by a consecutive decoupling in terms of a sequence of unitary transformations $U = U_0U_1U_2U_3\cdots$, which block-diagonalizes H_D of Eq. (4-11) stepwise.

$$H_D^U = \cdots U_3^\dagger U_2^\dagger U_1^\dagger U_0^\dagger H_D U_0 U_1 U_2 U_3 \cdots = \sum_{k=0}^{\infty} \mathcal{E}_k. \tag{4-41}$$

It requires the construction of a sequence of unitary transformations $U_i, i = 1, 2, 3, ...$ which eliminate the lowest order odd terms in the ith step in order to arrive at the block-diagonal Hamiltonian H_D^U. This order by order block diagonalization assumes the existence of an expansion of the block-diagonal Hamiltonian in terms of a suitable expansion parameter, which allows to identify block-diagonal (so called even) operators, $\mathcal{E}_k$, of a given order k. Once all these even operators are added we obtain the block-diagonal Hamiltonian H_D^U.

The most general ansatz to construct a unitary transformation $U = f(W)$ as an analytical function of an antihermitian operator W is a power series expansion,

$$U = a_0\mathbf{1} + a_1W + a_2W^2 + a_3W^3 + \cdots = a_0\mathbf{1} + \sum_{k=1}^{\infty} a_k W^k \tag{4-42}$$

which is assumed to converged within a suitable number of steps. The analytic expansion of U_m in Eq. (4-42) is the most general form of a parametrization of a unitary matrix with W being the parameter. Exploiting the antihermiticity ($W^\dagger = -W$) the power series expansion of the hermitian conjugate transformation can be given as

$$U^\dagger = a_0\mathbf{1} - a_1W + a_2W^2 - a_3W^3 + \cdots = a_0\mathbf{1} + \sum_{k=1}^{\infty} (-1)^k a_k W^k \tag{4-43}$$

The coefficients a_k have to satisfy a set of constraints such that U is unitary, i.e., $U^\dagger U = \mathbf{1}$. The use of these most general parametrization of the unitary matrices has led to the term *generalized* Douglas–Kroll–Hess transformation as the resulting Hamiltonian make no reference to a specific parametrization All these parametrizations lead to the same DKH$_m$ Hamiltonian which results from a certain truncation of Eq. (4-41) after the term $\mathcal{E}_m$ (see the details in Refs. [30–32]).

4.2.4. Infinite Order Two-Component (IOTC) Method

Recently Barysz et al. has proposed [19, 33] a method for the generation of two-component solutions of arbitrarily high accuracy which are formally equivalent to solutions of the Dirac equation for the discrete electronic part on its eigenspectrum. The method is formally of infinite order in the fine structure constant and has been acronymed as the IOTC (infinite-order two-component) theory. Its equivalence to the four-component Dirac approach has been documented by calculations of spin-orbital energies and some selected atomic properties [34, 35]. In the IOTC method the preliminary fpFW transformation U_0 (4-35) of the Dirac Hamiltonian H_D is followed by the second unitary transformation U_1 which is meant to block-diagonalize H_1, (i.e.) to bring it to the form (4-40). Thus, the total unitary transformation U of H_D is factorized into two transformations U_0 and U_1, $U = U_1 U_0$, with U_1 defined [21, 24]

$$U_1 = \begin{pmatrix} \Omega_+ & R_-\Omega_- \\ R_+\Omega_+ & \Omega_- \end{pmatrix} \tag{4-44}$$

where

$$\Omega_+ = (1 + R_+^\dagger R_+)^{-1/2},\ \Omega_- = -(1 + R_-^\dagger R_-)^{-1/2},\ R_- = -R_+^\dagger, \tag{4-45}$$

and $R_+ = R$ is the root of the following operator equation [24],

$$\{H_1\}_{21} + \{H_1\}_{22} R - R\{H_1\}_{11} - R\{H_1\}_{12} R = 0. \tag{4-46}$$

The subscripts of H_1 denote the appropriate 2×2 blocks of the fpFW-transformed Hamiltonian:

$$\begin{aligned} H_1 &= U_0^\dagger H_D U_0 \\ &= \begin{pmatrix} T_p + A(V + \alpha^2 BVB)A & \alpha A[V, B]A \\ \alpha A[B, V]A & -2\alpha^{-2} - T_p + A(V + \alpha^2 BVB)A \end{pmatrix} \end{aligned} \tag{4-47}$$

For the purpose of its iterative solutions Eq. (4-46) can be written in the form,

$$R = [\{H_1\}_{22}]^{-1} [-\{H_1\}_{21} + R\{H_1\}_{11} + R\{H_1\}_{12} R] \tag{4-48}$$

and corresponds to the assumption that the R operator is a 'small' operator as compared to the R-independent term in the r.h.s. of Eq. (4-46).

After substituting the H_1 blocks into Eq. (4-48) one finds that the determination of R requires that the following equation

$$2R + \alpha^2 T_p R + \alpha^2 R T_p = e_p R + R e_p = \\ = \alpha^3 A[B, V]A + \alpha^2 [AVA, R] + \alpha^4 [BAVAB, R] \\ + \alpha^3 R[B, AVA]R \tag{4-49}$$

is solved.

Once the solution $R_+ = R$ of Eq. (4-49) is known, the *exact* two-component 'electronic' Hamiltonian h_+ becomes:

$$h_+ = \Omega_+^\dagger \left[\{H_1\}_{11} + \{H_1\}_{12} R + R^\dagger \{H_1\}_{21} + R^\dagger \{H_1\}_{22} R \right] \Omega_+. \tag{4-50}$$

No closed-form solution of Eq. (4-49) have been available until the IOTC method has been formulated and different truncated iterative solutions have been proposed [33,36,37], leading to explicit analytic approximations to the exact Hamiltonian h_+. All of them can be classified [33, 36] according to what is called the *leading order* with respect to α^2.

4.2.4.1. Matrix Approximation to the Unitarly Transformed Dirac Equation

When Hess presented his work he followed the momentum–space representation of Douglas–Kroll. The origin of the momentum–space presentation of the DKH method may be traced back to the square-root operator in e_p, *i.e.*, $e_p = \sqrt{1 + \alpha^2 p^2}$ Eq. (4-37). This term requires the calculation of the square root of the momentum operator. Such a square-root expression can hardly be evaluated in a position–space representation with linear momentum operators as differential operators. In momentum–space representation however, the momentum operator takes a simple multiplicative form. Finally, we then have to Fourier-transform, together with the momentum–space operators all operators which possess in position space a simple multiplicative form like the scalar potential V, and obtain integral operators defined by their operator kernels. However, if the DKH method remained in its original formulation [23] with the need for the Fourier transforms of operators defined in coordinate, its use in relativistic quantum chemistry would be rather limited. The success of the DKH2 and related approximations is mostly due to excellent and rather bold idea of Hess [25, 26] to replace the explicit Fourier transforms by some basis set which diagonalizes the p^2 operator. Consequently, the matrix approximation of the IOTC method is based on converting the R-operator equation (4-49) into such a form that it can be solved by standard algebraic techniques. The first step is the generation of eigenvectors of the p^2; this is done by using a finite coordinate-dependent basis set $\{\zeta_\alpha(\mathbf{r})\}$ in which the eigenvectors $\mid k\rangle$ of p^2:

$$\mid k\rangle = \sum_\alpha c_{\alpha k} \zeta_\alpha(\mathbf{r}) \tag{4-51}$$

are determined, i.e.,

$$\langle k \mid p^2 \mid k' \rangle = w_k \delta_{kk'}. \tag{4-52}$$

In the basis set $\{|\, k\rangle\}$ the approximate identity resolution is built:

$$1 \approx \sum_k |\, k\rangle\langle k\,| \tag{4-53}$$

and inserted between operators defined in the coordinate and momentum spaces. Then, for any function of the p^2 operator, say $f(p^2)$ the following approximation is introduced:

$$\langle k \mid f(p^2) \mid k'\rangle = f(w_k)\delta_{kk'}, \tag{4-54}$$

whereas the matrix elements of V and $\boldsymbol{\sigma p} V \boldsymbol{\sigma p}$ can be evaluated directly in the **r**-space. What remains are the operators of the form:

$$\boldsymbol{\sigma p} V f(p^2) V \boldsymbol{\sigma p}. \tag{4-55}$$

They will lead to integrals with linear terms in $\boldsymbol{\sigma p}$ whose accurate enough evaluation would require large basis sets with high angular momentum functions. Hess avoided this problem by using the identity:

$$\frac{\boldsymbol{\sigma p \sigma p}}{p^2} = 1, \tag{4-56}$$

whose insertion into (4-55) gives:

$$\boldsymbol{\sigma p} V \boldsymbol{\sigma p}\, p^{-2} f(p^2) \boldsymbol{\sigma p} V \boldsymbol{\sigma p}. \tag{4-57}$$

The use of eigenvectors of the p^2 operator determined in the **r**-dependent basis set and of the identity (4-56) reduces most of the terms needed for the evaluation of (4-49) to rather elementary integrals in the coordinate representation. However, this method will not remove the cumbersome terms which are linear in $\boldsymbol{\sigma p}$. This means that one needs an additional steps before Eq. (4-49) can be solved.

4.2.4.2. The Exact Separation of Electronic Solutions of the Dirac Equation

The problem of solving the Eq. (4-49) lies in the presence of linear terms in $\boldsymbol{\sigma p}$ in this equation and has been solved recently [33]. It opened the possibility to solve this equation in a purely numerical way. Let us multiply Eq. (4-49) from the left by the operator $p^{-1}\boldsymbol{\sigma p}$, where p^{-1} denote the inverse square root of p^2 and is a scalar operator. One obtains then:

$$\begin{aligned} e_p Y + Y e_p = {} & \alpha^3 (pAbVA - p^{-1} A \boldsymbol{\sigma p} V \boldsymbol{\sigma p} bA) \\ & + \alpha^2 (p^{-1} A \boldsymbol{\sigma p} V \boldsymbol{\sigma p}\, p^{-1} AY - YAVA) \\ & + \alpha^4 (pAbVbApY - YAb \boldsymbol{\sigma p} V \boldsymbol{\sigma p} bA) \\ & + \alpha^3 Y (Ab \boldsymbol{\sigma p} V \boldsymbol{\sigma p} Ap^{-1} - AVAbp) Y, \end{aligned} \tag{4-58}$$

where

$$b = \frac{1}{e_p + 1} \tag{4-59}$$

and the operator Y is

$$Y = p^{-1}\boldsymbol{\sigma p} R. \tag{4-60}$$

Converting the R-operator equation into (4-58) means that all its matrix elements can be easily evaluated by using the method surveyed in Section 4.2.4.1. Thus, the equation for matrix elements $Y_{kk'}$:

$$\begin{aligned} Y_{kk'} = \frac{1}{E_k + E_{k'}} \Bigg[& \alpha^3 \langle k \mid pAbV\, A - p^{-1} A\boldsymbol{\sigma p} V \boldsymbol{\sigma p} bA \mid k' \rangle \\ & + \alpha^2 \sum_{k''} \left(\langle k \mid p^{-1} A\boldsymbol{\sigma p} V \boldsymbol{\sigma p} p^{-1} A \mid k'' \rangle Y_{k''k'} - Y_{kk''} \langle k'' \mid AVA \mid k' \rangle \right) \\ & + \alpha^4 \sum_{k''} \left(\langle k \mid pAbVbAp \mid k'' \rangle Y_{k''k} - Y_{kk''} \langle k'' \mid Ab\boldsymbol{\sigma p} V \boldsymbol{\sigma p} bA \mid k' \rangle \right) \\ & + \alpha^3 \sum_{k''k'''} Y_{kk''} \langle k'' \mid Ab\boldsymbol{\sigma p} V \boldsymbol{\sigma p} Ap^{-1} - AVAbp \mid k''' \rangle Y_{k'''k'} \Bigg] \end{aligned} \tag{4-61}$$

can be solved to arbitrarily high accuracy by using standard iterative approaches. Once this numerical (algebraic) solution for the matrix representation of Y is found, the corresponding matrix representation of h_+ can be calculated as well [33].

The numerical (algebraic) solution of Eq. (4-61) followed by the evaluation of the matrix elements of h_+ gives the infinite-order solution for the block-diagonalization of the Dirac Hamiltonian. The numerical accuracy of the IOTC method have been demonstrated many times [19, 33, 34, 36, 38, 39]. The IOTC method is nowadays a part of the commonly used molecular code Molcas [40].

4.2.4.3. The Ricatti Equation Method

An alternative route to the iterative IOTC method based on the diagonalization of $(2n) \times (2n)$ IOTC matrix Hamiltonian may be defined as well [42]. The method based on the diagonalization helps to avoid the slow convergence or divergences which may occur in the iterative scheme [33, 34].

The IOTC method is based on converting the R-operator equation into a matrix representation in a basis set. If this is done the form of the R-operator Eq. (4-46) becomes equivalent to what is known in algebra as the non-symmetric algebraic Ricatti equation (n-ARE) [41]. This does not seem to have been exploited until

recently [42]. Though relatively trivial, this observation immediately opens several new or at least alternative routes to the solution of Eq. (4-46).

It can be shown [41] that solutions of (4-46) are associated with the eigenvectors of the matrix representation of the H_1 operator expressed in some spinor (or bi-spinor) basis set,

$$\mathbf{H_1} = \begin{bmatrix} (\mathbf{H_1})_{11} & (\mathbf{H_1})_{12} \\ (\mathbf{H_1})_{21} & (\mathbf{H_1})_{22} \end{bmatrix}, \tag{4-62}$$

In the present case the eigenvectors $\mathbf{V}$ of (4-62) can be assumed to be composed of $n \times n$-dimensional invertible blocks $\mathbf{V_{ij}}$:

$$\mathbf{V} = [\mathbf{V_1}, \mathbf{V_2}] = \left[\begin{pmatrix} \mathbf{V_{11}} \\ \mathbf{V_{21}} \end{pmatrix}, \begin{pmatrix} \mathbf{V_{12}} \\ \mathbf{V_{22}} \end{pmatrix} \right], \tag{4-63}$$

where the $2n \times n$ matrices $\mathbf{V_1}$ and $\mathbf{V_2}$ correspond to positive and negative eigenvalues of $\mathbf{H_1}$, respectively. Thus, the eigenvalue problem of the $\mathbf{H_1}$ matrix may be written as:

$$\mathbf{H_1 V_1} = \mathbf{V_1 E_1}, \tag{4-64}$$

$$\mathbf{H_1 V_2} = \mathbf{V_2 E_2}, \tag{4-65}$$

where $\mathbf{E_1}$ and $\mathbf{E_2}$ are the diagonal matrices of the positive and negative eigenvalues of $\mathbf{H_1}$. Thus, one finds that,

$$\mathbf{H_{11} V_{11}} + \mathbf{H_{12} V_{21}} = \mathbf{V_{11} E_1} \tag{4-66}$$

and

$$\mathbf{H_{21} V_{11}} + \mathbf{H_{22} V_{21}} = \mathbf{V_{21} E_1}. \tag{4-67}$$

Since the $\mathbf{V_{ij}}$ blocks are assumed to be invertible, the eigenvalue matrix $\mathbf{E_1}$ can be determined from (4-66) and then inserted into (4-67). This leads to the following result:

$$(\mathbf{H_{21}} + \mathbf{H_{22} V_{21} V_{11}^{-1}} - \mathbf{V_{21} V_{11}^{-1} H_{11}} - \mathbf{V_{21} V_{11}^{-1} H_{12} V_{21} V_{11}^{-1}})\mathbf{V_{11}} = \mathbf{0}, \tag{4-68}$$

which is the non-symmetric algebraic Ricatti equation, associated with the $\mathbf{H_1}$ matrix:

$$\mathbf{H_{21}} + \mathbf{H_{22} R} - \mathbf{R H_{11}} - \mathbf{R H_{12} R} = \mathbf{0}, \tag{4-69}$$

associated with the $\mathbf{H_1}$ matrix and $\mathbf{R}$,

$$\mathbf{R} = \mathbf{V_{21} V_{11}^{-1}}, \tag{4-70}$$

is the matrix representation of the operator R. Once the $\mathbf{V}$ matrix is obtained by the diagonalization of the $2n \times 2n$ matrix $\mathbf{H_1}$, the solution for the matrix representation of the operator R can be determined. The diagonalization of the $\mathbf{H_1}$ is carried out only once and the eigenvectors of this matrix are used then to build the matrix representation of the h_+ Hamiltonian. One should stress that all this is done for one-electron operators. The many-electron theory with the one-electron part given by h_+ is the *two-component theory* and represents the infinite-order extension of the usual (many-electron) Douglas–Kroll methods [33, 34, 43, 44].

4.2.4.4. The Performance of the Two-Component IOTC Method

Numerical accuracy of the infinite-order two-component method has been studied and documented in other papers [19,34,35,38,42]. In this section we will show some selected results which confirm the excellent performance of the IOTC method.

We will start the numerical investigations of the numerical accuracy of the IOTC method with the $1s_{1/2}$ energy level in one-electron ions with different values of the nuclear charge Z. The tabulated data will be given in terms of the parameter γ which is defined by the orbital energy ϵ.

$$\gamma = -\epsilon/Z^2 \tag{4-71}$$

The data of the Table 4-1, which are copied from the earlier paper [42], show that the $1s_{1/2}$ energies are essentially the same as the corresponding Dirac energies. This confirms that the IOTC method recovers the spectrum of the Dirac operator.

One of the important features of the hydrogenic Dirac Hamiltonian is that its spectrum forms a super-symmetric pattern [45–47]. This is reflected by the so-called accidental degeneracy [1, 47] of all but the lowest energy levels with the same absolute value of the quantum number $\kappa = \pm(j + 1/2)$. The origin of this degeneracy can be analysed [47] in terms of the Johnson–Lippmann (JL) operator [48] which is the relativistic counterpart of the Runge–Lenz vector of the non-relativistic Kepler problem [49, 50]. For the hydrogenic problem the JL operator commutes with the Dirac Hamiltonian h_D (4-11) and with the square (J^2) of the total angular momentum operator $\mathbf{J}$ and its Cartesian components. On the other hand, the JL operator can be shown to anti commute with the Dirac (K) and inversion operators [47]. These features of the hydrogenic Dirac Hamiltonian give its (positive) energy spectrum

Table 4-1 $1s_{1/2}$ Energies for H-like ions expressed in terms of the parameter γ defined by Eq. (4-71) (see the text)

Z	IOTC	Dirac
80	0.5519050236	0.5519050236
100	0.5939195384	0.5939195384
120	0.6743599667	0.6743599667
130	0.7596994464	0.7596994934

in the form of degenerate stacks of the energy levels [47]. This degeneracy in the positive-energy Dirac spectrum for hydrogenic systems is been referred to as the κ-degeneracy.

Since the infinite-order two-component theory is based on exact equations, it is obvious that it must reproduce all features of the positive-energy Dirac spectrum, including its supersymmetric pattern. However, the way this theory is used introduces the algebraic approximation. It has been shown that with sufficiently large and flexible Gaussian basis sets the supersymmetric pattern of bound energy levels is fully restored [51], The majority of methods based on approximate two-component Hamiltonians cannot reproduce the supersymmetric features of the Dirac Hamiltonian. Among these methods one should also list the otherwise very efficient Douglas–Kroll–Hess (DKH) scheme [25,26,30,32]. In consequence the degeneracy pattern for example, for $ns_{1/2}$ and $np_{1/2}$ or $np_{3/2}$ and $nd_{3/2}$ levels is not reproduced by the DKH2 method. In consequence, this method cannot give the right values of the spin–orbit splittings in the np shells. For the illustration see the Tables 4-2–4-3. Results presented in Tables 4-2–4-3 are taken from our earlier publications [51].

Finally one should stress that the infinite-order two-component theory (IOTC) presented in this review gives all of the positive-energy spectrum of the Dirac Hamiltonian. Thus, within this part of the Dirac spectrum the IOTC two-component method is exactly equivalent to the exact four-component theory.

Table 4-2 A study of κ degeneracy in one-electron ions and comparison of IOTC and DKH results with the corresponding Dirac energies. Energies are expressed in the parameter γ defined by Eq. (4-71) (see text)

Z		IOTC	DKH2	Dirac
80	$2s_{1/2}$	0.14138247	0.14120194	0.14138247
	$2p_{1/2}$	0.14138247	0.14130478	0.14138247
100	$2s_{1/2}$	0.15486562	0.15440847	0.15486562
	$2p_{1/2}$	0.15486562	0.15450851	0.15486562
120	$2s_{1/2}$	0.18117521	0.17987940	0.18117521
	$2p_{1/2}$	0.18117520	0.17953312	0.18117521
80	$3p_{3/2}$	0.05720980	0.05720927	0.05720980
	$3d_{3/2}$	0.05720980	0.05720975	0.05720980
100	$3p_{3/2}$	0.05821391	0.05821247	0.05821391
	$3d_{3/2}$	0.05821391	0.05821368	0.05821391
120	$3p_{3/2}$	0.05952362	0.05952047	0.05952362
	$3d_{3/2}$	0.05952362	0.05952285	0.05952362

Table 4-3 Spin–orbit splittings for $np_{3/2}$-$np_{1/2}$ in eV

Z	IOTC	DKH2	Dirac
2p			
80	2368.45	2355.21	2368.45
100	6912.41	6816.46	6912.41
120	19407.99	18768.48	19407.99
7p			
80	53.846	53.506	53.846
100	153.60	151.46	153.61
120	411.49	400.12	411.49

4.2.4.5. Change of Picture Effect

The transformation of the Dirac Hamiltonian to two-component form is accompanied by a corresponding reduction of the wave function. The four-component Dirac spinor has only two non-vanishing components, as soon as the complete decoupling of the electronic and positronic degrees of freedom is achieved, and can thus be used as a two-component spinor. The so called change of picture problem arises in this context in the calculations of the expectation values of operators. Let U be the exact unitary transformation defined by Eq. (4-30) that decouples the Dirac Hamiltonian. The transformed wave function has thus only non-vanishing upper component and is given by Eq. (4-33). Every physical observable O within the Dirac theory is described by a self-adjoint (4×4) operator, which can be written as

$$\mathbf{O} = \begin{pmatrix} \mathbf{O}_{11} & \mathbf{O}_{12} \\ \mathbf{O}_{21} & \mathbf{O}_{22} \end{pmatrix}. \tag{4-72}$$

Its expectation value $\bar{O}$ should be written as

$$\bar{\mathbf{O}} = \langle \mathbf{\Psi}_\mathbf{D} | \mathbf{O} | \mathbf{\Psi}_\mathbf{D} \rangle \tag{4-73}$$

Thus in terms of two-component solutions (4-33), the corresponding expression becomes

$$\begin{aligned} \bar{\mathbf{O}} &= \left\langle \mathbf{\Psi}_\mathbf{D} | \mathbf{U}\mathbf{U}^\dagger \mathbf{O} \mathbf{U}\mathbf{U}^\dagger | \mathbf{\Psi}_\mathbf{D} \right\rangle = \left\langle \mathbf{\Psi}_\mathbf{D}^\mathbf{U} | \mathbf{U}^\dagger \mathbf{O} \mathbf{U} | \mathbf{\Psi}_\mathbf{D}^\mathbf{U} \right\rangle \\ &= \left\langle \mathbf{\Psi}_\mathbf{D}^\mathbf{U} | \mathbf{O}^\mathbf{U} | \mathbf{\Psi}_\mathbf{D}^\mathbf{U} \right\rangle = \left\langle \mathbf{\Psi}_+ | \mathbf{O}^\mathbf{U}{}_{11} | \mathbf{\Psi}_+ \right\rangle \end{aligned} \tag{4-74}$$

where

$$\mathbf{O}^{\mathrm{U}} = \mathbf{U}^{\dagger}\mathbf{O}\mathbf{U} \tag{4-75}$$

and $\mathbf{O}^{\mathrm{U}}{}_{11}$ denotes its (1, 1) block. This expression is still exact and no approximation has been introduced yet. However, in two-component approximation, which leaves the non-relativistic philosophy of quantum chemical calculations, this expectation value is calculated as:

$$\bar{\mathbf{o}} = \langle \mathbf{\Psi}_{+} | \mathbf{O}_{11} | \mathbf{\Psi}_{+} \rangle \tag{4-76}$$

That is, the change of picture of the operator O is neglected completely, and the difference $\bar{O} - \bar{o}$ is referred to as the picture change effect on the expectation value. In general, whenever a unitary transformation is applied to the Hamiltonian in order to block-diagonalise it, but not to other physical observables, some picture change effect will occur. For operators which assume large values in the vicinity of nuclei, this effect is expected to be quite large. Indeed, it has been found that for electric field gradients at heavy nuclei, as the nuclear quadruple moments, the picture change contribution is not negligible [52, 53]. The picture change effect has been also found to be quite large for dipole moments derivatives with respect to nuclear coordinates. The same is true for the dipole polarizability derivatives [52]. These findings show that two-component calculations of infrared and Raman intensities for heavy systems need to take into account the picture change of the relevant operators. In the case of major molecular electric properties, i.e., multiple moments and multiple polarizabilities, the change of picture should be rather small [38, 54, 55].

4.2.4.6. Back-Transformation

The two-component IOTC method is formally of infinite order and its equivalence to the four-component Dirac approach has been documented by calculations of spinorbital energies. However, the implementation of the method introduces certain approximations while moving to the matrix approximation to the unitarly transformed Dirac equation (see Section 4.2.4.1). It may affect the exact equivalence. It can be demonstrated [38] that the two-component IOTC wave function which is the upper component of the unitarly transformed four-component Dirac spinor Ψ

$$\Phi = \mathcal{U}_1^{\dagger}\mathcal{U}_0^{\dagger}\Psi = \begin{pmatrix} \phi^{IOTC} \\ 0 \end{pmatrix}, \tag{4-77}$$

can be back transformed and one obtains the exact Dirac solution which corresponds to the given IOTC solution:

$$\Psi = \mathcal{U}_0\mathcal{U}_1\Phi \tag{4-78}$$

Because of the approximate determination of U_1 the inverse transformation (4-78) may not exactly reproduce the Dirac bi-spinors. In order to check how exact is the back-transformed function Ψ, the transformed two-component solutions can than be used to evaluate different moments $< r^k >$ of the electron distribution.

The transformation matrices which enter (4-78) has been defined earlier by Eqs. (4-35) and (4-44). The transformation of (4-78) will therefore read

$$\begin{aligned} U_0 U_1 \left|\Phi\right\rangle &= \begin{pmatrix} A\Omega_+ + \alpha AB R_+ \Omega_+ & AR_-\Omega_- + \alpha AB\Omega_- \\ \alpha AB\Omega_+ - AR_+\Omega_+ & \alpha ABR_-\Omega_- - A\Omega_- \end{pmatrix} \begin{pmatrix} \phi^{IOTC} \\ 0 \end{pmatrix} \\ &= \begin{pmatrix} A\Omega_+ + \alpha AB R_+ \Omega_+ \\ \alpha AB\Omega_+ - AR_+\Omega_+ \end{pmatrix} \left|\phi^{IOTC}\right\rangle \end{aligned} \tag{4-79}$$

For the operator Y defined by (4-60) one obtains

$$R_- = -R_+^\dagger = -Y^\dagger \boldsymbol{\sigma}\mathbf{p}p^{-1} \tag{4-80}$$

and the form of the inverse transformation of the IOTC wave function (4-78) becomes

$$\left|\Psi\right\rangle = \begin{pmatrix} A\Omega_+ + \alpha A \frac{1}{e_p+1} pY\Omega_+ \\ \boldsymbol{\sigma p}\left(\alpha A \frac{1}{e_p+1}\Omega_+ - Ap^{-1}Y\Omega_+\right) \end{pmatrix} \left|\phi^{IOTC}\right\rangle \tag{4-81}$$

The approximate algebraic Dirac wave function (4-81) calculated with the algebraic approximation is then used to evaluate expectation values of different operators $\hat{O}$. These expectation values can be compared with the exact Dirac values and will give the measure of the accuracy of the algebraic IOTC approximation.

Let $\hat{O}$ be a diagonal operator defined in the Dirac picture. Then its expectation value for the approximate algebraic Dirac state (4-78) will be given by:

$$\begin{aligned} \left\langle \hat{O} \right\rangle &= \left\langle \Psi \left| U_1^\dagger U_0^\dagger \hat{O} U_0 U_1 \right| \Psi \right\rangle \\ &= \left\langle \phi^{IOTC} \left| \left(\Omega_+ A + \alpha \Omega_+ Y_+^\dagger p \frac{1}{e_p+1} A \left(\alpha \Omega_+ A \frac{1}{e_p+1} - \Omega_+ Y_+^\dagger p^{-1} A \right) \boldsymbol{\sigma p} \right) \right. \right. \\ &\quad \left. \left. \hat{O} \begin{pmatrix} A\Omega_+ + \alpha A \frac{1}{e_p+1} pY_+\Omega_+ \\ \boldsymbol{\sigma p}\left(\alpha A \frac{1}{e_p+1}\Omega_+ - Ap^{-1}Y_+\Omega_+\right) \end{pmatrix} \right| \phi^{IOTC} \right\rangle \\ &= \left\langle \phi^{IOTC} \left| \left\{ \Omega_+ A + \alpha \Omega_+ Y_+^\dagger p \frac{1}{e_p+1} A \right\} \hat{O} \left\{ A\Omega_+ + \alpha A \frac{1}{e_p+1} pY_+\Omega_+ \right\} \right. \right. \\ &\quad + \left\{ \alpha \Omega_+ A \frac{1}{e_p+1} - \Omega_+ Y_+^\dagger p^{-1} A \right\} \\ &\quad \left. \left. \boldsymbol{\sigma p} \hat{O} \boldsymbol{\sigma p} \left\{ \alpha A \frac{1}{e_p+1}\Omega_+ - Ap^{-1}Y_+\Omega_+ \right\} \right| \phi^{IOTC} \right\rangle \end{aligned} \tag{4-82}$$

In the algebraic approximation the evaluation of (4-82) can be carried out by using the approximate identity resolution in terms of eigenfunctions of the p^2 operator in the selected basis set [19,25,26,33]. As it has been shown recently [38] with sufficiently large basis set of Gaussian functions, the Dirac values of the $< r^k >$ moments calculated with the formula (4-82) can be fully recovered. Hence, it may be conclude that the IOTC approach for time-independent problems is as relativistic as the four-component wave function.

4.3. INTERACTIONS

The attention of the present study was focused on the electronic part of the Dirac spectrum and this appears to be sufficient for the majority of relativistic studies in quantum chemistry. However, since both the h_+ and h_- spectra can be generated in the same way one can, if needed, proceed towards quantum electrodynamics formulated in finite basis sets. The first step in this direction will be the appropriate definition of the electron–electron interaction. The theory investigated in this review is the one electron theory. However, the electron–electron interaction can be included by passing to the field-theoretic formalism. A Hamiltonian of an N electron system may be written as

$$H(1,2,\ldots,N) = \sum_{j=1}^{N} h_1(j) + \sum_{i<j}^{N} h_2(i,j) \tag{4-83}$$

where h_1 are the one-electron Hamiltonians and h_2 describe the interactions between electrons. In the non-relativistic case, $h_1 = h_1^S$ and $h_2(i,j) = \frac{e^2}{r_{ij}}$ is the inter-electron Coulomb interaction. In the relativistic theory defining an N-electron Hamiltonian is a major fundamental problem. A Lorentz-invariant quantum mechanics of many particles cannot be formulated.

The operator (4-83) is referred to as the Dirac–Coulomb (H_{DC}) Hamiltonian and represents the lowest order approximation of the electron– electron interactions.

The two-electron Dirac–Coulomb equation can be shown to have no bound states. Thus, there is no protection against the variational collapse into negative energy states. The ill-conditioned form of the Dirac–Coulomb Hamiltonian has been first recognized by Brown and Ravenhall and is usually termed as the 'Brown–Ravenhall disease'. This follows from the fact that a bound state of two non-interacting Dirac electrons, is degenerate with a continuum of non-normalizable states having one electron in the positive energy state and another one in the negative energy state. When the Coulomb interaction is included, the initial wave function of non-interacting electrons gains contributions from all those continuum states and becomes 'dissolved in continuum'.

Inspite of its rather obscure meaning and mathematical features the Dirac–Coulomb Hamiltonian is underlying the majority of relativistic techniques in quantum chemistry.

A rigorous formulation of a two-electron theory is only possible at the level of quantum electrodynamics [56]. However, using the correspondence principle, one may obtain the same result from classical electrodynamics. Classically, the scalar and the vector potentials generated at the point $\mathbf{r}_j$ by a charge e located at the point $\mathbf{r}_i$ and moving with velocity $\mathbf{v}_i$ (Lienard–Wiechert potentials) are given by

$$V_i^{LW}(\mathbf{r}_j) = \frac{e^2}{r_{ij}}\left[1 + \frac{(\mathbf{v}_i \cdot \mathbf{r}_{ij})}{c\, r_{ij}}\right]^{-1} \tag{4-84}$$

and

$$\mathbf{A}_i^{LW}(\mathbf{r}_j) = \frac{\mathbf{v}_i}{c}\, V_i^{LW}(\mathbf{r}_j) \tag{4-85}$$

respectively. By substituting these potentials into the classical relativistic Hamilton function with the vector potential $\mathbf{A}$

$$H = mc^2\sqrt{1 + \frac{1}{m^2c^2}\left(\mathbf{p} - \frac{e}{c}\mathbf{A}\right)^2} + V \tag{4-86}$$

and expanding into a power series with respect to $\frac{v}{c}$ we get

$$H = \sum_{j=1}^{N} H_1(j) + \sum_{i<j}^{N} \frac{e^2}{r_{ij}}\left[1 - \frac{\mathbf{v}_i \cdot \mathbf{v}_j}{2c^2} - \frac{(\mathbf{v}_i \cdot \mathbf{r}_{ij})(\mathbf{v}_j \cdot \mathbf{r}_{ij})}{2c^2 {r_{ij}}^2}\right] + \\ + O\left(\left(\frac{v}{c}\right)^2\right) \tag{4-87}$$

where

$$H_1(j) = mc^2\sqrt{1 + \frac{1}{m^2c^2}\left[\mathbf{p}_j - \frac{e}{c}\mathbf{A}(\mathbf{r}_j)\right]^2} + V(\mathbf{r}_j) \tag{4-88}$$

Now, according to the correspondence principle, we substitute:

$$H_1(j) \Rightarrow h_1^D(j) = c\alpha_j\left[\mathbf{p}_j - \frac{e}{c}\mathbf{A}(\mathbf{r}_j)\right] + V(\mathbf{r}_j) \tag{4-89}$$

and

$$\mathbf{v} \Rightarrow c\alpha \tag{4-90}$$

The resulting Hamiltonian reads:

$$H_{DB}(1, 2, \ldots, N) = \sum_{j=1}^{N} h_1^D(j) + \sum_{i<j}^{N}\left[h_2(i, j) + h_2^{mag}(i, j) + h_2^{ret}(i, j)\right] \tag{4-91}$$

where

$$h_2^{mag}(i,j) = -\frac{e^2}{2r_{ij}}(\alpha_i \cdot \alpha_j) \tag{4-92}$$

and

$$h_2^{ret}(i,j) = -\frac{e^2}{2{r_{ij}}^3}(\alpha_i \cdot \mathbf{r}_{ij})(\alpha_j \cdot \mathbf{r}_{ij}) \tag{4-93}$$

are, respectively, corrections due to two-electron magnetic interactions and due to retardation resulting from the finite velocity of propagation of the interaction. A relativistic Hamiltonian (4-91) is called the Dirac–Breit many-electron Hamiltonian. This replacement, however, does not remove the 'Brown–Ravenhall disease' problem. Moreover, the Dirac–Breit Hamiltonian is derived perturbationally and there may be some objections against its use in variational calculations. Thus, it is frequently suggested that the Breit correction to the Coulomb interaction should be considered in the perturbation framework and evaluated as the first-order contribution to the energy which follows from H_{DC} Since the Hamilton function (4-87) is correct up to $\left(\frac{v}{c}\right)^2$ terms, also the quantum-mechanical Hamiltonian is correct up to this accuracy and the formulation based on this Hamiltonian is only approximately Lorentz invariant (see the details in [56]).

In the context of the two-electron Breit operator (4-91) one should also mention its approximate form known as the Gaunt interaction V^G:

$$V^G(i,j) = \frac{1}{r_{ij}} + \frac{\alpha_i \cdot \alpha_j}{\mathbf{r}_{ij}} \tag{4-94}$$

which leads to the Dirac–Gaunt (H^{DG}) many-electron Hamiltonian:

$$H_{DG}(1,2,\ldots,N) = \sum_{j=1}^{N} \hat{h}_1^D(j) + \sum_{i<j}^{N} V^G(i,j) \tag{4-95}$$

The derivation of the two-component Hamiltonians neglects all effect related to the creation of virtual electron–positron pairs. Also the effects of virtual photons are neglected.

4.4. SUMMARY AND CONCLUSION

The present review is primarily intended to introduce the concept of the two-component relativistic methodology. With the development of efficient infinite-order IOTC method in its truly two-component form and the design of the corresponding codes, one may expect it to become a the powerful tool for the molecular computational chemistry. However, in the context of applications of relativistic

quantum chemistry, one has to mention that actually most of the corresponding calculations are carried out in the spin-free approximation. This permits that standard non-relativistic codes can be used with a simple modification of the core Hamiltonian. The future still seems to be in the development of the true two-component codes which will be able to deal with the spin–orbit interaction effect. The present alternative is to include the spin–orbit coupling terms in a posteriori way in the form of the configuration interaction calculations [57].

ACKNOWLEDGMENTS

The author wishes to thank Prof. Jacek Karwowski for the valuable discussion.

REFERENCES

1. Moss, R.E.: Advanced Molecular Quantum Mechanics. Chapman and Hall, London (1973)
2. Bethe, H.A., Salpeter, E.E.: Quantum Mechanics of One- and Two-Electron Atoms. Springer, Heidelberg (1957)
3. Foldy, L.L., Wouthuysen, S.A.: Phys. Rev. **78**, 29 (1950)
4. Feynman, R.P.: Quantum Electrodynamics. A Lecture Note. Benjamin, New York (1961)
5. Ryder, L.H.: Quantum Field Theory. Cambridge University Press, Cambridge (1992)
6. Grant, I.P., Quiney, H.M.: Adv. At. Mol. Phys. **23**, 37 (1988)
7. Lindgren, L., Persson, H., Salomonsson, S., Labzovsky, L.: Phys. Rev. A, **51** , 1167 (1995)
8. Balasubramanian, K. Relativistic Effects in Chemistry. Wiley, New York (1997)
9. Sakurai, J.J.: Advanced Quantum Mechanics. Addison-Wesley, Reading, MA (1967)
10. Dyall, K.G., Faegri, K.: Introduction to the Relativistic Quantum Chemistry. Oxford University Press, Oxford (2007)
11. Chang, Ch., Pélissier, M., Durand, P.: Phys. Scripta **34**, 394 (1986)
12. van Lenthe, E., Baerends, E.J., Snijders, J.G.: J. Chem. Phys. **99**, 4597 (1993)
13. van Lenthe, E., Baerends, E.J., Snijders, J.G.: J. Chem. Phys. **101**, 9783 (1994)
14. van Lenthe, E., Ehlers, A., Baerends, E.J.: J. Chem. Phys. **110**, 8943 (1999)
15. van Wuellen, Ch.: J. Chem. Phys. **109**, 392 (1998)
16. Filatov, M., Cremer, D.: J. Chem. Phys. **122**, 044104 (2005)
17. Dyall, K.G.: J. Chem. Phys. **106**, 9618 (1997); J. Chem. Phys. **109**, 4201 (1998); Dyall, K.G., Enevoldsen T.: J. Chem. Phys. **111**, 10000 (1999)
18. Kutzelnigg, W.: Z. Phys. D **15**, 27 (1990)
19. Barysz, M.: Theoretical Chemistry and Physics of Heavy and Superheavy Elements, Progress in Theoretical Chemistry and Physics, p. 349. Kluwer, Boston (2003)
20. Greiner, W.: Theoretische Physik, Bd. 6, Relativistische Quantenmechanik – Wellengleichungen, Harri Deutsch, Thun (1987)
21. Barysz, M., Sadlej A.J., Snijders J.G.: Int. J. Quantum Chem. **65**, 225 (1997)
22. Sucher, J.: Phys. Rev. A **22**, 348 (1980)
23. Douglas, M., Kroll, N.M.: Ann. Phys. **82**, 89 (1974)
24. Heully, J.-L., Lindgren I., Lindroth E., Lundquist S., Mårtenson–Pendril, A.-M.: J. Phys. B **19**, 2799 (1986)
25. Hess, B.A.: Phys. Rev. A **32**, 756 (1985)
26. Hess, B.A.: Phys. Rev. A **33**, 3742 (1986)

27. Almlöf, J., Faegri, K. Jr., Grelland, H.H.: Chem. Phys. Lett. **114**(53), (1985)
28. Almlöf, J., Groppen, O.: In: K.B. Lipkowitz, D.B. Boyd (eds.) Reviews in Computational Chemistry, Volume 8. VCH Publishers, New York (1996)
29. Nakajima, T., Hirao T., K.: J. Chem. Phys. **113**, 7786 (2000)
30. Wolf, A.: Reiher, M.: Hess, B.A.: J. Chem. Phys. **117**, 9215 (2002)
31. Wolf, A., Reiher, M., Hess, B.A.: In: P. Schwerdtfeger (ed.) Relativistic Electronic Structure Theory: Part 1. Fundamentals, p. 622. Elsevier, Amsterdam (2002)
32. Reiher, M.: Wolf, A.: J. Chem. Phys. **121**, 2037 (2004)
33. Barysz, M., Sadlej, A.J.: J. Chem. Phys. **116**, 2696 (2002)
34. Kędziera, D., Barysz, M.: J. Chem. Phys. **121**, 6719 (2004)
35. Kędziera, D., Barysz, M., Sadlej, A.J.: Struct. Chem. **15**, 369 (2004)
36. Barysz, M.: J. Chem. Phys. **116**, 2704 (2001)
37. Barysz, M.: Acta Physica Polonica A **101**, 815 (2002)
38. Barysz, M., Mentel, Ł., Leszczyński J.: J. Chem. Phys. **130**, 164114 (2009)
39. Barysz, M., Leszczyński J.: J. Chem. Phys. **126**, 154106 (2007)
40. Andersson, K., Barysz, M., Bernhardsson, A., Blomberg, M.R.A., Carissan, Y., Cooper, D.L., Cossi, C., Devararajan, A., Fülscher, M., Gaenko, A., Gagliardi, L., de Graaf, C., Hagberg, D., Hess, B.A., Karlström, G., J.W. Krogh, J.W., Lindh, R., Malmquist, P.-Å., Nakajima, T., Neogrády, P., Olsen, J., Pedersen, T.B., Raab, J., Roos, B.O., Schimmelpfennig, B., Schütz, M., Seijo, L., Serrano-Andrés, L., Siegbahn, P.E.M., Stålring, J., Thorsteinsson, T., Veryazov, V., Widmark, P.-O.: Molcas Version 6.5., Lund University, Sweden (2006)
41. Freiling, G.: Linear Algebra Appl. **351**, 243 (2002)
42. Kędziera, D., Barysz, M.: Chem. Phys. Lett. **446**, 176 (2007)
43. Reiher, M.: Theor. Chem. Acc. **116**, 241 (2006)
44. Barysz, M., Sadlej, A.J.: J. Mol. Struct. (Theochem) **573**, 181 (2001)
45. Sukumar, C.V.: J. Phys. A **18**, L697 (1985)
46. Jarvis, P.D., Stedman, G.E.: J. Phys. A **19**, 1373 (1986)
47. Dahl, J.P., Jørgensen, T.: Int. J. Quantum Chem. **53**, 161 (1995)
48. Johnson, M.H., Lippmann, B.A.: Phys. Rev. **78**, 329A (1950)
49. Schiff, L.: Quantum Mechanics, p. 236. McGraw-Hill, Singapore (1968)
50. Adams, B.G., Čižek J., Paldus J.: Int. J. Quantum Chem. **21**, 153 (1982)
51. Kędziera, D., Barysz, M.: Chem. Phys. Lett. **393**, 521 (2004)
52. Kellö, V.: Sadlej, A.J., Int. J. Quant. Chem. **68**, 159 (1998)
53. Kellö, V.: Sadlej, A.J.: Hess, B.A., J. Chem. Phys. **105**, 1995 (1996)
54. Wolf, A., Reiher, M.: J. Chem. Phys. **124**, 064102 (2006)
55. Wolf, A., Reiher, M.: J. Chem. Phys. **124**, 064103 (2006)
56. Karwowski, J.: Quantum chemical models. In: S. Wilson, G.H.F. Diercksen (eds.) Problem Solving in Computational Molecular Science: Molecules in Different Environments, Kluwer, NATO ASI Series, Dordrecht, pp. 37–84 (1997)
57. Malmqvist, P.-Å., Roos, B.O., Schimmelpfenning, B.: Chem. Phys. Letters **357**, 230 (2002)

CHAPTER 5

RELATIVISTIC DENSITY FUNCTIONAL THEORY

CHRISTOPH VAN WÜLLEN

Fachbereich Chemie and Forschungszentrum OPTIMAS, Technische Universität Kaiserslautern, Erwin-Schrödinger-Straße, 67663 Kaiserslautern, Germany
e-mail: vanwullen@chemie.uni-kl.de

Abstract: This review starts with the basics of nonrelativistic density functional theory, followed by the foundation of the relativistic variant. How to formulate a relativistic spin density functional theory is shown through the comparison of the non-collinear and collinear approximations. It is shown where relativistic corrections to the exchange-correlation functionals are important and that they have a sizeable influence on total energies but are not so important for valence properties. After discussing some four-component Dirac–Kohn–Sham implementations, quasirelativistic methods are reviewed with emphasis on the zeroth-order regular approximation and the Douglas–Kroll–Hess method. This review contains 163 references.

Keywords: Relativistic, Density functional theory, Electron gas, Collinear, Four-current, Dirac equation

5.1. NONRELATIVISTIC DENSITY FUNCTIONAL THEORY BASICS

Computational schemes based on density functional theory (DFT) range among the most important methods for the quantum mechanical modeling of atoms, molecules, and solids. While DFT has been a standard computational method in solid state physics for nearly four decades, it became popular for molecular systems in the second half of the 1980s, after second-generation gradient-corrected exchange-correlation functionals had been developed based on the so-called generalized gradient approximation (GGA). For extended systems (large molecules or solids with large unit cells), the accuracy and the efficiency of DFT makes it a highly competitive method. The cornerstones of DFT are the Hohenberg–Kohn theorem [1] and the Kohn–Sham kinetic energy functional [2]. The Hohenberg–Kohn theorem establishes that for electrons moving in an external potential $v(\mathbf{r})$, different potentials give rise to different ground-state electron densities, such that the external potential is a functional of the electron density. Since the knowledge of the ground state density then also uniquely determines (via the external potential) the Hamiltonian of the system, the ground state energy and other properties (including those of excited states!) are a functional of the electron density.

M. Barysz and Y. Ishikawa (eds.), *Relativistic Methods for Chemists*,
Challenges and Advances in Computational Chemistry and Physics 10,
DOI 10.1007/978-1-4020-9975-5_5,

A variational principle holds for the energy functional, such that the exact ground state density is obtained by minimizing the energy functional. This is of little practical use since the evaluation of this energy functional is as difficult as solving the Schrödinger equation. DFT becomes a computational method through the introduction of *approximate* energy functionals for which one is able to find the density which minimizes this functional. This contrasts with wave function based methods where one strives for approximate solutions to the exact Hamiltonian.

For a given electron density $\rho(\mathbf{r})$, one can easily separate off the interaction with the external potential and the electrostatic Coulomb energy of the electronic charge distribution and thus rewrites the energy functional $E[\rho]$ as

$$E[\rho] = \int v(\mathbf{r})\rho(\mathbf{r})d\mathbf{r} + \frac{1}{2}\int\int \frac{\rho(\mathbf{r}_1)\rho(\mathbf{r}_2)}{|\mathbf{r}_1 - \mathbf{r}_2|} d\mathbf{r}_1 d\mathbf{r}_2 + G[\rho] \qquad (5\text{-}1)$$

The second term is usually called the Hartree energy, and we will follow this nomenclature although it is not quite correct – the self-interaction present here is excluded in Hartree's method. The functional $G[\rho]$ is *universal* as it no longer depends on the external potential, and for the exact ground state density its value contains, as the largest part, the kinetic energy of the system. Any attempts to express the kinetic energy of an atomic or molecular system as an explicit functional of the density have been unsuccessful until today, and the breakthrough came with the suggestion by Kohn and Sham [2] of an implicit functional for the kinetic energy which is the kinetic energy T_S of a fictious system of noninteracting electrons having the same density:

$$E[\rho] = T_S[\rho] + \int v(\mathbf{r})\rho(\mathbf{r})d\mathbf{r} + \frac{1}{2}\int\int \frac{\rho(\mathbf{r}_1)\rho(\mathbf{r}_2)}{|\mathbf{r}_1 - \mathbf{r}_2|} d\mathbf{r}_1 d\mathbf{r}_2 + E_{xc}[\rho] \qquad (5\text{-}2)$$

The exchange-correlation functional E_{xc} thus defined is now what one has to approximate as accurately as possible while keeping a form that makes the determination of the minimizing density computationally tractable. Note that E_{xc} not only contains the difference between the (true) electron interaction energy and the electrostatic Coulomb energy, but also the difference between the true kinetic energy and the kinetic energy of the noninteracting reference system. The Kohn–Sham procedure was a dramatic step forward: even when neglecting E_{xc} altogether, this method applied to atoms yields a density which decays exponentially and shows the atomic shell structure, important properties which the Thomas–Fermi model and all its elaborations fail to reproduce. To evaluate T_S, a set of single-particle Schrödinger equations have to be solved self-consistently, yielding the Kohn–Sham orbitals, such that the Kohn–Sham and Hartree–Fock methods result in very similar computational schemes. Note that while T_S is only quite indirectly (or: *implicitly*) a functional of the electron density, it can of course easily and explicitly be written down as a functional of the orbitals.

Because the complete neglect of E_{xc} already gives answers that are physically reasonable, one can hope to get useful results from approximate exchange-correlation functionals with quite simple mathematical forms. The simplest one is the *local density approximation* (LDA)

$$E_{xc}[\rho] = \int \rho(\mathbf{r})\epsilon_{xc}(\rho(\mathbf{r}))d\mathbf{r} \tag{5-3}$$

where $\epsilon_{xc}(\rho)$ is the exchange-correlation energy per electron of a homogeneous electron gas with constant density ρ. Let us stress that no matter how difficult accurate calculations for a homogeneous electron gas might be, these have to be done once and for ever for a set of densities such that a reliable fit of the resulting one-parameter function $\epsilon_{xc}(\rho)$ can be constructed. From then on, the evaluation of E_{xc} for any system merely involves a three-dimensional (numerical) integration. The resulting method is exact (by construction) for a homogeneous electron gas, but also gave surprisingly good results for atomic and molecular systems despite their electron density being strongly inhomogeneous. LDA quickly became a standard method in solid state physics but was also quite successful for atomic and molecular systems [3]. LDA is uniquely defined. Based on quantum calculations of the homogeneous electron gas [4], there are two different but essentially equivalent parametrizations of the function $\epsilon_{xc}(\rho)$ [5, 6].

In an attempt to improve upon LDA, in the next step one requires that E_{xc} is exact for an inhomogeneous electron gas with a (very) slowly varying density. This approximation is called *gradient expansion approximation* (GEA). The lowest order gradient expansion is problematic for the correlation part [7] and brings no improvement over LDA. The origin of this failure lies in the fact that LDA, being exact for at least one system (the homogeneous electron gas) fulfills all the (surprisingly many known [8]) scaling properties and sum rules exact functionals do obey, and which are violated by GEA. So one gave up the requirement that a gradient-corrected functional should be asymptotically correct for a system with very slowly varying density, but rather kept the functional form of the lowest-order gradient expansion

$$E_{xc}[\rho] = \int F_{xc}(\rho(\mathbf{r}), |\nabla\rho(\mathbf{r})|)d\mathbf{r} \tag{5-4}$$

which involves a two-parameter function F_{xc} that depends on the density as well as its gradient. Rotational invariance implies that only the length of the gradient should enter the working equation. A good reason for keeping such a functional form is, of course, that it generates no extra computational effort compared to LDA. Constructions of such functions F_{xc} have been described starting from purely first-principles considerations, but there are also quite successful semi-empirical approaches [9]. This so called *generalized gradient approximation* (GGA) was pioneered in Ref. [10] and from then on, a large number of different GGAs have been proposed. In

this chapter, we will not be concerned with a discussion of various GGAs. While the introduction of GGAs was certainly an important step and increased the accuracy such that DFT was also accepted as a standard tool in quantum chemistry, it is disappointing that there are so many GGAs around without a clear answer which one is the best. More recently, extensions have been introduced which use part of the Hartree–Fock exchange energy [11, 12] or add the kinetic energy density as an additional variable [13–15]. In both cases, the exchange-correlation energy can no longer be written as an explicit functional of the density but rather of the orbitals. These are however implicitly a functional of the density through the Kohn–Sham procedure. There are also attempts to construct orbital-dependent correlation functionals [16], but these have not yet had much influence on the mainstream of DFT applications.

A magnetic field couples to the charge current and the spin of the electrons, and therefore the Hohenberg–Kohn theorems are no longer valid if there is an external magnetic field. The density as the basic variable is not enough, one has to add the current density and the spin density. A current-density functional theory has been formulated [17, 18] targeted at systems in strong magnetic fields, but usually only the coupling of the magnetic field to the electron spin is taken into account. This yields spin density functional theory, in which the spin-up and spin-down densities are treated as two independent variables. The local approximation analogous to Eq. (5-3) is called the *local spin density approximation* (LSDA). Since the exchange energy of a spin-polarized electron gas of a given density is larger (in absolute value) than of a spin-unpolarized electron gas of the same density, it is easily seen that LSDA will give a different (usually: lower) energy for a molecular system with unpaired electrons (i.e., uncompensated spins) than LDA in the limit of a vanishing magnetic field. The Hohenberg–Kohn theorem states that the electron density is "sufficient" in the absence of magnetic fields, but if there it are uncompensated spins, then approximate functionals work much better if they "look" not only at the density but also at the spin density (difference between spin-up and spin-down density) [19]. The reason is, that a working functional has to extract information on the two-particle density from $\rho(\mathbf{r})$. While for example an open-shell singlet and a triplet from the same electron configuration have quite similar densities $\rho(\mathbf{r})$, their two-particle densities are different because the Pauli exclusion principle (antisymmetry of the wave function) reduces the probability of finding two same-spin electrons close to each other beyond of what results from their Coulombic repulsion. While LSDA can easily "detect" such a situation (singlet and triplet have different spin densities), LDA fails to do so. The same holds if one goes beyond the local (spin) density approximation: open shell systems require GGAs that depend on the spin-up and spin-down densities as well as their gradients.

5.2. RELATIVISTIC EXTENSION OF DFT

For systems containing heavy elements (elements with nuclear charge $Z > 36$), the Schrödinger equation (even if it could be solved exactly) does not give the "right" answer (that is, it differs from results obtained experimentally) because its

classical limit is nonrelativistic mechanics. Therefore, the Schrödinger equation is not compatible with Einstein's special relativity, and from classical mechanics we know that this gives rise to noticeable discrepancies if velocities v are no longer small compared to the speed of light (c), the leading (relative) error being of the order $\frac{v^2}{c^2}$. In a quantum mechanical treatment of an atom, the leading error of a nonrelativistic treatment is $(Z\alpha)^2$, α begin the dimensionless fine structure constant ($\alpha \approx \frac{1}{137}$). Nonrelativistic calculations on heavy-element compounds thus produce errors that cannot be accepted, and an relativistic extension of DFT is required. Such an extension is not straightforward as there is no relativistic Hamiltonian for many-electron systems, one rather has to use a quantum field theory for electrons, positrons and photons (which mediate the interaction between charged particles). The basics of relativistic density functional theory were laid out by Rajagopal and Callaway [20], Rajagopal [21], MacDonald and Vosko [22], and Ramana and Rajagopal [23]. Leaving aside the issue of renormalization which is necessary in quantum field theories to get finite expressions for charge, energy, etc., the main message here is that there *is* a relativistic generalization of the Hohenberg–Kohn theorem, and that the basic variable in the relativistic case is the four-current. Moreover, in the so-called *electrostatic limit* where the external potential is time-independent and purely electrostatic, the time component of the four-current (essentially: the charge density) alone is sufficient as the basic variable. Within the Born–Oppenheimer approximation, the nuclei are at rest and are the sources of the external potential, such that we are in the electrostatic limit (unless there is an external magnetic field). We note in passing that the Born–Oppenheimer approximation also singles out a specific Lorentz frame (that where the nuclei are at rest), such that the question of relativistic invariance does not play a central role. However, as in the nonrelativistic case, also in the electrostatic limit the three spatial components of the four-current are non-zero if there are unpaired electrons, such as in open-shell atoms or molecules. We should thus expect that for systems in which the spatial parts of the four-current do not vanish, an approximate energy functional of the four-current is more accurate than a functional of the charge density alone. In this chapter we will not use four-vectors and covariant notation, and use ρ and $\mathbf{j} = (j_x, j_y, j_z)$ for the charge density and the spatial part of the four-current. Note that $\mathbf{j}$ still contains contributions both from displacement currents and spin. The Kohn–Sham procedure can also be generalized to the relativistic case, and thus we have in analogy to Eq. (5-2)

$$\begin{aligned} E[\rho,\mathbf{j}] = T_S[\rho,\mathbf{j}] &+ \int v(\mathbf{r})\rho(\mathbf{r})d\mathbf{r} \\ &+ \frac{1}{2}\int\int \frac{\rho(\mathbf{r}_1)\rho(\mathbf{r}_2)}{|\mathbf{r}_1-\mathbf{r}_2|}d\mathbf{r}_1 d\mathbf{r}_2 - \frac{1}{2c^2}\int\int \frac{\mathbf{j}(\mathbf{r}_1)\cdot\mathbf{j}(\mathbf{r}_2)}{|\mathbf{r}_1-\mathbf{r}_2|}d\mathbf{r}_1 d\mathbf{r}_2 \\ &+ E_{xc}[\rho,\mathbf{j}] \end{aligned} \tag{5-5}$$

Some remarks are in order here. T_S is the kinetic energy of a reference system of noninteracting Dirac particles, therefore the Kohn–Sham procedure leads to the self-consistent solution of a one-particle Dirac equation, and the Kohn–Sham orbitals are (four-component) Dirac spinors ψ_i

$$\begin{pmatrix} mc^2 + v_{\text{eff}} & c\sigma \cdot (\mathbf{p} + \mathbf{A}_{\text{eff}}) \\ c\sigma \cdot (\mathbf{p} + \mathbf{A}_{\text{eff}}) & -mc^2 + v_{\text{eff}} \end{pmatrix} \begin{pmatrix} \phi_i \\ \chi_i \end{pmatrix} = \epsilon_i \begin{pmatrix} \phi_i \\ \chi_i \end{pmatrix}, \quad \psi_i = \begin{pmatrix} \phi_i \\ \chi_i \end{pmatrix} \tag{5-6}$$

Here, m is the mass of the electron, c the speed of light, $\mathbf{p} = -\mathrm{i}\nabla$ the operator of the linear momentum, $\sigma = (\sigma_x, \sigma_y, \sigma_z)$ the vector of the Pauli spin matrices. Many texts substitute $\sigma = g_e \mathbf{s}$ in the final equations, with s the electron spin and the electron g value ($g_e = 2$ in Dirac theory). Atomic (Hartree) units are used throughout, in which $\hbar$, m, the elementary charge e and $4\pi\epsilon_0$ assume unit value although we keep the electron mass m in some of the equations for convenience. There is still an ambiguity for the unit of the magnetic field strength, and we adopt the convention followed by the SI, where there is no factor $\frac{1}{c}$ in the Lorentz force. In these units, the value of the speed of light is $c \approx 137$ and the value of the Bohr magneton is $\mu_B = \frac{1}{2}$, while that of the vacuum permeability is $\mu_0 = \frac{4\pi}{c^2}$. The effective Kohn–Sham scalar and vector potentials v_{eff}, $\mathbf{A}_{\text{eff}}$ are

$$\begin{aligned} v_{\text{eff}}(\mathbf{r}) &= v(\mathbf{r}) + \int \frac{\rho(\mathbf{s})}{|\mathbf{r} - \mathbf{s}|} d\mathbf{s} + \frac{\delta E_{xc}}{\delta \rho}(\mathbf{r}) \\ \mathbf{A}_{\text{eff}}(\mathbf{r}) &= -\frac{1}{c^2} \int \frac{\mathbf{j}(\mathbf{s})}{|\mathbf{r} - \mathbf{s}|} d\mathbf{s} + \frac{\delta E_{xc}}{\delta \mathbf{j}}(\mathbf{r}) \end{aligned} \tag{5-7}$$

The three terms in v_{eff} are the external potential (usually, the electrostatic potential generated by the nuclear framework, multiplied by the electron charge), the Hartree potential v_H (second term) and the scalar exchange-correlation potential v_{xc} which is a functional derivative of the exchange-correlation energy. In the absence of external magnetic fields, $\mathbf{A}_{\text{eff}}$ only contains two terms, arising from the current–current part of the Hartree energy and a vector exchange-correlation part which is again a functional derivative of E_{xc}. The first question is what are the *occupied* Kohn–Sham orbitals ψ_i that are needed to evaluate the kinetic energy, the density and the current

$$\begin{aligned} T_S &= \sum_i^{\text{occ}} \left\langle \begin{pmatrix} \phi_i \\ \chi_i \end{pmatrix} \middle| \begin{pmatrix} mc^2 & c\sigma \cdot \mathbf{p} \\ c\sigma \cdot \mathbf{p} & -mc^2 \end{pmatrix} \begin{pmatrix} \phi_i \\ \chi_i \end{pmatrix} \right\rangle \\ \rho(\mathbf{r}) &= \sum_i^{\text{occ}} \psi_i^\dagger(\mathbf{r}) \psi_i(\mathbf{r}) = \sum_i^{\text{occ}} \phi_i^\dagger(\mathbf{r}) \phi_i(\mathbf{r}) + \chi_i^\dagger(\mathbf{r}) \chi_i(\mathbf{r}) \\ \mathbf{j}(\mathbf{r}) &= \sum_i^{\text{occ}} \psi_i^\dagger(\mathbf{r}) \begin{pmatrix} 0 & c\cdot\sigma \\ c\cdot\sigma & 0 \end{pmatrix} \psi_i(\mathbf{r}) = c \sum_i^{\text{occ}} \phi_i^\dagger(\mathbf{r}) \sigma \chi_i(\mathbf{r}) + \chi_i^\dagger(\mathbf{r}) \sigma \phi_i(\mathbf{r}) \end{aligned} \tag{5-8}$$

since the Dirac operator has both positive and negative energy eigenfunctions. Somewhat in the line of Dirac's original interpretation that the negative-energy levels are completely filled (*"Dirac sea"*) the negative-energy states are reinterpreted in a field-theoretical approach which leads to the definition of a physical vacuum. While we cannot go into the details here, it should be noted that there are non-vanishing vacuum contributions to the expectation values of the kinetic energy and the four-current which are neglected in the above expression, where the summation over the occupied orbitals goes over positive-energy spinors only. Such vacuum effects are present even in a one-electron system and are the origin of the Lamb shift, that is the removal of the degeneracy of the $2s$ and $2p_{\frac{1}{2}}$ energy levels in hydrogenlike ions. In many-electron systems, vacuum effects also arise from the electron-electron interaction. To get a computationally feasible scheme for many-electron systems, we will ignore vacuum effects although they could be incorporated by perturbational methods after self-consistency has been achieved. Such calculations or even estimations for many-electron systems are rare (e.g., Refs. [24–27]). Operationally, and from the physics contained, the Dirac–Kohn–Sham (DKS) scheme Eqs. (5-5–5-8) relates to the Dirac–Fock–Breit method in the same manner nonrelativistic Kohn–Sham relates to Hartree–Fock.

If there were additionally an external magnetic field, it would not make much difference: the vector potential $\mathbf{A}(\mathbf{r})$ describing the external magnetic field must be added to $\mathbf{A}_{\text{eff}}$. In other words, the absence of an external magnetic field does not simplify the formulation. If we restrict ourselves to exchange-correlation functionals that only depend on the charge density and neglect the current–current term of the Hartree energy (second term in the second line of Eq. (5-5)) then $\mathbf{A}_{\text{eff}}$ will disappear from the DKS equation. In (nearly) neutral systems, the current–current contribution to the Hartee term is usually small (unpaired electrons only in the valence shell) so this term is neglected in most cases. For stationary closed shell systems, it vanishes exactly since $\mathbf{j} = 0$ everywhere. To a good approximation, it can be evaluated after self-consistency has been achieved. Although this contribution may be negligible for a single molecule it is not unimportant in physics: it is the origin of the magnetocrystalline shape anisotropy (through the spin-dipolar interaction contained therein) and the magnetic force between two (macroscopic) wires where an electric current is passed through. The prefactor $c^{-2} = \frac{\mu_0}{4\pi}$ comes from the Biot–Savart law and shows that the current–current interaction vanishes in the nonrelativistic limit:[1] it arises

[1] In a nonrelativistic (Galilei-invariant) world, the Lorentz force (exerted by a magnetic field on a moving charge) and the Biot–Savart law (the generation of a magnetic field through currents of moving charges) cannot coexist. In the nonrelativistic limit, we have to choose which one survives, the other being a "relativistic effect". We follow the SI such that the Lorentz force is independent of the speed of light, and absorb the factor $4\pi\epsilon_0$ in the definition of the charge, but then $\mu_0 \sim c^{-2}$, the prefactor in the Biot–Savart law, vanishes in the nonrelativistic limit. Whatever choice is made, the current–current interaction, which involves *both* laws, is of order $\mathcal{O}(c^{-2})$. In the c.g.s. unit system, frequently used in theoretical physics, this apparent asymmetry is removed and a factor c^{-1} is found both in the Lorentz force and in the Biot–Savart law. This causes a lot of confusion when comparing equations from different texts.

from the transverse part of the electron interaction which we (loosely speaking) identify with the Breit interaction in wave function based methods, which considers magnetic interactions and retardation. Actually, the Hartree term only involves the magnetic (Gaunt) part. Note that Breit contributions to the exchange-correlation energy also arise for closed shell systems. Therefore the Breit contributions to E_{xc} are much more substantial than to the Hartree energy. Given the success of the Dirac–Coulomb operator in wave function based methods, it is legitimate to use a relativistic density functional scheme that consistently neglects the Breit interaction and will be related to the Dirac–Fock–Coulomb method. In this case, it is even justified to use exchange-correlation functionals known from nonrelativistic theory since the relativistic corrections to the exchange-correlation functional are dominated by the transverse terms.

5.3. RELATIVISTIC SPIN DENSITY FUNCTIONAL THEORY: COLLINEAR AND NONCOLLINEAR APPROXIMATION

We postpone the discussion of relativistic corrections to the exchange correlation functional until the next section. From nonrelativistic theory we know that the accuracy of a functional depending on the density only will be quite limited if the system under consideration is not closed shell. On the other hand, current-dependent functionals have not met great success even in nonrelativistic theories [28–30]. Although in principle one could obtain current-dependent functionals from spin-dependent functionals [31] since a relativistic framework establishes a connection between them, much effort has been made to take over spin density functional theory in a straightforward way into the relativistic regime. To this end, one uses a Gordon decomposition of the current density [20, 32, 33] and obtains in the absence of an external magnetic field

$$\mathbf{j}(\mathbf{r}) = \mathbf{j}_{\mathrm{orb}}(\mathbf{r}) + \frac{1}{2m}\nabla \times \mathbf{m}(\mathbf{r}) \tag{5-9}$$

where $\mathbf{j}_{\mathrm{orb}}$ is an orbital current which we will not discuss further, and $\mathbf{m}(\mathbf{r})$ the spin (magnetization) density[2]

$$\mathbf{m}(\mathbf{r}) = \sum_i^{\mathrm{occ}} \psi_i^\dagger(\mathbf{r}) \begin{pmatrix} \sigma & 0 \\ 0 & -\sigma \end{pmatrix} \psi_i(\mathbf{r}) = \sum_i^{\mathrm{occ}} \phi_i^\dagger(\mathbf{r})\sigma\phi_i(\mathbf{r}) - \chi_i^\dagger(\mathbf{r})\sigma\chi_i(\mathbf{r}) \tag{5-10}$$

[2] Spin and magnetization density is not the same. The magnetization density contains an additional prefactor, the Bohr magneton. However, this distinction is not always made in the literature. The two minus signs in Eq. (5-10) imply that not even a one-electron system can be fully spin polarized except in the nonrelativistic limit. While the minus signs follow from the Gordon decomposition, some authors define the spin densities with plus signs here. Numerically, it seems to make little difference.

Neglecting orbital currents, one gets for the interaction with a magnetic field $\mathbf{B} = \nabla \times \mathbf{A}$

$$-\int \mathbf{j} \cdot \mathbf{A}\, d\mathbf{r} \approx -\frac{1}{2m} \int (\nabla \times \mathbf{m}) \cdot \mathbf{A}\, d\mathbf{r} = -\mu_B \int \mathbf{m} \cdot \mathbf{B}\, d\mathbf{r} \tag{5-11}$$

(the minus signs come from the negative charge of the electron). After neglecting the transverse Hartree energy one rewrites the energy functional for vanishing external magnetic fields in terms of ρ and $\mathbf{m}$

$$E[\rho, \mathbf{m}] = T_S[\rho, \mathbf{m}] + \int v(\mathbf{r})\rho(\mathbf{r}) d\mathbf{r} + \frac{1}{2} \int \int \frac{\rho(\mathbf{r}_1)\rho(\mathbf{r}_2)}{|\mathbf{r}_1 - \mathbf{r}_2|} d\mathbf{r}_1 d\mathbf{r}_2 + E_{xc}[\rho, \mathbf{m}] \tag{5-12}$$

and re-derives the Kohn–Sham single-particle equations within this approximation as

$$\begin{pmatrix} mc^2 + v_{\text{eff}} - \mu_B\, \sigma \cdot \mathbf{B}_{xc} & c\sigma \cdot \mathbf{p} \\ c\sigma \cdot \mathbf{p} & -mc^2 + v_{\text{eff}} + \mu_B\, \sigma \cdot \mathbf{B}_{xc} \end{pmatrix} \begin{pmatrix} \phi_i \\ \chi_i \end{pmatrix} = \epsilon_i \begin{pmatrix} \phi_i \\ \chi_i \end{pmatrix} \tag{5-13}$$

with an exchange-correlation magnetic field as a functional derivative of E_{xc}

$$\mathbf{B}_{xc} = -\mu_B^{-1} \frac{\delta E_{xc}}{\delta \mathbf{m}} \tag{5-14}$$

A local approximation to $E_{xc}[\rho, \mathbf{m}]$ would require a four-parameter function ϵ_{xc}. In practice, only two parameters are used like in the nonrelativistic case, where one has the density and the spin density. The reason is twofold. First, this reduction allows that one uses the functionals known from nonrelativistic DFT in relativistic calculations. Second, all or a large part of the functional is derived from the homogeneous electron gas where there is no directional dependence. There are two different variants to perform this reduction, called the *collinear* and the *noncollinear* approximation. Some consequences of these approximations have been analyzed by the present author [34]. In the *collinear approximation*, one uses, at each point in space, the projection of $\mathbf{m}$ on to a fixed axis. Conventionally, one uses the z axis (although one could use any direction) and has

$$E_{xc}[\rho, \mathbf{m}] = \int \rho(\mathbf{r}) \epsilon_{xc}\big(\rho(\mathbf{r}), m_z(\mathbf{r})\big) d\mathbf{r} \tag{5-15}$$

This generates an exchange-correlation magnetic field $\mathbf{B}_{xc}$ which is parallel to the z axis in each point (i.e., collinear):

$$\mathbf{B}_{xc} = -\mu_B^{-1} \frac{\delta E_{xc}}{\delta \mathbf{m}} = -\mu_B^{-1} \left(0, 0, \frac{\partial E_{xc}}{\partial m_z}\right) = -\mu_B^{-1} \left(0, 0, \rho \frac{\partial \epsilon_{xc}}{\partial m_z}\right) \quad (5\text{-}16)$$

The spinor potential, that is, the terms $\sigma \cdot \mathbf{B}_{xc}$ in the Kohn–Sham equation, exert a driving force for the (open shell) orbitals to align their spins along the collinear axis, because any component of $\mathbf{m}$ perpendicular to it remains unnoticed by the functional. Since a nonvanishing spin density usually increases the exchange-correlation energy density, aligning the spins is favourable (energy-lowering). In the *non-collinear* approximation, one uses the length of the magnetization density vector $\mathbf{m}(\mathbf{r})$ as variable:

$$E_{xc}[\rho, \mathbf{m}] = \int \rho(\mathbf{r}) \epsilon_{xc}\big(\rho(\mathbf{r}), |\mathbf{m}(\mathbf{r})|\big) d\mathbf{r} \quad (5\text{-}17)$$

which generates a field $\mathbf{B}_{xc}(\mathbf{r})$ that is no longer aligned but parallel to $\mathbf{m}$ at each point in space:

$$\mathbf{B}_{xc} = -\mu_B^{-1} \frac{\delta E_{xc}}{\delta \mathbf{m}} = -\mu_B^{-1} \rho \frac{\partial \epsilon_{xc}}{\partial |\mathbf{m}|} \frac{\mathbf{m}}{|\mathbf{m}|} \quad (5\text{-}18)$$

Even in the recent literature, it is stated that the noncollinear approximation is rather involved (for a recent example, see [35]), but in my opinion this does not hold: the spinor potential ($\sigma \cdot \mathbf{B}_{xc}$ terms) in Eq. (5-13) are diagonal 2×2 matrices in the collinear approximation but full 2×2 matrices in the noncollinear case. This makes a factor of two (both in storage and in floating point operations) in the exchange-correlation part of the computation. This can be considered immaterial since the other parts of the computation (matrix elements of the Hartree potential, diagonalizations) usually require the largest part of the CPU time. Note that in the above equations, any value for the electron spin magnetic moment ($-\mu_B$) will give the same final result (no external magnetic fields), thus this factor is often omitted.

If there is a single unpaired s electron outside a closed-shell atomic core, the consequence of the collinear approximation is the alignment of the magnetization along the z axis and that's it. The situation is different for a singly occupied $p_{\frac{1}{2}}$ orbital: if no mixing with the $p_{\frac{3}{2}}$ orbitals is possible (large spin–orbit splitting), then $\mathbf{m}$ will strongly deviate from the z axis in large regions of space, and therefore the collinear approximation will find a smaller amount (in absolute value) of exchange-correlation energy than the noncollinear treatment. The energy difference is $\sim$0.1 eV for heavy p-block elements like thallium and lead [32, 34] and translates into the same difference for computed ionization energies because there is no difference between both approximations for closed-shell ionic cores. Another consequence of the collinear approximation is that it breaks rotational invariance, and the total energy of simple open-shell molecules like I_2^+ or PbF vary by $\sim$0.1 eV depending on the orientation of the molecule [34]. This makes calculations

of molecular interactions meaningless with the collinear approximation, at least if one is interested in the orientational dependence of this interaction. The reason for the dependence of the total energy on the orientation of the molecule is that the Dirac energy (in DFT: T_S) is only invariant to simultaneous rotations in real and spin space, and that a rotation in spin space changes the exchange-correlation energy in the collinear approximation. In the noncollinear approximation, all energy contributions remain unchanged by a Dirac rotation.

On the other hand, using the collinear approach is beneficial if one is interested in magnetic anisotropy energies [36–38], that is, the variation of the total energy when changing the direction of the magnetization. This quantity, related to zero field splitting, is important for the ability of a system to "store" information which has been "written" by aligning the magnetization by an external magnetic field to a preferred direction. If the "writing" is over, and the external magnetic field switched off, spin–orbit coupling imposes a barrier for the magnetization to change its orientation. In a recent application [37] the collinear approach was used to impose (partial) spin alignment on the unpaired electrons and to investigate the dependence of the total energy with respect to the direction of the collinear axis.

There is an alternative approach to define a relativistic spin density, namely the moment polarization approach [39]. Unfortunately the present author has not understood how it can uniquely be defined for multiple open shells and in the absence of any symmetry in the molecule, so no details will be given here. We can only mention here that this approach allows for a restricted version, in which the Dirac spinors form Kramers pairs even in open-shell systems. If properly exploited, this constraint leads to computational savings.

Non-collinear computational schemes have also been developed in the context of nonrelativistic density functional theory [40–43]: while noncollinear magnetization is usually a consequence of spin–orbit coupling, it can arise in nonrelativistic theory as a consequence of spin frustration, leading to non-collinear magnetic structures.

5.4. RELATIVISTIC EXCHANGE-CORRELATION FUNCTIONALS

We start this chapter with a qualitative discussion. In classical mechanics, relativistic corrections are of the order β^2 with $\beta = \frac{v}{c}$. In a nonrelativistic homogeneous electron gas, the highest momentum encountered (the Fermi momentum k_F) is

$$k_F = (3\pi^2\rho)^{\frac{1}{3}} \tag{5-19}$$

and equals the highest "velocity" in atomic units, such that the parameter which measures the importance of relativistic effects is (in atomic units)

$$\beta = \frac{1}{mc}(3\pi^2\rho)^{\frac{1}{3}} \approx 0.0226\,\rho^{\frac{1}{3}} \tag{5-20}$$

Table 5-1 Critical 'core' radius r_{crit} (in Bohr) and number of electrons N_e contained in the critical region for various atoms (see text), from four-component Dirac–Kohn–Sham calculations

Atom	Z	r_{crit}	N_e
O	8	0.07	0.2
S	16	0.11	1.5
Pd	46	0.20	11.3
Hg	80	0.25	29.1
(114)	114	0.30	55.0

In the homogeneous electron gas, relativistic effects start to become non-negligible if the density is $\rho \approx 100\, a_0^{-3}$ (that is, $\beta \approx 0.1$) or higher. In the atomic cores, the density exceeds this critical value. To which extent this affects the exchange-correlation energy depends on the size of the critical region and how much charge is contained therein. Table 5-1 displays for various atoms the radius r_{crit} below which the density exceeds $100\, a_0^{-3}$, and the integrated charge density N_{crit}

$$\rho(r) > 100\, a_0^{-3} \text{ for } r < r_{crit}, \quad N_{crit} = \int_0^{r_{crit}} 4\pi r^2 \rho(r) dr \tag{5-21}$$

The values have been obtained from four-component atomic Dirac–Kohn–Sham calculations. While the size of the core region does not vary very much, the number of electrons contained therein is quite large for heavy elements. This means, that corrections to the exchange-correlation functional will have substantial impact on the *total energy* of systems containing heavy elements. Of course, valence properties, that is, energy differences between states that have the same electronic structure in the atomic cores, are much less affected by the Breit interaction. At high densities, where relativistic effects are important, exchange dominates correlation, therefore the most important correction (in terms of absolute energies) requires the calculation of the exchange energy of a relativistic homogeneous electron gas. This calculation has been reported several times (see Ref. [22] and the references cited there). Here we give a plot of the exchange energy density $\epsilon_x(\rho)$ for a nonrelativistic (dottet line) and relativistic homogeneous electron gas (Figure 5-1): High-density regions contribute less exchange energy (in absolute value) in a relativistic treatment. Note that the relativistic $-\epsilon_x(\rho)$ curve has a maximum at $\rho \approx 91{,}776\, a_0^{-3}$ and becomes negative at $\rho = 1.4 \times 10^6\, a_0^{-3}$. One further sees that neglecting the Breit interaction, one only gets a small correction (dashed line). Ellis [44] has calculated this quantity (i.e., the exchange energy of an electron gas at Dirac–Fock–Coulomb level) and erroneously concluded that relativistic corrections are unimportant – because he did not realize that the dominant contribution comes indeed from the Breit interaction. The correlation energy density of a relativistic gas is only known from the random phase approximation (RPA) that is accurate for high densities, but since relativistic corrections are not so important at low densities, this is not severe: a nonrelativistic

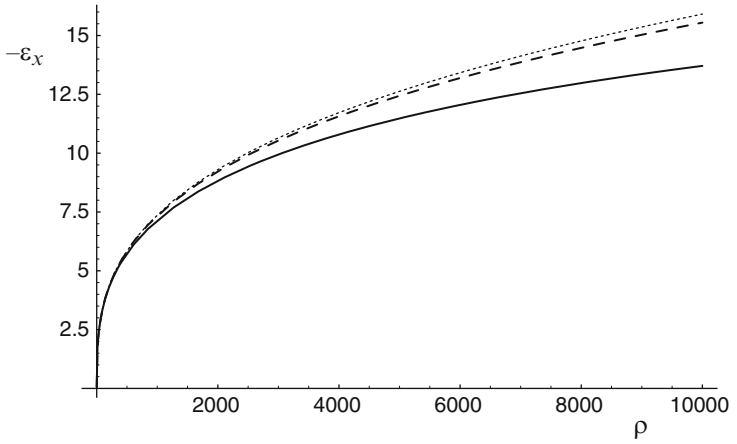

Figure 5-1. Exchange energy density of a nonrelativistic (*dotted line*) and relativistic (*thick line*) homogeneous electron gas. The *dashed line* neglects the Breit interaction in the relativistic calculation. All quantities are given in atomic (Hartree) units

correlation functional, augmented by a relativistic correction from RPA (that vanishes for low densities) [45], is probably accurate enough. A plot of the relativistic correlation potential can be found in Ref. [46]. However, the correlation energy density is not uniquely defined and depends, for example, how the negative-energy states are treated [47]. Extensions to spin-polarized systems are also available, mostly for exchange [48–51]. The first results from relativistic LDA functionals where rather disappointing: for neutral closed-shell atoms, the Breit contributions to the total energy were overestimated by a factor of $1.5 \cdots 2.0$ (see the compilation of results in Ref. [45], but this has been found much earlier, already in Ref. [22]). It has been argued that this error is intrinsic to the local density approximation because retardation effects are naturally much more important in an (infinite) electron gas compared to an atom or small molecule.

Because gradient expansion did not result in useful functionals in the nonrelativistic case, this can also not be expected in the relativistic case. Relativistic GGA functionals have been proposed [52] based on a semiempirical approach: the gradient-dependent part of a nonrelativistic GGA for exchange is multiplied by a density-dependent relativistic correction factor, which is chosen such that exact relativistic corrections to atomic exchange energies can be reproduced. Because the functional form of the nonrelativistic functional is maintained, relativistic effects such as the spin-other-orbit interaction, which should be represented by the "true" relativistic functional, are not recovered. Because the number of closed-shell atoms is not much larger than the number of fitting parameters (8), it is not clear how successful relativistic GGAs really are. Perhaps this issue is not yet fully settled.

The above considerations relate to total energies, and these are not too important in "chemical" applications. Here it is of interest to which extent properties like bond dissociation energies, valence ionization potentials, equilibrium bond

lengths and vibrational frequencies are affected by relativistic corrections to E_{xc}. Some systematic comparisons are available [53–55]. From these studies it seems that relativistic corrections to the exchange-correlation functional are not too important: corrections to the exchange part may affect valence properties on the 1% level, while relativistic corrections to the correlation functional can be neglected. In some sense, this is the expected result, given the success of the Dirac–Coulomb operator in wavefunction based quantum chemical methods. Furthermore, note that quantum electrodynamical corrections (vacuum polarization, self energy, etc.), which are neglected anyway in the Dirac–Kohn–Sham scheme, affect valence properties by the same amount [24, 25]. For valence properties, relativistic effects are by no means small, but they are almost completely recovered if the relativistic kinematics of the electron is properly described, that is, if the calculation is based on the Dirac equation. The relativistic corrections to the electron interaction (Breit operator in wave function based methods, relativistic corrections to E_{xc} in DFT) are much less important. This is probably the reason why most "relativistic density functional calculations" performed today are oblivious of relativistic density functional theory in its proper sense. What is often termed "relativistic DFT" is a Dirac–Kohn–Sham computational scheme with a nonrelativistic (spin-dependent) exchange-correlation functional. The collinear or noncollinear approach (or the moment polarization approach, see above) are used to define the spin density.

5.5. DIRAC–KOHN–SHAM IMPLEMENTATIONS

It is probably not worth the effort to compile a comprehensive list of Dirac–Kohn–Sham programs that have been described in the literature, so the selection presented here is strongly affected by my personal view. Nevertheless the reader may find it useful to have the references to some Dirac–Kohn–Sham programs at hand, because by searching those articles which cite these references, one may quickly locate applications of these methods.

Probably the first *molecular* Kohn–Sham program was presented by Rosen and Ellis [56] (there were earlier atomic programs, see Refs. [57,58]). The Ellis program (see also Ref. [39]) used Slater's exchange functional ($X\alpha$), that was later relativistically corrected [44]. Because this relativistic correction was obtained from a Dirac–Fock–Coulomb treatment of the electron gas, the important Breit contributions were missing. The Ellis program has found widespread use: it was further improved in the group of Fricke and applied to the chemistry of superheavy elements [59], with a relatively new extension to spin-density functionals [60, 61]. In the last version, density fitting techniques are used to evaluate the matrix elements of the Hartree potential[60].

A group in China also started from Ellis' program but meanwhile the code ("BDF", for *Beijing Density Functional program*) seems to be largely rewritten [62–65]. To evaluate the matrix elements of the Hartree potential, a multicenter multipolar expansion of the density is used: first, the density is decomposed first into disjoint atomic contributions, from which a multipolar (partial wave) expansion is made. While the Hartree potential of each partial wave at each of the grid

points can easily be evaluated quite accurately using a one-dimensional numerical integration and possibly some sort of extrapolation, the multipolar expansion itself has to be truncated. This truncation is the key parameter controlling the numerical accuracy (see the discussion in Ref. [66]).

The computational procedure of Dirac–Kohn–Sham largely parallels that of Dirac–Hartree–Fock. One difference is, that the nonlocal exchange operator present in Hartree–Fock is absent in DFT (but only as long as one does not use hybrid functionals!). On the other hand, the matrix elements of the exchange-correlation potential involve a numerical integration that has to be added to a Dirac–Fock code to enable it to do Dirac–Kohn–Sham calculations. How to do this is well known from nonrelativistic methods. Therefore several Dirack–Fock programs have been extended to include DFT as an option. Such codes do not have optimal efficiency because there are faster ways to evaluate the matrix elements of the Hartree potential than via four-center two-electron integrals, as done in Dirac–Fock methods. There, one needs these integrals anyway for the nonlocal exchange part. Without Fock exchange, one can use e.g. density fitting techniques to evaluate the matrix elements of the Hartree potential, which are well known from nonrelativistic theory [67–71]. However, some of the most often exchange-correlation functions used today such as B3LYP [72–75] are hybrid functionals that *do* include nonlocal Fock exchange.

Saue [76] presented such a Dirac–Kohn–Sham code which emerged from a Dirac–Fock program, used later to calculate properties (in particular response properties) at a relativistic level [77–84]. Similarly, Nakajima [85–87] coded Dirac–Kohn–Sham derived from their Dirac–Fock program [88–90], and their program was optimized later on for DFT adopting the pseudospectral approach described by Friesner [91, 92] to Dirac–Kohn–Sham [93, 94]. This implementation also features a treatment for relativistic double group symmetry for high symmetries such as C_{6h} [89].

The implementation by Quiney and Belpassi [95, 96] originally was also based on a Dirac–Fock program, later density fitting techniques were added [97–100]. Few applications have been reported so far [101–104].

5.6. QUASIRELATIVISTIC METHODS

Methods are termed *quasirelativistic* if they are conceptually based on Dirac spinors, but do not (explicitly) deal neither with the negative-energy orbitals nor with the small components of the orbitals of positive energy: hence the alternate name *two-component methods*. There is an abundant literature on quasirelativistic methods, some kind of overview can be found in Ref. [105], see also the preceding chapter in this Book. This looks like a crude approximation only at first sight: quasirelativistic methods can reproduce, in principle exactly, the positive-energy branch of the Dirac spectrum. This contrasts with the so-called scalar-relativistic (or *one-component*) approaches, which go one step further but then the spin–orbit interaction is neglected, which is important in heavy-element compounds, and for example determines the chemistry of the superheavy p-block elements (element

113 through 118) [106]. We cannot discuss in detail effective core potential (ECP) methods, in which electrons of the inner atomic cores are not explicitly treated but replaced by the ECP. We only mention here that, although the vast majority of ECP applications is scalar-relativistic, spin-dependent ECPs that cover also spin–orbit effects have been successfully developed and tested [107], the coding of their matrix elements is not difficult [108] and these techniques can be used in density functional calculations [109, 110]. The discussions of quasirelativistic methods are mostly restricted to one-particle systems, but the techniques can easily be used for relativistic density functional calculations because the Dirac–Kohn–Sham equations only involve a local effective potential v_{eff} and have therefore the same structure as the Dirac equation one particle.

For about a decade, quasirelativistic density functional theory was dominated by the zeroth-order regular approximation (ZORA) [111, 112] and Douglas–Kroll–Hess (DKH) [113] methods. A two-component relativistic DKH density functional method was first proposed by Rösch [114, 115]: the initial implementation was scalar-relativistic [116] but later results from the full two-component version were also reported [117–119]. Noteworthy is the treatment of relativistic symmetry [120]. Rösch uses density fitting techniques to evaluate the matrix elements of the Hartree potential. A similar implementation has been described, with the application to solids in mind, by Boettger [121–123]. He suggested the so-called *screened nucleus spin–orbit* (SNSO) approximation, which compensates for the neglect of the Hartree-Potential in the Douglas–Kroll transformation. The underlying problem is the following: taking the Douglas–Kroll method literally, one must construct the Douglas–Kroll Hamiltonian $\hat{H}_{DK}$, which is an effective one-particle operator in a DFT computational scheme, in each iteration of the self-consistency loop because it depends, through the Hartree potential v_H and the exchange-correlation potential v_{xc} on the density:

$$v_{\text{eff}}(\mathbf{r}) = v(\mathbf{r}) + v_H(\mathbf{r}) + v_{xc}(\mathbf{r}), \quad \hat{H}_{DK} = \hat{H}_{DK}(v_{\text{eff}}) \tag{5-22}$$

Ignoring for a moment the problem that the density (and therefore, the effective potential) cannot easily be calculated from the two-component orbitals, this means that $\hat{H}_{DK}$ has to be re-constructed in each iteration. Arguing that the nuclear attraction potential dominates the effective potential in the vicinity of the nuclei, where relativistic effects are important, one approximates

$$\hat{H}_{DK}(v_{\text{eff}}) \approx \hat{H}_{DK}(v) + v_H + v_{xc} \tag{5-23}$$

that is, one performs the Douglas–Kroll transformation *using the nuclear potential only* and adds the Hartree and exchange-correlation potentials later. By virtue of this approximation, the Douglas–Kroll transformation need only be done once and not in each cycle of the iteration. While this approximation was more or less successful in scalar-relativistic applications, two-component results showed that there is a problem [117, 123]: spin–orbit splittings of high-angular-momentum atomic shells were greatly overestimated, with a small error for p shells, a substantial error

(∼15%) for d shells and a large error (∼50%) for f shells. In scalar relativistic calculations, adding the Hartree potential later partly compensates for doing a Douglas–Kroll transformation with the nuclear potential only. However, since the Hartree potential is scalar (has no spin–orbit parts), the approximate Douglas–Kroll operator is identical to the nuclear-only DK operator in its spin–orbit part, in other words: the spin–orbit operator still contains the full (unscreened) nuclear potential. Because there is a centrifugal potential which prevents electrons in high-angular-momentum atomic orbitals coming close to the nucleus, electrons in these orbitals do not "see" the naked but a screened nucleus, the screening being more important the higher the angular momentum. In the SNSO approximation [119, 123] the nuclear charge is empirically reduced to an effective nuclear charge when calculating the spin–orbit matrix elements, depending on the angular momentum of the basis functions whose matrix element is to be calculated. Note that the SNSO approximation, as originally presented, is somewhat inconsistent: only the first-order spin–orbit contributions to the Douglas–Kroll operator are modified while the second-order contributions remain unchanged. This cannot be generalized to higher-order Douglas–Kroll operators. A better suggestion is to scale the spin–orbit matrix elements before they go into the Douglas–Kroll "machine" [124]. Another two-component implementation going up to fourth-order Douglas–Kroll has been reported by Scuseria [125] and applied to heavy-element chemistry [126–128].

A more fundamental problem that potentially limits the accuracy of quasirelativistic methods is the so-called *picture change* problem, which means that one has to use properly transformed operators before one calculates expectation values using the two-component spinors [129–131]. In this context, the problem is that the electron density, which is *the* central quantity in DFT, is *not* given by the sum of the absolute squares of the two-component orbitals ("two-component density"). Rather, one should back-transform the two-component spinors to four-component Dirac spinors before one calculates the ("four-component" or "physical") electron density. Such a consistent treatment of the electron interaction in the DKH framework [132] would of course spoil all the computational savings of the quasirelativistic approach and is therefore of no practical use. What helps is the observation that at least for certain quasirelativistic operators, the two- and four-component density differ only in the atomic cores and are transferable from atoms to molecules, such that with a density correction calculated once and for ever for each atom in the periodic table, one can obtain, to a very good approximation, the four-component electron density directly from the two-component orbitals [124]. Note that even an exact quasirelativistic operator which reproduces the positive-energy branch of the Dirac spectrum is only defined up to a unitary transformation. Such a transformation leaves the energy spectrum invariant but may change the two-component density. Among the manifold of (nearly) exact quasirelativistic operators, those which produce a two-component density that is very similar to the "true" four-component density at least outside the atomic cores are to be preferred. In this respect Foldy–Wouthuysen type operators may be superior to methods which produce two-component orbitals that are renormalized upper Dirac components.

The ZORA method is in fact a re-derivation of a quasirelativistic Hamiltonian discovered earlier by Chang et al. [111]. It has been derived by Baerends, van Lenthe et al. [112, 133–135] as the leading contribution of a regular relativistic expansion, hence the name ZORA. It is interesting that a four-component procedure fully equivalent to ZORA can be derived applying perturbation theory directly to the Dirac equation [136]. Two-component ZORA DFT calculations were reported soon thereafter [137,138]. The main problem with ZORA is that it is not gauge invariant [133]. Because the ZORA kinetic energy operator $\hat{T}_{ZORA}$

$$\hat{T}_{ZORA} = \sigma\mathbf{p}\frac{c^2}{2mc^2 - v_{\text{eff}}}\sigma\mathbf{p}, \quad \hat{H}_{ZORA} = \hat{T}_{ZORA} + v_{\text{eff}} \tag{5-24}$$

depends on the effective potential, a constant shift of this potential affects the total energy in the wrong way (because $\hat{H}_{ZORA}$ does *not* experience a constant shift). Upon formation of a chemical bond, and more pronounced upon ionizing an atom, such nearly constant potential shifts occur in the region of the atomic core, and one can estimate that the error introduced by the gauge dependence of ZORA is much too large to be acceptable. For example, the calculated first ionization potential of gold with ZORA where the kinetic energy operator depends on the effective potential is 5.21 eV [139], far off the experimental value of 9.22 eV. All implementations of ZORA work around this problem in one way or the other. Originally the *electrostatic shift approximation* (ESA) was proposed [133]. Here, the total energy of a molecule only defined as an atomization energy, that is, with respect to the constituent atoms. These atoms are then calculated using ZORA where the effective potential used to construct the kinetic energy operator $\hat{T}_{ZORA}$ is fixed and taken from the self-consistent molecular calculation. The ZORA(MP) method (MP stands for *model potential*) works in some sense the other way round: To construct the kinetic energy operator in the molecule, a superposition of the densities of the neutral atoms constituting the molecule is used, and a Hartree and exchange-correlation potential derived thereof [139]. The advantage is that it is somewhat easier to compute forces [140] (i.e., geometry gradients), although gradients for ZORA(ESA) have also been presented soon thereafter [141]. There is also a variant called *strictly atomic* ZORA [140], where relativistic corrections to the matrix elements are only considered if both basis functions "sit" on the same atom. Furthermore, only the nuclear potential of that atom is used to construct $\hat{T}_{ZORA}$. This fixes the gauge and removes unphysical contributions from the tails of the nuclear potential of the other atoms. Likewise, no relativistic corrections enter the calculation of forces other than implicitly through the shape of the orbitals and their energy. This way, a nonrelativistic program can be used unmodified to compute the forces. Newer variants of ZORA avoid the numerical integration to compute the matrix elements of $\hat{T}_{ZORA}$ [142]. They rely on the resolution of the identity (RI).

In the last few years, many more quasirelativistic approaches have been proposed, for example the so-called relativistic elimination of the small component (RESC) [85,87,143]. Most likely, the development of new quasirelativistic operators has come to an end through the advent of quasirelativistic *infinite order* operators

that are exact within a given basis set. The first proposal in this direction came probably from Barysz and coworkers [144–147]. The issue has been thoroughly discussed by Kutzelnigg and Liu [148–151] although computational schemes at least very similar to theirs been in use elsewhere [152–154]. Two- and four-component methods can be made fully equivalent, but then two-component methods offer no advantages in terms of computational efficiency. However, one can invoke a hierarchy of approximations [155] starting either from a two- or a four-component formulation and restore computational efficiency.

The section on quasirelativistic Hamiltonians should not be closed without emphasizing that there is a price to pay for the (possible) gain in computational efficiency: two-component Hamiltonians are usually much more complicated than the Dirac operator. This is especially true if it comes to the calculation of magnetic properties like the chemical shift. It is perhaps not accidental that Kaupp, after some experimentation with quasirelativistic schemes [156], finally gave preference to a full four-component formulation [157]. So one can be somewhat pessimistic about the future of quasirelativistic *all electron* methods. Possibly, the two-component programs will only find applications when using spin-dependent ECPs, since this is certainly much more efficient than all-electron methods, let it be four- or two-component. At least for valence properties, two-component DFT calculations with ECPs seem to give the same answers as two- and four-component all-electron methods [109, 158]. Core properties like chemical shifts and electric field gradients at the nucleus should of course not be calculated with ECPs.

5.7. THE PRESENCE, AND THE FUTURE

While four-component approaches have gained a lot in efficiency in the last decade, the so-called infinite order two-component methods (at matrix level) get more and more similar, at least from an operational point of view, to a four-component treatment. The distinction between these methods, which sometimes went even somewhat emotional,[3] is fading away. Especially for properties that depend on the wave function in the atomic core, four-component methods are superior simply because too much effort has to be done to get this correct in a two-component formulation. After all, there are aspects beyond accuracy and computational efficiency: the development of two-component methods is (perhaps: has been) an intellectual challenge and thus a rewarding research field in its own right. Note that the separation into scalar and spin–orbit effects, although not uniquely defined [160–162], is important for qualitative discussion and understanding, and this separation is rooted in a two-component formulation. My prediction is that we will see more and more routine applications of the four-component Dirac–Kohn–Sham method in the not too distant future.

[3] In a speech (witnessed by the present author) given by W. Nieuwpoort at a conference dinner in 1999, the difference between four-component and two-component methods was characterized as the difference between a four-course and a two-course dinner. See also the title of Ref. [159]!

What surprises somewhat if one reviews "relativistic DFT" calculations is how little impact relativistic density functional theory in its narrower sense (see the first sections of this chapter) has had on these calculations. This will probably only change if more physics, such as two-electron spin–orbit effects beyond the screening of the nuclei (which comes from the Hartree term, not from the exchange-correlation functional), is included in new relativistic functionals. These effects are especially important in systems containing only *light* atoms, as the one-particle relativistic effects are small here. Note that the same holds in wavefunction based quantum chemistry, where the Breit interaction is an important contribution to the relativistic effects only for light atoms, while it is often neglected for heavy-element compounds where one-particle (kinematic) effects dominate. Quasirelativistic methods have so often been combined with density functional theory because this is straightforward to formulate: only effective one-particle equations with a local potential occur. This also means that it is only a small step from an implementation of a quasirelativistic method for one-electron systems to a many-electron algorithm based on DFT (see Ref. [163] which shows that ZORA becomes (much) more complicated for Hartree–Fock than for DFT).

Most likely, Dirac–Kohn–Sham will become cornerstone of heavy-element quantum chemistry, just as nonrelativistic Kohn–Sham is for compounds where relativistic effects are still unimportant. It is well possible that on the long run, two-component algorithms will only be of interest in conjunction with spin–orbit ECPs.

REFERENCES

1. Hohenberg, P., Kohn, W.: Phys. Rev. **136**, B864 (1964)
2. Kohn, W., Sham, L.J.: Phys. Rev. **140**, A1133 (1965)
3. Jones, R.O., Gunnarsson, O.: Rev. Mod. Phys. **61**, 689 (1989)
4. Ceperley, D.M., Alder, B.J.: Phys. Rev. Lett. **45**, 566 (1980)
5. Vosko, S.H., Wilk, L., Nusair, M.: Can. J. Phys. **58**, 1200 (1980)
6. Perdew, J.P., Zunger, A.: Phys. Rev. B **23**, 5048 (1981)
7. Ma, S.K., Brueckner, K.A.: Phys. Rev. **165**, 18 (1968)
8. Levy, M., Perdew, J.P.: Int. J. Quantum Chem. **49**, 539 (1994)
9. Becke, A.D.: J. Comput. Chem. **20**, 63 (1999)
10. Langreth, D.C., Mehl, M.J.: Phys. Rev. B **28**, 1809 (1983)
11. Becke, A.D.: J. Chem. Phys. **98**, 1372 (1993)
12. Becke, A.D.: J. Chem. Phys. **98**, 5648 (1993)
13. Ghosh, S.K., Parr, R.G.: Phys. Rev. A **34**, 785 (1986)
14. Becke, A.D., Roussel, M.R.: Phys. Rev. A **39**, 3761 (1989)
15. Tao, J.M., Perdew, J.P., Staroverov, V.N., Scuseria, G.E.: Phys. Rev. Lett. **91**, 146401 (2003)
16. Engel, E., Dreizler, R.M.: J. Comput. Chem. **20**, 31 (1999)
17. Vignale, G., Rasolt, M.: Phys. Rev. Lett. **59**, 2360 (1987)
18. Vignale, G., Rasolt, M.: Phys. Rev. B **37**, 10685 (1988)
19. Gunnarsson, O., Lundqvist, B.I.: Phys. Rev. B **13**, 4274 (1976)
20. Rajagopal, A.K., Callaway, J.: Phys. Rev. B **7**, 1912 (1973)
21. Rajagopal, A.K.: J. Phys. C **11**, L943 (1978)
22. Macdonald, A.H., Vosko, S.H.: J. Phys. C **12**, 2977 (1979)

23. Ramana, M.V., Rajagopal, A.K.: Adv. Chem. Phys. **54**, 231 (1983)
24. Pyykkö, P., Tokman, M., Labzowsky, L.N.: Phys. Rev. A **57**, R689 (1998)
25. Labzowsky, L., Goidenko, I., Tokman, M., Pyykkö, P.: Phys. Rev. A **59**, 2707 (1999)
26. Dyall, K.G., Bauschlicher, C.W., Schwenke, D.W., Pyykkö, P.: Chem. Phys. Lett. **348**, 497 (2001)
27. Pyykkö, P., Dyall, K.G., Csazar, A.G., Tarczay, G., Polyansky, O.L., Tennyson, J.: Phys. Rev. A **6302**, 024502 (2001)
28. Colwell, S.M., Handy, N.C.: Chem. Phys. Lett. **217**, 271 (1993)
29. Lee, A.M., Colwell, S.M., Handy, N.C.: Chem. Phys. Lett. **229**, 225 (1994)
30. Lee, A.M., Handy, N.C., Colwell, S.M.: J. Chem. Phys. **103**, 10095 (1995)
31. Capelle, K., Gross, E.K.U.: Phys. Rev. Lett. **78**, 1872 (1997)
32. Eschrig, H., Servedio, V.D.P.: J. Comput. Chem. **20**, 23 (1999)
33. Eschrig, H.: The Fundamentals of Density Functional Theory. Teubner, Stuttgart (1996)
34. van Wüllen, C.: J. Comput. Chem. **23**, 779 (2002)
35. Engel, E., Auth, T., Dreizler, R.M.: Phys. Rev. B **64**, 235126 (2001)
36. Jansen, H.J.F.: Phys. Rev. B **59**, 4699 (1999)
37. Fritsch, D., Koepernik, K., Richter, M., Eschrig, H.: J. Comput. Chem. **29**, 2210 (2008)
38. van Wüllen, C.: J. Chem. Phys. **139**, 194109 (2009)
39. Ellis, D.E., Goodman, G.L.: Int. J. Quantum Chem. **25**, 185 (1984)
40. Kübler, J., Hoeck, K.H., Sticht, J., Williams, A.R.: J. Appl. Phys. **63**, 3482 (1988)
41. Kübler, J., Hoeck, K.H., Sticht, J., Williams, A.R.: J. Phys. F **18**, 469 (1988)
42. Nordstrom, L., Singh, D.J.: Phys. Rev. Lett. **76**, 4420 (1996)
43. Sandratskii, L.M.: Adv. Phys. **47**, 91 (1998)
44. Ellis, D.E.: J. Phys. B-At. Mol. Opt. Phys. **10**, 1 (1977)
45. Engel, E., Keller, S., Bonetti, A.F., Müller, H., Dreizler, R.M.: Phys. Rev. A **52**, 2750 (1995)
46. Ramana, M.V., Rajagopal, A.K.: Phys. Rev. A **24**, 1689 (1981)
47. Bonetti, A.F., Engel, E., Dreizler, R.M., Andrejkovics, I., Müller, H.: Phys. Rev. A **58**, 993 (1998)
48. Ramana, M.V., Rajagopal, A.K.: J. Phys. C **12**, L845 (1979)
49. Ramana, M.V., Rajagopal, A.K.: J. Phys. C **14**, 4291 (1981)
50. Macdonald, A.H.: J. Phys. C **16**, 3869 (1983)
51. Xu, B.X., Rajagopal, A.K., Ramana, M.V.: J. Phys. C **17**, 1339 (1984)
52. Engel, E., Keller, S., Dreizler, R.M.: Phys. Rev. A **53**, 1367 (1996)
53. Mayer, M., Häberlen, O.D., Rösch, N.: Phys. Rev. A **54**, 4775 (1996)
54. Varga, S., Engel, E., Sepp, W.D., Fricke, B.: Phys. Rev. A **59**, 4288 (1999)
55. Schmid, R.N., Engel, E., Dreizler, R.M., Blaha, P., Schwarz, K.: Adv. Quantum Chem. **33**, 209 (1998)
56. Rosen, A., Ellis, D.E.: J. Chem. Phys. **62**, 3039 (1975)
57. Liberman, D., Waber, J.T., Cromer, D.T.: Phys. Rev. **137**, A27 (1965)
58. Liberman, D.A., Cromer, D.T., Waber, J.T.: Comput. Phys. Commun. **2**, 107 (1971)
59. Fricke, B., Sepp, W.D., Bastug, T., Varga, S., Schulze, K., Anton, J., Pershina, V.: Adv. Quantum Chem. **29**, 109 (1997)
60. Anton, J., Fricke, B., Engel, E.: Phys. Rev. A **69**, 012505 (2004)
61. Anton, J., Fricke, B., Schwerdtfeger, P.: Chem. Phys. **311**, 97 (2005)
62. Liu, W.J., Hong, G.Y., Dai, D.D., Li, L.M., Dolg, M.: Theor. Chem. Acc. **96**, 75 (1997)
63. Liu, W.J., Dolg, M.: Phys. Rev. A **57**, 1721 (1998)
64. Wang, F., Li, L.M.: J. Mol. Struct. (Theochem) **586**, 193 (2002)
65. Liu, W.J., Wang, F., Li, L.M.: J. Theor. Comput. Chem. **2**, 257 (2003)
66. Liu, W., van Wüllen, C.: J. Chem. Phys. **113**, 2506 (2000)
67. Whitten, J.L.: J. Chem. Phys. **58**, 4496 (1973)
68. Baerends, E.J., Ellis, D.E., Ros, P.: Chem. Phys. **2**, 41 (1973)

69. Dunlap, B.I., Connolly, J.W.D., Sabin, J.R.: J. Chem. Phys. **71**, 3396 (1979)
70. Dunlap, B.I.: Phys. Chem. Chem. Phys. **2**, 2113 (2000)
71. Dunlap, B.I.: J. Mol. Struct. (Theochem) **529**, 37 (2000)
72. Stephens, P.J., Devlin, F.J., Chabalowski, C.F., Frisch, M.J.: J. Phys. Chem. **98**, 11623 (1994)
73. Becke, A.D.: J. Chem. Phys. **98**, 5648 (1993)
74. Becke, A.D.: Phys. Rev. A **38**, 3098 (1988)
75. Lee, C., Yang, W., Parr, R.G.: Phys. Rev. B **37**, 785 (1988)
76. Saue, T., Helgaker, T.: J. Comput. Chem. **23**, 814 (2002)
77. Henriksson, J., Saue, T., Norman, P.: J. Chem. Phys. **128**, 024105 (2008)
78. Salek, P., Helgaker, T., Saue, T.: Chem. Phys. **311**, 187 (2005)
79. Gaston, N., Schwerdtfeger, P., Saue, T., Greif, J.: J. Chem. Phys. **124**, 044304 (2006)
80. Fossgaard, O., Gropen, O., Valero, M.C., Saue, T.: J. Chem. Phys. **118**, 10418 (2003)
81. Fossgaard, O., Gropen, O., Eliav, E., Saue, T.: J. Chem. Phys. **119**, 9355 (2003)
82. Gourlaouen, C., Piquemal, J.P., Saue, T., Parisel, O.: J. Comput. Chem. **27**, 142 (2006)
83. Thierfelder, C., Schwerdtfeger, P., Saue, T.: Phys. Rev. A **76**, 034501 (2007)
84. Bast, R., Hesselmann, A., Salek, P., Helgaker, T., Saue, T.: Chem. Phys. Chem. **9**, 445 (2008)
85. Nakajima, T., Suzumura, T., Hirao, K.: Chem. Phys. Lett. **304**, 271 (1999)
86. Yanai, T., Iikura, H., Nakajima, T., Ishikawa, Y., Hirao, K.: J. Chem. Phys. **115**, 8267 (2001)
87. Nakajima, T., Yanai, T., Hirao, K.: J. Comput. Chem. **23**, 847 (2002)
88. Yanai, T., Nakajima, T., Ishikawa, Y., Hirao, K.: J. Chem. Phys. **114**, 6526 (2001)
89. Yanai, T., Harrison, R.J., Nakajima, T., Ishikawa, Y., Hira, K.: Int. J. Quantum Chem. **107**, 1382 (2007)
90. Yanai, T., Nakajima, T., Ishikawa, Y., Hirao, K.: J. Chem. Phys. **116**, 10122 (2002)
91. Friesner, R.A.: Chem. Phys. Lett. **116**, 39 (1985)
92. Friesner, R.A.: J. Chem. Phys. **85**, 1462 (1986)
93. Nakajima, T., Hirao, K.: J. Chem. Phys. **121**, 3438 (2004)
94. Nakajima, T., Hirao, K.: Mon. Chem. **136**, 965 (2005)
95. Quiney, H.M., Belanzoni, P.: J. Chem. Phys. **117**, 5550 (2002)
96. Belpassi, L., Tarantelli, F., Sgamellotti, A., Quiney, H.M.: J. Chem. Phys. **122**, 184109 (2005)
97. Quiney, H.M., Belanzoni, P., Sgamellotti, A.: Theor. Chem. Acc. **108**, 113 (2002)
98. Belpassi, L., Tarantelli, F., Sgamellotti, A., Quiney, H.M.: J. Chem. Phys. **128**, 124108 (2008)
99. Belpassi, L., Tarantelli, F., Sgamellotti, A., Quiney, H.M.: J. Chem. Phys. **124**, 124104 (2006)
100. Belpassi, L., Tarantelli, F., Sgamellotti, A., Quiney, H.M.: Phys. Rev. B **77**, 233403 (2008)
101. Belpassi, L., Infante, I., Tarantelli, F., Visscher, L.: J. Am. Chem. Soc. **130**, 1048 (2008)
102. Belpassi, L., Tarantelli, F., Sgamellotti, A., Gotz, A.W., Visscher, L.: Chem. Phys. Lett. **442**, 233 (2007)
103. Belpassi, L., Tarantelli, F., Sgamellotti, A., Quiney, H.M.: J. Phys. Chem. A **110**, 4543 (2006)
104. Belpassi, L., Tarantelli, F., Sgamellotti, A., Quiney, H.M., van Stralen, J.N.P., Visscher, L.: J. Chem. Phys. **126**, 064314 (2007)
105. Kutzelnigg, W.: Chem. Phys. **225**, 203 (1997)
106. Liu, W., van Wüllen, C., Han, Y.K., Choi, Y.J., Lee, Y.S.: Adv. Quantum Chem. **39**, 325 (2001)
107. Lee, Y.S.: In: P. Schwerdtfeger Relativistic Electronic Structure Theory: Part 2. Applications, p. 352. Elsevier, Amsterdam (2004)
108. Pitzer, R.M., Winter, N.W.: Int. J. Quantum Chem. **40**, 773 (1991)
109. Mitin, A.V., van Wüllen, C.: J. Chem. Phys. **124**, 064305 (2006)
110. Armbruster, M.K., Weigend, F., van Wüllen, C., Klopper, W.: Phys. Chem. Chem. Phys. **10**, 1748 (2008)
111. Chang, C., Pelissier, M., Durand, P.: Phys. Scr. **34**, 394 (1986)
112. van Lenthe, E., Baerends, E.J., Snijders, J.G.: J. Chem. Phys. **99**, 4597 (1993)

113. Hess, B.A.: Phys. Rev. A **33**, 3742 (1986)
114. Knappe, P., Rösch, N.: J. Chem. Phys. **92**, 1153 (1990)
115. Rösch, N., Häberlen, O.D.: J. Chem. Phys. **96**, 6322 (1992)
116. Häberlen, O.D., Rösch, N.: Chem. Phys. Lett. **199**, 491 (1992)
117. Mayer, M., Krüger, S., Rösch, N.: J. Chem. Phys. **115**, 4411 (2001)
118. Garcia-Hernandez, M., Lauterbach, C., Krüger, S., Matveev, A., Rösch, N.: J. Comput. Chem. **23**, 834 (2002)
119. Majumder, S., Matveev, A.V., Rösch, N.: Chem. Phys. Lett. **382**, 186 (2003)
120. Matveev, A.V., Mayer, M., Rösch, N.: Comput. Phys. Commun. **160**, 91 (2004)
121. Boettger, J.C.: Int. J. Quantum Chem. **65**, 565 (1997)
122. Boettger, J.C.: Phys. Rev. B **57**, 8743 (1998)
123. Boettger, J.C.: Phys. Rev. B **62**, 7809 (2000)
124. van Wüllen, C., Michauk, C.: J. Chem. Phys. **123**, 204113 (2005)
125. Peralta, J.E., Scuseria, G.E.: J. Chem. Phys. **120**, 5875 (2004)
126. Batista, E.R., Martin, R.L., Hay, P.J., Peralta, J.E., Scuseria, G.E.: J. Chem. Phys. **121**, 2144 (2004)
127. Melo, J.I., de Azua, M.C.R., Peralta, J.E., Scuseria, G.E.: J. Chem. Phys. **123**, 204112 (2005)
128. Peralta, J.E., Batista, E.R., Scuseria, G.E., Martin, R.L.: J. Chem. Theory Comput. **1**, 612 (2005)
129. Thaller, B.: The Dirac Equation. Springer, Heidelberg (1992)
130. Baerends, E.J., Schwarz, W.H.E., Schwerdtfeger, P., Snijders, J.G.: J. Phys. B-At. Mol. Opt. Phys. **23**, 3225 (1990)
131. Kellö, V., Sadlej, A.J.: Int. J. Quantum Chem. **68**, 159 (1998)
132. Matveev, A., Rösch, N.: J. Chem. Phys. **118**, 3997 (2003)
133. van Lenthe, E., Baerends, E.J., Snijders, J.G.: J. Chem. Phys. **101**, 9783 (1994)
134. van Leeuwen, R., van Lenthe, E., Baerends, E.J., Snijders, J.G.: J. Chem. Phys. **101**, 1272 (1994)
135. van Lenthe, E., van Leeuwen, R., Baerends, E.J., Snijders, J.G.: Int. J. Quantum Chem. **57**, 281 (1996)
136. Sadlej, A.J., Snijders, J.G., van Lenthe, E., Baerends, E.J.: J. Chem. Phys. **102**, 1758 (1995)
137. van Lenthe, E., Snijders, J.G., Baerends, E.J.: J. Chem. Phys. **105**, 6505 (1996)
138. Philipsen, P.H.T., van Lenthe, E., Snijders, J.G., Baerends, E.J.: Phys. Rev. B **56**, 13556 (1997)
139. van Wüllen, C.: J. Chem. Phys. **109**, 392 (1998)
140. van Wüllen, C.: J. Comput. Chem. **20**, 51 (1999)
141. van Lenthe, E., Ehlers, A., Baerends, E.J.: J. Chem. Phys. **110**, 8943 (1999)
142. Filatov, M.: Chem. Phys. Lett. **365**, 222 (2002)
143. Fedorov, D.G., Nakajima, T., Hirao, K.: Chem. Phys. Lett. **335**, 183 (2001)
144. Barysz, M., Sadlej, A.J., Snijders, J.G.: Int. J. Quantum Chem. **65**, 225 (1997)
145. Barysz, M., Sadlej, A.J.: J. Mol. Struct. (Theochem) **573**, 181 (2001)
146. Barysz, M., Sadlej, A.J.: J. Chem. Phys. **116**, 2696 (2002)
147. Kedziera, D., Barysz, M.: J. Chem. Phys. **121**, 6719 (2004)
148. Kutzelnigg, W., Liu, W.J.: Mol. Phys. **104**, 2225 (2006)
149. Kutzelnigg, W., Liu, W.J.: J. Chem. Phys. **123**, 241102 (2005)
150. Liu, W.J., Peng, D.L.: J. Chem. Phys. **125**, 044102 (2006)
151. Liu, W.J., Kutzelnigg, W.: J. Chem. Phys. **126**, 114107 (2007)
152. Dyall, K.G.: J. Chem. Phys. **106**, 9618 (1997)
153. Filatov, M.: J. Chem. Phys. **125**, 107101 (2006)
154. Ilias, M., Saue, T.: J. Chem. Phys. **126**, 064102 (2007)
155. Peng, D.L., Liu, W.J., Xiao, Y.L., Cheng, L.: J. Chem. Phys. **127**, 104106 (2007)
156. Komorovsky, S., Repisky, M., Malkina, O.L., Malkin, V.G., Malkin, I., Kaupp, M.: J. Chem. Phys. **124**, 084108 (2006)

157. Komorovsky, S., Repisky, M., Malkina, O.L., Malkin, V.G., Ondik, I.M., Kaupp, M.: J. Chem. Phys. **128**, 104101 (2008)
158. van Wüllen, C., Langermann, N.: J. Chem. Phys. **126**, 114106 (2007)
159. Quiney, H.M., Skaane, H., Grant, I.P.: Adv. Quantum Chem. **32**, 1 (1999)
160. Dyall, K.G.: J. Chem. Phys. **100**, 2118 (1994)
161. Sadlej, A.J., Snijders, J.G.: Chem. Phys. Lett. **229**, 435 (1994)
162. Visscher, L., van Lenthe, E.: Chem. Phys. Lett. **306**, 357 (1999)
163. Faas, S., Snijders, J.G., van Lenthe, J.H., van Lenthe, E., Baerends, E.J.: Chem. Phys. Lett. **246**, 632 (1995)

CHAPTER 6

RELATIVISTIC PSEUDOPOTENTIALS

XIAOYAN CAO AND MICHAEL DOLG

Institut für Theoretische Chemie, Universität zu Köln, Greinstr. 4, 50939 Köln, Germany
e-mail: x.cao@uni-koeln.de;m.dolg@uni-koeln.de

Abstract: A brief overview over the foundations and modern variants of the relativistic effective core potential method, i.e., energy-consistent and shape-consistent ab initio pseudopotentials as well as ab initio model potentials, is given. The energy-consistent ab initio pseudopotential approach is discussed in more detail, focussing on the uranium atom as an example. The selection of appropriate relativistic reference data, the choice of the core and the fitting procedure are discussed. Results of atomic and molecular test calculations, e.g., for the low-lying electronic states of uranium hydride, are summarized. Whereas the 5f-in-core large-core approximation provides an efficient approximate treatment of larger actinide systems without having to struggle with complexities arising from the open 5f shell, the 5f-in-valence small-core approach allows to reach a similar accuracy as the best available relativistic all-electron calculations.

Keywords: Effective core potentials, Model potentials, Pseudopotentials, Pseudo-valence orbitals, Core-polarization potentials, Dirac–Coulomb–Hamiltonian, Breit interaction, Wood–Boring–Hamiltonian, Frozen-core errors, Uranium, Uranium hydride, Electronic structure, Excited states, Calibration

6.1. INTRODUCTION

The effective core potential (ECP) approach is one of the most successful approximate methods in relativistic quantum chemistry with an almost uncountable number of applications in the field of computational chemistry for heavy element systems. By means of restricting the explicitly treated electrons and orbitals to those belonging to the valence shells of the constituting atoms of a system, not only computational resources are saved, but also the major relativistic effects can be included implicitly in the calculation. In the ECP approaches the atomic cores, i.e., the nucleus and the electrons in the chemically inert inner shells of each atom, are replaced by a suitably parametrized relatively simple one-electron operator acting on the remaining valence electrons, the effective core 'potential'. Besides the modelling of core-valence Coulomb and exchange interactions as well as core-valence orthogonality constraints the ECP can be designed to account for relativistic corrections at essentially any computational level, for which accurate atomic all-electron (AE) reference calculations are feasible.

M. Barysz and Y. Ishikawa (eds.), *Relativistic Methods for Chemists*,
Challenges and Advances in Computational Chemistry and Physics 10,
DOI 10.1007/978-1-4020-9975-5_6,

Essentially two main variants of the ECP method exist. The so-called model potential (MP) approach can be viewed as an attempt to model as accurately as possible the frozen-core (FC) Hartree–Fock (HF) operator acting on the valence electron system, i.e., the radial nodal structure of the valence orbitals of an atom is unchanged with respect to the AE case. The so-called pseudopotential (PP) approach formally uses a transformation from the AE valence orbitals with the correct nodal structure to pseudo-valence orbitals with a simplified radial nodal structure, i.e., a reduced number of radial nodes leading to smaller demands with respect to the one-particle basis sets but also requiring a modified form of some operators acting on the explicitly treated valence space. Clearly, ECPs are mainly constructed to reproduce the results of AE calculations for properties determined by the spatial valence region of a system. Properties related to the spatial core region are beyond the original scope of the method, especially for the PP approach.

Although it should not be forgotten that ECPs are a tool for approximate relativistic quantum chemical calculations, not necessarily every AE calculation, also those using a formally better Hamiltonian than the one modelled by the ECP, yield a superior result. This is due to the fact that ECPs allow to concentrate the computational resources on the important parts of the system, e.g., they shift computational effort from the chemically unimportant core region to the chemically decisive valence region. This is not only related to the computational savings with respect to the one-particle basis sets, but also due to the fact that, by choosing appropriate, not necessarily identical, core definitions for a scalar-relativistic PP and a related spin–orbit (SO) operator the expensive large-scale correlation treatment may be essentially kept at the scalar-relativistic level, accounting for SO effects only within the framework of an effective Hamiltonian built in the basis of the LS or ΛS states. In addition, the explicit evaluation of core-valence correlation effects, i.e., dynamic core polarization, can be avoided by augmenting the ECP Hamiltonian by an effective core-polarization potential (CPP), correcting also for static core-polarization contributions. Highly accurate ECPs can even implicitly account for relativistic terms in the AE Hamiltonian which are difficult to deal with in standard atomic and especially molecular AE calculations, e.g., the ‘full’ Breit interaction, instead of merely the Gaunt term included frequently in molecular AE Dirac–Hartree–Fock (DHF) calculations and subsequent correlation treatments, or even higher corrections from quantum electrodynamics.

The present overview aims at computational chemists and is restricted to relativistic ECPs used in atomic and molecular ab initio electronic structure theory using Gaussian basis sets, e.g., related methods originating from solids state physics and applying plane wave expansions are not considered here. Moreover, the emphasis is put on PPs, especially those of the so-called energy-consistent variety. For more detailed information about the other approaches the reader is referred to review articles which appeared during the last decade, e.g., reviews focussing on MPs by Klobukowski, Huzinaga and Sakai [74] as well as by Seijo and Barandiáran [126], and on PPs by Pyykkö and Stoll [112] and by Schwerdtfeger [122]. The recentreview papers of the current authors on PPs and partly also on

MPs [20, 30, 31, 33, 60] provide a relatively complete list of older reviews, which might be of interest for those who wish to learn more about the field and its development. For a deeper discussion of relativistic effects or relativistic AE methods we refer the reader to the other chapters in this book.

In the following we will first summarize the basic concepts underlying the PP method and explain the most important equations. We will then describe in detail the method of energy-consistent PPs and continue with a brief discussion of frequently used alternative approaches developed by other groups, e.g., shape-consistent PPs as well as MPs. At the end we will have a look at an example, i.e., various energy-consistent PPs for the uranium atom and their applications.

6.2. THEORETICAL CONSIDERATIONS

The following sections give a brief overview over the basic equations underlying the pseudopotential (PP) approach and discuss the commonly used analytical forms of the valence-only (VO) model Hamiltonian.

6.2.1. Phillips–Kleinman Equation

In 1959 Phillips and Kleinman developed a rigorous formulation of the "empirical potential" approach within an effective one-electron framework for the calculation of wavefunctions in crystals and molecules [105]. The so-called Phillips–Kleinman equation, which is described below, provided the first sound theoretical basis for all PP methods.

Let us imagine an (effective) one-electron Hamiltonian $\hat{H}_{eff}$ with one upper energy eigenfunction $|\varphi_v>$, that we will call valence (v) eigenfunction, and several lower energy eigenfunctions $|\varphi_c>$, that we will call core (c) eigenfunctions.

$$\hat{H}_{eff}|\varphi_a> = \varepsilon_a|\varphi_a>, \qquad a \in \{v, c\} \tag{6-1}$$

We assume that all eigenfunctions are orthonormal.

$$<\varphi_a|\varphi_{a'}> = \delta_{aa'}, \qquad a, a' \in \{v, c\} \tag{6-2}$$

Due to the orthogonality requirements the valence orbital $|\varphi_v>$ will have radial nodes, if core orbitals $|\varphi_c>$ of the same symmetry are present. In order to derive a scheme with which we can save computational effort by treating only the valence electron(s) in the field of the core(s) and further by reducing the basis set requirements for the description of the valence space by reducing the number of radial nodes, we define an arbitrary, unnormalized function $|\varphi_p>$ as a linear combination of valence and core eigenfunctions:

$$|\varphi_p> = |\varphi_v> + \sum_c a_c|\varphi_c> \tag{6-3}$$

Using the orthogonality constraints between the $|\varphi_c>$ and $|\varphi_v>$ in Eq. (6-2) we can easily get the coefficients a_c by acting on Eq. (6-3) from the left with $<\varphi_c|$

$$a_c =<\varphi_c|\varphi_p> \tag{6-4}$$

Using this result one can solve Eq. (6-3) for the valence eigenfunction:

$$|\varphi_v>=|\varphi_p>-\sum_c <\varphi_c|\varphi_p>|\varphi_c> \tag{6-5}$$

Substituting $|\varphi_v>$ in Eq. (6-1) by this expression and using Eq. (6-1) for $|\varphi_c>$ yields

$$\hat{H}_{eff}|\varphi_p>-\sum_c \varepsilon_c|\varphi_c><\varphi_c|\varphi_p>=\varepsilon_v[|\varphi_p>-\sum_c |\varphi_c><\varphi_c|\varphi_p>] \tag{6-6}$$

If we define the so-called Phillips–Kleinman (PK) 'potential' $\hat{V}^{PK}$ as

$$\hat{V}^{PK}=\sum_c(\varepsilon_v-\varepsilon_c)|\varphi_c><\varphi_c| \tag{6-7}$$

we can rearrange Eq. (6-6) to give the so-called Phillips–Kleinman equation:

$$(\hat{H}_{eff}+\hat{V}^{PK})|\varphi_p>=\varepsilon_v|\varphi_p> \tag{6-8}$$

Since $\hat{V}^{PK}$ is not a usual potential, i.e., a function depending on a position $\mathbf{r}$, it is called pseudopotential (PP). It is important to note that the operator $\hat{V}^{PK}$ is energy-dependent because it depends on ε_v, and it is nonlocal because it depends on $|\varphi_v>$. Now both the core functions $|\varphi_c>$ and the valence function $|\varphi_v>$, as well as any linear combination $|\varphi_p>$ defined by Eq. (6-3), are eigenfunctions of the PK equation (6-8) with an eigenvalue ε_v. Note that the PK Hamiltonian implicitly takes care of core-valence orthogonality conditions and that one can use any arbitrary trial wavefunction $|\tilde{\varphi}_p>$ in a variational procedure to approach ε_v from above, without danger to collapse to the core energy levels. The linear combination Eq. (6-3) may e.g., be used to eliminate from $|\varphi_v>$ the nodal structure arising from core-valence orthogonality, yielding a smooth and nodeless pseudo-valence function $|\varphi_p>$. Unfortunately, the construction of the PK potential would require the knowledge of $|\varphi_a>$ and ε_a $(a \in v,c)$, i.e., the full problem still has to be solved and no computational savings arise so far. In addition the pseudo-valence function $|\varphi_p>$ constructed according to Eq. (6-3) is neither the single solution with the eigenvalue ε_v nor is it unique. It also could have the undesirable property that it shows significantdeviations from $|\varphi_v>$ in the chemically important spatial valence

region. For a recent attempt to explicitly apply PK theory as well as additional references to previous work in this field we refer the reader to articles by Schwartz and coworkers [129, 130].

The Phillips–Kleinman pseudopotential formalism was generalized in 1968 by Weeks and Rice [145] to cases, where $|\varphi_v>$ is eigenfunction of the (effective) one-electron Hamiltonian, whereas the $|\varphi_c>$ are not, as well as to cases where more than one valence electron is present. The extension of Eq. (6-8) for the many-electron pseudo-valence eigenfunction $|\Phi_p>$ is

$$(\hat{H}_v + \hat{V}^{GPK})|\Phi_p >= E_v|\Phi_p > \tag{6-9}$$

where the so-called generalized Phillips–Kleinman (GPK) PP $\hat{V}^{GPK}$ is a nonlocal, energy-dependent many-electron operator

$$\hat{V}^{GPK} = -\hat{H}_v\hat{P} - \hat{P}\hat{H}_v + \hat{P}\hat{H}_v\hat{P} + E_v\hat{P} \tag{6-10}$$

constructed from the Hamiltonian for the valence electrons $\hat{H}_v$, the total valence energy E_v and a projection operator $\hat{P}$, which projects out from the many-electron pseudo-valence eigenfunction $|\Phi_p>$ any core components, thus yielding the original valence eigenfunction $|\Phi_v>$ of $\hat{H}_v$ for the eigenvalue E_v, i.e.,

$$|\Phi_v >= (1 - \hat{P})|\Phi_p > \tag{6-11}$$

Equations (6-9) to (6-11) are formidable, and no computational savings would result compared to a standard all-electron (AE) treatment since the derivation merely corresponds to a rewriting of the original problem in a quite complicated form. However, the PK and GPK methods provide a formal theoretical basis for the subsequent development of PPs applied nowadays in quantum chemical calculations. Weeks and Rice state: "... it seems to us that the advantage of a pseudopotential formalism lies not in the formal exact solution but in the physical insights it gives and the models it suggests." Thus we keep in mind that in principle it is possible to find a 'potential' which, when added to a valence Hamiltonian, allows the variational solution of the corresponding Schrödinger equation without variational collapse by using a pseudo-valence wavefunction without explicit orthogonality requirements to the wavefunction describing the core system. We note here, that by getting rid of the core electron system we formally perform a core-valence separation and apply the frozen-core (FC) approximation. The former means that from now on we neglect core- and core-valence correlation effects, and the latter requires that we assume the core electron system to be unaffected by any changes the rest of the system may undergo. We now continue and discuss in the next sections how a suitable valence-only model Hamiltonian yielding such a pseudo-valence wavefunction for an atom could look like.

6.2.2. Valence Electron Model Hamiltonian for an Atom

For an atom with n_v valence electrons the valence-only Hamiltonian H_v is given by

$$\hat{H}_v = -\frac{1}{2}\sum_i^{n_v} \nabla_i^2 + \sum_i^{n_v}\sum_{j>i}^{n_v} \hat{g}(i,j) - \sum_i^{n_v} \frac{Q}{r_i} + \sum_i^{n_v} \hat{V}'_{cv}(i) \tag{6-12}$$

Here $\hat{g}(i,j)$ stands for the electron-electron interaction, e.g., in the simplest case $\hat{g}(i,j) = 1/r_{ij}$ for the Coulomb interaction. Q is the core charge, i.e., $Q = Z - n_c$ when n_c electrons and a nucleus of charge Z form the core, and $\hat{V}'_{cv}(i)$ denotes the core-valence interactions for the electron i not represented by the leading $-Q/r_i$ Coulomb attraction. The GPK equation (6-9) tells us, that when a pseudo-valence wavefunction as solution is sought $\hat{H}_v$ has to be supplemented with the GPK pseudopotential $\hat{V}^{GPK}$ equation (6-10)

$$\hat{H}_v^{GPK} = -\frac{1}{2}\sum_i^{n_v} \nabla_i^2 + \sum_i^{n_v}\sum_{j>i}^{n_v} \hat{g}(i,j) - \sum_i^{n_v} \frac{Q}{r_i} + \sum_i^{n_v} \hat{V}'_{cv}(i) + \hat{V}^{GPK} \tag{6-13}$$

We define an effective one-electron potential for valence electron i

$$\hat{V}_{cv}(i) = -\frac{Q}{r_i} + \Delta\hat{V}_{cv}(i) \tag{6-14}$$

using the approximation that $\hat{V}^{GPK}$ can be written as a sum over one-electron contributions $\hat{V}^{GPK}(i)$

$$\Delta\hat{V}_{cv}(i) = \hat{V}'_{cv}(i) + \hat{V}^{GPK}(i) \tag{6-15}$$

The atomic valence-only Hamiltonian Eq. (6-13) for pseudo-valence wavefunction calculations is now simplified to:

$$\hat{H}_v^{PP} = -\frac{1}{2}\sum_i^{n_v} \nabla_i^2 + \sum_i^{n_v}\sum_{j>i}^{n_v} \hat{g}(i,j) + \sum_i^{n_v} \hat{V}_{cv}(i) \tag{6-16}$$

Here $\hat{V}_{cv}(i)$ has to account for all interactions of the valence electron i with the nucleus and the (removed) core electron system, as well as for the neglect of explicit core-valence orthogonality constraints. In the following we will refer to $\Delta\hat{V}_{cv}(i)$ as a pseudopotential (PP). The analytical form and the construction of $\Delta\hat{V}_{cv}(i)$ for practical calculations will be discussed in the next section.

6.2.3. Analytical Form of Non-relativistic Pseudopotentials

The first PP was proposed by Hellmann in 1935 [59]. For treating potassium as a one-valence electron atom he assumed a simple local functional form for the complete potential acting on the valence electron:

$$\hat{V}_{cv}(\mathbf{r}) = V_{cv}(r) = -\frac{1}{r} + \frac{2.74}{r} e^{-1.16r} \tag{6-17}$$

Later it was found that simple r-dependent spherical PPs are not accurate enough for atoms containing valence orbitals of various angular symmetries, especially for first-row atoms [7]. Starting with the work of Abarenkov and Heine in 1965 [1] an increasing number of researchers took besides the r-dependency also a l-dependency into account, i.e., a dependency of the PP on the angular momentum quantum number l. We note that such a r and l dependency is already suggested in the PK pseudopotential Eq. (6-7), e.g., when core orbitals of different l are present. Kahn and Goddard [69] suggested unified PPs $\Delta\hat{V}_{cv}(\mathbf{r}_i)$

$$\Delta\hat{V}_{cv}(\mathbf{r}_i) = \sum_{l,m} V_l(r_i)|lm><lm| = \sum_{l=0}^{l=\infty} V_l(r_i)\hat{P}_l(i) \tag{6-18}$$

with the angular momentum projection operator based on spherical harmonics $|lm>$:

$$\hat{P}_l(i) = \sum_{m=-l}^{m=l} |lm><lm| \tag{6-19}$$

For $l \geq L$, where typically $(L-1)$ is the largest angular momentum used by the core orbitals, the PPs $V_l(r_i)$ are only slightly different [69], i.e.,

$$V_l(r_i) \cong V_L(r_i) \qquad \text{for} \qquad l \geq L \tag{6-20}$$

In general, if we assume $V_l(r_i) = V_L(r_i)$ for $l \geq L$, we can use the closure property of the projection operators to write the expression [69]

$$\Delta\hat{V}_{cv}(\mathbf{r}_i) \cong V_L(r_i) + \sum_{l=0}^{L-1} [V_l(r_i) - V_L(r_i)]\hat{P}_l(i) \tag{6-21}$$

The operator $\Delta\hat{V}_{cv}(\mathbf{r}_i)$ in Eq. (6-21) is a so-called semilocal PP, i.e., it mainly consists of a sum of local potentials $V_l(r_i) - V_L(r_i)$ acting on each angular momentum symmetry $0 \leq l \leq L-1$ separately up to a maximum angular momentum $L-1$ present in the core, beyond which a common local potential $V_L(r_i)$ acts on all angular momentum symmetries $l \geq L$.

The potentials $V_l(r_i)$ and $V_L(r_i)$ were written by Kahn et al. [70] as linear combinations of Gaussian type functions r_i multiplied by powers of r_i,

$$V_m(r_i) = \sum_k A_{km} r_i^{n_{km}} e^{-a_{km} r_i^2} \qquad \text{with} \qquad m = l, L \tag{6-22}$$

where r_i denotes the electron-core distance. The choice was made mainly because of computational convenience and efficiency for the further calculations, i.e., the matrix elements over the PP operators may then be readily evaluated in a cartesian Gaussian basis [8, 70, 84, 108].

In 1976 Kahn et al. [70] proposed a prescription for obtaining ab initio PPs from finite-difference HF atomic orbitals. The basic idea is to construct according to Eq. (6-3) a pseudo-valence orbital φ_p for each angular symmetry l as a linear combination of the AE valence and core orbitals, plug it in the radial Fock equation together with the appropriate orbital energy ε_v and to solve the resulting expression for the unknown potential $V_m(r_i)$ ($m = l, L$). Three conditions were imposed in addition to Eq. (6-3) on the pseudo-valence orbital φ_p:

1. The (energetically lowest) pseudo-valence orbital φ_p (in each angular symmetry) should have no radial nodes (a node or zero at r = 0 is not considered a radial node).
2. The pseudo-valence orbital φ_p should be as close as possible to the original valence orbital φ_v.
3. The pseudo-valence orbital φ_p should have a minimal number of spatial undulations.

These conditions mainly arise from the wish that the basis set used to represent the pseudo-valence orbital φ_p can be reduced comparing to the original basis set used to describe the true valence orbital φ_v. In order to impose these conditions in practice, Kahn et al. constructed a functional which had to be minimized with respect to the expansion coefficients a_c in Eq. (6-3). After the potentials were numerically generated on a grid, they were fitted to the expansion Eq. (6-22) in a least-squares sense. The powers n_{kl} of the electron-core distance r_i were restricted to the values -2, -1, and 0, because these values were found to adequately cover of the behavior of $\Delta\hat{V}_{cv}(\mathbf{r}_i)$ at the origin [70]. The work of Kahn et al. was a very important step forward in the development of ab initio PPs, however the pseudo-valence orbitals generated with their prescription often deviated too much from the AE valence orbitals in the chemically relevant spatial valence region and thus lead to defects of the PPs derived from them. This defect was actually already overcome by the work of Durand and Barthelat [40] as well as thereafter of Christansen et al. [24] evolving in the shape-consistent PP approach (cf. Section 6.4.1).

6.2.4. Analytical Form of Scalar-Relativistic Pseudopotentials

As reader may have noticed relativistic effects have not been taken into account so far. One distinguishes direct and indirect relativistic effects. The direct effects arise from substituting the non-relativistic Hamiltonian by a relativistic one and have been shown to originate in the spatial core region, i.e., near the nucleus, and to act on all orbitals which have a significant amplitude in this region. They always lead to a contraction and stabilization, as well as for angular momentum symmetry $l > 0$ to a spin–orbit (SO) splitting yielding states with total angular momentum quantum number $j = l - 1/2$ and $j = l + 1/2$. In a many-electron atom the direct effects are especially strong for the innermost shells of mainly s and p symmetry, which are strongly contracted and thus shield the nuclear charge for more diffuse orbitals more efficiently. The reduced effective nuclear charge acting on all further out orbitals leads for these to an expansion and destabilization. For the valence orbitals of a many-electron atom one finds usually that the valence s and p shells are stabilized and contracted, mainly by dominating direct relativistic effects, whereas the d and f shells are destabilized and expanded, mainly by dominating indirect relativistic effects.

In a PP approach, where the pseudo-valence orbitals have as low function values in the spatial core region as possible, it is not possible to generate accurately direct relativistic contributions by an operator acting in this region. Since electron density is shifted from the spatial core region towards the valence region, a modified relativistic operator has to be constructed anyhow. The indirect effects cause so to say a modification of the core charge seen by the valence orbitals, an effect which easily can be accommodated by the ansatz used in the non-relativistic case so far. Thus, PPs taking into account relativistic effects are constructed essentially along the same lines as in the non-relativistic case, however SO interaction causes some modifications of the analytical form, if it is taken into account. In case that only so-called scalar-relativistic contributions are to be incorporated in the PP, i.e., SO effects are neglected or averaged out, the so far described non-relativistic formalism can be kept and only the reference data for parametrization has to be adapted accordingly. Kahn et al. described in 1978 the first derivation of scalar-relativistic ab initio PPs [71] based on atomic Cowan–Griffin AE calculations [25]. Relativistic, e.g., two-component, PPs were first published at the same time by Hafner and Schwarz [55] at a semiempirical level and independently by Lee et al. [79] at the ab initio level. The analytical form of such relativistic PPs will be described in the next section.

6.2.5. Analytical Form of Relativistic Pseudopotentials

In a description of an atom at the non-relativistic Hartree–Fock level (HF) all orbitals belonging to a shell with main quantum number n and angular momentum quantum number l are degenerate, thus leading to a semilocal PP with a l-dependence by means of a projection operator $\hat{P}_l$ based on spherical harmonics. At the relativistic

Dirac–Hartree–Fock (DHF) level the degeneracy is reduced and depends in addition to n and l also on the total angular momentum j of the orbital (or spinor), implying a semilocal PP with a lj-dependence by means of a projection operator $\hat{P}_{lj}$ set up with spinor-spherical harmonics $|ljm>$:

$$\Delta\hat{V}_{cv}(\mathbf{r}_i) = \sum_{l,j,m} V_{lj}(r_i)|ljm><ljm| = \sum_{l=0}^{l=\infty}\sum_{j=|l-\frac{1}{2}|}^{j=l+\frac{1}{2}} V_{lj}(r_i)\hat{P}_{lj}(i) \tag{6-23}$$

with

$$\hat{P}_{lj}(i) = \sum_{m=-j}^{m=j} |ljm><ljm| \tag{6-24}$$

By using the same strategy as Kahn and Goddard [69] did for the non-relativistic case (cf. Section 6.2.3), $\Delta V_{cv}(\mathbf{r}_i)$ may be written as

$$\Delta\hat{V}_{cv}(\mathbf{r}_i) \cong V_L + \sum_{l=0}^{l=L-1}\sum_{j=|l-\frac{1}{2}|}^{j=l+\frac{1}{2}} [V_{lj}(r_i) - V_L(r_i)]\hat{P}_{lj} \tag{6-25}$$

Note that

$$\hat{P}_l(i) = \sum_j \hat{P}_{lj}(i) = \hat{P}_{l,|l-\frac{1}{2}|}(i) + \hat{P}_{l,l+\frac{1}{2}}(i) \tag{6-26}$$

and

$$V_l(r_i) = \frac{1}{2l+1}[l\,V_{l,|l-\frac{1}{2}|}(r_i) + (l+1)V_{l,l+\frac{1}{2}}(r_i)] \tag{6-27}$$

The relativistic PP in Eq. (6-25) may thus be rewritten as the sum of a spin-free averaged (av) and a spin-dependent (so) term [42]

$$\Delta\hat{V}_{cv}(\mathbf{r}_i) = \Delta\hat{V}_{cv,av}(\mathbf{r}_i) + \Delta\hat{V}_{cv,so}(\mathbf{r}_i) \tag{6-28}$$

where

$$\Delta\hat{V}_{cv,so}(\mathbf{r}_i) = \sum_{l=1}^{L-1} \frac{\Delta V_l(r_i)}{2l+1}[l\,\hat{P}_{l,l+1/2}(i) - (l+1)\hat{P}_{l,l-1/2}(i)] \tag{6-29}$$

$\Delta\hat{V}_{cv,av}(\mathbf{r}_i)$ is a scalar-relativistic PP, i.e., without inclusion of SO coupling, and it corresponds to $\Delta\hat{V}_{cv}(\mathbf{r}_i)$ defined in Eq. (6-21) if the difference between $V_{LJ}(r_i)$ and $V_L(r_i)$ is neglected [42]. The $\Delta\hat{V}_{cv,so}(\mathbf{r}_i)$ is called SO PP. A simpler form especially suited for use in SO configuration interaction (CI) calculations following s scalar-relativistic HF solution was derived by Pitzer and Winter [108]

$$\Delta\hat{V}_{cv,so}(\mathbf{r}_i) = \sum_{l=1}^{L-1} \frac{2\Delta V_l(r_i)}{2l+1}\hat{P}_l(i)\hat{\mathbf{l}}_i \cdot \hat{\mathbf{s}}_i\,\hat{P}_l(i). \tag{6-30}$$

Here $\hat{\mathbf{l}}_{\lambda i} = \hat{\mathbf{r}}_{\lambda i} \times \hat{\mathbf{p}}_i$ and $\hat{\mathbf{s}}_i$ stand for the operators of orbital angular momentum and spin, respectively. We note here in passing that relativistic (two-component) PPs can be averaged and thus also used in scalar-relativistic (one-component) calculations, whereas the usage of a scalar-relativistic PP together with a SO term optimized only for the valence orbitals, and not for the semi-core orbitals, in variational two-component calculations usually leads to errors.

6.2.6. Molecular Pseudopotentials

By using steps similar to the ones described in Section 6.2.2 for an atom one can obtain a corresponding molecular valence electron model Hamiltonian (cf. Eqs. 6-14–6-16)

$$\hat{H}_v = -\frac{1}{2}\sum_i^{n_v} \nabla_i^2 + \sum_i^{n_v}\sum_{j>i}^{n_v} \hat{g}(i,j) + \sum_i^{n_v} \hat{V}_{cv}(i) + V_{cc} \tag{6-31}$$

where

$$\hat{V}_{cv}(i) = -\sum_\lambda \frac{Q_\lambda}{r_{\lambda i}} + \Delta\hat{V}_{cv}(i) \tag{6-32}$$

and

$$V_{cc} = \sum_{\lambda<\mu}[\frac{Q_\lambda Q_\mu}{r_{\lambda\mu}} + \Delta V_{cc}^{\lambda\mu}(r_{\lambda\mu})] \tag{6-33}$$

The sums in Eqs. (6-32) and (6-33) run over all nuclei λ, μ with the core charge Q_λ, Q_μ. In principle one obtains the molecular PP as a superposition of atomic PPs

$$\hat{V}_{cv}(i) = \sum_\lambda \hat{V}_{cv}^\lambda(i) = \sum_\lambda[-\frac{Q_\lambda}{r_{\lambda i}} + \Delta\hat{V}_{cv}^\lambda(i)] \tag{6-34}$$

plus some non-additive correction V_{cc}. This new term V_{cc} compared to the case of one atom (cf. 6-16) denotes the interaction between nuclei and/or cores, written as the point charge approximation for the leading term and additional pair-wise corrections ΔV_{cc} for deviations from the Coulomb repulsion, e.g., for mutually penetrating cores, where besides modified electrostatic contributions also orthogonality constraints and the Pauli-repulsion between the electron shells localized on different cores has to be taken into account. It is hoped that a suitable parametrization of $\Delta\hat{V}_{cv}^\lambda$ and $\Delta V_{cc}^{\lambda\mu}$ is able to compensate for all errors resulting from the simplifications of the original valence Hamiltonian.

6.2.7. Core-Polarization Potentials

The derivation of the valence electron model Hamiltonian for an atom as well as a molecule sketched above has been done at the independent-particle level, i.e., using HF-type determinant wavefunctions built from orbitals. Thus electron

correlation effects are not considered. When the cores are actually replaced by local or semi-local potentials the contributions of core and core-valence correlation necessarily have to be neglected, whereas an explicit correlated treatment of the valence electrons is still possible. We note that the leading contribution for core-valence correlation in an AE CI treatment would be single excitations from the core orbitals coupled to single and higher excitations from the occupied valence orbitals to the virtual ones.

If we suppose that the (spherically symmetric) core of an atom will not be affected when the atom bonds to the other atoms, i.e., the FC approximation is valid, one can just take the PPs determined for each atom in the system (cf. 6.2.5) to construct the molecular PP by means of their superposition (cf. Eq. 6-34). Contributions arising from the deformation of the atomic cores under the field of the other cores and all valence electrons in the system, i.e., static core-polarization effects, are thus neglected. The induced error may become especially significant for systems with large, easily polarizable cores and only a few valence electrons, e.g., for large-core PPs in case of group 1 and 2 or 11 and 12 elements. At the AE level, starting with spherical mutually orthogonalized cores, the static core-polarization could be accounted for in a CI treatment by single excitations from the core orbitals to the virtual ones.

Since in the ECP approximation the core electrons have been removed from the system, the above mentioned single excitations cannot be performed explicitly, but only taken into account in form of an effective operator acting on the valence electrons. Therefore, a so-called core-polarization potential (CPP) $\hat{V}_{cpp}$ is frequently added to the valence electron model Hamiltonian.

$$\hat{H}_v = -\frac{1}{2}\sum_i^{n_v} \nabla_i^2 + \sum_i^{n_v}\sum_{j>i}^{n_v} \hat{g}(i,j) + \sum_i^{n_v} \hat{V}_{cv}(i) + V_{cc} + \hat{V}_{cpp} \qquad (6\text{-}35)$$

The $\hat{V}_{cpp}$ accounts for both static core-polarization, i.e., polarization of the core at the HF level, as well as dynamic core polarization, i.e., core-valence correlation. It has been demonstrated in PP calculations that by including the dipole polarization of the core charge density one can also takes care of the largest part of the core-valence correlation contributions [53].

For a core λ the dipole moment $\hat{\mu}_\lambda$ induced by an external electric field $\hat{\mathbf{f}}_\lambda(\mathbf{r})$ generated by all other cores and nuclei as well as all valence electrons in the system at a core λ with dipole polarizability α_λ amounts to

$$\hat{\mu_\lambda} = \alpha_\lambda \hat{\mathbf{f}}_\lambda \qquad (6\text{-}36)$$

We note here in passing that the application of a CPP will also contribute to the dipole moment of a system. The interaction of such induced dipoles with the external electric field yields an expression for the CPP

$$\hat{V}_{cpp} = -\frac{1}{2}\sum_\lambda \hat{}_\lambda \cdot \hat{\mathbf{f}}_\lambda = -\frac{1}{2}\sum_\lambda \alpha_\lambda \hat{\mathbf{f}}_\lambda^2 \qquad (6\text{-}37)$$

Equation (6-37) strictly applies only to large distance(s) of the polarizing charge(s) from the polarized core(s) and even diverges in the limit vanishing distances. Therefore Müller et al. [94] have suggested to multiply the field $\mathbf{f}_\lambda$ with a cut-off functions F removing the singularities. The field at a core λ then reads as

$$\hat{\mathbf{f}}_\lambda = -\sum_i \frac{\mathbf{r}_{i\lambda}}{r_{i\lambda}^3} F(r_{i\lambda}, \delta_e^\lambda) + \sum_{\mu \neq \lambda} Q_\mu \frac{\mathbf{r}_{\mu\lambda}}{r_{\mu\lambda}^3} F(r_{\mu\lambda}, \delta_c^\lambda) \tag{6-38}$$

where the cut-off functions can be chosen, e.g., as follows

$$F(r_{i\lambda}, \delta_e^\lambda) = [1 - exp(-\delta_e^\lambda r_{i\lambda}^2)]^{n_e} \tag{6-39}$$

$$F(r_{\mu\lambda}, \delta_c^\lambda) = [1 - exp(-\delta_c^\lambda r_{\mu\lambda}^2)]^{n_c}. \tag{6-40}$$

The exponents n_e and n_c for the electronic and nuclear contributions are usually 1 or 2, and the corresponding cut-off parameters δ_e^λ and δ_c^λ can be used for the adjustment to suitable reference data. We note that the CPP is not a simple one-electron operator as the usual ECPs, but contains one- and two-particle contributions arising from the valence electrons as well as the cores/nuclei. The integral evaluation over Cartesian Gaussian functions is quite complex [123, 120] and energy gradients for geometry optimizations are still missing. CPPs of the type described here often accompany large-core PPs for main group elements [67, 68] as well as group 11 and 12 transition metals [66, 133]. For the latter systems quadrupole corrections have also been developed [134].

6.2.8. Core–Core/Nucleus Repulsion Corrections

For small cores, where the overlap effects between cores are not significant, the point-charge repulsion model is often a good approximation for the core–core interaction V_{cc} (cf. the first term in Eq. (6-33)). However if the large cores are used the core–core repulsion (CCRC) correction for "verlapping" or "Mutually penetrating" cores, i.e., the second term in Eq. (6-33), is necessary. A similar core-nucleus repulsion correction (CNRC) has to be applied for the interaction between nuclei of atoms treated without PPs and centers with large-core PPs. A Born–Mayer-type ansatz proved to be quite successful to model the pairwise repulsive correction [66, 133]

$$\Delta V_{cc}^{\lambda\mu}(r_{\lambda\mu}) = B_{\lambda\mu} exp(-b_{\lambda\mu} r_{\lambda\mu}) \,. \tag{6-41}$$

The parameters can be derived, e.g., from FC HF calculations on pairs of atomic cores.

6.3. ENERGY-CONSISTENT PSEUDOPOTENTIALS

In the following we will describe in more detail the methodology of energy-consistent ab initio pseudopotentials (PPs). Although a few hints to earlier work in this field are given, including also semiempirical parametrizations, we will focus on

the currently mainly used Wood–Boring (WB) adjusted scalar-relativistic ab initio PPs as well as the recently developed, presumably more accurate relativistic ab initio PPs adjusted to multi-configuration (MC) Dirac–Hartree–Fock (DHF) reference data obtained by using the Dirac–Coulomb (DC) Hamiltonian self-consistently and the Breit term in first-order perturbation theory (+B). We refer to these potentials as multi-configuration Dirac–Hartree–Fock/Dirac–Coulomb–Breit (MCDHF/DC+B) adjusted relativistic ab initio PPs. At the end of this chapter we describe these two types of PPs, their adjustment and some selected applications in more detail for the uranium atom.

6.3.1. Some Historical Aspects

The development of the energy-consistent PPs, previously called energy-adjusted PPs, originated from the early work of Preuss in 1955 [109] and thus initially mainly energy-adjusted semiempirical large-core PPs were derived [110]. Since about 1982, starting with the work of Fuentealba, the PPs were often supplemented by core-polarization potentials (CPPs) [52,53] of the type Meyer and coworkers applied in all-electron (AE) calculations [94]. The adjustment was usually performed for a multitude of one-valence electron states (SEFIT, *single electron fit*) using experimental reference data. Parametrizations are available for most of the main group elements [67, 68] as well as group 11 and 12 transition metals [66, 133, 134]. Schwerdtfeger developed besides semiempirical also several relativistic ab initio PPs for heavy main group elements by taking the reference data from relativistic single-configuration DHF calculations using the DC Hamiltonian [121, 124, 125].

Initial adjustments of ab initio PPs for transition metal elements at the non-relativistic Hartree–Fock (HF) level by Wedig soon revealed that a large-core approximation, e.g., a Ar-core in case of Ti, leads to too large frozen-core (FC) errors and a non-satisfactory transferability of the PPs [144]. However, in addition it was found for a small core that FC errors introduced in the SEFIT adjustment for a highly charged ion lead to unacceptably large errors when the PP was used for a neutral atom. Thus an adjustment of small-core PPs to ab initio HF data for a multitude of many-valence electron states (MEFIT, *many electron fit*) of the neutral atom and the low-charged ions became the method of choice [35, 144]. Relativistic contributions have been included initially by adding correction terms to the PP obtained at the one-valence electron level from single configuration DHF calculations using the DC Hamiltonian for the highly charged single valence electron ion.

Motivated mainly by the work of Hay and Wadt on shape-consistent relativistic ab initio PPs [57, 58, 142], who applied the Cowan–Griffin (CG) scalar-relativistic HF approach [25] to generate the reference orbitals and orbital energies, the related Wood–Boring (WB) scalar-relativistic Hamiltonian [150] was implemented in the HF method [36, 37] and from there on used routinely to generate relativistic reference energies for many-valence electron states within the LS coupling scheme. Energy-consistent PPs relying on this approximate relativistic approach were derived for main group elements [11, 76, 96], 4d and 5d transition metals [3] as

well as lanthanides [36, 37, 39] and actinides [77, 88, 90, 91], thus together with the previously derived parametrization for the 3d transition metals [35] covering essentially the whole periodic table. For transition metals as well as lanthanides and actinides an accurate small-core approach has been adapted, however for both lanthanides and actinides a computationally efficient albeit quite approximate and, for inexperienced users, possibly even dangerous large-core parametrization attributing the open f shell to the PP core is also available. Some of the small-core PPs are accompanied by spin–orbit (SO) operators, either parametrized on the basis of one-electron splittings calculated with the spin-dependent WB Hamiltonian [3] or by using reference data obtained at the DHF level [18, 36].

Most of the WB-adjusted PPs are accompanied by energy-optimized valence basis sets, however usually only one basis set size and contraction pattern was supplied in the original publications. Additional systematic correlation-consistent valence basis sets of augmented valence triple- and quadruple-zeta quality were published by Martin and Sundermann for the main group element PPs for Ga–Kr and In–Xe [83]. For the small-core f-in-valence lanthanide and actinide PPs generalized contracted atomic natural orbital (ANO) basis sets of polarized valence double- to quadruple-zeta quality as well as related segmented contracted basis sets of polarized valence quadruple-zeta quality are available [17–19, 21].

Recently, scalar-relativistic PPs, especially adapted for use in quantum Monte-Carlo (QMC) calculations due to a removed Coulomb singularity at the nucleus, based on the WB HF approach were presented by Burkatzki et al. for main group elements as well as 3d transition elements [14, 15]. These potentials are accompanied by correlation-consistent valence basis sets of valence double- to quintupel-zeta quality for the first and second row main group elements, double- and triple-zeta quality for the third to fifth row main group elements as well as triple- and quadruple-zeta quality for the 3d transition metals. Although primarily designed for the use within the QMC approach, these PPs and valence basis sets can also be used in standard wavefunction-based quantum chemical calculations and possibly also in density functional theory (DFT) computations.

The PPs originating from the WB scalar-relativistic HF approach are up to now the most widely used energy-consistent PPs. Their main deficiency is probably the absence of a similarly consistent set of accompanying SO operators. Especially in view of the various recent developments of two-component HF and Kohn–Sham (KS) density functional (DF) codes as well as large-scale configuration interaction (CI) codes allowing for SO terms in the Hamiltonian, it became necessary to extend the energy-adjustment to a two-component formalism. After an initial study of the super-heavy transition metal element hahnium Ha (now named dubnium Db) in 1993 [38], the direct adjustment to MCDHF reference data for a multitude of many-electron states obtained with the DC or DCB Hamiltonian in the intermediate coupling scheme has been applied to main group elements [80, 81, 85, 86, 135], the group 11 and 12 elements [47, 127] as well as the 3d and 4d transition metals [32, 104, 128]. Ongoing work in the groups of Stoll (Stuttgart), Dolg (Cologne)as

well as Schwerdtfeger (Auckland) deals with energy-consistent ab initio PPs for 5d transition metals, lanthanides and actinides as well as superheavy elements. These new sets of PPs are often accompanied by sequences of correlation-consistent atomic natural orbital (ANO) basis sets of the Dunning type systematically converging to the basis set limit [47, 101–104]. In a number of calibration studies it was shown, that the PPs and accompanying valence basis sets yield results of similar quality to the best currently feasible relativistic AE calculations [48].

6.3.2. Method of Parametrization

The parametrization of energy-consistent PPs requires three steps, i.e., a decision on the size of the core, the generation of the reference data and the actual adjustment of the PP parameters.

Step 1 As a first step of a PP parametrization a decision with respect to the separation between valence and core space has to be made. Let us take the scandium atom, i.e., the lightest transition metal, as an example. Here one essentially has two choices: a computationally very attractive although not very accurate large-core PP (LPP) and a computationally more demanding and more accurate small-core PP (SPP). These options are illustrated in Figure 6-1. The orbital energies ε exhibit a clear separation between the 3d,4s valence orbitals (the chemical valence shells) and the 3s,3p semi-core orbitals ($\varepsilon_{3p}/\varepsilon_{3d} \approx 4.6$), i.e., from an energetic point of view the large-core approach appears to be a reasonable choice. However, when looking at the radial expectation values $< r >$ it becomes obvious that the 3d shell is very compact and has a much more similar radial extension with 3s,3p shells than with

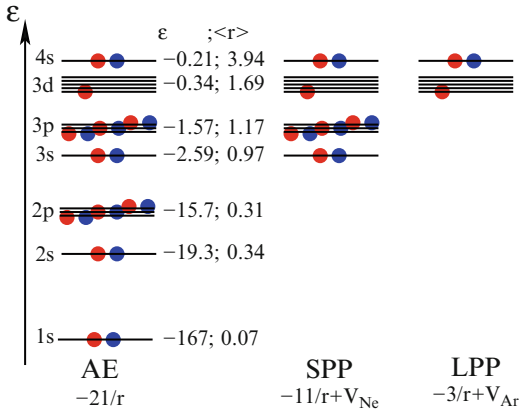

Figure 6-1. Schematic plot of the ground state orbital energy levels for Sc for an all-electron (AE; nuclear charge $Z = 21$) approach as well as a small-core pseudopotential (SPP; [Ne]-core; core charge $Q = 11$) and large-core pseudopotential (LPP; [Ar]-core; core charge $Q = 3$). The orbital energies ε (Hartree) and radial expectation values $< r >$ (Bohr) were taken from scalar-relativistic Wood–Boring all-electron calculations

the 4s shell ($< r >_{3d} / < r >_{3p} \approx 1.4$). Thus from a spatial point of view the 3s,3p shells should be included in the valence space together with 3d and 4s. Since both energetically and spatially a clear separation is visible between the 1s,2s,2p core shells and the 3s,3p,3d,4s semi-core/valence shells, a small-core approach is implied ($\varepsilon_{2p}/\varepsilon_{3s} \approx 6.1$, $< r >_{3s} / < r >_{2p} \approx 3.1$). In fact experience for transition metals shows so far, that the small-core PP approach is more reliable than the large-core one. This aspect is discussed in more detail for uranium below, where additional options for the size of the core come into play (cf. Section 6.5).

Step 2 Having decided on the size of the core the necessary reference data has to be derived. The energy-consistent ab initio PP approach relies only on quantum mechanical observables in the determination of the adjustable parameters in the PP, i.e., total valence energies. Since no quantities such as orbitals and orbital energies defined only in an effective one-particle model, e.g., the HF or DHF scheme, are used, the reference calculations could in principle also be carried out at the correlated level. In general the total valence energies used here can always be written as sums of observable contributions, e.g., the electron affinity, ionization potentials and excitation energies of the atom/ion. For an atom/ion a set of configurations, LS states or J levels is selected. The selection should cover all charge states and electron configurations which are relevant for the species which should be treated with the resulting PP. Usually the ground state of the neutral atom, of the anion if it exists, as well as the low-charged cations are included. In addition to the ground states the easily accessible low-energy excited states should also be included. Usually such a selection, which may be also motivated by the experimentally observed low-lying states [97], leads to about 10–30 reference configurations or LS states, corresponding to a few hundred or thousand J levels. Recent parametrizations also included reference configurations or states with higher energy, e.g., with ionizations or excitations from semi-core orbitals or excitation into higher virtual orbitals. The most extensive parametrization for uranium discussed below comprised 100 reference configurations and more than 30,000 J levels (cf. Section 6.5).

For the selected configurations, LS states or J levels as well as for the core system AE reference calculations have to be carried out and the total valence reference energies have to be calculated by building the appropriate differences. In case of the energy-consistent ab initio PPs besides the non-relativistic HF method essentially only the scalar-relativistic HF scheme using the WB Hamiltonian [150], similar to the CG HF approach [25] applied by other groups, was used for the calculation of energies for configurations or LS states. An extensively modified version of the finite difference atomic HF code MCHF77 of Froese Fischer [51] was applied in order to avoid any finite basis set effects in the reference data. In principle other scalar-relativistic schemes such as the Douglas–Kroll–Hess (DKH) Hamiltonian [60] could also be used to generate reference data for one-component relativistic PPs, however to our knowledge a corresponding finite difference code is not at hand. In case of two-component relativistic PPs we applied the four-component finite-difference MCDHF code GRASP1 [41] to generate referencedata for the J levels in

the intermediate coupling scheme. Usually the DC or the DCB Hamiltonian and a finite nucleus model, e.g., a Fermi charge distribution, was applied.

Step 3 In order to determine the free parameters in the valence-only model Hamiltonian we perform for a given set of initially guessed parameters atomic finite-difference PP calculations for all reference configurations, LS states or J levels using essentially the same machinery as for the AE calculations. Accordingly modified versions of MCHF77 [51] and GRASP1 [41] are used for this purpose. The sum over squared deviations of the PP total valence energies E_I^{PP} from the AE reference values E_I^{AE} is evaluated,

$$S = \sum_I w_I (E_I^{PP} - E_I^{AE} + \Delta E_{shift})^2 := min, \tag{6-42}$$

and the first and second derivatives (or approximations for them) with respect to the free parameters are determined. The least-squares minimization with respect to the free parameters is then achieved iteratively with various standard optimization methods. Due to the high speed of the atomic structure codes involved a few hundred or thousand optimization steps can be performed if needed.

The achieved accuracy depends critically on the size of the core as well as within the limits of accuracy of the semilocal ansatz also on the number of adjustable parameters. Typical requirements for the accuracy are 0.1 eV for the total valence energies of many-electron configurations or LS states with one or two Gaussian functions per radial potential of each l- or lj-value included in the projection operators. For a reasonable choices of the cores PP adjustments for single-electron cases reach an accuracy in the valence energies of 0.001 eV or better.

The procedure described so far requires that, e.g., the total valence energy of the ground state of an atom corresponds to the sum of all ionization potentials when going from the neutral atom to the highly charged core. Especially for small-core PPs, the quantitatively correct description of the complete removal of electrons from the semi-core orbitals is not a necessary requirement for a reliable PP, especially since the core of the neutral atom will be considerably different from the free highly charged core and thus FC errors in the sum of the ionization potentials are unavoidable. It was found that a global shift of the AE reference energies ΔE_{shift}, typically of the order of 1% or less of the ground state total valence energy, can improve the accuracy of the fit by one or two orders of magnitude. ΔE_{shift} can also be viewed as a shift of the AE core energy, as illustrated schematically in Figure 6-2 for the Sc atom in case of a small-core ([Ne]-core) parametrization. It is obvious that the quantities of interest in this context, i.e., all possible energy differences between configurations, LS states of J levels included as references, remain unchanged. Recent adjustments with up to four Gaussian functions in each radial potential for uranium apply such a global shift and achieve an accuracy of better than 0.01 eV for configurational averages (cf. Section 6.5).

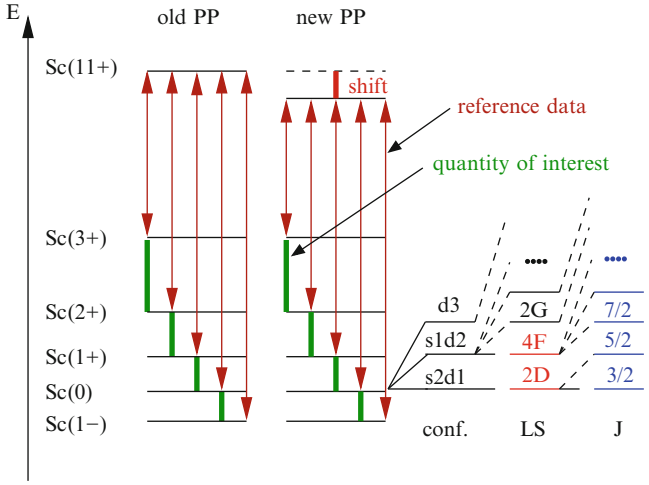

Figure 6-2. Schematic presentation of the selected reference data (*vertical double-sided arrows*) as well as the data usually of interest, i.e., electron affinity, ionization potentials (and excitation energies) (*vertical bars*), in the multi-electron multi-state adjustment of a Sc small core pseudopotential. The reference energies can be obtained for configurational averages (conf.), LS states or J levels. The shift of the core energy ΔE_{shift} included in newer pseudopotential adjustments (amounting typically to $\approx 1\%$ of the total valence energy) changes the reference data, but not the actual quantities of interest

6.3.3. Availability of Pseudopotentials and Valence Basis Sets

The primary source for energy-consistent PPs and the corresponding valence basis sets is, besides the original publications, the www-pages of the Stuttgart group of H. Stoll [136]. These offer input formats for different standard quantum chemistry codes such as MOLPRO [147], GAUSSIAN [50] and TURBOMOLE [2] and should be fairly complete, except for the SO terms. Similarly, energy-consistent PPs form QMC calculations are available from the www-pages of the Cologne group [16]. PP parameters and corresponding valence basis sets are also partly available from the data bases included in the above mentioned as well as other computer programs, although maybe not in the most up-to-date versions. In addition, due to the different acronyms and names used in programs and publications (e.g., Stuttgart–Dresden PPs (SDD) [50]; Stuttgart–Dresden-Bonn PPs (SDB) [83], Stuttgart–Bonn PPs [17, 21]; Stuttgart–Cologne PPs [19, 147]) it might be difficult for the user/reader to realize that identical approaches are used.

For convenience the most frequently used energy-consistent ab initio PPs and the corresponding valence basis sets are summarized in Table 6-1 for main group elements and Table 6-2 for transition metals, lanthanides and actinides. The groups in Stuttgart (Stoll), Cologne (Dolg) and also Auckland (Schwerdtfeger) are currently adjusting further small-core two-component relativistic energy-consistent PPs modelling DHF/DC+B data and try to fill the gaps for the heavierelements in

Table 6-1 Energy-consistent relativistic ab initio pseudopotentials and valence basis sets for main group elements[a]

Elements	Reference data	Core size	Ref.	Basis sets	Ref.	Comments
H-He	WB		[14]	cc-pVXZ (X = D,T,Q,5), seg., ANO CI	[14]	srel. "PPs" for QMC
B-F	WB	1s	[11]	(4s4p)/[2s2p], seg., HF	[11]	srel. PPs
Ne	HF,WB	1s	[96]	(7s7p)/[4s4p], seg., HF; +1d; +3d1f	[96]	nrel. and srel. PPs, SO, CPP
Li-Ne	WB	1s	[14]	cc-pVXZ (X = D,T,Q,5), seg., ANO CI	[14]	srel. PPs for QMC
Al-Cl	WB	1s-2p	[11]	(4s4p)/[2s2p], seg., HF	[11]	srel. PPs
Ar	HF,WB	1s-2p	[96]	(7s7p)/[4s4p], seg., HF; +1d; +3d1f	[96]	nrel. and srel. PPs, SO, CPP
Na-Ar	WB	1s-2p	[14]	cc-pVXZ (X = D,T,Q,5), seg., ANO CI	[14]	srel. PPs for QMC
Ga-Kr	DHF/DC+B	1s-2p	[86, 103]	(12s12p9d3f2g)/[6s6p4d3f2g], gen.	[86]	rel. PPs
				aug-cc-pVXZ (X = D,T,Q,5), gen., ANO CI	[101, 103]	
Ga-Br	WB	1s-3d	[11]	(4s4p)/[2s2p], seg., HF	[11]	srel. PPs
				cc-pVXZ (X = T,Q), seg., ANO CI	[83]	
Kr	HF,WB	1s-3d	[96]	(7s7p)/[4s4p], seg., HF; +1d; +3d1f	[96]	nrel. and srel. PPs, SO, CPP
				cc-pVXZ (X = T,Q), seg., ANO CI	[83]	
K, Ca; Ga-Kr	WB	1s-3p; 1s-3d	[14]	cc-pVXZ (X = D,T), seg., ANO CI	[14]	srel. PPs for QMC
In-Xe	DHF/DC+B	1s-3d	[86, 103]	(12s12p9d3f2g)/[6s6p4d3f2g], gen.	[86]	rel. PPs
				aug-cc-pVXZ (X = D,T,Q,5), gen., ANO CI	[101, 103]	
In-I	WB	1s-4f	[11]	(4s4p)/[2s2p], seg., HF	[11]	srel. PPs
				cc-pVXZ (X = T,Q), seg., ANO CI	[83]	
Xe	HF,WB	1s-4f	[96]	(7s7p)/[4s4p], seg., HF; +1d; +3d1f	[96]	nrel. and srel. PPs, SO, CPP
				cc-pVXZ (X = T,Q), seg., ANO CI	[83]	
Rb, Sr; In-Xe	WB	1s-4p; 1s-4d	[14]	cc-pVXZ (X = D,T), seg., ANO CI	[14]	srel. PPs for QMC
Tl-Rn	DHF/DC+B	1s-4f	[85, 86, 103]	(12s12p9d3f2g)/[6s6p4d3f2g], gen.	[85, 86]	rel. PPs
				aug-cc-pVXZ (X = D,T,Q,5), gen., ANO CI	[101, 103]	
Cs, Ba; Tl-Rn	WB	1s-4d5s5p; 1s-5d	[14]	cc-pVXZ (X = D,T), seg., ANO CI	[14]	srel. PPs for QMC
Tl-Rn	HF,WB	1s-5d	[76]	(4s4p), HF; +1d	[76]	nrel. and srel. PPs, SO, CPP

[a] DHF/DC+B-adjusted 9- and 10-valence electron PPs for group 1 (K-119) and group 2 (Ca-Ra) with quite large basis sets are also available [80, 81].
basis set: seg.: segmented contraction scheme; gen.: generalized contraction scheme.
pseudopotentials: nrel.: nonrelativistic; srel.: scalar-relativistic (one-component); rel.: relativistic (two-component).
SO: spin–orbit operator to be added to srel. PPs to be used in, e.g., in perturbation theory.
CPP: core-polarization potential.

Table 6-2 Energy-consistent relativistic ab initio pseudopotentials and valence basis sets for transition metals, lanthanides and actinides

Elements	Reference data	Core size	Ref.	Basis sets	Ref.	comments
Sc-Zn	HF,HF+DHF/DC	1s-2p	[35]	(8s7p6d)/[6s5p3d], seg., HF; +1f	[35]	nrel. and srel. PP
Sc-Cu	WB	1s-2p	[15]	cc-pVXZ (X = T,Q), gen., ANO CI	[15]	srel. PP for QMC
Sc-Ni	DHF/DC+B	1s-2p	[32]			rel. PP
Cu, Zn	DHF/DC+B	1s-2p	[47]	aug-cc-pwCVXZ (X = D,T,Q,5), gen., ANO CI	[102]	rel. PP
Y-Cd	HF,WB	1s-3d	[3]	(8s7p6d)/[6s5p3d], seg., HF; +1f	[3]	nrel. and srel. PP, SO
Y-Pd	DHF/DC+B	1s-3d	[104]	aug-cc-pwCVXZ (X = D,T,Q,5), gen., ANO CI	[104]	rel. PP
Ag, Cd	DHF/DC+B	1s-3d	[47]	aug-cc-pwCVXZ (X = D,T,Q,5), gen., ANO CI	[102]	rel. PP
Hf-Hg	HF,WB	1s-4f	[3]	(8s7p6d)/[6s5p3d], seg., HF; +1f	[3]	nrel. and srel. PP, SO
Hf-Pt	DHF/DC+B	1s-4f	[49]	aug-cc-pwCVXZ (X = D,T,Q,5), gen., ANO CI	[49]	rel. PP
Au, Hg	DHF/DC+B	1s-4f	[47]	aug-cc-pwCVXZ (X = D,T,Q,5), gen., ANO CI	[102]	rel. PP
111, 112	HF,DHF/DC+B	1s-5f	[127]	[9s7p7d4f], [10s7p7d4f]	[127]	nrel. and rel. PP
La-Lu	HF,WB	1s-3d	[36, 17]	(14s13p10d8f6g)/[6s6p5d4f3g], gen., ANO CI	[17]	nrel. and srel. PP, SO
				p-VQZ reducable to p-VTZ, p-VDZ		reduction by omitting contractions
				(14s13p10d8f6g)/[10s8p5d4f3g], seg., ANO CI	[18]	seg. basis set derived from gen. basis set
La-Lu	HF,WB	1s-4f^n	[37, 39, 143]	(7s6p5d)/[5s4p3d]; seg., HF; +1f/+2f	[37]	nrel. and srel. PP, CPP; modelling Ln(III)
				(8s7p6d)/[6s5p5d,5s4p4d],	[151]	
				(7s6p5d)/[6s5p4d,5s4p4d], seg., HF; sol.		

(continued)

Table 6-2 (continued)

Elements	Reference data	Core size	Ref.	Basis sets	Ref.	Comments
La-Yb	HF,WB	1s-4f^{n+1}	[37, 39, 143]	(7s6p5d)/[5s4p3d]; seg., HF; +1f/+2f	[37]	nrel. and srel. PP, CPP; modelling Ln(II)
Ce,Pr,Nd,Tb,Dy	WB	1s-4f^{n-1}	[62]	(6s5p4d,7s6p5d)/p-VXZ, X = D,T,Q, seg., HF; +2f1g; sol.	[62]	srel. PP; modelling Ln(IV)
Ac-Lr	HF,WB	1s-4f	[77, 21]	(12s11p10d8f)/[8s7p6d4f], seg., HF	[77]	nrel. and srel. PP, SO
				(14s13p10d8f6g)/[6s6p5d4f3g], gen., ANO CI	[21]	
				p-VQZ reducable to p-VTZ, p-VDZ		reduction by omitting contractions
				(14s13p10d8f6g)/[10s9p5d4f3g]	[19]	seg. basis set derived from gen. basis set
Ac-Lr	WB	1s-5f^{n}	[90]	(6s5p4d,7s6p5d,8s7p6d)/p-VXZ, X = D,T,Q, seg., X = D,T,Q, seg., HF; +2f1g; sol.	[90]	srel. PP, CPP; modelling An(III)
Th-Cf	WB	1s-5f^{n-1}	[91]	(6s5p4d,7s6p5d)/p-VXZ, X = D,T,Q, seg., X = D,T,Q, seg., HF; +2f1g; sol.	[91]	srel. PP, CPP; modelling An(IV)
Pu-No	WB	1s-5f^{n+1}	[91]	(6s5p4d,7s6p5d)/p-VXZ, X = D,T,Q, seg., X = D,T,Q, seg., HF; +2f1g; sol.	[91]	srel. PP, CPP; modelling An(II)

basis set: seg.: segmented contraction scheme; gen.: generalized contraction scheme; sol.: reduced basis sets for solid state calculations available.
pseudopotentials: nrel.: nonrelativistic; srel.: scalar-relativistic (one-component); rel.: relativistic (two-component).
SO: spin–orbit operator to be added to srel. PP to be used in, e.g., in perturbation theory.

the periodic table, including the lanthanides and actinides. It is hoped that these potentials are useful in quantum chemical calculations including SO effects from the outset, i.e., already at the HF level.

6.4. OTHER EFFECTIVE CORE POTENTIAL METHODS

In the following we briefly outline some other effective core potential (ECP) approaches which are in use besides the energy-consistent pseudopotential (PP) method.

6.4.1. Shape-Consistent Pseudopotentials

In contrast to the method of energy-consistent pseudopotentials (PPs) where quantum mechanical observables such as all-electron (AE) total valence energies are used as reference data for the adjustment, quantities defined within an effective one-electron picture, i.e., AE valence orbitals and orbital energies, are taken as reference data for the method of shape-consistent PPs [24, 40]. In the shape-consistent PP approach the pseudo-valence orbital φ_p is required to retain the correct radial distribution of charge given by the AE valence orbital φ_v in the valence region outside a critical radius r_c and the corresponding PP pseudo-valence orbital energy ε_p is set equal to the AE valence orbital energy ε_v, i.e., for a given lj one requires that

$$\varphi_{p,lj}(r) = \begin{cases} \varphi_{v,lj}(r) \text{ for } r \geq r_c \\ f_{lj}(r) \text{ for } r < r_c \end{cases} \qquad \text{and} \qquad \varepsilon_{p,lj} = \varepsilon_{v,lj} \quad (6\text{-}43)$$

The auxiliary function f_{lj} is required to be radially nodeless and smooth in the core region ($r < r_c$). Except for the normalization and continuity conditions for the $\varphi_{p,lj}(r)$ the choice of r_c as well as the choice of f_{lj} is in certain limits arbitrary and a matter of experience.

For the $\varphi_{p,lj}$ defined in Eq. (6-43) the shape-consistent PP $\Delta\hat{V}_{cv}$ has to be constructed which, when inserted into the valence Hamiltonian $\hat{H}_v$, Eq. (6-16), should yield the $\varphi_{p,lj}$ as HF orbitals for the chosen atomic reference state. By using the semi-local PPs defined in Eq. (6-23), i.e., restricting the $\Delta\hat{V}_{cv}$ to the form of a radially multiplicative potential $V_{lj}(r)$ for each lj-set, a radial Fock equation can be set up

$$[-\frac{1}{2}\frac{d^2}{dr^2} + \frac{l(l+1)}{2r^2} + V_{lj}^{PP}(r) + \hat{W}_{p,lj}(\{\varphi_{p',l'j'}\})]|\varphi_{p,lj}(r) >= \varepsilon_{v,lj}|\varphi_{p,lj}(r) > \quad (6\text{-}44)$$

The first two terms in the parentheses are the radial kinetic energy operator, the term $\hat{W}_{p,lj}$ stands for an effective valence Coulomb and exchange potential for $\varphi_{p,lj}$. With a given $\varphi_{p,lj}$ and $\varepsilon_{v,lj}$, $V_{lj}^{PP}(r)$ can be determined pointwise by inversion. Relativistic effects are implicitly included in V_{lj}^{PP} since the AE reference calculation explicitly describes these effects. Repeating this procedure for each

lj-set, the resulting potentials V_{lj}^{PP} are tabulated on a grid and are usually fitted by means of a least-squares criterion to a linear combination of Gaussian functions according to

$$\hat{\tilde{V}}^{PP}(\mathbf{r}_i) = -\frac{Q}{r} + \sum_{lj}\left(\sum_k A_{lj,k} r^{n_{lj,k}-2} e^{-\alpha_{lj,k} r^2}\right)\hat{P}_{lj} \,. \tag{6-45}$$

The separation into scalar-relativistic and spin–orbit (SO) potentials, $\Delta\hat{V}_{cv,av}$ and $\Delta\hat{V}_{cv,so}$, according to Eq. (6-28) is the same as we have discussed in Section 6.2.3 and 6.2.5. Shape-consistent PPs including SO operators based on single-configuration Dirac–Hartree–Fock (DHF) AE calculations using the Dirac–Coulomb (DC) Hamiltonian have been generated by Christiansen, Ermler and coworkers [12, 43, 44, 61, 78, 98, 95, 115, 116, 149].

A very popular set for main group and transition elements based on scalar-relativistic Cowan–Griffin (CG) AE calculations [25] was published by Hay and Wadt [57, 58, 142]. Their recently revised basis sets [117] are especially suitable for density functional theory (DFT) investigations. In their procedure for obtaining PPs the r_c is chosen to be near the outermost maximum of the φ_l and the following radial function f_l is adopted for $r < r_c$

$$f_l(r) = r^b(a_0 + a_1 r + a_2 r^2 + a_3 r^3 + a_4 r^4) \tag{6-46}$$

$b = l + 3$ in the non-relativistic case, and $b = \lambda + 2$ in the relativistic case, where

$$\lambda + 1 = \frac{1}{2}(1 - \delta_{0,l}) + \sqrt{l(l+1) + \frac{1}{4}(1 + \delta_{l,0})^2 + (\alpha Z)^2} \tag{6-47}$$

and α is the fine structure constant. For relativistic s orbitals the choices of $b = \lambda + 3$ and f as 6th degree polynomial have been found to lead to smoother s pseudo-orbitals. The five coefficients a_i are determined by requiring that

1. $\varphi_p(r)$ remains normalized.
2. $f_l(r)$ and its first three derivatives match φ_v and its first three derivatives at r_c.

For subsequent usage in molecular valence-only calculations compact valence basis sets were generated, i.e., the pseudo-valence orbitals were fitted by using a nonlinear least-squares procedure, similar to the one for fitting the potentials, to a linear combination of Gaussian functions, i.e.,

$$\varphi_{p,l} = \sum_i C_i r^l e^{-\alpha_i r^2} \tag{6-48}$$

In order to arrive at more compact Gaussian expansions for $\hat{\tilde{V}}^{PP}$ the Toulouse group [8] proposed a quite useful criterion, i.e., the minimization of the following operator norm

$$||\hat{\mathcal{O}}|| = < \varphi_{p,lj} | \hat{\mathcal{O}}^2 | \varphi_{p,lj} >^{1/2} \quad \text{with} \tag{6-49}$$

$$\hat{\mathcal{O}} = \tilde{\varepsilon}_{v,lj} | \tilde{\varphi}_{p,lj} >< \tilde{\varphi}_{p,lj} | - \varepsilon_{v,lj} | \varphi_{p,lj} >< \varphi_{p,lj} | \, . \tag{6-50}$$

Here the quantities without tilde are obtained with the exact V_{lj}^{PP} tabulated on a grid from the radial Fock equation (6-44), whereas those with tilde are calculated with the analytical potential $\tilde{V}_{lj}^{PP}$. Typically only three or less terms per lj combination are needed, the overlap $< \tilde{\varphi}_{p,lj} | \varphi_{p,lj} >$ deviates from 1 by less than 10^{-5} and the eigenvalue difference $\tilde{\varepsilon}_{v,lj} - \varepsilon_{v,lj}$ is less than 10^{-3} Hartree. An almost complete set of shape-consistent PPs using this prescription, based also on DHF AE calculations applying the DC Hamiltonian for the heavier atoms, has been published by Stevens and coworkers [26, 131, 132].

Small cores have to be used in case of transition metals, lanthanides and actinides in order to keep frozen-core errors in PP calculations below a required accuracy. For small cores, however, more than a single occupied pseudo-valence orbital of the same lj combination may be present in suitable reference states. Therefore one or more pseudo-valence orbitals may have a radial node, which leads to singularities in the PP if it is determined by inversion of the Fock equation (6-44). Most shape-consistent PPs are derived for positive ions, which are chosen in such a way that this problem can not occur. If the ions are sufficiently highly charged this has the disadvantage that frozen-core (FC) errors arise for the derived PP when transferring it from the ions to the neutral atom or molecule. A possible solution to this problem is attempted in the so-called generalized relativistic ECP (GRECP) approach of Titov, Mosyagin, and coworkers [92, 138–140]. The GRECPs combine the standard semilocal form of the PPs with additional nonlocal terms to take into account the difference between the effective potentials acting on the outer core and valence electrons with the same l and j quantum numbers. A number of GRECPs accounting also for contributions of the Breit interaction have been published recently for U, Pu, and the superheavy elements 112, 113, 114 [93]. Since the GRECP ansatz is at present not supported by most of the standard quantum chemistry codes, it is interesting to check if the addition of a nonlocal term to the standard semilocal PP ansatz will yield clear benefits with respect to accuracy (see also Section 6.5 for a comparison).

6.4.2. Model Potential Method

Another important category of ECP methods is called the model potential (MP) method and was originally proposed by Bonifacic and Huzinaga [13]. It originated from the so-called Huzinaga–Cantu equation [63, 64]

$$[\hat{H}_{eff} + \sum_{c} (-2\varepsilon_c) | \varphi_c >< \varphi_c |] | \varphi_v >= \varepsilon_v | \varphi_v > \tag{6-51}$$

Here $\hat{H}_{eff}$ again denotes an (effective) one-electron Hamiltonian, e.g., a Fock operator, and the valence function $|\varphi_v>$ and the core functions $|\varphi_c>$ fulfill the conditions defined in Eqs. (6-1) and (6-2). The sum over projection operators guarantees that the eigenvalues of the core orbitals $|\varphi_c>$ appear at an energy $-\varepsilon_c > 0$ in the spectrum, i.e., at higher energies than the valence orbital eigenvalues. The Huzinaga–Cantu equation is very similar to the Phillips–Kleinman equation, Eqs. (6-7) and (6-8), but one must observe that the pseudo-orbital $|\varphi_p>$ in the Phillips–Kleinmann equation does not necessarily have radial nodes (cf. Section 6.2.2), whereas the valence orbital $|\varphi_v>$ in the Huzinaga–Cantu equation keeps its correct nodal structure. Of course valence basis sets applied in MP calculations should be able to represent the nodal structure correctly and thus are usually larger than those used in PP calculations.

For an atom with core charge Q and n_v valence electrons ($Q = Z - n_v$, with Z being the nuclear charge) the valence-electron model Hamiltonian is given by

$$\hat{H}_v = -\frac{1}{2}\sum_i^{n_v} \nabla_i^2 + \sum_i^{n_v}\sum_{j>i}^{n_v} \hat{g}(i,j) - \sum_i^{n_v} \frac{Q}{r_i} + \sum_i^{n_v} [\Delta\hat{V}_C(i) + \Delta\hat{V}_X(i)] \quad (6\text{-}52)$$

with $\Delta\hat{V}_C(i)$ being the Coulomb (C) interaction between the core and the valence electrons

$$\Delta\hat{V}_C(i) = -\frac{n_c}{r_i} + 2\sum_c \hat{J}_c(i) \quad (6\text{-}53)$$

and $\Delta\hat{V}_X(i)$ representing the core-valence exchange (X) interaction

$$\Delta\hat{V}_X(i) = -\sum_c \hat{K}_c(i) \quad (6\text{-}54)$$

$\hat{J}_c(i)$ and $\hat{K}_c(i)$ stand for the usual Coulomb and exchange operators related to the core orbital $|\varphi_c>$. In order to prevent the valence electrons from collapsing into the core the projection/shift operator $\hat{P}(i)$ has to be included in the last sum of the Hamiltonian $\hat{H}_v$ of Eq. (6-52)

$$\hat{P}(i) = \sum_c (-2\varepsilon_c)|\varphi_c(i)><\varphi_c(i)| \quad (6\text{-}55)$$

Defining the model potential (MP) $\hat{V}_{MP}(i)$ for electron i as

$$\hat{V}^{MP}(i) = \Delta\hat{V}_C(i) + \Delta\hat{V}_X(i) + \hat{P}(i) \quad (6\text{-}56)$$

one obtains the atomic valence-electron model Hamiltonian

$$\hat{H}_v^{MP} = -\frac{1}{2}\sum_i^{n_v} \nabla_i^2 + \sum_i^{n_v}\sum_{j>i}^{n_v} \hat{g}(i,j) - \sum_i^{n_v} \frac{Q}{r_i} + \sum_i^{n_v} \hat{V}_{MP}(i) \quad (6\text{-}57)$$

A molecular MP is considered to contain an assembly of non-overlapping core levels, and thus the molecular valence-electron model Hamiltonian may be written as [74]

$$H_v^{\hat{M}P} = -\frac{1}{2}\sum_i^{n_v}\nabla_i^2 + \sum_i^{n_v}\sum_{j>i}^{n_v}\hat{g}(i,j) + \sum_{\lambda<\mu}\frac{Q_\lambda Q_\mu}{r_{\lambda\mu}} + \sum_i\sum_\lambda[-\frac{Q^\lambda}{r_{\lambda i}} + \hat{V}^{MP,\lambda}(i)] \tag{6-58}$$

where the terms in $\hat{V}^{MP,\lambda}(i)$ are the analogues for the core λ of the corresponding terms in Eqs. (6-56) and (6-55).

Due to the different choices of the analytical form of $\hat{V}^{MP,\lambda}(i)$ there are three versions of the MP approach in current use [65, 73, 118, 119]. Readers interested in further details are recommended to read the review articles written by Klobukowski, Huzinaga and Sakai [74] as well as by Seijo and Barandiarán [126].

Probably the most successful and widely used variant of the MP method are the "ab initio model potentials" (AIMP) of Huzinaga, Seijo, Barandiarán and coworkers [65]. These authors have suggested a linear combination of Gaussians with prefactors $1/r$, i.e., a local spherically symmetric model potential, to represent the Coulomb core-valence interaction, $\Delta\hat{V}_C^\lambda(\mathbf{r}_i)$

$$\Delta\hat{V}_C^\lambda(\mathbf{r}_i) = \Delta V_C^\lambda(r_{\lambda i}) = \frac{1}{r_{\lambda i}}\sum_k C_k^\lambda e^{-\alpha_k^\lambda r_{\lambda i}^2} \tag{6-59}$$

The exponents α_k^λ and coefficients C_k^λ are adjusted to the all-electron (AE) potential in a least-squares sense under the constraint that $\sum_k C_k^\lambda = Z_\lambda - Q_\lambda = n_c^\lambda$ in order to enforce the correct asymptotic behavior of the MP. Since the evaluation of integrals over such a local potential is not costly, essentially any desired accuracy can be easily achieved by using a sufficiently long expansion.

The nonlocal exchange part $\Delta\hat{V}_X^\lambda(i)$ is substituted by its spectral representation in the space defined by a set of functions χ_p^λ centered on core λ

$$\Delta\hat{V}_X^\lambda(\mathbf{r}_i) = \sum_{p,q}|\chi_p^\lambda(i) > A_{pq}^\lambda < \chi_q^\lambda(i)| \tag{6-60}$$

It should be noted that this model potential operator yields the same one-center integrals as the true AE core-exchange operator as long as the basis functions can be represented by the set of the χ_p^λ. Two- and three-center integrals are approximated. Since, in contrast to the Coulomb part, the exchange part is short-ranged, only a moderate number of functions χ_p^λ is needed and the one-center approximation is expected to be very good, at least for not too large cores. In practical applications the basis used in the spectral representation is chosen to be identical to the primitive functions of the valence basis set used for the atom under consideration and the A_{pq}^λ are calculated during the input processing of each AIMP calculation.

The core shifting operator $\hat{P}(i)$ is kept as it stands in Eq. (6-55). For practical calculations the core orbitals $|\varphi_c>$ are represented by sufficiently large (AE) basis sets.

For taking into account SO coupling a one-electron SO operator, which is a representation of the AE WB SO operator [150], is added to the AIMPs [126]

$$\Delta\hat{V}^{\lambda}_{cv,so}(\mathbf{r}_i) = \sum_l (\sum_k \frac{B^{\lambda}_{lk}}{r^2_{\lambda i}} e^{-\beta^{\lambda}_{lk} r^2_{\lambda i}}) \hat{P}^{\lambda}_l(i) \hat{\mathbf{l}}_{\lambda i} \cdot \hat{\mathbf{s}}_i \hat{P}^{\lambda}_l(i) \tag{6-61}$$

where $\hat{\mathbf{l}}_{\lambda i} = \hat{\mathbf{r}}_{\lambda i} \times \hat{\mathbf{p}}_i$ and $\hat{\mathbf{s}}_i$ denote the operators of orbital angular momentum and spin, respectively. $\hat{P}^{\lambda}_l$ stands for the projection operator onto the subspace of angular quantum number l with respect to core λ. The coefficients B^{λ}_{lk} and exponents β^{λ}_{lk} are determined by means of a least-squares fit to the radial components of the WB SO term.

Recently AIMPs for explicit usage of the second- and third-order Douglas–Kroll–Hess (DKH) approximation in the valence have been developed for transition metals [113, 114] and lanthanides as well as actinides [99, 141], respectively. A corresponding SO treatment using the DKH-type atomic mean-field approximation in a state-interaction method was also proposed [100].

6.4.3. DFT-Based Effective Core Potentials

Although the ab initio ECPs introduced above were adjusted to wavefunction-based AE HF or DHF reference data, they also perform quite well when combined with various DFT methods, especially when a small core is used. Nevertheless several DFT-based ECP sets have been worked out too [4–6, 27, 54].

We start with a brief introduction to the DFT-based MP method advocated by Andzelm et al. [4] for usage in combination with the LSD-VWN approach. Starting from the Kohn–Sham (KS) equations for a spin-polarized system of n_v valence electrons and assuming orthogonality between valence φ^{σ}_v and core orbitals φ^{σ}_c of spin σ ($\sigma = +, -$), one can rewrite the Huzinaga–Cantu equation (6-51) as

$$[\hat{F}^{\sigma} + \sum_c (-2\varepsilon^{\sigma}_c)|\varphi^{\sigma}_c >< \varphi^{\sigma}_c|]|\varphi^{\sigma}_v >= \varepsilon^{\sigma}_v|\varphi^{\sigma}_v > \tag{6-62}$$

where

$$\hat{F}^{\sigma} = \hat{F}^{\sigma}_v + \Delta\hat{V}^{\sigma,MP} \tag{6-63}$$

and

$$\hat{F}^{\sigma}_v(\mathbf{r}) = -\frac{1}{2}\nabla^2 - \sum_{\lambda} \frac{Q_{\lambda}}{r_{\lambda}} + \int \frac{\rho_v(\mathbf{r}')d\mathbf{r}'}{|\mathbf{r} - \mathbf{r}'|} + v_{xc}[\rho_{+,v}, \rho_{-,v}] \tag{6-64}$$

Q_λ is the charge of core λ, $\rho_{+,v}$ and $\rho_{-,v}$ denote the spin-up and spin-down densities for the valence orbitals, $\rho_v = \rho_{+,v} + \rho_{-,v}$, and v_{xc} represents the exchange-correlation potential. The density $\rho_{\sigma,v}$ is defined in terms of the valence orbitals φ_i^σ

$$\rho_{\sigma,v}(\mathbf{r}) = \sum_i^{n_v} f_i^\sigma |\varphi_i^\sigma(\mathbf{r})|^2 \tag{6-65}$$

where f_i^σ is an occupation number. The model potential $\hat{V}^{\sigma,MP}$ is defined as

$$\hat{V}^{\sigma,MP} = \Delta\hat{V}^{\sigma,MP} + \hat{P} \tag{6-66}$$

$$\hat{P} = \sum_c (-2\varepsilon_c^\sigma)|\varphi_c^\sigma >< \varphi_c^\sigma| \tag{6-67}$$

We suppose that the frozen-core approximation is valid here, i.e., the core orbitals of the atoms do not overlap with each other and that cross terms in the exchange and correlation potentials can be neglected. Then $\hat{V}^{\sigma,MP}$ may be written as a sum over the atomic MPs $\hat{V}_\lambda^{\sigma,MP}$

$$\hat{V}^{\sigma,MP} = \sum_\lambda \hat{V}_\lambda^{\sigma,MP} = \sum_\lambda (\Delta\hat{V}_\lambda^{\sigma,MP} + \hat{P}_\lambda) \tag{6-68}$$

where

$$\Delta\hat{V}_\lambda^{\sigma,MP} = -\frac{n_c^\lambda}{r_\lambda} + \int \frac{\rho_c^\lambda(\mathbf{r}')d\mathbf{r}'}{|\mathbf{r}-\mathbf{r}'|} + v_{xc}[\rho_{+,c}^\lambda, \rho_{-,c}^\lambda] \tag{6-69}$$

The analytical expression for $\Delta\hat{V}_\lambda^{\sigma,MP}$ may be written as [4]

$$\Delta\hat{V}_\lambda^{\sigma,MP} = \sum_k A_k^\lambda \frac{e^{-\alpha_k^\lambda r^2}}{r} \tag{6-70}$$

with the constraint $\sum_k A_k^\lambda = Z^\lambda - Q^\lambda = n_c^\lambda$ enforcing the correct asymptotic behavior. The core orbitals for the projection operator $\hat{P}_\lambda$ are approximated by a least squares fit procedure using an expansion of Gaussian functions. The reference atomic orbitals were obtained from CG/WB-type [25] LSD-VWN finite-difference atomic calculations.

Similarly, one can apply the ab initio shape-consistent PP generation procedure to derive DFT-based PPs. For a prototype atomic configuration the method yields the $\varphi_{p,lj}$ as radial KS orbitals, at the original AE orbital energies $\varepsilon_{v,lj}$. When both scattering-type partial waves and bound states are considered Hamann, Schlüter, and Chiang (HSC) required that pseudo partial waves have to exhibit the so-called norm-conserving properties [56], i.e.,

1. The AE and pseudo valence eigenvalues agree.
2. The AE and pseudo valence wavefunctions agree for $r > r_c$.
3. The integrals from 0 to r of the AE and pseudo valence charge densities agree for $r > r_c$.
4. The logarithmic derivatives of the AE and pseudo valence partial waves and their first energy derivatives agree for $r > r_c$.

In the local density functional framework Bachelet, Hamann and Schlüter have published relativistic PPs for H through Pu [5, 6]. When only bound states are considered the norm-conservation requirements are related and can be replaced by a simplified set of conditions essentially corresponding to the ones for shape-consistency defined in Eq. (6-43). Considering only bound states Delley presented so-called density functional semi-core PPs (DSPP) for all elements from H to Am for use with local orbital methods [27]. The DSPPs are based on a minimization of errors with respect to the norm conservation conditions for two to three relevant ionic configurations of the atom (hardness conservation). The primary density functional used to define the AE reference data was the Perdew–Burke–Ernzerhof (PBE) gradient corrected functional, but DSPPs optimized for both the PBE functional as well as the local density approximation (LDA) using the Perdew–Wang local correlation were also generated. In order to improve the numerical stability and transferability a model core density is added (non-linear core correction) [27, 82]. Delley concludes that the PP approximation is less severe than the approximations made in DFT, however his results shed some doubt on the common practise to use ab initio adjusted ECPs also within DFT.

6.5. EXAMPLE: URANIUM

After the previous discussion of the effective core potential (ECP) approaches in general, we want to go through one example for the generation of relativistic energy-consistent ab initio pseudopotentials (PPs) and the accompanying energy-optimized valence basis sets explicitly. For this purpose we selected one of the most interesting elements for a theoretician, i.e., the uranium atom. This choice is motivated mainly by the large relativistic effects observed for this heavy atom, the high complexity of its electronic structure due to the presence of open d and f shells already in the atomic ground state and the possibility to adjust PPs with entirely different core definitions as well as different ranges of applicability, i.e., 5f-in-valence as well as 5f-in-core PPs. We hope that the detailed description given here will provide the reader with a deeper understanding of the previous sections of this contribution. Our discussion is concluded by a brief summary of selected recent applications using the described PPs and basis sets, highlighting their reliability but also stating their limitations.

6.5.1. Choice of the Reference Data

We begin with a discussion of the reference data to be used in the PP adjustment, i.e., the relativistic computational model we want to parametrize. We restrict ourselves to multi-configuration (MC) Dirac–Hartree–Fock/Dirac–Coulomb (DHF/DC) and Dirac–Coulomb–Breit (DHF/DC+B) as well as Wood–Boring (WB) all-electron (AE) reference data. In Table 6-3 results from relativistic AE DHF calculations applying the DC Hamiltonian for the neutral to sixfold positively charged uranium atom are listed in the first data column. The DC Hamiltonian is a standard approximation used in four-component relativistic AE calculations for atoms, molecules and solids which captures the most important relativistic contributions for chemical investigations and thus it is a convenient starting point for our discussion. Several sets of PPs, e.g., the shape-consistent PPs by Christiansen and coworkers [24, 43], have been adjusted to DHF/DC reference data. The energy differences in Table 6-3 refer to the averages over all J-levels (included in the MC treatment) of the listed non-relativistic configurations. Only the energetically lowest configuration of each charge state and possible 5f occupation is listed. Note that the entries are ordered according to increasing 5f occupation, and for each 5f occupation according to increasing 6d occupation.

The second data column gives the deviations of non-relativistic Hartree–Fock (HF) results [51] from the MCDHF/DC reference data [41], i.e., differential 'non-relativistic' contributions. We note that states with high 5f occupancy are lowered and those with lower 5f occupancy are raised in energy when going from a relativistic to a non-relativistic description. The reason are dominating indirect relativistic effects which destabilize and expand the 5f shell when relativity is switched on. For a given 5f occupation a similar albeit less pronounced behavior is observed for the 6d shell, which is less affected by dominating indirect relativistic effects. Finally, for a given 5f and 6d occupation the configurations with a lower 7s occupation are more lowered in energy than those with a high one when going from a relativistic to a non-relativistic description. Here direct relativistic effects dominate, stabilize and contract the 7s shell when relativity is switched on. A closer look at the table reveals that uranium would probably have a [Rn] $5f^4\ 7s^2$ ground state configuration, i.e., in a non-relativistic world uranium would be preferably divalent (as also the lanthanides and the other actinides), with low-lying mono- and trivalent oxidation states.

In the third data column the deviations of scalar-relativistic one-component WB results from the MCDHF/DC reference data are listed. The WB approach [150], as well as the closely related Cowan–Griffin (CG) approach [25], was used for a large number of PPs and model potentials (MPs) as reference data, e.g., PPs of Hay and Wadt [57, 58, 142] or the 'Stuttgart' group [30, 135] as well as MPs of Seijo and coworkers [126]. In contrast to the four-component MCDHF scheme the WB approach allows to extract reference data for scalar-relativistic ECPs in the LS coupling scheme. Analyzing the data listed in Table 6-3 we learn that although the method captures to a large extent the relativistic contributions, it introduces some inaccuracies especially when the 5f occupation is changed and leads to smaller errors when for a fixed 5f occupation the charge state is changed.

Table 6-3 Relative point nucleus (pn) Dirac–Hartree–Fock/Dirac–Coulomb (DHF/DC) energies ΔE (eV) of the 2J+1-weighted average of all J levels belonging to a nonrelativistic configuration with respect to the energy of the U [Rn] $5f^3 6d^1 7s^2$ ground state configuration. For each 5f occupation number only the energetically lowest configuration for each ionization level is listed. Deviations (eV) from the DHF/DC pn data are given for nonrelativistic Hartree–Fock (HF) and scalar-relativistic Wood-Boring (WB) pn calculations. Contributions of the Breit interaction (→B) at the DHF/DC pn level as well as of a finite nucleus (→fn) with a Fermi charge distribution at the DHF/DC+B level are also listed

Charge	Configuration			ΔE	Deviation		Contribution	
	5f	6d	7s	DHF DC,pn	HF pn	WB pn	DHF DC,pn →B	DHF DC+B →fn
6+				167.9498	22.6562	1.1844	0.3263	0.0246
5+	1			118.1617	20.5056	1.0225	0.3208	0.0179
4+	2			78.6962	18.5789	0.8886	0.3138	0.0124
3+	3			49.0026	16.9078	0.7795	0.3061	0.0079
2+	4			28.4542	15.5332	0.6999	0.2984	0.0045
1+	4	1		16.0181	17.6511	0.7258	0.3111	0.0217
0	4	2		9.7540	19.0413	0.7549	0.3200	0.0337
5+	1			107.4044	13.7992	0.7393	0.1997	0.0084
4+	1	1		69.4125	11.9319	0.6044	0.1942	0.0030
3+	1	2		41.0364	10.3181	0.4994	0.1878	−0.0014
2+	1	3		21.6260	9.0010	0.4226	0.1812	−0.0046
1+	1	3	1	9.6394	10.9340	0.4456	0.1929	0.0111
0	1	3	2	3.6701	12.1736	0.4714	0.2007	0.0218
4+	2			62.9423	5.7708	0.3564	0.0850	−0.0058
3+	2	1		35.8785	4.2312	0.2524	0.0804	−0.0100
2+	2	1	1	17.5395	6.3608	0.2596	0.0938	0.0071
1+	2	1	2	5.7548	7.8467	0.2722	0.1031	0.0194
0	2	2	2	0.4682	5.8033	0.2236	0.0933	0.0105
3+	3			33.3768	−1.2986	0.0278	−0.0147	−0.0178
2+	3		1	15.7154	0.6234	0.0334	−0.0015	−0.0023
1+	3		2	4.4832	1.9041	0.0435	0.0073	0.0084
0	3	1	2	0.0000	0.0000	0.0000	0.0000	0.0000
2+	4			17.2536	−7.1634	−0.2183	−0.0932	−0.0268
1+	4		1	6.8681	−5.8095	−0.1977	−0.0817	−0.0156
0	4		2	2.0435	−5.1113	−0.1784	−0.0749	−0.0094
1+	5			12.5023	−11.2231	−0.3303	−0.1358	−0.0313
0	5		1	8.1022	−10.2666	−0.2698	−0.1171	−0.0231

The fourth data column lists the contributions of the Breit interaction, in its frequency-dependent form as implemented in the GRASP1 [41] atomic structure package, evaluated in first-order perturbation theory based on a MCDHF solution obtained with the DC Hamiltonian (denoted as DC+B). We see that these contributions, which are often omitted or only partly taken into account in molecular AE calculations, i.e., in form of the Gaunt interaction (accounting for the magnetic interaction, but neglecting retardation terms), are non-negligible if a good accuracy is aimed at. In fact the WB (and probably also the CG) approach accidentally agree better with results obtained with the DCB Hamiltonian than with the DC Hamiltonian. Test calculations on U and U^+ revealed that the self-consistent treatment of the Breit term (denoted as DCB) makes only contributions to relative energies as listed in Table 6-3 of at most 0.0005 eV [93], i.e., a perturbative treatment (denoted as DC+B) is sufficiently accurate to generate AE reference data for PP adjustments.

Finally, in the fifth data column the contributions of a finite nuclear model, i.e., a Fermi nuclear charge distribution, are listed. These contributions are quite small and possibly the effect of the nuclear model is of little importance for studies of the valence electronic structure, which is the goal of ECP methods. For the time being we assume that contributions arising from quantum electrodynamics are smaller than those of the nuclear model and thus can be neglected when constructing a valence model Hamiltonian aiming at chemical accuracy, i.e., 1 kcal/mol (0.04 eV). The more recent so-called 'Stuttgart' energy-consistent relativistic PPs rely on reference data obtained at the MCDHF/DC+B level applying a finite nuclear model.

6.5.2. Choice of the Core

Let us continue the discussion with the choice of the core, where in case of uranium we essentially have three possibilities: small, medium and large. Since the frozen-core (FC) approximation is underlying the PP approach, one might expect that the choice of the PP core can be guided by relativistic atomic FC AE calculations. In case of uranium results of such calculations, carried out at the state-averaged MCDHF/DC level, are available from literature [20]. Here we present in Table 6-4 a slightly extended tabulation for the same configurations as listed in Table 6-3.

We tacitly assume that the conclusions about FC errors arrived for the DC Hamiltonian will essentially be valid for other Hamiltonians too.

The frozen core in our example was taken from a state-averaged MCDHF/DC calculation for the U [Rn] $5f^3 6d^1 7s^2$ ground state configuration, i.e., our conclusions with respect to FC errors will have to take into account a bias favoring configurations of the neutral atom with a $5f^3$ occupation. Clearly, in order to achieve computational savings one desires to have a core as large as possible. If we look at Table 6-4 we observe that treating U with only 6 valence electrons (Q = 6), i.e., assuming a large core (1s-5d, 6s, 6p) in line with qualitative chemical models, quantitatively leads to FC errors of up to 0.35 eV when staying within configurations with a $5f^3$ occupation. In comparison to this a medium-sized core (1s-5d), attributing the

Table 6-4 Relative energies (eV) of the 2J+1-weighted average of all J levels belonging to a nonrelativistic configuration of U with respect to the U [Rn] $5f^3 6d^1 7s^2$ ground state configuration from all-electron (AE) point nucleus (pn) state-averaged multi-configuration Dirac–Hartree–Fock (DHF) calculations using the Dirac–Coulomb (DC) Hamiltonian. Frozen-core errors (eV) are listed for three choices of the core (core charges Q = 32, 14, 6) treating the 5f shell in the valence adapted from the neutral U atom in its [Rn] $5f^3 6d^1 7s^2$ ground state configuration. The last column lists frozen-core errors for a core including the partially occupied 5f shell taken from the lowest energy configuration with the same 5f occupancy (core charge $Q = 14 - n_{5f}$, with the 5f occupation number n_{5f})

Charge	Configuration			AE DHF	Frozen-core error			
	5f	6d	7s	DC,pn	Q = 32	Q = 14	Q = 6	$Q = 14 - n_{5f}$
6+				167.9498	0.0077	1.2479	15.4283	0.0059
5+		1		118.1617	0.0058	1.0291	11.3885	0.0129
4+		2		78.6962	0.0048	0.8850	8.2895	0.0040
3+		3		49.0026	0.0043	0.7963	6.0066	0.0013
2+		4		28.4542	0.0040	0.7488	4.4237	0.0010
1+		4	1	16.0181	0.0039	0.7379	3.8610	0.0002
0		4	2	9.7540	0.0038	0.7365	3.5686	0.0000
5+	1			107.4044	0.0021	0.4545	7.1973	0.1523
4+	1	1		69.4125	0.0014	0.3779	4.8002	0.0626
3+	1	2		41.0364	0.0014	0.3359	3.1180	0.0175
2+	1	3		21.6260	0.0013	0.3179	2.0282	0.0023
1+	1	3	1	9.6394	0.0013	0.3082	1.6778	0.0003
0	1	3	2	3.6701	0.0013	0.3046	1.5126	0.0000
4+	2			62.9423	0.0003	0.0886	2.3845	0.1796
3+	2	1		35.8785	0.0002	0.0765	1.2558	0.0535
2+	2	1	1	17.5395	0.0002	0.0682	0.8277	0.0260
1+	2	1	2	5.7548	0.0001	0.0636	0.5841	0.0126
0	2	2	2	0.4682	0.0002	0.0678	0.3493	0.0000
3+	3			33.3768	0.0000	0.0006	0.3479	0.1458
2+	3		1	15.7154	0.0000	0.0006	0.1366	0.0698
1+	3		2	4.4832	0.0000	0.0009	0.0412	0.0306
0	3	1	2	0.0000	0.0000	0.0000	0.0000	0.0000
2+	4			17.2536	0.0002	0.0467	0.2082	−0.0399
1+	4		1	6.8681	0.0001	0.0450	0.2224	−0.0193
0	4		2	2.0435	0.0002	0.0426	0.2430	0.0000
1+	5			12.5023	0.0004	0.0945	0.6651	0.1921
0	5		1	8.1022	0.0004	0.0761	0.5418	0.0000

Frozen cores: U Q = 6: 1s-5d, 6s, 6p; Q = 14: 1s-5d; Q = 32: 1s-4d; $Q = 14 - n_{5f}$: 1s-5f.

6s and 6p semi-core orbitals to the valence shell, which now comprises 14 valence electrons (Q = 14), yields negligible FC errors below 0.001 eV as does a small core (1s-4f) treating 32 electrons in the valence (Q = 32).

Clearly, if we stay within configurations with a U $5f^3$ occupation the medium-core approximation or even the large-core approximation will be sufficiently accurate, as judged from these results. One of the chemically interesting features of the early actinides however is their ability to adopt various oxidation states, which correspond to different 5f occupation numbers in the independent particle picture such as the DHF approach. Decreasing the 5f occupation by one to $5f^2$ or increasing it by one to $5f^4$ shows that the chemically motivated choice of a large core leads to FC errors of up to 2.4 eV, i.e., this approximation is more or less useless for quantitative investigations and ECPs using it are probably bound to fail. Especially large errors occur for the chemically interesting differences between tri- and tetravalent uranium. For the medium-core case the FC errors are clearly below 0.1 eV and still might be acceptable for studies aiming at chemical accuracy. If an accuracy better than 0.1 eV is desired, the small-core approximation leading to errors smaller than 0.001 eV has to be used.

The conclusions drawn for a comparison of the $5f^3$, $5f^2$ and $5f^4$ occupied configurations are supported by the results for the configurations with two or three electrons removed from the 5f shell, i.e., $5f^1$ or $5f^0$, or two electrons added to the 5f shell, i.e., $5f^5$, with respect to the ground state configuration. Especially in the chemically important cases corresponding to penta- and hexavalent uranium the FC errors for the chemically motivated large-core approximation are huge and amount to several electron volts. Even the medium-core approximation exhibits 5f occupation dependent errors of up to about 1.25 eV. Thus, the whole variety of uranium oxidation states and configurations with corresponding 5f occupation can only be accurately described by the small-core approximation, where an accuracy of 0.008 eV or better is achieved. We note that the findings obtained with regard to the FC errors for the approximately 30 configurations listed in Table 6-4 remain valid when looking at an extended set of over 60 configurations (18, 15, 12, 9, 6, and 3 with $5f^0$, $5f^1$, $5f^2$, $5f^3$, $5f^4$ and $5f^5$, respectively), which contains for each 5f occupation several different 6d occupations. From the extended set for a given 5f occupation a small dependency of the FC errors on the 6d occupation can be observed especially for the medium- and large-core case, however the dependency is less strong than the one on the 5f occupancy apparent from Table 6-4.

One might argue that 32 valence electrons are too many and one could possibly include e.g., the 5s and 5p shells into the core, i.e., treat only 24 valence electrons explicitly. However one has to keep in mind that the savings arising from the eliminated 5s and 5p shells are not very large and that at the correlated level, when pseudo-valence orbitals are used, larger errors in correlation energies may arise due to the larger number of eliminated radial nodes in the 6s and 6p semi-core orbitals as well as the 7s and 7p valence orbitals. No detailed investigation of these effects exists for the uranium atom, however studies of main group elements [28, 29, 106, 137] point to a possible overestimation of exchange integrals between,

e.g., the (5f, 6d) and (7s, 7p) shells and thus a possible overestimation of related correlation contributions as well as multiplet splittings.

In the following we try to give a simple explanation of the observed behavior of the FC errors. In Figures 6-3 and 6-4 the uranium orbital energies as well as the corresponding radial orbital densities and core densities are displayed. First, it is clear from a comparison of the non-relativistic and relativistic one-particle energies that

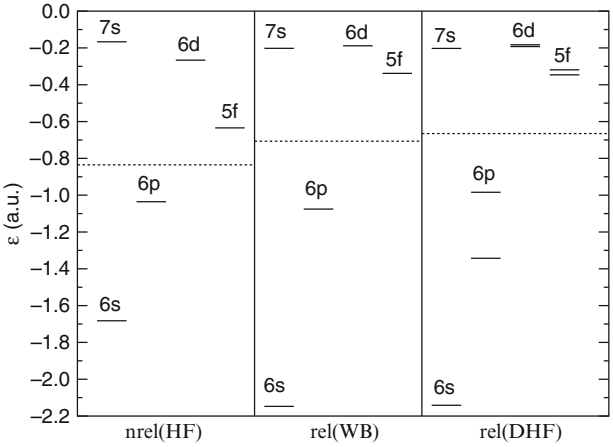

Figure 6-3. Orbital energies of uranium in its [Rn] $5f^3 6d^1 7s^2$ ground state configuration at the nonrelativistic Hartree–Fock, the scalar-relativistic Wood–Boring and the relativistic Dirac–Hartree–Fock/Dirac–Coulomb level

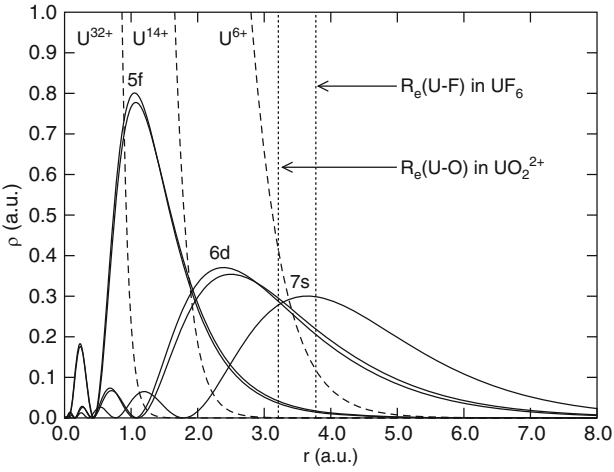

Figure 6-4. Relativistic radial orbital densities of uranium in its [Rn] $5f^3 6d^1 7s^2$ ground state configuration for the relativistic 5f, 6d and 7s orbitals as well as corresponding U^{6+}, U^{14+} and U^{32+} core densities from Dirac–Hartree–Fock/Dirac–Coulomb calculations

relativistic effects are significant and cannot be neglected. Whereas the 5f shell is energetically well separated from the other valence shells, i.e., 6d and 7s, it becomes almost degenerate with them at the relativistic level due to a dominant indirect relativistic destabilization. Similarly, the 6d shell is slightly destabilized whereas the 7s shell is slightly stabilized due to dominating direct relativistic effects. A very large relativistic stabilization and a large spin–orbit (SO) splitting is observed for the 6s and 6p shell, respectively, which have to be included in the valence as discussed above. The core-valence separation based only on energetic arguments, indicated by the dotted line in Figure 6-3, attributes 5f, 6d and 7s to the valence space and 1s-6s, 2p-6p, 3d-5d as well as 4f to the core space. However Figure 6-4 indicates, that from a spatial point of view the 6d shell is more compact than the U^{6+} core density and 5f is even more compact than the U^{14+} core density. Any change in the 5f occupation will change the effective nuclear charge acting on the more diffuse 6s and 6p 'core' orbitals by a corresponding amount and thus lead to the concomitant stabilization and contraction or destabilization and expansion of these shells, i.e., the shape and energy of the 6s and 6p is 5f occupation number dependent, indicating that these orbitals are not really core-like. In order to remind of the energetic core and spatial valence character the term semi-core shells is frequently used. Although the 6d shell is more diffuse than 5f, it has its density maximum in the same spatial region as 6s and 6p. Therefore the 6d occupation also influences the 6s and 6p semi-core orbitals, but to a lesser extent than the 5f occupation. Similarly, the 5f shell has its density maximum in the same spatial region as the 4s, 4p and 4d shells and a change in the 5f occupation will change the effective nuclear charge acting on these shells, although not as much as for the 6s and 6p shells. Thus, from a spatial point of view it is clear that for accurate calculations all orbitals with main quantum number $n > 4$ have to be treated in the valence space. The currently available small-core PPs for the actinides use this core definition [77] and an analogous core-valence separation is made for the corresponding small-core lanthanide PPs [17,36], i.e., all shells with main quantum number $n > 3$ are treated in the valence space. However, both sets of PPs have been adjusted to relativistic AE data obtained with the WB relativistic HF approach and deviations between the WB and MCDHF/DC or MCDHF/DC+B reference energies are usually larger than the FC errors. The generation and performance of a uranium small-core PP adjusted directly to MCDHF/DC+B reference data [34] will be discussed below.

The results summarized in Table 6-4 for the medium core imply that FC errors for energy differences are smaller when calculated only between configurations with the same 5f occupation as compared to errors for configurations with different 5f occupation. In view of the high complexity of the electronic structure arising from open f shells and the fact that for many questions the individual electronic state arising from a specific coupling of the open shell electrons is not of high importance, one might be tempted to construct PPs modelling an uranium atom with a specific valency, corresponding to a specific 5f occupation number, and attributing the corresponding partially occupied 5f shell to the PP core. Thus, one does not only have one PP for every atom, but one for every valency of every atom. The rightmost column in Table 6-4 presents FC errors for configurations of each of the

listed 5f occupation numbers, where the frozen core always has been taken from the lowest energy configuration with the specific 5f occupation number. Thus for a uranium 5f occupation of n_{5f} electrons only $14 - n_{5f}$ electrons are treated explicitly in the valence shell. It is apparent that the FC errors amount to at most 0.2 eV for all choices of the core and the valency. In case of a $5f^0$ occupation the errors for intra-configurational energy differences are smaller than for the medium-core case, adopting the core from the neutral uranium atom in its [Rn] $5f^3 6d^1 7s^2$ ground state. In case of the $5f^1$ configurations the corresponding errors for the 5f-in-core and medium-core 5f-in-valence cases are very similar, whereas for the higher $5f^n$ occupations ($n > 1$) they are somewhat larger for the 5f-in-core case than for the medium-core 5f-in-valence case. A clear dependency of the 5f-in-core FC errors on the 6d occupation number is observed.

We note that when attributing the partially occupied 5f shell to the PP core, the computational effort of calculations of actinides is essentially reduced to the one for treating an early transition metal. In case of uranium and other actinides 5f-in-core PPs for trivalent [90], di- and tetravalent [91] as well as penta- and hexavalent [89] situations have been generated and tested in molecular calculations, including studies of actinocenes [88], the hydration of trivalent actinide ions [148] or extended porphyrin complexes such as actinide (III) texaphyrins and motexafins [22]. Corresponding 4f-in-core PPs for di- and trivalent [37] as well as tetravalent [62] lanthanides are available too.

Clearly any information which depends on the details of the electronic structure of the open shell attributed to the PP core is lost, however the computational savings in cases where the open f shell remains core-like in a molecular or solid environment are quite large. Trends along the lanthanide and actinide series can be studied on equal footing, although only for an average over all states having the same valence substate and the same f subconfiguration, i.e., a so-called superconfiguration. The concept of a superconfiguration was proposed by Field more than two decades ago in order to rationalize the extremely complex spectra of lanthanide diatomics [46].

6.5.3. Pseudopotential Adjustment

Let us now turn to the generation of the relativistic energy-consistent uranium PPs. We briefly discuss the WB-adjusted (small-core) 5f-in-valence [77] and (large-core) 5f-in-core [89–91] PPs as well as a MCDHF/DC+B-adjusted (small-core) 5f-in-valence PP [34]. The latter PP is adjusted according to the most recent developments [32, 38, 135].

6.5.3.1. Wood–Boring-Adjusted 5f-in-Valence Pseudopotential

The discussion of FC errors listed in Table 6-4 yielded the result that for accurate calculations of energy differences between states with different 5f occupation a small-core PP, i.e., 60 core electrons (in shells with $n < 5$) and 32 valence electrons (in shells with $n \geq 5$), has to be generated. The WB-adjusted PP [77] uses in Eq. (6-22) one Gaussian term with $n_m = 0$ for each of the angular symmetries

$l = 0$ to 4, i.e., a total of ten adjustable parameters. The eight parameters up to f symmetry were adjusted to 12 energetically low-lying LS states of U and U^+ with varying 5f, 6d, 7s and 7p occupation in a multi-state multi-electron adjustment. The parameters were adjusted in a least-squares fit according to Eq. (6-42) so that the total valence energies obtained in finite difference PP calculations [51] agree best with corresponding scalar-relativistic AE WB reference energies. The parameters for g symmetry were adjusted in a multi-state single-electron adjustment to g^1 states of U^{31+} with virtually no errors. Atomic test calculations for 21 LS states of U and 15 LS states of U^+ (occupation numbers 5f: 2 - 6, 6d: 0 - 4, 7s: 0 - 2, 7p: 0 - 1) gave errors of at most 0.06 eV compared to the AE WB reference data. In Table 6-5 we compile results for a different test, i.e., for relative average energies of configurations of U - U^{6+} as used in Tables 6-3 and 6-4 . The accuracy obtained in the fit for LS states of U and U^+ is retained in the corresponding test calculations of configurational averages. For all listed configurations of U - U^{4+} an absolute (relative) accuracy of better than 0.09 eV (0.8%) is achieved. The absolute errors are significantly larger for U^{5+} and U^{6+}, i.e., up to 0.43 eV, but the relative errors remain quite small, i.e., below 0.3%. In total the mean absolute error with respect to the WB AE data is 0.07 eV, whereas with respect to MCDHF AE data using the DC and DCB Hamiltonian it is 0.50 eV and 0.33 eV, respectively.

The SO operators of the WB-adjusted PP were originally derived from perturbatively determined WB orbital SO splittings [77]. Later MCDHF/DC-adjusted SO terms for the 5f, 6d and 7p shell were derived from multi-state multi-electron SO splittings for use in first-order perturbation theory based on the scalar-relativistic solution as well as for two-component variational calculations keeping a 5s, 5p, 5d, 6s, 6p core frozen at the scalar-relativistic level [21]. The latter operators should also be used in large-scale SO configuration interaction (CI) calculations with excitations from the 5f, 6d (, 7s) and 7p valence shells. It is important to use the SO operators in the correct framework: whereas the former parametrization accounts implicitly for the orbital relaxation of the 5f, 6d and 7p valence shells under the SO term, the latter one assumes that this effect is explicitly considered in the calculations. Both operators assume the 5s, 5p, 5d, 6s, 6p core/semi-core shells to remain at the scalar-relativistic level. Large errors may result, when the valence SO terms are allowed to act on these shells.

Although the performance of the original small-core WB-adjusted PP was found to be quite satisfactory in numerous molecular studies, e.g., [9, 10], both the disagreements with the WB AE data for the higher oxidation states U^{5+} and U^{6+} not included in the adjustment as well as the deviations of the WB AE data itself from results obtained with the best available method, i.e., MCDHF calculations based on the DCB Hamiltonian, motivated a readjustment of the PP [34]. The main reason, however, was the fact that only valence SO operators were available, which are allowed to act on the 5f, 6d, 7p actual valence shells, but not on the 5d, 5p and 6p semi-core shells included in the valence space of the small-core PP. Thus no two-component HF calculations or SO CI calculations allowing excitations from these inner shells were possible.

Table 6-5 As Table 6-3, but for all-electron point nucleus (pn) Wood–Boring and finite Fermi nucleus (fn) Dirac–Hartree–Fock/Dirac–Coulomb–Breit (DHF/DC+B) energy differences ΔE (eV) with respect to the uranium ground state. The errors $\Delta\Delta E$ (eV) are listed for a Wood–Boring (WB) adjusted (old) [77] as well as a Dirac–Hartree–Fock/Dirac–Coulomb–Breit adjusted (new) [34] small-core pseudopotential (SPP). For comparison available data from literature for a generalized relativistic effective core potential (GRECP) adjusted to fn DHF/DCB data is listed too [93]

Charge	Configuration			ΔE	$\Delta\Delta$E	ΔE	$\Delta\Delta$E	
	5f	6d	7s	WB	SPP	DHF	SPP	
				pn	old	DC+B,fn	new	GRECP
6+				169.1342	0.4290	168.3200	0.0045	
5+		1		119.1842	0.2071	118.5177	0.0025	
4+		2		79.5848	0.0491	79.0378	0.0010	
3+		3		49.7821	−0.0468	49.3303	−0.0010	
2+		4		29.1540	−0.0913	28.7693	−0.0039	
1+		4	1	16.7440	−0.0173	16.3620	−0.0045	
0		4	2	10.5089	0.0404	10.1180	−0.0038	
5+	1			108.1437	0.2395	107.6258	0.0020	
4+	1	1		70.0169	0.0820	69.6211	0.0032	
3+	1	2		41.5358	−0.0181	41.2325	0.0032	
2+	1	3		22.0486	−0.0653	21.8109	0.0018	
1+	1	3	1	10.0850	−0.0093	9.8506	0.0009	0.0843
0	1	3	2	4.1415	0.0344	3.8992	0.0012	0.0843
4+	2			63.2986	0.0826	63.0292	−0.0014	
3+	2	1		36.1309	−0.0139	35.9551	0.0013	
2+	2	1	1	17.7842	0.0184	17.6451	0.0005	
1+	2	1	2	6.0270	0.0453	5.8808	0.0012	0.0467
0	2	2	2	0.6918	0.0095	0.5751	0.0014	0.0449
3+	3			33.4046	−0.0047	33.3473	−0.0038	
2+	3		1	15.7488	0.0129	15.7131	−0.0033	
1+	3		2	4.5267	0.0273	4.4993	−0.0017	0.0011
0	3	1	2	0.0000	0.0000	0.0000	0.0000	0.0000
2+	4			17.0353	−0.0169	17.1327	−0.0026	
1+	4		1	6.6705	0.0010	6.7689	−0.0011	−0.0454
0	4		2	1.8651	0.0129	1.9568	0.0005	−0.0450
1+	5			12.1721	0.0459	12.3320	0.0034	−0.0832
0	5		1	7.8323	0.0617	7.9585	0.0043	

6.5.3.2. Dirac–Hartree–Fock-Adjusted 5f-in-Valence Pseudopotential

The newest uranium PP is directly adjusted to MCDHF data using the DCB Hamiltonian and a Fermi nuclear charge distribution [34]. Two-component finite difference MCHF PP calculations applying the same (intermediate) coupling

scheme are performed in order to eliminate possible errors due to the use of finite basis sets. The reference data set used to determine the PP up to f symmetry comprised now 100 non-relativistic configurations yielding a total of 30,190 J levels. The reference data was obtained for U - U^{7+} and included a wider spectrum of occupations in the 5f, 6d, 7s and 7p valence shell (occupation numbers 5f: 0 - 5, 6d: 0 - 4, 7s: 0 - 2, 7p: 0 - 1), but also additional configurations with holes in the core/semi-core shells 5s, 5p, 5d, 6s, 6p as well as configurations with electrons in the 6f - 9f, 7d - 9d, 8p - 9p and 8s - 9s shells. A global shift was applied to all reference energies, cf. Eq. (6-42), and treated as an additional parameter to be optimized. For g symmetry the adjustment was analogous to the scalar-relativistic case, i.e., a multi-state single-electron adjustment to $g^1_{7/2}$ and $g^1_{9/2}$ states of U^{31+} was performed.

Due to the SO splitting of the shells with angular quantum number $l > 0$ V_l is divided into two components: $V_{l,j=l-1/2}$ and $V_{l,j=l+1/2}$. Therefore the minimum number of parameters for a PP up to f symmetry with one Gaussian per lj term is now 14 instead of 8 and a selection of m Gaussians per lj value leads to $14m$ parameters. However, test calculations revealed that for the reference states included in the adjustment at least two Gaussians have to be used in s symmetry in order to get a satisfactory accuracy, i.e., at least 16 adjustable parameters were used.

Since the number of reference energies is now significantly higher than in the WB case (30,190 vs. 12), higher accuracy can now be achieved by using more adjustable parameters. Figure 6-5 shows the development of the root mean squared errors of the energies of the non-relativistic configurations as well as of the individual J levels when the number of adjustable parameters increases. Whereas the error with respect

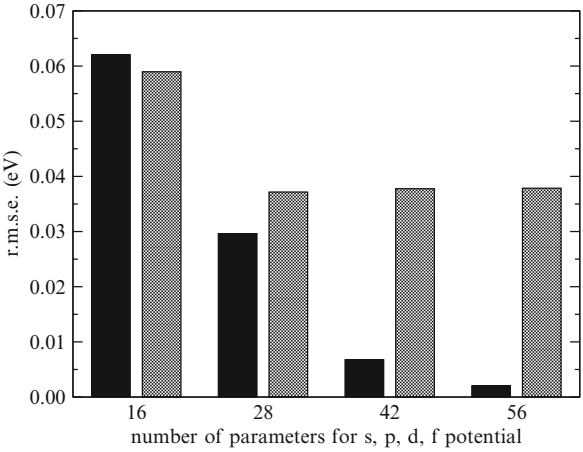

Figure 6-5. Root mean squared errors (eV) for the configurational average (*black*) and the individual J levels (*grey*) of Dirac–Hartree–Fock/Dirac–Coulomb–Breit point nucleus adjusted small core pseudopotentials for uranium with different number of parameters. The entries 16, 28, 42 and 56 on the abscissa correspond roughly to one, two, three and four Gaussian terms per lj value in the radial expansion of the s, p, d and f pseudopotentials (cf. text). The reference data sets comprised 98 non-relativistic configurations and the associated 30,035 J levels

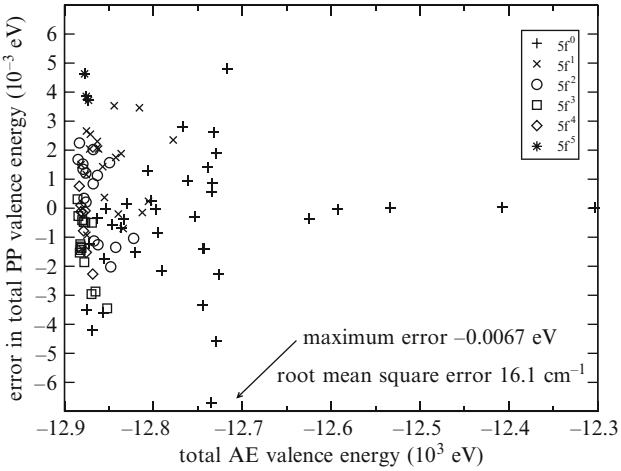

Figure 6-6. Errors (eV) in total valence energies of 100 non-relativistic configurations for the multi-configuration Dirac–Hartree–Fock/Dirac–Coulomb–Breit Fermi nucleus adjusted small-core pseudopotential for uranium [34]

to the individual J levels seems to be converged already with two Gaussians per lj term to about 300 cm^{-1} (0.037 eV), the one for the averages of the configurations can be further reduced to 16 cm^{-1} (0.002 eV) by applying four Gaussians per lj value. Figure 6-6 gives an overview of the errors for the configurational averages for the most extensive parametrization with 4 Gaussians per lj term (56 parameters). One can see that in contrast to the AE FC errors listed in Table 6-4 the PP errors exhibit a less systematic behavior with respect to the 5f occupancy, however their magnitude is comparable and stays below 0.012 eV for any energy difference between two of the configurations in a total energy interval of approximately 600 eV.

Table 6-5 compares PP relative energies to corresponding AE data. It should be noted that the configurations listed there form a subset of the reference configurations used in the PP adjustment. For comparison results published for a shape-consistent (generalized) relativistic effective core potential (GRECP) are also listed [93]. This PP was also adjusted to DHF/DCB reference data, however not at the MC level. It combines the traditional semilocal with a nonlocal ansatz. PPs of this school exhibit a fairly high accuracy, but the number of adjustable parameters is significantly larger than for the energy-consistent case and the additional nonlocal term cannot be handled by most quantum chemistry codes, including the ones accessible to us. Thus our conclusions are only based on the data available from the original publication. It can be seen that a characteristic pattern of errors, i.e., a clear dependency on the f occupancy n with roughly $(3 - n) \times 0.043$ eV, results.

The behavior of the errors for the individual J levels is displayed in Figure 6-7 for the MCDHF/DC+B-adjusted PP. The root mean squared error is 0.038 eV, whereas the largest error is 0.27 eV and occurs for a very high-lying J level of a chemically probably not too important configuration with a 5f^4 occupation. If only J levels with a relative energy of 5 eV with respect to the lowest J level of the configuration

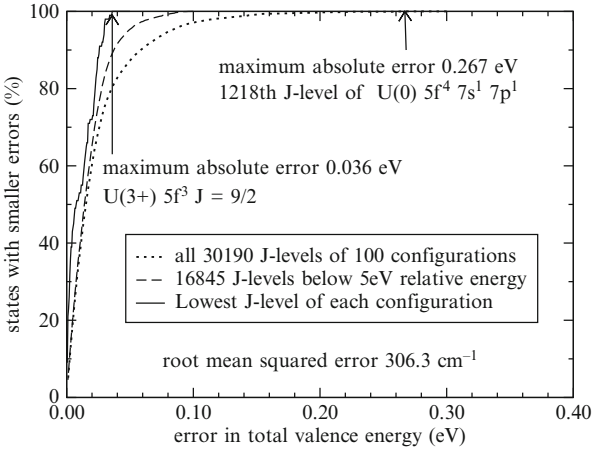

Figure 6-7. Percentage (%) of J levels with errors in the total valence energies below the threshold (eV) indicated on the abscissa for the multi-configuration Dirac–Hartree–Fock/Dirac–Coulomb–Breit Fermi nucleus adjusted small-core pseudopotential for uranium [34]

Table 6-6 Relative energies ΔE (cm^{-1}) for single-determinant J levels calculated at the Dirac–Hartree–Fock/Dirac–Coulomb–Breit (DHF/DC+B,DCB) level using a Fermi charge distribution for the finite nucleus and errors $\Delta\Delta E$ (cm^{-1}) of calculations with a small-core energy-consistent pseudopotential (SPP) [34] and a generalized relativistic effective core potential (GRECP) [93] modelling such all-electron calculations. Mean absolute errors (cm^{-1}) are listed in the last line

J	$5f^3\_6d^1\_7s^2_+$				$5f^2\_6d^2\_7s^2_+$			
	ΔE DHF DC+B	$\Delta\Delta E$ SPP	ΔE DHF DCB	$\Delta\Delta E$ GRECP	ΔE DHF DC+B	$\Delta\Delta E$ SPP	ΔE DHF DCB	$\Delta\Delta E$ GRECP
0	10,767.4	366.0	10,767	416	39,561.1	422.6	39,562	724
1	29,342.5	311.6	29,343	553	20,452.5	101.2	20,453	292
2	20,477.0	413.4	20,477	556	24,250.8	228.8	24,252	422
3	18,515.7	208.6	18,516	359	15,905.0	−38.9	15,906	126
4	17,458.4	194.0	17,458	339	13,548.7	−20.7	13,549	86
5	2,762.4	−55.4	2,762	−23	7,017.3	−116.5	7,018	−30
6	0.0	0.0	0	0	0.0	0.0	0	0
m.a.e.		258.2		374.3		158.4		280.0

are considered, the maximum error is below 0.1 eV, and if only the lowest J levels of each configuration are considered, it is at most 0.036 eV. Again we compare to the GRECP, restricting ourselves to two data sets out of three taken from the original publication [93]. It can be seen from Table 6-6 that for the individual J levels, when described as a single determinant in the jj coupling scheme, the errors of the energy-consistent PP are slightly smaller than the ones obtained for the GRECP. The same is true for the third data set not shown here.

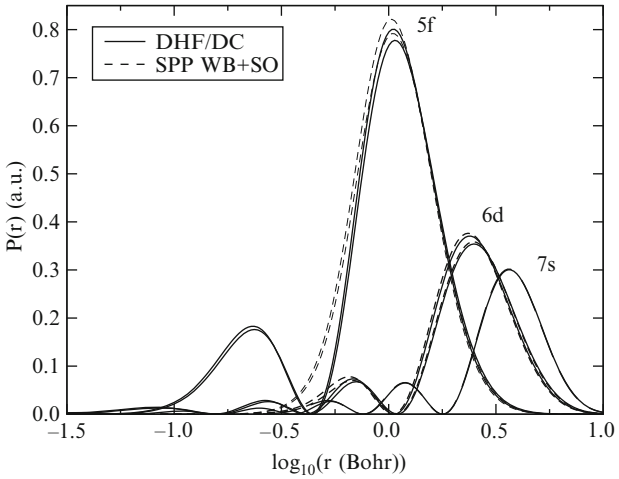

Figure 6-8. Radial orbital densities of uranium in the [Rn] $5f^3 6d^1 7s^2$ ground state configuration from state-averaged multi-configuration Dirac–Hartree–Fock/Dirac–Coulomb calculations [41] in comparison to pseudo-valence functions obtained from corresponding valence-only calculations with a scalar-relativistic Wood–Boring adjusted small-core pseudopotential [77] and a spin–orbit term designed to act on the 5f and 6d shells [21]

It is interesting to have a look at the shape of the radial functions, especially for energy-consistent PPs, where the agreement with corresponding AE orbitals is not enforced for a specific electronic state. In Figure 6-8 radial densities for the 5f, 6d and 7s shells obtained with the scalar-relativistic WB PP supplemented by a SO term designed for a variational treatment of the 5f, 6d (, 7s) and 7p shells in the field of a 5s, 5p, 5d, 6s and 6p scalar-relativistic core [21, 77] are compared for the neutral uranium atom ground state to corresponding radial densities of the large components evaluated at the MCDHF/DC level. The simplified radial structure (lower number of radial nodes) is clearly obvious in case of the 5f and 6d shells, whereas the differences for the 7s shell are virtually invisible, including the different nodal structure for abscissa values smaller than ≈ -0.3. It is apparent that in the valence region the pseudo-valence orbitals reproduce the AE orbitals fairly well. Figure 6-9 shows the same comparison for the MCDHF/DC+B Fermi nucleus adjusted PP [34], where an even better agreement is observed. In this context we want to note that in the shape-consistent formalism the exact agreement between pseudo-valence orbitals and all-electron orbitals in the spatial valence region is only guaranteed for a single reference state.

6.5.3.3. 5f-in-Core Pseudopotentials

Let us now turn to a much more approximate treatment of uranium in molecules or solids. The rightmost column in Table 6-3 indicates, that it might be possible to include the open 5f shell as well as all other shells with main quantum number $n < 6$ into the PP core. Similar sets of such PPs attributing the 4f shell to the core have been

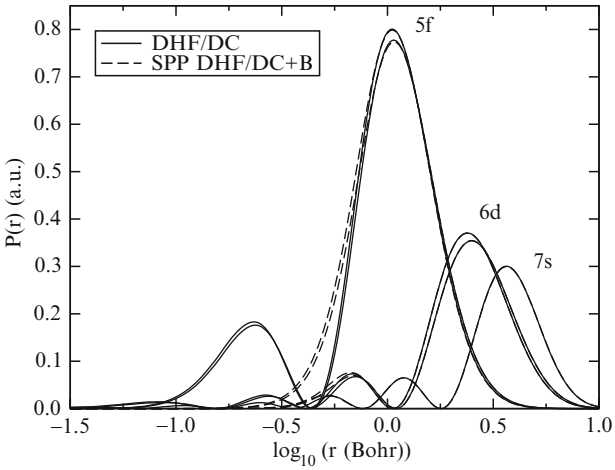

Figure 6-9. As Fig. 6-8 but for a two-component Dirac–Hartree–Fock/Dirac–Coulomb–Breit adjusted small-core pseudopotential [34]

in use for almost two decades for the lanthanides [37, 39] and fit into the concept of a superconfiguration advocated by Field [46]. The adjustment and application of 5f-in-core PPs for the actinides has only been attempted recently [22, 89–91]. In case of uranium PPs for tri-, tetra-, penta- and hexavalent situations corresponding to a 5f occupation with 3, 2, 1 and 0 electrons, respectively, are available. The reference data has been obtained for configurational averages at the WB scalar-relativistic AE level using a extensively modified version of the finite difference HF code MCHF77 of Froese-Fischer in order to avoid basis set errors [51]. The PPs were adjusted using the same code, i.e., again errors due to finite basis sets or differences in the coupling schemes at the AE and PP level were avoided.

For the terms up to d symmetry two Gaussians per l value were applied in the expansion of the radial PP. Thus 12 parameters were adjusted to up to 18 reference energies for each given 5f occupation. Despite that fact that the 5f shell was attributed to the core and instead of LS states the configurational average was taken into account, the adjustment procedure is equivalent to the 5f-in-valence WB small-core PP described above. The accuracy of the adjustment was better than 0.1 eV for all reference energies, cf. e.g., Table 6-7 for the $5f^3$-in-core PP of (trivalent) uranium. The rightmost column in this table shows that this accuracy not only holds for a comparison to WB AE reference data but also for one to corresponding MCDHF/DC data.

Special care had to be taken for the f symmetry. For a given 5f occupation of m electrons a potential V_1 was adjusted to reference energies of the $5f^{m+1}$, $5f^m\ 6f^1$, $5f^m\ 7f^1$ and $5f^m\ 8f^1$ configurations. For $m = 0$, i.e., the element at the beginning of a set of actinides with a given valency, the adjustment of V_1 corresponds to a multi-state single-electron fit similar to the one performed for the g potentials in the 5f-in-valence case. A second potential V_2 was adjusted to the $5f^m\ 6f^1$, $5f^m\ 7f^1$ and $5f^m$

Table 6-7 Relative energies (eV) of U configurations with a $5f^3$ occupation with respect to the U [Rn] $5f^36d^17s^2$ ground state configuration from all-electron state-averaged multi-configuration Dirac–Hartree–Fock calculations using the Dirac–Coulomb Hamiltonian (AE DHF/DC). Frozen-core errors (eV) are listed for a 1s-$5f^3$ core adapted from the neutral U atom [Rn] $5f^36d^17s^2$ ground state configuration (Q = 11). All-electron Wood–Boring (AE WB) average energy differences (eV) with respect to the U [Rn] $5f^36d^17s^2$ ground state configuration and corresponding errors (eV) of $5f^3$-in-core pseudopotential values with respect to the all-electron Wood–Boring (LPP) as well as to the Dirac–Hartree–Fock/Dirac–Coulomb (LPP′) data

Charge	Configuration			DHF/DC		WB		
	5f	6d	7s	AE	Q = 11	AE	LPP	LPP[a]
3+	3			33.3768	0.1458	33.4046	−0.0296	−0.0018
2+	3		1	15.7154	0.0698	15.7488	−0.0445	−0.0111
1+	3		2	4.4832	0.0306	4.5267	−0.0342	0.0093
2+	3	1		16.2232	0.0194	16.1849	−0.0670	−0.1053
1+	3	1	1	5.2615	0.0029	5.2419	−0.0309	−0.0505
0	3	1	2	0.0000	0.0000	0.0000	0.0000	0.0000
1+	3	2		6.8058	0.0075	6.7365	0.0004	−0.0689
0	3	2	1	1.6538	0.0049	1.6090	0.0360	−0.0088
0	3	3		3.8822	0.0264	3.8072	0.0766	0.0005

Frozen cores: U Q = 11: 1s-5f.

$8f^1$ configurations. For $m = 14$, i.e., the element at the end of a set of actinides/post-actinides with a given valency, the adjustment of V_2 also corresponds to a multi-state single-electron fit. In contrast to V_1 the occupation of the 5f shell with an additional electron is explicitly forbidden when using V_2. In order to get a smooth transition from V_1 to V_2 when moving along a hypothetical series of elements with a fixed valency, the actually used f term of the PP was obtained as a superposition

$$V = \left(1 - \frac{m}{14}\right) V_1 + \frac{m}{14} V_2. \tag{6-71}$$

It is clear that the superconfiguration model of Field [46] applied to the actinides would require an integral 5f occupation, i.e., the use of V_2. However, due to the diffuse character of the 5f shell, it is accessible to the chemical environment and in fact the 5f shell might accept electron density from neighboring atoms, i.e., $5f^{m+\delta m}$ occupations may arise. The purpose of the linear combination of potentials above is to allow, by means of mixing in of V_1, also 5f occupancies slightly larger than the integral value m intended to be modelled by the 5f-in-core PP. Of course δm has to be sufficiently small for this approximation to be valid, e.g., $0 \leq \delta m \ll 1$. Various molecular test calculations (vide infra) in fact show that δm can deviate from zero by several tenths of an electron when counted in a Mulliken population without a breakdown of the model. Clearly the approach is not designed for 5f occupations less than the one attributed to the PP core, i.e., $\delta m < 0$, and thus a charge transfer from the actinide 5f shell into other orbitals is not covered by the approximation.

6.5.4. Valence Basis Set Optimization

As important as the PP parametrization itself is the optimization of reliable valence basis sets. It should be noted that due to the different radial shape of the pseudo-valence orbitals in the core region valence basis sets cannot be transferred from one PP to another, even for the same element and the same core size, i.e., PPs should only be used in connection with valence basis sets optimized specifically for them. This is especially true for contracted basis sets, but significant errors might also already arise for not too large uncontracted basis sets.

6.5.4.1. 5f-in-Valence Pseudopotentials

For the uranium example described here (14s13p10d8f6g)/[6s6p5d4f3g] basis sets exist for both WB- and MCDHF/DC+B-adjusted 5f-in-valence small-core PPs [21,34]. Since 5s, 6s, 5p, 6p and 5d have to be attributed to the semi-core orbitals and are described with one contraction each, a [4s4p4d4f] set is left for the description of the 5f, 6d, 7s and 7p valence shells, i.e., a set of overall valence quadruple-zeta quality arises. The basis sets for uranium and the other actinides were generated as described in the following. First a (14s11p8d8f) set of exponents was energy-optimized in atomic PP HF calculations [107] for the [Rn] $5f^4 7s^2\ ^5$I state of the neutral uranium atom. In the second step two diffuse d functions for the description of the 6d shell were HF energy-optimized for the [Rn] $5f^3 6d^1 7s^2\ ^5$L state. In order to describe the 7p shell two diffuse p functions obtained in case of the WB PPs by linear interpolation from HF energy-optimized functions for the [Rn] $5f^0 7s^2 7p^1\ ^2$P and [Rn] $5f^{14} 7s^2 7p^1\ ^2$P states of Ac and Lr, respectively, were added in the third step. In case of the MCDHF/DC+B-adjusted PP the two exponents were optimized for the [Rn] $5f^3 7s^2 7p^1\ ^5$I state. In order to guarantee an unbiased description of states with different 5f occupation, the contraction coefficients for the resulting (14s13p10d8f)/[6s6p5d4f] sets were obtained in the fourth step from averaged density matrices for the lowest LS states of the [Rn] $5f^3 6d^1 7s^2$ and [Rn] $5f^4 7s^2$ configurations. Symmetry-breaking at the CASSCF level was avoided by averaging over all components of each LS state. Whereas it was feasible to perform CASSCF/MRCI calculations for the [Rn] $5f^4 7s^2\ ^5$I state, the [Rn] $5f^3 6d^1 7s^2\ ^5$L state was only treated at the CASSCF level. In the MRCI calculations the 5s, 5p and 5d shells were kept frozen, i.e., the sets are suitable for correlating the 5f and $n > 5$ shells, whereas additional functions should be added when a correlation of the 5s, 5p and 5d shells is also desired. Finally, as the fifth and last step six g exponents were chosen identically to the six largest f exponents, reflecting their importance in the g ANOs obtained from MRCI calculations for the [Rn] $5f^4 7s^2\ ^5$I state using the (14s13p10d8f)/[6s6p5d4f] ANO basis set augmented by eight g functions identical to the f set. A generalized ANO contraction was derived as described above for the [Rn] $5f^4 7s^2\ ^5$I state, yielding the final (14s13p10d8f6g)/[6s6p5d4f3g] set of roughly polarized valence quadruple-zeta quality. [5s5p4d3f2g] and [4s4p3d2f1g] sets of polarized triple- and double-zeta quality as well as a [3s3p2d1f] minimal basis set can be created by omitting contractions with small ANO occupation numbers.

Table 6-8 Basis set errors (milli-Hartree) in total valence energies for the generalized contracted (14s13p10d8f)/[6s6p5d4f] and segmented contracted (14s13p10d8f6g)/[10s9p5d4f3g] ANO valence basis sets for the uranium small-core pseudopotentials (SPP) [77, 21, 34]

		SPP WB			SPP DC+B	
State		Uncontr.	Gen. contr.	Seg. contr.	Uncontr.	Fen. contr.
$5f^3\ 6d^1\ 7s^2$	^{5}L	2.31	2.32	4.11	0.72	0.73
$5f^4\ 7s^2$	^{5}I	1.59	1.59	2.82	0.46	0.46

The basis set errors in the total valence energies at the HF level amount to less than 3 milli-Hartree for all these basis sets, cf. Table 6-8.

Since a generalized contraction pattern cannot be efficiently dealt with in several commonly used quantum chemistry codes, segmented contracted (14s13p10d8f6g)/[10s9p5d4f3g] basis sets have been derived from the generalized contracted sets. Note that the number of contracted functions of the computationally expensive d, f and g sets is the same as for the generalized contracted sets, however for the less demanding s and p sets a larger number of contracted functions had to be used to achieve roughly the same accuracy. The basis set errors in the total valence energies at the HF level amount to less than 5 milli-Hartree for all these basis sets, cf. Table 6-8.

6.5.4.2. 5f-in-Core Pseudopotentials

For the 5f-in-core PPs for the trivalent actinides first (4s4p3d), (5s5p5d) and (6s6p6d) primitive sets have been HF optimized for the An^{2+} [Rn $5f^n$] $6s^2 6p^2 6d^1$ superconfiguration ($n = 0-14$ for Ac - Lr). For usage in solid state calculations the most diffuse exponent in each angular symmetry was restricted to 0.15 in order to avoid linear dependencies. An additional diffuse 2s1p1d set was then HF optimized for the An [Rn $5f^n$] $6s^2 6p^2 6d^1 7s^2$ superconfiguration and segmented contractions of VXZ (X=D,T,Q) quality were derived. The errors in the HF energies were at most 0.2 eV and 0.1 eV for the VDZ and VTZ, VQZ basis sets, respectively. Finally a 2f1g set CI optimized for the An [Rn $5f^n$] $6s^2 6p^2 6d^1 7s^2$ was added [90].

6.5.5. Calibration and Application

6.5.5.1. 5f-in-Valence Pseudopotentials

Recent studies compared results obtained with the WB [77] and MCDHF/DC+B [34] adjusted relativistic small-core PPs and AE data derived with the scalar-relativistic Douglas–Kroll–Hess Hamiltonian (DKH) [60] augmented by the Breit-Pauli (BP) SO Hamiltonian for uranium monohydride UH [23, 34]. Due to the different AE approaches modelled by the PPs an exact agreement cannot be expected. Table 6-9 shows selected data for the $^4I_{9/2}$ ground state. We note that the selection of the active space used in the CASSCF reference calculations has noticeable effects on the equilibrium distance R_e and the vibrational constant ω_e. For the compromise

Table 6-9 Selected results for the UH $5f^3\ \sigma^2\ \sigma^2\ ^4I$ ($\Omega = 9/2$) ground state [23, 34]

Method	R_e (Å)	ω_e (cm^{-1})	D_e (eV)
SPP WB/CASSCF[a]	2.159	1,330	
SPP WB/CASSCF[b]	2.076	1,442	
SPP WB/CASSCF[c]	2.073	1,431	
SPP WB/MRCI+Q	2.008	1,501	3.06[e]
SPP MCDF/DC+B/MRCI+Q	2.021	1,499	3.04[e]
DKH/MRCI+Q	2.019	1,495	2.99[e]
SPP WB/MRCI+Q/SO	2.011	1,497	2.85
SPP MCDF/DC+B/MRCI+Q/SO	2.025	1,505	2.82
DKH/MRCI+Q/SO	2.021	1,483	2.79
exp.[d]		1,424	

[a] Minimum active space in CASSCF: 3 electrons in 7 orbitals (U 5f).
[b] Applied active space in CASSCF: 5 electrons in 12 orbitals.
[c] Ideal active space in CASSCF: 7 electrons in 17 orbitals (U 5f, 6d, 7s, 7p, H 1s).
[d] Andrews and coworkers (1997), UH in Argon matrix.
[e] $D_e(UH) = E_l(UH,R = 50\ Bohr)\text{-}E_l(UH,R_e)$; $E_l(UH,R = 50\ Bohr) \approx E_s(U^+H^-,R = 50\ Bohr) + E_l(U)\text{-}E_s(U^+) + E(H)\text{-}E(H^-) + 1/50$; U: $5f^3 6d^1 7s^2\ ^5L$, U^+: $5f^3 7s^2\ ^4I$; *s*: small active space[b], *l*: large active space[c].

active space CASSCF/MRCI calculations for UH at the equilibrium distance were feasible, however not for the separated neutral atoms at large distance. Thus an approximation had to be used to evaluate the binding energies (cf. footnote *f* in Table 6-9). At the correlated level, without taking into consideration SO coupling, the deviations of the WB PP ($\Delta R_e = -0.011$ Å, $\Delta\omega_e = 6\ cm^{-1}$, $\Delta D_e = 0.07$ eV) and the MCDHF/DC+B PP ($\Delta R_e = 0.002$ Å, $\Delta\omega_e = 4\ cm^{-1}$, $\Delta D_e = 0.05$ eV) results from the DKH data are quite small.

Table 6-10 lists vertical excitation energies for the ground state internuclear equilibrium distance. For the lowest five states the PP term energies agree within 0.003 eV with the AE DKH/BP data and the ΛS state contributions deviate by at most 1%. For the next group of states the agreement is somewhat worse with at most 0.09 eV and 2%. Finally, the largest disagreement with up to 0.15 eV and 5% is observed for the last group of states. Here the agreement is better for the MCDHF/DC+B PP than for the WB PP, probably due to the improved adjustment of the SO term in a two-component manner. The high accuracy of the MCDHF/DC+B PP was also demonstrated in intermediate Hamiltonian Fock-space coupled cluster calculations, in which the experimental fine structure splitting of U^{5+} $5f^1$ was exactly reproduced and the term energies of the J levels of U^{4+} $5f^2$ reaching up to $\approx$44,000 cm^{-1} were obtained with a mean absolute error of 420 cm^{-1} [146].

Besides applications in a larger number of molecular calculations, cf. the compilation listed in a recent review [20], the WB-adjusted small-core PPs for uranium

Table 6-10 Term energies (eV) of UH from calculations with spin–orbit coupling (state interaction approach) [23, 34]

		SPP WB	SPP		AE DKH +BP
			WB	DC+B	
No.	Ω	LS(%)	ΔE	ΔE	ΔE
1.	4.5	^{4}I(80) + ^{4}H(17)+$^4\Gamma$(3)	0.000	0.000	0.000
2.	3.5	^{4}H(60) + $^4\Gamma$(30) + $^4\Phi$(9) + $^4\Delta$(1)	0.032	0.029	0.032
3.	2.5	$^4\Gamma$(43) + $^4\Phi$(38) + $^4\Delta$(16) + $^4\Pi$(3)	0.046	0.046	0.049
4.	1.5	$^4\Delta$(40) + $^4\Phi$(31) + $^4\Pi$(23) + $^4\Sigma$(6)	0.057	0.058	0.060
5.	0.5	$^4\Pi$(49) + $^4\Sigma$(30) + $^4\Delta$(21)	0.068	0.070	0.071
6.	5.5	^{4}I(72) + ^{4}H(22) + $^6\Lambda$(3) + $^4\Gamma$(1) + ^{4}K(1)	0.336	0.380	0.419
8.	4.5	^{4}H(38) + $^4\Gamma$(36) + ^{4}I(18) + $^4\Phi$(8)	0.363	0.405	0.447
9.	3.5	$^4\Phi$(39) + ^{4}H(32) + $^4\Delta$(16) + $^4\Gamma$(13)	0.378	0.424	0.464
10.	2.5	$^4\Gamma$(40) + $^4\Delta$(35) + $^4\Pi$(23) + $^4\Phi$(2)	0.392	0.436	0.480
11.	1.5	$^4\Phi$(43) + $^4\Sigma$(30) + $^4\Pi$(27)	0.402	0.454	0.491
12.	0.5	$^4\Pi$(43) + $^4\Delta$(42) + $^4\Sigma$(15)	0.404	0.452	0.494
7.	5.5	$^6\Lambda$(83) + ^{6}K(13) + ^{4}I(3) + ^{4}H(1)	0.341	0.271	0.190
13.	4.5	^{6}K(100)	0.463	0.412	0.353
14.	6.5	$^6\Lambda$(79) + ^{6}K(21)	0.579	0.562	0.517

AE DKH + BP basis set: U (30s26p18d14f7g)/[10s9p7d5f3g]; H aug-cc-pVQZ.

and plutonium were also applied in scalar-relativistic density functional (DF) calculations of crystalline UO_2, PuO_2 and Pu_2O_3 [75, 111]. The Mott insulator UO_2 has a CaF_2-like structure, characterized by U^{4+} $5f^2$ triplet-coupled centers, with an antiferromagnetic coupling between nearest neighbor U^{4+} $5f^2$ ions. It was found that the screened hybrid DF of Heyd, Scuseria and Ernzerhof (HSE) yields results superior to other hybrid DFs as well as those of the generalized gradient approximation and local density approximation (LDA) type. The uranium small-core PP was accompanied by a (8s8p6d5f) uncontracted valence basis set, which was obtained from the original atomic basis set by omitting some of the most tight and the most diffuse functions. Oxygen was treated at the AE level and described by a 6-31G basis set. For other technical details of these calculations, further references as well as a broader discussion of the results cf. the original papers [75, 111]. A summary of the various DF results is given in Table 6-11: the experimentally observed antiferromagnetic ordering is correctly reproduced in the HSE calculations, the calculated result for the lattice constant a_0 is only 0.007 Å (0.1%) larger than the experimental value, and the band gap Δ and the bulk modulus B_0 are overestimated by 0.2 eV (13.8%) and 11 GPa (5.3%), respectively.

6.5.5.2. 5f-in-Core Pseudopotentials

Next we want to discuss the performance of the 5f-in-core PP approach for uranium as well as the other actinides in molecular calculations. Clearly, the underlying approximation is only valid if the 5f shell stays core-like and does not participate in bonding in the MO-LCAO sense. For AnF_n (n = 2, 3, 4, 5, 6) the accuracy of

Table 6-11 Calculated and experimental properties of UO_2 [111] obtained with the scalar-relativistic Wood–Boring adjusted pseudopotential for uranium [77]: band gap Δ (eV), equilibrium lattice constant a_0 (Å), bulk modulus B_0 (GPa) and energy difference ΔE (meV) between the ferromagnetic (FM) and antiferromagnetic (AFM) solutions per formula unit. A null for Δ indicates a metal

Method	Δ		a_0		B_0		ΔE
	FM	AFM	FM	AFM	FM	AFM	
LSDA	0	0	5.317	5.289	239	216	−98
PBE	0	0	5.425	5.445	206	186	−123
TPSS	0	0	5.437	5.445	202	191	−124
PBE0	2.23	3.13	5.455	5.454	220	219	+2
HSE	1.56	2.39	5.463	5.463	226	218	+7
Exp.	2.1		5.470		207		>0

Table 6-12 U–F bond distances R_e (Å), binding energies D_e (eV) and Mulliken f populations n_f from 5f-in-core pseudopotential (large-core pseudopotential, LPP) Hartre-Fock calculations of uranium polyfluorides UF_m in comparison to corresponding 5f-in-valence pseudopotential (small-core pseudopotential, SPP) multi-configuration self-consistent field calculations modelling an average over all states arising from the open U 5f shell [90]. The number m indicates the number of fluorine atoms, whereas $6 - m$ denotes the number of 5f electrons attributed to the uranium core (LPP) or explicitly treated in the valence space (SPP)

m	R_e		D_e		n_f	
	LPP	SPP	LPP	SPP	LPP	SPP
3	2.17	2.12	4.94	5.05	3+0.08	3.02
4	2.09	2.07	5.31	5.38	2+0.16	2.22
5	2.03	2.03	5.26	5.39	1+0.42	1.55
6	1.98	1.98	5.36	5.65	0+0.96	1.16

the 5f-in-core PP approach has been demonstrated by comparison to corresponding 5f-in-valence PP results and its limitations have been discussed, e.g., cases for which the actual 5f occupation in 5f-in-valence calculations is either below or significantly higher than the integral value modelled by the 5f-in-core PP [89–91]. The corresponding results for the uranium fluorides UF_n ($n = 3, 4, 5, 6$) are summarized in Table 6-12. In HF test calculations the mean absolute (relative) errors of 5f-in-core results with respect to 5f-in-valence reference values for the three series AnF_2 (An = Pu - No; divalent actinides), AnF_3 (An = Ac - Lr; trivalent actinides) and AnF_4 (An = Th - Cf; tetravalent actinides) for the bond lengths are at most 0.03 Å (1.0%), those for the binding energies at most 0.09 eV (2.5%). For AnF_5 (An = Pa - Am; pentavalent actinides) the errors are at most 0.04 Å (1.8%) and 0.09 eV (1.7%), i.e., still acceptable, whereas for AnF_6 (An = U - Am; hexavalent actinides) the 5f-in-core approach obviously reaches its limitations and only yields reasonable results

for UF_6. Here the errors in the bond length and in the binding energy are only 0.001 Å (< 0.1%) and –0.29 eV (–5.1%), respectively. The 5f-in-core f population of 0.96 electrons still agrees quite well with the corresponding 5f-in-valence result of 1.16 electrons, however the large deviation of about one electron from the $5f^0$ occupation modelled by the 5f-in-core PP indicates already a potential source of error. These deviations become even larger for the heavier actinides and much larger discrepancies between both sets of calculations arise. We note here that the 5f-in-core PP modelling hexavalent uranium corresponds simply to a uranium medium-core PP (Q = 14 in Table 6-4) with a usage restriction to formally hexavalent uranium compounds, motivated mainly by its adjustment of the s-, p- and d-projectors to configurations with a $5f^0$ occupation only.

An interesting field of application of 5f-in-core PPs is the hydration of actinides, e.g., actinide (III) ions [148]. Calibration calculations for actinide(III) mono-water complexes at the HF level using valence triple-zeta basis sets show quite satisfactory agreement between 5f-in-core and 5f-in-valence PP results [90]. The trends for actinide-oxygen bond lengths and actinide(III)-water binding energies are displayed in Figures 6-10 and 6-11, respectively.

The PP results agree also reasonably well with AE DHF results of Mochizuki and Tatewaki using the DC Hamiltonian and large basis sets for the actinides, but only double-zeta basis sets for hydrogen and oxygen [87]. We note that the agreement becomes even better, when double-zeta instead of triple-zeta basis sets are applied in the PP calculations. Mochizuki and Tatewaki estimated a basis set superposition error of 0.2 eV in the metal(III)-water binding energies of the corresponding

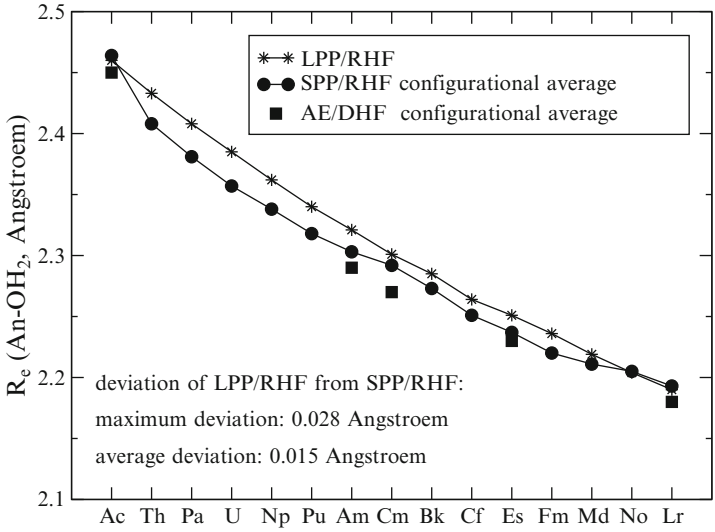

Figure 6-10. Actinide-oxygen distances (Å) of actinide ion water complexes $An^{3+}H_2O$ (An = Ac - Lr) calculated at the Hartree–Fock level with 5f-in-core (LPP) and 5f-in-valence (SPP) pseudopotentials using standard basis sets of An pVTZ and O, H cc-pVTZ quality. The all-electron Dirac–Hartree-Fock/Dirac–Coulomb results [87] use An (30s25p19d13f2g) and H, O cc-pVDZ basis sets

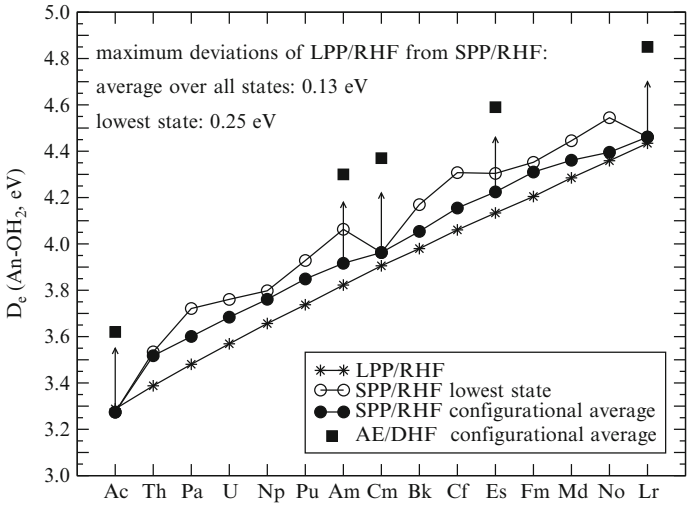

Figure 6-11. Binding energies (eV) of actinide ion water complexes $An^{3+}H_2O$ (An = Ac − Lr) calculated at the Hartree–Fock level with 5f-in-core (LPP) and 5f-in-valence (SPP) pseudopotentials using standard basis sets of An pVTZ and O, H cc-pVTZ quality. The all-electron Dirac–Hartree–Fock/Dirac–Coulomb results [87] use An (30s25p19d13f2g) and H, O cc-pVDZ basis sets and are most likely affected by basis set superposition errors of 0.2 eV or more (cf. text). The effect of reducing the H, O basis sets from cc-pVTZ to cc-pVDZ quality is indicated by the arrows

lanthanide(III) mono-water complexes, but did not report corresponding numbers in case of the actinide systems. Their total energies for the actinides obtained in the finite basis set deviate twice as much as for the lanthanides from finite difference DHF/DC limit values, i.e., the basis set superposition errors might even be slightly larger in the actinide systems than in the lanthanide systems.

Besides the above systems the 5f-in-core PP approach was also tested for actinocenes $An(C_8H_8)_2$ [88]. The stability of these systems arises from both the involvement of the actinide 6d and 5f orbitals in metal-ring bonding. Whereas the former is explicitly accounted for in the 5f-in-core PP approach, the latter is only taken into account implicitly. For a partially occupied $5f^n$ shell ($n < 14$ and integral) implicitly included in the PP core, the f projector of a 5f-in-core PP allows by construction to accommodate explicitly a small additional fraction of δn electrons in the 5f shell, i.e., a $5f^{n+\delta n}$ occupation. In case of uranocene $U(C_8H_8)_2$ the central U^{4+} $5f^2$-in-core ion can accept some additional charge from the two aromatic $C_8H_8^{2-}$ ligands explicitly in e_{2g} symmetry and implicitly in e_{2u} symmetry in the D_{2h} point group. At the HF level 5f-in-core and 5f-in-valence PP results for $An(C_8H_8)_2$ (An = Th - Pu) deviate on average by 0.025 Å (1.2%) for the metal-ring distances and 0.92 eV (1.1%) for the ionic metal-ring binding energies. These differences could be even decreased when adding a core-polarization potential (CPP) to the 5f-in-core pseudopotential. At the coupled cluster level using basis sets of polarized double-zeta quality for carbon and hydrogen the metal-ring distances of thorocene and uranocene agree within 0.012 and 0.042 Å, respectively, with the experimental results.

A borderline case for the application of 5f-in-core PPs are uranyl UO_2^{2+} as well as the related ion UO_2^{+} [89]. In the former case the hexavalent uranium 5f-in-core PP was found to work reasonably well, however as explained above, it is merely a uranium medium-core PP which has been adjusted exclusively for the description of situations with a hexavalent uranium with a formal $5f^0$ occupation. Due to the large structural differences of the individual states (linear $^2\Delta_u$ and $^2\Phi_u$ as well as bent $^2A_1$, $^2B_1$ and $^2B_2$ states) belonging to the modelled superconfiguration as well as the fact that the 5f occupation in small-core PP calculations for some of these states is clearly below the value of one modelled by a PP for a pentavalent uranium, the 5f-in-core PP approach clearly fails for UO_2^{+}. The molecular 5f-in-core PP results reveal that the danger of failure increases with an increasing oxidation number of the actinide. 5f-in-valence PP or AE test calculations at the HF level are recommended for checking if the assumption of a near-integral 5f occupation made in the 5f-in-core PP approach is fulfilled.

We want to end our brief survey of selected applications with the application of the 5f-in-core PP modelling trivalent uranium to the NaCl-structured UN crystal. Evarestov et al. applied the Perdew–Wang (PW) exchange-correlation parametrization of the generalized-gradient approximation and used various scalar-relativistic uranium PPs [45]. The chemical bonding in UN was found to be of metallic-covalent nature, i.e., the uranium 5f orbitals contribute noticeably to the top of the valence band as well as to the bottom of the conduction band, whereas the uranium 6d and 7s orbitals are involved in covalent interactions with the nitrogen 2p orbitals. For various 5f-in-valence medium-core PPs binding energies in the range of 8.6–9.3 eV were found, in strong contrast to the experimental value of 13.6 eV. The 5f-in-core PP modelling trivalent uranium with a $5f^3$ occupation gives a value of 9.9 eV and yields very similar results for the charge distribution as the 5f-in-valence medium-core PPs. Significantly better agreement with the experimental cohesive energy was obtained for the WB-adjusted small-core PP [77] as well as an approximation to the GRECP of Mosyagin and Titov [93] (cf. Table 6-5 for an atomic comparison of the WB-adjusted small-core PP and the full GRECP), i.e., 12.8 eV and 14.9 eV, respectively. The authors attribute the worse performance of the medium-core PPs to large relaxation and polarization effects of the [Rn] $5s^25p^65d^{10}$ semi-core shells, which are only included explicitly in the calculations when a small core is chosen. In addition errors arise most likely from the PW DFT approach, which yields a uranium [Rn] $5f^47s^2$ instead of the experimentally observed [Rn] $5f^36d^17s^2$ ground state configuration. Additional smaller errors are due to the applied truncated uranium basis sets as well as the neglect of SO coupling. We note that for crystalline GdN a 4f-in-core PP modelling a trivalent Gd atom with a $4f^7$ occupation yielded results within a few percent of the experimental values for the lattice constant and the cohesive energy, when a wavefunction-based coupled cluster correlation treatment using the so-called incremental scheme was performed following the periodic HF calculations [72].

All 5f occupations calculated by medium-core PPs were between 3.25 and 3.36 electrons, whereas those obtained from the WB-adjusted small-core PP and the approximate GRECP were 2.77 and 3.07 electrons, respectively. Especially the

former value points to a possible reason for a failure of the 5f-in-core PP, which only can model 5f occupations of three electrons and slightly more, but not less. Further theoretical studies are needed to clarify if a system like crystalline UN with relatively itinerant 5f orbitals is still within the scope of a 5f-in-core PP approach.

6.6. CONCLUSIONS

The present introductory article gave a brief overview of currently used effective core potential (ECP) methods, focussing especially on the energy-consistent pseudopotential (PP) approach. With the development of efficient relativistic all-electron (AE) approaches at the four-, two- and also one-component level and the design of the corresponding computer codes, one might think that ECPs soon will become an outdated approximate computational scheme. It may well be true that the time is gone when ECP ab initio studies of diatomic molecules containing one heavy atom were state-of-the-art in relativistic quantum chemistry, however the accurate treatment of systems with two or more heavy atoms still appears to be a field where ECPs can be very useful. Thus, after almost 75 years of development since the initial work of Hellmann there is still ongoing research by several groups. The emphasis today seems to be mainly on accurate small-core ab initio ECPs modelling rigorous AE calculations, e.g., Dirac–Hartree–Fock (DHF) using the Dirac–Coulomb (DC) or Dirac–Coulomb–Breit (DCB) Hamiltonian, or also Hartree–Fock with the more approximate Douglas–Kroll–Hess Hamiltonian. Since it will become more routine to include spin–orbit (SO) coupling already at the self-consistent field level, or at least in large-scale SO configuration interaction calculations, corresponding reliable two-component instead of merely the scalar-relativistic ECPs are now more frequently developed. During the last decades the accuracy of most ECP approaches has been further increased, so that besides the inclusion of the relativistic effects arising from the DC Hamiltonian also smaller contributions like the Breit interaction or, for heavy elements, the finite nucleus can be taken into account. Thus, in very accurate ECP parametrizations even some effects, which can not be routinely taken into account in AE calculations, can be implicitly included.

In the energy-consistent PP approach a new parametrization of small-core two-component PPs directly adjusted to MCDHF/DC+B finite nucleus reference data is currently performed. The recent development of systematic series of correlation-consistent valence basis sets for these PPs is very beneficial. Although the accuracy of these PPs is higher than the perviously derived Wood–Boring (WB) adjusted PPs, some deficiencies inherent to all PP methods still remain. For example, the overestimation of (some) exchange integrals due to the usage of pseudo-valence orbitals with a simplified radial nodal structure can lead to small errors, which are now nevertheless noticeable, e.g., in some fine-structure splittings, due to the improved overall accuracy of the fit. It remains to be explored in the future, how this small defect can be corrected in a way which does not destroy the computational simplicity of the method.

ACKNOWLEDGEMENTS

The authors are grateful to the German Research Foundation (Deutsche Forschungsgemeinschaft) for support. M.D. thanks H. Stoll as well as P. Schwerdtfeger for long-standing collaborations on the field of energy-consistent relativistic pseudopotentials.

REFERENCES

1. Abarenkov, I.V., Heine, V.: The model potential for positive ions. Phil. Mag. **12**, 529–537 (1965)
2. Ahlrichs, R., et al.: TURBOMOLE, quantum chemistry program system. http://www.turbomole.com
3. Andrae, D., Häußermann, U., Dolg, M., Stoll, H., Preuß, H.: Energy-adjusted ab initio pseudopotentials for the second row and third row transition elements. Theor. Chim. Acta **77**, 123–141 (1990)
4. Andzelm, J., Radzio, E., Salahub, D.R.: Model potential calculations for second-row transition metal molecules within the local-spin-density method. J. Chem. Phys. **83**, 4573–4580 (1985)
5. Bachelet, G.B., Schlüter, M.: Relativistic norm-conserving pseudopotentials. Phys. Rev. B **25**, 2103–2108 (1982)
6. Bachelet, G.B., Hamann, D.R., Schlüter, M.: Pseudopotentials that work: From H to Pu. Phys. Rev. B **26**, 4199–4228 (1982)
7. Barthelat, J.C., Durandi, Ph.: Recent progress of pseudo-potential methods in quantum chemistry. Gaz. Chim. Ital. **108**, 225–236 (1978)
8. Barthelat, J.C., Durand, P., Serafini, A.: Non-empirical pseudopotentials for molecular calculations. I. The PSIBMOL algorithm and test calculations. Mol. Phys. **33**, 159–180 (1977)
9. Batista, E.R., Martin, R.L., Hay, P.J., Peralta, J.E., Scuseria, G.E.: Density functional investigations of the properties of UF_6 and UF_5 using valence-electron and all-electron approaches. J. Chem. Phys. **121**, 2144–2150 (2004)
10. Batista, E.R., Martin, R.L., Hay, P.J.: Density functional investigations of the properties and thermochemistry of UF_n and UCl_n (n = 1 – 6). J. Chem. Phys. **121**, 11104–11111 (2004)
11. Bergner, A., Dolg, M., Küchle, W., Stoll, H., Preuß, H.: Ab initio energy-adjusted pseudopotentials for elements of groups 13 through 17. Mol. Phys. **80**, 1431–1441 (1993)
12. Blaudeau, J.P., Curtiss, L.A.: Optimized Gaussian basis sets for use with relativistic effective (core) potentials: K, Ca, Ga-Kr. Int. J. Quant. Chem. **61**, 943–952 (1997)
13. Bonifacic, V., Huzinaga, S.: Atomic and molecular calculations with the model potential method. I. J. Chem. Phys. **60**, 2779–2786 (1974)
14. Burkatzki, M., Filippi, C., Dolg, M.: Energy-consistent pseudopotentials for Quantum Monte Carlo calculations. J. Chem. Phys. **126**, 234105-1–234105-8 (2007)
15. Burkatzki, M., Filippi, C., Dolg, M.: Energy-consistent small-core pseudopotentials for 3d-transition metals adapted to quantum Monte Carlo calculations. J. Chem. Phys. **129**, 164115-1–164115-7 (2008)
16. Burkatzki, M., et al.: Cologne QMC PPs. http://www.tc.uni-koeln.de/data/psdb/intro.html
17. Cao, X., Dolg, M.: Valence basis sets for relativistic energy-consistent small-core lanthanide pseudopotentials. J. Chem. Phys. **115**, 7348–7355 (2001)
18. Cao, X., Dolg, M.: Segmented contraction scheme for small-core lanthanide pseudopotential basis sets. J. Molec. Struct. (Theochem) **581**, 139–147 (2002)
19. Cao, X., Dolg, M.: Segmented contraction scheme for small-core actinide pseudopotential basis sets. J. Molec. Struct. (Theochem) **673**, 203–209 (2004)

20. Cao, X., Dolg, M.: Relativistic energy-consistent ab initio pseudopotentials as tools for quantum chemical investigations of actinide systems. Coord. Chem. Rev. **250**, 900–912 (2006)
21. Cao, X., Dolg, M., Stoll, H.: Valence basis sets for relativistic energy-consistent small-core actinide pseudopotentials. J. Chem. Phys. **118**, 487–496 (2003)
22. Cao, X., Li, Q., Moritz, A., Xie, Z., Dolg, M., Chen, X., Fang, W.: Density functional studies of actinide (III) motexafins (An-Motex^{2+}, An = Ac, Cm, Lr). Structure, stability and comparison with lanthanide (III) motexafins. Inorg. Chem. **45**, 3444–3451 (2006)
23. Cao, X., Moritz, A., Dolg, M.: All-electron Douglas-Kroll-Hess and pseudopotential study on the low-lying states of uranium hydride UH. Chem. Phys. **343**, 250–257 (2008)
24. Christiansen, P.A., Lee, Y.S., Pitzer, K.S.: Improved ab initio effective core potentials for molecular calculations. J. Chem. Phys. **71**, 4445–4450 (1979)
25. Cowan, R.D., Griffin, D.C.: Approximate relativistic corrections to atomic radial wave functions. J. Opt. Soc. Am. **66**, 1010–1014 (1976)
26. Cundari, T.R., Stevens, W.J.: Effective core potential methods for the lanthanides. J. Chem. Phys. **98**, 5555–5565 (1993)
27. Delley, B.: Hardness conserving semilocal pseudopotentials. Phys. Rev. B **66**, 155125-1–155125-9 (2002)
28. Dolg, M.: On the accuracy of valence correlation energies in pseudopotential calculations. J. Chem. Phys. **104**, 4061–4067 (1996)
29. Dolg, M.: Valence correlation energies from pseudopotential calculations. Chem. Phys. Lett. **250**, 75–79 (1996)
30. Dolg, M.: Effective core potentials. In: J. Grotendorst (ed.) Modern Methods and Algorithms of Quantum Chemistry, John Neumann Institute for Computing, NIC Series, Volume. 1, pp. 479–508, Jülich (2000); Volume 3, pp. 507–540, Jülich (2000)
31. Dolg, M.: Relativistic effective core potentials. In: P. Schwerdtfeger (ed.) Relativistic Electronic Structure Theory, Part 1: Fundamentals; Theoretical and Computational Chemistry, Volume 11, ch. 14, pp. 793–862. Elsevier, Amsterdam (2002)
32. Dolg, M.: Improved relativistic energy-consistent pseudopotentials for 3d transition metals. Theor. Chem. Acc. **114**, 297–304 (2005)
33. Dolg, M., Cao, X.: The relativistic energy-consistent ab initio pseudopotential approach and its application to lanthanide and actinide compounds. In: K. Hirao, Y. Ishikawa (eds.) Recent Advances in Computational Chemistry, Volume 6, pp. 1–35. World Scientific, New Jersey (2004)
34. Dolg, M., Cao, X.: Accurate relativistic small-core pseudopotentials for actinides. Energy adjustment for uranium and first applications to uranium hydride. J. Phys. Chem. A **113**, 12573–12581 (2009)
35. Dolg, M., Wedig, U., Stoll, H., Preuß, H.: Energy-adjusted ab initio pseudopotentials for the first row transition elements. J. Chem. Phys. **86**, 866–872 (1987)
36. Dolg, M., Stoll, H., Preuß, H.: Energy-adjusted ab initio pseudopotentials for the rare earth elements. J. Chem. Phys. **90**, 1730–1734 (1989)
37. Dolg, M., Stoll, H., Savin, A., Preuß, H.: Energy-adjusted pseudopotentials for the rare earth elements. Theor. Chim. Acta **75**, 173–194 (1989)
38. Dolg, M., Stoll, H., Preuß, H., Pitzer, R.M.: Relativistic and correlation effects for element 105 (Hahnium Ha). A comparative study of M and MO (M = Nb, Ta, Ha) using energy-adjusted ab initio pseudopotentials. J. Phys. Chem. **97**, 5852–5859 (1993)
39. Dolg, M., Stoll, H., Preuß, H.: A combination of quasirelativistic pseudopotential and ligand field calculations for lanthanoid compounds. Theor. Chim. Acta **85**, 441–450 (1993)
40. Durand, P., Barthelat, J.C.: A theoretical method to determine atomic pseudopotentials for electronic structure calculations of molecules and solids. Theor. Chim. Acta **38**, 283–302 (1975)

41. Dyall, K.G., Grant, I.P., Johnson, C.T., Parpia, F.A., Plummer, E.P.: GRASP – a general-purpose relativistic atomic structure program. Comput. Phys. Commun. **55**, 425–456 (1989). Dolg, M., Metz, B.: Modifications for PP calculations/optimizations
42. Ermler, W.C., Lee, Y.S., Christiansen, P.A., Pitzer, K.S.: Ab initio effective core potentials including relativistic effects. A procedure for the inclusion of spin-orbit coupling in molecular wavefunctions. Chem. Phys. Lett. **81**, 70–74 (1981)
43. Ermler, W.C., Ross, R.B., Christiansen, P.A.: Spin-orbit coupling and other relativistic effects in atoms and molecules. Adv. Quantum. Chem. **19**, 139–182 (1988)
44. Ermler, W.C., Ross, R.B., Christiansen, P.A.: Ab initio relativistic effective potentials with spin-orbit operators. VI. Fr through Pu. Int. J. Quant. Chem. **40**, 829–846 (1991)
45. Evarestov, R.A., Losev, M.V., Panin, A.I., Mosyagin, N.S., Titov, A.V.: Phys. Stat. Sol. B **245**, 114–122 (2008)
46. Field, R.W.: Diatomic molecule electronic structure beyond simple molecular constants. Ber. Bunsenges. Phys. Chem. **86**, 771–779 (1982)
47. Figgen, D., Rauhut, G., Dolg, M., Stoll, H.: Energy-consistent pseudopotentials for group 11 and 12 atoms: adjustment to multi-configuration Dirac-Hartree-Fock data. Chem. Phys. **311**, 227–244 (2005)
48. Figgen, D., Wedig, A., Stoll, H., Dolg, M., Eliav, E., Kaldor, U.: On the performance of two-component energy-consistent pseudopotentials in atomic Fock-space coupled cluster calculations. J. Chem. Phys. **128**, 024106-1–024106-9 (2008)
49. Figgen, D., Peterson, K.A., Dolg, M., Stoll, H.: Energy-consistent pseudopotentials and correlation consistent basis sets for the 5d elements Hf – Pt. J. Chem. Phys. **130**, 164108-1–164108-12 (2009)
50. Frisch, M., et al.: GAUSSIAN, quantum chemistry program system. http://www.gaussian.com
51. Froese-Fischer, C.: The Hartree-Fock Method for Atoms, Wiley, New York (1977). MCHF77, atomic numerical multi-configuration HF program package. Dolg, M.: modifications for PP calculations/optimizations and WB calculations
52. Fuentealba, P.: On the reliability of semiempirical pseudopotentials: dipole polarizability of the alkali atoms. J. Phys. B: At. Mol. Phys. **15**, L555–L558 (1982)
53. Fuentealba, P., Preuss, H., Stoll, H., v. Szentpály, L.: A proper account of core-polarization with pseudopotentials: single valence-electron alkali compounds. Chem. Phys. Lett. **89**, 418–422 (1982)
54. Gutsev, G.L.: Numerical pseudopotentials within DV-X_α framework. Adv. Quant. Chem. **29**, 137–157 (1997)
55. Hafner, P., Schwarz, W.H.E.: Pseudopotential approach including relativistic effects. J. Phys. B: At. Mol. Phys. **11**, 217–233 (1978)
56. Hamann, D.R., Schlüter, M., Chiang, C.: Norm-conserving pseudopotentials. Phys. Rev. Lett. **43**, 1494–1497 (1979)
57. Hay, P.J., Wadt, W.R.: Ab initio effective core potentials for molecular calculations. Potentials for the transition metal atoms Sc to Hg. J. Chem. Phys. **82**, 270–282 (1985)
58. Hay, P.J., Wadt, W.R.: Ab initio effective core potentials for molecular calculations. Potentials for K to Au including the outermost core orbitals. J. Chem. Phys. **82**, 299–310 (1985)
59. Hellmann, H.: A new approximation method in the problem of many electron electrons. J. Chem. Phys. **3**, 61 (1935)
60. Hess, B.A., Dolg, M.: Relativistic quantum chemistry with pseudopotentials and transformed Hamiltonians. In: B.A. Hess (ed.) Relativistic Effects in Heavy-Element Chemistry and Physics, Wiley Series in Theoretical Chemistry, Volume 12, ch. 3, pp. 89–122. Wiley, New York (2002)
61. Hurley, M.M., Pacios, L.F., Christiansen, P.A., Ross, R.B., Ermler, W.C.: Ab initio relativistic effective potentials with spin-orbit operators: II. K through Kr. J. Chem. Phys. **84**, 6840–6853 (1986)

62. Hülsen, M., Weigand, A., Dolg, M.: Quasirelativistic energy-consistent 4f-in-core pseudopotentials for tetravalent lanthanide elements. Theor. Chem. Acc. **122**, 23–29 (2009)
63. Huzinaga, S., Cantu, A.A.: Theory of separability of many-electron systems. J. Chem. Phys. **55**, 5543–554 (1971)
64. Huzinaga, S., McWilliams, D., Cantu, A.A.: Projection operators in Hartree-Fock theory. Adv. Quantum. Chem. **7**, 187–220 (1973)
65. Huzinaga, S., Seijo, L., Barandiarán, Z., Klobukowski, M.: The ab initio model potential method. Main group elements. J. Chem. Phys. **86**, 2132–2145 (1987)
66. Igel, G., Wedig, U., Dolg, M., Fuentealba, P., Preuß, H., Stoll, H., Frey, R.: Cu and Ag as one-valence-electron atoms: Pseudopotential CI results for CuO and AgO. J. Chem. Phys. **81**, 2737–2740 (1984)
67. Igel-Mann, G., Stoll, H., Preuss, H.: Pseudopotentials for main group elements (IIIa through VIIa). Mol. Phys. **65**, 1321–1328 (1988)
68. Igel-Mann, G., Stoll, H., Preuss, H.: Pseudopotential study of monohydrides and monoxides of main group elements K through Br. Mol. Phys. **65**, 1329–1336 (1988)
69. Kahn, L.R., Goddard, W.A.: Ab initio effective potentials for use in molecular calculations. J. Chem. Phys. **56**, 2685–2701 (1972)
70. Kahn, L.R., Baybutt, P., Truhlar, D.G.: Ab initio effective core potentials: Reduction of all-electron molecular structure calculations to calculations involving only valence electrons. J. Chem. Phys. **65**, 3826–3853 (1976)
71. Kahn, L.R., Hay, P.J., Cowan, R.D.: Relativistic effects in ab initio effective core potentials for molecular calculations – applications to uranium atom. J. Chem. Phys. **68**, 2386–2397 (1978)
72. Kalvoda, S., Dolg, M., Flad, H.-J., Fulde, P., Stoll, H.: Ab initio approach to cohesive properties of GdN. Phys. Rev. B **57**, 2127–2133 (1998)
73. Katsuki, S., Huzinaga, S.: An effective Hamiltonian method for valence-electron molecular calculations. Chem. Phys. Lett. **152**, 203–206 (1988)
74. Klobukowski, M., Huzinaga, S., Sakai, Y.: Model core potentials: Theory and application. In: J. Leszczynski (ed.) Computional chemistry: Reviews of current trends, Volume 3, pp. 49–74. World Scientific, Singapore (1999)
75. Kudin, K.N., Scuseria, G.E., Martin, R.L.: Hybrid density-functional theory and the insulating gap of UO_2. Phys. Rev. Lett. **26**, 266402-1–266402-4 (2002)
76. Küchle, W., Dolg, M., Stoll, H., Preuss, H.: Ab initio pseudopotentials for Hg through Rn. I. Parameter sets and atomic calculations. Mol. Phys. **74**, 1245–1263 (1991)
77. Küchle, W., Dolg, M., Stoll, H., Preuss, H.: Energy-adjusted pseudopotentials for the actinides. Parameter sets and test calculations for thorium and thorium monoxide. J. Chem. Phys. **100**, 7535–7542 (1994)
78. LaJohn, L.A., Christiansen, P.A., Ross, R.B., Atashroo, T., Ermler, W.C.: Ab initio relativistic effective potentials with spin-orbit operators. III. Rb through Xe. J. Chem. Phys. **87**, 2812–2824 (1987)
79. Lee, Y.S., Ermler, W.C., Pitzer, K.S.: Ab Initio Effective Core Potentials Including Relativistic Effects. I. Formalism and Applications to the Xe and Au Atoms. J. Chem. Phys. **67**, 5861–5876 (1977)
80. Lim, I.S., Schwerdtfeger, P., Metz, B., Stoll, H.: All-electron and relativistic pseudopotential studies for the group 1 element polarisabilities from K to element 119. J. Chem. Phys. **122**, 104103-1–104103-12 (2005)
81. Lim, I.S., Stoll, H., Schwerdtfeger, P.: Relativistic small-core energy-consistent pseudopotentials for the alkaline-earth elements Ca to Ra. J. Chem. Phys. **124**, 034107-1–034107-9 (2006)
82. Louie, S.G., Froyen, S., Cohen, M.L.: Nonlinear ionic pseudopotentials in spin-density-functional calculations. Phys. Rev. B **26**, 1738–1742 (1982)

83. Martin, J.M., Sundermann, A.: Correlation consistent valence basis sets for use with the Stuttgart-Dresden-Bonn relativistic effective core potentials: The atoms Ga-Kr and In-Xe. J. Chem. Phys. **114**, 3408–3420 (2001)
84. McMurchie, L.E., Davidson, E.R.: Calculation of integrals over ab initio pseudopotentials. J. Comput. Chem. **4**, 289–301 (1981)
85. Metz, B., Schweizer, M., Stoll, H., Dolg, M., Liu, W.: A small-core multiconfiguration Dirac-Hartree-Fock-adjusted pseudopotential for Tl. Application to TlX (X = F, Cl, Br, I). Theor. Chem. Acc. **104**, 22–28 (2000)
86. Metz, B., Stoll, H., Dolg, M.: Small-core multiconfiguration Dirac-Hartree-Fock-adjusted pseudopotentials for post-d main group elements: Application to PbH and PbO. J. Chem. Phys. **113**, 2563–2569 (2000)
87. Mochizuki, Y., Tatewaki, H.: Four-component relativistic calculations on the complexes between a water molecules and trivalent lanthanoid and actinoid ions. Chem. Phys. **273**, 135–148 (2001)
88. Moritz, A., Dolg, M.: Quasirelativistic 5f-in-core pseudopotential study of the actinocenes $An(C_8H_8)_2$, An = Th-Pu. Chem. Phys. **327**, 48–54 (2007)
89. Moritz, A., Dolg, M.: Quasirelativistic energy-consistent 5f-in-core pseudopotentials for pentavalent and hexavalent actinide elements. Theor. Chem. Acc. **121**, 297–306 (2008)
90. Moritz, A., Cao, X., Dolg, M.: Quasirelativistic energy-consistent 5f-in-core pseudopotentials for trivalent actinide elements. Theor. Chem. Acc. **117**, 473–481 (2007)
91. Moritz, A., Cao, X., Dolg, M.: Quasirelativistic energy-consistent 5f-in-core pseudopotentials for divalent and tetravalent actinide elements. Theor. Chem. Acc. **118**, 2763–2774 (2007)
92. Mosyagin, N.S., Titov, A.V., Latajka, Z.: Generalized relativistic effective core potential: Gaussian expansion of potentials and pseudospinors for atoms Hg through Rn. Int. J. Quant. Chem. **63**, 1107–1122 (1997)
93. Mosyagin, N.S., Petrov, A.N., Titov, A.V., Tupitsyn, I.I.: Generalized RECP accounting for Breit effects: Uranium, plutonium and superheavy elements 112, 113, 114. In: J.P. Julien, J. Maruani, D. Mayou (eds.) Recent Advances in the Theory of Chemical and Physical Systems, Progress in Theoretical Chemistry and Physics, Part II, Volume 15, pp. 253–284. Springer, Berlin (2006)
94. Müller, W., Flesch, J., Meyer, W.: Treatment of intershell correlation effects in ab initio calculations by use of core polarization potentials. Method and application to alkali and alkaline earth atoms. J. Chem. Phys. **80**, 3297–3310 (1984)
95. Nash, C.S., Bursten, B.E., Ermler, W.C.: Ab initio relativistic potentials with spin-orbit operators. VII. Am through element 118. J. Chem. Phys. **106**, 5133–5142 (1994)
96. Nicklass, A., Dolg, M., Stoll, H., Preuß, H.: Ab initio energy-adjusted pseudopotentials for the noble gases Ne through Xe: Calculation of atomic dipole and quadrupole polarizabilities. J. Chem. Phys. **102**, 8942–8952 (1995)
97. National Institute of Standards and Technology (NIST). http://www.nist.gov
98. Pacios, L.F., Christiansen, P.A.: Ab initio relativistic effective potentials with spin-orbit operators. I. Li through Ar. J. Chem. Phys. **82**, 2664–2671 (1985)
99. Paulovič, J., Nakajima, T., Hirao, K., Seijo, L.: Third-order Douglas-Kroll ab initio model potential for actinide elements. J. Chem. Phys. **117**, 3597–3604 (2002)
100. Paulovič, J., Nakajima, T., Hirao, K., Lindh, R., Malmqvist, P.A.: Relativistic and correlated calculation on the ground and excited states of ThO. J. Chem. Phys. **119**, 798–805 (2003)
101. Peterson, K.A.: Systematically convergent basis sets with relativistic pseudopotentials. I. Correlation consistent basis sets for the post-d group 13-15 elements. J. Chem. Phys. **119**, 11099–11112 (2003)
102. Peterson, K.A., Puzzarini, C.: Systematically convergent basis sets for transition metals. II. Pseudopotential-based correlation consistent basis sets for the group 11 (Cu, Ag, Au) and 12 (Zn, Cd, Hg) elements. Theor. Chem. Acc. **114**, 283–296 (2005)

103. Peterson, K.A., Figgen, D., Goll, E., Stoll, H., Dolg, M.: Systematically convergent basis sets with relativistic pseudopotentials. II. Small-core pseudopotentials and correlation consistent basis sets for the post-d group 16-18 elements. J. Chem. Phys. **119**, 11113–11123 (2003)
104. Peterson, K.A., Figgen, D., Dolg, M., Stoll, H.: Energy-consistent relativistic pseudopotentials and correlation consistent basis sets for the 4d elements Y-Pd. J. Chem. Phys. **126**, 124101-1–124101-12 (2007)
105. Phillips, J.C., Kleinman, L.: New method for calculating wave functions in crystals and molecules. Phys. Rev. **116**, 287–294 (1959)
106. Pittel, B, Schwarz, W.H.E.: Correlation energies from pseudopotential calculations. Chem. Phys. Lett. **46** 121–124 (1977)
107. Pitzer, R.M.: ATMSCF, Atomic Electronic Structure Code. The Ohio State University, Columbus (2003)
108. Pitzer, R.M., Winter, N.W.: Electronic-structure methods for heavy-atom molecules. J. Phys. Chem. **92**, 3061–3063 (1988)
109. Preuss, H.: Untersuchungen zum kombinierten Näherungsverfahren. Z. Naturf. **10a**, 365–373 (1955)
110. Preuss, H., Stoll, H., Wedig, U., Krüger, T.: A combination of pseudopotentials and density functionals. Int. J. Quant. Chem. **19**, 113–130 (1981)
111. Prodan, I.D., Scuseria, G.E., Martin, R.L.: Assessment of metageneralized gradient approximation and screened Coulomb hybrid density functionals on bulk actinide oxides. Phys. Rev. B. **73**, 045104-10–045104-10 (2006)
112. Pyykkö, P., Stoll, H.: Relativistic Pseudopotential Calculations, 1993–June 1999. In: A. Hincliffe (ed.) R.S.C. Spec. Period. Rep., Chemical Modelling, Applications and Theory, Volume 1, pp. 239–305. Cambridge (2000)
113. Rakowitz, F., Marian, C.M., Seijo, L., Wahlgren U.: Spin-free relativistic no-pair ab initio core model potentials and valence basis sets for the transition metal elements Sc to Hg. I. J. Chem. Phys. **110**, 3678–3686 (1999)
114. Rakowitz, F., Marian, C.M., Seijo, L.: Spin-free relativistic no-pair ab initio core model potentials and valence basis sets for the transition metal elements Sc to Hg. II. J. Chem. Phys. **111**, 10436–10443 (1999)
115. Ross, R.B., Powers, J.M., Atashroo, T., Ermler, W.C., LaJohn, L.A., Christiansen, P.A.: Ab initio relativistic effective potentials with spin-orbit operators. IV. Cs through Rn. J. Chem. Phys. **93**, 6654–6670 (1990)
116. Ross, R.B., Gayen, S., Ermler, W.C.: Ab initio relativistic effective potentials with spin-orbit operators. V. Ce through Lu. J. Chem. Phys. **100**, 8145–8155 (1994)
117. Roy, L.E., Hay, P.J., Martin, R.L.: Revised basis sets for the LANL effective vore potentials. J. Chem. Theor. Comput. **4**, 1029–1031 (2008)
118. Sakai, Y.: New developments in the model potential method. J. Chem. Phys. **75**, 1303–1308 (1981)
119. Sakai, Y., Huzinaga, S.: The use of model potentials in molecular calculations. I. J. Chem. Phys. **86**, 2132–2145 (1982)
120. Smit, M.J.: Multicenter integrals over polarization potential operators. Int. J. Quant. Chem. **73**, 403–416 (1999)
121. Schwerdtfeger, P.: Relativistic effects in molecules: Pseudopotential calculations for TlH^+, TlH and TlH_3. Phys. Scr. **36**, 453–459 (1987)
122. Schwerdtfeger, P.: Relativistic Pseudopotentials. In: U. Kaldor, S. Wilson (eds.) Progress in Theoretical Chemistry and Physics – Theoretical chemistry and physics of heavy and superheavy element, pp. 399–438. Kluwer, Dordrecht (2003)
123. Schwerdtfeger, P., Silberbach, H.: Multicenter integrals over long-range operators using Cartesian Gaussian functions. Phys. Rev. A **37**, 2834–2842 (1988). Erratum: ibidem, **42**, 665 (1990)

124. Schwerdtfeger, P., v.Szentpaly, L., Vogel, K., Silberbach, H., Stoll, H., Preuss, H.: Relativistic and correlation effects in pseudopotential calculations for Br, I, HBr, HI, Br_2 and I_2. J. Chem. Phys. **84**, 1606–1612 (1986)
125. Schwerdtfeger, P., v.Szentpaly, L., Stoll, H., Preuss, H.: Relativistic pseudopotential calculations for HBr^+, HBr, HBr^-, HI^+, HI, HI^-. J. Chem. Phys. **87**, 510–513 (1987)
126. Seijo, L., Barandiarán, Z.: The ab initio model potential method: a common strategy for effective core potential and embedded cluster calculations. In: J. Leszczynski (ed.) Computional chemistry: Reviews of current trends, Volume 4, pp. 55–152. World Scientific, Singapore (1999)
127. Seth, M., Schwerdtfeger, P., Dolg, M.: The chemistry of the superheavy elements. I. Pseudopotentials for 111 and 112 and relativistic coupled cluster calculations for $(112)H^+$, $(112)F_2$ and $(112)F_4$. J. Chem. Phys. **106**, 3623–3632 (1997)
128. Sheu, J.-H., Lee, S.-L., Dolg, M.: Calibration of relativistic energy-consistent small-core pseudopotentials for 3d-transition metals. J. Chin. Chem. Soc. **50**, 583–592 (2003)
129. Smallwood, C.J., Larsen, R.E., Glover, W.J., Schwartz, B.J.: A computationally efficient exact pseudopotential method. I. Analytic reformulation of the Phillips-Kleinman theory. J. Chem. Phys. **125**, 074102-1–074102-9 (2006)
130. Smallwood, C.J., Meija, C.N., Glover, W.J., Larsen, R.E., Schwartz, B.J.: A computationally efficient exact pseudopotential method. II. Application to the molecular pseudopotential of an excess electron interacting with tetrahydrofuran (THF). J. Chem. Phys. **125**, 074103-1–074103-9 (2006)
131. Stevens, W.J., Basch, H., Krauss, M.: Compact effective potentials and efficient shared-exponent basis sets for the first- and second-row atoms. J. Chem. Phys. **81**, 6026–6033 (1984)
132. Stevens, W.J., Krauss, M., Basch, H., Jasien, P.J.: Relativistic compact effective potentials and efficient, shared-exponent basis sets for the third-, fourth-, and fifth-row atoms. Can. J. Chem. **70**, 612–630 (1992)
133. Stoll, H., Fuentealba, P., Dolg, M., Flad, J., v. Szentpály, L., Preuß, H.: Cu and Ag as one-valence-electron atoms: Pseudopotential results for Cu_2, Ag_2, CuH, AgH, and the corresponding cations. J. Chem. Phys. **79**, 5532–5542 (1983)
134. Stoll, H., Fuentealba, P., Schwerdtfeger, P., Flad, J., v. Szentpály, L., Preuß, H.: Cu and Ag as one-valence-electron atoms: CI results and quadrupole corrections for Cu_2, Ag_2, CuH, AgH. J. Chem. Phys. **81**, 2732–2736 (1984)
135. Stoll, H., Metz, B., Dolg, M.: Relativistic energy-consistent pseudopotentials — recent developments. J. Comput. Chem. **23**, 767–778 (2002)
136. Stoll, H., et al.: Stuttgart-Cologne PPs. http://www.theochem.uni-stuttgart.de/pseudopotentials
137. Teichteil, C., Malrieu, J.P., Barthelat, J.C.: Non-empirical pseudopotentials for molecular calculations. 2. basis set extension and correlation effects on X_2 molecules (X = F, Cl, Br, I). Mol. Phys. **33**, 181–197 (1977)
138. Titov, A.V., Mosyagin, N.S.: Generalized relativistic effective core potential: Theoretical ground. Int. J. Quant. Chem. **71**, 359–401 (1999)
139. Titov, A.V., Mosyagin, N.S.: The generalized relativistic effective core potential method: Theory and calculations. Russ. J. Phys. Chem. **74**, S376–S387 (2000)
140. Titov, A.V., Mosyagin, N.S., Isaev, T.A., Petrov, A.N.: Accuracy and efficiency of modern methods for electronic structure calculation on heavy- and superheavy-elements compounds. Phys. At. Nucl. **66**, 1188–1198 (2003)
141. Tsuchiya, T., Nakajima, T., Hirao, K., Seijo, L.: A third-order Douglas-Kroll ab initio model potential for the lanthanides. Chem. Phys. Lett. **361**, 334–340 (2002)
142. Wadt, W.R., Hay, P.J.: Ab initio effective core potentials for molecular calculations. Potentials for main group elements Na to Bi. J. Chem. Phys. **82**, 284–298 (1985)
143. Wang, Y., Dolg, M.: Pseudopotential study of the ground and excited states of Yb_2. Theor. Chem. Acc. **100**, 124–133 (1998)

144. Wedig, U., Dolg, M., Stoll, H.: Energy-adjusted pseudopotentials for transition-metal elements. In: A. Veillard (ed.) Quantum Chemistry: The Challenge of Transition Metals and Coordination Chemistry, NATO ASI Series, Series C, Mathematical and Physical Sciencies, Volume 176, pp. 79–89. Reidel, Dordrecht (1986)
145. Weeks, J.D., Rice, S.A.: Use of pseudopotentials in atomic-structure calculations. J. Chem. Phys. **49**, 2741–2755 (1968)
146. Weigand, A., Cao, X., Vallet, V., Flament, J.-P., Dolg, M.: Multiconfiguration Dirac-Hartree-Fock adjusted energy-consistent pseudopotential for uranium: Spin-orbit configuration interaction and Fock-space coupled-cluster study of U^{4+} and U^{5+}. J. Phys. Chem. A **113**, 11509–11516 (2009)
147. Werner, H.-J., Knowles, P.J., et al.: MOLPRO, quantum chemistry program system. http://www.molpro.net
148. Wiebke, J., Moritz, A., Cao, X., Dolg, M.: Approaching actinide (III) hydration from first principles. Phys. Chem. Chem. Phys. **9**, 459–465 (2007)
149. Wildman, S.A., DiLabio, G.A., Christiansen, P.A.: Accurate relativistic effective potentials for the sixth-row main group elements. J. Chem. Phys. **107**, 9975–9979 (1997)
150. Wood, J.H., Boring, A.M.: Improved Pauli Hamiltonian for local-potential problems. Phys. Rev. B **18**, 2701–2711 (1978)
151. Yang, J., Dolg, M.: Valence basis sets for lanthanide 4f-in-core pseudopotentials adapted for crystal orbital ab initio calculations. Theor. Chem. Acc. **113**, 212–224 (2005)

CHAPTER 7

FOUR-COMPONENT ELECTRONIC STRUCTURE METHODS

EPHRAIM ELIAV AND UZI KALDOR
School of Chemistry, Tel Aviv University, 69978 Tel Aviv, Israel
e-mail: ephraim@tau.ac.il, kaldor@tau.ac.il

Abstract: Four-component relativistic methods are the most accurate available for heavy atoms and molecules. Their history, current status and perspectives for further development are reviewed. Their main application is for benchmark calculations of heavy element compounds. Benchmarking requires continued improvement of the relativistic Hamiltonian towards the goal of fully covariant description, as well as development of high level correlation methods suitable for general open shell systems. One of the best relativistic many-body approaches available for the purpose is the multi-root, multi-reference Fock space coupled cluster (FSCC) method. It is size extensive, and usually gives the most precise results within the four-component no-virtual-pair approximation (NVPA). The relativistic FSCC method and its recent applications are described. Relativistic effects beyond NVPA may be studied using quantum electrodynamics (QED). We discuss the challenges of introducing covariant many-body QED methods suitable for use in quantum chemistry. Mathematical and physical foundations for merging many-body relativistic approaches, in particular FSCC, with QED theory are presented. A promising technique is Lindgren's covariant evolution operator (CEO) method, in combination with the generalized Fock space with variable numbers of electrons and uncontracted virtual photons. The relationship of the CEO approach to the Bethe-Salpeter covariant equation and other QED schemes is discussed. Size-consistent computational schemes, combining variational treatment of first order QED effects (Lamb shifts) at the SCF step with infinite order treatment of QED and correlation, are under development. For cases of quasidegenerate levels, common in heavy systems, multireference approaches must be used. Double (electronic and photonic) Fock-space CC, a covariant multireference multi-root many-body-QED approach, is presented.

Keywords: Four-component relativistic methods, Coupled cluster, Fock-space methods, Quantum electrodynamics

7.1. INTRODUCTION

Notation and Units All mathematical expressions appearing in this chapter are in atomic units, unless otherwise stated. In these units, the electron mass m and the elementary charge e are unity. However, we retain their symbols in equations in

M. Barysz and Y. Ishikawa (eds.), *Relativistic Methods for Chemists*,
Challenges and Advances in Computational Chemistry and Physics 10,
DOI 10.1007/978-1-4020-9975-5_7,

order to demonstrate how the fundamental characteristics of the electrons enter the equations and clearly distinguish equations describing electrons from those describing its antiparticle, the positron. Operators carry operator hats, and three-component vectors appear in bold characters. The Einstein summation convention or implicit summation is used, so that a repeated index is summed over.

The chapter starts with an overview of relativistic four-component methodology (Section 7.2). We then proceed to describe the relativistic Fock-space coupled cluster (Section 7.3.1) and intermediate Hamiltonian approaches (Section 7.3.2), followed by applications to heavy (Section 7.4) and superheavy (Section 7.5) atoms. The methods described have also been used to study heavy molecules such as UO_2 (Section 7.4), nuclear quadrupole moments (Section 7.4.6) and adsorption behavior of superheavy elements produced in accelerators, crucial for their separation and identification (Section 7.5.6). The last part (Section 7.6) delineates directions under development which promise, in our opinion, exciting progress in the foreseeable future.

7.2. FOUR-COMPONENT METHODOLOGY

The building blocks of the four-component methods are described in this Section. We start with the Dirac equation, then discuss the many-body QED Hamiltonian and its no-virtual-pair approximation. The later subsections describe the ways and means of applying this formalism to atomic and molecular systems.

7.2.1. Dirac Equation – Historical Overview

The revolution in physics at the beginning of the twentieth century revealed two fundamental facts, namely that our reality is quantum and relativistic. Theoretical chemistry was one of the first sciences to recognize the overwhelming importance of the first fact, namely the quantum nature of matter, and adopt non-relativistic quantum theory in the form of the many-body Schrödinger equation (SE) for calculation of atomic and molecular systems. Since then, a whole arsenal of powerful many-body approaches and efficient computer codes has been developed by the quantum chemical community, with the aim of solving the non-relativistic stationary Schrödinger equation with the highest precision possible. Many high-level quantum-chemical methods used to solve the SE, including configuration interaction (CI), many-body perturbation theory (MBPT), multi-configuration self consistent field (MCSCF) and coupled cluster (CC), became standard; they are available in off-the-shelf, user-friendly chemical software, and are used routinely in high-quality or even benchmark calculations of many systems. Properties of small molecules composed of first- and second-row atoms, with states having single-reference character, can now be obtained with accuracy rivaling that of experiment, as demonstrated, e.g., in the recent book of Helgaker et al. [1]. All the standard many-body approaches exploit the fact that interactions in non-relativistic Hamiltonians can be expressed in closed analytical form and are at most two-body and instantaneous (e.g., the classical Coulomb potential). The most precise and systematic of these

approaches are based on many-body perturbation theory. Advanced MBPT schemes can treat electron correlation effects to essentially all orders, using methods of the coupled cluster type. CC approaches are based on exponential parameterization of the wave operator, which leads to coupled nonlinear equation, solved iteratively. The Rayleigh–Schrödinger formulations of MBPT and CC benefit from being size-consistent (giving correct dissociation limits for the energy and wave function) and size-extensive (have linear energy scaling with the size of the system). Using a time-independent diagrammatic technique of the Goldstone type in the MBPT/CC methods [2] permits direct summation of the size-extensive energy contributions (expressed by connected diagrams) of instantaneous electron–electron interactions to infinite order. The MBPT and CC methods also have multireference variants, capable of treating difficult to calculate quasi-degenerate atomic and molecular structures. Among the multireference MBPT/CC approaches, the multi-root methods, based on effective Hamiltonians and "extended model-spaces technique" [2], are probably the most efficient, universal and precise, due to balanced treatment of non-dynamic (quasi-degeneracy) and dynamic correlation effects.

Relativity has been introduced to the realm of physics, including the micro scale, even before quantum theory. In fact, Schrödinger himself derived a relativistic equation prior to publishing his famous nonrelativistic wave equation. The relativistic equation was found in his notebooks from late 1925, and he appears to have prepared a manuscript applying it to the hydrogen atom [3]. However, he later discarded the relativistic equation, because it yielded incorrect fine structure levels for the hydrogen atom. It was also plagued by some strange features, very difficult for physical interpretation: the equation appeared to give negative probabilities and allow negative energy states. The equation Schrödinger discarded was rederived independently in 1926 by several physicists, including Klein, Fock, and de Broglie (for an exciting historical review see [4] and references therein), and has later proved to describe spinless bosonic particles. This equation is known as the Klein–Gordon equation, and may be written in the following covariant (independent of Lorentz frame transformations) form [5]:

$$\left(\Box^2 + m^2c^2\right)\psi = 0, \quad \text{where} \quad \Box^2 = \partial_\mu \partial^\mu = \partial^2/c^2\partial t^2 - \boldsymbol{\nabla}^2. \tag{7-1}$$

The relativistic quantum equation for fermionic particles with spin $\frac{1}{2}$, which serve as the building blocks of atoms and molecules, has been proposed by Dirac in 1928 [6], just two years after publication of the Schrödinger and Klein–Gordon equations. Dirac's celebrated equation constitutes the foundation of relativistic quantum mechanics. Detailed accounts of the mathematical properties and physical interpretation of the Dirac equation, important for quantum chemistry, may be found in several recently published books [7–13], and will not be repeated here. Some important points will be addressed below, closely following [14].

It is convenient to write the Dirac equation in covariant form,

$$\left(i\,\gamma_\mu \partial^\mu - mc\right)\psi = 0, \tag{7-2}$$

where γ_μ are related to the Dirac matrices,

$$\gamma_\mu = \beta\,(\boldsymbol{\alpha}\,, iI_4)\,, \quad \boldsymbol{\alpha} = \begin{pmatrix} 0_2 & \boldsymbol{\sigma} \\ \boldsymbol{\sigma} & 0_2 \end{pmatrix}, \quad \beta = \begin{pmatrix} I_2 & 0_2 \\ 0_2 & -I_2 \end{pmatrix}. \tag{7-3}$$

$\boldsymbol{\sigma}$ are the Pauli spin matrices. The four-gradient ∂^μ is

$$\partial^\mu = \left(\boldsymbol{\nabla}, -\frac{i}{c}\frac{\partial}{\partial t}\right). \tag{7-4}$$

This equation resolves some of the problems of the Klein–Gordon equation, but still allows for negative energy states. A more familiar form of the free-particle Dirac equation is obtained upon multiplication by βc from the left,

$$\left(\hat{h}_{D;0} - i\frac{\partial}{\partial t}\right)\psi = 0, \quad \hat{h}_{D;0} = \beta mc^2 + c\,(\boldsymbol{\alpha}\cdot\mathbf{p}) \tag{7-5}$$

External fields are introduced through the principle of minimal electromagnetic action [15],

$$p_\mu \to \pi_\mu = p_\mu - qA_\mu, \tag{7-6}$$

in which the 4-momentum $p_\mu = -i\,\partial_\mu$ and the 4-potential $A_\mu = (\mathbf{A}, \frac{i}{c}\phi)$ appear. For electrons, the particles of interest here, the charge is $q = -e$; for positrons it would be $q = +e$. The electronic Dirac equation is then

$$\hat{D}\psi = \left(\hat{h}_{D;A_\mu} - i\frac{\partial}{\partial t}\right)\psi = 0, \tag{7-7}$$

where $\hat{h}_{D;A\mu}$ is the Dirac Hamiltonian of a single electron in an external field,

$$\hat{h}_{D;A\mu} = \beta mc^2 + c\,(\boldsymbol{\alpha}\cdot\boldsymbol{\pi}) - e\phi. \tag{7-8}$$

The operators appearing in the Dirac equation (7-7) are 4×4 matrix operators, and the corresponding wave function is therefore a four-component vector function,

$$\psi = \begin{pmatrix} \psi^L \\ \psi^S \end{pmatrix}; \quad \psi^X = \begin{pmatrix} \psi^{X\alpha} \\ \psi^{X\beta} \end{pmatrix}, \quad X = L, S. \tag{7-9}$$

The four degrees of freedom reflect the fact that the Dirac equation describes both electrons and positrons and explicitly includes spin. For a given external potential and the chosen charge $q = -e$, both the positive energy and negative energy solutions correspond to the *electronic* states. In the non-relativistic limit, the lower two components of the positive energy solutions go to zero, whereas the upper two components reduce to a spin orbital in which the spatial part solves the non-relativistic electronic Schrödinger equation. The upper and lower two components

are therefore generally referred to as the large (marked 'L' in (7-9)) and small components ('S' in (7-9)), respectively. For the same potential, the negative energy branch of the spectrum gives the positronic solutions indirectly, either by charge conjugation of the electronic solutions (see, e.g., [13, 14]) or, following the original idea of Dirac, by filling all negative energy continuum states with electrons using the Pauli principle (so called Dirac's filled sea) and then regarding the positrons as hole states in this electron-filled continuum. Looking at the positronic solutions in the non-relativistic limit, the large components are those going to zero. It is therefore more logical to speak about upper and lower components rather than large and small ones [16]. However, since the focus in chemistry is on electronic solutions, the common terminology will be used. It is important to note that the large components of the positive energy solutions of the Dirac equation are large by a factor c only in an average sense; there may be regions in space where the small components dominate [14].

While relativity became a fundamental working concept and tool in quantum physics, it was not until the 1970s that quantum chemists realized the importance of relativity in chemistry and applied relativistic quantum chemistry to many-electron atomic and molecular systems. Some of the reasons for this delay are discussed below.

At the early stages of the development of fundamental quantum theory, many outstanding scientists, including Dirac himself, believed that relativity cannot play any substantial role in describing atomic and molecular systems (see [17] for relevant quotations). The triumphal success of non-relativistic quantum chemical methodology has been reached in describing systems composed of light elements (including many organic compounds) and initially confirmed those beliefs. Compounds of light elements were the only systems computationally treatable during the first three decades of quantum chemistry. Not until the mid-1970s did computers become powerful enough to produce quantitative calculations of heavy species, and more precise calculations of light systems revealed deviations from experiment in many cases. Attempts to understand some discrepancies led to realizing the importance of relativity in chemistry and to the eventual development of relativistic many-body methodology. It is now well established and illustrated by many calculations and experiments that the structure, spectroscopy and chemical activity of heavy atoms and molecules exhibit large relativistic effects. These effects play an important role in lighter element compounds too, showing up in phenomena such as fine or hyperfine structure of electronic states. Relativistic effects in chemistry are described in the books listed above [7–13]. A comprehensive catalog of relativistic quantum chemistry literature has been compiled by Pyykkö [18–20]; a regularly updated version may be found online [21].

Another reason for the relatively late (and still uncompleted) development of the many-body relativistic methodology are the theoretical difficulties and inconsistencies encountered when trying to combine the principles of relativity and quantum many-body theory in a consistent and usable scheme. Soon after the development of Dirac's electronic theory it became obvious that a relativistically covariant and consistent quantum description of many-body micro-world phenomena is possible only

if matter (electrons), radiation field (photons) and their interactions are described on equal footing. Fundaments of the theory based on the principles formulated above were introduced by Feynman, Dyson, Schwinger, Tomonaga and others in the late 1940s [22–25]. The theory is commonly dubbed quantum electrodynamics (QED), a relativistically consistent quantum description of all electromagnetic processes, neglecting other fundamental interactions, i.e., weak, strong and gravitational forces. This neglect is supported by many low- and high-energy scattering experiments of elementary particles and photons as well as spectral analysis. QED is probably the most successful fundamental physical theory developed to date. It can describe almost all observed microscopic events of size greater than 10^{-13} cm, and may thus be regarded as a natural basis for the development of relativistic quantum chemistry. However, for reasons discussed below, the impact of QED on the development of quantum chemistry till now has been rather limited. The physical interpretation of wave functions described by relativistic equations and, consequently, the methodology of solving these equations in QED, is substantially different from the many-body technique used in quantum chemistry. The QED is, in principle, an infinite-body theory, or, more precisely, it describes systems with infinite numbers of degrees of freedom, namely fields, which are relativistically and gauge invariant. Quantum field theory, a whole system of mathematical tools developed especially for solving QED and other gauge theory problems, must thus be adapted to the objects of quantum chemistry, which are finite size atomic and molecular systems in stationary states. It would be logical to carry out this adaptation, which is still far from complete, using the Hamiltonian formalism, widespread in quantum chemistry but less popular in QED. The next subsection shows a very brief derivation of the QED Hamiltonian in a form suitable for developing a covariant many-body procedure, with the aim of applying this procedure later in molecular electronic structure calculations.

7.2.2. QED Hamiltonian

The QED Hamiltonian is usually derived by a quantization procedure of the classical electrodynamic (CED) counterpart. The CED theory describes the classical radiation (electromagnetic) and matter (fermionic) fields, as well as their interactions, in covariant manner. The quantization, as shown below, leads to a form identical with the CED equations, but the interpretation of the QED fields differs substantially from both the CED and Dirac's theory. Thus, Dirac's four-component spinor ψ does not describe in QED a single electronic state, but is rather interpreted as an electronic field operator, which can create and destroy particles. The number of particles is not conserved in a QED system, contrary to the situation in an isolated molecular system; only the electric charge is a constant of motion.

The starting point for CED, and therefore also for QED field theory, is the Lagrangian formalism, which allows the correct identification of conjugate momenta appearing in the Hamiltonian [26]. Below we present a very brief introduction of the QED Lagrangian and Hamiltonian formalisms, following Labzowsky's

book [27] and two more recent reviews [14, 28]. The classical Lagrangian density for interacting electromagnetic and fermionic fields has the form

$$\mathcal{L}_{\text{QED}} = \mathcal{L}_{\text{rad}} + \mathcal{L}_{\text{mat}} + \mathcal{L}_{\text{int}}\,. \tag{7-10}$$

The first term describes the electromagnetic degrees of freedom,

$$\mathcal{L}_{\text{rad}} = -\frac{1}{16\pi} F^{\mu\nu} F_{\mu\nu}, \tag{7-11}$$

where $F^{\mu\nu} = \partial^\mu A^\nu - \partial^\nu A^\mu$ is the antisymmetric electromagnetic field tensor. The second term $\mathcal{L}_{\text{mat}}$ is the Dirac 4-spinor matter (fermionic) field ψ,

$$\mathcal{L}_{\text{mat}} = \overline{\psi}\left(i\gamma_\mu \partial^\mu - mc\right)\psi, \tag{7-12}$$

where $\overline{\psi} = \psi^+\gamma_0 = (\psi_1^*, \psi_2^*, -\psi_3^*, -\psi_4^*)$ is the adjoint spinor. Note that the minimal substitution, used in (7-6), follows from the last term $\mathcal{L}_{\text{int}}$ in the Lagrangian, which describes the interaction between the fermionic and electromagnetic fields as the product of the 4-current $j_\mu = (\mathbf{j}, ic\rho)$ and the 4-potential $A^\mu = \left(\mathbf{A}, i\frac{\varphi}{c}\right)$,

$$\mathcal{L}_{\text{int}} = j_\mu A^\mu. \tag{7-13}$$

This term was first proposed by Schwarzschild [29] to satisfy Lorentz covariance, and is employed on an ad hoc basis in the non-relativistic domain, even though it does not represent the proper non-relativistic limit, which is electrostatics (see [30] and references therein). Comparing (7-7), regarded now as a classical covariant equation of motion for the fermionic field (see also (7-23) below), and (7-13), we can identify the 4-current as

$$j_\mu = -ec\psi^\dagger\beta\gamma_\mu\psi; \quad \rho = -e\psi^\dagger I_4\psi; \quad \mathbf{j} = -ec\psi^\dagger\boldsymbol{\alpha}\psi. \tag{7-14}$$

The scalar ϕ and vector $\mathbf{A}$ potentials define the electric (E) and magnetic (B) fields,

$$\mathbf{E} = -\nabla\phi - \frac{\partial \mathbf{A}}{\partial t}; \quad \mathbf{B} = \nabla \times \mathbf{A}. \tag{7-15}$$

The freedom of gauge [31] allows the coice of the most convenient form of the potentials. Usually, a uniform electric field is represented by $A_\mu = \left(0, -\frac{i}{c}\mathbf{E}\cdot\mathbf{r}\right)$, since it can be handled by time-independent theory [32]. The most popular gauge in quantum chemistry is the Coulomb gauge $\nabla\cdot\mathbf{A} = 0$. From Maxwell's equations and the definitions (7-15), the field equations in the presence of a density ρ and a current $\mathbf{j}$ can then be expressed as [33]

$$\nabla^2\phi = -4\pi\rho \tag{7-16}$$

$$\left(\nabla^2\mathbf{A} - \alpha^2\frac{\partial^2\mathbf{A}}{\partial t^2}\right) - \nabla\alpha^2\frac{\partial\phi}{\partial t} = -4\pi\alpha^2\mathbf{j}, \tag{7-17}$$

where α is the fine-structure constant. The equation for the scalar potential is simply the Poisson equation with the solution

$$\phi(\mathbf{r},t) = \int \frac{\rho(\mathbf{r}',t)}{|\mathbf{r}-\mathbf{r}'|} d\tau'. \tag{7-18}$$

The scalar potential is given in the Coulomb gauge by the *instantaneous* charge density. The effects of retardation, as well as magnetic interactions, enter through the vector potential as higher-order terms in a perturbation expansion of the total interaction in terms of the fine-structure constant α [34]. Thus, the interaction between two point charges q_1 and q_2 with velocities $\mathbf{v}_1$ and $\mathbf{v}_2$ is given to second order in Coulomb gauge by [31,35,36]

$$\mathcal{L}_{\text{int}} = \frac{q_1 q_2}{r_{12}} \left[-1 + \frac{1}{2c^2} \left\{ (\mathbf{v}_1 \cdot \mathbf{v}_2) + \frac{1}{r_{12}^2} (\mathbf{r}_{12} \cdot \mathbf{v}_1)(\mathbf{r}_{12} \cdot \mathbf{v}_2) \right\} \right]. \tag{7-19}$$

The first term may be identified as a charge-charge interaction, whereas the second term is a current-current interaction.

In electronic structure theory we employ $\hat{h}_{D;V}$, the Dirac operator in the molecular field. It corresponds to the introduction of the 4-potential

$$\phi(\mathbf{r}_i) = \sum_A \frac{Z_A e}{|\mathbf{r}_i - \mathbf{R}_A|}; \quad \mathbf{A}(\mathbf{r}_i) = 0, \tag{7-20}$$

where $Z_A e$ and $\mathbf{R}_A$ are the charge and position, respectively, of nucleus A. The nuclei are treated as sources of external scalar potentials, and nuclear spins are ignored. This "clamped nucleus" approximation is essentially the same as the one introduced by Born and Oppenheimer [37] in non-relativistic theory, in which the main assumption is that electrons follow the slower movements of nuclei adiabatically.

The Lagrangian $\mathcal{L}_{\text{QED}}$ describes both the electromagnetic and fermionic degrees of freedom, as well as interactions between them, simultaneously and on equal footing as dynamic variables. The Lagrangian has all necessary symmetry properties for correctly formulated one dimensional gauge-field theory: it is Lorentz covariant and gauge invariant, since local gauge transformations of the form

$$A_\mu(x) \to A'_\mu(x) = A_\mu(x) + \partial_\mu \lambda(x) \tag{7-21}$$

$$\psi(x) \to \psi'(x) = \exp[-i\lambda(x)]\psi(x), \tag{7-22}$$

with $\lambda(x)$ an arbitrary gauge function, leave the Lagrangian (7-10) invariant. The gauge transformation of the fermionic field spinor $\psi(x)$ describes rotations in the complex plane, which is the reason for calling QED an Abelian

U(1) gauge theory. The least action principle, $\delta S = \delta \int d^4x \; \mathcal{L}_{\text{QED}} = 0$, under arbitrary infinitesimal variations of the dynamic field variables A_μ and ψ, yields the coupled equations of motion

$$\begin{aligned} \partial_\mu F^{\mu\nu} &= 4\pi j^\nu \\ \left(i\gamma_\mu \partial^\mu - mc\right)\psi &= e\gamma_\mu A^\mu \psi. \end{aligned} \tag{7-23}$$

The first of these equations is the most general covariant form of the inhomogeneous Maxwell equations, written previously in the more standard form (7-16) and (7-17). It implies immediately the continuity equation $\partial_\mu j^\mu = 0$. The second equation in (7-23) is the covariant Dirac equation in the presence of an external electromagnetic field. This equation has been presented earlier in slightly different form (7-7) as the relativistic quantum mechanical one electron equation. Note that the Dirac equation has now been derived from the classical least action principle, and is thus interpreted as an Euler–Lagrange classical equation for the spinor field ψ rather than a quantum mechanical wave equation.

The quantization procedure is usually done in the Hamiltonian formulation. Our next step is therefore the transition of the QED theory from the Lagrangian to the Hamiltonian formulation, using the Legendre transformation. This step requires the definition of the conjugate momenta

$$\pi = \frac{\partial \mathcal{L}_{\text{QED}}}{\partial \dot{\psi}} = i\psi, \qquad \Pi_\mu = \frac{\partial \mathcal{L}_{\text{QED}}}{\partial \dot{A^\mu}} = \frac{1}{4\pi} F_{\mu 0}. \tag{7-24}$$

After some tedious mathematical manipulations, the final classical Hamiltonian density is given by

$$\begin{aligned} \Re_{QED} &= \Pi_\mu \dot{A^\mu} + \pi\dot{\psi} - \mathcal{L}_{\text{QED}} \\ &= \frac{1}{8\pi}(\mathbf{E}^2 + \mathbf{B}^2) + \frac{1}{4\pi}\mathbf{E}\cdot\nabla\varphi - \overline{\psi}\left(i\gamma_\mu\partial^\mu - mc\right)\psi + e\overline{\psi}\gamma^\mu\psi A_\mu. \end{aligned} \tag{7-25}$$

This expression for the Hamiltonian density is no longer manifestly Lorentz or gauge invariant. However, all physical observables, including energies, field gradients, transition amplitudes, etc., which can be deduced from this Hamiltonian density, are Lorentz and gauge invariant. After integration over all space, using partial integration in the second term of (7-25) and the Gauss law, the classical Hamiltonian is obtained,

$$\begin{aligned} H_{QED} &= \int dr^3 \Re_{QED} \\ &= \int dr^3 \left\{ \frac{1}{8\pi}(\mathbf{E}^2 + \mathbf{B}^2) + \psi^+ \left[\boldsymbol{\alpha}\cdot(-i\nabla - e\mathbf{A}) + \beta mc + e\varphi\right]\psi \right\}. \end{aligned} \tag{7-26}$$

Dirac's $\boldsymbol{\alpha}$ matrices have been introduced here for convenience, $\boldsymbol{\alpha} = \gamma^0\boldsymbol{\gamma}$. Expression (7-26) is the classical Hamiltonian of the U(1) gauge field theory of interacting dynamical electromagnetic and fermionic fields, written in a particular gauge independent form. This Hamiltonian is now ready to be quantized, although this is not technically simple, and is gauge dependent. Consistent quantization of this field theory may be achieved by a constrained canonical procedure [38] or the manifestly covariant Gupta–Bleuler formalism [39, 40]. The resulting quantum field theory of QED properly describes the structure and interactions of the quanta of fermionic fields (e.g., electrons and positrons) with quanta of electromagnetic fields (e.g., photons). The second quantized quantum mechanical Hamiltonian in QED has exactly the same form as (7-26), but all fields have now been upgraded to field operators, acting on occupation number vectors in an appropriate Fock space with variable numbers of electrons/positrons and photons. One of the options in this canonical formalism is to express all physical observables by particle-antiparticle creation/destruction operators arranged in normal order, renormalizing the vacuum energy to zero. The problem of negative energy states is completely removed, since both electrons and positrons have positive energies due to normal ordering. QED approaches are time-dependent, due to the retarded character of interactions. Standard QED methods, such as Green functions and S-matrix, are based on the time-dependent Feynman diagrams technique. These methods suffer from some methodological problems, described at the end of the current subsection, which prevent their use in quantum chemical calculations of stationary states. A novel powerful QED method, with structure resembling that of stationary many-body approaches, has been developed recently by Lindgren and coworkers [41–46]. It offers the possibility of being merged with quantum chemical machinery based on the Bloch equation to provide a unified tool suitable for application to general quasidegenerate atomic and molecular configurations. This so-called covariant evolution operator (CEO) method is described in Section 7.6.2.

The total number of particles in QED is not conserved, and electron–positron pair creation processes are included in calculations. The number of photons is also variable, depending on the particular process. The CEO method has a particularly simple form when formulated in generalized Fock space with variable numbers of fermions and so-called uncontracted virtual photons. This is why we consider it a natural framework for implementing Fock-space many-body quantum chemical approaches, capable of describing systems with a variable number of particles. In particular, the relativistic Fock-space coupled cluster (FSCC) approach, which is an all-order, size extensive, multi-root, multi-reference method (for a recent review see [47]), is an ideal candidate for merging with CEO. The relativistic FSCC method and its recent applications in the effective and intermediate Hamiltonian formulations are described in Section 7.3–7.5. In the last Section we present briefly a double Fock-space CC method, based on CEO-QED. Another promising option, which can be applied within the algebraic approximation, is to use (at least at the SCF step) the so-called variational QED procedure [14]: the explicitly filled Dirac negativeenergy sea is included in the system core states, thus defining the HF state

formally as having large but finite charge and mass. The renormalization procedure is then included in the SCF iterations explicitly. A modification of this procedure, described in Section 7.6.1 below, is based on using negative energy states of the free electron as well as single retarded photon exchange effective potential. This will incorporate the leading radiation effects (Lamb shifts) in the renormalized HF energy and wave function self-consistently, so that the appropriate reducible multiphotonic part of the vacuum polarization and the self energy will be included in the direct and exchange SCF terms, respectively,

There are still fundamental problems which make the merging of QED and quantum chemistry a difficult theoretical task. These problems, which have been solved only partially, fall in two categories, interpretational and methodological:

(1) *Interpretational Problems* A second quantization approach based on electron–positron operators invalidates the direct interpretation of the field operators $\widehat{\psi}$ as the usual quantum mechanical wave functions, since superposition of states with variable numbers of particles is not compatible with simple probabilistic interpretation of the wave function. In interpreting the field operators $\widehat{\psi}$ several other serious problems are encountered, as discussed early on by Dyson [48], Wick [49], and Goldstein [50]. Dyson was particularly concerned about the meaning of the wave function in relativistic quantum mechanics, characterizing this as a subject "full of obscurities and unsolved problems". Solving the QED many-particle problem leads to a description with individual times for the different particles. This description is manifestly relativistically covariant, but is not in accordance with the standard quantum mechanical picture, where we have a common time for all particles. The divergence from the "normal" quantum mechanical picture leads to "spurious" or "abnormal" solutions in QED without physical significance or nonrelativistic counterpart [51]. Another fundamental problem, discussed by Gross [52], is that the QED equations do not reduce to the correct "one-body limit" when one of the particles becomes infinitely heavy, which is important for proper implementation of the Born–Oppenheimer approximation. However, it was later found that problems of this kind are most pronounced in the scattering of strongly interacting particles, and not as important for bound-state systems in weak coupling [53–57].

(2) *Methodological Problems* The traditional QED techniques, such as S-matrix, are very different from many-body methods used in quantum chemistry for describing stationary states. The main computational drawback of existing QED methods from the point of view of quantum chemistry is their concentration on calculating the energy shifts while not including the QED effects in the wave function in a consistent and clear manner. Another important point is that most QED methods (with a few exceptions, see [41, 58]) cannot treat degenerate or quasi-degenerate configurations, which are common in open shell heavy species. In quantum chemistry, the derivation of the Hamiltonian is distinct from solving for its eigenvalues; in contrast, the same QED approach is often used both for deriving the potential and calculating the energy shift caused by it.

7.2.3. Particle–Particle Interaction and the No-Virtual-Pair approximation

Due to the theoretical problems enumerated above, and the long-going practice (justified in many cases) of ignoring many-body relativistic and QED effects, the evolution of quantum chemical tools for calculating relativistic effects has been historically directed more by the well developed non-relativistic many-body methodology than by QED. QED was used post factum, if at all, e.g., for justifying already developed relativistic methodology. The very "philosophy" and structure of relativistic quantum chemistry methods, mostly adopted from the non-relativistic realm, are different from those of QED. Atomic and molecular systems are described in chemistry as systems with a finite number of particles interacting via instantaneous, energy independent two-body potentials. This picture ignores partially or fully some fundamental phenomena, such as the existence of the negative energy states continuum, radiative effects and retardation of the inter particle interactions, which are important for a fully covariant description. Fortunately, many of these QED corrections are numerically small for real atomic and molecular systems, explaining the relative success of "naive" and direct schemes of constructing relativistic many-body Hamiltonians by simple summation of one-electron Dirac Hamiltonians and inter-particle two-body "classical" instantaneous potentials. The most rigorous of such four-component Hamiltonians is the Dirac–Coulomb (DC) Hamiltonian, which uses the non-relativistic Coulomb form of interparticle interactions,

$$\hat{H} = \sum_i \hat{h}_{D;V}(i) + \frac{1}{2}\sum_{i\neq j} \hat{g}^{\text{Coulomb}}(i,j) + \hat{V}_{nn};\quad \hat{V}_{nn} = \frac{1}{2}\sum_{A\neq B} \frac{Z_A Z_B e^2}{|\mathbf{R}_A - \mathbf{R}_B|}, \tag{7-27}$$

where $\hat{h}_{D;V}(i)$ are the one-electron four-component Dirac operators in the molecular field, and $\hat{V}_{nn}$ is the classical internuclear potential. The inter-electronic potential $\hat{g}^{\text{Coulomb}}(i,j)$ is the Coulomb term

$$\hat{g}^{\text{Coulomb}}(i,j) = e^2 \frac{I_4 \cdot I_4}{r_{ij}}, \tag{7-28}$$

where the 4×4 identity matrices I_4 have been inserted to stress that, although the Coulomb term looks like the non-relativistic electron–electron interaction, its physical content is different. Upon reduction to non-relativistic form [59–63] through a Foldy–Wouthuysen transformation, one finds that the relativistic operator contains for instance spin-own orbit interaction in addition to the instantaneous Coulomb interaction. The first scheme based on the DC Hamiltonian was developed in 1935 by Swirles [64], who generalized the SCF approach of her scientific adviser Hartree to the relativistic realm. However, as pointed out above, practical relativistic quantum chemical calculations did not appear until the 1970s.

The transformation of the inter-electronic interaction to covariant form may be made by adding the missing effects of retardation and magnetic interaction to the non-relativistic limit represented by the instantaneous Coulomb interaction. The necessary correction terms can be obtained rigorously by invoking the full machinery of QED, where the interactions are described in terms of the exchange of virtual photons. However, the first derivations of such corrections were done in the semiclassical limit, using continuous electromagnetic fields. The lowest order relativistic corrections to the Coulomb electrostatic interaction between the electrons were considered for the first time in the Feynman (Lorentz) gauge ($\partial^\mu A_\mu = 0$) by Gaunt in 1929 [65], when a magnetic interaction of order α^2 was added to the DC Hamiltonian (7-27). This magnetostatic term is called the Gaunt interaction and has the form

$$\hat{g}^{\text{Gaunt}}(1,2) = -e^2 \frac{c\boldsymbol{\alpha}_1 \cdot c\boldsymbol{\alpha}_2}{c^2 r_{12}}. \tag{7-29}$$

The Gaunt interaction is instantaneous, similar to the Coulomb term. One can furthermore show by reduction to the non-relativistic form that the Gaunt term carries all spin-other orbit interactions [66]. It was later shown by Breit [67] that the retardation of the Coulomb interaction gives rise to effects of the same order, α^2. This leads, together with the magnetic interaction, to the so-called Breit interaction [67]

$$\hat{g}^{\text{Breit}}(1,2) = -\frac{e^2}{2c^2 r_{12}} \left[(c\boldsymbol{\alpha}_1 \cdot c\boldsymbol{\alpha}_2) + \frac{1}{r_{12}^2} (c\boldsymbol{\alpha}_1 \cdot \mathbf{r}_{12}) (c\boldsymbol{\alpha}_2 \cdot \mathbf{r}_{12}) \right]. \tag{7-30}$$

The Breit term is written here in a slightly unusual form [14], using explicitly the relativistic velocity operator $c\boldsymbol{\alpha}$. It is thus shown to be the quantum mechanical analogue of the classical expression (7-19). While the Breit term can be derived as the low-frequency limit of the single virtual photon exchange interaction in the Coulomb gauge as described by QED (see Section 7.6.2), it can equally well [61] be derived from the quantization of (7-19), which is essentially the way used by Breit. The final form of the Dirac–Coulomb–Breit (DCB) Hamiltonian is

$$\hat{H}_{\text{DCB}} = \sum_i \hat{h}_{D;V}(i) + \frac{1}{2} \sum_{i \neq j} \{ \hat{g}^{\text{Coulomb}}(i,j) + \hat{g}^{\text{Breit}}(i,j) \} + \hat{V}_{nn}. \tag{7-31}$$

The Breit interaction (7-30) is instantaneous, although it compensates for the leading effect of the retardation of the Coulomb interaction. In a full QED treatment (see Section 7.6.2) there is an additional time/energy dependent retardation effect of the Breit interaction of order α^3. If energy is conserved, the exchange of a single transverse retarded photon (Figure 7-1) yields the following form of the frequency dependent Breit interaction for the case of "on shell" interactions,

$$\hat{g}_\omega^{\text{Breit}}(1,2) = -\frac{e^2}{2c^2 r_{12}} \left[(c\boldsymbol{\alpha}_1 \cdot c\boldsymbol{\alpha}_2) - \frac{(c\boldsymbol{\alpha}_1 \cdot \boldsymbol{\nabla}_1) (c\boldsymbol{\alpha}_2 \cdot \boldsymbol{\nabla}_2) (\exp(i|\omega|r_{12}) - 1)}{\omega^2} \right]. \tag{7-32}$$

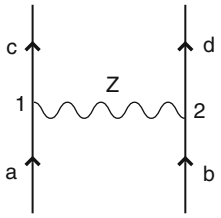

Figure 7-1. The exchange of a single photon between two electrons can be simulated by an effective potential $g_\omega(1,2)$. The heavy lines represent the electronic states in the bound-interaction SCF picture

In the SCF approximation, the photon frequency ω is defined by the orbital energy difference $\omega = (\varepsilon_a - \varepsilon_c)/c = (\varepsilon_d - \varepsilon_b)/c$ (see Figure 7-1 for notation). In the zero-frequency or energy independent limit $\omega \to 0$, the expression (7-32) transforms into (7-30).

In the alternative Feynman gauge, the frequency dependent Gaunt interaction has the form

$$\hat{g}_\omega^{\text{Gaunt}}(1,2) = -e^2 \frac{c\boldsymbol{\alpha}_1 \cdot c\boldsymbol{\alpha}_2 \exp(i|\omega|r_{12})}{c^2 r_{12}}. \tag{7-33}$$

In the zero frequency (energy independent) limit this interaction is transformed into the instantaneous Gaunt interaction (7-29). As we saw before, the instantaneous Gaunt interaction does not contain any retardation, and therefore the retardation correction to this interaction is of the order α^2, an order of magnitude larger than energy independent interaction in the Coulomb gauge, which is the Breit term (7-30). This implies that when the frequency independent Gaunt potential (Feynman gauge) is used in the quantum chemical calculations of heavy element compounds, considerable errors may be introduced [68–71]. In QED calculations, on the other hand, when the retardation is properly taken care of, this error is eliminated, and the Feynman gauge is often used due to its simplicity.

The first quantum chemists to implement four-component calculations regarded the DCB Hamiltonian as the best theoretical framework for relativistic many-body methods. Most of the approaches implemented were adapted from the non-relativistic realm by using special relativistically invariant double point groups, as well as Kramers (time-reversal) symmetry when applicable. In the atomic case, the high symmetry allows the separation of radial and angular degrees of freedom. The angular part can be solved analytically with the help of Racah algebra [72], whereas the radial equations can be solved by finite difference methods. In molecular calculations one has to resort to the *algebraic approximation*, the use of finite basis set expansions. This approximation is often used for atoms too. The first basis set calculations led to rather disastrous results (see [73] for references), caused by the fact that the relativistic four-component Hamiltonian (7-27) is not bounded from below. This is due to the existence of the negative energy continuum, which in the usual quantum chemical practice is kept unfilled and may be used for relaxation of occupied atomic/molecular electronic levels. Special caremust be

taken for correct formulation of the SCF and correlation methods based on such a Hamiltonian. The main numerical problems of the DCB Hamiltonian, with possible solutions, are listed below, sorted by the steps of solving the four-component relativistic equation.

1. *SCF and Orbital Generation Step* The standard SCF procedure used in non-relativistic calculations is based on a Hamiltonian bounded from below and directed by the variational theorem toward reaching the energy minimum. This standard procedure cannot be applied to four-component Hartree–Fock calculations, because the states of interest are electron-like and therefore excited states in the spectrum of the relativistic Hamiltonian. However, variational theory is also applicable to *stationary* states, so it may be used in the relativistic Hartree–Fock theory. Talman [74] and LaJohn and Talman [75] pointed out that it is feasible to find the electron-like positive energy solutions by using a minimax principle, where the energy is minimized with respect to rotations in the virtual positive energy spinor space (the optimization process used in the non-relativistic approach) and maximized with respect to rotations in the negative energy spinor space. The positive and negative energy parts of the spectrum are well separated energetically, and the optimization procedure is feasible. The coupling of the large and small components of the Dirac equation leads to a difference in parity of the two components, and thus requires separate basis set expansions for each component. However, the small and large component basis sets should not be chosen independently. In order to make the minimax variational procedure stable, one has to impose a special condition, known as "kinetic balance", connecting the small and large component basis sets, or else face the so called "variational collapse" [73] or "basis set disease" [76] (see Section 7.2.5).
2. *Electron Correlation Step* There has been considerable discussion as to the stability of the Dirac–Coulomb–(Breit) Hamiltonian in the correlation step, particularly in variational procedures. The discussion originated from an argument put forward by Brown and Ravenhall [77], who considered the interaction of two electrons described by this Hamiltonian. In a perturbation treatment of the He atom, one may start with the non-interacting system and form a Slater determinant consisting of the 1s orbitals obtained by solving the hydrogenic atom with $Z = 2$. This Slater determinant is, however, degenerate with an (in principle) infinite number of Slater determinants built of one orbital from the positive continuum and one from the negative continuum. When the electron–electron interaction is turned on in the correlation step, all these determinants will mix in and lead to what has been called a continuum dissolution or "Brown–Ravenhall disease", meaning that no bound state is obtained. Brown and Ravenhall proposed to put the interelectronic interactions between projection operators onto the positive energy spectrum, Λ^+, to avoid the mixing in of these continuum determinants. This proposal has beenfurther explored by Sucher and

others (see [78] for a review), on the basis of QED theory. The final projected Dirac–Coulomb–(Breit) Hamiltonian has the form

$$\hat{H}^{+}_{\mathrm{DCB}} = \sum_i \hat{h}_{D;V}(i) + \frac{1}{2}\sum_{i\neq j} \Lambda_i^{+}\{\hat{g}^{\mathrm{Coulomb}}(i,j) + \hat{g}^{\mathrm{Breit}}(i,j)\}\Lambda_j^{+} + \hat{V}_{nn}$$

$$\Lambda_i^{+} = \sum_n^{+} \psi_n^{+}(x_i)\psi_n(x_i). \tag{7-34}$$

H^{+}_{DCB} is correct to second order in the fine-structure constant α, but is not covariant. This Hamiltonian is expected to be highly accurate for most neutral and weakly ionized atoms and molecules [79]. Higher quantum electrodynamic (QED) terms are required for benchmark calculations of multiply ionized species of heavy-element compounds; they will be considered in the last Section of this chapter. If one constructs the projection operators from the same independent particle basis used in the expansion of the second quantized form of H^{+}_{DCB}, which is almost always the case, the effect of the projection operators is simply to limit the eigenfunction of H^{+}_{DCB} to configurations with positive energy spinors only. In practice, the continuum dissolution problem was solved in the algebraic approximation by simply ignoring the negative energy branch in the correlation step, and four-component relativistic molecular calculations are routinely carried out today. When the finite difference method is used for atoms, the two problems listed above are solved by imposing the electron-like boundary conditions at $r = 0$ and $r \to \infty$ for bound solutions [80]. The approximation based on H^{+}_{DCB} is called no-virtual pair approximation (NVPA), since the virtual electron–positron pairs which cause the Brown–Ravenhall disease are eliminated.

The H^{+}_{DCB} Hamiltonian is not unique, since the distinction between electron and positron creation and annihilation operators, as well as the operators Λ^{+}, depend on the orbital set in which the field operators are expanded. One possible choice is the eigenorbitals of the free-particle Dirac equation (7-5), giving the "free" picture. Another choice is the solutions of the Dirac equation in the molecular field (7-20), leading to the Furry picture [81]. A third possibility is to continuously update the projection operators in each SCF iteration, so that they correspond at convergence to the solutions of the combined molecular and mean-field potentials of the Hartree–Fock equations. This "fuzzy" picture, proposed by Mittleman [82], corresponds to the standard four-component approach. Some authors do not distinguish between the "fuzzy" and "Furry" pictures (see, for instance [27]). The optimal choice of the projection operators is discussed in [83].

Properly designed four-component many-electron NVPA methods are currently the most elaborate and precise approaches for molecules and most atoms, and are used for benchmark calculations. The separate basis set expansion of the large and small components used in NVPA leads to higher computational cost compared with non-relativistic or more approximate relativistic methods. Careful

analysis shows that the cost difference between four-component NVPA schemes and non-relativistic methods is in the prefactor, not in the scaling [14]. Still, this difference is large enough to encourage the use of more cost-efficient relativistic approximations, which replace four-component approaches by two- or one-component schemes. One-component methods include only the so-called scalar (or kinematic) relativistic effects. Two-component approaches incorporate, in addition, electron spin effects. Exact (or infinite order) two-component (X2C) methods have been developed recently ([84–89] and references therein). Most X2C methods are iterative and based on either elimination techniques for the small component or special unitary transformations which decouple the NVPA Hamiltonian. They are capable of reproducing the energies of four-component NVPA in the iterative numerical limit if the same projection operators are used in the NVPA Hamiltonian. This condition is not trivial to satisfy. Four-component methods usually allow the continuous update of the NVPA Hamiltonian, and therefore the complete relaxation of the electronic wave function, whereas in most X2C approaches this relaxation is absent, due to the use of predefined projection operators before performing an approximate decoupling of the electronic and positronic degrees of freedom. X2C may lead to excellent approximations and allow relativistic calculations at reduced computational cost, but it is incorrect to state that it provides complete equivalence with the four-component methods. It should also be noted that the reduction of computational cost relative to four-component NVPA occurs only at the SCF and integral transformation steps; the correlation step has the same computational scaling in two- and four-component methods [14].

A different approach to computational cost saving retains the four-component framework and seeks savings by the reduction or elimination of intermediate quantities (e.g., two-electron integrals) appearing in the calculations, exploiting the atomic nature of the small component density. The current status and perspectives of this approach are discussed in [14].

The four-component approach is mandatory if one wishes to go beyond the NVPA approximating and formulate a strictly covariant many-body theory. Such formulations, which may have a fundamental character and impact quantum chemistry science, are not available as yet. This is mainly due to the impossibility of expressing covariant particle-particle interactions in closed analytical energy-independent form, of the type used in building quantum mechanical Hamiltonians for stationary atomic and molecular states. As stated before, deriving a covariant relativistic many-body method requires switching to the QED framework instead of the quantum mechanics basis. The QED description includes four-component fermionic quantum fields and explicit treatment of photons. The evident drawback is that the already high computational scaling with system size of four-component methods becomes even worse, due to the photonic degrees of freedom. This would make many-body-QED methods applicable to benchmark calculations of small systems only. The rapidly increasing computational resources and algorithm improvements make it, however, feasible to follow this rather uncompromising route.

It will be demonstrated in Sections 7.6.1 and 7.6.2 that the recently developed covariant evolution operator method of Lindgren [41–44], in combination with the

modified variational QED–SCF procedure [14], which includes the leading radiation effects self-consistently, makes possible the development of rigorous and feasible many-body QED methodology with updatable WF. The QED methods under development have a structure similar to all-order effective Hamiltonian many-body NVPA approaches, and are suitable for use in quantum chemistry, including the most complicated quasi-degenerate situations. Not all many-body NVPA methods should be considered for merging with novel QED methodology, but only those with the appropriate structure and properties. In the next subsection we overview high-level relativistic many-body NVPA approaches, emphasizing all-order Fock-space methods which are suitable for merging with QED. Recent methodological developments and applications of relativistic FSCC within NVPA are presented in Section 7.3. A plan is then drawn for going beyond NVPA and incorporating the QED effects in consistent and systematic manner, using the covariant evolution operator approach and generalized Fock space with variable numbers of electrons and photons. In Section 7.6.2 we present a short review of the CEO method, and then discuss an efficient way of simultaneously including the most important correlation and QED effects in "all-order" and size-extensive fashion, using summation of the many electron and photon contributions in a double (electronic and photonic) Fock space coupled cluster procedure.

7.2.4. The NVPA Hamiltonian and Benchmarking of Four-Component Methods

The general form of the molecular many-electron Hamiltonian is

$$\hat{H} = \sum_i \hat{h}(i) + \frac{1}{2}\sum_{i\neq j} \hat{g}(i,j) + \hat{V}_{nn}, \tag{7-35}$$

where $\hat{h}(i)$ are one-electron operators, $\hat{g}(i,j)$ represents the two-electron interaction, and $\hat{V}_{nn}$ is the classical repulsion of fixed nuclei. This form is valid in both the relativistic and non-relativistic domains, to the extent that three-particle and higher interactions can be ignored, together with the negative energy spectrum and radiative corrections. The last two demands are applicable to the four-component relativistic case, when the one-electron part $\hat{h}(i)$ is represented by the Dirac operator. The negative energy branch of the spectrum is treated as a virtual subspace in the SCF minimax procedure and is eliminated later in the correlation step, using NVPA. The NVPA is realized by "surrounding" the $\hat{g}(i,j)$ potential with projection operators Λ^+, which project out the positive energy spinors. For the development of quantum chemistry methods it is rarely necessary to be more specific regarding the form of the many-electron Hamiltonian. This holds particularly true if the operator is recast in second quantized form. As noted above, all interparticle potential energy terms in the Hamiltonian are expressed in closed analytical time/energy independent form in both the non-relativistic and relativistic NVPA formalism. This is very different from the situation in QED, where the potential can be expressed *approximately* as an infinite sum of energy/time dependent many-body terms, usually evaluated numerically.

Four-component methods are the most precise and expensive quantum-chemical techniques, and are mostly used for benchmark calculations. Benchmarking these methods includes convergence studies, involving in some cases extrapolation techniques, of three aspects of the application:

(1) *Quality of Hamiltonian* It includes higher order nuclear and QED effects. We shall discuss the possibility of increasing the level of the QED treatment of interelectron interactions towards the fully covariant description. Consideration of different nuclear corrections may be found in [90].

(2) *Quality of the Hamiltonian Eigenvalues and Eigenfunctions* This involves mainly the treatment of electron correlation, including higher orders of the dynamic correlation effects, always treated approximately, as well as increasing the size of the active space, treated "exactly" by diagonalization, which is particularly important when quasidegeneracy is significant. Correlation methods used in the relativistic domain are similar to those of nonrelativistic quantum chemistry. A short list, with representative references to atomic and molecular applications, is given here:

- Density Functional Theory (DFT) [91–96]
- Multi-Configuration Self Consistent Field (MCSCF): atoms [97–103], molecules [104–106]
- CI: atoms [99, 107, 108], molecules [106, 109, 110]
- MBPT: atoms [111–114], molecules [115, 116]
- Coupled Cluster (CC): atoms [117–123], molecules [124–130]

The history, benefits, drawbacks, technical features and suitability to the QED framework of those methods in their four-component implementation are discussed briefly below.

(3) *Quality of Algebraic Approximation* This involves mainly the development and application of better and more complete one-electron basis sets. Some aspects of the use of basis sets are presented in Section 7.2.5. A recent review of basis sets suitable for four-component atomic and molecular electronic structure calculations may be found in [13].

The quality and usefulness of specific computational schemes is largely determined by these three aspects, but also by what may seem of technical nature, the quality of algorithms and software used in the implementation. Highly efficient algorithms must be developed and coded, including parallelization and distribution procedures. The most advanced four-component computer programs, together with some of their important features, are listed here for atoms (Table 7-1) and molecules (Table 7-2).

The first method used extensively to include correlation in relativistic four-component calculations was the numerical atomic multiconfiguration Dirac–Fock (MCDF) scheme [97–99]. This method gives, in general, good atomic term energies and transition probabilities. It is particularly successful in treating nondynamic correlation, where a few hundred configuration state functions are sufficient; the many thousands of CSFs required for accurate description of dynamic correlation are sometimes beyond its reach (see, e.g., the recent calculation of Rodrigues et al. [138] for atomic Cs, where the MCDF results could not be converged with respect to configuration space). Atomic MCSCF has been implemented in a Gaussian basis

Table 7-1 Atomic four-component programs

Program name {main authors}	Methods	Basis sets	Ref.
GRASP {Grant, Quiney, Dyall, Parpia, Froese-Fischer, Fritzsche}	MCSCF, CI	Numerical	[98–100]
MCDFGME {Desclaux, Indelicato}	MCSCF	Numerical	[131]
{Ishikawa, Koc, Vilkas}	MCSCF, MRMP2	GTO, STO	[103, 113]
{Johnson, Sapirstein, Blundell, Derevyanko, Safronova}	MBPT, CC	B-splines	[112, 118]
{Lindgren, Salomonson, Lindroth, Mårtensson-Pendrill}	MBPT, CC	Numerical	[117, 120]
{Eliav, Kaldor, Ishikawa}	FSCC	GTO, STO	[121]
{Das, Sahoo, Chaudhuri, Mukherjee}	FSCC	GTO	[123]
{Flambaum, Sushkov, Dzuba, Kozlov}	MBPT, CC, CI	Numerical	[114]

Table 7-2 Molecular four-component programs

Program name	Hamiltonian	Methods	Ref.
MOLFDIR	DC, DCG	CI, CCSD(T), MP2	[132]
DIRAC	DC, DCG	CI, CC, FSCC, MP2, MCSCF, DFT	[133]
UTCHEM	DC	CC,CI	[134]
DREAMS	DC	MP2	[135]
BERTHA	DC, DCB	MBPT, CC	[136]
PROPHET4R	DC	CI	[137]
BDF	DC	DFT	[92]

by Vilkas et al. [103]. Four-component molecular MCSCF has been developed and implemented recently [104–106]. Four-component CI approaches in atomic [99, 107, 108] and molecular [106, 109, 110] versions are available in many codes (see Tables 7-1 and 7-2) and used routinely. Both MCSCF and CI methods are not size-extensive and require corrections when used in benchmark calculations for many electron systems.

Another class of methods, which have the advantage of size-extensivity, goes under the heading "many-body (perturbation) methods", reviewed recently by Sapirstein [139] for atoms and by Saue and Visscher [14] for molecules. For highly ionized atoms, second-order many-body perturbation theory (2nd-order MBPT, better known to chemists as Mller–Plesset or MP2 theory) is accurate enough to see QED effects from differences between calculated and experimental values for highly ionized atoms. Neutral or weakly ionized atoms and molecules, on the other hand, require higher order treatment of correlation. One approach to the problem is relativistic multireference MBPT, implemented recently in a Gaussian basis for atoms by Ishikawa and coworkers [113]. An alternative scheme involves infinite-order summation of perturbation terms, accomplished by the coupled cluster method [140–142]. A numerical procedure for solving the relativistic many-body Dirac–Coulomb equation, based on the pair approximation of the CC approach, has been developed by Lindgren and coworkers [117]. A different approach employs discrete basis sets of local or global functions. Summation over an infinite set of bound states

and integration over the positive energy continuum are replaced by finite summation over the pseudospectrum. The implementation of the projection operators is made easy by the clean separation of positive and negative energy states; it amounts to limiting summations to the positive energy branch of the one-electron pseudospectrum. A relativistic CC technique based on local splines (piecewise polynomial fitting) has been developed and implemented to a number of atoms [118, 119]. Another kind of local basis sets has been introduced to relativistic CC by Salomonson and ster [120], who discretized the radial space. This technique is similar in spirit to the spline method and may be regarded as its limiting case (single-point representation rather than polynomial fitting). Single reference relativistic four-component methods for molecules were introduced in the 1990s [124, 125].

A particularly powerful, multi-root multireference variant of the coupled cluster method, called Fock-space or valence-universal [143, 144], gave remarkable agreement with experiment for many transition energies of heavy atoms (see review in [122]) and molecules [126–129]. This success makes the scheme a useful tool for reliable prediction of the structure and spectrum of superheavy elements, which are difficult to access experimentally. The FSCC method is the only quantum chemical approach suitable for treatment of systems with a variable number of particles. This and other methodological benefits of the FSCC approach make it an ideal candidate for merging with QED theory to create an infinite order size-extensive covariant many-body method.

A brief description of the relativistic NVPA FSCC method is given in Section 7.3.1. A more flexible and general scheme with higher accuracy and extended applicability, the intermediate Hamiltonian Fock-space coupled cluster approach, is shown in Section 7.3.2, followed by representative applications. The novel double Fock space coupled cluster method, still under development, is presented briefly in Section 7.6.3. This approach is based on the covariant evolution operator approach of Lindgren [41], and is a further step on the way to a covariant many-body technique suitable for benchmark electronic structure calculations.

7.2.5. Standard Four-Component SCF Procedure for Atoms and Molecules

The no-pair DCB Hamiltonian (7-34) is used to solve the one-electron SCF equations and get orbitals and orbital energies, as a starting point for relativistic many-body correlation calculations [82]. The energy functional used in the SCF procedure is the expectation value of the N-electron Slater determinant $|\Phi\rangle$, given in the second quantized form

$$|\Phi\rangle = a_1^\dagger a_2^\dagger \cdots a_N^\dagger \, |0\rangle \,, \tag{7-36}$$

where the vacuum state is defined by

$$a_i \, |0\rangle = 0; \quad \forall a_i \,. \tag{7-37}$$

The SCF energy is

$$E = \left\langle \Phi \left| \hat{H} \right| \Phi \right\rangle = h_{ii} + \frac{1}{2}\langle ji||ji\rangle, \tag{7-38}$$

where

$$h_{pq} = \int \varphi_p^\dagger(\mathbf{r}_1)\hat{h}_{D;V}(1)\varphi_q(\mathbf{r}_1)d\tau_1 \tag{7-39}$$

and the two electron integrals are

$$\langle pr||sq\rangle = \langle pr|sq\rangle - \langle pr|qs\rangle, \tag{7-40}$$

$$\langle pr|sq\rangle = \int d\mathbf{r}_1 d\mathbf{r}_2 \varphi_p^\dagger(\mathbf{r}_1)\varphi_r^\dagger(\mathbf{r}_2)\hat{g}(1,2)\varphi_s(\mathbf{r}_1)\varphi_q(\mathbf{r}_2). \tag{7-41}$$

In the algebraic approximation, orbitals are spanned in a set of basis functions $\varphi_p = \chi_\mu c_{\mu p}$, where Greek indices are used for the AO-basis. The energy (7-38) can then be expressed as

$$E = D_{\mu\nu}h_{\nu\mu} + \frac{1}{2}D_{\mu\nu}\langle \nu k||\mu\lambda\rangle D_{\kappa\lambda}; \quad D_{\lambda\kappa} = c_{\lambda i}c_{\kappa i}^*, \tag{7-42}$$

in which the AO-density matrix D appears. The Hartree–Fock SCF equations may be derived from (7-38) or (7-42) using the variational principle. The final form of the SCF equations is

$$\widehat{F}\phi_q = \varepsilon_q\phi_q\,, \tag{7-43}$$

where there is no summation on the right hand side. The Fock matrix is defined in the algebraic approximation as a basis set representation of the Fock operator $\widehat{F}$,

$$F_{pq} = h_{pq} + \langle p\lambda||qk\rangle D_{\lambda\kappa}. \tag{7-44}$$

The standard relativistic SCF procedure is similar to the nonrelativistic case, with the Hartree–Fock orbitals replaced by the four-component Dirac–Fock–Breit (DFB) functions. The spherical symmetry of atoms leads to the separation of the one-electron equation into radial and spin-angular parts [145], with the latter solved analytically. The SCF equation for the radial part of one-electron spinors is solved either numerically or in a basis. In the case of molecules, the algebraic approximation must be used. Here we discuss briefly the features of atomic SCF. The radial four-spinor has the large component $P_{n\kappa}$ in the upper two places and the small component $Q_{n\kappa}$ in the lower two. The quantum number κ (with $|\kappa| = j + 1/2$) comes from the spin-angular equation, and n is the principal quantum number, which counts the solutions of the radial equation with the same κ. Defining

$$\phi_{n\kappa} = \begin{pmatrix} P_{n\kappa}(r) \\ Q_{n\kappa}(r) \end{pmatrix}, \tag{7-45}$$

the radial SCF equation has the form

$$F_\kappa \phi_{n\kappa} = \varepsilon_{n\kappa} \phi_{n\kappa}, \tag{7-46}$$

where the one-electron Hartree–Fock operator F_κ is [112, 146–149]

$$F_\kappa = \begin{pmatrix} V_{\text{nuc}} + U^{LL} & c\Pi_\kappa + U^{LS} \\ c\Pi_\kappa^+ + U^{SL} & V_{\text{nuc}} + U^{SS} - 2c^2 \end{pmatrix}, \tag{7-47}$$

with

$$\Pi_\kappa = -d/dr + \kappa/r \tag{7-48}$$

and

$$\Pi_\kappa^+ = d/dr + \kappa/r. \tag{7-49}$$

Three types of two-electron integrals over the Coulomb operator (7-28) appear, $U^{LL} \equiv \langle LL||LL\rangle$, $U^{SL} \equiv \langle SL||SL\rangle$ and $U^{SS} \equiv \langle SS||SS\rangle$. There are also integrals over the Breit term (7-30), e.g., $U_B^{SL} \equiv \langle SS||LL\rangle$. V_{nuc} is the nuclear attraction potential. The point-charge model employed in light atom calculations gives significant errors for heavy elements, and the finite extent of the nucleus must be considered. Several models for the distribution of the nuclear charge are commonly used [150, 151]. In the uniform charge distribution model, the charge of a nucleus of atomic mass A is distributed uniformly over a sphere with radius $R = 2.2677 \times 10^{-5} A^{-1/3}$. The nuclear potential for a nucleus with charge Z is then

$$V_{\text{nuc}} = \begin{cases} -Z/r & \text{for } r > R \\ -(Z/2R)(3 - r^2/R^2) & \text{for } r \le R. \end{cases} \tag{7-50}$$

Two other commonly used potentials employ Fermi or Gaussian charge distributions. Dirac–Fock calculations for all elements up to Mt (E109) [151] found that significant differences exist between point-charge and finite nuclei, while the three finite nuclei models give very close values. A finite nucleus should therefore be used, but the choice of the exact model is secondary.

The terms U^{LL}, etc. in (7-47) represent the one-body mean-field potential, which approximates the two-electron interaction in the Hamiltonian, as is the practice in SCF schemes. In the DFB equations this interaction includes the Breit term (7-30) in addition to the electron repulsion $1/r_{ij}$. The radial functions $P_{n\kappa}(r)$ and $Q_{n\kappa}(r)$ may be obtained by numerical integration [152, 153] or by expansion in a basis (for more details see [154, 155]). Since the Dirac Hamiltonian is not bound from below, failure to observe correct boundary conditions leads to "variational collapse" [156, 157], where admixture of negative energy solutions may yield energies below experimental. To avoid this failure, the basis sets used for expanding the large and small components must maintain "kinetic balance" [158–160]. In the nonrelativistic limit ($c \to \infty$), the small component is related to the large component by (see below and [156])

$$Q_{n\kappa}(r) = (2c)^{-1} \Pi_\kappa^+ P_{n\kappa}(r), \tag{7-51}$$

where Π_κ^+ is defined in (7-49). In the case of numerical solution of the radial SCF equation, the relationship (7-51) serves as asymptotic boundary conditions.

Molecules cannot be solved by separating the radial from the angular-spin coordinates. Instead, basis sets $\{\chi_\mu\}$ are used, and the large and small components are expanded by

$$\psi_p^X = \chi_\mu^X c_{\mu p}^X; \quad X = L, S. \tag{7-52}$$

The SCF equations are then [14]

$$\begin{pmatrix} V^{LL} + U^{LL} & c\Pi^{LS} + U^{LS} \\ c\Pi^{SL} + U^{SL} & V^{SS} + U^{SS} - 2mc^2 S^{SS} \end{pmatrix} \begin{pmatrix} \mathbf{c}_p^L \\ \mathbf{c}_p^S \end{pmatrix} = \begin{pmatrix} S^{LL} & 0 \\ 0 & S^{SS} \end{pmatrix} \begin{pmatrix} \mathbf{c}_p^L \\ \mathbf{c}_p^S \end{pmatrix} \epsilon_p \tag{7-53}$$

with the matrix elements

$$S_{\mu\nu}^{XY} = \left\langle \chi_\mu^X \mid \chi_\nu^Y \right\rangle; \quad V_{\mu\nu}^{XY} = \left\langle \chi_\mu^X \left| \hat{V} \right| \chi_\nu^Y \right\rangle; \quad \Pi_{\mu\nu}^{XY} = \left\langle \chi_\mu^X \left| (\boldsymbol{\sigma} \cdot \mathbf{p}) \right| \chi_\nu^Y \right\rangle. \tag{7-54}$$

To satisfy kinetic balance, the small component basis must span the functions

$$\chi_\mu^S(\mathbf{r}) = (\boldsymbol{\sigma} \cdot \mathbf{p}) \chi_\mu^L(\mathbf{r}). \tag{7-55}$$

More details may be found in [14].

7.3. THE NVPA MULTI-ROOT MULTI-REFERENCE FOCK-SPACE COUPLED CLUSTER METHOD

Here we describe the FSCC method, followed by the more recent and stronger intermediate Hamiltonian approach. The latter is illustrated by representative applications demonstrating its capabilities.

7.3.1. Basic FSCC Method

The NVPA Dirac–Coulomb–Breit Hamiltonian H_{DCB}^+ may be rewritten in second-quantized form [149, 161] in terms of normal-ordered products of spinor creation and annihilation operators $\{a_r^+ a_s\}$ and $\{a_r^+ a_s^+ a_u a_t\}$, corresponding to the "fuzzy" picture,

$$H = H_{\mathrm{DCB}}^+ - \langle 0|H_{\mathrm{DCB}}^+|0\rangle = \sum_{rs} f_{rs}\{a_r^+ a_s\} + \frac{1}{4}\sum_{rstu} \langle rs||tu\rangle \{a_r^+ a_s^+ a_u a_t\}. \tag{7-56}$$

Here f_{rs} and $\langle rs||tu\rangle$ are, respectively, elements of the one-electron Dirac–Fock–Breit and antisymmetrized two-electron Coulomb–Breit interaction matrices over Dirac four-component spinors. The effect of the projection operators Λ^+ is now

taken over by normal ordering, denoted by the curly braces in (7-56), which requires annihilation operators to be moved to the right of creation operators as if all anticommutation relations vanish. The Fermi level is set at the top of the highest occupied positive energy state, and the negative energy states are ignored.

The development of a general multi-root multireference scheme for treating electron correlation effects usually starts from consideration of the Schrödinger equation for a number (d) of target states,

$$H\Psi^{\alpha} = E^{\alpha}\Psi^{\alpha}, \quad \alpha = 1, ..., d. \tag{7-57}$$

The physical Hamiltonian is divided into two parts,

$$H = H_0 + V, \tag{7-58}$$

so that V is a small perturbation to the zero-order Hamiltonian H_0, which has known eigenvalues and eigenvectors,

$$H_0|\mu\rangle = E_0^{\mu}|\mu\rangle. \tag{7-59}$$

The case of exact or quasi-degeneracy, occurring in many open shell heavy compound systems, involves the equality or near equality of some energy values E_0^{α}. By adopting the NVPA approximation, a natural and straightforward extension of the nonrelativistic open-shell CC theory emerges. The multireference valence-universal Fock-space coupled-cluster approach is presented here briefly; a fuller description may be found in [143, 144]. FSCC defines and calculates an effective Hamiltonian in a d-dimensional model space $P = \sum |\mu\rangle \langle\mu|$, $\mu = 1, .., d$, comprising the most strongly interacting zero order many electron wave functions. All other functions are in the complementary Q-space, so that $P + Q = 1$. All d eigenvalues of H_{eff} coincide with the relevant eigenvalues of the physical Hamiltonian,

$$H_{\text{eff}}\Psi_0^{\alpha} = E^{\alpha}\Psi_0^{\alpha}, \quad \alpha = 1, ..., d. \tag{7-60}$$

There is no summation over the index α, and

$$\Psi_0^{\alpha} = C_{\mu}^{a}|\mu\rangle, \quad \alpha = 1, ..., d. \tag{7-61}$$

Ψ_0^{α} describes the major part of Ψ^{α} for all $\alpha = 1, ..., d$,

$$P\Psi^{\alpha} = \Psi_0^{\alpha}, \quad \alpha = 1, ..., d. \tag{7-62}$$

The effective Hamiltonian has the form [2, 117]

$$H_{\text{eff}} = PH\Omega P, \; H_{\text{eff}} = H_0 + V_{\text{eff}}. \tag{7-63}$$

Ω is the normal-ordered wave operator, mapping the eigenfunctions of the effective Hamiltonian onto the exact ones, $\Omega\Psi_0^\alpha = \Psi^\alpha, \alpha = 1, ..., d$. It satisfies intermediate normalization,

$$P\Omega P = P. \tag{7-64}$$

The effective Hamiltonian and wave operator are connected by the generalized Bloch equation, which for a complete model space P may be written in the compact linked form [2]

$$Q[\Omega, H_0]P = Q(V\Omega - \Omega H_{\text{eff}})_{\text{linked}} P. \tag{7-65}$$

Ω is parameterized exponentially in the coupled cluster method. A particularly compact form is obtained by using the normal ordered form,

$$\Omega = \{\exp(S)\}. \tag{7-66}$$

The Fock-space approach starts from a reference state (closed-shell in our applications, but other single-determinant functions may also be used), correlates it, then adds and/or removes electrons one at a time, recorrelating the whole system at each stage. The sector (m, n) of the Fock space includes all states obtained from the reference determinant by removing m electrons from designated occupied orbitals, called valence holes, and adding n electrons in designated virtual orbitals, called valence particles. The practical limit is $m+n \leq 2$, although higher sectors have also been tried [162]. The excitation operator S, serving as the variable of exponential parameterization of the wave operator Ω, is partitioned into sector operators

$$S = \sum_{m\geq 0}\sum_{n\geq 0} S^{(m,n)}. \tag{7-67}$$

This partitioning allows for partial decoupling of the open-shell CC equations according to the so called subsystem embedding condition [143]. The equations for the (m, n) sector involve only S elements from sectors (k, l) with $k \leq m$ and $l \leq n$, so that the very large system of coupled nonlinear equations is separated into smaller subsystems, which are solved consecutively: first, the equations for $S^{(0,0)}$ are iterated to convergence; the $S^{(1,0)}$ (or $S^{(0,1)}$) equations are then solved using the known $S^{(0,0)}$, and so on. This separation, which does not involve any approximation, reduces the computational effort significantly. The effective Hamiltonian (7-63) is also partitioned by sectors. An important advantage of the method is the simultaneous calculation of a large number of states.

Each sector excitation operator is, in the usual way, a sum of virtual excitations of one, two, ..., electrons,

$$S^{(m,n)} = \sum_l S_l^{(m,n)}, \tag{7-68}$$

with l going, in principle, to the total number of electrons. In practice, l has to be truncated. The level of truncation reflects the quality of the approximation, i.e., the

extent to which the complementary Q space is taken into account in the evaluation of the effective Hamiltonian. The series (7-68) is truncated at $l = 2$ in the applications described below. The resulting CCSD (coupled cluster with single and double excitations) scheme involves the fully self-consistent, iterative calculation of all one- and two-body virtual excitation amplitudes, and sums all diagrams with these excitations to infinite order. These FSCC equations for a particular (m, n) sector of the Fock space are derived by inserting the normal-ordered wave operator (7-66) with Fock space exponential parameterization of the excitation operator (7-68) into the Bloch equation (7-65). The final form of the FSCC equation for a complete model space includes only *connected* terms [2, 117],

$$Q[S_l^{(m,n)}, H_0]P = Q\{(V\Omega - \Omega H_{\text{eff}})_l^{(m,n)}\}_{\text{conn}} P, \tag{7-69}$$

$$H_{\text{eff}}^{(m,n)} = P(H\Omega)_{\text{conn}}^{(m,n)} P \ . \tag{7-70}$$

As negative energy states are excluded from the Q space, the diagrammatic summations in the CC equations are carried out only within the subspace of the positive energy branch of the DF spectrum. After converging the FSCC equation (7-69), the effective Hamiltonian (7-70) is diagonalized, yielding directly transition energies. The effective Hamiltonian in the FSCC approach has "diagonal" structure with respect to the different Fock-space sectors. From (7-70) it follows that two Fock space sectors belonging to a common Hilbert space (with the same number of particles) do not mix even if they have strongly interacting states. This means that important nondynamic correlation effects are approximated. The mixed-sector CC presented below avoids this problem.

The FSCC equation (7-69) is solved iteratively, usually by the Jacobi algorithm. As in other CC approaches, denominators of the form $(E_0^P - E_0^Q)$ appear, originating in the left-hand side of the equation. The well-known intruder state problem, appearing when some Q states are close to and strongly interacting with P states, may lead to divergence of the CC iterations. The intermediate Hamiltonian method solves this problem in many cases and allows much larger and more flexible P spaces.

7.3.2. The Intermediate Hamiltonian CC Method

7.3.2.1. Need and Formulation

The accuracy and convergence of the Fock-space coupled cluster method depends on an appropriate partitioning of the function space into P and Q subspaces. Ideally, the P space should include all functions important to the states considered, since the effective Hamiltonian is diagonalized in P, whereas Q-space contributions are included approximately. On the other hand, convergence of the coupled cluster iterations is enhanced by maximal separation and minimal interaction between P and Q. These requirements are not always easy to reconcile. Relatively high P functions have often strong interaction with or are energetically close to Q states, making

convergence slow or impossible. The offending functions are usually included in P because of their significant contribution to the lower P states, and we may not be particularly interested in the correlated states generated from them by the wave operator; however, the FSCC is an all-or-nothing method, and lack of convergence means that no states at all are obtained. The intermediate Hamiltonian coupled cluster method developed recently [163] addresses this problem, making possible larger and more flexible P spaces, thereby extending the scope of the coupled cluster method and increasing its precision.

An additional advantage of the ability to use extended model spaces may be reducing the need for including high excitation levels in the formalism. The need for high excitations (triple and higher) is usually limited to a small group of virtual orbitals. If such orbitals are brought into P, all excitations involving them are included to infinite order by diagonalizing the effective Hamiltonian, avoiding the need for the (usually expensive) treatment of their contribution to dynamical correlation.

The intermediate Hamiltonian method has been proposed by Malrieu [164] in the framework of degenerate perturbation theory. The P space is partitioned into the main P_m subspace, which includes all the states of interest, and the intermediate P_i subspace, serving as a buffer between P_m and the rest of the functional space Q. The corresponding operators satisfy the equations

$$P_m + P_i = P \ , \qquad P + Q = 1 \ . \tag{7-71}$$

The rationale for this partitioning is the following: the relatively high states in P contribute significantly to the states of interest, which evolve from the lower P states, but couple strongly with intruders from Q and spoil the convergence of the iterations; they should therefore be treated differently from the lower states. This goal is achieved by partitioning P and allowing more approximate treatment of P_i states. The intermediate Hamiltonian H_I is constructed in P according to the same rules as the effective Hamiltonian,

$$H_I = PH\Omega P, \tag{7-72}$$

but only $|\Psi_m\rangle$ states with their largest part in P_m are required to have energies E_m closely approximating those of the physical Hamiltonian,

$$H_I P|\Psi_m\rangle = E_m P|\Psi_m\rangle \ . \tag{7-73}$$

The other eigenvalues, which correspond to states $|\Psi_i\rangle$ with the largest components in P_i, may be more or less accurate. This leads to some freedom in defining the relevant eigenfunctions and eigenvalues, and, therefore, in the evaluation of problematic QSP_i matrix elements. To limit this freedom and make the approach more general and flexible, we also use the partitioning

$$Q = Q_i + Q_m. \tag{7-74}$$

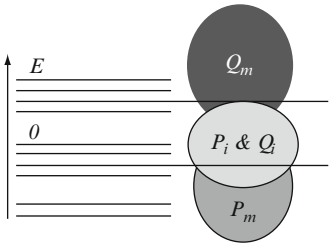

Figure 7-2. Model spaces in the modified intermediate Hamiltonian method

This additional partitioning narrows the overlap of the P and Q energies, and only P_i and Q_i subspaces can now overlap (see Figure 7-2) The number of problematic amplitudes, now $Q_i SP_i$, is thus reduced.

Partitioning the P and Q projectors of the FSCC equation (7-69) into the main and intermediate parts by formulas (7-71,7-74) yields four coupled CC equations,

$$Q_m[S, H_0]P_m = Q_m\{V\Omega - \Omega H_{\text{eff}}\}_{\text{conn}} P_m \tag{7-75}$$

$$Q_i[S, H_0]P_m = Q_i\{V\Omega - \Omega H_{\text{eff}}\}_{\text{conn}} P_m \tag{7-76}$$

$$Q_m[S, H_0]P_i = Q_m\{V\Omega - \Omega H_{\text{eff}}\}_{\text{conn}} P_i \tag{7-77}$$

$$Q_i[S, H_0]P_i = Q_i\{V\Omega - \Omega H_{\text{eff}}\}_{\text{conn}} P_i\,. \tag{7-78}$$

Only the last of these can cause convergence problems. Successful replacement of this equation by another, based on physical considerations, is the central point of the IH method. The new equation to be used instead of (7-78) will be called the *IH condition* (IHC). Ideally, it should satisfy the following demands:

- Be free of convergence problems.
- Have minimal impact on the other coupled equations (7-75–7-77).

Subject to these demands, we would like the IHC to be as close to (7-78) as possible.

Several IH FSCC methods have been developed and applied recently, based on different IH conditions. The first such approach [163], denoted IH1, uses the condition

$$Q_i \Omega P_m H \Omega P_i = Q_i H \Omega P_i, \tag{7-79}$$

which is similar to the equation proposed by Malrieu and applied up to the 3rd order of degenerate perturbation theory [164]. While Malrieu's scheme could not go beyond 3rd order because terms with small denominators appear, the IH CC variants developed in our group are all-order and may be used in the framework of any multireference CC formulation.

The next IH FSCC scheme (IH2) is based on the perturbation theory expansion of the problematic $Q_i SP_i$ amplitudes. In the lowest order we simply take

$$Q_i SP_i = 0. \tag{7-80}$$

This type of IH condition has also been used for developing a new type of hybrid multireference coupled cluster schemes, including the mixed sector CC presented below.

Another IH condition leads to the most flexible and useful scheme, the extrapolated IH (XIH) [165, 166], which can yield correct solutions both for P_m and P_i, thus recovering the whole effective Hamiltonian spectrum in the extended model space P. This can be accomplished even when the standard FSCC approach using the same model space P has intruder states leading to divergence. The IH condition for the XIH approach has the form

$$Q_i[S, H_0 + P_i \Delta P_i]P_i = Q_i\{\beta\Delta S + V\Omega - \Omega H_{\text{eff}}\}_{\text{conn}} P_i\,. \tag{7-81}$$

Δ is an energy shift parameter, correcting small energy denominators for the problematic intruder states. A compensation term with the multiplicative parameter β ($\beta \leq 1$) is added on the right-hand side. For $\beta = 1$, the $P_i \Delta P_i$ term on the left-hand side is fully compensated, so that (7-81) is equivalent to (7-78). Proper choice of the two parameters makes it possible to reach convergence in (7-81) and thus in the non-problematic equations (7-75–7-77). Several calculations with different values of the parameters allow extrapolation of both P_m and P_i level energies to the limit $\Delta \to 0$ or $\beta \to 1$. This extrapolation was found to be robust, in most cases linear for P_m states and quadratic for states in P_i. In the extrapolation limit the IH method transforms into the effective Hamiltonian approach. The XIH approach is asymptotically size extensive and in many cases size consistent, even for incomplete P_m, requiring only that the entire model space P is complete. A somewhat similar IH FSCC scheme has been proposed by Mukhopadhyay et al. in 1992 [167], but to the best of our knowledge has never been implemented.

The intermediate Hamiltonian approaches presented here may be applied within any multi-root multireference infinite order method. Recently [168] we implemented the XIH scheme to another all-order relativistic multi-root multireference approach, the Hilbert space or state universal CC, which is the main alternative to and competitor of Fock-space CC. The HSCC is based on the Jeziorsky–Monkhorst parameterization of the wave operator [169],

$$\Omega = \sum_{\mu=1}^{d} \Omega_\mu = \sum_{\mu=1}^{d} \{\exp(S^\mu)\} P^\mu;\;\; P^\mu = |\mu\rangle \langle\mu|\,. \tag{7-82}$$

Here every determinant μ belonging to the P space serves as a reference state (Fermi vacuum), and the excitation operators S^μ are vacuum dependent. The nature of the determinants in the model space may be general; the only requirement is that all determinants belong to the same Hilbert space. The most useful scheme is probably the HSCC approach with a model space built of general MCSCF solutions. This

will make the HSCC method suitable for global potential surface calculations. The XIH-HSCC equation in the case of complete model space P is

$$\begin{aligned}[S^{\mu}, H_0 + P_i \Delta P_i] P^{\mu} &= \{\beta \Delta S^{\mu} P_i P^{\mu} + V\{\exp(S^{\mu})\} P^{\mu} \\ &\quad - \{\exp(S^{\nu})\} P^{\nu} H_{\text{eff}} P^{\mu}\}_{\text{conn}} \\ P^{\nu} H_{\text{eff}} P^{\mu} &= P^{\nu} (H\{\exp(S^{\mu})\})_{\text{conn}} P^{\mu}. \end{aligned} \tag{7-83}$$

The HSCC effective Hamiltonian (7-83), unlike the FSCC effective Hamiltonian, has non-diagonal structure, coupling different Fock-space sectors belonging to the same Hilbert space. This leads to better treatment of nondynamic correlation. A *mixed sector coupled cluster* (MSCC), which may be regarded as a hybrid approach combining the advantages of FSCC and HSCC, has recently been derived [170] within the IH2 method based on IHC (7-80). The MSCC exponential parameterization of the wave operator Ω and the working equation are formally similar to those of FSCC (see (7-66)–(7-69)), but the subsystem embedding condition is now relaxed and several sectors of Fock space belonging to the same Hilbert space mix and are diagonalized together. MSCC may thus yield the most balanced inclusion of dynamic and nondynamic correlation effects. Implementation of the XIH method to higher sectors (up to six valence electrons/holes [162]) of the Fock space is also in progress [171]. All the multireference multiroot CC methods described above may be used for the challenging task of benchmark calculations for heavy quasidegenerate systems with more than two electrons/holes in the valence open shell. Another challenging, long-term project is to apply the IH method within the double FSCC, a covariant MRCC based on QED, presented in Section 7.6.3. This method can be applied to highly charged heavy ions, which exhibit large QED effects.

Summing up, we conclude that the IH method is an efficient and universal tool, applicable to all multi-root multireference methods. It avoids intruder states, while at the same time allowing the use of large, complete model spaces, improving significantly the accuracy of the calculation.

7.3.2.2. Selection of P_m and P_i Model Spaces

A major advantage of the intermediate Hamiltonian approach is the flexibility in selecting the model space. This has been a major problem in applying the Fock-space scheme, as noted at the beginning of this section. While in the Fock-space coupled cluster method one may feel lucky to find any partitioning of the function space into P and Q with convergent CC iterations, the intermediate Hamiltonian method makes it possible for the first time to vary the model space systematically and study the effect upon calculated properties. An example is given in Table 7-3, which shows the dependence of the calculated electron affinity of Cs on the model spaces P_m and P_i [172]. The calculations used the IH1 method, based on the IH condition (7-79).

Orbitals defining P_m and P_i are selected largely in order of increasing orbital energies. The electron affinities in Table 7-3 show that P_m reaches optimal size and

Table 7-3 Electron affinity of Cs with different model spaces (meV) [172]. The experimental value is 472 meV (Ref. [173])

Model space	P_m orbitals	P_i orbitals	EA
A	6*s*	–[a]	516
B	6*s*,6*p*,5*d*	7-11*s*,7-10*p*,6-9*d*,4-6*f*	511
C	6-7*s*,6-7*p*,5-6*d*	8-11*s*,8-10*p*,7-9*d*,4-6*f*	490
D	6-9*s*,6-8*p*,5-7*d*,4*f*	10-12*s*,9-11*p*,8-9*d*,5-6*f*	481
E	6-10*s*,6-9*p*,5-7*d*,4-5*f*	11-12*s*,10-11*p*,8-9*d*,6*f*	480
F	6-9*s*,6-8*p*,5-7*d*,4*f*	10-13*s*,9-12*p*,8-9*d*,5-6*f*	475
G	6-9*s*,6-8*p*,5-7*d*,4*f*	10-12*s*,9-11*p*,8-10*d*,5-7*f*	480

[a]FSCC, no P_i space.

convergence with set D, and further increase (set E) has little effect. Augmenting P_i by s and p orbitals (set F) leads to further change, whereas adding d and f functions (set G) has little effect, as do other attempts to augment set F. The model spaces of set F are therefore used in the calculation. Note that the model spaces are not determined by agreement with experiment; they are extended until the relevant physical properties converge.

7.3.2.3. Atomic Excitation Energies Not Accessible by FSCC

The selection of the model space P determines the states calculated. The effective Hamiltonian in the (m,n) sector is constructed and diagonalized in the corresponding $P^{(m,n)}$, giving correlated energies of $P^{(m,n)}$ states relative to the correlated reference state. A more flexible model space leads to greatly extended range of applicability, as demonstrated by the two examples below.

- Excited states of Ba and Ra were calculated by FSCC in the (0,2) sector, starting from M^{2+} as reference [174]. The model space in the 2-electron sector for Ba included all states with two electrons in the $5d$, $6s$ and $6p$ orbitals, except the $6p^2$ states; inclusion of the latter led to intruder states and divergence, so that incomplete model spaces had to be employed. The IH method made possible larger model spaces, giving many more states as well as higher accuracy [175]. We could put all states the states used in FSCC, plus $6p^2$, in P_m; P_i was defined by adding states with occupied $7s$–$10s$, $7p$–$10p$, $6d$–$9d$, and $4f$–$6f$ orbitals, yielding a very large P $(= P_m + P_i)$ space. The average error in states accessible to both methods was reduced from 742 cm^{-1} (relative error 3.11%) for FSCC to 139 cm^{-1} (relative error 0.69%) for IH. In addition, many more states, including those belonging to the $6p^2$ term, were obtained [175]. Similar results were obtained for Ra.
- In the rare gases Xe and Ar, the neutral closed-shell atoms provide a natural choice for reference state, and the excited states are therefore in the (1,1) sector. The excitation energies are relatively high and not too far apart, and we could not find *any* partitioning leading to convergence of the Fock-space coupled cluster iterations. The improved convergence properties of the intermediate Hamiltonian

approach solved this problem [176]. Over 20 excitation energies of each atom were obtained, with an average error of 0.06 eV (0.6%). The original publication may be consulted for details.

7.4. APPLICATIONS: HEAVY ELEMENTS

High-level inclusion of both relativity and correlation is essential if a quantitative description of a heavy atom is desired. It should be emphasized that correlation and relativistic effects (by the latter we mean the difference between results of relativistic and equivalent nonrelativistic formulations) are non-additive for heavy atoms. The cause is clear: since the relativistic spatial distribution of the orbitals differs significantly from that of nonrelativistic counterparts (s and p orbitals undergo contraction, whereas d and f orbitals expand), correlation energy changes. This affects in particular inner shells, but more diffuse orbitals are not exempt. This is demonstrated in Section 7.4.2 for the gold atom [121].

Representative applications of the Fock-space coupled cluster method to heavy atoms are presented below. The spherical symmetry of atoms, which leads to angular decomposition of the wave function and coupled-cluster equations, is used at both the Dirac–Fock–Breit [149] and CC [121, 177] stages of the calculation. The energy integrals and CC amplitudes, which appear in the Goldstone-type diagrams defining the CC equations, are decomposed in terms of vector-coupling coefficients, expressed by angular-momentum diagrams, and reduced Coulomb–Breit or S matrix elements, respectively. The reduced equations for single and double excitation amplitudes are derived using the Jucys–Levinson–Vanagas theorem [117] and solved iteratively. This technique makes possible the use of large basis sets with high l values, as a basis orbital gives rise to two functions at most, with $j = l \pm 1/2$, whereas in Cartesian coordinates the number of functions increases rapidly with l. Typically we go up to h ($l = 5$) or i ($l = 6$) orbitals, but higher orbitals (up to $l = 8$) have been used. To account for core-polarization effects, which may be important for many systems, we correlate at least the two outer shells, usually 20–40 electrons. Finally, uncontracted Gaussians are used, since contraction leads to problems in satisfying kinetic balance and correctly representing the small components. On the other hand, it has been found that high-energy virtual orbitals have little effect on the transition energies we calculate, since these orbitals have nodes in the inner regions of the atom and correlate mostly the inner-shell electrons, which we do not correlate anyway. These virtual orbitals, with energies above 80 or 100 hartree, are therefore eliminated from the CC calculation, constituting in effect a post-SCF contraction.

The Fock-space coupled cluster and its intermediate Hamiltonian extension have been incorporated into the DIRAC package [133], opening the way to *molecular* applications. The heavy species NpO_2^+, NpO_2^{2+}, and PuO_2^{2+} were calculated, giving access to the ground and many excited states and leading to reassignment of some of the observed spectroscopic peaks [128]. A later application addressed UO_2 and UO_2^+ [129], with less conclusive results, due to the highly complicated open-shell character of these species.

Most of the applications involved heavy atomic systems, and proved the power of the method. Some examples are described in the current Section. These successes make the FSCC and IH approaches a useful tool for predicting properties of superheavy elements, not easy to access experimentally. Applications to these elements may be found in Section 7.5.

7.4.1. When Is an Atom "Heavy"? Ionization Potentials of Alkali Atoms

An obvious question is when do atoms start to be "heavy", requiring relativistic treatment for accurate description of their energy levels. An indicative criterion may be derived by comparing high-level relativistic and nonrelativistic calculations with experimental values. Such a comparison is given in Table 7-4, where errors in the first ionization potentials of alkali atoms, calculated by the Fock-space coupled cluster scheme within the four-component Dirac–Coulomb or the Schrödinger framework, are collected [177]. While the errors in the IPs calculated relativistically are small and do not change much with the atomic number, the nonrelativistic values become progressively worse as the atom gets heavier.

Alkali atoms are basically one-valence-electron systems, and correlation would therefore not be expected to play a major role in the determination of properties such as ionization potentials. Nevertheless, a Hartree–Fock (or, for the heavier alkali atoms, a Dirac–Fock) calculation gives sizable errors for this property. In particular, if accuracy below the one percent level is desired, as would be needed, for example, in studies of parity nonconservation effects [178], high-level treatment of correlation is essential. Large basis set calculations of several IPs were carried out by the Notre Dame group in second-order MBPT for Li to Cs [179] and in CCSD for Cs [180], using large B-spline basis sets. The Fock-space CC method in an extensive Gaussian-type basis was applied to all atoms by Eliav et al. [177]. Results for atomic cesium, collected in Table 7-5, show that all-order summation is indeed necessary to obtain highly accurate ionization potentials. The better values obtained by Eliav et al. are probably due to the superiority of Gaussian-type orbitals over

Table 7-4 Experimental and FSCC ionization potentials of alkali atoms (cm^{-1}). Errors of calculated values with respect to experiment are given

			Calc. error	
Atom	Z	Expt.	Rel.	Nonrel.
Li	3	43,487	−3	−6
K	19	35,010	18	−26
Rb	37	33,691	30	535
Cs	55	31,407	36	1163
Fr	87	32,849	−10	2780

Table 7-5 Comparison of Cs ionization potentials calculated by different methods (hartree). Percent error in parentheses

	$6s_{1/2}$	$6p_{1/2}$	$6p_{3/2}$	$7s_{1/2}$
DF [179]	0.12737 (11%)	0.08562 (7.1%)	0.08378 (6.5%)	0.05519 (5.9%)
MBPT-2 [179]	0.14511 (1.4%)	0.09253 (0.4%)	0.08996 (0.4%)	0.05939 (1.3%)
CC [180]	0.14257 (0.4%)	0.09198 (0.2%)	0.08951 (0.15%)	0.05845 (0.3%)
FSCC [177]	0.14326 (0.11%)	0.09212 (0.05%)	0.08962 (0.02%)	0.05867 (0.03%)
Expt. [184]	0.14310	0.09217	0.08964	0.05865

B-spline functions. The Fock-space CC values are within 0.02–0.11% of experiment. Fine structure splittings are also reproduced well: 548 cm^{-1} for the $6p$ level (experimental 554) and 96.5 cm^{-1} for $5d$ (experimental 97.6).

7.4.2. Gold Atom: Local Maximum of Relativistic Effects

The gold atom exhibits very large relativistic effects on its chemical and physical properties, due to the contraction and stabilization of the $6s$ orbital. The compactness of the atom relative to its neighbors leads to a local maximum in relativistic effects, called by Pyykkö the "gold maximum" [181]. Nonrelativistic calculations lead to large errors, including the reversal of the two lowest excited states [182,183]. Gold serves therefore as a stringent test for methods aspiring to provide accurate values for heavy elements, and was one of the first atoms tested by the relativistic coupled cluster scheme [121]. Two closed-shell states can be used as starting points for the Fock-space treatment, defining the (0,0) sector, namely Au^+ or Au^-. Electrons are then added or removed according to the schemes

$$Au^+(0,0) \rightarrow Au(0,1) \rightarrow Au^-(0,2), \tag{7-84}$$

or

$$Au^-(0,0) \rightarrow Au(1,0) \rightarrow Au^+(2,0). \tag{7-85}$$

The basis consisted of $21s17p11d7f$ Gaussian spinors [183], and correlated shells included $4spdf5spd6s$. Table 7.6 shows the nonrelativistic, Dirac–Coulomb, and Dirac–Coulomb–Breit total energies of the two ions. As expected, relativistic effects are very large, over 1100 hartree. The nonadditivity of relativistic and correlation corrections to the energy, apparent in Table 7-6, has been noted above.

The various transition energies of the gold atom and its ions are shown and compared with experiment [184] in Table 7-7. The nonrelativistic results have errors of several eV. The relativistic CC values, on the other hand, are highly accurate, with an average error of 0.06 eV. More recent (unpublished) values, obtained with a larger $31s26p21d17f14g11h8i$ basis, are even closer to experiment, giving 9.21 eV for the IP and 2.29 eV for the EA. The inclusion of the Breit effect does not change the results by much, except for some improvement of the fine-structure splittings.

Table 7-6 CCSD transition energies in Au (eV). IP is the ionization potential, EA denotes electron affinity, and EE – excitation energy relative to the ground state. FS denotes fine-structure splittings

			NR	DC	DCB	Expt.[184]
IP	$5d^{10}6s$	$^2S_{1/2}$	6.981	9.101	9.086	9.226
EE	$5d^96s^2$	$^2D_{3/2}$	5.301	2.661	2.669	2.658
	$5d^96s^2$	$^2D_{5/2}$	5.301	1.115	1.150	1.136
	$5d^{10}6p_{1/2}$	$^2P_{1/2}$	3.313	4.723	4.720	4.632
	$5d^{10}6p_{3/2}$	$^2P_{3/2}$	3.313	5.193	5.184	5.105
FS		^2D	0	1.546	1.519	1.522
		^2P	0	0.470	0.466	0.473
EA	$5d^{10}6s^2$	$^1S_0$	1.267	2.278	2.269	2.31

Table 7-7 Total energies of the closed-shell systems Au^+ and Au^- (hartree), with nonrelativistic, DC, and DCB Hamiltonians. Correlation includes $4s$ and higher shells

	Au^+		Au^-	
	Uncorrelated	Correlation	Uncorrelated	Correlation
NR	−17863.46301	−1.29756	−17863.68392	−1.37018
DC	−19029.01322	−1.36150	−19029.32077	−1.46436
DCB	−19007.42385	−1.36430	−19007.73063	−1.46690

7.4.3. The f^2 Levels of Pr^{3+}: Importance of Dynamic Correlation

Lanthanides and actinides possess open f shells, which give rise to large manifolds of closely spaced states. As an example of these systems we discuss the energy levels of the Pr^{3+} ion, which has an f^2 ground state configuration. The spectrum is well characterized experimentally [185] and provides a good test for high-accuracy methods incorporating relativity and correlation. The system has been studied by both MCDF and Fock-space CC, and comparison between these methods can therefore be made.

The MCDF calculations [186] involved between 354 and 1708 CSFs for the different J states. The number of CSFs was much larger in the CC calculations [187], since all excitations from the $4spdf5sp$ orbitals to virtual orbitals with energies up to 100 hartree, as well as excitations from $4spd5sp$ to the partially filled $4f$, were included. Thus, a much larger part of dynamic correlation was accounted for. The Pr^{5+} closed shell state served as reference, and two electrons were added in the $4f$ shell to obtain the levels of interest. Three basis sets were used, with l going up to 4, 5 and 6. The calculated excitation energies are compared with experiment [185] in Table 7-8.

The Fock-space CC excitation energies are in better agreement with experiment than MCDF values, and improve with the size of the basis. All 13 levels appear in the correct order (in MCDF the $^3P_2$ level appears 1200 cm^{-1} below the $^1I_6$ instead of 950 cm^{-1} above it). Convergence with respect to the l value in the virtual space

Table 7-8 Excitation energies of Pr^{3+} $4f^2$ levels (cm^{-1}). The ground state is $^3H_4$

Level	Expt. [185]	MCDF [186]	CCSD [187]		
			$l \leq 4$	$l \leq 5$	$l \leq 6$
$^3H_5$	2,152.09	2,337	2,273	2,273	2,270
$^3H_6$	4,389.09	4,733	4,645	4,641	4,635
$^3F_2$	4,996.61	4,984	4,749	4,832	4,843
$^3F_3$	6,415.24	6,517	6,266	6,345	6,354
$^3F_4$	6,854.75	6,950	6,808	6,844	6,843
$^1G_4$	9,921.24	10,207	10,019	10,014	10,001
$^1D_2$	17,334.39	18,153	16,803	16,961	16,998
$^3P_0$	21,389.81	22,776	20,802	21,109	21,155
$^3P_1$	22,007.46	23,450	21,443	21,747	21,791
$^1I_6$	22,211.54	25,854	22,267	22,061	22,010
$^3P_2$	23,160.61	24,653	22,719	23,009	23,051
$^1S_0$	50,090.29	50,517	48,448	49,072	49,194
Avrg. error		853	394	245	222

Table 7-9 Fine structure in Pr^{3+} (cm^{-1})

	Expt. [185]	MCDF	DC $l \leq 4$	DC $l \leq 5$	DCB $l \leq 5$	DC $l \leq 6$
$^3H_5 - {}^3H_4$	2,152	2,337	2,273	2,273	2,081	2,270
$^3H_6 - {}^3H_5$	2,237	2,396	2,369	2,368	2,169	2,365
$^3F_3 - {}^3F_2$	1,419	1,533	1,517	1,513	1,373	1,511
$^3F_4 - {}^3F_3$	440	433	542	499	465	489
$^3P_1 - {}^3P_0$	618	674	631	638	585	636
$^3P_2 - {}^3P_1$	1,153	1,203	1,276	1,262	1,090	1,260
Avrg. error		95	98	89	51	86

seems good, and the best basis gives an average error of 222 cm^{-1} for the excitation energies. A full half of the total error is due to the high $^1S_0$ state; these states are notoriously difficult to calculate. While inclusion of the Breit term has a rather small effect on the excitation energies of Pr^{3+}, it improves the fine-structure splittings (Table 7-9). This is a general phenomenon, and may be traced to the spin-other-spin interaction in the two-electron Breit term [188]. Fine-structure splittings are less sensitive to the amount of correlation retrieved.

7.4.4. Electron Affinities of Alkali Atoms – Accuracy at the 1 meV Level

Alkali atoms are conceptually simple one-valence-electron systems, and have consequently attracted many experimental and theoretical studies. The electron affinities of the atoms up to Cs are known with great precision [173]; only a semiempirical

value of 492 meV (with an uncertainty of 2.2%) is available for Fr [189]. An interesting aspect of these systems is the suggestion made some years ago [190–192] that Cs^- might have bound excited states, an idea refuted by more recent experimental [193] and theoretical [189] work. One of the first applications of the relativistic Fock-space coupled cluster (FSCC) method described above has been to transition energies of alkali atoms [177]. Excellent agreement with experiment was obtained for ionization potentials (an average error of 0.09%) and excitation energies (0.2% error), but electron affinities, particularly those of the heavier elements in the group, were less satisfactory, with errors of 4–9% for K, Rb, and Cs. The newly developed intermediate Hamiltonian method made possible more extensive calculations with much larger P spaces, and the problem was therefore revisited [172].

The effect of the model space upon the calculated EA was studied as described above (Section 7.3.2, Table 7-3). The model spaces employed are believed to converge to within a few meV; they are listed in Table 7-10. The number of correlated electrons in the cation reference states varied from 8 in Na^+ to 50 in $E119^+$ (see Table 7-10); corresponding anions have two additional correlated electrons.

Calculated electron affinities are collected and compared with experiment in Table 7-11. The power of the intermediate Hamiltonian method is demonstrated by the excellent agreement with experiment. The Fock space values start well for Na, but errors increase to 5%, 7% and 9% for the heavier K, Rb and Cs, respectively. IHFSCC values, on the other hand, are all within 5 meV or 1% of experiment. It

Table 7-10 Correlated electrons in the reference cations and structure of model spaces

Atom	Correlated electrons		P_m orbitals	P_i orbitals
	Number	Orbitals		
Na	8	$2s2p$	3-6s,3-5p,3-5d,4f	7-10s,6-9p,6-7d,5-7f
K	16	$2s2p3s3p$	4-7s,4-6p,3-5d,4f	8-11s,7-10p,6-7d,5-6f
Rb	26	$3s3p3d4s4p$	5-8s,5-7p,4-6d,4f	9-12s,8-11p,7-8d,5-6f
Cs	26	$4s4p4d5s5p$	6-9s,6-8p,5-7d,4f	10-13s,9-12p,8-9d,5-6f
Fr	40	$4f5s5p5d6s6p$	7-10s,7-9p,6-8d,5f	11-14s,10-13p,9-10d,6-7f
E119	50	$4f5d6s6p6d7s7p$	8-11s,8-10p,7-9d,5-6f	12-15s,11-13p,10-11d,7-8f

Table 7-11 Electron affinities of the alkali atoms (meV). Fock-space (FS), intermediate Hamiltonian (IH) and extrapolated intermediate Hamiltonian (XIH) compared with experimental [173] (semiempirical [189] for Fr) values

	FSCC	IH1	XIH					Expt.
			$\Delta = 8$	$\Delta = 6$	$\Delta = 4$	$\Delta = 0$	+QED	
Li	–	–	618.38	618.28	618.19	618.01	617.84	618.05(2)
Na	549.1	549.9	549.02	548.87	548.72	548.42	548.04	547.93(3)
K	525.4	506.8	503.94	503.85	503.77	503.60	503.08	501.46(1)
Rb	519.3	490.8	487.39	487.34	487.29	487.19	485.90	485.92(2)
Cs	516.0	474.6	473.07	473.02	472.96	472.85	470.75	471.63(3)
Fr	542.2	491.3	490.34	490.26	490.17	490.00	486.03	492(10)
119	717.1	662.5	661.97	661.75	661.51	661.05	648.70	–

should be noted that the FSCC function of the anions includes only one determinant in the P space, whereas the IHFSCC P space includes several thousand. The importance of these additional determinants (and of excitations from them to Q) increases with the size of the alkali anion.

Even higher accuracy became possible with the development of the extrapolated intermediate Hamiltonian method [165]. Whereas some of the matrix elements belonging to the P_i space are "fudged" in the IH1 scheme and affect the energies, the XIH approach recovers the energies of the exact H_{eff} in the full, extended P space. Eq. (7-81) was used with the parameter Δ only, and the energies were calculated for $\Delta = 8, 6, 4$ and extrapolated to $\Delta = 0$, which gives the full H_{eff} results. As the table shows, energies vary linearly with Δ and the extrapolation is robust. Adding QED corrections, the mean absolute error of the calculated EAs is 0.6 meV, with the largest error 1.6 meV. Similar accuracy was obtained for the IPs of alkali atoms, with 45 IPs of Rb, Cs and Fr giving a mean absolute error of 1.4 meV [166].

7.4.5. Electron Affinities in Group 13

The Hotop and Lineberger tables [173], a standard source for electron affinities, show reliable values for the two lightest elements, B and Al; other values have error limits of 50–100%. High-precision measurements for all five elements were reported in 1998–2000 [194–198]. Few calculations have appeared for the latter atoms before 1997. These include the multireference configuration interaction (MRCI) of Arnau et al. using pseudopotentials [199], the Fock-space coupled cluster work on Tl [200], and the multiconfiguration Dirac–Fock computation of Wijesundera [201].

MRCI values for Al (0.45 eV) and MCDF results for B (0.26 eV) and Al (0.43 eV) are in good agreement with experimental values. MRCI and MCDF EAs for the other atoms agree with each other (0.29 and 0.30 eV for Ga, 0.38 and 0.39 eV for In, 0.27 and 0.29 eV for Tl). The CC EA of Tl is much higher at 0.40(5) eV. A major difference between the CC and the other two methods lies in the number of electrons correlated. While Arnau and Eliav et al. [199, 201] correlate valence electrons only, three for the neutral atom and four for the anion, Eliav et al. [200] correlated 35 electrons in Tl and 36 in Tl^-. A FSCC study of all five elements was undertaken [202], with the aim of determining their EAs and, in particular, the effect of inner-shell correlation and virtual space used on the calculated values.

Large basis sets of Gaussian-type orbitals (up to $35s27p21d9g6h4i$) were used, taken from the universal basis set of Malli et al. [203]. Many electrons were correlated (5 in B, 11 in Al, 27 in Ga, 21 in In, and 35 in Tl), to account for core polarization. The calculated EAs are shown in Table 7-12 and compared with experiment [194–198]. Agreement with experimental values for B, Al and In is very good, but a significant deviation is observed for Ga. A detailed analysis of the calculation [204] did not come up with an acceptable explanation for this disagreement. When the EA of Tl was measured with high precision it was found to be 0.377(13) eV [198], in good agreement with the FSCC value but not with the significantly lower MRCI and MCDF results. The advantage of the FSCC calculation

Table 7-12 Group 13 electron affinities (eV)

Atom	Expt.		CCSD [202]
B	0.279 723(25)	[194]	0.279
Al	0.432 83(5)	[195]	0.427
Ga	0.43(3)	[196]	0.301
In	0.404(9)	[197]	0.419
Tl	0.377(13)	[198]	0.40(5)

lies in correlating both valence and inner shells, so that core polarization and correlation are included properly, while only valence electrons are correlated in the other applications. Results show that inner-shell correlation contributes about one quarter or 0.1 eV of the total affinity. The rather large error limit quoted in the FSCC result appears because two Fock-space schemes, starting from Tl^+ and Tl^- respectively, give significant differences. The remaining disagreement between FSCC and measured values for Ga is still a puzzle [204].

7.4.6. Properties Other Than Energy: Nuclear Quadrupole Moments

The knowledge of nuclear quadrupole moments (NQM) is of considerable interest in chemical spectroscopy. They are also required in nuclear physics for testing nuclear models. One of the best ways to determine the nuclear quadrupole moment Q is by combining the experimental nuclear quadrupole coupling constant B, also known as the electric quadrupole hyperfine interaction constant, with accurate calculations of the electric field gradient (EFG) at the nucleus, q. The nuclear quadrupole coupling constant is given by the relation

$$B = -eqQ/h, \tag{7-86}$$

where e is the absolute value of the electron charge and h is Planck's constant.

Atomic and molecular properties, such as the nuclear quadrupole moment, are usually observed via the energy shifts generated by coupling to an external field. The desired property is the derivative of the energy with respect to the external field. We used the finite field method [205] to calculate the EFG at the relevant nuclei. The interaction with an arbitrary NQM Q is added to the Hamiltonian $\hat{H}_0$, giving

$$\hat{H}(Q) = \hat{H}_0 - eqQ/h. \tag{7-87}$$

The Dirac–Coulomb Hamiltonian for the atom served as $\hat{H}_0$. The energy, which is the expectation value of $\hat{H}(Q)$, may be expanded as

$$E(Q) = \langle \Psi(Q)|\hat{H}(Q)|\Psi(Q)\rangle = E_0 + Q\left(\frac{dE(Q)}{dQ}\right)_0 + \frac{Q^2}{2}\left(\frac{d^2E(Q)}{dQ^2}\right)_0 + \cdots . \tag{7-88}$$

Differentiating and invoking the Hellmann–Feynman theorem, one obtains

$$\left.\frac{dE(Q)}{dQ}\right|_{Q=0} = -\frac{e}{h}\langle\Psi_0|\hat{q}_{zz}|\Psi_0\rangle. \tag{7-89}$$

Conflicting considerations determine the value of Q used in practice. The energy change must be large enough not to disappear in the precision of the calculations, but too large a perturbation may go beyond the linear regime and introduce errors in the derivative. Linearity is therefore monitored throughout the application.

The calculations were carried out using the DIRAC relativistic ab initio electronic structure program [133]. Nuclei were described by the Gaussian finite nucleus model, and the uncontracted well tempered basis set of Huzinaga and Klobukowski [206] was employed. The Hamiltonian used includes the external field from the start, so that the Dirac–Hartree–Fock orbitals already see it. Previous attempts of adding the field at the perturbative (coupled cluster) step were less satisfactory.

The first application addressed the halogen atoms Cl, Br and I [207]. The electric field splits the $P_{3/2}$ atomic levels into two sublevels separated by $2B$, and the size of the splitting as function of Q gives the required derivative, from which the electric field gradient is calculated. Using the splitting rather than the energy shift of individual levels has the advantage that the second-derivative term in Eq. (7-88) cancels out, and deviation from linearity starts with the cubic term. An additional advantage is that the splitting vanishes identically for $Q = 0$. The effect of the Gaunt term, the major part of the Breit interaction, is obtained at the Dirac–Hartree–Fock level by taking the expectation value of the relevant operator. The total size of the effect is small, well below 1%, and the neglect of interaction between Gaunt and correlation contributions is not significant.

The basis sets were extended until the EFG values converged. Table 7-13 shows EFG values obtained for the larger iodine basis sets. We believe convergence is better than 1%. The final EFG values were determined from calculations using the last basis sets listed in the Table with $Q = 1.25 \times 10^{-5}$ a.u., and nonlinearity was estimated by comparing with $Q = 2.5 \times 10^{-5}$. Deviation from linearity was below 0.5% in all cases. Considering all sources of error, we estimate the total error at 1.5%.

Using the calculated EFG values and the experimental B values [208–210], the following NQM values are obtained: $Q(^{35}\mathrm{Cl}) = -81.1(1.2)$ mb, $Q(^{79}\mathrm{Br}) = 302(5)$ mb, and $Q(^{127}\mathrm{I}) = -680(10)$ mb. The Q of Cl agrees with the previous reference value of $-81.65(80)$ mb [211], while that of Br differs somewhat from the accepted 313(3) mb. Iodine shows the largest correction to the previous $-710(10)$ mb, in line with the $-696(12)$ mb obtained from molecular calculations [212]. A more detailed discussion may be found in [207].

An even more interesting case is that of ^{179}Au, where the long accepted muonic value of 547(16) mb [211] has been challenged [213]. Gold presents a particularly tough case, possibly because of relatively small EFG at its nucleus. Experimentally, the EFG is highly sensitive to the molecular environment, as shown by the large

Table 7-13 Dependence of the EFG at the iodine nucleus on the basis set and number n_{corr} of correlated electrons in I^-

Basis	*s*	*p*	*d*	*f*	*g*	*h*	n_{corr}	EFG(a.u.)
$28s23p18d8f4g$	1–28	6–28	9–26	18–25	22–25		26	7.10439
$28s23p18d8f5g$	1–28	6–28	9–26	18–25	21–25		26	7.10402
$28s23p18d9f5g$	1–28	6–28	9–26	18–26	22–26		26	7.09632
$28s23p19d9f5g$	1–28	6–28	9–27	18–26	22–26		26	7.08905
$28s23p18d8f4g2h$	1–28	6–28	9–26	18–25	22–25	23–24	26	7.13261
$28s23p18d8f4g2h$	1–28	6–28	9–26	18–25	22–25	23–24	44	7.17009
$28s23p18d8f4g2h$	1–28	6–28	9–26	18–25	22–25	23–24	54	7.17104
$28s23p19d8f4g2h$	1–28	6–28	9–27	18–25	22–25	23–24	54	7.16368
$28s23p20d8f4g2h$	1–28	6–28	9–28	18–25	22–25	23–24	54	7.16368
$28s23p20d9f4g2h$	1–28	6–28	9–27	18–26	22–25	23–24	54	7.15757
$28s24p20d9f4g2h$	1–28	5–28	9–27	18–26	22–25	23–24	54	7.15905
$28s24p21d9f4g2h$	1–28	5–28	8–27	18–26	22–25	23–24	54	7.15917

NQCC differences between AuCl (9.6 MHz) and its noble gas complexes (−259.8 for Ar-AuCl, −349.9 MHz for Kr-AuCl) [214]. Computationally, very strong dependence on the gold-containing molecule and the particular method used has been observed [215], with the EFG varying between −0.374 and +0.746 a.u. for the AuX molecules (X=F,Cl,Br,I) calculated with the Dirac–Coulomb and Douglas–Kroll Hamiltonians at the CCSD(T) level, yielding NQM values from −1.51 to +0.65 b. A recent molecular calculation [216] obtained 510(15) mb.

The method described above was applied [217], using both the well-tempered [206] and universal [203] basis sets. An intrinsic check is provided by the availability of two independent sets of quadrupole coupling constants for the $^2D_{5/2}$ and $^2D_{3/2}$ states [218]. Indeed we found that medium size basis sets gave a difference of ∼1% between the NQMs calculated for the two states, going down to 0.1% for the largest basis sets. Our final result is $Q(^{197}\text{Au}) = 521(7)$ mb, in good agreement with the molecular 510(15) mb [216].

7.5. APPLICATIONS: SUPERHEAVY ELEMENTS

As can be expected, the effect of relativity increases when we go to superheavy elements. This term is usually applied to elements with atomic number above 100 (trans-fermium elements). The chemistry of some of these elements has been studied [219, 220]. An important relativistic effect involves changes in the level ordering, leading sometimes to a ground state configuration which differs from that of lighter atoms in the same group and, consequently, to different chemistry.

7.5.1. Ground State Configuration of Roentgenium (E111)

A major relativistic effect in the gold atom is the stabilization of the 6*s* orbital. This is manifested by the energy separation between the $5d^{10}6s\ ^2S$ ground state and

the $5d^9 6s^2\ ^2D$ excited state. Looking at group 11 (coinage metal) atoms, the ^2D excitation energies of Cu are 1.389 ($J = 5/2$) and 1.642 ($J = 3/2$) eV, increasing to 3.749 and 4.304 eV for Ag [184]. Were it not for relativity, one would expect even higher energies for Au. Indeed, nonrelativistic CCSD (Table 7-6) puts the ^2D energy at 5.301 eV above the ^2S ground state, in line with expectations. Relativistic effects reduce this value radically, giving 1.150 and 2.669 eV for the excited ^2D sublevels, within 0.015 eV of experiment [184]. Even larger stabilization may be expected for the next member of the group, element 111. The question arose whether this stabilization would be sufficient to push the ^2D level below the ^2S and make it the ground state of the atom.

The calculations were carried out as for gold above, starting with the $E111^-$ anion as reference [221]. As expected, very large relativistic effects are observed, demonstrated by the large contraction of the 7*s* orbital of neutral E111 (Figure 7-3). The 7*s* orbital energy of the anion goes down from −0.018 to −0.136 hartree, while the 6*d* goes up from −0.355 to −0.186 ($j = 3/2$) and −0.080 ($j = 5/2$) hartree. Atomic energies also show dramatic changes (see Table 7-14). Of particular interest to us is the $6d^9 7s^2\ ^2D_{5/2}$ state, predicted by nonrelativistic CCSD to lie 5.43 eV above the $6d^{10}7s\ ^2S$ state, but reduced relativistically to 3 eV *below* the ^2S, thus becoming the ground state. Ionization potentials of the atom show relativistic effects of 12–15 eV! Similar effects were observed in eka-mercury (E112) [222] and eka-thallium (E113) [200].

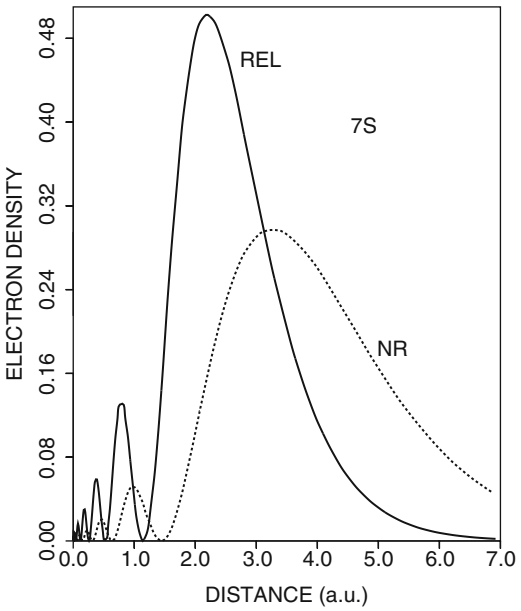

Figure 7-3. Relativistic and nonrelativistic densities of element 111 7*s* orbital

Table 7-14 CCSD excitation energies, electron affinity and ionization potentials of element 111 (eV)

Transition		DC	DCB	NR
EE	$6d^9 7s^2\ ^2D_{5/2} \rightarrow 6d^9 7s^2\ ^2D_{3/2}$	2.719	2.687	0
	$6d^9 7s^2\ ^2D_{5/2} \rightarrow 6d^{10} 7s\ ^2S_{1/2}$	3.006	2.953	−5.430
EA	$6d^9 7s^2\ ^2D_{5/2} \rightarrow 6d^{10} 7s^2\ ^1S_0$	1.542	1.565	6.484
IP	$6d^9 7s^2\ ^2D_{5/2} \rightarrow 6d^8 7s^2\ ^3D_4$	10.57	10.60	22.98
	$6d^9 7s^2\ ^2D_{5/2} \rightarrow 6d^9 7s\ ^3D_3$	12.36	12.33	0.92
	$6d^9 7s^2\ ^2D_{5/2} \rightarrow 6d^{10}\ ^1S_0$	15.30	15.23	−0.44

7.5.2. Ground State of Rutherfordium – Relativity vs. Correlation

The nature of the rutherfordium ground state has been a subject of interest for a long time. Rutherfordium is the first atom after the actinide series, and in analogy with the lighter group-4 elements it should have the ground-state configuration $[\mathrm{Rn}]5f^{14}6d^2 7s^2$. Keller [223] suggested that the relativistic stabilization of the $7p_{1/2}$ orbital would yield a $7s^2 7p_{1/2}^2$ ground state. MCDF calculations [224, 225] found that the $7p^2$ state was rather high; they indicated a $6d\,7s^2 7p$ ground state, with the lowest state of the $6d^2 7s^2$ configuration higher by 0.5 [224] or 0.24 eV [225]. The two calculations are similar, using numerical MCDF [97] in a space including all possible distributions of the four external electrons in the $6d$, $7s$ and $7p$ orbitals, and the difference may be due to the different programs used or to minor computational details. These MCDF calculations take into account nondynamic correlation only, which is due to near-degeneracy effects and can be included by using a small number of configurations. A similar approach by Desclaux and Fricke [226] gave errors of 0.4–0.5 eV for the energy differences between $(n-1)d$ and np configurations of Y, La and Lu, with the calculated np energy being too low. Desclaux and Fricke corrected the corresponding energy difference in Lr by a similar amount [226]. If a shift of similar magnitude is applied to the MCDF results for Rf, the order of the two lowest states may be reversed. It should also be noted that dynamic correlation, largely omitted from MCDF, has been shown to play a significant role in determining atomic excitation energies, reducing the average error in calculating Pr^{3+} excitation energies by a factor of four relative to MCDF results. The FSCC method was therefore applied to Rf [227]. Starting from Rf^{2+} with the closed-shell configuration $[\mathrm{Rn}]5f^{14}7s^2$, two electrons were added, one at a time, in the $6d$ and $7p$ orbitals, to form the low-lying states of Rf^+ and Rf. A large basis set of $34s24p19d13f8g5h4i$ G-spinors was used, and the external 36 electrons were correlated, leaving only the $[\mathrm{Xe}]4f^{14}$ core uncorrelated. A series of calculations, with increasing l values in the virtual space, was performed to assess the convergence of the results. Some of the calculated transition energies are shown in Table 7-15. Others may be found in the original publication [227].

The salient feature of the calculated transition energies is their monotonic behavior with the amount of correlation accounted for. The correlation of the $5f$ electrons and the gradual inclusion of higher l spaces all increase the four transition energies

Table 7-15 Transition energies in Rf^+ and Rf (eV)

	Rf^+		Rf	
	$7s^2 6d_{3/2}$ $^2D_{3/2}$ IP	$7s^2 6d_{5/2}$ $^2D_{5/2}$ EE	$7s^2 6d^2$ $^3F_2$ IP	$7s^2 7p6d$ $^3D_2$ EE
MCDF [225]	13.47		5.30	−0.24
MCDF [224]				−0.50
CCSD				
$l \leq 2$[a]	13.37	0.79	5.15	−0.60
$l \leq 3$[a]	13.95	0.82	5.65	−0.11
$l \leq 3$	14.05	0.87	5.76	0.03
$l \leq 4$	14.20	0.90	5.90	0.17
$l \leq 5$	14.34	0.92	5.99	0.25
$l \leq 6$	14.37	0.92	6.01	0.27
$l \leq 5$[b]	14.34	0.87	5.99	0.27

[a] $5f$ electrons not correlated.
[b] With Breit interaction.

in Table 7-15, as well as those not shown here. The MCDF results fall invariably between the d and f limits. This makes sense, since the MCDF function optimizes the orbitals and CI coefficients in a space including configuration state functions which correspond to all possible distributions of the four external electrons in the $6d$, $7s$ and $7p$ orbitals. Nondynamic correlation, resulting from interactions of configurations relatively close in energy, is thus described very well; the dynamic correlation, which is more difficult to include and requires many thousands of configurations, is not described as well, leading to an error in the identification of the Rf ground state. The latter is determined by the sign of the excitation energy in the last column of Table 7-15. A negative energy means that the $7s^2 7p6d$ configuration is lower than $7s^2 6d^2$, and is therefore the ground state. From the calculations reported, we estimate the CCSD converged value for this energy at 0.30–0.35 eV, making the $7s^2 6d^2$ state the ground state of atomic Rf. Recent state-of-the-art experiments with Rf confirmed [228] that the chemistry of the atom is similar to that of Hf, which has a $6s^2 5d^2$ ground state.

This example shows the intricate interplay of relativity and correlation. It is well known that relativity stabilizes p vs. d orbitals, and correlation has the opposite effect. When both effects are important and the result not obvious *a priori*, one must apply methods, such as relativistic CC, which treat relativity and correlation simultaneously to high order.

7.5.3. Eka-Lead (Element 114) – How Inert Is It?

Great progress has been made in recent years in creating new superheavy elements. After the synthesis of elements 110–112 in 1994–96 [229–232], elements 114 and 116 were reported in 1999 and 2000 [233–235]. The latter atoms are the subject

of great interest, as they fall within the "island of stability" predicted by nuclear physics. The exact location of this island is not certain. There seems to be general agreement that the next neutron magic number is 184, but the proton magic number (which determines the atomic number of the element) is variously predicted at 114 [236], 120 [237], or 126 [238]. Current technology produces isotopes with too few neutrons to get maximum stability; nevertheless, longer lifetimes than for other superheavy elements have been reported. One reason for studying these elements, apart from the nuclear physics involved, is the hope that the strong relativistic effects for the heavier elements would lend them exotic chemical properties, unknown for their lighter homologues. The discussion of roentgenium above provides an example where the ground-state configuration of a superheavy element differs from that of the lighter atoms in the group; another case of unusual behavior of a superheavy element is given in the next Subsection. Here we compare the properties of eka-lead with those of lead and lighter group-4 elements. The IHFSCC method is used to obtain high accuracy.

Two series of calculations were carried out [239]. The first started from the closed-shell M^{4+} ion, adding two electrons in the Fock-space scheme

$$M^{4+}(\text{sector } 0) \rightarrow M^{3+}(\text{sector } 1) \rightarrow M^{2+}(\text{sector } 2). \tag{7-90}$$

Thirty two electrons $[(n-1)s^2(n-1)p^6(n-1)d^{10}(n-2)f^{14}$, with $n = 6$ for Pb and 7 for E114] are correlated in the reference state. We were interested in the few lowest states only for these sectors, so a relatively small P_m was taken, including only states with ns and np electrons added to the reference. The P space was considerably larger, including in addition the next four s, four p, four d, three f and two g orbitals. In this case, the traditional FSCC converges with a model space constructed from the ns and np orbitals, and the advantage of IHFSCC lies in enhancing accuracy by allowing a larger P space.

The closed-shell M^{2+} ns^2 state is taken as reference in the second Fock-space sequence,

$$M^{2+}(\text{sector } 0) \rightarrow M^{+}(\text{sector } 1) \rightarrow M(\text{sector } 2). \tag{7-91}$$

Here 34 electrons are correlated in the reference state. Basis sets going to $l = 8$ were used, with $35s26p21d16f11g9h9i7k7l$ Gaussian orbitals. The FSCC iterations converge only when the np orbitals serve as the sole valence particles, i.e., only ns^2np^2 states could be obtained. The IHFSCC method allows many more valence orbitals and, consequently, many more states. The P_m for lead included all states constructed from the $7s$, $8s$, $6p$, $7p$, and $6d$ orbitals; P included, in addition, states with occupied $9s-12s$, $8p-11p$, $7d-9d$, $5f-7f$, and $5g$ orbitals. For E114 we were interested in fewer states, so that P_m was smaller, with $8s$, $7p$, and $8p$ orbitals; $9s-13s$, $9p-12p$, $7d-10d$, $6f-8f$, and $5g$ orbitals complete the P space.

The ionization potentials and low excitation energies of the lead and eka-lead cations are reported, together with Pb experimental values [184], in Table 7-16. For easy comparison, terms are listed in the LS coupling as in Moore's Tables [184], although the validity of this coupling scheme for Pb, and even more so for

Table 7-16 Ionization potentials (IP) and excitation energies (EE) of lead and eka-lead cations (cm^{-1}). $n = 6$ for Pb, 7 for E114

Transition				Pb		E114
				Expt. [184]	Calc.	Calc.
M^{3+}. Ground state $(n-1)d^{10}ns\ ^2S_{1/2}$						
IP	→	$(n-1)d^{10}$	$^1S_0$	341,350	341,748	373,208
EE	→	$(n-1)d^{10}np_{1/2}$	$^2P_{1/2}$	76,158	76,839	86,676
	→	$(n-1)d^{10}np_{3/2}$	$^2P_{3/2}$	97,219	97,803	138,047
M^{2+}. Ground state $(n-1)d^{10}ns^2\ ^1S_0$						
IP	→	$(n-1)d^{10}ns$	$^2S_{1/2}$	257,592	257,617	288,256
EE	→	$(n-1)d^{10}nsnp_{1/2}$	$^3P_0$	60,397	60,396	73,135
	→		$^3P_1$	64,391	64,451	79,832
	→	$(n-1)d^{10}nsnp_{3/2}$	$^3P_2$	78,985	78,964	119,597
	→		$^1P_1$	95,340	95,716	135,170
	→	$(n-1)d^{10}np_{1/2}^2$	$^3P_0$	142,551	143,412	166,645
M^{+}. Ground state $(n-1)d^{10}ns^2np_{1/2}\ ^2P_{1/2}$						
IP	→	$(n-1)d^{10}ns^2$	$^1S_0$	121,243	121,077	136,074
EE	→	$(n-1)d^{10}ns^2np_{3/2}$	$^2P_{3/2}$	14,081	13,885	39,355
	→	$(n-1)d^{10}ns^2(n+1)s$	$^2S_0$	59,448	59,253	71,993

E114, is questionable; the only good quantum number in the reported levels (and the calculation procedures) is J. The average deviation of the Pb results from experiment is 334 cm^{-1}, and the largest error is 861 cm^{-1}. This close agreement indicates that the eka-lead values provide good predictions for the electronic spectrum of this superheavy element. Table 7-17 gives the transition energies of the neutral atoms. It is noteworthy that many Pb states can be obtained accurately by the IHFSCC method (the average error for the 22 P_m excitations is 602 cm^{-1} or 1.6%), while only the $6s^26p^2$ states are accessible by traditional FSCC. There are many P_i states above 51,000 cm^{-1}; these come out less well, as expected from theory. In contrast, the higher P_m states are roughly as accurate as the lower levels. The predicted transition energies of E114 given in the same table show ionization potentials higher by 0.2–0.3 eV than those reported by Seth et al. [240]. Our values are probably more accurate, due to the inclusion of the Breit term and the use of a larger basis and a much extended model space, which more than compensates for the perturbative inclusion of triples. The transition energies reported here should be roughly as accurate as those of Pb, with errors of a few hundredths of an eV, and provide therefore good predictions for future experimental values.

The prominent feature of the energies collected in Tables 7-16 and 7-17 is that ionization potentials and excitation energies of E114 are much higher than analogous Pb values. Table 7-18 collects the first four ionization potentials of all group-14 elements (experimental values [241] for C–Pb, calculated for Pb and E114), and Figure 7-4 shows the first IP for these elements. The usual trend of IPs decreasing for heavier atoms holds from C to Sn; reversal of this trend begins in Pb and increases greatly for E114, with IPs surpassing those of Si. This reversal is due to relativistic stabilization of the valence s and $p_{1/2}$ orbitals, which becomes stronger

Table 7-17 Ionization potential (IP) and excitation energies (EE) of neutral lead and eka-lead (cm^{-1}). States belong to P_m, unless noted otherwise. The ground state is $(n-1)d^{10}ns^2np_{1/2}^2\ {}^3P_0$, with $n = 6$ for Pb, 7 for E114

Transition				Pb		E114
				Expt. [184]	Calc.	Calc.
IP	→	$ns^2np_{1/2}$	$^2P_{1/2}$	59,821	59,276	68,868
EE	→	ns^2np^2	$^3P_1$	7,819	7,531	26,342
	→		$^3P_2$	10,650	10,307	28,983
	→		$^1D_2$	21,458	20,853	60,956
	→		$^1S_0$	29,467	29,259	67,817
	→	$ns^2np_{1/2}(n+1)s$	$^3P_0$	34,960	34,405	43,111
	→		$^3P_1$	35,287	34,711	43,441
	→	$ns^2np_{1/2}(n+1)p$	$^3P_0$	42,919	42,255	52,487
	→		$^3P_1$	44,401	43,655	54,647
	→		$^3D_1$	44,675	43,969	51,302
	→		$^3D_2$	44,809	44,089	54,814
	→	$ns^2np_{1/2}nd$	$^3F_2$	45,443	44,525	56,026[a]
	→		$^3F_3$	46,328	45,627	56,494[a]
	→		$^3D_2$	46,060	45,173	56,418[a]
	→		$^3D_1$	46,068	45,165	56,456[a]
	→	$ns^2np_{3/2}(n+1)s$	$^3P_2$	48,188	47,414	79,473
	→		$^1P_1$	49,439	48,682	80,455
	→	$ns^2np_{1/2}(n+2)s$	$^3P_1$	48,687	47,988	
	→		$^3P_0$	48,726	48,031	
	→	$ns^2np_{3/2}(n+1)p$	$^3D_3$	57,372	57,336	92205
	→	$ns^2np_{3/2}nd$	$^3D_3$	58,518	58,080	95,851[a]
	→		$^3P_1$	59,427	59,291	
	→	$ns^2np_{3/2}(n+2)s$	$^3P_2$	62,621	61,728	

[a] P_i state.

Table 7-18 Ionization potentials of group 14 elements (eV). Experimental data from the Handbook [241], calculated data: present work

	Experimental					Calculated	
	C	Si	Ge	Sn	Pb	Pb	E114
IP1	11.260	8.152	7.900	7.344	7.417	7.484	8.539
IP2	24.383	16.346	15.935	14.632	15.032	15.012	16.871
IP3	47.888	33.493	34.224	30.503	31.937	31.941	35.739
IP4	64.494	45.142	45.713	40.735	42.322	42.372	46.272

in the superheavy elements. The higher IPs of eka-lead, together with the closed shell character of its $7p_{1/2}^2$ configuration, indicate it will be more inert and less metallic than lead.

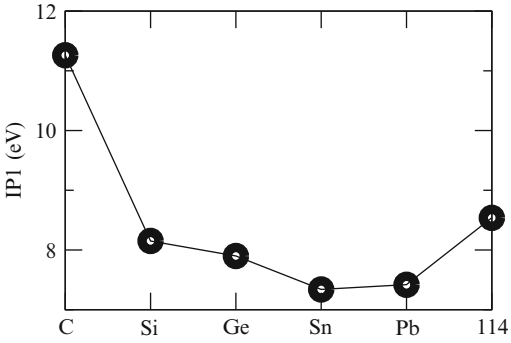

Figure 7-4. First ionization potentials of group 14 elements

7.5.4. Electronic Spectrum of Nobelium (Z = 102) and Lawrencium (Z = 103)

The spectroscopic study of superheavy atoms ($Z \gtrsim 100$) presents a severe challenge to the experimentalist. While certain chemical properties of these elements may be elucidated in single-atom experiments [219, 220], spectra can be measured only in sizable samples. The first such study of a superheavy atom [242] used 2.7×10^{10} atoms of ^{255}Fm with a half life of 20.1 h, long enough to make possible shipment of the sample from Oak Ridge, Tennessee, where it was produced, to the Max-Planck-Institut für Kernphysik in Heidelberg, where the spectrum was taken. Spectroscopic measurements are planned for No and Lr, which have shorter lifetimes, by a collaboration based at GSI [243], with production and measurement taking place in the same site. Such measurements must be accompanied by high-level calculations. The low production rates of the atoms in nuclear fusion reactions, below 10 per second, and short lifetimes, on the order of seconds, necessitate reliable prediction of the position of transition lines, to avoid the need for broad wavelength scans. In addition, theoretical studies are crucial for identifying the lines. Indeed, the Fm measurements [242] were accompanied and guided by multiconfiguration Dirac–Fock (MCDF) calculations. Four-component FSCC calculations were undertaken for No [244] and Lr [245]. The accuracy of the predicted spectra for these elements was estimated by applying the same method to ytterbium [244] and lutetium [245], their lighter homologues, where experimental transition energies are available.

Large, converged basis sets ($37s31p26d21f16g11h6i$) and P spaces (up to $8s6p6d4f2g1h$) were used in the framework of the IH-FSCC method. Many electrons (42 for No, 43 for Lr) were correlated, so that any core polarizations effects were included. The mean absolute error for the twenty lowest excitation energies was 0.04 eV for Yb, 0.05 eV for Lu. The calculated IP of No was 6.632 eV, in agreement with the semiempirically extrapolated value of 6.65(7) eV [246].

The transition energies and amplitudes of No are shown in Table 7-19. The energies were obtained by IH-FSCC, and their expected accuracy is $\sim$800 cm^{-1}. The amplitudes were calculated by relativistic CI and have lower accuracy, which is,

Table 7-19 RCI electric dipole transition amplitudes of the strongest transitions of nobelium. τ is the lifetime of the upper level

λ(Å)	Upper state	τ(s)	Lower state	A(s^{-1})
2,365	$7s8p\ ^1P_1$	2.9×10^{-8}	$7s^2\ ^1S_0$	3.2×10^7
2,457	$7s8p\ ^3P_1$	2.9×10^{-8}	$7s^2\ ^1S_0$	1.0×10^7
3,327	$7s7p\ ^1P_1$	2.0×10^{-9}	$7s^2\ ^1S_0$	5.0×10^8
4,103	$7s9s\ ^3S_1$	1.2×10^{-8}	$7s7p\ ^3P_1$	1.8×10^7
4,484	$7s7d\ ^3D_2$	4.5×10^{-8}	$7s7p\ ^3P_1$	1.4×10^7
5,140	$7s9s\ ^3S_1$	1.2×10^{-8}	$7s7p\ ^3P_2$	4.2×10^7
5,663	$7s7d\ ^3D_3$	6.1×10^{-8}	$7s7p\ ^3P_2$	1.7×10^7
6,168	$7s8s\ ^3S_1$	1.4×10^{-8}	$7s7p\ ^3P_0$	1.1×10^7
6,832	$7s8s\ ^3S_1$	1.4×10^{-8}	$7s7p\ ^3P_1$	3.3×10^7
7,679	$7s7d\ ^1D_2$	8.0×10^{-8}	$7s7p\ ^3P_1$	1.2×10^7
8,171	$7s8p\ ^3P_0$	3.7×10^{-8}	$7s6d\ ^3D_1$	1.6×10^7
10,290	$7s8s\ ^3S_1$	1.4×10^{-8}	$7s7p\ ^3P_2$	2.8×10^7
15,427	$7s8s\ ^1S_0$	8.9×10^{-8}	$7s7p\ ^1P_1$	1.1×10^7
18,235	$7s8p\ ^3P_0$	3.7×10^{-8}	$7s8s\ ^3S_1$	1.1×10^7

however, sufficient for the purpose of identifying the strongest lines. The simulated spectrum is shown in Figure 7-5. The salient feature of the spectrum is a strong line at $30{,}100 \pm 800\ \text{cm}^{-1}$, with an amplitude of $A = 5\times10^8\ \text{s}^{-1}$. There are other lines, with amplitudes at least one order of magnitude lower.

Table 7-20 shows the transition energies of lawrencium. Its ground state ($7s^2 7p\ ^2P_{1/2}$) is different from that of lutetium ($6s^2 5d\ ^2D_{3/2}$), as relativity pushes the $7p$ orbital below the $6d$. The QED corrections to the transition energies are small, below 30 cm^{-1}. This small contribution reflects the fact that the $7s$ population does not change for the transitions reported. Some excitations involving holes in the $7s$ shell were calculated by the RCI method; they exhibit larger QED effects, between 200 and 400 cm^{-1}. The prime region for observing transitions in the planned experiment is between 20,000 and 30,000 cm^{-1}. Our calculations predict several excitations with large transition amplitudes in this region. The strongest lines in the range of the experiment will correspond to $7p \rightarrow 8s$ at 20,100 cm^{-1} and $7p \rightarrow 7d$ at 28,100 cm^{-1}. The $7p \rightarrow 9s$ transition at 30,100 cm^{-1} is also dipole allowed, but the very different spatial distribution of the two orbitals is expected to make it weaker than the other two. The transition amplitudes are shown in Table 7-20. Note that some excited states, in particular those with a single $7s$ electron, have large contributions from several configurations. Thus, the first two states in Table 7-20 have RCI coefficients between 0.4–0.5 for each of the $7s7p_{1/2}7p_{3/2}$, $6d_{3/2}6d_{5/2}7s$, and $7s6d_{5/2}^2$ configurations, and their assignment is somewhat arbitrary. The simulated spectrum, obtained by convolution with a Gaussian function with 20 Å full width at half maximum, is shown in Figure 7-6. The two states with the largest RCI transition amplitudes are outside the range of the planned experiment. They are dominated by the $6d^2 7s$ and $7s7p^2$ configurations, which cannot at present be included in the P

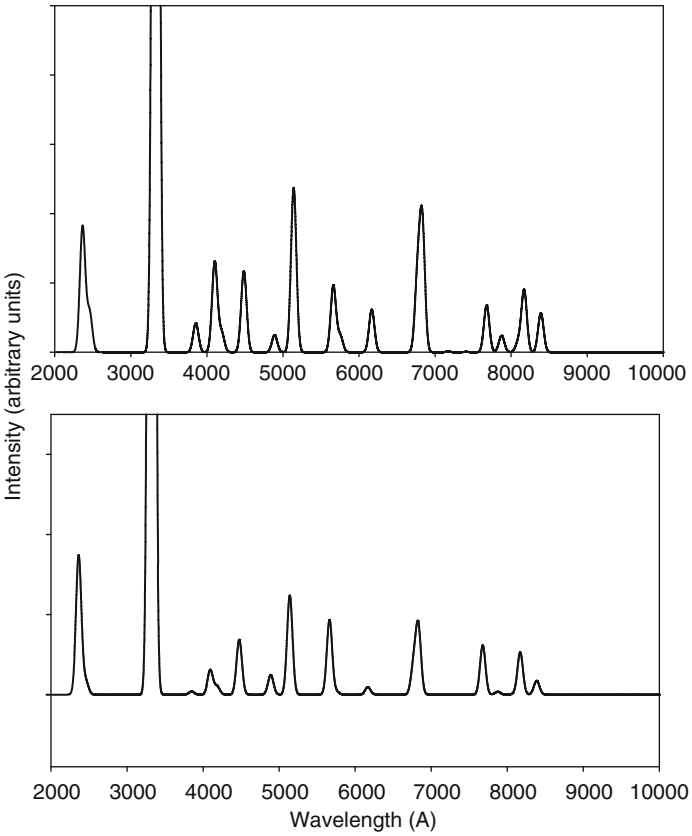

Figure 7-5. Simulated E1 spectrum of No, assuming equal population of all excited levels. The lower panel is corrected for the total lifetime of the levels

Table 7-20 RCI amplitudes of E1 transitions to the $7s^2 7p_{1/2}$ ground state of Lr. The upper levels are designated by the dominant electron configurations; other configurations may contribute substantially

λ (Å)	Upper level	J	A(s^{-1})
2,637.7	$6d_{3/2}6d_{5/2}7s$	1/2	3.6×10^8
2,911.3	$6d^2_{5/2}7s$	3/2	2.2×10^8
2,988.9	$7s^2 8d_{3/2}$	3/2	9.4×10^6
3,151.8	$6d^2_{3/2}7s$	3/2	8.6×10^6
3,319.5	$7s^2 9s$	1/2	6.0×10^5
3,559.2	$7s^2 7d_{3/2}$	3/2	3.5×10^7
3,616.2	$7s7p_{1/2}7p_{3/2}$	1/2	2.7×10^6
4,306.4	$7s7p^2_{1/2}$	1/2	1.4×10^7
4,967.5	$7s^2 8s$	1/2	2.7×10^7

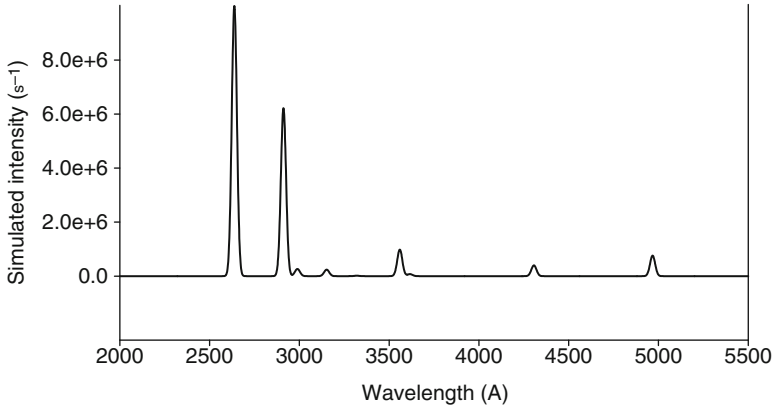

Figure 7-6. Simulated E1 spectrum of Lr

space. Consequently, these states do not appear in the FSCC calculations, and their energies may have larger errors than states obtained by FSCC. The transitions at 20,100 and 28,100 cm^{-1} carry the next highest amplitudes, and are the most likely to be observed.

7.5.5. Can a Rare Gas Atom Bind an Electron?

One of the most dramatic effects of relativity is the contraction and concomitant stabilization of s orbitals. An intriguing question is whether the $8s$ orbital of element 118, the next rare gas, would be stabilized sufficiently to give the atom a positive electron affinity. Using the neutral atom Dirac–Fock orbitals as a starting point raises a problem, since the $8s$ orbital has positive energy and tends to "escape" to the most diffuse basis functions. This may be avoided by calculating the unoccupied orbitals in an artificial field, obtained by assigning partial charges to some of the occupied shells. The nonphysical fields are compensated by including an appropriate correction in the perturbation operator. A series of calculations with a variety of fields gave electron affinities differing by a few wave numbers [247], from which an electron affinity of −0.056(10) eV was deduced. More recently, the issue of possible quantum electrodynamic effects on this quantity was raised. The impetus was a calculation of QED effects on the ionization potential of E119, which was estimated at 0.0173 eV [248], of the same order as the calculated EA of 118. Thus, QED effects could change the EA significantly, and their treatment has been undertaken [249].

An improved basis set with $36s32p24d22f10g7h6i$ uncontracted Gaussian-type orbitals was used and all 119 electrons were correlated, leading to a better estimate of the electron affinity within the Dirac–Coulomb–Breit Hamiltonian, 0.064(2) eV [249]. Since the method for calculating the QED corrections [248] is

based on the one-electron orbital picture, the 8*s* orbital of E118 was extracted from the correlated wave functions Ψ_{118}^{CC} and Ψ_{118-}^{CC} by

$$\phi_{8s}(r) = \frac{\langle \Psi_{118}^{CC} | \Psi_{118-}^{CC} \rangle}{\left(\langle \Psi_{118}^{CC} | \Psi_{118}^{CC} \rangle \langle \Psi_{118-}^{CC} | \Psi_{118-}^{CC} \rangle \right)^{1/2}} . \tag{7-92}$$

The integration in the numerator is over 118 electrons, giving a one electron orbital; the normalization integrals in the denominator are over all electrons. Using ϕ_{8s} and the total electron density, the self-energy and vacuum polarization terms were calculated, giving a total Lamb shift of 0.0059(5) eV, reducing the electron affinity by 9% (for details see Ref. [249]). This is the largest QED effect found so far for neutral or weakly ionized species, confirming the importance of QED corrections for superheavy elements.

It should be emphasized that correlated nonrelativistic or relativistic uncorrelated calculations yield no electron affinity for element 118. The Rn atom does not show a bound state of the anion even at the relativistic CC level.

7.5.6. Adsorption of Superheavy Atoms on Surfaces – Identifying and Characterizing New Elements

One of the exciting fields in nuclear physics is the production of new superheavy elements. The newly produced atoms coming out of the accelerator must be separated from other reaction products and identified to establish their atomic number. Identification is relatively easy if the nucleus decays by a series of α emissions. However, many of the neutron rich isotopes, which have relatively long lifetimes and may therefore be amenable to chemical studies, decay by spontaneous fission to unknown products. This is the case for the recently produced $^{283}112$ ($t_{1/2}$=3.8 s), $^{287}114$ ($t_{1/2}$ = 0.5 s), and $^{288}114$ ($t_{1/2}$=0.5 s) [250], as well as $^{284}113$ ($t_{1/2}$=0.48 s) [251]. Elements 112 and higher are expected to be volatile, and their adsorption behavior can be used by gas-phase chromatography, whereby atoms are deposited on detectors located along a chromatography column according to their volatility. The deposition temperatures are measured and associated with the adsorption enthalpies ΔH_{ads}. Transition metals, mainly gold, are generally used as detector surfaces, since they stay clean of oxide layers.

The volatility of element 112 relative to that of Hg was studied by this technique [252]. The two elements showed similar behavior on gold-covered detectors. The adsorption behavior of element 114 relative to Pb is currently being studied, and similar experiments may be expected for element 113 and others. Prediction of the adsorption behavior of these elements and their lighter homologues on different surfaces is important in designing the experiments, choosing appropriate adsorption surfaces, etc. Calculations pertaining to elements 112–114 and118 have

recently been carried out [253–255]. Required atomic properties, in particular polarizabilities, were calculated by the finite field method (see Section 7.4.6). Adding a static uniform electric field $\mathbf{F}$ to the Hamiltonian gives the energy

$$E(\mathbf{F}) = E(0) + \mathbf{F} \cdot \frac{\partial E(\mathbf{F})}{\partial \mathbf{F}}\bigg|_{\mathbf{F}=\mathbf{0}} + \frac{1}{2} \cdot \mathbf{F}^2 \frac{\partial^2 E(\mathbf{F})}{\partial^2 \mathbf{F}}\bigg|_{\mathbf{F}=\mathbf{0}} + \cdots . \tag{7-93}$$

The first derivative is the atomic dipole moment, which vanishes, and the polarizability is obtained by

$$\alpha_{ij} = - \frac{\partial^2 E(\mathbf{F})}{\partial F_i \, \partial F_j}\bigg|_{\mathbf{F}=\mathbf{0}}, \quad i, j = x, y, z. \tag{7-94}$$

For a uniform electric field $F = F_z$ in the z direction,

$$\alpha = - \frac{\partial^2 E(F)}{\partial^2 F}\bigg|_{F=0}. \tag{7-95}$$

The ground state energies of the atoms, $E(F)$, were calculated for $F = 0, 0.001, 0.002$ a.u., and the derivative with respect to F^2, multiplied by 2, gave the polarizability. The calculated values are shown in Table 7-21. Good agreement with experimental polarizabilities of the lighter elements was obtained. The values in the last column of the table were obtained by correcting the calculated polarizability of the superheavy atom by the (small) error for the corresponding lighter homologue.

These values were used in a physisorption model to obtain adsorption enthalpies. It was found that the ΔH_{ads} values of Hg and 112 on inert surfaces (quartz, ice, Teflon) were too close (∼2 kJ/mol differences) to distinguish between the two elements experimentally. The differences between Pb and 114 are somewhat larger, 7 kJ/mol on quartz and ice, 3 kJ/mol on Teflon. Element 118 is also problematic, giving adsorption enthalpies very close to those of Rn both on noble metals and inert surfaces. A possible candidate for separating these two elements is charcoal; further studies are needed to explore this possibility.

Table 7-21 Experimental [241, 256] and calculated [253–255] polarizabilities (a.u.)

Atom	Expt.	DF	MP2	CCSD	CCSD(T)	Corrected[a]
Hg	33.91	44.90	27.47	35.31	34.15	
112		29.46	25.11	27.66	27.64	27.40
Pb	45.89	49.91	46.75	46.98	46.96	
114		29.78	30.72	30.28	30.59	29.52
Rn		34.99	34.96	34.78	35.04	
118		50.01	44.45	46.64	46.33	

[a]See text.

7.6. DIRECTIONS FOR FUTURE DEVELOPMENT

The methods and applications described above show that much progress has taken place in the field. Still, there are many open problems, and we are far from being able to apply relativistic quantum chemistry routinely to large classes of systems and states. Recent developments by Saue and Visscher [14] and by Lindgren and coworkers [41–46] show great promise for overcoming at least some of these problems. These developments are described briefly in the current Section; the full details may be found in the original publications. Based on these novel schemes, we propose in Section 7.6.3 a new double Fock-space formalism, with variable numbers of electrons and photons.

7.6.1. Beyond Standard Four-Component Hartree–Fock Method: the QED–SCF Procedure

Here we discuss steps beyond the standard four-component Hartree–Fock approach, towards a practical variational QED SCF formulation [14]. This will allow us to consider the extension of the one electron picture to the correlated level of many-body QED theory in the next subsection.

According to Dirac's theory, the excitation of an electron from the Dirac sea to a positive energy orbital, requiring an energy on the order of $2mc^2$, leaves a hole with opposite charge, identified later as the positron. Creation of electron–positron pairs out of the vacuum is thus allowed at sufficiently high energies. Such processes do not conserve particle number, but do conserve charge. The energies of interaction in chemistry are generally too low for real pair creation processes, but the Dirac sea manifests itself in the calculation of heavy elements through vacuum polarization (VP) and, together with retardation effect, self energy (SE) shifts of the energy levels. If the Dirac sea is regarded as filled core and the interparticle interactions are in covariant form, the Lamb shift (the sum of the VP and SE) may be understood, at least in the leading order, via the single particle SCF picture. As shown in [14], the variational QED procedure corresponds to a *true minimum* of the ground energy at the closed-shell Hartree–Fock level. In contrast, the electronic ground state in the standard approach is characterized by a *minimax principle*. The standard approach vacuum is then empty, and the negative-energy orbitals are treated as an orthogonal complement to the electron orbitals. This orthogonal complement, which is an additional (positronic) degree of freedom, allows nearly complete relaxation of the electronic ground state. This relaxation procedure in the standard SCF approach missed the SE and VP terms.

Let us consider the variatianal QED–SCF procedure with the explicitly filled Dirac sea in more detail. It is convenient to define the reference bare vacuum as filled with all the negative-energy solutions of the free-particle Dirac equation,

$$\left|0^{(\mathrm{ref})}\right\rangle = a^{\dagger}_{[-1]} a^{\dagger}_{[-2]} \ldots a^{\dagger}_{[-\infty]} \left|\mathrm{empty}\right\rangle . \tag{7-96}$$

The empty state $|\text{empty}\rangle$ corresponds to the vacuum of the standard approach of the four-component relativistic molecular theory. Square brackets around indices (e.g., $a^\dagger_{[-l]}$) are used to indicate negative energy solutions of the *free-particle* Dirac equation. We consider the description of bound electronic states in terms of a single Slater determinant with all the negative-energy orbitals included explicitly among the occupied orbitals,

$$|\Phi\rangle = a^\dagger_{-\infty} \cdots a^\dagger_{-2} a^\dagger_{-1} a^\dagger_1 a^\dagger_2 \cdots a^\dagger_N |\text{empty}\rangle \tag{7-97}$$

This form of determinant is convenient to implement in the algebraic approximation, where the continuum spectrum becomes a quasi-continuum. What we lose by this approach is the physical picture of electron–positron pair creation provided by the particle-hole formalism. Following [14], the total SCF energy and Fock matrix of the standard approach are replaced by their renormalized QED counterparts E^{QED} and F^{QED},

$$\begin{aligned} E^{\text{QED}} &= \langle \Phi | H | \Phi \rangle - \left\langle 0^{(\text{ref})} | H | 0^{(\text{ref})} \right\rangle \\ &= D^{\text{QED}}_{\mu\nu} h_{\nu\mu} + \frac{1}{2} D^{\text{QED}}_{\mu\nu} \langle \nu\kappa || \mu\lambda \rangle D^{\text{QED}}_{\kappa\lambda} \end{aligned} \tag{7-98}$$

$$F^{\text{QED}}_{pq} = h_{pq} + \langle p\lambda || q\kappa \rangle D^{\text{QED}}_{\lambda\kappa} \tag{7-99}$$

Here the AO density matrix of QED appears,

$$D^{\text{QED}}_{\kappa\lambda} = D_{\kappa\lambda} + D^{\text{LS}}_{\kappa\lambda}; \quad D_{\kappa\lambda} = \sum_i^{(+)} c_{\kappa i} c^*_{\kappa i}; \quad D^{\text{LS}}_{\kappa\lambda} = \sum_i^{(-)} \left(c_{\kappa i} c^*_{\kappa i} - c_{\kappa[i]} c^*_{\kappa[i]} \right). \tag{7-100}$$

Comparing with (7-42) and (7-44), one sees that the standard AO density matrix D has been replaced by the renormalized QED counterpart D^{QED}, obtained by adding the *Lamb shift density* D^{LS}; this reflects the modification of the vacuum density relative to the reference vacuum upon the introduction of the actual potential. If the potential includes only the unretarded Coulomb interaction, as in [14], then $D^{\text{LS}} \equiv D^{\text{pol}}$, where D^{pol} is pure vacuum polarization density, corresponding to the core polarization part in electronic structure calculations. If the potential includes, in addition to the Coulomb term, an effective interaction corresponding to covariant exchange with a single transverse photon, e.g., energy dependent Breit interaction, the radiative self-energy correction density D^{se} is added to the vacuum polarization term giving $D^{\text{LS}} \equiv D^{\text{pol}} + D^{\text{se}}$.

Going from the standard approach to QED means that the negative-energy orbitals count as core orbitals, and are therefore included in the summation in (7-99). The HF equations in the variational QED have the same form as in (7-53), but with the substitution $F \rightarrow F^{\text{QED}}$. The first order irreducible self energy and vacuum polarization corrections are automatically included in the exchange and direct

(Coulomb) parts, respectively, of the HF energy in every SCF iteration. This reflects the topological equivalence of the direct and exchange HF diagrams to the VP and SE Feynman diagrams, respectively.

7.6.2. Beyond NVPA: QED Many-Body Description and the Covariant Evolution Operator Approach

The QED description is fully covariant and, in principle, time dependent. To make connection between stationary infinite order many-body NVPA and QED, let us consider a time dependent perturbation theory approach, which provides a convenient way to get rid of time dependence in a rigorous and elegant manner, following [41–46]. The figures below are taken from [46].

The QED Hamiltonian may be written as $\widehat{H}_{QED} = \widehat{H_0} + \widehat{V}$. Here $\widehat{H}_0$ includes the sum of the noninteracting quantized electronic and photonic field densities,

$$\widehat{H}_0 = \frac{1}{8\pi}(\mathbf{E}^2 + \mathbf{B}^2) - \overline{\psi}\left(i\gamma_\mu \partial^\mu - mc\right)\psi, \tag{7-101}$$

and the perturbation

$$\widehat{V} = -e\overline{\psi}\gamma^\mu A_\mu \psi \tag{7-102}$$

represents the electron interaction with the electromagnetic field A_μ.

The basic tool in time-dependent perturbation theory is the time-evolution operator, which in the interaction picture defines the evolution of the field operators,

$$|\Psi(t)\rangle = \widehat{U}(t, t_0)\,|\Psi(t_0)\rangle\,, \quad (t > t_0). \tag{7-103}$$

Perturbative description of the evolution operator $\widehat{U}(t, t_0)$ leads to the expansion

$$\widehat{U}(t, t_0) = \sum_{n=0}^{\infty} \frac{(-i)^n}{n!} \int_{t_0}^{t} dx_1 \cdots \int_{t_0}^{t} dx_n\, T[\widehat{V}(x_1) \cdots \widehat{V}(x_n)]. \tag{7-104}$$

T is the time-ordering operator. The contraction of two $\widehat{V}$ interactions using Wick's theorem [257] corresponds to the exchange of a single retarded photon. The operator (7-104) is non-covariant, since only positive energy states are involved, and time moves only in the positive direction (Figure 7-7, left). It can be made covariant by inserting electron propagators on the in- and outgoing lines. By definition, operators act to the right on unperturbed model states, which implies that with adiabatic damping we can set the initial time $t_0 = -\infty$, so that no propagators on incoming lines are needed. Time can then flow in both directions on outgoing lines, and both positive and negative energy states are accounted for (Figure 7-7, right). The covariant evolution operator for single-photon exchange is now expressed by

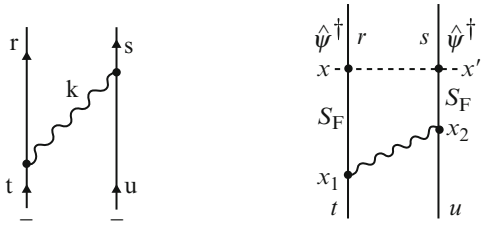

Figure 7-7. The non-covariant and covariant evolution operators for single-photon exchange

$$\widehat{U}_{\mathrm{Cov}}(t,-\infty) = -\int\int d^3x d^3x' \widehat{\psi}^\dagger(x)\widehat{\psi}^\dagger(x') \times \int\int d^4x_1 d^4x_2 S_F(x;x_1) S_F(x';x_2) V_{sp}(x_1;x_2)\widehat{\psi}(x_1)\widehat{\psi}(x_2). \tag{7-105}$$

The energy-dependent single photon potential V_{sp} is given in the Fourier transform by

$$\langle rs\,|V_{sp}(E)|\,tu\rangle = \left\langle rs\left|\int_0^\infty dk f(k)\Big(\frac{1}{E-\varepsilon_t-\varepsilon_u-\mathrm{sgn}(\varepsilon_t)(k-i\gamma)} + \frac{1}{E-\varepsilon_s-\varepsilon_r-\mathrm{sgn}(\varepsilon_s)(k-i\gamma)}\Big)\right|tu\right\rangle, \tag{7-106}$$

where ε is the orbital energy. Orbitals are generated by the Dirac equation in the nuclear field (Furry picture) or by the SCF procedure described in the previous subsection (fuzzy picture). k is the photon momentum, and $f(k)$ is a known gauge-dependent function [41]. The important point is that the expression for the interaction potential V_{sp} is valid even when energy is not conserved between initial and final states. This feature is needed for treating quasi-degeneracy with the extended model space technique, based on the effective or intermediate Hamiltonians described in Sections 7.3.1 and 7.3.2. If energy is conserved,

$$\varepsilon_r + \varepsilon_s = \varepsilon_t + \varepsilon_u, \tag{7-107}$$

(7-106) becomes the standard S-matrix result (7-32,7-33).

The covariant evolution operator is generally singular, due to intermediate model space states. Eliminating the singularities leads to the *Green's operator* $\widehat{G}$ [43]. Green's operator is closely related to the field theoretical Green's function, used extensively in QED (see for instance [58]). The Green's function is nothing but the zero-body term in the second-quantized representation of the Green's operator.

The Green's operator is separated into open and closed parts, $\widehat{G} = 1 + Q\widehat{G}_{op}P + P\widehat{G}_{cl}P$, where $\widehat{G}_{op}$ operates outside and $\widehat{G}_{cl}$ inside the model space, as indicated

by the projection operators P and Q. $\widehat{G}_{op}$ is essentially the wave operator, used in the many-body approaches in quantum chemistry and presented in Section 7.3.1, and $\widehat{G}_{cl}$ yields the effective Hamiltonian [41,43]

$$\Omega = P + Q\widehat{G}_{op}P \tag{7-108}$$

$$\widehat{V}_{\text{eff}} = P(i\frac{\partial}{\partial t}\widehat{G}_{cl}(t))_{t=0}P\ . \tag{7-109}$$

The Green's operator can be applied also to energy-dependent interactions of the QED type, and forms therefore a link between many-body electronic structure and quantum field theory. Eliminating the singularity from the covariant evolution operator leaves some finite residuals [41–43],

$$\widehat{G}(t) = \widehat{G}_0(t) + \sum \frac{\delta^n \widehat{G}_0(t)}{\delta E^n}(\widehat{V}_{\text{eff}})^n, \tag{7-110}$$

where $\widehat{G}_0(t)$ represents the Green's operator without any intermediate model-space states,

$$\widehat{G}_0 = 1 + \mathbb{R}_Q\widehat{W} + \mathbb{R}_Q\widehat{W}\mathbb{R}_Q\widehat{W} + \cdots; \quad \mathbb{R}_Q = \frac{Q}{E_0 - H_0}. \tag{7-111}$$

$\widehat{W}$ is the sum of all irreducible multi-photon interactions (Figure 7-8), and $\mathbb{R}_Q$ is the zero order resolvent operator. The difference ratios transform into derivatives in the case of complete degeneracy. These terms represent the model space contributions and are analogous to the folded diagrams of open-shell FSCC (see Section 7.3.1), but also contain energy derivatives (difference ratios) of the energy-dependent interaction. Summing the contributions to all orders gives the generalized Bethe–Salpeter (BS) equation in the form of the Schrödinger equation with energy dependent potential,

$$(E - \widehat{H}_0)\,|\Psi\rangle = \widehat{W}(E)\,|\Psi\rangle\,. \tag{7-112}$$

A similar covariant equation has been derived in 1951 by Bethe and Salpeter for the complete solution of the two-body relativistic problem [258]. The BS equation may be solved self-consistently, using, e.g., the Brillouin–Wigner perturbation

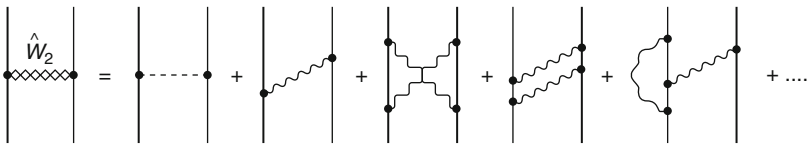

Figure 7-8. The two-body part of the effective potential $\widehat{W}$ in the Bethe–Salpeter–Bloch equation (7-113) contains all irreducible two-body potential diagrams, including the Coulomb interaction as well as all retardation and radiative effects

theory. For many-body considerations, such as size-extensivity [2], we prefer to work with the Rayleigh–Schrdinger theory and the linked-diagram representation, as in standard MBPT. This may be achieved by transforming the BS equation to the corresponding Bloch equation (7-65)

$$(E_0 - \widehat{H}_0)\widehat{\Omega}P = (\widehat{W}(E)\widehat{\Omega} - \widehat{\Omega}\widehat{W}_{\text{eff}}(E))_{\text{linked}}P, \quad \widehat{W}_{\text{eff}} = P\widehat{W}\widehat{\Omega}P, \quad (7\text{-}113)$$

referred to as the generalized Bethe–Salpeter–Bloch (BSB) equation. Note that the energy parameter of the BS potential $\widehat{W}$ and the BS effective interaction $\widehat{W}_{\text{eff}}$ is the target state energy E, and not the model state energy E_0, as one might have expected. This shift is due to the derivative terms in the expansion (7-110). The Bloch equation (7-113) may be used to generate a perturbative expansion of the wave operator for energy-dependent interactions. The difficulty here is in evaluating the energy derivatives of the (multi-photon) perturbation $\widehat{W}(E)$, which is itself calculated numerically. This difficulty may be overcome by working in the extended Fock space with variable numbers of so called uncontracted virtual photons (Figure 7-9). These photons may be described by Feynman diagrams corresponding to the time after they have been radiated by one electron but not yet absorbed by another (or the same) electron. Matrix elements describing these diagrams are derived using CEO. These matrix elements are energy independent [41], and the standard many-body machinery may therefore be used. After the absorption (or contraction) of the virtual photons, the exchange interactions become energy-dependent (see, e.g., (7-106)). If the virtual photon is absorbed by the same electron it has been radiated from, we get radiative effects, which should be properly renormalized. The renormalization procedure for radiative multiphoton diagrams is not fully developed yet [41].

The photonic Fock space treatment may be combined with consideration of electron (and positron) processes and interactions, using the fermionic Fock space formalism presented in Section 7.3.1. A generalized ("double") Fock space CC approach, which treats the electronic and photonic degrees of freedom on equal footing, thus ensuring covariance, is presented below.

7.6.3. Generalized Fock Space. Double Fock-Space CC

With the uncontracted interactions (7-102), the wave function lies in an extended Fock space with a variable number of (virtual) photons or photonic Fock-space sectors (Figure 7-9). The Bloch equation (7-65) will have a particularly simple structure,

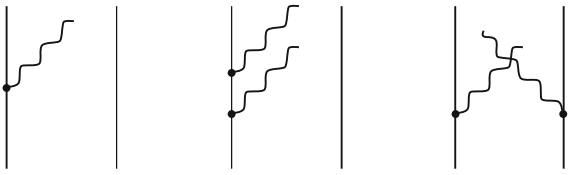

Figure 7-9. The wave function with uncontracted photons lies in an extended Fock space

$$[\widehat{\Omega}, H_0]P = (\widehat{V}\widehat{\Omega} - \widehat{\Omega}\widehat{V}_{\text{eff}})_{\text{linked}}P, \tag{7-114}$$

$$\widehat{V}_{\text{eff}} = P\widehat{V}\widehat{\Omega}P. \tag{7-115}$$

$\widehat{V}$ is the energy-independent perturbation (7-102), which may be divided in parts according to the number of uncontracted virtual photons,

$$\widehat{V} = \sum_{\mu\geq 0} {}^{(\mu)}\widehat{V}(k_1 l_1, ..., k_\mu l_\mu). \tag{7-116}$$

(μ) is the number of retarded uncontracted photons, k_ν and l_ν stand for the energy and momentum of photon ν. Expressions for ${}^{(\mu)}\widehat{V}(k_1 l_1, ..., k_\mu l_\mu)$ were derived using CEO [41], and are not shown here.

We consider here explicitly for the first time the exponential form of the wave operator $\widehat{\Omega} = \{\exp(\widehat{S})\}$ in the generalized Fock space with a variable number of uncontracted virtual photons and electrons/positrons. This parametrization leads to the double Fock-space CC method, presented below. The double Fock-space excitation amplitudes have the structure

$$\widehat{S} = \sum_{m\geq 0}\sum_{n\geq 0}\sum_{\mu\geq 0} {}^{(\mu)}\widehat{S}^{(m,n)}(k_1 l_1, ..., k_\mu l_\mu), \tag{7-117}$$

where (m, n) is the electronic valence sector, and (μ) is the number of retarded uncontracted photons (photonic sectors). The double FSCC equation is

$$Q[{}^{(\mu)}S_l^{(m,n)}, H_0]P = Q\{{}^{(\mu)}(V\Omega - \Omega V_{\text{eff}})_l^{(m,n)}\}_{\text{conn}}P. \tag{7-118}$$

Note that only *connected* diagrams appear on the right-hand side of (7-118), whereas the Bloch equation (7-114) includes all linked diagrams, both connected and disconnected.

The Fock-space excitation operator ${}^{(\mu)}S_l^{(m,n)}$ and resolvent ${}^{(\mu)}R_Q$ are divided into components acting in the subspaces with zero, one, ... uncontracted photons ($\mu = 0, 1, \ldots$). The generalized double FSCC equation (for μ going up to 2) may then be separated into

$${}^{(0)}S_l^{(m,n)} = \tag{7-119}$$

$${}^{(0)}R_{l,Q}^{(m,n)}\{{}^{(0)}V^{(0)}\Omega + \overbrace{{}^{(1)}V^{(1)}\Omega} + \overbrace{\overbrace{{}^{(2)}V^{(2)}\Omega}} - {}^{(0)}\Omega V_{\text{eff}})_l^{(m,n)}\}_{\text{conn}}P,$$

$${}^{(1)}S_l^{(m,n)} =$$

$${}^{(1)}R_{l,Q}^{(m,n)}\{{}^{(1)}V^{(0)}\Omega + {}^{(0)}V^{(1)}\Omega + \overbrace{{}^{(2)}V^{(1)}\Omega} + \overbrace{{}^{(1)}V^{(2)}\Omega} - {}^{(1)}\Omega V_{\text{eff}})_l^{(m,n)}\}_{\text{conn}}P,$$

$${}^{(2)}S_l^{(m,n)} =$$

$${}^{(2)}R_{l,Q}^{(m,n)}\{{}^{(2)}V^{(0)}\Omega + {}^{(0)}V^{(2)}\Omega + {}^{(1)}V^{(1)}\Omega + \overbrace{{}^{(2)}V^{(2)}\Omega} - {}^{(2)}\Omega V_{\text{eff}})_l^{(m,n)}\}_{\text{conn}}P.$$

The upper curly brackets stand for numerical integration over the photonic energy k and momentum l. Thus, multi-photonic retarded energy-dependent interactions are evaluated numerically in the generalized Fock-space by contraction of the photonic uncontracted lines of ${}^{(\mu)}\widehat{V}$ with those of ${}^{(\mu)}\widehat{S}^{(m,n)}$ in all possible ways. Note that an exponential form of $\widehat{\Omega}$ will introduce powers of $\widehat{S}$ in (7-119); the integration (unlike the more familiar contraction) is carried out over V and the first S in the term. Multiphotonic terms describing the interelectronic potential are evaluated by an efficient all-order CC procedure. The effective potential derived by iterative solution of the FSCC equations in the photonic sectors is used in the equation for the electronic sectors. The energy dependence is introduced either by the energy denominators or by the folded diagrams with a double energy denominator. After reaching convergence in the double FSCC equations (7-119), the effective (or intermediate) Hamiltonian in the pure electronic valence sectors, $H_{\text{eff}} = H_0 + V_{\text{eff}}$, is diagonalized to yield directly electronic transition energies.

An example of applying the method with the Bloch equation, without an explicit exponential parametrization of Ω, has been given by Lindgren and coworkers [43–45]. The truncation to single and double excitations gives the so called all order pair equation. It is convenient to describe the scheme using the diagrammatic representation. Starting by iterating the Coulomb interaction in the Furry picture leads to the standard (relativistic) pair-correlation (Ω_2) function (Figure 7-10a). A new pair function with one uncontracted photon (b) is then generated, and additional Coulomb interactions may be added before and after closing the photon (c-e). This leads to one retarded Breit interaction with any number of Coulomb interactions. Absorbing the photon on the same electron leads instead, after proper renormalization, to the electron self energy and vertex corrections (f). The whole procedure can then be repeated (g). In principle, it is possible to create a second photon before the first in absorbed (Figure 7-9), which would generate irreducible multi-retarded photon exchange. This would rapidly exceed currently available computational capabilities, but the effect may be estimated analytically.

The double Fock-space CC approach presented here is under development. In addition to the Furry picture, we implemented the fuzzy picture, based on the variational QED–SCF procedure described in Section 7.6.1. In the fuzzy picture approach, single electronic spinors are "radiatively dressed"; they include first order VP and SE diagrams, as well as higher order reducible diagrams generated from

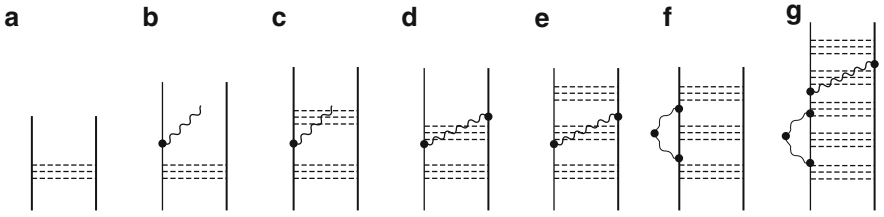

Figure 7-10. Single- and double-photon exchange

them by the SCF procedure. This makes it possible to avoid highly complicated calculations of renormalized contributions to radiative terms at the correlation stage. Another feature is that the exchange with one transverse photon is added to the instantaneous Coulomb interaction in the photonic Fock-space 0-sector (with no uncontracted virtual photons). This way, many irreducible two-photon diagrams may be evaluated numerically in a single uncontracted photonic sector. This and some other recent developments of covariant many-body methods will be reported in a future publication [259].

7.7. SUMMARY AND CONCLUSION

The no-virtual-pair Dirac–Coulomb–Breit Hamiltonian, correct to second order in the fine-structure constant α, provides the framework for four-component methods, the most accurate approximations in electronic structure calculations. The status, features and perspectives for further development of benchmark NVPA many-body methods have been reviewed. Infinite order many-body methods, in particular the coupled cluster scheme, are the most successful approaches to the treatment of electron correlation within the NVPA framework. When applied within the effective or intermediate Hamiltonian technique, these methods give remarkably high-quality results for the most complicated cases of dense quasidegenerate open shell levels in heavy atomic and molecular systems. The IH Fock-space coupled cluster method has structure and features highly suitable for benchmark calculation within NVPA, as well as for extrapolation transcending NVPA towards proper merging with QED theory. Representative calculations included in this review demonstrate the power and reliability of the FSCC method. Transition energies of heavy atoms calculated by NVPA FSCC, including ionization potentials, excitation energies and electron affinities, usually agree with experiment within a few hundredths of an eV. The frequency independent Breit term must be included in the Hamiltonian for this level of accuracy; it is particularly important for hyperfine splittings [121, 187] and for transitions affecting the occupancy of f shells [260]. The latter transitions also require high l basis functions, with i ($l = 6$) orbitals contributing up to 0.1 eV in the case of La. The ability of these methods to reproduce available spectroscopic data lends credence to predictions made regarding the structure and spectroscopy of superheavy elements, which are gradually becoming accessible to experimental study. Among the elements with chemistry expected to be different from that of the lighter homologues are roentgenium (E111), with a ground state electron configuration unlike that of the lighter coinage metals; eka-lead (E114), with an ionization potential higher than any group-14 atom except carbon; and eka-radon (E118), which is the first rare gas to bind an electron. Four-component NVPA molecular calculations, while not reaching the accuracy obtained for atoms, are the most precise available for schemes with similar scaling and computational cost.

While NVPA correlated four-component methods provide excellent results where applicable, they are less accurate for highly ionized heavy and superheavy systems, due to large QED effects. Most current QED approaches can

only be applied in single-particle approximations, and cannot incorporate electron correlation and quasidegeneracy effects to high order. The recently developed covariant evolution operator method of Lindgren [41] is free of these drawbacks, and opens new perspectives for deriving truly covariant many-body methods. As an example of such methods, we presented a double Fock-space CC method, which couples electronic and photonic degrees of freedom in rigorous manner. Less computationally demanding methods can be derived from this many-body QED theory. These approximations are expected to be similar to the NVPA and other, less expensive relativistic methods, which have proved to be of great value in the study of atomic and molecular systems, as shown in the present and other chapters of this book. Nevertheless, QED four-component benchmark calculations for carefully selected systems will be necessary to test and calibrate the less expensive and more widely applicable schemes, currently available or developed in the future.

ACKNOWLEDGMENTS

Many of the atomic results reported here were obtained in collaboration with Yasuyuki Ishikawa of the University of Puerto Rico. Molecular FSCC calculations has been done in collaboration with Lucas Visscher of the Free University in Amsterdam. The authors are grateful to Ingvar Lindgren and Trond Saue for many stimulating discussions. We had fruitful collaboration with Bernd Hess, Valeria Pershina, Pekka Pyykkö, Peter Schwerdtfeger, and with our past and present graduate students Arik Landau, Tal Koren, Nastya Borschevsky and Hani Yakobi; we thank all of them. Permission to use Figs. 7–10, taken from Lindgren's lecture [46], is gratefully acknowledged. Financial support has been provided by the Israel Science Foundation and the U.S.-Israel Binational Science Foundation.

REFERENCES

1. Helgaker, T., Jrgensen, P., Olsen, J.: Molecular Electronic Structure Theory. Wiley, Chichester (2000)
2. Lindgren, I., Morrison, J.: Atomic Many-Body Theory, 2nd edn. Springer, Berlin (1986)
3. Kragh, H.: Centaurus **26**, 154 (1982)
4. Kragh, H.: Am. J. Phys. **52**, 1024 (1984)
5. Sakurai, J.J.: Advanced Quantum Mechanics. Addison-Wesley, Reading, MA (1967)
6. Dirac, P.A.M.: Proc. Roy. Soc. London A **117**, 714 (1928)
7. Hess, B.A. (ed.): Relativistic Effects in Heavy-Element Chemistry and Physics. Wiley, Chichester (2002)
8. Schwerdtfeger, P. (ed.): Relativistic Electronic Structure Theory. Part 1. Fundamentals. Elsevier, Amsterdam (2002)
9. Schwerdtfeger, P. (ed.): Relativistic Electronic Structure Theory. Part 2. Applications. Elsevier, Amsterdam (2004)
10. Kaldor, U., Wilson, S. (eds.): Theoretical Chemistry and Physics of Heavy and Super-Heavy Elements. Kluwer, Amsterdam (2003)

11. Grant, I.P.: Relativistic quantum theory of atoms and molecules. Theory and computation. Springer, New York (2007)
12. Hirao, K., Ishikawa, Y. (eds): Recent Advances in Relativistic Molecular Theory. World Scientific Publishing, Singapore (2004)
13. Dyall, K.G., Faegri, K.: Introduction to Relativistic Quantum Chemistry. Oxford University Press, New York (2007)
14. Saue, T., Visscher, L.: in Theoretical Chemistry and Physics of Heavy and Superheavy Elements [10], p. 211 ff
15. Gell-Mann, M.: Nuovo Cimento Suppl. **4**, 848 (1956)
16. Kutzelnigg, K.: Chem. Phys. **225**, 203 (1997)
17. Desclaux, J.P.: in Relativistic Electronic Structure Theory. Part 1. Fundamentals, p. 1
18. Pyykkö, P.: Relativistic Theory of Atoms and Molecules, Volume I – A Bibliography 1916-1985. Springer, Berlin (1986)
19. Pyykkö, P.: Relativistic Theory of Atoms and Molecules, Volume II – A Bibliography 1986-1992. Springer, Berlin (1993)
20. Pyykkö, P.: Relativistic Theory of Atoms and Molecules, Volume III – A Bibliography 1993-2000. Springer, Berlin (2000)
21. Pyykkö, P.: Database RTAM (relativistic quantum chemistry database 1915–2007); Version 13.0 (October 5, 2007); http://rtam.csc.fi/
22. Schwinger, J.: Phys. Rev. **75**, 1912 (1949); Phys. Rev. **75**, 651 (1949)
23. Feynman, R.: Phys. Rev. **76**, 749 (1949); Phys. Rev. **76**, 769 (1949)
24. Tomonaga, S.: Phys. Rev. **74**, 224 (1948)
25. Dyson, F.: Phys. Rev. **75**, 486 (1949); Phys. Rev. **75**, 1736 (1949)
26. Craig, D.P., Thirunamachandran, T.: Molecular Quantum Electrodynamics. Dover, New York (1998)
27. Labzowsky, L.: The Theory of Atom. QED of Electronic Shells and Radiation Processes (in Russian), Nauka, Moscow (1996)
28. Wolf, A., Reiher, M., Hess, B.A.: Transgressing theory boundaries: The generalized Douglas-Kroll transformation, in Recent Advances in Relativistic Molecular Theory [12], pp. 137–190
29. Schwarzschild, K.: Gött. Nach. Math.-Phys. Kl. 26 (1903)
30. Saue, T.: in Relativistic Electronic Structure Theory. Part 1. Fundamentals [8], p. 332
31. Jackson, J.D., Okun, L.B.: Rev. Mod. Phys. **73**, 663 (2001)
32. Bloch, F.: In: F. Bopp (ed.) W. Heisenberg und die Physik unserer Zeit. Vieweg & Sohn, Braunschweig (1961)
33. Griffith, D.J.: Introduction to Electrodynamics, Prentice-Hall, Upper Saddle River, NJ (1999)
34. Cohen-Tannoudji, C.: Dupont-Roc, J., Grynberg, G.: Photons et atomes, Savoirs Actuels, New York (1987)
35. Heaviside, O.: Philos. Mag. Ser. 5 **27**, 324 (1889)
36. Darwin, C.G.: Phil. Mag. **39**, 537 (1920)
37. Born, M., Oppenheimer, J.R.: Ann. Phys. **84**, 457 (1927)
38. Weinberg, S.: The Quantum Theory of Fields, Volume I: Foundations. Cambridge University Press, Cambridge (1995)
39. Gupta, S.N.: Proc. Phys. Soc. (London) **A63**, 681 (1950)
40. Bleuler, K.: Helv. Phys. Acta **23**, 567 (1950)
41. Lindgren, I., Salomonson, S., sn., B.: Phys. Rep. **389**, 161 (2004)
42. Lindgren, I., Salomonson, S., Hedendahl., D.: Can. J. Phys. **83**, 183 (2005)
43. Lindgren, I., Salomonson, S., Hedendahl., D.: Phys. Rev. A **73**, 062502 (2006)
44. Lindgren, I., Salomonson, S., Hedendahl., D.: Int. J. Mod. Phys. E **16**, 1221 (2007)
45. Lindgren, I., Salomonson, and S., Hedendahl., D.: Int. J. Quantum Chem. **12**, 2272 (2008)

46. Lindgren, I.: http://fy.chalmers.se/∼f3ail/Publications/Corfu.pdf; http://fy.chalmers.se/∼f3ail/Publications/CorfuProc.pdf
47. Kaldor, U., Eliav, E., Landau, A.: In: E.J. Brandas, E.S. Kryachko (eds.) Fundamental World of Quantum Chemistry, Volume III. Kluwer (2004), p. 365
48. Dyson, F.J.: Phys. Rev. **91**, 1543 (1953)
49. Wick, G.C.: Phys. Rev. **96**, 1124 (1953)
50. Goldstein, J.S.: Phys. Rev. **91**, 1516 (1953)
51. Sazdjian, H.: J. Math. Phys. **28**, 2618 (1987)
52. Gross, F.: Phys. Rev. **186**, 1448 (1969); Phys. Rev. C **26**, 2203 (1982)
53. Todorov, I.T.: Phys. Rev. D **3**, 2351 (1971)
54. Caswell, W.E., Lepage, G.P.: Phys. Rev. A **18**, 810 (1978)
55. Connell, J.H.: Phys. Rev. D **43**, 1393 (1991)
56. Phillips, D.R., Wallace, S.J.: Phys. Rev. C **54**, 507 (1996)
57. Bijtebier, J.: Nucl. Phys. **696A**, 581 (2001)
58. Shabaev, S.M.: Phys. Rep. **356**, 119 (2002)
59. Chraplyvy, S.V.: Phys. Rev. **91**, 388 (1953); ibid. **92** 1310 (1953)
60. Barker, W.A., Glover, F.R.: Phys. Rev. **99**, 317 (1955)
61. Moss, R.E.: Advanced Molecular Quantum Mechanics. Chapmann and Hall, London (1973)
62. Itoh, T.: Rev. Mod. Phys. **37**, 159 (1965)
63. Sjovoll, M., Fagerli, H., Gropen, O., Almlöf, J., Saue, T., Olsen, J., Helgaker, T.: J. Chem. Phys. **107**, 5496 (1997)
64. Swirles, B.: Proc. Roy. Soc. (London) A **152**, 625 (1935)
65. Gaunt, J.A.: Proc. Roy. Soc. (London) A **122**, 513 (1929)
66. Saue, T.: Doctor of Philosophy Thesis, University of Oslo (1996)
67. Breit, G.: Phys. Rev. **34**, 553 (1929); Phys. Rev. **36**, 383 (1930); Phys. Rev. **39**, 616 (1932)
68. Gorceix, O., Indelicato, P.: Phys. Rev. A **37**, 1087 (1988)
69. Lindroth, E., Martensson-Pendrill, A.-M.: Phys. Rev. A **39**, 3794 (1989)
70. Sucher, J.: J. Phys. B **66**, L585 (1988)
71. Lindgren, I.: J. Phys. B **23**, 1085 (1990)
72. Grant, I.P.: Proc. R. Soc. London A **262**, 555 (1961)
73. Schwarz, W.H.E.,Wallmeier, H.: Mol. Phys. **46**, 1045 (1982)
74. Talman, J.D.: Phys. Rev. Lett. **57**, 1091 (1986)
75. LaJohn, L., Talman, J.D.: Chem. Phys. Lett. 195, **184** (1992)
76. Schwarz, W.H.E., Wechsel-Trakowski, E.: Chem. Phys. Lett. **85**, 94 (1984)
77. Brown, G.E., Ravenhall, D.G.: Proc. Roy. Soc. London A **208**, 552 (1951)
78. Kutzelnigg, W.: Phys. Scr. **36**, 416 (1987)
79. Lindgren, I.: In: U. Kaldor (ed.) Many-Body Methods in Quantum Chemistry, Lecture Notes in Chemistry, Volume 52, p. 293. Springer, Heidelberg (1989); Nucl. Instrum. Methods **B31**, 102 (1988)
80. Grant, I.P., Quiney, H.M.: Adv. At. Mol. Phys. **23**, 37 (1988)
81. Furry, W.H.: Phys. Rev. **81**, 115 (1951)
82. Mittleman, M.H.: Phys. Rev. A **24**, 1167 (1981)
83. Visscher, L.: in Relativistic Electronic Structure Theory. Part 1. Fundamentals [8], p. 291
84. Dyall, K.G.: J. Chem. Phys. **106**, 9618 (1997); J. Chem. Phys. **111**, 10000 (1999)
85. Filatov, M., Dyall, K.G.: Theor. Chem. Acc. **117**, 333 (2007)
86. Barysz, M., Sadlej, A.: J. Mol. Struct. (Theochem) **573**, 181(2001)
87. Wolf, A., Reiher, M., Hess, B.A.: J. Chem. Phys. **117**, 9215 (2002)
88. Kutzelnigg, W., Liu, W.: J. Chem. Phys. **123**, 241102 (2005)
89. Iliaš, M., Saue, T.: J. Chem. Phys. **126**, 064102 (2007)

90. Mohr, P.J., Plunien, G., Soff, G.: Phys. Rep. **293**, 227 (1998)
91. Varga,, S., Engel, E., Sepp, W.D., Fricke, B.: Phys. Rev. A **59**, 4288 (1999)
92. Liu, W.J., Hong, G.Y., Dai, D.D., Li, L.M., Dolg, M,: Theor. Chem. Acc. **96**, 75 (1997)
93. Yanai, T., Iikura, H., Nakajima, T., Ishikawa, Y. Hirao, K.: J. Chem. Phys. **115**, 8267 (2001)
94. Saue, T., Helgaker, T.: J. Comp. Chem. **23**, 814 (2002)
95. Matveev, A.V., Mayer, M., Rosch, N.: Chem. Phys. Chem. **160**, 91 (2004)
96. Belpassi, L., Tarantelli, F., Sgamellotti, A., Quiney, H.M.: Phys. Rev, **77**, 233403/1 (2008)
97. Grant, I.P.: Adv. Phys. **19**, 747 (1970); Grant, I.P., Quiney, H.M.: Adv. Atom. Molec. Phys. **23**, 37 (1988)
98. Dyall, K.G., Grant, I.P., Johnson, C.T., Parpia, F.A., Plummer, E.P.: Comput. Phys. Commun. **55**, 425 (1989)
99. Parpia, F.A., Froese-Fischer, C., Grant, I.P.: Comput. Phys. Commun. **94**, 249 (1996)
100. Fritzsche, S., Froese Fischer, C., Dong, C.Z.: Comp. Phys. Commun. **124**, 340 (2000)
101. Desclaux, J.P.: Comp. Phys. Commun. 9, 31 (1975)
102. Reiher, M., Hinze, J.: J Phys. B 32, 5489 (1999)
103. Vilkas, M.J., Koc, K., Ishikawa, Y.: Chem. Phys. Lett. **280**, 167 (1997); Vilkas, M.J., Ishikawa, Y., Koc, K.:Phys. Rev. E **58**, 5096 (1998); Vilkas, M.J., Ishikawa, Y., Koc, K.: Intern. J. Quantum Chem. **70**, 813 (1998)
104. Jensen, H.J.Aa., Dyall, K.G., Saue, T., Faegri, K.: jr., J. Chem. Phys. **104**, 4083 (1996)
105. Thyssen, J.: Doctor of Philosophy Thesis, University of Southern Denmark (2001)
106. Fleig, T., Jensen, H.J., Olsen, J., Visscher, L.: J. Chem. Phys. **124**, 104106/1 (2006)
107. Jauregui, R., Bunge, C.F., Ley-Koo, E.: Phys. Rev. A **55**, 1781 (1997)
108. Watanabe, Y., Tatewaki, H.: J. Chem. Phys. **123**, 074322/1 (2005)
109. Visscher, L., Saue, T., Nieuwpoort, W.C., Fgri, K., Gropen, O.: J. Chem. Phys. **99**, 6704 (1993)
110. Kato, M., Hado, M., Fukuda, R., Nakatsuji, N.: Chem. Phys. Lett. **408**, 150 (2005)
111. Chen, M.H., Cheng, K.T., Johnson, W.R.: Phys. Rev. A **47**, 3692 (1993);
112. Johnson, W.R., Sapirstein, J., Phys. Rev. Lett. **57**, 1126 (1986); Johnson, W.R., Idrees, M., Sapirstein, J.: Phys. Rev. A **35**, 3218 (1987); Blundell, S.A., Johnson, W.R., Liu, Z.W., Sapirstein, J., Phys. Rev. A **39**, 3768 (1989); Johnson, W.R., Blundell, S.A., Sapirstein, J.: Phys. Rev. A **37**, 307 (1988); Phys. Rev. A **37**, 2764 (1988); Phys. Rev. A **41**, 1689 (1990)
113. Vilkas, M.J., Ishikawa, Y., Koc, K.: Phys. Rev. A **60**, 2808 (1999); Ishikawa, Y., Vilkas, M.J., Koc, K.: Intern. J. Quantum Chem. **77**, 433 (2000)
114. Dzuba, V.A., Flambaum, V.V., Sushkov, O.P.: J.Phys. B, **16**, 715(1983); Dzuba, V.A., Flambaum, V.V., Kozlov, M.G.: JETP Letteres **63**, 882 (1996); Dzuba, V.A., Flambaum, V.V., Kozlov, M.G.: Phys. Rev. A **54**, 3948 (1996)
115. K.G. Dyall, Chem. Phys. Lett. **224**, 186 (1994)
116. Laerdahl, J.K., Saue, T., Faegri, K.: Theor. Chem. Acc. **97**, 177 (1997)
117. Salomonson, S., Lindgren, I., Mrtensson, A.-M.: Phys. Scr. **21**, 351 (1980)
118. S.A. Blundell, W.R. Johnson, Z.W. Liu, and J. Sapirstein, Phys. Rev. A **39**, 3768 (1989); Phys. Rev. A **40**, 2233 (1989); Blundell, S.A., Johnson, W.R., Sapirstein, J., Phys. Rev. Lett. **65**, 1411 (1990); Phys. Rev. A **43**, 3407 (1991)
119. Liu, Z.W., Kelly, H.P.: Phys. Rev. A **43**, 3305 (1991)
120. Salomonson , S., ster, P.: Phys. Rev. A **40**, 5548 (1989)
121. Eliav, E., Kaldor, U., Ishikawa, Y.: Phys. Rev. A **49**, 1724 (1994)
122. Kaldor, U., Eliav, E.: Adv. Quantum Chem. **31**, 313 (1998)
123. Das, B.P., Latha, K.V.P., Sahoo, B.K., Sur, C., Chaudhuri, R.K., Mukherjee, D.: J. Theor. Comp. Chem. **1**, 1 (2005)
124. Eliav, E., Kaldor, U.: Chem. Phys. Lett. **248**, 405 (1996)
125. Visscher, L., Lee, T.J., Dyall, K.G.: J. Chem. Phys. **105**, 8769 (1996)

126. Visscher, L., Eliav, E., Kaldor, U.: J. Chem. Phys. **115**, 759 (2001)
127. Eliav, E., Kaldor, U., He, B.A.: J. Chem. Phys. **108**, 3409 (1998)
128. Infante, I., Gomes, A.S.P., Visscher, L.: J. Chem. Phys. **125**, 074301 (2006)
129. Infante, I., Eliav, E., Visscher, L., Kaldor, U.: J. Chem. Phys. **127**, 124308 (2007)
130. Fleig, T., Sorensen, L.K., Olsen, J.: Theo. Chem. Acc. **118**, 347 (2007)
131. MCDFGME, a MultiConfiguration Dirac Fock and General Matrix Elements program, release 2005, written by J.P. Desclaux and P. Indelicato (http://dirac.spectro.jussieu.fr/mcdf)
132. Aerts, P.J.C., Visser, O., Visscher, L., Merenga, H., de Jong, W.A., Nieuwpoort, W.C.: MOLFDIR, University of Groningen, The Netherlands; Visscher, L., Lee, T.J., Dyall, K.G.: RELCCSD, NASA Ames Research Center, Moffett Field, CA
133. DIRAC, a relativistic ab initio electronic structure program, Release DIRAC04.0 (2004), written by H.J. Aa. Jensen, T. Saue, and L. Visscher with contributions from V. Bakken, E. Eliav, T. Enevoldsen, T. Fleig, O. Fossgaard, T. Helgaker, J. Laerdahl, C.V. Larsen, P. Norman, J. Olsen, M. Pernpointner, J.K. Pedersen, K. Ruud, P. Salek, J.N.P. van Stralen, J. Thyssen, O. Visser, and T. Winther. (http://dirac.chem.sdu.dk)
134. T. Yanai, H. Nakano, T. Nakajima, T. Tsuneda, S. Hirata, Y. Kawashima, Y. Nakao, M. Kamiya, H. Sekino, and K. Hirao: UTChem – A Program for Ab Initio Quantum Chemistry, in Lecture Notes in Computer Science, **2660**, 712 (2003)
135. DREAMS is a Dirac-based relativistic electronic atomic and molecular structure program suite consisting of a version of MOLECULE a vectorized integral program developed by J. Almlöf, P.R. Taylor, adapted by P.R. Taylor, K. Fægri Jr. and a Dirac–Hartree–Fock and MP2 program developed by K.G. Dyall
136. Quiney, H.M., Scaane, H., Grant, I.P., Adv. Quant. Chem. **32**, 1 (1999)
137. Matsuoka, O., Watanabe, Y.: in Recent Advances in Relativistic Molecular Theory [12], p. 247
138. Rodrigues, G.C., Ourdane, M.A., Bieroń, J., Indelicato, P., Lindroth, E.: Phys. Rev. A **63**, 012510 (2000)
139. Sapirstein, J.: Rev. Mod. Phys. **70**, 55 (1998)
140. Coester, F.: Nucl. Phys. **7**, 421 (1958); Coester, F., Kmmel, H.: Nucl. Phys. **17**, 477 (1960)
141. Čižek, J.: Adv. Chem. Phys. **14**, 35 (1969)
142. Bartlett, R.J.: Theor. Chim. Acta **80**, 71 (1991)
143. Pal, S., Mukherjee, D.: Adv. Quantum Chem. **20**, 292 (1989)
144. Kaldor, U.: Theor. Chim. Acta **80**, 427 (1991)
145. Davydov, A.S.: Quantum Mechanics. NEO Press, Peaks Island, Maine (1966) Chap. VIII
146. Kim, Y.K.: Phys. Rev. **154**, 17 (1967)
147. Kagawa, T.: Phys. Rev. A **12**, 2245 (1975); Phys. Rev. A **22**, 2340 (1980)
148. Quiney, H.M., Grant, I.P., Wilson, S.: J. Phys. B **20**, 1413 (1987); Phys. Scr. **36**, 460 (1987); In: U. Kaldor (ed.) Many-Body Methods in Quantum Chemistry, Lecture Notes in Chemistry, Volume 52. Springer, Heidelberg, 1989; J. Phys. B **23**, L271 (1990); I.P. Grant and H.M. Quiney, Adv. Atom. Molec. Phys. **23**, 37 (1988)
149. Ishikawa, Y., Binning, R.C., Sekino, H.: Chem. Phys. Lett. **160**, 206 (1989); Ishikawa, Y.: Phys. Rev. A **42**, 1142 (1990); Chem. Phys. Lett. **166**, 321 (1990); Ishikawa, Y., Quiney, H.M.: Phys. Rev. A **47**, 1732 (1993); Ishikawa, Y., Koc, K.: Phys. Rev. A **50**, 4733 (1994)
150. Johnson, W.R., Soff, G., At. Data Nucl. Data Tables **33**, 405 (1985)
151. Visscher, L., Dyall, K.G.: At. Data Nucl. Data Tables **67**, 207 (1997)
152. Desclaux, J.-P.: Comput. Phys. Commun. **9**, 31 (1975)
153. Grant, I.P., McKenzie, B.J., Norrington, P.H., Mayers, D.F., Pyper, N.C.: Comput. Phys. Commun. **21**, 207 (1980)
154. Ishikawa, Y., Kaldor, U.: In: J. Leszczynski (ed.) Computational Chemistry: Review of Current Trends, Volume I, p. 1. World Scientific, Singapore (1996)

155. Kaldor, U., Eliav, E.: Adv. Quantum Chem. **31**, 313 (1998)
156. Lee, Y.S., McLean, A.D., J. Chem. Phys. **76**, 735 (1982)
157. Aerts, P.J.C., Nieuwpoort, W.C.: Chem. Phys. Lett. **113**, 165 (1985); ibid. **125**, 83 (1986)
158. Stanton, R.E., Havriliak, S.: J. Chem. Phys. **81**, 1910 (1984)
159. Ishikawa, Y., Baretty, R., Binning, R.C.: Intern. J. Quantum Chem. Symp. **19**, 285 (1985); Ishikawa, Y., Sekino, H.: Chem. Phys. Lett. **165**, 243 (1990)
160. Ishikawa, Y., Binning, R.C., Sando, K.M.: Chem. Phys. Lett. **101**, 111 (1983); Chem. Phys. Lett. **105**, 189 (1984); Chem. Phys. Lett. **117**, 444 (1985); Ishikawa, Y., Baretty, R., Binning, R.C.: Chem. Phys. Lett. **121**, 130 (1985); Ishikawa, Y., Quiney, H.M: Intern. J. Quantum Chem. Symp. **21**, 523 (1987)
161. Sucher, J., Phys. Scr. **36**, 271 (1987)
162. Hughes, S.R., Kaldor, U.: Chem. Phys. Lett. **194**, 99 (1992); ibid. **204**, 339 (1993); Phys. Rev. A **47**, 4705 (1993); J. Chem. Phys. **99**, 6773 (1993); Intern. J. Quantum Chem. **55**, 127 (1995)
163. Landau, A., Eliav, E., Kaldor, U.:Chem. Phys. Lett. **313**, 399 (1999); Landau, A., Eliav, E., Kaldor, U.: Adv. Quantum Chem. **39**, 172 (2001)
164. Malrieu, J.P., Durand, Ph., Daudey, J.P.: J. Phys. A **18**, 809 (1985)
165. Eliav, E., Vilkas, M.J., Ishikawa, Y., Kaldor, U.: J. Chem. Phys. **122**, 224113 (2005)
166. Eliav, E., Vilkas, M.J., Ishikawa, Y., Kaldor, U.: Chem. Phys. **311**, 163 (2005)
167. Mukhopadhyay, D., Datta, B., Mukherjee, D.: Chem. Phys. Lett. **197**, 236 (1992)
168. Eliav, E., Borschevsky, A., Shamasundar, R.K., Pal, S., Kaldor, U.: Int. J. Quantum Chem. **109**, 2909 (2009)
169. Jeziorsky, B., Monkhorst, H.J.: Phys. Rev. A **24**, 1668 (1981)
170. Landau, A., Eliav, E., Ishikawa, Y., U. Kaldor, U.: J. Chem. Phys. **121**, 6634 (2004)
171. Eliav, E., Borschevsky, A., Yakobi, H., Kaldor, U.: Unpublished.
172. Landau, A., Eliav, E., Ishikawa, Y., Kaldor, U., J. Chem. Phys. **115**, 2389 (2001)
173. Hotop, H., Lineberger, W.C.: J. Phys. Chem. Ref. Data **4**, 539 (1975); J. Phys. Chem. Ref. Data **14**, 731 (1985)
174. Eliav, E., Kaldor, U., Ishikawa, Y.: Phys. Rev. A **53**, 3050 (1996)
175. Landau, A., Eliav, E., Ishikawa, Y., Kaldor, U.: J. Chem. Phys. **113**, 9905 (2000)
176. Landau, A., Eliav, E., Ishikawa, Y., Kaldor, U.: J. Chem. Phys. **115**, 6862 (2001)
177. Eliav, E.: Kaldor, U.: Ishikawa, Y.: Phys. Rev. A **50**, 1121 (1994)
178. Mrtensson-Pendrill, A.M.: In: S. Wilson (ed.) Methods in Computational Chemistry, Volume 5, p. 99. Plenum, New York (1992)
179. Johnson, W.R., Liu, Z.W., Sapirstein, J.: At. Data Nucl. Data Tables **64**, 279 (1996)
180. Blundell, S.A., Johnson, W.R., Sapirstein, Z.: Phys. Rev. D **45**, 1602 (1992)
181. Pyykkö, P.: Chem. Rev. **88**, 563 (1988)
182. Hay, P.J., Wadt, W.R., Kahn, L.R., Bobrowicz, F.W.: J. Chem. Phys. **69**, 984 (1978)
183. Pizlo, A., Jansen, G., Hess, B.A.: J. Chem. Phys. **98**, 3945 (1993)
184. Moore, C.E.: Atomic Energy Levels, Natl. Bur. of Stand. (U.S.) Circ. No. 467. U.S. GPO, Washington, DC (1948)
185. Martin, W.C., Zalubas, R., L. Hagan, L.: Atomic Energy Levels – The Rare-Earth Elements, Natl. Bur. Stand. Ref. Data Series, NBS Circ. No. 60. U.S. GPO, Washington, DC (1978)
186. Cai, Z., Meiser Umar, V., Froese Fischer, C.: Phys. Rev. Lett. **68**, 297 (1992)
187. Eliav, E., Kaldor, U., Ishikawa, Y.: Phys. Rev. A **51**, 225 (1995)
188. Hess, B.A., Marian, C.M., Peyerimhoff, S.D.: In: D.R. Yarkony (ed.) Modern Electronic Structure Theory, p. 152. World Scientific, Singapore (1995)
189. Bahrim, C., Thumm, U.: Phys. Rev. A **61**, 022722 (2000)
190. Fabrikant, I.I.: Opt. Spektrosk. **53** 223 (1982); Opt. Spectrosc. (USSR) **53** (1982) 131
191. Froese Fischer, C., Chen, D.: J. Mol. Struct. **199**, 61 (1989)

192. Greene, C.H.: Phys. Rev. A **42**, 1405 (1990)
193. Scheer, M., Thøgersen, J., Bilodeau, R.C., Brodie, C.A., Haugen, H.K., Andersen, H.H., Kristensen, P., Andersen, T.: Phys. Rev. Lett. **80**, 684 (1998)
194. Scheer, M., Bilodeau, R.C., Haugen, H.K.: Phys. Rev. Lett. **80**, 2562 (1998)
195. Scheer, M., Bilodeau, R.C., Thøgersen, J., Haugen, H.K.: Phys. Rev. A **57**, R1493 (1998)
196. W.W. Williams, D.L. Carpenter, A.M. Covington, M.C. Koepnick, D. Calabrese, and J.S. Thompson, J. Phys. B **31**, L341 (1998)
197. Williams, W.W., Carpenter, D.L., Covington, A.M., Thompson, J.S., Kvale, T.J., Seely, D.G.: Phys. Rev. A **58**, 3582 (1998)
198. Carpenter, D.L., Covington, A.M., Thompson, J.S.: Phys. Rev. A, **61**, 042501 (2000)
199. Arnau, F., Mota, F., Novoa, J.J.: Chem. Phys. **166**, 77 (1992)
200. Eliav, E., Kaldor, U., Ishikawa, Y., Seth, M., Pyykk, P.: Phys. Rev. A **53**, 3926 (1996)
201. Wijesundera, W.P.: Phys. Rev. A **55**, 1785 (1997)
202. Eliav, E., Ishikawa, Y., Pyykkö, P., Kaldor, U.: Phys. Rev. A **56**, 4532 (1997)
203. Malli, G.L., Da Silva, A.B.F., Ishikawa, Y.: Phys. Rev. A, **47**, 143 (1993)
204. D. Sundholm, D., Tokman, M., Pyykkö, P., Eliav, E., Kaldor, U.: J. Phys. B **32**, 5853 (1999)
205. Kunik, D., Kaldor, U.: J. Chem. Phys. **55**, 4127 (1971); Monkhorst, H.J.: Int. J. Quantum Chem. **11**, 421 (1977)
206. Huzinaga, S., Klobukowski, M.: Chem. Phys. Lett. **212**, 260 (1993)
207. Yakobi, H., Eliav, E., Visscher, L., Kaldor, U.: J. Chem. Phys. **120**, 054301 (2007)
208. Davis, L., Feld, B.T., Zabel, C.W., Zacharias, J.R., Phys. Rev. **76**, 1076 (1949); Jaccarino, V., King, J.G.: Phys. Rev. **83**, 471 (1951)
209. King, J.G., Jaccarino, V.: Phys. Rev. **94**, 1610 (1954)
210. Jaccarino, V., King, J.G., Satten R.A., Stroke, H.H.: Phys. Rev. **94**, 1798 (1954)
211. Pyykkö, P.: Mol. Phys. **99**, 1617 (2001)
212. van Stralen, J.N.P., Visscher, L.: Mol. Phys. **101**, 2115 (2003)
213. Sundholm, D., Olsen, J.: Phys. Rev. Lett. **68**, 927 (1992)
214. Evans, C.J., Lesarri, A., Gerry, M.C.L.: J. Am. Chem. Soc. **122**, 6100 (2000)
215. Schwerdtfeger, P., Bast, R., Gerry, M.C.L., Jacob, C.R., Jansen, M., Kellö, V., Mudring, A.V., Sadlej, A.J., Söhnel, T., Wagner, F.E.: J. Chem. Phys. **122**, 124317 (2005)
216. Belpassi, L., Tarantelli, F., Sgamelloti, A., Quiney, H.M., van Stralen, J.N.P., Visscher, L.: J. Chem. Phys. **126**, 064314 (2007)
217. Yakobi, H., Eliav, E., Kaldor, U.: J. Chem. Phys. **126**, 184305 (2007)
218. Childs, W.G.: Goodman, L.S.: Phys. Rev. **141**, 176 (1966); Blachman, A.G., Landman, D.A., Lurio, A: ibid. **161**, 60 (1967)
219. Pershina, V., Hoffman, D.C.: Theoretical Chemistry and Physics of Heavy and Superheavy Elements, p. 55. Kluwer, Dordrecht (2003)
220. Schädel M. (ed.): The Chemistry of Superheavy Elements. Kluwer, Dordrecht (2003)
221. Eliav, E., Kaldor, U., Schwerdtfeger, P., Hess, B.A., Ishikawa, Y.: Phys. Rev. Lett. **73**, 3203 (1994)
222. Eliav, E., Kaldor, U., Y. Ishikawa, Y.: Phys. Rev. A **52**, 2765 (1995)
223. Keller, O.L.: Radiochim. Acta **37**, 169 (1984). See also Mann, J.B., quoted by Fricke B., Waber, J.T.: Actinides Rev. **1**, 433 (1971)
224. Glebov, V.A., Kasztura, L., Nefedov, V.S., Zhuikov, B.L.: Radiochim. Acta **46**, 117 (1989)
225. Johnson, E., Fricke, B., Keller, O.L., Nestor, C.W., Tucker, T.C.: J. Chem. Phys. **93**, 8041 (1990)
226. Desclaux, J.P., Fricke, B.: J. Phys. **41**, 943 (1980)
227. Eliav, E., Kaldor, U., Ishikawa, Y.: Phys. Rev. Lett. **74**, 1079 (1995)
228. Schädel, M.: Radiochim. Acta **70/71**, 207 (1995)
229. Hofmann S. et al.: Z. Phys. A **350**, 277 (1995)
230. Hofmann S. et al.: Z. Phys. A **350**, 281 (1995)

231. Hofmann, S. et al.: Z. Phys. A **354**, 229 (1996)
232. For a recent review see Hofmann, S.: Rep. Progr. Phys. **61**, 639 (1998)
233. Oganessian, Yu.Ts. et al.: Phys. Rev. Lett. **83**, 3154 (1999)
234. Oganessian, Yu.Ts. et al.: Phys. Rev. C **63**, 011301(R) (2000)
235. Oganessian, Yu.Ts.: Nucl. Phys. A **685**, 17c (2000)
236. Sobiczewski, A.: Phys. Part. Nuclei **25**, 295 (1994); Möller, P., Nix, J.R.: J. Phys. G **20**, 1681 (1994); Smolanczuk, R., Skalski, J., Sobiczewski, A.: Phys. Rev. C **52**, 1871 (1995)
237. Rutz, K., Bender, M., Bürvenich, T., Schilling, T., Reinhard, P.G., Maruhn, J.A., Greiner, W.: Phys. Rev. C **56**, 238 (1997)
238. Ćwiok, S., Dobaczewski, J., Heenen, P.H., Magierski, P., Nazarewicz, W.: Nucl. Phys. A **611**, 211 (1996)
239. Landau, A., Eliav, E., Ishikawa, Y., Kaldor, U.: J. Chem. Phys. **114**, 2977 (2001)
240. Seth, M., Fgri, K., Schwerdtfeger, P.: Angew. Chem. Intern. Ed. **37**, 2493 (1998)
241. Lide, D.R. (ed.): Handbook of Chemistry and Physics, 74th edn. CRC Press, Boca Raton, FL (1993)
242. Sewtz, M., Backe, H., Dretzke, A., Kube, G., Lauth, W., Schwamb, P., Eberhardt, K., Grüning, C., Thörle, P., Trautmann, N., Kunz, P., Lassen, J., Passler, G., Dong, C.Z., Fritzsche, S., Haire, R.G.: Phys. Rev. Lett. **90**, 163002 (2003)
243. Backe, H. et al.: Eur. Phys. J D **45**, 99 (2007)
244. Borschevsky, A., Eliav, E., Vilkas, M.J., Ishikawa, Y., Kaldor, U.: Phys. Rev. A **75**, 042514 (2007)
245. Borschevsky, A., Eliav, E., Vilkas, M.J., Ishikawa, Y., Kaldor, U.: Eur. Phys. J D **45**, 115 (2007)
246. Sugar, J.: J. Chem. Phys. **60**, 4103 (1974)
247. Eliav, E., Kaldor, U., Ishikawa, Y., Pyykkö, P., Phys. Rev. Lett. **77**, 5350 (1996)
248. Pyykkö, P., Tokman, M., Labzowsky, L.: Phys. Rev. A **57**, R689 (1998); Labzowsky, L., Goidenko, I., Tokman, M., Pyykkö, P.: Phys. Rev. A **59**, 2707 (1999)
249. Goidenko, I., Labzowsky, L., Eliav, E., Kaldor, U., Pyykk, P.: Phys. Rev. A **67**, 020101(R) (2003)
250. Oganessian, Yu. Ts. et al.: Phys. Rev. C **74**, 044602 (2006)
251. Oganessian, Yu. Ts.: J. Phys. G: Nucl. Part. Phys. **34**, R165 (2007)
252. Eichler, R. et al.: Nature **447**, 72 (2007)
253. Pershina, V., Borschevsky, A., Eliav, E., Kaldor, U.: J. Chem. Phys. **128**, 024707 (2008)
254. Pershina, V., Borschevsky, A., Eliav, E., Kaldor, U.: J. Phys. Chem. **112**, 13712 (2008)
255. Pershina, V., Borschevsky, A., Eliav, E., Kaldor, U.: J. Chem. Phys. **119**, 144106 (2008)
256. Goebel, D., Hohm, U.: J. Phys. Chem. **100**, 7710 (1996)
257. Wick, G.C.: Phys. Rev. **80**, 268 (1950)
258. Salpeter, E.E., Bethe, H.A.: Phys. Rev. **84**, 1232 (1951)
259. Eliav, E.: unpublished
260. Eliav, E., Shmuliyan, S., Kaldor, U., Ishikawa, Y.: J. Chem. Phys. **109**, 3954 (1998)

CHAPTER 8

THE EFFECTS OF RELATIVITY IN MATERIALS SCIENCE: CORE ELECTRON SPECTRA

R. BROER

Theoretical Chemistry, Zernike Institute for Advanced Materials, University of Groningen, Nijenborgh 4, 9747AG Groningen, The Netherlands
e-mail: r.broer@rug.nl

Abstract: Core electron spectroscopies like X-ray photo-electron spectroscopy, X-ray absorption spectroscopy and electron energy loss spectroscopy are powerful tools to investigate the electronic structure of transition metal, lanthanide and rare earth materials. On the other hand, the interpretation of the spectra is often not straightforward. Relativistic effects and in particular spin-orbit interactions, electron-electron interaction in the valence shell and between core and valence electrons, solid state effects may all play a role in the core electron spectra. Dynamical and non-dynamical electron correlation effects may also be non-negligible. The spectra can be interpreted and predicted using first principles computational methods that take into account both relativity and electron correlation. Furthermore, such approaches enable the interpretation of the complex processes in terms of physical mechanisms. This chapter discusses the effects of relativity on the core spectra of transition metal, lanthanide and actinide materials and a number of much used computational approaches to describe and interpret the spectra.

Keywords: X-ray photo-electron spectra, X-ray absorption spectra, Electron energy loss spectra, Ab initio relativistic quantum chemical methods, Spin-orbit effects, Branching ratios

8.1. INTRODUCTION

In many cases the consequences of relativity in materials manifest themselves clearly in the electronic, magnetic and optical and properties. In this chapter we focus on the interpretation of relativistic effects on spectroscopic properties, in particular on core and deep valence excitation and ionization spectra of transition metal, lanthanide and actinide materials. For excitation from p, d,... shells spin-orbit angular momentum coupling is a prominent relativistic effect. Core spectroscopies like X-ray Photo-electron Spectroscopy (XPS), X-ray absorption spectroscopy (XAS) and Electron Energy Loss Spectroscopy (EELS) can nowadays in many cases give very accurate information on the electronic structure of matter. On the other hand, the interpretation of the spectra is often rather complicated, especially in materials

M. Barysz and Y. Ishikawa (eds.), *Relativistic Methods for Chemists*,
Challenges and Advances in Computational Chemistry and Physics 10,
DOI 10.1007/978-1-4020-9975-5_8,

that contain open shell ions. For example, the relative intensities of spin-orbit split peaks in electron energy-loss spectroscopy and near edge X-ray absorption spectroscopy can only in special cases be roughly deduced from the statistical weights of the core levels. In most cases the angular momentum couplings of the open shell valence electrons, the external crystal field and covalent effects strongly affect these ratios [1–3]. A quantitative estimate of these effects on the branching ratios cannot be found without the aid of computational results.

The shifts of core electron binding energies as observed in X-ray photo-electron spectra (XPS) of an ion in a particular chemical environment with respect to a chosen reference can also provide detailed information about the ground state electronic structure of the materials. Especially in the case of XPS the effects of charge transfer (CT) present a complication for the interpretation of the spectra. The creation of a hole in one of the core orbitals of an atom lowers the excitation energy of so-called charge transfer states, in which an electron is transferred from the neighboring atoms to the core-ionized atom. Hence, the hole may become screened through CT, depending on the electron affinity of the ionized atom.

It is clear that a definite interpretation of X-ray spectra is often not possible without the aid of computational results. Semi-empirical methods using effective integrals and Hamilton matrix elements have been quite successful in reproducing experimental spectra, see for example the reviews [4,5] and references therein. However, semi-empirical approaches cannot be used for an independent prediction of the excitation spectra, because essential parameters are adjusted to fit experimental data. Standard density functional theory (DFT) has the problem that it is a ground state theory. Time-dependent DFT is only recently being explored as a possible tool for the analysis of spin-orbit-split core excitations [6] in materials. The availability of *ab initio* methods that are able to include relativistic as well as atomic and solid-state many-electron effects from the outset is therefore of great importance.

In recent years *first principles* four-component methods based on solving the Dirac-Fock configuration interaction (CI) equations and applied to embedded clusters of adequate size have been shown to be well suited for the study of core electron spectra [3, 7, 8]. The four-component CI methods allows for a balanced treatment of relativistic and electron correlation effects. Traditionally the severe computational demands have formed an important drawback for using these four-components methods, but with the increased availability of massive compute power and the increased efficiency of the program packages built for these methods [9], Dirac-Fock-CI studies for clusters of moderate size have come within reach.

A more economic approach is to start with non-relativistic orbitals and wavefunctions [10–12] and add scalar relativistic corrections (the mass-velocity and Darwin terms) by modifying the one-electron Hamiltonian before [12] or after [10, 11] orbital optimization, while spin-orbit effects are included in a second step via a spin-orbit-coupling CI treatment. These approximate approaches to include relativistic effects have the important practical advantage that standard quantum chemical program packages can be used. A disadvantage is that the orbitals are determined without taking the spin-orbit effects into account.

The need for accurate computational investigations to complement experimental studies can be further illustrated by two examples, both concerning XPS data. The spectra for metallic Zn show that the Zn 2s and 2p binding energies are quite similar to those in ZnO, although Zn is in its oxidation state zero in the metal and two in ZnO. The experimental $2p_{3/2}$ binding energy values are close to 1,021.8 eV for both compounds [13, 14]. With the aid of quantum chemical *ab initio* cluster calculations Rössler *et al*. [10, 11] were able to find an explanation: although the initial state effects, which represent the chemical bonding situation of the Zn atoms (ions) before ionization, and the final state effects, which account for relaxation and screening effects after ionization, are quite different in metal and oxide, they accidentally add up to practically identical binding energy shifts with respect to a free Zn atom [10, 11]. The second example concerns the 3s XPS of NiO and MnO: both spectra show a secondary peak at about 6 eV higher binding energy than the main peak and it is tempting to assume that the secondary peaks are of common origin. First principles many-electron studies of embedded clusters revealed however that in the case of NiO both peaks are associated with high spin final states, which both have considerable CT character, while in the case of MnO the contribution of CT effects is much smaller and the secondary peak corresponds to a lower spin final state [15,16].

The importance of many-electron theories for electronic transition processes in materials science is also emphasized in a recent review by Adachi and Ogasawara [17]. A discussion using *ab initio* Green's function results for the XPS of several levels of atoms from calcium to uranium, with the emphasis on the effects of Coster-Kronig processes, can be found in a review paper by Ohno [18]. Moore, Van der Laan and co-workers [19–21] combined relativistic atomic many-electron calculations [22], theoretical spin-orbit sum rules derived by Thole and Van der Laan [1, 2] with branching ratios observed in XAS and EELS to obtain valence spin-orbit interactions in transition metal, lanthanide and actinide materials. An extended review of this approach, with applications to actinides, is given in [21].

In atomic systems there are two standard ways to interpret relativistic angular momentum couplings, Russell-Saunders coupling and j-j coupling. If the spin-orbit coupling is weak compared to the electron-electron interactions, the Russell-Saunders scheme is used, in which first the orbital momenta l of the individual electrons are coupled to a total angular momentum L and the spin momenta s of the individual electron are coupled to a total spin S. Then L and S are coupled to a total angular momentum J. The j-j coupling scheme is used in cases where the spin-orbit coupling is strong compared to the electron-electron interactions. Here the angular momentum l and the spin s of each electron are coupled to give an individual angular momentum for each electron. The individual j for each electron are then coupled to give a total angular momentum J. Relativistic many-electron calculations are able to treat the entire range of angular momentum couplings, from negligible spin-orbit coupling to dominant spin-orbit coupling. The results, often said to be obtained in "intermediate coupling" [20] can be expressed in terms of Russell-Saunders states or in j-j coupled states, whatever representation gives better insight [4, 7]. When the core spin-orbit coupling is large, but the valence spin-orbit coupling is small, it may be useful to use a mixed coupling scheme, in which an open core shell is j-j

coupled and the open valence shell is Russell-Saunders coupled. Examples of all three schemes, Russell-Saunders, j-j and mixed coupling, appear in Section 8.3 and 8.4, where we discuss a few representative examples of core ionization spectra and core excitation spectra. Section 8.2 gives a concise description of four-component computational methods that enable accurate treatment of the relativistic effects in initial and final states of core electron spectra.

8.2. COMPUTATIONAL METHODS

The preferred material model for the prediction and interpretation of core excitation spectra in crystalline materials is the embedded cluster model. In the embedded cluster approximation a small part of the crystal is represented by atoms at lattice positions. This cluster is embedded in an effective potential accounting for the rest of the crystal. Since the cluster model enables the use of many-electron quantum chemical methods, it allows for an accurate account of the local electronic response, i.e. of the differential electron correlation and relaxation effects that accompany the excitation and ionization processes. The most straightforward way to treat relativistic effects is to use a four-component relativistic many-electron method. The four-component Dirac-Fock-CI method has the advantage that it can treat relativistic effects, electron correlation effects and relaxation effects from the outset and on the same footing. The method is used in various examples given in the next two sections. We start therefore with a very brief review of this method, following Visscher, Visser and co-workers [23, 24].

The one-electron Dirac equation describes the motion of an electron in an electromagnetic field in accordance with the theory of special relativity as well as the theory of quantum mechanics. The time-independent version of this equation reads

$$(c\boldsymbol{\alpha} \cdot \boldsymbol{p} + \beta mc^2)\psi = \varepsilon\psi \tag{8-1}$$

The α and β matrices are 4×4 matrices given by

$$\alpha_x = \begin{pmatrix} 0_2 & \sigma_x \\ \sigma_x & 0_2 \end{pmatrix}, \alpha_y = \begin{pmatrix} 0_2 & \sigma_y \\ \sigma_y & 0_2 \end{pmatrix}, \alpha_z = \begin{pmatrix} 0_2 & \sigma_z \\ \sigma_z & 0_2 \end{pmatrix}, \beta = \begin{pmatrix} I_2 & 0_2 \\ 0_2 & -I_2 \end{pmatrix} \tag{8-2}$$

The σ's are 2×2 Pauli matrices, I_2 and O_2 are $\times 2$ identity and null matrices. The spectrum of the four-component free electron Dirac Eq. (8-1) is unbounded from above, as well as from below, so there is no state of lowest energy. Solutions occur with eigenvalues above mc^2 (the electron solutions) as well as with eigenvalues below $-mc^2$ (the positron solutions). The existence of the negative eigenvalue solutions gives rise to conceptual difficulties, but fortunately the problems connected with the negative eigenvalue solutions are in practice not very prominent [23, 24]. The Dirac equation is often written as a two-component equation for two-component spinors (single particle functions),

$$\begin{pmatrix} mc^2 I_2 & c\sigma.\boldsymbol{p} \\ c\sigma.\boldsymbol{p} & -mc^2 I_2 \end{pmatrix} \begin{pmatrix} \psi^L \\ \psi^S \end{pmatrix} = \varepsilon \begin{pmatrix} \psi^L \\ \psi^S \end{pmatrix}. \tag{8-3}$$

This equation clearly shows the different character of the electron and positron solutions. It can be shown that for the positive energy solutions the two-component spinor ψ^L has an amplitude of order c larger than the two-component spinor ψ^S [23, 24]. In the Born-Oppenheimer approximation, the Dirac equation for an electron in the static field ϕ due to nuclei is then

$$\begin{pmatrix} (mc^2 - e\phi) I_2 & c\sigma.\boldsymbol{p} \\ c\sigma.\boldsymbol{p} & (-mc^2 - e\phi) I_2 \end{pmatrix} \begin{pmatrix} \psi^L \\ \psi^S \end{pmatrix} = \varepsilon \begin{pmatrix} \psi^L \\ \psi^S \end{pmatrix}. \tag{8-4}$$

The positive potential due to the nuclei leads to bound electron states. Finally we shift all energies in this one-particle Dirac equation by $-mc^2$ to ease comparison of the electron eigenvalues with the values found in nonrelativistic theory [23, 24] giving:

$$\begin{pmatrix} -e\phi I_2 & c\sigma.\boldsymbol{p} \\ c\sigma.\boldsymbol{p} & (-2mc^2 - e\phi) I_2 \end{pmatrix} \begin{pmatrix} \psi^L \\ \psi^S \end{pmatrix} = \varepsilon \begin{pmatrix} \psi^L \\ \psi^S \end{pmatrix} \tag{8-5}$$

The above equations are valid for one particle, so the next step is to find a many-particle equation that can be used for many-electron systems. This means that we have to define an appropriate electron-electron interaction operator. The Coulomb operator by it self has the problem that it is not invariant under Lorentz operations. Therefore approximate invariance corrections, like the Breit term [25] or the Gaunt term [26] are often added. We can then formulate a many-electron Hamiltonian

$$H = \sum_{i}^{n} h_i + \sum_{j>i}^{n} g_{ij} \tag{8-6}$$

in which h_i is the Dirac operator of Eq. (8-5) for electron i and g_{ij} is the electron-electron interaction operator. The corresponding many-electron equation of motion

$$H\Psi = E\Psi \tag{8-7}$$

is called the Dirac-(Gaunt/Breit) equation, depending on which operator g_{ij} is used [23]. In the Dirac-Fock-CI approach the many-electron wavefunction is approximated by a sum of Slater-determinants built from orthonormal spinors ψ:

$$\Psi = \sum_{I} \Phi_I C_I \tag{8-8}$$

$$\Phi_I = (n!)^{-1/2} \det |\psi_{I1}(1)\psi_{I2}(2) \ldots \psi_{In}(n)| \tag{8-9}$$

The spinors ψ are commonly optimized in restricted open shell Dirac-Fock calculations. For the description of core electron spectra it is important to use optimized

spinors not only for the initial state but also for the final states. This final state orbital optimization allows for a compact representation of the orbital relaxation after core excitation. This orbital relaxation is especially important for the outer shell spinors, which become more contracted in the presence of a core hole.

Often the orbitals are not optimized for each state separately, but instead for a weighted average (WA) over all states of a particular configuration. Having one common orbital set for all states of a configuration has important computational and conceptual advances, while the energy increase with respect to fully optimized orbitals for each state is usually only minor. Whether the WA approach is can be used, depends on the case at hand.

The energies of the various angular momentum coupled states of each electronic configuration can be obtained from a complete open shell CI (COS-CI) calculation: a full CI in the space of the open shell orbitals [23]. In a ground state COS-CI calculation the valence electrons are distributed in all possible ways over the open valence orbitals, while all other electrons are in doubly occupied orbitals. Core ionized or core excited states have not only open shell valence electrons, but also open shell core electrons. In a COS-CI calculation of such states the core hole is also distributed in all possible ways over the open core orbitals. Depending on the problem at hand, the core hole may also be kept fixed in one particular core orbital. The COS-CI allows accounting for the electron-electron interactions of the valence shell electrons and, for the final states, also for the electron-electron interactions amongst the open shell core electrons as well as the electron-electron interactions between core and valence electrons. The COS-CI accounts for the electron correlation within the valence shell, it does not include dynamical electron correlation. This dynamical correlation is in most cases predominantly an atomic effect and the consequences of neglecting this correlation can be estimated from accurate free ion/atom studies.

In order to obtain theoretical spectra, not only relative energies but also relative intensities have to be computed. This implies that overlap matrix elements (for XPS) or dipole matrix elements (for XAS and EELS) between initial and final wavefunctions need to be evaluated. The non-orthogonality between the spinors of the initial and final states makes that these computations are non-trivial. Moreover, the matrix elements have to be calculated for a large number of final states, that are each expanded in many Slater-determinants. With the aid of the cofactor method of Prosser and Hagström [27] the computations of relative intensities become feasible.

Since the core electrons have their density close to the nuclei, we also need to consider the model to be used for the nuclei. In non-relativistic theory it is common to take a simple point charge model. The radial solutions of the Schrödinger equation for the point-charge potential can be exactly represented by Slater type functions $r^n e^{-\lambda r}$. In relativistic theory one can also find exact solutions of the Dirac equation for the point-nucleus potential. For example, the radial part of the $1s^{1/2}$ solution for a point nucleus is given by

$$R(r) = r^{\gamma-1} e^{-\lambda r} \text{ with } \gamma = \sqrt{1 - \frac{Z^2}{c^2}} \tag{8-10}$$

where Z is the charge of the nucleus [24]. We see that the finite speed of light gives rise to a non-integer power of r. This causes a weak singularity at the origin. Because this singularity is just an artifact of the point-charge model, the use of the point-charge model in Dirac-Fock calculations is not recommendable. Moreover, such singularities are hard to describe with Slater type basis functions and even harder with Gaussian type functions. Therefore, the choice of a finite nuclear model is also computationally favourable [23, 24, 28]. A slight disadvantage is that there is no agreement yet on a standard finite nuclear model, so that different models and parameterisations are in use, such as a uniform nuclear charge distribution over a finite sphere or a charge distribution over a narrow Gaussian function. Careful Dirac-Fock studies [28] showed that for properties that do not directly involve the nuclei, the choice of a particular nuclear model has no important consequences, except that finite nucleus models give a higher total energy than the point-charge model. This is mostly due to an increase in energy of the innermost s-spinors. Differences between different popular finite size models are only minor. The influence of the chosen nuclear model on the spin-orbit splitting of the one-electron levels is small [28]. For example, for uranium ($Z = 92$) the average energy of the 2p levels is unaffected and the 2p spin-orbit splitting decreases by 3.1 eV from 3,834.5 to 3,831.4 eV, when a finite nucleus model is chosen instead of a point nucleus. The 4f levels are stabilized by 0.08 eV, while the spin-orbit splitting is unchanged. In the 3d transition metal manganese both 2p-levels are stabilized by 0.0004 eV with a finite nucleus model as compared to a point nucleus, the 10.62 eV spin-orbit splitting is unaffected.

Presently only a few computer packages are well suited to perform four-component calculations for molecules and embedded clusters. The first is the MOLFDIR suite for relativistic Dirac-Fock-CI calculations, developed at the University of Groningen [23]. The generation of one and two electron integrals over basis functions, a necessary step in all wavefunction based *ab initio* calculations, is rather slow in MOLFDIR. The package is capable of handling up to the Dirac-Fock level all double groups that are subgroups of the O_h double group. At the CI level the highest Abelian subgroup of the point group under consideration is used. For systems with high symmetry exploiting this symmetry is helpful to keep the calculations feasible. Moreover the point group representations may be used to label the different states and to clarify the interpretation. The DIRAC program suite can also perform relativistic Dirac-Fock-CI calculations [29]. It is capable of handling only Abelian symmetry groups, but on the other hand it has a much faster integral generator. Four-component multi-reference methods have been developed by Ishikawa *et al*. [30].

Van der Laan and co-workers [2, 4, 19, 20] make use of the relativistic atomic program package of Cowan [22]. They combine the results of relativistic Hartree-Fock calculations with branching ratios observed in near-edge XAS or EELS data. With the aid of a spin-orbit sum rule [1], information is obtained for the valence shell spin-orbit splittings. This procedure is further outlined and illustrated in Section 8.4. Recently a DFT-CI method has been developed [31, 32] in which Kohn-Sham (or Dirac-Kohn-Sham) orbitals instead of Hartree-Fock (or Dirac-Fock) orbitals form the one-electron basis for the CI calculations. In this approach electronic

correlations among selected orbitals are "explicitly correlated", i.e. taken into account by the CI scheme, while correlations amongst other orbitals are treated within the framework of DFT. Clearly the quality of the DFT-CI results depends on the exchange-correlation potentials used in the calculations as well as on the choice of the orbitals to be correlated through CI [16]. The CI results discussed in the next sections are obtained from calculations in the conventional (four-component) wavefunction based CI approach, where the spinors are determined in Hartree-Fock (Dirac-Fock) self-consistent field (SCF) or multi-configuration SCF calculations.

8.3. X-RAY PHOTOELECTRON SPECTRA

The X-ray spectra of transition metal, lanthanide and actinide materials are quite complex. Most of these materials are open shell compounds: they contain atoms or ions with incompletely filled electron shells. Atomic many-body effects, many-body effects relating to inter-atomic charge-transfer and relativistic effects all play a role. Spin-orbit interactions must be included in the treatment of ionization from shells with non-zero orbital angular momentum. Even in 3p XPS of 3d-transition metal compounds, spin-orbit couplings determine the spectra to some extent. For sufficiently large core-spin-orbit splittings the X-ray spectra show doublets that correspond to excitations from different spin-orbit-split core levels.

To analyze this in more detail we consider the Mn 2p and 3p XPS of MnO, following Freeman *et al*. [15] and Bagus *et al*. [7, 8]. MnO is an ionic material, which crystallizes in a simple rock salt crystal structure. Each Mn ion is coordinated by six oxygen ligands and has octahedral (O_h) site symmetry, likewise each oxygen ion is surrounded by an octahedron consisting of six Mn ions. Bagus and co-workers analyzed the spectra using *ab initio* four-component relativistic CI wavefunctions for embedded cluster models of MnO. The simplest model for representing Mn in MnO consists of a single Mn^{2+} ion embedded in a point charge array that reproduces the Madelung potential of an ideal MnO crystal. This purely ionic model allows the testing of the importance of atomic relativistic and electron correlation effects. Of course, in compounds that are less ionic than MnO, such as rock salt NiO, core excitations cannot be treated without accounting also for ligand-to-metal charge transfer effects (see [16] and references therein). In MnO, however, the atomic relativistic and correlation effects are dominant over the charge transfer effects and therefore the single embedded ion is a reasonable first approximation.

The ground state of Mn^{2+} is dominated by the $1s^2 2s^2 2p^6 3s^2 3p^6 3d^5$ configuration, which is often abbreviated as $KLM3d^5$, here we use the shorthand notation $3d^5$. Likewise, the leading configurations of the *2p* and *3p* hole states are denoted $2p^5 3d^5$ and $2p^5 3d^5$, respectively. We use atomic symmetry notations that neglect the covalent mixing of the Mn orbitals and the crystal-field splitting of the orbital levels. However, the calculations quoted below [7, 8, 15] take account of the appropriate double group symmetry representations. The *2p* XPS spectra in MnO are qualitatively different from the *3p* spectra. The $3p_{3/2}$–$3p_{1/2}$ spin-orbit splitting is only $\sim$1.4 eV in Mn^{2+}, so the 3p hole spectra can well be analyzed in terms of

spin-orbit-split Russell-Saunders (RS) multiplets $^{2S+1}$L. The 2p hole spectra cannot be analyzed in this way because the $2p_{3/2}$–$2p_{1/2}$ spin-orbit splitting is much larger, ~10.6 eV. The high spin initial state of Mn^{2+} is ^6S while the allowed final states are ^5P and ^7P, arising from $p^5(^2P)d^5(^6S)$. In order to determine the relative XPS intensities I_{rel} the sudden approximation (SA) [33] can be used. The SA assumes that at the instant of photo-ionization, the ionized state is described by a "frozen" wavefunction Ψ^F that results from annihilating one electron from the initial state wavefunction. The transition probability towards a final wavefunction Ψ_k is considered to be proportional to the square of the many electron overlap integral between the Ψ_k and the "frozen" wavefunction,

$$P_k \sim \left\langle \Psi k \middle| \Psi^F \right\rangle^2 \tag{8-11}$$

We consider first Mn 3p ionization in MnO. The 3p XPS shows an intense first peak at ~47.5 eV binding energy, a shoulder at ~2.5 eV higher binding energy and a very broad, about 20 eV wide, peak centered at ~20 eV above the first peak [8, 35]. Nonrelativistic results for Mn^{2+} have already been obtained over 30 years ago by Freeman *et al.* [15], who performed Hartree-Fock calculations followed by COS-CI: a full CI in the space of the five 3d valence orbitals. In this configuration space the final ^7P state can only be built from $3p^5(^2P)3d^5(^6S)$. The leading configuration of the final ^5P state is also $3p^5(^2P)3d^5(^6S)$, but two other valence shell angular momentum couplings, $3p^5(^2P)3d^5(^4P)$ and $3p^5(^2P)3d^5(^4D)$ also give terms of ^5P symmetry. These last two terms, whose angular momentum coupling within the 3d shell is different from that of the initial state, are not "allowed": they do not carry intensity. However, these configurations do have the same total symmetry as the allowed $3p^5(^2P)3d^5(^6S)$ configuration and therefore they can mix with the allowed configuration. This mixing of configurations yields states, which "steal" intensity from the allowed configurations and this leads to the distribution of intensities over various final states and therefore over a range of energies.

The four-component Dirac-Fock-CI results were obtained by Bagus *et al.* [7] with the MOLFDIR program system [29]. Table 8-1 shows the nonrelativistic energies and intensities [15] with the corresponding relativistic results [7] for 3p-hole states of Mn^{2+}. The Mn orbitals were optimized separately for the initial $3d^5$ and for the final $3p^53d^5$ configurations. The CI was a COS-CI with the 3d-orbitals as active valence orbitals. The SA relative intensities are normalized so that the I_{rel} of the final state of lowest energy is equal to its degeneracy. The lowest ^{7}P multiplet has a degeneracy of 7×3 and it is split into J = |S + L|...|S–L| levels, in this case into J = 4, 3, 2, each with degeneracy 2J + 1 = 9, 7, 5. The three ^{5}P states resulting from the COS-CI mentioned above each have a degeneracy of $5 \times 3 = 15$. The J values corresponding to each of these multiplets are 3, 2 and 1. Each of the three ^{5}P states carries intensity, since the "allowed" ^{5}P configuration originating from $3p^5(^2P)3d^5(^6S)$ contributes to each of the three CI wavefunctions. The nonrelativistic results in Table 8-1 show that the lowest ^{5}P final state at about 4 eV carries

Table 8-1 Comparison of nonrelativistic Hartree-Fock-CI results [15] and relativistic Dirac-Fock-CI results [7] for 3p-hole states of Mn^{2+}. Relative energies (eV) and relative intensities

	Nonrelativistic			Relativistic		
	E_{rel}(eV)	Nr. of states	I_{rel}	E_{rel}(eV)	Nr. of states	I_{rel}
^{7}**P**	0	21	21	0	9	9
				0.50	7	7.0
				0.93	5	5.0
^{5}**P**	4.0	15	4.9	4.0–4.5	52	4.8
^{5}**P**	9.4	15	0.2	9.3–9.5	49	0.2
^{5}**P**	23.8	15	10.0	23.1–24.4	25	9.9

$\sim$25% of $I_{rel}(^7\mathrm{P})$ and the state at $\sim$24 eV gets $\sim$50%. Of course, other $3p^5d^5$ states are also present in this energy region, but due to their symmetries they carry zero intensity. The computed $^7P - {}^5P$ energy splitting is about 1.5 eV larger than the experimental splitting of about 2.5 eV. This error is well understood: the energies of d^5 multiplets with respect to the lowest ^{6}S multiplet are overestimated due to the approximate treatment of the atomic electron correlation in the calculations shown here.

Turning now to the relativistic calculations [7], we observe that the lowest Russell-Saunders multiplet is split into three different levels, with intensities that are consistent with the degeneracies of the J = 4, 3, 2 levels. Their energy separations are in reasonable agreement with the Landé-interval rule [36,37], which states that the energy separations between three J levels corresponding to one RS multiplet are approximately given by

$$\frac{E_J - E_{J-1}}{E_{J-1} - E_{J-2}} = \frac{J}{J-1} \tag{8-12}$$

In the energy range from 4 to 4.5 eV about 50 relativistic final states are present, whose intensities sum to roughly that of the non-relativistic ^{4}P multiplet at 4 eV. These states are best described as a mixing of different occupations of the *3p* and *3d* spinors, rather then as pure J = 2, 1 and 0 levels [7]. Likewise, there are also about 50 different relativistic states around 9.5 eV and 25 relativistic states around 24.8 eV. Comparing the nonrelativistic and relativistic results reveals that not only the relative energies and but also the relative intensities I_{rel} are quite similar in the two cases. Of course, J can be only a good quantum number in an isolated ion. There the states of a given J level are degenerate. In a crystal, the crystalline environment lowers the site symmetry and the energies of the states are split by ligand and crystal field effects so J is only an approximate quantum number. Moreover, a real crystal is never purely ionic, there are always effects of covalency. Accurate four-component calculations for an embedded $[MnO_6]$ cluster model [8] showed splittings of only $\sim$0.1 eV within the three approximate J-levels of the ^{7}P state (T_{1u} in the O_h site

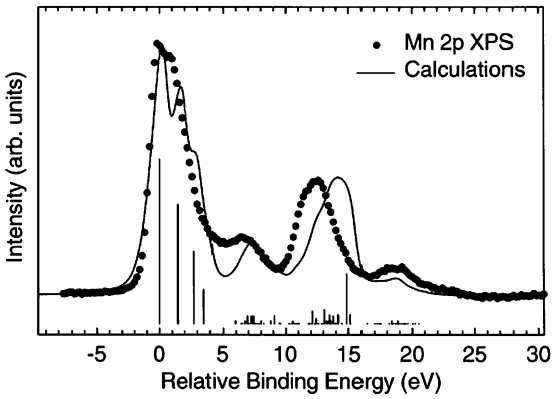

Figure 8-1. Experimental 2p level XPS spectra of MnO taken from [35] and theoretical spectra taken from [7]. The spectra were aligned so that the first experimental peak and the first theoretical peak with J = 4 are at zero energy

symmetry). This is not surprising since the 3p electrons are quite localized. The conclusion is that the Mn $3p$ XPS of MnO can be well interpreted in terms of spin-orbit-split atomic Russell-Saunders terms. It is clear that the origin of the structure of the $3p$ XPS of MnO is the angular momentum recoupling of the $3d$ shell. In particular, the shoulder at $\sim$2.5 eV in the spectrum can be viewed as a $3d$ angular momentum recoupled low spin atomic peak.

The interpretation for the $2p$ XPS of MnO is quite different. Single crystal Al $-$ K_α spectra taken by Parmigiani and Sangaletti [35] are shown in Figure 8-1. The spectrum shows four main features. The main peak and the feature at $E_{rel} \approx 7$ eV are ascribed to 2p hole states where the $2p^5$ shell is j-j coupled to $j = 3/2$; the two features above 10 eV are ascribed to $j = 1/2$ coupling of the $2p^5$ shell.

Clearly, it is not possible to make an analysis of the 2p hole spectra in terms of spin-orbit-split RS multiplets ^{2S+1}L. This is because the $2p_{1/2}$–$2p_{3/2}$ spin-orbit splitting is large. It is, however, possible to use a mixed coupling scheme, in which the $2p^5$ core shell is j-j coupled and the $3d^5$ valence shell is Russell-Saunders coupled. In the 2p hole states of lowest energy the $2p^5$ shell is j-j coupled to $j = 3/2$ and the $3d^5$ shell is coupled to $^6S_{5/2}$. This leads to four levels with J = 4, 3, 2, 1. The computed energies of the four lowest 2p hole states, calculated with the same four-component full valence CI model as used above for the 3p hole states, have indeed J = 4, 3, 2, 1. These energies are shown as a line spectrum in Figure 8-1. The relative intensities of the three higher states, with J = 3, 2, 1, are somewhat lower than expected from the degeneracies corresponding to their J values. This is due to configuration mixing with other d^5 multiplets with the same J values.

It is customary to construct a theoretical spectrum from the theoretical energies and SA intensities, by convoluting the intensities to take account of the core-hole lifetimes and of the experimental resolution. In the present case, the lifetime broadening has been represented by a Lorentzian function with a half width at half maximum of 0.35 eV; the experimental broadening by a Gaussian function with

0.5 eV half width at half maximum. In the so obtained theoretical spectrum the four main features in the MnO spectra are reproduced with roughly the correct width and intensity, see Figure 8-1. The main difference is that the theoretical E_{rel} are $\sim$2 eV higher than observed. As for the 3p-hole states, this error is due, at least in part, to the use of a formalism that overestimates the width of the d^5 multiplet energies. It is important that all four main features of the *2p* XPS spectra are present in the theoretical spectrum [7] that was obtained for a single Mn^{2+} ion embedded in point charges. In earlier semi-empirical studies [38] the second and fourth feature were assigned as arising from solid state effects, in particular from mixing of d^5 with ligand-to-metal charge transfer configurations. A recent *ab initio* four-component study in the same spirit as shown here, but for a larger MnO_6 cluster [8] confirmed that all main features of the Mn 2p and 3p XPS in MnO can be understood by considering relativistic and electron correlation effects of the Mn ions.

So far we have considered relative electron binding energies, taking the position of the first peak as $E_{rel} = 0$. In materials science it is quite useful to discuss binding energy shifts, for example with respect to the binding energies of the corresponding levels in the free atom or ion. In order to facilitate the physical interpretation of the various energy effects contributing to the binding energy shifts, it is helpful to separate the various contributions to the binding energy into initial state effects and final state effects. Initial state effects can be said to be due to the environment of the electron to be excited or ionized, while final state effects are due to changes of the environment in response to the core excitation or ionization. Rössler *et al*. [10, 11] considered Zn *2s* and *2p* core level binding energies in atomic Zn, a series of Zn containing compounds and ZnO. The *2s* binding energies were studied within Hartree-Fock theory. The *2p* binding energies were computed with a small multi-configuration expansion. Scalar relativistic relativistic corrections and spin-orbit coupling were included in a "spin-orbit coupling configuration interaction", SOC-CI. The $2p_{3/2}$–$2p_{1/2}$ splitting is 23.3 eV both for atomic Zn and ZnO. For atomic Zn the non-relativistic Koopman's value (i.e. with all orbitals frozen) for the *2s* ionization energy is 1,206.36 eV. In this value the electronic relaxation energy, i.e. the energy gain obtained when all orbitals are allowed to adapt to the new situation is neglected. This relaxation energy is large, $\sim$25 eV. Yet the Koopman 2s binding energy is very close to the best theoretical result of 1,206.51 eV [10]. This is because the scalar relativistic shift is as large as the relaxation energy but opposite in sign. While the relaxation energy lowers the 2s binding energy, the scalar relativistic effect increases the binding energy by about the same amount. Similar compensating effects are seen for the 2p binding energies. At the Koopman level a shift of $\sim$9 eV towards higher binding energy was found between Zn and Zn^+ and a further shift of about 11 eV between Zn^+ and Zn^{2+}, quite independent of the state under consideration, 2s, $2p_{1/2}$ or $2p_{3/2}$. After inclusion of electron relaxation and relativistic corrections the shifts are slightly larger, 10.5 and 12 eV, respectively.

For the study of ZnO, which crystallizes in the wurtzite structure in which each ion is tetrahedrally coordinated, Rössler *et al*. [11] used similar wavefunction expansions, but now for embedded clusters of various radii. This approach enabled an extrapolation towards extremely large clusters. At the Koopman level a decrease in

the binding energy of $\sim 2.1 \pm 0.1$ eV with respect to atomic Zn is obtained. This negative shift is at first sight surprising, since it occurs despite the ionic character of ZnO. The reason for this negative initial state shift is the strong Madelung field generated by the crystalline environment of the ionized Zn atom, which destabilizes the Zn 2s and 2p levels. In other words, the increase in binding energy due to the decrease in number of Zn valence electrons is overcompensated by the Madelung field. After accounting for relaxation the decrease is reduced to $\sim 1.0 \pm 0.1$ eV. Inclusion of relativistic effects brings the decrease in binding energy with respect to the free atom at $\sim 3.1 \pm 0.2$ eV, in good agreement with the experimental values. These examples make clear that scalar relativistic effects on absolute core electron binding energies and binding energy shifts are non-negligible. Yet, the most prominent effects of relativity on the spectra are due the spin-orbit splitting of core hole levels with non-zero orbital angular momentum.

8.4. X-RAY ABSORPTION AND ELECTRON ENERGY LOSS SPECTRA

X-ray absorption spectroscopy (XAS) and Electron Energy Loss Spectroscopy (EELS) can give very accurate information on the electronic structure of condensed matter. In transition metal, lanthanide and actinide materials the excitation of an electron from a core level with non-zero angular momentum into the valence band gives rise to complicated spectra with a set of high-intensity peaks, the so-called "white lines", at the threshold of the absorption edges. Spin-orbit coupling plays a central role in the appearance of these spectra. For sufficiently large core-spin-orbit splittings the spectra show doublets corresponding to excitations from different spin-orbit-split core levels. For example, the two transition metal *2p* absorption edges in 3d transition metal materials are due to transitions from $3d^n$ to $2p^5_{3/2}3d^{n+1}$ and to $2p^5_{1/2}3d^{n+1}$. Just as in transition metal *2p* XPS, the two features are well separated in energy. The fractions of the total intensity going into either of these two spin-orbit-split manifolds are called "branching ratios". Different from XPS, these branching ratios can in most cases not be estimated simply from the fraction of final state levels in that branch. Due to the dipole selection rules the branching ratios depend also on the valence spin-orbit interactions and on the electron-electron interactions in the final state [2]. If solid state effects like covalency and crystal field splitting are small compared to these interactions, J is a good quantum number and the transition probabilities are determined by atomic dipole selection rules and hence by the final state core-valence angular momentum couplings. When covalency increases J ceases to be a good quantum number and the branching ratio will change towards the statistical value [1]. The influence of the valence shell on the branching ratio can be nicely illustrated for the simple case of $L_{2,3}$ (i.e. $2p \rightarrow 5d$) absorption in Pt with a final $KLMN5d^9$ configuration [1]. For Pt the valence spin-orbit splitting is so large that j-j coupling is appropriate. If the character of the 5d-holes in platinum is $5d_{5/2}$, then dipole transitions are forbidden for $2p_{1/2}$ hole states but allowed for $2p_{3/2}$ hole states. However, the more $5d_{3/2}$ character is mixed in, the more I_{rel} for

$2p_{1/2}$ hole states increases. Hence the absence of a $2p_{1/2}$ edge indicates the absence of $5d_{3/2}$ holes in the valence shell.

Thole and van der Laan [1] showed that the branching ratios in XAS and EELS can serve as local probes of the valence spin-orbit interactions of a material [20]. Assuming that large core spin-orbit interactions divide the spectra into two branches, then the branching ratio's for transitions from the two core levels $j^+ = c + 1/2$ and $j^- = c - 1/2$ are defined by the area's of the white-line peaks: $B = A_{j+}/(A_{j+} + A_{j-})$. Thole and van der Laan [1, 2] derived for dipole transitions from the core shell c to a valence shell l, $l^n \rightarrow cl^{n+1}$, a linear relation between the theoretical branching ratio B_j and the expectation value of the angular part of the valence spin-orbit operator $\langle w^{110} \rangle$ in the initial state Ψ:

$$B = B_0 - \frac{c}{2c+1} \frac{\langle w^{110} \rangle}{n_h}. \tag{8-13}$$

Here n_h is the number of holes in the valence shell l. B_0 is the branching ratio in the absence of valence spin-orbit interaction. B_0 depends on the core-valence electron-electron interactions, but if these interactions are neglected B_0 is equal to the statistical value $\frac{c+1}{2c+1}$. For example, for p^5 final states the statistical value for B_0 is $2/3$ and for d^9 final states it is $3/5$. A simple relation for $\langle w^{110} \rangle$ in terms of the occupations numbers n_{j1} and n_{j1} of the $j_1 = l - 1/2$ and $j_2 = l + 1/2$ valence shell levels was also derived [20]:

$$\langle w^{110} \rangle = n_{j_2} - \frac{l+1}{l} n_{j_1} \tag{8-14}$$

Table 8-2 shows the branching ratios and spin-orbit expectation values $\langle w^{110} \rangle$ for $N_{4,5}$ actinide transitions, obtained from relativistic atomic Hartree-Fock calculations in a study by Moore *et al.* [20] with the code of Cowan [22]. It is clear from Table 8-2 that the deviation of $\mathbf{B_0}$ from the statistical value 3/5 is only minor, but the deviation of B from 3/5 is considerable. Experimental values for $\langle w^{110} \rangle$ may be obtained from the sum rule Eq. (8-13) by substitution of the measured B values.

Table 8-2 The number of 5f electrons (n), branching ratio (B) of the actinide $N_{4,5}$ edge spectra, 5f spin–orbit expectation value $\langle w^{110} \rangle$, electron occupation numbers of the $5f_{5/2}$ level ($n_{5/2}$) and the $5f_{7/2}$ level ($n_{7/2}$), in intermediate coupling, branching ratio without 5f spin–orbit interaction (B_0) (Taken from Moore *et al.* [20])

n	B	$\langle w^{110} \rangle$	$n_{5/2}$	$n_{7/2}$	B_0
0	0.592	0	0	0	0.592
1	0.634	−1.33	1	0	0.583
2	0.680	−2.57	1.96	0.04	0.594
3	0.723	−3.50	2.79	0.21	0.596
4	0.760	−4.04	3.45	0.55	0.598
5	0.817	−4.88	4.23	0.77	0.600

Next, values for the occupations n_{j1} and n_{j2} can be deduced by using Eq. (8-14). Moore *et al*. [20] used the computational results of Table 8-2 with the experimental branching ratio's for U, Th and Pu to show that the $f_{5/2}$ and $f_{7/2}$ occupation numbers of Th and Pu are consistent with intermediate coupling, while those of U are consistent with Russell-Saunders coupling.

In this approach the differences in the radial character of the $c - 1/2$ and $c + 1/2$ core levels are neglected. We will see later that this is not fully justified, especially for heavy atoms. Nevertheless, the branching ratios observed in X-ray absorption and electron energy loss spectra have with the spin-orbit sum rules of Thole and van der Laan been used successfully to determine the valence shell spin-orbital interactions of transition metal, rare earth and actinide compounds [1, 2, 4, 19–21]. For the $L_{2,3}$ edge in 3d transition metals the application of the sum rules is hampered by the large 2p-3d exchange interaction that is of similar size as the 2p spin-orbit interaction [2]. The same problem occurs for the $M_{4,5}$ edge of the lanthanides where the 3d-4f exchange interaction is strong compared to the 3d spin-orbit interaction. Still, even in the case of lanthanides the trend in the branching ratios can be used to obtain the relative population of the spin-orbit split states [20]. For the $L_{2,3}$ edges in 4d and 5d transition metals the sum rule should hold quite well, just like for the $M_{4,5}$ and $N_{4,5}$ edges of the light actinides discussed above [20].

Bagus *et al*. [3] also used atomic models for their four-component Dirac-Fock-CI studies of near-edge XAS. They discussed the results of relativistic CI studies for two different closed shell ions: V^{5+}, modeling V_2O_5, and U^{6+}. Following this work we consider three different cases. The first is the 2p edge of V^{5+}, where the $2p^5 3d^1$ final states involve significant $p_{3/2}$–$p_{1/2}$ mixing due to the 2p-3d multiplet splitting. The second case is the 4d edge of U^{6+}, where the 4d spin–orbit splitting of $\sim$40 eV is so large that the $4d^9 5f^1$ excited states are almost pure $d_{5/2}$ and $d_{3/2}$ hole states. The third case is for the 5d edge of U^{6+} where Russell-Saunders coupling dominates the character of the $5d^9 5f^1$ excited states leading to one single peak rather than a doublet. Relativistic wavefunctions for the initial and final states were calculated with the DIRAC program package [29]. The spinors were optimized with Dirac-Fock calculations for ground and excited state wavefunctions separately. Both V^{5+} and U^{6+} have a closed shell $^1S_0$ ground state. For the excited states the Dirac-Fock spinors were used in a CI calculation with the core-hole distributed in all possible ways over the spinors of the core shell and the excited electron distributed in all possible ways over the spinors of the initially empty valence shell, details of the calculations can be found in [3]. The relative intensities I_{rel} were obtained by calculating transition dipole matrix elements between the initial and final state wavefunctions.

The dipole selection rules for J levels are $\Delta J = 0, \pm 1$, with $J = 0 \rightarrow J = 0$ forbidden. The ground state of both V^{5+} and U^{6+} is a closed shell $J = 0$ level, therefore the allowed final states have $J = 1$. In the case of V^{5+} the $2p^5 3d^1$ final configuration has the following RS multiplets: $^3F_{4,3,2}$; $^1F_3$; $^3D_{3,2,1}$; $^1D_2$; $^3P_{2,1,0}$ and $^1P_1$. The allowed final states have $J = 1$ and are hence linear combinations of only $^3D_1$, $^3P_1$ and $^1P_1$. Likewise, the $nd^9 5f^1$ final configurations of U^{6+} have

Table 8-3 Properties of the three J = 1 levels of the $2p^5 3d^1$ configuration of V^{5+} (Reproduced from [3])

			Weight of j–j Configurations			Multiplet Character (%)		
Level	E_{rel}(eV)	I_{rel}	$2p_{1/2}{}^{-1}3d_{3/2}{}^{1}$	$2p_{3/2}{}^{-1}3d_{3/2}{}^{1}$	$2p_{3/2}{}^{-1}3d_{5/2}{}^{1}$	^1P	^3P	^3D
1	0	0.02	0.02	0.74	0.24	0.5(0.02)	91.0	8.5
2	4.8	1	0.13	0.25	0.62	28.3(1)	4.4	69.3
3	11.9	2.44	0.85	0.00	0.15	71.2(2.52)	4.6	24.2

The relative energy, E_{rel}, is set to zero for the first level and the relative intensity, I_{rel}, is arbitrarily normalized to one for the second level. The weights of the j–j coupled J = 1 configurations and the projections, in percentage, of the Russell–Saunders multiplets on the relativistic CI wavefunctions are also given
The ^1P multiplet projections normalized to one for the second level are given in parenthesis

many RS multiplets, but again only the multiplets $^3D_1$, $^3P_1$ and $^1P_1$ contribute to the $J = 1$ final states. The selection rules in terms of RS multiplets are $\Delta S = 0$, and $\Delta L = 0, \pm 1$. Since the ground state is a $^1S_0$ state, the only allowed excited Russell-Saunders multiplet is $^1P_1$. This multiplet can contribute to each of the three final J = 1 levels, and it is this contribution that can give intensity to the levels. The final J = 1 levels can also be analysed in terms of j-j coupled configurations. In the case of V^{5+} the final configurations that can couple to J = 1 are $2p_{1/2}{}^{-1}3d_{3/2}{}^{1}$, $2p_{3/2}{}^{-1}3d_{3/2}{}^{1}$ and $2p_{3/2}{}^{-1}3d_{5/2}{}^{1}$, the three J = 1 final wavefunctions can be written as linear combinations of these three j-j configurations. The $2p_{1/2}{}^{-1}3d_{5/2}{}^{1}$ final configuration cannot be coupled to J = 1. Analogously, for U^{6+} the three final configurations that can couple to J = 1 are $nd_{3/2}{}^{-1}5f^1_{5/2}$, $nd_{5/2}{}^{-1}5f_{5/2}{}^{1}$ and $nd_{5/2}{}^{-1}5f_{7/2}{}^{1}$ but the $nd_{3/2}{}^{-1}5f_{7/2}{}^{1}$ final configuration cannot be coupled to J = 1.

The properties of the three lowest final J = 1 levels resulting from the 2p → 3d transitions of V^{5+} are summarized in Table 8-3. The first column labels the three levels, the second column shows the relative energies E_{rel} and the third column shows the relative intensities I_{rel}. In the next three columns the relativistic wavefunctions are analysed in terms of j-j coupled configurations. The last three columns show the analysis through a projection of the RS multiplets ^1P,^{3} P and ^3D on these relativistic wavefunctions. The wavefunctions corresponding to the RS multiplets were obtained from a non-relativistic calculation, i.e. a Dirac-Fock-CI calculation with extremely large light speed. The projections are normalized to give a total of 100% for each J level, for a detailed description of the projections, see ref. [3].

The relative energy, E_{rel}, is set to zero for the first level and the relative intensity, I_{rel}, is arbitrarily normalized to one for the second level. The weights of the j–j coupled J = 1 configurations and the projections, in %, of the Russell–Saunders multiplets on the relativistic CI wavefunctions are also given.

The ^1P multiplet projections normalized to one for the second level are given in parenthesis.

The first level at $E_{rel} = 0$ has very little intensity. It is an almost pure $2p_{3/2}$ level. The reason for the weak intensity becomes clear from the analysis in terms of RS multiplets: this level is dominated by the ^3P level and the dipole allowed ^1P multiplet contributes less than 1%. The second level at 4.8 eV has significant ^1P character and

Table 8-4 Properties of the three J = 1 levels of the $4d^9 5f^1$ configuration of U^{6+}; see the caption to Table 8-3 (Reproduced from [3])

			Weight of j–j		Configurations	Multiplet	Character (%)	
Level	E_{rel}(eV)	I_{rel}	$4d_{3/2}{}^{-1}5f_{5/2}{}^{1}$	$4d_{5/2}{}^{-1}5f_{5/2}{}^{1}$	$4d_{5/2}{}^{-1}5f_{7/2}{}^{1}$	^{1}P	^{3}P	^{3}D
1	0	0.01	0.00	0.90	0.10	0.5(0.01)	73.2	26.4
2	2.3	1	0.00	0.10	0.90	57.7(1)	8.1	34.1
3	44.4	0.55	1.00	0.00	0.00	41.7(0.72)	18.5	39.7

the third level at 11.9 eV even more. This explains the large I_{rel} for these two levels. It is interesting to compare the ^{1}P contributions of the three levels to their relative intensities I_{rel}. To facilitate this comparison these contributions were renormalized to one for the second level (the renormalized values are given in parenthesis). If the radial parts of the spinors for the different j values were identical, as assumed in the sum rules of Thole and Van der Laan [1, 2], then the relative contributions of the ^{1}P multiplet would be the same as the relative intensities [3]. For V^{5+} this is nearly true. We will see below that this approximation holds less well for U^{6+}. It is clear from the projections that the excited state wavefunctions do not simply correspond to RS coupled states. On the other hand, the analysis in terms of j-j coupled configurations shows that it is also not reasonable to associate each of the two levels that carry intensity with one particular j-j coupling. This is obviously a case where intermediate coupling is appropriate. The energy difference of 7.1 eV between the two levels with significant I_{rel} compares well with the energy separation of ~7 eV between two structures with large intensities that have been associated with V 2p – 3d transitions in near edge XAS spectra of V_2O_3 [3]. Obviously, the results for the atomic model cannot reproduce the details of an experiment for V_2O_3, because solid-state effects are neglected. Nevertheless, the results do explain the existence of two intense peaks.

Table 8-4 shows the same properties as given for the 2p → 3d transitions of V^{5+}, but now for the three lowest final J = 1 levels resulting from the 4d → 5f transitions of U^{6+}. Again the first level has little intensity, but in this case the second level at 2.3 eV higher energy carries most of the intensity. The weights of the j-j configurations show that there is almost no $4d_{3/2}$–$4d_{5/2}$ mixing. The energy difference of 42.1 eV between the two intense peaks reflects the large $4d_{3/2}$–$4d_{5/2}$ spin-orbit splitting. There is some mixing of the $5f_{5/2}$ and $5f_{7/2}$ occupations, driven by the electrostatic integrals between 4d and 5f spinors, but the states can be considered as almost pure j-j coupled states [3, 36]. The nearly pure j-j coupling implies that all wavefunctions show significant mixing of the three RS multiplets. The deviation between the I_{rel} and the normalized ^{1}P contributions is substantially larger than in the case of V^{5+}. The reason is that the spatial extent of the $4d_{3/2}$ is appreciably smaller than that of $4d_{5/2}$. Bagus *et al.* [3] used the $\langle r^2 \rangle$ of the initial state spinors as a convenient measure: $\langle r^2 \rangle$ for $4d_{3/2}$ is over 6% smaller than $\langle r^2 \rangle$ for $4d_{5/2}$.

The branching ratio obtained from the relative intensities in Table 8-4, $B = I_{5/2}/(I_{5/2} + I_{3/2}) = 0.64$, deviates more from the statistical value of 0.6 than

Table 8-5 Properties of the three J = 1 levels of the $5d^9 5f^1$ configuration of U^{6+} (Reproduced from [3])

			Weight of j–j Configurations			Multiplet	Character (%)	
Level	E_{rel}(eV)	I_{rel}	$5d_{3/2}{}^{-1}5f_{5/2}{}^{1}$	$5d_{5/2}{}^{-1}5f_{5/2}{}^{1}$	$5d_{5/2}{}^{-1}5f_{7/2}{}^{1}$	^{1}P	^{3}P	^{3}D
1	0	0.00	0.03	0.83	0.14	0.1(0.00)	86.5	13.5
2	6.9	0.03	0.42	0.15	0.43	2.2(0.02)	12.9	84.8
3	31.2	1	0.55	0.02	0.43	97.8(1)	0.6	1.7

The relative energy, E_{rel}, is set to zero for the first level and the relative intensity, I_{rel}, is normalized to one for the third level. The weights of the j–j coupled J = 1 configurations and the projections, in percentage, of the Russell–Saunders multiplets on the relativistic CI wavefunctions are also given. The ^{1}P multiplet projections normalized to one for the third level are given in parenthesis

the value obtained from projection, B = 0.58, and the value B = 0.59 obtained from the sum rule analysis of van der Laan *et al.* [19, 20] (see Table 8-2). This shows that not considering the dipole integrals, either by using projection or by using sum rules, introduces a significant error in the branching ratio for the 4d → 5f transitions of U^{6+}.

The results for the 5d → 5f transitions of U^{6+}, reproduced from Ref. [3] in Table 8-5, are very different from the 4d → 5f results. The only transition that carries significant intensity is to the third level, which is predominantly ^{1}P, at 31 eV higher energy than the first level which is mainly ^{3}P. The energy difference between them is largely due to ^{3}P $-^1$ P exchange splitting. The level at 7 eV is mainly ^{3}D. It is not a pure Russell-Saunders state, some ^{1}P character is mixed in, giving the level some intensity. The near edge X-ray absorption fine structure for the $O_{4,5}$ edge of the formally hexavalent UO_3 show indeed one strong peak with a very weak satellite at lower energy [3, 39]. This analysis for the three different cases, which is based on the work of Bagus *et al.* [3], shows that the relative energies and intensities of X-ray absorption peaks at core-level edges can be well understood by examining the final state RS multiplets.

Of course, the atomic models as used by Thole *et al.* and Bagus *et al.* are adequate only for those systems where solid-state effects like covalency and crystal field splitting are weak enough to enable an interpretation in terms of atomic-like orbitals. Furthermore, CT effects cannot be included in an atomic model. In the introduction we noted that in the case of XPS screening through CT might be especially important in the final states, because the core hole causes a strong potential that lowers the excitation energy of states, in which an electron is transferred from the neighboring atoms to the core-ionized atom. In near edge XAS and EELS final states the effects of such CT states are much less prominent, because the excited electron is transferred to a local valence shell, so that a strong electron attracting potential is avoided.

8.5. SUMMARY

XPS, XAS and EELS core spectra of some transition metal, lanthanide and actinide materials have been discussed, with emphasis on effects of relativity. The spectra can give detailed information on the electronic structure of the materials, but the interpretation of the spectra is often complicated. Relativistic effects, core-valence electrostatic interactions, valence electrostatic interactions and solid-state effects may all play a role. Transitions from core levels with non-zero angular momentum and large core-spin-orbit splittings lead to branched spectra, which cannot be explained without explicitly considering the core and valence spin-orbit interactions. Accurate first principle methods that are able to take all these effects into account are in most cases needed for a proper interpretation of the complicated spectra.

The relativistic four component Dirac-Fock-CI method [23,24] is well suited for this purpose, because the effects of relativity and electron correlation are treated from the outset, in a well-balanced way. With the increased availability of massive compute power and the increased efficiency of the program packages built for these methods, Dirac-Fock-CI studies for clusters of moderate size are nowadays feasible. A brief description of the Dirac-Fock-CI has been included and it is argued that finite-size nuclear models are better suited for Dirac-Fock studies than the point charge model. A more economic but also more approximate approach is to start with non-relativistic orbitals and wavefunctions and add scalar relativistic corrections by modifying the one-electron Hamiltonian, while spin-orbit effects are included via a spin-orbit-coupling CI treatment [10–12]. This approach to include relativistic effects has the important practical advantage that standard quantum chemical program packages can be used.

The effects of relativity on X-ray photoelectron spectra have been discussed using the Dirac-Fock-CI results of Bagus and coworkers [7, 8] for MnO as a guide. It was shown that all main features of the Mn 2p and 3p XPS in MnO can be understood by considering relativistic and electron correlation effects of a single embedded Mn ion. The most prominent relativistic effects are the effect due to spin-orbit coupling in transitions from core levels with non-zero angular momentum. The work of Rössler *et al*. [10,11] showed that scalar relativistic effects on absolute core electron binding energies and on binding energy shifts due to different chemical environments are also non-negligible.

In transition metal, lanthanide and actinide materials the excitation of an electron from a core level with non-zero angular momentum into the valence band gives rise to complicated near-edge XAS and EELS spectra with a set of high-intensity peaks, the so-called "white lines", at the threshold of the absorption edges. For sufficiently large core-spin-orbit splittings the spectra show doublets (branches) corresponding to excitations from different spin-orbit-split core levels. Different from XPS, the relative intensities of the individual branches cannot be estimated simply from the statistical value (the fraction of final state levels in the branch). Due to the dipole selection rules the branching ratios depend also on the valence spin-orbit interactions and on the electron-electron interactions in the final state. Moore, Van der Laan and co-workers [2, 20, 21] demonstrated that the deviation of the

experimental branching ratio from the statistical value, combined with relativistic Hartree-Fock results, may be used in the sum rules of Thole and Van der Laan [1] to give information on the valence-spin-orbit coupling. This work was briefly discussed.

The results of relativistic many-electron calculations can in principle be expressed either in terms of Russell-Saunders states or in j-j coupled states, whatever representation gives better insight. A new analysis of branching ratios by Bagus *et al*. [34] is discussed. With the aid of Dirac-Fock-CI results for near edge XAS for V^{5+} and U^{6+} it was shown that the relative energies and intensities of X-ray absorption peaks at core-level edges can be well understood by examining the final state Russell-Saunders multiplets.

ACKNOWLEDGMENTS

Dr. P.S. Bagus, Dr. L. Sangaletti, Dr. K.T. Moore and Dr. G. van der Laan are thanked for making their results available for this publication.

REFERENCES

1. Thole, B.T., Van der Laan, G.: Phys. Rev. A **38**, 1943 (1988); Phys. Rev. B **38**, 3158 (1988); Van der Laan, G., Thole, B.T.: Phys. Rev. Lett. **60**, 1977 (1988)
2. Van der Laan, G., Thole, B.T.: J. Electron Spectrosc. **86**, 57 (1997)
3. Bagus, P.S., Freund, H., Kuhlenbeck, H., Ilton, E.S.: Chem. Phys. Lett. **455**, 331 (2008)
4. De Groot, F.M.F.: J. Electron Spectrosc. **67**, 529 (1994)
5. Ikeno, H., De Groot, F.M.F., Stavitski, E., Tanaka, I.I.: J. Phys.- Condens. Mat. **21**, 104208 (2009)
6. Fronzoni, G., De Francesco, R., Stener, M., Causa, M.: J. Phys. Chem. B **110**, 9899 (2006)
7. Bagus, P.S., Broer, R., De Jong, W.A., Nieuwpoort, W.C., Parmigiani, F., Sangaletti, L.: Phys. Rev. Lett. **84**, 2259 (2000)
8. Bagus, P.S., Ilton, E.S.: Phys. Rev. B **73**, 155110 (2006)
9. Pernpointner, M., Visscher, L., De Jong, W.A., Broer, R.: J. Comput. Chem. **21**, 1176 (2000); Pernpointner, M., Visscher, L.: J. Comput. Chem. **24**, 754 (2003)
10. Rössler, N., Staemmler, V.: Phys. Chem. Chem. Phys. **5**, 3580 (2003)
11. Rössler, N., Kotsis, K., Staemmler, V.: Phys. Chem. Chem. Phys. **8**, 697 (2006)
12. Roos, B.O., Malmqvist, P.A.: Phys. Chem. Chem. Phys. **6**, 2919 (2004)
13. Hüfner, S.: Photoelectron Spectroscopy, Springer Series in Solid-State Sciences, 2nd edn., vol. 82. Springer, Berlin (1996)
14. Wagner, C.D.: In: D. Briggs, M.P. Seah (eds.) Practical Surface Analysis, 2nd edn., vol. 1. Wiley, Chichester, UK (1996)
15. Freeman, A.J., Bagus, P.S., Mallow, J.V.: Int. J. Magn. **4**, 35 (1973)
16. Hozoi, L., De Vries, A.H., Broer, R., De Graaf, C., Bagus, P.S.: Chem. Phys. **331**, 178 (2006)
17. Adachi, H., Ogasawara, K.: Adv. Quantum Chem. **42**, 1 (2003)
18. Ohno, M.: J. Electron Spectrosc. **131–132**, 3 (2003)
19. Van der Laan, G., Moore, K.T., Tobin, J.G., Chung, B.W., Wall, M.A., Schwartz, A.J.: Phys. Rev. Lett. **93**, 097401 (2004)
20. Moore, K.T., Van der Laan, G., Tobin, J.G., Chung, B.W., Wall, M.A., Schwartz, A.J.: Ultramicroscopy **106**, 261 (2006)

21. Moore, K.T., Van der Laan, G.: Rev. Mod. Phys. **81**, 235 (2009)
22. Cowan, R.D.: The Theory of Atomic Structure and Spectra. University of California Press, Berkeley, CA (1981)
23. Visser, O., Aerts, P.J.C., Hegarty, D., Nieuwpoort, W.C.: Chem. Phys. Lett. **134**, 34 (1987); Visser, O.: PhD Thesis, University of Groningen, The Netherlands (1992)
24. Visscher, L., Visser, O., Aerts, P.J.C., Merenga, H., Nieuwpoort, W.C.: Comput. Phys. Commun. **81**, 120 (1994); Visscher, L.: PhD Thesis, University of Groningen, The Netherlands (1993)
25. Breit, G.: Phys. Rev. **34**, 553 (1929)
26. Gaunt, J.A.: Proc. R. Soc. A **122**, 513 (1929)
27. Prosser, F., Hagström, S.: Int. J. Quantum Chem. **2**, 89 (1968); J. Chem. Phys. **48**, 4807 (1968)
28. Visscher, L., Dyall, K.G.: Atom. Data Nucl. Data **67**, 207 (1997)
29. Saue, T., Bakken, V., Enevoldsen, T., et al.: DIRAC, a relativistic ab initio electronic structure program (2000)
30. Recent Advances in Relativistic Molecular Theory, K. Hirao, Y. Ishikawa (eds.). World Scientific Publishing, Singapore (2004)
31. Ogasawara, K., Ishii, T., Tanaka, I.I., Adachi, H.: Phys. Rev. B **61**, 143 (2000)
32. Ogasawara, K., Iwata, T., Koyama, Y., Ishii, T., Tanaka, I.I., Adachi, H.: Phys. Rev. B **64**, 115413 (2001)
33. Åberg, T.: Phys. Rev. **156**, 35 (1967)
34. Bagus, P.S., Schrenk, M., Davis, D.W., Shirley, D.A.: Phys. Rev. A **9**, 1090 (1974)
35. Parmigiani, F., Sangaletti, L.: J. Electron Spectrosc. **98–99**, 287 (1999)
36. Griffith, J.S.: The Theory of Transition-Metal Ions. Cambridge University Press, Cambridge (1971)
37. Condon, E.U., Shortly, G.H.: The Theory of Atomic Spectra. Cambridge University Press, Cambridge (1951)
38. Taguchi, M., Uozumi, T., Kotani, A.: J. Physical Soc. Japan **66**, 247 (1977) and references therein
39. Kalkowski, G., Kaindl, G., Brewer, W.D., Krone, W.: Phys. Rev. B **35**, 2667 (1987)

CHAPTER 9

RELATIVISTIC SYMMETRIES IN THE ELECTRONIC STRUCTURE AND PROPERTIES OF MOLECULES

DEVASHIS MAJUMDAR[1], SZCZEPAN ROSZAK[2], AND JERZY LESZCZYNSKI[1]

[1]*Department of Chemistry, Jackson State University, Jackson, MS 39217, USA*
e-mail: devashis@icnanotox.org;jerzy@icnanotox.org
[2]*Institute of Physical and Theoretical Chemistry, Wroclaw University of Technology, Wybrzeze Wyspianskiego 27, 50-370 Wroclaw, Poland*
e-mail: szczepan.roszak@pwr.wroc.pl

Abstract: Double groups and time reversals are finding increasing attention in recent years to calculate molecular electronic properties including relativistic effects. In the present review we have initially developed the concept of double groups for diatomic and polyatomic systems and demonstrated the use of double groups in diverse molecular properties. The concept of time reversal has been introduced as a symmetry property to mitigate the problem of CP (C: charge conjugation; P: parity) violation. The applications of time reversal in explaining molecular electronic properties have been collected together with a discussion on its role in double group symmetry.

Keywords: Double groups, Spin-orbit coupling, Relativistic configuration interaction, Correlation group table, Crystal field theory, Ligand field theory, Iodine oxide, MRSDCI, SnTe, Au_2, Pb_3, $Pb_3{}^+$, $Pt(thpy)_2$, MCSCF, SOCI, Time reversal, Parity, Charge conjugation, CPT theorem

Abbreviations

C	Charge conjugation
C_2	Twofold axis of symmetry
C_3	Threefold axis of symmetry
C_4	Fourfold axis of symmetry
CASMCSCF	Complete active space multiconfiguration self-consistent field
CFT	Crystal field theory
D^s	Spin multiplet
D^j	Rotational state of a spherical top molecule according to the j value

M. Barysz and Y. Ishikawa (eds.), *Relativistic Methods for Chemists*,
Challenges and Advances in Computational Chemistry and Physics 10,
DOI 10.1007/978-1-4020-9975-5_9,

E	Identity operation in point group
$\overline{E}$	New operation corresponding to E in the double group
$\hat{E}$	Identity operator
EPR	Electron paramagnetic resonance
ESR	Electron spin resonance
g	Any irreducible representation in point or double group
H	Hamiltonian
$H^{(l)}$	Magnetic perturbation energy
I	Identity matrix
J	Total angular momentum
L	Total spatial angular momentum
$\boldsymbol{l}$	Orbital angular momentum
l_x, l_y, l_z	x, y, z components of l
Λ	Spatial angular momentum for a diatomic
$\chi(\varphi)$	Character of rotation through an angle φ
LFT	Ligand field theory
LST	Linear synchronous transit
$M_{J_i}(I = 1, 2)$	Projection of j quantum number to two atoms in a diatomic
MCSCF	Multiconfiguration self-consistent field
MRSDCI	Multireference singles and doubles configuration interaction
$\boldsymbol{\mu}$	Electric dipole moment
$\boldsymbol{m}$	Magnetic dipole moment
NMR	Nuclear magnetic resonance
OLED	Organic light emitting diode
Ω	Angular momentum for a diatomic
P	Parity operator
$Pt(thpy)_2$	Bis-[2-(2-thienyl)-pyridine] platinum
q	Sum of the orbital quantum number of electrons in an atom
R	New group element R (in a double group) representing rotation by 2π
RCI	Relativistic configuration interaction
$R_h(3)$	Three-dimensional rotation-reflection group
S	Total spin momentum
SO	Spin-orbit
SOCI	Second-order configuration interaction
SM	Spin-mixed
s	Spin momentum
σ	Reflection operator in a point group
T	Time reversal
U	Unit operator
V(r)	Potential

9.1. INTRODUCTION

Symmetry arguments are quite popular among chemists to elucidate the structure and reactivity of molecular systems. The arguments are not only systematic in their approach to understand the molecular properties but also they have some aesthetic appeal. These symmetry considerations are mostly based on the spatial point groups. However, such point group-based arguments have several limitations. It may lead to wrong or less accurate information of molecular properties, which depend on the orbital and spin motions of the constituent atoms. Such properties of the molecules come under the purview of relativistic theory and are treated in a way, which is not very conventional in classical chemical problems.

The spin of an electron gives rise to a magnetic dipole. The movement of electrons in its orbit, on the other hand, also produces the magnetic dipole. Thus an interaction between these two magnetic dipoles is possible and the effect is called *spin-orbit* interaction. These orbital and spin motions could further be influenced by an external magnetic field. An example is represented by molecular magnetism. This property is dependent on the orbital and spin motions of the constituent electron and nuclei and the external magnetic field generated by the motion of the electrons through a coil. Thus there could be two motion-dependent properties of a molecule. The former case, where no external field effect is present, influences the stability and spectroscopic behavior of the molecule. This *relativistic effect* generates a symmetry property known as *double group* symmetry [1–8]. Spatial symmetry must be augmented with arguments based on *time reversal* to deal with the later kind of property [3, 7, 9, 10]. The purpose of the present review is not to describe the details of double group characteristics or the time reversal effects. These are available in several books and publications [1–10]. We intend to define only the basic points related to these properties and then discuss the use of these two special relativistic features in diverse chemical problems with a special emphasis on the properties explained under double group framework.

9.2. SPIN-ORBIT INTERACTION AND DOUBLE GROUP

The spin-orbit effect arises due to the interaction of the magnetic dipole of the electronic spin and the movement of electron in its orbit. This feature is connected with relativistic effect and Dirac showed [8] that the magnetic perturbation energy ($H^{(1)}$) of a spin in a central field could be expressed as

$$H^{(1)} = \xi(r)\, \boldsymbol{l}.\boldsymbol{s}, \text{ with } \xi(r) = \frac{\hbar^2}{2m^2c^2r}\frac{\partial V(r)}{\partial(r)} \tag{9-1}$$

Here $\boldsymbol{l}$ and **s** are the orbital and spin momentum respectively and V(r) is the potential in which the electron moves. If more than one electron is involved $H^{(1)}$ turns out to be

$$H^{(1)} = \sum_i \xi(r_i)\, \boldsymbol{l}_i.\boldsymbol{s}_i \tag{9-2}$$

In this expression the interaction of spins with orbits other than their own is neglected. This is a valid approximation as long as the central field is stronger than the interelectronic interactions. It could be proved without much difficulty that the matrix elements of $H^{(1)}$ is proportional to **L.S** (**L**: total spatial angular momentum $= \boldsymbol{l}_1 + \boldsymbol{l}_2 + \ldots + \boldsymbol{l}_i$; **S**: total spin momentum $= \boldsymbol{s}_1 + \boldsymbol{s}_2 + \ldots + \boldsymbol{s}_i$). The **L.S** terms could be obtained from the total angular momentum **J** from the relation

$$\mathbf{J} = \mathbf{L} + \mathbf{S} \tag{9-3}$$

The above expressions are central in all relativistic calculations of atoms and molecules. The energy expressions and their implementations for the single and multiple electronic systems, in this context, have already been discussed in several articles of this book and elsewhere [8, 11, 12]. Here our motivation is to review the information regarding the use of double group in such calculations.

The atomic wavefunctions are, in general, made up of both orbital and spin part. Whereas the orbital part is always characterized by having integer values of $\boldsymbol{l}$, this is not the case for the spin part. Coming back to the last expression (9-3) where J characterizes the state system, the two possible spin states are α (1/2, 1/2) and β (1/2, −1/2) states. The spin of an electron can always be described as linear combination of these two functions α and β, and it is independent of the choice of the axis of quantization. Since $s = 1/2$ for an electron, J is a half-integer in systems with an odd number of electrons. The transformation properties of systems with half-integer angular momentum should be treated in a special way.

Let us consider the expression for the character of rotation through an angle ϕ.

$$\begin{aligned}
\chi(\phi) &= \frac{\sin(j + 1/2)\phi}{\sin 1/2\phi} \\
\chi(\phi) &= \chi(\phi + 2\pi)(\text{when } j \text{ is an integer}) \\
&= -\chi(\phi + 2\pi)(\text{when } j \text{ is half-integer})
\end{aligned} \tag{9-4}$$

Thus a rotation of 2π brings any physical system back to itself and so the transformation matrix and characters for the rotation of ϕ and $\phi + 2\pi$ ought to be equal. But when j is half-integer, the signs of representation is double-valued in the rotation group and thus they are not true representations. Every character changes sign when one performs a rotation of 2π. On the other hand, rotation by 4π is equivalent to the identity operator $\hat{E}$.

$$\begin{aligned}
\text{For}, \phi = 0, \quad \chi(0) &= \frac{(j + 1/2)\cos(j + 1/2)0}{1/2.\cos 1/2.0} = 2j + 1; \\
\text{and, when} \quad \phi = 2\pi, \quad \chi(2\pi) &= \frac{(j + 1/2)\cos(j + 1/2)2\pi}{1/2\cos\pi} \\
&= 2j + 1(\text{when } j \text{ is integer}) \\
&= -(2j + 1)(\text{when } j \text{ is half-integer}).
\end{aligned} \tag{9-5}$$

The only character with unique value is the character for rotation by π for j half-integer.

$$\chi(\pi) = \chi(3\pi) = 0 \tag{9-6}$$

In order to obtain the double-valued representation, we introduce that the molecule is to go into itself not upon a rotation by 2π around an axis, but only upon a rotation by 4π. This, of course, makes no difference in physical sense and is to be considered a mathematical device. A new group element R, the rotation by 2π, is now defined and the elements of single-valued groups are expanded by means of multiplication be R. The double group thus contains more classes than single group but not twice as many.

The double groups are usually denoted in terms of the respective point group symmetry with some specific superscripts. For example double-groups of C_{2v} and D_{2h} symmetries could either be denotes as C_2v^2, D_{2h}^2 [8], or $C_2v(M)^2$, $D_{2h}(M)^2$ [3] or C'_{2v}, D'_{2h} [2]. Throughout the manuscript we will use the first convention. The purpose of this review is to show how these double groups are actually used in relativistic treatments of molecules. Explicit treatments on the generation of double group character tables are available in literature [2, 3, 8]. A brief discussion on this topic is available in Appendix to show that the above discussion could be extended to generate double group character tables of different symmetries.

9.3. DOUBLE GROUPS AND RELATIVISTIC TREATMENT OF MOLECULES

9.3.1. Diatomic Systems

The formation of a diatomic molecule leads to the lowering of the spherical symmetry of individual atoms to cylindrical and hence any angular momentum of a diatomic along the internuclear axis is meaningful. This angular momentum along the internuclear axis is defined as Λ and for given L quantum number, $\Lambda = 0, 1, 2, 3\ldots$ L. The electronic states of a diatomic molecule are determined by these Λ values and are designated as Σ, Π, Δ, $\Phi\ldots$ etc. The spin-orbit coupling changes the symmetry of the relativistic problem to the double group. The coupling of the spin angular momentum (S) and the spatial angular momentum (Λ) along the internuclear axis leads to a net angular momentum (Ω), which is given by (analogous to Eq. (9-3)):

$$\Omega = |\Lambda + S| \tag{9-7}$$

The possible Ω states could be obtained by combining Λ with spin or directly from the individual j states.

$$\Omega = |M_{J_1} + M_{J_2}| \tag{9-8}$$

The M_J values are the individual projection of the j quantum numbers of the two atoms.

In order to assign the relativistic states and the nature of wavefunction of a diatomic system, we need to introduce several terminologies regarding the nature

of the spin-orbit states, direct product correlation of both single and double valued representation of the double groups and the corresponding Ω states, and the correlation of spin multiplets (D^s) with double groups. Detailed discussion of these topics is out of the scope of this review. We will present here only a brief account of them for the interest of this review. Interested readers should use the available literatures [1, 3, 8] to have complete account of these topics.

As it could be seen from any $C^2_{\infty v}$ double group character table [2–4, 8] of a diatomic, the irreducible representations are Σ^+, Σ^-, Π, Δ,..., $E_{1/2}$, $E_{3/2}$,..., $E_{n/2}$.The Σ^+, Σ^-, Π, Δ,... are single valued irreducible representations while $E_{1/2}$, $E_{3/2}$,..., $En_{/2}$ are double-valued. The Ω states corresponding to these non-relativistic states are represented as 0^+, 0^-, 1, 2,..., 1/2, 3/2,..., n/2 [1] respectively. Thus using these notations of the Ω states, one can represent the direct product correlations of a diatomic double group in terms of relativistic states. For example, the $\Sigma^+ \otimes \Sigma^+$ direct product of a $C^2_{\infty v}$-symmetry has irreducible representation of Σ^+ and hence the corresponding Ω state is 0^+. Similarly, the direct product of Δ and Π states in $C^2_{\infty v}$ double group generates $\Phi \otimes \Pi$ irreducible representations and the corresponding Ω states are 3 and 1. These states could also be derived from vectorial coupling scheme [1, 8]. In the case of two-valued representations, let consider the product of $E_{1/2} \otimes E_{1/2}$ states in $C^2_{\infty v}$ double group. The direct product would produce Σ^+, Σ^-, and Π irreducible representations and the corresponding Ω states are 0^+, 0^-, and 1. Similarly, $E_{1/2} \otimes E_{3/2}$ product yields 2 and 1 Ω states. The next thing one needs to establish is how the spin multiplets (D^s) correlate with the irreducible representation of a double group. The transformation of D^s is isomorphic with the transformation of the rotation state j (D^j) in molecular spectroscopy. The irreducible representations spanned by the D^s representation of the spin multiplets with quantum number s, are determined once the characters of the various operations of the double group are obtained. These are given by:

$$\begin{aligned}
\chi^s(\phi) &= \frac{\sin(s+1/2)\varphi}{\sin(\phi/2)}, \text{ if} \varphi \neq 0, \\
\chi^s(0) &= 2s+1, \text{ if } \varphi = 0, \\
\chi^s(C_n R) &= \chi^s(C_n), \text{ if s is an integer,} \\
\chi^s(C_n R) &= -\chi^s(C_n), \text{ if s is a half-integer}
\end{aligned} \tag{9-9}$$

Thus $D^0(s = 0)$ corresponds to Σ^+ irreducible representation of the $C^2_{\infty v}$ double group. Similarly use of Eq. (9-9) shows that $D^{1/2}$ and D^3 correspond to $E_{1/2}$ and $\Sigma^- \oplus \Pi \oplus \Delta \oplus \Phi$ irreducible representations of the $C^2_{\infty v}$ double group. Thus any transformation of D^s could be determined with respect to the irreducible representations of the $C^2_{\infty v}$ double group (these are also valid for $D^2_{\infty h}$ double group). It should be further noted that although the D^s and D^j transformations are isomorphic, there is a notable difference. The spin states can contain only g (gerade) representation for a homonuclear diatomic. Thus if l (angular momentum) is odd, all u representations appearing in spherical harmonics should be changed to g in correlating electronic spin states.

The determination of a relativistic state arising from a given non-relativistic state involves two steps. Firstly, the irreducible representations spanned by the spin multiplets using double group correlation (as discussed above) are found out. These irreducible representations are then multiplied with the spatial symmetry of the non-relativistic state in the next step. The resulting set of the irreducible representations is then transformed to the Ω state. As an example, for the $^3\Pi$ non-relativistic state of diatomic molecule, $s = 1$ and hence D^1 corresponds to Σ^- and Π irreducible representations. Now,

$$\Sigma^-(\text{spin}) \otimes \Pi(\text{spatial}) = \Pi$$
$$\Pi(\text{spin}) \otimes \Pi(\text{spatial}) = \Sigma^- + \Sigma^+ + \Delta$$

Thus the $^3\Pi$ non-relativistic state yields Π, Σ^-, Σ^+, and Δ relativistic states and their assignments according to Ω quantum numbers are 1, 0^+, 0^-, and 2. In the case of homonuclear diatomics the non-relativistic states are characterized by either *g* or *u* parities. Thus the assignments should be made according to these parities.

The above background gives us a basis to analyze the wavefunctions of the relativistic electronic states. The discussion here would be on the basis of Cartesian representation of orbitals, which means real representation of π and δ orbitals. A π orbital of a diatomic molecule could have either +1 (notation: π^+) or –1 (notation: π^-) angular momentum projection along the internuclear axis. These orbitals are actually complex, analogous to $l = 1$ and $l = -1$ complex representation of p orbitals of an atom [12]. Like the conversion of p orbital to p_x, p_y, and p_z, π^+ and π^- orbitals could be converted to π_x and π_y orbitals through the following transformations:

$$\pi_x = \frac{1}{\sqrt{2}}(\pi^+ + \pi^-); \pi_y = \frac{-i}{\sqrt{2}}(\pi^+ + \pi^-) \tag{9-10}$$

The dπ and dδ orbitals can also be transformed into real orbitals through analogous transformations. Since most of the electronic structure computations are done in real representation, the spin-orbit matrix elements should be treated as complex. The matrix elements, which are usually encountered, are shown below along with their characteristics (using appropriate representations of the terms α, β, s_x, s_y, and s_z; l_x, l_y and l_z represent components of l):

$$\langle\sigma\alpha|l_x s_x|\pi_y\beta\rangle = \left\langle \sigma \begin{pmatrix}1\\0\end{pmatrix} \middle| l_x \frac{1}{2}\begin{pmatrix}0 & 1\\1 & 0\end{pmatrix} \middle| \pi_y \begin{pmatrix}0\\1\end{pmatrix} \right\rangle = \frac{1}{2}\langle\sigma|l_x|\pi_y\rangle(\text{Real}),$$
$$\langle\sigma\alpha|l_y s_y|\pi_x\beta\rangle = \left\langle \sigma \begin{pmatrix}1\\0\end{pmatrix} \middle| l_x \frac{1}{2}\begin{pmatrix}0 & i\\-i & 0\end{pmatrix} \middle| \pi_x \begin{pmatrix}0\\1\end{pmatrix} \right\rangle = \frac{-i}{2}\langle\sigma|l_y|\pi_x\rangle(\text{Imaginary}),$$
$$\langle\pi_x\alpha|l_z s_z|\pi_y\alpha\rangle = \left\langle \pi_x \begin{pmatrix}1\\0\end{pmatrix} \middle| l_z \frac{1}{2}\begin{pmatrix}1 & 0\\0 & -1\end{pmatrix} \middle| \pi_y \begin{pmatrix}1\\0\end{pmatrix} \right\rangle = \frac{1}{2}\langle\pi_x|l_z|\pi_y\rangle(\text{Real}) \tag{9-11}$$

Let us consider $^2\Pi$ electronic state of heteronuclear diatomic system. It yields 1/2 and 3/2 Ω states. The 1/2 state can be expressed as [13]:

$$\frac{1}{2} = \pi^+\beta = \left(\pi_x\beta + i\pi_y\beta\right)$$

Thus there are two states with β spin of which $\pi_x\beta$ is real and $\pi_y\beta$ is imaginary. They have the same sign and hence represent a 1/2 angular momentum state. This 1/2 state is doubly degenerate as it belongs to $E_{1/2}$ two-dimensional representation of the $C^2_{\infty v}$ double group. Thus there is one more representation, which corresponds to $-1/2$ projection.

$$-\frac{1}{2} = \pi^-\alpha = (\pi_x\alpha - i\pi_y\alpha)$$

A degenerate state is thus obtained for the 1/2 state through spin flipping and changing the sign of the imaginary wavefunction.

The 3/2 state is higher in energy compared to 1/2 state although their spin-orbit components originate from the same non-relativistic state. The relativistic wavefunction of the 3/2 state is determined as follows:

$$\frac{3}{2} = \pi^+\alpha = (\pi_x\alpha + i\pi_y\alpha)$$

Thus the 3/2 state arising from the $^2\Pi$ state consists of two configurations — both with α spins and same signs and the second one is imaginary. Hence both signs and spins are important in deciding the assignment of relativistic electronic states. The difference between the various electronic states is thus dependent on the spin of the wavefunction and sign of both real and imaginary configuration. A detailed account of these features is available in ref [8]. Balasubramanian and coworkers [14] have further extended these ideas of characterizing the wave functions in relativistic configuration interaction (RCI) as flexible correlation group table (CGT) method to deal with more complex nature of relativistic states.

9.3.2. Polyatomic Systems

The analysis of the relativistic wavefunction of a polyatomic molecule primarily needs the correlation of the spin states in the double group and the determination of the relativistic states. The basic operations are more or less similar to the diatomics. The essential steps are as follows:

(a) Correlation of the spin multiplets (D^s) of the electronic states into the double group of the molecular point group.
(b) Multiplication of the spatial symmetry of the non-relativistic electronic state by the irreducible representations spanned by the spin multiplets in a direct product relation.

Table 9-1 C_{2v}^2 Double group character table with correlation of spin functions

		$\overline{C_2}$	$\overline{\sigma_{yz}}$	$\overline{\sigma_{xz}}$	$\overline{E}$	
$C_{\infty v}^2$	**E**	$\mathbf{C_2}$	$\boldsymbol{\sigma}_{\mathbf{yz}}$	$\boldsymbol{\sigma}_{\mathbf{xz}}$		
A_1	1	1	1	1	1	z, $\alpha\beta - \beta\alpha$
A_2	1	1	−1	−1	1	l_z, s_z, $\alpha\beta - \beta\alpha$
B_1	1	−1	−1	1	1	x, l_y, s_y, $\alpha\alpha + \beta\beta$
B_2	1	−1	1	−1	1	y, l_x, s_x,$\alpha\alpha - \beta\beta$
$E_{1/2}$	2	0	0	0	−2	(α, β)

(c) The decomposition of the representation thus obtained into irreducible components using standard direct product relations for the irreducible representations.

Let us exemplify the above discussion using the case of an open shell triatomic system with C_2v symmetry (e.g. PbH_2). Let us consider the $^3B_1$ state (S = 1). The character values for the various members of C_{2v} group are obtained by using standard procedure for any D^j representation.

C_{2v}^2	E	C_2	σ_{xz}	σ_{yz}	$\overline{E}$
D^1	3	−1	−1	−1	3

Thus from C_{2v}^2 character table (Table 9-1) it is obvious that $D^1 = A_2 + B_1 + B_2$. Now $(A_2 + B_1 + B_2) \otimes B_1 = B_2 + A_1 + A_2$. As a consequence, the spin orbit coupling term splits $^3B_1$ into B_2, A_1 and A_2 components. This example required only single-valued representations as the triplet state has integral spin multiplicity. Let us consider a half-integral spin multiplicity such as $^2A_1$:

C_{2v}^2	E	C_2	σ_{xz}	σ_{yz}	$\overline{E}$
$D^{1/2}$	2	0	0	0	−2

Thus $D^{1/2}$ correlates with $E_{1/2}$ representation and $E_{1/2} \otimes A_1 = E_{1/2}$. Since in the double group of C_{2v}^2, there is only one two-valued irreducible representation, all spin multiplets correlate into one or more $E_{1/2}$ representations.

The above discussion provides the basis of correlating a spin state in a double group. The method could be extended to any double group with the primary knowledge of D^s of the electronic states into the double group. A complete form of such correlations for various double groups is available in references [3, 8]. The relativistic computation of polyatomic systems further needs, like the diatomic case, a set of spin functions for a given spatial and spin-orbit state. We will present a brief discussion of this subject here. Complete discussions with all the necessary results are available in reference [8].

First we consider the case of even number of electrons. The state could be singlet, triplet, quintet or higher. The spin correlation function corresponding to a

singlet state for two electrons is $1/\sqrt{2}\ (\alpha\beta - \beta\alpha)$; for the triplet states these spin functions could be $1/\sqrt{2}\alpha\alpha, 1/\sqrt{2}\beta\beta$, and $1/2\ (\alpha\beta + \beta\alpha)$. As discussed earlier in connection with the C_{2v}^2 double group, the triplet state correlates with one or more single valued representation of the double group. For the C_{2v}^2 double group, one can summarize the results in the following Table 9-1 [8, 15].

From the C_{2v}^2 double group Table 9-1, the spin function for a single open shell, viz. α and β, transforms as degenerate $E_{1/2}$ representation. The spin function of the two open shells thus transform as:

$$E_{1/2} \otimes E_{1/2} = A_1 \oplus A_2 \oplus B_1 \oplus B_2$$

The A_1 representation corresponds to singlet, while the A_2, B_1, and B_2 representations are for triplets. The symmetry-adapted spin function $A_2(\alpha\beta + \beta\alpha)$ transform in the same way as l_z operator, while $B_2(\alpha\alpha - \beta\beta)$ and $B_1(\alpha\alpha + \beta\beta)$ transforms as l_x and l_y operator respectively.

All of the odd number of electrons transform as $E_{1/2}$ degenerate representation. Since $E_{1/2}$ representation is two-dimensional, there should be two degenerate spin-orbit states with same energy. If one represents α spin as E_+ and β spin as E_-, all the spin-functions with total M_s values given by $2k + 1/2$, $k = 0, \pm1, \pm2, \ldots$ would transform as E_+, while spin-functions obtained by flipping the spin function would yield E_-. Thus, as an example, the quartet spin functions with ααβ, αβα, βαα, and βββ would transform as E_+, while ββα, βαβ, αββ, and ααα will transform as E_-.

The following direct product rules are useful to determine the spatial symmetries and spin contributions that will mix in either E_+ or E_-.

$$\begin{aligned} A_1 \otimes E_+ &= E_+ & A_2 \otimes E_+ &= E_+ \\ B_1 \otimes E_+ &= E_- & B_2 \otimes E_+ &= E_- \\ A_1 \otimes E_- &= E_- & A_2 \otimes E_- &= E_- \\ B_1 \otimes E_- &= E_+ & B_2 \otimes E_- &= E_+ \end{aligned}$$

Thus, for example, a $^2A_1$ state with an open spin yields E_+ representation and this mix with $^2B_1(\beta)$, $^2A_2(\alpha)$, $^4A_1(\beta\alpha\alpha, \alpha\beta\alpha, \alpha\alpha\beta, \beta\beta\beta)$, $^4A_2(\beta\alpha\alpha, \alpha\beta\alpha, \alpha\alpha\beta, \beta\beta\beta)$, $^4B_1(\alpha\beta\beta, \beta\alpha\beta, \beta\beta\alpha, \alpha\alpha\alpha)$, $^4B_2(\alpha\beta\beta, \beta\alpha\beta, \beta\beta\alpha, \alpha\alpha\alpha)$ states, and so on. It is to be noted that B_1 and B_2 spatial symmetries represent E_- functions and thus are flipped relative to the A_1 and A_2 spin functions. However, the total symmetry of the spin-orbit state, thus obtained, is E_+. This distinction is necessary as the spin-orbit states E_+ and E_-, although are degenerate, do not mix with other because of their mutual orthogonal nature.

The above brief discussions give a background to analyze and interpret the spin-orbit calculation results in any relativistic configuration interaction (RCI), and any other multireference calculations. The results are also helpful to understand the basic inputs for codes (where explicit inclusion of double group characteristic is not available) to calculate spin-orbit effects in molecular systems using double group

symmetry. For all these purposes it would be quite handy to have all these results in tabular forms. There are lots of articles available at present, where these results are explicitly tabulated [3, 8]. With this background of double group symmetry it is now worthwhile to discuss several applications of the double group symmetry in spin-orbit calculations of diatomic and polyatomic systems.

9.4. APPLICATIONS OF DOUBLE GROUP SYMMETRY IN CALCULATING MOLECULAR PROPERTIES

The results of the inclusion of spin-orbit effect in the calculation of the electronic properties of transition metal are available since 1950s. The effect was included in crystal field theory (CFT) and later in ligand field theory (LFT) to study the electronic structure and properties of high-spin and low-spin transition metal complexes and double group symmetry was included for the assignment and splitting pattern of the electronic states [16]. The method is still used in specific cases to interpret the spectral characteristics of the heavy transition metal complexes [17]. The literature in this filed is quite extensive and we will not discuss the details in this review. The discussions presented here are mostly on diatomic and polyatomic clusters with substantial spin-orbit effects. Multi-reference relativistic calculations were used in the framework of double group symmetry to interpret the electronic properties of such systems. We will present also the case of coordination complexes, where double group symmetry has been successfully used in the framework multireference calculations to interpret the splitting pattern of the observed spectra.

9.4.1. Diatomics

An extensive literature is available on the application of relativistic calculations on diatomics including double group symmetry to assign the Ω states. These molecules are either M-X ($C_{\infty v}$ point group) or M-M ($D_{\infty h}$ point group) types. Balasubramanian and co-workers, Roszak, Das and others [8, 18–30] have theoretically investigated a large number of such systems. Most of the studies focus on the spin-orbit stabilization of the systems and interpretation of their observed photoelectron spectra. Here we intend to show how our previous discussions on the use of double group symmetry are being used to assign Ω states of such molecules and interpret the nature of the diatomic relativistic states. For this purpose we will select a few systems with $C_{\infty v}$ and $D_{\infty h}$ symmetries.

9.4.1.1. Diatomics of $C_{\infty v}$ Symmetry

(a) *Iodine oxide (IO)*: Iodine oxide is formed in the troposphere through the reaction of iodine with ozone. This molecule can absorb ultraviolet light and display a rich excited state properties. More importantly, the presence of the heavy atom (I) in the diatomic molecule complicates the excited state spectrum of such molecules due to spin-orbit effect. This is an example of a molecule with odd

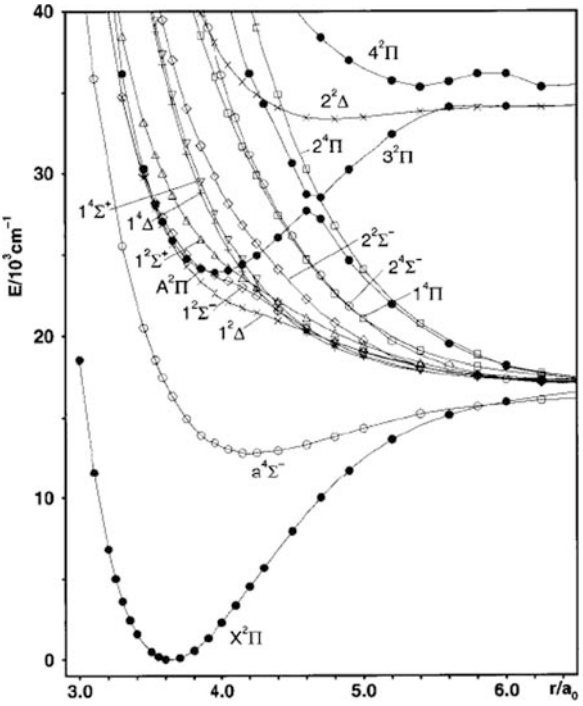

Figure 9-1. Potential energy curves of the low-lying Λ-S states of the IO radical calculated without including spin-orbit coupling

number of electrons with $C_{\infty v}$ symmetry. Roszak and coworkers [19] carried out an extensive analysis of the ground and excited state energy surfaces of this molecule using multireference single and double-excitation configuration interaction (MRSDCI) including spin-orbit effect. Figure 9-1 represents the energy surfaces of several ground and excited states of this molecule without spin-orbit effect.

Let us consider the cases of first three low-lying states $^2\Pi$, $^4\Sigma^-$, and $^2\Delta$. The corresponding D^s for these states are $D^{1/2}$, $D^{3/2}$, and $D^{1/2}$ and they represent $E_{1/2}$, $E_{1/2} \oplus E_{3/2}$, $E_{1/2}$ irreducible representations of the $C^2_{\infty v}$double group. Now following our previous discussions:

$$E_{1/2}(spin) \otimes \Pi(spatial) = E_{1/2} \otimes E_{1/2}$$
$$E_{1/2}(spin) \otimes \Sigma^-(spatial) = E_{1/2}$$
$$E_{3/2}(spin) \otimes \Sigma^-(spatial) = E_{3/2}$$
$$E_{1/2}(spin) \otimes \Delta(spatial) = E_{5/2} \otimes E_{3/2}$$

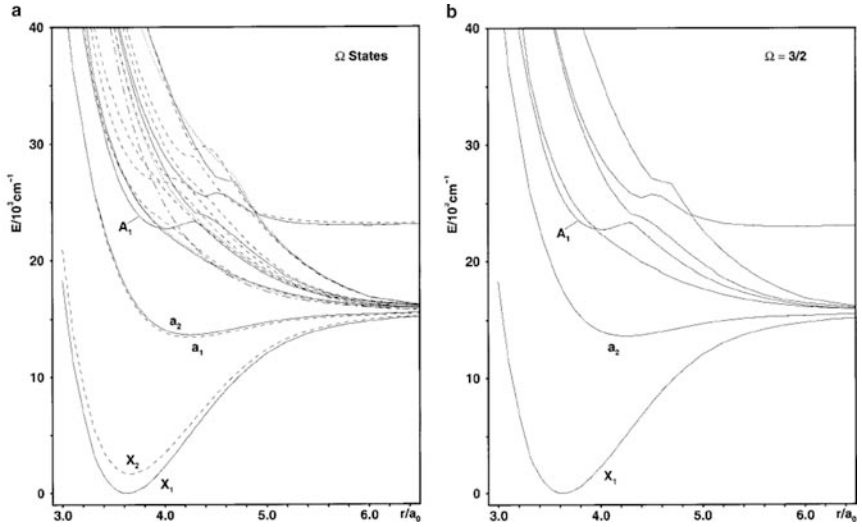

Figure 9-2. Potential energy curves for (**a**) the lowest electronic states of the IO radical calculated including spin-orbit coupling (solid lines for $\Omega = 3/2$ states, dashed lines for $\Omega = 1/2$, dotted lines for $\Omega = 5/2$, and a dot-dashed line for $\Omega = 7/2$) and (**b**) for $\Omega = 3/2$ states

Thus the Ω states corresponding to the $^2\Pi$, $^4\Sigma^-$, and $^2\Delta\Lambda$-S states are (1/2, 3/2), (1/2, 3/2), and (3/2, 5/2). This also represents the splitting patterns of the corresponding Λ-S states. The splitting patterns of the other states could also be similarly worked out. Thus there could be numerous Ω states and the energy surfaces of 1/2, 5/2, and 7/2 are shown in Figure 9-2a. The energy surfaces of the 3/2 states are shown in Figure 9-2b.

The results of the calculations showed that $\Pi_{3/2}\Omega$ ground state is $1,683\,\text{cm}^{-1}$ more stable than the nearest low-lying $\Pi_{1/2}(\Omega)$ state and it is supported by experimental observations ($2,091\,\text{cm}^{-1}$) [19]. If we qualitatively analyze the nature of the wave functions using the configuration (π^3) of the $^2\Pi$ state (already discussed in Section 3.1) we can get an idea of the relative stabilities of the $\Pi_{3/2}$ and $\Pi_{1/2}\Omega$ states. The $\Pi_{3/2}$ state could be represented as $(\pi_x\alpha - i\,\pi_y\alpha)$ and the $\Pi_{1/2}$ state as $(\pi_y\beta - i\,\pi_y\beta)$. Now we have shown in Section 3.1 that this $\Pi_{3/2}$ wave function corresponds to $-1/2(\Pi)$ state, which is degenerate with $\Pi_{1/2}$ state arising from the $^2\Pi$ state with π^1 configuration. The $\Pi_{1/2}$ state wavefunction likewise represents the $-3/2$ degenerate state of the 3/2-state with π^1 configuration. Since 1/2 state is lower in energy than 3/2 with π^1 configuration (Section 3.1), the energy situation is flipped in the present case of $\Pi_{3/2}$ state with higher stability. This argument is valid here since the $\Pi_{3/2}$ and $\Pi_{1/2}$ is not mixed with other states [18]. It is to be mentioned in this connection, that the $\Omega = 3/2$ energy surfaces show lots of avoided crossings (Figure 9-2b). This feature of the 3/2 state is attributed to the different compositions of these Ω states at different I-O bond distances [18]. Since our

concern here is to confine the discussion only to the application of double group formalism in the framework of relativistic calculations, we will not discuss any other results related to the relative energies and frequencies of the various states and their other calculated physical properties here. The details are available in the published work [18].

(b) *SnTe*: This particular example of $C_{\infty v}$ system is representative of diatomic systems with even number of electrons. The binary SnTe systems find technological importance to detect infrared and visible radiations. Barrow and coworkers have experimentally analyzed the band systems of SnTe in both absorption and emission cases [31, 32]. Das and coworkers [26] have carried out the theoretical calculations of this diatomic molecule at the MRSDCI level including spin-orbit effect. The calculated Λ-S states of SnTe are shown in Figure 9-3. The combination of the ground states (^3P_g) of both Sn and Te gives rise to 18 singlet, triplet and quintet states. The first excited states of Sn and Te are both ^1D_g. The combination of Sn (^1D_g) + Te(^3P_g) or Sn (^3Pg) + Te(^1D_g) correlate nine triplets of Σ^+, $\Sigma^-(2)$, $\Pi(3)$, $\Delta(2)$, and Φ symmetries. Figure 9-3 represents only the low-lying electronic states.

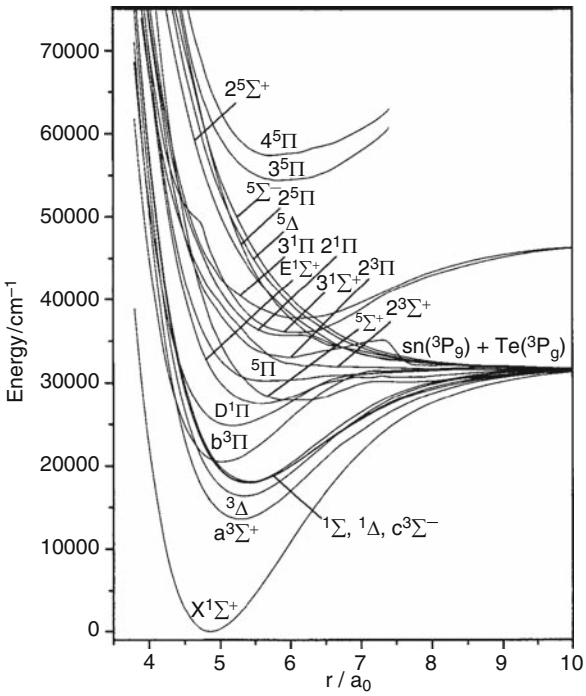

Figure 9-3. Computed potential energy curves of low-lying Λ-S states of SnTe

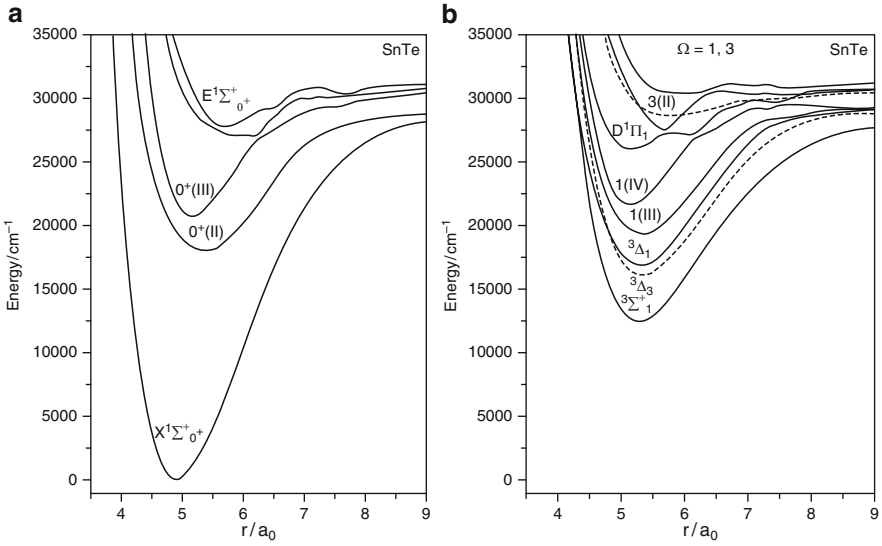

Figure 9-4. (**a**) Computed potential energy curves of (**a**) 0^+ states and (**b**) of 1 and 3 states of SnTe

If we use our previous scheme (Section 3.1) we can find that $X^1\Sigma^+(\sigma^2\pi^4)$, $^1\Sigma^-(\sigma^2\pi^2\pi*^2)$, $^3\Sigma^-$ $(\sigma^2\pi^2\pi*^2)$, and $E^1\Sigma^+(\pi^3\pi*^1)$ states as well as the $^1\Pi$ and the $^3\Pi(\sigma^1\pi^4\pi^{*1})$ states produce $0^+\Omega$ states. Actually there are as many as 50 Ω states possible and all of them were taken into account for spin-orbit calculations. The potential energy curves of the $\Omega = 0^+$ states are shown in Figure 9-4a and b represent $\Omega = 1$ and 3 states. The origin of 1 and 3 states in Figure 9-4b could also be explained following the above analysis of the corresponding Λ-S states. The $X^1\Sigma^+_{0^+}\Omega$ state has a small imaginary part contribution in the wave function due to $^3\Pi(\sigma\pi : \sigma\alpha\pi^-\alpha + \sigma\beta\pi^+\beta = \sigma\alpha(\pi_x - i\pi_y)\alpha + \sigma\beta(\pi_x + i\pi_y)\beta)$ as it is composed through mixing of $X^1\Sigma^+$ (98%; all real) and $^3\Pi$ 2% Λ-S states. The other Ω states are always mixed with high-energy Λ-S states and so they form the higher electronic states in energy spectrum.

9.4.1.2. Systems with $D_{\infty h}$ Symmetry: The Case of Au_2

Au_2 dimer is an even electron system. The gas-phase absorption spectra of Au_2 showed spin-obit stabilization of the ground state and this state was assigned as $X0^+_g$. Das and Balasubramanian [20] have calculated 24 electronic states of Au_2 using relativistic configuration interaction (RCI) technique. The energy surfaces of the singlet and triplet Λ-S states of Au_2 are shown in Figure 9-5a and b respectively. The complete description of these states is available in the original paper [20]. We will discuss here only the formation of a few spin-orbit states (from these Λ-S states) using double group technique.

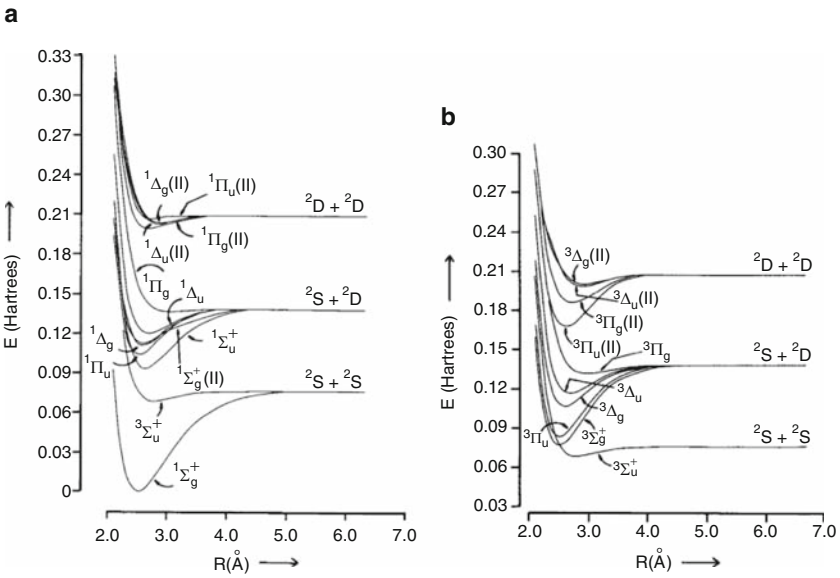

Figure 9-5. Potential energy curves of some of the (**a**) singlet and (**b**) triplet states of Au_2 (CASSCF/FOCI level) without spin-orbit effect

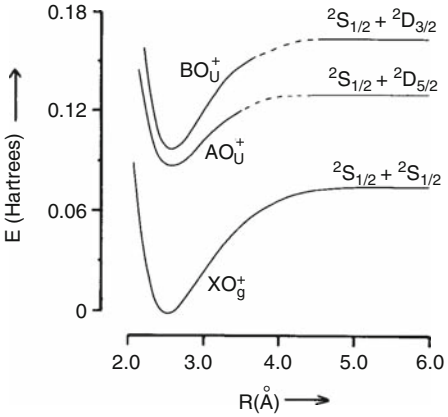

Figure 9-6. Potential energy curves for the three Ω-states of Au_2

The ground state $X\,^1\Sigma_g^+(\sigma_g{}^2)$, and $^3\Sigma_g^+(1\sigma_u{}^1 2\sigma_u{}^1)$, $^3\Sigma_u^+(\sigma_g{}^1\sigma_u^1)$, $^3\Pi_u(\sigma_u{}^1\pi_g{}^3)$, $^1\Sigma_u^+(\sigma_g{}^1\sigma_u{}^1)$ are the first few low-lying electronic states (Figure 9-5a and b). The low-lying excited states are within $20,000\,cm^{-1}$ energy separation (ΔE) with respect to the ground $X\,^1\Sigma_g^+$ state. These states represent (using the procedure described in Section 3.1) $0_g{}^+$, $0_g{}^-$, 1_g, $0_u{}^-$, 1_u, $0_u{}^+$, $0_g{}^+$, 1_g, and 2_g Ω states. The other Ω states arising from the higher Λ-S states [20] could be similarly worked out. All of these Ω states have been computed, but only three of them have been experimentally detected [33]. Figure 9-6 represents the energy surfaces of these

three states and the corresponding configuration of the atoms at the dissociation limit. The results tally quite well with the experiment in terms of the energy separation of the respective states. The $X0_g^+$ state is made up of 96% $^1\Sigma_g^+(\sigma_g^2)$, and 2% $^1\Sigma_g^+(\sigma_u^2)\Lambda$-S states, while $A0_u^+$ (49% $^3\Pi_u(\sigma_u^1\pi_g^3)$, 8% $^3\Pi_u(\sigma_g^1\pi_u^3)$, 21% $^1\Sigma_u^+(2\sigma_g1\sigma_u)$, 12% $^1\Sigma_u^+(1\sigma_g1\sigma_u)$, 7% $^1\Sigma_u^+(1\sigma_g2\sigma_u)$) and $B0_u^+$ (49% $^1\Sigma_u^+(\sigma_g\sigma_u)$, 33% $^3\Pi_u(\sigma_u^1\pi_g^3)$, 3% $^3\Pi_u(\sigma_g^1\pi_u^3)$) Ω states have substantial mixing with the higher Λ-S states. Thus one can qualitatively predict the nature of ΔE between these spin-orbit states through consideration of the mixing of the different Λ-S states in a particular Ω state.

9.4.2. Polyatomic Systems

Polyatomic systems showing spin-orbit stabilization of the ground and higher electronic states cover a large group of clusters/molecules. To name a few are the heavy transition metal clusters [18, 34–36], the carbides, oxides, halides of such metals [37–41] and their metal-ligand complexes [42, 43]. Substantial theoretical investigations have been carried out on such systems to study the relativistic effect on the different electronic states and to help in turn to interpret their observed electronic spectra. In this section we will illustrate a few cases where interesting electronic properties have been explained through inclusion of double group formalism in relativistic calculations.

9.4.2.1. Enhancement and Quenching of Jahn-Teller Distortion due to Spin-Orbit Effect: Pb_3 and Pb_3^+

The Pb_3 and Pb_3^+ clusters represent even and odd electron systems respectively and are ideal systems to demonstrate the relativistic effect on the various electronic states using the formalism of double group theory. When the calculations are carried out without spin-orbit effect, both of these clusters show Jahn-Teller distortion of different electronic states. Inclusion of spin-orbit effect enhances the Jahn-Teller effect in the case of Pb_3 and quenching effect is observed for Pb_3^+ [36].

Pb_3: Figure 9-7a shows the energy surfaces of the various electronic states of $Pb_3(C_{2v})$ as a function of Pb-Pb-Pb angle (θ) at the complete active space multiconfiguration self-consistent field (CASMCSCF) level [36]. Thus the energetics of both angular as well as linear structures of Pb_3 is taken care of. The potential energy curves of these states in Figure 9-7a indicate that the $^1A_1$ and $^1B_2$ curves cross each other around $\theta = 60.0°$. The $^3A_2$ and $^3B_1$ potential energy curves also exhibit the same feature. Both the $^1A_1$ and $^1B_2$ states in the D_{3h} symmetry correlate into $^1E'(1a_1'^2 2a_1'^2 1a_2''^2 1e'^4 2e'^2)$, whereas the $^3B_1$ and $^3A_2$ states correlate into $^3E'(1a_1'^2 2a_1'^2 1a_2''^1 1e'^4 2e'^3)$. As a result one can infer that the $^1A_1$ and $^1B_2$ states are the Jahn–Teller components of the $^1E'$ doubly degenerate state, whereas the $^3B_1$ and $^3A_2$ states are the Jahn–Teller components of the $^3E'$ state. All of these states distorts to a significant extent through $E \otimes e$ Jahn–Teller coupling [44] when spin-orbit effect is not taken into account (Figure 9-7a).

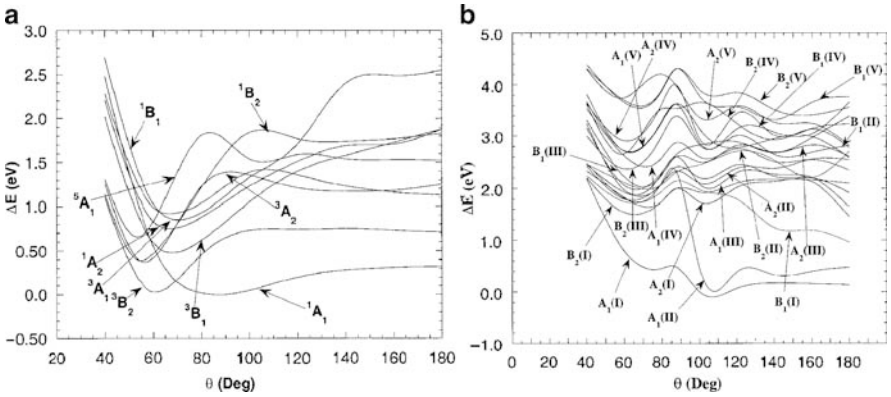

Figure 9-7. (**a**) Potential energy curves for the low-lying electronic states of Pb_3 (CASMCSCF level). The curves are drawn as a function of the Pb-Pb-Pb bond-angle (θ). (**b**) Potential energy curves (as a function of θ) for the low-lying relativistic states of Pb_3 using relativistic configuration interaction (RCI) calculations

Figure 9-7b shows the potential energy surfaces for the relativistic states of Pb_3 (C_{2v}^2 double group) as a function of θ using RCI calculations. All the low-lying states with appropriate spin combinations yielding the state of desired double group symmetry were included. Following our previous discussion in Section 9.3.2, the $^1A_1$ state yields the A_1 state in C_{2v}^2 double group. The lowest $^3B_2$ (D^1 spin multiplet) state yields $(A_2 + B_1 + B_2) \otimes B_2 = B_1 + A_2 + A_1$ states in the double group. Thus an A_1 component of $^3B_2$, which has the spin combination $\alpha\beta - \beta\alpha$, mixes with the $^1A_1$ state.

The bending potential energy surfaces of these relativistic states reveal several interesting features. First, when compared with the energy surfaces of the electronic states of Pb_3 without SO effect (Figure 9-7a), it is obvious that the spin–orbit effect completely changes the energy surface's profile. Most of the potential energy curves have multiple minima due to avoided crossings induced by the spin–orbit coupling. This difference of the energy profiles of relativistic states with respect to the nonrelativistic states is comprehensible in view of the nonadiabatic nature of the surface due to strong SO coupling. The lowest two relativistic states, A_1(I) and A_1(II) exhibit avoided crossings. In fact these two states are so interesting in that they are allowed to cross nonrelativistically, as one is a dominant $^1A_1$ state and the other is a $^3B_2$ state. However, from our previous discussion, one of the spin–orbit components of the $^3B_2$ state is A_1 in the C_{2v}^2 double group and thus the A_1 component of the $^3B_2$ state mixes with the A_1 component of the $^1A_1$ state when SO effects are included. It has been reveled from the analysis of the composition of these states [36] that they have varying compositions at different θ values through the mixing of the $^1A_1$ and $^3B_2$ states. Thus although these states compete for ground state in nonrelativistic domain, the mixing separates them relativistically. As a result both of these potential energy surfaces look like asymmetric double well due to several avoided crossings.

The interplay between the Jan-Teller distortion and the spin-orbit coupling gives rise to more than one potential minimum in the curves in Figure 9-7b. Figure 9-7a shows that the $^3B_2$ state has D_{3h} symmetry at the potential minimum and correlates with the $^3A_2{}'$ state. This state correlates into $A_1{}' \oplus E''$ states in the $D_{3h}{}^2$ double group. The $^1A_1{}'$ state on the other hand, correlates into $A_1{}'$ state of the $D_{3h}{}^2$ double group. Consequently at the D_{3h} geometry, the $A_1{}'$ states arising from the $^3A_2{}'$ and the $^1A_1{}'$ states can mix. In the C_{2v} group this is manifested as spin–orbit mixing in the A_1 and B_2 components and it is quite substantial [36]. Thus the first minimum in the A_1(I) curve is due to the mixing of these triplet and single states through spin–orbit coupling. The second minimum in the A_1(I) curve is due to the interplay between Jahn–Teller distortion and spin–orbit coupling. Many other electronic states behave in a similar manner due to the strong interplay between the Jahn–Teller and spin–orbit couplings and thus giving rise to unusual shapes in the bending potential energy curves of the excited electronic states in Figure 9-7b. Although rigorous theoretical argument cannot be given at present for the enhancement of the Jahn-Teller distortion, the avoided crossing of the A_1(I) and A_1(II) due to mixing of the $^1A_1$ and $^3B_2$ states could be considered as a key factor for this phenomenon.

Pb_3^+: Figure 9-8a shows the energy surfaces of the various electronic states of $Pb_3{}^+(C_{2v})$ as a function of θ at the CASMCSCF level [36]. It is evident from the potential energy curves, that the $^2B_2$ and $^2A_1$ states have almost the same energy at $\theta = 60°$. This situation is also true for the $^2B_1$ and $^2A_2$ states. The $^2A_1$ and $^2B_2$ state correlate into $^2E'$ in the D_{3h} symmetry $(1a_1{}'^2 2a_1'^2 1a_2{}''^2 1e'^4 2e'^1)$, whereas the $^2B_1$ and $^2A_2$ states become $^2E''(1a_1{}'^2 2a_1{}'^2 1a_2{}''^1 1e'^4 2e'^2)$. As a result one can infer that the $^2A_1$ and $^2B_2$ states are the Jahn–Teller components of the $^2E'$ state, while the $^2B_1$ and $^2A_2$ states are the Jahn–Teller components of the $^2E''$ state in D_{3h} group.

The bending potential energy curves of $Pb_3{}^+$ with SO effects are presented in Figure 9-8b. The first ten roots of the relativistic E state are plotted as a function

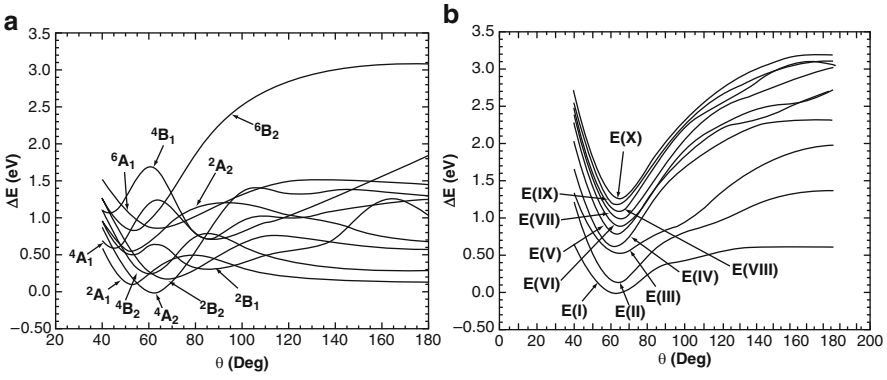

Figure 9-8. (**a**) Potential energy curves for the low-lying electronic states of $Pb_3{}^+$ (CASMCSCF level). The curves are drawn as a function of θ as defined in Figure 9-7. (**b**) Potential energy curves (as a function of θ) for the low-lying relativistic states of $Pb_3{}^+$ using RCI calculations

of the apex angle θ of the triangular geometry. The calculated compositions showed that the spin states of different multiplicities are mixed to generate these states [36]. All the states presented here have minimum at θ = 60°. The E(I) state at θ = 60° is formed through mixing of the $^2A_1$, $^2B_2$, $^4B_1$, and $^4A_2$ (with major contribution from $^2A_1$) states, whereas the E(II) state (at θ = 60°) is formed through mixing of the $^4A_2$, $^2B_1$, $^4A_1$, and $^6B_2$ (with major contribution from $^4A_2$) states. As a result their minima are within 0.1 eV energy separations (Figure 9-8b).

The Pb_3^+ ion is very interesting in that the Jahn–Teller distortion is completely quenched by the spin–orbit coupling. When two states are degenerate at θ = 60°, they undergo avoided crossing at θ = 60° due to spin–orbit mixing. The spin–orbit stabilization becomes larger and thus overcomes the Jahn–Teller stabilization. The ground state of Pb_3^+ is a $^4A_1''$ state (correlates with the minima $^4A_2$ state in Figure 9-8a) in the absence of spin–orbit coupling. It has been found that the first excited $^2E'$ and $^4A_2'$ states in D_{3h} structure [36] are virtually degenerate and close to the ground state. The $^2E'$ state undergoes Jahn–Teller distortion into the $^2A_1$ and $^2B_2$ C_{2v} pairs in the absence of spin–orbit coupling. However, when spin–orbit effects are included the $^4A_1''$ state can be expressed as the direct product $(E_{1/2} \oplus E_{3/2}) \otimes A_1''$, which correlates into $E_{5/2} \oplus E_{3/2}$ spin–orbit states. The spin–orbit states of the $^2E'$ state are obtained as the direct product $E_{1/2} \otimes E'$, which correlates into $E_{3/2} \oplus E_{5/2}$. Thus the spin–orbit states arising from the $^2E'$ state have identical symmetries to the spin–orbit states arising from the $^4A_1''$ state. The other $^4A_2''$ state can be expressed as the direct product $(E_{1/2} \oplus E_{3/2}) \otimes A_2''$, which correlates into $E_{1/2} \oplus E_{3/2}$ spin–orbit states. Therefore the $E_{3/2}$ components of all three states can strongly couple, thereby quenching the Jahn–Teller distortion completely. Likewise the $E_{5/2}$ state of the $^2E'$ state can interact strongly with the 5/2 state of the $^4A_1''$ state. The calculated stabilization due to Jahn–Teller distortion is only about 0.5–1 kcal/mol for the $^2E'$ state. But the spin–orbit stabilization is substantially larger (9 kcal/mol), and thus overcomes the Jahn–Teller stabilization. Consequently all of the electronic states of Pb_3^+ retain their D_{3h} structures due to strong spin–orbit coupling in the electronic states.

9.4.2.2. Emission Properties of Metal Complexes

Cyclometalated Pt(II) complexes might be phosphorescent, since, for instance, bis-[2-(2-thienyl)-pyridine] platinum ($Pt(thpy)_2$) has a strong emission from the triplet states at 580 nm in both the photoluminescence and electroluminescence spectra [45, 46]. Such properties of the organic ligand coordinated transition metal complexes are important in the fields of organic light emitting diodes (OLED) [46]. Strong spin-orbit coupling among the low-lying states is the key factor of an efficient OLED, as the spin-orbit coupling provides a fast intersystem crossing between states of different multiplicities. $Pt(thpy)_2$ (Figure 9-9) is such a model system and was investigated at the MCSCF and second-order configuration interaction (SOCI) level of theories to study the spin-orbit coupling [43].

The $Pt(thpy)_2$ complex has a C_2 point group symmetry. Thus the spin-orbit calculations are to be carried out under C_2^2 double group formalism. In absence of

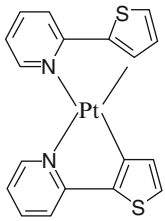

Figure 9-9. The schematic structure of $Pt(thpy)_2$

spin-orbit effect the ground state of this molecule is singlet, $S_0(^1A)$. The lowest excited state triplet, $T_1(^3A)$, is 2.36 eV above the ground state. The other low lying states $T_2(^3B)$, $T_3(^3B)$, $S_1(^1A)$, $S_2(^1B)$, and $S_3(^1B)$ are respectively 2.55, 2.70, 2.73, 2.97, and 3.24 eV above the ground state [43]. Thus these low-lying states are quite closely spaced with respect to the low-lying T_1 and can mix through spin-orbit coupling.

The $D^0(S = 0)$ and $D^1(S = 1)$ correlates respectively with the A and A + 2B irreducible representations of the C_2^2double group. Therefore the relativistic states constructed from ^1A and ^1B are A or B respectively. For the triplet states (^3A or ^3B) the splitting patterns will be either A + 2B (for ^3A) or B + 2A (for ^3B). The appropriate spin combinations for the singlet and triplet states could be derived as in case of C_{2v}^2 double group (Table 9-1). Considering the correlation between the irreducible representations of the C_{2v} and C_2 group, the job could be simplified further. Since the irreducible representation A in C_2 correlates with A_1 or A_2 in C_{2v} point group, the appropriate spin function for the singlet should be (αβ–βα). The triplet combinations should be (αβ + βα) for A and (αα + ββ) or (αα–ββ) for B irreducible representation of the C_2^2 double group.

Figure 9-10 shows the energy surfaces of the first ground and first 12 low-lying spin orbit states of $Pt(thpy)_2$ along the linear synchronous transit (LST) path (between a C_2 and C_{2v} structures). For simplicity, the spin-mixed (SM) states are named by their energetic order at the energy minimum of the adiabatic S0 state, such as SM0, SM1, SM2, and so on. As mentioned in the previous section, the lowest spin-mixed state SM0 consists of the adiabatic ground state $S0(^1A[A])$ with the weight of 99%, where the spin function $1/\sqrt{2}\ (\alpha\beta - \beta\alpha)$ belongs to the A representation of C_2^2double group indicated by [A]. The lowest excited state SM1 has $T_1(^3A[A])$ as a main configuration, where the spin function $1/\sqrt{2}\ (\alpha\beta + \beta\alpha)$ also belongs to the A representation of C_2^2double group symmetry. Since this state does not have a large singlet component, the transition dipole moment (TDM) is very small (0.0007 eÅ), and as a result, the transition probability is considerably small. The second lowest state SM2 also has $T_1(^3A[B])$, where its spin function is $1/\sqrt{2}\ (\alpha\alpha + \beta\beta)$ and is only 21 cm^{-1} higher than SM1. The TDM between SM0 and SM2 (0.0904 eÅ) is larger than that between SM0 and SM1, as SM2 has a small component of $S_3(^1B[A])$ and the adiabatic TDM (1.4 eÅ) between $S0(^1A[A])$ and $S_3(^1B[A])$ is remarkably larger than the others. As a result, the transition probability

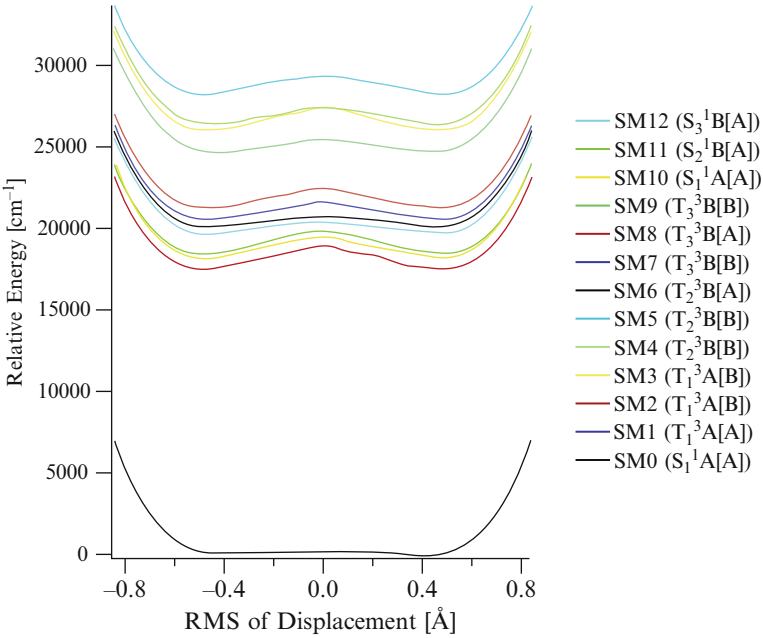

Figure 9-10. Potential energy curves for 13 low-lying spin-mixed states in $Pt(thpy)_2$ obtained at the MCSCF+SOCI/SBKJC+p level of theory. The main adiabatic component in each spin-mixed state is shown in parentheses

between SM2 and SM0 is higher that that between AM1 and SM2 [43]. SM1 and SM2 should be recognized as the sublevels of T_1 as both of the states contain irreducible components of ^{3}A-state (A + 2B, as discussed earlier). The third sublevel of T_1 appears as SM3 (containing the B component of ^{3}A). Using the similar argument of the splitting patterns of the triplet state, SM4, SM5, and SM6 are the sublevels of T_2 (^{3}B[B]), and SM7, SM8, and SM9 are the sublevels of T_3 (^{3}B[A]). SM8 has a large TDM to the ground state SM0 (0.6652 eÅ), but it may be possible that the nonradiative transition from these states to lower excited spin-mixed states would be very fast because the state is high in energy, so that the emission from these states would not be observed. Thus the outcome of the theoretical investigations is that the emission from SM2 would be observed rather than from SM1, and the main peak of the emission would appear at the energy of 2.18 eV [43]. In addition, because SM2 has large adiabatic triplet components, this emission should be recognized as *phosphorescence*. SM10, SM11, and SM12 have adiabatic S_1 (^{1}A[A]), S_2 (^{1}B[A]), and S_3 (^{1}B[A]) components as a main configuration, respectively. These states have large TDMs to the ground state, but fast nonradiative relaxation (or intersystem crossings) is expected to occur from these states to low-lying *excited* states (the Kasha rule) and, as a result, no emission would be observed from these states.

This conclusion was supported by several experiments. A strong emission was observed at $\lambda_{max} = 580\,nm$ (2.13 eV) in both the photoluminescence and electroluminescence spectra of $Pt(thpy)_2$ [45, 46]. Yersin et al. also reported that the transition between the lowest triplet sublevel, and the ground state is forbidden, and that the radiative transition from the next low-lying triplet sublevel is faster, when the complex was dissolved in Shpolskii matrix [47].

9.4.2.3. More Recent Developments in the Applications of Double Group Theory

Recently Balasubramanian [48] has developed the character theory of relativistic double group spinor representations in order to represent the total rovibronic states of nonrigid molecules. It is shown that the double groups can be represented in terms of *wreath products* and powerful matrix cycle type generators that are used to construct their character tables. It is shown that these tables are of use when spin–orbit coupling is included in the Hamiltonian even for molecules containing lighter atoms. Several examples of double groups of wreath products such as $\{S_2[S_2] \times I\}^2$, $\{S_2[S_3]\}^2$, $\{S_4[S_2]\}^2$, etc., were considered as representatives of nonrigid Tl_2H_4, $Pb_2(CH_3)_6$, $(PoH_2)_4$, etc. molecules (S_n: symmetric permutation group; I: isodynamic group; see ref. [4] for their definitions). It is shown that the tunneling splittings and the nuclear spin statistical weights can be obtained for such species using the character tables thus constructed.

9.5. TIME REVERSAL

In quantum mechanics, the invariance of physical laws under an associated transformation often generates conservation laws or selection rules that follow from the invariance of the Hamiltonian H under transformation. The idea of time reversal occurs in order to conserve certain properties, which is occurring due to a phenomenon called CP violation (C: charge conjugation operator; P: parity operator). Thus it is worthwhile to introduce the definitions of these terminologies first before discussing time reversal.

9.5.1. Parity

Let V be a potential, which is symmetric about the origin (i.e. $V(-x) = V(x)$). This implies that if $\psi(x)$ is a solution of the Schrödinger equation so is $\psi(-x)$. For one-dimensional case, it could be written,

$$-\frac{\hbar^2}{2m}\frac{d^2\psi(-x)}{dx^2} + V(-x)\psi(-x) = E\psi(-x) \tag{9-12}$$

And for $V(-x) = V(x)$,

$$-\frac{\hbar^2}{2m}\frac{d^2\psi(-x)}{dx^2} + V(x)\psi(-x) = E\psi(-x) \tag{9-13}$$

If both $\psi(x)$ and $\psi(-x)$ solve the Schrödinger equation with the same eigenvalue E, they must be related to each other as,

$$\psi(x) = \alpha\psi(-x) \tag{9-14}$$

Letting $x \to -x$ generates $\psi(-x) = \alpha\psi(x)$, and insertion of it in Eq. (9-14) gives, $\psi(x) = \alpha\psi(-x) = \alpha(\alpha\psi(x)) = \alpha^2\psi(x)$ which leads to $\alpha = \pm 1$. Then either $\psi(-x) = \psi(x)$ (wavefunction of even parity) or $\psi(-x) = -\psi(x)$ (wavefunction of odd parity), and this leads to the concept of parity operator P. It causes change in sign when $x \to -x$ in the wave function.

$$P\psi(x) = \psi(-x) \tag{9-15}$$

Generally even powers lead to a function with even parity, while the odd powers lead to odd parity. Some of the properties of P are as follows.

1. Applying the parity operator twice in succession brings the original wave function back.

$$P^2\psi(x) = P\psi(-x) = \psi(x) \tag{9-16}$$

2. Reflection through y-axis brings back the original state. If ψ is even, one sees same function values through y-axis reflection and for odd ψ, the negative of the function values is observed under the same operation. It follows that $P^2 = I$ (identity matrix), and the eigenstates of the parity are $\pm 1 (P|\psi\rangle = \pm|\psi\rangle)$.
3. If $|\psi\rangle$ is an angular momentum state with angular momentum $L(i.e.|\psi\rangle = |L, m_z\rangle)$ (m_z is the component of the magnetic quantum number), then

$$P|L, m_z\rangle = (-1)^L|L, m_z\rangle \tag{9-17}$$

Since if $\alpha = \pm 1$, both ψ(x) and ψ(–x) solve the Schrödinger equation with same eigenvalue, the generalization is if P and H commute (i.e. [P,H] = PH – HP = 0), the parity is conserved. Thus a state with parity α cannot evolve into a state with parity –α, since the Hamiltonian governs the true evolution of the states.
$P(H|\psi\rangle) = P(E|\psi\rangle) = EP|\psi\rangle$ if $|\psi\rangle$ is a non-degenerate eigenstate of H with eigenvalue E and for the commutation of P and H, $P(H|\psi\rangle) = H(P|\psi\rangle) = E(P|\psi\rangle)$. So the eigenstates of H are also the eigenstates of the parity operator and the eigenvalues of P are $\alpha = \pm 1$. This precludes states of mixed or infinite parity and physically this mathematical constraints means that particles are either fermions or bosons.
4. In the case of fermions, particles with spin 1/2 have positive parity, while particles with spin –1/2 have negative parity. Thus electrons have α = +1 while positrons have α = –1. Bosons have same intrinsic parity for both particles and anti-particles.
5. Parity is a multiplicative quantum number. If $|\psi\rangle = |a\rangle|b\rangle$ defines a composite system and if the parities of the individual states are P_a and P_b respectively, the

parity of the composite state (P_ψ) is given by $P_a P_b$. Parity is *conserved* in electromagnetic and strong interactions but is *not conserved* for weak interactions.

9.5.2. Charge Conjugation

Charge conjugation, represented by an operator C, converts particles into antiparticles. If $|\psi\rangle$ represents a particle and $|\overline{\psi}\rangle$ an antiparticle state, then $C|\psi\rangle = |\overline{\psi}\rangle$, and $C|\overline{\psi}\rangle = |\psi\rangle$. It thus follows that,

$$C^2|\psi\rangle = CC|\psi\rangle = C|\overline{\psi}\rangle = |\psi\rangle \tag{9-18}$$

This implies $C = \pm 1$. The charge conjugation is also like a parity operator in that it is multiplicative quantum number. Since charge conjugation converters particles into antiparticles and vice versa, it reverses the sign of all quantum numbers (also changes the sign of magnetic moment). It has also conservation properties similar to the parity i.e. C is not conserved for weak interactions and conserved for strong interactions.

The individual violation of charge conjugation and parity in weak interactions led to the hope that combination of them would be conserved. It is almost a rigorous rule, but there is a slight violation and it is known as CP violation. An example is the case of long-lived 'K' meson state. It has been observed [49] that the amount of CP violation is of the order of 2.3×10^{-3}. This CP violation happens because, for a small fraction of time, the long-lived neutral 'K' meson state $|K_L\rangle$ is found to be in $|K_1\rangle$, giving the unexpected decay.

9.5.3. CPT Theorem and Concept of Time Reversal

The concept of time reversal symmetry was needed to restore the invariance due to CP violation. This is another discrete transformation that changes a state $|\psi\rangle$ into $|\psi'\rangle$, which evolves with time in the negative direction. Momentums change sign i.e. linear momentum $p \rightarrow -p$ and angular momentum $L \rightarrow -L$, but all other quantities retain the same sign. The time reversal operator T acts to transform the state as

$$T|\psi\rangle = |\psi'\rangle \tag{9-19}$$

The operator T is *antiunitary* and *antilinear*, which means

$$T(\alpha|\psi\rangle + \beta|\varphi\rangle) = \alpha^*|\psi'\rangle + \beta^*|\varphi'\rangle \tag{9-20}$$

$$\text{and } \langle T\varphi|T\psi\rangle = \langle\varphi|\psi\rangle^* \tag{9-21}$$

The operator T could be written as product of an operator Θ (that converts states into their complex conjugates, $\Theta\psi = \psi^*$) and a unitary operator U (defined as $\langle U\varphi|U\psi\rangle = \langle\varphi|\psi\rangle$) as,

$$T = U\Theta \tag{9-22}$$

If the T commutes with H ([T, H] = 0) and if $|\psi\rangle$ satisfies the Schrödinger equation, $T|\psi\rangle$ will also satisfy Schrödinger equation when $t \rightarrow -t$ (hence the name time reversal operator). If the laws of physics are unchanged under time reversal, then they are symmetry of the system. It is to be further noted that for a spinless particle U is the unit operator in Eq. (9-22) and for a particle with spin $T = i\sigma_y\Theta$ (in the Pauli matrix representation).

Now according to CPT theorem, if C, P and T are taken together, we have an exact symmetry and so the laws of physics are invariant. This means that if matter is replaced by antimatter (charge conjugation), momentum is reversed with spatial inversion (parity conjugation) and time is reversed, the result would be universe indistinguishable for one we live in. For CPT theorem to be valid, all three symmetries must be valid. If one or two symmetries are violated, the third must also be violated. For example, in the case of weak interactions there is CP violation and to compensate it there must be T violation.

9.5.4. Properties of T and Its Implication in Molecular Properties

T does not have eigenvalues, so it is not possible to classify a quantum state as being even or odd under time reversal. An illustration is the effect of T on the atomic state $|J, M\rangle$, where the total angular momentum is specified by the usual quantum numbers J and M and can have both orbital and spin contributions. Using a particular phase convention, it is found that,

$$T|J, M\rangle = (-1)^{J-M+q}|J, -M\rangle \tag{9-23}$$

where q is the sum of the orbital quantum numbers of all the electrons in the atom. For the special case of the spin states $\alpha = |(1/2)\,,\ (1/2)\rangle$ and $\beta = |(1/2)\,, -(1/2)\rangle$ for a single electron (9-23) gives

$$\begin{aligned} T\alpha &= \beta \\ T\beta &= -\alpha \end{aligned} \tag{9-24}$$

Hence, T interconverts the two spin states (within an essential phase factor ± 1).

Unlike states, quantum-mechanical operators can be classified as even or odd under time reversal. Time-even (+) and time-odd (−) operators are defined by

$$\begin{aligned} TA(+)T^{-1} &= A(+)^{\dagger} \\ TA(-)T^{-1} &= -A(-)^{\dagger} \end{aligned} \tag{9-25}$$

Operators usually have the same behavior under time reversal as the associated observables. From (9-25), the expectation values of a time-even operator have the same magnitude and sign in ψ and $T\psi$, whereas those of a time-odd operator have

the same magnitude but opposite sign. Hence, the expectation value of a time-odd operator is zero in a non-degenerate state since ψ and $T\psi$ must be the same state in this case.

Although T does not have eigenvalues, the operator T^2 has the eigenvalue $\varepsilon = \pm 1$ for a system with an even number of electrons and –1 for an odd number. This leads to Kramers theorem [3, 7]. According to this theorem, in the presence of any static electric potential, but in the absence of an external magnetic field, the energy levels of a system with an odd number of electrons (or half odd-integral angular momentum) must have even-fold degeneracy. Pairs of such degenerate states are interconverted by T, with $T\psi$ called the Kramer's conjugate of ψ. Equation (9-23) is an example. The time reversal converts $|J, M\rangle$ into the new state $|J, -M\rangle$, which is orthogonal to and degenerate with the original one and corresponds to a reversal of the angular momentum.

As we have seen in Eq. (9-17), parity does not convert $|J, M\rangle$ into a new state as P, unlike T and has eigenvalues of ± 1. If two states of opposite parity, such as ψ_{2s} and ψ_{2p_0} in atomic hydrogen, are degenerate, or nearly so, the system can exist in a state of mixed parity and as such can support odd-parity observables such as the electric dipole moment. Since pairs of mixed parity states such as $\psi_{\pm} = {}^{1}\!\Big/\!_{\sqrt{2}}\left(\psi_{2s} \pm \psi_{2p_0}\right)$ are interconverted by P, it suggests a loose analogy, where states such as $|J, M\rangle$ and $|J, -M\rangle$ could be thought of having *mixed time parity* because of their interconversion by time reversal (even though associated states of definite time parity do not exist). *Mixed time parity* is an essential requirement for a state to support time-odd observables.

This distinct behavior of general angular momentum states under $P$and Tlies at the heart of the different behavior of atoms and molecules in electric and magnetic fields, exemplified by the Stark and Zeeman effects. In the Stark phenomena, the first order effects require a permanent electric dipole moment, which has odd parity but is time-even. In the Zeeman case it requires a permanent magnetic dipole moment, which has even parity but is time-odd. Time reversal finds application in the behavior of molecules in electric and magnetic field, antisymmetric light scattering, Raman EPR, optical activity and related degeneracy, magneto-chiral phenomena, optical NMR and ESR, spin-dependent intermolecular forces, velocity-dependent property surfaces and vibrational circular dichroism, true and false chirality and photon static magnetic field. A comprehensive review of such applications is available in an earlier article of Barron and Buckingham [10]. We will not go into the details of them. Our main interest here is the symmetry related use of time reversal. We thus intend to conclude our present review with a brief discussion on the relation of time reversal with group theory.

9.5.5. Time Reversal in Group Theory

Spatial symmetry operations could be augmented with time reversal to encompass some of the more subtle aspects of molecular behavior. Permanent electric ($\boldsymbol{\mu}$) and magnetic ($\boldsymbol{m}$) dipole moments provide an example. As far as spatial symmetry is

concerned, the difference between electric and magnetic dipole moments is that $\boldsymbol{\mu}$ is a polar vector and so transforms like a translation, whereas $\boldsymbol{m}$ is an axial (pseudo) vector and so transforms like a rotation. In the elementary theory, if the integrand in $\langle\psi_n|\mu_a|\psi_n\rangle$ contains the totally symmetric irreducible representation, the molecule in the quantum state ψ_n is able to support the α-component of an electric dipole moment. Because the operator $\boldsymbol{\mu}$ is time-even, this gives the correct answer, but because $\boldsymbol{m}$ is time-odd, the same argument applied to $\langle\psi_n|m_a|\psi_n\rangle$ can give the wrong answer because it only has nonzero expectation values in degenerate states.

The usual selection rules for transition matrix elements between states of *different* levels are unchanged whatever the behavior under time reversal of the operators and wave functions, but for matrix elements between component states of the *same* degenerate level, the group-theoretical background to the selection rules must be modified. From the discussions of the previous section (Section 9.5.4),

$$\langle T\psi_j|V|\psi_k\rangle = \varepsilon\lambda\langle T\psi_k|V|\psi_j\rangle \tag{9-26}$$

where ε, the eigenvalue of T^2, equals $+1$ or -1, depending on whether there is an even or odd number of electrons, and λ equals $+1$ or -1, depending on whether the operator V is time-even or time-odd. Hence, depending on whether $\varepsilon\lambda$ is positive or negative, $\langle T\psi_j|V|\psi_k\rangle$, and therefore also $\langle\psi_j|V|\psi_k\rangle$ belong to the representation $[\mathrm{R}^2]\otimes\mathrm{R_V}$ or $\{\mathrm{R}^2\}\otimes\mathrm{R_V}$ [3,10]. The R terms represent the irreducible representations and the square and curly brackets denote the symmetrized and antisymmetrized parts of the direct product, respectively. In the odd-electron case, the representation refers to the appropriate double group. Formalisms are available for the construction of relativistic symmetry-adapted molecular basis functions under consideration of time reversal invariance. The theory is applicable to the finite double point groups $\mathrm{C_n}^2$, $\mathrm{C_{nh}}^2$, $\mathrm{S_n}^2$, $\mathrm{C_{nv}}^2$, $D_{\mathrm{n}}{}^2$, $\mathrm{D_{nd}}^2$, $D_{nh}{}^2$, T^2, $\mathrm{T_h}^2$, $\mathrm{T_d}^2$, O^2, and $\mathrm{O_h}^2$. It is based on the linear combination of atomic orbital (LCAO) method and projection operator technique is employed to construct molecular symmetry orbitals from atomic orbitals [50,51].

9.6. CONCLUDING REMARKS

The present review is primarily motivated to introduce the concept of double groups in the calculations and interpretation of relativistic properties of molecules. After a brief introduction to the basic concepts of double groups and the ways to characterize the spin-mixed molecular states using the double group concept, several illustrative cases have been discussed, which included diatomic and polyatomic systems with diverse electronic properties. The use of time reversal in studying molecular properties and related spectra is relatively new. In the present article we have briefly discussed the concept and use of this relativistic property. The concept of time reversal has been introduced by considering it as a symmetry property to mitigate the problem due to CP violation. The special fields of applications of time reversal have been indicated with the relation of it to the double group concept.

Although not very popular yet, the applications of these relativistic symmetries to explain diverse molecular electronic properties are drawing attention in recent times and we believe that this article would be useful to the readers (especially beginners) to cope up with the basic concepts of this increasing developing field.

ACKNOWLEDGEMENTS

The authors acknowledge the support of NSF CREST funding (No. HRD-0833178).

APPENDIX

Construction of a double group: The definition of a double group and its basic characteristics has already been discussed in Section 9.2. Here we will make a brief discussion on the procedure for generation of the character table of a double group taking illustrations of $D_3{}^2$ and $D_4{}^2$ double groups. The character table could be derived from the corresponding point group. The procedure involves determination of the number of elements, the number of classes and the number of irreducible representations. The dimension of the irreducible representation is obtained by requiring that the sum of the squares of the irreducible representations (g) is equal to the order of the double group. Once the dimension is known, the characters can be obtained from a mapping of the corresponding representations of the three-dimensional rotation-reflection ($R_h(3)$) group (for definition of such group see, e.g. [4]) on to the elements in question.

If a set of elements R forms a class in an ordinary point group, there is a class R and class $\overline{R}$ in the double group. If, of course, R corresponds to C_2, and if there is C_2' perpendicular to original C_2, then $\overline{C_2}$ and $\overline{C_2}'$ belong to the same class of C_2 and C_2'. For a two-dimensional representation, the relation $\overline{C_2} = SC_2S^{-1}$ is satisfied if S is a rotation by 180° about an axis perpendicular to C_2. If there are no such orthogonal sets of C_2's, then the double group will have twice as many classes as well as irreducible representations as the ordinary group. If there are such sets of C_2's, then the double group will have correspondingly fewer classes and irreducible representations. For example the D_3 point group has classes $\{E, 2C_3, 3C_2\}$ and since there are no C_2''s orthogonal to C_2's, the $D_3{}^2$ double group will have classes $\{E,\ 2C_3,\ 3C_2,\ \overline{E},\ 2\overline{C_3},\ 3\overline{C_2}\}$. The D_4 group on the other hand has classes $\{E,\ 2C_4,\ C_2(C_4{}^2), 2C_2',\ 2C_2''\}$. The class structure of the double group is,

$$\left\{\begin{array}{r} \overline{C_2},\ 2\overline{C_2'},\ 2\overline{C_2''},\ \overline{E},\ 2\overline{C_4}, \\ E,\ 2C_4,\ C_2,\ 2C_2',\ 2C_2'' \end{array}\right\}$$

Concerning the dimensionalities, we have for $D_3{}^2$

$$\sum_{i=1}^{6} g_i^2 = 12 \tag{9-27}$$

For the D_3 point group there are three irreducible representations and the group order is 6. Consequently, for the new representations we have

$$\sum_{i=1}^{3} g_i^2 = 6 \tag{9-28}$$

The only solution of this gives us two one-dimensional and one two-dimensional $(1^2 + 1^2 + 2^2)$ representation.

The ${D_4}^2$ group has seven irreducible representations. The D_4 point group has order 8 with five irreducible representations. This means that for representation we have

$$\sum_{i=1}^{2} g_i^2 = 8 \tag{9-29}$$

This leads to two two-dimensional representations.

All the other proper groups and proper groups with inversion can be treated similarly. The last thing remains the generation of the characters of the double groups. The procedure could be summarized as follows.

1. The characters for the original elements in the new even dimensional irreducible representations can be obtained by substituting the proper angles in to the character of C(φ) etc. in the even dimensional representation of $R_h(3)$ [4]. The characters for the new elements have opposite sign.
2. If more than one representation of given dimension occurs, the angle is increased by successive increment of $2\pi/n$ until all irreducible representations are accounted for. This is equivalent to increasing the multiple of φ along the half integer series 1/2, 3/2, 5/2, and so on.
3. The notation for the two-dimensional representation is E, four-dimensional G and six-dimensional H (Herzberg notation [2]). The letters are subscripted by half integer that was used to derive it.

The new two-dimensional irreducible representations of D_4 are $E_{1/2}$ and $E_{3/2}$. The characters could be written as follows.

$$E_{1/2} : \left\{ E : 2, 2C_4 : 2\cos\frac{90^\circ}{2} = \sqrt{2}, \left\{ \frac{\overline{C_2'}}{C_2} : 2\cos\frac{180^\circ}{2} = 0, \right.\right.$$

$$\left\{ \begin{matrix} 2\overline{C_2'} \\ 2C_2' \end{matrix} : 2\cos\frac{180^\circ}{2} = 0, \right.$$

$$\left.\left\{ \begin{matrix} 2\overline{C_2''} \\ 2C_2'' \end{matrix} : 2\cos\frac{180^\circ}{2} = 0, \overline{E} : -2, 2\overline{C_4} : -2\cos\frac{90^\circ}{2} = -\sqrt{2} \right\}\right.$$

$$E_{3/2} : \Big\{E : 2, 2C_4 : 2\cos\frac{3\times 90^\circ}{2} = -\sqrt{2},\ \begin{Bmatrix}\overline{C_2'}\\ C_2\end{Bmatrix} : 2\cos\frac{3\times 180^\circ}{2} = 0,$$

$$\begin{Bmatrix}2\overline{C_2'}\\ 2C_2'\end{Bmatrix} : 2\cos\frac{3\times 180^\circ}{2} = 0,$$

$$\begin{Bmatrix}2\overline{C_2''}\\ 2C_2''\end{Bmatrix} : 2\cos\frac{3\times 180^\circ}{2} = 0, \overline{E} : -2, 2\overline{C_4} : -2\cos\frac{3\times 90^\circ}{2} = \sqrt{2}\Big\}$$

The new one-dimensional representations that appear in $D_3{}^2$ double group occur in pair, since there is an even number of them. The characters of the two components can be taken directly from the diagonal forms of the two-dimensional transformation matrices corresponding to various symmetry elements. Thu for j = 3/2 in $D_3{}^2$ we have,

$$R(E) = \begin{pmatrix}1 & 0\\ 0 & 0\end{pmatrix} \tag{9-30}$$

$$R(C_3) = \begin{pmatrix}e^{i(3/2)(2\pi/3)} & 0\\ 0 & e^{-i(3/2)(2\pi/3)}\end{pmatrix} = \begin{pmatrix}-1 & 0\\ 0 & -1\end{pmatrix} \tag{9-31}$$

$$R(C_2) = \begin{pmatrix}e^{i(3/2)(2\pi/2)} & 0\\ 0 & e^{-i(3/2)(2\pi/2)}\end{pmatrix} = \begin{pmatrix}-i & 0\\ 0 & i\end{pmatrix} \tag{9-32}$$

The treatment of two-dimensional $E_{1/2}$ representation of $D_3{}^2$ is just as in $D_4{}^2$. This generates the characters of the new irreducible representations of $D_3{}^2$ as follows.

$$E_{1/2} : \{E : 2, 2C_3 : 1, 3C_2 : 0, \overline{E} : -2,\ 2\overline{C_3} : -1, 3\overline{C_2} : 0\}$$

$$E_{3/2} : \left\{E : \begin{matrix}1\\1\end{matrix}, 2C_3 : \begin{matrix}-1\\-1\end{matrix}, 3C_2 : \begin{matrix}-i\\i\end{matrix}, \overline{E} : \begin{matrix}-1\\-1\end{matrix}, 2\overline{C_3} : \begin{matrix}1\\1\end{matrix}, 3\overline{C_2} : \begin{matrix}i\\-i\end{matrix}\right\}$$

(The two numbers in this case indicates the double values of the irreducible representations). The methods described here could be used to other double groups also. The detailed analysis could be found in refs [3, 4, 8].

REFERENCES

1. Herzberg, G.: Molecular Spectra and Molecular Structure, Volume 1: Spectra of Diatomic Molecules. Van Nostrand Reinhold, New York (1950)
2. Herzberg, G.: Molecular Spectra and Molecular Structure, Volume 3: Electronic Spectra and Electronic Structure of Polyatomic Molecules. Van Nostrand Reinhold, New York (1996)
3. Bunker, P.R., Jensen, P.: Molecular Symmetry and Spectroscopy. NRC Research Press, Ottawa, Canada (1998)

4. Flurry, R.L. Jr.: Symmetry Groups, Theory and Applications. Prentice-Hall, Upper Saddle River, NJ (1980)
5. Bethe, H.A.: Splitting of terms in crystals. Ann. Physik **3**, 133–206 (1929)
6. Hammermesh, M.: Group Theory and Its Application to Physical Problems. Dover, New York (1989)
7. Tinkham, M.: Group Theory and Quantum Mechanics. McGraw Hill, New York (1997)
8. Balasubramanian, K.: Relativistic Effects in Chemistry, Part A. Wiley, New York (1997)
9. Stedman, G.E., Butler, P.H.: Time reversal symmetry in applications of point group theory. J. Phys. A **13**, 3125–3140 (1980)
10. Barron, L.D., Buckingham, A.D.: Time reversal and molecular properties. Acc. Chem. Res. **34**, 781–789 (2001)
11. Sadlej, A.J.: Methods of relativistic quantum chemistry. In: B.O. Roos (ed.) Lecture Notes in Quantum Chemistry II, pp. 203–230. Springer, Heidelberg (1994)
12. McGlynn, S.P., Vanquickenborne, L.G., Kinoshita, M., Carroll, D.G.: Introduction to Applied Quantum Chemistry. Holt, Rinehart & Winston, New York (1972)
13. Balasubramanian, K., Pitzer, K.S.: Electron structure calculations including CI for ten low lying states of Pb_2 and Sn_2. Partition function and dissociation energy of Sn_2. J. Chem. Phys. **78**, 312 (1983)
14. Hang, T., Liao, M., Wang, Y., Wu, G., Balasubramanian, K.: A flexible correlation group table (CGT) method for the relativistic configuration interaction wavefunctions. J. Math. Chem. **28**, 213–239 (2000)
15. Pitzer, R.M., Winter, N.W.: Electronic structure methods for heavy-atom molecules. J. Phys. Chem. **92**, 3061–3063 (1988)
16. Ballhusen, C.J.: Introduction to Ligand Field Theory. McGraw Hill, New York (1962)
17. Newman, D.J., Ng, B.K.C. (Eds.).: Crystal Field Hand Book. Cambridge University Press, Cambridge (2000)
18. Balasubramanian, K.: Relativistic Effects in Chemistry, Part B. Wiley, New York (1997)
19. Roszak, S., Krauss, M., Alekseyev, A.B., Liebermann, H.-P., Buenker, R.J.: Spin-orbit configuration interaction calculation of the potential energy curves of iodine oxide. J. Phys. Chem. A **104**, 2999–3003 (2000)
20. Das, K.K., Balasubramanian, K.: Spectroscopic properties of low-lying electronic states of Au_2. J Mol. Spectrosc. **140**, 280–294 (1990)
21. Chattopadhyay, A., Das, K.K.: Electronic states of TlX (X = As, Sb, Bi): A configuration interaction study. J. Phys. Chem. A **108**, 7306–7317 (2004)
22. Chattopadhya, S., Das, K.K.: Electronic spectrum of $SiSe^+$: A MRDCI study. Chem. Phys. Lett. **399**, 140–146 (2004)
23. Giri, D., Das, K.K.: Theoretical studies of the electronic spectrum of SnSe. Chem. Phys. Lett. **411**, 144 (2005)
24. Giri, D., Das, K.K.: Electronic states of SnS and SnS^+: A configuration interaction study. J. Phys. Chem. A **109**, 7207–7215 (2005)
25. Banerjee, A., Pramanik, A., Das, K.K.: Ab initio configuration interaction study of the low-lying electronic states of InF. Chem. Phys. Lett. **429**, 62–67 (2006)
26. Giri, D., Pati, K., Das, K.K.: Relativistic configuration interaction study of the electronic spectrum of SnTe and $SnTe^+$. J. Chem. Phys. **124**, 154301–154313 (2006)
27. Chakrabarti, S., Das, K.K.: Electronic states and spectroscopic properties of GeSi. J. Mol. Spectrosc. **252**, 160–168 (2008)
28. Alekseyev, A.B., Liebermann, H.-P., Buenker, R.J.: Spin-orbit configuration interaction study of ultraviolet photofragmentation of XeH^+. Phys. Chem. Chem. Phys. **10**, 5706–5713 (2008)

29. Alekseyev, A.B., Buenker, R.J., Liebermann, H.-P.: Ab-initio study of the KrH^+ photodissociation. J. Chem. Phys. **128**, 234308 (2008)
30. Majumdar, D., Balasubramanian, K.: A theoretical study of the potential energy curves and spectroscopic constants of VC. Mol. Phys. **101**, 1369–1376 (2003)
31. Barrow, R.F.: The band spectrum of SnTe emission. Proc. Phys. Soc. (London) **52**, 380–387 (1940)
32. Barrow, R.F.: The absorption spectrum of SnTe. Proc. Phys. Soc. (London) **56**, 78–85 (1944)
33. Klotzbucher, W.E., Ozin, G.A.: Optical spectra of hafnium, tungsten, rhenium and ruthenium atoms and other heavy transition metal atoms and clusters (Zr 1,2, Pd 1,2, Au 1,2,3) in noble gas mixtures. Inorg. Chem. **19**, 3767–3776 (1980)
34. Majumdar, D., Dai, D., Balasubramanium, K.: Theoretical study of the electronic states of platinum trimer (Pt_3). J. Chem. Phys. **113**, 7919–7927 (2000)
35. Majumdar, D., Dai, D., Balasubramanium, K.: Theoretical study of the electronic states of platinum pentamer (Pt_5). J. Chem. Phys. **113**, 7928–7938 (2000)
36. Balasubramanian, K., Majumdar, D.: Spectroscopic properties of lead trimer (Pb_3 and Pb_3^+): Potential energy surfaces, spin-orbit and Jahn-Teller effects. J. Chem. Phys. **115**, 8795–8809 (2001)
37. Roszak, S., Balasubramanian, K.: Electronic structure and thermodynamic properties of LaC_2. J. Phys. Chem. **100**, 11255–11259 (1996)
38. Wielgus, P., Majumdar, D., Roszak, S., Leszczynski, J.: Structure and properties of the low-lying electronic states of CeC_2 and CeC_2^+. J. Chem. Phys. **127**, 124307–124313 (2007)
39. Majumdar, D., Balasubramanian, K., Nitche, H.: A comparative theoretical study of bonding in UO_2^{++}, UO_2^+, UO_2, UO_2^-, OUCO, $O_2U(CO)_2$ and UO_2CO_3. Chem. Phys. Lett. **361**, 143–151 (2002)
40. Galiardi, L., Heaven, M.C., Krogh, W., Roos, B.O.: The electronic spectrum of UO_2 molecule. J. Am. Chem. Soc. **127**, 86–91 (2005).
41. Hargittai, M.: Structural effects in molecular metal halides. Acc. Chem. Res. **42**, 453–462 (2008)
42. Majumdar, D., Roszak, S., Balasubramanian, K.: Interaction of benzene (B_z) with Pt and Pt_2: A theoretical study on $Bz - Pt_2$, $Bz_z - Pt$, Bz_zPt_2 and Bz_3Pt_3 clusters. J. Chem. Phys. **114**, 10300–10310 (2001)
43. Matsusita, T., Asada, T., Koseki, S.: Relativistic study on emission mechanism in palladium and platinum complexes. J. Phys. Chem. A **110**, 13295–13302 (2006)
44. Bersuker, I.B.: Modern aspects of Jahn-Teller effect theory and application. Chem. Rev. **101**, 1067–1114 (2001)
45. Brooks, J., Babayan, Y., Lamansky, S., Djurovich, P.I., Tsybam, I., Bau, R., Thomson, M.E.: Synthesis and characterizations of phosphorescent cyclometalated platinum complexes. Inorg. Chem. **41**, 3055–3066 (2002)
46. Cocchi, M., Kalinowski, J.: Highly efficient electrophosphorescent light emitting diodes with reduced quantum efficiency roll off at large current densities. Appl. Phys. Lett. **84**, 1052–1054 (2004)
47. Schmidt, J., Strasser, J., Yersin, H.: Determination of relaxation paths in the manifold of excited states of $Pt(2\text{-thpy})_2$ and $[Ru(bpy)_3\}^{2+}$ by time-resolved excitation and emission. Inorg. Chem. **36**, 3957–3965 (1997)
48. Balasubramanian, K.: Relativistic double group spinor representations of nonrigid molecules. J. Chem. Phys. **120**, 5524–5535 (2004)
49. Christenson, J.H., Cronin, J.W., Fitch, V.L., Turlay, R.: Evidence for the 2π decay of the $K_2{}^0$ meson. Phys. Rev. Lett. **13**, 138–140 (1964)
50. Mayer, J.: Construction of linearly independent relativistic symmetry orbitals for finite double-point groups including time reversal symmetry. Int. J. Quantum Chem. **33**, 445–465 (1988)
51. Mayer, J.: Addendum to construction of linearly independent relativistic symmetry orbitals for finite double-point groups including time reversal symmetry. Int. J. Quantum Chem. **61**, 929–933 (1997)

CHAPTER 10

RELATIVISTIC STRING-BASED ELECTRON CORRELATION METHODS

TIMO FLEIG

Laboratoire de Chimie et Physique Quantiques, I.R.S.A.M.C., Universitė Paul Sabatier, Toulouse III, 118, Route de Narbonne, F-31062 Toulouse, Cedex 4, France
e-mail: timo.fleig@irsamc.ups-tlse.fr

Abstract: Highly-accurate relativistic electronic-structure studies on heavy elements require general and efficient many-body methods. In order to achieve spectroscopic accuracy, the description of in particular dynamic electron correlation is of crucial importance. Modern wavefunction-based electron correlation approaches of high efficiency are typically based on a string representation of many-particle quantities. The focus in this chapter lies on the introduction to a suite of new relativistic electronic-structure methods which treat electron correlation and relativistic effects on the same footing and to a number of concepts of importance for relativistic many-body methods. Several applications to small heavy-element systems are discussed where the presented methods are put to critical tests in direct comparison with other modern approaches of relativistic electronic-structure theory.

Keywords: Relativistic many-body theory, time-reversal symmetry, multi-reference theory, spin–orbit interaction, configuration interaction, multi-configuration self-consistent-field, coupled cluster, heavy-element properties

10.1. INTRODUCTION

The majority of all published results in quantum chemistry is today obtained by application of density functional theory (DFT). The reason lies in the great efficiency of DFT in the treatment of electron correlation which makes it applicable even to very large molecules. Quantum chemical models based on the electronic wave function, on the other side, allow for a systematic improvement of the level of sophistication and therefore a more complete understanding of electronic structure in general. This naturally comes with an increased computational expense of wave-function based methods, and highly accurate electronic-structure studies are often only feasible for comparatively small molecules.

The rigorous treatment of special relativity and electron correlation in wave-function based quantum-chemical methods applied to heavy-element systems

M. Barysz and Y. Ishikawa (eds.), *Relativistic Methods for Chemists*,
Challenges and Advances in Computational Chemistry and Physics 10,
DOI 10.1007/978-1-4020-9975-5_10,

comprises a central topic of this chapter. From a modern point of view the essence of these two aspects may be somewhat rephrased: The central problem lies in an accurate and at the same time efficient treatment of dynamic electron correlation in a rigorously relativistic framework. With the advent of ever more advanced relativistic Hamiltonian operators for the electronic-structure problem (such as infinite-order/exact two-component operators [1–3]) the focus has shifted toward improving the less-developed technology for the treatment of electron correlation.

The furthering of relativistic electron correlation methods faces various difficulties. The most prominent is the reduction of non-relativistic symmetries (spatial and spin symmetries) in the relativistic framework due to magnetic couplings, the most important of which is the spin–orbit interaction. Beside further contraction/expansion effects of orbitals it partially lifts the non-relativistic energetic degeneracies of states. Second, particularly d and f elements and their compounds often exhibit states, even ground states, which are characterized by several unpaired electrons, i.e., open shells. The treatment of such states surpasses the use of a single Hartree–Fock determinant as a reference function for the correlation step of the calculations. Instead, the multi-reference character of the states must be accounted for, and this calls for methods going beyond standard single-reference implementations (this applies in particular to coupled cluster approaches).

Many electronic-structure approaches are based on the assumption that spin–orbit interaction may be included in an approximate fashion. This is sometimes reasonable, but restricts those methods in their applicability. The separation is carried out in more or less rigorous ways and may take place at different stages of the calculation. In most instances, orbital optimizations neglect spin–orbit coupling [4–7]. In this case the polarization of electronic shells due to the presence of spin–orbit interaction has to be described by the correlation expansion since it is not incorporated into the orbitals. The use of real-valued (spin-) orbitals is indeed a computational advantage in relativistic correlation methods. For molecules with certain symmetries, however, the use of real-valued integrals is possible by construction (see Section 10.2.4) which makes the *entire calculation* real-valued not only the orbitals. Since usually the computational cost is much higher at the correlation step of a calculation, the more costly orbital optimization using a spin-dependent Hamiltonian is in these cases well justified. In general, spinors from such a calculation form a significantly improved one-particle basis in heavy-element calculations [8] and facilitate as well as improve the subsequent correlation treatment. Regarding four-component methods in this respect, the explicit treatment of the small component degrees of freedom can become too inefficient here. Two-component Hamiltonians are then a favorable choice. Another (additional) place to separate off spin–orbit coupling is at the later stage of the calculation, the post-Hartree–Fock step. There exist a number of different "shadings" of how rigorous the separation is carried out, e.g., in references [9, 10]. The models seem to work well in many cases where the coupling between correlation and spin–orbit interaction is not decisive in the description of a given property of the system. To name one example, the spin–orbit-(SO-) CASPT2 method [11, 9] draws advantage from its efficient (perturbative) treatment of electron correlation, but spin–orbit

interaction is considered only after the orbital optimization and not simultaneously with (dynamic) electron correlation. A rigorous assessment of its accuracy remains an open issue and relies on the direct comparison with non-separating methods (an example is presented in Section 10.5.3).

Spin–orbit interaction effects in heavy elements, however, may be as drastic as to give rise to the change of a ground state (PtH, [12]), the qualitatively different description of a dissociation process (Tl_2, [13], see Section 10.5.1), or the variance of an atomic electric polarizability on the order of 35% (Tl, [14]). In general, therefore, it is desirable to treat spin–orbit interaction and electron correlation on the same footing.

The emphasis in this chapter lies on the discussion of wave-function based correlation approaches which incorporate spin–orbit interaction a priori, i.e., already in the Hartree–Fock or Multi-Configuration (MC) SCF optimization. With respect to the latter method, a certain distinction should be made: Liu and Kutzelnigg published in 2000 a "relativistic MCSCF by means of quasidegenerate direct perturbation theory" [15, 16]. However this is not relativistic MCSCF in the present sense as relativistic effects in their approach are added on top of a non-relativistic MCSCF optimization. Regarding relativistic methods treating dynamic electron correlation (post-HF or -MCSCF step) the discussion focusses on spinor-based approaches. These methods have all been developed from non-relativistic precursor implementations which allow for the highest-level treatment of correlation, i.e., approaching the exact solution of the relevant many-particle equations with a given one-particle basis set (Full Configuration Interaction, General-Order Coupled Cluster), if desired and computationally feasible. This is seldomly done in practice, but these wave-function based methods allow for a systematic improvement of the correlation level and therefore a detailed assessment of electron correlation contributions typically via benchmark studies.

The chapter is organized as follows: In the following section principles of crucial importance to the understanding of a number of relativistic electron correlation approaches are reviewed. A short section introducing many-particle wave functions touches on strings representing relativistic wave functions. The purpose of these introductory presentations is also to make the following sections accessible in a self-contained manner. These elaborate on essentials of string-based relativistic electron correlation methods without going into great detail. In the final section some sample applications are presented including a critical comparison with other approaches.

10.2. GENERAL PRINCIPLES

10.2.1. Time-Reversal Symmetry

In the absence of external magnetic fields the time-reversal operation comprises a symmetry in the quantum-mechanical description of many-particle systems such as atoms and molecules. Time-reversal or Kramers symmetry (TRS) is often exploited in relativistic many-particle theory where spin-dependent Hamiltonian operators

are employed. It may be implemented for significant reductions of the number of independent parameters and, therefore, the ensuing computational effort. Since the following methodological elaborations are based on the use of TRS, a brief introduction to the concept and the notation shall be given in advance. Further background information and details can be found in the literature, e.g. [17–19].

The time-reversal operator $\hat{K}$ is defined as an antiunitary operator, i.e., it is unitary, $\hat{K}^\dagger = \hat{K}^{-1}$, implying

$$\hat{K}\hat{K}^\dagger = \hat{K}^\dagger\hat{K} = \mathbf{1} \tag{10-1}$$

and moreover satisfies

$$\hat{K}c = c^*\hat{K} \tag{10-2}$$

where c is a complex number. For the general case of the four-component Dirac equation, it may be conveniently defined as

$$\hat{K} := -\imath\,\boldsymbol{\Sigma}_y\hat{K}_0 \tag{10-3}$$

with $\hat{K}_0$ a complex conjugation operator, $\boldsymbol{\Sigma}_y = \mathbf{1}_2 \otimes \boldsymbol{\sigma}_y$ a four-component operator and $\boldsymbol{\sigma}_y$ a (two-dimensional) spin–Pauli matrix.

Using this definition, it may be shown [20,21] that, for instance, the free-particle Dirac operator $\hat{h}_D$, the one-particle Dirac operator including an external electric potential (such as that of a nucleus) $\hat{H}_D$, or the Dirac–Coulomb operator $\hat{H}_{DC}$ are invariant under unitary transformation according to

$$\hat{K}^\dagger\,\hat{h}_D\,\hat{K} = \hat{h}_D \tag{10-4}$$

and equivalently for the other operators. This means that such Hamiltonian operators commute with the Kramers operator, $\left[\hat{K}, \hat{H}\right] = 0$, and thus TR is consequently a fundamental symmetry that can be exploited in the respective eigenvalue equations.

10.2.2. Kramers-Paired Spinors

In order to understand the implications of TRS, it suffices to consider two-component functions such as non-relativistic spin-orbitals. If we define "unbarred" and "barred" spin-orbitals, respectively, as

$$\begin{aligned}\Phi_i &:= \phi_i\alpha = \phi_i\begin{pmatrix}1\\0\end{pmatrix} = a_i^\dagger \mid\ \rangle \\ \Phi_{\bar{i}} &:= \phi_i\beta = \phi_i\begin{pmatrix}0\\1\end{pmatrix} = a_{\bar{i}}^\dagger \mid\ \rangle\end{aligned} \tag{10-5}$$

the Kramers operator in two-component form, $-\imath\boldsymbol{\sigma}_y\hat{K}_0$, is seen to relate the functions to each other, according to

$$\hat{K}\Phi_i = -\imath\begin{pmatrix}0 & -\imath\\ \imath & 0\end{pmatrix}\hat{K}_0\,\phi_i\begin{pmatrix}1\\0\end{pmatrix} = \phi_i\begin{pmatrix}0 & -1\\ 1 & 0\end{pmatrix}\begin{pmatrix}1\\0\end{pmatrix} = \phi_i\beta = \Phi_{\bar{i}}$$
$$\hat{K}\Phi_{\bar{i}} = -\phi_i\alpha = -\Phi_i \tag{10-6}$$

here assuming real spatial parts ϕ_i, and thus for the action on a fermionic function $\hat{K}^2 = -\mathbf{1}$. The physical interpretation of this behavior is that a reversal of time affects the direction of velocities, and therefore angular momenta, which is reflected by the above spin flips. We introduce an auxiliary quantity M_K which takes the value $M_K = \frac{1}{2}$ for the spin-orbital Φ_i and $M_K = -\frac{1}{2}$ for the spin-orbital $\Phi_{\bar{i}}$. Obviously, M_K corresponds to the spin projection M_S in the non-relativistic case and will therefore be called Kramers projection in the general case.

In relativistic theory, where due to the spin–orbit interaction neither the orbital angular momentum nor the spin comprise good quantum numbers and instead the total angular momentum j is relevant, the one-particle functions are generalized and replaced by either 2- or 4-spinors. These are the solutions of the ensuing relativistic equations and appear as some (complex) linear combinations of the above spin-orbitals, e.g., in the case of atomic p 2-spinors as

$$\Phi_p\left(j, m_j\right) = \Phi_p\left(\frac{1}{2}, \frac{1}{2}\right) = \sqrt{\frac{1}{3}}\,p_z\alpha + \sqrt{\frac{1}{3}}\left(p_x + \imath\,p_y\right)\beta$$
$$\Phi_{\overline{p}}\left(j, -m_j\right) = \Phi_{\overline{p}}\left(\frac{1}{2}, -\frac{1}{2}\right) = \sqrt{\frac{1}{3}}\,p_z\beta - \sqrt{\frac{1}{3}}\left(p_x - \imath\,p_y\right)\alpha \tag{10-7}$$

and correspondingly for other quantum numbers j, m_j. Applying Eqs. 10-6, $\hat{K}^2 = -\mathbf{1}$ is seen to be satisfied, and $\hat{K}$ relates functions of equal j and principal quantum number n, but flips the sign of m_j. We therefore have established a one-particle basis of Kramers-paired spinors for the relativistic description of many-electron atoms. The Kramers projection remains $M_K = \frac{1}{2}$ for a spinor m_j and $M_K = -\frac{1}{2}$ for the corresponding spinor $-m_j$, but the correspondence to M_S is lost.

In the case of molecules where j is no longer valid, one may still conserve the Kramers pairing of relativistic molecular spinors by resorting to a Kramers-restricted formalism [22]. A molecular Kramers pair now consists of two functions which are related by $\hat{K}$, the unbarred function Φ_i having $M_K = \frac{1}{2}$, the barred function $\Phi_{\bar{i}}$ having $M_K = -\frac{1}{2}$. The relevance of M_K will be discussed in greater depth in the section on many-particle states (Section 10.3).

10.2.3. Integrals Over Kramers-Paired Spinors

The computational demand of spinor-based relativistic electronic structure methods is increased compared to their non-relativistic counterparts. This is for one part due to the spin-dependence of the relativistic Hamiltonian and the consequences discussed in Section 10.4, for the other due to additional classes of non-vanishing integrals which must be considered. For example, the one-particle integral $h_{i\bar{j}}$ vanishes due to spin integration in the non-relativistic case where i and j refer to spin-orbitals, but not in general in the relativistic case where i and j refer to spinors.

Without the use of symmetries, all blocks in Figure 10-1 would have to be calculated and stored. However, the introduction of a Kramers-restricted formalism which implies the use of Kramers-paired one-particle functions allows for exploiting TRS. The upper left and lower right blocks are related to each other by virtue of

$$\begin{aligned} h_{\bar{i}\bar{j}} &= \left\langle \Phi_{\bar{i}} | \hat{h} | \Phi_{\bar{j}} \right\rangle = \left\langle \hat{K}\Phi_i | \hat{h} | \hat{K}\Phi_j \right\rangle = \left\langle \Phi_i | \hat{K}^\dagger \hat{h} \hat{K} | \Phi_j \right\rangle^* = \left\langle \Phi_i | \hat{h} | \Phi_j \right\rangle^* \\ &= \left\langle \hat{h}\Phi_j | \Phi_i \right\rangle = \left\langle \Phi_j | \hat{h}^\dagger | \Phi_i \right\rangle = \left\langle \Phi_j | \hat{h} | \Phi_i \right\rangle = h_{ji} \end{aligned} \tag{10-8}$$

where Eqs. (10-2), (10-4), and the hermiticity of the Hamiltonian have been used. The lower left and upper right blocks are related if complex conjugation and time-reversal symmetries are taken into account, according to

$$h_{\bar{i}j} = \left\langle \hat{K}\Phi_{\bar{i}} | \hat{h} | \Phi_j \right\rangle = -\left\langle \Phi_i | \hat{K}^\dagger \hat{h} \hat{K} \hat{K} | \Phi_j \right\rangle^* = -\left\langle \Phi_i | \hat{h} | \Phi_{\bar{j}} \right\rangle^* = -h^*_{i\bar{j}} \tag{10-9}$$

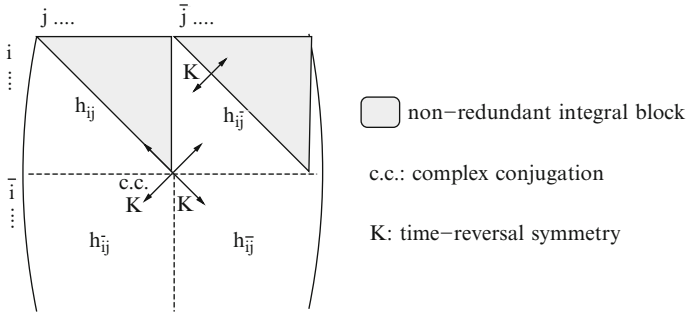

Figure 10-1. Reduction to non-redundant set of one-particle integrals by exploiting time-reversal and complex conjugation symmetry in a Kramers-paired spinor basis

where in addition $\hat{K}^\dagger = \hat{K}^{-1}$ has been used. Finally, Kramers symmetry reduces the upper right block to triangle form:

$$\begin{aligned} h_{i\bar{j}} &= \left\langle \Phi_i | \hat{h} \hat{K} | \Phi_j \right\rangle = \left\langle \Phi_i | \hat{K}^\dagger \hat{h} \hat{K} \hat{K} | \Phi_j \right\rangle \\ &= -\left\langle \Phi_i | \hat{K}^\dagger \hat{h} | \Phi_j \right\rangle = -\left\langle \hat{K} \Phi_i | \hat{h} | \Phi_j \right\rangle^* = -\left\langle \Phi_{\bar{i}} | \hat{h} | \Phi_j \right\rangle^* \\ &= -\left\langle \Phi_j | \hat{h} | \Phi_{\bar{i}} \right\rangle = -h_{j\bar{i}} \end{aligned} \tag{10-10}$$

Hence, we have shown that the unique types of one-particle integrals in a Kramers basis reduce to

$$h_{ij} \qquad h_{i\bar{j}}. \tag{10-11}$$

Likewise, the original set of classes of two-particle integrals can be reduced to the following unique set by applying the same principles

$$(ij|kl) \qquad (\bar{i}j|kl) \qquad (\bar{i}j|\bar{k}l) \qquad (\bar{i}j|k\bar{l}) \tag{10-12}$$

and in addition particle exchange symmetry. Naturally, the computational savings are much more important in the case of two-body integrals.

TRS has been used in a variety of different many-particle models, e.g., Dirac-Hartree-Fock theory [22], relativistic Multi-Configuration Self-Consistent-Field theory (MCSCF) [23–25] and approaches accounting for dynamic particle correlations such as relativistic density-functional theory (DFT) [26, 27], configuration interaction (CI) methods [28, 21], and coupled-cluster (CC) approaches [29].

10.2.4. Double Group Symmetry

A rigorously relativistic implementation of many-body methods requires the use of double point groups if molecular symmetry is to be exploited. Most often, the binary groups are implemented, i.e., D_{2h}^* and its subgroups [30]. The most sophisticated implementation of double point group symmetry is possible when the units of quaternion numbers are used in the representation of basis functions. The details which are to be found in the literature [22, 31] are beyond the scope of this presentation. However, the implications for integrals over Kramers-paired spinors shall be discussed in an exemplifying case.

As expounded in reference [31], the double group of C_{2h}^* is a complex-valued group, i.e., matrix elements over basis functions classified according to the symmetry representations of this group remain complex-valued, despite the use of quaternion algebra. The character table of C_{2h}^* reads as [32] (Table 10.1).

Any spinor now transforms as to one of the fermion-type irreducible representations E. Moreover, in a basis of Kramers-paired spinors the functions of a given pair are related by time-reversal and span ${}^1E$ and ${}^2E$, either *gerade* or *ungerade* which is also obvious from the relationship of the respective characters,

Table 10-1 Character table of the double point group C_{2h}^*

	E	C_2	σ_h	I	$\overline{E}$	$\overline{C_2}$	$\overline{\sigma_h}$	$\overline{I}$
A_g	1	1	1	1	1	1	1	1
B_g	1	−1	−1	1	1	−1	−1	1
A_u	1	1	−1	−1	1	1	−1	−1
B_u	1	−1	1	−1	1	−1	1	−1
${}^1E_g$	1	i	i	1	−1	−i	−i	−1
${}^2E_g$	1	−i	−i	1	−1	i	i	−1
${}^1E_u$	1	i	−i	−1	−1	−i	i	1
${}^2E_u$	1	−i	i	−1	−1	i	−i	1

which is given by complex conjugation. Since also in the case of double groups the relativistic Hamiltonian transforms as to the totally symmetric representation, the above-identified unique type of one-particle integrals $h_{i\bar{j}}$ vanishes due to double group and time-reversal symmetries, as ${}^1E_g \otimes A_g \otimes {}^1E_g = B_g$. The remaining set of two-particle integrals is in this case given as $(ij|kl), (\bar{i}j|\bar{k}l), (\bar{i}j|k\bar{l})$. Corresponding considerations are valid for the other complex-valued double groups, C_2^*, and C_s^*.

The described savings are in the same way achieved for the real-valued binary double groups, D_{2h}^*, D_2^*, and C_{2v}^*, but here it can be shown [22] that matrix elements can be constructed being purely real. These considerations are, however, not valid for the so-called quaternionic matrix groups, C_i^* and C_1^*, where the spinors of a Kramers pair span the same symmetry irrep and the matrix elements remain complex valued.

Double group symmetry has been implemented in a large number of relativistic electronic-structure methods. A detailed discussion can be found in the textbook by Dyall and Fægri [33], and a complete set of character tables in the monograph by Koster et al. [32].

10.2.5. Generalized Active Spaces

A powerful concept to construct the electronic wave function is to introduce an arbitrary number of orbital spaces and to group the orbitals of a given system into these spaces in accord with physical and chemical arguments. This makes is possible to restrict the electronic occupation of the subspaces in constructing the wave function such that the expansion is limited to those terms which are considered most important for properly describing the physical/chemical properties of the system. The procedure of Generalized Active Spaces (GAS) has been introduced by Olsen in the context of non-relativistic quantum chemistry [34] and can be regarded as the complete generalization of the Restricted Active Space (RAS) concept [35] used for instance in the *MOLCAS* program package [36] both with respect to the number of subspaces as well as the electronic occupation of these.

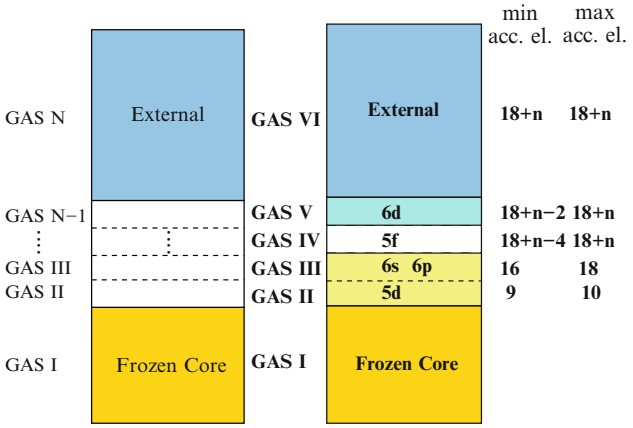

Figure 10-2. Subdivision of atomic or molecular orbitals into Generalized Active Spaces. *Left-hand side:* General case. *Right-hand side:* Example for an actinide atom. n is the number of electrons in the $5f$ shell of the atom, min./max. acc. el. specifies the minimum/maximum number of accumulated electrons after consideration of this subspace. The 'Frozen Core' space can be omitted when a core Fock matrix is generated for these orbitals

Heavy elements and their compounds often exhibit a complicated electronic structure even in their electronic ground state. Here the GAS concept offers the flexibility to account for the typical near-degeneracies of atomic orbital shells of different angular momenta and the frequently encountered large number of unpaired electrons in ground and excited states. Figure 10-2 displays the basic ideas and shows the particular subdivision and occupation constraints for an actinide atom. The present example is a showcase for calculations on heavy-element compounds. It comprises all Slater determinants (or a reference state plus all excitations in the case of a coupled cluster calculation) meeting the occupation restraints given for the various active spaces. One or zero holes are allowed in the space of the $5d$ orbitals; zero, one or two holes are allowed in the combined spaces of the $5d$, $6s$, and $6p$ orbitals, etc. The specification '$18 + n - 4$' denotes that up to four particles may be excited from the combined spaces II–IV into the following spaces. Accordingly, '$18 + n - 2$' denotes that up to two particles may be excited from the combined spaces II–V into the external space, yielding a typical Multi-Reference (MR) setup with up to two particles in the external space.

In physical terms, this model space accounts for the following effects and interactions: The reference space takes into consideration that for actinide atoms commonly various $5f - 6d$ mixed configurations are important for describing the low-lying electronic states. In the present example, all configurations ranging from $5f^n, 6d^0$ up to $5f^{n-4}, 6d^4$ are accounted for in the reference space. Since there may be up to two holes in the $6s$, $6p$ shells, the dynamic electron correlation effects (which are treated since double excitations into the external space are allowed) among these electrons and among them and those of the valence shells are considered. Thus, electron correlation effects are treated in a Core-Core (C-C) type

fashion in the case of the $6s$, $6p$ electrons and in a Core-Valence (C-V) type fashion in the case of the $5d$ electrons, which may also be regarded as a core polarization model for the latter shells.

Clearly, certain qualitative knowledge of the electronic structure of a system in question is required prior to the construction of appropriate spaces and constraints. The generality of the GAS approach, however, allows for its application in a number of wave-function based (relativistic) electronic-structure methods such as Configuration Interaction (CI), MCSCF, and CC models which will be described in Section 10.4. Its power unfolds in a variety of applications to electronic-structure problems and the determination of atomic and molecular properties. Some examples will be shown in Section 10.5.

10.3. MANY-PARTICLE WAVEFUNCTIONS

10.3.1. Spinor Strings

Many modern quantum-chemical methods capable of performing large-scale many-body calculations are based on a representation of the many-particle wavefunctions in terms of strings of creation operators in second quantization (string-based methods), e.g. [37–42]. The advantages of string-based approaches are manifold. First and foremost, they allow for an efficient evaluation of coupling coefficients in CI theory or of connections in CC theory. Moreover, methods implementing higher-order excitations (such as triple (T), quadruple (Q) replacements etc.) are more easily obtained, and they do not suffer from a reduced efficiency in the treatment of these higher excitations. Furthermore, multi-reference approaches are more straightforwardly accessible as demonstrated e.g. in references [43,44]. All of these issues are of importance in the treatment of heavy-element systems due to the typically large number of electrons to be correlated and the ubiquity of open-shell electronic structures.

The rigorous generalization of string-based approaches to the relativistic domain is, e.g., described in references [21,45,46]. Two sets of strings are defined, a set composed of Kramers-unbarred spinors and a set composed of Kramers-barred spinors

$$\begin{aligned} \mathcal{S}^\dagger \mid \ \rangle &= a_i^\dagger a_j^\dagger \dots a_n^\dagger \mid \ \rangle \\ \overline{\mathcal{S}}^\dagger \mid \ \rangle &= a_{\bar{i}}^\dagger a_{\bar{j}}^\dagger \dots a_{\bar{n}}^\dagger \mid \ \rangle \end{aligned} \tag{10-13}$$

where $i, j, \dots$ denote indices of Kramers pairs. Since the individual operators can be labelled according to their symmetry in the double group and furthermore the active (GAS) space they refer to, strings are blocked into symmetry groups and symmetry-occupation groups.

The graphical representation of such creator strings is akin to an ordering algorithm for the individual strings and therefore the key to an efficient implementation of a many-body method. One possibility of employing graphical techniques is to invoke group theoretical approaches such as the Symmetric Group Approach

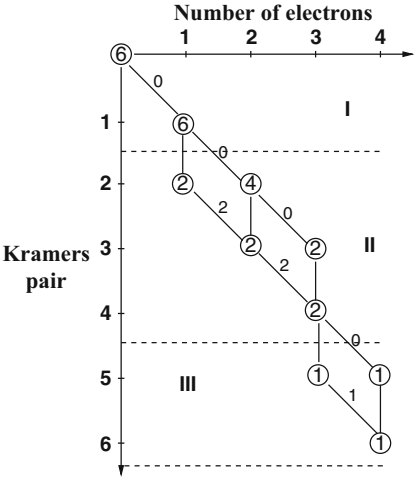

Figure 10-3. Sample string graph for Kramers unbarred spinor strings, 4 electrons in 6 Kramers pairs subdivided into three active spaces (GAS); numbers in *circles* correspond to vertex weights, numbers along paths to arc weights

(SGA) or the Unitary Group Approach (GUGA) as has been done for the case of a spin-adapted basis within the spin–orbit configuration interaction method [47] in the COLUMBUS program suite [4]. Alternatively, the graphical approach introduced in reference [35] can be generalized to the relativistic case and a basis of Kramers-paired spinors [8]. A sample string graph for a subset of strings with one particle in GAS I (one Kramers pair), two particles in GAS II (three Kramers pairs) and one particle in GAS III (two Kramers pairs) is shown in Figure 10-3 (an arbitrary number of active spaces and their respective occupations may be introduced). The vertex weights indicate how many unique strings originate from a given vertex. The arc weights define an ordering of the individual strings such that a string index is given by the sum of weights of the arcs it passes. In the example in Figure 10-3 six Kramers unbarred strings are obtained, where the first one is represented by $a_1^\dagger a_2^\dagger a_3^\dagger a_5^\dagger \mid \quad \rangle$. In a corresponding fashion Kramers barred spinor strings are obtained. Since relativistic Hamiltonian operators may couple alpha and beta spin-orbitals or, concomitantly, Kramers unbarred and barred spinors, the unbarred and barred sets of strings are generated and stored separately.

In CI-type models [21, 8] a Kramers-unbarred and a Kramers-barred string are combined to form a Slater determinant according to

$$\mathcal{S}_I^\dagger \overline{\mathcal{S}}_J^\dagger \mid \quad \rangle \tag{10-14}$$

where I and J denote individual strings. In (general-order) CC-type of models the individual strings are combined to form excitation operators acting on a reference state (Fermi vacuum) according to

$$\tau_\mu^\dagger = \mathcal{S}_I^\dagger \overline{\mathcal{S}}_J^\dagger \, \mathcal{S}_K \overline{\mathcal{S}}_L \tag{10-15}$$

where $\mathcal{S}$ is a corresponding string of annihilation operators. The essentials of the relativistic string-based implementations of these many-body methods will be discussed in Sections 10.4.2 and 10.4.4.

For a given combination of strings, the Kramers projection may now be given as

$$M_K := \frac{N_p - N_{\overline{p}}}{2} \tag{10-16}$$

with N_p the number of creation operators of electrons in Kramers unbarred spinors. As an example, the state $a_1^\dagger a_2^\dagger a_3^\dagger a_{\overline{5}}^\dagger \mid \rangle$ has an associated Kramers projection of $M_K = +1$. Correspondingly, the string operator itself $a_1^\dagger a_2^\dagger a_3^\dagger a_{\overline{5}}^\dagger$ changes the Kramers projection by $\Delta M_K = +1$. With the definitions in Eqs. (10-3) and (10-6) it is readily shown that $\hat{K}^2 = (-\mathbf{1})^n$ for the action of $\hat{K}$ on a many-particle state, where n is the number of fermions.

10.3.2. Relativistic Excitation Classes

The creation of excitation manifolds based on a reference state - be it single- or multi-reference – is a substantial issue both in CC and CI theory. The concept of excitation classes applies to both the wave function, where the type of excitation relative to the reference state is characterized, as well as the Hamiltonian which in second quantization carries out one- and two-particle displacements. The introduction of GA spaces calls for an efficient and transparent handling of the arising excitation types because the excitation level is linked to the chosen occupations of the active spaces. In the second quantization picture this is ideally achieved by labelling all unique excitation types and bookkeeping the number of creation and annihilation operators referring to that excitation type. As a simple example, consider Table 10-2.

Table 10-2 Two exemplifying excitation classes of a one- and a two-particle operator

Exc. class		Elementary operator	GAS I	GAS II	GAS III
A	$\hat{a}_i^\dagger$	Creation of unbarred spinor	0	0	1
	$\hat{a}_{\overline{j}}^\dagger$	Creation of barred spinor	0	0	0
	$\hat{a}_k$	Annihilation of unbarred spinor	1	0	0
	$\hat{a}_{\overline{l}}$	Annihilation of barred spinor	0	0	0
		⋮			
E	$\hat{a}_i^\dagger$	Creation of unbarred spinor	0	1	1
	$\hat{a}_{\overline{j}}^\dagger$	Creation of barred spinor	0	0	0
	$\hat{a}_k$	Annihilation of unbarred spinor	1	0	0
	$\hat{a}_{\overline{l}}$	Annihilation of barred spinor	1	0	0
		⋮			

Excitation class A represents an annihilation of an electron in GAS I and a creation in GAS III, where both operators refer to the Kramers unbarred set of one-particle functions. The type of excitation therefore generates determinants (in the CI case) with an occupation lowered by one spinor in the first space and increased by one spinor in the third space and the same Kramers projection M_K as the reference state.

An excitation class for a two-particle operator is shown in the lower half of Table 10-2. Two electrons in an unbarred and a barred spinor of space I – not necessarily forming a Kramers pair! – are annihilated and created in two unbarred spinors of spaces II and III, respectively. The complete operator in normal ordering and the associated integral read

$$\hat{a}^{\dagger}_{i\,II}\hat{a}^{\dagger}_{j\,III}\hat{a}_{k\,I}\hat{a}_{\bar{l}\,I}\,(i\bar{l}|jk). \tag{10-17}$$

Therefore, this operator may be classified as flipping the Kramers projection by one unit, according to $\Delta M_K = +1$. The information given by ΔM_K, the number of particles and their occupation of active spaces may now be compiled to define an excitation class.

Excitation classes become an important means of classifying quantities occurring in relativistic many-particle theory. In CI theory the value of a CI coupling coefficient (deciding whether a matrix element of the Hamiltonian vanishes or not) is determined by the excitation class of the left-hand and right-hand string combinations and the excitation class of the Hamiltonian operator. In relativistic CC theory, correspondingly, connections can be determined by the excitation classes of the involved strings for the excitation/deexcitation operators and the Hamiltonian [44]. It becomes obvious that there is no essential distinction between various excitation levels such as the singles and doubles excitations which are typically employed in second-order methods, and higher excitations. Due to the treatment of all excitation levels on the same footing, the implementation of general excitation level (or general-order) methods is facilitated. Further implications of the excitation-class formalism will be addressed in the following sections.

10.4. WAVEFUNCTION-BASED ELECTRON CORRELATION METHODS

10.4.1. Hamiltonian Operators

10.4.1.1. General Considerations

We shall at first focus on the applicability of the electron correlation methods discussed here and the use of various relativistic Hamiltonian operators which define the physical framework of a given method. Particular attention will be paid to the distinction between four- and two-component Hamiltonians used at the correlation stage, since this issue persists to be a source of some confusion.

Four-component electronic-structure theory is very often based on the so-called "empty Dirac" picture [33], e.g., as the implementations in the DIRAC quantum-chemistry program package [48] where the Dirac–Coulomb Hamiltonian is frequently used. This means that the states of negative energy, described by some finite basis set, are treated as virtual orbitals in the Hartree–Fock optimization [22] and a minmax variation principle is employed [49]. Here the energy is minimized with respect to spinor transformations among positive-energy spinors and maximized with respect to spinor transformations involving positive- and negative-energy spinors. After this step, the negative-energy states may be discarded which can be viewed as a *no-pair approximation a posteriori* [50] since a coupling between negative- and positive-energy states is now explicitly ruled out. The positive-energy states (+), however, are nonetheless described by four-component spinors which in general have a non-vanishing small (S) component

$$\psi_i^+ = \begin{pmatrix} \psi_i^L \\ \psi_i^S \end{pmatrix}, \tag{10-18}$$

where ψ_i^L is a two-component spinor (bi-spinor). The other common approach to no-pair theories is to invoke the decoupling of positive- and negative-energy states *a priori*, i.e., to transform the four-component operators to a two-component form with an action only on positive-energy states. Examples are the Infinite-Order Two-Component (IOTC) [1, 3], Exact Two-Component (X2C) [2], or the widely-known Douglas–Kroll–Hess (DKH) theory [51, 52] .

The point to be made in the present context is that electron correlation methods based on spinors optimized with any of the above (spin-dependent) Hamiltonians are structurally entirely independent of the choice of this Hamiltonian. This is for example understood by considering the ensuing integral transformation into the basis of atomic or molecular spinors after a four-component Hartree–Fock (or MCSCF) calculation. The positive-energy spinors in Eq. (10-18) are then expanded into some one-particle basis set ϕ according to

$$\begin{aligned} \psi_i^L &= \sum_{J=1}^{N^L} c_{iJ}^L \phi_J^L \\ \psi_i^S &= \sum_{J=1}^{N^S} c_{iJ}^S \phi_J^S \end{aligned} \tag{10-19}$$

where N^L is the number of Large-component basis functions. The set of integrals transformed into the atomic or molecular basis required to describe the positive-energy states is then cast as (sampling only one-particle integrals)

$$
\begin{aligned}
h^{+}_{mn} &= \left\langle \psi^{+}_{m} | \hat{h} | \psi^{+}_{n} \right\rangle = \left\langle \begin{pmatrix} \psi^{L}_{m} & \psi^{S}_{m} \end{pmatrix} | \begin{pmatrix} \hat{h}_{11} & \hat{h}_{12} \\ \hat{h}_{21} & \hat{h}_{22} \end{pmatrix} | \begin{pmatrix} \psi^{L}_{n} \\ \psi^{S}_{n} \end{pmatrix} \right\rangle \\
&= \left\langle \psi^{L}_{m} | \hat{h}_{11} | \psi^{L}_{n} \right\rangle + \left\langle \psi^{L}_{m} | \hat{h}_{12} | \psi^{S}_{n} \right\rangle + \left\langle \psi^{S}_{m} | \hat{h}_{21} | \psi^{L}_{n} \right\rangle + \left\langle \psi^{S}_{m} | \hat{h}_{22} | \psi^{S}_{n} \right\rangle \\
&= \sum_{J=1}^{N^L} \sum_{K=1}^{N^L} c^{L*}_{mJ} \left\langle \phi^{L}_{J} | \hat{h}_{11} | \phi^{L}_{K} \right\rangle c^{L}_{nK} + \sum_{J=1}^{N^L} \sum_{K=1}^{N^S} c^{L*}_{mJ} \left\langle \phi^{L}_{J} | \hat{h}_{12} | \phi^{S}_{K} \right\rangle c^{S}_{nK} \\
&\quad + \sum_{J=1}^{N^S} \sum_{K=1}^{N^L} c^{S*}_{mJ} \left\langle \phi^{S}_{J} | \hat{h}_{21} | \phi^{L}_{K} \right\rangle c^{L}_{nK} + \sum_{J=1}^{N^S} \sum_{K=1}^{N^S} c^{S*}_{mJ} \left\langle \phi^{S}_{J} | \hat{h}_{22} | \phi^{S}_{K} \right\rangle c^{S}_{nK} \quad (10.20)
\end{aligned}
$$

Therefore, contributions from the Large and Small component parts of the spinors are summed up in the transformation step. In any two-component approach, now, the terms involving the small component functions in Eq. (10.20) are obsolete and one obtains a transformed integral h'^{+}_{mn} which may be numerically different from h^{+}_{mn}. However, the obtained set of integrals has exactly the same size in both cases which essentially is due to the no-pair approximation, be it a priori or a posteriori. From Kramers-restricted optimizations we thus obtain a set of transformed (non-redundant) integrals h^{+}_{mn}, $h^{+}_{\overline{mn}}$, $(kl|mn)^{+}\ldots$ as given in Eqs. (10-11) and (10-12), both in the four- and two-component case. The relativistic electron correlation approaches presented here may therefore be used with four- and two-component Hamiltonians without modification, which opens the way for direct comparison.

10.4.1.2. Relativistic Formulations

The generality of the excitation class formalism introduced in Section 10.3.2 allows for the definition of different relativistic frameworks, both with respect to the Hamiltonian used in the orbital/spinor optimization step as well as the step accounting for dynamic electron correlation. We may envisage five commonly occurring cases, labelled by the excitation class manifold M, which are displayed in Table 10-3. Notably, there is no distinction between four- and two-component Hamiltonians. M = 1 refers to a non-relativistic Hamiltonian or a scalar relativistic Hamiltonian which does not include spin-dependent terms and therefore disallows for a change in the Kramers projection. As this environment always implies the use of (restricted) spin-orbitals, the Kramers pairs are simply comprised by a pair of

Table 10-3 Manifolds of excitation classes depending on the relativistic Hamiltonian and framework

	Excitation classes		
M	1-Particle terms	2-Particle terms	Relativistic framework
1	$\Delta M_K = 0$	$\Delta M_K = 0$	Non-relativistic or "scalar" relativistic
2	$\Delta M_K = 0, \pm 1$	$\Delta M_K = 0$	Orbitals, mean-field spin–orbit
3	$\Delta M_K = 0, \pm 1$	$\Delta M_K = 0, \pm 1, \pm 2$	Orbitals, full spin–orbit
4	$\Delta M_K = 0$	$\Delta M_K = 0, \pm 2$	Spinors, real/complex double groups
5	$\Delta M_K = 0, \pm 1$	$\Delta M_K = 0, \pm 1, \pm 2$	Spinors, quaternion double groups

α and β spin functions and a common spatial function. M = 2 defines a widely-used type of operators where the spin-dependent two-particle terms are approximated by an atomic mean-field (AMFI) [53]. This approach has proven to be reliable both for heavy [54] and also light elements [8, 55]. M = 3 comprises the generalization of M = 2 to a fully spin-dependent Hamiltonian, especially its two-particle terms, but still referring to a scalar one-particle basis. This type of approach has disadvantages compared to the formalism designated by M = 4 and M = 5 where a spinor basis is used. It is less efficient than the mean-field approach defined by M = 2 and less accurate than the spinor-based methods. In fact, in considering the discussion on the distinction between four- and two-component Hamiltonians (above) we may state that it is to a larger degree a question of *when* (i.e., at which stage of the calculation) spin–orbit interactions are introduced into relativistic methodology rather than *how*. In the framework of orbitals the relaxation of the wave function due to spin–orbit interaction has to be described by the correlation expansion. This is certainly viable and has been implemented in a number of quantum-chemical approaches, e.g., in references [5, 4, 21]. It has, however, been shown that in the case of CI models results at a given excitation level for the wave function are significantly more accurate if a spinor basis is used from the outset [8]. The latter of course comes with the price of having to deal with an extended set of transformed integrals (compared with approaches of type M = 2), even if these can be brought to (quaternion) real form. The problem of relaxation due to spin–orbit interaction at the correlated stage appears to be less pronounced in CC methods [7].

10.4.1.3. Hamiltonian in Kramers-Adapted Form

For the following discussions we shall focus on the four-component Dirac–Coulomb Hamiltonian $\hat{H}_{DC}$ which is the most exact representative of the types of Hamiltonians in the present context. Further formal elaborations on the Breit interaction giving rise to the spin and other orbit interaction in a two-component framework are presented in complete form elsewhere [33, 56].

In order to preserve the time-reversal property given by Eq. (10-4) for the individual terms of $\hat{H}_{DC}$ in second quantization, two possible operator bases will be discussed here. The basis introduced by Aucar et al. [19]

$$\hat{X}^{+}_{pq} = a^{\dagger}_{p} a_{q} + a^{\dagger}_{\overline{q}} a_{\overline{p}}$$

$$\hat{X}^{-}_{pq} = a^{\dagger}_{p} a_{q} - a^{\dagger}_{\overline{q}} a_{\overline{p}} \tag{10-21}$$

$$\hat{X}^{++}_{pqrs} = \hat{X}^{+}_{pq} \hat{X}^{+}_{rs} - \delta_{qr} a^{\dagger}_{p} a_{s} - \delta_{\overline{p}r} a^{\dagger}_{\overline{q}} a_{s} - \delta_{q\overline{s}} a^{\dagger}_{p} a_{\overline{r}} - \delta_{\overline{p}\overline{s}} a_{\overline{q}^{\dagger}} a_{\overline{r}} \tag{10-22}$$

etc.,

meets the requirements and has been used in relativistic MCSCF [23, 45, 24] and CI theory [21, 8]. The corresponding operators for Kramers-barred spinors are obtained by applying the Kramers replacement operator

$$\hat{K}_{pq}\, a^{\dagger}_{p} a_{q} := a^{\dagger}_{\overline{p}} a_{\overline{q}}. \tag{10-23}$$

For a consistent representation of the formalism, it is desirable to cast all occurring operators in terms of this basis, i.e., also the operators manipulating states such as orbital transformation and excitation operators with respect to a reference state. Since the $\hat{X}$ operators comprise combinations of excitations and deexcitations, an alternative representation purely in terms of excitation operators

$$\hat{E}^{v}_{pq} = \imath^{f(v)} \left(\hat{1} + v\hat{K}_{pq}\right) a^{\dagger}_{p} a_{q} \tag{10-24}$$

with

$$f(v) = \frac{3}{2}v + \frac{5}{2}v^{2} \tag{10-25}$$

for expressing the prefactor may be preferred for the case of relativistic CC theory. This is discussed in reference [57].

For most purposes $\hat{H}_{DC}$ may now be reformulated [33, 21] in the basis given by Eqs. (10-21) and (10-22) yielding

$$\begin{aligned}
\hat{H}_{DC} = & \sum_{pq} \left[\mathbf{h_{pq}} \hat{\mathbf{X}}^{+}_{\mathbf{pq}} + \frac{1}{2} \left(h_{\overline{p}q} \hat{X}^{+}_{\overline{p}q} + h_{p\overline{q}} \hat{X}^{+}_{p\overline{q}} \right) \right] \\
& + \frac{1}{2} \sum_{pqrs} \left[(\mathbf{pq}|\mathbf{rs}) \hat{\mathbf{x}}^{++}_{pqrs} + (\overline{p}q|rs) \hat{x}^{++}_{\overline{p}qrs} + (p\overline{q}|rs) \hat{x}^{++}_{p\overline{q}rs} \right] \\
& + \frac{1}{4} \sum_{pqrs} (\overline{p}q|r\overline{s}) \hat{x}^{++}_{\overline{p}qr\overline{s}} \\
& + \frac{1}{8} \sum_{pqrs} \left[(\overline{p}q|\overline{r}s) \hat{x}^{++}_{\overline{p}q\overline{r}s} + (p\overline{q}|r\overline{s}) \hat{x}^{++}_{p\overline{q}r\overline{s}} \right].
\end{aligned} \tag{10-26}$$

In a non-relativistic framework – due to spin integration – only the terms given in boldface symbols would be non-vanishing. It is clear from the discussion in Section 10.2.3 that the operator in this form contains redundant types of integrals over Kramers-paired spinors. Also in order to describe the advantages of string-based implementations in the present framework, the operator in the above form will undergo further modification as discussed in Section 10.4.2.2.

10.4.2. Configuration Interaction

10.4.2.1. Matrix Representations

Given a basis of Kramers-restricted optimized spinors we may first discuss general structural properties of the Hamiltonian matrix [23]. A matrix representation of the relativistic Hamiltonian using determinants formed from the spinor strings introduced in Section 10.3.1 is displayed schematically for a six-particle system in Figure 10-4. For all types of double groups discussed in Section 10.2.4 the unshaded blocks are zero as the Hamiltonian is at most a two-particle operator. The plain

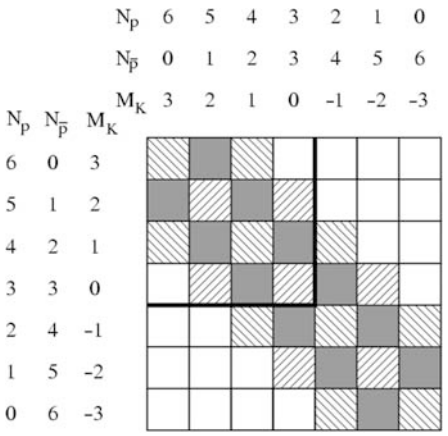

Figure 10-4. Hamiltonian matrix for a 6-particle system. N_p is the number of electrons in unbarred Kramers pairs, $N_{\overline{p}}$ the number of electrons in barred Kramers pairs (from reference [23]; reprinted by permission of the publisher.)

grey shaded blocks are zero for real-valued and complex valued groups, essentially because here the spinors of a Kramers pair transform according to different fermion irreducible representations of the double group. The different types of striped blocks represent non-vanishing but disjoint sections. Finally, time-reversal symmetry may be exploited also at the many-particle level to reduce the Hamiltonian matrix to the non-redundant part in the box in the upper left corner. This applies to an even total number of electrons. For systems with an odd total number of electrons, time-reversal symmetry is exploited since the wave function transforms according to a fermion irreducible representation of the double group.

10.4.2.2. String-Based Relativistic CI

Before turning to the actual algorithms and implementations of relativistic configuration interaction it is appropriate to highlight the essential differences between non-relativistic and relativistic approaches. This will make the extensive use of available symmetries and the need for highly efficient algorithms obvious.

10.4.2.2.1. Computational Demand Due to the loss of non-relativistic symmetries like spatial and spin symmetry, rigorously relativistic electron correlation calculations are significantly more demanding than their non-relativistic counterparts [50]. This increase in computational cost is best illustrated by virtue of a representative example featuring a typical multi-reference CI calculation.

We may again consider the CI expansion for an actinide atom with the valence electronic configuration $5f^7$ in a basis set comprising 67 and 68 virtual Kramers pairs in symmetries g and u, respectively. Using the highest abelian subgroup of the binary double point group D^*_{2h} which is C^*_{2h}, the various states arising from the ground electronic configuration $5f^7$ are obtained in the irreducible representation ^1E_u, see Table 10-4.

Table 10-4 Typical multi-reference singles and doubles CI expansion in the non-relativistic and relativistic frameworks for an actinide atom. The sum of all determinants in the non-relativistic case (counting $n = 1 \ldots 3$) equals the number of determinants in the relativistic case

	Non-relativistic			Relativistic	
State	# of dets.	Symmetry	State	# of dets.	Symmetry
^8X_u	23.433	A_u	(all states)	18.315.011	^1E_u
	23.771	B_{nu}			
^6X_u	324.314	A_u			
	325.795	B_{nu}			
^4X_u	1.419.874	A_u			
	1.422.304	B_{nu}			
^2X_u	2.804.408	A_u			
	2.809.124	B_{nu}			

The reference space in this example is given by all determinants which can be formed from distributing seven to five electrons among the $5f$ Kramers pairs and zero to two electrons among the virtual Kramers pairs, respectively. All states of octet through doublet symmetry are obtained by at most eight distinct calculations in the non-relativistic case, the largest of which comprises roughly 2.8 million Slater determinants. In the relativistic case all states are obtained in a single calculation, however comprising more than 18 million Slater determinants. Calculations of this size are still two orders of magnitude smaller than what is feasible today with modern implementations of string-driven relativistic CI [24, 58, 59]. The relativistic calculation in symmetry ^2E_u is not required since it is degenerate with ^1E_u. Double group and time-reversal symmetries therefore lead to important computational savings which must be exploited in efficient rigorous relativistic computer implementations. Beside the reduction of symmetry which makes relativistic calculations more demanding, a second factor comes into play: Due to the increased couplings of relativistic states among each other (caused by spin–orbit interaction) the CI Hamiltonian matrix is significantly more dense in the relativistic case (see Figure 10-4), i.e., it contains less zero-valued matrix elements. This structural change of the Hamiltonian matrix adds to the computational demand beside the actual size of the calculation, because the determination of projected vectors becomes more time-consuming.

10.4.2.2.2. Large-Scale Relativistic CI Algorithms The treatment of large CI expansions where at the same time only a few (lowest) eigensolutions are required has become a standard problem in non-relativistic frameworks. For example, for large sparse matrices modern variants [60, 42] of the Davidson algorithm [61] can be used which are also straightforwardly adapted for the treatment of complex matrix eigenvalue problems [45]. By virtue of the use of quaternion algebra and double group symmetry (as indicated in Section 10.2.4) the real-valued optimization algorithms can be used without modification also in the relativistic framework which

applies to atoms, all linear molecules, and to non-linear molecules of at least C_{2v} or D_2 symmetry. In all other cases, the formalism remains algebraically complex.

10.4.2.2.3. Sigma-Vector Fragmentation When it comes to computational efficiency in large-scale applications the decisive step in all types of above-mentioned algorithms is the determination of projected (sigma) vectors from a set of trial (C) vectors in a given iteration:

$$\boldsymbol{\sigma} = \mathbf{HC}.$$

where $\mathbf{H}$ is the Hamiltonian in matrix representation. It is the appearance of a wider class of integrals in the relativistic spinor basis beside the implementation of relativistic symmetries which comprise the essential changes requiring special attention.

Since the sigma vector can also be written in the fashion

$$\boldsymbol{\sigma} = \sum_{\Delta M_K=-2}^{+2} \boldsymbol{\sigma}^{\Delta M_K} \tag{10-27}$$

it is convenient to split the Hamiltonian operator (10-26) into five corresponding fractions:

$$\hat{H}^{DC}_{\Delta M_K=+2} = \sum_{pqrs} \frac{1}{8}(p\overline{q}|r\overline{s})\hat{x}^{++}_{p\overline{q}r\overline{s}} = \sum_{pqrs} \frac{1}{2} p^\dagger r^\dagger \overline{s}\overline{q}\ (p\overline{q}|r\overline{s}) \tag{10-28}$$

$$\begin{aligned}\hat{H}^{DC}_{\Delta M_K=+1} &= \sum_{pq} \frac{1}{2} h_{p\overline{q}} \hat{X}^{+}_{p\overline{q}} + \sum_{pqrs} \frac{1}{2}(p\overline{q}|rs)\hat{x}^{++}_{p\overline{q}rs} \\ &= \sum_{pq} \frac{1}{2} h_{p\overline{q}} \hat{X}^{+}_{p\overline{q}} \\ &\quad + \sum_{pqrs} \left[p^\dagger r^\dagger s\overline{q}\ (p\overline{q}|rs) + p^\dagger \overline{r}^\dagger \overline{s}\overline{q}\ (s\overline{p}|qr) \right]\end{aligned} \tag{10-29}$$

$$\begin{aligned}\hat{H}^{DC}_{\Delta M_K=0} &= \sum_{pq} h_{pq} \hat{X}^{+}_{pq} + \sum_{pqrs} \left[\frac{1}{2}(pq|rs)\hat{x}^{++}_{pqrs} + \frac{1}{4}(\overline{p}q|r\overline{s})\hat{x}^{++}_{\overline{p}qr\overline{s}} \right] \\ &= \sum_{pq} h_{pq} \hat{X}^{+}_{pq} \\ &\quad + \sum_{pqrs} \Big\{ \frac{1}{2} \left[p^\dagger r^\dagger sq(pq|rs) + \overline{p}^\dagger \overline{r}^\dagger \overline{s}\overline{q}(qp|sr) \right] \\ &\qquad + p^\dagger \overline{r}^\dagger \overline{s}q\ [(pq|sr) + (\overline{r}q|s\overline{p})] \Big\}\end{aligned} \tag{10-30}$$

$$\hat{H}^{DC}_{\Delta M_K=-1} = \sum_{pq} h_{\overline{p}q}\hat{X}^{+}_{\overline{p}q} + \sum_{pqrs}\frac{1}{2}(\overline{p}q|rs)x^{++}_{\overline{p}qrs}$$
$$= \sum_{pq} h_{\overline{p}q}\hat{X}^{+}_{\overline{p}q}$$
$$+ \sum_{pqrs}\left[\overline{p}^{\dagger}r^{\dagger}sq(\overline{s}p|rq) + \overline{p}^{\dagger}\overline{r}^{\dagger}\overline{s}q(\overline{p}q|sr)\right] \quad (10\text{-}31)$$

$$\hat{H}^{DC}_{\Delta M_K=-2} = \sum_{pqrs}\frac{1}{2}(\overline{p}q|\overline{r}s)x^{++}_{\overline{p}q\overline{r}s}$$
$$= \sum_{pqrs}\frac{1}{2}\overline{p}^{\dagger}\overline{r}^{\dagger}sq(\overline{p}q|\overline{r}s) \quad (10\text{-}32)$$

Before turning to the algorithm, we may with the help of Figure 10-4 summarize the properties of the iterative procedure in the relativistic case. The first CI iteration yields the Hartree–Fock determinant in the closed shell case or a simple linear combination of a few determinants in the open-shell case. Assuming that the initial wave function corresponds to a non-relativistic or scalar relativistic Hamiltonian, this initial wave function has a well-defined Kramers projection value M_K. In the second iteration, all possible couplings from the initial determinants to all singly and doubly excited determinants are included, necessarily having Kramers projection values from M_K to $M_K \pm 2$. This step can be viewed as a first order coupling in terms of perturbation theory. The third iteration includes all the determinants that can be obtained from the initial wave function with up to quadruple excitations and Kramers projection from M_K to $M_K \pm 4$. In the case depicted in Figure 10-4 this comprises the full determinant space, but in cases with more open-shell orbitals, a larger number of iterations may be required to include the full determinant space.

10.4.2.2.4. Excitation-Class-Driven Algorithm Using the concept of excitation classes introduced in Section 10.3.2 the connections between right-hand and left-hand string types may now be determined by their corresponding excitation types and those of the Hamiltonian (respectively its fragment in question). Due to the generality of this approach, the evaluation of structurally similar quantities is straightforwardly possible, in particular linearly transformed vectors (sigma vectors) and CI density matrices.

Labelled with M_K and a real/imaginary index as $\boldsymbol{\sigma}_r^{M_K}$ a specific element ($\mathcal{T}, \overline{\mathcal{T}}$; string indices are dropped for convenience[1]) of the sigma vector fragment reads

$$\sigma_r^{+2}(\mathcal{T}, \overline{\mathcal{T}}) = \sum_{ijkl}\sum_{\mathcal{S},\overline{\mathcal{S}}}(p\overline{q}|r\overline{s})^{r/i}\, A^{\mathcal{T}\overline{\mathcal{T}},\mathcal{S}\overline{\mathcal{S}}}_{p\overline{q}r\overline{s}} C^{r/i}_{\mathcal{S},\overline{\mathcal{S}}} \quad (10\text{-}33)$$

[1] Therefore, $\hat{K}\mathcal{T}$ is in general NOT equal to $\overline{\mathcal{T}}$ in the present context.

where $\mathcal{S}\overline{\mathcal{S}}$ denote unbarred and barred strings as defined in Eq. (10-13). $A^{\mathcal{T}\overline{\mathcal{T}},\mathcal{S}\overline{\mathcal{S}}}_{p\overline{q}r\overline{s}} = \langle\ |\mathcal{T}\overline{\mathcal{T}}p^\dagger r^\dagger \overline{sq}\mathcal{S}^\dagger\overline{\mathcal{S}}^\dagger|\ \rangle$ is the CI coupling coefficient for the bra ($\mathcal{T}\overline{\mathcal{T}}$) and ket ($\mathcal{S}\overline{\mathcal{S}}$) determinant. The actual evaluation of the coupling coefficient and the ensuing contractions can be implemented in a very general fashion based on the manipulation of the involved spinor strings [8].

CI density matrices are likewise obtained by replacing the integrals $(p\overline{q}|rs)^{r/i}$ used in the contraction for the sigma vector (10-33) with expansion coefficients of the left-hand determinants $C_{\mathcal{T},\overline{\mathcal{T}}}$, for example according to

$$\rho^r(2)\,(p\overline{q}rs) = \sum_{\mathcal{S},\overline{\mathcal{S}}}\sum_{\mathcal{T},\overline{\mathcal{T}}} C^{r/i}_{\mathcal{T},\overline{\mathcal{T}}} A^{\mathcal{T}\overline{\mathcal{T}},\mathcal{S}\overline{\mathcal{S}}}_{p\overline{q}rs} C^{r/i}_{\mathcal{S},\overline{\mathcal{S}}}. \tag{10-34}$$

We may now turn to the essential question of how the coupling coefficients are determined in an efficient manner, since this issue is decisive for the large-scale applicability of the methods presented in this chapter.

10.4.2.2.5. Coupling Coefficients Via Strings For simplicity we drop the indexing of real and imaginary parts and restrict the summations in Eq. (10-33) to obtain

$$\sigma^{+2}(\mathcal{T},\overline{\mathcal{T}}) = \sum_{\substack{p\geq r\\ s\geq q}}\sum_{\mathcal{S}\overline{\mathcal{S}}} \langle\ |\mathcal{T}\overline{\mathcal{T}}\ p^\dagger r^\dagger \overline{sq}\ \mathcal{S}^\dagger\overline{\mathcal{S}}^\dagger|\ \rangle \cdot [(p\overline{q}|r\overline{s}) - (r\overline{q}|p\overline{s})] \cdot C^{(\mathcal{T}\overline{\mathcal{T}})}_{\mathcal{S},\overline{\mathcal{S}}} \tag{10-35}$$

We may now insert a resolution of the identity in the spinor string basis

$$\mathbf{1} = \sum_{\mathcal{U}\overline{\mathcal{U}}} \mathcal{U}^\dagger\overline{\mathcal{U}}^\dagger|\ \rangle\langle\ |\mathcal{U}\overline{\mathcal{U}} \tag{10-36}$$

into the matrix element for the coupling coefficient and obtain for this part of the expression

$$\begin{aligned}&\sum_{\mathcal{S}\overline{\mathcal{S}}} \langle\ |\mathcal{T}\overline{\mathcal{T}}\ p^\dagger r^\dagger \overline{sq}\ \mathcal{S}^\dagger\overline{\mathcal{S}}^\dagger|\ \rangle\\ &= \sum_{\mathcal{S}\overline{\mathcal{S}}}\sum_{\mathcal{U}\overline{\mathcal{U}}} \langle\ |\mathcal{T}\overline{\mathcal{T}}\ p^\dagger r^\dagger\ \mathcal{U}^\dagger\overline{\mathcal{U}}^\dagger|\ \rangle\langle\ |\mathcal{U}\overline{\mathcal{U}}\ \overline{sq}\ \mathcal{S}^\dagger\overline{\mathcal{S}}^\dagger|\ \rangle.\end{aligned} \tag{10-37}$$

The string of annihilation operators $\overline{\mathcal{T}}$ can now be permuted to the right of the spinor creation operators, whereby a sign $(-1)^{2N}$ arises, N being the length of the barred/unbarred string:

$$\prod_{i=1}^{N} a_{\mathcal{T}}(\bar{i})\ a^\dagger(p) = \prod_{i=2}^{N} a_{\mathcal{T}}(\bar{i}) \left[\delta_{\bar{i}p} - a^\dagger(p)\ a_{\mathcal{T}}(\bar{i})\right] = (-1)^N\ a^\dagger(p) \prod_{i=1}^{N} a_{\mathcal{T}}(\bar{i}) \tag{10-38}$$

This manipulation becomes possible due to the use of a Kramers-restricted spinor basis. We perform the same permutations with the string $\mathcal{U}^\dagger$ and obtain for Eq. (10-37)

$$\begin{aligned}
&\sum_{\mathcal{S}\overline{\mathcal{S}}}\sum_{\mathcal{U}\overline{\mathcal{U}}} \langle \quad | \mathcal{T}\, p^\dagger r^\dagger\, \overline{\mathcal{T}}\mathcal{U}^\dagger\overline{\mathcal{U}}^\dagger | \quad \rangle \langle \quad | \mathcal{U}\overline{\mathcal{U}}\, \overline{sq}\, \mathcal{S}^\dagger\overline{\mathcal{S}}^\dagger | \quad \rangle \\
&= \sum_{\mathcal{S}\overline{\mathcal{S}}}\sum_{\mathcal{U}\overline{\mathcal{U}}} \langle \quad | \mathcal{T}\, p^\dagger r^\dagger\, \overline{\mathcal{T}\mathcal{U}}^\dagger\mathcal{U}^\dagger | \quad \rangle \langle \quad | \overline{\mathcal{U}}\mathcal{U}\, \overline{sq}\, \mathcal{S}^\dagger\overline{\mathcal{S}}^\dagger | \quad \rangle \\
&= \sum_{\mathcal{S}\overline{\mathcal{S}}}\sum_{\mathcal{U}\overline{\mathcal{U}}} \langle \quad | \mathcal{T}\, p^\dagger r^\dagger\, \overline{\mathcal{T}\mathcal{U}}^\dagger\mathcal{U}^\dagger | \quad \rangle \langle \quad | \overline{\mathcal{U}}\, \overline{sq}\, \mathcal{U}\mathcal{S}^\dagger\overline{\mathcal{S}}^\dagger | \quad \rangle . \qquad (10\text{-}39)
\end{aligned}$$

Here we have exploited that the sign from the permutation of $\mathcal{U}^\dagger\overline{\mathcal{U}}^\dagger$ is reproduced by the permutation of $\mathcal{U}\overline{\mathcal{U}}$. Executing the sums over resolution strings $\mathcal{U}\overline{\mathcal{U}}$ finally yields

$$\sum_{\mathcal{S}\overline{\mathcal{S}}} \langle \quad | \mathcal{T}\; p^\dagger r^\dagger\, \mathcal{S}^\dagger | \quad \rangle \langle \quad | \overline{\mathcal{T}}\; \overline{sq}\; \overline{\mathcal{S}}^\dagger | \quad \rangle . \qquad (10\text{-}40)$$

Using this expression the partition of the sigma vector becomes

$$\sigma^{+2}(\mathcal{T},\overline{\mathcal{T}}) = \sum_{\substack{p\geq r\\ s\geq q}}\sum_{\mathcal{S}\overline{\mathcal{S}}} \langle \quad | \mathcal{T}\; p^\dagger r^\dagger\, \mathcal{S}^\dagger | \quad \rangle \langle \quad | \overline{\mathcal{T}}\; \overline{sq}\; \overline{\mathcal{S}}^\dagger | \quad \rangle \cdot [(p\overline{q}|r\overline{s}) - (r\overline{q}|p\overline{s})] \cdot C^{(\mathcal{T}\overline{\mathcal{T}})}_{\mathcal{S},\overline{\mathcal{S}}} \qquad (10.41)$$

which exhibits the principal form required to understand string-graphical approaches to evaluating coupling coefficients or connections. By inserting a resolution of the identity the coupling coefficients have been split into two disjoint matrix elements which only involve unbarred or barred spinors, respectively. In an analogous manner the other sigma vector partitions may be treated, yielding disjoint coupling coefficients over spinor operator strings of individual lengths between zero and two, respectively. The two-particle creation mappings for the above element $\langle \quad | \mathcal{T}\; p^\dagger r^\dagger\; \mathcal{S}^\dagger | \quad \rangle$ and the two-particle annihilation mappings for the element $\langle \quad | \overline{\mathcal{T}}\; \overline{sq}\; \overline{\mathcal{S}}^\dagger | \quad \rangle$ are now obtained separately by exploiting the organization of n-particle strings for active subspaces as introduced in Section 10.3.1. It is thus possible to exploit the same efficiency gain in relativistic CI as has been obtained in the case of non-relativistic CI approaches by splitting Slater determinants into ordered strings of alpha/beta (unbarred/barred) types [62, 35, 42]. This will be demonstrated for sample applications discussed in Section 10.5.

10.4.3. Multi-Configuration SCF

Theory and formalism of truly relativistic molecular (or atomic) MCSCF for application in both the four-component (empty-Dirac picture) and two-component frameworks have been presented already in the mid 1990s [23]. In 2003 Kim

and Lee published a partial implementation of a genuine second-order Kramers restricted MCSCF method for two-component spinors and relativistic effective core potentials (RECP) including spin–orbit interactions [25]. Their work documents some of the benefits of a fully variational KR-MCSCF method for static correlation. In the present the first full implementation of a Kramers-restricted second-order relativistic four-component MCSCF model for molecules is described.

The implementation of this method [45] has made it possible to optimize molecular Kramers-paired spinors under full account of spin–orbit interaction. The advantages of such an approach are twofold: (1) Due to the treatment of spin–orbit coupling a priori the determination of potential energy curves/surfaces includes the most important relativistic effects already in the orbital optimization, which is for instance of importance in the qualitatively correct description of many dissociation processes where heavy elements are involved. (2) In general, MCSCF spinors represent a much better wave function approximation for subsequent treatments of dynamic electron correlation than Hartree–Fock spinors. In particular for the description of electronically excited states of heavy-element compounds with complicated electronic structure, state-specific MCSCF wave functions may be of great advantage in the process of obtaining a quantitatively correct picture of these states.

Since the MCSCF method [63] is a multi-configurational approach, a CI module of preferrably large-scale applicability is highly desirable. Calculations on heavy-element compounds often necessitate the use of large active spaces, which is due to the frequently occurring energetic near-degeneracy of orbitals in heavy elements and the also often occurring large number of unpaired electrons, especially in electronically excited states. It is for these reasons that string-driven relativistic CI is of importance for an efficient and widely applicable relativistic MCSCF method, as well as for a subsequent treatment of dynamic electron correlation. The central features of the approaches presented in references [23, 45, 24] shall therefore be summarized here. An emphasis will be put on those features relevant to string-based relativistic CI.

10.4.3.1. MCSCF Algorithm

In order to achieve a good approximation to the exact energy functional $E(\boldsymbol{\lambda})$ energy variations are expressed through a second-order Taylor expansion around the current expansion point in the parameter space ($\boldsymbol{\lambda} = \mathbf{0}$),

$$E^{(2)}(\boldsymbol{\lambda}) = E(\mathbf{0}) + \boldsymbol{\lambda}^{\dagger}\boldsymbol{E}^{[1]} + \frac{1}{2}\boldsymbol{\lambda}^{\dagger}\boldsymbol{E}^{[2]}\boldsymbol{\lambda} \tag{10-42}$$

with the energy gradient $\boldsymbol{E}^{[1]}$ and the energy Hessian matrix $\boldsymbol{E}^{[2]}$. The optimal second-order step for minimization is the step giving the lowest predicted energy value from the second-order expansion, yielding a modified Newton type of equation

$$\boldsymbol{\lambda}^{\nu} = -(\boldsymbol{E}^{[2]} - \nu\boldsymbol{I})^{-1}\boldsymbol{E}^{[1]} \tag{10-43}$$

with a level shift parameter ν. The solution of this equation defines one macro iteration.

In order to allow for large relativistic MCSCF expansions with millions of configurations and hundreds of basis functions, the energy Hessian matrix $E^{[2]}$ is never calculated explicitly [64]. The solution vector is instead found by an iterative algorithm, where the solution vector is approximately expanded in a set of trial vectors $\{b_n\}$

$$\boldsymbol{\lambda}^j = \sum_n^{N_b^j} a_n^j b_n \tag{10-44}$$

where N_b^j is the dimension of the trial vector space in micro iteration j. The solution $\boldsymbol{\lambda}^\nu$ to the full linear equation in Eq. (10-43) is found to the required accuracy by means of successive linear transformations

$$\boldsymbol{\sigma}_n = E^{[2]} b_n \tag{10-45}$$

for each $\boldsymbol{b}_n$. The optimal coefficients $\{a_n^j\}$ in Eq. (10-44) are found by solving the *projected* linear equations, where Eq. (10-43) is projected onto the reduced vector space of trial vectors

$$\boldsymbol{a}^j = -(E^{[2j]} - \nu_j I)^{-1} E^{[1j]}. \tag{10-46}$$

The reduced Hessian and gradient elements are thus

$$E_{mn}^{[2j]} = b_m^\dagger E^{[2]} b_n = b_m^\dagger \sigma_n \tag{10-47}$$

$$E_n^{[1j]} = b_n^\dagger E^{[1]}. \tag{10-48}$$

All sigma vectors $\boldsymbol{\sigma}_n$ have configurational and orbital contributions, as the Hessian couples all subspaces. This separation of configurational and orbital rotations is not necessary, but it has been shown to be advantageous with respect to computation time [65].

10.4.3.2. Electronic Gradient and Hessian

The configurational part of Eq. (10-48) for a determinant $\left|\Phi_\mu\right\rangle$ reads

$$E_\mu^{[1]c} = \left\langle \Phi_\mu \left| \hat{H} \right| c^{(k)} \right\rangle - E^{[0]} c_\mu^{(k)} \tag{10-49}$$

and the expression $\hat{H}\left|c^{(k)}\right\rangle$ needs to be determined from the current expansion point vector $\left|c^{(k)}\right\rangle$. For the orbital part one obtains expressions of the type

$$E_{rs}^{[1]o} = -\left\langle \mathbf{c}^k \left| \left[\hat{X}_{sr}^-, \hat{H} \right] \right| \mathbf{c}^k \right\rangle \tag{10-50}$$

where $\hat{X}_{sr}^-$ is defined by Eq. (10-21).

Likewise, writing Eq. (10-45) in terms of configurational and orbital parts, one obtains

$$\begin{pmatrix} \sigma^{c} \\ \sigma^{o} \\ \sigma^{c^*} \\ \sigma^{o^*} \end{pmatrix} = \begin{pmatrix} E^{[2]c^*,c} & E^{[2]c^*,o} & E^{[2]c^*,c^*} & E^{[2]c^*,o^*} \\ E^{[2]o^*,c} & E^{[2]o^*,o} & E^{[2]o^*,c^*} & E^{[2]o^*,o^*} \\ E^{[2]c,c} & E^{[2]c,o} & E^{[2]c,c^*} & E^{[2]c,o^*} \\ E^{[2]o,c} & E^{[2]o,o} & E^{[2]o,c^*} & E^{[2]o,o^*} \end{pmatrix} \cdot \begin{pmatrix} b^{c} \\ b^{o} \\ b^{c^*} \\ b^{o^*} \end{pmatrix}, \quad (10\text{-}51)$$

The configurational parts of the sigma vectors comprise the contributions

$$\boldsymbol{\sigma}^{c}_{\mu} = \langle \Phi_{\mu} | \hat{H} | \mathbf{B} \rangle + \langle \Phi_{\mu} | \tilde{\hat{H}} \left| \mathbf{c}^{k} \right\rangle, \quad (10\text{-}52)$$

where $|\mathbf{B}\rangle = \sum_{\mu} b_{\mu} |\Phi_{\mu}\rangle$ is a configurational trial vector and $\tilde{\hat{H}}$ is a one-index transformed Hamiltonian [23,45]. For the orbital parts one obtains [23,45]

$$\boldsymbol{\sigma}^{o}_{rs} = -\left\{ \left\langle \mathbf{c}^{k} \left| \left[\hat{X}^{-}_{sr}, \hat{H} \right] \right| \mathbf{B} \right\rangle + \left\langle \mathbf{B} \left| \left[\hat{X}^{-}_{sr}, \hat{H} \right] \right| \mathbf{c}^{k} \right\rangle \right\} - \left\langle \mathbf{c}^{k} \left| \left[\hat{X}^{-}_{sr}, \tilde{\hat{H}} \right] \right| \mathbf{c}^{k} \right\rangle. \quad (10.53)$$

It is therefore obvious that the applicability of relativistic (as well as non-relativistic) MCSCF crucially depends on the direct CI technique employed to evaluate these expressions. The configuration space vectors, both current expansion point or CI trial vectors, which are required in the linear transformations (sigma vectors) and the density matrices may have very large dimensions. Table 10-5 summarizes the quantities evaluated by string-driven direct CI and relates them to their origin in the MCSCF equations. The evaluation of sigma vectors, density and transition density matrices proceeds as expounded in Section 10.4.2.2.4.

As an efficient option, integrals with two indices referring to negative-energy states may be neglected in the calculation of sigma vectors. Although this is then consequently not a fully second-order optimization, it gives satisfactory convergence at a significantly lower cost in the integral transformation [45,23] which needs to be carried out once for every macro iteration.

The MCSCF approach is its current form [45] is directly applicable using the four-component or two-component Hamiltonian operators implemented in the `DIRAC` program system [48]. In contrast to the methods presented here

Table 10-5 Direct CI contributions to the MCSCF gradient and Hessian

Gradient $E^{[1]}$	Config. part $E^{[1]c}$	CI sigma vector $\hat{H} \left\| c^{(k)} \right\rangle$
Gradient $E^{[1]}$	Orbital part $E^{[1]o}$	CI density matrices $\left\langle c^{(k)} \right\| \left[\hat{X}^{-}_{sr}, \hat{H} \right] \left| c^{(k)} \right\rangle$
Hessian $E^{[2]}$	Config. part $E^{[2]c,c/o}$	CI sigma vector $\hat{H} \left\| c^{(k)} \right\rangle$
		CI sigma vector $\hat{H} \|\mathbf{B}\rangle$
Hessian $E^{[2]}$	Orbital part $E^{[2]o,c/o}$	CI density matrices $\left\langle c^{(k)} \right\| \left[\hat{X}^{-}_{sr}, \hat{H} \right] \left| c^{(k)} \right\rangle$
		CI transition densities $\left\langle c^{(k)} \right\| \left[\hat{X}^{-}_{sr}, \hat{H} \right] \|\mathbf{B}\rangle$

which treat dynamic electron correlation, two-component approximations lead to significant computational savings in relativistic MCSCF applications since the (computationally expensive) integral transformations only include integrals over the large-component parts of spinors.

10.4.4. Coupled Cluster

Relativistic CC calculations for molecules containing heavy elements can presently not attain the same accuracy as non-relativistic CC calculations for molecules containing light elements. The limiting factors are the number of electrons which need to be correlated, the size of the required one-particle basis sets, the more complicated electronic structure of many heavy-element compounds, and the less-developed methodology for relativistic CC calculations. Also and especially in the relativistic domain, general-order and multi-reference approaches are highly desirable. This pertains to the occurrence of unpaired electrons, not only when dissociation processes are to be described but very often in the ground- and excited-state electronic structures close to equilibrium geometries. General-order and multi-reference implementations are therefore related, and advances in relativistic CC methodology are likely to touch upon both these issues.

There is still no general consensus on how a multi-reference coupled cluster theory should be formulated. Modern developments including iterative excitation levels higher than CC doubles, e.g., [37, 44, 66–68] and various multi-reference (MR) approaches [44, 43, 69, 70] have been presented in the non-relativistic framework. Generalizations to a relativistic formalism, which is here to be understood as also including spin–orbit interaction terms, remain rare. Hirata et al. [71] describe higher-order electron correlation methods including coupled cluster approaches where spin–orbit interaction is introduced by means of relativistic effective core potentials with spin–orbit effective potentials. The four-component implementations by Visscher et al., Kramers-restricted [29] and unrestricted [72], respectively, are not generally applicable to open-shell/multi-reference states. The only genuinely relativistic multi-reference approaches for molecules reported to the date are the Fock-Space CC implementations by Landau et al. [73] and Visscher et al. [74]. These methods, as the Fock-space approach in general, use a common orbital basis for all of the occurring ionized systems. Relativistic FSCC approaches have been applied to systems with few unpaired electrons and in this domain are likely to be the most accurate relativistic molecular many-body methods currently available.

Alternatively, the multi-reference problem may be approached by exploiting the GAS concept in the construction of CC model spaces [44, 75], leading to variants of so-called state-specific MRCC. This formulation retains the advantages of single-reference approaches such as the commutativity of cluster operators and allows for a flexible definition and robust treatment of open-shell and multi-reference problems [76].

10.4.4.1. Active-Space Coupled Cluster

The original idea for the type of multi-reference CC approach presented here is ascribed to Oliphant and Adamowicz [77, 78]. The present approach is based on the generalized implementation of these ideas by Olsen [44, 76] where the projection manifold is extended to simulate excitations from additional reference functions beside those from the Fermi vacuum state. Figure 10-5 gives an illustration of how the CC model spaces are constructed. We resort to a simple case with undefined number of Kramers pairs in GAS I, one valence (e.g., bonding) Kramers pair in GAS II, another Kramers pair, e.g., of antibonding character, in GAS III, and an undefined number of Kramers pairs in the external space GAS IV. The arising model space is best understood by explicitly considering the CC excitation manifold $\langle\mu|$ obtained by these definitions. Since the number of holes in GAS I is restricted to two, the excitation manifold can be written as

$$\langle\mu| = \left\langle\mu^{S(\mathrm{III}^1)}\right| + \left\langle\mu^{S(\mathrm{IV}^1)}\right| + \left\langle\mu^{D(\mathrm{III}^2)}\right| + \left\langle\mu^{D(\mathrm{IV}^2)}\right| + \left\langle\mu^{D(\mathrm{III}^1+\mathrm{IV}^1)}\right| + \left\langle\boldsymbol{\mu}^{\mathbf{T}(\mathbf{III}^1+\mathbf{IV}^2)}\right| + \left\langle\mu^{T(\mathrm{III}^2+\mathrm{IV}^1)}\right| + \left\langle\boldsymbol{\mu}^{\mathbf{Q}(\mathbf{III}^2+\mathbf{IV}^2)}\right|. \quad (10\text{-}54)$$

The term $\left\langle\mu^{S(\mathrm{III}^1)}\right|$ now indicates that relative to the (in this case) closed-shell reference state, where GAS I and GAS II are fully occupied, Single (S) replacements with one electron occupying GAS III have been included. Likewise, the other terms of the extended excitation manifold are interpreted. Particular attention should be paid to the two terms given in boldface symbols: $\left\langle\boldsymbol{\mu}^{\mathbf{T}(\mathbf{III}^1+\mathbf{IV}^2)}\right|$ denotes triple excitations

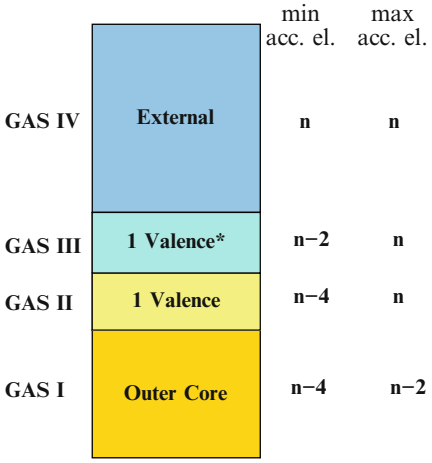

Figure 10-5. Generalized Active Space model for a CC wave function. *n* is the total number of electrons, min./max. acc. el. specifies the minimum/maximum number of accumulated electrons after consideration of this subspace

with respect to the reference state where two particles reside in the external space. Compared with the term $\left\langle \mu^{D(\mathrm{IV}^2)} \right|$ which "correlates" the reference state it is seen that in the Triples term a single excitation is "correlated", as Double excitations into the external space are combined with these Single excitations. In an analogous manner, the term $\left\langle \mu^{Q(\mathrm{III}^2+\mathrm{IV}^2)} \right|$ describes the correlation of the one doubly-excited state within spaces II and III. Essentially, GAS CC therefore simulates a genuine multi-reference CC treatment by including a selected set of higher excitations in the excitation manifold. In the same way the cluster operators are constructed such that they include all excitations defined by the active space constraints. A description of this CC Ansatz is presented in reference [81].

The drawback of this formalism – in contrast to FSCC or the state-universal Ansatz [69, 79] or a new multi-reference exponential ansatz by Hanrath [80] – is the variance with respect to the choice of the Fermi vacuum since the various conceivable reference functions are not strictly treated on the same footing. The straightforward remedy, a separate cluster expansion for every reference function, leads to the state-universal Hilbert-space CC theory which is far less efficient [79]. The loss of Fermi vacuum invariance, however, does not appear to be of crucial importance in application and problems can be avoided by proper choices of reference spaces [40].

10.4.4.2. Relativistic Cluster Operators

The cluster operators $\hat{T} = \sum_m \hat{T}_m$ are now generalized to the relativistic framework, which entails the possibility of flipping the Kramers projection along with the excitation [46]:

$$\hat{T}_1 = \sum_{ia} \left\{ t_i^a \hat{\tau}_i^a + t_{\bar{i}}^a \hat{\tau}_{\bar{i}}^a + t_i^{\bar{a}} \hat{\tau}_i^{\bar{a}} + t_{\bar{i}}^{\bar{a}} \hat{\tau}_{\bar{i}}^{\bar{a}} \right\}$$

$$\begin{aligned}\hat{T}_2 = \sum_{ij,ab} \Bigg\{ & \frac{1}{4} t_{ij}^{ab} \hat{\tau}_{ij}^{ab} + \frac{1}{2} t_{\bar{i}\bar{j}}^{ab} \hat{\tau}_{\bar{i}\bar{j}}^{ab} + \frac{1}{2} t_{i\bar{j}}^{ab} \hat{\tau}_{i\bar{j}}^{ab} + \frac{1}{2} t_{ij}^{\bar{a}\bar{b}} \hat{\tau}_{ij}^{\bar{a}\bar{b}} + \frac{1}{2} t_{ij}^{a\bar{b}} \hat{\tau}_{ij}^{a\bar{b}} \\ & + \frac{1}{4} t_{\bar{i}\bar{j}}^{\bar{a}\bar{b}} \hat{\tau}_{\bar{i}\bar{j}}^{\bar{a}\bar{b}} + t_{i\bar{j}}^{\bar{a}\bar{b}} \hat{\tau}_{i\bar{j}}^{\bar{a}\bar{b}} + t_{i\bar{j}}^{a\bar{b}} \hat{\tau}_{i\bar{j}}^{a\bar{b}} + t_{\bar{i}j}^{\bar{a}\bar{b}} \hat{\tau}_{\bar{i}j}^{\bar{a}\bar{b}} + t_{\bar{i}j}^{a\bar{b}} \hat{\tau}_{\bar{i}j}^{a\bar{b}} + \frac{1}{4} t_{ij}^{\overline{ab}} \hat{\tau}_{ij}^{\overline{ab}} \\ & + \frac{1}{2} t_{\bar{i}\bar{j}}^{\bar{a}\bar{b}} \hat{\tau}_{\bar{i}\bar{j}}^{\bar{a}\bar{b}} + \frac{1}{2} t_{\bar{i}\bar{j}}^{a\bar{b}} \hat{\tau}_{\bar{i}\bar{j}}^{a\bar{b}} + \frac{1}{2} t_{\bar{i}j}^{\overline{ab}} \hat{\tau}_{\bar{i}j}^{\overline{ab}} + \frac{1}{2} t_{i\bar{j}}^{\overline{ab}} \hat{\tau}_{i\bar{j}}^{\overline{ab}} + \frac{1}{4} t_{\bar{i}\bar{j}}^{\overline{ab}} \hat{\tau}_{\bar{i}\bar{j}}^{\overline{ab}} \Bigg\} \\ & \text{etc.} \end{aligned} \tag{10-55}$$

In the case of spin orbitals, the Kramers flipping would correspond to the introduction of terms accounting for spin–orbit interaction. In the present, this special case is generalized to be applicable with any kind of one-particle space of Kramers-paired spinors. As here no restrictions on the amplitudes regarding time-reversal symmetry in the many-particle space are introduced, this approach is termed *Kramers-unrestricted* relativistic CC, referring to the many-particle but not the

one-particle space. The excitations are categorized according to the change in the Kramers projection M_K, e.g., $\hat{\tau}_i^{\overline{a}}$ corresponds to $\Delta M_K = -1$, $\hat{\tau}_{i\overline{j}}^{ab}$ to $\Delta M_K = +1$, $\hat{\tau}_{\overline{ij}}^{\overline{ab}}$ to $\Delta M_K = 0$, etc.

10.4.4.3. Coupled Cluster Vector Function

The central quantity to be evaluated in the course of a coupled cluster optimization is the coupled cluster vector function Ω_μ for a given element μ of the excitation manifold:

$$\Omega_\mu = \left\langle \mu \left| e^{-\hat{T}} \hat{H} e^{\hat{T}} \right| \mathrm{Ref} \right\rangle \tag{10-56}$$

The evaluation of the CC vector function proceeds in an analogous fashion as described in reference [44], where the CC vector function is obtained in four steps which are based on CI expansions and string manipulations. Some care has to be taken regarding the term "string-based" in this context. Strictly speaking, the presented approach is string-based because the CI expansions are performed in a string-based manner, as expounded in Section 10.4.2.2. However, genuinely string-based CC is usually understood as determining connections and performing contractions based directy on the manipulation of (spinor) strings, not intermediate CI expansions. An approach of the latter type is currently under development [81]. Although the CI-based formalism is not very efficient, it is generally applicable and exploits the advantages of string-based relativistic CI.

Based on relativistic CI expansions the CC vector function may be constructed in essentially four steps.

Step 1: $|a\rangle = e^{\hat{T}} |\mathrm{Ref}\rangle$*, expansion of the reference vector*

$$\begin{aligned} |a\rangle &= \left(\sum_{n=0} \frac{1}{n!} \hat{T}^n \right) |\mathrm{Ref}\rangle \\ &= |\mathrm{Ref}\rangle + \hat{T} |\mathrm{Ref}\rangle + \frac{1}{2} \hat{T} \left\{ \hat{T} |\mathrm{Ref}\rangle \right\} + \frac{1}{6} \cdots \end{aligned} \tag{10-57}$$

The expansion is carried out by calculating a CI sigma vector repeatedly, i.e. once for each term $\hat{T} |\mathrm{Ref}\rangle$, as described in Section 10.4.2.2.4. In this step, the contraction is not performed with integrals, however, but with the CC amplitudes of the current iteration.

A restricted set of excitations may be defined by reducing the range of allowed M_K values for the construction of excitations. This leads to approximate CC calculations within a reduced coupling scheme. The expansion in step 1 is otherwise truncated when the highest excitation level has been reached which may couple to the excitation manifold.

Step 2: $|b\rangle = \hat{H}\,|a\rangle$*: linear transformation of the expanded reference vector* This step again corresponds to the calculation of a CI sigma vector of the expanded reference vector $|a\rangle$. The contraction is now carried out with integrals over Kramers-paired spinors which are classified according to excitation classes and the associated change of M_K, as discussed in Section 10.3.2. As demonstrated in reference [46], the vector $\hat{H}e^{\hat{T}}\,|Ref\rangle$ should be in the space of atmost n-fold excitations whereas $e^{\hat{T}}\,|Ref\rangle$ may be in the space of $n+2$-fold excitations. The operation count of this step thus scales as $O^{n+2}V^{n+2}$, where O is the number of occupied Kramers pairs, V is the number of virtual Kramers pairs, and n is the maximum excitation level.

Step 3: $|c\rangle = e^{-\hat{T}}\,|b\rangle$*, expansion of the transformed reference vector*

$$\begin{aligned} |c\rangle &= \left(\sum_{n=0} \frac{(-1)^n}{n!}\,\hat{T}^n\right)|b\rangle \\ &= |b\rangle - \hat{T}\,|b\rangle + \frac{1}{2}\hat{T}\left\{\hat{T}\,|b\rangle\right\} - \frac{1}{6}\ldots \end{aligned} \tag{10-58}$$

The expansion is carried out in complete analogy with step 1. It is assured that the expansion is restricted to the excitation manifold $\langle\mu|$.

Step 4: $\Omega_\mu = \langle\mu|c\rangle$*, evaluation of transition density matrix elements*

$$\Omega_\mu = \left\langle \mathrm{Ref}\left|\hat{\tau}_\mu^\dagger\right| c\right\rangle$$

The projection of the excitation manifold $\langle\mu|$ against the expanded transformed reference vector $|c\rangle$ corresponds to the calculation of transition density matrix elements and yields the CC vector function. Employing the concise implementation presented in Section 10.4.2.2.4 the evaluation becomes equivalent to the calculation of CI sigma vectors, where instead of a contraction with integrals a contraction with expansion coefficients is performed. For the present case, the left-hand vector of expansion coefficients is a unit vector. As this step is carried out in the space of atmost n-fold excitations, it scales as $O^n V^{n+2}$ and is therefore significantly faster than step 2.

Due to the computational limitations imposed by the scaling of step 2, the method in its current form is not applicable on a large scale. Although general electronic structures can be treated and the efficiency of the CI steps makes expansions on the order of hundreds of millions of terms possible, the steep increase in computational cost with the number of correlated electrons limits the applicability to roughly 15 active electrons. Approaches ameliorating the computational scaling are currently under development [82, 81].

10.5. SAMPLE APPLICATIONS

10.5.1. Tl_2 Ground and Excited States

For the dithallium molecule the inclusion of spin–orbit interaction is imperative for a qualitatively correct description of bonding and dissociation [13]. The reasons for this are a weakening of the bond through σ-π mixing and a drastic energetic lowering of the atomic limit due to the strong spin–orbit splitting of the Tl $6p_{1/2}$ and $6p_{3/2}$ spinors. Both these effects can be described by relativistic MCSCF approaches [45].

The results in Figure 10-6 have been obtained with Dyall's uncontracted triple-zeta basis set [83] augmented with all valence-correlating functions and the infinite-order two-component Barysz–Sadlej–Snijders (BSS) Hamiltonian [84,3,85] including the one- and two-electron spin–orbit interaction terms for Hartree–Fock and relativistic MCSCF calculations through the atomic mean-field approximation [53, 86]. Since for this Hamiltonian only integrals over Large-component functions are included, the computational effort is greatly reduced in relativistic MCSCF calculations.

The potential-energy curves of the 0_g^+ molecular state obtained from a closed-shell Hartree–Fock (csHF) calculation and two types of MCSCF calculations, one with a minimal (GAS1) and one with a larger active space (GAS2), are shown in

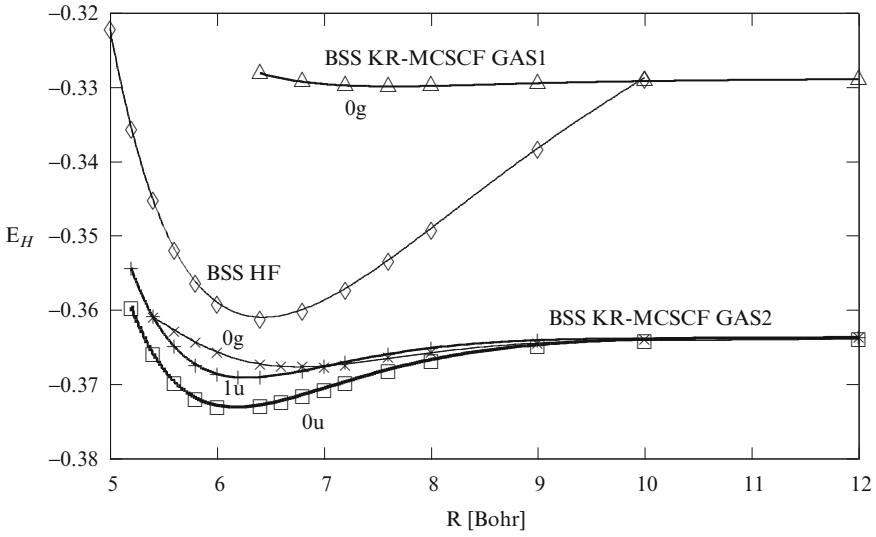

Figure 10-6. Potential energy curves of Tl_2 using the BSS Hamiltonian including one- and two-electron spin–orbit terms. BSS HF denotes a closed-shell Hartree–Fock calculation (shifted by -0.09 E_H for better comparison), BSS MCSCF are generalized active space Kramers-Restricted (KR)-MCSCF calculations. GAS1 is a static correlation calculation with 6 valence electrons, where single and double excitations are allowed out of space 1 holding the 6*s* electrons into a CAS space with two electrons consisting of the $6p$ molecular orbitals. GAS2 allows some dynamic electron correlation by adding an orbital space 3 with up to to two electrons in 9 *gerade* and 9 *ungerade* Kramers pairs. All energy offsets are -40530.0 E_H (from reference [45]; reprinted by permission of the publisher)

Table 10-6 (from reference [45]; reprinted by permission of the publisher)

State and method	R_e [Å]	ω_e [cm^{-1}]	D_e [eV]
0_g^+ BSS KR-MCSCF GAS1	4.04	16.8	0.03
0_g^+ BSS KR-MCSCF GAS2	3.59	35.5	0.11
0_g^+ DC-CASPT2 [87]	2.90	79	0.36
1_u BSS KR-MCSCF GAS2	3.32	51.8	0.14
1_u DC-CASPT2 [87]	3.07	79	0.37
0_u^- BSS KR-MCSCF GAS2	3.27	59.3	0.25
0_u^- DC-CASPT2 [87]	3.04	84	0.51
0_u^- CASPT2-SO [11]	3.09	75	0.43
0_u^- AREP CCSD(T) [88]	2.84	109	0.97
0_u^- REP KRCCSD(T) [88]	3.16	64	0.28
0_u^- Experiment [89]	3.00	80	0.43

Figure 10-6, and the derived spectral constants are compiled in Table 10-6 along with a selection of results from the literature. The GAS2 calculation has in addition been carried out also for states of *ungerade* symmetry with 0_u^- as the molecular ground state, in accord with previous CASPT2 calculations [11, 87]. The small-space MCSCF gives a well which is much too shallow, resulting in too small a harmonic frequency and dissociation energy. The curve from the large-space MCSCF shows how an inclusion of (some) dynamic electron correlation greatly improves the results, as the occupation of antibonding Kramers pairs becomes more realistic (i.e., smaller) compared to the small-space calculation. The trend of dynamic electron correlation to be important in obtaining spectroscopic accuracy for Tl_2 is substantiated by comparison with results obtained from multi-reference perturbative (DC-CASPT2, CASPT2-SO) and coupled cluster treatments in Table 10-6. It is interesting to note that the overall deviation from experimental values is larger in the highly correlated – but spin–orbit free – AREP CCSD(T) calculation than in the present GAS2 MCSCF calculation which includes spin–orbit interaction rigorously. The inadequacy of a spin–orbit free treatment is particularly obvious in the much too large dissociation energy in the AREP CCSD(T) treatment (from reference [88]). The different relativistic CASPT2 approaches perform well for the spectral constants of this system. In view of the relativistic CC results, however, the CASPT2-SO [11] values appear to be somewhat fortuitous and are likely to be due to error cancellations of spin–orbit stabilizations.

Although spectroscopic accuracy is not achieved in most relativistic MCSCF calculations, the resulting MCSCF wave function is a significantly improved starting point for highly correlated relativistic calculations as demonstrated, e.g., in reference [24].

10.5.2. Br_2^{2+}

The theoretical and experimental study [90] of double photoionization of molecular bromine comprises a sample application to a large number of electronically excited states where spectroscopic accuracy is imperative. Relativistic GASCI based on configuration-averaged DCHF has in the present case been employed. This type of configuration averaging is very often a good option when many electronically excited states (or all) of interest are derived from a set of electronic configurations involving energetically close-lying orbitals. This is the case in Br_2^{2+} and also in the following sample applications.

The lowest electronic states are shown in Table 10-7 along with an analysis of the essential part of the corresponding relativistic CI wave functions in terms of Kramers-paired molecular spinors. On the basis of these results it has been possible to assign the main part of the double photoionization spectrum of Br_2 as shown in Figure 10-7. It should be noted that many more electronically excited states come to lie between the assigned peaks, but only those are shown in the figure which are experimentally accessible, i.e., which result from the removal of two electrons from the ground-state electronic configuration of neutral Br_2. This type of study combines the difficulties of electron correlation effects in excited states, high density of states, and the need for a treatment of special relativity on the same footing. This becomes particularly obvious in the vertical excitation spectra where spin–orbit coupling is seen to have the same order of magnitude as state separations within an

Table 10-7 Lowest vertical excitation energies of Br_2^{2+} from relativistic GASCI calculations. Dirac–Coulomb Hamiltonian, CI CAS8in6 SD8, distance 2.22 Å

T_v [eV]	Omega/symmetry	Corresp. term(s)	Configuration(s)
3.702	3g	$^3\Phi_3$, $^1\Phi_3$, $^5\Pi_3$	$0.96\pi_u^1\pi_g^1\pi_g^1\sigma_u^1$
3.393	2u	$^3\Pi_2$	$0.89\pi_{g(2)}^1\sigma_u^1$
3.174	1u	$^3\Pi_1$, $^1\Pi_1$	$0.71\pi_{g(1)}^1\sigma_u^1$
3.044	0u	$^3\Pi_0$	$(0.63+0.63)\pi_{g(1)}^1\sigma_u^1$
3.041	0u	$^3\Pi_0$	$(-0.62+0.62)\pi_{g(1)}^1\sigma_u^1$
2.410	1u	$^3\Sigma_1$, $^3\Delta_1$	$0.96\pi_{u(1)}^1\pi_{g(1)}^1$
2.395	0u	$^1\Sigma_0$	$(0.67+0.67)\pi_{u(1)}^1\pi_{g(1)}^1$
2.139	1u	$^3\Delta_1$, $^3\Sigma_1$	$-0.67\pi_{u(2)}^1\pi_{g(1)}^1+0.68\pi_{u(1)}^1\pi_{g(2)}^1$
2.050	2u	$^3\Delta_2$, $^1\Delta_2$	$0.68\pi_{u(1)}^1\pi_{g(2)}^1-0.68\pi_{u(2)}^1\pi_{g(1)}^1$
1.693	3u	$^3\Delta_3$	$0.96\pi_{u(2)}^1\pi_{g(2)}^1$
1.644	0u	$^3\Sigma_0$	$(0.67+0.67)\pi_{u(2)}^1\pi_{g(2)}^1$
1.128	0g	$^1\Sigma_0$	$0.35\pi_{g(1)}^2+0.82\pi_{g(2)}^2$
0.661	2g	$^1\Delta_2$	$0.91\pi_{g(1)}^1\pi_{g(2)}^1$
0.141	1g	$^3\Sigma_1$	$0.93\pi_{g(1)}^1\pi_{g(2)}^1$
0.000	0g	$^3\Sigma_0$	$0.84\pi_{g(1)}^2-0.39\pi_{g(2)}^2$

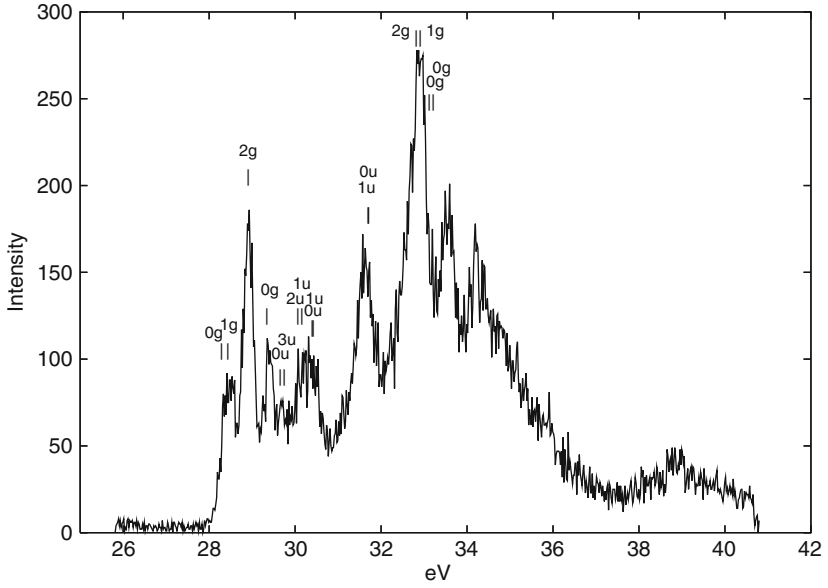

Figure 10-7. Double photoionization spectrum of Br_2. The assignments of the bands are given in terms of the final electronic states in the dication. The theoretical values have been adjusted so that the lowest 2_g state corresponds to the strong peak at 28.91 eV. (from reference [90]; reprinted by permission of the publisher.)

electronic configuration which are predominantly due to electron correlation effects. First-order splittings are on the order of 0.5 eV, and even second-order splittings may be as large as 0.2 eV.

10.5.3. I_3 and I_3^-

As a more rigorous example for the comparison [91] of different modern relativistic electron correlation methods the lowest electronic excitation for the I_3 molecule are shown in Figure 10-8. All three presented methods, SO-CASPT2 [9, 11], GASCI [8, 24], and IHFSCC [74, 92, 93], yield excitation energies in good agreement with gas phase experiments [94, 95], with absolute errors smaller than 0.1 eV (with one exception, $\frac{3}{2}g$ state, IHFSCC). Time-Dependent Density Functional Theory (TDDFT) has not been applicable to this open-shell species. For IHFSCC the adiabatic excitation energies are given in addition where the deviations are seen to diminish significantly. Whereas SO-CASPT2 shows some unsystematic behavior, GASCI tends to overshoot the experimental energies by roughly equal amounts. The similarity between GASCI and IHFSCC arises from the fact that for the $(1h, 0p)$ Fock-space sector used the exponential parametrization of IHFSCC for the excited states is truncated after the linear term and is therefore essentially the same as in MRCI. Given these similarities in error trends for IHFSCC and GASCI

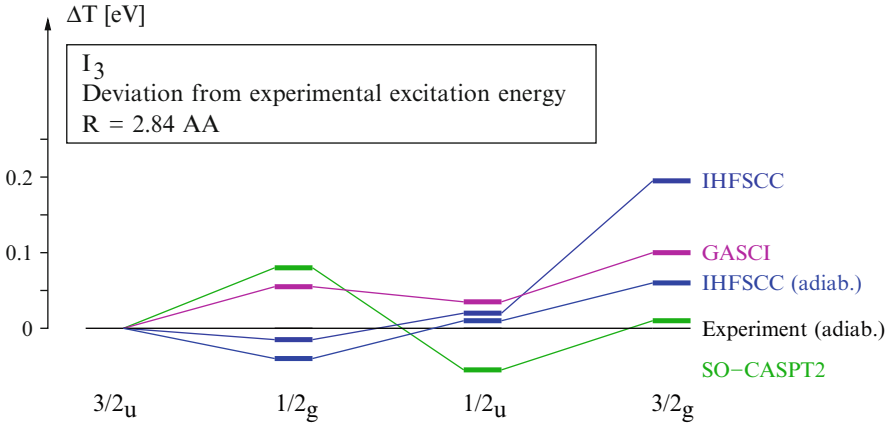

Figure 10-8. Comparison of excitation energies T_v and T_e (in eV) for different methods CASPT2/TZP, IHFSCC/aVTZ/Q_1, GASCI/aCVTZ/CAS_SD15 for I_3 at $r_1 = r_2 = 2.84$ Å

approaches and accounting for the downward shift of excitation energies by the adiabatic correction, GASCI is expected to yield very accurate adiabatic excitation energies, with errors on the order of only a few hundred wavenumbers.

For the triiodide ion the comparison included in addition relativistic TDDFT [96]. Vertical excitation energies are compiled in Table 10-8 and shown in graphical form in Figure 10-9.

In the figure, IHFSCC results are taken as reference values for the respective states, and the deviations of the other methods from IHFSCC are given. The GASCI calculations tend to yield higher excitation energies than the corresponding IHFSCC ones, with an average deviation of 0.18 eV which, in absolute terms, is rather similar to the difference between SO-CASPT2 and IHFSCC. The discrepancies between GASCI and IHFSCC vary in a similar fashion to that between SO-CASPT2 and IHFSCC, particularly for excited states 6–17. While TDDFT seems to capture the essential trends of the other, more sophisticated methods, it is seen to be significantly less reliable from a quantitative point of view.

The differences between IHFSCC and GASCI can likely be understood on the basis of a comparison with Linear Response Coupled Cluster (LRCC) [97] method which like the CI method is based upon a linear parameterization for the description of excited states. In contrast to LRCC (or equivalently the Equation-of-Motion (EOM) CC approach), IHFSCC is fully size-extensive also for excited states due to the inclusion of higher-order connected diagrams [98, 99] for Fock-space sectors with more than one quasiparticle. With respect to the trend of the differences there is evidence [100] that LRCC excitation energies are systematically shifted upwards compared to IHFSCC ones, in line with what is observed here for the difference between IHFSCC and GASCI results.

Table 10-8 Comparison of vertical excitation energies T_v (in eV) obtained with different methods (TDDFT/TZ2P, SO-CASPT2/TZP, IHFSCC(aVTZ/Q_1), GASCI (aCVTZ/SD6_CAS_SD22); Three active spaces are used in the GASCI setup: SD excitations from GAS I (iodine 5*s* spinors), a CAS space for GAS II with 16 electrons in nine Kramers pairs, and up to two particles in the external GAS III) for I_3^- at $r_1 = r_2 = 2.93$ Å. States of the same symmetry as those for the optically active excited states are shown in boldface

	TDDFT		GASCI		SO-CASPT2		IHFSCC	
State	Ω	T_v	Ω	T_v	Ω	T_v	Ω	T_v
1	2_g	1.92	2_g	2.30	2_g	2.03	2_g	2.10
2	1_g	2.04	0_u^-	2.40	1_g	2.14	1_g	2.23
3	0_u^-	2.42	1_u	2.41	0_u^-	2.28	0_u^-	2.26
4	1_u	2.43	1_g	2.41	1_u	2.29	1_u	2.27
5	0_g^-	2.50	0_g^-	2.91	0_g^-	2.54	0_g^-	2.68
6	0_g^+	2.56	0_g^+	2.95	0_g^+	2.61	0_g^+	2.73
7	1_g	2.70	1_g	3.08	1_g	2.72	1_g	2.90
8	2_u	2.61	2_u	3.21	2_u	2.94	2_u	3.22
9	1_u	2.72	1_u	3.25	1_u	2.98	1_u	3.30
10	$\mathbf{0_u^+}$	**3.14**	$\mathbf{0_u^+}$	**3.66**	$\mathbf{0_u^+}$	**3.34**	$\mathbf{0_u^+}$	**3.52**
11	2_g	3.50	0_u^-	3.98	0_u^-	3.62	0_u^-	3.95
12	0_u^-	3.42	1_u	4.02	1_u	3.66	2_g	3.96
13	1_g	3.63	2_g	4.16	2_g	3.82	1_u	4.03
14	1_u	3.56	1_g	4.25	1_g	3.93	1_g	4.07
15	$\mathbf{0_u^+}$	**4.46**	$\mathbf{0_u^+}$	**4.75**	$\mathbf{0_u^+}$	**4.29**	$\mathbf{0_u^+}$	**4.33**
16	0_g^-	4.10	0_g^-	4.77	0_g^-	4.37	0_g^-	4.54
17	0_g^+	4.11	0_g^+	4.78	0_g^+	4.38	0_g^+	4.54

10.6. CONCLUDING REMARKS

For the treatment of smaller molecules containing heavy elements, relativistic wavefunction-based methods are tools of high reliability. Perturbative approaches such as SO-CASPT2 are very efficient, especially in the treatment of dynamic electron correlation. Since this is a problem of crucial importance also and particularly in heavy-element chemistry, approaches of these types are the method of choice for many applications. Similar and more rigorous new developments are, e.g., four-component CASPT2 [87], but their applicability and performance still require more testing. Relativistic CI models such as the presented GASCI approach have advantages since they treat spin–orbit interaction a priori and in a rigorous manner. They are very generally applicable and flexible due to the active space concept. For systems containing three or more heavy elements, relativistic GASCI studies

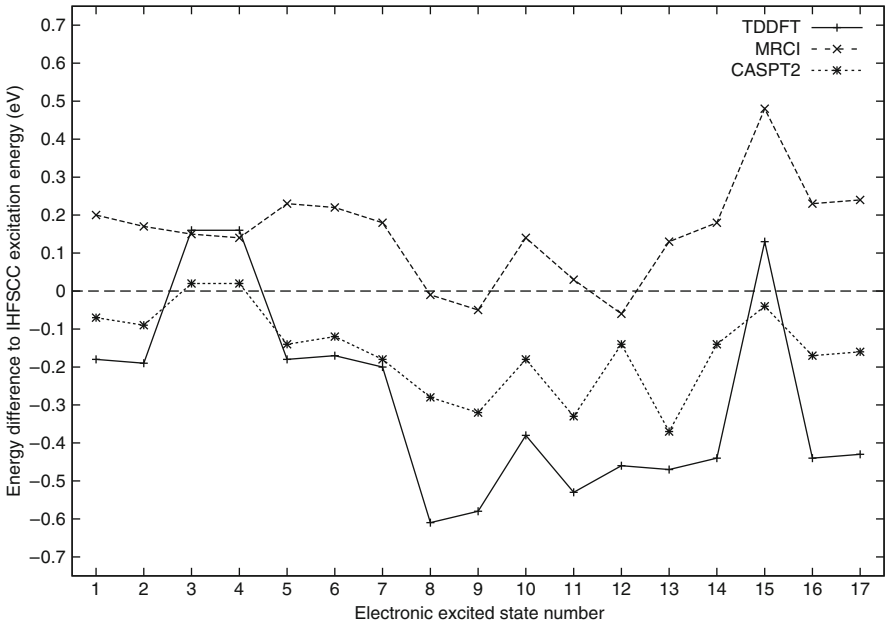

Figure 10-9. Plot of the differences in excitation energies in Table 10-8 between IHFSCCSD (reference values) and SO-CASPT2, GASCI (MRCI), and TDDFT at $R = 2.93$ Å, as a function of the different excited states

are quite costly and are therefore often only applied at selected nuclear geometries. Recent improvements including efficient parallelization [58,59] have enhanced their competitiveness.

Regarding relativistic CC approaches general applicability remains an essential problem. Fock-space approaches are probably the most accurate methods for relativistic electonic-structure studies to the date, but molecules with a large number of unpaired electrons in the reference system are still out of reach. Other multi-reference CC approaches such as the GASCC method introduced here have the potential of being generally applicable, but have yet to prove that they can also successfully treat complicated open-shell problems. The same is true for a recent real-orbital based implementation by Wang et al. [7] and the approaches by Hirata et al. [71]. Despite the remaining difficulties, relativistic wavefunction-based quantum chemistry has recently made progress at a good pace and has continued to close the methodological gap between the treatment of molecules with light atoms and the treatment of molecules with heavy atoms.

ACKNOWLEDGEMENTS

I am grateful to Andre S. P. Gomes for making results on I_3 and I_3^- available prior to publication.

REFERENCES

1. Kędziera, D., Barysz, M.: Two-component relativistic methods for the heaviest elements. J. Chem. Phys. **121**, 6719 (2004)
2. Kutzelnigg, W., Liu, W.: Quasirelativistic theory equivalent to fully relativistic theory. J. Chem. Phys. **123**, 241102 (2005)
3. Iliaš, M., Saue, T.: An infinite-order two-component relativistic hamiltonian by a simple one-step transformation. J. Chem. Phys. **126**, 064102 (2007)
4. Lischka, H., Shepard, R., Pitzer, R.M., Shavitt, I., Dallos, M., Müller, T., Szalay, P.G., Seth, M., Kedziora, G.S., Yabushita, S., Zhang, Z.: High-level multireference methods in the quantum-chemistry program system COLUMBUS: Analytic MR-CISD and MR-AQCC gradients and MR-AQCC-LRT for excited states, GUGA spin-orbit CI and parallel CI density. Phys. Chem. Chem. Phys. **3**, 664 (2000)
5. Vallet, V., Maron, L., Teichteil, C., Flament, J-P.: A two-step uncontracted determinantal effective Hamiltonian-based SO-CI method. J. Chem. Phys. **113**, 1391 (2000)
6. Kleinschmidt, M., Tatchen, J., Marian, C.M.: SPOCK.CI: A multireference spin-orbit configuration interaction method for large molecules. J. Chem. Phys. **124**, 124101 (2006)
7. Wang, F., Gauss, J., van Wüllen, C.: Closed-shell coupled cluster theory with spin-orbit coupling. J. Chem. Phys. **129**, 064113 (2008)
8. Fleig, T., Olsen, J., Visscher, L.: The generalized active space concept for the relativistic treatment of electron correlation. II: Large-scale configuration interaction implementation based on relativistic 2- and 4-spinors and its application. J. Chem. Phys. **119**, 2963 (2003)
9. Malmqvist, P.-Å., Roos, B.O., Schimmelpfennig, B.: The restricted active space (RAS) state interaction approach with spin-orbit coupling. Chem. Phys. Lett. **357**, 230 (2002)
10. Miyajima, M., Watanabe, Y., Nakano, H.: Relativistic quasidegenerate perturbation theory with four-component general multiconfiguration reference functionss. J. Chem. Phys. **124**, 044101 (2006)
11. Roos, B.O., Malmqvist, P.-Å.: Relativistic quantum chemistry: The multiconfigurational approach. Phys. Chem. Chem. Phys. **6**, 2919 (2004)
12. Fleig, T., Marian, C.M.: Relativistic all-electron ab initio calculations on the platinum hydride molecule. Chem. Phys. Lett. **222**, 267 (1994)
13. Christiansen, P.A.: Dissociation curves for nine low lying states of Tl_2 from REP CI calculations. J. Chem. Phys. **79**, 2928 (1983)
14. Fleig, T.: Spin-orbit resolved static polarizabilities of group 13 atoms. 4-component relativistic configuration interaction and coupled cluster calculations. Phys. Rev. A **72**, 052506 (2005)
15. Kutzelnigg, W., Liu, W.: Relativistic MCSCF by means of quasidegenerate direct perturbation theory. I. Theory. J. Chem. Phys. **112**, 3540 (2000)
16. Liu, W., Kutzelnigg, W., van Wüllen, C.: Relativistic MCSCF by means of quasidegenerate direct perturbation theory. II. Preliminary applications. J. Chem. Phys. **112**, 3559 (2000)
17. Messiah, A.: *Quantenmechanik*, Volume 1, 2, 2nd Auflage edn. Walter de Gruyter & Co., Berlin (1991)
18. Rösch, N.: Time-reversal symmetry, Kramers degeneracy and the algebraic eigenvalue problem. Chem. Phys. **80**, 1 (1983)
19. Aucar, G.A., Jensen, H.J. Aa., Oddershede, J.: Operator representations in Kramers bases. Chem. Phys. Lett. **232**, 47 (1995)
20. Saue, T., Visscher, L.: Four-component electronic structure methods for molecules. In: U. Kaldor, S. Wilson (eds.), *Theoretical Chemistry and Physics of Heavy and SuperHeavy Elements*. Kluwer, Dordrecht (2003)

21. Fleig, T., Olsen, J., Marian, C.M.: The generalized active space concept for the relativistic treatment of electron correlation. I. Kramers-restricted two-component configuration interaction. J. Chem. Phys. **114**, 4775 (2001)
22. Saue, T., Jensen, H.J. Aa.: Quaternion symmetry in relativistic molecular calculations: The Dirac-Hartree-Fock method. J. Chem. Phys. **111**, 6211 (1999)
23. Jensen, H.J. Aa., Dyall, K.G., Saue, T., Fægri, K.: Relativistic four-component multiconfigurational self-consistent field theory for molecules: Formalism. J. Chem. Phys. **104**, 4083 (1996)
24. Fleig, T., Jensen, H.J. Aa., Olsen, J., Visscher, L.: The generalized active space concept for the relativistic treatment of electron correlation. III: Large-scale configuration interaction and multiconfiguration self-consistent-field four-component methods with application to UO_2. J. Chem. Phys. **124**, 104106 (2006)
25. Kim, Y.S., Lee, Y.S.: The Kramers' restricted complete active-space self-consistent field method for two-component molecular spinors and relativistic effective core potentials including spin-orbit interactions. J. Chem. Phys. **119**, 12169 (2003)
26. Saue, T., Helgaker, T.U.: Four-component relativistic Kohn-Sham theory. J. Comp. Chem. **23**, 814 (2002)
27. Matveev, A.V., Majumder, S., Rösch, N.: Efficient treatment of the Hartree interaction in the relativistic Kohn-Sham problem. J. Chem. Phys. **123**, 164104 (2005)
28. Schwerdtfeger, P. (ed.): Relativistic Electronic Structure Theory, Volume 1. Fundamentals, chapter 6, p. 291. Elsevier, Amsterdam (2002) (L. Visscher, Post Dirac-Hartree-Fock methods – Electron correlation)
29. Visscher, L., Dyall, K.G., Lee, T.J.: Kramers-restricted closed-shell CCSD theory. Int. J. Quantum Chem. Quantum Chem. Symp. **29**, 411 (1995)
30. Visscher, L.: On the construction of double group molecular symmetry functions. Chem. Phys. Lett. **253**, 20 (1996)
31. Visscher, L., Saue, T.: Approximate relativistic electronic structure methods based on the quaternion modified Dirac equation. J. Chem. Phys. **113**, 3996 (2000)
32. Koster, G.F., Dimmock, J.O., Wheeler, R.G., Statz, H.: Properties of the Thirty-Two Point Groups. Massachusetts Institute of Technology, Cambridge, MA (1963)
33. Dyall, K.G., Fægri, K.: *Introduction to Relativistic Quantum Chemistry*. Oxford, Oxford University Press (2007)
34. Program LUCIA.: A general CI code written by Olsen, J., University of Aarhus, with contributions from Larsen, H. and Fülscher, M.
35. Olsen, J., Roos, B.O., Jørgensen, P., Jensen, H.J. Aa.: Determinant based configuration interaction algorithms for complete and restricted configuration interaction spaces. J. Chem. Phys. **89**, 2185 (1988)
36. Karlström, G., Lindh, R., Malmqvist, P.-Å., Roos, B.O., Ryde, U., Veryazov, V., Widmark, P-O., Cossi, M., Schimmelpfennig, B., Neogrády, P., Seijo, L.: MOLCAS: A program package for computational chemistry. Comp. Mater. Scien. **28**, 222 (2003)
37. Kállay, M., Surján, P.: Higher excitations in coupled-cluster theory. J. Chem. Phys. **115**, 2945 (2001)
38. MRCC.: A string-based quantum-chemical program suite written by Kállay, M.
39. Hirata, S.: Symbolic algebra in quantum chemistry. Theoret. Chim. Acta **116**, 2 (2006)
40. Köhn, A., Olsen, J.: Coupled-cluster with active space selected higher amplitudes: Performance of seminatural orbitals for ground and excited state calculations. J. Chem. Phys. **125**, 174110 (2006)
41. Ansaloni, R., Bendazzoli, G.L., Evangelisti, S., Rossi, E.: A parallel full-ci algorithm. Comp. Phys. Commun. **128**, 496 (2000)

42. Olsen, J., Jørgensen, P., Simons, J.: Passing the one-billion limit in full configuration interaction (FCI) calculations. Chem. Phys. Lett. **169**, 463 (1990)
43. Kállay, M., Szalay, P., Surján, P.: A general state-selective multireference coupled-cluster algorithm. J. Chem. Phys. **117**, 980 (2002)
44. Olsen, J.: The initial implementation and applications of a general active space coupled cluster method. J. Chem. Phys. **113**, 7140 (2000)
45. Thyssen, J., Fleig, T., Jensen, H.J. Aa.: A direct relativistic four-component multiconfiguration self-consistent-field method for molecules. J. Chem. Phys. **129**, 034109 (2008)
46. Fleig, T., Sørensen, L.K., Olsen, J.: A relativistic 4-component general-order multi-reference coupled cluster method: Initial implementation and application to HBr. Theoret. Chem. Acc. **118**, 347 (2007) erratum Theor. Chem. Acc. **118**, 979 (2007)
47. Yabushita, S., Zhang, Z., Pitzer, R.M.: Spin-orbit configuration interaction using the graphical unitary group approach and relativistic core potential and spin-orbit operators. J. Phys. Chem. **103**, 5791 (1999)
48. DIRAC.: A relativistic ab initio electronic structure program, Release DIRAC08 (2008), written by Visscher, L., Jensen, H.J. Aa., Saue, T., with new contributions from Bast, R., Dubillard, S., Dyall, K.G., Ekström, U., Eliav, E., Fleig, T., Gomes, A.S. P., Helgaker, T.U., Henriksson, J., Iliaš, M., Jacob, C.R., Knecht, S., Norman, P., Olsen, J., Pernpointner, M., Ruud, K., Sałek, P., and Sikkema, J., (see http://dirac.chem.sdu.dk)
49. Talman, J.D.: Minimax Principle for the Dirac Equation. Phys. Rev. Lett. **57**, 1091 (1986)
50. Visscher, L.: The dirac equation in quantum chemistry: Strategies to overcome the current computational problems. J. Comp. Chem. **23**, 759 (2002)
51. Heß, B.A.: Relativistic electronic-structure calculations employing a two-component no-pair formalism with external field projection operators. Phys. Rev. A **33**, 3742 (1986)
52. Reiher, M.: Douglas-Kroll-Hess Theory: A relativistic electrons-only theory for chemistry. Theoret. Chim. Acta **116**, 241 (2006)
53. Heß, B.A., Marian, C.M., Wahlgren, U., Gropen, O.: A mean-field spin-orbit method applicable to correlated wavefunctions. Chem. Phys. Lett. **251**, 365 (1996)
54. Heß, B.A., Marian, C.M.: Relativistic effects in the calculation of electronic energies. In: P. Jensen, P.R. Bunker (eds.) *Computational Molecular Spectroscopy*. Wiley & Sons, Sussex (1999)
55. Tatchen, J., Marian, C.M.: On the performance of approximate spin-orbit Hamiltonians in light conjugated molecules: The fine-structure splitting of HC_6H^+, NC_5H^+, and NC_4N^+. Chem. Phys. Lett. **313**, 351 (1999)
56. Reiher, M., Wolf, A.: *Introduction to Relativistic Quantum Chemistry*. Wiley, Weinheim (2007)
57. Fleig, T.: Time-reversal symmetry in general coupled cluster theory. Phys. Rev. A **77**, 062503 (2008)
58. Knecht, S., Jensen, H.J. Aa., Fleig, T.: Large-scale parallel configuration interaction. I. Nonrelativistic and scalar-relativistic general active space implementation with application to $(Rb\text{-}Ba)^+$. J. Chem. Phys. **128**, 014108 (2008)
59. Knecht, S., Jensen, H.J. Aa., Fleig, T.: Large-scale parallel configuration interaction. II. Four-component double-group general active space implementation with application to BiH. J. Chem. Phys. **132** (2010) xxxx, in press
60. Liu, B.: The Simultaneous Expansion Method. In *Numerical algorithms in chemistry: Algebraic methods. Proceedings from a workshop of the National Resource for Computation in Chemistry*, Berkeley (1978)
61. Davidson, E.R.: The iterative calculation of a few of the lowest eigenvalues and corresponding eigenvectors of large real-symmetric matrices. J. Comput. Phys. **17**, 87 (1975)
62. Handy, N.: Multi-root configuration interaction calculations. Chem. Phys. Lett. **74**, 280 (1980)

63. Roos, B.O.: The multiconfigurational (mc) self-consistent field (scf) theory. In: B.O. Roos (ed.) Lecture Notes in Quantum Chemistry. Springer, Berlin (1992)
64. Jensen, H.J. Aa., Ågren, H.: A direct, restricted-step, second-order mcscf program for large scale ab initio calculations. Chem. Phys. **104**, 229 (1986)
65. Jensen, H.J. Aa., Jørgensen, P., Ågren, H.: Efficient optimization of large scale mcscf wave functions with a restricted step algorithm. J. Chem. Phys. **87**, 451 (1987)
66. Fan, P-D., Hirata, S.: Active-space coupled-cluster methods through connected quadruple excitations. J. Chem. Phys. **124**, 104108 (2006)
67. Hirata, S.: Higher-order equation-of-motion coupled-cluster methods. J. Chem. Phys. **121**, 51 (2004)
68. Kállay, M., Gauss, J.: Approximate treatment of higher excitations in coupled-cluster theory. J. Chem. Phys. **123**, 214105 (2005)
69. Kowalski, K., Piecuch, P.: New classes of non-iterative energy corrections to multi-reference coupled-cluster energies. Mol. Phys. **102**, 2425 (2004)
70. Abrams, M.L., Sherrill, C.D.: General-order single and multi-reference configuration interaction and coupled-cluster theory: Symmetric dissociation of water. Chem. Phys. Lett. **404**, 284 (2005)
71. Hirata, S., Yanai, T., Harrison, R.J., Kamija, M., Fang, P.-D.: High-order electron-correlation methods with scalar relativistic and spin-orbit corrections. J. Chem. Phys. **126**, 024104 (2007)
72. Visscher, L., Lee, T.J., Dyall, K.G.: Formulation and implementation of a relativistic unrestricted coupled-cluster method including noniterative connected triples. J. Chem. Phys. **105**, 8769 (1996)
73. Landau, A., Eliav, E., Kaldor, U.: Intermediate Hamiltonian Fock-space coupled-cluster method. Chem. Phys. Lett. **313**, 399 (1999)
74. Visscher, L., Eliav, E., Kaldor, U.: Formulation and implementation of the relativistic Fock-space coupled-cluster method for molecules. J. Chem. Phys. **115**, 9720 (2001)
75. Köhn, A., Olsen, J.: Coupled-cluster with active space selected higher amplitudes: Performance of seminatural orbitals for ground and excited state calculations. J. Chem. Phys. **125**, 174110 (2006)
76. Krogh, J.W., Olsen, J.: A general coupled cluster study of the N_2 molecule. Chem. Phys. Lett. **344**, 578 (2001)
77. Oliphant, N., Adamowicz, L.: Multireference coupled-cluster method using a single-reference formalism. J. Chem. Phys. **94**, 1229 (1991)
78. Oliphant, N., Adamowicz, L.: The implementation of the multireference coupled-cluster method based on the single-reference formalism. J. Chem. Phys. **96**, 3739 (1991)
79. Jeziorski, B., Monkhorst, H.J.: Coupled-cluster method for multideterminantal reference states. Phys. Rev. A **24**, 1668 (1981)
80. Hanrath, M.: An exponential multireference wave-function *ansatz*. J. Chem. Phys. **123**, 084102 (2005)
81. Sørensen, L.K., Fleig, T., Olsen, J.: A relativistic four- and two-component generalized-active-space coupled cluster method. Z. Phys. Chem. **224**, 999 (2010)
82. Sørensen, L.K., Fleig, T., Olsen, J.: Spectroscopic and electric properties of the LiCs molecule: A coupled cluster study including higher excitations. J. Phys. B. At. Mol. Opt. Phys. **42**, 165102 (2009)
83. Dyall, K.G.: Relativistic and nonrelativistic finite nucleus optimized triple-zeta basis sets for the 4p, 5p and 6p elements. Theoret. Chem. Acc. **108**, 335 (2002) erratum Theor. Chem. Acc. **109**, 284 (2003); revision Theor. Chem. Acc. **115**, 441 (2006). Basis sets available from the Dirac web site, http://dirac.chem.sdu.dk
84. Jensen, H.J. Aa., Iliaš, M.: Two-component relativistic methods based on the quaternion modified dirac equation: From the Douglas-Kroll to the Barysz-Sadlej-Snijders infinite order, 2005. unpublished

85. Barysz, M., Sadlej, A.J., Snijders, J.G.: Nonsingular two/one-component relativistic hamiltonians accurate through arbitrary high order in alpha(2). Int. J. Quantum Chem. **65**, 225 (1997)
86. AMFI.: An atomic mean-field spin-orbit integral program, 1996 and 1999. University of Stockholm
87. Abe, M., Nakajima, T., Hirao, K.: The relativistic complete active-space second-order perturbation theory with the four-component dirac hamiltonian. J. Chem. Phys. **125**, 234110 (2006)
88. Lee, H-S., Han, Y-K., Kim, M.C., Bae, C., Lee, Y.S.: Spin-orbit effects calculated by two-component coupled-cluster methods: Test calculations on AuH, Au_2, TlH and Tl_2. Chem. Phys. Lett. **293**, 97 (1998)
89. Froben, F.W., Schulze, W., Kloss, U.: Raman-spectra of matrix-isolated group IIIA dimers - Ga-2, In-2, Tl-2. Chem. Phys. Lett. **99**, 500 (1983)
90. Fleig, T., Edvardsson, D., Banks, S.T., Eland, J.H.D.: A theoretical and experimental study of the double photoionisation of molecular bromine and a new double ionisation mechanism. Chem. Phys. **343**, 270 (2008)
91. Gomes, A.S.P., Visscher, L., Bolvin, H., Saue, T., Knecht, S., Fleig, T., Eliav, E.: The electronic structure of the triiodide ion from relativistic correlated calculations: A comparison of different methodologies, 2009. to be submitted
92. Landau, A., Eliav, E., Ishikawa, Y., Kaldor, U.: Intermediate hamiltonian fock-space coupled-cluster method: Excitation energies of barium and radium. J. Chem. Phys. **113**, 9905 (2000)
93. Landau, A., Eliav, E., Ishikawa, Y., Kaldor, U.: Mixed-sector Intermediate Hamiltonian Fock-space coupled-cluster approach. J. Chem. Phys. **121**, 6634 (2004)
94. Taylor, T.R., Asmis, K.R., Zanni, M.T., Neumark, D.M.: Characterization of the i3 radical by anion photoelectron spectroscopy. J. Chem. Phys. **110**, 7607–7609 (1999)
95. Choi, H., Taylor, T.R., Bise, R.R., Hoops, A.A., Neumark, D.M.: Excited states and photodissociation dynamics of the triiodine radical (i_3). J. Chem. Phys. **113**, 8608–8614 (2000)
96. Gross, E.K.U., Kohn, W.: Adv. Quant. Chem. **21**, 255 (1990)
97. Helgaker, T.U., Jørgensen, P., Olsen, J.: Molecular Electronic Structure Theory. Wiley, Chichester (2000)
98. Meissner, L., Bartlett, R.J.: Transformation of the hamiltonian in excitation energy calculations: Comparison between fock-space multireference coupled-cluster and equation-of-motion coupled-cluster methods. J. Chem. Phys. **94**, 6670 (1991)
99. Meissner, L., Bartlett, R.J.: A dressing for the matrix elements of the singles and doubles equation-of-motion coupled-cluster method that recovers additive separability of excitation energies. J. Chem. Phys. **102**, 7490 (1995)
100. Musial, M., Bartlett, R.J.: Intermediate Hamiltonian Fock-space multireference coupled-cluster method with full triples for calculation of excitation energies. J. Chem. Phys. **129**, 044101 (2008)

CHAPTER 11

ELECTRONIC STRUCTURE AND CHEMISTRY OF THE HEAVIEST ELEMENTS

V. PERSHINA

GSI Helmholtzzentrum für Schwerionenforschung GmbH, Planckstr. 1, D-64291 Darmstadt, Germany
e-mail: V.Pershina@gsi.de

Abstract: Investigations of chemical properties of the heaviest elements are among the most fundamental in all of chemistry. They seek to probe the uppermost reaches of the periodic table of the elements where the nuclei are unstable and relativistic effects on the electronic shells are very strong. Theoretical research in this area is extremely important. It is often the only source of useful chemical information. It also enables one to predict behaviour of the heaviest elements in the sophisticated and expensive experiments with single atoms. Spectacular developments in the relativistic quantum theory and computational algorithms allowed for accurate predictions of properties of the heaviest elements and their experimental behaviour. The works on the relativistic electronic structure calculations for the heaviest elements are overviewed. Preference is given to those related to the experimental research. Role of relativistic effects is discussed.

Keywords: Heaviest elements, Relativistic effects, Electronic structure, Chemical properties, Volatility, Complex formation

11.1. INTRODUCTION

Elements considered in this chapter are those with $Z = 104$ and heavier. They are called transactinides, since they are located after the actinide element series which ends with element 103, Lr. The heaviest among them, whose production was confirmed by the IUPAC and IUPAP, is element 112. Observation of even heavier elements, 113 through 118 with the exception of 117, has been claimed but not yet confirmed and approved by the commissions.

The heaviest elements are very special: Located at the bottom of the periodic table of the elements, their nuclei are extremely unstable and electronic shells are influenced by strong relativistic effects [1–10].

Due to the instability of isotopes of these elements and low production rates, experimental chemical research in this area is very complex: Special techniques had to be developed that allow for studying macrochemical properties on the basis

M. Barysz and Y. Ishikawa (eds.), *Relativistic Methods for Chemists*,
Challenges and Advances in Computational Chemistry and Physics 10,
DOI 10.1007/978-1-4020-9975-5_11,

of single atom events. Not less challenging is the theoretical chemical research in this area. It should be based on the most accurate relativistic atomic and molecular calculations in order to reliably predict properties and experimental behaviour of the new elements. It needs also development of special approaches which bridge calculations with quantities that cannot be predicted in a straightforward way via quantum-chemical calculations.

Due to recent developments in the relativistic quantum theory, calculational algorithms and computer techniques, very accurate calculations of heavy element properties became possible. In this chapter, we will overview advances in the theoretical studies of chemical properties of the heaviest elements and predictions of their experimental behaviour. We will pay particular attention to the influence of relativistic effects on chemical properties and trends in the periodic table.

11.2. PRODUCTION AND IDENTIFICATION OF THE HEAVIEST ELEMENTS

Elements heavier than U (Z = 92) are all produced by man-made nuclear reactions. The first members of the transactinides series, Z = 104 through 106 were discovered (in 1969 through 1974) in heavy-ion accelerators by bombardment of heavy actinide (Pu-Cf) targets with light ions (carbon, boron, neon, oxygen), so called "hot-fusion" reactions. The institutions involved in the production of these elements were the LBNL (USA) and the JINR (Russia) (see [11–13] for reviews).

In the 1970s, a different type of fusion reaction was discovered and later used in the discovery of elements with Z larger than 106. These so called "cold-fusion" reactions were based on targets in the vicinity of doubly-magic ^{208}Pb (mainly lead and bismuth) and beams of the complementary medium-mass projectiles with Z $\geq$ 24. Elements with Z = 107 through 112 were produced and identified in this way between 1981 and 1996 at the GSI in Darmstadt (see [14,15] for reviews). Recently, the RIKEN laboratory (Japan) has announced the production of element 113 in the reaction of the ^{70}Zn beams with a ^{209}Bi target [16].

The lifetime of the heaviest elements was found to be very short, for example, the half-life of ^{277}112 is only 0.7 ms (Figure 11-1). The cross-section was also found to decrease rapidly with increasing Z. It is, for example, only ~0.5 pb for ^{277}112. It was, therefore, concluded that it would be very difficult to reach even heavier elements in this way.

More recently, production of the superheavy elements 112 through 118 (except for 117) using "hot" fusion reactions between ^{48}Ca ions and ^{238}U, ^{242,244}Pu, ^{243}Am, ^{245,248}Cm, and ^{249}Cf targets was reported by a Dubna/Livermore collaboration working at the JINR (see [17] for a review). These results are of considerable interest for chemical studies because the reported half-lives are much longer (many orders of magnitude) than those of the isotopes produced by "cold" fusion reactions which lead to more neutron-deficient isotopes. Thus, e.g., $t_{1/2}(^{283}112) = 3.8$ s, and $t_{1/2}(^{287}114) = 0.48$ s. The first chemistry experiments have already been performed with this isotope of element 112 (see below) and experiments for the heavier

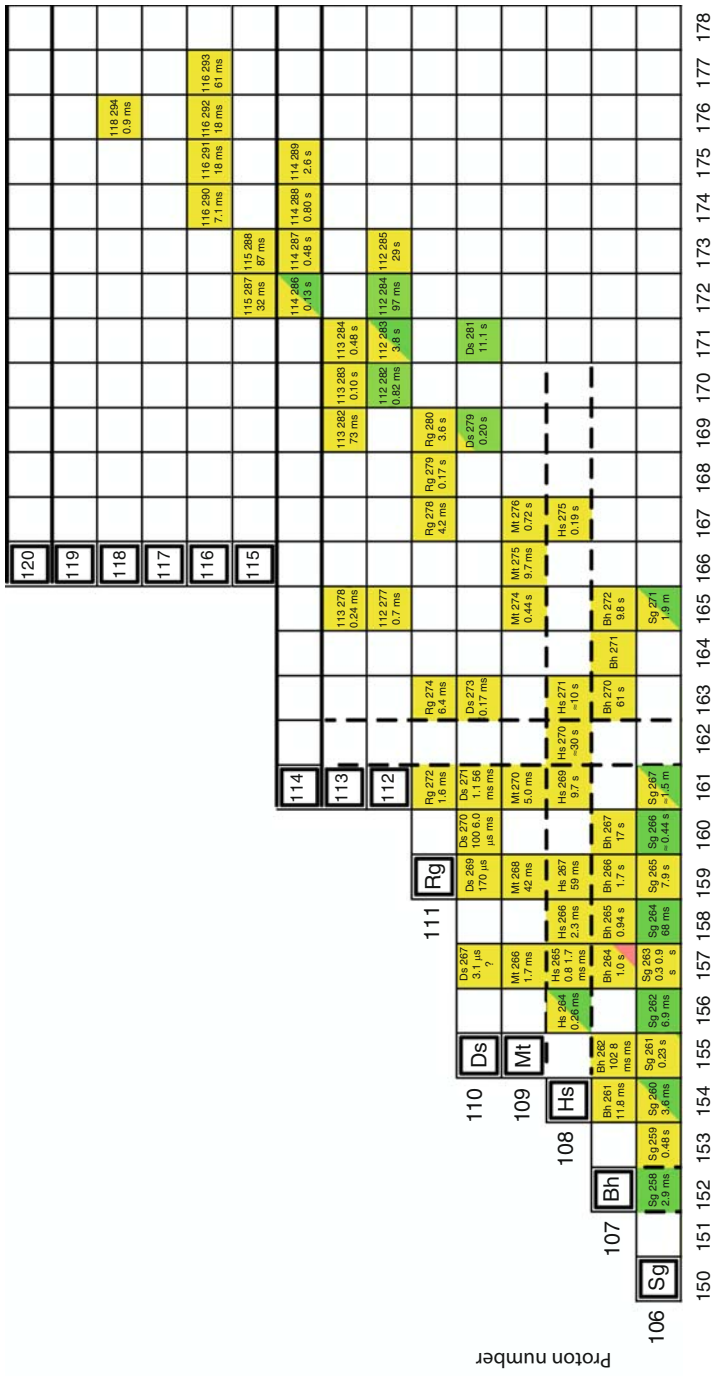

Figure 11-1. The upper part of the chart of nuclides (Light grey – α decay, dark grey – spontaneous fission)

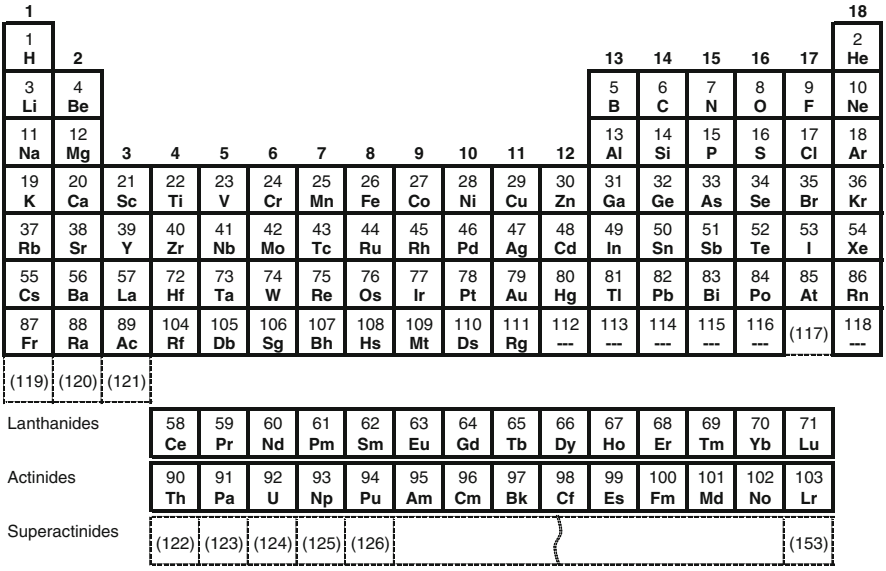

Figure 11-2. The periodic table of the elements 2008

elements 113 and 114 are scheduled. The modern chart of nuclides at its upper end is shown in Figure 11-1. The periodic table as of 2008 is shown in Figure 11-2.

The names and symbols for the transactinide elements approved by the IUPAC are: rutherfordium (Rf) for $Z = 104$, dubnium (Db) for $Z = 105$, seaborgium (Sg) for $Z = 106$, bohrium (Bh) for $Z = 107$, hassium (Hs) for $Z = 108$, meitnerium (Mt) for $Z = 109$, darmstadtium (Ds) for $Z = 110$, and röntgenium (Rg) for $Z = 111$ [18]. As discovery claims on elements with $Z \geq 112$ are under review, these elements are still awaiting naming.

In order to positively identify a new element and place it in its proper position in the periodic table, its atomic number, Z, must be determined or deduced in some way. The elements beyond 101 have been identified first by "physical" techniques because of their very small production rates and short half-lives. One widely used technique is that of $\alpha - \alpha$ correlation of the element's α-decay to a known daughter and/or granddaughter nucleus that also decays by α-emission. For example, elements 111 and 112 produced in "cold-fusion" reactions were identified in this way. Positive identification becomes even more difficult for species that decay predominantly by spontaneous fission (SF). Although detection of SF is a very sensitive technique, it is to date impossible to determine what the nuclear charge Z of the fissioning species might have been since only the fission fragments are detected. The nuclear charge Z of *both primary fragments* would have to be identified in coincidence in order to obtain the total Z of the new element. For example, the claimed α-decay chain associated with $^{292}116$ produced in the $^{248}\mathrm{Cm}(^{48}\mathrm{Ca}, 4n)$ reaction and its daughters goes through $^{288}114$ and $^{284}112$, which undergoes SF. In this case the α chain ends up at an unknown isotope, so that a firm assignment is not possible.

Thus, chemical experiments designed so that the behavior of the unknown isotope will be compared to that of a lighter homolog in a chemical group will help to identify Z (see [11–15] for reviews on experimental techniques for the transactinide elements synthesis and characterization).

The possibility of discovery of even heavier elements is presently a matter of theoretical discussions, and predictions of centers of stabilities in the superheavy element region depend on the model used and are often in disagreement with each other. About 50 years ago it was assumed that the periodic table would end at about $Z = 100$, since the attractive strong interactions can no longer counter-balance the Coulomb repulsion between the many protons. It was then realized that shell-closing effects would increase the nuclear stability substantially. It was, indeed, shown that the stability of nuclei with $Z > 102$ is due to quantum shell effects. Consequently, calculations based on shell correction method (macroscopic-microscopic models, which depend on a large number of parameters, since the form of the potential for strong attractive interactions is not known) predicted the peak of an island of stability at $Z = 114$, $N = 184$ ($^{298}114$) due to both, proton- as well as neutron-shell closures at these numbers [19, 20]. Only in the 1990s, this point of view was challenged by calculations based on more refined models such as self-consistent-field theory and realistic effective nucleon-nucleon interactions. Most of the self-consistent calculations suggest that the center of the proton shell stability should be around higher proton numbers, $Z = 120$, 124, or 126. For the neutrons, relativistic mean-field theory predicts $N = 172$, in contrast to the nonrelativistic prediction for $Z = 184$, which neglects spin-orbit interaction. For reviews on those theoretical works, see [21, 22]. It will be a matter of future investigations to confirm or contradict these theoretical predictions by experiment.

11.3. EXPERIMENTAL CHEMICAL STUDIES

Even though the atomic number can be positively assigned by α-decay chains, no knowledge is obtained about electronic configurations or chemical properties of a new element from these physical methods. The elements are just placed in the periodic table in corresponding chemical groups or periods according to its atomic number and the calculated electronic structures. Thus, it is a matter of experimental chemistry to attempt to validate or contradict these predictions: By assessing similarity in the chemical behaviour with that of lighter homologs a unique position of the new element in a chemical group can be confirmed. It is also essential to establish whether trends in the chemical groups observed for the lighter elements is continued with the transactinides, or whether deviations occur due to the strong relativistic effects. Fundamental properties which enable one to decide about such similarity are oxidation states, ionic radii and complex formation.

Experimental studies of the heaviest elements require use of isotope with a half-life long enough to permit chemical separation and a reasonable production and detection rate. This may range for the heaviest elements from a few atoms per minute for Rf to only an atom per week in the case of element 112. The chemical

procedures used in atom-at-a-time studies must be fast enough to be accomplished in times comparable to the half-lives of the isotopes used in those studies and must give the same results as for macro amounts.

Chemical methods in which a single atom rapidly participates in many identical chemical interactions to two-phase systems with fast kinetics that reach equilibrium quickly have proven to be valid. Thus, it is sufficient to combine the results of many separate one-atom-at-a-time experiments, or identical experiments with only one atom, in order to get statistically significant results [23]. The two main types — gas phase and liquid chemistry — of separations are based on this principle.

11.3.1. Gas-Phase Chemistry

Gas-phase chromatography experiments allow for studying volatility of single chemical species. The measure of this property of macroamounts is the sublimation enthalpy, ΔH_{sub}. A pioneer experiment that allowed an approximation to the sublimation process by adsorption of single species on metallic columns was designed in Dubna [24]. Many assumptions are involved in this approach allowing for a loose correlation between the heat of adsorption and the heat of sublimation. In this method, a longitudinal, negative temperature gradient is established along the chromatography column through which a gas stream is conducted. It contains the volatile species of interest (atoms or molecules) that deposit on the surface of the chromatography column according to their volatilities. The deposition zones are registered by detectors along the column, which are associated with specific deposition (adsorption) temperatures, T_{ads}. The obtained T_{ads} are then used to deduce the adsorption enthalpy ΔH_{ads} using adsorption models and a Monte Carlo simulation.

The first investigations of volatility of the heaviest element compounds were performed in Dubna for Rf (kurchatovium, Ku, in the Russian works at that time), in the form of a chloride, $RfCl_4$ (since it is impossible to stabilize the heaviest 6d elements in the atomic state) using this chromatography technique [25]. Later, volatility of HsO_4 [26] and of element 112 [27], which is stable in the elemental state, was studied in this way. Volatile elements 113 and 114 are to be studied next.

In another technique, isothermal chromatography, the entire column is kept at a constant temperature. Volatile species pass through the column undergoing numerous adsorption-desorption steps. Their retention time is indicative of the volatility at a given temperature. A series of temperatures is run and the chemical yield of the species is studied as a function of the temperature. The temperature, $T_{50\%}$, at which 50% of the species pass through the column, i.e. 50% of the chemical yield, is taken as a measure of volatility in a comparative study. A Monte Carlo program is used to deduce ΔH_{ads} from the measured $T_{50\%}$ using a thermodynamic model of adsorption. The volatility of the Rf, Db, Sg and Bh compounds was successfully studied using this technique [28–31]. Reviews of the gas-phase experimental techniques and applications can be found in [8, 32, 33].

11.3.2. Liquid-Phase Chemistry

Liquid-liquid or ion (cation, CIX, or anion, AIX) exchange chromatography experiments are used to study the complex formation of the heaviest elements and their homologs in aqueous solutions.

An anionic complex $ML_i{}^{z-i}$ is formed according to the reaction

$$M^{z+} + iL^- = ML_i{}^{z-i}, \tag{11-1}$$

with the complex formation constant $\beta_i = [ML_i][M]^{-1}[L]^{-i}$. It is extracted from aqueous solutions by an anion-exchanger according to the following reaction

$$pRB^+L^-(org) + ML_i{}^{-p} = (RB^+)_p(ML_i)^{p-}(org) + pL^-, \tag{11-2}$$

with the equilibrium constant K_{DM}. The distribution coefficient is then

$$K_d = \frac{K_{DM}[RB^+L^-]^p_{org}\beta_i[L^-]^{i-p}}{\sum\limits_0^N \beta_n[L^-]^n}, \tag{11-3}$$

where $p = i - z$, z is the metal formal charge and N is the maximum coordination number. Obtained distribution coefficients K_d (usually plots of K_d values (vs.) acid concentration) are used to judge stabilities of the formed complexes. Also, knowing the K_d values, the complex formation β_i can be obtained.

In experiments with radioactive species, K_d is measured as a ratio of the activity of a studied species in the organic phase to that in the aqueous phase [34–36]. It is closely related to the key observable, the retention time, t_r, in the chromatography column

$$K_d = (t_r - t_0)\frac{V}{M}, \tag{11-4}$$

where t_0 – column hold-up time due to the free column volume, V – flow rate of the mobile phase, and M is the mass of the ion exchanger. In this way, complex formation of Rf, Db and Sg in various acidic solutions has been studied using the AIX and CIX separations [34, 35].

A promising method of separation of the heaviest elements is the electrochemical deposition from aqueous solutions. Electrochemical deposition produces an almost ideal sample for α-spectrometry and at the same time, as least a partial separation from interfering nuclides is achieved. It is presently tested for the homologs of elements 108 and 112 and heavier, e.g., Os, Hg, Pb, Bi and Po. The measured quantities in this method are E_{cri} and $E_{50\%}$ which are the critical potential and the electrode potential when 50% of the atoms are deposited. They both are a measure of the stability of a specific oxidation state and the strength of the metal-metal interaction of the studied metal atom with the electrode material [34, 35]. Reviews of the aqueous chemistry experimental studies can be found in [8, 9, 33–36].

11.4. THEORETICAL STUDIES

11.4.1. Role of Theoretical Studies

Except for the few properties, like volatility or complex formation, many others cannot be directly measured for the heaviest element. They can only be evaluated. For example, chemical composition of compounds can only be assumed on the basis of analogy in the experimental behaviour with that of the lighter congeners in the chemical groups. Ionisation potentials (IP), electron affinities (EA), dissociation energies (D_e) or geometrical structures (e.g., bond lengths, R_e) can not presently be measured at all. They can only be calculated. Thus, in the area of the heaviest elements, theory becomes extremely important and is often the only source of useful chemical information. Finally, it is only the theory that can reveal relativistic effects influence on chemical properties and experimental behaviour: only by comparing the observed behaviour with that predicted on the basis of relativistic (vs.) nonrelativistic calculations, can the importance and magnitude of relativistic effects be established.

Earlier predictions of chemical properties of the heaviest elements were based on results of the relativistic Dirac-Slater (DS) and Dirac-Fock (DF) atomic calculations and extrapolations of periodic trends (see reviews [5,37–40]). These and later works have revealed that use of the relativistic quantum theory and most advanced relativistic methods is mandatory for calculations of properties of the heaviest elements where relativistic effects become most important. Early molecular calculations have shown that trends in properties in the chemical groups can be predicted in an erroneous way for the heaviest elements by using nonrelativistic codes. Some simple extrapolations of the periodic trends, though sometimes useful, must also be made cautiously. Previous reviews of the theoretical works on molecular calculations for the heaviest elements are those of [6–10,41–43].

11.4.2. Relativistic and QED Effects on Atomic Electronic Shells of the Heaviest Elements

Relativistic effects on atomic orbitals (AOs) are well known: this is the contraction and stabilization of the s and $p_{1/2}$ AOs, the destabilisation and expansion of the $p_{3/2}$, d and f AOs, and the spin-orbit (SO) splitting of the AOs with $l > 0$. All the three effects change approximately as Z^2 for valence shells down a column of the periodic table. For the heaviest elements with large Z, these effects are of paramount importance. Figure 11-3 shows, e.g., the relativistic stabilization of the ns and $np_{1/2}$ AO and the SO splitting of the np AOs of the group 14 elements, with the latter amounting to 50 eV for element 164 [5].

Figure 11-4 shows the relativistic contraction $\Delta_R\langle r\rangle_{7s} = (\langle r\rangle_{nr} - \langle r\rangle_{rel})/\langle r\rangle_{nr} = 25\%$ of the 7s AO in Db. (See also Figure 7-3 in the Chapter of E. Eliav and U. Kaldor for the relativistic contraction of the 7s(Rg) AO.)

The relativistic contraction and stabilization of the ns AO reach the maximum in the seventh row at element 112 [6] (Figure 11-5). The shift of the maximum to

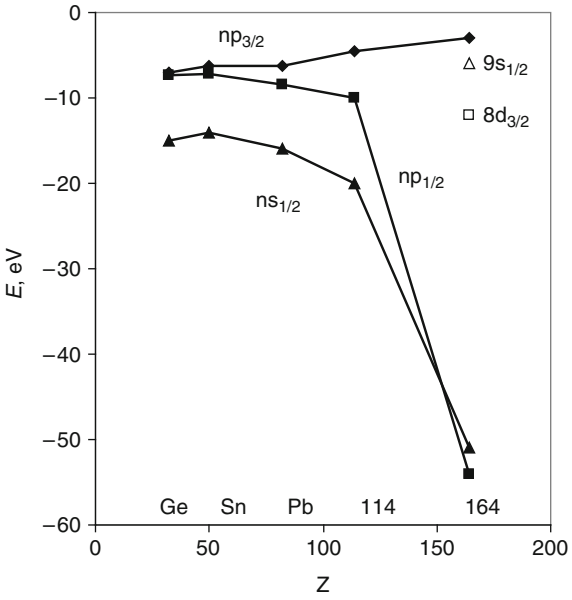

Figure 11-3. DS eigenvalues of the valence electrons of group 14 elements in the sp^2p configuration (Re-drawn from [5])

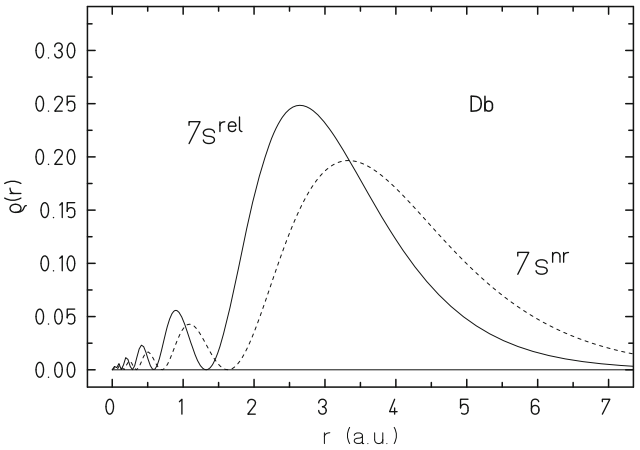

Figure 11-4. Relativistic (solid line) and nonrelativistic (dashed line) radial distribution of the 7s valence electrons in element 105, Db (From [43])

element 112 in the seventh row in contrast to gold in the sixth row [44] is due to the fact that in both elements 111 and 112 the ground state electronic configuration is d^qs^2, while the electronic configuration changes from Au($d^{10}s^1$) to Hg($d^{10}s^2$).

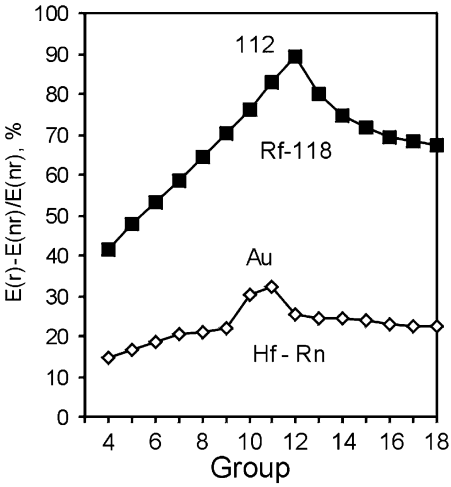

Figure 11-5. The relativistic stabilization of the 6s and 7s orbitals in the sixth and seventh row of the periodic table (Re-drawn from [6]). The DF data are from [45]

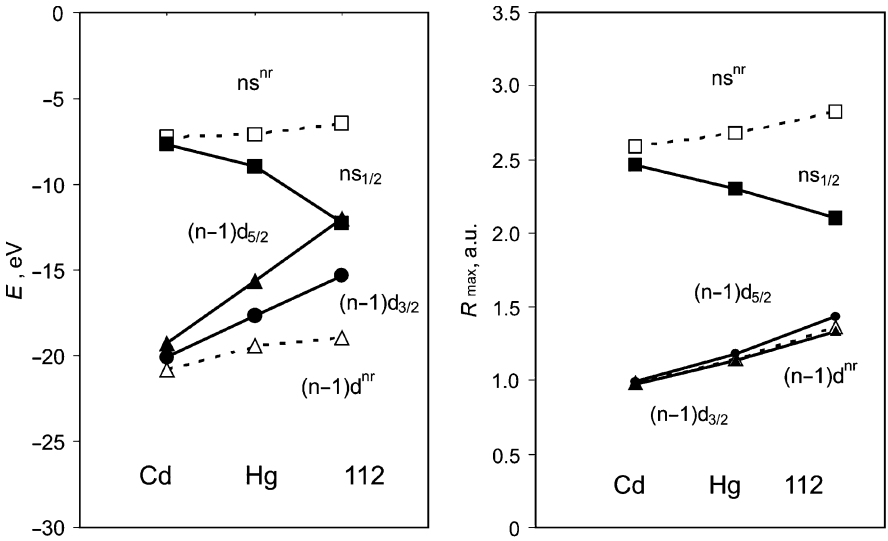

Figure 11-6. Relativistic DF (full lines) and non-relativistic HF (dashed lines) AO energies, E, and radii of the maximum electronic charge density, R_{max}, of the valence AO of group 12 elements [6, 45] (From [46])

The 7s(112) AO stabilization is ∼10 eV, according to the DF calculations [6, 45] (Figure 11-6).

The relativistic destabilization of the 6d AOs increases along the 6d series and reaches its maximum at element 112 with the SO splitting of 3.3 eV (Figure 11-6).

Together with the stabilization of the 7s AOs, this results in the inversion of the 7s and 6d energy levels, so that the first ionized electron of element 112 is $6d_{5/2}$ and not 7s as in Hg. (An inversion of the 7s and 6d levels in the seventh row starts already at Hs.) Figure 11-6 also shows that trends in the relativistic and non-relativistic energies of the ns AOs (the same is valid for the $np_{1/2}$ AOs) become opposite as one proceeds from the sixth to the seventh row of the periodic table, which will result in opposite trends in relativistic and nonrelativistic properties defined by those AOs.

In the 7p series of the elements, the stabilization of the $7s^2$ is so large that it becomes practically an inert pair. The stabilization of the $7p_{1/2}$ AO and the SO splitting of the 7p AOs is also very large for these elements reaching 11.8 eV for element 118. For the heavier elements, relativistic effects on their valence orbitals are even more pronounced and could lead to properties which are very different to those of the lighter homologs. The periodic table up to element 172 and relativistic effects on properties of these elements are discussed in [5].

Breit effects (accounting for magnetostatic interaction) on valence orbital energies and IP of the heaviest elements are small, for example, only 0.02 eV for element 121 [47]. They can, however, reach few % for the fine structure level splitting in the 7p elements and are of the order of correlation effects there. In element 121, they can be as large as 0.1 eV for transition energies between states including f orbitals [47].

Quantum electrodynamic (QED) effects are known to be very important for inner-shells, for example, in accurate calculations of X-ray spectra [48]. For highly charged few electron atoms they were found to be of similar size as the Breit correction to the electron-electron interaction [49]. Importance of the QED effects was also shown for valence ns electrons of neutral alkali-metal and coinage metal atoms: They are of the order of 1–2% of the kinetic relativistic effects there [50]. The result for the valence ns electron is a destabilization, while for $(n - 1)$d electron is an indirect stabilization. In the middle range ($Z = 30$–80) both the valence-shell Breit and the Lamb-shift terms behave similarly to the kinetic relativistic effects scaling as Z^2. For the highest Z values the increase is faster. Nuclear volume effects grow even faster with Z. Consequently, for the superheavy elements its contribution to the orbital energy will be the second important one after the relativistic contribution.

For element 118, QED effects (self-energy and vacuum polarization corrections to the binding energy of the 8s electron) were found to amount to 9% reduction (0.0059 eV) of the EA [51].

11.5. RELATIVISTIC QUANTUM CHEMICAL METHODS

The most appropriate quantum chemistry methods for the heaviest elements are those which treat both relativity and correlation at the highest level of theory. Most of them are described in this volume, as well as they were overviewed recently [52]. Thus, only those which were applied to the heaviest elements and their compounds will be mentioned here.

11.5.1. Atomic Codes

The best theoretical level for the many-body methods if the Dirac-Coulomb-Breit (DCB) Hamiltonian

$$h_{DCB} = h_{DC} + \sum_{i<j} B_{ij}. \tag{11-5}$$

It contains the one-electron Dirac Hamiltonian h_D plus the nuclear potential, V^n, and the operator $V_{ij} = 1/r_{ij}$ for the instantaneous Coulomb interaction between electrons

$$h_{DC} = \sum_i (c\boldsymbol{\alpha}_i \boldsymbol{\rho}_i + (\beta_i - 1)) + V^n + \sum_{i<j} 1/r_{ij}. \tag{11-6}$$

B_{ij} is the Breit term

$$B_{ij} = -1/2[(\boldsymbol{\alpha}_i \boldsymbol{\alpha}_j) r_{ij}^{-1} + (\boldsymbol{\alpha}_i \boldsymbol{r}_{ij})(\boldsymbol{\alpha}_j \boldsymbol{r}_{ij}) r_{ij}^{-3}]. \tag{11-7}$$

The V^n includes the effect of the finite nuclear size, while some finer effects, like QED, can be added to h_{DCB} perturbatively. The DCB Hamiltonian in this form contains all effects through the second order in α, the fine-structure constant. Correlation effects are taken into account by the configuration interaction (CI), many-body perturbation theory (MBPT) and, presently at the highest level of theory, the coupled cluster single double excitations (CCSD) technique.

The Fock-space (FS) DCB CC method [53] is presently the most powerful method which was applied to heavy and the heaviest elements (see the Chapter of E. Eliav and U. Kaldor in this issue). The method has an accuracy of few hundredths of an eV for excitation energies in heavy elements, since it takes into account most of the dynamic correlation (states with high l). Calculations using this method have shown, for example, a principally different ground state electronic configuration of Rf ($7s^2 6d^2$) [54] in contrast to the multiconfiguration (MC) DF calculations ($6d^2 7s 7p_{1/2}$) [55, 56]. The heaviest element treated by this method is 122 [57]. Due to the present limitation of the FS CCSD method in treating electronic configurations with no more than two electrons (holes) beyond the closed shell, the calculations for the middle of the 6d-series (elements 105 through 110) have not yet been performed.

Further developments are under way to remove this limitation. Thus, high-sectors FSCC code is under development which will allow for treating systems with up to six valence electrons/holes in an open shell. Relativistic Hilbert space CC (HSCC) method is also worked on, which could be used for systems with more than a couple of electrons/holes in the active valence shell. The mixed sector CC (MSCC) method will be a generalization of the previous two (FSCC and HSCC) and will combine their advantages.

The DC FS CCSD and CCSD(T) methods incorporated in the DIRAC package [58] have a slightly lower accuracy than the DCB FSCC one. They were used for calculations of properties of the heaviest elements 112 through 118 (see below). The used basis sets are the universal ones [59], those of Visscher [60], and Faegri [61].

The latter proved to be the most suitable for the heaviest elements. The prolapse-free relativistic Gaussian basis sets for the superheavy elements up to Z = 119 suitable for four-component ($4c$) molecular calculations were also published recently [62].

A practical instrument for many-electron open-shell system is the MCDF method [63, 64]. Based on the CI technique, it accounts for most of the correlation effects while retaining a relatively small number of configurations. It omits, however, dynamic correlation which makes it less accurate than the DC(B) CCSD one. Calculations of multiple IPs for Lr through Hs, and of elements 112 and 114 and their homologs were performed with its use [55, 56, 65–69]. Results are discussed below.

Atomic calculations for the heaviest elements were also performed using other approaches. Thus, e.g., the electronic states of element 114 were calculated using the relativistic complete active space MCSCF (CASMCSCF) CI method [70]. Also, many atomic calculations were performed while calculating molecular properties with the use of molecular codes (see below).

Overall, results of the modern accurate atomic calculations agree rather well with predictions made with the use of the earlier DF and DS methods, where the calculated energy terms were corrected by the difference with experiment for the lighter homologs [5]. Elements up to Z = 172 were treated with the use of the latter methods [71]. Element 184 was also considered in [5], as an example of an even heavier element.

11.5.2. Molecular Methods

The most accurate way to solve the Dirac many-electron Eq. (11-5) is that without approximation. Nevertheless, the problems of electron correlation and proper basis sets make the use of *ab initio* DF methods very limited with respect to the heavy-element systems. Most of the molecular *ab initio* DF calculations account for correlation via the CI, Møller-Plesset, MP2, or CCSD(T) techniques [72]. The DC method suitable for molecular calculations is also implemented in the DIRAC package [58]. The basis sets are described in [61].

The *ab initio* DF methods are still too computer time intensive and not sufficiently economic to be applied to the heaviest element systems in a routine manner, especially to the complex systems studied experimentally. Mostly small molecules, like hydrides or fluorides, were studied at this level of theory [73–78]. The main aim of those calculations was to study relativistic and correlation effects on model systems. The DF calculations without correlation were performed for some heaviest element molecules, like $RfCl_4$, $SgBr_6$ or HsO_4 [79, 80], though binding energies are up to 50% inaccurate. Pioneer calculations of Pyykkö and Desclaux for RfH_4 and SgH_6 using the DF one center expansion method should also be mentioned [81].

Effective core potentials (ECP) were successfully applied to the heaviest element systems (see the Chapter of M. Dolg in this issue): the energy-adjusted pseudo potentials (PP) [82] known as Stuttgart ones and the relativistic ECP (RECP) [83].

The PPs were used for calculations of the electronic structures and properties of compounds of elements 111 through 114 [75, 84–87]. Performed at different levels of theory for relativity (HF, spin-average relativistic effective core potentials, AREP, AREP + SO) and correlation (MP2, CCSD(T)), they enabled one to establish the influence of relativistic and correlation effects on properties of chemically interesting molecules and complexes.

The RECP at different levels of theory for correlation (MP2, complete active space MSCF (CAS-MCSCF), CCSD(T)), were also used for a number of chemically interesting gas-phase chlorides and oxychlorides of elements Rf through Sg, as well as for some hydrides and fluorides of the 7p elements including element 118 [88–97]. The RECPs are published by Nash [98]. Generalized RECPs accounting for Breit effects were developed for elements 112, 113 and 114 [99].

The density functional theory (DFT) was applied at most for the heaviest element compounds, complexes in solutions and solid state. Due to its overall simplicity and efficiency of the calculational algorithms, the DFT methods are well suited for treating chemically interesting large systems, adsorption processes, solid state and solutions. (Thus, e.g., the computing time in the DFT for a system of many atoms grows as $N_{at}{}^2$ or $N_{at}{}^3$, while in traditional methods as $\exp(N_{at})$.) The modern DFT theory is exact [100] and the accuracy depends on the adequate choice of the exchange-correlation potential [101].

The Dirac-Slater Discrete Variational (DS-DV) method [102] was extensively used in the past for calculations of ground state properties of the heaviest element compounds — gas-phases molecules and complexes in solutions (see [10] for a review). Even though it was inaccurate with respect to binding energies, it allowed for reliable predictions of ionization energies and character of chemical bonding.

Introduction of the RGGA approximation for the exchange-correlation potential, improvement in the integration scheme and basis set technique [103] allowed for accurate calculations of binding energies and geometry optimization. The most recent version used nowadays for the heaviest element compounds is the 4*c*-DFT one combined with the noncollinear spin-polarized formalism [104] (see examples below). According to this method, the total energy of a molecular system is given by the following expression

$$E = \sum_{i=1}^{M} n_i \langle \phi_i | \hat{t} | \phi_i \rangle + \int V^N \rho d^3\vec{r} + \frac{1}{2} \int V^H \rho d^3\vec{r} + E^{xc}[\rho, \vec{m}] + \sum_{p>q} \frac{Z_p Z_q}{|\vec{R}_p - \vec{R}_q|} \tag{11-8}$$

with the electronic density, ρ

$$\rho(\vec{r}) = \sum_{i=1}^{M} n_i {\phi_i}^+(\vec{r}) \phi_i(\vec{r}) \tag{11-9}$$

and the magnetization density, m

$$\vec{m}(\vec{r}) = -\mu_B \sum_{i=1}^{M} n_i \phi_i^+(\vec{r}) \beta \vec{\Sigma} \phi_i(\vec{r}). \tag{11-10}$$

Here, n_i are the occupation numbers, $\vec{r}$ is the electronic coordinates, respectively, and μ_B is the Bohr-magneton. The index i runs over all occupied molecular orbitals M, which are four-component Dirac spinors. The four-component spin operator $\vec{\sum} = (\sum_x, \sum_y, \sum_z)$ is built from two-component Pauli matrix σ. The Dirac kinetic energy operator has the form

$$\hat{t} = c\vec{\alpha} \cdot \vec{p} + c^2(\beta - I), \tag{11-11}$$

where $\vec{\alpha} = (\alpha_x \alpha_y \alpha_z)$ and β are the four-component Dirac matrices in the standard representation, and I is the four-component unit matrix. V^N is the nuclear potential, E^{xc} is the exchange correlation energy functional and V^H is the electronic Hartree potential

$$V^H(\vec{r}) = \int \frac{\rho(\vec{r'})}{|\vec{r} - \vec{r'}|} d_3\vec{r'}. \tag{11-12}$$

Application of the variational principle with the constraint that the number of electrons in the system should be conserved leads to the single particle Kohn-Sham equations in their non-collinear form

$$\left\{ \vec{t} + V^N + \tilde{V}^H + \frac{\delta E^{xc}[\rho, \vec{m}]}{\delta \rho} - \mu_B \beta \vec{\Sigma} \frac{\delta E^{xc} \lfloor \rho, \vec{m} \rfloor}{\delta \vec{m}} \right\} \phi_i = \varepsilon_i \phi_i \, {}^{i=1\ldots M'} \tag{11-13}$$

Here $\tilde{V}^H$ is the Hartree potentials from the model-density and $M' \geq M$ is the number of molecular orbitals.

Self-consistent, all-electron calculations are performed within the relativistic local density approximation (LDA). The nonlocal corrections (i.e., the generalized gradient approximation, GGA) are then included perturbatively using the Becke 1988 [105] functional for exchange and the Perdew 1986 [106] functional for correlation. Many other functionals are also included in the method, though the B88/P86 one was found to be the most appropriate. (In the following, results of the 4c-DFT calculations will be given for this potential.)

The non-collinear approximation allows the magnetization density to point at any direction at any point of the system under consideration. Accordingly, nearly each electron is treated by its own wavefunction with a quantum number j and magnetic number m_j. This permits treatment of open shell system. (The collinear approximation is also implemented in the method.)

The method uses numerical wave-functions. The basis set optimization procedure is described in [104]. It is developed for very large systems, e.g., clusters with up to more than 100 atoms and is, therefore, suitable for treatment of adsorption process and complex formation.

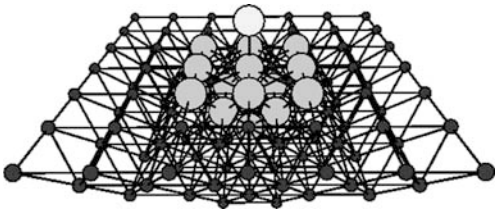

Figure 11-7. Embedded M-M_{14} system

A possibility to treat even a larger number of atoms economically is achieved via the embedded cluster procedure [107] (Figure 11-7).

According to the embedding technique, the total density of a system can be divided into two parts

$$\tilde{\rho}(\vec{r}) = \tilde{\rho}^{cl} + \tilde{\rho}^{env}(\vec{r}). \tag{11-14}$$

The action of the environment on the cluster can be treated as an external potential due to the external charge density $\tilde{\rho}^{env}(\vec{r})$. The external potential V^{ext} is

$$V^{ext} = V^{n}_{ext} + V^{C}_{ext} + V^{ex}_{ext}, \tag{11-15}$$

where V^{n}_{ext} is the Coulomb potential of the nuclei, V^{C}_{ext} is the Coulomb potential of the electronic charge density of the environment, and V^{xc}_{ext} is the exchange-correlation potential. The original KS-equation then reads

$$\left(\hat{t} + V^{n}_{cl}(\rho^{cl}) + V^{C}_{cl}(\rho^{cl}) + V^{xc}_{cl}(\rho^{cl}) + V^{ext}\right)\phi_i(\vec{r}) = \varepsilon_i \phi_i(\vec{r}). \tag{11-16}$$

This equation is solved self-consistently with respect to ρ^{cl} given by Eq. (11-9) where i runs over all cluster electrons. The embedded cluster method was used, e.g., for studying adsorption of Hg and element 112 on gold (see Section 11.7.3.3).

Another 4*c*-DFT method used for some heaviest element compounds is the Beijing one (BDF) [108–111]. It differs from the 4*c*-DFT method [104] by the basis set technique: 4*c*-numerical atomic spinors obtained by finite-difference atomic calculations are used for cores, while basis sets for valence spinors are a combination of numerical atomic spinors and kinetically balanced Slater-type functions. The non-relativistic GGA for the exchange-correlation potentials is used. Results for the same systems, like e.g. $(114)_2$, obtained with the use of the 4*c*-DFT [104] and BDF [111] methods are very similar.

Several quasi-relativistic approximations, e.g., 2*c*-DFT using Douglas-Kroll (DK) approach [112], or zero-order regular approximation (ZORA) [108], also implemented in the Amsterdam density functional (ADF) method [113], were used for the heaviest element compounds as well. The SO ZORA demonstrated very good agreement with the 4*c*-DFT results, as is shown in [108].

Some other methods like, e.g., Douglas-Kroll-Hess [114], were also applied to small heaviest element species. Examples of the calculations with the use of the various methods are considered in the following sections.

11.6. ATOMIC PROPERTIES OF THE HEAVIEST ELEMENTS AND RELATIVISTIC EFFECTS

11.6.1. Electronic Configurations

Results of the atomic relativistic calculations have shown that the relativistic stabilization of the 7s-AO in the seventh row results in the availability of the $7s^2$ electron pair in the ground state of the 6d and 7p elements, $7s^26d^q$ and the $7s^27p^q$, respectively. This is in contrast to the sixth row, where Pt and Au have different, $5d^96s$ and $5d^{10}6s$, ground states, respectively (Table 11-1). The first excited states also differ for the two series: those for the 6d-elements contain the $7s^2$ pair all. Relativistic stabilization of the $7p_{1/2}$ AO results in the ground state of Lr different to that of the lighter homolog Lu (Table 11-1).

It is remarkable that the controversy about ground states of Lr and Rf was finally solved with the use of the DCB FS CCSD method. The DCB CCSD calculations for Lr [115] confirmed the MCDF $7s^27p_{1/2}$ state [116], but corrected the MCDF $7s^27p6d$ one for Rf [55, 56] giving the $7s^26d^2$ state as ground [54]. A very high level of correlation with the $l = 6$ was needed to reach this accuracy. The DF calculations [45] have revealed that element 120 has the $7p^68s^2$ relativistic ground state in difference to the non-relativistic $7p^67d8s$ state [6]. According to the DCB CCSD result [47], element 121 should have a $8s^28p_{1/2}$ ground state (in agreement with earlier DF results [5]) which is 0.4 eV lower in energy than the $8s^27d$ state, which is the ground state for the lighter group-3 homologs. Element 122 should have the $8s^27d8p$ state in contrast to the $7s^26d^2$ state of Th [57]. Thus, the relativistic stabilization of the $8p_{1/2}$ is responsible for this unusual configuration.

For the heavier elements, the older DS and DF [5] data are available. The DFT + QED calculations were recently performed for elements 121–131 [117]. The proximity of the 7d, 6f and 5g levels, and their partial filling makes the usual classification on the basis of a simple electronic configuration difficult, so that the placement of these elements in the periodic table becomes problematic. It will be a challenge for theoreticians to accurately predict electronic states of those superheavy elements.

Table 11-1 Ground state electronic configurations of the 5d and 6d elements. Lu and Lr are also included

Lu	Hf	Ta	W	Re	Os	Ir	Pt	Au	Hg
$5d6s^2$	$5d^26s^2$	$5d^36s^2$	$5d^46s^2$	$5d^56s^2$	$5d^66s^2$	$5d^76s^2$	$5d^96s$	$5d^{10}6s$	$5d^{10}6s^2$
Lr	Rf	Db	Sg	Bh	Hs	Mt	Ds	Rg	112
$7s^27p_{1/2}$	$6d^27s^2$	$6d^37s^2$	$6d^47s^2$	$6d^57s^2$	$6d^67s^2$	$6d^77s^2$	$6d^87s^2$	$6d^97s^2$	$6d^{10}7s^2$

11.6.2. Ionization Potentials, Electron Affinities and Stable Oxidation States

The first IPs of elements 104 through 166 were calculated using the DF and DS methods (see [5] for a review). The multiple IPs of Rf through Hs, and of elements 112 and 114, as well as the first IPs for elements 113–119 were calculated using the MCDF method [56, 65–69, 118]. The DCB CCSD results were reported for IPs of elements 104, 111–115, 121 and 122 [47, 54, 57, 119–123].

The IPs for the seventh row of the elements in comparison with those for the sixth row are shown in Figure 11-8. The values can be found in [8].

Relativistic effects on IPs reflect those on the valence AOs responsible for the ionisation. Thus, the relativistic destabilization of the 6d-AOs is a reason for the first IPs of Rf through Mt being lower compared to the 5d homologs. In elements 110 through 112, the first ionized electron is also 6d in contrast to the lighter homologs Pt through Hg, though the ionisation energies are higher. In elements 113 through 118, the first ionized electron is 7p as expected. A large 7p AO SO splitting explains a drastic decrease in the IP from element 114 to 115 due to the filling of the $7p_{3/2}$ shell for element 115, which is more destabilized than the $6p_{3/2}$ shell of Bi. A large 7p AO SO splitting also explains the smaller IPs of elements 115 through 118 in comparison with their homologs Bi through Rn.

Element 118 is expected to be the most electronegative in the group of the noble gases: Its outer 8s orbital is relativistically stabilized to give the atom a positive EA of 0.058 eV according to DCB CCSD + QED calculations [51, 125]. The inclusion of both relativistic and correlation effects was required to obtain this result. Similar calculations did not give a ^2S bound state for Rn^-. The DC CCSD(T) IP(118) is 8.92 eV [126], the smallest in group 18.

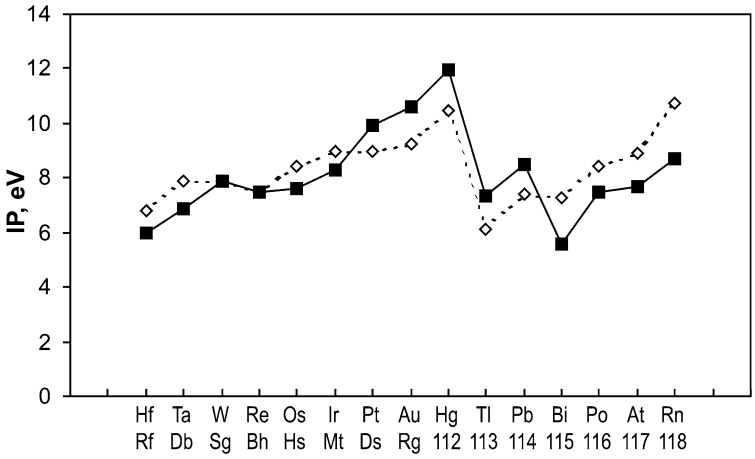

Figure 11-8. Ionization potentials of the sixth row elements (dashed line, experimental values [124]) and the seventh row (solid line, calculated values)

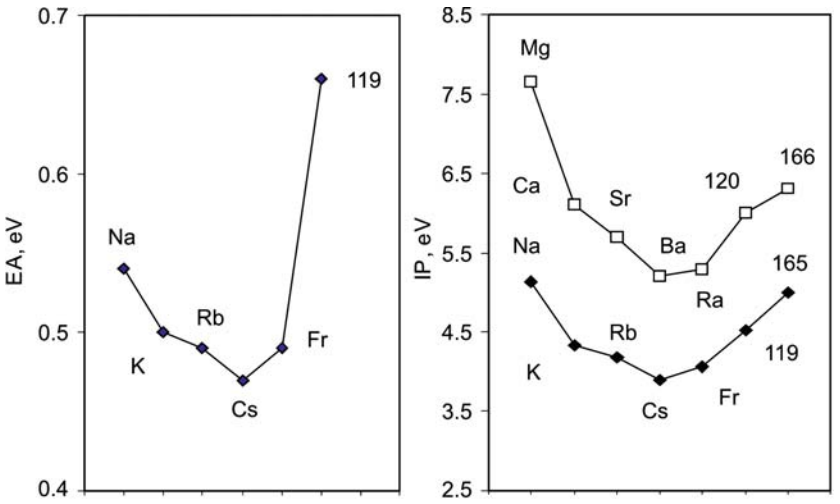

Figure 11-9. Electron affinities, EA, and ionisation potentials, IP, for alkali and alkaline-earth elements. The data for Na through Fr and Mg through Ra are experimental [124]

The relativistic stabilization of the $np_{1/2}$ AOs in group 13 and 14 is also responsible for a trend reversal in the decreasing IPs beyond In and Sn, respectively. Similarly, an upturn in the IPs is observed from Sc to element 119 and Ba to element 120 in group 1 and 2 due to the relativistic stabilization of the outer $ns_{1/2}$ electrons. The IP of element 119 is relativistically increased from 3.31 to 4.53 eV, as DK CCSD calculations show [127].

The decreasing trend in EA in the group of alkali elements from Na to Cs (Figure 11-9) is reversed beyond Cs due to the relativistic stabilization of the 7s(Fr) and 8s(119) AOs.

Due to the relativistic stabilization of the 8s AO, EA(119) is 662 meV, being also the highest in group 1, according to DCB CCSD calculations [128]. The CCSD IP(121) = 4.45 eV and EA(121) = 0.57 eV, the highest in group 3 [47]. The DCB CCSD IP(122) = 5.59 eV [57] as compared to the IP(Th) = 6.52 eV: this relative decrease is due to the relativistically stabilized $8p_{1/2}$ electron of element 122. The DF and DS IPs of even heavier elements can be found in [5].

IPs of internal conversion electrons (1s and 2s) for the element 112, 114, 116 and 118 are predicted to an accuracy of a few 10 eV using DHF theory and taking into account QED and nuclear-size effects [48]. The $K_{\alpha 1}$ transition energies for different ionization states of Mt were accurately predicted using the same approach and compared with recent experiments in the α-decay of ^{272}Rg [129].

The relativistic stabilization of the 7s AO and destabilization of the 6d AOs over the 6d series of the elements results in the increased stability of higher oxidation states, in agreement with the observed trends in the chemical groups. The MCDF calculations of the multiple IPs for elements Rf through Hs [56,65–67] have, indeed, shown a decrease in IP($0 \rightarrow Z^{+}{}_{max}$), as illustrated in Figure 11-10. Due to the same

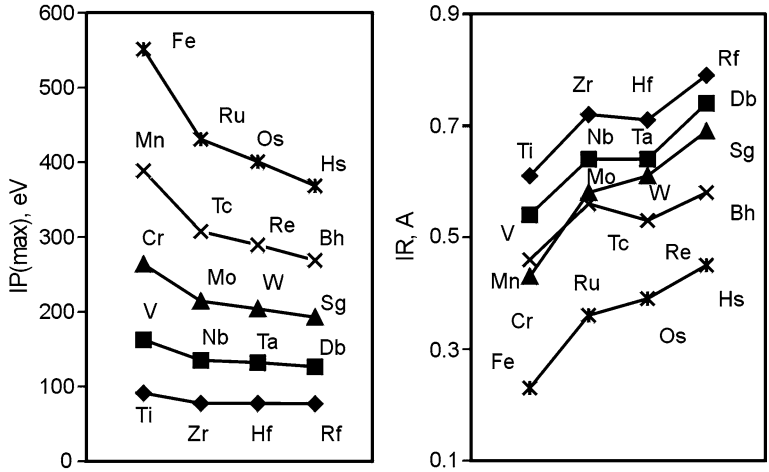

Figure 11-10. Multiple ionization potentials: IP(0 → 4+) for group-4, IP(0 → 5+) for group-5, IP(0 → 6+) for group-6, IP(0 → 7+) for group-7, and IP(0 → 8+) for group-8 elements, as well as ionic radii, IR, for these elements in their maximum oxidation states obtained from the MCDF calculations [56, 65–67] (From [43])

reason, lower oxidation states at the beginning of the 6d series will be unstable: the step-wise ionization process results, for example, in the $6d^2$ and not in the $7s^2$ configurations for Db^{3+} or Sg^{4+}. Since the 6d orbitals of the 6d elements are more destabilized than the (n − 1)d orbitals of the 4d and 5d elements, Db^{3+} and Sg^{4+} will even be less stable than Ta^{3+} and W^{4+}, respectively.

A trend to an increase in the stability of the 3+ and 5+ oxidation states of Rg was also attributed to relativistic effects. Due to a relatively high EA of Rg, the 1− oxidation state may be accessible with appropriate ligands. The 4+ state of element 112 should also be more stable than those of Au and Hg, respectively. The 0 oxidation state will dominate for element 112 due to its closed shell (the EA is 0 [120]).

The large relativistic stabilization of the $7s^2$ electrons and, hence, a large 7s-7p gap hindering hybridization, is the reason for enhanced stability of lower oxidation states at the beginning of the 7p-series. Thus, the 1+ oxidation state will be more important than the 3+ state for element 113. Due to the relativistic stabilization of the $7p_{1/2}$ electrons of element 114, the 2+ state should predominate over the 4+ state to a greater extent than in the case of Pb. The 6d AOs should be still accessible for hybridization for elements 113 and 114 and should take part in bonding leading to the formation of compounds of these elements in higher oxidation states like, e.g., $113F_6^-$ [78] or $114F_6^{2-}$ [77]. For elements 115 through 118, on the contrary, lower oxidation states should be more stable than those of the lighter homologs due to the inaccessibility of the relativistically stabilized $7p_{1/2}$ AO for bonding. For element 115, the 1+ state should be more important due to the SO destabilized $7p_{3/2}$ electron. The 3+ state should also be possible, while 5+ not. For element 116,

a decrease in the stability of the 4+ oxidation state is expected due to a large SO splitting of the 7p AOs, and the 2+ state should be important due to the two destabilized $7p_{3/2}$ electrons. For element 117, the 1+ and 3+ oxidation states should be the most important, while 5+ and 7+ are less. The 1- state of element 117 having one electron hole on the $7p_{3/2}$ AO should therefore be less important (its EA is the smallest in the group). For element 118, 2+ and 4+ states are possible, while the 6+ one will be less important, because of the strong binding of the $7p_{1/2}$ electrons. Oxidation states of heavier elements are discussed in [5].

11.6.3. Atomic/Ionic/Covalent Radii and Polarizability

Atomic (AR) and ionic radii (IR) are defined by the maximum of the radial charge density, $R_{\max}$, of the outer valence AO. The DF $R_{\max}$ values for elements up to Z = 120 were tabulated by Desclaux [45]. The MCDF $R_{\max}$ for Rf through Hs and their lighter homologs in the chemical groups in various oxidation states were calculated by Johnson, Fricke et al. [56, 65–67]. In those works, IR of the transactinides were obtained via a linear correlation between $R_{\max}$ and known IR [130] in the chemical groups. The IR of elements Rf through Hs in the highest oxidation states are shown in Figure 11-10.

Figure 11-10 shows that the IR of the 4d and 5d elements are almost equal due to the lanthanide contraction (of 0.020 Å) which is roughly 86% a nonrelativistic effect: The diminished shielding of the nucleus charge by the 4f electrons causes the contraction of the valence shells. The IR of the transactinides are about 0.05 Å larger than the IR of the 5d elements. This is due to an orbital expansion of the outer $6p_{3/2}$ orbitals responsible for the size of the ions. The IR of the transactinides are, however, still smaller than the IR of the actinides due to the actinide contraction (0.030 Å), being larger than the lanthanide contraction, which is mostly a relativistic effect: The 5f shells are more diffuse than the 4f shells, so that the contraction of the outermore valence shells is increased by relativity to a larger extent in the case of the 6d elements as compared to the 5d elements. The DF and HF calculations [85] for the 5d and 6d elements with and without the 4f and 5f shells, respectively, have shown that the shell-structure contraction is, indeed, enhanced by relativistic effects and that the orbital and relativistic effects are not additive.

A set of atomic single and triple bond covalent radii (CR) for most of the elements of the periodic table including the heaviest ones till Z = 118 and 112, respectively, are given in [131, 132]. They were deduced from the calculated molecular bond lengths of various covalent compounds. The obtained single bond CR for the group 4 through 8 6d-elements are consistent with their IR: they are about 0.06 Å on the average larger than the CR of the 5d elements (Figure 11-11). (The triple bond CR are slightly larger, i.e., 0.08 Å on the average.) An important finding of those works is a decrease in the CR_{6d}-CR_{5d} difference starting from group 9, reaching negative values in groups 11 and 12, as a result of the relativistic bond contraction. This was called a “transactinide break” [132].

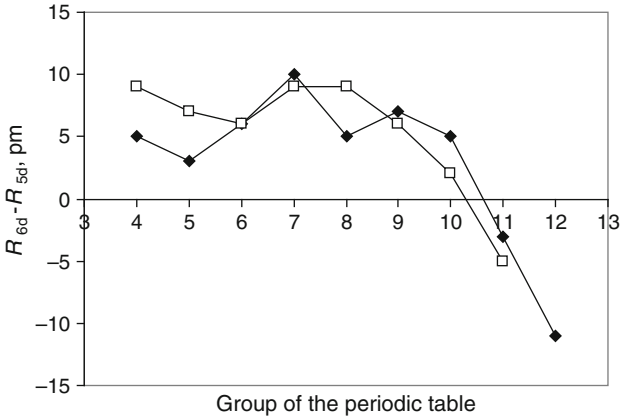

Figure 11-11. The difference in the lengths of the single (filled rhomboids) and triple (open squares) bonds between the 6d and 5d metals [131, 132]

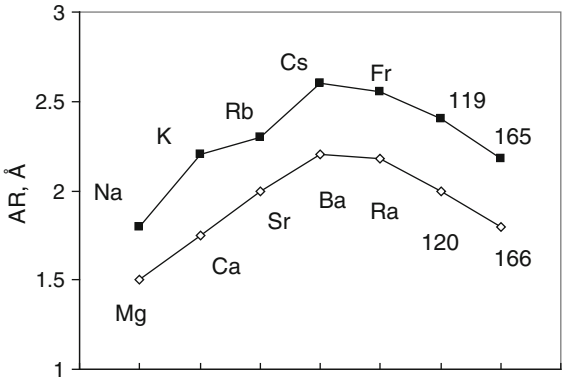

Figure 11-12. Atomic radii, AR, of alkali and alkaline earth elements. The data for Na through Cs and Mg through Ra are experimental. The other data are from DS calculations (Re-drawn from [133])

Thus, the calculations for elements 111 and 112 have shown that they should have the smallest AR and CR in the respective chemical groups due to the relativistic contraction of the 7s AO.

The DS/DF calculations [5] have also shown that within the alkaline and alkaline earth series of elements a reversal of increasing AR occurs beyond Cs and Ba, respectively (Figure 11-12). The shell-contraction effects are, however, much smaller in the group-1 series of elements compared to the group-11 ones.

The static dipole polarizabilities α were calculated most accurately at the DC CCSD(T) level for elements 112 through 118 [126, 134–136]. As a comparison of results of several calculations for Hg and element 112 shows (Table 11-2), relativistic effects significantly decrease α of both species, with the effect being much more

Table 11-2 Polarizabilities, α (in a.u.), of Hg and element 112 calculated within different approximations

Atom	Method	α				Ref.
		HF	MP2	CCSD	CCSD(T)	
Hg	NR	82.25	–	–	37.83	[86]
	PP					
	AR	44.78	28.33	35.26	34.42	[86]
	PP					
	ECP	32.46	27.13	28.82	28.48	[95]
	DC	44.90	27.47	35.31	34.15	[134]
	Exp.	–	–	–	33.91	[137]
112	NR	107.85	–	–	74.66	[86]
	PP					
	AR	29.19	23.57	25.84	25.82	[86]
	PP					
	ECP	30.30	27.67	28.61	28.68	[95]
	DC	29.46	25.11	27.66	27.64	[134]

pronounced for the heavier element (a relativistic decreased from 74.7 to 25.8 a.u., as was shown by the PP CCSD(T) calculations [86]). Correlation also decreases α in both cases much more at the nonrelativistic level.

According to the calculations, α of element 112 should be the smallest in group 12 due to the relativistic contraction of the outer 7s AO. Polarizabilities of elements 113 and 114 are also smaller than those of In and Tl, and Sn and Pb, respectively, which is due to the relativistic stabilization of the outer $7p_{1/2}$ AO (see below). A reversal of the trends in α is observed in group 13 and 14 beyond In and Sn, respectively, similarly to those in AR, or $R_{\max}(np_{1/2})$-AO. Correlation effects on α of group 13 and 14 elements are similar to those of group 12 elements. For elements 115 through 118, α are the largest in the respective chemical groups [136] due to the largest $R_{\max}(np_{3/2})$-AO [45]. The polarizability of element 118 is the largest among all the rare gases [126]. For element 119, α is also relativistically decreased from 693.9 to 184.8 a.u., as calculated at the DK CCSD(T) level. An improved basis set has given l65.98 a.u. for the latter [127].

11.7. GAS-PHASE CHEMISTRY

11.7.1. Rf Through Hs

11.7.1.1. Electronic Structures and Properties of Group 4 Through 8 Compounds

The 4*c*-DFT electronic structure calculations were performed for MF_4, MCl_4, MBr_4(M = Zr, Hf and Rf), MCl_5, MBr_5, $MOCl_3$ (M = Nb, Ta and Db), MCl_6, MO_3, $MOCl_4$, MO_2Cl_2 and $M(CO)_6$ (M = Mo, W and Sg), MO_3Cl (M = Tc, Re and Bh), and MO_4 (M = Ru, Os and Hs) (see [7,43] for reviews) and the RECP ones

for some group 4 through 6 halides and oxyhalides [83, 88]. Covalent compounds of the type MX (X = H, N, B and C) and some others were also considered in various studies (see [131, 132] for a summary). One of the aims of these works was clarifying role of relativistic and correlation effects.

The calculations have shown that the compounds of the heaviest elements are, indeed, homologs of the lighter elements in the chemical groups and that bonding is defined by the valence (n − 1)d AOs. An important finding was an increase in the stability of the maximum oxidation state in the chemical groups. A comparison of the relativistic with non-relativistic results for MCl_5 (M = Nb, Ta and Db) [138, 139], for example, has shown that this is a pure relativistic effect. Relativistic effects increase the energy gap ΔE between the bonding MO of the ligand character and antibonding MO of the (n − 1)d character due to the relativistic destabilization of the (n − 1)d AOs. This results in an increase in the energies of the electron charge-transitions which are associated with the reduction of the metal [139].

The calculations have also shown that relativistic effects are responsible for an increase in covalence of the group 4 through 8 compounds. Figure 11-13 shows relativistic and non-relativistic values of the effective metal charges, Q_M, and overlap populations (OP) obtained from a Mulliken analysis of the electronic density distribution in MCl_5 (M = V, Nb, Ta and Db), as an example [138]. One can see that the relativistic and non-relativistic values are opposite from Ta to Db.

A partial OP analysis shows that this behaviour is due to the opposite relativistic and orbital effects on the ns and $np_{1/2}$ AOs, while in the case of the (n − 1)d AO, relativistic effects enhances the orbital one (Figure 11-14).

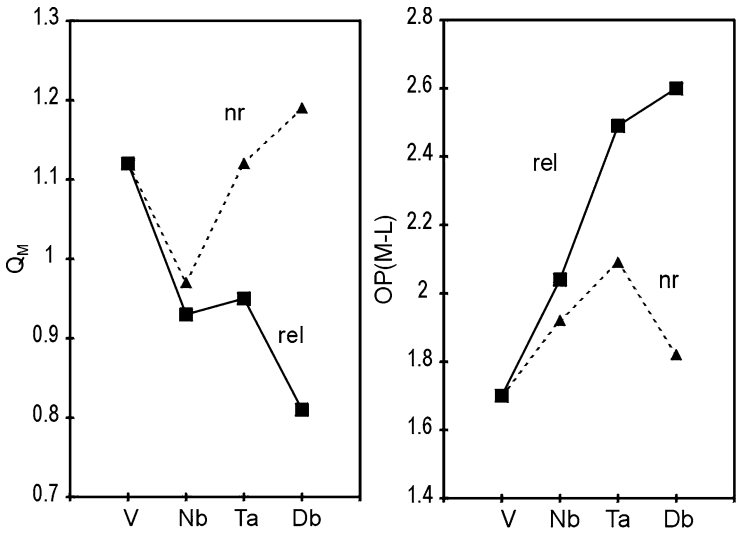

Figure 11-13. Relativistic (solid lines) and nonrelativistic (dashed lines) effective charges, Q_M, and overlap populations, OP, for MCl_5 (M = V, Nb, Ta and Db) [138]. L denotes the ligand (From [43])

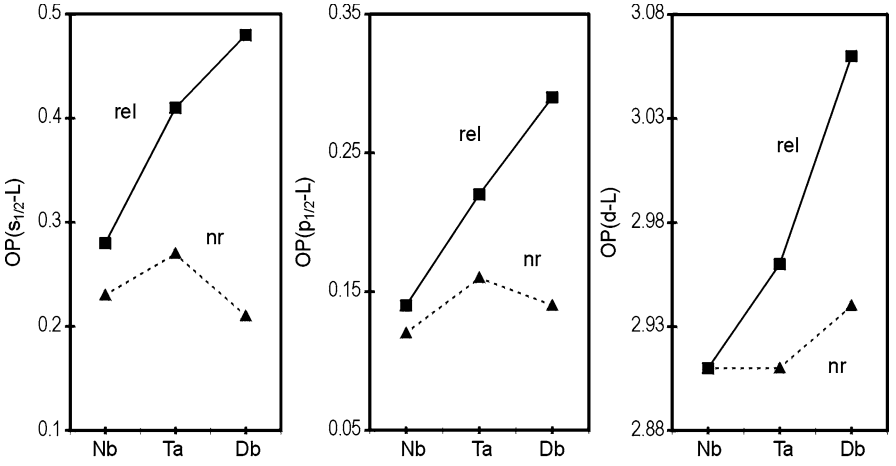

Figure 11-14. Relativistic (solid lines) and nonrelativistic (dashed lines) partial overlap populations in MCl_5 (M = Nb, Ta and Db). L denotes valence orbitals of the ligand. The data are from [138] (From [43])

Table 11-3 Atomization energies of WO_2Cl_2 and SgO_2Cl_2 calculated at various levels of approximation using the RECP method [88]. The additional SO effect is shown in the parentheses

Molecule	HF (AREP)	MP2	CCSD	CCSD(T)	Exp.[a]
WO_2Cl_2	11.7	24.4	20.9	22.1	23.5
SgO_2Cl_2	14.6 (−0.4)	24.8 (−1.3)	21.6 (−1.4)	22.5 (−1.6)	–

[a]Calculated via a Born-Haber cycle

The RECP CCSD(T) calculations for the group 6 oxyhalides [88] without and with SO coupling have shown that a slight decrease in D_e of the 6d compounds with respect to the 5d ones occurs due to the SO splitting of the 6d-AOs. A comparison of the average relativistic HF (AREP) and CCSD values has also demonstrated importance of electron correlation, accounting for about 65% in the D_e of SgO_2Cl_2 (Table 11-3).

Both the 4*c*-DFT [140] and RECP [88] calculations agreed on the most stable type of compound among the group 6 oxychlorides, MO_2Cl_2 (M = Mo, W and Sg). Gas-phase chromatography experiments were then conducted with these species [30]. The DS-DV calculations were performed for $M(CO)_6$ (M = Mo, W, Sg and U) [141]. $Sg(CO)_6$ was found to be very similar to $W(CO)_6$ and different from $U(CO)_6$.

Geometry optimization calculations for various group 4–8 halides, oxyhalides, oxides and other compounds [88, 131, 132, 142–146] have shown that R_e of the 4d and 5d compounds are almost equal as a result of the lanthanide contraction, while those of the 6d compounds are about 0.05–0.06 Å larger (Figures 11-11 and 11-15). The latter is due to the both orbital and relativistic effects on the (n-1)d AOs.

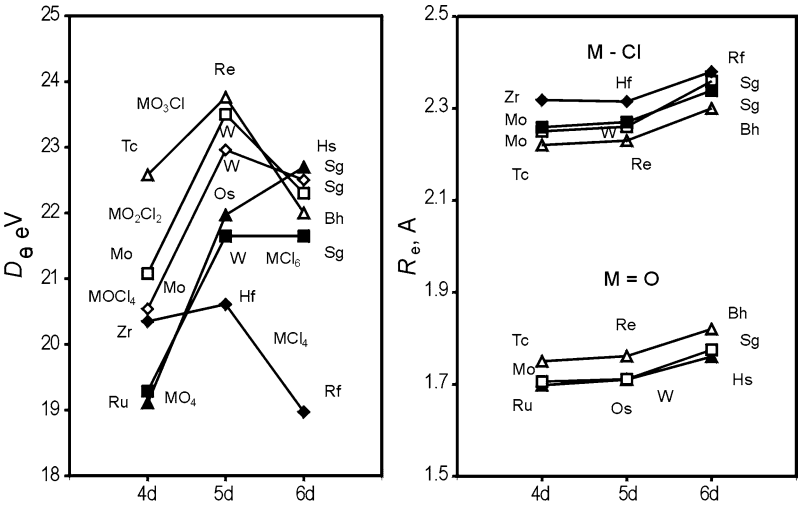

Figure 11-15. The 4*c*-DFT [142–146] and RECP [88] atomization energies, D_e, and optimized bond lengths, R_e, for various gas-phase compounds of group-4 through 8 elements (From [43])

11.7.1.2. Predictions of Experimental Behaviour

Prediction of ΔH_{ads} of a heavy-element molecule on a surface is presently still a formidable task for first principle calculations. A way was, therefore, suggested in [143–146] to obtain it with the use of physisorption models and accurately calculated molecular properties. The models are based on a principle of the molecule-slab interaction, where the interaction is subdivided into usual types for the long-range forces: dipole-dipole, dipole-induced dipole and van der Waals (dispersion) one. Thus, e.g., for a molecule with a dipole moment interacting with a (metal) surface charge Q, the interaction energy is [143]

$$E(x) = -\frac{2Qe\mu_{mol}{}^2}{x^2} - \frac{Q^2e^2\alpha_{mol}}{2x^4} - \frac{3}{2}\frac{\alpha_{mol}\alpha_{slab}}{\left(\frac{1}{IP_{mol}} + \frac{1}{IP_{slab}}\right)x^6}, \qquad (11\text{-}17)$$

where the electric dipole moment, μ_{mol}, IP_{mol} and α_{mol} belong to the molecule, while those with the index "slab" to the surface atom, and x is the molecule-surface separation distance. The latter is well approximated by the van der Waals radius, R_{vdW}.

For a molecule without dipole moment interacting with a dielectric surface, the energy is [144]

$$E(x) = -\frac{3}{16}\left(\frac{\varepsilon - 1}{\varepsilon + 2}\right)\frac{\alpha_{mol}}{\left(\frac{1}{IP_{slab}} + \frac{1}{IP_{mol}}\right)x^3}, \qquad (11\text{-}18)$$

where ε is the dielectric constant of the adsorbent material. All the molecular properties except of x can be accurately calculated using relativistic codes. The x can be deduced from the measured ΔH_{ads} for the lighter compounds using equations of the types (11-17) and (11-18) and the calculated molecular properties. The unknown x values for the heaviest element compounds are then evaluated with respect to the x for the lighter homologs using molecular R_{vdW}. The latter is obtained from the calculated R_e values and radii of the ligand spheres. As an example, the 4*c*-DFT calculated energy contributions to ΔH_{ads} for the group 7 MO_3Cl (M = Tc, Re and Bh) [143] are given in Table 11-4.

On their basis, $-\Delta H_{ads}$ of 78.5 kJ/mol and of 48.2 kJ/mol were calculated for BhO_3Cl and TcO_3Cl, respectively, relative to the measured 61 kJ/mol for ReO_3Cl. This gives a trend in volatility as $TcO_3Cl > ReO_3Cl > BhO_3Cl$. The calculations have shown that this trend is defined by the trend in the dipole moments of these molecules.

Experimental investigations of volatility of the group 7 oxychlorides performed using the isothermal gas-phase chromatography [31] has, indeed, confirmed the theoretically predicted trend (Figure 11-16). Also, the deduced by a Monte Carlo simulation $-\Delta H_{ads}$ of 75 and 51 kJ/mol for BhO_3Cl and TcO_3Cl, respectively, are in perfect agreement with the theoretical values.

Table 11-4 Contributions to the interaction energy, $E(x)$, between the MO_3Cl molecules (M = Tc, Re, and Bh) and Cl^Q (surface) for $Q = -0.4$ (From [143])

	μ-*Q*e	α-*Q*e	α-α(Cl)
Molecule	$E10^{16}x^2$, eV cm^2	$E10^{32}x^4$, eV cm^3	$E10^{48}x^6$, eV cm^6
TcO_3Cl	2.23	5.69	379.1
ReO_3Cl	3.10	6.81	460.6
BhO_3Cl	4.67	8.64	591.2

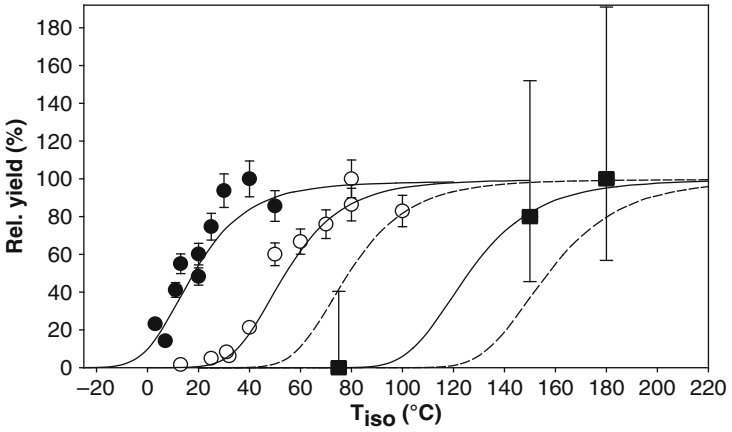

Figure 11-16. The relative yields of TcO_3Cl (filled black circles), ReO_3Cl (open circles) and BhO_3Cl (filled black squares) as a function of the isothermal temperatures, T_{iso} (From [31])

Prediction of the energy of weak interactions of the very similar MO_4 (M = Ru, Os, and Hs) species with an inert surface required, however, a much higher level of accuracy of the calculated properties than in the case of relatively strong dipole-dipole interactions of MO_3Cl (M = Tc, Re and Bh). Thus, the 4*c*-DFT calculations with extremely extended basis sets (e.g., a minimal set plus the 7p7d6f8s8p5g one for Hs) had to be performed to achieve the required accuracy [146] (see Table 11-5 for the calculated and experimental values).

The obtained IP and α for MO_4 (M = Ru, Os and Hs), in perfect agreement with experimental data for the Ru and Os oxides, show a reversal of the trend in group 8, while R_e increases steadily in the group (Figure 11-17).

Table 11-5 Ionization potentials, *I* (in eV), polarizabilities, α (in a.u.), bond lengths, R_e (in Å), vibrational frequencies, *ν*, of the M-O bond (in cm^{-1}), molecule-surface separation distances, *x* (in Å), and adsorption enthalpies, $-\Delta H_{ads}$ (in kJ/mol) on quartz for MO_4 (M = Ru, Os, and Hs)

Property	Method	RuO_4	OsO_4	HsO_4	Ref.
I	Calc.	12.21	12.35	12.29	[146]
	Exp.	12.19	12.35	–	[147]
α	Calc.	58.07	55.28	65.99	[146]
	Exp.	58.64	55.13	–	[137]
R_e	Calc.	1.712	1.719	1.779	[146]
	Exp.	1.706	1.711	–	[148]
ν	Calc.	851	900	989	[146]
	Exp.	880	965	–	[148]
x	Calc.	2.23	2.23	2.25	[146]
$-\Delta H_{ads}$	Calc.	41.0 ± 1	39.0 ± 1	45.4 ± 1	[146]
	Exp.	–	39 ± 1	46 ± 2	[26]

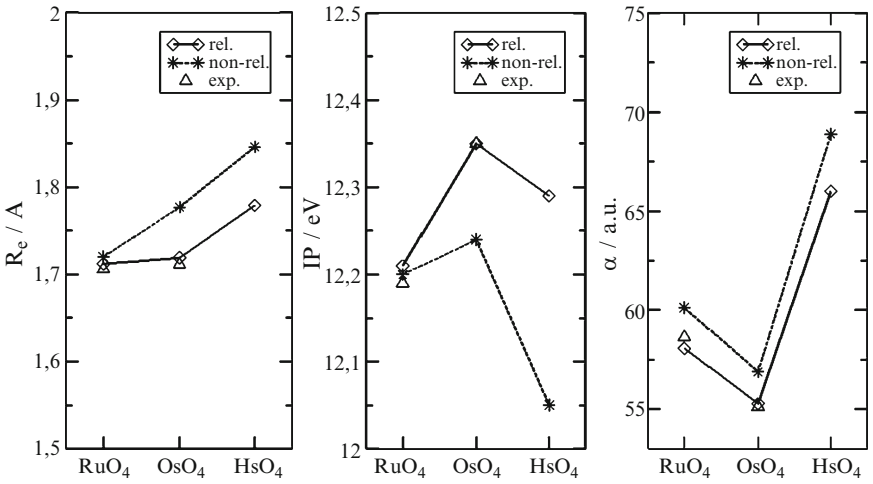

Figure 11-17. Relativistic (rel.) and nonrelativistic (non-rel.) bond lengths, R_e, ionization potentials, IP, and polarizabilities, α, in MO_4 (M = Ru, Os, and Hs) (From [146])

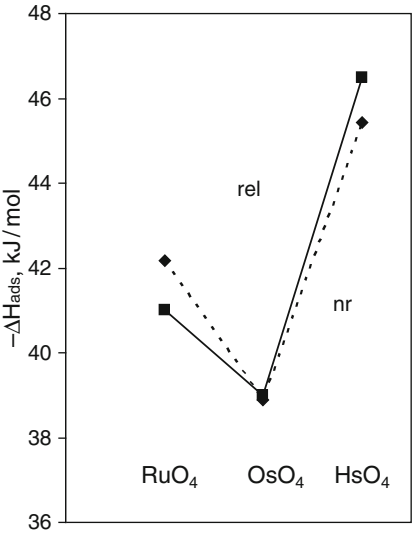

Figure 11-18. Relativistic (solid line) and nonrelativistic (dashed line) adsorption enthalpies of MO_4 (M = Ru, Os, and Hs) on quartz [146]

The trends in these properties proved to be in agreement with the trends in the energies and R_{max} of the (n − 1)d AO in group 8, respectively.

Using the calculated molecular properties and the physisorption model (Eq. 11-18), ΔH_{ads} on quartz (silicon nitride) were calculated for RuO_4 and HsO_4 with respect to OsO_4 (see Table 11-5 and Figure 11-18). They have indicated the same reversal of the trend in group 8 as that in α (Figure 11-17).

Thermochromatography experiments on volatility of OsO_4 and HsO_4 revealed that HsO_4 is, indeed, about 6 kJ/mol stronger adsorbed on the silicon nitride surface of detectors than OsO_4 [26]. (RuO_4 was not experimentally studied due to its decomposition). Also, the measured ΔH_{ads} of HsO_4 is very close to the calculated one (Table 11-5). The experimentally observed adsorption positions of the tetroxides is shown in Figure 11-19.

Thus, both theoretical and experimental studies have established a reversal of the trend in volatility of the group 8 tetroxides in line with the trend in the polarizabilities of these molecules. This remarkable case demonstrates importance of both accurate calculations and statistically meaningful experiments. It also shows that straightforward extrapolations of properties in the chemical groups can be unreliable.

In the same work [146], influence of relativistic effects on spectroscopic properties and volatility of the MO_4 species was studied with the help of additional non-relativistic calculations (Figure 11-17). The non-relativistic values revealed the same trends in group 8 as relativistic, since the orbital and relativistic effects on the (n-1)d-AO act in the same direction. Relativistic effects on ΔH_{ads} were shown to

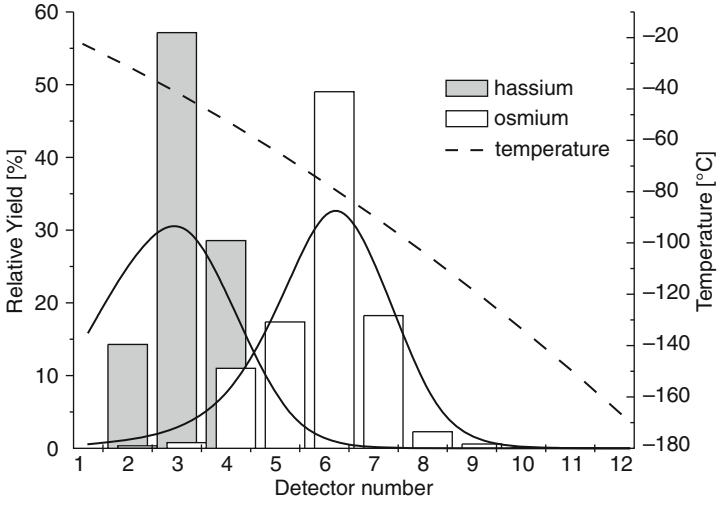

Figure 11-19. Observed adsorption behaviour of OsO_4 and HsO_4 in the gas-phase thermochromatography experiments [26]

be negligible (Figure 11-18). There were some other attempts to interpret volatility of HsO_4 [80,149]. These works reveal, however, some deficiency of the calculations, as discussed in [145].

11.7.2. Rg

In group 11, relativistic stabilization of the ns AO results in the change of the ground state electronic configuration from $d^{10}s^1$ for Cu, Ag and Au to d^9s^2 for Rg [119], which should influence dissociation energies of compounds of these elements. The maximum of relativistic effects on the 7s-shell of Rg in group 11 is also a reason to observe anomalous properties of its low coordination compounds. The large relativistic destabilization and expansion of the 6d AOs is expected to enhance the stability of higher coordination compounds of this element.

A number of molecular relativistic calculations were performed for simple compounds of Rg at various levels of theory. The electronic structure of the simplest molecule RgH, used as a test system for benchmark calculations as AuH, was studied in detail with the use of various methods, DF, DK, PP, and DFT (see Table 11-6). A comparison of the relativistic (ARPP) with the nonrelativistic (NRPP) calculations shows that scalar relativistic effects double D_e, though the SO splitting for the Rg atom ($7s^26d^9$) diminishes it by 0.7 eV (the ARPP CCSD – SOPP CCSD difference) [75]. Thus, the trend to an increase in D_e from AgH to AuH turned out to be inversed from AuH to RgH (Figure 11-20).

The PP CCSD calculations [75] have also shown that the bond in RgH is substantially shortened by relativity ($\Delta R_e = -0.4$ Å) and it is the shortest in the series AgH, AuH and RgH, so that the trend to a decrease in R_e is continued with RgH.

Table 11-6 Bond lengths (in Å) in AuH and RgH

Molecule	R_e	Method	Ref.
AuH	1.5236	Experiment	[150]
RgH	1.499	SO PP CCSD(T)	[75]
	1.523	DHF CCST(T)	[75]
	1.503	SO PP-CCSD(T)	[75]
	1.529	PP CCSD(T)	[151]
	1.506	SC-PP CCSD(T)[a]	[152]
	1.543	ADF ZORA	[131]
	1.546	BDF	[110]
	1.520	4*c*-DFT	[153]

[a]Shape-consistent (SC)

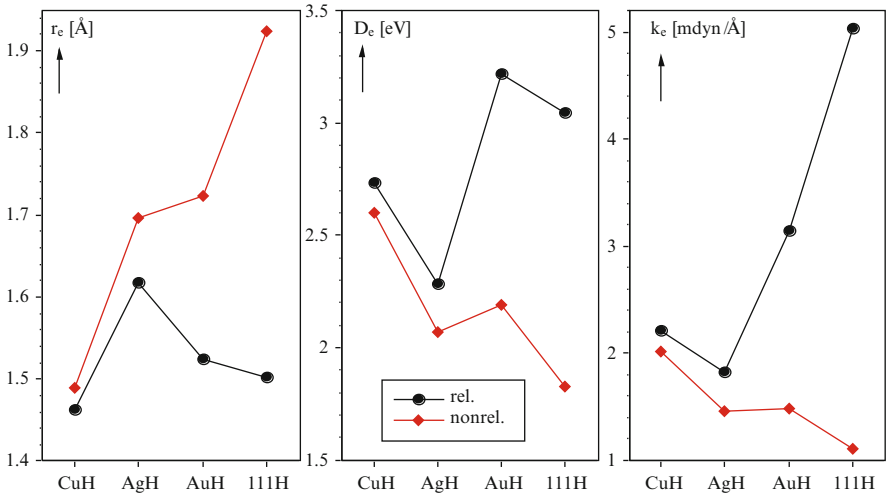

Figure 11-20. Nonrelativistic and relativistic bond lengths, r_e (see also Table 11-6 for various values for RgH), dissociation energies, D_e, and force constants, k_e, of the group-11 hydrides (From [75])

The BDF calculations [110] have, however, revealed that R_e(RgH) is slightly larger than R_e(AuH). The different trends in R_e obtained in these two types of the calculations are obviously connected to a different contribution of the contracted 7s and expanded 6d AOs to bonding (though the 6d contribution was found to be predominant in both cases). Results of various calculations for R_e(RgH) are summarized in Table 11-6 (see also [75, 131]). They indicate that R_e(RgH) should be similar to R_e(AuH).

Both the PP and DFT calculations established that the trend to an increase in k_e is continued with RgH having the largest value of all known diatomic molecules (Figure 11-20).

The μ_e was shown to decrease relativistically from AgH to AuH and to RgH, indicating that RgH is more covalent and element Rg(I) is more electronegative than Au(I). Large SO effects were found on R_e (SO increased) and k_e (SO decreased) [110].

Results of the 4*c*-BDF [110] and 4*c*-DFT calculations [153] for other dimers, AuX and RgX (X = F, Cl, Br, O, Au, Rg), indicate that relativistic effects follow a similar pattern to that for RgH except for RgF and RgO, where the SO splitting increases D_e. The PP calculations for RgH, RgLi and RgF [75] have, however, shown that the SO effects on R_e are very small, but they are large for D_e, decreasing it in all the cases, in difference to the BDF calculations for RgF [110]. The scalar relativistic effects increase D_e(RgLi), but decrease D_e(RgF). They decrease R_e by about 0.4 Å in all the cases. The singlet state was found to be the ground for Rg_2 in comparison to the triplet [153]. The dissociation energy was found to change in the following order: $Au_2 > RgAu > Rg_2$.

To study the stability of higher oxidation states, energies of the $MF_6^- \rightarrow MF_4^- + F_2$ and $MF_4^- \rightarrow MF_2^- + F_2$ (M = Cu, Ag, Au and Rg) decomposition reactions were calculated at the PP MP2 and CCSD levels of the theory [84, 87]. Relativistic effects were shown to stabilize higher oxidation states in the high-coordination compounds of Rg due to a destabilization of the 6d AOs and their larger involvement in bonding. RgF_6^- was shown to be the most stable in this group. SO coupling stabilizes the molecules in the following order: $RgF_6^- > RgF_4^- > RgF_2^-$. This order is consistent with the relative involvement of the 6d electrons in bonding for each type of molecule.

11.7.3. Element 112

It is known that with increasing relativistic stabilization and contraction of the ns AO in group 12, elements become more inert. Thus, bulk Hg is known to be a liquid, however, very different from the condensed noble gases. In the case of element 112, relativistic effects are expected to be further amplified.

Earlier, Pitzer [154] suggested that the very high excitation energy $6d^{10}7s^2 \rightarrow 6d^{10}7s7p_{1/2}$ of about 8.6 eV of element 112 into the configuration of the metallic state will not be compensated by the energy gain of the metal-metal bond formation. An extrapolation of ΔH_{sub} of metals in group 12 has given 22.2 kJ/mol for element 112, which is the lowest in group 12 [155]. The questions to the electronic structure theory, therefore, were: Is element 112 metallic in the solid state, or is it more like a solid noble gas? How volatile and reactive is the element 112 atom in comparison with Hg and Rn?

11.7.3.1. Relativistic Effects on Atomic Properties

Atomic properties of Hg and element 112 were calculated at various levels of theory: 4*c*-BDF with the Perdew-Burke-Ernzerhof (PBE) functionals, and the PB self-interaction correction (PBESIC) [156], QR-PP CCSD(T), ARPP CCSD(T) [86], ECP CCSD(T) [95] and DC(B) CCSD(T) [120,134]. The results are summarized in Tables 11-7 and 11-8.

Table 11-7 Polarizabilities, α (in a.u.), and ionization potentials, IP (in eV), of Hg and element 112

	Hg		112		
Method	α	IP	α	IP	Ref.
4*c*-BDF PBE	35.1	10.61	29.0	11.78	[156]
4*c*-BDF PBESIC	36.4	10.40	29.8	11.40	[156]
QR-PP CCSD(T)	34.2	10.37	28.0	13.17	[156]
AR-PP CCSD(T)	34.42	–	25.82	–	[86]
ECP CCSD(T)	28.48	10.39	28.68	11.675	[95]
DC CCSD(T)	34.15	–	27.64	–	[134]
DCB CCSD	–	10.445	–	11.97	[120]
Exp.	33.919	10.4375	–	–	[137]

Table 11-8 Spectroscopic properties: bond lengths, R_e (in Å), and dissociation energies, D_e (in eV), of Hg_2 and $(112)_2$

	Hg_2		$(112)_2$		
Method	R_e	D_e	R_e	D_e	Ref.
4*c*-BDF PBE	3.439	0.053	3.089	0.156	[156]
4*c*-BDF PBESIC	3.904	0.025	3.363	0.075	[156]
QR-PP CCSD(T)	3.769	0.044	3.386	0.097	[156]
4*c*-DFT(B88/P86)	3.63	0.01	3.45	0.05	[153]
Exp.	3.63	0.043	–	–	[158, 159]

AR was obtained as a half of $R_e[(112)_2]$ (see below) [46, 153]. $R_{vdW}(112) = 3.76 \pm 0.03$ a.u. was estimated with respect to $R_{vdW}(Hg) = 3.95 \pm 0.02$ a.u. [157] using a ratio of their R_{max}(ns)-AOs [45].

Additional non-relativistic calculations [46, 84, 86] have shown that relativistic IP(112) is 4 eV larger than the non-relativistic one, because relativistically, the first ionized electron is $6d_{5/2}$, while nonrelativistically, it is the destabilized 7s one. The α is 45 a.u. decreased due to the relativistic contraction of the 7s AOs. Thus, IP(112) is the largest in group 12, while α is the smallest [46] reflecting the AO energies and R_{max}, respectively (Figure 11-6). Due to the same reason, AR(112) is 0.5 a.u. relativistically contracted and it is the smallest in group 12. The CR show the same trend in the group [131, 132]. The non-relativistic values have opposite trends beyond Cd (Figure 11-21).

11.7.3.2. Volatility as Sublimation: Van der Waals Systems

Homonuclear dimers. The first step to treat the sublimation process of the element 112 "macroamount" is to find out how strong element 112 is bound to itself. Accordingly, calculations of the spectroscopic properties of Hg_2 and $(112)_2$ were performed with the use of various methods: 4*c*-BDF PBE, ECP CCSD(T), QP-PP CCSD(T) [156] and 4*c*-DFT [46, 153]. The results are summarized in Table 11-8.

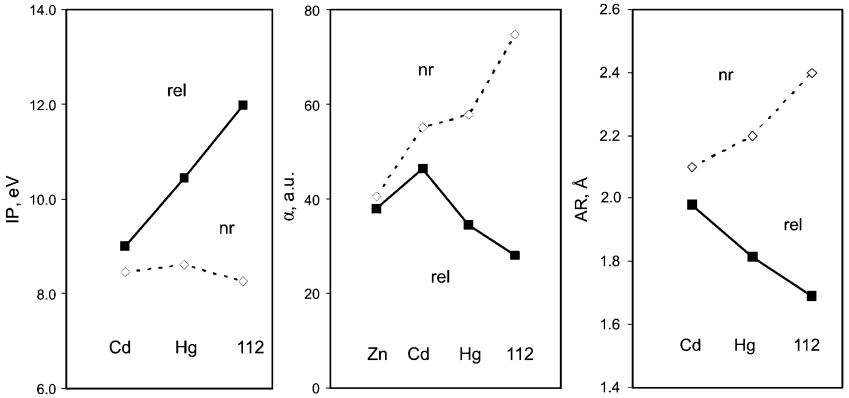

Figure 11-21. Relativistic (solid lines) and non-relativistic (dashed lines) ionization potentials, IP, atomic radii, AR, and polarizabilities, α, of group 12 element [46]

The 4*c*-DFT calculations for $(112)_2$ [153] have shown that the 6d(112)-AOs are active and mixing up with the 7s-AOs in the highest occupied MOs. The 4*c*-DFT $R_e(Hg_2)$ perfectly agrees with the experimental value [158], though $R_e[(112)_2]$ is larger than that of the PP calculations [156]. $D_e(Hg_2)$ is better reproduced by the PP calculations [156], as is expected for the preferentially van der Waals type of bonding. Both the DFT and PP calculations agree on an increase in D_e of about 0.04 eV from the Hg to element 112 dimer with shortening of the bond, in line with the smaller R_{max}[7s(112)] AO with respect to R_{max}[6s(Hg)] AO (Figures 11-22 and 11-6). Thus, due to the relativistic 7s AO contraction $(112)_2$ should be more bound than Hg_2. The PP calculations for Hg_2 [160] have shown that bonding in this molecule is not of pure van der Waals type, and a partial overlap occurs. The same was found for $(112)_2$ [153]. Thus, a half of the $R_e(M)_2$ (M = Hg and element 112) gives, therefore, rather AR than R_{vdW}.

Solid state. The LDA DFT (non-relativistic, scalar relativistic, SR, and 4*c*-relativistic) band structure calculations were performed on the element 112 solid state [161]. It was found that element 112 prefers the *hcp* structure (as that of Zn and Cd) in difference to Hg (*fcc*). Thus, it should differ from its lighter homolog Hg on a structural level and resemble the solid state noble gases. A cohesive energy of 1.13 eV was obtained for element 112 at the SR-level of theory, which is larger than that of Hg (0.64 eV) and is an order of magnitude larger than those of the solid noble gases. This result is consistent with the larger $D_e[(112)_2]$ with respect to $D_e(Hg_2)$ (see Table 11-8). It was concluded that element 112 is not a metal, but rather a semiconductor with a band gap of at least 0.2 eV. (The results of the LDA calculations were considered as a lower bound.) In this sense, element 112 resembles the group 12 metals more closely than it does the noble gases.

Adsorption on inert surfaces. Knowledge of ΔH_{ads} of element 112 on inert surfaces such as quartz and ice was desired for designing gas-phase chromatography

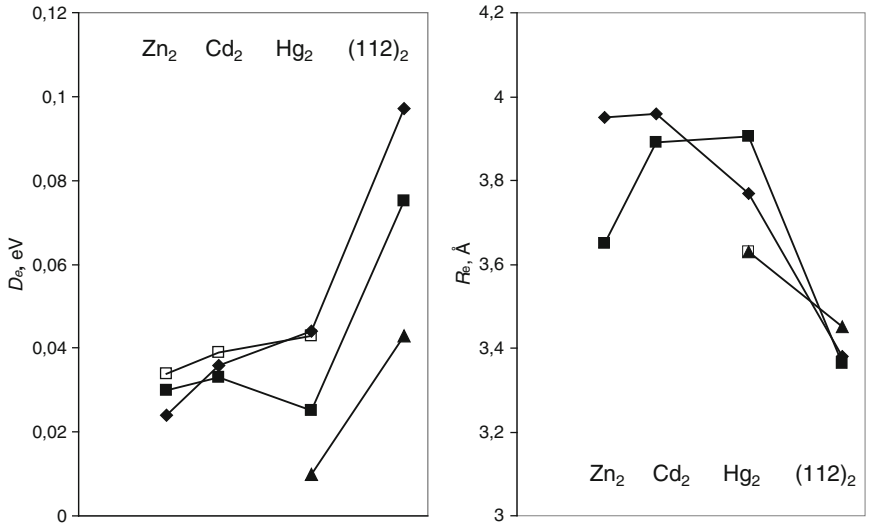

Figure 11-22. The QR PP CCSD(T) (filled rhomboids), 4*c*-BDF PBESIC (filled squares) [156], 4*c*-DFT (filled triangles) [153] and experimental (open squares) dissociation energies, D_e, and bond lengths, R_e, respectively, in the group 12 dimers (see Table 11-8)

experiments. With this aim in view, ΔH_{ads} of Hg and element 112, as well as Rn for comparison purposes, on quartz and ice were calculated using the adsorption model (Eq. (11-18)) and calculated atomic properties [46, 134] (Table 11-7). Since bonding of Hg and element 112 with inert surfaces was assumed to be similar to that in M_2(M = Hg and element 112), x was taken as half of the bond length in M_2, and not as R_{vdW}. The obtained $-\Delta H_{ads} = 40.5$ kJ/mol for Hg on quartz and 25.20 kJ/mol on ice are in very good agreement with the experimental values of 42 ± 2 and 25.5 ± 2 kJ/mol, respectively [162]. For element 112, $-\Delta H_{ads} = 43.2 \pm 0.2$ kJ/mol (for AR) on quartz and $-\Delta H_{ads} = 26.3 \pm 0.1$ kJ/mol on ice were predicted. Thus, element 112 was expected to be somewhat stronger adsorbed on inert surfaces than Hg, i.e., it was expected to be deposited on ice in the thermochromatography column at slightly higher temperatures than Hg.

By using relativistic (vs.) non-relativistic values of the atomic properties (Figure 11-21), influence of relativistic effects on ΔH_{ads} and its trend in group 12 was elucidated [46]. Since α is proportional to 1/IP, the different trends in the relativistic (vs.) nonrelativistic values in the group (Figure 11-21) cancel in the product αIP, so that the trends in the relativistic (vs.) non-relativistic $E(x)$ are finally determined by trends in the relativistic (vs.) non-relativistic x, or AR values. Consequently, the relativistic contraction of the AR (due to the contraction of the 7s(112) AO) results in an increase in $-\Delta H_{ads}$ from Hg to element 112, while non-relativistically, it is the other way around.

An important conclusion for the chemistry is that element 112 is stronger bound by van der Waals forces than Hg both in the homonuclear dimer, solid state and adsorbed state on an inert surface, and this is a relativistic effect caused by the contraction of the 7s AO (see Figure 11-26 below).

11.7.3.3. Volatility as Measured in the Gas-Phase Experiments: Interaction with Metals

In the gas-phase thermochromatography experiments, volatility of element 112, as well as of Hg and Rn, for comparison purposes, was studied as adsorption on gold plated silicon detectors of the chromatography column [27]. Prediction of ΔH_{ads} of these elements on a gold surface was, therefore, desirable.

Heteronuclear dimers. As a first step to study adsorption of Hg and element 112 on noble metal surfaces, electronic structure calculations were performed for HgM and 112M, where M = Ag, Au, Pt, Pd and Cu using the 4*c*-DFT [163]. It was demonstrated that element 112 forms chemical bond with Au primarily due to the interaction between the double occupied 7s(112) AO and the single occupied 6s(Au) AO (see Figure 11-23).

The ground state of 112Au is $^2\Sigma^+$ $d_{Au}{}^{10}\sigma_{Au}{}^2\sigma^*{}_{112}{}^1$. A Mulliken analysis indicates that the σ^* HOMO is a mixture of the 7s(112) and 6s(Au) AOs. Below are two non-bonding π MOs of the $5d_{5/2}$(Au) AOs. The composition of the bonding σ MO lying at −6.76 eV is (in %): (1.2)7s(112) + (4)$6d_{5/2}$(112) + (87)$5d_{5/2}$(Au) + (4)6s(Au). Thus, one can see that the 6d(112)AOs are also active in 112Au. A comparison of D_e(112M) with D_e(HgM) shows that element 112 is about 0.1–0.2 eV weaker bound with a transition metal atom M, depending on the metal, than Hg and the bonds are longer.

Relativistic effects influence on the properties of HgAu and 112Au was investigated via additional nonrelativistic calculations [46]. The results are presented in Table 11-9. Relativistic effects were shown to increase D_e in HgAu by 0.13 eV,

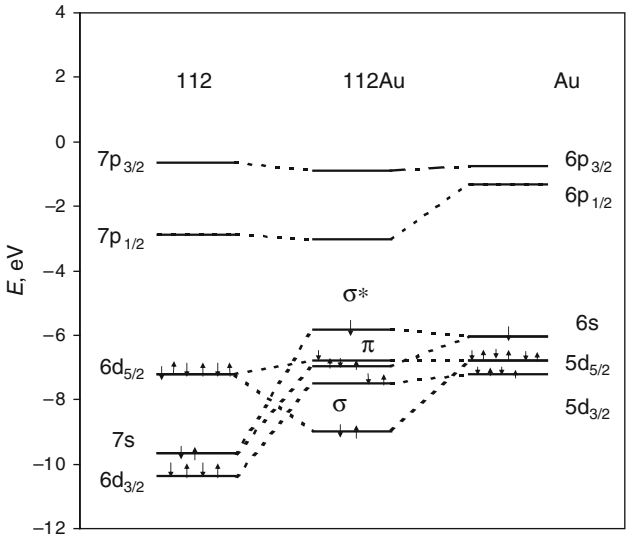

Figure 11-23. Bond formation (principal MOs) of the 112Au molecule

Table 11-9 Nonrelativistic and relativistic spectroscopic properties of AuHg and 112Au: dissociation energies, D_e (in eV), bond lengths, R_e (in a.u.), vibrational frequencies, w_e (in cm^{-1}), effective charges, Q_M, and overlap populations, OP [46]

Molecule	Case	R_e	D_e	w_e	Q_M	OP
HgAu	Nr	5.44	0.36	75.89	0.05	0.44
	Rel	5.04	0.49	102.96	0.10	0.34
112Au	Nr	5.65	0.47	77.19	0.08	0.48
	Rel	5.15	0.36	81.74	0.01	0.24

but decrease it by about the same value (0.12 eV) in 112Au. This makes trends in the nonrelativistic (vs.) relativistic D_e values opposite from HgAu to 112Au, so that $D_e{}^{nr}(112Au) > D_e{}^{nr}(HgAu)$, while $D_e{}^{rel}(112Au) < D_e{}^{rel}(HgAu)$. R_e is decreased by relativistic effects in both systems. The trends are, however, the same both for the non-relativistic and relativistic R_e. Relativistic effects increase vibrational frequencies w_e in each compound, but to a much lesser extent in 112Au than in HgAu, which makes trends in the relativistic and non-relativistic values opposite from HgAu to 112Au. Trends in the relativistic and non-relativistic values of Q_M and OP are also different from HgAu to 112Au: $Q_{Hg}{}^{rel}(HgAu) > Q_{112}{}^{rel}(112Au)$ and $OP^{rel}(HgAu) > OP^{rel}(112Au)$, while $Q_{Hg}{}^{nr}(HgAu) < Q_{112}{}^{nr}(112Au)$ and $OP^{nr}(HgAu) < OP^{nr}(112Au)$.

A partial OP analysis shows that such a decrease in both the ionic and covalent contributions of element 112 to bonding is a result of a decreasing involvement of the relativistically stabilized 7s AO.

Interaction with gold clusters. To proceed further to the description of the adsorption of Hg and element 112 on a gold surface, calculations for metal atom — gold cluster systems were performed using the 4*c*-DFT method [46, 164, 165, 168]. Since the structure of the gold layers covering the silicon detectors is not known, two types of the ideal surface were considered: Au(100) and Au(111). Accordingly, clusters of various size, from very small ones of nine and 14 atoms to very large once of more than 100 atoms (in order to reach the convergence for binding energies with the cluster size), were constructed to simulate these types of surfaces.

For the Au(100) surface, results of the calculations for the M-Au_n and embedded M-Au_nAu_m (M = Hg and element 112, $n_{max} = 36$ and m = 156) systems [165] have shown that element 112 is 0.1–0.3 eV weaker bound with gold than Hg depending on the adsorption position, and that the bridge position should be preferential (Table 11-10). Potential energy curves are shown in Figure 11-24. Using the difference between the calculated $E_b = 1.52$ eV and experimental $-\Delta H_{ads} = 1.03$ eV for Hg on gold [166], $-\Delta H_{ads}(112) = 0.65$ eV of element 112 was given as an early prediction (Table 11-10).

The absolute value of E_b(Hg) in the bridge position on the Au_nAu_m cluster obtained in this way is, however, about 0.5 eV larger than the experimentally observed $-\Delta H_{ads}$(Hg) on gold evidencing that the Au(100) surface is obviously not the one used in the experiments. The LDA DFT calculations [167] demonstrated that

Table 11-10 Calculated binding energies, E_b (in eV), for the M-Au_n and M-Au_nAu_m systems (m = 156), where M = Hg and element 112 [165]

M	E_b(M-Au_n)			E_b(M-Au_nAu_{156})			$-\Delta H_{ads}$
	Top n = 14	Bridge n = 14	Hollow n = 9	Top n = 34	Bridge n = 36	Hollow n = 29	Exp.
Hg	0.86	1.00	0.85	1.02	1.52	0.84	1.03[a]
112	0.71	0.82	0.79	0.65	1.14(0.65)[b]	0.74	0.54[c]

[a]Ref. [166]
[b]Predicted value of $-\Delta H_{ads}$
[c]Ref. [27]

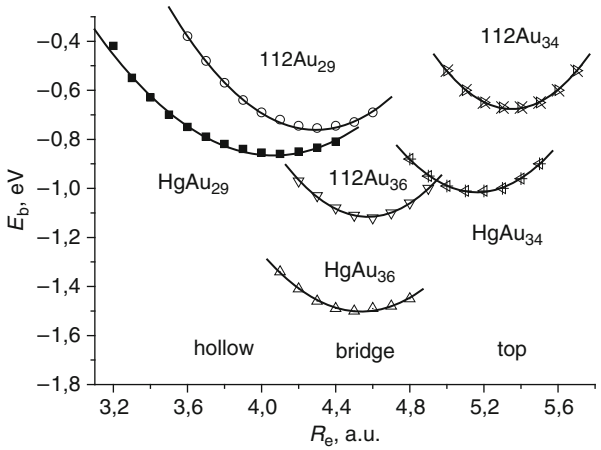

Figure 11-24. The 4*c*-DFT calculated potential energy curves for M-Au_nAu_{156} clusters (M = Hg and element 112) in the three adsorption positions: top, hollow and bridge [165]

Au(111) surface should be about 0.4 eV more stabilized than the Au(100) one. Consequently, $-\Delta H_{ads}$(M) on the Au(111) surface should be about this value smaller, which fits better to the experimental $-\Delta H_{ads}$(Hg) [166].

The 4*c*-DFT calculations for Hg and element 112 interacting with large gold clusters (n = 95 for the top, n = 94 for the bridge, n = 120 for the hollow1 and n = 107 for the hollow2 positions) simulating the Au(111) surface have also been completed [168]. Results show the same relation between E_b of Hg and element 112 as for the Au(100) surface: element 112 is about 0.1–0.2 eV weaker bound to gold than Hg. Overall, E_b with the clusters simulating the Au(111) surface are smaller than those with clusters simulating the Au(100) surface. $E_b(112) = 0.46$ eV.

In the first thermochromatography experiment with element 112 [27], two decay chains attributed to the 112 isotope were observed in two separate experiments with difference temperature gradients. (Earlier, experiments using a slightly different technique were performed, showing that element 112 is very volatile [169].) Later, four more events were observed attributed to element 112 [170]. From the observed

T_{ads}, $-\Delta H_{ads} = 52^{+4}_{-3}$ kJ/mol was deduced using a Monte Carlo simulation. Rn was deposited at the last detectors in the column giving $-\Delta H_{ads} = 20$ kJ/mol. Thus, the experiments demonstrated that element 112 does not behave like Rn. It obviously forms chemical bonding with gold similarly, though weaker than, to Hg. (The deposition of Hg took place right on the first detectors in the column, at the highest temperatures.) This finding was in agreement with the theoretical predictions [163–165, 168] indicating that element 112 is not a rare gas-like, but a 6d-metal-like. Also, the observed and calculated [168] ΔH_{ads} are very close to each other.

In [46], influence of relativistic effects on the adsorption process of Hg and element 112 on metal surfaces was investigated on the example of small metal-gold cluster systems. Two extreme cases were considered: the ad-atom in the top position and in the hollow one: In the first case, the ns and $np_{1/2}$ AOs of the adsorbed atom should be active, while in the second case, the (n-1)d ones. Accordingly, additional non-relativistic calculations were performed for the M-Au_{14} and M-Au_9 systems (Figure 11-25). Results are presented in Table 11-11. They indicate that upon adsorption in the top position, relativistic effects increase E_b by 0.22 eV in $HgAu_{14}$, while they do not increase E_b in $112Au_{14}$ due to the relativistic stabilization of the 7s(112) AO. This is similar to the case of the dimers HgAu and 112Au (Table 11-9). Relations between $E_b(HgAu_{14})$ and $E_b(112Au_{14})$

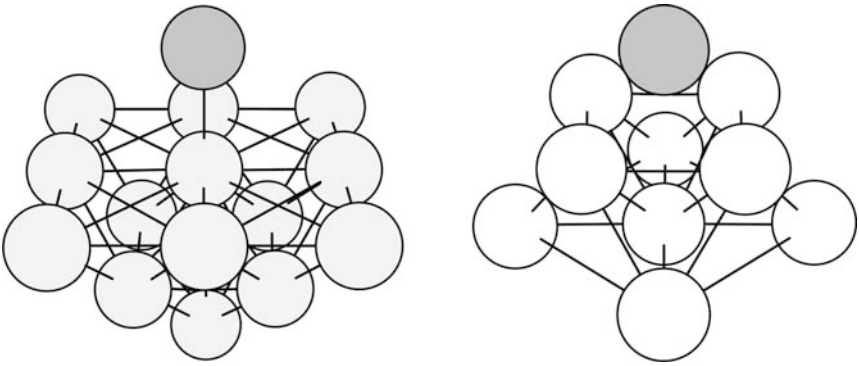

Figure 11-25. The M-Au_{14} and M-Au_9 systems simulating adsorption of M in the top and hollow positions on the Au(100) surface, respectively

Table 11-11 Relativistic and non-relativistic binding energies, E_b (in eV), and the M-Au_n separation distance, R_e (in a.u.), in the M-Au_{14} and M-Au_9 systems [46]

System	Case	M-Au_{14}(top)		M-Au_9 (hollow)	
		R_e	D_e	R_e	D_e
$HgAu_n$	Nr	5.5	0.64	4.6	0.41
	Rel	5.0	0.86	3.8	0.85
$112Au_n$	Nr	5.8	0.70	4.9	0.52
	Rel	5.2	0.71	4.2	0.79

for non-relativistic and relativistic cases are also similar to those for the dimers: $E_b^{rel}(HgAu_{14}) > E_b^{rel}(112Au_{14})$, while $E_b^{nr}(HgAu_{14}) < E_b^{nr}(112Au_{14})$.

For adsorption in the hollow position, even though the trends in E_b are the same as for the top position, e.g. $E_b^{rel}(HgAu_9) > E_b^{rel}(112Au_9)$ and $E_b^{nr}(HgAu_9) < E_b^{nr}(112Au_9)$, relativistic effects increase E_b in both $HgAu_9$ and $112Au_9$. This makes the difference in E_b between $HgAu_9$ and $112Au_9$ (0.06 eV) smaller than for the top position case (0.15 eV). Such a relative small decrease in bonding from Hg to element 112 is connected with the larger involvement of the relativistically destabilized 6d(112) AOs in the hollow position. Relativistic effects were shown to decrease the distance of the ad-atom to the surface, R_e, in all the systems.

To conclude, the relativistic calculations for various M–Au_n (M = Hg and element 112) systems demonstrated that bonding of element 112 with gold is about 20–40 kJ/mol weaker than that of Hg. This is a relativistic effect caused by the contraction and stabilization of the 7s AOs, which is less accessible for bonding than the 6s(Hg) AO. This case is different to the case where element 112 is bound by van der Waals forces, e.g., in the homonuclear dimer, solid state and adsorbed state on an inert surface. There, element 112 is stronger bound than Hg due to the relativistically contracted AR.

Plots summarising all the cases are shown in Figure 11-26. One can see that a linear correlation between ΔH_{sub} and $-\Delta H_{ads}$ (as that used in [170]) is not

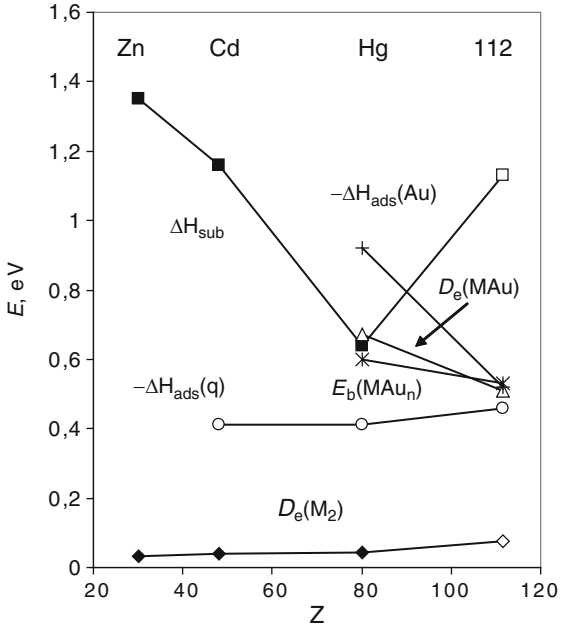

Figure 11-26. Binding energies of group 12 elements in various systems: $D_e(M_2)$ in the dimers M_2 (rhomboids), $-\Delta H_{ads}(q)$ on quartz (circles), $\Delta H_{sub}(M)$ of metals (squares), $D_e(MAu)$ of the dimers MAu (triangles); E_b of M-Au_n (stars); experimental $-\Delta H_{ads}(Au)$ on gold (crosses), where M = Zn, Cd, Hg and element 112. Filled symbols are experiment, open ones are calculations

generally valid, since bonding between atoms of the same type and atoms of various types may be different. Also, ΔH_{sub} of element 112 obtained via a straightforward extrapolation in group 12 is obviously underestimated [155].

The RECP + DFT (SO corrected) calculations for the Hg and element 112 interacting with small gold clusters (n = 1 till 4, and 10) were also reported [171]. Performed at a lower level of theory, they have overall confirmed the earlier 4*c*-DFT results [46, 163, 164]: element 112 should be less bound than Hg with the gold clusters.

11.7.3.4. Other Compounds

The relativistic contraction of the 7s AO is expected to manifest itself also in properties of other element 112 compounds. The PP calculations [86] have shown that the relativistic bond length contraction in $112H^+$ is similar to that in RgH, and that $R_e(112H^+)$ is the smallest among all others, CdH^+, HgH^+ and $112H^+$, and is similar to $R_e(ZnH^+)$, in agreement with the GRECP calculations [172]. (The RECP CCSD(T) calculations [95] for HgH^+ and $112H^+$ have, however, given a larger R_e for the latter compound.) Another interesting point is that, in contrast to the group-11 hydrides, the trend in the dissociation energies from Cd to Hg is continued with element 112, i.e. $D_e(CdH^+) < D_e(HgH^+) < D_e(112H^+)$, but $D_e(AgH) < D_e(AuH) > D_e(RgH)$ [85, 95, 172]. The reason for this difference is greater relativistic effects in $112H^+$ than in RgH.

The second (DK2) and third-order DK (DK3) method was also applied to 112H, $112H^+$ and $112H^-$ [173]. It was shown that scalar relativistic effects on the properties of $112H^-$ are similar to those on 113H and are smaller than those on $112H^+$ and 112H. The DK results for 112H differ, however, from the GRECP ones [172]: according to the former, $R_e(HgH) < R_e(112H)$, and $D_e(HgH) > D_e(112H)$, while the latter give $R_e(HgH) > R_e(112H)$, and $D_e(HgM) \approx D_e(112H)$ (see discussions in [172]).

The destabilization of the 6d AOs should result in their larger involvement in bonding in high-coordination compounds of element 112. Thus, higher oxidation states of element 112 should also be observed. The PP CCSD(T) calculations of the energies of the $MF_4 \rightarrow MF_2 + F_2$ and $MF_2 \rightarrow M + F_2$ (M = Zn, Cd, Hg and element 112) decomposition reactions supported this assumption [86]. The results are presented in Table 11-12 and depicted in Figure 11-27.

Thus, the 2+ state is important for all three molecules, ZnF_2, CdF_2 and HgF_2, though the first two are more stable than HgF_2. The latter decomposes at 645°C. The small energy of the decomposition reaction of MF_2 into M and F_2 confirms the prediction that element 112 will be more inert than Hg, though the difference to Hg is not that large. Comparison with non-relativistic results shows that this is a pure relativistic effect: non-relativistically, $112F_2$ would be by far more stable (comparable to CdF_2) with decomposition energy of 509.8 kJ/mol.

The 4+ oxidation state is not known for Zn, Cd and Hg. Results of the PP calculations suggested that HgF_4 should be thermodynamically stable [174]. The energy

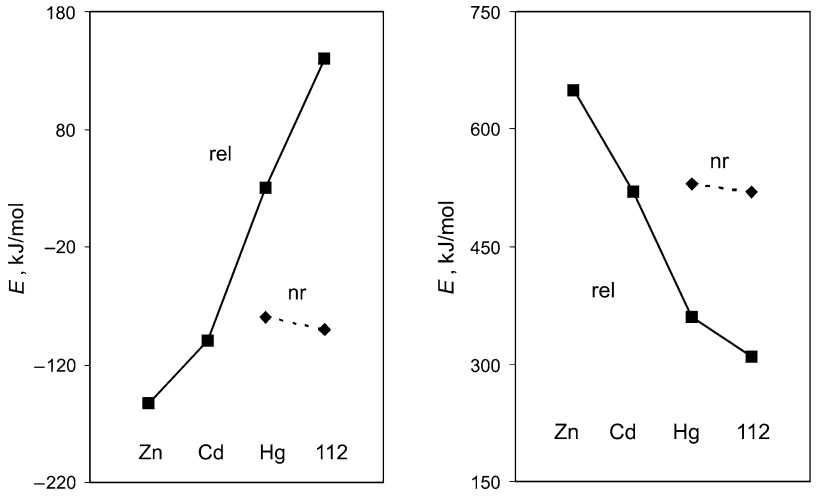

Figure 11-27. Relativistic (solid lines) and nonrelativistic (dashed lines) energies of the decomposition reactions $MF_4 \rightarrow MF_2 + F_2$ and $MF_2 \rightarrow M + F_2$ (M = Zn, Cd, Hg and element 112) (Re-drawn from the data of [86])

Table 11-12 Decomposition reaction energies for the element 112 fluorides (in kJ/mol) obtained in the PP calculations [84, 86]

	$MF_4 \rightarrow MF_2 + F_2$		$MF_2 \rightarrow M + F_2$	
Method	ARPP	NRPP	ARPP	NRPP
CCSD(T) + SO	129.5	–	315.2	–
CCSD(T)	95.0	−93.9	250.1	509.8
HF	66.4	−334.7	248.8	556.5

of the decomposition reaction of $112F_4$ of 129.5 kJ/mol indicates that the molecule should be thermodynamically more stable than HgF_4 (Figure 11-27). However, no definite conclusion about the existence of $112F_4$ can be drawn, since its decomposition energy is between 100 and 200 kJ/mol: experimentally, few compounds with the energy below 100 kJ/mol are known in the solid state. Nonrelativistically, $112F_4$ would be definitely unstable with the energy of the decomposition reaction of −93.9 kJ/mol. SO coupling increases energies of both reactions significantly (Table 11-12).

A Mulliken population analysis for MF_2 and MF_4 (M = Hg and 112) suggests that the 6d AOs of element 112 are involved in bonding to a larger extent than the 5d AOs of Hg [84, 86]. It was also found that the addition of F^- ions to HgF_2 and to HgF_4 is energetically favorable [174]. By analogy, it is assumed that in combination with appropriate polar solvent, $112F_5^-$ and/or $112F_3^-$ may be formed [86].

11.7.4. Element 113

11.7.4.1. Atomic Properties and Volatility

The ground electronic state of element 113 is $7s^2 7p_{1/2}$. The 7s AO is relativistically stabilized to such an extent that it becomes inaccessible for bonding. Properties of element 113 will, therefore, be defined by the $7p_{1/2}$ AO, which is also relativistically stabilized and contracted, not therefore favoring strong covalent bonds.

The best DCB FSCC calculated IP and EA of element 113 are 7.306 and 0.68 eV, respectively [121]. Both quantities are relativistically stabilized and larger than those of Tl of 6.11 and 0.4 eV, respectively (Figure 11-28). The best calculated α of Tl and element 113 are those via the DC FS CCSD method [135] (Table 11-13). The atomic properties were shown to exhibit a reversal of the trend in group 13 beyond In (Figure 11-28). This is caused by the strong contraction and stabilization of the outer $np_{1/2}$ AOs of Tl and element 113. The effect is strongest for element 113,

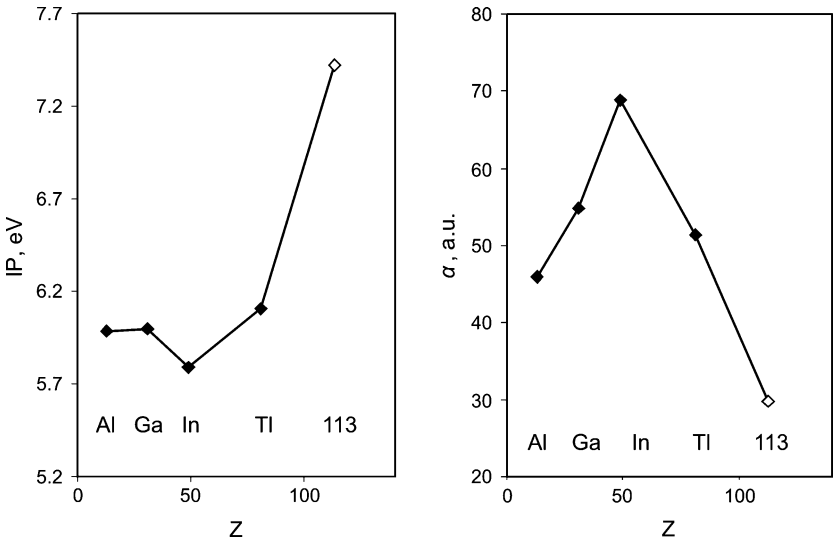

Figure 11-28. Ionization potentials, IP, and polarizabilities, α, of group 13 elements. The data for element 113 are from the DC(B) FSCC calculations [121, 135]

Table 11-13 Selected values of the Tl and element 113 properties: ionization potentials, IP (in eV), electron affinities, EA (in eV), polarizabilities, α (in a.u.), atomic radii, AR, and van der Waals radii, R_{vdW} (in Å)

Element	Method	IP	EA	α	AR	R_{vdW}	Ref.
Tl	Calc.	6.108[a]	0.40(5)[a]	51.29	1.38	1.90	[135]
	Exp.	6.110	0.377(13)	51(7)	–		[137]
113	Calc.	7.306[a]	0.68(5)[a]	29.85	1.22	1.84 ± 0.01	[135]

[a]DCB RCC [121]

resulting in the smallest α, AR and R_{vdW} in group 13 (except for B), while the IP and EA are the largest. R_{vdW} of Tl and element 113 were also obtained in [135] via a correlation of the known R_{vdW} in group 13 with $R_{max}(np_{1/2})$-AO [45].

Results of the best calculations for the properties of Tl and element 113 are summarized in Table 11-13. A comparison with other calculations is given in [135].

As the other 7p-elements, element 113 is expected to be volatile. Its adsorption on quartz and gold is, therefore, to be studied using the same gas-phase thermochromatography technique as that used for element 112 [27]. Test experiments have already been conducted on its nearest homolog, Tl [175]. Knowledge of ΔH_{ads} of element 113 and Tl on gold and ice was, therefore, required. Besides, ΔH_{ads} on Teflon or polyethylene (PE), of which the transport capillaries are made, should be known to guarantee its delivery from the target chamber to the chemistry set up.

In [135], ΔH_{ads} of group 13 elements Al through element 113 on Teflon and PE were predicted with the use of the adsorption model (Eq. (11-18)) and calculated atomic properties (Table 11-13). The obtained ΔH_{ads} are shown in Figure 11-29 where $-\Delta H_{ads}(113) = 14$ kJ/mol on Teflon and 16 kJ/mol on PE. These $-\Delta H_{ads}$ are about 6 kJ/mol smaller than the corresponding Tl values, making possible the separation and identification of the heavier element by the use of these surfaces.

The obtained ΔH_{ads} (Figure 11-29) exhibit a trend reversal beyond In in group 13, as that in the atomic properties (Figure 11-28). The extremely small α of element 113 is the main reason for its very low ΔH_{ads} on inert surfaces. This will allow for easy transport of element 113 through the Teflon capillaries.

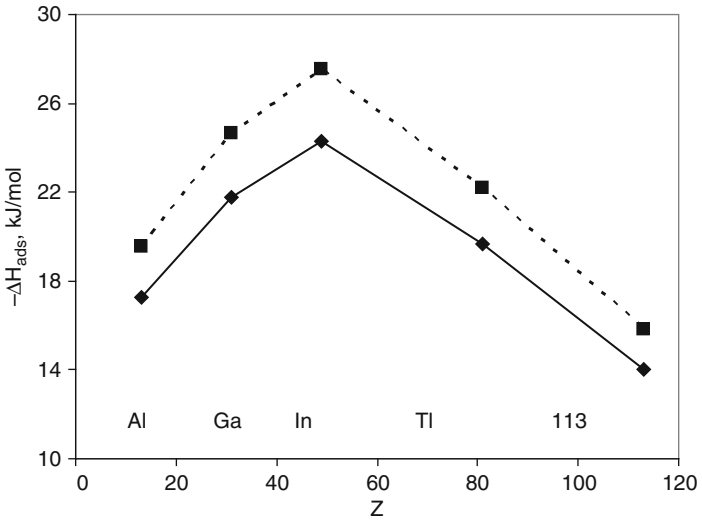

Figure 11-29. Calculated adsorption enthalpies of group 13 elements on Teflon (solid line) and polyethylene (dashed line) (From [135])

11.7.4.2. Properties of Compounds

A very large SO splitting of the 7p AOs is expected to influence properties of compounds of all the 7p elements, 113 through 118. The DFC, PP, RECP and 2*c*- and 4*c*-DFT calculations [78, 89, 91–93, 97, 111, 153, 176] were performed for MH (M = 113–118) and their lighter homologs in the chemical group. One of the aims of the studies was investigation of the influence of relativistic effects on molecular spectroscopic properties.

The 2*c*- and 4*c*-DFT results for 113H [176] are almost identical, and both are similar to the ECP CCSD(T) SO ones [97], as a comparison in [89, 108] shows. According to them, the 6d and 7s AOs participate little in bonding and all the effects are defined by the $7p_{1/2}$ shell. A large relativistic contraction of the $7p_{1/2}$ AO results in a large contraction of the 113-H bond: $\Delta R_e(\mathrm{SO}) = -0.206$ Å according to RECP CCSD(T) calculations [91] and $\Delta R_e(\mathrm{SO}) = -0.16$ Å according to DFC CCSD(T) and PP SO CCSD(T) calculations [78] (Figure 11-30). The RECP CI calculations [93, 97] show similar values. Such a bond contraction is not found in the other MH (M = elements 113–118): For 114H through 118H, both the relativistically contracted $7p_{1/2}$ and expanded $7p_{3/2}$ AOs take part in bonding, with the contribution of the $7p_{1/2}$ AO gradually decreasing along the 7p series, as expected.

In the series of the group-13 hydrides, a reversal of the trend in increasing R_e and μ_e was predicted from TlH to 113H [78, 91]. Element 113 was found to be more electronegative than Ga, In, Tl and even Al. D_e(113H) was shown to be destabilized by the large atomic SO splitting: RECP $\Delta D_e(\mathrm{SO}) = -0.93$ eV [91] and PP $\Delta D_e(\mathrm{SO}) = -0.97$ eV [78], in good agreement with each other. A decreasing trend in D_e and k_e from BH to 113H was predicted.

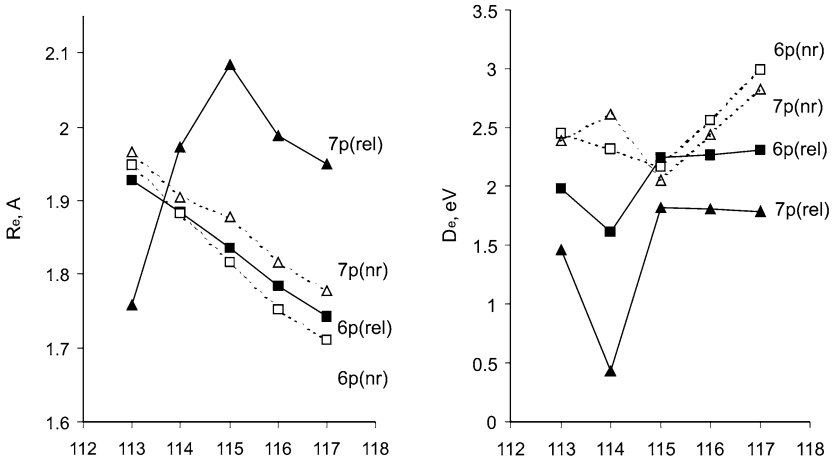

Figure 11-30. Bond lengths, R_e, and dissociation energies, D_e, for the 6p (Tl through At) and 7p (elements 113 through 117) element hydrides, MH [91–93, 111]

The dimer $(113)_2$ should also be weakly bound, as the DF calculations indicated [177]: the $7p_{1/2}$ electron yields a weak bond having $2/3\pi$ bonding and $1/3\sigma$ antibonding character. More recent, the $2c$- and $4c$-DFT calculations [176] have also shown that the binding energy is very small ($D_e = 0.08$ eV and $R_e = 3.51$ a.u. for the ground 1_u state for the BP potential, though the PBESCC result gives the 0_g^+ state as a ground with $D_e = 0.11$ eV and $R_e = 3.744$ a.u.).

The PP, DCB, RECP and $4c$-DFT calculations [78,84,89,153] for MF (M stands for all group 13 metals) have given increasing R_e and μ_e from TlF to 113F, in contrast to the decreasing values from TlH to 113H. These different trends in R_e and μ_e for the MF compounds as compared to MH are explained by a more ionic nature of the MF molecules.

An interesting case of the (113)(117) molecule was studied at the DF level [76]. There, both the low lying $7p_{1/2,1/2}(113)$ AO and the destabilized $7p_{3/2,1/2}(117)$ AO contribute to electron transfer to the group 13 atom. Thus, rather than the single electron of the group 13 atom completing the valence p shell of the group 17 atom, the electron flow is more the other way around: the high-lying $7p_{3/2,1/2}$ shell donates into the low-lying $7p_{1/2,1/2}$ shell of the group 13 atom. This results in a reversal of the dipole direction and a change of the sign of the dipole moment.

As was mentioned earlier, the relativistic destabilization of the 6d AOs is expected to influence properties of high-coordination compounds of element 113. This was confirmed by the PP and RECP calculations [78, 89, 92] for $113X_3$ (X = H, F, Cl, Br and I). As a consequence of the involvement of the 6d AOs, a T-shaped rather than trigonal planar geometric configuration was predicted for these molecules showing that the valence shell electron pair repulsion (VSERP) theory is not applicable to the heaviest elements. Relativistic effects on bond angles were assumed to be small. However, if Jahn-Teller distortions are involved, relativistic effects may significantly change bond angles, as was shown for AtF_3 [178].

The stable high-coordination compound $113F_6^-$ with the metal in the 5+ oxidation state is also foreseen. $113F_5$ will probably be unstable since the energy of the reaction $113F_5 \rightarrow 113F_3 + F_2$ is less than -100 kJ/mol [78]. The calculated energies of the decomposition reaction $MX_3 \rightarrow MX + X_2$ (from M = B, Al, Ga, In, Tl to element 113) suggest a decrease in the stability of the 3+ oxidation state in this group.

11.7.5. Element 114

11.7.5.1. Atomic Properties and Volatility

The electronic ground state of element 114 is a quasi-closed shell $7s^2 7p_{1/2}{}^2$ being a result of the strong relativistic stabilization of the $7p_{1/2}$ AO and a large SO splitting of the 7p AOs (Figure 11-3). Properties of element 114 and its compounds should, therefore, be determined by the relativistically stabilized and contracted, doubly occupied $7p_{1/2}$ AO. It is, therefore, expected to be rather inert and volatile.

Unusual properties of element 114 were predicted as early as in 1970 via an extrapolation in the periodic table [179]: A correlation of ΔH_f of gaseous atoms,

equal to ΔH_{sub} of metals, in group 14 (vs.) a raw of the periodic table has given 41.8 kJ/mol for element 114. A more grounded correlation of ΔH_f (vs.) Z has given a larger value of 71.5 ± 15 kJ/mol [155]. Both values are, however, the smallest among the group 14 elements.

Properties of element 114 predicted on the basis of atomic relativistic calculations also indicate its relative inertness. The DCB CCSD IP(114) = 8.539 eV [122] is in very good agreement with the predicted earlier DF value of 8.5 eV [5]. Polarizabilities of Pb and element 114 were calculated at various levels of theory [95, 134, 180]. The best results [134, 180], in agreement with each other, are shown in Table 11-14 (a more detailed comparison in given in [180]). The DC CCSD(T) value [134] (obtained with an additional 2h function in the basis set) for Pb is in very good agreement with experiment [180] and that for element 114 is recommended.

The SO coupling was shown to lead to a significant reduction of the polarizability of element 114 from 47.9 a.u. at the scalar-relativistic DK level to 31.5 a.u. at the DC level [180].

The data of Table 11-14 demonstrate that the influence of correlation on α of the group 14 elements with the outer $np_{1/2}$ AOs is much smaller than on α of the group 12 elements Hg and element 112 with the outer ns AO (Table 11-2), i.e., −3 a.u. for Pb and +1 a.u for element 114; again, the change is less negative for the heavier atom similarly to Hg and element 112. The polarizability of element 114 proved to be the smallest in group 14 due to the relativistic stabilization and contraction of the outer $7p_{1/2}$ AO (Figures 11-3 and 11-31).

R_{vdW} of element 114 was obtained via a correlation of known R_{vdW} in group 14 with $R_{max}(np_{1/2})$-AO [134]. The best calculated atomic properties for Pb and element 114 are given in Table 11-15.

Using the data of Table 11-15 and the adsorption model (Eq. (11-18)), ΔH_{ads} of group 14 elements on Teflon and PE were predicted [134]. The calculated $-\Delta H_{ads}$ for Pb and element 114 are 27.34 and 20.97 kJ/mol on PE, and 13.65 and 10.41 kJ/mol on Teflon, respectively. The enthalpies show the same reversal of the

Table 11-14 Electronic configurations, basis sets and polarizabilities, α (in a.u.), for Pb and element 114

Atom	Method	Basis set	α				Ref.
			HF	MP2	CCSD	CCSD(T)	
Pb	DC CCSD(T)[a]	26s24p18d13f5g2h	49.91	46.75	46.98	46.96[c]	[134]
	KR CCSD(T)[b]	37s33p25d19f2g	49.71	47.63	47.36	47.34[d]	[180]
	Calc.		–	–	–	45.89	[137]
	Exp.		–	–	–	47.1 ± 7	[180]
114	DC CCSD(T)[a]	26s24p18d13f5g2h	29.78	30.72	30.28	30.59[e]	[134]
	KR CCSD(T)[b]	32s31p24d18f3g	30.13	32.02	31.05	31.49[f]	[180]

[a] DIRAC04 code

[b] DC with Kramers symmetry in the CC procedure

[c,d,e,f] The values with Gaunt contribution are: 47.7; 47.3; 31.87; 31.0, respectively

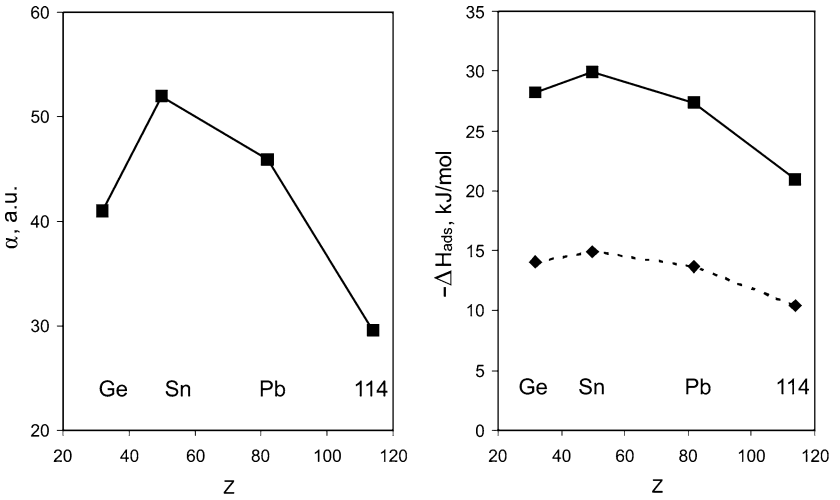

Figure 11-31. The DC CCSD(T) calculated polarizabilities, α, and adsorption enthalpies, $-\Delta H_{ads}$, of the group 14 elements on polyethylene (solid line) and Teflon (dashed line) [134]

Table 11-15 Selected values of the Pb and element 114 properties: ionization potentials, IP (in eV), electron affinities, EA (in eV), polarizabilities, α (in a.u.), atomic radii, AR, and van der Waals radii, R_{vdW} (in a.u.)

Element	Method	IP	α	AR	R_{vdW}	Ref.
Pb	Calc.	7.349[a]	46.96[b]	3.40[c]	4.06[c]	[134]
	Exp.	7.417	47.1 ± 7	3.40	4.16	[137, 180]
114	Calc.	8.539[a]	30.59[b]	3.30[c]	3.94[c]	[134]

[a]DCB CCSD [122]
[b]DC CCSD(T)
[c]Via correlation with $R_{max}(np_{1/2})$

trend as that for the $R_{max}(np_{1/2})$-AO and α of group 14 elements (Figure 11-31). According to these values, element 114 should be well transported from the target chamber to the chemistry set up through the Teflon capillary.

11.7.5.2. Homonuclear Dimers

Keeping in mind that bonding in the homonuclear dimers is a first indication about bonding in the solid state, the calculations of the electronic structures of M_2 (M = Ge, Sn, Pb and element 114) were performed with the use of various methods: 4*c*-BDF [111], 4*c*-DFT [181] and RECP CCSD(T) [95, 111]. The results for Pb and element 114 are summarized in Table 11-16. R_e and D_e for M_2 (M = Ge, Sn, Pb and element 114) are also depicted in Figure 11-32. Except for the calculations [95], performed with insufficiently large basis sets, where $(114)_2$ was obtained too bound, the other calculations agree with each other (see discussion in [181]). All the calculations agree on the fact that $(114)_2$ is stronger bound than a typical van der

Table 11-16 Bond lengths, R_e (in Å), dissociation energies, D_e (in eV), and vibrational frequencies, w_e (in cm^{-1}) of M_2 (M = Pb and element 114)

Molecule	Method	R_e	D_e	w_e	Ref.
Pb_2	ECP CCSD(T)	3.06	0.64	111	[111]
	RECP CCSD(T)	2.98	0.68	–	[95]
	4*c*-BDF	2.98	1.14	108	[111]
	2*c*-DFT SO ZORA	2.97	1.16	106	[108]
	4*c*-DFT	2.97	1.18	107	[181]
	Exp.	2.93	0.86	110	[182]
	Exp.	–	1.17	–	[183]
$(114)_2$	ECP CCSD(T)	3.73	0.07	26	[111]
	RECP CCSD(T)	3.07	0.38	–	[95]
	4*c*-BDF	3.49	0.12	50	[111]
	2*c*-DFT SO ZORA	3.46	0.12	40	[108]
	4*c*-DFT	3.49	0.13	26	[181]

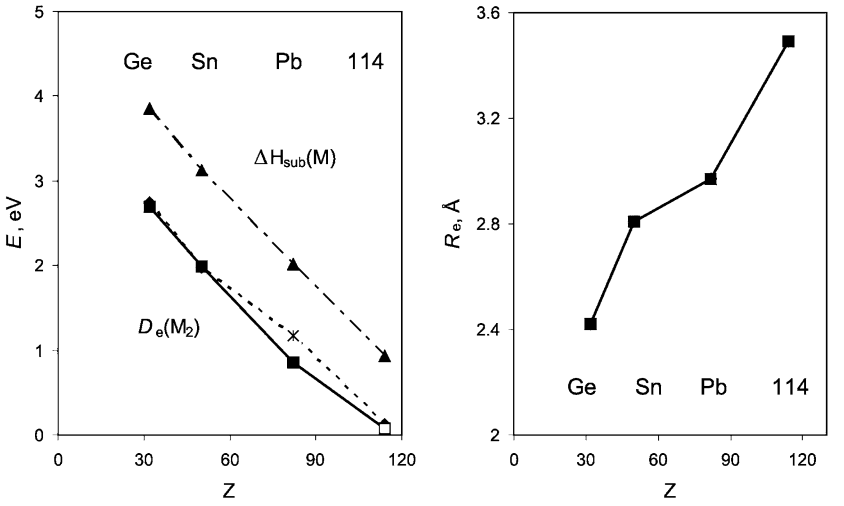

Figure 11-32. Dissociation energies, $D_e(M_2)$ (experimental for Ge_2 through Pb_2: two points for Pb_2 are two different experimental values [182, 183]; and calculated for $(114)_2$: two points are two different types of the calculations, 4*c*-DFT [181] and REC CCSD(T) [111]); sublimation enthalpies, $\Delta H_{sub}(M)$, and calculated bond lengths, $R_e(M_2)$ [181], where M = Ge, Sn, Pb and element 114

Waals system. It is stronger bound than $(112)_2$, but weaker than Pb_2. A Mulliken population analysis indicates that both the $7p_{1/2}$ and $7p_{3/2}$ AO take part in the bond formation: the HOMO of σ character is composed of 98% ($7p_{1/2}$) and 2%($7p_{3/2}$).

D_e and R_e for the group 14 dimers and ΔH_{sub} of the corresponding metals are shown in Figure 11-32.

One can see that the $D_e(M_2)$ and $\Delta H_{sub}(M)$ (M = Ge, Sn, Pb and element 114) plots are parallel (slightly better for the experimental D_e = 0.86 eV of Pb_2 [182])

and follow that of the energy of the $np_{1/2}$(M)-AO (Figure 11-3). This in another evidence that bonding in these species is, indeed, defined by the $np_{1/2}$ AO and its relativistic stabilization with increasing Z in group 14.

Using the correlation between $D_e(M_2)$ and $\Delta H_{sub}(M)$, and the calculated $D_e[(114)_2]$, $\Delta H_{sub}(114) = 1.22$ eV (118 kJ/mol) is predicted. (Using another experimental $D_e(Pb_2)$ value of 1.17 eV [183] for the correlation, $\Delta H_{sub}(114) = 0.80$ eV is obtained.)

11.7.5.3. Intermetallic Systems

Volatility of element 114 as adsorption on a metal surface is supposed to be studied using the same gas-phase thermochromatography column with gold covered detectors, as that used for element 112. (The feasibility experiments with Pb have already been conducted [184].) Accordingly, the 4*c*-DFT electronic structure calculations were performed for the MM′ dimers, where M = Ge, Sn, Pb and element 114, and M′ = Ni, Pb, Pt, Cu, Ag and Au [181]. (All these noble metals were considered, because some of them will be used as electrode materials in the experiments on the electrochemical deposition of element 114 from aqueous solution [34,35].) The obtained spectroscopic properties of PbM′ and 114M′ (M′ = Ni, Pd and Pt; Cu, Ag and Au) are summarized in Table 11-17.

Element 114 was shown to form a rather strong chemical bond with the group 10 and 11 metal atoms. In 114Au, the doubly occupied $7p_{1/2}(114)$ and the single occupied 6s(Au) AO form one double-occupied σ bonding MO and one single-occupied σ* untibonding MO, so that the ground state is $^2\Sigma^+ \; d_{Au}{}^{10}\sigma_{Au}{}^2\sigma \; *_{114}{}^1$. A Mulliken

Table 11-17 Calculated bond lengths, R_e (in Å), dissociation energies, D_e (in eV), and harmonic vibrational frequencies, w_e (in cm^{-1}), for PbM′ and 114M′, where M′ are group 10 and 11 elements [181]

Molecule	R_e	D_e	w_e
PbNi	2.37	1.84	238.9
PbPd	2.50	1.95	201.8
PbPt	2.45	3.53	213.5
PbCu	2.53	1.60	180.5
PbAg	2.67	1.22	231.8
PbAu	2.64	2.15	152.7
		1.29[a]	158.6[a]
114Ni	2.47	0.30	245.7
114Pd	2.69	0.79	137.82
114Pt	2.56	1.11	157.37
114Cu	2.74	0.47	283.6
114Ag	2.95	0.30	151.5
114Au	2.88	0.73	96.70

[a]Spectroscopic measurements (a low limit) [185]

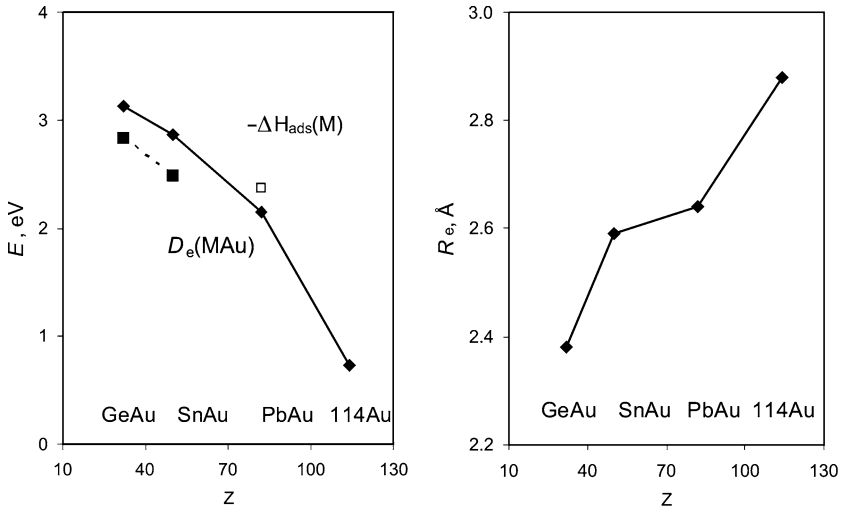

Figure 11-33. Dissociation energies, D_e (solid line – calculations [181], dashed line – experiment), and calculated bond lengths, R_e, in the MAu dimers (M = Ge, Sn, Pb and element 114). The measured $-\Delta H_{ads}$ of Pb on gold [184] is shown with an open square

population analysis shows that both the $7p_{1/2}(114)$ and $7p_{3/2}(114)$ AOs overlap with the 6d(Au) AOs. The type of bonding is similar to that of 112Au, though D_e(114Au) is about 0.2 eV larger than D_e(112Au). Among all the considered metals, bonding with Pt should be the strongest, while with Ag and Ni the weakest. The trends in the D_e and R_e values of PbM′ and 114M′ as a function of M′ were shown to be determined by the trends in the energies and R_{max} of the valence (n-1)d AO of the M′ atoms, respectively, and are similar for PbM′ and 114M′ (except for the Ni dimers) [181].

Figure 11-33 shows D_e and R_e for MAu as a function of Z(M), where M = Ge, Sn, Pb and element 114. The D_e plot has a pattern – a decrease with Z(M) – similar to that for $D_e(M_2)$ (Figure 11-32). This means that in group 14 the type of the M-M bonding is similar to the M-Au one (in difference to group 12): it is defined preferentially by the $np_{1/2}$(M) AO becoming less accessible for bonding with increasing Z (Figure 11-3). The R_e, however, increases with Z(M) due to the involvement of also the $np_{3/2}$(M) AO.

There is one measured value of $-\Delta H_{ads}$(Pb) = 2.37 eV on gold [184]. Assuming, that $-\Delta H_{ads}$(M) correlates with D_e(MAu), as ΔH_{sub}(M) does with $D_e(M_2)$, $\Delta H_{ads}(114) = -0.95$ eV on gold is predicted using the measured $-\Delta H_{ads}$(Pb) and the calculated D_e(114Au). This value is in very good agreement with $-\Delta H_{ads}(114) = 0.97$ eV obtained using semi-empirical models of adsorption on metals [186].

The 4*c*-DFT calculations for Pb and element 114 interacting with large gold clusters simulating the Au(111) surface have also been performed [168]. Results for M-Au_n (M = Pb and element 114, and n = 95 for the top, n = 94 for the bridge,

n = 120 for the hollow1 and n = 107 for the hollow2 positions) indicate that element 114 is about 1.3 eV weaker bound with gold than Pb, similarly to the dimers. A comparison with group 12 elements shows that bonding with gold should change in the following order: 112 < Hg < 114 ≪ Pb, as it was obtained for the gold dimers of these elements. Thus, in the thermochromatography gas-phase experiments, element 114 should be adsorbed at the very beginning of the chromatography column with an entrance temperature of 35°C, similarly to Hg.

At the end of this section, it is worth giving a summary of the predicted adsorption behaviour of elements 112 and 114 on different types of surfaces, since chemical experiments are to be performed using the same chemistry set up and nuclear production mode. Thus, on inert surfaces, element 112 should be 6 kJ/mol stronger adsorbed by van der Waals forces than element 114, since $R_{vdW}(112) < R_{vdW}(114)$. On the contrary, on transition metal surfaces, element 112 should be about 20 kJ/mol weaker adsorbed than element 114 by chemical forces, since the 7s(112) AO is more stabilized than the $7p_{1/2}(114)$ AO.

11.7.5.4. Other Compounds

A decreased involvement of the $7p_{1/2}$ electrons of element 114 in bonding in comparison with lighter homologs in the group was also demonstrated by calculations for other molecular systems. $D_e(114H)$ of about 0.4 eV (0.40 eV for BDF [111] and 0.43 eV for RECP CI [93]) is the smallest in the considered MH series and the smallest in group 14 (Figure 11-30). $D_e(114H)$ was shown to be drastically decreased by the SO interaction ($\Delta_{SO}(D_e) = -2.18$ eV for RECP CCSD(T) [91, 92], −2.07 for RECP CI [93] and −2.02 for BDF [111]). Thus, the small $D_e(114H)$ is a result of both the 7p SO splitting and the double occupancy of the $7p_{1/2}$ spinor. The influence of the SO interaction on R_e is relatively small (Figure 11-30) due to the contribution of both the contracted $7p_{1/2}$ and expanded $7p_{3/2}$ AOs. This is also, obviously, the reason why $R_e(114H) = 1.96$ Å is larger than $R_e(PbH) = 1.88$ Å [91, 92]. The RECP CCSD(T) calculations [95] for PbH^+ and $114H^+$ have also given a 0.48 eV stronger bond in the latter molecule, though 0.18 Å shorter. The CAS-SCF/SOCI RECP calculations for $114H_2$ demonstrated breakdown of the conventional singlet (X^1A_1) and triplet ($^3B_1$) states due to large relativistic effects including SO ones [187]. The SO effects are shown to destabilize $114H_2$ by almost 2.6 eV.

Results of an earlier work [188] (based on atomic calculations) on the stability of some 114^{2+} and 114^{4+} compounds also lead to the conclusion of a lower reactivity of element 114. All tetravalent compounds were considered to be unstable towards decomposition. Some divalent inorganic salts were predicted to be, however, stable.

The electronic structures of 114X (X = F, Cl, Br, I, O) and $114O_2$ were calculated using the 2*c*-RECP CCSD(T), 2*c*-DFT SO ZORA and 4*c*-BDF methods [108, 111]. Better agreement with experiment for the known compounds of Pb was shown by the RECP CCSD(T) values. Trends in R_e and D_e for the halides and oxides from Pb to element 114 were found to be similar to those for the hydrides. In contrast to PbO_2 ($D_e = 5.60$ eV), $114O_2$ ($D_e = 1.64$ eV) was predicted to be

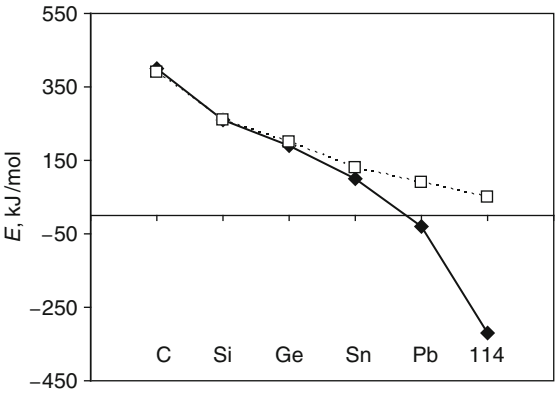

Figure 11-34. Relativistic DFC (solid line) and nonrelativistic HF (dashed line) calculated energies of the reaction $MH_4 \rightarrow MH_2 + H_2$ (M = C, Si, Ge, Sn, Pb and element 114) (From [77])

thermodynamically unstable with respect to the decomposition into the metal atom and O_2. Using results of these calculations, it was shown that element 114 should not react with O_2 at the experimental conditions [134].

The *ab initio* DF and PP calculations [76,77,84] for the decomposition reactions $MX_4 \rightarrow MX_2 + X_2$ and $MX_2 \rightarrow M + X_2$ (M = Si, Ge, Sn, Pb and element 114; X = H, F and Cl) also predicted a decrease in the stability of the 4+ oxidation state in agreement with earlier works [5]. The instability was shown to be a relativistic effect (see Figure 11-34 for MH_4, as an example). The neutral state was found to be more stable for element 114 than that for Pb. As a consequence, element 114 is expected to be less reactive than Pb, but about as reactive as Hg. This is similar to the predicted adsorption behaviour of the elements on gold: element 114 should be much weaker adsorbed than Pb, but slightly stronger than Hg. The possibility of the existence of $114F_6^{2-}$ was suggested [77].

11.7.6. Elements 115–118

11.7.6.1. Chemical Properties of Elements 115–117

Element 115 and 116. The chemistry of elements 115 and 116 has received little attention so far, though it is expected to be very interesting due to strong SO effects in the 7p AOs. Early studies based on extrapolations of properties and atomic DF calculations are summarized in [5,189].

The 4*c*-BDF and SO ZORA calculations were performed for 115H and $(115)_2$ in good agreement with each other [108,176]. The same 0_g^+ ground state was found for Bi_2 and $(115)_2$. The 115 dimer was found to be weaker bound than the Bi one: $D_e(115_2) = 0.83\,\text{eV}$ and $R_e = 3.08$ Å, while $D_e(Bi_2) = 2.45\,\text{eV}$ and $R_e = 2.69$ Å. Bonding in $(115)_2$ should be stronger than in $(113)_2$ and $(114)_2$.

Results of the RECP and BDF calculations [91,93,111] for R_e and D_e of 116H and PoH and influence of relativistic effects are shown in Figure 11-30. It was found that $D_e(\text{PoH}) > D_e(116\text{H})$, and $R_e(\text{PoH}) < R_e(116\text{H})$. Relativistic effects increase

R_e(116H) and decrease D_e(116H), as discussed in Section 11.7.4.2. The RECP were also applied to $116H_2$ [96]. The SO interaction was found to lengthen the 116-H bond and lead to a significant H-116-H bond angle increase in comparison with PoH_2. It was suggested that the result is a rehybridization of the valence 7p AO with a "supervalent" 8s AO of element 116.

A hypothesis of the decreasing stability of the 4+ oxidation state of element 116 was supported by estimates of formation enthalpies of MX_2 and MX_4 (M = Po and element 116; X = F, Cl, Br, I, SO_4^{2-}, CO_3^{2-}, NO_3^- and PO_4^{3-}) using results of the atomic MCDF calculations [188]. The chemistry of element 116 is expected to be mainly cationic: an ease of formation of the divalent compounds should approach that of Be or Mn, and tetravalent compounds should be formed with the most electronegative atoms, e.g., $116F_4$.

Element 117. The DF and RECP molecular calculations have shown that element 117 forms H117 by analogy with the other group-17 halogens [74, 92]. The bond in H117 should be weaker than in the other HM compounds (M = group 17 elements) in line with a decreasing trend in group 17. The bond length should be larger in H117 than in HAt, also in line with the trend (Figure 11-30). The reason for that is a decreasing contribution of the $np_{1/2}$ AO with increasing Z(M) in the group: bonding in H117 is formed predominantly by the $7p_{3/2}$ AO and is, therefore, 2/3 of the bonding of the 7p AOs without SO splitting. The DHF [74] and RECP [92] calculations for H117 have given the SO effects on R_e as 0.13 and 0.17 Å, respectively.

Analogously to the lighter homologs, element 117 should also form the dimer $(117)_2$. The DCB CCSD(T) calculations for X_2 (X = F through At) [190] found a considerable antibonding σ character of the HOMO of At_2 due to SO coupling (without the SO coupling, it is an antibonding π orbital). Thus, bonding in $(117)_2$ is predicted to have considerable π character. 117Cl is also predicted to be bound by a single π bond with a SO increased bond length [191]. The IF, AtF and 117F molecules were also considered at various levels of theory: DC and RECP plus HF/MP2/CCSD/CCSD(T) [83]. D_e(117F) was shown to be the largest among the group 17 fluorides. It was found that D_e(117F) is 0.1 eV increased by SO effects in contrast to the other group 17 fluorides. The SO effects are opposite for all the three spectroscopic constants for 113F and 117F. The RECP calculations have shown that the D_{3h} geometry is not the proper one for the $117F_3$ molecule, in difference from the sixth period compound of At, thus again indicating that the VSERP theory is not applicable to the heaviest elements.

11.7.6.2. Chemistry of Element 118

The chemistry of element 118 should be interesting due to the very large SO splitting of the 7p AO of 11.8 eV [45]. The destabilization of the four $7p_{3/2}$ electrons suggests that element 118 should be relatively reactive, in line with an increasing trend in the reactivity in group 18. It should also be the most electronegative element among the rare gases due to the relativistic stabilization of the 8s AO. (The DCB CCSD + QED calculations has given EA(118) = 0.058 eV [51].) The DC CCSD(T) α(118)

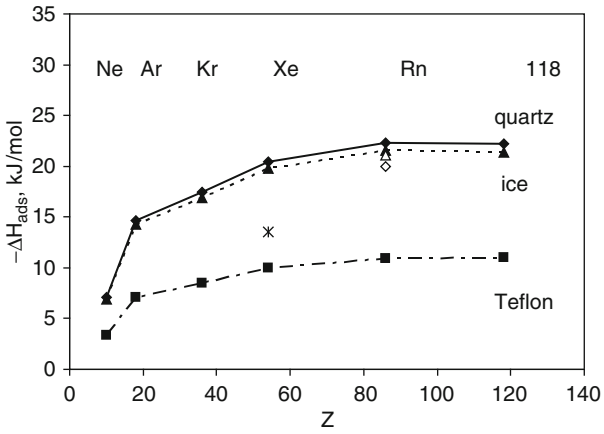

Figure 11-35. Calculated adsorption enthalpies of the noble gas atoms on quartz (rhomboids, solid line), ice (triangles, dashed line) and Teflon (squares, dashed-dotted line). Experimental data are: for Rn on quartz (an open rhomboid [192]) and ice (an open triangle [162]); for Xe on ice (a star) [193] (From [126])

= 46.3 a.u. is the largest in group 18, as also AR = 4.55 a.u., while IP = 8.92 eV is the smallest [126]. (The RECP + CCSD(T) $\alpha(118) = 52.43$ a.u. is overestimated due to the smaller basis set [95].) These extreme values reflect, in addition to the general trends in the periodic table, the relativistic expansion and destabilization of the outer valence $7p_{3/2}$ AO.

Volatility. Using calculated atomic properties and the adsorption model (Eq. (11-18)), van der Waals coefficients C_3 and ΔH_{ads} of Ne through element 118 on noble metal and inert surfaces, such as quartz, ice, Teflon and graphite, were calculated [126] (Figure 11-35).

The C_3 coefficients were shown to steadily increase in group 18, while the increase in $-\Delta H_{ads}$ from Ne to Rn does not continue to element 118: The larger AR of element 118 is responsible for its equal ΔH_{ads} with Rn. It was, therefore, predicted that experimental distinction between Rn and 118 by adsorption on these types of surfaces will not be feasible. A possible candidate for separating the two elements is charcoal; further study is needed to test this possibility.

Chemical compounds. As was mentioned above, the destabilization of the $np_{3/2}$ AOs should also result in the increasing stability of the 2+ and 4+ oxidation states in group 18. The RECP calculations for the reactions $M + F_2 \rightarrow MF_2$ and $MF_2 + F_2 \rightarrow MF_4$, where M = Xe, Rn and element 118, confirmed an increasing stability of the fluorides in the raw, as a result of the increasing polarizability of the central atom [83,89]. The SO effects were shown to stabilize $118F_4$ by a significant amount of about 2 eV, though they elongate R_e by 0.05 Å. Thus, the trends in increasing R_e and D_e are continued with element 118. Also, the following trends in the stability of the fluorides were established: $RnF_2 < HgF_2 < PbF_2$, while $112F_2 < 114F_2 < 118F_2$.

Influence of the SO interaction on the geometry of MF_4 was investigated by the RECP-SOCI [94, 194] and RECP CCSD calculations [89]. It was shown that a D_{4h} geometrical configuration for XeF_4 (calculated in agreement with experiment) and for RnF_4 (calculated) becomes slightly unstable for $118F_4$. A T_d configuration becomes more stable than the D_{4h} one in $118F_4$ by 0.25 eV [94, 194] or 0.17 eV [83, 89]. The reason for this unusual geometry was the availability of only the stereochemically active $7p_{3/2}$ electrons for bonding. This is another example of the inapplicability of the VSERP theory for the heaviest elements. An important observation was made that the fluorides of element 118 will most probably be ionic rather than covalent, as in the case of Xe. This prediction might be useful for future gas-phase chromatography experiments.

The RECP calculations [92] for 118H have shown the van der Waals bond to be stabilized by about 2.0 meV by SO effects with $\Delta R_e(\mathrm{SO}) = -0.019$ Å. Trends in the stability of hydrides was predicted as follows: RnH << HgH < PbH, 118H << 114H < 112H. The RECP calculations for a single-charge ions give $D_e(\mathrm{RnH}^+) > D_e(118\mathrm{H}^+)$ and $R_e(\mathrm{RnH}^+) < R_e(118\mathrm{H}^+)$ [95].

11.7.7. Elements with Z > 118

From element 122, a very long, unprecedented transition series that is characterized by the filling of not only 6f but also 5g AOs with partially filled $8p_{1/2}$ AO begins. These elements were called "superactinides" by Seaborg in 1968 [13]. Quite a number of theoretical calculations of the ground state electronic configurations were performed for this region (see [5] for a review and a recent work [117]). At the beginning of the superactinides, not only two but four electron shells, namely $8p_{1/2}$, $7d_{3/2}$, $6f_{5/2}$ and $5g_{7/2}$ are expected to complete simultaneously. These open shells, together with the 8s electrons, will determine the chemistry. According to the DS calculations, the g electrons appear in element 125 [5], while the relativistic DFT with QED corrections (Breit interaction) [117] found that g electrons in the atom first appear from element 126. It was also shown that the QED corrections are important for studying electronic configurations of superheavy elements. Even more accurate *ab initio* calculations are needed to accurately predict electronic states of those elements.

Due to the very strong relativistic effects, the chemistry of those elements will be much more different to anything known before. However, without relativistic effects, it would also be very different due to the very large orbital effects. Until now, no studies have been performed at the MO level for compounds of these elements, except for DF calculations (without correlation) for fluorides of element 126 [195]. Accurate predictions of properties of specific compounds will be quite a challenging task in this area. This may need inclusion of the QED effects to reach the desired accuracy.

Experimental investigations are still a matter of a far future and are dependent on discoveries of longer-lived isotopes. The evolution of the periodic table was discussed by Seaborg last in 1996 [196].

Table 11-18 Trends in volatility of the heaviest element compounds and their lighter homologs in the chemical groups

Group	Compounds	Theoretically predicted	Ref.	Experimentally observed	Ref.
4	MCl_4, MBr_4	Hf < Rf	[139]	Hf < Rf	[28]
5	ML_5 (L = Cl, Br)	Nb < Ta < Db	[197]	(DbO_3Br)	[29]
		$DbCl_5 > DbOCl_3$	[197]	$DbCl_5 > DbOCl_3$	[29]
6	MO_2Cl_2	Mo > W > Sg	[140]	Mo > W > Sg	[30]
7	MO_3Cl	Tc > Re > Bh	[143]	Tc > Re > Bh	[31]
8	MO_4	Ru < Os > Hs	[146]	Os > Hs	[26]
12	M	Hg < 112	[165, 168]	Hg < 112	[27]
14	M	Pb << 114 < 112	[168, 181]	–	–

11.7.8. Summary of Predictions of Volatility of the Heaviest Elements and Their Compounds

Predicted trends in volatility of the heaviest elements and their compounds compared to the experimental observations are summarized in Table 11-18. One can see that all the predicted trends for group 4 through 8 and 12 were confirmed by the experiments. Also, the absolute values of the adsorption enthalpies are in very good agreement with the experimental ones, as discussed above. Predictions for element 114 are still awaiting experimental verification.

11.8. AQUEOUS CHEMISTRY

11.8.1. Redox Potentials and Reduction Experiments

The stability of oxidation states of the heaviest elements is tested by reduction experiments. For that purpose, knowledge of the redox potentials E° is of crucial importance. For a reduction reaction

$$M^{z+n} + ne \leftrightarrow M^{z+}, \tag{11-19}$$

the redox potential E° is

$$E^\circ = -\Delta G^\circ / nF, \tag{11-20}$$

where F is the Faraday constant and n in the number of the transferred electrons. In reality, components of reaction (11-19) are high-coordinated hydrated, hydrolyzed and complex species, so that calculations of E° via the total energy differences may not be sufficiently accurate. Another way to obtain E° was, therefore, suggested in [198] using a linear correlation between IP and E°, since

$$\Delta G^\circ = -E^\circ nF = -(\mathrm{IP} + \Delta G^\circ{}_{\mathrm{hydr}}). \tag{11-21}$$

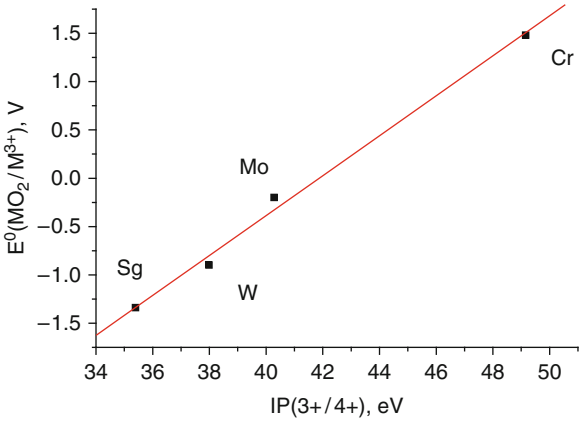

Figure 11-36. Correlation between MCDF IP(3+/4+) [66] and standard potentials $E°(MO_2/M^{3+})$ [201], where M = Cr, Mo, W, and Sg (From [200])

Here, $\Delta G°_{hydr}$ is a free energy of hydration, which is a smooth function of the atomic number and can, therefore, be evaluated. In this way, $E°$ for Rf, Db and Sg in various oxidation states were determined [198–200] using the MCDF multiple IPs [55, 65, 66] and experimental $E°$ for lighter homologs [201]. One of those correlations for the group-6 species is shown in Figure 11-36, as an example [200].

Results of those investigations have, indeed, shown that the stability of the maximum oxidation state increases in group 4 through 6, while that of lower oxidation states decreases. Along the 6d series, the stability of the maximum oxidation state decreases: $E°(Lr^{3+}/Lr^{2+}) = -2.6\,V$, $E°(Rf^{4+}/Rf^{3+}) = -1.5\,V$, $E°(Db^{5+}/Db^{4+}) = -0.93\,V$, and $E°(Sg^{6+}/Sg^{5+}) = -0.05\,V$. The redox potentials for Lr, Rf, Db and Sg and their homologs are given in [8].

A comparison of the relativistic with nonrelativistic calculations shows that the increasing stability of the maximum oxidation state is a relativistic effect due to the destabilization of the 6d AOs. The estimates of redox potentials have also demonstrated that the 3+ and 4+ states for Db and Sg, respectively, will not be stable: the ionisation process results in the $6d^2$ and not the $7s^2$ state in Db^{3+} and Sg^{4+} [200]. Since the 6d AOs are more destabilized than the 4d and 5d ones, the 3+ and 4+ states in Db and Sg, respectively, will even be less stable than those states in their lighter homologs. Based on these predictions, experiments to attempt to reduce Sg with a strongly reducing metal such as Al ($E° = -1.662\,V$) are planned.

11.8.2. Complex Formation and Extraction by Liquid Chromatography

A number of aqueous chemistry separation experiments have been conducted for Rf, Db and Sg and their homologs [202–211]. These experiments demonstrated a basic similarity in the behaviour of the heaviest elements and their lighter homologs, although they have revealed a number of controversies (see reviews

[9,34,36]). Many theoretical works based on the 4*c*-DFT calculations were devoted to predictions of the extraction behaviour of these elements [212–219]. The main features of the method used in those works are given in the following.

A model to predict hydrolysis/complex formation. For a complex formation reaction (11-1), the complex formation constant K_i is

$$\log K_i = -\Delta G^r / 2.3RT, \tag{11-22}$$

where ΔG^r is a free energy change of the reaction. Since it is almost impossible to calculate $\Delta G^r = \Delta G^f(\text{products}) - \Delta G^f(\text{reagents})$ with sufficient accuracy for large, highly coordinated aqueous species of the heavy-element complexes, the following model has been used. The formation energy ΔG^f of the $M_xO_u(OH)_v(H_2O)_w^{(z-2u-v)+}$ species can be decomposed in the following way [220]

$$\begin{aligned} &-\Delta G^f(u,v,w)/2.3RT \\ &\quad = \sum a_i + \sum a_{ij} + \log P - \log(u!v!w!2^w) + (2u+v+1)\log 55.5 \end{aligned} \tag{11-23}$$

The first term on the right hand side of Eq. (11-23), $\sum a_i$, is the non-electrostatic contribution from M, O, OH, and H_2O, related to OP of the species. For a reaction,

$$\Delta \sum a_i = \Delta E^{\text{OP}} = k\Delta\text{OP}, \tag{11-24}$$

where k is an empirical coefficient. The next term, $\sum a_{ij}$, is a sum of each pairwise electrostatic (Coulomb) interaction

$$E^C = \sum a_{ij} = -B \sum_{ij} Q_i Q_j / d_{ij}, \tag{11-25}$$

where d_{ij} is the distance between the moieties i and j; Q_i and Q_j are their effective charges and $B = 2.3RTe^2/\varepsilon$, where ε is the dielectric constant. For a reaction, ΔE^{C} is the difference in E^{C} for the species in the left hand and right hand parts. P in Eq. (11-23) is the partition function representing the contribution of structural isomers if there are any. The last two terms are statistical: one is a correction for the indistinguishable configurations of the species and the other is a conversion to the molar scale of concentration for the entropy. $\sum a_{ij}$ and $\sum a_i$ for each compound are then calculated via Mulliken numbers obtained as a result of the electronic structure calculations of complexes on interest. To predict $\log K_i$ or $\log\beta_i$ for transactinide complexes, coefficients k and B should be defined by fitting $\log K_i$ to experimental values for the lighter homologs, as it is shown in [217]. Using the suggested model in the combination with 4*c*-DFT calculations, hydrolysis and complex formation constants were predicted for a large number of aqueous compounds of Rf, Db, Sg and Hs and their group-4, 5, 6 and 8 lighter homologs [212–219].

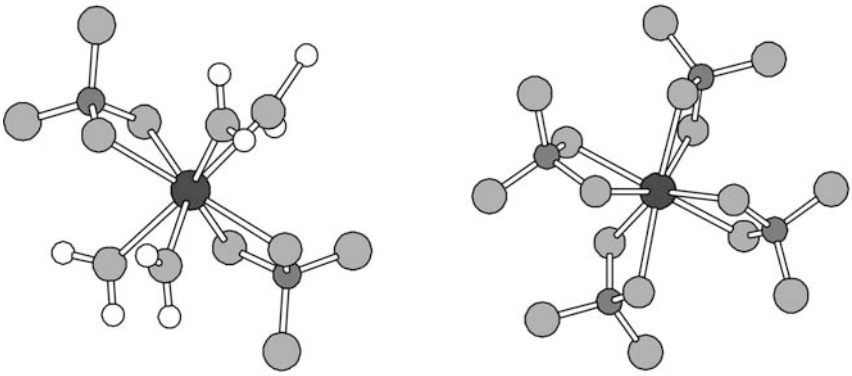

Figure 11-37. $M(SO_4)_2(H_2O)_4$ and $M(SO_4)_4{}^{4-}$ complexes of Zr, Hf and Rf (From [213])

Table 11-19 Coulomb part of the free energy change, ΔE^C (in eV) of the complex formation reactions [213]

Reaction	Zr	Hf	Rf	Trend
$M(H_2O)_8{}^{4+} \Leftrightarrow M(SO_4)_2(H_2O)_4$	−35.72	−35.84	−33.60	Hf > Zr >> Rf
$M(H_2O)_8{}^{4+} \Leftrightarrow M(SO_4)_3(H_2O)_2{}^{2-}$	−42.43	−42.43	−39.37	Zr = Hf >> Rf
$M(H_2O)_8{}^{4+} \Leftrightarrow M(SO_4)_4{}^{4-}$	−45.14	−45.02	−41.38	Zr > Hf >> Rf
$M(H_2O)_8{}^{4+} \Leftrightarrow R_4M(SO_4)_4$	−41.04	−40.78	−37.65	Zr > Hf >> Rf

As an example, a process of step-wise complexation of group-4 elements Zr, Hf, and Rf in H_2SO_4 solutions is considered here. In [213], relative values of the free energy change of the $M(SO_4)_2(H_2O)_4$, $M(SO_4)_3(H_2O)_2{}^{2-}$ and $M(SO_4)_4{}^{4-}$ (M = Zr, Hf, and Rf) formation reactions from hydrated and partially hydrolyzed cations have been calculated using the 4*c*-DFT method. (Figure 11-37 shows geometrical configurations of two of these complexes.) The obtained ΔE^C and trends for one type of complex formation reaction starting from the hydrated species $M(H_2O)_8{}^{4+}$ are given in Table 11-19.

Analogously, ΔE^C were obtained for a complex formation reaction starting from hydrolyzed complexes, i.e., $MOH(H_2O)_7{}^{3+} \Leftrightarrow M(SO_4)_n(H_2O)_{8-2n}$. The results have indicated the same trend in the complex formation, Zr > Hf >> Rf, as for the former type of reaction (Table 11-19). The obtained on their basis $\log K_d$ values for extraction of Zr, Hf and Rf by amines are shown in Figure 11-38.

The experiments on the extraction of Zr, Hf and Rf from H_2SO_4 solutions by amines confirmed the predicted trend Zr > Hf >> Rf in the complex formation and have given the K_d(Rf) values closed to the predicted ones [207].

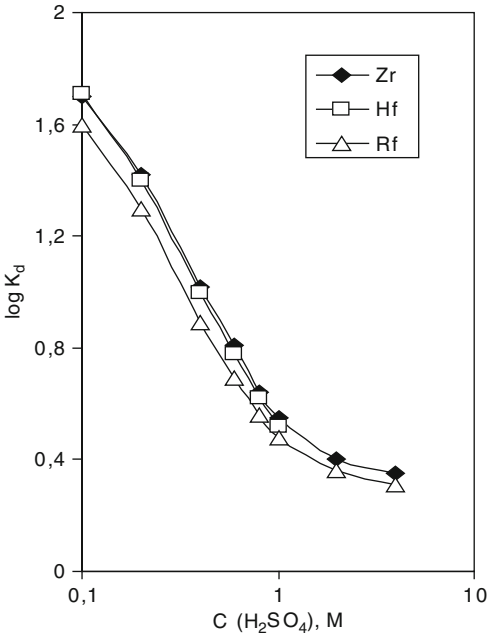

Figure 11-38. Predicted log K_d values for the extraction of Hf and Rf by amines with respect to the measured one for Zr (From [213])

11.8.3. Summary of Predictions of the Complex Formation

A summary of the predicted trends in hydrolysis, complex formation and extraction of the heaviest element complexes and their homologs as compared to the experimental results is given in Table 11-20. As one can see there, most of the predictions were confirmed by the experiments for the heaviest elements and their homologs, while some of them are still awaiting confirmation, as in the case of Sg in HF solutions.

The calculations have shown that the theory of hydrolysis [208] based on the relation between the cation size and charge does not explain all the experimental behaviour, like, e.g., the difference between Nb and Ta, or Mo and W. Only by performing relativistic calculations for real equilibria in solutions, can the complex formation or hydrolysis constants, K_d and their order in the chemical groups be correctly predicted.

Results of the calculations have also shown the predominant contribution in ΔG^r to be a change in the electrostatic metal-ligand interaction energy, ΔE^C (Eq. (11-25)). Thus, by calculating only this term trends in the complex formation can be reliably predicted.

Experimental aqueous phase studies of chemical properties of elements heavier than Sg have not yet been performed. They will depend on the development of experimental techniques which cope with production rates of less than one atom per hour and short half-lives.

Table 11-20 Trends in hydrolysis and complex formation of the heaviest element compounds and their lighter homologs in chemical groups

Group	Complexes	Theoretically predicted	Ref.	Experimentally observed	Ref.
4	Hydrolysis of M^{4+}	Zr > Hf > Rf	[212]	Zr > Hf > Rf	[202]
	$MF_x(H_2O)^{z-x}{}_{8-x}$ ($x \leq 4$)	Zr > Hf > Rf	[212]	Zr > Hf > Rf	[203, 204]
	$MF_6{}^{2-}$	Rf ≥ Zr > Hf	[212]	Rf ≥ Zr > Hf	[205]
	$MCl_6{}^{2-}$	Zr > Hf > Rf	[212]	Rf > Zr > Hf	[206]
	$M(SO_4)_4{}^{4-}$	Zr > Hf >> Rf	[213]	Zr > Hf >> Rf	[207]
5	Hydrolysis of M^{5+}	Nb > Ta > Db	[214]	Nb > Ta	[202]
	$MOCl_4{}^-$, $MCl_6{}^-$	Nb ≥ Db > Ta	[215]	Nb ≥ Db >Ta	[209]
	$MF_6{}^-$, $MBr_6{}^-$	Nb > Db > Ta	[216]	Nb > Db > Ta	[209]
6	Hydrolysis of M^{6+}	Mo > W > Sg	[217]	Mo > W > Sg	[210]
	Hydrolysis of $MO_2(OH)_2$	Mo > Sg > W	[217]	Mo > W	[210]
	$MO_2F_2(H_2O)_2$	Mo > Sg > W	[218]	Mo > W	[221]
	$MOF_5{}^-$	Mo < W < Sg	[218]	Mo < W	[221]
8	$MO_4(OH)_2{}^{2-}$	Os > Hs >> Ru	[219]	Os ≥ Hs	[211]

11.9. SUMMARY AND OUTLOOK

Many accurate calculations of atomic and molecular properties of the heaviest elements and their homologs have nowadays become available. The most accurate atomic calculations for the heaviest elements up to $Z = 122$ were performed with the use of the DC and DCB FSCC methods. Reliable electronic configurations were obtained assuring the position of the superheavy elements in the periodic table. Accurate ionization potentials, electron affinities and energies of electronic transitions are presently available and can be used to assess the similarity between the heaviest elements and their lighter homologs in the chemical groups.

The most valuable information about molecular properties of the chemically interesting compounds was obtained with the use of the 4*c*-DFT and RECP/PP CCSD(T) methods. They proved to be complimentary, both conceptually and quantitatively in studies of molecular properties, and their combination is obviously the best way to investigate properties of the heaviest elements. The calculations with the use of these methods allowed for predicting valence states, geometries, and types of stable compounds of the heaviest elements. They permitted the establishment of important trends in chemical bonding, stabilities of oxidation states, crystal-field and SO effects, complexing ability and other properties in the periodic table in going over to the heaviest elements, as well as the role and magnitude of relativistic and correlation effects.

It was shown that the heaviest elements are basically homologs of their lighter congeners in the chemical groups, though their properties may be rather different due to very large relativistic effects. This is also a reason why trends in atomic and molecular properties may change in going over to the heaviest elements. Thus, straightforward extrapolations in the chemical groups may result in erroneous predictions. Relativistic calculations also proved to be the most reliable tool

in predicting the outcome of the gas-phase and aqueous phase experiments with Rf, Db, Sg, Bh, Hs, and element 112. The synergism between theoretical and experimental research in the last decade led to a better understanding of the chemistry of these exotic species.

Although rich information has been collected, a number of open questions still remain. For elements which were chemically identified, a more detailed study, both theoretical and experimental, shall follow. New compounds of the chemically identified elements, e.g., carbonyls of Sg, or organometallic ones of Hs, should be synthesized and chemically investigated. For those elements, not yet studied, like Mt, Ds, Rg and those 114 through 118, isotopes suitable for chemical studies should be found, as well as their nuclear decay properties should be known, so that they can be positively identified. Their separation will also need new technological developments to cope with the very low production rates and short half-lives. In this area, theoretical chemistry will have a number of exciting tasks to predict the experimental behaviour in the chemical separation experiments.

For elements heavier than $Z = 118$, investigations of chemical properties is a matter of future. They will be even more exciting than those which have already been performed, since resemblance with their lighter homologues will be even less pronounced. Some further methodical developments in the relativistic quantum theory, like, e.g., inclusion of the QED effects on a SCF basis, may be needed to achieve a required accuracy of the calculations.

ACKNOWLEDGEMENTS

The author acknowledges a fruitful collaboration with J. Anton, T. Jacob, T. Bastug, A. Borschevsky, E. Eliav, U. Kaldor, and D. C. Hoffman. She appreciates many fruitful discussions with her colleagues at the GSI, Darmstadt. She thanks S. Hofmann for the chart of nuclides and Ch. E. Düllmann for the periodic table of the elements. She also acknowledges help of B. Schausten in preparing the pictures.

REFERENCES

1. Schädel, M. (ed.).: The Chemistry of the Superheavy Elements. Dordrecht, The Netherlands/Boston, MA/London (2003)
2. Proceedings of "The Robert A. Welch Foundation Conference on Chemical Research XXXIV. Fifty Years with Transuranium Elements", Houston, TX, 22–23 October 1990, pp. 255–276 (1990)
3. Greiner, W., Gupta, R.K. (eds.).: Heavy Elements and Related New Phenomena. World Scientific, Singapore (1999)
4. Wilson, S., Kaldor, U. (eds.).: Theoretical Chemistry and Physics of Heavy and Superheavy Elements, pp. 55–114. Kluwer, Dordrecht (2003)
5. Fricke, B.: Struct. Bond. **21**, 89 (1975)
6. Schwerdtfeger, P., Seth, M.: Relativistic effects on the superheavy elements. In: Encyclopedia on Calculational Chemistry, vol. 4, pp. 2480–2499. Wiley, New York (1998)
7. Pershina, V.: The chemistry of the superheavy elements and relativistic effects. In: P. Schwerdtfeger (ed.) Relativistic Electronic Structure Theory, Part II, pp. 1–80. Elsevier, Amsterdam (2002)

8. Hoffman, D.C., Lee, D.M., Pershina, V.: Transactinide elements and future elements. In: L.R. Morss, N.M. Edelstein, J. Fuger (eds.) The Chemistry of the Actinide and Transactinide Elements, 3rd edn, Ch. 14, pp. 1652–1752. Springer, Dordrecht (2006)
9. Pershina, V., Kratz, J.V.: Experimental and theoretical studies of the chemistry of the heaviest elements. In: B.A. Hess (ed.) Relativistic Effects in Heavy-Element Chemistry and Physics, pp. 219–244. Wiley, New York (1997)
10. Pershina, V.: Chem. Rev. **96**, 1977 (1996)
11. Barber, R.C., Greenwood, N.N., Hrynkiewicz, A.Z., Jeannin, Y.P., Lefort, M., Sakai, M., Ulehla, I., Wapstra, A.H., Wilkinson, D.H.: Prog. Part. Nucl. Phys. **29**, 453 (1992)
12. Flerov, G.N., Ter-Akopian, G.M.: Rep. Prog. Phys. **46**, 817 (1983)
13. Seaborg, G.T., Loveland, W.D.: The Elements Beyond Uranium. Wiley, New York (1990)
14. Münzenberg, G., Hofmann, S.: Discovery of the heaviest elements. In.: W. Greiner, R.K. Gupta (eds.) Heavy Elements and Related New Phenomena, pp. 9–42. World Scientific, Singapore (1999)
15. Hofmann, S., Münzenberg, G.: Rev. Mod. Phys. **72**, 733 (2000)
16. Morita, K., Morimoto, K., Kaji, D., Akiyama, T., Goto, S., Haba, H., Ideguchi, E., Katori, K., Koura, H., Kikunaga, H., Kudo, H., Ohnishi, T., Ozawa, A., Sato, N., Suda, T., Sieki, K., Tokanai, F., Yamaguchi, T., Yoneda, A., Yoshida, A.: J. Phys. Soc. Jpn. **76**, 045001 (2007)
17. Oganessian, Yu.: J. Phys. G: Nucl. Part. Phys. **34** R165 (2007)
18. Commission on nomenclature of inorganic chemistry. Pure & Appl. Chem. **69**, 2471; www.iupac.org (1997)
19. Möller, P., Nix, J.R.: J. Phys. G., Nucl. Part. Phys. **20**, 1681 (1994)
20. Myers, W.D., Swiatecki, W.J.: Nucl. Phys. A **601**, 141 (1996); Liran, S., Marinov, V., Zeldes, N.: Phys. Rev. C **63**, 017302–1 (2000)
21. Heenen, P.H., Nazarewicz, W.: Europhys. News, Febr. 2002, p. 5; Bender, M., Nazarewicz, W., Reinhard, P.-G.: Phys. Lett. B **515**, 42 (2001); Bender, M., Rutz, K., Reinhard, P.-G., Maruhn, J.A., Greiner, W.: Phys. Rev. C **60**, 034304 (1999)
22. Kruppa, A.T., Bender, M., Nazarewicz, W., Reinhard, P.G., Vertse, T., Cwiok, S.: Phys. Rev. C **61**, 034313–1 (2000); Cwiok, S., Dobaczewski, J., Heenen, P.H., Magierski, P., Nazarewicz, W.: Nucl. Phys. A **611**, 211 (1996)
23. Adloff, J.P., Guillaumont, R.: Fundamentals of Radiochemistry, pp. 327–52. CRC Press, Boca Raton, FL (1993)
24. Hübener, S., Zvara, I.: Radiochim. Acta **31**, 89 (1982)
25. Zvara, I., Eichler, B., Belov, V.Z., Zvarova, T.S., Korotkin, Yu.S., Shalaevsky, M.R., Shegolev, V.A., Hussonnois, M.: Sov. Radiochem. **16**, 709 (1974)
26. Düllmann, Ch.E., Brüchle, W., Dressler, R., Eberhardt, K., Eichler, B., Eichler, R., Gäggeler, H.W., Ginter, T.N., Glaus, F., Gregorich, K., Hoffman, D.C., Jäger, E., Jost, D.T., Kirbach, U.W., Lee, D.E., Nitsche, H., Patin, J.B., Pershina, V., Piguet, D., Qin, Z., Schädel, M., Schausten, B., Schimpf, E., Schött, H.J., Soverna, S., Sudowe, R., Thörle, P., Timokhin, S.N., Trautmann, N., Türler, A., Vahle, A., Wirth, G., Yakushev, A.B., Zielinski, P.M.: Nature **418**, 859 (2002)
27. Eichler, R., Aksenov, N.V., Belozerov, A.V., Bozhikov, G.A., Vhepigin, V.I., Dmitriev, S.N., Dressler, R., Gäggeler, H.W., Gorshkov, V.A., Haenssler, F., Itkis, M.G., Laube, A., Lebedev, V.Ya., Malyshev, O.N., Oganessian, Yu.Ts., Petrushkin, O.V., Piguet, D., Rasmussen, P., Shishkin, S.V., Shutov, S.V., Svirikhin, A.I., Tereshatov, E.E., Vostokin, G.K., Wegrzecki, M., Yeremin, A.V.: Nature Lett. **447**, 72 (2007)
28. Kadkhodayan, B., Türler, A., Gregorich, K.E., Baisden, P.A., Czerwinski, K.R., Eichler, B., Gäggeler, H.W., Hamilton, T.M., Jost, D.T., Kacher, C.D., Kovacs, A., Kreek, S.A., Lane, M.R., Mohar, M.F., Neu, M.P., Stoyer, N.J., Sylwester, E.R., Lee, D.M., Nurmia, M.J., Seaborg, G.T., Hoffman, D.C.: Radiochim. Acta **72**, 169 (1996)
29. Türler, A.: Radiochim. Acta **72**, 7 (1996)

30. Schädel, M., Brüchle, W., Dressler, R., Eichler, B., Gäggeler, H.W., Günther, R., Gregorich, K.E., Hoffman, D.C., Hübener, S., Jost, D.T., Kratz, J.V., Paulus, W., Schumann, D., Timokhin, S., Trautmann, N., Türler, A., Wirth, G., Yakushev, A.B.: Nature (Lett.) **388**, 55 (1997); Türler, A., Brüchle, W., Dressler, R., Eichler, B., Eichler, R., Gäggeler, H.W., Gärtner, M., Glatz, J.-P., Gregorich, K.E., Hübener, S., Jost, D.T., Lebedev, V.Ya., Pershina, V., Schädel, M., Taut, S., Timokhin, N., Trautmann, N., Vahle, A., Yakushev, A.B.: Angew. Chem. Int. Ed. Engl. **38**, 2212 (1999)
31. Eichler, R., Brüchle, W., Dressler, R., Düllman, Ch.E., Eichler, B., Gäggeler, H.W., Gregorich, K.E., Hoffman, D.C., Hübener, S., Jost, D.T., Kirbach, U.W., Laue, C.A., Lavanchy, V.M., Nitsche, H., Patin, J.B., Piguet, D., Schädel, M., Shaughnessy, D.A., Strellis, D.A., Taut, S., Tobler, L., Tsyganov, Y.S., Türler, A., Vahle, A., Wilk, P.A., Yakushev, A.B.: Nature **407**, 63 (2000)
32. Gäggeler, H.W., Türler, A.: Gas-phase chemistry. In: Ref. 1, pp. 237–290; Türler, A., Gregorich, K.E. (eds.).: Experimental techniques, ibid., pp. 117–158
33. Hoffman, D.C.: Chem. Eng. News May 24 (1994); Hoffman, D.C.: J. Chem. Ed. **76**, 331 (1999)
34. Kratz, J.V.: Liquid-phase chemistry. In: Ref. 1, pp. 159–104
35. Kratz, J.: Chemistry of transactinides. In: S. Nagy, Z. Klencsar (eds.) Handbook of Nuclear Chemistry, pp. 323–396. Kluwer, Norwell, MA (2003)
36. Schädel, M.: Angew. Chem. Int. Ed. Engl. **45**, 368 (2006)
37. Penneman, R.A., Mann, J.B., Jørgensen, C.K.: Chem. Phys. Lett. **8**, 321 (1971)
38. Jørgensen, C.K.: Angew. Chem. Int. Ed. Engl. **12**, 12 (1973)
39. Haissinski, M.: Radiochem. Radioanal. Lett. **8**, 107 (1971)
40. Seaborg, G.T., Keller, O.L.: In: J.J. Katz, G.T. Seaborg, L.R. Morss (eds.) The Chemistry of the Actinides, 2nd edn., vol. 2, p. 1629. Chapman & Hall, New York (1986)
41. Bonchev, D., Kamenska, V.: J. Phys. Chem. **85**, 1177 (1981)
42. Cotton, S.A.: Chem. Soc. Rev. 219 (1996)
43. Pershina, V.: Theoretical chemistry of the heaviest elements. In: Ref. 1, pp. 31–94
44. Pyykkö, P.: Chem. Rev. **88**, 563 (1988)
45. Desclaux, J.P.: Atom. Data Nucl. Data **12**, 311 (1973)
46. Pershina, V., Bastug, T.: Chem. Phys. **311**, 139 (2005)
47. Eliav, E., Shmulyian, S., Kaldor, U., Ishikawa, Y.: J. Chem. Phys. **109**, 3954 (1998)
48. Gaston, N., Schwerdtfeger, P., Nazarewicz, W.: Phys. Rev. A **66**, 062505 (2002)
49. Lindgren, I.: Int. J. Quantum Chem. **57**, 683 (1996)
50. Pyykkö, P., Tokman, M., Labzowsky, L.N.: Phys. Rev. A **57**, R689 (1998)
51. Goidenko, I., Labsowsky, L., Eliav, E., Kaldor, U., Pyykkö, P.: Phys. Rev. A **67**, 020102(R) (2003)
52. Schwerdfeger, P. (ed.).: Relativistic Electronic Structure Theory, Parts I and 2. Elsevier, Amsterdam (2002)
53. Kaldor, U., Eliav, E., Landau, A.: Accurate relativistic Fock-Space calculations for many-electron atoms. In: Ref. 52, vol. 2, pp. 81–119
54. Eliav, E., Kaldor, U., Ishikawa, Y.: Phys. Rev. Lett. **74**, 1079 (1995)
55. Glebov, V.A., Kasztura, L., Nefedov, V.S., Zhuikov, B.L.: Radiochim. Acta **46**, 117 (1989)
56. Johnson, E., Fricke, B., Keller, Jr. O.L., Nestor, Jr. C.W., Ticker, T.C.: J. Chem. Phys. **93**, 8041 (1990)
57. Eliav, E., Landau, A., Ishikawa, Y., Kaldor, U.: J. Phys. B**35**, 1693 (2002)
58. DIRAC Package. Dirac, a relativistic *ab initio* electronic structure program, Release DIRAC04.0 (2004)", written by Jensen, H.J.Aa., Saue, T., Visscher, L. with contributions from Bakken, V., Eliav, E., Enevoldsen, T., Fleig, T., Fossgaard, O., Helgaker, T., Laerdahl, J., Larsen, C.V., Norman, P., Olsen, J., Pernpointner, M., Pedersen, J.K., Ruud, K., Salek, P., van Stralen, J.N.P., Thyssen, J., Visser, O., Winther, T. (http://dirac.chem.sdu.dk) (2004)
59. Malli, G., Da Silva, A.B.F., Ishikawa, Y.: J. Chem. Phys. **101**, 6829 (1994)
60. Visscher, L., Aerts, P.J.C., Visser, O., Nieuwpoort, W.C.: Int. J. Quantum Chem. **25**, 131 (1991)

61. Faegri, K.: Theor. Chem. Acta **105**, 252 (2001); Faegri, K., Dyall, K.G.: Basis sets for relativistic calculations. In: Ref. 52, pp. 259–290
62. de Macedo, L.G.M., Borin, A.C., da Silva, A.B.F.: Atom. Data Nucl. Data **93**, 931 (2007)
63. Desclaux, J.P.: Comput. Phys. Commun. **9**, 31 (1975)
64. Grant, I.P.: J. Phys. B **19**, 3187 (1986)
65. Fricke, B., Johnson, E., Rivera, G.M.: Radiochim. Acta **62**, 17 (1993)
66. Johnson, E., Pershina, V., Fricke, B.: J. Phys. Chem. **103**, 8458 (1999)
67. Johnson, E., Fricke, B., Jacob, T., Dong, C.Z., Fritzsche, S., Pershina, V.: J. Phys. Chem. **116**, 1862 (2002)
68. Yu, Y.J., Li, J.G., Dong, C.Z., Ding, X.B., Fritsche, S., Fricke, B.: Eur. Phys. J. D **44**, 51 (2007)
69. Yu, Y.J., Dong, C.Z., Li, J.G., Fricke, B.: J. Chem. Phys. **128** 124316 (2008)
70. Balasubramanian, K.: Chem. Phys. Lett. **341**, 601 (2001); ibid, **351**, 161 (2002)
71. Fricke, B., Greiner, W., Waber, J.T.: Theor. Chim. Acta (Berlin) **21**, 235 (1971)
72. Visscher, L.: Post-Dirac-Fock methods. In: Ref. 52, Part 1, pp. 291–331; Saue, T.: Post Dirack-Fock-methods-properties, ibid., pp. 332–400
73. Wood, C.P., Pyper, N.C.: Chem. Phys. Lett. **84**, 614 (1981)
74. Saue, T., Faegri, K., Gropen, O.: Chem. Phys. Lett. **263**, 360 (1996)
75. Seth, M., Schwerdtfeger, P., Dolg, M., Faegri, K., Hess, B.A., Kaldor, U.: Chem. Phys. Lett. **250**, 461 (1996); Seth, M., Schwerdtfeger, P.: Chem. Phys. Lett. **318**, 314 (2000)
76. Faegri, K., Saue, T.: J. Chem. Phys. **115**, 2456 (2001)
77. Seth, M., Faegri, K., Schwerdtfeger, P.: Angew. Chem. Int. Ed. Engl. **37**, 2493 (1998); Schwerdtfeger, P., Seth, M.: J. Nucl. Radiochem. Sci. **3**, 133 (2002)
78. Seth, M., Schwerdtfeger, P., Faegri, K.: J. Chem. Phys. **111**, 6422 (1999)
79. Malli, G.L., Styszynski, J.: J. Chem. Phys. **109**, 4448 (1998); Malli, G.: J. Chem. Phys. **116**, 5476 (2002)
80. Malli, G.: J. Chem. Phys. **117**, 10441 (2002)
81. Pyykkö, P., Desclaux, J.P.: Chem. Phys. Lett. **50**, 503 (1977); Nature **226**, 336 (1977); Chem. Phys. **34**, 261 (1978)
82. Dolg, M.: Relativistic effective core potentials. In: Ref. 52, Part 1, pp. 793–862
83. Lee, Y.S.: Two-component relativistic effective core potential calculations for molecules. In: Ref. 52, Part 2, pp. 352–416
84. Seth, M.: The chemistry of superheavy elements. Thesis, University of Auckland (1998)
85. Seth, M., Dolg, M., Fulde, P., Schwerdtfeger, P.: J. Am. Chem. Soc. **17**, 6597 (1995)
86. Seth, M., Schwerdtfeger, P., Dolg, M.: J. Chem. Phys. **106**, 3623 (1997)
87. Seth, M., Cooke, F., Schwerdtfeger, P., Heully, J.L., Pelissier, M.: J. Chem. Phys. **109**, 3935 (1998)
88. Han, Y.K., Son, S.K., Choi, Y.J., Lee, Y.S.: J. Phys. Chem. A **103**, 9109 (1999)
89. Han, Y.K., Lee, Y.S.: J. Phys. Chem. A **103**, 1104 (1999)
90. Han, Y.K., Bae, C., Lee, Y.S.: J. Chem. Phys. **110**, 8986 (1999)
91. Han, Y.K., Bae, C., Son, S.K., Lee, Y.S.: J. Chem. Phys. **112**, 2684 (2000)
92. Choi, Y.J., Han, Y.K., Lee, Y.S.: J. Chem. Phys. **115**, 3448 (2001)
93. Nash, C.S., Bursten, B.E.: J. Phys. Chem. A**103**, 632 (1999)
94. Nash, C.S., Bursten, B.E.: **103**, 402 (1999); Nash, C.S., Bursten, B.E.: Angew. Chem. Int. Ed. Engl. **38**, 151 (1999)
95. Nash, C.S.: J. Phys. Chem. A **109**, 3493 (2005)
96. Nash, C.S., Crockett, W.W.: J. Phys. Chem. A **110**, 4619 (2006)
97. Balasubramanian, K.: Chem. Phys. Lett. **361**, 397 (2002)
98. Nash, C.S., Bursten, B.E., Ermler, W.C.: J. Chem. Phys. **106**, 5153 (1997)

99. Mosyagin, N.S., Petrov, A.N., Titov, A.V., Tupitsyn, I.I.: In: J.-P. Julien et al. (eds.) Recent Advances in the Theory of Chemical and Physical Systems, pp. 229–251. Springer, The Netherlands (2006)
100. Kohn, W., Becke, A.D., Parr, R.G.: J. Phys. Chem. **100**, 12974 (1996)
101. Engel, E.: Relativistic density functional theory: Foundations and basic formalism. In: Ref. 52, Part 1, pp. 523–621
102. Rosen, A., Ellis, D.E.: J. Chem. Phys. **62**, 3039 (1975); Rosen, A.: Adv. Quantum Chem. **29**, 1 (1997)
103. Bastug, T., Sepp, W.D., Kolb, D., Fricke, B., te Velde, G., Baerends, E.J.: J. Phys. B **28**, 2325 (1995)
104. Anton, J., Fricke, B., Engel, E.: Phys. Rev. A **69**, 012505 (2004)
105. Becke, A.D.: Phys. Rev. A **38**, 3098 (1988)
106. Perdew, J.P.: Phys. Rev. B **33**, 1822 (1986); ibid **34**, 7406 (1986)
107. Jacob, T., Geschke, D., Fritzsche, S., Sepp, W.D., Fricke, B., Anton, J., Varga, S.: Surf. Sci. **486**, 194 (2001)
108. van Wüllen, C.: Relativistic density functional calculations on small molecules. In: Ref. 52, Part 2, pp. 598–655
109. Liu, W., Hong, G., Dai, D., Li, L., Dolg, M.: Theor. Chem. Acc. **96**, 75 (1997)
110. Liu, W., van Wüllen, Ch.: J. Chem. Phys. **110**, 3730 (1999)
111. Liu, W., van Wüllen, W.Ch., Han, Y.K., Choi, Y.J., Lee, Y.S.: Adv. Quantum Chem. **39**, 325 (2001)
112. Mayer, M., Krüger, S., Rösch, N.: J. Chem. Phys. **115**, 4411 (2001)
113. van Lenthe, E., Ehlers, A., Baerends, E.J.: J. Chem. Phys. **110**, 8943 (1999); te Velde, G., Baerends, E.J.: J. Comput. Phys. **99**, 84 (1992)
114. Hess, B.A.: Phys. Rev. A **33**, 3742 (1986)
115. Eliav, E., Kaldor, U., Ishikawa, Y.: Phys. Rev. A **52**, 291 (1995)
116. Desclaux, J.P., Fricke, B.: J. Phys. **41**, 943 (1980)
117. Umemoto, K., Saito, S.: J. Phys. Soc. Jpn. **65**, 3175 (1996)
118. Pyper, N.C., Grant, I.P.: Proc. R. Soc. Lond., Ser A **376**, 483 (1981)
119. Eliav, E., Kaldor, U., Schwerdtfeger, P., Hess, B.A., Ishikawa, Y.: Phys. Rev. Lett. **73**, 3203 (1994)
120. Eliav, E., Kaldor, U., Ishikawa, Y.: Phys. Rev. A **52**, 2765 (1995)
121. Eliav, E., Kaldor, U., Ishikawa, Y., Seth, M., Pyykkö, P.: Phys. Rev. A **53**, 3926 (1996)
122. Landau, A., Eliav, E., Ishikawa, Y., Kaldor, U.: J. Chem. Phys. **114**, 2977 (2001)
123. Eliav, E., Kaldor, U., Ishikawa, Y.: Mol. Phys. **94**, 181 (1998)
124. Moore, C.E.: Atomic Energy Levels. Natl. Stand. Ref. Data Ser., Natl. Bur. Stand., Washington, DC (1971)
125. Eliav, E., Kaldor, U., Ishikawa, Y., Pyykkö, P.: Phys. Rev. Lett. **77**, 5350 (1996)
126. Pershina, V., Borschevsky, A., Eliav, E., Kaldor, U.: J. Chem. Phys. **129**, 144106 (1–9) (2008)
127. Lim, I., Pernpointer, M., Seth, M., Schwerdtfeger, P.: Phys. Rev. A **60**, 2822 (1999); Lim, I.S., Schwerdtfeger, P., Metz, B., Stoll, H.: J. Chem. Phys. **122**, 194103 (2005)
128. Landau, A., Eliav, E., Ishikava, Y., Kaldor, U.: J. Chem. Phys. **115**, 2389 (2001)
129. Thierfeld, C., Schwerdtfeger, P., Hessberger, F.P., Hofmann, S.: Eur. Phys. J. A **36**, 227 (2008)
130. Shannon, R.D.: Acta Crystallogr., Sect. A **32**, 751 (1976)
131. Pyykkö, P., Atsumi, M.: Chem. Eur. J. **15**, 186 (2009)
132. Pyykkö, P., Riedel, S., Patzsche, M.: Chem. Eur. J. **11**, 3511 (2005)
133. Fricke, B., Waber, J.T.: J. Chem. Phys. **56**, 3246 (1972)
134. Pershina, V., Borschevsky, A., Eliav, E., Kaldor, U.: J. Chem. Phys. **128**, 024707 (2008)
135. Pershina, V., Borschevsky, A., Eliav, E., Kaldor, U.: J. Phys. Chem. A **112**, 13712 (2008)
136. Borschevsky, A., Pershina, V., Eliav, E., Kaldor, U.: Chem. Phys. Lett. **480**, 49 (2009)

137. CRC Handbook of Chemistry and Physics, 86th edn., by D.R. Lide (ed.). CRC Press, Boca Raton, FL (2005); Goeben, D., Hohm, U.: J. Phys. Chem. **100**, 7710 (1996)
138. Pershina, V., Fricke, B.: J. Chem. Phys. **99**, 9720 (1993)
139. Pershina, V., Fricke, B.: Electronic structure and chemistry of the heaviest elements. In: Ref. 3, pp. 194–262
140. Pershina, V., Fricke, B.: J. Phys. Chem. **99**, 144 (1995); Pershina, V., Fricke, B.: ibid. **100**, 8748 (1996)
141. Nash, C.S., Bursten, B.E.: New J. Chem. **19**, 669 (1995)
142. Varga, S., Fricke, B., Hirata, M., Bastug, T., Pershina, V., Fritzsche, S.: J. Phys. Chem. **104**, 6495 (2000)
143. Pershina, V., Bastug, T.: J. Chem. Phys. **113**, 1441 (2000)
144. Pershina, V., Bastug, T., Fricke, B., Varga, S.: J. Chem. Phys. **115**, 1 (2001)
145. Pershina, V., Bastug, T., Fricke, B.: J. Chem. Phys. **122**, 124301 (2005)
146. Pershina, V., Anton, J., Jacob, T.: Phys. Rev. A **78**, 032518 (2008)
147. Burroughs, P., Evans, S., Hamnett, A., Orchard, A.F., Richardson, N.V.: J. Chem. Soc., Faraday Trans. **2** 70, 1895 (1974)
148. Krebs, B., Hasse, K.D.: Acta Crystallogr., Sect. B: Struct. Crystallogr. Cryst. Chem. **32**, 1334 (1976); Müller, A., Krebs, B.: J. Mol. Spectrosc. **24**, 180 (1967)
149. Filatov, M., Cremer, D.: J. Chem. Phys. **119**, 1412 (2003)
150. Seto, J.Y., Morbi, Z., Charron, F., Lee, S.K., Bernath, P.F., Le Roy, P.J.: J. Chem. Phys. **110**, 11756 (1999)
151. Dolg, M., Stoll, H., Seth, M., Schwerdtfeger, P.: Chem. Phys. Lett. **345**, 490 (2001)
152. Han, Y.K., Hirao, K.: Chem. Phys. Lett. **328**, 453 (2000)
153. Anton, J., Fricke, B., Schwerdtfeger, P.: Chem. Phys. **311**, 97 (2005)
154. Pitzer, K.S.: J. Chem. Phys. **63**, 1032 (1975)
155. Eichler, B.: Kernenergie **10**, 307 (1976)
156. Liu, W., Dolg, M., Schwerdtfeger, P.: unpublished
157. Pyykkö, P.: Chem. Rev. **97**, 597 (1997)
158. Zee, R.D., Blankespoor, S.C., Zweier, T.S.: J. Chem. Phys. **88**, 4650 (1988)
159. Huber, K.P., Herzberg, G.: Constants of Diatomic Molecules. Reinhold, New York (1979)
160. Schwerdtfeger, P., Li, J., Pyykkö, P.: Theor. Chim. Acta **87**, 313 (1994); Dolg, M., Flad, H.J.: J. Phys. Chem. **100**, 6147 (1996)
161. Gaston, N., Opahle, I., Gäggeler, H.W., Schwerdtfeger, P.: Angew. Chem. Int. Ed. Engl. **46**, 1663 (2007)
162. Soverna, S.: Doctoral Thesis, Universität Bern (2004); Soverna, S., Dressler, R., Düllmann, C.E., Eichler, B., Eichler, R., Gäggeler, H.W., Haenssler, F., Niklaus, J.P., Piguet, D., Qin, Z., Türler, A., Yakushev, A.: Radiochim. Acta **93**, 1 (2005)
163. Pershina, V., Bastug, T., Fricke, B., Jacob, T., Varga, S.: Chem. Phys. Lett. **365**, 176 (2002)
164. Sarpe-Tudoran, C., Pershina, V., Fricke, B., Anton, J., Sepp, W.D., Jacob, T.: Eur. Phys. J. D **24**, 65 (2003); Pershina, V., Bastug, T., Sarpe-Tudoran, C., Anton, J., Fricke, B.: Nucl. Phys. A **734**, 200 (2004)
165. Sarpe-Tudoran, C., Fricke, B., Anton, J., Pershina, V.: J. Chem. Phys. **126**, 174702 (2007)
166. Niklaus, J.P., Eichler, R., Soverna, S., Gäggeler, H.W., Tobler, L.: PSI Annual Report, p. 8. (2000)
167. Boisvert, G., Lewis, L.J., Puska, M.J., Nieminen, R.M.: Phys. Rev. B **52**, 9078 (1995)
168. Pershina, V., Anton, J., Jacob, T.: J. Chem. Phys. **131**, 084713 (2009)
169. Yakushev, A.B., Buklanov, G.V., Chelnokov, M.L., Chepigin, V.I., Dmitriev, S.N., Gorshkov, V.A., Hübener, S., Lebedev, Y.Ya., Malyshev, O.N., Popeko, A.G., Sokol, E.A., Timokhin, S.N., Türler, A., Vasko, V.M., Yeremin, A.V., Zvara, I.: Radiochim. Acta **89**, 743 (2001)

170. Eichler, R., Aksenov, N.V., Belozerov, A.V., Bozhikov, G.A., Chepigin, V.I., Dmitriev, S.N., Dressler, R., Gäggeler, H.W., Gorshkov, A.V., Itkis, M.G., Haenssler, F., Laube, A., Lebedev, V.Ya., Malyshev, O.N., Oganessian, Y.Ts., Petrushkin, O.V., Piguet, D., Popeko, A.G., Rasmussen, P., Shishkin, S.V., Serov, A.A., Shutov, A.V., Svirikhin, A.I., Tereshatov, E.E., Vostokin, G.K., Wegrzecki, M., Yeremin, A.V.: Angew. Chem. Int. Ed. Engl. **47**(17), 3262 (2008)
171. Rykova, E.A., Zeitsevskii, A., Mosyagin, N.S., Isaev, T.A., Titov, A.V.: J. Chem. Phys. **125**, 241102 (2006); Zaitsevskii, A., Rykova, E.A., Mosyagin, N.S., Titov, A.V.: Cent. Eur. J. Phys. **4,** 448 (2006)
172. Mosyagin, N.S., Isaev, T.A., Titov, A.V.: J. Chem. Phys. **124**, 224302 (2006)
173. Nakajima, T., Hirao, K.: Chem. Phys. Lett. **329**, 511 (2000)
174. Kaupp, M., von Schering, H.G.: Angew. Chem. Int. Ed. Engl. **32**, 861 (1993); Kaupp, M., Dolg, M., Stoll, H., von Schnering, H.G.: Inorg. Chem. **33**, 2122 (1994)
175. König, S., Gäggeler, H.W., Eichler, R., Haenssler, F., Soverna, S., Dressler, R., Friedrich, S., Piguet, D., Tobler, L.: PSI Annual Report (http://lch.web.psi.ch/pdf/anrep05/03.pdf) (2005)
176. Liu, W., van Wüllen, C., Wang, F., Li, L.: J. Chem. Phys. **116**, 3626 (2002)
177. Wood, C.P., Pyper, N.C.: Chem. Phys. Lett. **84**, 614 (1981)
178. Schwerdtfeger, P.: J. Phys. Chem. **100**, 2968 (1996)
179. Keller, Jr. O.L., Burmett, J.L., Carlson, T.A., Nestor, Jr. C.W.: J. Phys. Chem. **74**, 1127 (1970)
180. Thierfelder, C., Assadollahzadeh, B., Schwerdtfeger, P., Schäfer, S., Schäfer, R.: Phys. Rev. A **78**, 052506 (2008)
181. Pershina, V., Anton, J., Fricke, B.: J. Chem. Phys. **127**, 134310 (2007)
182. Pitzer, K.S., Balasubramanian, K.: J. Phys. Chem. **86**, 3068 (1982)
183. Heaven, M.C., Miller, T.A., Bondybey, V.E.: J. Phys. Chem. **87**, 2071 (1983)
184. Haenssler, F., Eichler, R., Gäggeler, H.W., Soverna, S., Dressler, R., Piguet, D., Schippering, M.: PSI Annal Report, p. 3 (2004); Eichler, R.: Private communication
185. Houdart, R., Schamps, J.: J. Phys. B **6**, 2478 (1873)
186. Rossbach, H., Eichler, B.: Akademie der Wissenschaft der DDR, Report No. ZFK-527 (1984)
187. Balasubramanian, K.: J. Chem. Phys. **117**, 7426 (2002)
188. Grant, I.P., Pyper, N.C.: Nature **265**, 715 (1977)
189. Keller, Jr. O.L., Nestor, Jr. C.W., Fricke, B.: J. Phys. Chem. **78**, 1945 (1974)
190. Visscher, L., Dyall, K.G.: J. Chem. Phys. **104**, 9040 (1996)
191. Malli, G.L.: In: Relativistic and Electron Correlation Effects in Molecules and Solids, NATO ASI Series, vol. 318. Plenum, New York (1994)
192. Eichler, B.: Private communication
193. Graham, A.P., Toennies, J.P.: J. Chem. Phys. **118**, 2879 (2003)
194. Nash, C.S., Bursten, B.E.: Angew. Chem. Int. Ed. Engl. **38**, 151 (1999)
195. Malli, G.L.: J. Chem. Phys. **124**, 071102 (2006); Malli, G.: Theor. Chem. Acc. **118**, 473 (2007)
196. Seaborg, G.T.: J. Chem. Soc., Dalton Trans. 760 (1996)
197. Pershina, V., Sepp, W.D., Bastug, T., Fricke, B., Ionova, G.V.: J. Chem. Phys. **97**, 1123 (1992)
198. Ionova, G.V., Pershina, V., Johnson, E., Fricke, B., Schädel, M.: J. Phys. Chem. **96**, 11096 (1992)
199. Pershina, V., Fricke, B.: J. Phys. Chem.**98**, 6468 (1994)
200. Pershina, V., Johnson, E., Fricke, B.: J. Phys. Chem. A **103**, 8463 (1999)
201. Bratsch, S.G.: J. Phys. Chem. Ref. Data **18**, 1 (1989)
202. Czerwinski, K.R.: Studies of fundamental properties of Rutherfordium (Element 104) using organic complexing agents. Doctoral Thesis, LBL Berkeley, CA (1992)
203. Strub, E., Kratz, J.V., Kronenberg, A., Nähler, A., Thörle, P., Zauner, S., Brüchle, W., Jäger, E., Schädel, M., Schausten, B., Schimpf, E., Zongwei, L., Kirbach, U., Schumann, D., Jost, D., Türler, A., Asai, M., Nagame, Y., Sakara, M., Tsukada, K., Gäggeler, H.W., Glanz, J.P.: Radiochim. Acta **88**, 265 (2000)

204. Ishii, A., Toyoshima, A., Tsukada, K., Asai, M., Toume, H., Nishinaka, I., Nagame, Y., Miyashita, S., Mori, T., Suganuma, H., Haba, H., Sakamaki, M., Goto, M.S., Kudo, H., Akiyama, K., Oura, Y., Nakahara, H., Tashiro, Y., Shinohara, A., Schädel, M., Brüchle, W., Pershina, V., Kratz, J.V.: Chem. Lett. **37**, 288 (2008)
205. Trubert, D., Le Naour, C., Hussonois, M., Brillard, L., Montroy Gutman, F., Le Du, J.F., Constantinescu, O., Barci, V., Weiss, B., Gasparro, J., Ardisson, G.: In: Abstracts of the 1st International Conference on Chemistry and Physics of the Transactinides, Seeheim, September 26–30 (1999)
206. Haba, H., Tsukada, K., Asai, M., Goto, S., Toyoshima, A., Nishinaka, I., Akiyama, K., Hirata, M., Ichikawa, S., Nagame, Y., Shoji, Y., Shigekawa, M., Koike, T., Iwasaki, M., Shinohara, A., Kaneko, T., Matuyama, T., Ono, S., Kudo, H., Qura, Y., Sueki, K., Nakahara, H., Sakama, M., Yokoyama, A., Kratz, J.V., Schädel, M., Brüchle, W.: J. Nucl. Radiochem. Sci. **3**, 143 (2002)
207. Omtwedt, J.P., Polyakova, D., Alstad, J., Bjornstad, T., Düllmann, C.E., Folden, C.M. III, Garcia, M.A., Gates, J., Gregorich, K.E., Hoffman, D.C., Nelson, S.L., Nitsche, H., Omtwedt, L., Pershina, V., Samadani, F., Skarnemark, G., Stavsetra, L., Sudove, R., Wilson, R.E., Zheng, L., Zielinski, P.M.: Radiochim. Acta (to be submitted)
208. Baes, Jr. C.F., Mesmer, R.E.: The Hydrolysis of Cations. Wiley, New York (1976)
209. Paulus, W., Kratz, J.V., Strub, E., Zauner, S., Brüchle, W., Pershina, V., Schädel, M., Schausten, B., Adams, J.L., Gregorich, K.E., Hoffman, D.C., Caption Lane, M.R., Laue, C., Lee, D.M., McGrath, C.A., Shaughnessy, D.K., Strellis, D.A., Sylwester, E.R.: Radiochim. Acta **84**, 69 (1999)
210. Schädel, M., Brüchle, W., Jäger, E., Schausten, B., Wirth, G., Paulus, W., Günther, R., Eberhardt, K., Kratz, J.V., Seibert, A., Strub, E., Thörle, P., Trautmann, N., Waldek, W., Zauner, S., Schumann, D., Kirbach, U., Kubica, B., Misiak, R., Nagame, Y., Gregorich, K.E.: Radiochim. Acta **83**, 163 (1998)
211. von Zweidorf, A., Angert, R., Brüchle, W., Bürger, S., Eberhartdt, K., Eichler, R., Hummrich, H., Jäger, E., Kling, H.O., Kratz, J.V., Kuczewski, B., Langrock, G., Mendel, M., Rieth, U., Schädel, M., Schausten, B., Schimpf, E., Thörle, P., Trautmann, N., Tsukada, K., Wiehl, N., Wirth, G.: Radiochim. Acta **92**, 855 (2004)
212. Pershina, V., Trubert, D., Le Naour, C., Kratz, J.V.: Radiochim. Acta**90**, 869 (2002)
213. Pershina, V., Polakova, D., Omtvedt, J.P.: Radiochim. Acta **94**, 407 (2006)
214. Pershina, V.: Radiochim. Acta **80**, 65 (1998)
215. Pershina, V.: Radiochim. Acta **80**, 75 (1998)
216. Pershina, V., Bastug, T.: Radiochim. Acta **84**, 79 (1999)
217. Pershina, V., Kratz, J.V.: Inorg. Chem.**40**, 776 (2001)
218. Pershina, V.: Radiochim. Acta **92**, 455 (2004)
219. Pershina, V.: Radiochim. Acta **93**, 373 (2005)
220. Kassiakoff, A., Harker, D.: J. Am. Chem. Soc. **60**, 2047 (1938)
221. Kronenberg, A., Mohapatra, P.K., Kratz, J.V., Pfrepper, G., Pfrepper, R.: Radiochim. Acta **92**, 395 (2004)

CHAPTER 12

RELATIVISTIC EFFECTS ON MAGNETIC RESONANCE PARAMETERS AND OTHER PROPERTIES OF INORGANIC MOLECULES AND METAL COMPLEXES

JOCHEN AUTSCHBACH

Department of Chemistry, University at Buffalo, State University of New York, Buffalo, NY 14260-3000, USA

e-mail: jochena@buffalo.edu

Abstract: This chapter is concerned with relativistic effects on molecular properties other than energy and structure. The chapter has two parts: The first part consists of a brief overview of theoretical formalisms to calculate energy-derivative properties. In the second part benchmark data and selected case studies are presented. The examples emphasize inorganic and organometallic systems but data for some popular benchmark series of molecules with main group atoms are also included. Molecular properties that are discussed in detail this chapter include NMR and EPR parameters, electric field gradients, electronic spectra, and polarizabilities.

Keywords: Molecular response properties, Nuclear magnetic resonance, Electron paramagnetic resonance, Chemical shift, Electric field gradient, Nuclear quadrupole coupling, Hyperfine tensor, g-tensor, Dipole moment, Polarizability, Absorption spectra, Relativistic effects, Spin–orbit coupling

12.1. INTRODUCTION

Energy is central to the understanding of Chemistry. The potential energy surface (PES) of a molecule or a set of molecules defines chemical structure and reactivity. In other chapters the influence of relativity on the energy (the PES) and therefore structure, reactivity, chemical bonding, and other chemical behavior, is demonstrated by numerous examples.

Derivatives of the energy of a molecule or a set of molecules with respect to suitably defined parameters are intimately related to a large number of important *molecular properties* other than the energy. The derivative parameters can be nuclear coordinates, or static and time-dependent electric and magnetic fields, or nuclear spin magnetic moments, among others. For example, the fundamental parameters for electronic and vibrational spectroscopies (such as IR, Raman, UV–Vis, along with their chiroptical counterparts), electric, magnetic, and mixed

M. Barysz and Y. Ishikawa (eds.), *Relativistic Methods for Chemists*,
Challenges and Advances in Computational Chemistry and Physics 10,
DOI 10.1007/978-1-4020-9975-5_12,

polarizabilities, nuclear and electron paramagnetic (spin) resonance (NMR and EPR) parameters, nonlinear optical properties, and many others, can be conveniently defined via energy or quasi-energy derivatives, and computed accordingly from first principles using quantum chemical methods. We will also call these derivatives "response properties". Pure nuclear-position derivatives relate to the shape of the PES (harmonic and higher order force constants) and will not be considered here.

The concept of a *response property* has to do with the the molecule responding to the influence of an external field. For instance, electric dipole moments or linear and higher order polarizabilities can be defined and computed via derivatives of the energy with respect to electric field strengths (field amplitudes). For ordinary field strengths the most suitable approach is to consider the field as a small perturbation of the molecule's ground state and use perturbation theory to compute static or frequency-dependent response. The properties of interest are then given by first, second, and higher derivatives of the energy with respect to the field strengths. Hence, the terms "response property" or "derivative property" may be used interchangeably.[1]

Other molecular properties can be defined by differentiation with respect to suitably defined parameters that are not necessarily the amplitudes of an actual electric or magnetic field. For convenience, we may consider these perturbation parameters as generalized field strengths.

Examples: The electric polarizability is proportional to the second derivative of the energy with respect to the electric field amplitudes. The magnetizability is the magnetic analog defined as the second derivative with respect to a magnetic field. Although not observable, one may define relativistic effects on the binding energy of a molecule via an expansion of the energy in powers of c^{-2} and consider the effects in various orders as a molecular property. Instead of an electromagnetic field, it is c^{-2} that plays a similar role as the derivative (perturbation) parameter. Another example is the Raman absorption intensity where one of the derivative parameters is a vibrational normal coordinate. In NMR, one of the perturbations used to compute chemical shifts and nuclear spin–spin coupling is the nuclear spin magnetic moment, not directly the magnetic field that is associated with this moment.

As long as the energy includes relativistic effects, so do these derivative/response properties. That is, they can be derived and computed from a relativistic energy expression. For heavy element compounds, reliable methods for computations of molecular properties such as the ones mentioned above should be based on the same relativistic quantum chemical methods that are now in widespread use for the determination of molecular structure and bond energies. Alternatively, relativistic correction terms of order $c^{-2}, c^{-4}, \ldots$ to a molecular property can be computed by applying perturbation theory also for the "relativity" part of the energy. This chapter will focus on the first approach where special relativity is already considered in the unperturbed energy.

[1] The orders differ by one, however, if "response" refers to a perturbation of a molecular property which is in turn defined as a first-order energy derivative. Then a linear property response is a second-order energy derivative, and so on.

The leading order of relativistic effects on the properties is c^{-2} just like for the energy, but their magnitude relative to the nonrelativistic property can be very large in some cases. This tends to be the case in particular when the property of interest is determined by features of the electronic structure near heavy atomic nuclei (we will specify in more detail in Section 12.2.7 what is meant by "... the property is determined by ..."). If the property of interest is defined quantum-mechanically via operators that are very large near the nuclei, the property may afford very large relativistic corrections, percentage-wise. As an example, relativistic effects on NMR spin–spin coupling constants involving "relativistic" heavy nuclei such as Pt or Hg can be as large as, or even larger than, their total magnitude computed from a nonrelativistic theory. In such a situation, one might want to abandon the notion of a relativistic "correction" (which suggests that the relativistic effect is small) and simply consider the relativistic versus nonrelativistic results as *correct* (or at least approximately correct) versus *deficient*, as far as comparison with experiment is concerned. Other "nuclear" properties can have large relativistic contributions as well. For instance, nuclear quadrupole coupling constants or EPR nuclear hyperfine coupling constants for heavy elements are heavily influenced by relativity. The EPR Δg tensor might be considered a purely relativistic property in the same sense that spin–orbit coupling is relativistic effect. Relativistic effects on other molecular properties may not be quite as spectacular but some form of a relativistic formalism is still required to obtain correct results for molecules with heavy atoms.

For the interested reader, in Section 12.2 the theoretical background for computations of molecular response properties will be outlined. This section covers some relativistic methods, variational perturbation theory for energy and quasienergy, derivations of some of the most important perturbation operators, and a list of response properties that are of particular interest in chemistry (Table 12-1 on page 543). Readers who are mainly interested in case studies may safely skip this section, although the subsection on perturbation operators (12.2.5) and the subsection on analyses of properties (12.2.7) will be helpful to rationalize why relativistic effects on some properties can be particularly large. In Section 12.3 a range of properties will be discussed in more detail, and benchmark data and some selected case studies will be provided. This section is concerned mainly with NMR and EPR parameters, electric field gradients, and polarizabilities. Brief concluding remarks can be found in Section 12.4.

12.2. COMPUTING MOLECULAR PROPERTIES

In this section a brief overview of methods for computing molecular properties in a relativistic framework will be provided. To render this chapter reasonably self-contained Section, 12.2.1, provides a synopsis of (some) relativistic methods that may be used to compute molecular energies, and wavefunctions or electron densities, relativistically. Section 12.2.1 is not meant to cover all of the methods that are currently popular to treat molecules within a relativistic framework since this is covered in other chapters. However, it will facilitate the discussion about properties that follows, while keeping the chapter somewhat self-contained. The

zeroth-order regular approximation (ZORA) will often be used as an example for an approximate variationally stable two-component relativistic method, mainly for two reasons: First, the quantum mechanical operators needed to define properties can be derived comparatively easily, and the connection of the relativistic formalism with the nonrelativistic limit is very transparent. The author hopes that many of the typical features of a relativistic formalism will in this way be presented to the reader in a straightforward and non technical manner. The second reason is that the calculation of many molecular response properties within the ZORA–DFT framework has been reported in the literature (this includes developments by the author and collaborators). Examples for relativistic property-computation methods that were developed within the ZORA framework are NMR chemical shifts [1–3] and spin–spin coupling constants J [4, 5], EPR $\boldsymbol{g}$- [6] and $\boldsymbol{A}$-tensors [7], polarizabilities [8], electric field gradients [9], or the calculation of excitation energies based on time-dependent DFT [10]. This does not mean that the ZORA is necessarily the best method to use – after all it is an approximate two-component method, and alternatives that may offer better performance (in particular for core-orbital properties) are available. However, for many properties the ZORA was shown to be a good approximation to the fully relativistic treatment. Core orbitals of heavy atoms are not well described by an unmodified ZORA scheme but fortunately this is of little consequence for many of the aforementioned properties. Good performance can be expected in describing valence orbitals and excitations, for instance, and properties that depend on such excitations when formulated in a "sum-over-states" (SOS) approach, see Eq. (12-26) below. Examples where an accurate treatment of the core orbitals would be vital are core excitations, naturally, or computations of absolute shielding constants (but not chemical shifts which should be considered valence shell properties).

Regarding units, in the theoretical section Hartree atomic units (au) are used. In these units the electron mass $m_e = 1$, unit of charge $e = 1$, the proportionality constant in Coulomb's law $1/(4\pi\varepsilon_0) = 1$, Planck's constant $h = 2\pi$, and speed of light $c \approx 137.036$ atomic units. Factors of one $(e, m_e, 1/(4\pi\varepsilon_0), h/(2\pi)$ will usually be dropped. In a universe with an infinite speed of light there would be no difference between Einstein's special relativity and Galilei relativity and the Schrödinger equation would provide the correct description of chemical phenomena. Therefore, the nonrelativistic limit of a particular equation will be obtained from letting the speed of light $c \to \infty$. For magnetic properties we follow the choice of McWeeny's textbook [11] here, based on equations in SI units that are converted to atomic units using the conversion factors above. Factors of $\mu_0/(4\pi)$ appear in au as $1/c^2$.

The Born–Oppenheimer approximation is assumed throughout, i.e., the focus will be on electronic properties. Corrections terms due to nuclear vibrations may be computed separately. Moreover, electromagnetic fields are treated semi-classically, not as quantized fields. Most program implementations that are presently available to compute molecular properties for heavy element systems quantum mechanically are based on these approximations.

12.2.1. Relativistic Methods in Quantum Chemistry

Details of how to include relativistic effects into quantum chemistry are extensively discussed in other chapters. For convenience, a brief overview will be given here to facilitate the derivation of the molecular property operators in various relativistic schemes and in the nonrelativistic limit (Section 12.2.5). Much of this discussion has also been provided in [12a] and more recently in an updated form in [12b], but with a restriction to frequency-independent properties.

"Ordinary" nonrelativistic quantum chemistry deals with the solution of the nonrelativistic time-independent many-electron Schrödinger equation

$$\hat{\mathcal{H}}_{\text{nrel}}\Psi = \Psi E, \tag{12-1}$$

or approximations thereof. Here, Ψ is the many-electron wavefunction of an atom or molecule with fixed nuclei, and E is the total energy. Further,

$$\hat{\mathcal{H}}_{\text{nrel}} = \sum_i \frac{\hat{\boldsymbol{p}}_i^2}{2} + V_{Ne} + V_{ee} + V_{\text{NN}} \tag{12-2}$$

is the nonrelativistic Hamiltonian which contains the nonrelativistic kinetic energy operator $\hat{\boldsymbol{p}}_i^2/2$ for each electron i, the electron–nucleus attraction potential $V_{Ne} = -\sum_{A,i} Z_A/r_{Ai}$ added up for for each electron–nucleus pair, the nonrelativistic electron–electron Coulomb repulsion $V_{ee} = \sum_{j>i} 1/r_{ij}$, and the internuclear repulsion potential $V_{\text{NN}} = \sum_{B>A} Z_A Z_B/R_{AB}$. We use i, j for electron labels, $\boldsymbol{r}$ for electron coordinates (absolute values r), labels A, B for nuclei, and uppercase $\boldsymbol{R}$ for nuclear coordinate vectors. Further, r_{Ai} indicates an electron–nucleus distance, r_{ij} an electron–electron distance, and R_{AB} and nucleus–nucleus distance. Z_A is a nuclear charge, and $\hat{\boldsymbol{p}} = -i\boldsymbol{\nabla}$ is the momentum operator in real-space representation. Since analytic solutions of Eq. (12-1) for many electron systems are not known, approximations have to be made.

In relativistic quantum chemistry, $\hat{\mathcal{H}}_{\text{nrel}}$ in Eq. (12-1) is replaced by its relativistic counterpart and Ψ by a two- or four-component wavefunction. All of the problems of the nonrelativistic many-electron theory are present in the relativistic formulation as well. Hence, similar techniques are common in order to find approximate solutions; in particular the use of orbital models, replacing the wave function calculation by Density Functional Theory (DFT), treating the electron correlation problem by perturbation theory or the coupled cluster ansatz, or other common methods. However, relativistic quantum chemistry has its own specific challenges associated with it. To begin with, a relativistic many-particle Hamiltonian for general molecules should be derived from quantum electrodynamics (QED) [13]. See, for instance, [14, 15] for work on how to embed magnetic property calculations within a QED framework. Relativistic many-electron atomic and molecular computations often

rely on the use of the four-component no-pair Dirac–Coulomb–Breit Hamiltonian (DCB) or some approximation obtained from it:

$$\hat{\mathcal{H}}_{\mathrm{DCB}} = \sum_{i=1}^{N} \left(c\vec{\alpha}_i \hat{\boldsymbol{p}}_i + \beta_i c^2 \right) + V_{Ne} + V_{ee} + \sum_{j>i=1}^{N} \hat{\mathcal{H}}_{ij}^{\mathrm{B}} + V_{\mathrm{NN}} \qquad (12\text{-}3)$$

Here, $\vec{\alpha}$ and β are 4×4 matrices introduced by Dirac in order to obtain a relativistic wave equation for spin-1/2 particles from the "classical" relativistic Hamilton function. In its standard representation, $\vec{\alpha}$ is written in terms of the well known Pauli spin-matrices $\vec{\sigma}_s$ (not to be confused with the symbol for the nuclear shielding tensor). These matrices have x, y, and z components; we will use the vector arrow to indicate this. Thus, $\vec{\alpha}_i \hat{\boldsymbol{p}}_i$ indicates the scalar product of the alpha matrix–vector with the momentum vector operator for electron number i. The $\hat{\mathcal{H}}_{ij}^{\mathrm{B}}$ (Breit interaction, see, e.g., [16]) represents relativistic corrections to V_{ee} from magnetic interactions and further accounts for the fact that the electron–electron interaction is not instantaneous but is transmitted with a finite speed. Some of the problematic features of the Dirac–Coulomb(–Breit) operator can be avoided by restricting its solutions to the positive energy spectrum, the eigenfunctions of which are identified with the desired electronic states (no-pair approximation [17, 18]). Although $\hat{\mathcal{H}}_{\mathrm{DCB}}$ is in general not truly Lorentz-invariant, it "provides an excellent approximation to the full theory" [19]. QED corrections may be added, e.g., based on perturbation theory calculations. For simplicity of notation we will in the following not explicitly consider the Breit-interaction. Its relative importance to, e.g., total atomic energies was found to decrease with increasing nuclear charge from ~50% in He to ~2% in Hg relative to the one-electron relativistic corrections [20].

As a starting point for practical computations, the N-electron equation is usually separated into N effective one-electron equations for one-particle wavefunctions ψ_i (atomic or molecular orbitals (AOs, MOs). An explicit treatment of correlation may follow in wavefunction based methods. In DFT correlation effects are included via the effective potential. For simplicity, we will implicitly refer to one-electron equations with an effective one-electron potential (or true one-electron systems) in the following, and use the symbol ψ for a one-electron wavefunction or orbital. Particular details of common approximations to treat the correlation problem will not be discussed here.

One way of performing a relativistic molecular computation in order to obtain a starting point for calculating energy-derivative properties is to use directly the Dirac equation

$$\hat{\mathcal{H}}_{\mathrm{D}} \psi_{\mathrm{D}} = \psi_{\mathrm{D}} E \qquad (12\text{-}4)$$

with

$$\hat{\mathcal{H}}_{\mathrm{D}} = c\vec{\alpha}\,\hat{\boldsymbol{p}} + \beta c^2 + V. \qquad (12\text{-}5)$$

Note that we have adopted here the aforementioned notation for (effective) one-electron equations. Because of $\vec{\alpha}$ and β being 4×4 matrices, the orbital ψ_{D} has to be a four-component object (a spinor) for which each component is in general a

complex function of space. Due to the four components, such molecular computations tend to be quite expensive compared to nonrelativistic ones, and the explicit inclusion of electron correlation is a formidable task.

Many attempts have been made to transform the four-component Eq. (12-4) into two-component form, in order to keep interpretations more simple[2] and to reduce the computational effort. Here we will give an account of some of these methods to illustrate the general idea. Writing $\vec{\alpha}$ explicitly in terms of the 2×2 Pauli spin-matrices $\vec{\sigma}$, the four component Dirac equation (12-4) reads

$$(\hat{\mathcal{H}}_{\mathrm{D}} - E)\psi_{\mathrm{D}} = \begin{pmatrix} V - E & c\vec{\sigma}\,\hat{\boldsymbol{p}} \\ c\vec{\sigma}\,\hat{\boldsymbol{p}} & V - E - 2c^2 \end{pmatrix} \begin{pmatrix} \varphi \\ \chi \end{pmatrix} = 0. \tag{12-6}$$

The zero of the energy scale has been shifted in Eq. (12-6) to $+mc^2, m = 1$, the rest mass energy of the electron, so that bound states have negative energy as usual in nonrelativistic quantum chemistry. Here, φ and χ are the "upper" and "lower" components of the four-component orbital ψ_{D}. In turn, each of these two components is itself made up of two components. The spinors φ and χ are also frequently referred to as the "large" and "small" components because of the $1/2c$ prefactor in Eq. (12-7) below.[3] Because of the $c\vec{\sigma}\,\hat{\boldsymbol{p}}$ terms the nonrelativistic limit of the Dirac equation is not immediately obvious from Eq. (12-6) but it leads indeed to the nonrelativistic limit for $c \to \infty$ as will be seen shortly.

From the second row of the 2×2 matrix in Eq. (12-6) one obtains the equation

$$\chi = X\,\varphi = \frac{1}{2c} k\vec{\sigma}\,\hat{\boldsymbol{p}}\,\varphi, \tag{12-7}$$

where

$$k = \left(1 - \frac{V - E}{2c^2}\right)^{-1}, \quad X = \frac{1}{2c} k\vec{\sigma}\,\hat{\boldsymbol{p}} \tag{12-8}$$

Equation (12-7) provides the relation between the upper an the lower component for an exact solution of the Dirac equation. It means that, in principle, the knowledge of φ should be sufficient since χ can be determined from it, or vice versa. Hence, it ought to be possible to obtain a relativistic equation for φ or χ alone, the solutions of which contain the same information as ψ_{D} (i.e., no further approximations). We may call this the fully relativistic two-component relativistic approach as compared to the fully relativistic four-component approach based on the Dirac equation.

---

[2] However, so-called picture change effects occur which may complicate certain operators. See, e.g., [16, 21, 22].

[3] Note however that, depending on the potential and the location, the "small component" can be much larger than the "large" one, e.g., for $p_{1/2}$ orbitals close to the nucleus and therefore the terms "upper" and "lower" component will be used here.

In the ESC scheme (elimination of the small component), Eq. (12-7) is directly substituted in the equation obtained from the 1st row of the matrix in (12-6). This yields the two-component ESC Hamiltonian:

$$\hat{\mathcal{H}}^{\mathrm{ESC}} = V + \frac{1}{2}(\vec{\sigma}\hat{\boldsymbol{p}})k(\vec{\sigma}\hat{\boldsymbol{p}}) \tag{12-9}$$

with k being defined in Eq. (12-8). In the nonrelativistic limit, for $c \to \infty$ one finds that $k \to 1$. We also note that $(\vec{\sigma}\hat{\boldsymbol{p}})^2 = \hat{\boldsymbol{p}}^2\,\mathbb{1}$, i.e., the nonrelativistic Schrödinger Hamiltonian is recovered from the ESC operator (12-9) as

$$\hat{\mathcal{H}}_{\mathrm{nrel}} = V + \frac{1}{2}(\vec{\sigma}\hat{\boldsymbol{p}})^2. \tag{12-10}$$

It is convenient to leave the spin-dependent terms in (12-10) for the derivation of certain nonrelativistic magnetic property operators where electron–spin interactions are needed. Although the ESC equation is a fully relativistic two-component equation, its Hamiltonian depends (via k) on the unknown energy E. It is therefore not suitable for linear variational calculations. For a description of alternative approaches to construct an exact two-component operator see the chapter by Barysz and [23–25].

In order to arrive at an energy-independent two-component equation, a [Foldy-Wouthuysen (FW)] transformation of $\hat{\mathcal{H}}_{\mathrm{D}}$ to block-diagonal form can be devised as

$$\hat{\mathcal{H}}^{\mathrm{FW}} = U\hat{\mathcal{H}}_{\mathrm{D}}U^{-1}. \tag{12-11}$$

In the case that the transformation makes $\hat{\mathcal{H}}^{\mathrm{FW}}$ block-diagonal and does not introduce an energy-dependence of the operator, this would completely uncouple the equations for the upper and the lower component and yield the desired two-component relativistic equation, along with $\chi = X\varphi$, an energy-independent relation between upper and lower component (see Eqs. (12-7,12-8)). U can be written in terms of X as shown in other chapters. For many-electron systems, the exact form of X and U and therefore the exact form of $\hat{\mathcal{H}}^{\mathrm{FW}}$ are not known. Different approximations for X yield different approximate two-component Hamiltonians in which the decoupling of the two components is not complete but the lower component is neglected anyway. These approximate two-component Hamiltonians are sometimes collectively denoted as "quasi relativistic".

A rather simple approach is to expand k in (12-7) to zeroth order in c^{-2}. The speed of light is large compared to velocities normally encountered in everyday life and therefore an expansion in inverse powers of c or c^2 may appear straightforward.[4] Letting $k \to 1$ yields $X \approx c\vec{\sigma}\hat{\boldsymbol{p}}/(2c^2)$, which results in the famous Pauli Hamiltonian [26] after carrying out the transformation (12-11) with $U(X)$:

[4] However, $c \approx 137$ atomic units and the Bohr "velocity" of an electron in the field of a nucleus with charge Z is equal to Z atomic units. Relativistic corrections, which are of order $(Z/c)^2$, cannot be expected to be small for atoms and molecules with heavy nuclei.

$$\hat{\mathcal{H}}_{\text{Pauli}} = \hat{\mathcal{H}}_{\text{nrel}} - \frac{\hat{\boldsymbol{p}}^4}{8c^2} - \frac{(\hat{\boldsymbol{p}}^2 V)}{8c^2} + \frac{\imath}{4c^2}\vec{\sigma}\big[(\hat{\boldsymbol{p}}V)\times\hat{\boldsymbol{p}}\big] \tag{12-12}$$

(here and elsewhere $\imath^2 = -1$). The second, third, and fourth term on the r.h.s. of (12-12) are the mass–velocity (MV), Darwin (DAR), and spin–orbit (SO) term, respectively. See, for instance, the chapter by Schwarz for further details. The MV, DAR, and so operators represent corrections of order c^{-2} to the nonrelativistic Hamiltonian. They modify the kinetic energy of the electron, the electron–nucleus potential, and introduce the coupling between spin- and angular momentum of an electron. Close to a nucleus the magnitude of the electron–nuclear attraction potential in V is very large (it goes to $-\infty$ for point-like nuclei). In this case the term $(V - E)/2c^2$ in k of Eq. (12-8) is not small and expanding k in Eq. (12-7) in powers of c^{-2} is not justified. As a result, the Pauli operator affords undesirable singularities. Moreover, it is not variationally stable and permits only a perturbational treatment to first order [27, 28]. Higher order contributions yield diverging terms. Variational computations based on the Pauli operator have been carried out, by using frozen cores and minimal basis sets in the core regions for valence orbitals, under which circumstances the variational instability can be kept somewhat under control. Such pseudo variational procedures are now deprecated. A *scalar relativistic* or *spin-free relativistic* approach is obtained by omitting the SO term in (12-12) and other two-component methods. This yields a one-component formalism analogous to the nonrelativistic scheme with pure α- and β- spin orbitals.[5]

A better justified expansion of k is used to construct the ZORA (zeroth order regular approximation) [29] or Chang–Pélissier–Durand [30] Hamiltonian. The ZORA operator can be obtained from the zeroth-order term of an expansion of k in Eq. (12-8) in powers of $E/(2c^2 - V)$, or by letting $X \approx \frac{c\boldsymbol{\sigma}\hat{\boldsymbol{p}}}{2c^2-V}$ as the main approximation when performing the transformation of Eq. (12-11). If we write k from Eq. (12-8) as

$$k = \left(1 - \frac{V-E}{2c^2}\right)^{-1} = \frac{2c^2}{2c^2 - V}\left(1 + \frac{E}{2c^2 - V}\right)^{-1} \tag{12-13}$$

the inverse $(\cdots)^{-1}$ may be expanded in a power series in $E/(2c^2 - V)$. The two-component ZORA Hamiltonian represents the zeroth-order term of this expansion, i.e., one uses $(1 + \text{small})^{-1} \approx 1$, leading to the Hamiltonian

$$\hat{\mathcal{H}}_{\text{ZORA}} = V + \frac{1}{2}(\vec{\sigma}\hat{\boldsymbol{p}})\mathcal{K}(\vec{\sigma}\hat{\boldsymbol{p}}) \tag{12-14a}$$

$$= V + \frac{1}{2}\hat{\boldsymbol{p}}\mathcal{K}\hat{\boldsymbol{p}} + \frac{\imath}{2}\vec{\sigma}\big[(\hat{\boldsymbol{p}}\mathcal{K})\times\hat{\boldsymbol{p}}\big] \tag{12-14b}$$

[5] It is also possible to separate off a spin–orbit part in the Dirac equation and in four-component perturbation theories which leaves two components to be determined.

where

$$\mathcal{K} = \frac{2c^2}{2c^2 - V} = \frac{1}{1 - V/(2c^2)}. \tag{12-15}$$

The third term in (12-14b) is the ZORA spin–orbit (SO) operator. The ZORA operator has the desirable feature of being variationally stable. The expansion of k in terms of $E/(2c^2 - V)$ is justified not only in regions where V is small compared to c^2 but also where V is very large in magnitude and negative, as long as E remains small. Therefore, the ZORA provides a good relativistic approximation for valence orbitals and outer core orbitals with comparatively small energy, even in the near-nucleus region of a heavy atom. For core orbitals of heavy atoms with very large E the ZORA affords substantial errors. Note the formal similarity to the ESC Hamiltonian in (12-9), with k replaced by $\mathcal{K}$. The nonrelativistic limit corresponds to letting $\mathcal{K} \to 1$ in which case we also have $(\hat{\boldsymbol{p}}\mathcal{K}) = 0$ and the SO operator vanishes. The ZORA operator affords contributions beyond c^{-2} in the relativistic perturbation order, yet some other contributions of order c^{-2} and higher are missing due to the approximate nature of the operator. For the limiting case of small V, one may further expand $\mathcal{K}$ in Eq. (12-15) in terms of $V/(2c^2)$ to obtain $\mathcal{K} \approx 1 + V/(2c^2)$. I.e., in the valence regions in atoms and molecules where the potential is small, $\hat{\boldsymbol{p}}\mathcal{K} \approx \hat{\boldsymbol{p}}V/2c^2$. By comparison with (12-12) one can see that in this case the ZORA spin–orbit operator becomes identical to the Pauli spin–orbit operator. One can further show that with $\hat{\boldsymbol{p}}\mathcal{K} \approx \hat{\boldsymbol{p}}V/(2c^2)$ the first-order relativistic correction to the orbital energy, $(1/2)\langle\psi_{\rm nrel}|\hat{\boldsymbol{p}}\mathcal{K}\hat{\boldsymbol{p}}|\psi_{\rm nrel}\rangle \approx (1/4c^2)\langle\psi_{\rm nrel}|\hat{\boldsymbol{p}}V\hat{\boldsymbol{p}}|\psi_{\rm nrel}\rangle$ is the same as that of the scalar relativistic part of the Pauli operator (MV + DAR). Close to a nucleus, the ZORA and Pauli operators differ substantially. Conceptually, the ZORA operator has the disadvantage of not being invariant with respect to a change of the origin of the energy scale (gauge invariance), as can be seen from the fact that only V but not $(V - E)$ occurs in the operator. The standard choice for the potential is $V(\boldsymbol{r}) \to 0$ for $\boldsymbol{r} \to \infty$. Some of the resulting problems can be circumvented by a "scaling" procedure or by the use of frozen core potentials or model potentials for the construction of $\mathcal{K}$. For example, the "sum-of-atomic-potentials approximation" (SAPA) [31] was shown to be a good approximation. In the SAPA one uses $V = \sum_A V^A$, where local atomic potentials V^A are taken, for instance, from density functional computations of the neutral atoms. It also simplifies ZORA computations since the operator does not have to be updated during SCF iterations.

Improved regular approximations have been developed to cure certain deficiencies of ZORA. Dyall et al. [32] introduced an "infinite order regular approximation" (IORA). IORA is not the same as an infinite-order expansion of Eq. (12-13). In contrast to ZORA, the IORA Hamiltonian includes all relativistic terms of order c^{-2} correctly. Unfortunately, the development effort in particular for magnetic properties appears to be more involved than when using the simpler ZORA operator [33]. To the author's knowledge no full spin–orbit implementation of magnetic properties has yet been reported at the IORA level.

A different way of transforming the Dirac Hamiltonian to two-component form is used in the Douglas–Kroll (DKH) method. Here, U in Eq. (12-11) is obtained via

subsequent transformations that uncouple the upper and lower components to some order n in c^{-2} which can be written as

$$U_n = \sqrt{1 + W_n^2} + W_n \quad \text{or} \quad U_n = e^{W_n} \tag{12-16}$$

or by using other possible parameterizations [34] for U, with W_n being anti-hermitian. For U_0, the FW transformation for the free electron is used. To higher orders, equations for W_n have to be solved in order to achieve further uncoupling. Already with U_1 (the DKH1 level), a large fraction of the relativistic effects on orbital energies is recovered. We refer the reader to, e.g., [19] for details and original references. For molecular property calculations, mainly those that depend on core orbitals or core tails of semi-core and valence orbitals it is better to go to DKH2 or beyond. In particular due to the work of Hess and coworkers, the DKH method has been established as a reliable tool in quantum chemistry for the computation of heavy element compounds. To some extent, the ZORA and the DKH method to lowest order yield quite comparable results for many molecular properties. As an advantage, the DKH method does not suffer from a gauge invariance problem and it is significantly more accurate for core orbitals. The improved accuracy comes at the expense of a somewhat more complicated formalism in particular when incorporating terms from external or internal magnetic fields. Fortunately, a number of developments for magnetic properties within the DKH framework have been reported in recent years [35–40].

In order to arrive at a relativistic perturbation theory that avoids the infinities of the Pauli Hamiltonian to higher orders, so-called "direct" or "Dirac" four-component perturbation theory (DPT) can be employed. By a change of metric between upper and lower components in the Dirac-equation (12-6), an expansion of the resulting four-component equation in powers of c^{-2} is straightforward and leads to non singular first- and higher order expressions for E and ψ [41,42]. A treatment of magnetic properties has been described in detail [43]. For an implementation of magnetic properties see. e.g., [44]. Perturbation expansions tend to become computationally rather expensive to evaluate in high order. At the same time first-order relativistic perturbation theory may not be sufficient to describe relativistic effects on properties of molecules with such "strongly relativistic" elements as, Au, Pt, Hg, Pb, etc. A variational procedure (Dirac, regular approximations, DKH, etc.) might be easier to implement and computationally less expensive than a higher-order perturbational method for relativistic effects.

As an alternative to the aforementioned methods which incorporate special relativity directly in the calculations, the use of relativistic effective core potentials (ECPs) also allows for consideration of relativistic effects in molecular computations. Inclusion of spin–orbit coupling is also possible in these methods. Extensive benchmark calculations [45] have shown that ECPs can yield very reliable properties of heavy element compounds. For genuine valence properties (see Section 12.2.7) where the core tails of the valence orbitals are not of concern pseudopotentials are straightforward to apply in property computations. For magnetic properties such as NMR shifts or spin–spin coupling the all-electron electronic structure near

the nuclei needs to be reconstructed. Some authors have taken such an approach in projector-augmented plane wave computations [46, 47]. In this chapter we will not discuss the use of ECP methods but focus on computational approaches where relativity is directly taken into consideration in the Hamiltonian.

As already mentioned, the potential V in the equations in this section might not simply refer to the external potential (e.g., V_{Ne}) for one-electron systems but to an effective many-electron potential. In this case, V appearing in the relativistic operators accounts in a mean-field sense for some relativistic effects on the electron–electron Coulomb repulsion $1/r_{ij}$. For instance, the explicit transformation of $1/r_{ij}$ to two-component form yields in order c^{-2} a two-electron Breit–Pauli spin–orbit and a two-electron Darwin operator. The transformation of the $\hat{\mathcal{H}}_{ij}^{\boldsymbol{B}}$ terms of Eq. (12-3) to two-component form yields further two-electron terms. Use of an effective (mean-field) electron-repulsion potential in V in the one-electron SO and Darwin operators accounts, to some extent, for some of the two-electron terms. Indeed, upon formal substitution of the potential V_N in the Pauli spin–orbit operator (12-12) by the electrostatic potential $V_{ij} = 1/r_{ij}$ between two electrons, one obtains the electron–electron SO operator

$$\hat{\mathcal{H}}^{eeSO} = \frac{l}{4c^2} \sum_{i \neq j} \vec{\sigma}_s(i) \big[(\hat{\boldsymbol{p}}_i V_{ij}) \times \hat{\boldsymbol{p}}_i \big] \tag{12-17}$$

(analogously for the two-electron Darwin operator). The correct derivation would involve an order-c^{-2} transformation of the DCB Hamiltonian to two-component form [16]. Using an effective potential in the one-electron kinetic energy and SO operators of other two-component Hamiltonians (e.g., ZORA) also yields mean-field approximations of their corresponding two-electron operators. Other two-electron terms have to be added explicitly, i.e., their contributions are not covered in a mean-field sense when an effective potential is used in the one-electron part of a two-component relativistic operator. For example the interaction of the spin of one electron with the orbital angular momentum of another electron (the spin–other orbit (SOO) interaction) is often considered in its Breit–Pauli form:

$$\hat{\mathcal{H}}^{SOO} = -\frac{i}{2c^2} \sum_{i \neq j} \vec{\sigma}_s(i) \big[(\hat{\boldsymbol{p}}_i V_{ij}) \times \hat{\boldsymbol{p}}_j \big] \tag{12-18}$$

Mean-field approximations to compute matrix elements of this operator efficiently have been successfully applied in molecular property computations as well [48].

12.2.2. Molecular Response Properties: A Brief Survey. Energy and Quasi-Energy Perturbations

Suppose that we have chosen a method to compute the energy of a molecule using a relativistic Hamiltonian. For simplicity, assume that a variational approach was

used, i.e., the energy is stationary with respect to small variations in the wavefunction (or the electron density in DFT). In practice, approximations have to be employed in the computations, for instance for treating the electron correlation problem. Moreover, the level of treating relativistic corrections has to be selected e.g., by adopting one of the methods discussed in Section 12.2.1. The result is a computed energy E incorporating relativistic effects, along with a relativistic wavefunction Ψ (for wavefunction based methods) or a set of relativistic molecular orbitals ψ_i (MOs) used to parameterize the electron density $\rho(\boldsymbol{r})$ in Kohn–Sham DFT. The computations generally involve some type of discretization of the wavefunction or the MOs, typically by adopting basis sets such as atomic orbital (AO) basis sets which are commonly used in quantum chemistry, or plane wave basis sets which are more common in solid state physics. In this case a set of wavefunction parameters or MO coefficients is computed.

We consider static (time independent) perturbations first. The following paragraphs provide a brief summary of variational perturbation theory: Consider the energy as a function of a set of perturbation parameters $\mathcal{F}_i$. These are the generalized field amplitudes that were mentioned in the Introduction. They represent the amplitudes of actual electric or magnetic fields perturbing the molecule, or they may represent some other perturbation parameter. Vector notation will be used to indicate a whole set of amplitudes simultaneously, i.e., $\boldsymbol{\mathcal{F}} = (\mathcal{F}_1, \mathcal{F}_2, \ldots)$. The wavefunction Ψ or the electron density ρ, as well as the Hamiltonian $\hat{\mathcal{H}}$ or the Kohn–Sham Fock operator, in general also depend on the $\mathcal{F}_i$. We will choose wavefunction notation from now on; similar derivative schemes can be devised within density functional theory. The unperturbed ground state is obtained for $\boldsymbol{\mathcal{F}} = 0$. To obtain the effects from the perturbations in various orders, the energy, wavefunction, and Hamiltonian are expanded in power series around the unperturbed ground state, i.e.,

$$E(\boldsymbol{\mathcal{F}}) = E^{(0)} + \sum_i E^{(\mathcal{F}_i)}\mathcal{F}_i + \frac{1}{2}\sum_{i,j} E^{(\mathcal{F}_i,\mathcal{F}_j)}\mathcal{F}_i\mathcal{F}_j + \cdots \tag{12-19a}$$

$$\Psi(\boldsymbol{\mathcal{F}}) = \Psi^{(0)} + \sum_i \Psi^{(\mathcal{F}_i)}\mathcal{F}_i + \frac{1}{2}\sum_{i,j} \Psi^{(\mathcal{F}_i,\mathcal{F}_j)}\mathcal{F}_i\mathcal{F}_j + \cdots \tag{12-19b}$$

$$\hat{\mathcal{H}}(\boldsymbol{\mathcal{F}}) = \hat{\mathcal{H}}^{(0)} + \sum_i \hat{\mathcal{H}}^{(\mathcal{F}_i)}\mathcal{F}_i + \frac{1}{2}\sum_{i,j} \hat{\mathcal{H}}^{(\mathcal{F}_i,\mathcal{F}_j)}\mathcal{F}_i\mathcal{F}_j + \cdots \tag{12-19c}$$

For each of these quantities $A = E$, Ψ, or $\hat{\mathcal{H}}$, the notation

$$A^{(0)} = A(\boldsymbol{\mathcal{F}})\Big|_{\boldsymbol{\mathcal{F}}=0}: \quad A^{(\mathcal{F}_i)} = \frac{\partial A(\boldsymbol{\mathcal{F}})}{\partial \mathcal{F}_i}\Big|_{\boldsymbol{\mathcal{F}}=0}; \quad A^{(\mathcal{F}_i,\mathcal{F}_j)} = \frac{\partial^2 A(\boldsymbol{\mathcal{F}})}{\partial \mathcal{F}_i \partial \mathcal{F}_j}\Big|_{\boldsymbol{\mathcal{F}}=0} \tag{12-20}$$

etc. has been used to indicate the various derivatives at the expansion point needed to construct the power series. For reasons of notational brevity a partial-derivative notation was adopted [49]. It implies that in molecular properties defined as energy derivatives any implicit dependencies on the perturbation via wavefunction parameters are to be resolved. Some authors prefer to use a total-derivative notation where necessary [50]. Another way of avoiding notational ambiguities in a variational formalism has been suggested by King and Komornicki [51] which allows to retain a partial-derivative notation throughout.

The various energy derivatives in (12-19a) are the molecular response properties of interest here. Expressions to compute them can be obtained formally by expanding the energy expectation value $E(\boldsymbol{\mathcal{F}}) = \langle\Psi(\boldsymbol{\mathcal{F}})|\hat{\mathcal{H}}(\boldsymbol{\mathcal{F}})|\Psi(\boldsymbol{\mathcal{F}})\rangle$ (assuming a normalized wavefunction) and collecting terms of various orders:

$$E^{(0)} = \langle\Psi^{(0)}|\hat{\mathcal{H}}^{(0)}|\Psi^{(0)}\rangle \quad \text{[no perturbation present]} \tag{12-21a}$$

$$E^{(\mathcal{F}_i)} = \langle\Psi^{(0)}|\hat{\mathcal{H}}^{(\mathcal{F}_i)}|\Psi^{(0)}\rangle + \langle\Psi^{(\mathcal{F}_i)}|\hat{\mathcal{H}}^{(0)}|\Psi^{(0)}\rangle + \langle\Psi^{(0)}|\hat{\mathcal{H}}^{(0)}|\Psi^{(\mathcal{F}_i)}\rangle \tag{12-21b}$$

$$E^{(\mathcal{F}_i,\mathcal{F}_j)} = \ldots \text{ higher order equations } \ldots$$

The equation by which the wavefunction and energy are determined (Schrödinger equation, Dirac equation, ZORA or DKH equation, ..., depending on the choice of relativistic level in $\hat{\mathcal{H}}$), may also be expanded in a similar way. I.e., taking $\hat{\mathcal{H}}\Psi = \Psi \cdot E$ and substituting for each quantity the expansions (12-19) yields the unperturbed wave equation and a set of *response equations* that determine the wavefunctions to various orders:

$$\hat{\mathcal{H}}^{(0)}\Psi^{(0)} = \Psi^{(0)} \cdot E^{(0)} \tag{12-22a}$$

$$\hat{\mathcal{H}}^{(0)}\Psi^{(\mathcal{F}_i)} + \hat{\mathcal{H}}^{(\mathcal{F}_i)}\Psi^{(0)} = \Psi^{(\mathcal{F}_i)} \cdot E^{(0)} + \Psi^{(0)} \cdot E^{(\mathcal{F}_i)} \tag{12-22b}$$

$$\ldots \text{ higher order equations } \ldots$$

The wavefunction is usually considered to be normalized at all levels of the perturbation treatment. Expanding Ψ in $\langle\Psi(\boldsymbol{\mathcal{F}})|\Psi(\boldsymbol{\mathcal{F}})\rangle = 1$ leads to constraints that needs to be considered when the response equations are solved:

$$\langle\Psi^{(0)}|\Psi^{(0)}\rangle = 1 \tag{12-23a}$$

$$\langle\Psi^{(0)}|\Psi^{(\mathcal{F}_i)}\rangle + \langle\Psi^{(\mathcal{F}_i)}|\Psi^{(0)}\rangle = 0 \tag{12-23b}$$

$$\ldots \text{ higher order equations } \ldots$$

For program developments of response solvers within a given approximation for relativity and electron correlation such constraints are conveniently worked into the formalism by setting up and minimizing a functional with Langrange multipliers (the "Langrangian"). In a framework of a non-variational theory (such as coupled-cluster methods or Moller–Plesset perturbation theory to treat the electron

correlation) there is typically a set of auxiliary equations that need to be solved to obtain the correct derivatives of a non-variational energy [50]. In DFT, the perturbation expansion is formally carried out for the electron density, the DFT energy, and the Kohn–Sham Fock operator. In practice, response equations are solved for the Kohn–Sham MOs or the Kohn–Sham density matrix. For properties that require the knowledge of the density matrix instead of the density (magnetic properties, typically, or the ground state kinetic energy) one should keep in mind that the Kohn–Sham DFT treatment represents an approximation as one does not know the density matrix of the interacting electronic system, only that of the noninteracting Kohn–Sham system. Presently not much attention is paid to this issue since other approximations in DFT, for instance those that lead to incomplete treatment of correlation and introduce self-interaction errors, remain major issues limiting the accuracy of DFT response computations. It is possible that once the Kohn–Sham noninteracting versus interacting kinetic energy becomes an accuracy bottleneck for DFT this issue will also have to be addressed in response property computations. At the time of writing this article, it is fair to state that DFT and TD–DFT are far from having reached that point.

The number of terms in the expressions of the energy derivatives in Eqs. (12-21) can be reduced significantly. For instance, substituting (12-22a) into (12-21b) and utilizing (12-23b) simplifies the equation for $E^{(\mathcal{F}_i)}$ to

$$E^{(\mathcal{F}_i)} = \langle \Psi^{(0)} | \hat{\mathcal{H}}^{(\mathcal{F}_i)} | \Psi^{(0)} \rangle \tag{12-24}$$

This is the famous *Hellmann–Feynman theorem* [52] for energy derivatives. The first derivative has the form of a simple expectation value for a property B, i.e., $B = \langle \Psi | \hat{B} | \Psi \rangle$. That is, the operator for property B can be obtained by considering a first-order derivative of the Hamiltonian with respect to a suitably defined perturbation parameter $\mathcal{F}_i$. Examples for such properties are the electric or magnetic dipole moment of a molecule, or higher order moments, or the energy gradient with respect to nuclear displacements (intramolecular force). Since the wavefunction in (12-24) is the zeroth-order wavefunction, i.e., the electronic structure is unperturbed, one may also call the property $B = E^{(\mathcal{F}_i)}$ a zeroth-order response property.[6]

Using similar substitutions that led to (12-24) considerably simplifies the expression for the second energy derivatives. Consider two different perturbations. Elimination of a number of terms that cancel each other or integrate to zero yields

$$\begin{aligned} E^{(\mathcal{F}_i,\mathcal{F}_j)} &= \langle \Psi^{(0)} | \hat{\mathcal{H}}^{(\mathcal{F}_i,\mathcal{F}_j)} | \Psi^{(0)} \rangle + \langle \Psi^{(\mathcal{F}_j)} | \hat{\mathcal{H}}^{(\mathcal{F}_i)} | \Psi^{(0)} \rangle + \langle \Psi^{(0)} | \hat{\mathcal{H}}^{(\mathcal{F}_i)} | \Psi^{(\mathcal{F}_j)} \rangle \\ &= \langle \Psi^{(0)} | \hat{\mathcal{H}}^{(\mathcal{F}_i,\mathcal{F}_j)} | \Psi^{(0)} \rangle + 2\,\mathrm{Re} \langle \Psi^{(\mathcal{F}_j)} | \hat{\mathcal{H}}^{(\mathcal{F}_i)} | \Psi^{(0)} \rangle \end{aligned} \tag{12-25}$$

[6] A serious technical limitation of using Eq. (12-24) and its derivatives is that, generally, in an incomplete basis the equation is only valid if the basis set is independent of the perturbation parameters. This is the case for standard AO basis sets and electric fields or nuclear spins, but not for nuclear-position derivatives if the AO basis is nucleus-centered as usual. We will keep using expressions that are valid for complete basis sets but keep in mind that the computation might involve additional terms to account for basis set incompleteness.

The same expression is also obtained from (12-24) by now considering each term to be a function of a second perturbation $\mathcal{F}_j$, expanding in a power series in that parameter, and collecting all terms of first order in $\mathcal{F}_j$. I.e., the expression (12-25) is also the *first* derivative of a molecular property B, described by an operator $\hat{B}$, with respect to $\mathcal{F}_j$, i.e., $B^{(\mathcal{F}_j)} = E^{(\mathcal{F}_i,\mathcal{F}_j)}$. This second energy derivative/first property derivative requires the linear terms of the wavefunction in $\mathcal{F}_j$, i.e., we may label it as a double perturbation of the energy or the *linear response* of the property B. Expressions for higher order derivatives can be derived in a similar way. The case studies of Section 12.3 will focus on first- and second-order derivative properties.

Equation (12-25) can be rewritten as follows: By using the complete set of unperturbed wavefunctions for ground and excited states as a basis set, the first order equation (12-22b) can be solved for $\Psi^{(\mathcal{F}_j)}$ in this basis. Substituting the result back into (12-25) yields a "sum-over-states" (SOS) equation for the second-order property:

$$E_n^{(\mathcal{F}_i,\mathcal{F}_j)} = \langle \Psi_n^{(0)} | \hat{\mathcal{H}}^{(\mathcal{F}_i,\mathcal{F}_j)} | \Psi_n^{(0)} \rangle + 2\,\mathrm{Re} \sum_{k \neq n} \frac{\langle \Psi_n^{(0)} | \hat{\mathcal{H}}^{(\mathcal{F}_j)} | \Psi_k^{(0)} \rangle \langle \Psi_k^{(0)} | \hat{\mathcal{H}}^{(\mathcal{F}_i)} | \Psi_n^{(0)} \rangle}{E_n - E_k} \tag{12-26}$$

where the property is computed for state number n (usually the ground state) and the sum runs over all other excited states. The Ramsey equation for NMR parameters [53] is an example of such a SOS formulation of linear response.

The $(2n + 1)$ theorem states that the availability of the nth order perturbation of the wavefunction or electron density allows the calculation of the perturbed energy up to order $2n + 1$. The simplifications leading to (12-24) and (12-25) are examples of this theorem where the nth order wavefunction derivative has been eliminated. Another useful theorem states that the perturbation order is arbitrary. For time-dependent perturbations as discussed below care must be taken to permutate the frequencies along with the field if a particular ordering of perturbation is desired [54].

In the case that relativistic effects on response properties are computed as a perturbation, this increases the required overall order of perturbation theory by one to include effects of order c^{-2}, by two to include effects of order c^{-4}, and so on. For literature on computations of relativistic effects on NMR parameters by perturbation theory the reader is referred to [55–58] as representative examples.

Often the perturbations of a molecule are considered to be *time-dependent* perturbations of an otherwise stationary system (usually assumed to be in its ground state). For example, the fields that are perturbing the molecule are oscillating with frequencies $\omega_i, \omega_j, \ldots$ and one is interested in the derivative properties as functions of the applied frequencies. A typical example is the polarizability (linear, and nonlinear) of a molecule where the frequency-dependence if often one of the prime interests. In the presence of a time-dependent perturbation the energy is not well

defined. One possible approach to computing properties within a derivative scheme that is similar to the one outlined above for static properties is to consider the *quasi-energy* Q as the basic quantity [54,59,60]. Writing the time-dependent ground state wavefunction as a product of a time-dependent phase factor and a time-periodic phase-free function Φ,

$$\Psi = \Phi \cdot \exp\left[-\imath \int_{t_0}^{t} dt' \cdot \langle \Phi | \hat{\mathcal{H}} - \imath \frac{\partial}{\partial t'} | \Phi \rangle\right] \tag{12-27}$$

and substituting this ansatz into the time-dependent wave-equation

$$\hat{\mathcal{H}}\Psi = \imath \frac{\partial}{\partial t}\Psi \tag{12-28}$$

yields an equation (depending on $\hat{\mathcal{H}}$) for Φ,

$$\left(\hat{\mathcal{H}} - \imath \frac{\partial}{\partial t}\right)\Phi = \Phi \cdot Q(t) \tag{12-29}$$

that resembles an eigenvalue equation for the operator $\hat{\mathcal{H}} - \imath\partial/\partial t$, and an expression for the *quasi-energy*

$$Q(t) = \langle \Phi | \hat{\mathcal{H}} - \imath \frac{\partial}{\partial t} | \Phi \rangle \tag{12-30}$$

that resembles an energy expectation value integral. The quasi-energy plays an analogous role as the energy of a stationary system. It is assumed, that Φ is normalized and in the unperturbed limit it satisfies the unperturbed time-independent equation

$$\hat{\mathcal{H}}^{(0)}\Phi^{(0)} = \Phi^{(0)} \cdot E^{(0)} \tag{12-31}$$

(i.e., $Q^{(0)} = E^{(0)}$ is static). Response properties can now be computed from the *time average* of the quasi energy. The wavefunction normalization is typically taken into consideration via a constraint $(\partial/\partial t)\langle \Phi | \Phi \rangle = 0; \langle \Phi^{(0)} | \Phi^{(0)} \rangle = 1$ which is used along with (12-30) in a quasi-energy Lagrangian $\tilde{Q}$ to be minimized (assuming variational methods, as already stated). If we imagine a periodic perturbation, the quasi-energy is a periodic function which oscillates around its time-average. This time-average is different from the ground state energy of the unperturbed system. The difference can be expanded into powers of the applied field amplitudes, as previously done for the energy, to extract frequency-dependent derivatives/response properties. The situation is illustrated qualitatively in Figure 12-1 for the situation of a second-order change in the quasi-energy due to an applied oscillating field of amplitude $\mathcal{F}$. For a zero-frequency perturbation, $Q^{(\mathcal{F}^2)} = E^{(\mathcal{F}^2)}$ would be static.

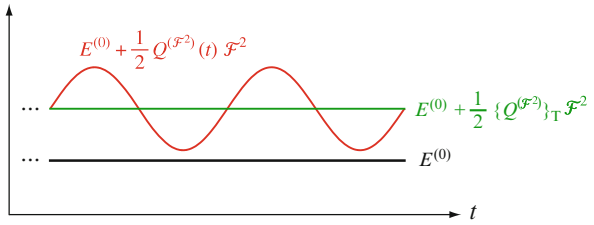

Figure 12-1. Stationary ground state energy of a system, $E^{(0)}$, and the quasi-energy of the perturbed system assuming a periodic perturbation to second order in the field strength $\mathcal{F}$. The perturbation is oscillating around the time average of $Q(t)$. For an electric field perturbation, $\{Q^{(\mathcal{F}^2)}\}_T$ is the negative dynamic polarizability

Suppose $Q(t)$ is periodic with a period of T. The time-average of the quasi-energy Lagrangian $\{\tilde{Q}\}_T$ is then

$$\{\tilde{Q}(t)\}_T = \frac{1}{T}\int_{-T/2}^{T/2} dt \cdot \tilde{Q}(t) \tag{12-32}$$

and response functions, instead of defined as energy derivatives, are obtained via computations of

$$\frac{\partial\{\tilde{Q}\}_T}{\partial\mathcal{F}_i(\omega_i)};\quad \frac{\partial^2\{\tilde{Q}\}_T}{\partial\mathcal{F}_i(\omega_i)\partial\mathcal{F}_j(\omega_j)};\quad \frac{\partial^3\{\tilde{Q}\}_T}{\partial\mathcal{F}_i(\omega_i)\partial\mathcal{F}_j(\omega_j)\partial\mathcal{F}_k(\omega_k)};\quad \cdots \tag{12-33}$$

which play a role analogous to the energy derivatives to various orders in (12-19a). Again, a partial derivative notation is used here but we keep in mind that implicit dependencies on the perturbation amplitudes, e.g., in the wavefunction parameters, need to be resolved when the results are computed. The response of the wavefunction parameters can be obtained from perturbation expansions of (12-28) or (12-29), collecting terms proportional to products of $\exp(\pm\imath\omega_i t)$ and solving the response equations as a function of the frequency/frequencies of the applied field(s). It would be beyond the scope of this chapter to provide details on how these equations are set up and solved, but we point out that similar techniques to develop response solvers for static properties can be applied to develop dynamic response equation solvers. For second-order properties, equations similar to the SOS equation (12-26) can be derived where in addition to energy differences the frequency also enters the denominator (and causing singularities where $\omega = (E_n - E_k)$). For further details see [61,62]. Regarding the time averaging: its main purpose is to provide a proper matching of frequencies for the applied fields to yield a nonzero response. As a mathematical consequence of the time-averaging, in the response functions of Eq. (12-33) the frequencies have to sum up to zero. The static limit is contained in this derivative scheme for all $\omega_i \to 0$.

12.2.3. Resonance: Computation of Excitation Spectra

It can be shown that a dynamic response property, as a function of the frequency ω of the applied perturbation, has to be complex. The real and the imaginary part form a Hilbert transform pair [63]. The imaginary part is associated with absorption processes, i.e., it yields some kind of spectrum, while the real part describes the dispersion of a refractive property.

As an example, consider the response of a molecule's dipole moment to an electric dipole field. The linear response is the (dynamic linear) dipole–dipole polarizability. If only the electronic degrees of freedom are considered in a computation one obtains the electronic dynamic polarizability of an atom or molecule, $\alpha(\omega)$. See Figure 12-2 for an illustration. If no damping is considered in the formalism, the frequency-dependent response is purely real except at the excitation frequencies ω_k. The real part becomes singular at the excitations much like a hypothetical undamped mechanical system such as a driven oscillator would experience a resonance catastrophe at its vibrational eigenfrequency. Right *at* the excitation frequencies, the response then switches from purely real to purely imaginary. The excitation spectrum would be obtained in form of δ-peaks. The singular behavior makes it impractical to compute $\alpha(\omega)$ and other dynamic response properties right at the excitations without using some form of damping. By introducing *damping* in the formalism (formally, for example, via finite lifetimes for excited states, or more pragmatically as a semi-empirical damping constant [65, 66]) one obtains nonsingular complex response functions instead. This is also analogous to a mechanical system such as a damped driven oscillator which shows large – but finite – oscillation amplitudes near its eigenfrequency. The imaginary part of the

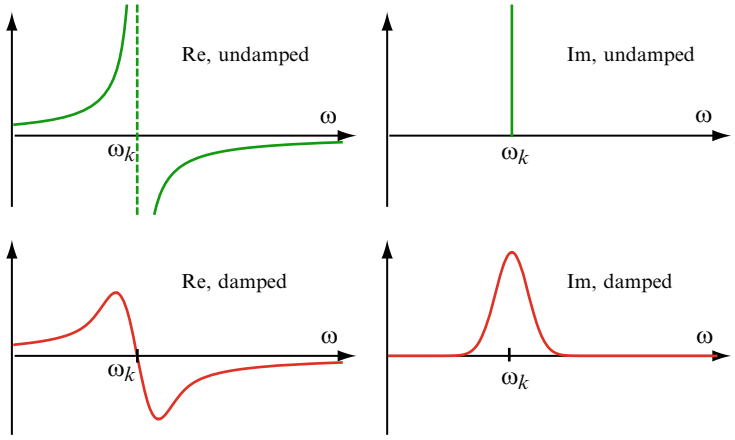

Figure 12-2. Qualitative behavior of a linear response function in the vicinity of an excitation with frequency ω_k. *Top:* no damping. The imaginary part would be a line-spectrum (δ-functions) with singularities in the real part at ω_k. *Bottom:* damped response corresponding to a Gaussian line shape of the imaginary part

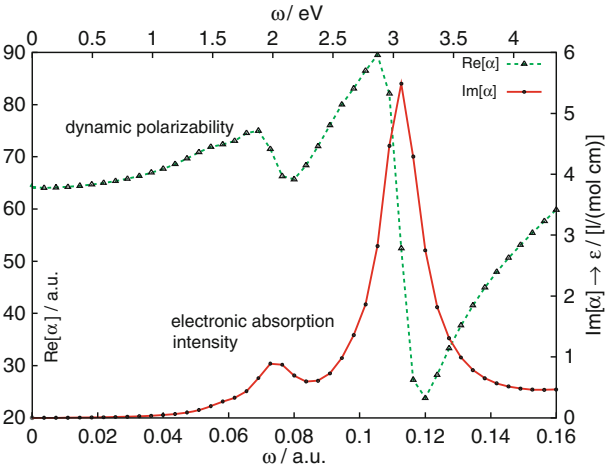

Figure 12-3. Real and imaginary part of the isotropic dipole polarizability $\alpha(\omega)$ of the Au_2 molecule, from ZORA spin–orbit DFT response computations with a local density functional and a damping constant of 0.2 eV [241]. $\mathrm{Im}[\alpha]$ converted to molar absorption coefficient

electronic polarizability, $\mathrm{Im}[\alpha]$, then describes the electronic absorption intensity in form of broadened absorption lines. Their width is proportional to the damping. Typically, the interest is in UV–Vis absorption but semi-core and core excitations can in principle also be modeled. $\mathrm{Im}[\alpha(\omega)]$ may be converted to the usual molar absorption coefficient used in spectroscopy. The case is illustrated in Figure 12-3 for the Au_2 molecule. DFT computations of the complex polarizability were performed with a semi-empirical damping parameter [66] to obtain a nonsingular response around the excitation energies and to obtain both the real and the imaginary part of $\alpha(\omega)$. The absorption spectrum is obtained from $\mathrm{Im}[\alpha]$ as a function of frequency. The real part shows the expected anomalous dispersion around the excitations, as illustrated – qualitatively – in Figure 12-2.

The singular behavior of undamped response functions offers an attractive way of computing excitation energies and transition moments directly. Of course, one way to compute excitation energies is to compute the wavefunction and energy for the ground state first, and next for a set of excited states, within a given computational approximation. Transition moments can subsequently be computed from these wavefunctions, and it is possible to compute excited states properties. This approach presently requires a wavefunction-based method since a generally applicable variational DFT method for excited states has not yet been developed.

Alternatively, one can take the following approach: An expression is derived for a dynamic response property such as $\alpha(\omega)$ within the desired formalism (Hartree–Fock, correlated wavefunction-based, DFT, within a given relativistic treatment) without considering damping terms. The equation is then transformed into a form that makes it obvious where the property becomes singular as a function of frequency. This is often accomplished by deriving the formal solution to the linear

response equations with the help of the inverse of a matrix or operator of the type $[E - \hat{A}]^{-1}$ (a Green's function) with $E = \hbar\omega$ and $\hat{A}$ being some operator. In a follow-up step this inverse is written in the basis of the complete set of eigenfunctions ϕ_i with eigenvalues f_i of the operator $\hat{A}$, which yields (for the discrete part of the spectrum of $\hat{A}$) a term of the type $[E - \hat{A}]^{-1} = \sum_i [\phi_i(\boldsymbol{\tau})\phi_i^*(\boldsymbol{\tau}')]/(E - f_i)$. This expression becomes singular if E equals one of the eigenvalues of $\hat{A}$ which means the eigenvalue f_i must be one of the excitation energies of the system. Therefore the solution to an eigenvalue-type problem $\hat{A}\phi_i = \phi_i \cdot f_i$ may provide access to the excitation energies. It is usually possible to obtain transition moments from the eigenvectors ϕ_i. Specific expressions for $\hat{A}$ depend on the computational method used and shall not be discussed here. It is important to keep in mind that, once the problem has been discretized, taking the response-singularity route to compute excitation energies offers computational advantages only in case the dimension of the problem at hand is less than, say, solving for the eigenvalues and eigenvectors of a Hamiltonian matrix directly. In exact theory different approaches are *formally* equivalent. However, one or another approach might offer distinct advantages for instance in the way how approximations can be introduced and how the solution can be constructed in approximate discretized form.

To summarize: The singularities (poles) of a response function can often be computed from an eigenvalue-type equation. In discretized form (basis set, numerical grid, or alike) the equation yields all excitation frequencies that are possible within a given basis set, as well as transition moments, at once. Implementations generally make use of Lanczos- or Davidson-type algorithms to select a range of (usually low lying) excitations to keep the computational effort manageable. This approach to obtain an excitation spectrum does not yield excited states wavefunctions or excited states densities. Properties of the excited states, or transition moments between excited states can be accessed by considering higher-order response functions. This route can also be used to obtain excitation energies and transition moments in DFT, which is formally a theory for the ground state only. Since the singularities are formally derived from considering where the response as a function of frequency becomes singular this approach has generally been associated with time-dependent DFT (TD–DFT). However, it should be kept in mind that the excitations are ultimately computed as properties of the *unperturbed* system and do not depend on the nature of the perturbation.

Presently, TD–DFT linear response excitation computations are the most suitable way to obtain first principles theory based spectra for larger molecules with heavy metal atoms due to its attractive balance of efficiency and accuracy. We note that the spectrum in Figure 12-3 which was obtained directly from $\mathrm{Im}[\alpha]$ on a frequency-grid agrees with the spectrum that is obtained from such a TD–DFT excitations computation with subsequent broadening of the absorption lines. For a reasonably small number of low-lying lying excitations (currently less than roughly a few hundred excitations in molecules with not more than a few hundred atoms) the TD–DFT/excitations approach tends to be more efficient for computing spectra. A frequency scan over $\mathrm{Im}[\alpha]$ might become more advantageous for very large

molecules with many excited states within a frequency window of interest [66], and it is also straightforward to apply to modeling core excitations. A combination of these methods can be used to obtain well-resolved dispersion curves for the real parts of a response function with a minimal number of frequency points [67].

For small heavy-atom molecules it is possible to apply very accurate wavefunction-based correlated methods for computing excitation spectra and excited states properties. Explicit computations of ground and excited states, as well as response-based methods involving static and time-dependent perturbations are in use here. For instance, equations-of-motion (EOM), propagator, and Green's function methods have been developed as general powerful tools in order to derive explicit expressions for perturbed properties within ab-initio wavefunction methods. For details see, e.g., [11, 68–70]. Unfortunately, these methods tend to scale unfavorably with system size.

The "singularity" route taken in DFT/TD–DFT for computations of excitation spectra can also be followed in Hartree–Fock theory. I.e., one applies time-dependent Hartree–Fock (TD–HF) perturbation theory and identifies singular terms as a function of frequency. It was shown that the approach is very similar to computing an excitation spectrum from singles – only configuration – interaction (CI singles, or CIS [71]). In general, TD–DFT is favored over TD–HF or CIS because it includes electron correlation so some extent. TD–DFT is formally exact for electric-field perturbations, but in practice approximations are of course made. Approximate TD–DFT with standard functionals is not without shortcomings and care should be taken that the computed response properties do not suffer from excessive self-interaction errors and problems that manifest in particular in charge-transfer excitations. Problems such as these can also severely impact static energy-derivative properties, in particular those of second and higher order. For a concise overview of TD–DFT related problems and how to avoid them see, for example, Ref [72].

12.2.4. Examples of Response Properties

Before investigating the various operators that are needed to compute energy derivative properties in relativistic and nonrelativistic theories, it is illustrative to take a look at a list of representative molecular properties that may be computed depending on the type and order of perturbation. In Table 12-1, various combinations of derivative parameters (generalized field amplitudes) are specified along with the type of molecular properties that can be obtained as a result. In many cases, the fields can be static or frequency dependent. Not all of the properties listed are observable. In some cases the property is only an observable under certain conditions, for example for a neutral molecule (dipole moment, etc.). The following notation is used: $R_A, R_B, \ldots$ = x, y, or z component of a nuclear position vector, nucleus A, B, …; $\mathcal{E}$ = electric field vector component (x, y, or z); $\mathcal{B}$ = magnetic field vector component; $m_A, m_B, \ldots$ = components of nuclear spin magnetic moment vectors; $\mathcal{S}$ = component of an effective electron spin vector (see Section 12.3.2),

Table 12-1 Some derivative properties that are of interest in chemistry

Derivative parameter(s)	Property that can be obtained from the derivative of the energy or quasi-energy
	First order derivatives
$\mathcal{E}$	Dipole moment
$\nabla\mathcal{E}$	Quadrupole moment
Q	Electric field gradient
$\mathcal{B}$	Magnetic moment
R_A	Intramolecular forces
c^{-2}	First-order relativistic energy correction
$\mathcal{B}$	EPR g-tensor if SO coupling is included in $\Psi^{(0)}$
m_A	EPR A-tensor if SO coupling is included in $\Psi^{(0)}$
	Second order derivatives
R_A, R_B	Harmonic force constants
	Harmonic vibrational frequencies
$\mathcal{E}$, $\mathcal{E}$	Dipole polarizability,
	Excitation energies, UV–VIS Intensities
	C_6 dispersion coefficients from imaginary ω
$\mathcal{E}$, R_A	Infrared intensities
$\mathcal{E}$, $\mathcal{B}$	Optical rotation, excitation energies, circular dichroism
$\mathcal{B}$, $\mathcal{B}$	Magnetizability, excitation energies,
	Magnetic transition moments
$\mathcal{B}$, m_A	NMR chemical shifts
m_A , m_B	NMR spin-spin coupling constants
$\mathcal{B}$, $\mathcal{S}$	EPR g-tensor if SO coupling not included in $\Psi^{(0)}$
m_A , $\mathcal{S}$	EPR A-tensor if SO coupling not included in $\Psi^{(0)}$
	Higher order derivatives
R_A, R_B, R_C,...	Cubic and higher order force constants
$\mathcal{E}$, $\mathcal{E}$, $\mathcal{E}$, ...	First and higher order hyperpolarizabilities,
	Two- and multi-photon absorption cross sections
$\mathcal{E}$, $\mathcal{E}$, R_A	Raman intensities
$\mathcal{E}$, $\mathcal{E}$, $\mathcal{B}$	Magneto-optical rotation, magneto-circular dichroism
$\mathcal{B}$, m_A, c^-2	Relativistic corrections to NMR chemical shifts to first order

Q = quadrupole moment. In some cases it is also specified what type of property can be obtained from studying the singularities of the response function (see Section 12.2.3). The list is not complete. It obviously includes a range of very important spectroscopic and optical properties.

12.2.5. Perturbation Operators

This section is intended to provide only a brief overview, mostly focussing on one-electron terms. As mentioned earlier, the ZORA operator will be used as an example to represent the class of approximate two-component methods. The usual way by

which to derive the perturbation operators in (12-19c) related to electromagnetic fields within a semi-classical treatment is to consider a scalar external potential ϕ and a vector potential $\boldsymbol{A}$. The scalar potential enters the Hamiltonian as $q_i\phi(\boldsymbol{r}_i)$ for each particle of charge q_i with position $\boldsymbol{r}_i$. Further, one makes the "minimal substitution" $\hat{\boldsymbol{p}}_i \rightarrow \hat{\boldsymbol{p}}_i - q_i\boldsymbol{A}$ for the momentum operator for each particle. Here, we will consider only the electronic degrees of freedom, with $q_i = -e$. The relation of ϕ and $\boldsymbol{A}$ with the electric field $\boldsymbol{E}$ and the magnetic field $\boldsymbol{B}$ are

$$\boldsymbol{E} = -\nabla\phi - \partial\boldsymbol{A}/\partial t, \tag{12-34a}$$

$$\boldsymbol{B} = \nabla \times \boldsymbol{A}. \tag{12-34b}$$

For a time-dependent electromagnetic wave with its electric and a magnetic field component the expressions for $\phi(\boldsymbol{r})$ and $\boldsymbol{A}(\boldsymbol{r})$ can be derived in closed form under certain circumstances. They are usually expanded around the coordinate origin $\boldsymbol{r} = 0$ to obtain perturbation operators of increasing powers of $\boldsymbol{r}$ (*multipole expansion*). This leads to much simplified operators for electromagnetic fields with optical, near IR, or larger wavelengths that are many times the dimension of the molecule. In this case the curvature radius of the field is large compared to the extension of the molecule and the multipole expansion can be truncated at low order.

For the properties of interest here, the fields arise from external time-dependent or time-independent electric and magnetic fields and from the magnetic fields associated with the spin magnetic moments of the nuclei and of the electrons. A multitude of terms arise upon consideration of all these effects in a four-component relativistic many-electron Hamiltonian after transformation to two-component form [11, 16, 73]. We will not consider all of these terms but mainly list expressions for some important one-electron operators and study the differences between the four-component formalism, an approximate two-component method, and the nonrelativistic limit.

Before proceeding, we note that a given magnetic field does not uniquely define the vector potential: adding the gradient ∇f of any scalar function $f(\boldsymbol{r})$ to $\boldsymbol{A}$ does not affect $\boldsymbol{B}$, because $\nabla \times \nabla f(\boldsymbol{r}) = 0$. Therefore $\boldsymbol{A}$ is undetermined up to adding ∇f. Often, f is chosen such that $\nabla\boldsymbol{A} = 0$ (Coulomb gauge). A different gauge of $\boldsymbol{A}$ can, e.g., be chosen implicitly by adopting a different origin for the coordinate representation of $\boldsymbol{A}$. For a range of variationally determined wavefunctions in a complete basis the calculated properties would not depend on the chosen gauge. This is not generally true for incomplete basis sets [11] and care needs to be taken that origin independent results are computed. Presently, the standard remedy is to adopt a "gauge including atomic orbital" (GIAO) basis set (also frequently referred to as "London AOs") [74, 75]. This eliminates the origin dependence in variational methods such as Hartree–Fock, Kohn–Sham DFT or multiconfigurational SCF (MCSCF), and often also leads to improved basis set convergence of the response property. Other methods to cure the origin problem are also in use, among them the "individual gauge of localized orbitals" (IGLO) [76], a "localized orbital/local origin" (LORG) [77], or applying a "continuous set of gauge transformations"

(CSGT) [78]. Magnetic properties computed with non-variational methods such as coupled cluster theory do not in general become origin invariant in a GIAO basis [79]. Typically, the origin problem alleviates when larger basis sets are employed. Sometimes, an origin problem is eliminated by using the "velocity gauge" relation between electronic momentum and electronic dipole operator. By using this trick, nuclear magnetic shielding constants can be made origin-independent [80, 81] but unfortunately the individual shielding tensor elements are still origin dependent. The velocity gauge is also popular for computations of optical rotation [79].

Applying the minimal substitution in the nonrelativistic one-electron part of the Schrödinger Hamiltonian of Eq. (12-2) and adding the external electric potential term yields the following perturbation terms in addition to $\hat{\mathcal{H}}^{(0)}$ (because the Hamiltonian contains $\hat{\boldsymbol{p}}^2$ there are no terms higher than second order in $\boldsymbol{A}$)

$$\hat{\mathcal{H}}^{\text{pert}}_{\text{nrel}} = \frac{1}{2}\left(\boldsymbol{A}\,\hat{\boldsymbol{p}} + \hat{\boldsymbol{p}}\boldsymbol{A} + i\vec{\sigma}[\hat{\boldsymbol{p}} \times \boldsymbol{A} + \boldsymbol{A} \times \hat{\boldsymbol{p}}] + \boldsymbol{A}^2\right) - \phi(\boldsymbol{r}). \tag{12-35}$$

We point out that these are the one-electron terms only. When considering perturbations by magnetic fields the expressions linear in $\boldsymbol{A}$ are usually called "paramagnetic" terms, while those proportional to $\boldsymbol{A}^2$ are called "diamagnetic" terms. The spin-dependent terms (terms containing $\vec{\sigma}$) are only obtained if the substitution $\hat{\boldsymbol{p}} \rightarrow \hat{\boldsymbol{p}} + \boldsymbol{A}$ is made in the nonrelativistic limit written as in Eq. (12-10) using $(\vec{\sigma}\,\hat{\boldsymbol{p}})^2$ instead of $\hat{\boldsymbol{p}}^2$ [see the text following Eq. (12-9). The explicit form of the operators depends on the type of perturbation; some frequently used expressions will be given below.

Electric property operators for static fields are obtained from the $-\phi$ term and, if needed, additional terms involving the gradient and higher derivatives of the electric field. Due to the linearity only terms involving first-order operator derivatives need to be considered when evaluating electric properties. Magnetic fields or time-dependent electromagnetic waves involve the vectorpotential $\boldsymbol{A}$. For first-derivative magnetic properties only the Hamiltonian terms linear in $\boldsymbol{A}$ are required. For second-derivative properties, one needs the linear terms in the Hamiltonian to determine $\Psi^{(\mathcal{F}_i)}$ for one of the perturbations [see Eq. (12-22b) from which the wavefunction is determined] and the pertubed Hamiltonian $\hat{\mathcal{H}}^{(\mathcal{F}_i)}$ is needed to compute the $2\,\text{Re}\langle\Psi^{(\mathcal{F}_j)}|\hat{\mathcal{H}}^{(\mathcal{F}_i)}|\Psi^{(0)}\rangle$ part of the response.[7] Hamiltonian terms that are bilinear in $\boldsymbol{A}$ enter the $\langle\Psi^{(0)}|\hat{\mathcal{H}}^{(\mathcal{F}_i,\mathcal{F}_j)}|\Psi^{(0)}\rangle$ (diamagnetic) part of a second-derivative property. Higher-order properties require linear and, if applicable, bilinear Hamiltonian terms. Depending on the overall order of perturbation and the expression used to compute the result, higher-order wavefunction perturbations might need to be computed as well.

[7] For magnetic properties, this part is the paramagnetic term and $\langle\Psi^{(0)}|\hat{\mathcal{H}}^{(\mathcal{F}_i,\mathcal{F}_j)}|\Psi^{(0)}\rangle$ which involves the $\boldsymbol{A}^2$ contribution is the diamagnetic term.

Now consider special relativity: Applying the minimal substitution in the one-electron part of the Dirac Hamiltonian (12-3) yields the following perturbation terms in addition to $\hat{\mathcal{H}}_{\mathrm{D}}^{(0)}$:

$$\hat{\mathcal{H}}_{\mathrm{D}}^{\mathrm{pert}} = c\vec{\alpha}\,\boldsymbol{A}(\boldsymbol{r}) - \phi(\boldsymbol{r}) \tag{12-36}$$

Note that there is no operator bilinear in $\boldsymbol{A}$ present. Consider a second-order magnetic perturbation: The nonrelativistic limit as well as relativistic two-component Hamiltonians yield a diamagnetic term if standard gauges for $\boldsymbol{A}$ are chosen. This term should be contained in order c^0 in a four-component result obtained with (12-36) but a corresponding bilinear operator is not present. It has been shown that a diamagnetic contribution to a second-order derivative property is indeed contained in the four-component scheme. It has been numerically traced back to the contributions from negative energy eigenfunctions of $\hat{\mathcal{H}}_{\mathrm{D}}$ if the complete spectrum of this operator is used as a basis set to represent $\Psi^{(\mathcal{F}_j)}$ in Eq. (12-25) [82], even though there is only a paramagnetic perturbation operator (12-36). The role of the negative energy states for diamagnetic shielding has also been emphasized by Pyykkö in early theoretical work on NMR chemical shifts [83]. Recent work by Liu et al. has aimed at ways to simplify the four-component treatment of nuclear magnetic shielding [84, 85]; the issue of diamagnetic terms has been addressed in some detail in these works. See also [86]. When a matrix formulation in a basis set or transformations at the operator level are employed, diamagnetic terms may appear explicitly if the formalism is suitably chosen [84, 85].

Spin-dependent terms arise via the action of the Dirac matrix $\vec{\alpha}$ in (12-36) on the four-component wavefunction. An example of how the nonrelativistic spin-dependent terms are obtained from the $c \to \infty$ limit of the four-component perturbation operator will be given below.

As it was shown in Section 12.2.1 the transformation from four- to two-component form involves the momentum operator (see Eq. (12-7)). Minimal substitution $\hat{\boldsymbol{p}} \to \hat{\boldsymbol{p}} + \boldsymbol{A}$ in the Dirac equation yields operators upon transformation to two-component form that include magnetic-field dependent terms (because of $\hat{\boldsymbol{A}}$) and sometimes the transformed magnetic perturbation operators can be identified straightforwardly (e.g., in the ZORA case which will be discussed below). In two-component formalisms, the effects of relativity in the perturbation operators tend to show up in two ways: First, spin-dependent terms are obtained straightforwardly. Second, compared to the nonrelativistic limit the operators are modified – sometimes severely – typically in the near-nucleus regions where these modifications take care of mass–velocity and other effects. One might think of those relativistic modifications as "kinematic terms" that take care of special relativity in regions where the electrons are very fast (near the nuclei). One may also conceptualize these modifications as picture change effects. The presence of $-\phi$ from external perturbing fields in the Dirac Hamiltonian gives rise to additional terms upon transformation to two-component form. Note that $-\phi$ appears both in the Dirac and in the nonrelativistic Hamiltonian. In two-component formalisms, the leading term is also $-\phi$, with

additional picture change corrections to the operator of order c^{-2} (which therefore vanish again when $c \to \infty$).

Consider the ZORA Hamiltonian as an example. Upon the substitution $\hat{\boldsymbol{p}} \to \hat{\boldsymbol{p}} + \boldsymbol{A}$ and consideration of a perturbing electric potential one obtains

$$\hat{\mathcal{H}}_{\text{ZORA}} = V + \frac{1}{2}[\vec{\sigma}_s(\hat{\boldsymbol{p}} + \boldsymbol{A})]\mathcal{K}[\vec{\sigma}_s(\hat{\boldsymbol{p}} + \boldsymbol{A})] - \phi + \text{p.c.t.} \tag{12-37}$$

where "p.c.t." denotes additional *p*icture *c*hange *t*erms of order c^{-2} resulting from the transformation of the electric potential to two component form (there is an electric field-dependence of $\mathcal{K}$) [87]. Perturbations of the metric are neglected here for brevity. By using $(\vec{\sigma}_s\hat{\boldsymbol{A}})(\vec{\sigma}_s\hat{\boldsymbol{B}}) = \hat{\boldsymbol{A}}\,\hat{\boldsymbol{B}} + i\vec{\sigma}_s \cdot \hat{\boldsymbol{A}} \times \hat{\boldsymbol{B}}$ for general vector operators $\hat{\boldsymbol{A}}$, $\hat{\boldsymbol{B}}$, Eq. (12-37) may be expanded as follows:

$$\hat{\mathcal{H}}_{\text{ZORA}} = V + \frac{1}{2}\Big(\hat{\boldsymbol{p}}\mathcal{K}\hat{\boldsymbol{p}} + i\vec{\sigma}_s(\hat{\boldsymbol{p}}\mathcal{K}) \times \hat{\boldsymbol{p}} \tag{12-38a}$$

$$+ \hat{\boldsymbol{p}}\mathcal{K}\boldsymbol{A} + \boldsymbol{A}\mathcal{K}\hat{\boldsymbol{p}} + i\vec{\sigma}_s[\hat{\boldsymbol{p}} \times (\mathcal{K}\boldsymbol{A}) + \boldsymbol{A} \times (\mathcal{K}\hat{\boldsymbol{p}})] \tag{12-38b}$$

$$+ \mathcal{K}\boldsymbol{A}^2\Big) - \phi + \text{p.c.t.} \tag{12-38c}$$

The first row, (12-38a), is the field-free ZORA operator $\hat{\mathcal{H}}^{(0)}_{\text{ZORA}}$ given in Eq. (12-14b). The remain terms arise from the presence of a field are therefore the ZORA perturbation terms:

$$\hat{\mathcal{H}}^{\text{pert}}_{\text{ZORA}} = \frac{1}{2}\Big([\hat{\boldsymbol{p}}\mathcal{K}\boldsymbol{A} + \boldsymbol{A}\mathcal{K}\hat{\boldsymbol{p}} + i\vec{\sigma}_s[\hat{\boldsymbol{p}} \times (\mathcal{K}\boldsymbol{A}) + \boldsymbol{A} \times (\mathcal{K}\hat{\boldsymbol{p}})] + \mathcal{K}\boldsymbol{A}^2\Big)$$

$$-\phi + \text{p.c.t.} \tag{12-39}$$

Just like in the nonrelativistic formalism, when using standard gauge choices for $\boldsymbol{A}$ the two-component method affords paramagnetic and diamagnetic terms when magnetic properties are considered. We can also see that the nonrelativistic limit, Eq. (12-35), is smoothly obtained from (12-39) when letting $\mathcal{K} \to 1$ (p.c.t. are of order c^{-2} and vanish in the nonrelativistic limit). The fact that the function $\mathcal{K}$ acts as a "kinematic correction factor" in the vicinity of the nuclei is seen in Figure 12-4 where $\mathcal{K}$ is plotted as a function of electron–nucleus distance for the Coulomb potential of a $Z = 50$ point nucleus. In regions of weak potential $\mathcal{K}$ is very close to unity but it drops to zero at the nucleus where the potential approaches $-\infty$. It is there that the ZORA and the nonrelativistic operators differ the most. For an extended nucleus $\mathcal{K}$ remains finite but it is very small at small r.

For many other types of variationally stable two-component relativistic Hamiltonians the operators are obtained via a series of successive transformations (typically implemented in discretized form as a series of matrix transformations), not as a closed form expression. In the presence of fields, modified transformations

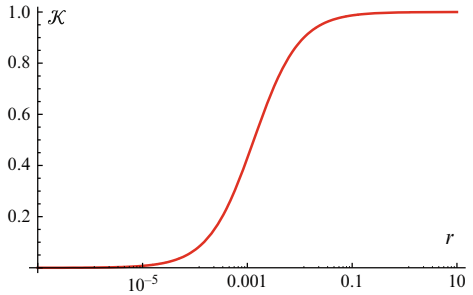

Figure 12-4. The function $\mathcal{K}$ of the ZORA operator plotted versus the electron–nucleus distance r for a Coulomb potential of a bare point nucleus of charge $Z = 50$, in atomic units. Note the logarithmic scale of the abscissa. For $\mathcal{K} \to 1$ the perturbation operators of Eq. (12-39) become equal to the nonrelativistic operators of Eq. (12-35)

have to be carried out to obtain the perturbation operators to account for the field effects. For examples of such transformations that were implemented within the DKH and IORA frameworks see, for example [33, 36–38, 40, 88]. We also point to work by Fukui et al. [40, 89] who reported a NMR nuclear shielding implementation based on the infinite-order Foldy–Wouthuysen transformation proposed by Barysz and Sadlej which is described in detail in another chapter. As an example, for comparison with ZORA where the relativistic corrections in the operator show up as relativistic "kinematic factors" $\mathcal{K}$ in the operators (which approach unity in the nonrelativistic limit), it is interesting to take a look at the magnetic perturbation operators in the DKH formalism. The discussion below closely follows the derivation of Melo et al. [38]. Let ($m_e = 1$)

$$E_p = c\sqrt{p^2 + c^2}; \quad K = \sqrt{\frac{E_p + c^2}{2E_p}}; \quad R = \frac{c}{E_p + c^2} \tag{12-40}$$

The perturbation operator in the DKH1 scheme (first-order DKH) is then [38]

$$\hat{H}^{\text{pert}}_{\text{DKH1}} = c\left(K[R\hat{\boldsymbol{p}}\boldsymbol{A} + \hat{\boldsymbol{p}}\boldsymbol{A}R]K + i\boldsymbol{\sigma}K[R\hat{\boldsymbol{p}} \times \boldsymbol{A} + \hat{\boldsymbol{p}} \times \boldsymbol{A}R]K\right) - \phi + \text{p.c.t.} \tag{12-41}$$

Here, K and R can also be thought of kinematic factors modifying the operators compared to the nonrelativistic limit. Because of the frequent occurrence of p^2 the DKH operators are usually computed in a basis where the operator p^2 is diagonal and subsequently transformed back to the original basis representation. A diamagnetic term of order $\boldsymbol{A}^2$ is not obtained at the DKH1 level. In the nonrelativistic limit, $E_p \to c^2$, $K \to 1$, $R \to 1/(2c)$, and the paramagnetic part of $\hat{H}^{\text{pert}}_{\text{nrel}}$ is obtained. The expressions for DKH2 are lengthier but also contain similar kinematic factors. At the DKH2 level a diamagnetic operator is obtained which

has the nonrelativistic operator $\boldsymbol{A}^2$ as its $c \to \infty$ limit. See [36, 38] for explicit expressions of the DKH2 perturbation operators and further details.

The Pauli operator affords severe singularities for Coulomb potentials (point nuclei) and the magnetic perturbation operators associated with it are not so well-behaved either. Within a first-order perturbation scheme to treat relativity, response functions for molecular properties can still be calculated in many cases. The perturbation operators can be derived analogous to the ZORA case, i.e., after minimal substitution in the Dirac Hamiltonian the resulting operator is transformed to the approximate two-component form. Some of the operators that arise from this transformation are obtained when substituting $\hat{\boldsymbol{p}} \to \hat{\boldsymbol{p}} + \boldsymbol{A}$ in the one-electron Pauli Hamiltonian, Eq. (12-12). An extensive list of operators relevant for magnetic resonance has been given by Manninen et al. [56]. See also the books by Moss [16] and Harriman [73].

Specific forms of the operators needed for computations of response properties depend on the type of perturbation. For electromagnetic fields, a low-order truncation of the multipole expansion yields for the scalar potential

$$\phi(\boldsymbol{r}) = -\boldsymbol{F} \cdot \boldsymbol{r} - \frac{1}{2}\boldsymbol{r}^T \mathbb{G} \boldsymbol{r} \tag{12-42}$$

where $\boldsymbol{F}$ and $\mathbb{G}$ are the electric field vector and the electric field gradient tensor at the coordinate origin, and superscript T indicates vector/matrix transposition. The electric field may be static or time dependent and characterized by an amplitude parameter $\mathcal{F}$ (which is then chosen as the perturbation parameter), a frequency ω, a wave vector $\boldsymbol{k}$, and a Jones vector which defines the wave's polarization. For a homogeneous static field there is only the dipole term present. As already mentioned, the potential ϕ enters the one-electron potential energy part of the Hamiltonian by multiplying with the electron charge $-e = -1$ au. Often, even for time-dependent fields only the first term, the electric dipole term, is retained when electric properties are to be evaluated which is justified in the limit of long wavelengths.

The vector potential for static or time-dependent electromagnetic fields may be chosen as

$$\boldsymbol{A}(\boldsymbol{r}) = -\frac{1}{2}\boldsymbol{r} \times \boldsymbol{B} \tag{12-43}$$

which, for electromagnetic waves corresponds to the lowest-order term of the multipole expansion of the vector potential around the origin. $\boldsymbol{B}$ is the static or time-dependent magnetic field which may also be characterized by an amplitude parameter $\mathcal{F}$, a frequency ω, a wave vector $\boldsymbol{k}$, and a Jones vector. The vector potential (12-43) is of the same order in the multipole expansion as (12-42). For a homogeneous static field the higher order terms vanish.

The vector potential associated with a point magnetic dipole $\boldsymbol{m}$ (e.g., a nuclear spin magnetic dipole moment) is given by

$$\boldsymbol{A}(\boldsymbol{r}) = \frac{1}{c^2}\frac{\boldsymbol{m}\times\boldsymbol{r}}{r^3} \tag{12-44}$$

where the dipole is located at $\boldsymbol{r} = 0$. For nuclear magnetic properties, for example, one needs the vector potential associated with the set of nuclear magnetic dipoles,

$$\boldsymbol{A}^{\mathrm{nuc}} = \sum_{A}^{\mathrm{Nuclei}} \boldsymbol{A}_A^{\mathrm{nuc}}(\boldsymbol{r}) = \frac{1}{c^2}\sum_{A}^{\mathrm{Nuclei}} \frac{\boldsymbol{m}_A\times\boldsymbol{r}_A}{r_A^3} \tag{12-45}$$

From (12-43), the corresponding magnetic field is $\boldsymbol{B}^{\mathrm{nuc}} = \nabla\times\boldsymbol{A}^{\mathrm{nuc}}$. If an extended nucleus is considered one needs to adopt a model for the shape of the nucleus. For instance, given its charge density ϱ_A^{nuc}, the vector potential is

$$\boldsymbol{A}_A^{\mathrm{nuc}}(\boldsymbol{r}) = -\frac{1}{c^2}\boldsymbol{m}_A\times\nabla\int d^3R\cdot\frac{\varrho_A^{\mathrm{nuc}}(\boldsymbol{R})/Z_A}{|\boldsymbol{r}-\boldsymbol{R}|} \tag{12-46}$$

We assume point nuclei later on for simplicity but keep in mind that finite-nucleus correction terms may be included in computations of "nuclear" properties by adopting a nuclear charge model and using Eq. (12-46) instead of (12-45). Note that (12-46) yields (12-45) for a point charge density $\varrho_A^{\mathrm{nuc}} = Z_A\cdot\delta(\boldsymbol{R}-\boldsymbol{R}_A)$. The consideration of effects from a finite nuclear volume on the hyperfine structure of heavy atoms has a long history. Conceptually, one may distinguish between two types of finite nucleus effects: One type stems from the change in the electronic structure due to the finite nuclear volume [90, 91] which is greatly amplified by relativistic effects. In DFT calculations, this concerns mainly the near nuclear tails of the Kohn–Sham orbitals. In response property calculations another effect arises from modifications of the perturbation operators due to the finite distribution of the nuclear current density causing the nuclear magnetic moment. Finite nucleus effects on hyperfine structure have been discussed in the literature as early as the nineteen thirties [92–99]. Consideration of finite nuclear current–density distributions affecting the hyperfine structure of heavy elements dates back to early nineteen fifties publications by A. Bohr and V. F. Weisskopf [95,96]. See also [97]. Recently, there have been two publications specifically devoted to computations finite nucleus effects in relativistic molecular property calculations, one on hyperfine coupling constants [100] and one on NMR spin–spin coupling [64]. Both used a spherical Gaussian nuclear model [44]

$$\rho_A^{\mathrm{Gauss}}(\boldsymbol{R}) = Z_A\left(\frac{\xi_A}{\pi}\right)^{3/2} e^{-\xi_A|\boldsymbol{R}-\boldsymbol{R}_A|^2} \tag{12-47}$$

where the parameter ξ_A defines the radial extension of the nucleus. The finite nucleus magnetic vector potential is in this model

$$\boldsymbol{A}_A^{\text{Gauss}} = \frac{1}{c^2}\frac{\boldsymbol{\mu}_A \times \boldsymbol{r}_A}{r_A^3} \cdot P(\tfrac{3}{2}, \tilde{r}_A^2) \tag{12-48}$$

where $\tilde{r}_A = \sqrt{\xi} r_A$. Further, P is the lower incomplete gamma function ratio

$$P(a,x) = \frac{1}{\Gamma(a)} \int_0^x dt\, t^{a-1} e^{-t} \tag{12-49}$$

which has the effect of 'damping' the point nucleus vector potential at distances very close to the nuclear radius [64]. At larger radii, $P(\frac{3}{2}, \tilde{r}_A^2)$ approaches one. Its effect is qualitatively somewhat similar to how the function $\mathcal{K}$ in Figure 12-4 regularizes the relativistic ZORA Hamiltonian.

We shall now provide expressions for some important operators that are relevant for many computations of molecular response properties. We begin with their non-relativistic form. The electronic Hamiltonian term due to a homogeneous electric field $\boldsymbol{F}$ (or, for inhomogeneous fields, to first order in the multipole expansion) is described by the one-electron operator $-\phi$ which therefore yields

$$\hat{\mathcal{H}}_{\text{nrel}}^{\text{elec}} = -\boldsymbol{F} \cdot \hat{\boldsymbol{d}}, \tag{12-50}$$

where $\hat{\boldsymbol{d}} = -\boldsymbol{r}$ is the electric dipole moment operator for an electron. Considering magnetic fields from the nuclear spins (needed for NMR and for EPR hyperfine tensors, for instance) and from an external field, upon substitution of $\boldsymbol{A} = \boldsymbol{A}^{\text{ext}} + \boldsymbol{A}^{\text{nuc}}$ into (12-35), with $\boldsymbol{A}^{\text{ext}}$ from Eq. (12-43) and $\boldsymbol{A}^{\text{nuc}}$ from Eq. (12-45), yields the magnetic perturbation operators

$$\hat{\mathcal{H}}_{\text{nrel}}^{\text{mag}} = \hat{\mathcal{H}}^{DM} + \hat{\mathcal{H}}^{OZ} + \hat{\mathcal{H}}^{SZ} + \hat{\mathcal{H}}^{OP} + \hat{\mathcal{H}}^{DS} + \hat{\mathcal{H}}^{FC} + \hat{\mathcal{H}}^{SD} + \hat{\mathcal{H}}^{OD} \tag{12-51}$$

with

$$\hat{\mathcal{H}}^{DM} = \frac{1}{4}(\boldsymbol{r} \times \boldsymbol{B}) \cdot (\boldsymbol{r} \times \boldsymbol{B}) \tag{12-52a}$$

$$\hat{\mathcal{H}}^{OZ} = -\hat{\boldsymbol{\mu}}_e \cdot \boldsymbol{B} = -\frac{1}{2}(\boldsymbol{r} \times \hat{\boldsymbol{p}}) \cdot \boldsymbol{B} \tag{12-52b}$$

$$\hat{\mathcal{H}}^{SZ} = -\hat{\boldsymbol{\mu}}_s \cdot \boldsymbol{B} = \frac{1}{2}\vec{\sigma}_s \cdot \boldsymbol{B} \tag{12-52c}$$

$$\hat{\mathcal{H}}^{OP} = \frac{1}{c^2}\sum_A \boldsymbol{m}_A\big(\frac{\boldsymbol{r}_A}{r_A^3} \times \hat{\boldsymbol{p}}\big) \tag{12-52d}$$

$$\hat{\mathcal{H}}^{DS} = \frac{1}{2c^2}\sum_A \left[(\boldsymbol{m}_A \cdot \boldsymbol{B})(\frac{\boldsymbol{r}_A}{r_A^3} \cdot \boldsymbol{r}) - (\boldsymbol{m}_A \cdot \boldsymbol{r})(\boldsymbol{B} \cdot \frac{\boldsymbol{r}_A}{r_A^3}) \right] \tag{12-52e}$$

$$\hat{\mathcal{H}}^{FC} + \hat{\mathcal{H}}^{SD} = \frac{1}{2}\vec{\sigma}_s \cdot \boldsymbol{B}^{\text{nuc}} = \frac{1}{2c^2}\sum_A \vec{\sigma}_s \left[\boldsymbol{m}_A(\nabla \cdot \frac{\boldsymbol{r}_A}{r_A^3}) - (\boldsymbol{m}_A \cdot \nabla)\frac{\boldsymbol{r}_A}{r_A^3} \right] \tag{12-52f}$$

$$\hat{\mathcal{H}}^{OD} = \frac{1}{2c^4}\sum_{B\neq A} \frac{(\boldsymbol{m}_A \cdot \boldsymbol{m}_B)(\boldsymbol{r}_A \cdot \boldsymbol{r}_B) - (\boldsymbol{m}_A \cdot \boldsymbol{r}_B)(\boldsymbol{m}_B \cdot \boldsymbol{r}_A)}{r_A^3 r_B^3}. \tag{12-52g}$$

Here, (12-52a) is the operator for the diamagnetic magnetizability, (12-52b) is the orbital Zeeman term, (12-52c) spin Zeeman, (12-52d) paramagnetic orbital, (12-52e) diamagnetic shielding, (12-52f) Fermi-contact + spin-dipole, (12-52g) diamagnetic orbital term, respectively. The terms (12-52d) to (12-52g) are the nuclear hyperfine terms. The individual FC and SD operators, in particular the well-known δ distribution term for FC, are obtained by explicitly carrying out the differentiation of $\boldsymbol{r}_A/r_A^3$ in (12-52f). The first term on the right hand side of (12-52f), yields 3/2 of the FC operator, while the second term yields -1/2 FC plus the SD operator. One obtains the more familiar expressions

$$\hat{\mathcal{H}}^{FC} = \frac{8\pi}{6c^2}\delta(\boldsymbol{r}_A)\boldsymbol{m}_A \cdot \vec{\sigma}_s \tag{12-53a}$$

$$\hat{\mathcal{H}}^{SD} = \frac{1}{2c^2} \cdot \frac{3(\vec{\sigma}_s \cdot \boldsymbol{r}_A)(\boldsymbol{m}_A \cdot \boldsymbol{r}_A) - r_A^2 \boldsymbol{m}_A \cdot \vec{\sigma}_s}{r_A^5} \tag{12-53b}$$

In (12-52b), $\hat{\boldsymbol{\mu}}_e = -(1/2)(\boldsymbol{r} \times \hat{\boldsymbol{p}})$ is the magnetic moment operator for an electron's orbital motion. By comparison of (12-52b) with (12-52c) the magnetic moment operator with respect to an electron spin degree of freedom is $\hat{\boldsymbol{\mu}}_s = -\vec{\sigma}_s/2$. The nonrelativistic limit has been obtained from the Dirac equation where the electronic g-factor is exactly 2 and not written explicitly. Experimental evidence and more sophisticated theoretical treatments show that the correct value is rather $g_e = 2.0023\ldots$ The electronic g-factor can be included via factors of $(g_e/2)$ in the spin-dependent operators where applicable. In the operator list the nuclear Zeeman terms, $-\boldsymbol{m}_A \cdot \boldsymbol{B}$ for each nucleus, were omitted because they do not contribute to the electronic energy of the molecule.

In two-component theories one obtains relativistic analogs of these operators, along with additional correction terms. The relativistic analogs of the FC term represent an extreme example for what might be called a picture change effect. With point nuclei, the two-component orbitals diverge at the nuclei as shown elsewhere in this book. Therefore, one must not use the nonrelativistic operators for relativistic computations of magnetic properties. The FC operator, for instance, would simply yield diverging matrix elements as the basis set approaches completeness,

and at best yield arbitrary results with a finite basis that does not include functions with singularities at the nuclei. The problem would be somewhat less severe when finite-nucleus models were used but there is still no justification for using the non-relativistic magnetic perturbation operators with a relativistic set of orbitals or a relativistic wavefunction.

As an example for how these operators are modified in a relativistic formalism consider the ZORA: substituting $\boldsymbol{A} = \boldsymbol{A}^{\text{ext}} + \boldsymbol{A}^{\text{nuc}}$ in the ZORA perturbation terms operators (12-39), with $\boldsymbol{A}^{\text{ext}}$ from Eq. (12-43) and $\boldsymbol{A}^{\text{nuc}}$ from Eq. (12-45) yields, among other terms, the ZORA analog of the sum of FC and SD operators:

$$\hat{\mathcal{H}}^{FC+SD}_{\text{ZORA}} = \frac{1}{2c^2}\sum_A \vec{\sigma}_S \left[\boldsymbol{m}_A(\nabla \cdot \left[\mathcal{K}\frac{\boldsymbol{r}_A}{r_A^3}\right]) - (\boldsymbol{m}_A \cdot \nabla)\left[\mathcal{K}\frac{\boldsymbol{r}_A}{r_A^3}\right]\right] \tag{12-54}$$

The ZORA analog of the Fermi-contact term itself is given by (2/3) of the first term in (12-54). For nuclear point-charge potentials with Z approximately 118 or less the factor of $\mathcal{K}$ in the ZORA hyperfine terms (see Figure 12-4) regularizes the operator and as a result there is no actual "contact" (delta-distribution like) term for point nuclei. Even with a relativistically diverging set of orbitals the matrix elements of these operators remain finite. The physical mechanism of the ZORA FC/SD is nonetheless quite similar to the nonrelativistic analogs: the operator induces/samples electronic spin density very close to the nuclei. Other magnetic-field operators are in the ZORA also modified by the presence of $\mathcal{K}$ in perturbation operators that otherwise look quite similar to their nonrelativistic analogs. As an example, using Coulomb gause the OP term (12-52d) appears in the ZORA formalism as

$$\hat{\mathcal{H}}^{OP}_{\text{ZORA}} = \frac{1}{2c^2}\sum_A \left(\boldsymbol{m}_A \cdot \mathcal{K}(\frac{\boldsymbol{r}_A}{r_A^3} \times \hat{\boldsymbol{p}}) + \boldsymbol{m}_A \cdot (\frac{\boldsymbol{r}_A}{r_A^3} \times \hat{\boldsymbol{p}})\mathcal{K} \right) \tag{12-55}$$

which also has a structure similar to the nonrelativistic operator except for the presence of $\mathcal{K}$. For the ZORA analogs of other magnetic perturbation operators we refer the reader to the original literature on ZORA NMR [1, 2, 4, 5].

In the four component formalism, using the standard gauge for the vector potential and assuming point nuclei, the magnetic-field perturbation operators are according to Eq. (12-36)

$$\hat{\mathcal{H}}^{\text{mag}}_{\text{Dirac}} = -\frac{c}{2}\vec{\alpha} \cdot (\boldsymbol{r} \times \boldsymbol{B}) + \frac{1}{2c}\vec{\alpha} \cdot \sum_A^{\text{Nuclei}} \frac{\boldsymbol{m}_A \times \boldsymbol{r}_A}{r_A^3} \tag{12-56}$$

As already mentioned, in this representation there are no perturbation operators bilinear in $\boldsymbol{A}$ to be considered. As it is the case for the nonrelativistic and the two-component methods, the nuclear hyperfine terms in the Dirac formalism heavily weigh the near-nuclear region. The electric-field perturbation operator is the same as in Eq. (12-50).

We note in passing that additional magnetic perturbation operators are obtained from making the minimal substitution in relativistic two-electron operators such as the two-electron spin–orbit and Darwin terms, or in the SOO term (12-18).

For electric-field perturbations, the operator modifications due to the transformation to two-component form tend to be less dramatic. Since $-\phi$ is the leading order one might use it directly as an approximation in two-component methods. For external electric-field operators, which may be written in terms of real spherical harmonics, it can be shown that the spin-free Pauli-operator picture-change term of order c^{-2} vanishes and only a spin–orbit correction term remains. Its presence is expected to lead to comparatively small effects on dipole moments, polarizabilities, and other electric-field related properties as long as a closed-shell molecule is considered [87]. Electric-field gradients (EFGs) and higher field-derivatives evaluated at the nuclear positions are an exception because of the large magnitude of the operators at the nuclei.

Instead of correcting the picture-change in the operator, it is also possible to reconstruct an approximate four-component density and its field-dependent perturbations. For example, for first-order derivative properties the four-component density or density matrix can then be integrated with the untransformed operator. This approach can eliminate picture-change effects of order c^{-2} and has been used, for example, by van Lenthe et al. to compute EFG tensors using the ZORA [9] (the method was termed ZORA-4). Recently, Mastalerz et al. have studied picture-change effects on EFGs using higher order DKH transformations [101] of the EFG operator. As an example, for the iodine EFG in the HI molecule scalar relativistic DKH result dropped by 11% upon inclusion of picture-change effects. This change amounted to about 39% of the total relativistic correction and is therefore highly significant. For comparison, the picture-change corrections between ZORA and ZORA-4 reported by van Lenthe et al. for the nuclear quadrupole coupling constant of iodine in HI amounted to 5% of the total. Spin–orbit effects were on the order of 3% in this case.

12.2.6. Hyperfine Operators: from Four to Two to One Component and the Nonrelativistic Limit

It is interesting to see how the nonrelativistic limit and approximate two-component versions for matrix elements of the magnetic perturbation operators are related. The transition from the nonrelativistic Fermi-contact hyperfine operator to its "non-contact" relativistic versions to its four-component version contained in (12-56) is perhaps one of the most drastic examples of a relativistic operator change. We therefore choose this operator for the following analysis. For simplicity, consider a one-electron atom with a point nucleus at the coordinate origin ($\boldsymbol{r} = 0$). The discussion shall be restricted to s-orbitals (for all other orbitals the nonrelativistic FC term yields vanishing matrix elements, and for s-orbitals one can ignore the other hyperfine operators). The following discussion has been adapted from [102]. See also

[103, 104] where analytic expressions of four-component hyperfine integrals and their nonrelativistic limits have been reported. Consider a hydrogen-like Dirac s-orbital for a point nucleus:

$$\psi_{\mathrm{D}}^{+} = \frac{1}{\sqrt{4\pi}} \begin{pmatrix} g_{\mathrm{D}}(r) \\ 0 \\ i f_{\mathrm{D}}(r) \cdot \cos\theta \\ i f_{\mathrm{D}}(r) \cdot \sin\theta e^{i\phi} \end{pmatrix}; \quad \psi_{\mathrm{D}}^{-} = \frac{1}{\sqrt{4\pi}} \begin{pmatrix} 0 \\ g_{\mathrm{D}}(r) \\ i f_{\mathrm{D}}(r) \cdot \sin\theta e^{-i\phi} \\ -i f_{\mathrm{D}}(r) \cdot \cos\theta \end{pmatrix} \tag{12-57}$$

where the indices + and − denote the sign of $m_j = \pm 1/2$ [16, 105]. The real radial functions for the upper (g_{D}) and lower (f_{D}) component are given by the coupled set of radial equations for $G_{\mathrm{D}} = r \cdot g_{\mathrm{D}}$ and $F_{\mathrm{D}} = r \cdot f_{\mathrm{D}}$:

$$\frac{d}{dr} F_{\mathrm{D}} - \frac{k}{r} \cdot F_{\mathrm{D}} - \left(\frac{V - \varepsilon_{\mathrm{D}}}{c} \right) \cdot G_{\mathrm{D}} = 0 \tag{12-58a}$$

$$\frac{d}{dr} G_{\mathrm{D}} + \frac{k}{r} \cdot G_{\mathrm{D}} + \left(\frac{V - \varepsilon_{\mathrm{D}}}{c} - 2c \right) \cdot F_{\mathrm{D}} = 0. \tag{12-58b}$$

where $k = -1, -2, -3, \ldots$ for $s_{1/2}$, $p_{3/2}$, $d_{5/2}$, ... orbitals, and $+1, +2, +3, \ldots$ for $p_{1/2}$, $d_{3/2}$, $f_{5/2}$, ... orbitals [106]. Further, $\varepsilon_{\mathrm{D}} = E_{\mathrm{D}} - c^2$, with E_{D} being the Dirac orbital energy that includes the rest-mass energy of $m_e c^2$. The normalization is chosen in the usual way such that

$$\int_0^\infty dr \cdot r^2 (g^2 + f^2) = 1. \tag{12-59}$$

The hyperfine perturbation operators relevant, for instance, for a computation of nuclear spin–spin coupling or spin–orbit contributions to nuclear magnetic shielding are obtained by differentiating the terms in $\hat{\mathcal{H}}^{\mathrm{mag}}$ with respect to a Cartesian component of the nuclear spin moment $\boldsymbol{m}_A$ (see the NMR Section 12.3.1). We select the z-component for convenience. I.e., we have from (12-53a) the nonrelativistic perturbation operator

$$\hat{\mathcal{H}}_{\mathrm{nrel}}^{(m_z)} = \frac{4\pi}{3c^2} \sigma_z \delta(\boldsymbol{r}) \tag{12-60}$$

(letting $\boldsymbol{r}_A = \boldsymbol{r}$ for the nucleus in the coordinate origin). From (12-54) one obtains for the isotropic part of the ZORA "contact" operator

$$\hat{\mathcal{H}}_{Z}^{(m_z)} = \frac{1}{3c^2} \left[\sigma_z \nabla \left(\mathcal{K} \frac{\boldsymbol{r}}{r^3} \right) \right], \tag{12-61}$$

and in the four-component case

$$\hat{\mathcal{H}}_{\mathrm{D}}^{(m_z)} = -\frac{1}{c} \left[\vec{\alpha} \times \frac{\boldsymbol{r}}{r^3} \right]_z, \tag{12-62}$$

In the nonrelativistic case, the expectation value of $\hat{h}^z_{\rm nrel}$ for s-orbitals is simply

$$\langle \psi^{\pm}_{\rm nrel} | \hat{\mathcal{H}}^{(m_z)}_{\rm nrel} | \psi^{\pm}_{\rm nrel} \rangle = \pm \frac{1}{3c^2} g_{\rm nrel}(0)^2 \tag{12-63}$$

where $g_{\rm nrel}(0)$ is the value of the nonrelativistic (one-component) radial function at the nucleus, and the $\pm$ signs refer to alpha or beta spin. The factor of 4π of Eq. (12-60) is canceled by the normalization factor of $\psi(\boldsymbol{r})$ due to the integration over the angles θ and ϕ. Equation (12-63) represents the well-known result that the matrix elements of the FC operator are proportional to the integrand *at* the point-nucleus and are therefore only nonzero for s-orbitals. For better comparison with the relativistic case it is convenient to employ $\nabla(\boldsymbol{r}/r^3) = 4\pi\delta(\boldsymbol{r})$, apply partial integration to move the derivatives from the operator to the orbital, and rewrite (12-63) as

$$\langle \psi^{\pm}_{\rm nrel} | \hat{\mathcal{H}}^{(m_z)}_{\rm nrel} | \psi^{\pm}_{\rm nrel} \rangle = \mp \frac{1}{3c^2} \int_0^\infty dr \cdot \left[\frac{dg_{\rm nrel}}{dr} g_{\rm nrel} + g_{\rm nrel} \frac{dg_{\rm nrel}}{dr} \right] \tag{12-64}$$

For the ZORA case, also after partial integration to shift the derivative in the operator to the orbital, we have for the matrix element of (12-61)

$$\langle \psi^{\pm}_{Z} | \hat{\mathcal{H}}^{(m_z)}_{Z} | \psi^{\pm}_{Z} \rangle = \mp \frac{1}{3c^2} \int_0^\infty dr \cdot \left[\frac{dg_Z}{dr} \mathcal{K} g_Z + g_Z \mathcal{K} \frac{dg_Z}{dr} \right]. \tag{12-65}$$

for $m_j = \pm 1/2$. Here, g_Z is the ZORA radial function which, as mentioned previously, has a logarithmic divergence at $r \to 0$ for a point nucleus. The nonrelativistic FC operator would therefore yield a diverging matrix element with g_Z but the $\mathcal{K}$ term in the ZORA operator regularizes the result (at the nucleus where $g_Z \to \infty$ we have $\mathcal{K} \to 0$). The nonrelativistic limit is straightforward: with $\mathcal{K} \to 1$ and $g_Z \to g_{\rm nrel}$ the result is identical to (12-64).

In the four-component case, we use in (12-62)

$$(\vec{\alpha} \times \boldsymbol{r})_z = \frac{\sin\theta}{r^2} \begin{pmatrix} 0 & 0 & 0 & \sin\varphi + \imath\cos\varphi \\ 0 & 0 & \sin\varphi - \imath\cos\varphi & 0 \\ 0 & \sin\varphi + \imath\cos\varphi & 0 & 0 \\ \sin\varphi - \imath\cos\varphi & 0 & 0 & 0 \end{pmatrix}$$

in spherical coordinates (r, φ, θ). One obtains with the four-component orbitals from Eq. (12-57) after integration over the angular variables

$$\langle \psi^{\pm}_{\rm D} | \hat{\mathcal{H}}^{(m_z)}_{\rm D} | \psi^{\pm}_{\rm D} \rangle = \mp \frac{2}{3c} \int_0^\infty dr \cdot (g^D f^D + f^D g^D) \tag{12-66}$$

(the integrand has intentionally been written in this form to resemble the nonrelativistic and ZORA result). There is no derivative term here but we will see shortly

that the nonrelativistic limit with its derivative term arises from the product of the upper and lower component in (12-66) which originates from the action of $\vec{\alpha}$ in the perturbation operator. Note that there is also a derivative term in the approximate two-component form (ZORA) which indicates that the derivative term must enter via the relationship between the upper and lower components of the Dirac orbital. This is indeed the case as can be seen from Eq. (12-7) where the derivative enters via $\hat{\boldsymbol{p}} = -\imath\boldsymbol{\nabla}$. The nonrelativistic limit of (12-66) can be obtained from the nonrelativistic limit for the coupled pair of radial equations for g and f, Eq. (12-58a,b). For $c \to \infty$, the $(V - \varepsilon_{\mathrm{D}})/c$ term in (12-58b) can be neglected and thus

$$F_{\mathrm{nrel}} = \frac{1}{2c}\left(\frac{dG_{\mathrm{nrel}}}{dr} + \frac{k}{r}\cdot G_{\mathrm{nrel}}\right). \tag{12-67}$$

For s-orbitals, $k = -1$. One obtains the following relationship between upper and lower component,

$$f_{\mathrm{nrel}} = \frac{1}{2c}\frac{dg_{\mathrm{nrel}}}{dr} \tag{12-68}$$

which indeed yields the derivative term. Substituting the last expression in the hyperfine integral, Eq. (12-66) finally recovers the nonrelativistic result (12-64).

In summary, the perturbation operators in the four-component picture cannot be directly compared to those arising from the two-component picture or in the nonrelativistic limit because part of their action is hidden in the coupling between the upper and lower components of the wavefunction or the orbitals, both at the unperturbed level as well as regarding the coupling between upper and lower components in the perturbed spinors. The apparent absence of derivative terms in the four-component perturbation operators or the apparent absence of a diamagnetic term is a manifestation of this situation.

12.2.7. Where in the Molecule Do the Properties "Originate" from?

In the Introduction and various other sections the "origin" of a property (energy, response property) of a molecule was mentioned. It is sometimes helpful to know which regions in a molecule contribute most to a given property in order to understand, for example, why it affords or does not afford large relativistic corrections. For this purpose, consider first the energy itself written as an expectation value in space representation ($\tau = 3N$ spatial electron coordinates, $s =$ spin coordinates of the electrons):

$$E = \langle\Psi|\hat{\mathcal{H}}|\Psi\rangle = \int d\tau ds \cdot \Psi^*(\tau, s)\hat{\mathcal{H}}\Psi^*(\tau, s) \tag{12-69}$$

This result is of course a single number, but the fact that it is obtained from an integral over $3N$ dimensional space suggests that one can learn something about the

origin of the energy in terms of spatial contributions.[8] Extended regions of space where the integrand is large will contribute more to the energy than regions where the integrand is small. The partitioning of the energy is arbitrary: no particular partitioning is made compulsory by the fundamental axioms of quantum theory. This allows a certain freedom of interpretation. However, for a property analysis to be useful it should not yield completely arbitrary interpretations from various different partitioning schemes. Some researchers reject energy and property analyses because of this freedom of interpretation. However, most chemists probably find them useful and quite intuitive as long as they are able to avoid strong elements of arbitrariness in such analyses.

For the energy above one may use the fact that in exact theory $\hat{\mathcal{H}}\Psi = \Psi \cdot E$ and therefore, after integrating (12-69) over all spin and all but one spatial coordinates, we have

$$E = \frac{E}{N} \int d^3r \cdot \rho(\boldsymbol{r}) \tag{12-70}$$

where N is the number of electrons and $\rho(\boldsymbol{r})$ the electron density. Based on this equation the main spatial contributions to the energy will be those where the electron density provides the largest contributions to the integral (irrespective of whether the energy expression is relativistic or nonrelativistic). The biggest contributions come from the ourter atomic core shells and from the valence regions of the molecule, not so much from spatial regions that are very close to the nucleus. The function $\varepsilon(\boldsymbol{r}) = (E/N)\rho(\boldsymbol{r})$ may be called the *energy density* for the molecule, i.e.,

$$E = \int d^3r \cdot \varepsilon(\boldsymbol{r}). \tag{12-71}$$

It must be emphasized again that the definition of the energy density is not unique. The chapter by Schwarz illustrates how a perturbation theory based formalism allows one to associate the core regions (where the electrons 'are fast') with the relativistic changes of orbital and binding energies in atoms and molecules.

One can follow a similar approach for a molecular property. For instance, suppose we have a first-derivative one-electron property P with operator $\hat{P}(\tau)$. The expectation value is

$$P = \langle\Psi|\hat{P}|\Psi\rangle = \int d\tau ds \cdot \Psi^*(\tau, s)\hat{P}\Psi^*(\tau, s) = \int d^3r \cdot P(\boldsymbol{r}) \tag{12-72}$$

where, after integration over spin and all but one spatial coordinates, the integrand of the remaining 3D integral may be called the "property density" function $P(\boldsymbol{r})$. Property densities can also be derived for higher-order derivative properties such as hyperpolarizabilities [107, 108]. Again, from (12-72) one can identify regions of

[8] If the momentum representation is chosen one obtains contributions from different electron momenta instead which can be useful, too, but may often be less intuitive for chemical applications.

space that contribute the most to the property. Different property density functions are obtained by manipulating the integrand without changing the integrated results. For instance, transformations like $\int dx \cdot f\nabla^2 g = -\int dx \cdot (\nabla f)(\nabla g)$ for square integrable functions might be employed to obtain somewhat different property densities. We also note that the integrand of the combined three terms in (12-21b) is different than that of the simpler Hellmann–Feynman equation (12-25) which means that spatial contributions to the first-derivative property will differ depending on which equation is used.

Another intuitive way for partitioning expectation value integrals is obtained in molecular orbital methods. Typically, in this case a property can be written as a sum over integrals involving the occupied orbitals or products of occupied with unoccupied orbitals. Instead of partitioning the total per spatial contributions from the integral, one carries out the integration for each MO separately and partitions the property per MO instead. For the MO basis, a localized or a delocalized description may be chosen which often yield complementary (but usually not contradictory) information about the origin of the property. In (Kohn–Sham) DFT an orbital partitioning of energy and properties is essentially "built into" the formalism since the electron density is constructed from the Kohn–Sham MOs. In correlated wavefunction-based methods one can, for instance, express the density matrix in terms of natural orbitals which would also lead to a convenient orbital-based partitioning of one-electron properties.

An orbital partitioning can be complementary to a space partitioning. For example, suppose the integrand in Eq. (12-72) indicates that a property has large contributions from the core regions in the molecule (the regions very close to the nuclei). An orbital analysis of the same property might indicate that the core orbitals are the main, or among the main, contributors. In this case it would be reasonable to identify the property as a core property. The NMR nuclear magnetic shielding is a good example for such a property. On the other hand, an orbital partitioning might determine instead that valence orbitals are the biggest contributors to a property for which a spatial analysis finds that core regions play a big role. This appears contradictory. We note, however, that valence orbitals have core tails. The two analyses can be reconciled if the core tails of the valence orbitals near the nuclei determine the major contributions to the property. In this case, the interpretation would rather be that the property is a "chemical" one determined by the valence orbitals, but that it strongly weighs the atomic core regions because the property operators are large there. A prime example for such a valence property determined by the core tails of the valence orbitals is the indirect NMR nuclear spin–spin coupling (J-coupling). In Section 12.3.1 spatial and orbital contributions to the nuclear spin–spin coupling in the PbH_4 molecule will be used as an example for the types of analyses discussed in this section. Another example is the NMR chemical shift for which most of the core-region–core-orbital contributions cancel and only the core-region–valence-orbital contributions are of importance (along with semi-core (outer core) contributions). Electric-field gradients also fall into this category, as well as some of the relativistic effects on molecular binding energies. A third, rather clear-cut scenario is one where the spatial analysis indicates that the origin of the property is the

valence region, and the orbital analysis finds that the valence orbitals are responsible for the property. In this case the property would reasonably be identified as a valence shell property. The electric polarizability is an example.

Core and valence orbitals are directly impacted by relativistic effects. For valence shell properties, particularly large relativistic effects are obtained if the property operators are large in the core regions of the heavy atoms. According to Section 12.2.5, large relativistic effects should therefore be expected for heavy nucleus chemical shifts or J-couplings of heavy nuclei or EFG tensors of heavy nuclei. For such properties relativistic effects can be very large indeed – to the point where relativistic "correction" becomes a questionable term, as already indicated in the introduction. Genuine core properties may also afford very large relativistic effects. For other valence properties, relativistic effects are often of similar relative magnitude as those on the binding energies. Examples are dipole moments, polarizabilities, vibrational frequencies, or excited state properties.

12.3. BENCHMARK DATA AND CASE STUDIES

In this section we provide some more details about the computation of specific properties: NMR, EPR, and EFG tensors, and polarizabilities along with linear-response based excitation spectra calculations. With the help of selected case studies, it will be shown how relativity influences these energy-derivative properties for molecules with heavy atoms. This section is not intended to provide a comprehensive coverage of the literature in this field, which is vast. There are a number of review articles available where the reader can find additional compilations of literature data and detailed overviews of the computational methodology for many different response properties which often include a survey of computational data obtained with relativistic methods. To list a selection of overview articles that include applications of computational methods in inorganic chemistry: Rosa et al. have reviewed the computation of excitation spectra of metal complexes [109]. Autschbach [61, 110], and Autschbach and Ziegler [62, 111] have reviewed computations of energy and many energy-derivative properties (NMR, EPR, optical, chiral, and others). We have also compiled the first dedicated review of relativistic NMR computations which covers the literature up to mid 2002 [12a], with a recent update covering literature up to 2009 [12b]. Bühl, Kaupp, et al. have reviewed the computation of NMR in metal systems [112, 113]; a number of relativistic NMR studies by Bagno et al. were summarized in [114]. Several researchers have reviewed computational work on NMR and EPR parameters in [115]; see for instance Neese's chapter on EPR applications in bioinorganic chemistry [116] and the EPR chapter by Patchkovskii and Schreckenbach [117], or the author's and Vaara et al.'s chapters on relativistic NMR [118–120]. [115] also contains a chapter on EFG calculations by Schwerdtfeger et al. [121]. NMR chemical shift computations using ab-initio methods were recently reviewed by Casabianca and de Dios [122]. A selection of reviews on a variety of topics including general aspects of transition metal complex modeling can be found,

for example, in the February 2000 thematic issue of *Chem. Rev.* entitled "Computational Transition Metal Chemistry" and in a "Theoretical and Computational Chemistry" special issue of *Coord. Chem. Rev.* (Vol. 238/239, March 2003). The "Chemist's Guide to Density Functional Theory" by Koch and Holthausen [123] provides numerous benchmark data for structure, energy, reactivity, and optical and spectroscopic data obtained with DFT including some for heavy atom systems and heavy metal complexes.

Because of the high computational cost of correlated wavefunction-based relativistic methods, and because of the rather poor performance of Hartree–Fock theory for many response properties other than first-derivative properties, there will be a strong emphasis on computational data obtained with density functional theory (DFT) in this section. DFT has become the major theoretical tool in this area which is clearly reflected in the available reviews.

The discussion begins with NMR parameters. This section will be particularly detailed because of the high importance of spin-free and spin–orbit relativistic effects as well as an abundance of experimental data. The computation of EPR parameters is conceptually related to those of NMR parameters and will be discussed next. Electric polarizabilities and electric field gradients will serve as representative examples of electric properties that have been studied extensively using relativistic methods. Some examples for computations of excitation energies via the TD–DFT response route will be included here as well.

Often, the (actual or generalized) fields perturbing the energy are 3-vectors, for example external electric and magnetic field vectors, or spin-vectors and nuclear magnetic moment vectors in 3D space. First derivative properties then have thre components which transform as rank-1 tensors (vectors). Second derivatives transform as rank-2 tensors, and so on. Often, for the rank-2 tensor properties we will focus on the isotropic averages given by 1/3 of the sum of the diagonal elements of the tensor. We will use the notation $\mathbb{A}$ for the tensor and A (math-italic) for the isotropic value. Sometimes an anisotropy value ΔA will also be of interest. Another property under consideration here is the electric field gradient which is a first-order energy derivative and a rank-2 tensor. Here, we will focus on the principal components, in particular on the one with the largest magnitude.

12.3.1. NMR Parameters

Two important NMR parameters, the nuclear magnetic shielding (tensor) and the "indirect" electron-mediated nuclear spin–spin coupling (tensor), are among the molecular properties that exhibit the most spectacular relativistic effects. We will forgo a discussion of the direct dipolar coupling between nuclei since (i) it does not involve the electronic structure and thus it is not affected by relativistic effects (other than indirectly, via relativistic effects on molecular structure) and (ii) it averages to zero for freely rotating molecules (gas phase and most solutions). As mentioned in Section 12.2.7, the origin of a molecular property can be analyzed spatially or by

orbital contributions. The NMR operators are large in the nuclear regions where relativistic effects on the electronic structure are strong, which helps to rationalize why relativistic effects are particularly large for these properties.

Consider the presence of nuclear spin magnetic moments $\boldsymbol{m}_A, \boldsymbol{m}_B, \ldots$ of nuclei $A, B, \ldots$ in a molecule, and a static homogeneous external magnetic field $\boldsymbol{B}$. The nuclear shielding σ_A and the indirect spin–spin coupling $\mathbb{K}_{AB}$ are rank-2 tensors that can be defined via the phenomenological Hamiltonians

$$H = -\boldsymbol{m}_A(1-\sigma_A)\boldsymbol{B} \tag{12-73a}$$

for the shielding tensor and

$$H = \boldsymbol{m}_A \mathbb{K}_{AB} \boldsymbol{m}_B \tag{12-73b}$$

for the spin–spin coupling. σ_A is dimensionless and usually reported in parts per million (ppm). $\mathbb{K}_{AB}$ is in SI units given in T^2/J or $\mathrm{kg}/(\mathrm{m}^2\mathrm{C}^2)$ and tends to be on the order of one to several thousand times 10^{19} SI units. The isotropic shielding σ_A and the isotropic spin–spin coupling constant $\mathbb{K}_{AB}$ are obtained from (1/3) of the sum of the diagonal elements of the tensors. The chemical shift δ is defined with respect to a reference (ref) nucleus. In terms of shielding constants the chemical shift is given as

$$\delta = \frac{\sigma^{\mathrm{ref}} - \sigma}{1 - \sigma^{\mathrm{ref}}} \tag{12-74}$$

which is to a very good approximation equal to $\sigma^{\mathrm{ref}} - \sigma$ for chemical shifts of light nuclei where $\sigma, \sigma^{\mathrm{ref}}$ are small. The latter equation is often also used for heavy element shifts where shielding constants can be as large as 10^4 ppm thus leading to deviations on the order of a percent compared to (12-74). The reference can also be a hypothetical shielding related to a well-defined spectrometer frequency, as it is customary, for example, for ^{103}Rh NMR [124].

Computationally, the problem is approached as follows: The energy of the molecule is considered in the presence of the external magnetic field and the nuclear spins. The spin–spin coupling and shielding are then, according to Eq. (12-73), given by the energy terms bilinear in the magnetic moments ($\mathbb{K}_{AB}$) and bilinear in one of the magnetic moments and the external field (σ_A). Therefore, if the energy is expanded in a perturbation series in the magnetic moments and the external field, the NMR parameters are given by second-order energy derivatives with respect to static perturbations, Eq. (12-25). NMR parameters are double perturbation properties.

The nuclear Zeeman term $-\boldsymbol{m}_A \cdot \boldsymbol{B}$ is not considered in the electronic energy. It accounts for the "1" in $(1-\sigma_A)$ of Eq. (12-73a). Thus,

$$\sigma_A = E^{(\boldsymbol{m}_A,\boldsymbol{B})} = \left.\frac{\partial^2 E}{\partial \boldsymbol{m}_A \partial \boldsymbol{B}}\right|_{\substack{\boldsymbol{m}_A=0 \\ \boldsymbol{B}=0}} \tag{12-75}$$

and

$$\mathbb{K}_{AB} = E^{(\boldsymbol{m}_A \boldsymbol{m}_B)} = \left.\frac{\partial^2 E}{\partial \boldsymbol{m}_A \partial \boldsymbol{m}_B}\right|_{\substack{\boldsymbol{m}_A=0 \\ \boldsymbol{m}_B=0}} \tag{12-76}$$

Both expressions are also in formal agreement with the phenomenological Hamiltonians (12-73). Measured J-coupling contstants are related to the rotational average of the $\mathbb{K}$-coupling tensor as

$$J_{AB} = \frac{\hbar}{2\pi} \gamma_A \gamma_B K_{AB} \tag{12-77}$$

with magnitudes typically on the order of a few to a few thousand Hz. The γs are the nuclear magneto-gyric ratios in units of radians/s.

It should be emphasized that chemical shifts σ and indirect nuclear spin–spin coupling constants K are response properties of the *electronic* system. Their measurement by NMR obviously relies on the presence of nuclear spins but the computational result is not dependent on the nuclear spins, or on the magneto-gyric ratios. Therefore, in the "clamped nucleus" approximation chemical shifts calculated for different isotopes of the same element are identical. Isotope effects on chemical shifts, spin–spin coupling, and other response properties can be obtained computationally from considering vibrational corrections or by treating the system dynamically. If calculated J-coupling constants are reported, then obviously the value depends on the isotopes via the magneto-gyric ratios (Eq. 12-77) whereas the indirect couplings K are not isotope-dependent (unless vibrational corrections are included).

The operators that are relevant for NMR parameters are the magnetic perturbation operators that depend on the nuclear spins and/or the external field $\boldsymbol{B}$. The nuclear magnetic moments $\boldsymbol{m}_A$ and the external field $\boldsymbol{B}$ are used directly as the perturbation parameters. For nuclear shielding, the $2\,\mathrm{Re}\langle\Psi^{(\mathcal{F}_j)}|\hat{\mathcal{H}}^{(\mathcal{F}_i)}|\Psi^{(0)}\rangle$ term of Eq. (12-25) involves operators that are *linear* in the external field and those linear in the magnetic moment $\boldsymbol{m}_A$. In nonrelativistic and two-component theories, these are for the $\boldsymbol{B}$ field the spin- and orbital-Zeeman terms, and for $\boldsymbol{m}_A$ the paramagnetic term (OP) and the FC + SC operators (or their two-component analogs). In four-component theory, the operators of Eq. (12-56) are used. We remind the reader that $\Psi^{(\mathcal{F}_j)}$ is computed from $\hat{\mathcal{H}}^{(\mathcal{F}_j)}$ [see Eq. (12-22b) and therefore both sets of operators are needed. Any operator that is bilinear in $\boldsymbol{m}_A$ and $\boldsymbol{B}$ will contribute to the $\langle\Psi^{(0)}|\hat{\mathcal{H}}^{(\mathcal{F}_i,\mathcal{F}_j)}|\Psi^{(0)}\rangle$ term of Eq. (12-25) for nuclear shielding. This is the "diamagnetic shielding" (DS) operator (12-52e) or its two-component analogs, while in 4-component theory these contributions are absorbed in the paramagnetic terms as mentioned earlier. For spin–spin coupling, the operators linear in $\boldsymbol{m}_A$, i.e., OP and FC + SD or their two-component analogs, contribute to the $2\,\mathrm{Re}\langle\Psi^{(\mathcal{F}_j)}|\hat{\mathcal{H}}^{(\mathcal{F}_i)}|\Psi^{(0)}\rangle$ term, and the bilinear OD term (12-52g) or its relativistic analogs contribute to the diamagnetic $\langle\Psi^{(0)}|\hat{\mathcal{H}}^{(\mathcal{F}_i,\mathcal{F}_j)}|\Psi^{(0)}\rangle$ term. Again, in four-component theory there are only the linear $c\vec{\alpha}\boldsymbol{A}^{\mathrm{nuc}}$ terms to consider.

Relativistic effects may show up in the results in several ways: (i) Via spin-free relativistic effects on $\Psi^{(0)}$ and $\Psi^{(\boldsymbol{m}_A)}$, $\Psi^{(\boldsymbol{B})}$ along with the relativistic modifications in the operators (the "kinematic terms" mentioned earlier). (ii) Via spin–orbit coupling terms. For instance, for a closed-shell system all cross terms between spin-free operators and spin-dependent operators cancel in the $2\,\mathrm{Re}\langle\Psi^{(\mathcal{F}_j)}|\hat{\mathcal{H}}^{(\mathcal{F}_i)}|\Psi^{(0)}\rangle$ term in the absence of spin–orbit coupling. However, these cross terms can become quite large if spin–orbit coupling is appreciable, such as for elements in the 5d block, for actinides, or for heavy p-block elements. (iii) Relativistic effects may substantially alter the *geometry* of the molecule. This may be considered an indirect effect that shall not be analyzed further in this chapter. I.e., here and in the following we assume that a comparison between relativistic and nonrelativistic results is made for the same (experimental or relativistically optimized) geometry.

This section represents an abridged version of Ref. [12b] where many more examples can be found. It is illustrative to first discuss a simple system to demonstrate the influence of relativity on NMR parameters. The plumbane molecule, PbH_4, has often served as a benchmark molecule for computations because it contains one of the heaviest NMR-active nuclei but does not have other electron-rich ligands that would lead to overly CPU intensive computations. Consider the Pb–H spin–spin coupling constant. Some benchmark data for the Pb–H coupling in PbH_4 and other plumbanes are listed in Table 12-2. In particular the more recent DFT computations based on hybrid DFT and including spin-free and SO effects reproduce the experimental data quite well. Regarding the overall significance of the relativistic effects: nonrelativistic computations typically yield results of only half the magnitude, i.e., with the nonrelativistic results as the reference the relativistic "corrections" are on the order of 100%. Spin–orbit effects on K(Pb–H) are quite noticeable but much smaller than the scalar relativistic effects. The MCSCF computation by Kirpekar and Sauer did not include scalar relativistic effects but it reproduced the magnitude of the SO effect on K(Pb–H) very well.

As we have seen, the "contact" operator (FC) is the one that samples the electronic structure right *at* the nuclei. Its relativistic analogs sample the very near-nuclear regions. This operator – because of its large prefactor – tends to dominate most coupling constants, including K(Pb–H) in PbH_4, and it should also be the one that samples relativistic effects most effectively. Figure 12-5 demonstrates the strong influence of relativity and the importance of the core regions on the Pb–H spin–spin coupling: In Figure 12-5 the FC-like contribution to the Pb–H coupling is partitioned spatially, as in Eq. (12-72), and shown as a radial integral around the Pb nucleus. We observe a number of details that are typical for spin–spin coupling involving heavy elements: Overall, there is a huge relativistic increase in K(Pb–H) which, percentage-wise, far exceeds relativistic effects usually found for structural parameters and bond energies of 6th row element compounds. Obviously, a bond will not contract 100% due to relativity, and a molecule that is only very weakly bound nonrelativistically, but moderately strongly bound in the relativistic case, might afford a very large percentage bond energy correction. But the large relativistic increase of

Table 12-2 Reduced Pb–H spin–spin coupling constant in plumbanes, in $10^{20}T^2J^{-1}$

	PbH_4	$Pb(CH_3)_2H_2$	$Pb(CH_3)_3H$
Spin-free ZORA			
PBE[a]	118	95.9	86.1
PBE0[a]	134	112	103
BP86/Xα[b]	132	107	97.8
Spin–orbit ZORA			
PBE[a]	110	88.0	78.6
PBE0[a]	126	104	95.0
BP86/Xα[b]	123	98.3	89.1
Selected other literature data[g]			
IORA BLYP[c]	127		109
IORA B3LYP[c]	137		121
Dirac HF[d]	182		167
MCSCF + Pauli SO[e]	48		
Nonrel. MCSCF[e]	56		
Expt.[f]	(112)	98.7	92.3

[a] Author's DFT data with nonhybrid PBE and hybrid PBE0 functional [125].
[b] Author's DFT data with nonhybrid BP86 potential and Xα response kernel [5].
[c] Spin-free DFT calculations using an infinite-order regular approximation (IORA), Filatov and Cremer [33].
[d] Four-component basis Hartree–Fock computations, Enevoldsen et al. [126]. A scaled value for PBH_4 to account for electron correlation was given as 138.3.
[e] Nonrelativistic MSCSF computations with first-order corrections from the Pauli SO operator, Kirpekar and Sauer [127].
[f] Experimental value for PbH_4 extrapolated from the experimental data for the methyl derivatives $Pb(CH_3)_3H$ and $Pb(CH_3)_2H_2$. Experimental data from [128]. An alternative experimental value for $Pb(CH_3)_3H$ is 94.6, from [129].
[g] For semiempirical data for PbH_4 see [130] and [131]. For a DFT study with frozen cores using the scalar Pauli operator variationally see [132].

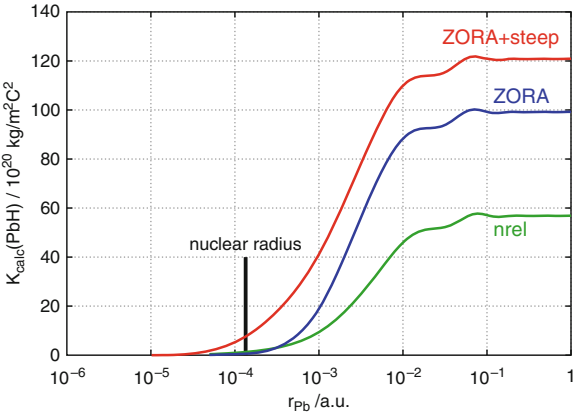

Figure 12-5. K(Pb–H) spin–spin coupling constant of PbH_4 obtained from a radial integral of a "coupling constant density" [cf. Eq. (12-72) around the Pb nucleus, from spin-free ZORA and nonrelativistic (nrel) DFT computations with a local density functional [4]. The total computed coupling constant is obtained as $r_{Pb} \to \infty$. FC type mechanism only. ZORA+steep means that a range of high-exponent ("steep", "tight") functions was added to the basis set in order to describe the relativistic effects near the Pb nucleus better. A point nucleus was used for the computations. The radius of the Pb nucleus is indicated in the figure

the already large Pb–H coupling constant indeed nicely illustrates the very strong effect that special relativity has on this NMR parameter.

Further note that most of the difference between ZORA and "nrel" results from regions less than about 1/100 bohr radii around the Pb nucleus. The nonrelativistic result is determined by this region to begin with, and most of the relativistic effects also contribute in this region. This finding highlights the fact that the operators that are involved are large near the nuclei. Another important finding is the large increase observed for K(Pb–H) when high-exponent basis functions are added to the basis set in order to describe the nuclear tails of the orbitals better. In general, computing relativistic NMR parameters requires basis sets that are particularly in the near nuclear region. For a point nucleus, the analytic solutions of the one-electron Dirac equation exhibit weak singularities for $s_{1/2}$ and $p_{1/2}$ orbitals. In a regular basis set this behavior can be approximated by adding high-exponent basis functions, which is necessary in particular if properties with "contact" -type operators are of interest. In Figure 12-5 it is seen that the additional increase in K(Pb–H) indeed results from regions very close to the nuclear radius. Although with finite nuclei no singular terms arise, the importance of the near nuclear regions – and therefore basis sets to describe the electronic structure there – is quite similar [64, 102].

The case is further illustrated in Figure 12-6 which shows the electron density of the Hg atom obtained from numerical and basis set DFT computations. In a previous paper [4] we argued that adding too many "tight" functions to a basis set to describe the strong increase of the density for radii less than the nuclear radius is not particularly desirable. Treating the point nucleus correctly in this respect would likely lead to an overestimation of the "contact" term magnitudes. The problem is somewhat alleviated if the basis set is restricted to provide good coverage

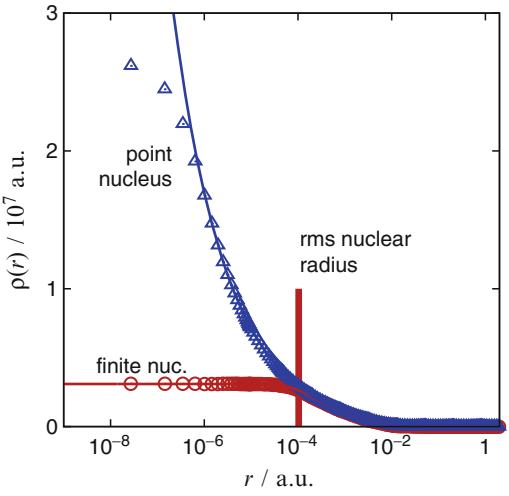

Figure 12-6. Two component electron density of the Hg atom in the near nucleus region, from numerical and basis set (markers) DFT computations [64]

for regions outside the nuclear radius. Numerical evidence has been provided in [64, 102]. Ultimately, though, when considering the data shown in Figure 12-5 it is clear that for computations of nuclear spin–spin coupling it would be best to adopt a finite-nucleus model. Such a study has very recently been undertaken [64] and confirmed that, when basis sets with many high exponent functions are used, one-bond J-couplings between a 6th row NMR nucleus and a light elements can be reduced on the order of 10% due to a finite nuclear volume (12% to 14% for Hg, Pb, and somewhat below 10%, for example, for Pt, based on a Gaussian nuclear model), mainly due to the modifications of the perturbation operators (see Eq. 12-48). Coupling constants between two 6th row atoms were in some cases reduced by more than 20%. Note, however, that most of the calculations presented here have been obtained with a point nuclear model and basis sets as described above.

We have recently revisited the PbH_4 case (along with other molecules) and studied the coupling constant with an analysis method based on using spin-free relativistic localized orbitals [133]. An analysis per canonical MO was also carried out. The results are illustrated in Figure 12-7. Both spin-free and spin–orbit results are provided. The important result from the orbital decomposition is that the coupling constant is determined by the Pb–H bonding orbitals (i.e., by the valence shell) along with sizeable contributions from the Pb 5s orbital. The result for this and other molecules studied in [133], results from other relativistic analyses of spin–spin coupling [135, 136], as well as, e.g., results from analyses of nonrelativistic spin–spin couplings performed by Ziegler et al. [137, 138], therefore demonstrate that spin–spin coupling is predominantly a valence-shell property [cf. Section 12.2.7]. Since the spatial analysis (Figure 12-5) yields most of the contributions from the core region, the origin of the property can be traced back to the core-tails of the valence orbitals. Indeed, very similar results are obtained for the spin–spin coupling

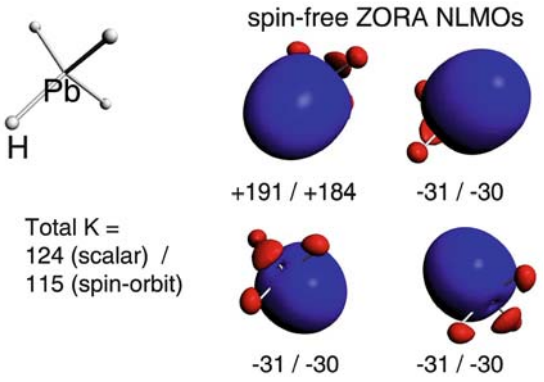

Figure 12-7. Pb–H spin–spin coupling in PbH_4 analyzed in terms of spin-free localized orbitals (here: natural localized MOs [134]). ZORA DFT computations from [133] with the PBE functional. Spin-free/spin–orbit results reported in units of $10^{20}T^2J^{-1}$. Contributions from the Pb 5s orbital are: spin-free 24, spin–orbit 24. The combined PBE results shown here differ slightly from those of Table 12-2 and Figure 12-5 because of a different basis set used for H and small differences in the geometries

in PbH_4 if a *frozen* core (1s–4d) is used (this was explicitly demonstrated in [4] for Hg–C coupling constants, the corresponding Pb data are unpublished). The main contribution is – as one might expect – from the Pb–H bonding orbital for the pair of nuclei under consideration. The analysis also finds three equivalent negative contributions from the other Pb–H bonds which are somewhat less intuitive and which do not show up in the light atomic analog methane. The computations indicated that the electronic structure in PbH_4 is quite a bit more delocalized than methane. In other words, each Pb–H bond is delocalized over the other three bonds. The loss of localized charge density in the bond shows up as negative contributions to K(Pb–H) from other orbitals as well as in a positive contribution from the Pb–H bonding orbitals that is significantly higher than the total K.

Large relativistic effects on one-bond heavy-atom–ligand spin–spin coupling constants have also consistently been calculated for other systems. Figure 12-8 shows a comparison of a number of tungsten–ligand coupling constants in comparison to their nonrelativistic counterparts and to experiment. Coupling constants involving other elements from the 6th row of the periodic table, such as Hg and Pt, are similarly strongly affected, mainly by spin-free relativistic effects [110].

Spin–orbit effects on one-bond couplings are often found to be relatively small in comparison to the spin-free effects. An exception is the series of Tl-X where X = F, Cl, Br, I. Figure 12-9 shows the isotropic K(Pb–X) as well as the coupling tensor anisotropy ΔK for the series as computed with hybrid DFT and the ZORA relativistic approach. Nonrelativistic data are not shown but were previously found to be only about half the magnitude of the scalar relativistic results [5]. For the isotropic coupling the spin-free relativistic computations only predict a weak trend along the series (or no trend at all depending on the functional used), while a very

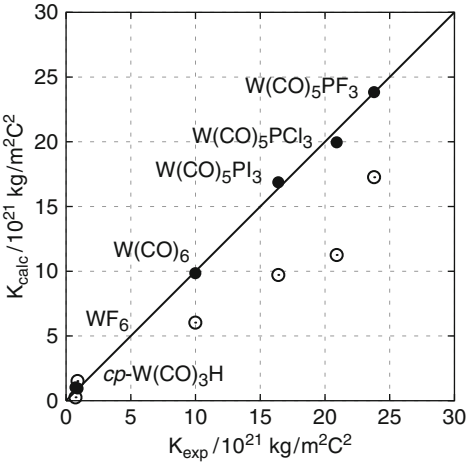

Figure 12-8. One-bond tungsten–ligand spin–spin coupling constants, computation versus experiment, from Reference [4]. *Filled markers* • indicate scalar relativistic ZORA, *open markers* ∘ nonrelativistic DFT results. The *straight thick line* indicates where calc. = expt.

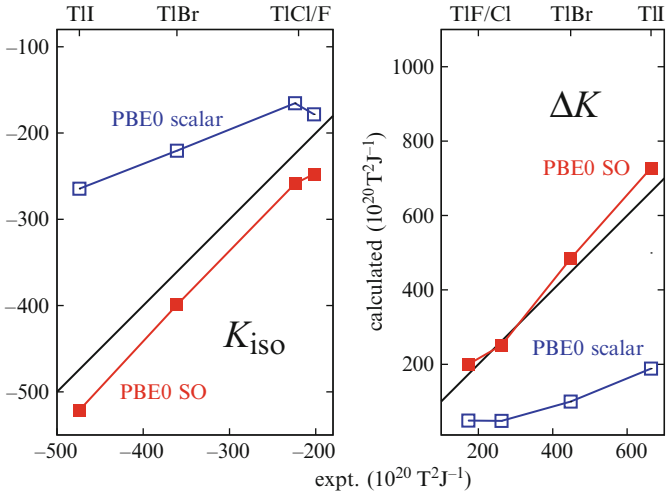

Figure 12-9. Spin–orbit effects on the nuclear spin–spin coupling in the series Tl-X, X = F, Cl, Br, I. ZORA hybrid DFT computations versus experiment. Isotropic coupling K and coupling tensor anisotropy ΔK. Computational data from [125]. Experimental data from [139–142]; see also [143] and [144]. The *straight thick line* indicates where calc. = expt.

strong trend is present in the SO results as well as the experiment. For Tl-I the spin–orbit OP-FC cross term is the largest individual term in the coupling tensor [5]. The available body of computational data indicates that SO effects on spin–spin coupling tend to be important when coupling between two heavy p-block elements is involved. We note in passing that nonhybrid functionals very strongly overestimate the coupling anisotropy while the hybrid DFT data shown in Figure 12-9 agree well with experiment.

Extremely large relativistic effects might be obtained for spin–spin coupling between two heavy nuclei. We have in the past studied metal–metal spin–spin coupling constants quite extensively, for instance for Pt–Pt [135], Pt–Tl [133, 136, 145–147], or Hg–Hg couplings [148, 149] and obtained good agreement with experiment from relativistic DFT computations whereas nonrelativistic computations cannot be meaningful for such couplings. For instance, Hg–Hg couplings can be as large as several hundred kilo-Hz, with the large magnitude caused by the s-sigma character of the Hg–Hg bonds and the fact that the hyperfine terms for the 6s Hg orbital increase relativistically by about a factor of three [102, 103]. For a pair of Hg nuclei, this would result in an order of magnitude increase of the 6s–6s orbital contributions in the coupling tensor just from the atomic hyperfine integrals alone. These and other studies on heavy metal–metal coupling constants [135, 136, 146, 147] have also shown that relativistic effects on the coupling constants tend to act as a *magnifying glass* for subtle effects in the metal–metal and metal–ligand bonds. This means that NMR is a particularly sensitive tool to study details of bonding in these heavy atomic systems.

Two- or higher-bond coupling constants have not yet been extensively investigated by relativistic computations. Kaupp has reported significant relativistic effects on the ^{31}P–^{31}P two-bond coupling constants in *cis*- and *trans*-$M(CO)_4(PH_3)_2$, M = Cr, Mo, W, leading to a reversal of the trend of increasing P–P coupling for the W complex as the metal becomes heavier [150]. Noticeable spin–orbit effects on a three-bond C–C coupling constant were reported by Autschbach and Ziegler for the complex $[(NC)_5Pt–Tl(CN)]^-$ [145]. It is likely that significant relativistic corrections on multi-bond coupling constants between light atoms will be obtained when the coupling path involves a heavy metal, as it is the case for the two examples mentioned. In this context, we highlight a recent study by Bagno and Saielli who computed nuclear spin–spin coupling constants between DNA base pairs mediated by a heavy metal (Hg) [151].

Interestingly, SO effects on nuclear magnetic shielding constants have been studied theoretically quite some time before scalar relativistic effects were considered. It has been known for a long time that the shielding of nuclei in the vicinity of a halogen strongly increases as the halogen nuclear charge increases. This leads to a decreasing shift of atoms neighboring X = F, Cl, Br, I, with increasing nuclear charge of X which is called "normal halogen dependence" (NHD). An example is the proton shift in the hydrogen halides H–X. It had been argued already in the late 1960s [153] that spin–orbit coupling must be responsible for the increasing shielding of the proton along the series. Computational studies of the proton shieldings in HX date back to the 1970s, when perturbation approaches employing the SO part of the Pauli operator together with semiempirical LCAO wavefunctions have been used [154–156]. Since then, numerous computations have confirmed that the NHD is induced by spin–orbit coupling. As an example, Figure 12-10 shows data

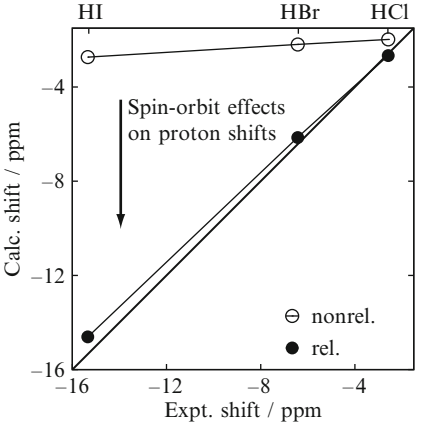

Figure 12-10. Proton chemical shift of HX, X = Cl, Br, I, with respect to HF. MCSCF computations including (rel) or excluding (nrel) first-order (Breit–Pauli) relativistic corrections to the shielding constant. Computational results were taken from from Manninen et al. [56]. Experimental data as quoted in [152]. The *straight thick line* indicates where calc. = expt.

from MCSCF computations by Manninen et al. who included relativistic effects perturbationally to first order in c^{-2} at the Breit–Pauli level [56]. The relativistic results are in excellent agreement with experiment and demonstrate the large spin–orbit effect in particular for HI. A compilation of literature data for the HX series can be found in [118]. The physical mechanism of NHD is related to that of spin–spin coupling in some sense [157,158]. Around a heavy atom where SO-coupling is strong, the external magnetic field not only induces a paramagnetic current–density but also a spin-density perturbation. This perturbation transfers through the chemical bonds and causes non-vanishing spin-dependent terms in the shielding tensor at light neighboring nuclei via the FC/SD mechanism. In computations of light-nucleus shieldings in heavy atom compounds it is therefore safest to use a spin–orbit relativistic method, although NHD-type effects may not always be present [159].

In transition metal chemistry, NHD-type effects have also been found. Several groups have investigated the carbon shifts in heavy transition metal carbonyls. Figure 12-11 shows a comparison of scalar and spin–orbit results obtained with the Pauli-operator (using frozen cores to avoid variational collapse) [152, 160]. The inclusion of SO coupling noticeably improves the agreement with experiment, in particular for the metals with higher group numbers/complexes with smaller shifts. Vaara et al. have also studied this series using a spin–orbit ECP for the metal and obtained similarly good agreement with experiment [161]. The spin–orbit effect for the shielding follows a somewhat unintuitive trend: like for all second-derivative properties the HOMO–LUMO gaps $\Delta\varepsilon$ and energy differences between other pairs of occupied and unoccupied orbitals enter denominators in the shielding tensor expression analogous to the energy differences in the denominator in Eq. (12-26). $\Delta\varepsilon$ increases from Hf to Ir, but so does the magnitude of SO term in the shielding. As it was analyzed by Wolff et al. [152], as the metal's oxidation state increases

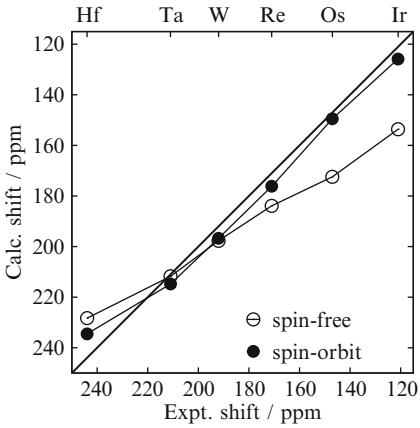

Figure 12-11. Carbon chemical shifts (reference: TMS) of transition metal carbonyls $[M(CO)_6]^n$ where n ranges from $+3$ (Ir) to -2 (Hf). Spin-free relativistic data from Ehlers et al. [160], SO and exp. data were taken from Wolff et al. [152]. The *straight thick line* indicates where calc. = expt.

from Hf to Ir, ligand–metal σ-bonding increases and π-back donation decreases.[9] The increase in σ character of the metal–ligand bond is able to transfer the spin-density more effectively from the metal to the carbon nucleus. This effect outweighs the increase in the orbital energy gap in the shielding expression. Such a balance of effects appears to be very typical in the NMR of transition metal complexes [110]. A balance between orbital gap trends and bonding characteristics was also noted, for example, for Pt chemical shifts [162].

For the shielding constant of a heavy metal nucleus both scalar and spin–orbit relativistic effects can be important [12, 118]. Relativistic effects on shielding constants are quite noticeable already for 4d metals and the main group elements up to around Xe. An increase of the scalar relativistic effects of the shielding of the heavy nucleus X with $\sim Z^{3.5}$ has been found for the HX series [163]. Other authors found a scaling of $Z^{2.3}$ for the metal shielding in the M-F series, where M = Cu, Ag, Au [164]. Benchmark data for absolute shieldings of atoms [165], in particular for the closed-shell are gas atoms [36, 40, 56, 84, 85, 166, 167], are available. One reason is that single atoms are very useful for benchmarks. There is also some interest in establishing absolute shielding scales for these systems. To this end, it should be noted that it is far from trivial to fully converge such calculations, and for the heavier nuclei it is also important to consider finite nucleus effects.

Often, large portions of the relativistic effects for shielding constants cancel when the chemical shift is evaluated. This happens to be the case when the relativistic effects in the shielding tensor mainly originate from the core and semi core orbitals. For 5d metals and the heaviest main group elements this is usually not the case anymore. Sizeable spin-free and spin–orbit relativistic effects on the chemical shifts of NMR nuclei such as W, Pt, Hg, Tl, or Pb are predicted in computations. The relative magnitudes of scalar versus SO effects depend on the element and the bonding environment. A selection of available computational studies of heavy metal chemical shifts where significant relativistic corrections were reported, and where results were compared with experimental data, is the following: [162, 168–172] for Pt chemical shifts, [1, 37, 173] for Hg [174–176] for W [174, 177] for Pb shifts [170, 136] for Tl chemical shifts. Metal NMR parameters in poly-oxo metallates have received significant interest from computational chemists in recent years [178–181]. Applications of relativistic DFT methods to model the NMR in these systems successfully shows that existing program implementations can handle systems with large numbers of electrons.

NMR tensor *anisotropies* are important in oriented samples (solid, partially oriented solutions). The tensorial properties of nuclear shielding and spin–spin coupling can be measured, for instance, in solid-state NMR experiments [182] or by liquid–crystal NMR (LCNMR). As an example for a strongly "relativistic" system, the LCNMR technique has been used by Jokisaari et al. to measure the anisotropy of the $^{13}C - ^{199}Hg$ coupling tensor in methyl mercury halides and $HgMe_2$ [183]

[9] In a computational analysis such changes in bonding tend to show up in significantly increased or reduced matrix elements in the numerator of the SOS expression, Eq. (12-26).

(Me = methyl). ZORA DFT computations were also performed which reproduced the experimental data within the rather large experimental error bars. Relativistic spin–orbit effects were found to increase the relative anisotropy $\Delta K/K$ as was predicted by Pyykkö already in 1977 [103], mainly due to FC/OP cross terms. In a related study, Jokisaari et al. investigated the ^{199}Hg shielding tensor anisotropy in these systems [184]. Scalar relativistic DFT computations predicted in this case the opposite trend for $\Delta\sigma$ than SO computations, with the latter being in agreement with the trend found experimentally: $\Delta\sigma$ decreases for Me–Hg–X along the series X = Me, Cl, Br, I.

Before moving on to discussing other types of properties it should be pointed out that the computational modeling of NMR parameters and other response properties can be quite challenging if solvent effects or crystal environments significantly perturb the electronic structure of a molecule. Single-molecule computations may not be sufficient in this case. For example, rather spectacular solvent effects on coupling constants and chemical shifts have been computed for Pt–Tl bonded systems [136, 146, 170], for Pt and Hg complexes [185], and more recently for the one-bond coupling in $[Hg–Hg–Hg]^{2+}$ [149]. These solvent effects cannot be described fully with a simple continuum model. For instance, in the Hg_3^{2+} case the computed gas-phase coupling constant is on the order of 240 kHz while the experimental value in the supposedly inert liquid SO_2 solvent is 140 kHz. By using molecular dynamics simulations it was shown that the presence of the solvent causes this difference. In a series of related Pt–Tl bonded systems coordination of one of the metals by water, along with bulk solvent effects, reversed the trend computed for K(Pt–Tl) in gas phase and reconciled theory and experiment [146]. Recent work on Pt chemical shifts has also indicated an importance of rather unspecific solvent effects which may influence the shift directly via electronic effects and indirectly via the geometry of the complex [149]. Computations can be very helpful in this respect to uncover if experimental data are strongly affected by such external influences, or if the observed trends are more of an intrinsic nature.

12.3.2. Electron Paramagnetic Resonance

In electron paramagnetic resonance two important molecular properties are the electronic $\mathcal{g}$-tensor and the nuclear hyperfine coupling tensor $\mathcal{A}$. Both arise from the interaction of a net electron–spin magnetic moment of the molecule with magnetic fields. In the case of the electronic g-tensor the interaction is with an external magnetic field. Usually the interest is in the deviation from the free electron g-value, i.e., $\mathcal{g} = g_e \mathbb{1} + \Delta\mathcal{g}$ and one considers $\Delta\mathcal{g}$ as a response property of the electronic structure in the molecule. The spin Zeeman term (12-52c) is is the interaction operator related to the free electron g value and will be omitted from the discussion.[10] In some formal analogy to the NMR shielding tensor, the EPR $\Delta\mathcal{g}$-tensor can be defined via an effective spin Hamiltonian that includes the interaction of a fictitious

[10] This is analogous to the (non) treatment of the nuclear Zeeman operator in NMR computations.

effective electron spin magnetic moment $\mathcal{S}$ with an external magnetic field and with each other via [73, 186]

$$H = \frac{1}{2}\boldsymbol{B}(g_e + \Delta g)\mathcal{S} + \mathcal{S}\mathbb{D}\mathcal{S}. \tag{12-78}$$

Equation (12-78) follows the usual sign conventions for Δg. Like the magnetic shielding, Δg is dimensionless and results are typically reported in parts per million (ppm) or parts per thousand (ppt). The factor 1/2 in Eq. (12-78) stems from the Bohr magneton converted to atomic units. It should also be noted that the "g-tensor" and some other tensors related to magnetic properties do not necessarily transform as proper tensors under spatial rotations, therefore the use of the word "tensor" in this context can be somewhat misleading [186]. Some authors prefer the term "g-matrix" instead [187]. The effective spin in Eq. (12-78) can be chosen to reproduce the observed multiplet structure of the EPR signal. The eigenvalues of the effective spin-Hamiltonian are intended to correspond to the experimentally observed energy levels. $\mathbb{D}$ is responsible for a zero-field splitting caused by electron–spin–electron–spin interactions It can be neglected from the discussion for the limit of a strong external field. Recent computational work dealing with zero-field splitting can be found in [188–192].

The hyperfine tensor $\mathbb{A}$ describes the interaction of a net electron–spin magnetic moment with the magnetic field from a nuclear spin. It can be defined by the effective spin–Hamiltonian [73, 186]

$$H = \mathcal{S}\mathbb{A}\boldsymbol{I}_A. \tag{12-79}$$

Here, $\boldsymbol{I}_A$ is the nuclear spin vector, which is related to the spin magnetic moment by $\vec{\mu}_A = \gamma_A \boldsymbol{I}_A$. Equation (12-79) follows a common convention for the definition of $\mathbb{A}$. Values are typically given in SI units of MHz, or in c.g.s. units of G (Gauss, with a conversion factor of approx. 2.8025 MHz/G [193]).

The Δg term in (12-78) connects the electronic spin magnetic moment and the external field with the response of the electronic system, which is somewhat analogous to the magnetic shielding tensor. Likewise, 12-79 describes the magnetic electronic spin–nuclear spin interaction which has some analogy to the nuclear spin–spin coupling. To rationalize the physical origin of the Δg-tensor, it is useful to recall that in a nonrelativistic theory there is no coupling between the electron spin and orbital magnetic moment. Consider an orbital model. In a nonrelativistic theory an orbital's spin is either α or β, independent of the spatial function of the orbital. However, when switching to a two-component relativistic formalism with spin–orbit coupling, the relative magnitude of the α and β component in the orbital varies as a function of position. In other words, the electron spin has now acquired a "sense" of where in the molecule it is (i.e., the α/β ratio depends on the potential which varies in space). Only in this situation can there be a change of the electron's g-tensor compared to the free-electron. It is therefore clear that spin–orbit coupling is a prerequisite for Δg calculations. In a sense, Δg may be considered

a purely relativistic property. The hyperfine coupling has a nonzero nonrelativistic limit. Depending on the formalism used to compute $\mathcal{A}$ spin–orbit coupling can be neglected in a first approximation but should be included for accurate results in heavy element systems.

Taking derivatives of the quantum mechanical energy expression expanded as a perturbation series in external field, nuclear spin, and the effective electron spin is not as straightforward as in the case of the NMR parameters because the effective spin $\mathcal{S}$ of Eqs. (12-78) and 12-79 does not appear in the operators of Section 12.2.5. Various ways of approaching the Δg-tensor problem were summarized in an overview article by Patchkovskii and Schreckenbach [117]. For hyperfine tensors see, e.g., the article by Eriksson [193]. See also the textbooks by Harriman and Abragam [73, 186]. In a nutshell, if spin–orbit coupling is included in the ground state computation then the EPR tensors can be computed from *first* derivatives of the molecular energy with respect to $\boldsymbol{B}$ for the Δg tensor and with respect to $\boldsymbol{m}_A$ (which is proportional to $\boldsymbol{I}_A$) for the $\mathcal{A}$-tensor. See also [6, 7, 194, 195]. If spin–orbit coupling is not included in the computation of $E^{(0)}$ then relativity needs to be treated as an additional perturbation. In this case, the EPR tensors are computed from a double perturbation equation of the type (12-25) where perturbation operators depending on the external field $\boldsymbol{B}$ or the nuclear spin moment $\boldsymbol{m}_A$, along with spin–orbit coupling operators and their field-dependent versions have to considered. In either case, an expression needs to be derived that allows to identify the eigenvalues of the effective spin Hamiltonians with the energy levels of the molecule's electron spin projection in the presence of the external or nuclear magnetic field. A "spin"-differentiation may also be conceptualized by considering a spin-dependent one-electron operator for spin-component u in the form $\hat{h} = \hat{a}_u(\boldsymbol{r})\sigma_u$. Examples are the spin–orbit operators in two-component formalisms, or the spin-dependent hyperfine terms (FC+SD and their relativistic analogs of Section 12.2.5). Suppose we start with a scalar relativistic reference system. The action of the spin-dependent operator on the wavefunction, after integration over spin, yields terms of the form

$$S_u \hat{a}_u(\boldsymbol{r}) Q_u(\tilde{\vec{r}}, \boldsymbol{r})\big|_{\tilde{\vec{r}}=\boldsymbol{r}} \tag{12-80}$$

with $Q_u(\tilde{\vec{r}}, \boldsymbol{r})$ being a normalized spin density [11] and S_u the maximum value of the projection of the spin onto the u-axis. A differentiation with respect to this spin-projection can now be carried out, leaving as the perturbation operator $\hat{a}_u$, the spin-free part of $\hat{h}$, acting on a normalized spin density. The $\hat{\mathcal{H}}^{(\mathcal{F}_i,\mathcal{F}_j)}$ operators needed for the bilinear ("diamagnetic") perturbation contributions can be derived in an analogous way from operators bilinear in spin-terms and $\boldsymbol{B}$ or $\boldsymbol{m}_A$, respectively. For the hyperfine coupling, the dominant term arises here from the FC operator and its relativistic analogs.

We shall discuss g-tensors first. A comparison of different nonrelativistic implementations reported up to 2001 can be found, e.g., [196]. Earlier work on Δg tensors with ab-initio (Hartree-Fock, MCSCF, CI) or semiempirical methods can be found, e.g., in [194, 197–202]. For further references on these approaches we

refer to the literature cited in [196, 203]. Scalar relativistic corrections can in principle be included in all these methods, either explicitly at the operator level or via ECPs. A first-derivative approach with spin–orbit coupling included variationally at the ZORA level has been implemented by van Lenthe et al. [6] (see also [194]). Applications of this approach have so far employed a spin-restricted unperturbed Kohn–Sham computation because of conceptual issues with the description of spin density in a spin–orbit coupled context. More recently, Malkin et al. reported an implementation within a two-component relativistic framework where the issue of defining the spin-polarization in a two-component framework has been addressed [39]. Four-component implementations have also been reported, for instance in [204, 205]. For a discussion of alternative ways to compute g-matrices, and applications to molecules containing metal atoms as heavy as uranium, we refer the reader to [187, 195].

A scalar relativistic method employing the Pauli operator with frozen cores [206] has been applied to d^1 transition metal complexes of the type MEX_4^{n-}, with M = V, Cr, Mo, W, Tc, and Re, E = O, N, and X = F, Cl, and Br [207]. The results are displayed in Figure 12-12. It can be seen that the correlation between the theoretically predicted and the experimental values is quite reasonable for the 3d and 4d metals. The $\Delta g_{\parallel}$ component of the tensor was systematically overestimated, though, in particular for the 5d metals, which unfavorably affected the isotropic averages shown in Figure 12-12. Density functional computations appear to perform reasonably well for EPR parameters of main group radicals. However, the performance of popular nonhybrid density functionals appears to be less satisfactory for transition metal complexes. This has been attributed in [207] to deficiencies of such functionals leading to an overestimation of covalent bonding between the metal and the ligands. This viewpoint has subsequently been corroborated by Malkina et al. [208]. Hybrid density functionals appear to perform somewhat better in comparison [196, 209].

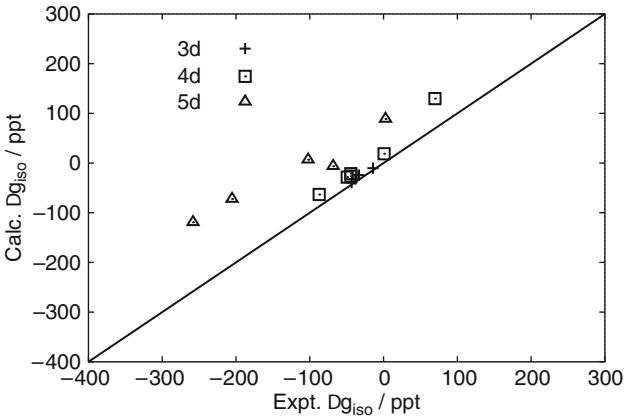

Figure 12-12. Isotropic average of the Δg tensor of 3d to 5d transition metal complexes MEX_4^{n-} with X = O, N, and X = halide, in ppt. Calculated results (DFT, Pauli operator, frozen cores) versus experiment. Data taken from Patchkovskii et al. [207]. The straight line indicates where calc. = expt.

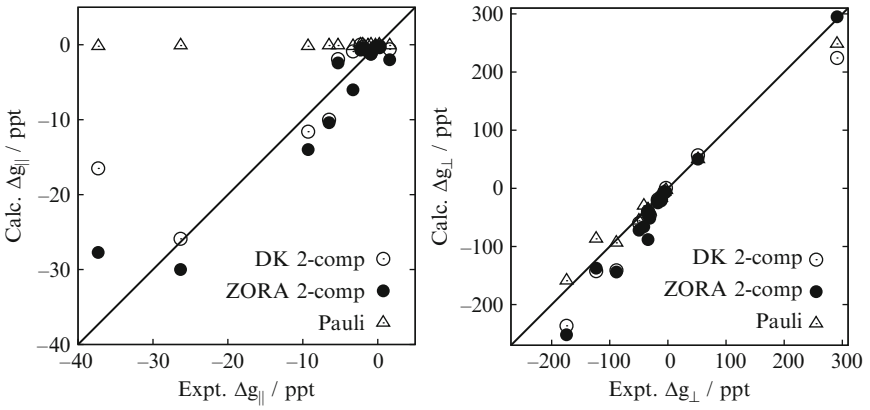

Figure 12-13. Comparison of various DFT computations (BP86 functional) of Δg tensors with experiment for the diatomic radicals RhC, PdH, ZnH, CdH, HgH, ZnF, CdF, HgF, ZnAg, CdAg, HgAg, LaO, ZnCN, CdCN, HgCN, and GaO. All data were taken from Table II of Malkin et al. [39]. ZORA results originally reported by Belanzoni et al. [210]. "Pauli" data from Patchkovskii and Schreckenbach [117] and Schreckenbach and Ziegler [206]. Data for the unique tensor components $\Delta g_{\parallel}, \Delta g_{\perp}$ are shown

EPR tensors of a series of diatomic radicals with heavy elements has been studied by various groups. Figure 12-13 gives an overview of some of the computational results obtained with variational two-component DFT (nonhybrid BP86 functional, DKH and ZORA) and a method where the Pauli operator was used in a second-order derivative approach (i.e., only the leading-order relativistic corrections are included). Data are shown for RhC, PdH, ZnH, CdH, HgH, ZnF, CdF, HgF, ZnAg, CdAg, HgAg, LaO, ZnCN, CdCN, HgCN, and GaO. For the parallel tensor component the Pauli perturbational approach fails to reproduce the negative $\Delta g_{\parallel}$ tensor components which are particularly large in magnitude for PdH and HgH. This issue has been discussed in [117, 210] and can be traced back to the following reason: When using a spin–orbit free unperturbed wavefunction the leading-order paramagnetic terms for the $\Delta g_{\parallel}$ component can be written in SOS form (Eq. 12.26) with the help of matrix elements $\langle \Psi_0 | \hat{L}_{\parallel} | \Psi_k \rangle$ multiplied by an effective spin–orbit coupling constant. Here, $\hat{L}_{\parallel}$ is the angular momentum operator along the molecule's axis. In the absence of spin–orbit coupling, the wavefunctions of a linear molecule are eigenfunctions of this operator and thus the leading paramagnetic contribution to $\Delta g_{\parallel}$ essentially vanishes in this approach. In the methods that include SO coupling variationally the wavefunctions are not eigenfunctions of $\hat{L}_{\parallel}$ and comparatively large matrix elements for the perturbation may result. It can be seen from Figure 12-13 that both variational two-component methods reproduce the negative $\hat{L}_{\parallel}$ reasonably well. For the $\Delta g_{\perp}$ component the situation is different. Here the leading-order contributions are those of order c^{-2} and the Pauli perturbational approach performs just as well as the variational methods [117]. The DKH implementation by Malkin et al.

has included effects from spin-polarization, which improved results for light-atomic systems. For the heavy-metal diatomics cases of Figure 12-13, the spin-restricted ZORA and the spin-polarized DKH data do not seem to differ dramatically.

Van Lenthe et al. have investigated $\mathcal{g}$-tensors in low spin Fe(I) and Fe(III) porphyrin complexes [211], using DFT and a ZORA implementation for the response calculations. The computational results for these systems, some of which afford very large $\mathcal{g}$-tensor anisotropies and isotropic g-values that differ strongly from the free-electron value, were in reasonable agreement with experiment. With the help of the calculations the validity of a simple and widely used model for the $\mathcal{g}$-tensor, based on writing the Kramers pair in terms of the Fe d_{xy}, d_{xz}, and d_{yz} orbitals, was tested. It was found that the model is indeed compatible with the first-principles calculations if one considers some amount of ligand orbital combinations of the same symmetry mixing with the d orbitals used to describe the unpaired electron.

Belanzoni et al. have computed hyperfine tensors using a spin-unrestricted scalar relativistic ZORA DFT approach as well as spin-restricted ZORA spin–orbit computations with a nonhybrid functional [210]. The methods are somewhat complementary, each neglecting some effects. The linear molecules of Figure 12-13 have been studied using the ZORA implementation of van Lenthe et al. [7]. The $\mathcal{A}$ tensors were also analyzed in quite some detail, based on Mulliken populations of the singly occupied molecular orbitals and semi-quantitative estimates of the orbital mixing due to spin–orbit coupling. Overall, the agreement with experiment was reasonable. In a recent article in which a modified four-component approach for EPR parameters (DKS2-RI) was reported, Komorovsky et al. noted that in particular for the HgH molecule spin-polarization effects on the hyperfine coupling turned out to be important [205]. Some isotropic ^{199}Hg hyperfine couplings are shown in Figure 12-14 for comparison of some of the theoretical methods mentioned in this paragraph. The data have been obtained using point-nucleus models and are therefore likely too high in magnitude. For comparison, the nonrelativistic isotropic hyperfine couplings from the ZORA SC-U data set reported by Belanzoni et al. are 3,763, 7,121, and 8,841 MHz for HgH, HgCN, and HgF, respectively. The experimental values were quoted as 7,002, 15,850, and 22,127 MHz, respectively. The overall quite reasonable agreement of the relativistic results shown in Figure 12-14 with experiment, and the $\sim$100% or more relativistic increase, once more highlights the enormous impact that relativity can have on properties involving nuclear hyperfine operators.

In the section on spin–spin coupling the finite size of nuclei was mentioned as a source of error in particular for treating the relativistic analogs of the FC "contact" operator. This operator is also an important ingredient for $\mathcal{A}$-tensor computations. Malkin et al. have calculated finite-nucleus effects for the related case of hyperfine coupling constants and found consistent improvement with experiment in DFT computations of group 11 atoms and small molecules with group 12 atoms [100]. As indicated in Section 12.3.1, the magnitudes of the FC-type integrals decrease when an extended nucleus is used. As an example for the impact on $\mathcal{A}$-tensors, the isotropic hyperfine coupling constant for ^{199}Hg in the Hg–F diatomic was calculated

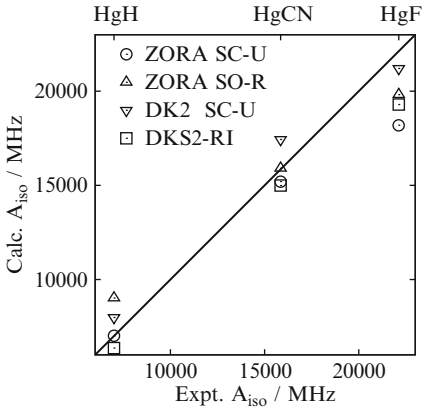

Figure 12-14. Isotropic ^{199}Hg EPR hyperfine coupling constants for HgH, HgCN and HgF. ZORA spin-restricted spin–orbit (SO-R) and scalar unrestricted (SC-U) DFT results (BP86 functional) taken from Belanzoni et al. [210]. Second-order DKH SC-U and four-component (DKS2-RI) DFT (LDA functional) data from Komorovsky et al. [205]

as 25102 MHz with a point nucleus and 21490 MHz with an extended nucleus (DFT, B3PW91 functional, second-order DKH). The experimental value is 22127 as already mentioned.

Regarding applications in coordination chemistry, Munzarová and Kaupp have compared DFT and coupled-cluster ab-initio methods for the computation of $\mathbb{A}$ tensors for 3d transition metal complexes [212]. A nonrelativistic formalism is often sufficient for these rather light atoms. Unfortunately, the authors stated that "none of the investigated functionals performs well for all complexes", including hybrid functionals. In comparison, coupled-cluster computations which were feasible for the smaller molecules in the test set yielded very accurate results, with a tendency to underestimate the experimental reference values. The problems with the density functionals have been attributed to difficulties obtaining the correct balance between spin polarization in the metal core regions (which determines the hyperfine coupling constants of the metals) and valence spin polarization, which causes problematic spin contamination [213]. Neese has subsequently also noted DFT-related problems with computations of hyperfine couplings for 3d metal complexes using an implementation where SO coupling terms were included to order c^{-2} [214].

The mechanism of ESR hyperfine coupling has been studied in detail in [215], highlighting the leading role of overlap between the singly occupied orbital of a doublet system with certain doubly occupied valence orbitals. Deviations between calculated results and experiment were approximately within 10–15% for most of the complexes and most of the functionals, allowing for a reliable interpretation of the results in comparison with experiments. A comparison between different program implementations for computations of EPR parameters by DFT has been recently made by Saladino and Larsen [216] with a focus on catalysis applications. Results for paramagnetic vanadium and copper model complexes were reported.

The authors also noted the problem with modeling the spin polarization in the metal 3d shell when calculating metal hyperfine couplings. On the positive side, experimental trends for systems with similar electronic structures were successfully reproduced.

12.3.3. Electric Field Gradients (EFGs)

The electronic and nuclear charges in a molecule create an electric field. We may refer to it as the "intrinsic" electric field of the molecule, as opposed to the electric field and field-gradient of an external perturbing field that was discussed in Section 12.2.5. The internal field's inhomogeneity is to first order given by its first derivative, the electric field gradient (EFG). In Section 12.2.5 it was shown that electric field gradients interact with electric quadrupole moments. To derive the expressions of the internal field gradient, imagine a (hypothetical or actual) point quadrupole with Cartesian quadrupole tensor elements G_{uv} as in Eq. (12-42) which is placed somewhere in the molecule as a probe. The quadrupole–electric field gradient interaction term has then to be added to the Hamiltonian analogous to the addition of $-\phi(\boldsymbol{r})$ and higher-order multipole terms for an electric field. Consider the first-order energy change $E^{(G_{uv})}G_{uv}$ due to the quadrupole–EFG interaction. The derivative $E^{(G_{uv})}$ is then – according to first-order perturbation theory – given by Eq. (12-24) with the unperturbed wavefunction, with $\hat{\mathcal{H}}^{(G_{uv})}$ being the molecule's electric field gradient operator at the position of the quadrupole. The electric field is given by the (negative) derivative of the scalar potential caused by the nuclei and the electrons. The electric field *gradient* operator for the quadrupole perturbation is defined accordingly as the (negative) *second* derivative of the scalar potential operator for the internal field,[11] i.e.,

$$\hat{V}_{uv}^{\mathrm{EFG}} = \frac{\partial^2 \phi}{\partial r_u \partial r_v} \quad u, v \in \{x, y, z\} \tag{12-81}$$

The internal EFG is then computed from an expectation value of the operator (12-81) where the second derivative can be considered at any point in space.[12] The EFG is a rank-2 tensor which may be characterized by three principal components, V_{ii}, and its principal axes. Important applications arise when considering the EFG at the position of a quadrupolar nucleus, and evaluating the interaction energy of the internal EFG with the nuclear quadrupolar charge distribution. This interaction

[11] The EFG proper is $-\hat{V}_{uv}$. We use the term 'EFG' but omit the negative sign here which is consistent with the definition of the quadrupole coupling used here.

[12] This is conceptually similar to the magnetic shielding tensor which may also be defined at any point in space by considering a point magnetic dipole $\boldsymbol{\mu}$ at a position $\boldsymbol{r}_X$ and using its vector potential $\boldsymbol{A}^X = \frac{1}{c^2}\frac{\boldsymbol{\mu}\times\boldsymbol{r}_X}{r_X^3}$ instead of the nuclear vector potential (12-45) in the derivation of the NMR shielding. In NMR the measurement relies on the presence of a nuclear spin and therefore the shielding tensor is measured at the position of the nucleus.

is important in NMR and Mössbauer spectroscopy, and it may be exploited directly in nuclear quadrupole resonance (NQR) spectroscopy. For instance, spectroscopic nuclear quadrupole coupling constants C_Q are related to the EFG tensor via

$$C_Q = \frac{eQV_{33}}{h} \tag{12-82}$$

where V_{33} is the largest-magnitude component of the EFG tensor and Q the nuclear quadrupole moment. Likewise, Mössbauer quadrupole splittings

$$\Delta E = (1/2)eQV^{\mathrm{EFG}} \tag{12-83}$$

are proportional to V^{EFG}. The nuclear quadrupole-field gradient interaction is very important in solid-state NMR [182] and, with modern ultra-high-field instruments, measurements of NMR parameters and C_Q of formerly inaccessible quadrupolar nuclei are now possible. With reliable EFG tensor computations at hand, a fit to experimental data might then in turn be used to obtain nuclear quadrupole moments. A large set of quadrupole moments based on literature data up to 2001 has been compiled by Pyykkö [217]. An updated compilation can be found in [218]. In these articles the reader can find references to relativistic computational work for many heavy nuclei including various actinides. We also point to an extensive review by Schwerdtfeger et al. [121] covering the literature up to 2003.

Taking the expectation value of (12-81) in the sense of Eq. (12-24) for a point quadrupole at a nuclear position $\boldsymbol{R}_A$ yields for an N-electron system

$$V_{uv}(\boldsymbol{R}_A) = -\int d\boldsymbol{r} \cdot \rho(\boldsymbol{r}) \left\{ \hat{V}_{uv}(\boldsymbol{r}, \boldsymbol{R}_A) - \frac{1}{N} \sum_{B \neq A}^{\text{Nuclei}} \hat{V}_{uv}(\boldsymbol{R}_B, \boldsymbol{R}_A) \right\} \tag{12-84}$$

with

$$\hat{V}_{uv}(\boldsymbol{x}, \boldsymbol{y}) = \frac{3(\boldsymbol{x} - \boldsymbol{y})_u (\boldsymbol{x} - \boldsymbol{y})_v - \delta_{u,v} |\boldsymbol{x} - \boldsymbol{y}|^2}{|\boldsymbol{x} - \boldsymbol{y}|^5} \tag{12-85}$$

There is an electronic and a nuclear contribution. Since the operator for the latter is not dependent on the electron coordinates the density integration can be carried out immediately to cancel the factor of $1/N$, but for analysis purposes based on a density decomposition it can be convenient to keep both terms together [219]. The term for the electronic part is valid in the four-component and the nonrelativistic regime. As already pointed out in Section 12.2.5, in two-component formalisms the perturbation operator has additional picture-change corrections of order c^{-2}. Moreover, the electronic contribution is affected by relativistic effects in the electron density. Given the large magnitude of the operator in the near-nucleus region from its overall $1/r_A^3$ behavior one should expect large relativistic effects on the EFG

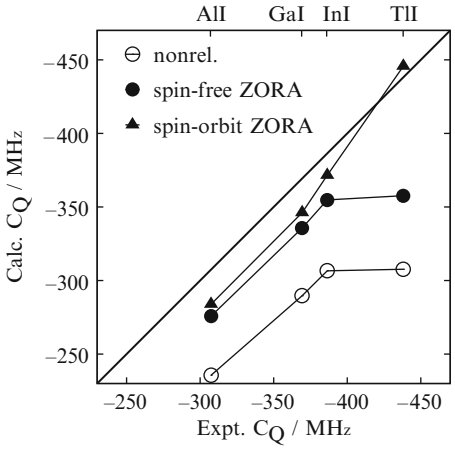

Figure 12-15. ^{127}I nuclear quadrupole coupling constants in group-13 iodide diatomics. ZORA DFT computations versus experiment. Data were taken from van Lenthe et al. [9]. The straight thick line indicates where calc. = expt.

percentage-wise. However, any filled and perfectly spherical atomic shell around the nucleus of interest does not contribute to the EFG.[13] Therefore, small deformations of the core orbitals in a molecular environment and the overall arrangement of the chemical bonds determine the magnitude of V which makes it overall a very useful "chemical" property.

The magnitude of relativistic effects on EFGs in heavy element systems is clearly demonstrated in Figure 12-15 for the iodine EFG in group-13 iodides [9]. Similar to the nuclear spin–spin coupling constants in TlX that were discussed earlier, both spin free as well as spin–orbit relativistic effects can be important for heavy p-block diatomics, in particular for TlI. If the bonding partner is not a heavy element, however, the scalar effects appear to be significantly more important which implies that for semi-quantitative results spin–orbit effects might be neglected for such systems. As an example, a range of ^{127}I C_Q results for iodine–halides reported in [9] agreed well with experiment both at the spin-free and the spin–orbit level. Marked improvements of iodine quadrupole coupling constants over nonrelativistic results were also obtained by Malkin et al. from second-order DKH scalar relativistic computations for the diatomics ICl, IBr, ICN, HI and IK [35].

The general (potential) importance of spin–orbit coupling for EFGs of heavy element molecules was pointed out by Visscher et al. [204] who performed four-component Hartree–Fock and correlated ab-initio computations for the H–X (X = F, Cl, Br, I) series of diatomics. For HI, the iodine EFG increased from 9.65 to 11.59 au at the Dirac HF level. An orbital contribution analysis was also carried out for HI and showed that most of the electronic contributions were due to valence-shell

[13] The EFG is also vanishing in highly symmetric environments such as tetrahedral or octahedral.

orbitals. The interpretation of the EFG mechanism was based on a model where a bond is formed between H^+ and a spherically symmetric (zero EFG) I^-. The bond formation amounts to forming a nonspherical hole in the iodine valence shell causing most of the EFG. Some semi-core- and core-polarization contributions were also seen in the EFG analysis for HI. Inclusion of spin–orbit coupling slightly lowered the magnitude of the EFG. This effect was attributed to the σ–π mixing in the bond: the electron hole on the iodine side acquires partial π character which is somewhat less asymmetric than the hole caused by a pure σ bond. Overall, the spin–orbit effect was small (−0.05 au) compared to the total relativistic increase. The H–X series of molecules has been very popular for theoretical benchmarks and has consequently been considered by many other authors as well. We cite reference [21] as an early numerical study of picture change effects which were demonstrated by computations of EFGs.

Picture-change effects on EFGs were studied by a number of researchers. As already mentioned, in a recent paper Mastalerz et al. revisited the series H–X where X = F, Cl, Br, I, At, and demonstrated that picture change effects can represent a considerable fraction of the relativistic correction to the EFG [101]. It should be noted that the bulk of the picture change effects were already obtained with the lowest-order transformation of the operator. A comparison was made with data obtained recently by other research groups, such as a study by Neese et al. [220] (four-component and DKH Hartree–Fock), by Malkin et al. [35] (DFT and Hartree–Fock with DKH), and Visscher et al. [204] (four-component Hartree–Fock, MP2, CCSD, CCSD(T)). All these studies have highlighted the importance of relativistic effects and of picture-change effects for this electric property.

The DKH method has recently been applied to calculate a large range of ^{119}Sn EFGs [221]. Scalar relativistic DFT calculations with the B3LYP functional were performed for 34 Sn complexes for which experimental Mössbauer quadrupole splitting parameters ΔE were available. The EFGs were in the range of −4 to +5 atomic units. It was noted that picture change effects entered the results as a systematic error of constant magnitude. Both picture-change corrected and picture-change uncorrected results showed an excellent linear correlation with the experimental ΔE. Based on the linear fit, a quadrupole moment of 13.2 ± 0.1 fm^2 was obtained for the ^{119}Sn nucleus, in good agreement with the 2001 reference value of 12.8 ± 0.7 [217].

For metal atom EFGs, Schwerdtfeger et al. pointed out problems with DFT to correctly describe the electron distribution in 3d transition metals [121]. As an example, for the CuCl molecule the Cu EFG varies between +0.67 and +0.15 for various functionals including hybrids while a CCSD(T) result of −0.34 au, likely to be very accurate, agrees well with experiment. It is known that 3d metals pose problems for many of the popular functionals and therefore it is no surprise that this is reflected in a rather poor performance in EFG computations. DFT results for heavier transition metal nuclei were not compared in this reference. Van Lenthe and Baerends also considered Cu–X (X = halide) diatomics in their ZORA study of EFGs cited earlier [9], along with Ag–X. The main focus has been on the halide C_Q; however, for the metal halides they did not agree as well with experiment

as those for the main group diatomics which also points towards deficient charge distributions for these systems obtained at the DFT level. Bast and Schwerdtfeger performed a DFT benchmark study of EFGs in 2003 [222] with a test set comprising various Sc, Cu, and Ga diatomics and concluded that "it is difficult (if not impossible in some cases) to obtain accurate [EFGs] for transition elements", while good performance of DFT was found for the main group element gallium. Willians et al. made a comparison between theory (ZORA DFT) and experiment for the ^{139}La C_Q [223]. Experimental data were derived from solid-state NMR. The agreement was poor irrespective whether SO coupling was included in the computations or not. However, the authors noted that the crystal environment was not modeled in the computations but might have a profound impact on the EFGs. Lanthanum chemical shifts computed at the same level of theory agreed reasonably well with experiment. Somewhat poor agreement with experiment for a Ru EFG both with hybrid and nonhybrid DFT was noted by Ooms and Wasylishen [224], albeit for a single carbonyl complex. Recently, Thierfelder et al. proposed to apply Coulomb-attenuated hybrid functionals for the computation of late transition metal EFGs [225]. The authors concluded that computations on the molecules CuH, AuH, and CuX, AuX, OC-CuX, OC-AuX, where X = H, F, Cl, Br, I, yielded reliable results with a CAM-B3LYP functional. Linear fits of the EFGs computed at this level of theory versus experimental C_Q yielded nuclear quadrupole moments that were in good agreement with experimental data.

Lantto and Vaara investigated the interplay of relativistic and electron correlation effects in a study of EFGs in noble gas (Ng) noble metal fluorides (Ng–M–F) [226]. Four-component MP2 calculations were performed to test the hypothesis whether relativistic effects and correlation effects are additive. It was found that treating these effects separately and adding them led to qualitatively correct noble gas quadrupole coupling constants. On the other hand, for the noble metal coupling constants a relativistic correlated treatment was found to be mandatory in order to get close to quantitative agreement with experiment. It is likely that these conclusions hold more generally as well. Relativistic effects in truly heavy metal atoms (with gold being one of the iconic examples) change the qualitative aspects of bonding. Therefore, one should expect that in such a situation correlation effects calculated at a nonrelativistic level of theory are not transferable to the bonding situation obtained at the relativistic level. Similar behavior has also been noted explicitly, for example, in calculations of heavy atom NMR chemical shifts and spin–spin couplings [118,119] as discussed earlier.

12.3.4. Dipole Moments, Polarizabilities, and Linear-Response Based Computations of Excitation Energies

The electronic contribution to the dipole moment of a molecule is given by a first-order derivative property of the electronic energy with respect to an electric

field.[14] The classical physics Hamiltonian for a dipole ($\boldsymbol{d}$)–electric field ($\boldsymbol{F}$) interaction is $H = -\boldsymbol{d} \cdot \boldsymbol{F}$. Accordingly, in quantum chemistry the intrinsic dipole moment of a molecule in the absence of a field (here: its electronic contribution) is

$$\boldsymbol{d} = -\left.\frac{\partial E}{\partial \boldsymbol{F}}\right|_{\boldsymbol{F}=0} \tag{12-86}$$

Induced dipole moments are obtained if one considers the dipole moment as being dependent on the electric field amplitudes, i.e.,

$$\boldsymbol{d}(\boldsymbol{F}) = \boldsymbol{d}^{(0)} + \left.\frac{\partial \boldsymbol{d}}{\partial \boldsymbol{F}}\right|_{\boldsymbol{F}=\boldsymbol{0}} \boldsymbol{F} + \cdots \tag{12-87}$$

for a static electric field. The first derivative is the linear dipole polarizability $\mathscr{\alpha}$, i.e., the linear response of the dipole moment. In terms of energy derivatives,

$$\mathscr{\alpha} = -\left.\frac{\partial^2 E}{\partial \boldsymbol{F}\, \partial \boldsymbol{F}'}\right|_{\substack{\boldsymbol{F}=\boldsymbol{0} \\ \boldsymbol{F}'=\boldsymbol{0}}} \tag{12-88}$$

is the static polarizability tensor, a double perturbation property. Using the quasienergy derivative formalism of Section 12.2.2, the approach may be generalized to oscillating fields and the *dynamic polarizability* $\alpha(\omega)$ may be computed as a function of frequency. As in previous sections, α denotes the isotropic average of the polarizability tensor $\mathscr{\alpha}$. Higher-order derivatives give access to various nonlinear optical (NLO) properties. The dynamic polarizability is a classic textbook example for a frequency-dependent molecular property. Molecular polarizabilities are often reported in atomic units, with a conversion factor to SI units of approximately $1.648 \cdot 10^{-41}$ C m $(\mathrm{V/m})^{-1}$/au [227], or in terms of polarizability volumes $\alpha' = \alpha/(4\pi\varepsilon_0)$ in volume units of $\mathrm{Å}^3$ or cm^3, respectively.

In Section 12.2.3 it was pointed out that the physical response is in general complex, with the imaginary part being related to an absorption property. In the case of the electronic dipole polarizability the imaginary part times the frequency is proportional to the electronic absorption coefficient (or cross section) corresponding to the dipole-allowed vertical transitions. A computation of the spectrum based on the "singularity route" outlined in Section 12.2.3 yields the electronic excitation energies, along with the nonzero or zero electric (and, if required, other) transition dipole moments. An example for a combined computation of $\mathrm{Re}[\alpha]$ and $\mathrm{Im}[\alpha]$ for the Au_2 molecule has already been discussed in this previous section.

In Section 12.2.5 the dipole moment operator for an electron was shown to be $\hat{\boldsymbol{d}} = -\boldsymbol{r}$ in the four-component and nonrelativistic formalisms. This operator

[14] According to the discussion of dynamic properties in Section 12.2.2 the only nonvanishing *first* quasienergy derivative is obtained if the field's frequency ω is zero, which is a consequence of the time averaging procedure.

does not have the inverse dependence on the nuclear distance like the ones relevant for the properties considered in previous sections. The polarizability at optical and lower frequencies is a valence shell–valence region property. As a consequence, the effects of relativity on polarizabilities are, percentage-wise, more similar to those on binding energies and other valence shell properties. Moreover, ECPs can be applied straightforwardly to compute polarizabilities including relativistic effects. Picture-change effects arising from the operator $\boldsymbol{r}$ are generally expected to be small for closed-shell systems [87].

Because the static polarizability can be computed also with finite-field techniques (i.e., analytical derivative techniques are not essential to obtain this property) literature data are abundant. To obtain accurate results for electric response properties such as the polarizability, however, it is important to include electron correlation in the computations. This is unlike its magnetic counterpart, the magnetizability, which is rather insensitive to electron correlation [228–230] but demanding on the basis set.

Static atomic polarizabilities have been computed already in the early days of relativistic quantum chemistry [231]. As an example, Desclaux et al. have studied static dipole polarizabilities of atoms from groups 1, 2, and 12 of the periodic table using numerical Dirac Hartree–Fock computations [232]. The authors noted that because of the lack of electron correlation the results were "mainly of technical interest". However, regarding the relativistic effects it was observed that the nonrelativistic trend of increasing polarizabilities with atom number reversed for the atom pairs Ba/Ra and Cd/Hg at the relativistic level. Such reversals of trends have in fact been found for many atomic properties; numerous examples were discussed by Pyykkö in a seminal review paper [233]. The relative decrease of the polarizability due to relativistic effects was found to be 12% and 32% for Ba and Ra, respectively. A decade later, Sadlej et al. have reinvestigated the polarizability of Ca, Sr, and Ba using correlated methods (MBPT and coupled cluster) [234]. The computed polarizabilities of 152, 190, and 273 au were in good agreement with experiment. The relativistic effect for Ba was largest, −12 au, and roughly comparable to the influence of electron correlation on the polarizability. In situations like this, one might also expect sizeable correlation–relativity cross terms.

As an example for polarizability computations both for real and imaginary frequencies, Hättig and Hess applied time-dependent scalar DKH computations with electron correlation treated at the MP2 level to obtain dynamic multipole polarizabilities of the noble gas atoms Ar–Rn [235]. From an integration of polarizability products along the imaginary frequency axis one can obtain dispersion coefficients C_6, C_8, C_{10}, and so forth. Relativistic effects on the static polarizabilities were rather small for the atoms up to Xe. For this atom, the dipole polarizability was calculated as 27.17 au with a relativistic correction of −0.22 (expt. quoted as 27.3). For the Xe–Xe C_6 coefficient the computation yielded 288.4 au with a relativistic correction of −3.8 (expt. quoted as 285.9).

Small molecules, in particular heavy diatomics, have been studied extensively since the advent of relativistic molecular methods. Computational data is abundant

and we will only quote a few studies to demonstrate the magnitude of relativistic effects on electric properties. Typically, sizeable relativistic effects both on dipole moments and polarizabilities of molecules should be expected for small molecules with heavy (6th row) atoms. As an example for relativistic effects on dipole moments, Kellö and Sadlej reported nonrelativistic dipole moments of 1.13, 1.35, and 1.21 au for CuH, AgH, and AuH, respectively, computed at the CCSD(T) level [236]. With relativistic corrections (MV + DAR) the dipole moments were 1.05, 1.14, and 0.64. Generally, for closed shell molecules and zero or low frequencies spin–orbit effects on polarizabilities α are considered to be very small [237]. Norman et al. compared four-component with scalar relativistic (DKH and ECP) Hartree–Fock computations for group-16 dihydrides (O-Po) and group-17 monohydrides (FAt) and found only small overall relativistic corrections, less than a few percent, which was attributed to the large excitation energies in these molecules [237]. This becomes apparent from the SOS equation for a second-derivative property, Eq. (12-26), which has the excitation energies in the denominator. However, it was noted that higher-order electric properties (first and second order hyperpolarizabilities) afford significant relativistic effects for the systems studied. Very large relativistic effects on quadratic response in *m*- and *o*-dihalobenzenes have also been reported recently by Henrikssson et al. [238]. In a 2004 computational study of the electric response of the Au_{20} cluster, Wu et al. reported remarkably large nonlinear polarizabilities which were obtained from DFT and TD–DFT computations using the scalar relativistic ZORA operator [8]. A static first hyperpolarizability of $\beta_{xyz} = 14.3 \cdot 10^{-30}$ esu was obtained. Linear polarizabilities were also reported, but a comparison with nonrelativistic results were not made. Although likely, it is unclear if β has been affected significantly by relativity.

The Hg dimer has received some attention because it is only very weakly bound in its electronic ground state and accurate computations require the treatment of relativity and correlation simultaneously. Accurate interatomic potentials between Hg_2 atoms used in simulations of bulk properties should help to better understand why Hg is liquid at room temperature and the role that relativistic effects play in the unique properties of mercury. Schwerdtfeger et al. have computed the Hg_2 potential curve and the polarizability tensor as a function of interatomic distance at the scalar relativistic coupled cluster level [239] (other correlation methods were applied in this work, too). The unique tensor components $\alpha_{\parallel}$ and $\alpha_{\perp}$ were both found to decrease by about 50% due to scalar relativistic effects. This very strong effect was attributed to a similarly strong relativistic reduction of the Hg atomic polarizability due to the relativistic contraction of the Hg 6s orbital [240]. See also the TD–DFT calculations [241] where the a reversal of the trend of increasing polarizability for Zn, Cd, Hg due to relativistic effects was explicitly noted. Gaston et al. have computed the polarizability of the Hg dimer using four-component DFT [242]. The authors noted good performance of the functionals (B3LYP and in particular VWN) to reproduce experimental data for the atomic and molecular polarizabilities despite their rather poor performance for predicting the PES: VWN overbinds strongly (as often) and B3LYP yields a repulsive potential curve for Hg_2. Despite these shortcomings, the polarizabilities were in good agreement with experiment,

and the location of the first two poles of the linear response on the real frequency axis also agreed reasonably well with experimental data for the two lowest excitation energies. For relativistic benchmark data see also Lim et al. [243] who calculated spectroscopic constants (R_e, ω_e, D_e, ionization potentials) and static polarizabilities for neutral and positively charged alkali dimers, using coupled cluster and density functional theory. Relativistic effects were dealt with by using pseudopotentials. The coupled-cluster results were found to be in very good agreement with experiment, while the DFT results showed quite a degree of variability. Among the functionals that were applied PW91 performed best.

A four-component DFT approach was applied by Salek et al. to compute static and dynamic polarizabilities of the isoelectronic series Hg, AuH, and PtH_2 [244]. For the Hg polarizability the authors noted large correlation effects of about 25% and an excellent performance of the VWN local density functional "superior to that of the BLYP and B3LYP functionals". The frequency range from 0 to 0.3 au was scanned in undamped computations of α for the Hg atom. The results exhibited very clearly the singular behavior as shown earlier in Figure 12-2. The locations of the poles at 0.20 and 0.24 au agreed quite well with experimental data of 0.18 and 0.25 au for the lowest $^3P_1$ and $^1P_1$ transitions, respectively. Atomic static and dynamic polarizabilities were recently revisited by Bast et al. [245] using four-component DFT with various functionals and including all closed-shell atoms up to Rn. The authors pointed out that rare-gas atoms are not a fully representative test set when calibrating functionals. Among the best performing functionals were asymptotically corrected hybrid functionals.

The OsO_4 molecule has been studied by a number of authors. Cundari et al. reported computations for a series of MO_4 and thiometalate species (M = 3d, 4d and 5d metal including Os) using ECPs [246, 247], with a focus on solvent effects and nonlinear polarizabilities. Hohm and Maroulis recently reported revised experimental data and wavefunction-based (MBPT and coupled-cluster) and DFT benchmark data for OsO_4 [249]. A static electronic polarizability of 51 au was derived from experimental data and estimated from computations as 52.2 ± 1.6 in the nonrelativistic limit. Filatov and Cremer [248] implemented polarizability computations using a modified IORA approach (IORAmm, Hartree–Fock and MP2) and reported computations for noble gas atoms, Hg, and the MO_4 series with M = Ru, Os, Hs. The relativistic correction for the static polarizability of OsO_4 was found to be rather small, −2.3 au The relativistic effect on the polarizability of HsO_4 was more pronounced, −6.5 au Filatov and Cremer reported IORAmm/MP2 polarizabilities of 59.2. 56.6, and 51.04 au and quoted an experimental value of 55.1 for OsO_4 from the CRC Handbook, 76th ed. Cundari's work indicated that medium effects on the polarizability might be pronounced [246]. Our group implemented a spin–orbit DFT and TD–DFT linear response program [241] and computed, inter alia, the static and frequency dependent polarizability of RuO_4 and OsO_4. The static isotropic polarizabilities computed with a local density approximation were 48.2 and 50.0 au, respectively. The value for OsO_4 is in good agreement with experiment.

As a last example for polarizability calculations we shall discuss the series of metallocenes, $M(C_5H_5)_2$, with M = Fe, Ru, Os. Experimental data for the group

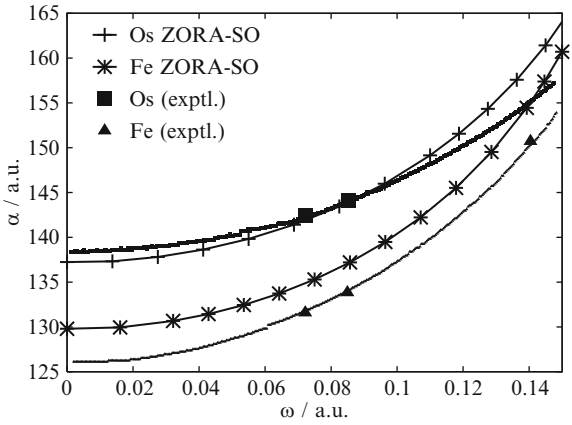

Figure 12-16. Frequency dependent electric polarizability of Ferrocene and Osmocene. Experimental data (points) and extrapolations (lines) extracted from figures published by Goebel and Hohm [250]. ZORA spin–orbit DFT computations, VWN functional [241]

8 metallocenes has been published in [250]. Figure 12-16 displays the frequency dependent polarizability for two of the metallocenes together with computed data that were published in [241]. The ferrocene data compare reasonably well with calculations published earlier in [227] which were performed at a nonrelativistic DFT level (B3LYP functional). The VWN polarizabilities shown in Figure 12-16 are roughly as much above the experimental values as the B3LYP values from [227] lie below. Overall, both the relativistic and the nonrelativistic computations for osmocene and ferrocene, respectively, appear to yield a good description of the polarizability dispersion. The relativistic increase of α from ferrocene to osmocene is quite well reproduced by the computations at frequencies below 0.1 au. For osmocene, the computations yield a stronger dispersion at higher energies which might indicate an underestimation of the energy of a nearby dipole-allowed transition. The solid line for the experimental data in Figure 12-16 represents an extrapolation from the measurements based on a Kramers–Heisenberg dispersion relation for α and its anisotropy, using a single effective excitation frequency and oscillator strength [250]. Between $\omega = 0.050$ and 0.095 au the fit yields an excellent match with a dispersion curve obtained by obtained by dispersive Fourier transform spectroscopy [250]. Instead of a possible underestimation of the computed excitation energies the computed results might alternatively indicate that the experimental fit is not flexible enough to describe the dispersion at higher frequencies.

Wang et al. have used the two-component ZORA framework for an implementation of the "singularity" route to excitation energies within TD–DFT that was discussed in Section 12.2.3 [10]. In the same year, Gao et al. reported a four-component TD–DFT implementation for excitation energies based on the same paradigm [251], and Peng et al. reported an alternative ZORA implementation [252]. Both groups of authors have focused on the correct treatment of non-collinear

spin-density perturbations in the perturbed exchange-correlation potential which is needed to correctly treat magnetic moment (spin) flipped transitions [253]. Wang et al. studied a number of systems, including various closed shell atoms (Zn, Cd, Hg, Cu^+, Pd, Ag^+, Au^+, noble gas atoms), and closed shell diatomics (AgI, Au_2, TlH, Bi_2) and obtained reasonable agreement with experimental excitation energies where available. It was also found that this TD–DFT approach can account for the fine structure splitting of the atomic np^6 to $np^5(n+1)s^1$ transitions, although it was noted that for Xe and Rn some of the splittings involving transitions from the $p_{1/2}$ orbitals were computed as too small [10]. This two-component ZORA implementation was recently applied to compute and analyze the excitation spectra of group-10 hexafluorides, MF_6 with M = Pd, Pt, Ds, along with four-component Hartree–Fock geometry optimizations which yielded octahedral structures in contrast to D_{4h} symmetric nonrelativistic geometries [254]. Comparisons with experimental data were made for PtF_6. Both structural data and the energies of the ligand-field transitions appeared to be in good agreement with experimental data.

Pierloot et al. recently computed the electronic spectra of uranyl UO_2^{2+} and uranyl-tetrachloride $[UO_2Cl_4]^{2-}$ with the TD–DFT ZORA approach [255] and compared to ab-initio CASPT2 data from [256]. TD–DFT computations with standard LDA and GGA XC potentials as well as the LB94 potential did not yield good agreement with CASPT2 in spin-free benchmark computations on UO_2^+ and $[UO_2Cl_4]^{2-}$. However, the shape-corrected SAOP potential performed very well, prompting the authors to conclude that the comparison "convincingly proves the quality of the DFT results". The agreement of the TD–DFT results with experiment and the CASPT2 results was indeed quite good, apart from the ordering of the first two states which are very close in energy. A comparison between ab-initio methods and TD–DFT for uranyl was also made by Réal et al. [257] who concluded that, while most functionals did not yield very accurate excitation energies, the geometries and relaxation energies of the excited states were reasonably well described. A range-separated functional (CAM–B3LYP) was shown to yield improvements for the excitation energies over the popular hybrid functional B3LYP. Ingram and Kaltsoyannis benchmarked non-hybrid functionals for TD–DFT excitation energy computations in three uranium compounds [258]. The researchers tested the PW91, LB94, and SAOP XC potentials and six basis set combinations. It was concluded that the use of large basis sets was not warranted for the systems studied and that SAOP reproduced the experimental data best.

12.4. CONCLUDING REMARKS

Molecular properties can be computed from energy or quasi-energy derivatives. Although much work remains to be done by method developers to improve the speed and accuracy of such computational methods, and to extend the list of properties that can be computed with two- or four-component relativistic methods, over the past 10 years a large number of publications have demonstrated the maturity and reliability of available relativistic methods for property computations. Relativistic effects

on "nuclear" properties can be very large. Examples are ∼100% or more relativistic increases of heavy-atom–light–atom nuclear spin spin couplings or of heavy nucleus EPR hyperfine couplings. NMR chemical shifts and nuclear quadrupole coupling constants can also be very strongly affected by relativistic modifications of the molecule's electronic structure. Even for valence shell properties such as polarizabilities, one might find very strong relativistic effects. A example is the comparatively small polarizability of the Hg atom noted earlier. There are now a number of program implementations available that researchers can use to compute such properties efficiently at some level of approximation for the treatment of relativistic kinematics, even for quite large molecules.

ACKNOWLEDGEMENTS

I would like to acknowledge support of my research by the National Science Foundation and the Department of Energy. I am indebted to the present and past members of my research group as well as many collaborators for their great contributions to the projects that we have been working on – some of which have been presented in this chapter. Dr. Ajitha Devarajan and Shaohui Zheng are thanked for preparing some of the data shown in this chapter. Special thanks to Profs. Markus Reiher and Michael Bühl for providing several re/preprints of their work.

REFERENCES

1. Wolff, S.K., Ziegler, T., van Lenthe, E., Baerends, E.J.: J. Chem. Phys. **110**, 7689 (1999)
2. Bouten,R., Baerends, E.J., van Lenthe, E., Visscher, L., Schreckenbach, G., Ziegler, T.: **104**, 5600 (2000)
3. Autschbach, J., Zurek, E.: J. Phys. Chem. A **107**, 4967 (2003)
4. Autschbach, J., Ziegler, T.: J. Chem. Phys. **113**, 936 (2000)
5. Autschbach, J., Ziegler, T.: J. Chem. Phys. **113**, 9410 (2000)
6. van Lenthe, E., Wormer, P.E.S., van der Avoird, A.: J. Chem. Phys. **107**, 2488 (1997)
7. van Lenthe, E., van der Avoird, A., Wormer, P.E.S.: J. Chem. Phys. **108**, 4783 (1998)
8. Wu, K., Li, J., Lin, C.: Chem. Phys. Lett. **388**, 353 (2004)
9. van Lenthe, E., Baerends, E.J.: J. Chem. Phys. **112**, 8279 (2000)
10. Wang, F., Ziegler, T., Van Lenthe, E., Van Gisbergen, S., Baerends, E.J.: J. Chem. Phys. **122**, 204103 (2005)
11. McWeeny, R.: Methods of Molecular Quantum Mechanics, 2nd edn. Academic Press, London (1992)
12. a) Autschbach, J., Ziegler, T.: In: D.M. Grant, R.K. Harris (eds.) Encyclopedia of Nuclear Magnetic Resonance, Volume 9, pp. 306–323. Wiley, Chichester (2002)
    b) Autschbach, J., Zheng, S., Ann. Rep. NMR Spectrosc., Volume 67, pp. 1–95, (2009)
13. Bethe, H.A., Salpeter, E.E.: Quantum Mechanics of One and Two Electron Atoms. Springer, Berlin (1957)
14. Romero, R.H., Aucar, G.A.: Int. J. Mol. Sci. **3**, 914 (2002)
15. Romero, R.H., Aucar, G.A.: Phys. Rev. A **65**, 053411 (2002)
16. Moss, R.E.: Advanced Molecular Quantum Mechanics. Chapman and Hall, London (1973)

17. Sadlej, A.J.: In: B.O. Roos (ed.) Lecture Notes in Chemistry II, Lecture Notes in Chemistry, Volume 64, pp. 203–230. Springer, Berlin (1994)
18. Almlöf, J., Gropen, O.: In: K.B. Lipkowitz, D.B. Boyd (eds.) Reviews in Computational Chemistry, Volume 8, Chap. 4, pp. 203–244. VCH Publishers, New York (1996)
19. Hess, B.A.: In: P. von Ragué Schleyer (ed.) Encyclopedia of Computational Chemistry, pp. 2499–2508. Wiley, Chichester (1998)
20. Okada, S., Shinada, M., Matsuoka, O.: J. Chem. Phys. **93**, 5013 (1990)
21. Kellö, V., Sadlej, A.J.: Int. J. Quantum Chem. **68**, 159 (1998)
22. Schwarz, W.H.E.: In: Z.B. Masic (ed.) The Concept of the Chemical Bond, Volume 2, pp. 559–643. Springer, Berlin (1990)
23. Barysz, M., Sadlej, A.J.: J. Mol. Struct. (THEOCHEM) **573**, 181 (2001)
24. Barysz, M., Sadlej, A.J.: J. Chem. Phys. **116**, 2696 (2002)
25. Ilias, M., Saue, T.: J. Chem. Phys. **126**, 064102 (2007)
26. Pauli, W.: Handbuch der Physik, volume 5. Springer, Berlin (1958)
27. Morrison, J.D., Moss, R.E.: Mol. Phys. **41**, 491 (1980)
28. Moss, R.E., Trivedi, H.P.: Mol. Phys. **38**, 1611 (1979)
29. van Lenthe, E., Baerends, E.J., Snijders, J.G.: J. Chem. Phys. **99**, 4597 (1993)
30. Chang, C., Pelissier, M., Durand, M.: Phys. Scr. **34**, 394 (1986)
31. Philipsen, P.H.T., van Lenthe, E., Snijders, J.G., Baerends, E.J.: Phys. Rev. B **56**, 13556 (1997)
32. Dyall, K., van Lenthe, E.: J. Chem. Phys. **111**, 1366 (1999)
33. Filatov, M., Cremer, D.: J. Chem. Phys. **120**, 11407 (2004)
34. Wolf, A., Reiher, M., Hess, B.A.: J. Chem. Phys. **117**, 9215 (2002)
35. Malkin, I., Malkina, O.L., Malin, V.G.: Chem. Phys. Lett. **361**, 231 (2002)
36. Fukuda, R., Hada, M., Nakatsuji, H.: J. Chem. Phys. **118**, 1015 (2003)
37. Fukuda, R., Hada, M., Nakatsuji, H.: J. Chem. Phys. **118**, 1027 (2003)
38. Melo, J.I., Ruiz de Azúa, M.C., Peralta, J.E., Scuseria, G.E.: J. Chem. Phys. **123**, 204112 (2005)
39. Malkin, I., Malkina, O.L., Malkin, V.G., Kaupp, M.: J. Chem. Phys. **123**, 244103 (2005)
40. Kudo, K., Fukui, H.: J. Chem. Phys. **123**, 114102 (2005)
41. Rutkowski, A.: J. Phys. B **19**, 149 (1986)
42. Kutzelnigg, W.: Z. Phys. D. **11**, 15 (1989)
43. Kutzelnigg, W.: J. Comput. Chem. **20**, 1199 (1999)
44. Hennum, A.C., Klopper, W., Helgaker, T.: J. Chem. Phys. **115**, 7356 (2001)
45. Schwerdtfeger, P., Brown, J.R., Laerdahl, J.K., Stoll, H.: J. Chem. Phys. **113**, 7110 (2000)
46. Van de Walle, C.G., Blöchl, P.E.: Phys. Rev. B **47**, 4244 (1993)
47. Pickard, C.J., Mauri, F.: Phys. Rev. B **63**, 245101 (2001)
48. Malkina, O.L., Schimmelpfennig, B., Kaupp, M., Hess, B.A., Chandra, P., Wahlgren, U., Malkin, V.G.: Chem. Phys. Lett. **296**, 93 (1998)
49. Epstein, S.T.: The Variation Method in Quantum Chemistry. Academic Press, New York (1974)
50. Gauss, J.: In: J. Grotendorst (ed.) Modern Methods and Algorithms of Quantum Chemistry, NIC, Volume 3, pp. 541–592. John von Neumann Institute for Computing, Jülich (2000)
51. King, H.F., Komornicki, A.: J. Chem. Phys. **84**, 5645 (1986)
52. Hellmann, H.: Z. Phys. **85**, 180 (1933)
53. Pyykkö, P.: Theor. Chem. Acc. **103**, 214 (2000)
54. Christiansen, O., Jørgensen, P., Hättig, C.: Int. J. Quantum Chem. **68**, 1 (1998)
55. Vaara, J., Manninnen, P., Lantto, P.: In: M. Kaupp, M. Bühl, V.G. Malkin (eds.) Calculation of NMR and EPR Parameters. Theory and Applications. Wiley, Weinheim (2003)
56. Manninen, P., Lantto, P., Vaara, J.: J. Chem. Phys. **119**, 2623 (2003)
57. Vaara, J., Ruud, K., Vahtras, O.: J. Chem. Phys. **111**, 2900 (1999)
58. Vaara, J., Ruud, K., Vahtras, O., AA gren, H., Jokisaari, J.: J. Chem. Phys. **109**, 1212 (1998)

59. Krykunov, M., Autschbach, J.: J. Chem. Phys. **123**, 114103 (2005)
60. Sasagane, K., Aiga, F., Itoh, R.: J. Chem. Phys. **99**, 3738 (1993)
61. Autschbach, J.: Coord. Chem. Rev. **251**, 1796 (2007)
62. Autschbach, J., Ziegler, T.: Coord. Chem. Rev. **238/239**, 83 (2003)
63. Byron, F.W., Fuller, R.W.: The Mathematics of Classical and Quantum Physics. Addison-Wesley, Reading, MA (1969)
64. Autschbach, J.: ChemPhysChem. Vol. 10, pp. 2274–2283 (2009)
65. Norman, P., Bishop, D.M., Jensen, H.J.A., Oddershede, J.: J. Chem. Phys. **115**, 10323 (2001)
66. Jensen, L., Autschbach, J., Schatz, G.C.: J. Chem. Phys. **122**, 224115 (2005)
67. Rudolph, M., Autschbach, J.: Chirality **20**, 995 (2008)
68. Jørgensen, P., Simons, J.: Second Quantization-Based Methods in Quantum Chemistry. Academic Press, New York (1981)
69. Oddershede, J.: Adv. Quantum Chem. **11**, 275 (1978)
70. Oddershede, J.: In: K.P. Lawley (ed.) Ab Initio Methods in Quantum Chemistry, Volume II, pp. 201–239. Wiley, London, (1987)
71. Foresman, J.B., Head-Gordon, M., Pople, J.A., Frisch, M.J.: J. Phys. Chem. **96**, 135 (1992)
72. Autschbach, J.: Spectroscopic Properties obtained from TD-DFT, in Encyclopedia of Inorganic Chemistry. Wiley. Chichester (2009)
73. Harriman, J.E.: Theoretical Foundations of Electron Spin Resonance. Academic Press, New York (1978)
74. London, F.: J. Phys. Radium **8**, 397 (1937)
75. Ditchfield, R.: Mol. Phys. **27**, 789 (1974)
76. Kutzelnigg, W.: Isr. J. Chem. **19**, 193 (1980)
77. Hansen, A.E., Bouman, T.D.: J. Chem. Phys. **82**, 5035 (1985)
78. Keith, T.A., Bader, R.F.W.: Chem. Phys. Lett. **210**, 223 (1993)
79. Pedersen, T.B., Koch, H., Boman, L., Sánchez de Merás, A.M.J.: Chem. Phys. Lett. **393**, 319 (2004)
80. Sauer, S.P.A., Oddershede, J.: Int. J. Quantum Chem. **50**, 317 (1994)
81. Geertsen, J.: J. Chem. Phys. **90**, 4892 (1989)
82. Aucar, G.A., Saue, T., Visscher, L., Jensen, H.J.A.: J. Chem. Phys. **110**, 6208 (1999)
83. Pyykkö, P.: Chem. Phys. **74**, 1 (1983)
84. Xiao, Y., Peng, D., Liu, W.: J. Chem. Phys. **126**, 081101 (2007)
85. Xiao, Y., Liu, W., Cheng, L., Peng, D.: J. Chem. Phys. **126**, 214101 (2007)
86. Komorovsky, S., Repisk, M., Malkina, O.L., Malkinand, V.G., Ondik, I.M., Kaupp, M.: J. Chem. Phys. **128**, 104101 (2008)
87. Dyall, K.G., Faegri, K., Jr.: Relativistic Quantum Chemistry. Oxford University Press, New York (2007)
88. Baba, T., Fukui, H.: Mol. Phys. **100**, 623 (2002)
89. Fukui, H., Baba, T., Shiraishi, Y., Imanishi, S., Kudo, K., Mori, K., Shimoji, M.: Mol. Phys. **102**, 641 (2004)
90. Andrae, D.: Phys. Rep. **336**, 413 (2000)
91. Visscher, L., Dyall, K.: At. Data Nucl. Data Tables **67**, 207 (1997)
92. Pyykkö, P.: Relativistic Theory of Atoms and Molecules, Lecture Notes in Chemistry, volume 60. Springer, Berlin (1993).
93. Rosenthal, J.E., Breit, G.: Phys. Rev. **41**, 459 (1932)
94. Crawford, M.F., Schawlow, A.L.: Phys. Rev. **76**, 1310 (1949)
95. Bohr, A., Weisskopf, V.F.: Phys. Rev. **77**, 94 (1950)
96. Bohr, A.: Phys. Rev. **81**, 331 (1951)
97. Stroke, H.H., Blin-Stoyle, R.J., Jaccarino, V.: Phys. Rev. **123**, 1326 (1961)

98. Rosenberg, H.J., Stroke, H.H.: Phys. Rev. A **5**, 1992 (1972)
99. Shabaev, V.M.: J. Phys. B **27**, 5825 (1994)
100. Malkin, E., Malkin, I., Malkina, O.L., Malkin, V.G., Kaupp, M.: Phys. Chem. Chem. Phys. **8**, 4079 (2006)
101. Mastalerz, R., Barone, G., Lindh, R., Reiher, M.: J. Chem. Phys. **127**, 074105 (2007)
102. Autschbach, J.: Theor. Chem. Acc. **112**, 52 (2004)
103. Pyykkö, P.: Chem. Phys. **22**, 289 (1977)
104. Lipas, P.O., Pyykkö, P., Pajanne, E.: J. Chem. Phys. **58**, 3248 (1973)
105. Reiher, M., Hinze, J.: In: B.A. Hess (ed.) Relativistic Effects in Heavy-Element Chemistry and Physics. Wiley, Chichester (2003)
106. Grant, I.P.: Adv. Phys. **19**, 747 (1970)
107. Ye, A., Autschbach, J.: J. Chem. Phys. **125**, 234101 (2006)
108. Ye, A., Patchkovskii, S., Autschbach, J.: J. Chem. Phys. **127**, 074104 (2007)
109. Rosa, A., Ricciardi, G., Gritsenko, O., Baerends, E.J.: In: N. Kaltsoyannis, J.E. McGrady (eds.) Principles and applications of density functional theory in inorganic chemistry I. Structure and Bonding, Volume 112, pp. 49–115. Springer, Heidelberg (2004)
110. Autschbach, J.: In: N. Kaltsoyannis, J.E. McGrady (eds.) Principles and applications of density functional theory in inorganic chemistry I, Structure and Bonding, Volume 112, pp. 1–48. Springer, Heidelberg (2004)
111. Ziegler, T., Autschbach, J.: Chem. Rev. **105**, 2695 (2005)
112. Bühl, M.: In: M. Kaupp, M. Bühl, V.G. Malkin (eds.) Calculation of NMR and EPR Parameters. Theory and Applications, pp. 421–431. Wiley, Weinheim (2004)
113. Kaupp, M., Malkin, V.G., Malkina, O.L.: In: P. von Ragué Schleyer Encyclopedia of Computational Chemistry, pp. 1857–1866. Wiley, Chichester, (1998)
114. Bagno, A., Saielli, G.: Theor. Chem. Acc. pp. 603–619 (2006)
115. Kaupp, M., Bühl, M., Malkin V.G. (eds.): Calculation of NMR and EPR Parameters. Theory and Applications. Wiley-VCH, Weinheim (2004)
116. Neese, F.: In: M. Kaupp, M. Bühl, V.G. Malkin (eds.) Calculation of NMR and EPR Parameters. Theory and Applications, pp. 581–589. Wiley-VCH, Weinheim (2004)
117. Patchkovskii, S., Schreckenbach, G.: In: M. Kaupp, M. Bühl, V.G. Malkin (eds.) Calculation of NMR and EPR Parameters. Theory and Applications, pp. 505–532. Wiley-VCH, Weinheim (2004)
118. Autschbach, J.: In: M. Kaupp, M. Bühl, V.G. Malkin (eds.) Calculation of NMR and EPR Parameters. Theory and Applications, pp. 227–247, Wiley-VCH, Weinheim (2004)
119. Autschbach, J., Ziegler, T.: In: M. Kaupp, M. Bühl, V.G. Malkin (eds.) Calculation of NMR and EPR Parameters. Theory and Applications, pp. 249–264, Wiley-VCH, Weinheim (2004)
120. Vaara, J., Manninen, P., Lantto, P.: In: M. Kaupp, M. Bühl, V.G. Malkin (eds.) Calculation of NMR and EPR Parameters. Theory and Applications, pp. 209–226. Wiley-VCH, Weinheim (2004)
121. Schwerdtfeger, P., Pernpointner, M., Nazarewicz, W.: In: M. Kaupp, M. Bühl, V.G. Malkin Calculation of NMR and EPR Parameters: Theory and Applications, pp. 279–291. Wiley-VCH, Weinheim (2004)
122. Casabianca, L.B., de Dios, A.C.: J. Chem. Phys. **128**, 052201 (2008)
123. Koch, W., Holthausen, M.C.: A Chemist's Guide to Density Functional Theory. Wiley, Weinheim (2001)
124. Mann, B.E.: In: P.S. Pregosin (ed.) Transition Metal Nuclear Magnetic Resonance, pp. 177–215. Elsevier, Amsterdam (1991)
125. Autschbach, J.: J. Chem. Phys. **129**, 094105 (2008) Erratum ibid. **130**, 209901 (2009)
126. Enevoldsen, T., Visscher, L., Saue, T., Jensen, H.J.A., Oddershede, J.: J. Chem. Phys. **112**, 3493 (2000)
127. Kirpekar, S., Sauer, S.P.A.: Theor. Chem. Acc. **103**, 146 (1999)

128. Schumann, C., Dreeskamp, H.: J. Magn. Reson. **3**, 204 (1970)
129. Flitcroft, N., Kaesz, H.D.: J. Am. Chem. Soc. **85**, 1377 (1963)
130. Pyykkö, P., Wiesenfeld, L.: Mol. Phys. **43**, 557 (1981)
131. Lobayan, R.M., Aucar, G.A.: J. Mol. Struct. **452**, 1 (1998)
132. Khandogin, J., Ziegler, T.: J. Phys. Chem. A **104**, 113 (2000)
133. Autschbach, J.: J. Chem. Phys. **127**, 124106 (2007)
134. Weinhold, F.: In: P. von Ragué Schleyer Encyclopedia of Computational Chemistry, pp. 1792–1811. John Wiley & Sons, Chichester (1998)
135. Autschbach, J., Igna, C.D., Ziegler, T.: J. Am. Chem. Soc. **125**, 1028 (2003)
136. Le Guennic, B., Matsumoto, K., Autschbach, J.: Magn. Res. Chem. **42**, S99 (2004)
137. Dickson, R.M., Ziegler, T.: J. Phys. Chem. **100**, 5286 (1996)
138. Khandogin, J., Ziegler, T.: Spectrochim. Acta **A 55**, 607 (1999)
139. Boeckh, R.V., Graeff, G., Ley, R.: Z. Phys. **179**, 285 (1964)
140. Dickinson, J.T., Stephenson, D.A., Zorn, J.C.: J. Chem. Phys. **53**, 1525 (1970)
141. Hammerle, R.H., Dickinson, J.T., VanAusdal, R.G., Stephenson, D.A., Zorn, J.C.: J. Chem. Phys. **50**, 2086 (1969)
142. Stephenson, D.A., Dickinson, J.T., Zorn, J.C.: J. Chem. Phys. **53**, 1529 (1970)
143. Bryce, D.L., Wasylishen, R.E.: J. Am. Chem. Soc. **122**, 3197 (2000)
144. Bryce, D.L., Wasylishen, R.E.: J. Autschbach, T. Ziegler, J. Am. Chem. Soc. **124**, 4894 (2002)
145. Autschbach, J., Ziegler, T.: J. Am. Chem. Soc. **123**, 5320 (2001)
146. Autschbach, J., Le Guennic, B.: J. Am. Chem. Soc. **125**, 13585 (2003)
147. Chen, W., Liu, F., Matsumoto, K., Autschbach, J., Le Guennic, B., Ziegler, T., Maliarik, M., Glaser, J.: Inorg. Chem. **45**, 4526 (2006)
148. Autschbach, J., Igna, C.D., Ziegler, T.: J. Am. Chem. Soc. **125**, 4937 (2003)
149. Autschbach, J., Sterzel, M.: J. Am. Chem. Soc. **129**, 11093 (2007)
150. Kaupp, M.: Untersuchung der Strukturen, Energien und NMR–Eigenschaften von Übergangsmetallverbindungen mit Hilfe quantenchemischer Methoden (1996). Habilitationsschrift, Universität Stuttgart, Germany
151. Bagno, A., Saielli, G.: J. Am. Chem. Soc. **129**, 11360 (2007)
152. Wolff, S.K., Ziegler, T.: J. Chem. Phys. **109**, 895 (1998)
153. Nomura, Y., Takeuchi, Y., Nakagawa, N.: Tetrahedron Lett. **8**, 639 (1969)
154. Morishima, I., Endo, K., Yonezawa, T.: J. Chem. Phys. **59**, 3356 (1973)
155. Volodicheva, M.I., Rebane, T.K.: Teoreticheskaya i Éksperimental'naya Khimiya (Engl. ed. Theor. and Exp. Chemistry) **14**, 348 (1978)
156. Cheremisin, A.A., Schastnev, P.V.: J. Mag. Res. **40**, 459 (1980)
157. Pyykkö, P., Görling, A., Rösch, N.: Mol. Phys. **61**, 195 (1987)
158. Kaupp, M., Malkina, O.L., Malkin, V.G., Pyykkö, P.: Chem. Eur. J. **4**, 118 (1998)
159. Alam, T., Clawson, J., Bonhomme, F., Thoma, S., Rodriguez, M., Zheng, S., Autschbach, J.: Chem. Mater. **20**, 2205 (2008)
160. Ehlers, A.W., Ruiz-Morales, Y., Baerends, E.J., Ziegler, T.: Inorg. Chem. **36**, 5031 (1997)
161. Vaara, J., Malkina, O.L., Stoll, H., Malkin, V.G., Kaupp, M.: J. Chem. Phys. **114**, 61 (2001)
162. Gilbert, T.M., Ziegler, T.: J. Phys. Chem. A **103**, 7535 (1999)
163. Fukui, H., Baba, T.: J. Chem. Phys. **108**, 3854 (1998)
164. David, J., Restrepo, A.: Phys. Rev. A **76**, 052511 (2007)
165. Kolb, D., Johnson, W.R., Shorer, P.: Phys. Rev. A **26**, 19 (1982)
166. Vaara, J., Pyykkö, P.: J. Chem. Phys. **118**, 2973 (2003)
167. Manninen, P., Ruud, K., Lantto, P., Vaara, J.: J. Chem. Phys. **122**, 114107 (2005)
168. Fowe, E.P., Belser, P., Daul, C., Chermette, H.: Phys. Chem. Chem. Phys. **7**, 1732 (2005)
169. Sterzel, M., Autschbach, J.: Inorg. Chem. **45**, 3316 (2006)

170. Autschbach, J., Le Guennic, B.: Chem. Eur. J. **10**, 2581 (2004)
171. Koch, K.R., Burger, M.R., Kramer, J., Westra, A.N.: Dalton Trans. pp. 3277–3284 (2006)
172. Autschbach, J., Zheng, S.: Magn. Reson. Chem. **46**, pp. S48–S55 (2008)
173. Nakatsuji, H., Hada, M., Kaneko, H., Ballard, C.C.: Chem. Phys. Lett. **255**, 195 (1996)
174. Rodriguez-Fortea, A., Alemany, P., Ziegler, T.: J. Phys. Chem. A **103**, 8288 (1999)
175. Hada, M., Kaneko, H., Nakatsuji, H.: Chem. Phys. Lett. **261**, 7 (1996)
176. Autschbach, J., Hess, B.A., Johansson, P.A., Neugebauer, J., Patzschke, M., Pyykkö, P., Reiher, M., Sundholm, D.: Phys. Chem. Chem. Phys. **6**, 11 (2004)
177. Dmitrenko, O., Bai, S., Beckmann, P.A., van Bramer, S., Vega, C., Dybowski, A.J.: J. Phys. Chem. A **112**, 3046 (2008)
178. Bagno, A., Bonchio, M., Sartorel, A., Scorrano, G.: ChemPhysChem **4**, 517 (2003)
179. Gracia, J., Poblet, J.M., Fernández, J.A., Autschbach, J., Kazansky, L.P.: Eur. J. Inorg. Chem. pp. 1149–1154 (2006)
180. Gracia, J., Poblet, J.M., Autschbach, J., Kazansky, L.P.: Eur. J. Inorg. Chem. pp. 1139–1148 (2006)
181. Bagno, A., Bonchio, M., Autschbach, J.: Chem. Eur. J. **12**, 8460 (2006)
182. Wasylishen, R.: In: M. Kaupp, M. Bühl, V.G. Malkin Calculation of NMR and EPR Parameters. Theory and Applications, pp. 433–447. Wiley-VCH, Weinheim (2004)
183. Autschbach, J., Kantola, A., Jokisaari, J.: J. Phys. Chem. A **111**, 5343 (2007)
184. Jokisaari, J., Järvinen, S., Autschbach, J., Ziegler, T.: J. Phys. Chem. A **106**, 9313 (2002)
185. Autschbach, J. Ziegler, T.: J. Am. Chem. Soc. **123**, 3341 (2001)
186. Abragam, A., Bleany, B.: Electron Paramagnetic Resonance for Transition ions. Clarendon Press, Oxford (1970)
187. Bolvin, H.: Chem. Phys. Chem. **7**, 1575 (2006)
188. Loboda, O., Minaev, B., Vahtras, O., Ruud, K., Agren, H.: J. Chem. Phys. **119**, 3120 (2003)
189. Loboda, O., Minaev, B., Vahtras, O., Schimmelpfennig, B., Agren, H., Ruud, K., Jonsson, D.: Chem. Phys. **286**, 127 (2003)
190. Ray, K., Begum, A., Weyhermuller, T., Piligkos, S., van Slageren, J., Neese, V., Wieghardt, K.: J. Am. Chem. Soc. **127**, 4403 (2005)
191. Reviakine, R., Arbuznikov, A.V., Tremblay, J.C., Remenyi, C., Malkina, O.L., Malkin, V.G., Kaupp, M.: J. Chem. Phys. **125**, 054110 (2006)
192. Hrobárik, P., Reviakine, R., Arbuznikov, A.V., Malkina, O.L., Malkin, V.G., Köhler, F.H., Kaupp, M.: J. Chem. Phys. **126**, 024107 (2007)
193. Eriksson, L.A.: In: P. von Ragué Schleyer (ed.) Encyclopedia of Computational Chemistry, pp. 952–958. John Wiley & Sons, Wiley, Chichester, UK (1998)
194. Jayatilaka, D.: J. Chem. Phys. **108**, 7587 (1998)
195. Chibotaru, L.F., Ceulemans, A., Bolvin, H.: Phys. Rev. Lett. **101**, 033003 (2008)
196. Neese, F.: J. Chem. Phys. **115**, 11080 (2001)
197. Lushington, G.H., Grein, F.: Theor. Chim. Acta **93**, 259 (1996)
198. Lushington, G.H., Grein, F.: Int. J. Quantum Chem. **106**, 3292 (1997)
199. Lushington, G.H.: J. Phys. Chem. A **104**, 2969 (2000)
200. Moores, W.H., McWeeny, R.: Proc. Roy. Soc. London A **332**, 365 (1973)
201. Ishii, M., Morihashi, V., Kikuchi, O.: J. Mol. Struct. (THEOCHEM) **325**, 99 (1991)
202. Vahtras, O., Minaev, B., AAgren, H.: Chem. Phys. Lett. **281**, 186 (1997)
203. Kaupp, M.: In: A. Lund, M. Shiotani (eds) EPR Spectroscopy of Free Radicals in Solids. Trends in Methods and Applications. Kluwer, Dordrecht, (2002)
204. Visscher, L., Enevoldsen, T., Saue, T., Oddershede, J.: J. Chem. Phys. **109**, 9677 (1998)
205. Komorovský, S., Repiský, M., Malkina, O.L., Malkin, V.G., Malkin, I., Kaupp, M.: J. Chem. Phys. **124**, 084108 (2006)
206. Schreckenbach, G., Ziegler, T.: J. Phys. Chem. A **101**, 3388 (1997)

207. Patchkovskii, S., Ziegler, T.: J. Chem. Phys. **111**, 5730 (1999)
208. Malkina, O.L., Vaara, J., Scimmelpfennig, B., Munzarová, M., Malkin,V.G., Kaupp, M.: J. Am. Chem. Soc. **122**, 9206 (2000)
209. Kaupp, M., Reviakine, R., Malkina, O.L., Arbuznikov, A., Schimmelpfennig, V., Malkin, V.G.: J. Comput. Chem. **23**, 794 (2002)
210. Belanzoni, P., van Lenthe, E., Baerends, E.J.: J. Chem. Phys. **114**, 4421 (2001)
211. van Lenthe, E., van der Avoird, A., Hagen, W.R., Reijerse, E.J.: J. Phys. Chem. A **104**, 2070 (2000)
212. Munzarová, M., Kaupp, M.: J. Phys. Chem. A **103**, 9966 (1999)
213. Schlegel, H.B.: In: P. von Ragué Schleyer (ed.) Encyclopedia of Computational Chemistry, pp. 2665–2671. Wiley, Chichester (1998)
214. Neese, F.: J. Chem. Phys. **118**, 3939 (2003)
215. Munzarová, M.L., Kubáček, P., Kaupp, M.: J. Am. Chem. Soc. **111**, 11900 (2000)
216. Saladino, A.C., Larsen, S.C.: Catalysis Today **1**, 122 (2005)
217. Pyykkö, P.: Mol. Phys. **99**, 1617 (2001)
218. Pyykkö, P.: Mol. Phys. **106**, 1965 (2008)
219. Rossini, A.J., Mills, R.W., Briscoe, G.A., Norton, E.L., Geier, S.J., Hung, I., Zheng, S., Autschbach, J., Schurko, R.W.: J. Am. Chem. Soc. **131**, 3317 (2009)
220. Neese, F., Wolf, A., Fleig, T., Reiher, M., Hess, B.A.: J. Chem. Phys. **122**, 204107 (2005)
221. Barone, G., Mastalerz, G., Reiher, M., Lindh, R.: J. Phys. Chem. A **112**, 1666 (2008)
222. Bast, R., Schwerdtfeger, P.: J. Chem. Phys. **119**, 5988 (2003)
223. Willans, M.J., Feindel, K.W., Ooms, K.J., Wasylishen, R.E.: Chem. Eur. J. **12**, 159 (2006)
224. Ooms, K.J., Wasylishen, R.E.: J. Am. Chem. Soc. **126**, 10972 (2004)
225. Thierfelder, C., Schwerdtfeger, P., Saue, T.: Phys. Rev. A **76**, 034502 (2007)
226. Lantto, P., Vaara, J.: J. Chem. Phys. **125**, 174315 (2006)
227. Hohm, U., Goebel, D., Grimme, S.: Chem. Phys. Lett. **272**, 328 (1997)
228. van Wüllen, C., Kutzelnigg, W.: Chem. Phys. Lett. **205**, 563 (1993)
229. Cybulski, S.M., Bishop, D.M.: J. Chem. Phys. **100**, 2019 (1994)
230. Krykunov, M., Autschbach, J.: J. Chem. Phys. **126**, 024101 (2007)
231. Konowalow, D.D., Rosenkrantz, M.E., Stevens, W.J., Krauss, M.: Chem. Phys. Lett. **64**, 317 (1979)
232. Desclaux, J.P., Laaksonen, L., Pyykkö, P.: J. Phys. B **14**, 419 (1981)
233. Pyykkö, P.: Chem. Rev. **88**, 563 (1988)
234. Sadlej, A.J., Urban, M., Gropen, O.: Phys. Rev. A **44**, 5547 (1991)
235. Hättig, C., Hess, B.A.: J. Phys. Chem. **100**, 6243 (1996)
236. Kellö, V., Sadlej, A.J.: Theor. Chim. Acta **92**, 253 (1995)
237. Norman, P., Schimmelpfennig, B., Ruud, K., Rgen Aa. Jensen, H.J., Gren, H.A.: J. Chem. Phys. **116**, 6914 (2002)
238. Henriksson, J., Saue, T., Norman, P.: J. Chem. Phys. **128**, 024105 (2008)
239. Schwerdtfeger, P., Söhnel, T., Pernpointner, M., Laerdahl, J.K., Wagner, F.E.: J. Chem. Phys. **115**, 5913 (2001)
240. Schwerdtfeger, P., Li, J., Pyykkö, P.: Theor. Chim. Acta **87**, 313 (1994)
241. Devarajan, A., Gaenko, A., Autschbach, J.: J. Chem. Phys. **130**, 194102 (2009)
242. Gaston, N., Schwerdtfeger, P., Saue, T., Greif, J.: J. Chem. Phys. **124**, 044304 (2006)
243. Lim, I.S., Schwerdtfeger, P., Söhnel, T., Stoll, H.: J. Chem. Phys. **122**, 134307 (2005)
244. Salek, P., Helgaker, T., Saue, T.: Chem. Phys. **311**, 187 (2005)
245. Bast, R., Heßelmann, A., Salek, P., Helgaker, T., Saue, T.: ChemPhysChem **9**, 445 (2008)
246. Cundari, T.R., Kurtz, H.A., Zhou, T.: J. Chem. Inf. Comput. Sci. **41**, 38 (2001)
247. Cundari, T.R., Kurtz, H.A., Zhou, T.: Chem. Phys. **240**, 205 (1999)
248. Filatov, M., Cremer, D.: J. Chem. Phys. **119**, 1412 (2003)
249. Hohm, U., Maroulis, G., J. Chem. Phys. **121**, 10411 (2004)

250. Goebel, D., Hohm, U.: J. Chem. Soc. Faraday Trans. **93**, 3467 (1997)
251. Gao, J., Zou, W., Liu, W., Xiao, Y., Peng, D., Song, B., Liu, C.: J. Chem. Phys. **123**, 054102 (2005)
252. Peng, D., Zou, W., Liu, W.: J. Chem. Phys. **123**, 144101 (2005)
253. Wang, F., Ziegler, T.: J. Chem. Phys. **121**, 12191 (2004)
254. David, J., Fuentalba, P., Restrepo, A.: Chem. Phys. Lett. **457**, 42 (2008)
255. Pierloot, K., van Besien, E., van Lenthe, E., Baerends, E.J.: J. Chem. Phys. **126**, 194311 (2007)
256. Pierloot, K., van Besien, E.: J. Chem. Phys. **123**, 204309 (2005)
257. Réal, F., Vallet, V., Marian, C., Wahlgren, U.: J. Chem. Phys. **127**, 214302 (2007)
258. Ingram, K., Kaltsoyannis, N.: Spec. Publ. R. Soc. Chem. **305**(Recent Advances in Actinide Science), 258 (2006) CAN 146:429319, 65–66

Index